Information for Contributors (See also A. I. P. Style Manual)

Manuscripts

Send manuscripts to S. A. Goudsmit, Brookhaven National Laboratory, Upton, Long Island, New York.

Each article submitted will in general consist of (a) textual material, i.e., all material which is to be set in type, and (b) drawings or photographs from which zinc etchings or copper half-tones will be made. Textual material will consist of an abstract, the body of the paper, tabular material, references, and figure captions. All of this material must be in English, typewritten (except mathematical expressions) double spaced with wide margins (for editorial instructions to the printer) on a durable, white paper, preferably letter size. The original copy, not the carbon, should be submitted.

For general style, spellings, abbreviations, and form, recent issues of this journal should be consulted.

The prime requisite is that the copy shall be clear to the typesetter, who is neither a physicist nor a mathematician.

Abstracts

An abstract must accompany each article. It should be adequate as an index and as a summary. As an index, it should give all subjects, major and minor, concerning which new information is presented. As a summary it should give the conclusions of the article and all numerical results of general interest.

Mathematical Expressions

All but the simplest mathematical expressions should be carefully printed in by hand. Be sure to distinguish between capital and small letters. Indicate clearly superscripts and subscripts by inverted carets and carets, respectively. Avoid complicated superscripts and subscripts. Avoid repetition of a complicated expression by representing it by some convenient symbol. Identify in the margin Greek letters and unusual symbols. Use fractional exponents instead of root signs. Use the solidus (/) for fractions wherever its use will save vertical space.

References

References should appear as footnotes, numbered consecutively, and arranged thus:

[4] A. B. Smith, Phys. Rev. 61, 832 (1932).

[5] H. Lamb, *Hydrodynamics* (Cambridge University Press, Cambridge, England, 1960), sixth edition, pp. 573, 645.

Tables

All but the simplest tabular material should be organized in tabular form rather than as a part of the running text. Tables may be written on sheets separate from the running text with indications in the margin of the running text where the table is to be inserted. Each table should have a caption which will make the data in the table intelligible without reference to the text. Avoid complicated column headings; if necessary, use symbols which are explained in the table caption.

Figures

Wherever possible figures should be planned for the width of a column of *The Physical Review* (3 inches). A convenient reduction ratio is about 2:1 or 3:1. The original drawings or photographs should therefore be in general about 6 to 9 inches wide and the lettering and symbols should be large enough on the original that when reduced they shall not be less than about $\frac{1}{16}$ in. (~1.5 mm). If the reduction is 3:1, the original lettering should be not less than $\frac{1}{32}$ in. high.

The process of making zinc etchings or copper half-tones is a black and white photographic one. Therefore line drawings must be in *india ink* on white paper or tracing cloth. Coordinate paper is not desirable but if used must be blue lined and the coordinate lines which are to show must be inked over.

Photographs should have maximum black and white contrast.

Plan figures to use space efficiently. Avoid wasting space, particularly at the top or bottom.

Identify on the back or other suitable place each original drawing or photograph with the author's name and the figure number. Figures should be numbered consecutively and their approximate position indicated in the margin of the running text. Figure captions should be typed and included with the manuscript (not as part of the figure).

Avoid round and oval photographs.

Alterations

Take great care that each manuscript is typographically accurate. A limited number of alterations in proof are unavoidable, but the cost of making extensive alterations after the article has been set in type will be charged to the author.

Proof and all correspondence concerning proof in the process of publication should be addressed to the Publication Manager, American Institute of Physics, 57 East 55 Street, New York 22, New York.

THE PHYSICAL REVIEW

A journal of experimental and theoretical physics established by E. L. Nichols in 1893

VOLUME 99

Second Series

JULY 1–SEPTEMBER 15, 1955

Published for the

AMERICAN PHYSICAL SOCIETY

by the

AMERICAN INSTITUTE OF PHYSICS

Incorporated

THE PHYSICAL REVIEW

A journal of experimental and theoretical physics established by E. L. Nichols in 1893

Published by the American Institute of Physics for the

AMERICAN PHYSICAL SOCIETY

Officers

President

R. T. BIRGE
University of California
Berkeley, California

Vice-President

E. P. WIGNER
Princeton University
Princeton, New Jersey

Secretary

K. K. DARROW
Bell Telephone Laboratories
Office:
Columbia University
New York 27, New York

Treasurer

G. B. PEGRAM
Columbia University
New York 27, New York

Local Secretary for the Pacific Coast

WILLIAM A. NIERENBERG
University of California
Berkeley, California

Managing Editor

S. A. GOUDSMIT
Brookhaven National Laboratory
Upton, Long Island
New York

BOARD OF EDITORS

Editor

S. A. GOUDSMIT

Assistant Editor

S. PASTERNACK

Associate Editors

1953–1955	*1954–1956*	*1955–1957*
W. A. FOWLER	P. G. BERGMANN	G. J. DIENES
KENNETH GREISEN	GREGORY BREIT	R. G. HERB
CHARLES KITTEL	F. J. DYSON	K. G. MCKAY
R. E. MARSHAK	P. KUSCH	J. R. PELLAM
W. K. H. PANOFSKY	R. SMOLUCHOWSKI	LEWI TONKS
V. F. WEISSKOPF	J. C. STREET	GREGOR WENTZEL

Manuscripts for publication should be submitted to S. A. GOUDSMIT, Brookhaven National Laboratory, Upton, Long Island, New York. The authors' institutions are requested to pay a publication charge of $25 per page which, if honored, entitles them to 100 free reprints. Instructions will be sent with galley proofs.

Proof and all correspondence concerning papers in the process of publication should be addressed to the Publication Manager, American Institute of Physics, 57 East 55 Street, New York 22, New York.

Subscription Price

United States and Canada $30.00
Elsewhere $32.00

Back Numbers [1]

Yearly back number rate when complete year is available:
Prior to 1949: $25.00
Thereafter: $33.00
Single copies: $3.00 each, prior to July, 1929;
$1.50 each, July, 1929–December, 1941;
$3.00 each, January, 1942–December, 1946;
$1.50 each, thereafter.
General index, 1893–1920: $4.00.
1921–1950: Paper binding, $10 (Members); $14 (Nonmembers)
Cloth binding, $12 (Members); $16 (Nonmembers)

Subscriptions, renewals, and orders for back numbers should be addressed to the American Institute of Physics, 57 East 55 Street, New York 22, New York.

Changes of address in the case of members of the American Physical Society should be addressed to the Treasurer; in the case of other subscribers to the American Institute of Physics.

[1] For Series 1 inquire of Physics Department, Cornell University, Ithaca, New York.

The Physical Review is published semi-monthly at Prince and Lemon Streets, Lancaster, Pennsylvania.

Entered as second-class matter March 6, 1947, at the Post Office at Lancaster, Pennsylvania, under the Act of March 3, 1879.

Acceptance for mailing at special rate of postage provided for in paragraph (d-2), section 34.40, P. L. & R. of 1948, authorized January 27, 1933.

Copyright 1955 by the American Physical Society

THE
PHYSICAL REVIEW

A journal of experimental and theoretical physics established by E. L. Nichols in 1893

SECOND SERIES, VOL. 99, NO. 1 JULY 1, 1955

Gamma-Ray Spectrum of Polonium-209

E. H. DAGGETT* AND G. R. GROVE
Mound Laboratory,† Monsanto Chemical Company, Miamisburg, Ohio
(Received November 10, 1954; revised manuscript received March 25, 1955)

A polonium sample was produced at Oak Ridge National Laboratory by the bombardment of bismuth targets with 20-Mev protons. The sample contained a mixture of the polonium isotopes of mass 208 and 209 with a negligible amount of the isotope of mass 210. Measurements were made of the isotopic ratio from the molecular spectrum and the alpha activity was determined by calorimetry. The spectrum obtained with a NaI(Tl) crystal and pulse-height analyzer showed the existence of gamma rays with energies of about 270, 570, and 865 kev. The 803-kev gamma ray of Po^{210} was not detected. This spectrum is attributed to Po^{209} since there is no gamma radiation from Po^{208}. The intensity of the 865-kev gamma ray relative to the gamma ray of a calibrated Po^{210} sample was estimated to be about 7.5×10^{-3} quanta per Po^{209} alpha particle. Coincidence measurements between various pairs of gamma rays indicated that only the 270- and 570-kev quanta were in cascade and existed with about the same relative intensity as the 865-kev gamma ray.

INTRODUCTION

A POLONIUM sample was produced at the Oak Ridge National Laboratory by bombardment of bismuth targets with cyclotron-produced protons having energies in the region of 20 Mev. At 20-Mev proton energy the $(p,2n)$ reaction predominates to yield polonium-208. The competing (p,n) reaction producing polonium-209 has a yield of the order of ten percent relative to the $(p,2n)$ reaction; while the radiative-capture reaction gives only a trace amount of polonium-210. The irradiated targets were dissolved in nitric acid and the polonium was plated on platinum foils. A small part of the polonium was volatilized into a quartz tube for spectroscopic determination of the isotopic ratios.[1] The remainder of the polonium was volatilized into another quartz tube which was sealed in an aluminum container about $\frac{1}{4}$ inch in diameter by $\frac{3}{4}$ inch long and constituted the sample which was used for calorimetric and gamma-ray measurements.

From the relative intensities of the band heads of the $Po^{208}-Po^{208}$ and the $Po^{208}-Po^{209}$ molecules obtained from the molecular spectrum of the small sample, it was estimated that the sample contained 14.5 ± 0.8 percent by weight of polonium-209 relative to the total polonium content. Only a trace amount of polonium-210 was detected. Calorimetric determinations of the power output of the large sample gave a value of very nearly one curie for the alpha activity, using a half-life value of 1070 days and an alpha energy of 5.14 Mev for polonium-208, and a half-life of 200 years and an alpha energy of 4.95 Mev for polonium-209. From the spectroscopic and calorimetric measurements it was estimated that about 2.4 millicuries of polonium-209 was present in the sample.

EXPERIMENTAL

The gamma-ray spectrum, Fig. 1, showed the existence of three gamma rays with energies of about 270, 570, and 865 kev. The 803-kev gamma ray of polonium-210 was not detectable from this sample. These three

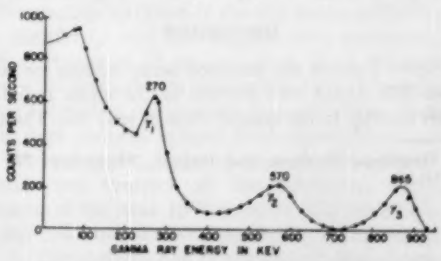

FIG. 1. Gamma-ray spectrum of polonium-209.

* Present address: Bell Telephone Laboratories, Murray Hill, New Jersey.
† Mound Laboratory is operated by Monsanto Chemical Company for the U. S. Atomic Energy Commission.
[1] D. J. Hunt and G. Pish, J. Opt. Soc. Am. (to be published).

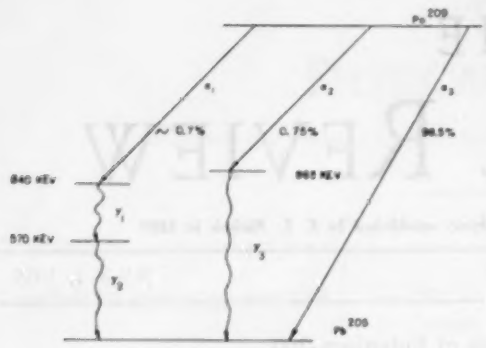

FIG. 2. Decay of polonium-209.

gamma rays are attributed to the decay of polonium-209 since it has been reported by Templeton, Howland, and Perlman[3] that there is no gamma radiation associated with the decay of polonium-208.

The gamma-ray spectrum from a pure polonium-210 standard sample was measured with the scintillation spectrometer using nearly the same geometry. The standard had an activity of 0.72 microcurie of the 803-kev gamma radiation. A comparison of the relative intensities of the 865- and 803-kev gamma rays corrected for differences of crystal efficiencies gave a value of 18 microcuries of 865-kev gamma radiation from the polonium-209 sample. Thus the alpha branching in the decay of polonium-209 to the 865-kev excited level of lead-205 is about 0.75 percent.

Coincidence measurements were made on the three different pair combinations of the 270, 570, and 865 kev gamma rays. The only combination giving a significant coincidence-counting rate within a resolving time of about 0.55 microsecond was the 270—570 kev pair. From the observed coincidence-counting rate corrected for the random contribution, the intensity of the coincident pair was estimated to be about 17 microcuries. This is an alpha-branching ratio of about 0.7 percent which gives rise to an 840-kev excited state of lead-205 that decays by cascade emission of the 270- and 570-kev gamma rays. The relative intensities of the three gamma rays and the alpha-branching ratios leading to their formation are consistent with the efficiency response of the crystal for gamma rays of these energies.

DISCUSSION

Figure 2 shows the proposed decay scheme for polonium-209. About 98.5 percent of the alpha radiation leads directly to the ground state of lead-205. The two fine-structure modes of decay of nearly equal intensity lead to excited states of lead-205 which differ in energy by only 25 kev.

This 25-kev difference in level spacing was verified by observing the spectrum in a well-type crystal, Fig. 3, which was thick enough to absorb a reasonable fraction of both of the cascade gamma rays emitted in the same event. This spectrum shows the peaks which are due to the sum of the 270- and 570-kev gamma rays and the 865-kev gamma ray. These peaks are separated by approximately 25 kev of energy which led to the proposed decay scheme instead of a single excited state which decayed by a single gamma ray or a cascade pair.

The existence of gamma rays following the decay of bismuth-205 by electron capture with energies of 0.431, 0.527, 0.550, 0.746, and 1.84 Mev have been reported by Karraker and Templeton.[3] Gamma-ray energies of

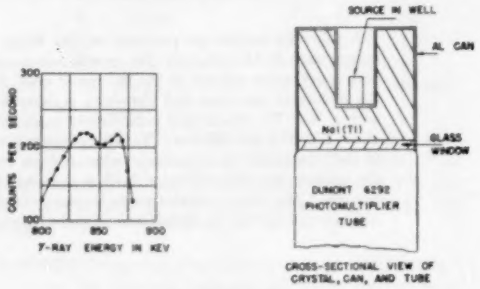

FIG. 3. Crystal counter and response.

284.4, 703.7, 911.6, 988.6, 1044.6, 1074.1, 1189.8, 1615.4, 1766.3, 1777.8, and 1864.2 kev were found by Alburger and Pryce[4] from conversion electron measurements using a source containing bismuth-205. These gamma rays result from transitions from excited states of lead-205 as do the three gamma rays observed in the decay of polonium-209. Inasmuch as these data are not mutually complementary, a level scheme for lead-205 is not as yet clearly defined.

ACKNOWLEDGMENTS

The authors wish to express their thanks to Dr. G. Pish and the other members of the X-Ray Group for the results of the spectroscopic analysis and to Mr. K. C. Jordan of the Calorimetry Research Group for the determination of the total alpha activity. Grateful acknowledgment is also made to Dr. D. L. Timma for his constant encouragement and stimulating discussions.

[3] Templeton, Howland, and Perlman, Phys. Rev. **72**, 758 (1947).

[3] D. G. Karraker and D. H. Templeton, Phys. Rev. **81**, 510 (1951).

[4] D. E. Alburger and M. H. L. Pryce, Phys. Rev. **95**, 1482 (1954).

Relative Intensities of the Radiations from Hf^{175}†

A. O. Burford, J. F. Perkins,* and S. K. Haynes
Vanderbilt University, Nashville, Tennessee

(Received November 8, 1954; revised manuscript received March 28, 1955)

The intensities of the electronic and electromagnetic radiations of Hf^{175} have been measured with a magnetic-lens spectrometer. The existence of transitions of 89.1, 113.4, 228, 318, 342.3, and 431 kev was confirmed. For the 89.1-kev transition $\alpha_K = 3.5_{-0.5}^{+1.5}$, $\alpha_K/\alpha_L = 6.0 \pm 1$, $\alpha_L/\alpha_M = 3.5 \pm 0.9$, and the transition is predominantly $M1$. For the 228-kev transition $\alpha_K/\alpha_{L+M} = 2.0 \pm 0.5$ and the transition is of the type $E2$. For the 342.3-kev transition $\alpha_K/\alpha_{L+M} = 4.94 \pm 0.5$, and the transition is a mixture of $M1$ and $E2$. A decay scheme is given in which the ground state of Lu^{175} is characterized as $\Omega = 7/2$, $I = 7/2$, parity even; the 113.4-kev state is the first rotational excited state with $\Omega = 7/2$, $I = 9/2$, parity even; the 342.3-kev state is a single-particle excited state with $\Omega = 5/2$, $I = 5/2$, parity even; and the 431-kev state is the first rotational excitation of the 342.3-kev state with $\Omega = 5/2$, $I = 7/2$, parity even.

I. INTRODUCTION

HAFNIUM-175 was discovered in 1949 by Wilkinson and Hicks[1] as a product of the reactions $Lu^{175}(p,n)Hf^{175}$ and $Lu^{175}(d,2n)Hf^{175}$. The half-life was measured and found to be 70 ± 2 days. They showed the presence of strong Lu K x-rays which indicated K capture and found a 350-kev gamma ray with a conversion coefficient of approximately 0.4. A 1.5-Mev gamma ray reported by these observers has not been found by others including ourselves. The assignment of the activity to Hf^{175} was confirmed by Hedgran and Thulin[2] and by Burson *et al.*[3] who produced the activity by neutron capture in separated isotopes of Hf. The conversion lines have been studied by Cork *et al.*[4] who discovered the K, L, and M lines of 89.1- and 342.3-kev gamma rays, by Burson *et al.*[3] who confirmed these lines and found conversion lines from gamma rays of 113.4 and 228.4 kev, and by Burson and Rutledge[5,6] who found lines from gamma rays of 318 and 431 kev and who measured the K/L conversion ratios of the four strongest lines to be ~3 for 89.1 kev, ~10 for 113.4 kev, ~2 for 228.4 kev, and 4.93 ± 0.20 for 342.3 kev. Later Bashilev *et al.*[7] obtained an $\alpha_K : \alpha_L : \alpha_M$ of 30:15:1.5 for the 89.1-kev transition and 100:20:5 for the 342.3-kev transition.

The studies reported here were designed as far as possible to provide more information on the relative intensities (a) of the electronic radiations by use of a magnetic-lens spectrometer, and (b) of the gamma radiations by measurement of the photoelectrons in the magnetic-lens spectrometer.

II. SOURCES

The Hf used was 20 mg of separated Hf^{174} obtained from the Isotopes Division, Oak Ridge, Tennessee, in the form of HfO_2. The analysis showed Hf^{174}, 7.85 percent; Hf^{176}, 16.70 percent; Hf^{177}, 27.29 percent; Hf^{178}, 24.07 percent; Hf^{179}, 8.24 percent; Hf^{180}, 15.84 percent, with impurities of a few hundredths of a percent of Cu, Mg, Na, and Si.

The sample was irradiated for one month in the Oak Ridge reactor during January 1953. No chemical purification was carried out with the result that certain weak impurity effects were encountered in the spectra. The material was dissolved in HF and a drop was placed on a tight 20-mil tungsten-wire coil in the evaporation apparatus previously described.[8] The wire was heated to a bright white heat for about 30 minutes. This operation was carried out three times. The resulting source was about 8 mm in diameter on a 120-$\mu g/cm^2$ aluminum foil and had a thickness of less than 50 $\mu g/cm^2$. This source was used for the electron spectrum in the magnetic spectrometer.

The remainder of the activity was enclosed in an Al capsule $\frac{3}{16}$ in. in diameter with 0.0158 in. of Al covering the active material as an electron absorber. This source was much stronger than the other and was used for the photoelectron spectrum of Hf^{175}. The converters were stuck on the end of the capsule with a small amount of very dilute cement.

III. ELECTRON SPECTRUM OF Hf^{175}

The electron spectrum of the thin source of Hf^{175} was run completely with the magnetic-lens spectrometer[8] with a window of 26 $\mu g\ cm^{-2}$ from 10 to 500 kev in June, 1953 and again in September, 1953. The average interval between the spectra was 105 days. Certain peaks were run again in April, 1954, about 180 days after the September run. By comparison it was possible to identify and subtract off the continuous beta-ray spectrum of the weak Hf^{181} impurity. The remainder of the electron spectrum as of September, 1953 is shown in Fig. 1. The identification of the various lines shown in

† This work was supported in part by contract with the U. S. Atomic Energy Commission whose assistance is gratefully acknowledged.

* U. S. Atomic Energy Commission Predoctoral Fellow. Present address: Lockheed Aircraft Corporation, Smyrna, Georgia.

[1] G. Wilkinson and H. Hicks, Phys. Rev. **75**, 696 (1949).
[2] A. Hedgran and S. Thulin, Phys. Rev. **81**, 1072 (1951).
[3] Burson, Blair, Keller, and Wexler, Phys. Rev. **83**, 62 (1951).
[4] Cork, Stoddard, Rutledge, Branyan, and Le Blanc, Phys. Rev. **78**, 299 (1950).
[5] S. B. Burson and W. C. Rutledge, Phys. Rev. **86**, 633 (1952).
[6] S. B. Burson and W. C. Rutledge, Argonne National Laboratory Report ANL-4746, 1951 (unpublished).
[7] Bashilev, Anton'eva, Dzhelepov, and Dolgentseva, Izvest. Akad. Naut. Ser. Fiz. U.S.S.R. **17**, 437 (1953).
[8] Broyles, Thomas, and Haynes, Phys. Rev. **89**, 715 (1953).

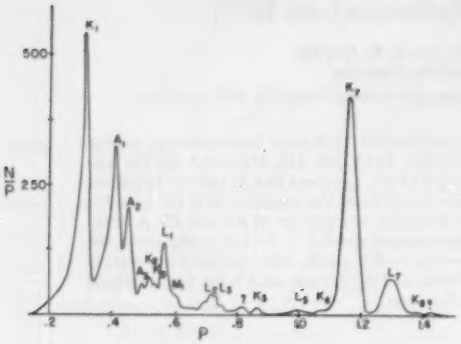

FIG. 1. Electron spectrum of Hf^{175} after subtraction of the continuous beta-ray spectrum of the Hf^{181} impurity.

the figure together with their relative intensities is given on the left-hand side of Table I.

All of the peaks assigned to Lu^{175} had a half-life of 70 days within experimental error except the Auger peaks. The peaks assigned to Hf^{181} had a half-life which agreed with Hf^{181} within experimental error. Two small unidentified peaks were also found. The one at $p=0.8$ did not appear in the June data. Further evidence of impurities was the failure of the Auger peaks to decay with the proper half-life. Between June and September these peaks decayed too fast, while between September and April they decayed too slowly. This difficulty combined with the fact that the K-conversion line of the 113-kev gamma ray should be under the A_2 peak makes the error in Auger intensity considerably larger than the errors in the determination of the areas under the peaks which are shown in the table.

From the third column of the table, the following important ratios can be obtained. For the 342.3-kev transition $\alpha_K/\alpha_{L+M}=4.94\pm0.5$; for the 228.4-kev transition, it is 2 ± 0.5; and for the 89.1-kev transition, α_K/α_L is 6.0 ± 1 and α_L/α_M is 3.5 ± 0.9.

The first of these ratios is about the same as that which Burson and Rutledge[6] and Bashilov[7] give for α_K/α_L. Although the difference is not great, we feel that it is greater than our experimental error. We estimate that our value of α_K/α_{L+M} is consistent with a value of about 6 for α_K/α_L.

The value of α_K/α_{L+M} for the 228.4-kev transition is in excellent agreement with Burson and Rutledge but the α_K/α_L ratio for the 89.1-kev transition is double their value and triple the value of Bashilov *et al.*[7] Both because Burson's value was obtained photographically over an energy range of 3 to 1 and because most of our errors would tend to make our value too small, we shall assume that the α_K/α_L ratio of 6 is substantially correct.

IV. PHOTOELECTRON SPECTRUM OF Hf^{175}

The spectrum of the strong source enclosed in an aluminum capsule was observed five times during the summer of 1953 in the following order; no converter, 1.53-mg cm^{-2} Au converter, no converter, 0.88-mg cm^{-2} Au converter, no converter. The no converter runs combined with the other runs between photoelectron lines made it possible to determine the Compton electron intensity under the photoelectron peaks. The three no-converter runs also helped identify parts of the spectrum which did not have the 70-day half-life of Hf^{175}. Figure 2 shows the spectrum obtained with the 0.88-mg cm^{-2} converter together with the Compton background under certain peaks. The 0.88 mg cm^{-2} was preferable for analysis both because, occurring later, there was less short lived impurity and also because it was desirable to have a converter which was reasonably thin for L and M photoelectrons from the 89.1- and 113-kev gamma rays.

The interpretation of Fig. 2 and the relative gamma-ray intensities are given on the right-hand side of

TABLE I. Magnetic spectrometer values for the electron and gamma-ray intensities.

Electron spectrum				Photoelectron spectrum		
Peak	Energy of gamma ray kev	Relative intensity	Nuclide	Peak	Energy of gamma ray kev	Relative intensity
K_1	89.1	10.0±5%	Lu^{175}	...	...	...
A_1	Lu $K-LL$	6.26±10%	Lu^{175}	$L_{K\alpha}$	Lu K_α	
A_2	Lu $K-LX$	2.92±10%	Lu^{175}	$L_{K\beta},M_{K\alpha}$	Lu $K_\alpha K_\beta$	61.1
A_3	Lu $K-XY$	0.61±25%	Lu^{175}	$M_{K\beta}$	Lu K_β	
K_2	133	...	Ta^{181}	...	...	...
K_3	136	...	Ta^{181}	...	...	...
L_1	89.1	1.67±15%	Lu^{175}	L_1	89.1	2.83±20%
M_1	89.1	0.5±25%	Lu^{175}	M_1	89.1	
L_2	133	...	Ta^{181}	...	...	...
L_3	136	...	Ta^{181}	...	...	...
...	...	...	Lu^{176}	K_4	113.4	...
...	...	...	Lu^{176}	L_4	113.4	0.46±30%
K_5	228.4	0.18±25%	Lu^{175}	...	...	...
L_5	228.4	0.088±50%	Lu^{175}	...	...	...
K_6	318	0.1±100%	Lu^{175}	...	...	...
K_7	342.3	8.5±2.5%	Lu^{175}	K_7	342.3	...
L_7	342.3	1.72±10%	Lu^{175}	L_7	342.3	89.8±8%
K_8	430	0.07±50%	Lu^{175}	...	...	...

Table I. The relative intensities were obtained by dividing the $L+M$ (or L) photoline areas by their photoelectric cross sections *relative* to that of the 342.3-kev gamma ray. These relative cross sections were assumed to be the same as the relative K photoelectron cross sections for the same binding energy. Thus we used the average of Heitler's[9] *relative* values for Al and Sn which agreed closely with each other and whose average K binding energy approximates the L binding energy of Au.

The most surprising result of the photoelectron spectrum is that the 113-kev gamma ray is so strong when it was completely undetectable in the conversion line spectrum. It seems clear that the conversion coefficient of this gamma ray is much smaller than that of the 89.1-kev gamma ray.

V. DISCUSSION AND DECAY SCHEME

A. Relative Gamma-Ray and Electron Intensities

In order to relate the relative electron and gamma-ray intensities, it is necessary to use either the known conversion coefficient of one of the gamma rays or the fluorescence yield of lutecium to relate the x-ray and Auger electron intensities.

The only conversion coefficients available are for the 342.3-kev line. McGowan[10] (0.095±0.015) and Kerr[11] (~0.118) have reported preliminary rough measurements. The experimental α_K/α_L ratios discussed in Sec. III, although not in agreement, seem to lie between 5 and 6. When combined with the theoretical values of α_K[12] and the various α_L,[13] these values seem to indicate

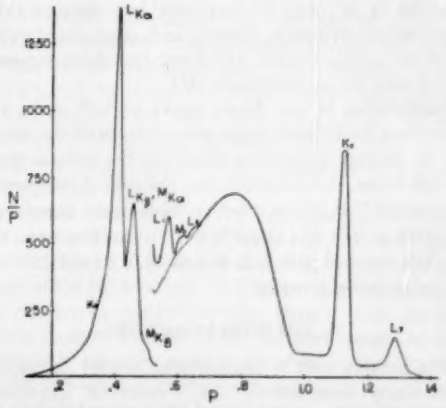

FIG. 2. Photoelectron spectrum of Hf^{178} from a 0.88-mg cm^{-2} radiator. The photoelectron peaks arising from the K x-rays are reduced in ordinate by a factor of 10.

[9] W. Heitler, *Quantum Theory of Radiation* (Oxford University Press, London, 1949), second edition, p. 124.
[10] F. K. McGowan (private communication).
[11] R. J. Kerr, Ph.D. thesis, Vanderbilt University, 1954 (unpublished).
[12] Rose, Goertzel, and Perry, Oak Ridge National Laboratory Report ORNL, 1023, 1951 (unpublished).
[13] M. E. Rose (privately circulated values).

TABLE II. Summary of data for transitions resulting from the decay of Hf^{178}.

Transition kev	Total intensity percent	α_K measured	α_K/α_L BPH[a]	α_K/α_L BR[b]	α_K/α_L B[c]
89.1	$15.0^{+4}_{-2.5}$	$3.5^{+1.5}_{-2.5}$	6.0±1	~3	2
113.4	~1	<1		~10	
228	~1		2.0±0.5[d]	~2	
318	<1				
342.3	100	0.095±0.015[e]	4.94±0.5[d]	4.93±0.2	5.0
430	~1				

[a] BPH refers to the present paper.
[b] BR refers to references 5 and 6.
[c] B refers to reference 7.
[d] Indicates α_K/α_{L+M} ratio.
[e] Reference 10.

a mixed $M1$, $E2$ transition with the proportion of $M1$ being between 49 and 79 percent and the K-converstion coefficient between 0.079 and 0.104. It would seem that McGowan's value is not far from the mean of these values and that his uncertainty represents pretty well the probable uncertainty of the mean of these values. In the following discussion McGowan's value has been used. The intensity values in Table I have been normalized using this value to make the total intensity of the 342.3-kev transition 100 percent.

In principle, the electron and photoelectron intensities could also be related by means of the K x-ray photoelectrons and the K-Auger electrons, by use of the fluorescence yield for Lu which is calculated to be 0.9326±0.003.[14] In Table I, the total number of empty K shells produced per disintegration comes out 1.45 from the Auger intensity and 0.650 from the x-ray intensity. Even with allowance for the uncertainty of the conversion coefficient of the Auger intensity, and the fluorescence yield, it is evident that the x-ray value is too low by a factor of about two. This discrepancy is probably due to the fact that the 0.88-mg cm^{-2} converter is not really thin for the 40- to 50-kev photoelectrons. Thus a substantial percentage of the photoelectrons produced are scattered out of the acceptance cone of the spectrometer by the converter. Another phenomenon which may contribute to this discrepancy is the change with energy of the mean angle of emission of the photoelectrons.[15] These phenomena undoubtedly occur to a lesser extent for the 76-, 86-, and 100-kev photoelectron peaks of the 89.1- and 113-kev gamma rays. Hence the intensities of these gamma rays given in Table II should be considered as lower limits. The 89.1-kev gamma-ray intensity may be as much as 50 percent greater and the 113-kev intensity as much as 25 percent greater than these given in the table.

Taking into account these uncertainties in gamma-ray intensities and the limits of detection of the photoelec-

[14] E. H. S. Burhop, Colloque du Centre National de la Recherche Scientifique, "Le Rôle du Cortège Electronique dans les Phénomènes Radioactifs," June, 1954. These results are to appear in J. phys. et radium.
[15] J. J. Murray, PhD thesis, California Institute of Technology, 1954 (unpublished).

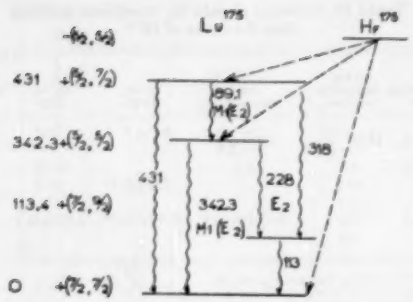

FIG. 3. Decay scheme of Hf^{175}. All energies are in kev. The parentheses opposite the states indicate the values of (Ω,I) where I is the total spin of the state and Ω is the component of the total spin along the axis of symmetry of the nucleus. The existence of capture disintegrations direct to the ground state of Lu^{175} is uncertain.

trons and conversion electrons which were not found, we get the total intensities and conversion coefficients given in Table II. This table also includes the previously discussed conversion ratios.

B. Decay Scheme

A proposed decay scheme for Hf^{175} is shown in Fig. 3.[16] The measured spin of the ground state of Lu^{175} is 7/2.[17] Since the 342.3-kev transition is in part $M1$, the 342.3-kev state must have a spin of 5/2, 7/2, or 9/2 with the same parity as the ground state. No 9/2 single-particle state exists in the subshell containing the 71st proton. Therefore if the spin were 9/2 the 342.3-kev state would have to be interpreted as a rotational excited state.[18] It is the 113.4-kev state, however, which is produced by Coulomb excitation[19] and to which the spin of 9/2 should be assigned.[16] Hence, 9/2 is eliminated as a possible value of the spin of the 342.3-kev state.

Our value for the ratio α_K/α_L for the 89.1-kev transition clearly indicates that it is also predominantly $M1$ by comparison with the curves of Goldhaber and Sunyar.[20] The conversion coefficient is also consistent with this interpretation. We estimate by extrapolating the curves of Rose *et al.*[13] from 150 kev to 89.1 kev that the theoretical K-conversion coefficient is between 4 and 5 for a pure $M1$ transition as compared with our value of 3.5 in Table II. The spin of the 431-kev state must therefore be 3/2, 5/2, 7/2, or 9/2.

A spin of 3/2 is excluded[21] because the 318-kev transition would have a spin change of 3 and would be unobservable. A spin of 5/2 is excluded because the 431-kev gamma ray would be more intense than the 89.1-kev gamma ray. Spins of 7/2 for both the 342.3- and the 431-kev states are excluded by the same reasoning applied to both the 431- and the 318-kev gamma rays. A spin of 9/2 is excluded for the same reason as for the 342.3-kev state.

If the spin of the 342.3-kev state is 5/2, the 431-kev state *can* have a spin of 7/2 as the first rotational level ($\Omega=5/2$, $I=7/2$)[18] of the 342.3-kev state. The 89.1-kev transition, being rotational, will have a much higher intensity[16] than the higher-energy 431- and 318-kev single-particle transitions of similar multipolarity. As a check on this interpretation, the energy of the transition between these two rotational states can be computed on the assumption that the effective moment of inertia of the nucleus is the same in the 342.3-kev state as in the ground state. The computed energy is 113.4 kev $(28/36)=88.2$ kev as compared with the experimental value of 89.1 kev.

The above assignment of spins makes the 228-kev radiation virtually pure $E2$ ($M3$ and $E4$ radiation being neglected). The experimental ratio $\alpha_K/\alpha_{L+M}=2.0\pm0.5$ is good agreement with the empirical curve of Goldhaber and Sunyar[20] for $E2$ radiation. The intensity of the K-conversion line of the 228-kev radiation is also about what would be expected for an $E2$ transition if about 20 percent of the 342.3-kev transitions are assumed to be $E2$ as indicated by our value of α_K for the latter. The 113.4-, 318- and 431-kev transitions are probably all mixtures of $M1$ and $E2$ radiation but there is little experimental evidence. Burson and Rutledge's[6] value of 10 for α_K/α_L for the 113.4-kev transition suggests that it may be predominantly $M1$.

Inaccuracies in the Auger peaks as well as in the conversion coefficients make any estimate of the intensity of capture transitions direct to the ground state of little value. It is probable that the spin of the ground state of Hf^{175} is 5/2 in order to have many transitions to states of spin 5/2 and 7/2 but virtually none to the 113/kev state of spin 9/2. A spin of 3/2 for Hf^{175} cannot be excluded however.

VI. ACKNOWLEDGMENTS

The authors wish to acknowledge helpful discussions with many members of the Vanderbilt University Physics Department and particularly with Dr. Henry Brysk. Mr. L. Velinsky and Mr. J. W. Gilbert were of great assistance in operating the spectrometer.

[16] The rotational aspects of this decay scheme were suggested to us by B. R. Mottelson in a private communication.
[17] H. Schuler and T. Schmidt, Naturwiss. **22**, 714 (1934).
[18] A. Bohr, thesis, Institute for Theoretical Physics of the University of Copenhagen, *Rotational States of Atomic Nuclei* (Ejnar Munksgaards Forlag, Copenhagen, 1954).
[19] N. P. Heydenburg and G. M. Temmer, Phys. Rev. **94**, 1399 (1954).
[20] R. Goldhaber and A. W. Sunyar, Phys. Rev. **83**, 906 (1951).
[21] This corrects an incorrect assignment made in a preliminary report of part of this work [Burford, Perkins, and Haynes, Phys. Rev. **95**, 303 (1954)].

Gamma Rays of Tellurium-131 and Tellurium-129

C. A. MALLMANN, A. H. W. ATEN, JR.,* D. R. BES, AND CLARA M. DE MCMILLAN
Comisión Nacional de la Energía Atómica, Buenos Aires, Argentina
(Received February 28, 1955)

The γ rays of Te^{131} and Te^{129} have been investigated by means of a crystal spectrometer.

EXPERIMENTAL

THE γ rays of Te^{131} and Te^{129} were studied in the laboratory for nuclear spectroscopy of this Institute by means of a crystal spectrometer equipped with a sliding channel. Energy and efficiency calibrations were performed by means of Hg^{203}, Cs^{137}, Na^{22}, and Y^{88}, and only photopeaks were used.

Most of the samples were prepared by irradiation of sodium tellurite with 26-Mev deuterons in the synchrocyclotron of this Institute. After iodine had been extracted twice, tellurium was precipitated in the presence of suitable hold-back carriers, and purified by a scavenging precipitation of ferric hydroxide and a second tellurium precipitation. In some cases Te^{129} was obtained free from Te^{131} via an antimony fraction separated by hydride formation from uranium oxide irradiated with deuterons. (These separations were performed in the Radiochemistry Laboratories.)

TELLURIUM-131

In the 25-minute period of Te^{131} the following γ energies were found: 145 ± 10 kev (100), 450 ± 10 kev (24), 595 ± 15 kev (about 6), 950 ± 15 kev (about 4) and 1140 ± 20 kev (about 8). The figures given in parentheses indicate relative intensities, the last three are only rough approximations. Measurements of the total γ energy by means of a Geiger counter with known γ sensitivity indicate that about one γ ray of 145 kev occurs per β decay, and therefore the intensity ratios also give a rough value of the numbers of each γ ray per β process.

In the 30-hour period of Te^{131} the energies observed were: 145 ± 10 kev, 770 ± 20 kev, and 1140 ± 20 kev. The intensity of the 770 kev is at least about as high as that of the 145 kev, and the 1140 kev is much stronger here relative to the 145-kev line than it is in the 25-minutes isomer. Because of the complex nature of the spectrum it was not possible to observe the 450-kev and the 595-kev γ rays here with certainty.

It should be mentioned that our results seem to be in agreement with the experiments of Geiger[1] if it is realized that the γ rays of higher energy cannot be recognized separately in absorption measurements.

It seems to be evident that the 145-kev transition goes to the ground state. It is tempting to assume that the 440-kev transition goes to the 145-kev level and that the 595-kev line represents the crossover of these two lines. From the difference in the intensity ratios in the 25-minute period and the 30-hours period, we may conclude that the 1140-kev γ ray and the 950-kev γ ray do not come from the same level. The main fraction of the 25-minute isomer seems to go to the 145-kev level.

In the decay of the 30-hour isomer the principal feature is the high intensity of the 770-kev γ ray, a line which we did not observe in the 25-minute period. Its occurrence is explained most easily by assuming a direct β decay of the metastable state of Te^{131} with a frequency comparable to that of the isomeric transition. Goldhaber and Hill[2] have given arguments for the possibility of such a direct β transition on the basis of the yield of the chemical separation of the two isomers. A very important fraction if not the main part of the direct β decay of the 30-hour isomer is followed by the 770 kev γ ray, a smaller fraction by the 1140-kev γ ray.

TELLURIUM-129

By far the larger part of the β decay of the 72-minute period of Te^{129} goes to the ground state, unless there should be a low-lying level in I^{129} with an energy below about 70 kev. A γ line of 435 ± 20 kev occurs in about 9 percent of the β transitions, and a γ line of 1080 ± 40 kev in about 0.7 percent.

ACKNOWLEDGMENTS

A fuller discussion of this work will be published in the *Publicaciones de la Comisión Nacional de la Energía Atómica, Argentina*. We wish to thank Ing. E. Galloni and Mr. Monneret de Villars for the cyclotron irradiations, Dr. K. Fraenz and Ing. Pinasco for help with the construction of the crystal spectrometer, and S. Mayo, J. Peyre, R. Norscini, and Dr. H. Bosch for assistance with the measurements.

* On leave of absence from the Instituut voor Kernphysisch Onderzoek, Amsterdam. Sincere thanks are due the Director of the Comisión Nacional de la Energía Atómica for a generous invitation which made possible this collaboration.

[1] K. Geiger, Z. Naturforsch. **7a**, 579 (1952).

[2] M. Goldhaber and R. D. Hill, Revs. Modern Phys. **24**, 179 (1952).

Alpha Spectrum in the Decay of Li^8†

R. T. Frost* and S. S. Hanna
Department of Physics, The Johns Hopkins University, Baltimore, Maryland
(Received February 28, 1955)

The alpha-particle spectrum in the successive beta-alpha decay of Li^8 was observed with magnetic analysis from 1 to 6.5 Mev, corresponding to excitation energies in Be^8 from 2 to 13 Mev. The only definite structure in the spectrum corresponds to the well-known broad state at 2.9 Mev.

IN the many reactions in which the unstable Be^8 nucleus is produced by the emission of a heavy particle, the large recoil momentum imparted to the Be^8 nucleus seriously alters the observed alpha-particle spectrum in the $Be^8(\alpha)\alpha$ disintegration.[1] In the beta decay of Li^8, however, the alpha spectrum can be studied without excessive distortion. In addition, since the half-life of the Li^8 nucleus is 0.85 sec,[1] it is possible to produce Li^8 nuclei and then observe the $Li^8(\beta)Be^8(\alpha)\alpha$ decay without interference from competing reactions or modes of decay.

Previous investigations of the alpha spectrum,[2] employing range analysis, have been conducted in two ways. In one, a study is made of the spectrum of one of the decay alpha particles emitted from a target in which Li^8 nuclei are embedded; in the other, the ranges of both alpha particles are measured in a cloud chamber or emulsion. The former method is subject to the intrinsic loss of resolution discussed below, while with the latter technique the task of obtaining good statistics is formidable. Because of the current interest in the existence of states of Be^8 above 3 Mev, we have examined the "single alpha" spectrum in some detail with good instrumental resolution. The loss of resolution inherent in the method of producing the alpha particles is less serious in the high-energy region of the spectrum.

Table I. Effect of target and center-of-mass motion on the energy and resolution in the alpha spectrum.

E_α Mev	Recoil broadening Mev	Target		Total broadening Mev
		Av loss Mev	Broadening[a] Mev	
1.5	±0.07	0.23	±0.11	±0.18
3.5	±0.07	0.14	±0.05	±0.12
6.0	±0.05	0.09	±0.03	±0.08

[a] This calculation takes into account the shape of the "line" already produced by the recoil effect, and gives the additional broadening introduced by the target.

The analysis is based on the observation of some 7×10^4 particles.

A convenient method of preparing Li^8 nuclei is with the $Li^7(d,p)Li^8$ reaction. Thin targets of natural lithium, deposited on nickel foils, were bombarded with a beam of deuterons of 0.68-Mev energy. At this energy the Li^8 nuclei are emitted at forward angles between 0° and 32° in the laboratory system. As the Li^8 nuclei come to rest at various depths in the target, set at 45°, the emitted alpha particles are degraded in energy by various amounts with a resulting loss of resolution. By assuming an isotropic emission of Li^8 nuclei[3] (in the center-of-mass system) and extrapolating a range-energy curve for Li^8 particles[4] to low energies, the average loss in energy and the effective broadening were computed for various alpha energies, with the results given in Table I.

The distortion of the spectrum arising from the disintegration in flight of the Be^8 nuclei may also be described in terms of an effective broadening or loss of resolution. For an isotropic beta-neutrino correlation[5] and an isotropic beta-alpha correlation,[6] the values in Table I are obtained.

The "prompt" radiations from the Li+d reactions were excluded from observation by means of a rotating shutter, designed so as to expose the target periodically to the beam, and in opposite phase the target to the alpha detector. The period of rotation was 2 sec. The delayed alpha particles were observed at 90° to the deuteron beam.

The spectrum was studied with a magnetic analyzer which has been used previously.[6] With recording in nuclear emulsions, no attempt was made to detect alpha particles much below 1.0 Mev. Four exposures were made covering the following energy intervals: 0.9–2.0, 1.1–2.3, 2.0–4.1, and 3.1–6.4 Mev. The energies were obtained from the known calibration of the instrument. The chief uncertainty in the actual energy scale of the alpha spectrum arises from the loss is energy in the target (Table I). In reading the plates in the microscope, the distribution in track length was measured

† Supported in part by the U. S. Atomic Energy Commission.
* Now at Knolls Atomic Power Laboratory, Schenectady, New York.

[1] For a summary of these reactions, see F. Ajzenberg and T. Lauritsen, Revs. Modern Phys. **24**, 321 (1952).

[2] W. A. Fowler and C. C. Lauritsen, Phys. Rev. **51**, 1103 (1937); Rumbaugh, Roberts, and Hafstad, Phys. Rev. **51**, 1106 (1937), Phys. Rev. **54**, 657 (1938); C. L. Smith and W. Y. Chang, Proc. Roy. Soc. (London) **A166**, 415 (1938); Bonner, Evans, Malich, and Risser, Phys. Rev. **73**, 885 (1948); C. W. Li and W. Whaling, Phys. Rev. **81**, 661 (1951) (this investigation employs magnetic analysis); Frye, Armstrong, and Rosen, Phys. Rev. **98**, 241(A) (1955); F. C. Gilbert, Phys. Rev. **93**, 499 (1954).

[3] The results of the computation are not very sensitive to this assumption.

[4] Neuendorffer, Inglis, and Hanna, Phys. Rev. **82**, 75 (1951); W. H. Barkas, Phys. Rev. **89**, 1019 (1953).

[5] Hanna, LaVier, and Class, Phys. Rev. **95**, 110 (1954).

[6] D. R. Inglis, Phys. Rev. **78**, 104 (1950); R. W. Gelinas and S. S. Hanna, Phys. Rev. **89**, 483 (1953).

at various positions on the plates. Throughout the spectrum, a well-defined peak in the track length distribution was obtained with negligible background.

Each exposure was corrected for the variation with particle momentum of the solid angle of the spectrograph. The observed α^{++} yield was converted to the total $\alpha^{+}+\alpha^{++}$ yield, using data from the literature.[7] This correction is small and is applicable only in the low-energy region. Since the exposures were not all made with the same target, and because of uncertainties in the monitoring introduced by the pulsing arrangement, no attempt was made to obtain absolute normalizations. Instead, the spectra were joined together by matching intensities in the regions of overlap. Finally, the complete momentum spectrum was converted to an energy spectrum.

The spectrum is shown in Fig. 1. The peak corresponding to the familiar 2.9-Mev state in Be^8 is prominently displayed, but shifted to lower energy because of the average energy loss in the target (Table I).

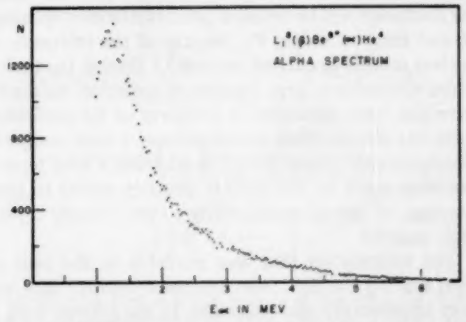

FIG. 1. Alpha spectrum from $Li^8(\beta)Be^{8*}(\alpha)He^4$. The vertical intensity scale is arbitrary. The numbers given indicate approximately the actual number of particles counted for the points below 3 Mev. Above 3 Mev the actual count is about twice that indicated by the numbers.

Other structure is not apparent in the spectrum. Considering the resolution as given in Table I and the statistical uncertainty in the data, it is estimated that a fairly sharp group in the vicinity of E_α=2.0, 4.0, or 6.0 Mev would have been detected if its intensity was greater than 2.5, 1.0, or 0.5 percent, respectively, of the total observed intensity which can be attributed principally to the 2.9-Mev state. Very broad states would, of course, be more difficult to observe.

In order to compare the present results with earlier measurements, the various spectra are plotted on a logarithmic scale in Fig. 2. Wherever necessary, the earlier data have been converted from a range to an energy spectrum, and the energy scale has been adjusted to compensate for an estimated average target loss. The agreement among the various curves is generally good. The discrepancies which appear, for the most part, can be traced to the different techniques employed. In the region of 4.5 Mev in the present data, there is perhaps an indication of very broad structure, but not as much as in the curve of Bonner *et al.*

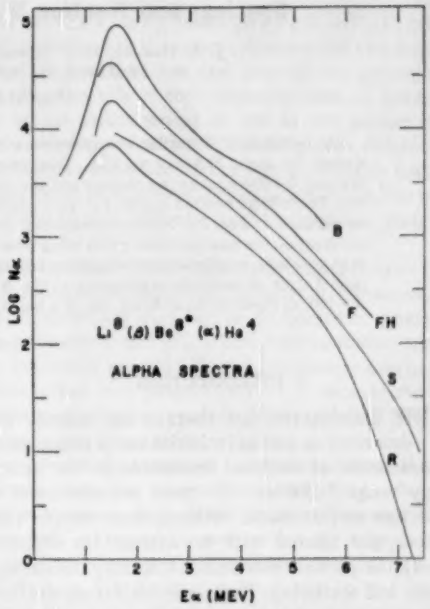

FIG. 2. Logarithmic plot of the curves of various authors. B=Bonner *et al.* FH=present authors. F=Fowler and Lauritsen. S=Smith and Chang. R=Rumbaugh, Roberts, and Hafstad. The vertical displacement of the curves is of course arbitrary.

In this experiment one does not expect to observe all states in Be^8. In detecting the alpha-particle decay, only states of even spin and even parity will be exhibited. In addition, there are limitations imposed by the well-established selection rules of beta decay. For example, the beta transition to the ground state of Be^8 is not detected,[8] which suggests a difference in spin between this state and the one at 2.9 Mev. One might reasonably expect, however, to detect states in Be^8 having the same spin and parity as the 2.9-Mev state.

We are greatly indebted to Mr. James Lambert for assistance in reading the plates.

[7] G. H. Briggs, Proc. Roy. Soc. (London) **114**, 431 (1927).

[8] W. F. Hornyak and T. Lauritsen, Phys. Rev. **77**, 160 (1950).

Spacings and Neutron Widths of Nuclear Energy Levels*

J. A. Harvey, D. J. Hughes, R. S. Carter, and V. E. Pilcher
Brookhaven National Laboratory, Upton, New York
(Received February 28, 1955)

The parameters of nuclear energy levels at excitation energy just above neutron binding have been studied for about 20 heavy nuclides. Total cross sections for neutrons of energy 0 to 700 ev were made utilizing the Brookhaven fast chopper and the transmissions were analyzed to obtain the resonance parameters. The reduced neutron widths, Γ_n^0, show a wide variation among the resonances in single nuclides relative to radiation widths, Γ_γ. Within experimental error, the size distribution of the reduced neutron widths is exponential, the most probable width being zero. The experimental level spacings, D, exhibit discontinuities at closed shells, an effect that remains after correction of the spacings for differences in excitation energy. The ratio Γ_n^0/D, of particular significance to the "cloudy crystal ball" nuclear model, has a maximum about $A=160$, as expected from theory, but of a much smaller magnitude than the computed peak.

I. INTRODUCTION

THE Brookhaven fast chopper has already been described as well as its initial use in measurement of parameters of neutron resonances in the neutron energy range 2–200 ev.[1] In these measurements the total cross section alone, obtained from sample transmission, was treated with no attempt to determine directly the partial cross sections, usually consisting of capture and scattering. The concentration on total cross sections was a result primarily of the nature of the fast chopper, in particular its small sample size and large detector area, which makes it particularly suitable for total cross section measurement by transmission.

Although the limitation to total cross section alone seems at first sight to neglect important parameters of levels, such as the partial widths Γ_n and Γ_γ, it has resulted that most of the level parameters can be obtained rapidly and with sufficient accuracy for comparison with theory by total cross section measurements alone. The analysis of the experimental data that makes possible the attainment of most of the level parameters is presented in Sec. II. It is indeed fortunate that so much information can be obtained from total cross sections because direct measurements of the partial cross sections, scattering[2] and capture,[3] are extremely difficult to perform and to interpret.

Because of these advantages, a vigorous program for measurement of total cross sections has been carried on for the past year, with the result that some 300 resonances have been studied during this period. The level parameters obtained represent a great increase in the available data for comparison with predictions of nuclear structure theory[4] relating to level widths and spacings. In addition, the measured parameters exhibit trends that have not been discussed theoretically, for example the "exponential Γ_n^0 distribution" presented in Sec. IV A; these results constitute the raw material for further theoretical development. In the present report the discussion will be devoted primarily to level spacings D, and neutron widths Γ_n, because of the relevance to nuclear models of current interest.[5,6] During the period under discussion a large number of radiation widths Γ_γ have also been measured; a summary of the earliest of these has already been published[7] and a more complete description will appear later.[8] In addition, a brief report[9] has been made on the ratio of neutron widths to level spacings, of special applicability to the "cloudy crystal ball" model.[6]

The information that was available in the past on level spacing obtained from neutron resonance data was very fragmentary and uncertain. In the present work it has been possible to measure enough resonances in a given energy interval in such a way that essentially all levels are located. In this way an unambiguous determination of the average level spacing[10] for the two possible spin states that can be formed by slow neutrons is made. The level spacings thus obtained are valuable for comparison with the predictions of various nuclear models because they are the spacings at neutron binding energy, hence about 7-Mev excitation, an energy at which the spacings were not well known previously. At the beginning of this work very little was known and nothing predicted by theory concerning the variation in neutron width from level to level, hence it was obviously desirable to measure individual Γ_n's for a number of levels.

* Work carried out under contract with U. S. Atomic Energy Commission.

[1] Seidl, Hughes, Palevsky, Levin, Kato, and Sjöstrand, Phys. Rev. **95**, 476 (1954).

[2] J. Tittman and C. Sheer, Phys. Rev. **83**, 746 (1951); H. L. Foote, Jr., Phys. Rev. **94**, 790 (1954); R. E. Wood, Phys. Rev. **95**, 644 (1954).

[3] Albert, Yeater, and Gaerttner, Phys. Rev. **95**, 644 (1954); Gaerttner, Yeater, and Albert, Knolls Atomic Power Laboratory Report KAPL-1084, March, 1954 (unpublished); E. Meservey, Phys. Rev. **96**, 1006 (1954).

[4] J. M. Blatt and V. F. Weisskopf, *Theoretical Nuclear Physics* (John Wiley and Sons, Inc., New York, 1952).

[5] Feshbach, Porter, and Weisskopf, Phys. Rev. **96**, 448 (1954).

[6] A. Bohr and B. R. Mottelson, Kgl. Danske Videnskab. Selskab, Mat.-fys. Medd **27**, 159 (1953).

[7] D. J. Hughes and J. A. Harvey, Nature **173**, 942 (1954).

[8] J. S. Levin (to be published).

[9] Carter, Harvey, Hughes, and Pilcher, Phys. Rev. **96**, 113 (1954).

[10] The symbol D is used through this paper to represent the level spacing for a single spin state.

Furthermore, the ratio of neutron width to level spacing was of obvious interest because predictions for this ratio did exist for the strongly absorbing or "black" nucleus and the partially transparent or "cloudy crystal ball" nuclear model. It is interesting that for both Γ_n and D large variations have been found, variations unexpected from current theory.

II. ANALYSIS OF DATA

The neutron resonance data are recorded in terms of sample transmission T, and the purpose of the analysis is to obtain all possible information about the level parameters from T as a function of neutron time-of-flight. Even though the transmission is a direct measure of the total cross section alone, the analysis gives much additional information concerning the parameters of the levels that appear as resonances in the total cross section. The partial cross sections for scattering and absorption that make up the total cross section (assuming no α or proton emission or fission) are given in terms of the level parameters by the Breit-Wigner single-level formula:

$$\sigma_s=4\pi\lambda_0^2 g\left|\frac{\Gamma_n/2}{E-E_0+i\Gamma/2}+\frac{R}{\lambda_0}\right|^2+4\pi(1-g)R^2, \quad (1)$$

and

$$\sigma_n=\pi\lambda_0^2 g\left(\frac{E_0}{E}\right)^{\frac{1}{2}}\frac{\Gamma_n\Gamma_\gamma}{(E-E_0)^2+(\Gamma/2)^2}, \quad (2)$$

where

$$g=\tfrac{1}{2}\left[1\pm\frac{1}{2I+1}\right]. \quad (3)$$

In these equations E is the energy of the neutron, $2\pi\lambda_0$ is the wavelength of a neutron with energy E_0, the energy at resonance, and Γ_n, Γ_γ, and Γ are the neutron, radiation, and total widths of the level. In practice the effect of levels other than that being analyzed, neglected in these equations, is often important but their effect can be subtracted by means described by Seidl *et al.*,[1] which will not be repeated here.

If the statistical factor g is known, the total cross section measurement alone gives the parameters of the level, Γ_γ and Γ_n (again assuming that other widths are negligible). This procedure is possible because the width of the cross section resonance at half-maximum is just Γ and the peak height σ_0 of the total cross section is given by

$$\sigma_0=4\pi\lambda_0^2 g\Gamma_n/\Gamma. \quad (4)$$

For a level at low neutron energy, where the instrumental resolution is very good, the procedure is relatively uncomplicated. In this region the *measured* peak height of the cross section resonance together with its width give Γ_γ and Γ_n (if g is known) after calculated corrections are made for the Doppler broadening of the level, as described by Seidl *et al.*[1]

If g is not known, as is usually the case, the method gives $g\Gamma_n$ rather than Γ_n. Measurement of the partial cross sections σ_s or σ_γ, which give Γ_n/Γ or Γ_γ/Γ, can be used to distinguish the correct choice of the two possible values of g in this case and thus all the parameters, including the spin of the compound state, J, are fixed. Use of the measurement of one of the partial cross sections (relative to the total) to fix g alone rather than to determine the other parameters is advisable because partial cross section measurements are inherently more complicated and difficult than transmission measurements.

As the partial cross-section measurements have been made for an exceedingly small number of resonances, the total cross-section work can be considered in general to give primarily Γ and $g\Gamma_n$ in the good resolution region. The important quantity Γ_γ can fortunately also be obtained rather well (from $\Gamma_\gamma=\Gamma-\Gamma_n$) because the uncertainty of g does not produce a large error in Γ_γ, as $g\Gamma_n$ is usually small compared to Γ.

For most of the measured Γ_γ's the experimental error is larger than the uncertainty arising from the two possible g values, even when this uncertainty is maximum, for $I=\frac{1}{2}$, in which case $g=\frac{1}{4}$ or $\frac{3}{4}$. A typical example of the $I=\frac{1}{2}$ case is the 17.6-ev level in thulium, described in III A, with a Γ of 63 ± 16 mv (millielectron volts) and a Γ_n of 1.5 or 4.5 mv depending on g. Here the uncertainty in Γ_γ arising from g (±1.5 mv) is less than the experimental uncertainty in Γ in spite of the fact that the two possible values of g have the maximum spread in this case. For other initial target spins the g uncertainty is less than it is for $I=\frac{1}{2}$, and there is no uncertainty for a zero-spin target nucleus, for which $g=1$. In contrast to Γ_γ values, the Γ_n's resulting from the measured $g\Gamma_n$'s contain an uncertainty that is a maximum of ±50 percent for $I=\frac{1}{2}$. However, the observed great range of measured Γ_n's implies that the uncertainty arising from g is not a serious handicap at the present stage of neutron spectroscopy.

Thus far we have considered only the case of good resolution, where results obtained with a single sample, usually thin, give all the needed information. For neutron energies somewhat higher than the good resolution region, however, the true shape of a resonance is greatly distorted by the resolution function and the analysis becomes extremely complicated. Nevertheless it is still possible, by measurement of both thin and thick samples, to obtain Γ and $g\Gamma_n$. The complication of the analysis is caused principally by the distorting effect of the Doppler broadening of the resonance and the change in the observed resonance shape with sample thickness. For the present work the method of analysis used in the poor resolution region is the same in principle as that described by Seidl *et al.*, but contains a few improvements. These improvements result in a great saving of time in the complicated analysis, which involves the areas of dips in transmission curves for two sample thicknesses and the Doppler broadening. This information is used to obtain σ_0 and Γ, the principle being illustrated by Fig. 1, and $g\Gamma_n$ and Γ_γ are then

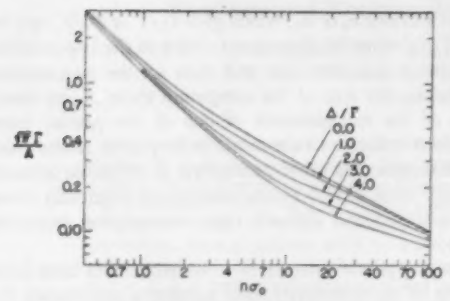

FIG. 1. Curves relating the measured area of transmission dips, A (ev), sample thickness n (atoms/cm²), and Doppler broadening Δ (ev) to the resonance parameters Γ and σ_0 (peak height). The principle of the method of resonance analysis is that values of A, n, and Δ for two sample thicknesses are consistent with only a particular location on a single curve, and this location determines Γ and σ_0. (See reference 1.) Because the desired parameters appear combined with the measured quantities, the method involves successive approximations.

calculated as already described for the good resolution case.

It is fortunate that the results obtained are still valuable when, for experimental reasons, two sample thicknesses cannot be used. In general, at high energy only a thick sample can be used because a thin sample would give a transmission too close to unity for accurate results. However there are cases even at high energy in which, because of overlapping of resonances, only a thin-sample result is obtained. If a thin-sample result alone is available the quantity $\sigma_0\Gamma$ is obtained, which quantity gives $g\Gamma_n$ for the resonance directly with no knowledge of Γ necessary, as is seen from Eq. (4). For a thick-sample run alone, on the other hand, one obtains $\sigma_0\Gamma^2$, that is, $g\Gamma_n\Gamma$, and from this combination $g\Gamma_n$ is obtained only if Γ_γ is assumed. For cases in which a single thickness is available in the intermediate thickness range, a dependence of the resulting $g\Gamma_n$ on the assumed Γ_γ is present but weaker than for the thick sample. Because the main objective in the present work is the measurement of neutron widths, the dependence of $g\Gamma_n$ on the assumed Γ_γ was studied for each level in order to estimate the error of the final neutron widths.

The general procedure followed in determining $g\Gamma_n$ was to measure both it and Γ when two sample thicknesses could be used to give a reasonably accurate value of the latter. For resonances for which Γ could be measured only with large error or where just one sample thickness could be used, Γ_γ was taken to be the average of the measured values for other resonances in the same nuclide. The use of this "assumed" Γ_γ in getting Γ and hence $g\Gamma_n$ is fortunately not a source of great error because of the fact that the radiation widths are relatively constant compared to the extremely wide range that was found in this work for the Γ_n's. In addition, for many samples of intermediate thickness the error resulting from the Γ_γ "assumed" is much less than the experimental error because of the weak dependence of $g\Gamma_n$ on Γ_γ, as will be exemplified in the next section.

For most of the elements investigated, a sufficiently large number of resonances was found so that some statistical information was obtained on the distribution of level parameters among the levels of single nuclides. It was possible to investigate the distribution of level spacings in a given nuclide as a function of neutron energy and to use this observed distribution to determine at which energy a significant fraction of the levels was missed. The number of levels for some of the elements was sufficiently large so that the distribution law of the neutron widths, which would range over a factor as large as 100 for a given isotope, could be determined. Some general conclusions about this statistical information will be given in Sec. IV after the measurements of individual elements are described in Sec. III. In connection with the description of measurements, the manner in which average neutron widths, spacings, and width-to-spacing ratios are determined will be discussed.

III. MEASUREMENTS

The fast chopper, neutron detectors, and timing equipment have already been described in reference 1 and were used in essentially the same form during the past year with the exception of a few improvements. The chopper is a rapidly rotating shutter that produces neutrons in bursts of about 1-μsec duration, from which individual neutron velocities are selected electronically by the flight time to detectors 20 meters distant. The rotor is now being used regularly at a speed of 10 000 rpm compared to the 6000 rpm described in reference 1.

Previously the principal contribution to timing uncertainty was the time involved in pulse collection in the 2-in. diameter BF_3 neutron counters. A faster neutron counter has now been developed[11] and is in routine use. It consists of 128 counters, $\frac{3}{4}$ in. in diameter, in a common BF_3 atmosphere and operating at the same high voltage. The spread in pulse collection time for this multiple BF_3 counter is about 0.5 μsec (full width at half-maximum), and this time does not constitute a serious contribution to the final resolution function. As the neutron flight path in the multiple BF_3 counter is $3\frac{1}{2}$ in., the corresponding flight time becomes serious for neutrons below 20 ev for at this energy the flight time in the counter is 1.4 μsec. The flight time in the counter is much smaller in a scintillation-type detector that has been under development in the past year, but this detector is not in routine use as yet.

At high energies, where the flight time in the counter is negligible, the resolution function (with the multiple BF_3 counter) has a full width at half-maximum of 1.4 μsec, giving a resolution of 0.07 μsec/m at 20 meters. This resolution represents an energy spread of 2.0 ev at 100 ev and 22 ev at 500 ev. Under these conditions, the

[11] H. Palevsky (to be published).

TABLE I. Levels in thulium ($_{69}Tm^{169}$) with resonance energies (E_0) less than 160 ev. The neutron widths (Γ_n) are obtained from the measured areas of transmission dips for sample thicknesses n (atoms/cm²); r is the ratio of the error in Γ_n arising from the uncertainty in Γ_γ (taken as 70±20 mv for each resonance) to that arising from the area measurement. The statistical weight factor, g, is assumed to be $\frac{1}{2}$; Δ is the Doppler broadening of the level.

E_0 (ev)	Δ (ev)	$(1/n)\times10^{24}$ (cm²/atom)	Area (% error) (ev)	Γ_n (% error) (mv)	r	Weighted Γ_n (mv)	Reduced width Γ_n^0 (mv)
3.92±0.03	0.047	1390	0.84 (9)	12 (30)	1.3	12±4	6±2
14.4±0.1	0.095	1390	0.33 (7)	5.7 (16)	0.7	5.7±0.8	1.5±0.2
		90	1.17 (6)	5.7 (29)	2.0		
17.6±0.2	0.10	1390	0.21 (10)	3.4 (15)	0.3	3.2±0.4	0.76±0.10
		90	0.81 (5)	3.0 (25)	2.1		
29.1±0.3	0.14	90	0.22 (27)	0.37 (36)	<0.1	0.37±0.13	0.07±0.02
35.2±0.4	0.15	1390	0.33 (12)	11.6 (20)	0.2	13±2	2.2±0.4
		90	1.39 (7)	16 (28)	1.3		
38.1±0.5	0.16	90	0.27 (16)	0.61 (20)	0.15	0.61±0.12	0.10±0.02
45.6±0.6	0.17	1390	0.19 (22)	6.8 (27)	<0.1	6.4±1.3	0.9±0.2
		90	0.84 (9)	5.9 (29)	0.7		
51.6±0.7	0.18	1390	0.19 (25)	7.8 (30)	<0.1	7.7±1.6	1.1±0.2
		90	0.90 (9)	7.6 (29)	0.7		
59.8±0.8	0.20	1390	0.38 (19)	22 (27)	0.11	24±5	3.1±0.6
		690	0.71 (12)	30 (25)	0.3		
		90	1.11 (15)	14 (42)	0.4		
66.8±1.1	0.20	1390	0.85 (13)	80 (22)	0.25	100±15	12±2
		690	1.36 (9)	105 (17)	0.3		
		90	3.9 (10)	119 (18)	0.6		
84.4±1.5	0.23	690	0.36 (29)	14 (38)	<0.1	11±3	1.2±0.4
		90	0.87 (16)	9 (42)	0.2		
96±2	0.24	690	1.04 (14)	79 (26)	0.25	74±11	7.6±1.1
		90	2.3 (9)	71 (19)	0.7		
104±2	0.25	90	0.43 (40)	2.7 (54)	<0.1	2.7±1.4	0.26±0.14
118±2	0.27	690	0.69 (22)	46 (33)	<0.1	41±12	3.8±1.1
		90	1.38 (20)	32 (50)	0.2		
128±3	0.28	90	0.84 (25)	10 (48)	0.12	10±5	0.9±0.4
139±3	0.29	90	1.6 (23)	45 (60)	0.2	45±30	4±2
158±4	0.31	690	1.43 (15)	180 (35)	0.12	160±40	13±3
		90	2.9 (16)	130 (30)	0.2		

upper energy limit at which resonances can be resolved depends greatly on the element under study, for the level spacing differs greatly from element to element as we shall see in the next section.

In describing the results of the measurements, we shall first consider thulium because the procedure applied to all the elements is here well illustrated without the complication of separated isotopes. Tin will be described next because the additional analysis necessary for separated isotopes can be made clear. The results of the remaining elements and isotopes can then be described briefly because of the similarity of the methods involved.

A. Thulium

Two grams of thulium oxide of 99.9 percent purity[12] were available for the transmission measurements. These measurements were made from 3 to 200 ev with the old bank of BF_3 counters and hence with a resolution poorer than now available. Three sample thicknesses were used, $\frac{1}{2}$ in., $\frac{1}{16}$ in., and $\frac{1}{32}$ in., the thickest sample requiring only 0.75 g of sample in each of the two sample-holders because of the small cross-sectional area of the two neutron beams. The number of atoms/cm² for each of the samples is given in Table I. The error in the thickness of the thickest sample was about 4 percent and in the others about 6 percent. Runs were made sufficiently long to obtain about 2 percent statistical accuracy per point, one-μsec timing channels being used above 20 ev, two-μsec channels from 20–10 ev, and four-μsec channels below 10 ev. It was not necessary to make long runs for the open beam because its shape was well known from earlier runs. The procedure for determining the background was discussed in reference 1.

Transmission curves for thick and thin samples from 30–80 ev are shown in Fig. 2 on a time-of-flight scale. The resolution inferred from the observed widths at half-maximum of the small transmission dips was 3.4 μsec or 0.17 μsec/m. Between resonances the transmission of the thick sample is 0.86±0.02, which value gives 8±2 b for the potential scattering after correcting for the oxygen contribution. The areas of the transmission dips were measured with a planimeter on the curve of

[12] Obtained from Dr. F. H. Spedding, Ames Laboratory, Iowa, who also supplied the Tb, Ho, and Lu samples.

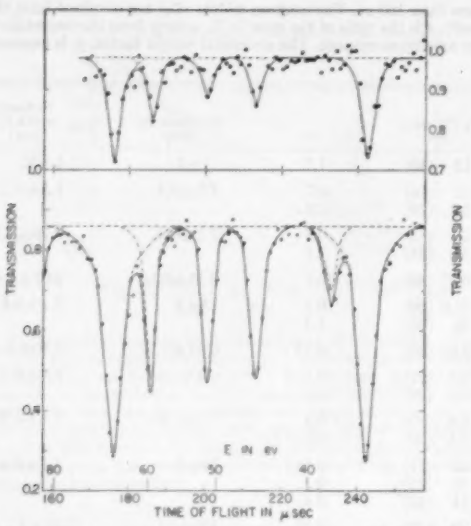

FIG. 2. The transmission as a function of time of flight at 20 m for thin ($1/n=1390$ cm³/atom, upper curve) and thick ($1/n=90$ cm³/atom, lower curve) samples of Tm_2O_3. The dotted straight line is the base line from which the areas of the resonances are measured. The analysis of these data by the method sketched in Fig. 1 is given in Table I.

Fig. 2, then normalized to unit transmission (i.e., divided by 0.86 for the resonances in the thick sample) and converted to ev. In the normalization, small corrections were made in the case of the 38.1- and 59.8-ev resonances because of the distorting effect of nearby large resonances. For each resonance, the area was measured over a limited energy interval, such that the wing correction (an area of $n\sigma_0\Gamma^2/\Delta E$, where ΔE is the energy interval) varied between 2 percent and 10 percent. The statistical errors quoted in Table I for the areas were calculated from the statistical accuracy of the points and the error in obtaining the "base line" used for normalization. The time-of-flight scale was accurate to ± 1 μsec.

For resonances where accurate data are available for both thick and thin samples, both Γ and σ_0 can be obtained since the thick and thin samples give approximately $\sigma_0\Gamma^2$ and $\sigma_0\Gamma$. In this case Γ_γ can be obtained even though the value of g ($\frac{1}{4}$ or $\frac{3}{4}$ for thulium) is not known, as discussed in Sec. II. For an intermediate sample, the power of Γ obtained is between 1 and 2. For example, the 35.2-ev resonance gave $\sigma_0\Gamma^{1.93}=59\pm10$ for the thick sample, and $\sigma_0\Gamma^{1.14}=310\pm50$ for the thin sample, by the technique illustrated in Fig. 1. From these numbers, Γ is obtained directly as 120 ± 40 mv and hence Γ_γ is 110 ± 40 mv, with negligible error arising from the assumption that $g=\frac{1}{2}$. For the 14.4- and 17.6-ev resonances the Γ's were calculated to be 75 ± 22 mv and 63 ± 16 mv, respectively, giving Γ_γ's of 69 ± 22 mv and 60 ± 16 mv, respectively. These three resonances thus give an average Γ_γ of 70 ± 12 mv for thulium.

Although thick and thin samples were measured for most of the other resonances in thulium the accuracy was not sufficient to give values of Γ_γ better than about 50 percent. Since radiation widths are known to be almost constant from resonance to resonance in a particular nuclide,[7] a radiation width of 70 ± 20 mv was used for all the thulium resonances to calculate $2g\Gamma_n$,[13] instead of Γ_γ's measured for particular resonances. Table I summarizes the results for thulium up to 160 ev, giving the pertinent experimental data used to obtain the neutron widths. The Doppler width Δ is calculated from the formula $\Delta=2(kTE_0m/M)^{\frac{1}{2}}$, with m/M the neutron-nucleus mass ratio, and kT expressed in ev. The error in $2g\Gamma_n$ is a result of the error in Γ_γ, taken as 70 ± 20 mv, and the error in A; the ratio of these contributions is given as r. For thin samples it can be seen that the error in $2g\Gamma_n$ arising from the uncertainty in Γ_γ is unimportant. For example, for an r even as large as 0.3, the Γ_γ uncertainty increases the error in $2g\Gamma_n$ above that resulting from the area error by only 5 percent. The reduced neutron width $2g\Gamma_n^0$ (reduced to 1 ev by division of $2g\Gamma_n$ by $E_0^{\frac{1}{2}}$) has the same error as the neutron width, since the energy of the resonance is measured quite accurately. The value of $\sigma_0\Gamma^2$ for the 3.92-ev resonance measured by Sailor *et al.*[14] together with a Γ_γ of 70 ± 20 mv give 14 ± 4 mv for $2g\Gamma_n$, which agrees with the present measurement.

In the energy range from 3–75 ev, 10 resonances were found compared to 6 in the range 75–150 ev. There are no resonances below 3 ev.[14] Above 75 ev it is quite apparent from the transmission curve that small levels may have been missed or that the transmission dips at the higher energies may not be single resonances. Below 75 ev any resonance larger than $\frac{1}{3}$ of the smallest observed would be sufficiently large for observation. Figure 3 illustrates the method of obtaining the level spacing D from the observed location of resonances in energy. The dropping away of the observed number of

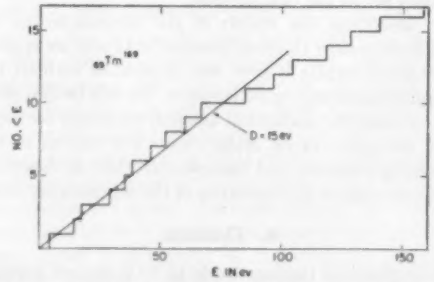

FIG. 3. The number of levels observed in thulium as a function of neutron energy. The slope of the straight line gives an observed spacing of 7.5 ev. On the assumption that the level spacing is the same for both spin states, D equals 15 ev for each spin state. It is apparent from the dropping away of the number of levels from the straight line that levels have been missed above 75 ev.

[13] Written thus because $2g$ is unity on the assumption that $g=\frac{1}{2}$.
[14] Sailor, Landon, and Foote, Phys. Rev. 96, 1014 (1954).

levels below the straight line indicates that some levels are missed above 75 ev. The slope of the straight line corresponds to a level spacing of 7.5 ev for resonances of the two possible spin states, $J=I\pm\frac{1}{2}$. Assuming that there are the same number of levels of spin 0 and 1 (I for Tm is $\frac{1}{2}$) a value for D of 15 ev for each spin state is obtained.

The reduced neutron widths of the resonances vary over a wide range (greater than a factor of 100). The average value of $2g\Gamma_n^0$ for the first 10 resonances (up to 75 ev) is 2.8±0.6 mv. In order to investigate the distribution of these ten reduced widths, the integral of the number of levels *versus* width is plotted in Fig. 4. It is seen that the integral distribution can be fitted by an exponential, implying that the differential distribution itself is exponential within experimental error. A complication in determining the distribution law arises because of the two possible values of g. For example, if the level spacings of the two spin states in thulium are the same, then (Sec. IV C) it is expected that the average reduced neutron widths, Γ_n^0, of the two kinds of levels would be the same. The distribution of $2g\Gamma_n^0$ would then actually contain two groups, of equal numbers of resonances and equal Γ_n^0 but differing by a factor of three in $2g\Gamma_n^0$ ($g=\frac{1}{4}$ or $\frac{3}{4}$). The observed composite distribution would then depart from an exponential behavior simply because of lack of knowledge of g.

Although the level spacing and the distribution law of the reduced neutron widths are obtained from the first 10 resonances, 15 resonances can be used to obtain the Γ_n^0/D ratio, whose significance is discussed in Sec. IV C. The greater usable energy range for Γ_n^0/D results from the fact that this ratio (averaged over the two spin states) is simply the sum of $g\Gamma_n^0$ for all the resonances in a certain energy range divided by the range. Thus if small resonances are missed above 75 ev they have a very small effect on the sum, hence on Γ_n^0/D. Also, for thin samples, if a transmission dip is really a combination of

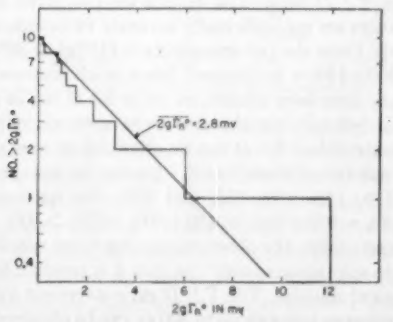

FIG. 4. The distribution of reduced neutron widths of the first 10 levels in thulium. The number of resonances with widths exceeding a particular value is plotted against this value. The straight line represents an exponential distribution with an average $2g\Gamma_n^0$ of 2.8 mv, which is the arithmetic average of the 10 widths. The slight curvature may be caused by the 2 spin states as discussed in the text.

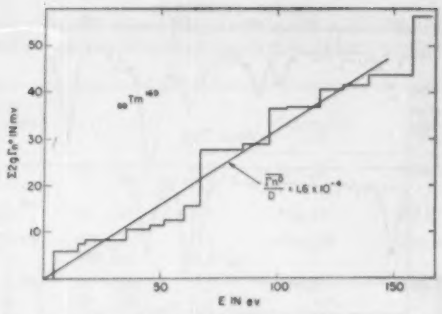

FIG. 5. The sum of the reduced neutron widths in thulium *vs* energy. A value of 1.6×10^{-4} for the Γ_n^0/D ratio is obtained from the straight line.

two unresolved resonances, the value of $g\Gamma_n^0$ computed in the analysis is just the sum of the two individual $g\Gamma_n^0$'s. Figure 5 is a plot of the sum of reduced neutron widths *vs* energy. The slope of the straight line gives directly the ratio Γ_n^0/D. In the energy range up to 75 ev the stepped curve deviates from the straight line more than it does in the D plot of Fig. 3 since the Γ_n^0's show large fluctuations. On the other hand, the data in Fig. 5 above 75 ev do not drop away from the straight line as much as the D plot for the reasons just given. The slope of the line in Fig. 5 corresponds to a value for Γ_n^0/D of $(1.6\pm0.3)\times10^{-4}$.

B. Tin

The total cross section of tin was first measured from 10–500 ev, using a thick sample (25.3 g/cm²) of metallic tin of 99.97 percent purity. The results showed many resonances above 35 ev. In order to identify the isotopes responsible for these resonances, samples (oxides) enriched in the isotopes[18] 112, 115, 116, 117, 118, 119, 120, and 122 were run from 35–500 ev, with no measurement being made on samples enriched in 114 and 124. These results will be discussed in three energy regions, below 92, 92–210, and above 210 ev.

Figure 6 shows the transmission of samples of normal tin and the enriched isotopes 117, 112, 116, and 119 in the energy range 92–210 ev. The normal and enriched 117 sample runs were made with the new BF_3 detector and $\frac{1}{2}$-μsec timing channels, hence with a resolution of 0.07 μsec/m, and the enriched 112, 116, and 119 samples with the old BF_3 counters with 1- and 2-μsec channels. Seven resonances were found in normal tin at 96.5, 112, 122, 125, 141, 149, and 197 ev. From the enriched isotope runs, the 122, 125, and 197-ev resonances were assigned to 117, the 96.5-ev resonance to 112, the 112 and 149-ev resonances to 116, and the 149-ev resonance to 119.

Thick samples of 118, 120, and 122 (~3 g/cm²) showed no resonances in the energy region of Fig. 6.

[18] Enriched isotopes were obtained on loan from the Isotope Research and Production Division of the Oak Ridge National Laboratory, Oak Ridge, Tennessee.

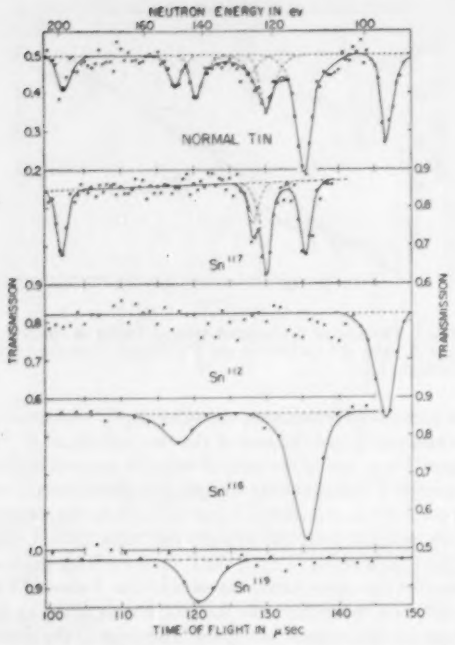

FIG. 6. The transmission as a function of neutron time of flight in the energy region 90 to 210 ev for samples of normal tin and enriched isotopes, illustrating the isotopic identification of resonances. The normal tin and 117 runs were made with a resolution of 0.07 μsec/m and the 112, 116, and 119 runs with a resolution of 0.2 μsec/m. The 112-ev resonance, actually in the 116 isotope, appears in the curve for the 117 sample because it contains appreciable 116. The fact that the base line is sloping in the 117 run is instrumental and does not introduce any error in the analysis of the resonances. The agreement between the parameters obtained from the normal run and the enriched isotope runs is obvious in Table II, where the experimental data and analysis are presented.

Although an enriched 124 sample was not run, the thick normal sample contained 1.58 g/cm² of 124 and any resonance in 124 would have been found. No 115 resonances were found in the 115 sample in the same energy range but this sample was enriched only to 14.0 percent in 115 (59.3 percent in 116) and only 0.5 g was available. It is possible that small resonances in 115 may have been missed, particularly near the large resonance in 116 at 112 ev. As the thick normal tin run contained 0.158 g/cm² of 114 and the 115 sample contained only 0.04 g/cm² of 114, it is possible that a small resonance may have been missed in 114. Thick- and thin-sample runs on the 112-ev resonance in 116 resulted in a Γ_γ of 110±40 mv.

There are three resonances in normal tin below 92 ev. No curve is shown for these resonances, which are at 39.4, 46.3, and 62.5 ev. From enriched isotope runs the 39.4-ev resonance is in 117 and the 46.3-ev resonance is in 118. The 62.5-ev resonance appeared in the 122 isotope run only, but the transmission dip was much too small to be assigned to 122. The 122 sample contained 3.07 percent 124, or 0.127 g/cm² of 124, and the observed dip for this sample thickness of 124 agrees with that calculated from the normal tin run on the assumption that the resonance is in 124. Thick and thin samples on the 39.4-ev resonance in 117 resulted in a Γ_γ of 106±25 mv. Any resonance larger than 1/100 of the observed resonances in the energy range below 92 ev would have been found.

In the energy range above 210 ev several of the observed transmission dips in the normal tin sample had contributions from more than one isotope. The transmission dip at 470 ev has contributions from 117 and 119, the dip at 425 ev has contributions from 117 and 120 and the 280-ev dip has contributions from 114 and 112. The fact that these dips have contributions from two isotopes is obvious from the enriched isotope runs. A large resonance in 118 at 268 ev also showed up in the enriched 117 sample, which contained 14.38 percent 118. The resonance at 222 ev was assigned to 119. Two small resonances at 260 and 340 ev which are barely seen in the normal tin run are reasonable resonances in the enriched 117 run. A resonance at 290 ev was found in the enriched 115 run but was too small to be seen in the normal tin run.

The pertinent data and the results of the analysis of the resonances are given in Table II in which a Γ_γ of 110±30 was used for each resonance. In addition to the columns explained for Table I, a column to indicate the sample (enriched isotope or normal) run is included. The agreement of the reduced neutron widths resulting from normal and enriched isotope runs is proof that the resonances have been correctly assigned to the various isotopes.

The level spacing and the Γ_n^0/D ratio for the Sn^{117} isotope was obtained by the same procedure described for thulium. There are five resonances below 300 ev in Sn^{117}, which give a D of 120±30 ev for each spin state, a $2g\Gamma_n^0$ of 1.2±0.4 mv, and a value of $(0.10\pm0.04)\times10^{-4}$ for the Γ_n^0/D ratio. The results for the three higher resonances are not sufficiently accurate to include in the analysis. From the two resonances in 119 below 300 ev, a D of 300±140 ev is obtained. Since small resonances in 115 may have been missed, no value for D can be given for this isotope. For the even-even isotopes, only approximate values for D can be obtained because of the small number of levels found. Thus for the isotopes 112, 114, 116, 118, 120, 122, and 124, the spacings are 150±80, ~300, 150±70, 200±100, ~500, >500, ~200 ev, respectively. The observed spacing is the spacing for a single spin state as only the spin ½ is possible for the compound nucleus. The Γ_n^0/D ratio averaged over all the even-even isotopes up to 300 ev can be obtained only with poor accuracy, giving $(0.20\pm0.08)\times10^{-4}$.

C. Other Elements

Molybdenum ($_{42}$Mo).—A thick sample (7.35 g/cm²) of metallic molybdenum of 99.9 percent purity was run

TABLE II. Levels in tin isotopes ($E_0<500$ ev) based on measurements with normal tin and samples enriched in the various isotopes. The g factor is assumed to be $\frac{1}{2}$ for the odd, and unity for the even isotopes; Γ_γ is taken as 110 ± 30 mv; a refers to the particular isotope; other symbols have the same significance as in Table I.

Isotope	E_0 (ev)	Δ (ev)	Sample	$(1/n)\times10^{21}$ (cm²/atom)	Area (% error) (ev)	Γ_n (% error) (mv)	r	Weighted Γ_n (mv)	Reduced width Γ_n^0 (mv)
Sn^{112}	96.5±2.0	0.29	112	880	1.53 (8)	95 (17)	0.5	85±10	8.7±1.0
			Normal	800	1.37 (10)	71 (19)	0.4		
	280±9	0.51	112	880	0.5 (40)	36 (48)	<0.1	36±17	2.2±1.0
Sn^{114}	280±9	0.50	Normal	1200	2.4 (20)	420 (23)	<0.1	450±90	27±5
			115	4600	1.3 (30)	540 (34)	<0.1		
Sn^{116}	112±2	0.32	116	79	3.3 (15)	62 (25)	0.5	58±6	5.5±0.6
			Normal	55.2	3.6 (8)	55 (19)	0.9		
			Normal	1250	0.90 (10)	54 (16)	0.2		
			117	1990	0.75 (12)	62 (17)	0.2		
	149±4	0.36	116	79	1.2 (30)	8 (70)	<0.1	4.5±1.4	0.37±0.11
			Normal	55.2	0.96 (20)	3.5 (34)	<0.1		
Sn^{118}	46.3±0.6	0.20	118	44.9	0.71 (15)	0.7 (30)	0.3	0.7±0.2	0.11±0.03
			Normal	29.8	0.91 (18)	0.8 (50)	0.3		
	368±14	0.57	118	40.7	10.7 (6)	410 (7)	0.4	420±30	22.0±1.3
			Normal	33.2	11.5 (9)	390 (11)	0.3		
			117	382	4.8 (12)	560 (17)	0.2		
Sn^{120}	425±18	0.61	120	71	3.9 (25)	44 (40)	0.3	44±18	2.1±0.8
Sn^{122}	No resonances								
Sn^{124}	62.5±0.9	0.23	Normal	130	1.35 (20)	11 (49)	0.4	12±2	1.5±0.3
			122	1620	0.22 (20)	12 (23)	<0.1		
Sn^{116}	290±10	0.50	115	670	1.6 (30)	260 (50)	<0.1	260±130	3.0±1.5
Sn^{117}	39.4±0.5	0.19	117	71	1.07 (6)	5.3 (24)	1.3	5.4±0.5	0.86±0.09
			117	1550	0.164 (10)	5.6 (11)	<0.1		
			Normal	94	0.87 (12)	4.3 (34)	0.4		
	122±3	0.33	117	91	1.09 (12)	13 (23)	0.3	15±3	1.4±0.3
			Normal	104	1.43 (20)	27 (52)	0.2		
	125±3	0.33	117	91	0.37 (30)	2.5 (36)	<0.1	2.8±0.8	0.25±0.08
			Normal	104	0.47 (50)	3.9 (65)	<0.1		
	197±6	0.42	117	91	1.48 (15)	30 (29)	0.2	35±9	2.5±0.6
			Normal	104	1.7 (25)	52 (61)	0.15		
	259±8	0.48	117	71	0.87 (25)	12 (36)	<0.1	12±4	0.8±0.3
	343±13	0.55	117	71	2.2 (30)	80 (80)	<0.1	80±60	4±3
	425±18	0.61	117	71	3.3 (22)	190 (40)	0.15	190±80	9±4
	460±20	0.64	117	71	2.4 (25)	120 (60)	0.1	120±70	6±4
Sn^{119}	141±3	0.35	119	138	1.6 (20)	52 (57)	0.2	30±12	2.5±1.0
			Normal	92	1.2 (20)	17 (48)	0.15		
	222±7	0.44	119	138	0.98 (22)	24 (33)	0.15	24±6	1.6±0.4
			Normal	92	1.25 (18)	24 (33)	0.1		
	460±20	0.63	119	138	2.6 (25)	200 (37)	0.1	200±70	9±3

from 10 to 750 ev with a resolution of 0.07 μsec/m. Twelve resonances were found and at the higher energies smaller resonances may have been missed. Samples of MoO_3 enriched in 95, 96, and 97 obtained from Oak Ridge were run over the same range. The other isotopes were not available in sufficient quantity to make suitable identification of resonances at the higher energies. The procedure for identifying the resonances is similar to that used for tin.

The data are summarized in Table III, based on a radiation width of 260±80 mv. For the 45-ev and 71.5-ev resonances, measurements for various sample thicknesses gave values for Γ_γ. The measurements on the 45-ev resonance give $\Gamma=392\pm50$ mv, $2g\Gamma_n=186\pm20$ mv, and hence $\Gamma_\gamma=206\pm60$ mv. The 71.5-ev resonance has $\Gamma=344\pm80$ mv, $2g\Gamma_n=16\pm2$ mv, and $\Gamma_\gamma=330\pm80$ mv. Concerning isotopic assignments, the 45, 71.5, 133, 367, and 478-ev resonances are in the isotopes 95, 97, 96, 100, and 98, respectively.[16] Two apparently single resonances in the normal sample have contributions from more than one isotope. The 570-ev resonance has contributions from Mo^{95} and Mo^{97} and the 406-ev resonance has contributions from Mo^{97} and another isotope. The three resonances at 406, 440, and 510 ev could not be assigned to a definite isotope. The calcula-

[16] The three lowest-energy resonances have been identified previously by S. P. Harris, Argonne National Laboratory Progress Report ANL-5031, February, 1953 (unpublished).

TABLE III. Neutron widths of resonances in the isotopes of molybdenum ($_{42}$Mo) based on a Γ_γ of 260±80 mv.

Isotope	E_0 (ev)	Δ (ev)	Sample	$(1/n)\times10^{24}$ (cm²/atom)	Area (% error) (ev)	Γ_n (% error) (mv)	r	Weighted Γ_n (mv)	Reduced width Γ_n^0 (mv)
Mo^{95}	45.0±0.6	0.22	Normal	18 490	0.39 (6)	177 (8)	0.4	174±10	26.0±1.6
			Normal	7830	0.83 (12)	184 (15)	0.3		
			Normal	1890	1.82 (5)	163 (14)	1.7		
			Normal	409	3.96 (4)	161 (11)	2.0		
			Normal	137	7.2 (10)	177 (17)	1.0		
	162±4	0.42	95	83	1.14 (10)	11.6 (19)	0.6	13.6±1.9	1.1±0.2
			Normal	137	1.00 (12)	15.6 (20)	0.5		
	570±30	0.79	95	83	2.6 (30)	120 (50)	0.1	120±60	5±3
	700±40	0.87	95	83	7.5 (20)	740 (18)	0.2	740±130	28±5
Mo^{96}	133±2	0.38	96	1890	1.90 (6)	215 (13)	0.8	200±15	17.3±1.3
			96	62.7	8.1 (8)	160 (22)	1.1		
			Normal	17 600	0.38 (20)	240 (21)	<0.1		
			Normal	295	4.07 (7)	170 (21)	1.2		
			Normal	131	6.7 (6)	200 (21)	1.2		
			95	1340	2.02 (12)	180 (23)	0.6		
Mo^{97}	71.5±1.2	0.28	97	122	1.67 (5)	17.8 (27)	2.2	16.6±1.8	2.0±0.2
			Normal	1010	0.42 (15)	17.2 (19)	0.2		
			Normal	690	0.57 (16)	17.6 (21)	0.2		
			Normal	520	0.60 (15)	14.2 (21)	0.3		
			Normal	232	1.19 (22)	17.3 (43)	0.4		
	292±10	0.56	97	122	2.4 (15)	94 (32)	0.4	75±15	4.4±0.9
			Normal	232	1.33 (15)	63 (24)	0.3		
	406±17	0.66	97	122	1.9 (35)	80 (55)	0.1	80±40	4±2
	580±30	0.79	97	122	6.3 (25)	670 (20)	0.2	670±130	28±6
Mo^{98}	480±20	0.71	Normal	93	10.5 (12)	640 (21)	0.3	740±110	34±5
			95	2060	3.0 (25)	1000 (36)	<0.1		
			96	1640	3.0 (25)	860 (36)	<0.1		
			97	815	3.3 (25)	570 (39)	<0.1		
Mo^{100}	367±15	0.62	Normal	238	10.5 (10)	960 (18)	0.4	1000±120	52±6
			95	1130	5.1 (12)	1050 (19)	0.2		
			96	5380	1.6 (30)	900 (35)	<0.1		
			97	8360	1.3 (40)	1100 (46)	<0.1		
$Mo^{92,94,98,100}$	406±17	0.66	Normal	148[a]	1.4 (40)	30 (60)	0.1	30±18	1.5±0.9
	440±20	0.69	Normal	148[a]	2.9 (20)	110 (40)	0.3	110±40	5±2
	510±20	0.74	Normal	148[a]	2.7 (30)	110 (56)	0.2	110±60	5±3

[a] Average for the isotopes 92, 94, 98 and 100 as explained in text.

tions for these three resonances in Table III were based on an isotopic abundance of 14.6 percent (the average of the isotopes 92, 94, 98, and 100). The transmission between resonances gives a value of 5.4±0.3 b for the potential scattering cross section of molybdenum.

In the entire energy range investigated, four resonances were found in Mo^{95} and the same number in Mo^{97}. The level spacing D thus equals 370±120 ev for each isotope. The $\bar{\Gamma}_n^0/D$ ratios for Mo^{95} and Mo^{97}, based on these four resonances, are $(0.40\pm0.14)\times10^{-4}$ and $(0.26\pm0.09)\times10^{-4}$, respectively. There are six resonances up to 600 ev assigned to the five even isotopes, which results in an average level spacing for the five isotopes of 500±150 ev. The average $\bar{\Gamma}_n^0/D$ for these five isotopes is $(0.38\pm0.11)\times10^{-4}$.

Indium ($_{49}$In).—The transmissions of three samples of indium metal of thicknesses 9.14, 1.10, and 0.87 g/cm² were measured from 3 to 150 ev, and a 0.102 g/cm² sample from 3 to 10 ev, with a resolution of 0.17 μsec/m. A sample of In_2O_3 enriched to 60 percent In^{113} was run from 3 to 150 ev and one enriched to 99.94 percent In^{115} (2.32 g/cm²) from 43 to 150 ev, with a resolution of 0.07 μsec/m. The resonances and their assignments up to 40 ev agree with previous work with the Brookhaven crystal spectrometer[17] and the Oak Ridge fast chopper.[18]

Thick- and thin-sample runs on the 9.1-, 12.1-, and 40-ev resonances in In^{115} result in Γ_γ's of 80±40, 140±60, and 140±50 mv, respectively. Recent work with the Brookhaven crystal spectrometer[19] gives values of Γ_γ of 81±4 mv for the 3.86-ev resonance and 72±2 mv for the 1.46-ev resonance (both in In^{115}). In computing the neutron widths for In^{115} in Table IV, an average value of 77±15 mv was used. Thick- and thin-sample runs on the 14.7- and 25.2-ev resonances in In^{113} result in Γ_γ's of 60±20 and 110±40 mv, respectively. For all resonances in In^{113} in Table IV, an average Γ_γ of 80±20 mv was used.

[17] V. L. Sailor and L. B. Borst, Phys. Rev. **87**, 161 (1952).
[18] G. S. Pawlicki and E. C. Smith, Oak Ridge National Laboratory Quarterly Progress Report ORNL-1289, March 1952 (unpublished).
[19] H. H. Landon and V. L. Sailor (private communication).

TABLE IV. Neutron widths of resonances in the isotopes of indium ($_{49}$In) based on a Γ_γ of 80±20 mv for In^{113} and 77±15 mv for In^{115}.

Isotope	E_0 (ev)	Δ (ev)	Sample	$(1/n)\times10^{24}$ (cm²/atom)	Area (% error) (ev)	Γ_n (% error) (mv)	r	Weighted Γ_n (mv)	Reduced width Γ_n^0 (mv)
In^{113}	4.71±0.04	0.065	113	196	0.173 (11)	0.104 (15)	0.4	0.104±0.016	0.048±0.007
	14.7±0.1	0.12	113	196	0.93 (6)	6.1 (27)	1.5	7.7±1.0	2.0±0.3
			Normal	498	0.72 (8)	8.1 (25)	1.1		
			Normal	5250	0.20 (15)	8.2 (19)	0.2		
	21.7±0.2	0.14	113	196	0.71 (11)	4.2 (30)	0.8	4.4±0.9	0.95±0.20
			Normal	498	0.42 (20)	3.8 (36)	0.3		
			Normal	5250	0.081 (27)	5.0 (30)	<0.1		
	25.2±0.2	0.15	113	196	0.99 (10)	10.2 (30)	0.8	9.7±1.6	1.9±0.3
			Normal	498	0.67 (10)	10.0 (25)	0.7		
			Normal	5250	0.123 (22)	9.1 (23)	<0.1		
	32.5±0.4	0.17	113	196	0.80 (6)	7.3 (23)	1.1	8.5±1.0	1.49±0.18
			Normal	498	0.55 (12)	8.0 (24)	0.4		
			Normal	5250	0.13 (25)	12.5 (28)	<0.1		
	45.6±0.6	0.20	113	196	0.59 (12)	4.7 (26)	0.4	4.7±1.2	0.69±0.18
	63.6±1.0	0.24	113	196	0.15 (40)	1.0 (44)	<0.1	1.0±0.4	0.13±0.06
	70.6±1.2	0.25	113	196	0.48 (9)	4.7 (15)	0.3	4.7±0.7	0.56±0.08
	82.5±1.5	0.27	113	196	0.30 (30)	2.9 (36)	<0.1	2.9±1.0	0.32±0.11
	93.2±1.8	0.29	113	196	1.34 (9)	40 (20)	0.5	40±8	4.1±0.8
	105±2	0.31	113	196	1.15 (14)	29 (30)	0.3	29±9	2.8±0.9
In^{115}	3.86±0.04	0.059	Normal	1950	0.075 (10)	0.31 (11)	0.2	0.34±0.03	0.173±0.014
			Normal	230	0.408 (5)	0.43 (17)	1.4		
			113	294	0.316 (7)	0.33 (17)	0.9		
	9.10±0.09	0.090	Normal	1950	0.163 (10)	1.78 (12)	0.3	1.73±0.17	0.57±0.06
			Normal	230	0.55 (7)	1.6 (20)	1.0		
			113	294	0.51 (10)	1.7 (25)	0.7		
	12.1±0.1	0.10	Normal	21.8	0.46 (8)	0.131 (20)	0.9	0.106±0.013	0.031±0.004
			Normal	230	0.076 (20)	0.115 (23)	<0.1		
			113	294	0.047 (17)	0.088 (16)	<0.1		
	23.0±0.2	0.14	Normal	21.8	0.71 (10)	0.5 (30)	0.6	1.0±0.2	0.21±0.04
			Normal	230	0.34 (15)	1.3 (21)	0.2		
	39.9±0.5	0.19	Normal	21.8	1.47 (12)	4.6 (31)	0.8	3.5±0.4	0.55±0.06
			Normal	182	0.48 (15)	2.8 (26)	0.2		
			113	294	0.41 (8)	3.5 (12)	0.3		
	46.3±0.6	0.20	115	82.4	0.20 (17)	0.43 (21)	<0.1	0.43±0.09	0.063±0.013
	48.6±0.7	0.21	Normal	21.8	0.60 (12)	0.59 (23)	0.3	0.65±0.08	0.093±0.012
			115	82.4	0.28 (13)	0.69 (17)	<0.1		
	63.2±1.0	0.24	115	82.4	0.34 (21)	1.1 (28)	<0.1	1.1±0.3	0.14±0.04
	83.3±1.5	0.27	Normal	21.8	1.98 (10)	15 (30)	0.5	11±2	1.2±0.2
			Normal	182	0.60 (25)	7 (41)	<0.1		
			115	82.4	1.07 (12)	11 (32)	0.3		
	95±2	0.29	115	82.4	0.51 (14)	2.8 (21)	<0.1	2.8±0.6	0.29±0.06

In In^{113} there are seven resonances (including the 1.80-ev resonance measured by Sailor and Borst)[17] up to an energy of 49 ev, resulting in a D of 14±2 ev. Above this energy small resonances may have been missed or the ones given in Table IV may not be single resonances. The Γ_n^0/D ratio for In^{113}, obtained from a plot like Fig. 5 for Tm, is $(0.60\pm0.11)\times10^{-4}$. In In^{115} there are eight resonances (including the 1.46-ev resonance)[17] up to 56 ev resulting in a D of 14±2 ev. The Γ_n^0/D ratio for In^{115} (including a value of 2.78 mv for the Γ_n^0 of the 1.46-ev resonance)[19] is $(0.31\pm0.06)\times10^{-4}$. The reduced neutron width of the 1.46-ev resonance is unusually great, being about six times the average reduced neutron width.

Cesium ($_{55}Cs^{133}$).—The transmission of a thick sample of $CsNO_3$ (99.9 percent purity) was measured from 10 to 600 ev with a resolution of 0.07 μsec/m. A thin sample was run only below 60 ev. Thick- and thin-sample measurements on the 22.6- and 47.8-ev resonances gave Γ_γ's of 120±40 and 140±60 mv. The 5.9-ev resonance has been reported to have a Γ_γ of 115±20 mv and a $2g\Gamma_n$ of 5.2±0.4 mv.[20] An average Γ_γ of 110±30 mv was used for all resonances in the computations of Table V. There are 12 resonances up to 250 ev resulting in a D of 42±5 ev. The Γ_n^0/D-ratio (including a value of 2.1 mv for the Γ_n^0 of the 5.9-ev resonance)[20] is $(1.0\pm0.2)\times10^{-4}$. The large resonance at 240 ev has a reduced neutron width about seven times the average reduced

[20] H. H. Landon and V. L. Sailor, Phys. Rev. **93**, 1030 (1954).

TABLE V. Neutron widths of resonances in cesium ($_{55}Cs^{133}$) based on a Γ_γ of 110±30 mv.

E_0 (ev)	Δ (ev)	$(1/n)\times10^{24}$ (cm²/atom)	Area (% error) (ev)	Γ_n (% error) (mv)	r	Weighted Γ_n (mv)	Reduced width Γ_n^0 (mv)
22.6±0.3	0.13	910	0.42 (12)	6.5 (21)	0.6	6.6±1.1	1.4±0.2
		75.2	1.44 (7)	6.7 (27)	1.8		
47.8±0.6	0.19	910	0.55 (12)	19 (19)	0.5	19±3	2.8±0.4
		75.2	1.88 (10)	20 (28)	1.4		
83.1±1.5	0.26	72.6	1.12 (13)	9 (33)	0.6	9±3	1.0±0.3
94.8±1.8	0.27	73.7	1.45 (10)	19 (29)	0.7	19±6	2.0±0.6
128±2	0.32	73.7	3.40 (7)	112 (17)	0.8	112±19	9.9±1.7
143±3	0.33	73.7	0.92 (25)	9 (45)	0.2	9±4	0.8±0.4
149±4	0.34	73.7	1.9 (20)	45 (43)	0.3	45±20	3.7±1.6
182±5	0.38	73.7	0.42 (25)	3.4 (30)	<0.1	3.4±1.1	0.25±0.08
204±6	0.40	73.7	2.0 (15)	57 (38)	0.4	57±22	4.0±1.5
224±6	0.42	73.7	1.8 (20)	49 (46)	0.2	49±22	3.3±1.5
240±7	0.44	73.7	8.1 (8)	480 (18)	0.3	480±90	31±6
301±10	0.49	73.7	3.5 (10)	190 (24)	0.4	190±40	11±2
370±14	0.54	73.7	3.0 (15)	160 (34)	0.2	160±60	8±3
407±16	0.56	73.7	7.3 (20)	570 (38)	0.1	570±200	28±11
443±19	0.59	73.7	4.2 (25)	290 (49)	0.1	290±140	14±6
530±25	0.64	73.7	9.0 (20)	800 (38)	<0.1	800±300	35±13

neutron width. The size distribution of the reduced neutron widths is shown in Fig. 7, in comparison with distributions for several other nuclides.

Europium ($_{63}$Eu).—Four thicknesses of europium oxide from 0.066 to 1.57 g/cm² of europium were run from 4 to 50 ev with a resolution 0.17 μsec/m. The europium oxide (reported to be 99.8 percent purity) was obtained from the Fordomes Trading Company. No analyses were made on the transmission of the thick samples at the higher energies since the resonances were not well resolved. Since Eu^{151} and Eu^{153} are nearly equally abundant, an average abundance of 50 percent was used to calculate the isotopic sample thickness. An average Γ_γ of 90±20 mv was used for all resonances in Table VI, this value being obtained from the average Γ_γ for the first three resonances.[21] Several of the small resonances listed in Table VI had not been observed in earlier work,[21] whereas the reported resonances at 6.3 and 7.4 ev have each been resolved into two resonances. A resonance was observed at 8.1 ev and is believed to be due to a Sm impurity since no resonance was found at this energy by Sailor, *et al.*[21] The area of the transmission dip corresponds to 1.7 percent Sm impurity. Although this is more than the reported purity of the sample would allow, we have omitted this resonance from Table VI. The other Sm resonances are not large enough to be observed in the Eu sample. It is possible that the 5.47-ev resonance is caused by a Dy impurity, for there is a strong Dy resonance at this energy.

If we include the eight resonances below 4 ev measured with the Brookhaven crystal spectrometer,[21] there are 14 resonances below 7.7 ev. Assuming the level spacing of each isotope and each spin state is the same, we obtain an average D of 2.2 ev for each spin state. Even though all resonances were not found above 8 ev, the ratio $\bar{\Gamma}_n^0/D$ obtained, as in Fig. 5 for Tm, utilizes all the data up to 30 ev since the samples were sufficiently thin. The ratio $\bar{\Gamma}_n^0/D$ thus obtained is $(2.3\pm0.3)\times10^{-4}$. The Γ_n^0 distribution is given in Fig. 7.

Terbium ($_{65}$Tb^{159}).—Two hundred milligrams of Tb_4O_7 of ~99 percent purity were obtained from Dr. F. H. Spedding. Three sample thicknesses (1.05, 0.53, and 0.205 g/cm²) were run from 3 to 200 ev with a resolution of 0.17 μsec/m. The data and the results are summarized in Table VII based on a Γ_γ of 90±30 mv. The Brookhaven crystal spectrometer group have recently studied the first three levels.[14] However, they also reported a resonance at 10.6±0.3 ev which we do not observe even though the thick sample run was sufficiently thick to see a good sized transmission dip if the resonance were as large as reported. There are 16 resonances up to 80 ev, whose size distribution is given in Fig. 7. The D is 10.0±1.0 ev, and the ratio $\bar{\Gamma}_n^0/D$ is $(1.5\pm0.2)\times10^{-4}$.

Holmium ($_{67}$Ho^{165}).—Thick and thin samples of holmium oxide (99.9 percent purity) were run from 3 to 200 ev with a resolution 0.17 μsec/m. In the thick sample run a small resonance was observed at 8.1 ev and is believed to be due to a Sm impurity. The data and the results are given in Table VIII based on a Γ_γ of 90±20 mv. This Γ_γ was obtained from the average value of the Γ_γ measured for six resonances. The measured values of Γ_γ for the 18.2, 35.9, 40.3, 48.5, 73.1, and 87.2-ev

[21] Sailor, Foote, and Landon, Phys. Rev. **93**, 1292 (1954) and private communication from H. H. Landon.

resonances were 180±90, 60±20, 60±30, 60±30, 140±70, and 260±130 mv.

In previous work on holmium,[14] the first four levels were measured. From the reported $\sigma_0\Gamma^2$ of 77±10[11] for the 3.9-ev resonance and a Γ_γ of 90±20, a value for $2g\Gamma_n^0$ of 2.5±0.7 can be obtained, which agrees with the value of 2.5±0.5 in Table VIII. The size distribution of the neutron widths of the 15 resonances up to 90 ev are given in Fig. 7. These levels give a D of 12.0±1.3 ev. The ratio of $\bar{\Gamma}_n^0/D$ is $(2.5\pm0.4)\times10^{-4}$.

Lutetium ($_{71}$Lu).—The transmissions of thick and thin samples of Lu_2O_3 (99.9 percent purity) were measured from 4 to 150 ev. Thick and thin runs on the 11.3, 20.7, 23.7, 37, and 42-ev resonances gave Γ_γ's of 40±20, 160±50, 70±20, 90±30, and 80±30 mv. The data and results are summarized in Table IX, based on a Γ_γ of 70±20 mv. Since the sample thickness (n) is given for the element, the neutron widths listed are less than the true values. Thus the neutron width listed in Table IX for a particular resonance would be increased by a factor of (1/0.976) if the resonance were assigned to Lu[175] and by a factor of (1/0.024) if assigned to Lu[176].

In addition to the 5 resonances previously reported[14] from 4 to 21 ev, five additional resonances were observed. The thick and thin measurements on the 57-ev resonance indicate that it is not a single resonance. If we assume that resonances with $\Gamma_n^0<0.1$ mv are in Lu[176], there are 13 resonances below 45 ev in Lu[175] and D equals 7±2 ev for Lu[175]. The ratio $\bar{\Gamma}_n^0/D$ for Lu[175] equals $(1.7\pm0.2)\times10^{-4}$. Since many resonances in Lu[176] must have been masked by Lu[175] resonances, no level spacing for Lu[176] is given.

Hafnium ($_{72}$Hf).—Four thick samples of HfO_2 (~1 g/cm²) enriched to 61.0 percent Hf[177], 80.9 percent Hf[178], 46.6 percent Hf[179], and 93.96 percent Hf[180] were run from 4 to 150 ev with a resolution of 0.07 μsec/m. A thick sample (~4 g/cm²) of normal hafnium metal was also run in the same energy range. The two low-energy resonances in Hf[177] at 1.08 and 2.38 ev were not measured. Since only 14 mg of 7.85 percent Hf[174] and only 58 mg of 48.46 percent Hf[176] were available, only thin samples of these isotopes could be measured. In order to get thin runs on the 7.8-ev resonance, samples of Zr containing 2 percent Hf were used as well as thin samples enriched in other isotopes. The data and results are summarized in Table X based on a Γ_γ of 56±15 mv for Hf[177] and 60±20 mv for the other isotopes. The resonances and their assignments are in agreement with Argonne work,[23] in which resonances up to 13 ev were measured. In this work a Γ_γ of 43±10 mv and a $2g\Gamma_n$ of 1.8±0.5 mv were found for the 1.08-ev resonance. Recent work by Levin[23] gives a Γ_γ of 63±8 mv and a $2g\Gamma_n$ of 6.8±0.6 mv for the 2.38-ev resonance, and a Γ_γ of 44±20 mv and a $2g\Gamma_n$ of 11±2 mv for the 6.5-ev resonance.

[23] Bollinger, Harris, Hibdon, and Muehlhause, Phys. Rev. **92**, 1527 (1953).
[23] J. S. Levin (to be published).

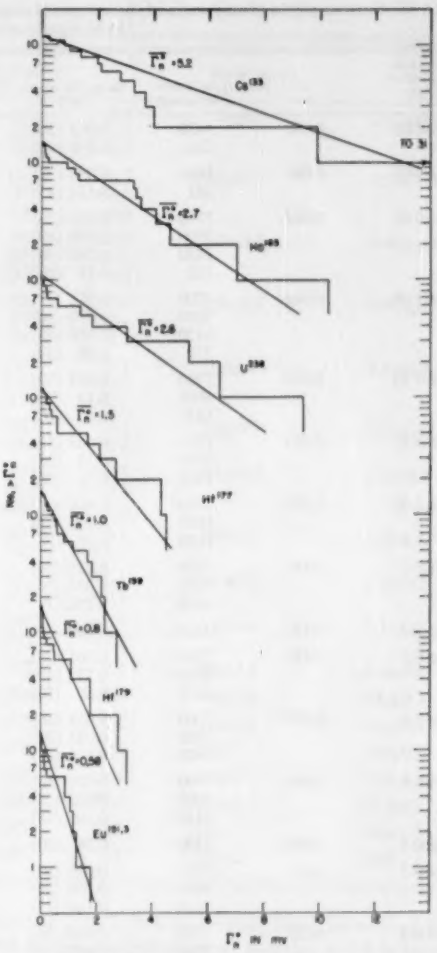

FIG. 7. The distribution in size of the reduced neutron widths for various nuclides, plotted in the same manner as Fig. 4. The slopes of the straight lines are computed from the arithmetic averages of the neutron widths.

The 12 resonances in Hf[177] found below 34 ev give a D of 5.6±0.6 ev. Their size distribution is given in Fig. 7. The ratio $\bar{\Gamma}_n^0/D$ for Hf[177] is $(3.0\pm0.4)\times10^{-4}$. In Hf[179] the wide spacing of the first few levels and the large number of small levels from 50–65 ev (see Fig. 7) complicates the determination of D, with a resulting value of 8±2 ev, somewhat less accurate than expected from the number of levels found. The ratio $\bar{\Gamma}_n^0/D$ is $(1.3\pm0.3)\times10^{-4}$. There is only one resonance in Hf[178] and one in Hf[180] up to 100 ev. One resonance was found in Hf[174], but since only a thin sample was available small resonances may have been missed. No resonances were found in Hf[176], but again since only a thin sample of enriched Hf[176] was available small resonances would not have been detected.

TABLE VI. Neutron widths of resonances of the isotopes of europium ($_{63}$Eu) based on a Γ_γ of 90±20 mv. The two isotopes are assumed to be equally abundant in computing $1/n$.

E_0 (ev)	Δ (ev)	$(1/n)\times10^{24}$ (cm²/atom)	Area (% error) (ev)	Γ_n (% error) (mv)	r	Weighted Γ_n (mv)	Reduced width Γ_n^0 (mv)
4.83±0.04	0.057	1420	0.015 (30)	0.051 (30)	<0.1	0.048±0.008	0.022±0.004
		322	0.056 (20)	0.047 (21)	<0.1		
5.47±0.05	0.061	1420	0.036 (20)	0.142 (20)	<0.1	0.133±0.018	0.057±0.008
		322	0.121 (15)	0.126 (18)	0.2		
6.03±0.08	0.064	7700	0.015 (25)	0.35 (25)	<0.1	0.35±0.05	0.14±0.02
		5000	0.030 (40)	0.46 (42)	<0.1		
		1420	0.080 (30)	0.37 (33)	0.1		
		322	0.17 (30)	0.20 (37)	0.1		
6.25±0.08	0.065	7700	0.017 (25)	0.43 (23)	<0.1	0.41±0.07	0.16±0.03
		5000	0.030 (40)	0.47 (40)	<0.1		
		1420	0.080 (30)	0.39 (33)	<0.1		
		322	0.24 (30)	0.35 (44)	0.2		
7.24±0.10	0.070	7700	0.065 (30)	2.0 (33)	<0.1	2.4±0.5	0.89±0.18
		5000	0.13 (25)	2.7 (30)	0.1		
		1420	0.30 (20)	2.4 (33)	0.3		
7.47±0.10	0.071	7700	0.065 (30)	2.0 (33)	<0.1	2.4±0.5	0.88±0.18
		5000	0.13 (25)	2.7 (30)	0.1		
		1420	0.30 (20)	2.5 (34)	0.3		
8.90±0.09	0.078	7700	0.090 (12)	3.4 (14)	0.1	4.2±0.4	1.41±0.14
		5000	0.19 (15)	5.4 (19)	0.1		
		1420	0.38 (7)	4.3 (18)	1.0		
10.5±0.1	0.085	7700	0.025 (30)	1.0 (32)	<0.1	1.90±0.13	0.59±0.04
		5000	0.075 (10)	2.14 (10)	<0.1		
		1420	0.192 (7)	1.81 (9)	0.3		
11.1±0.2	0.087	1420	0.060 (40)	0.5 (43)	<0.1	0.5±0.2	0.15±0.06
11.7±0.1	0.089	7700	0.061 (20)	3.0 (22)	<0.1	3.7±0.3	1.08±0.08
		5000	0.121 (10)	4.0 (11)	0.3		
		1420	0.30 (10)	3.7 (18)	0.5		
12.3±0.2	0.091	7700	0.018 (50)	0.9 (51)	<0.1	1.2±0.2	0.34±0.07
		5000	0.045 (30)	1.4 (30)	<0.1		
		1420	0.106 (25)	1.1 (29)	<0.1		
12.7±0.1	0.093	7700	0.020 (50)	1.0 (49)	<0.1	2.2±0.4	0.62±0.12
		5000	0.082 (20)	2.9 (20)	<0.1		
		1420	0.169 (15)	1.9 (17)	0.2		
13.6±0.2	0.096	1420	0.04 (50)	0.4 (53)	<0.1	0.4±0.2	0.11±0.06
14.8±0.2	0.10	7700	0.020 (50)	1.1 (51)	<0.1	1.9±0.3	0.49±0.07
		5000	0.056 (20)	2.2 (21)	<0.1		
		1420	0.150 (15)	1.8 (19)	0.2		
15.2±0.2	0.10	7700	0.039 (50)	2.3 (53)	<0.1	2.2±0.3	0.57±0.08
		5000	0.057 (20)	2.3 (20)	<0.1		
		1420	0.157 (15)	2.0 (18)	0.2		

Tantalum ($_{73}$Ta^{181}).—Two thick samples (7.80 and 0.89 g/cm²) of tantalum metal were measured from 7 to 150 ev with a resolution of 0.07 μsec/m. Two thin samples (0.0496 and 0.296 g/cm²) were run from 7 to 45 ev only. The 4.3-ev resonance was not measured since this resonance has been studied recently by the BNL crystal spectrometer group,[24] giving $\Gamma_\gamma=49\pm6$ mv and $2g\Gamma_n=4.3\pm0.7$ mv. The data are summarized in Table XI based on a Γ_γ of 50±10 mv. Thick and thin runs on the 10.4, 13.95, and 20.5-ev resonances give Γ_γ's of 49±11, 55±13, and 49±15 mv. Several resonances of Table XI below 40 ev had not been found in earlier work[25,26] in this energy range. For example, the previously reported resonances at 24 and 35 ev have each been resolved into two resonances, as was already shown in unpublished work by the MTR fast-chopper group at Arco, Idaho. A small resonance reported[27] at about 11 ev was not found in our work. The 10 resonances below 45 ev give a D of 9.0±1.0 ev. The Γ_n^0/D ratio is $(1.8\pm0.3)\times10^{-4}$.

Uranium ($_{92}$U^{238}).—The transmissions of eight different thicknesses (from 0.0266 to 36.0 g/cm²) of normal uranium were measured in various energy regions from 5 to 750 ev with a resolution of 0.07 μsec/m. Above 200 ev, however, only a single sample thickness of 18.0 g/cm² was used. A 12.0-g/cm² sample was run from 5 to 200 ev, as well as various thin samples. For example, in

[24] R. E. Wood (private communication).
[25] Melkonian, Havens, and Rainwater, Phys. Rev. 92, 702 (1953).
[26] R. L. Christensen, Phys. Rev. 92, 1509 (1953).
[27] Gaerttner, Yeater, and Albert, Knolls Atomic Power Laboratory Report KAPL-1084, March, 1954 (unpublished).

TABLE VI.—*Continued.*

E_0 (ev)	Δ (ev)	$(1/n)\times10^{24}$ (cm²/atom)	Area (% error) (ev)	Γ_n (% error) (mv)	r	Weighted Γ_n (mv)	Reduced width Γ_n^0 (mv)
16.8±0.2	0.11	7700	0.028 (50)	1.8 (51)	<0.1	1.5±0.2	0.37±0.05
		5000	0.045 (15)	1.9 (17)	<0.1		
		1420	0.093 (10)	1.2 (10)	<0.1		
18.0±0.2	0.11	7700	0.058 (25)	4.1 (25)	<0.1	5.0±0.5	1.18±0.13
		5000	0.106 (15)	5.2 (17)	<0.1		
		1420	0.287 (10)	5.2 (15)	0.4		
18.8±0.2	0.11	7700	0.030 (50)	2.2 (50)	<0.1	3.9±0.8	0.90±0.18
		5000	0.069 (30)	3.4 (31)	<0.1		
		1420	0.25 (20)	4.5 (25)	0.2		
19.3±0.2	0.11	7700	0.060 (30)	4.6 (32)	<0.1	4.3±0.8	0.98±0.19
		5000	0.069 (30)	3.5 (33)	<0.1		
		1420	0.25 (20)	4.6 (26)	0.2		
20.1±0.2	0.11	7700	0.110 (20)	9.3 (23)	<0.1	11.5±1.2	2.6±0.3
		5000	0.212 (7)	12.8 (10)	0.3		
		1420	0.42 (10)	10.0 (21)	0.6		
22.0±0.3	0.12	7700	0.037 (35)	3.2 (34)	<0.1	2.9±0.7	0.62±0.15
		1420	0.15 (30)	2.7 (34)	<0.1		
22.5±0.3	0.12	7700	0.060 (30)	5.3 (32)	<0.1	6.7±1.3	1.4±0.3
		5000	0.12 (25)	7.3 (30)	<0.1		
		1420	0.32 (20)	7.2 (28)	0.2		
24.1±0.3	0.13	7700	0.034 (40)	3.2 (42)	<0.1	3.0±0.8	0.61±0.15
		3460	0.068 (30)	2.9 (31)	<0.1		
25.0±0.3	0.13	7700	0.061 (30)	5.9 (31)	<0.1	5.8±1.2	1.2±0.3
		3460	0.12 (25)	5.7 (29)	<0.1		
27.0±0.4	0.14	3460	0.14 (25)	7.1 (28)	<0.1	6.7±1.4	1.3±0.3
		7700	0.061 (30)	6.5 (31)	<0.1		
29.5±0.4	0.14	3460	0.057 (50)	2.9 (52)	<0.1	2.9±1.5	0.5±0.3
30.8±0.4	0.14	3460	0.064 (50)	3.5 (52)	<0.1	3.5±1.8	0.6±0.3
31.8±0.4	0.15	3460	0.059 (50)	3.3 (52)	<0.1	3.3±1.7	0.6±0.3
35.1±0.5	0.16	3460	0.11 (30)	6 (33)	<0.1	6±2	1.0±0.3
36.9±0.5	0.16	3460	0.17 (30)	12 (33)	<0.1	12±4	2.0±0.7
38.3±0.6	0.16	3460	0.17 (30)	13 (34)	<0.1	13±4	2.1±0.7
42.2±0.7	0.17	3460	0.25 (25)	22 (32)	<0.1	22±7	3.4±1.1
47.4±0.8	0.18	3460	0.38 (20)	41 (30)	0.1	41±12	6±2

addition to the 12.0-g/cm² run, measurements were made on the 66.5-ev resonance with three other samples, of thicknesses 4.66, 0.925, and 0.123 g/cm². Two 36.0-g/cm² samples were run in the region of 90 ev to obtain data on the extremely weak resonance at 90 ev. A minor correction to the transmission was made for the U^{235} content when necessary.

The results are summarized in Table XII. The data on the 6.70-ev resonance were obtained from Levin[28] and are included for completeness. The measurements on the first four resonances are sufficiently accurate to give good results for Γ and hence Γ_γ. The Γ's obtained are 25.5±2.0, 33±5, 61±7, and 44±10 mv for the 6.7, 21, 37, and 66.5-ev resonances, respectively, hence the Γ_γ's are 24±2, 25±5, 29±9, and 17±10 mv. These values are all consistent with a single Γ_γ of 25 mv. Table XII summarizes the data based on a Γ_γ of 25±5 mv for all resonances, except the 6.7-ev resonance for which a Γ_γ of 24±2 mv was used.

There are eleven resonances up to 200 ev giving a D of 18±2 ev. The size distribution of their neutron widths is shown in Fig. 7. It is interesting that the ratio of the largest to the smallest reduced neutron width is about 10^3. Any resonance up to 100 ev with a Γ_n^0 of 1/500 of the average Γ_n^0 would have been found, as well as any resonance 1/100 of the average Γ_n^0 in the 100–200-ev range. Above 200 ev it is apparent that small resonances may have been missed or that some resonances listed may be two resonances. The ratio Γ_n^0/D up to 400 ev is $(1.2\pm0.2)\times10^{-4}$. The "resonance absorption integral," $\int\sigma_a dE/E$, where σ_a is the absorption cross section, is given by $\sum \pi\sigma_0\Gamma_\gamma/2E_0$ over the resonances. The value calculated from the resonances up to 420 ev is 265±12 b. As the additional contribution for the resonances above 420 ev (calculated from the average resonance parameters) amounts to 11±3 b, the resonance absorption integral is 276±12 b.

IV. DISCUSSION OF RESULTS

We have seen in the preceding section that the experimental total cross sections give the level spacings directly by a simple counting of levels, with an accuracy limited

TABLE VII. Neutron widths of resonances in terbium ($_{65}Tb^{159}$) based on a Γ_γ of 90±30 mv.

E_0 (ev)	Δ (ev)	$(1/n)\times10^{24}$ (cm²/atom)	Area (% error) (ev)	Γ_n (% error) (mv)	g	Weighted Γ_n (mv)	Reduced width Γ_n^0 (mv)
3.35±0.03	0.046	1290	0.158 (7)	0.43 (14)	0.7	0.43±0.05	0.24±0.03
		499	0.30 (6)	0.43 (23)	1.7		
4.99±0.05	0.057	1290	0.022 (23)	0.072 (25)	<0.1	0.055±0.008	0.025±0.004
		499	0.036 (14)	0.045 (16)	<0.1		
11.14±0.10	0.085	1290	0.512 (5)	7.4 (25)	1.9	9.2±1.8	2.8±0.6
		499	0.93 (5)	11.4 (30)	2.1		
14.4±0.2	0.096	499	0.131 (16)	0.54 (20)	0.2	0.54±0.11	0.14±0.03
21.4±0.2	0.12	1290	0.151 (12)	2.4 (15)	0.1	2.1±0.2	0.46±0.05
		499	0.240 (12)	1.7 (17)	0.2		
24.7±0.3	0.13	1290	0.272 (8)	5.7 (14)	0.3	5.8±0.7	1.17±0.14
		499	0.50 (10)	6.0 (24)	0.7		
27.8±0.3	0.13	499	0.108 (13)	0.82 (15)	<0.1	0.90±0.12	0.17±0.02
		252	0.24 (18)	1.08 (24)	0.2		
34.1±0.4	0.15	1290	0.160 (17)	4.0 (21)	<0.1	3.3±0.7	0.57±0.11
		499	0.244 (9)	2.6 (13)	0.2		
		252	0.52 (14)	4.2 (27)	0.4		
44.2±0.6	0.17	1290	0.16 (23)	5.3 (27)	<0.1	5.6±0.8	0.84±0.13
		499	0.34 (12)	5.1 (18)	0.2		
		252	0.63 (15)	7.3 (35)	0.3		
46.6±0.6	0.17	1290	0.45 (12)	21 (20)	0.3	15±3	2.2±0.4
		499	0.51 (9)	9.7 (17)	0.5		
		252	0.88 (11)	16 (32)	0.7		
51.1±0.7	0.18	499	0.21 (19)	3.1 (24)	<0.1	3.7±0.7	0.52±0.10
		252	0.47 (20)	4.7 (33)	0.2		
54.9±0.7	0.19	252	0.19 (30)	1.6 (36)	<0.1	1.6±0.6	0.21±0.08
58.7±0.8	0.20	499	0.26 (30)	4.5 (37)	<0.1	4.6±1.1	0.60±0.14
		252	0.43 (25)	4.6 (37)	0.1		
66.1±1.1	0.21	499	0.45 (15)	11 (22)	0.2	15±4	1.9±0.5
		252	1.04 (13)	31 (33)	0.6		
74.6±1.3	0.22	499	0.60 (17)	18 (28)	0.2	20±5	2.3±0.6
		252	1.04 (25)	30 (60)	0.2		
78.2±1.4	0.23	499	0.47 (18)	13 (26)	0.1	15±4	1.7±0.4
		252	0.92 (30)	23 (74)	0.2		
91.9±1.8	0.24	499	0.60 (20)	22 (31)	0.2	24±6	2.5±0.7
		252	1.00 (18)	29 (40)	0.3		
97.9±1.9	0.25	499	0.76 (18)	34 (30)	0.2	45±11	4.5±1.1
		252	1.48 (15)	65 (33)	0.5		
112.5±2.0	0.27	499	0.94 (30)	53 (53)	0.1	65±25	6.0±2.5
		252	1.6 (25)	80 (56)	0.2		
115±2	0.27	499	0.95 (30)	55 (53)	0.1	70±30	7±3
		252	1.7 (25)	90 (55)	0.2		
122±3	0.28	252	1.2 (30)	50 (70)	0.1	50±30	4±3
131±3	0.29	252	0.65 (35)	16 (50)	<0.1	16±8	1.4±0.7
144±3	0.30	499	1.08 (22)	80 (36)	0.2	120±30	10±3
		252	2.5 (20)	180 (35)	0.5		
156±4	0.32	499	1.03 (26)	80 (44)	0.2	160±40	13±3
		252	2.8 (15)	230 (30)	0.7		

primarily by the small number of levels observed, but affected also by the possibility of loss of levels by poor resolution. The reduced neutron widths (rather $2g\Gamma_n^0$) that are obtained are subject not only to experimental error but to uncertainty arising from lack of knowledge of Γ_γ for the individual levels. Although the lack of knowledge of Γ_γ at first sight seems serious, the final uncertainty is usually the experimental error itself, because of the weak dependence of $2g\Gamma_n^0$ on Γ_γ for average sample thicknesses. For comparison with theory, the reduced neutron width Γ_n^0 rather than $2g\Gamma_n^0$ is needed, and hence there is additional uncertainty for all but zero-spin target nuclei because $2g$ is not unity, in the worst case (spin-½ target nuclei) the two possible values being ½ and ⅔.

In spite of the limitation arising from the g value, several interesting features are clearly revealed by a survey of the measured neutron widths. The values that

TABLE VIII. Neutron width of resonances in holmium ($_{67}Ho^{165}$) based on a Γ_γ of 90±20 mv.

E_0 (ev)	Δ (ev)	$(1/n)\times10^{24}$ (cm²/atom)	Area (% error) (ev)	Γ_n (% error) (mv)	r	Weighted Γ_n (mv)	Reduced width Γ_n^0 (mv)
3.92±0.03	0.050	1470	0.406 (4)	2.5 (18)	1.8	2.5±0.5	1.3±0.2
12.8±0.1	0.089	1470	0.561 (3.3)	13.1 (16)	1.7	13.1±1.8	3.4±0.5
18.2±0.2	0.11	1470	0.050 (25)	0.69 (28)	<0.1	0.92±0.17	0.22±0.04
		72	0.61 (7)	1.11 (22)	1.1		
21.3±0.2	0.12	72	0.48 (7)	0.73 (16)	0.7	0.73±0.12	0.16±0.03
35.9±0.4	0.15	1470	0.25 (15)	8.4 (19)	0.1	7.5±1.1	1.20±0.18
		72	1.07 (6)	6.4 (22)	1.3		
37.9±0.5	0.15	72	0.22 (16)	0.36 (20)	<0.1	0.36±0.07	0.059±0.012
40.3±0.5	0.16	1470	0.48 (12)	23 (19)	0.3	21±3	3.3±0.5
		72	1.75 (7)	19 (22)	1.1		
48.5±0.6	0.17	1470	0.47 (11)	26 (18)	0.2	25±4	3.6±0.5
		72	1.77 (8)	22 (25)	0.9		
52.2+0.7	0.18	1470	0.73 (6)	55 (13)	0.6	51±6	7.0±0.8
		72	2.26 (11)	34 (26)	0.7		
55.3±0.8	0.19	72	0.96 (17)	6.6 (46)	0.3	7±3	0.9±0.4
66.3±1.1	0.20	1470	0.51 (12)	38 (19)	0.2	38±6	4.6±0.7
		72	1.74 (11)	38 (26)	0.6		
70.0±1.2	0.210	72	0.34 (30)	1.1 (38)	<0.1	1.1±0.4	0.13±0.04
73.1±1.3	0.21	1470	0.42 (17)	30 (25)	<0.1	35±6	4.1±0.7
		72	2.03 (9)	38 (22)	0.7		
83.4±1.5	0.23	72	0.32 (35)	1.2 (46)	<0.1	1.2±0.6	0.13±0.06
87.2±1.6	0.23	1470	0.73 (13)	79 (18)	0.2	96±10	10.3±1.1
		72	3.72 (8)	108 (13)	0.6		
96±2	0.24	1470	0.99 (11)	133 (18)	0.2	125±15	12.7±1.5
		72	3.9 (9)	119 (14)	0.6		
104±2	0.26	1470	0.52 (20)	54 (27)	<0.1	65±13	6.4±1.3
		72	2.7 (13)	75 (24)	0.4		
123±3	0.28	72	1.66 (18)	34 (45)	0.3	34±16	3.1±1.5
130±3	0.29	1470	0.79 (24)	110 (32)	<0.1	160±25	14±2
		72	4.7 (10)	180 (15)	0.4		

have been obtained in the present study reveal that Γ_n^0 varies over an extremely large range, a fact that lessens greatly the disadvantage of the g uncertainty simply because the values range over a much greater spread than results from the two possible g values. Of the many possible aspects of the statistics of level parameters that could be studied, only a few prominent characteristics will be discussed at present, omitting possible trends that cannot be delineated clearly at the present time because of insufficient data. The neutron widths will be considered first, then the level spacings, and finally the ratio $\Gamma_n^0/\bar{D}$ which has an important bearing on current nuclear models.

A. Neutron Widths

The neutron width of a level is related to the mean lifetime τ_n of the state relative to disintegration by emission of a neutron by the relationship,

$$\Gamma_n=\hbar/\tau_n. \tag{5}$$

The width can be considered crudely as being determined by the time required for concentration of the excitation energy on a particular neutron and by the probability that this neutron will penetrate the nuclear potential barrier. Thus the width Γ_n and the reduced width Γ_n^0 are given by

$$\begin{aligned}\Gamma_n&=\hbar p/t_0,\\ \Gamma_n^0&=\hbar p^0/t_0,\end{aligned} \tag{6}$$

where t_0 is the lifetime spent by the nucleus in the particular excitation state before the energy is concentrated on a single neutron, p is the actual barrier penetrability, and p^0 is the value for a 1-ev neutron.

As the barrier penetrability p^0 is expected to be practically the same from one level to another in a particular nucleus, the wide range in neutron widths observed must indicate a corresponding wide range of lifetimes for the individual nuclear states. As we shall see later, the barrier penetration (given by $2\pi\Gamma_n^0/D$) is of the order of 10^{-3} for the elements considered; hence the intrinsic nuclear lifetime, t_0, varies from about 10^{-13} to 10^{-16} sec for the observed range in Γ_n^0 of 0.01 mv to 10 mv. In spite of this wide range, the values of t_0 are always much greater than the time required for a nucleon to cross the nucleus, which is about 10^{-21} second.

The wide range in t_0 observed reflects the differences

TABLE IX. Neutron widths of resonances in lutetium ($_{71}$Lu) based on a Γ_γ of 70±20 mv. The sample thickness (1/n) is the atomic value (see text).

E_0 (ev)	Δ (ev)	(1/n) ×10^{24} (cm^2/atom)	Area (% error) (ev)	Γ_n (% error) (mv)	r	Weighted Γ_n (mv)	Reduced width Γ_n[a] (mv)
4.39±0.03	0.051	171	0.032 (35)	0.012 (47)	<0.1	0.012±0.006	0.006±0.003
4.78±0.03	0.053	980	0.10 (8)	0.28 (11)	0.4	0.28±0.03	0.128±0.014
		171	0.36 (15)	0.33 (33)	0.7		
5.22±0.04	0.056	980	0.285 (7)	1.3 (22)	1.4	1.2±0.2	0.52±0.09
		171	0.56 (15)	0.9 (36)	0.9		
6.17±0.05	0.060	980	0.022 (30)	0.081 (33)	<0.1	0.062±0.012	0.025±0.005
		171	0.080 (23)	0.047 (27)	0.1		
9.8±0.1	0.076	72.5	0.11 (22)	0.044 (26)	0.2	0.044±0.012	0.014±0.004
11.3±0.1	0.082	980	0.34 (7)	3.4 (18)	1.2	3.2±0.5	0.95±0.15
		72.5	1.04 (8)	2.8 (30)	1.8		
14.1±0.1	0.091	980	0.82 (5)	22 (19)	1.7	18±3	4.8±0.7
		72.5	2.00 (12)	12 (28)	1.0		
15.5±0.2	0.095	980	0.157 (8)	1.46 (11)	0.3	1.40±0.15	0.35±0.04
		72.5	0.54 (20)	0.9 (44)	0.5		
20.0±0.2	0.11	72.5	0.095 (20)	0.08 (25)	<0.1	0.08±0.02	0.018±0.005
20.7±0.2	0.11	980	0.161 (10)	2.0 (13)	<0.1	2.3±0.3	0.51±0.07
		72.5	0.92 (7)	3.6 (30)	1.5		
22.0±0.2	0.12	72.5	0.082 (24)	0.07 (29)	<0.1	0.07±0.02	0.015±0.004
23.7±0.2	0.12	980	0.29 (8)	5.0 (14)	0.6	4.9±0.7	1.01±0.14
		72.5	1.00 (7)	4.6 (29)	1.7		
24.8±0.3	0.12	72.5	0.15 (28)	0.17 (34)	<0.1	0.17±0.06	0.034±0.012
27.3±0.3	0.13	72.5	0.22 (22)	0.27 (30)	<0.1	0.27±0.08	0.052±0.016
28.2±0.3	0.13	980	0.090 (21)	1.4 (26)	<0.1	1.4±0.3	0.26±0.05
		72.5	0.56 (14)	1.4 (40)	0.6		
30.4±0.3	0.13	980	0.39 (11)	9.7 (20)	0.4	9.2±1.7	1.7±0.3
		72.5	1.11 (16)	7.4 (40)	0.7		
31.2±0.3	0.14	980	0.122 (22)	2.1 (30)	<0.1	2.3±0.6	0.41±0.10
		72.5	0.75 (20)	3.0 (50)	0.5		
37.1±0.4	0.15	980	0.26 (12)	6.2 (16)	0.2	6.4±0.9	1.05±0.14
		72.5	1.02 (9)	7.0 (30)	1.2		
41.5±0.5	0.16	980	0.59 (7)	22 (15)	1.0	24±3	3.7±0.4
		72.5	1.96 (7)	27 (18)	1.3		
46.2±0.6	0.17	72.5	0.20 (32)	0.39 (39)	<0.1	0.39±0.15	0.06±0.02
50.7±0.7	0.17	980	0.68 (6)	37 (14)	0.7	38±4	5.3±0.6
		72.5	2.25 (6)	39 (16)	1.1		
54.3±0.7	0.18	72.5	0.32 (28)	0.8 (39)	0.1	0.8±0.3	0.11±0.04
57.5±1.0	0.18	980	0.10 (20)	3.1 (23)	<0.1	3.7±0.7	0.49±0.09
(2 equal resonances)		72.5	0.77 (10)	4.6 (26)	0.4	3.7±0.7	0.49±0.09
63.0±1.0	0.19	72.5	0.39 (31)	1.3 (45)	<0.1	1.3±0.6	0.16±0.08
71.0±1.2	0.21	72.5	1.03 (10)	10 (30)	0.9	10±3	1.2±0.4
86.0±1.5	0.23	72.5	0.67 (25)	4 (50)	0.2	4±2	0.4±0.2
89.4±1.6	0.23	72.5	0.69 (25)	4 (50)	0.2	4±2	0.4±0.2
98.9±1.8	0.25	980	0.87 (17)	80 (30)	0.2	93±11	9.3±1.1
		72.5	3.1 (10)	97 (13)	0.5		
104±2	0.25	980	0.50 (30)	37 (45)	<0.1	36±11	3.5±1.1
		72.5	1.6 (18)	35 (32)	0.4		
110±2	0.26	980	0.53 (25)	41 (37)	<0.1	39±10	3.7±0.9
		72.5	1.70 (17)	38 (30)	0.5		
119±3	0.27	980	0.57 (25)	52 (38)	<0.1	83±11	7.6±1.0
		72.5	2.8 (11)	89 (13)	0.5		
132±3	0.28	980	1.17 (14)	148 (20)	0.2	150±15	13.1±1.3
		72.5	3.9 (10)	150 (11)	0.5		

TABLE X. Neutron widths of resonances in the isotopes of hafnium ($_{72}$Hf) based on a Γ_γ of 56±15 mv for Hf^{177} and 60±20 for the other isotopes.

Isotope	E_0 (ev)	Δ (ev)	Sample	$(1/n)\times10^{24}$ (cm²/atom)	Area (% error) (ev)	Γ_n (% error) (mv)	r	Weighted Γ_n (mv)	Reduced width Γ_n^0 (mv)
Hf^{174}	30.5±0.4	0.135	174	41 000	0.135 (20)	49 (24)	<0.1	49±6	8.9±1.2
			Normal	57 000	0.101 (15)	49 (16)	<0.1		
Hf^{177}	5.9±0.1	0.057	177	1080	0.48 (10)	5.1 (29)	1.2	5.1±1.5	2.1±0.6
	6.6±0.1	0.061	177	1080	0.66 (10)	11 (29)	0.9	11±3	4.3±1.3
	8.8±0.1	0.070	177	1080	0.49 (20)	7.5 (41)	0.6	8±3	2.7±1.1
	13.7±0.2	0.090	177	543	0.139 (11)	0.70 (13)	0.2	0.67±0.08	0.18±0.02
			Normal	537	0.128 (13)	0.62 (17)	0.2		
	14.1±0.2	0.090	177	543	0.30 (10)	2.2 (18)	0.4	2.2±0.3	0.59±0.08
			Normal	537	0.31 (10)	2.2 (18)	0.4		
	22.2±0.2	0.12	177	543	0.29 (11)	2.6 (19)	0.4	2.7±0.3	0.57±0.06
			Normal	537	0.295 (6)	2.7 (13)	0.6		
	23.5±0.2	0.12	177	543	0.20 (16)	1.6 (22)	0.1	1.6±0.4	0.33±0.07
	25.9±0.3	0.12	177	543	0.056 (17)	0.41 (19)	<0.1	0.41±0.08	0.08±0.02
	27.2±0.3	0.13	177	543	0.193 (8)	1.80 (10)	0.4	1.80±0.18	0.35±0.04
	33.2±0.4	0.14	177	543	0.121 (17)	1.2 (20)	<0.1	1.2±0.2	0.21±0.04
	37.2±0.5	0.15	177	543	0.75 (11)	23 (21)	0.6	23±5	3.8±0.8
	43.6±0.6	0.16	177	543	0.271 (8)	4.3 (12)	0.3	4.3±0.5	0.65±0.08
	45.7±0.6	0.16	177	543	0.28 (9)	4.6 (14)	0.2	4.6±0.6	0.68±0.10
	46.8±0.6	0.16	177	543	0.29 (10)	4.9 (17)	0.2	4.9±0.8	0.72±0.12
	49.4±0.7	0.17	177	543	1.10 (4)	55 (8)	1.0	55±5	7.8±0.6
	55.6±0.7	0.18	177	543	0.58 (9)	18 (21)	0.4	18±4	2.4±0.5
	57.2±0.8	0.18	177	543	0.50 (10)	13 (20)	0.4	13±3	1.7±0.3
	60.3±1.0	0.19	177	543	0.15 (25)	2.8 (30)	<0.1	2.8±0.8	0.36±0.11
	64.4±1.0	0.19	177	543	1.12 (5)	66 (11)	0.7	66±8	8.2±0.9
	67.7±1.1	0.20	177	543	0.79 (5)	36 (11)	0.7	36±4	4.4±0.5
	72.3±1.2	0.21	177	543	0.46 (15)	14 (26)	0.1	14±4	1.6±0.4
	77.2±1.3	0.21	177	543	0.48 (9)	16 (17)	0.2	16±3	1.8±0.3
	84.3±1.5	0.22	177	543	0.14 (25)	3.4 (28)	<0.1	3.4±0.9	0.37±0.10
	86.2±1.6	0.22	177	543	0.57 (9)	22 (18)	0.3	22±4	2.4±0.5
	93.6±1.8	0.23	177	543	0.22 (17)	6.4 (20)	<0.1	6.4±1.3	0.66±0.13
	98.5±1.9	0.24	177	543	0.37 (13)	13 (19)	<0.1	13±3	1.3±0.3
	103±2	0.25	177	543	0.47 (20)	20 (33)	<0.1	20±7	2.0±0.7
	105±2	0.25	177	543	0.65 (18)	32 (31)	0.1	32±10	3.1±1.0

in intrinsic properties of individual nuclear levels; hence some information can be obtained from the data on the nature of the distribution of the nuclear lifetimes, or more simply, as they are expressed by the reduced neutron widths. As already mentioned in connection with the discussion of thulium, the observed reduced neutron widths follow an exponential distribution as a function of size. Distributions similar to that shown in Sec. III for thulium have been found for other nuclides as well. In order to compare the distributions observed for various nuclides, the actual results for all cases in which at least 11 levels were observed are exhibited together in Fig. 7. While it is certainly true that the exponential distribution is a good approximation for the observations, it is not definitely established that this law is followed exactly.

The effect of lack of knowledge of g on the Γ_n^0 distribution was discussed in Sec. III A for the case of thulium where it was shown that equal spacings for the two spin states would give a curve concave upward when plotted as in Fig. 7, even if the exponential is strictly true for the levels of each spin state. If, on the other hand, the levels with higher g (thus higher compound nuclear spin J) should have a smaller level spacing, the g effect might cancel (it would exactly if the level spacing contains a $2J+1$ factor, see Sec. IV B). Some of the distribution curves are slightly concave upward and this behavior might be related to the g effect. However, in the light of the present limited amount of data, the exponential distribution holds surprisingly well, and seems firmly enough established to justify theoretical calculations. The distribution law of neutron widths has not been treated extensively in any published theory of nuclear level structure as yet.

TABLE X.—*Continued.*

Isotope	E_0 (ev)	Δ (ev)	Sample	$(1/n)\times10^{24}$ (cm²/atom)	Area (% error) (ev)	Γ_n (% error) (mv)	r	Weighted Γ_n (mv)	Reduced width Γ_n^0 (mv)
Hf^{178}	7.80±0.10	0.070	Zr	165 000	0.151 (7)	57 (9)	0.4	49±3	17.5±1.0
			Zr	190 000	0.117 (10)	49 (12)	0.2		
			179	8000	0.82 (5)	46 (13)	1.6		
			180	9300	0.71 (5)	41 (14)	2.0		
			Normal	2710	1.45 (5)	50 (13)	1.8		
Hf^{179}	5.69±0.05	0.056	179	1150	0.437 (5)	4.2 (32)	2.5	4.2±1.3	1.8±0.6
	17.8±0.2	0.10	179	324	0.307 (6)	1.5 (16)	1.1	2.0±0.2	0.47±0.05
			Normal	736	0.257 (8)	2.5 (15)	0.7		
	24.0±0.2	0.12	179	324	0.535 (5)	5.3 (25)	1.7	5.3±1.4	1.1±0.3
	27.0+0.3	0.12	179	324	0.216 (10)	1.25 (15)	0.3	1.25±0.19	0.24±0.04
	31.5±0.4	0.13	179	324	0.51 (6)	6.0 (21)	1.3	6.0±1.2	1.1±0.2
	36.8±0.5	0.15	179	324	0.80 (10)	17 (29)	0.9	17±5	2.8±0.8
	40.6±0.5	0.15	179	324	0.86 (5)	20 (20)	1.8	20±4	3.1±0.6
	42.8±0.6	0.16	179	324	0.68 (7)	13.1 (21)	1.0	11.9±1.7	1.8±0.2
			179	324	0.63 (4)	10.8 (18)	1.5		
	44.7±0.6	0.16	179	324	0.055 (25)	0.41 (27)	<0.1	0.41±0.12	0.06±0.02
	48.1±0.7	0.17	179	324	0.093 (25)	0.8 (30)	<0.1	0.8±0.2	0.12±0.03
	51.1±0.7	0.17	179	324	0.103 (20)	0.9 (22)	<0.1	0.9±0.2	0.13±0.03
	51.7±0.7	0.17	179	324	0.059 (20)	0.51 (20)	<0.1	0.51±0.10	0.07±0.02
	52.4±0.7	0.17	179	324	0.060 (20)	0.53 (20)	<0.1	0.53±0.10	0.07±0.02
	53.5±0.7	0.18	179	324	0.062 (20)	0.56 (21)	<0.1	0.56±0.12	0.08±0.02
	55.4±0.8	0.18	179	324	0.31 (10)	3.7 (14)	0.2	3.7±0.5	0.50±0.07
	61.2±1.0	0.19	179	324	0.062 (25)	0.63 (26)	<0.1	0.63±0.16	0.08±0.02
	63.0±1.0	0.19	179	324	0.069 (20)	0.73 (21)	<0.1	0.73±0.15	0.09±0.02
	70.1±1.2	0.20	179	324	0.45 (10)	8.1 (18)	0.3	8.1±1.5	1.0±0.2
	78.2±1.3	0.21	179	324	0.21 (15)	3.1 (16)	<0.1	3.1±0.5	0.35±0.06
	80.7±1.4	0.22	179	324	0.12 (20)	1.7 (22)	<0.1	1.7±0.4	0.19±0.04
	84.3±1.5	0.22	179	324	0.32 (15)	5.7 (21)	<0.1	5.7±1.2	0.62±0.13
	86.7±1.6	0.22	179	324	0.23 (15)	3.9 (19)	<0.1	3.9±0.7	0.42±0.08
	93.6±1.8	0.23	179	324	0.85 (10)	32 (26)	0.3	32±8	3.3±0.8
	103±2	0.24	179	324	1.58 (10)	99 (15)	0.4	99±15	9.8±1.4
	106±2	0.25	179	324	0.20 (25)	3.8 (30)	<0.1	3.8±1.1	0.37±0.11
	110±2	0.25	179	324	0.47 (15)	12 (24)	0.2	12±3	1.1±0.3
Hf^{180}	73.9±1.2	0.20	180	204	1.72 (10)	44 (19)	0.7	50±6	5.8±0.7
			Normal	298	1.50 (15)	46 (23)	0.9		
			179	590	1.29 (10)	58 (18)	0.7		

A casual inspection of the relationship of the neutron width to the spacing to the neighboring levels reveals no obvious correlation in the sense that strong levels correspond to large spacing of neighboring levels. The failure of this effect to appear implies that the simple derivation of the proportionality of Γ_n to D usually given[4] is not to be taken too literally, for it would lead one to expect a tendency for the size of Γ_n to be associated with the D in the immediate vicinity.

B. Level Spacing

For the neutron energies used in the present work the neutron resonances observed in a particular nuclide are limited to the two possible J values, $I\pm\frac{1}{2}$, that can be excited by $l=0$ neutrons. In some ways unfortunate, this limitation nevertheless aids in interpretation of the data because the spins of the levels excited, which would be difficult to measure, are known approximately.

The level spacing observed for a given isotope is determined by the spacing for the two sets of levels, with the contribution of each set somewhat uncertain because of lack of knowledge of their relative frequency. The general procedure in the present work has been to assume that $J=I+\frac{1}{2}$ and $J=I-\frac{1}{2}$ levels are equally probable and to determine the spacing for levels of a single J from the data simply by counting the levels in a given energy interval and multiplying by two. The symbol D without a subscript refers to this spacing for a single spin state. Although in principle D can easily be determined by counting the levels in a given energy interval, it is extremely important to determine if levels are being missed because of experimental conditions.

TABLE XI. Neutron widths of resonances of tantalum ($_{73}Ta^{181}$) based on a Γ_γ of 50±10 mv.

E_0 (ev)	Δ (ev)	$(1/n)\times10^{24}$ (cm²/atom)	Area (% error) (ev)	Γ_n (% error) (mv)	r	Weighted Γ_n (mv)	Reduced width Γ_n^0 (mv)
10.38±0.10	0.077	6050	0.118 (8)	4.6 (13)	0.2	4.5±0.5	1.40±0.17
		338	0.58 (7)	4.3 (24)	1.1		
13.95±0.12	0.090	1017	0.113 (10)	0.96 (9)	<0.1	1.04±0.08	0.28±0.02
		338	0.285 (8)	1.35 (16)	0.3		
		38.5	0.69 (10)	1.01 (28)	0.8		
20.5±0.2	0.11	1017	0.088 (12)	1.03 (13)	<0.1	1.12±0.10	0.25±0.02
		338	0.255 (10)	1.33 (16)	0.3		
		38.5	0.61 (6)	0.96 (22)	1.1		
		38.5	0.62 (10)	1.02 (28)	0.7		
22.8±0.3	0.12	338	0.107 (25)	0.48 (33)	<0.1	0.25±0.04	0.052±0.008
		38.5	0.29 (11)	0.20 (18)	0.3		
		38.5	0.30 (20)	0.22 (33)	0.2		
24.0±0.3	0.12	6050	0.092 (25)	7.5 (28)	<0.1	6.1±0.7	1.25±0.15
		1017	0.32 (10)	6.4 (18)	0.3		
		338	0.48 (12)	5.0 (27)	0.3		
		38.5	1.19 (10)	5.8 (25)	0.7		
		38.5	1.14 (15)	5.3 (31)	0.6		
30.1±0.3	0.13	38.5	0.27 (12)	0.23 (21)	0.1	0.23±0.05	0.042±0.009
35.4±0.4	0.14	6050	0.126 (15)	15 (22)	<0.1	17±2	2.9±0.4
		6050	0.156 (20)	20 (27)	<0.1		
		1017	0.49 (15)	18 (25)	0.2		
		338	0.76 (15)	17 (33)	0.3		
36.1±0.4	0.14	6050	0.135 (15)	17 (18)	0.1	18±2	3.0±0.4
		6050	0.156 (20)	21 (23)	0.1		
		1017	0.49 (15)	18 (28)	0.3		
		338	0.76 (15)	17 (32)	0.3		
39.3±0.5	0.15	6050	0.33 (15)	55 (19)	0.1	51±5	8.1±0.8
		6050	0.37 (20)	65 (21)	0.1		
		1017	0.82 (10)	48 (17)	0.3		
		338	1.25 (10)	43 (18)	0.3		
49.4±0.6	0.17	338	0.117 (20)	1.08 (27)	<0.1	1.1±0.3	0.16±0.04
57.5±0.7	0.18	38.5	0.52 (25)	0.5 (48)	0.3	0.5±0.2	0.07±0.03
62.9±0.8	0.19	338	0.39 (15)	8.6 (27)	0.1	10±2	1.25±0.25
		38.5	1.14 (15)	12 (34)	0.5		
77.2±1.3	0.21	338	0.77 (15)	27 (28)	0.2	40±7	4.6±0.8
		38.5	2.63 (10)	47 (19)	0.2		
83.4±1.4	0.22	338	0.69 (15)	21 (29)	0.2	21±6	2.3±0.7
91.3±1.8	0.23	338	0.33 (25)	7 (36)	<0.1	7±2	0.7±0.2
99.8±1.9	0.24	338	1.79 (10)	125 (21)	0.1	125±25	12.5±2.5
106±2	0.25	338	0.56 (20)	16 (38)	<0.1	16±6	1.6±0.6
116±2	0.26	338	1.14 (15)	64 (25)	0.2	64±16	6.0±1.5
127±3	0.27	338	0.70 (20)	28 (36)	<0.1	28±10	2.5±0.9

The analysis of Tm in Sec. III illustrates the method used to establish that all levels in a particular region have been found. In that case, for instance, investigation shows that a level with a Γ_n^0 only $\frac{1}{3}$ of the smallest Γ_n^0 actually obtained could have been identified if present. The absence of levels of this magnitude indicates that levels are not being missed simply because of their small size.

Levels will also be missed, of course, if they merge and are misinterpreted as single levels; this possibility was checked in the case of Tm by observing the rate of appearance of levels with neutron energy. This behavior, Fig. 3, indicates that levels are not missed in Tm until an energy of about 75 ev is reached. Still another way of considering the possibility of missed levels is by means of the size distribution of Γ_n^0, for one can extrapolate the distribution of Fig. 4 back to zero width to obtain the total number of levels in a given energy range, hence the spacing. As this extrapolation covers such a small range in neutron width, it cannot change the total number of levels greatly.

The level spacings thus obtained refer to an excitation energy just above the neutron binding energy, which energy is in the range 5 to 8 Mev for the nuclides considered. Because of the rapid change of D with excitation energy, it is useful to convert the observed spacings to a specific value of the excitation energy for comparison purposes. If very accurate spacings could be obtained for many isotopes by the present method, it might be possible, by comparing spacings for different isotopes, to

TABLE XII. Neutron widths of resonances of uranium ($_{92}U^{238}$) based on a Γ_γ of 25±5 mv for all resonances but the 6.7-ev resonance for which $\Gamma_\gamma = 24 \pm 2$ mv.

E_0 (ev)	Δ (ev)	$(1/n) \times 10^{24}$ (cm²/atom)	Area (% error) (ev)	Γ_n (% error) (mv)	r	Weighted Γ_n (mv)	Reduced width Γ_n^0 (mv)
6.70±0.06	0.054	22 500	0.039 (7)	1.59 (11)	<0.1	1.52±0.07	0.59±0.03
		7460	0.093 (5)	1.51 (8)	0.1		
		284	0.44 (2)	1.47 (9)	2.0		
		141	0.61 (2)	1.53 (9)	2.0		
20.9±0.2	0.096	7460	0.164 (6)	8.6 (7)	0.1	8.5±0.4	1.86±0.11
		7190	0.165 (7)	8.4 (10)	0.2		
		284	0.710 (3)	8.6 (12)	1.4		
37.0±0.3	0.13	14 970	0.193 (7)	33.7 (9)	0.1	32.5±1.9	5.3±0.3
		7190	0.32 (9)	32.5 (16)	<0.1		
		3230	0.46 (5)	31.0 (13)	0.4		
		284	1.30 (3)	32.7 (12)	1.1		
66.5±0.7	0.17	3230	0.34 (8)	26 (12)	0.2	25±2	3.1±0.3
		428	0.76 (12)	21 (31)	0.2		
		85.1	1.41 (7)	23 (20)	0.5		
		33.3	2.2 (15)	25 (33)	0.3		
81.6±0.9	0.19	428	0.18 (32)	1.8 (44)	<0.1	2.1±0.7	0.23±0.08
		33.3	0.77 (18)	2.4 (48)	<0.1		
90±2	0.20	11.1	0.25 (30)	0.08 (40)	<0.1	0.09±0.03	0.009±0.003
		11.1	0.31 (30)	0.11 (45)	<0.1		
104±2	0.21	3230	0.59 (15)	81 (27)	<0.1	65±9	6.4±0.9
		428	1.20 (5)	62 (17)	0.2		
		33.3	3.4 (18)	56 (33)	0.2		
118±2	0.23	428	0.54 (9)	12 (18)	<0.1	15±2	1.4±0.2
		33.3	1.84 (16)	26 (32)	0.3		
146±3	0.27	33.3	0.58 (35)	0.9 (43)	0.1	0.9±0.4	0.07±0.03
166±3	0.27	33.3	1.0 (30)	2.4 (46)	0.2	2.4±1.2	0.19±0.09
192±4	0.29	428	1.64 (8)	127 (20)	0.1	130±20	9.4±1.7
		33.3	5.7 (20)	150 (36)	<0.1		
212±5	0.30	22.2	3.0 (30)	57 (50)	0.1	60±30	4±2
242±6	0.32	22.2	3.0 (25)	60 (43)	0.1	60±30	4±2
258±6	0.33	22.2	0.72 (40)	1.3 (48)	0.1	1.3±0.6	0.08±0.04
278±7	0.35	22.2	2.3 (30)	40 (53)	0.1	40±20	2.4±1.3
297±8	0.36	22.2	2.2 (30)	40 (58)	<0.1	40±20	2.3±1.3
368±9	0.40	22.2	4.5 (25)	130 (42)	<0.1	130±50	7±3
418±10	0.42	22.2	3.0 (35)	80 (60)	<0.1	80±50	4±2

get information on the variation of spacing with excitation energy. However, because of the fact that the results at the present time are limited in number and statistical accuracy, the most profitable procedure seems to be to convert the spacings to a single excitation energy, using the usual empirical formula[4] for level density,

$$w = 10^6/D = a \exp(b\sqrt{E^*}). \quad (7)$$

Here w is the number of levels per Mev, E^* is the excitation energy, and a and b are parameters that vary slowly with atomic weight. The level spacings obtained from counting the levels in given energy regions are shown in Table XIII together with the excitation energies to which they correspond, the latter being obtained from neutron binding energies. The spacings converted to 6 Mev by means of Eq. (7) are also given in Table XIII; in most cases the energy correction is not large relative to the variation in D observed. It can be seen from the values of Table XIII and from Fig. 8, where the adjusted D's are given, that the level spacings at a given excitation energy are not a smooth function of atomic weight as would be expected[28] from the statistical model of the nucleus. Instead, a discontinuity of the order of 100 occurs at the 82 neutron shell. Recent unpublished results obtained with the Van de Graaff at Duke University and with fast choppers at Brookhaven and Argonne give a more pronounced discontinuity at 82 neutrons as well as one of about 10^3 at 126 neutrons.

Discontinuities in level spacing near ground at magic numbers is well known and the present results show definitely that the shell structure exerts a large effect on level spacings at 6-Mev excitation as well. The shell effect at high excitation had already been observed in the work of Hughes, Garth, and Levin[29] at excitation energy 1 Mev higher. In their work the level spacings were obtained from the absorption cross section in the

[28] J. M. B. Lang and K. J. Le Couter, Proc. Phys. Soc. (London) **A67**, 586 (1954).
[29] Hughes, Garth, and Levin, Phys. Rev. **91**, 1423 (1953).

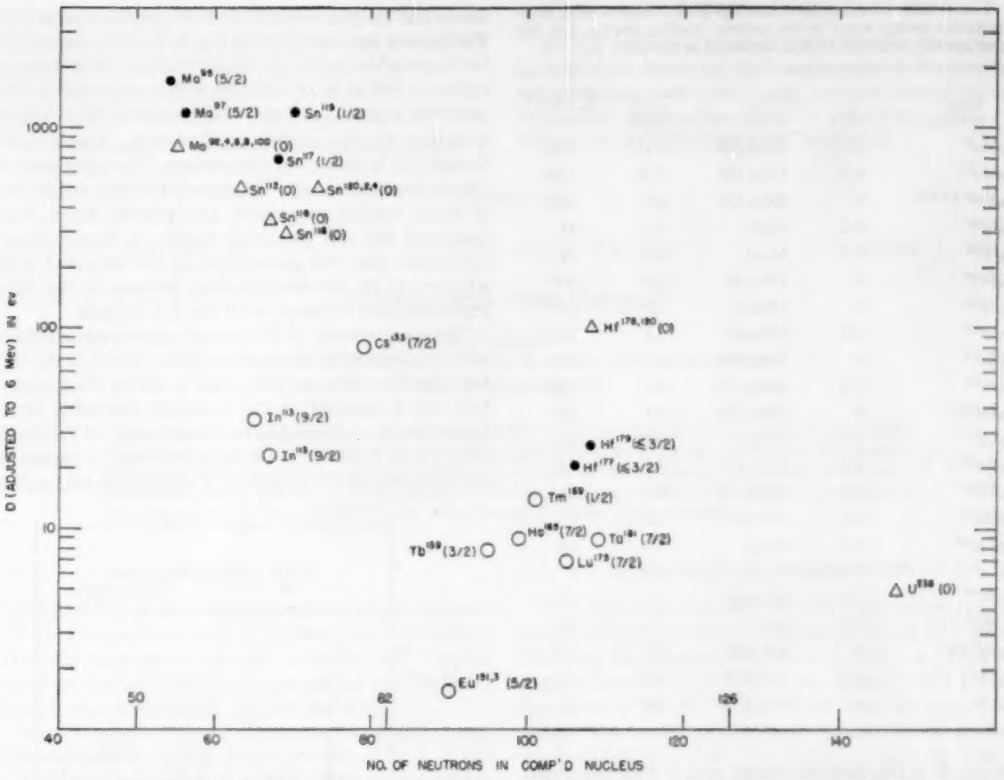

FIG. 8. The level spacings, D, adjusted to 6 Mev, as a function of neutron number in the compound nucleus. Each target nucleus is indicated and its spin is given in parentheses. The symbols ○, ●, and △ refer to odd Z-even N, even Z-odd N, and even Z-even N target nuclei, respectively. Points labeled with several isotopic numbers are averages for the isotopes.

Mev region but required knowledge of Γ_γ in the calculation. The recent measured Γ_γ's show that the assumed values of Γ_γ used by Hughes, Garth, and Levin were approximately correct; however, there is still some uncertainty in their D's because of the unknown contribution of higher l's in their measurements.

It would be very interesting to establish other level-density variations but unfortunately sufficiently many nuclei have not been investigated to establish definite trends. Although some even-odd effects seem to be present in Fig. 8, the data are not extensive enough to establish them definitely. However, one effect that seems definite is the higher D for even-Z nuclei. It would be of great interest to investigate the dependence of D on level spin J; the present data, while not extensive, do not seem to show an effect as large as the $1/(2J+1)$ factor expected theoretically.[28]

C. $\bar{\Gamma}_n^0/D$ Ratio

In addition to the intrinsic interest of $\bar{\Gamma}_n^0$ and D individually, their ratio has an important bearing at present on nuclear models. The significance of the $\bar{\Gamma}_n^0/D$ ratio follows directly from the discussion already given in IV A concerning the composition of neutron widths in terms of the intrinsic lifetime of a nuclear state and the penetrability of the nuclear surface. As the intrinsic lifetime of a state, t_0, is approximately given by h/D, it follows that division of the neutron width by D removes the specific nuclear part, leaving only the penetrability of the nuclear surface,

$$\Gamma_n/D = p/2\pi.$$

The relationship $t_0 = h/D$ follows directly[29] if the levels are considered to have equal spacing and it can be taken to hold approximately for actual level spacings as well, with D the average spacing.

For a strongly absorbing or "black" nucleus, the penetrability of the sharp potential discontinuity that represents the nuclear surface is simply the ratio of the neutron wave vector outside (k) to that inside (K) the nucleus,

$$p = 4k/K = 4(E/V)^{\frac{1}{2}},$$

[29] V. F. Weisskopf, Helv. Phys. Acta 23, 187 (1950).

TABLE XIII. Observed level spacings in ev, corresponding to an excitation energy equal to the neutron binding energy, and the spacings adjusted to 6 Mev as explained in the text.

Target isotope	Spin, I	D (ev)	Excitation energy (Mev)	D (adjusted to 6 Mev) (ev)
$_{42}Mo^{95}$	5/2	370±120	9.15	1700
$_{42}Mo^{97}$	5/2	370±120	8.29	1200
$_{42}Mo^{98,\,4,\,6,\,8,\,100}$	0	500±150	6.9	800
$_{49}In^{113}$	9/2	14±2	7.2	35
$_{49}In^{115}$	9/2	14±2	6.6	23
$_{50}Sn^{123}$	0	150±80	8.0	500
$_{50}Sn^{116}$	0	150±70	7.3	350
$_{50}Sn^{117}$	1/2	120±30	9.3	700
$_{50}Sn^{118}$	0	200±100	6.6	300
$_{50}Sn^{119}$	1/2	300±140	8.6	1200
$_{50}Sn^{120,\,2,\,4}$	0	500±200	6.1	500
$_{55}Cs^{133}$	7/2	42±5	6.73	80
$_{63}Eu^{151,\,3}$	5/2	2.2±0.3	5.7	1.6
$_{65}Tb^{160}$	3/2	10.0±1.0	5.8	8
$_{67}Ho^{165}$	7/2	12.0±1.3	5.7	9
$_{69}Tm^{169}$	1/2	15±2	5.9	14
$_{71}Lu^{175}$	7/2	7±2	6.0	7
$_{72}Hf^{177}$	≤3/2	5.6±0.6	7.6	21
$_{72}Hf^{179}$	≤3/2	8±2	7.4	26
$_{72}Hf^{178,\,180}$	0	100±50	6.1	100
$_{73}Ta^{181}$	7/2	9.0±1.0	6.03	9
$_{92}U^{238}$	0	18±2	4.87	5

where E is the neutron energy and V the well depth. Thus the ratio of the average reduced neutron width to the spacing D turns out to be a function of the well depth alone,

$$\frac{\Gamma_n^0}{D}=\frac{\langle\Gamma_n/E^{\frac{1}{2}}\rangle_{Av}}{D}=\frac{4}{2\pi}\left(\frac{1}{V}\right)^{\frac{1}{2}},$$

a ratio that is 1.0×10^{-4} for a 42-Mev well depth, for example.

For a partially transparent nucleus, represented by a potential with a small complex component, the Γ_n^0/D ratio is not constant with atomic weight but exhibits optical interference maxima. The cloudy crystal ball model gives a ratio with peaks at $A=57$ and 156, these positions being determined by the nuclear radius, R, possessing a simple relationship to the neutron wave number inside the nucleus (K),

$$KR=n\pi+\tfrac{1}{2}\pi,$$

with $n=2$ and 3 for the peaks quoted. The heights of the peaks in the Γ_n^0/D ratio are fixed by the complex component of the potential; hence it is desirable to check the magnitude and location of the peaks in an investigation of the validity of the model.

Results on the Γ_n^0/D ratio, based mainly on Brookhaven fast-chopper work, have been published recently.[9] The present data are given in Fig. 9, which is essentially the same as the published results,[9] with a few additional points as well as minor changes in the older results. The curve for a potential well $V=42(1+i0.03)$ Mev, corresponding to the model of Feshbach, Porter, and Weisskopf, is shown for comparison. The experimental results show a peak near the expected atomic weight but of much smaller magnitude and greater width than computed for this particular model. It should be remembered that the parameters of the potential were adjusted to fit the neutron cross sections in the Mev region and not adjusted to fit the Γ_n^0/D ratio.

The disagreement of the present experimental results with the theoretical curve is probably related to the fact that the Mev cross sections, used to obtain the parameters, are a measure of the potential scattering alone (gross elastic scattering in the terminology of Feshbach *et al.*). The Γ_n^0/D ratio on the other hand is related to the cross section for formation of the compound nucleus

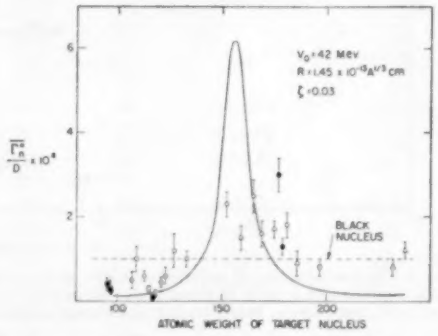

FIG. 9. Comparison of experimental values of Γ_n^0/D with theoretical predictions of the "black" and the "cloudy crystal ball" models of the nucleus. The symbols ○, ●, and △ refer to odd Z-even N, even Z-odd N, and even Z-even N target nuclei, respectively.

and in the present work is completely separated from the potential scattering. In the resonance energy region it is of course possible to obtain separately the cross section for compound nucleus formation, as is done here, and to get the potential scattering as well. The latter can be accomplished by means of a study of the cross section between resonances although very little has been done on this problem.

On the theoretical side there are several possibilities for modifications of the model that will reduce the compound nucleus formation cross section, and hence lower the Γ_n^0/D ratio, without changing the potential scattering, which already agrees with the Mev results. These possibilities include changing the sharp nuclear boundary to a diffuse boundary,[21] coupling of the incoming neutron to the low-lying rotational levels,[22]

[21] C. E. Porter and V. F. Weisskopf (private communication).
[22] A. Bohr and B. R. Mottleson (private communication).

and concentrating the cloudiness of the crystal at the nuclear surface.[32] Some of these theoretical possibilities can be tested by means of the Γ_n^0/D ratio but it would be necessary to increase the number of nuclides studied as well as the statistical accuracy for individual nuclides.

[32] H. Amster and V. F. Weisskopf (private communication).

V. ACKNOWLEDGMENTS

During the course of these measurements, the assistance of R. C. Garth, H. R. Muether, and A. Stolovy in taking data was of great value, as were discussions of theoretical implications with C. E. Porter, V. F. Weisskopf, A. Bohr, and B. R. Mottelson.

PHYSICAL REVIEW VOLUME 99, NUMBER 1 JULY 1, 1955

Photoprotons from Oxygen†

B. M. SPICER*
Physics Research Laboratory, University of Illinois, Champaign, Illinois
(Received January 6, 1955)

The cross section and angular distribution of the $O^{16}(\gamma,p)N^{15}$ reaction have been obtained for photon energies between 13.5 and 18.7 Mev, i.e., below the expected position of the giant resonance. The angular distribution indicated that the reaction proceeded predominantly through electric quadrupole or magnetic dipole absorption of photons, even though electric dipole transitions are allowed by isotopic spin selection rules. Suggestions are made regarding this forbiddenness of electric dipole absorption.

INTRODUCTION

STUDIES of photon absorption in oxygen have almost always used the (γ,α),[1] $(\gamma,4\alpha)$,[2] or (γ,n)[3,4] reactions. The only exception is the work of Wäffler and Younis,[1] who also obtained the (γ,p) cross section at 17.6 Mev, using γ rays from the $Li^7(p,\gamma)Be^8$ reaction.

It has been shown that if the assumption of the charge independence of nuclear forces is made, then it is expected that the (γ,α) reaction is forbidden to proceed via electric dipole absorption for energies below about 25 Mev.[5] This appears to be substantiated by experiment. The work of Penfold and the author[4] on the fine structure in the (γ,n) activation curve suggests that the (γ,n) reaction below 19 Mev proceeds by electric quadrupole and magnetic dipole absorption of photons. However, this suggestion was made on the basis of comparison of radiative widths to relatively inaccurate theoretical estimates. Therefore, it was deemed worthwhile to seek further information on the mechanism of photon absorption in oxygen below 20 Mev.

The experiment reported here was performed to obtain the cross-section and angular distribution for the $O^{16}(\gamma,p)N^{15}$ reaction between 13.5 and 18.7 Mev.

EXPERIMENTAL ARRANGEMENT

The photon source used in this experiment was a bremsstrahlung spectrum of maximum energy 18.7 Mev. The x-ray beam was collimated with lead to a pencil of angular diameter 0.012 radian, or a diameter of 1 cm at the center of the gas target, 90 cm from the source of x-rays. The scattering chamber used was similar to the one described by Fuller.[6] The line-up of the x-ray beam with respect to the scattering chamber was checked before each run by means of pictures of the beam taken on dental x-ray film. These films were positioned accurately with respect to the scattering chamber.

The scattering chamber contained oxygen gas at a pressure of one atmosphere. The gas acted as the target for the x-rays. Protons were detected in a pair of 1×3-inch 100-micron Ilford *G*-Special emulsions, which were placed parallel to, and to one side of, the x-ray beam. The emulsions were 0.87 cm apart, and their near edge was 2.40 cm from the center of the x-ray beam. Two sets of exposures were made, and in each case the dose at the scattering chamber was 5300 roentgens, as indicated by a Victoreen thimble at the center of an 8-cm cube of Lucite.

The emulsions were processed according to the dry development technique described by Beiser.[7] Observations on the tracks were made with two Leitz-Wetzlar binocular microscopes, using ×53 objective and ×8 ocular. This combination gave a field of view that was approximately 200 microns in diameter. Plates were searched by taking six-centimeter swaths along their long dimension.

Measurements made on the proton tracks were the

† Supported in part by the joint program of the Office of Naval Research and the U. S. Atomic Energy Commission.
* Fulbright Fellow, on leave from the Physics Department, University of Melbourne, Melbourne, Australia.
[1] H. Wäffler and S. Younis, Helv. Phys. Acta **22**, 614 (1949); Nabholz, Stoll, and Waffler, Phys. Rev. **86**, 1043 (1952).
[2] F. K. Goward and J. J. Wilkins, Proc. Phys. Soc. (London) **A65**, 671 (1952); C. A. Hsaio and V. L. Telegdi, Phys. Rev. **90**, 494 (1953); D. L. Livesey and C. L. Smith, Proc. Phys. Soc. (London) **A65**, 758 (1952).
[3] Katz, Haslam, Horsley, Cameron, and Montalbetti, Phys. Rev. **95**, 464 (1954).
[4] A. S. Penfold and B. M. Spicer (to be published).
[5] M. Gell-Mann and V. L. Telegdi, Phys. Rev. **91**, 169 (1953).
[6] E. G. Fuller, Phys. Rev. **79**, 303 (1950).
[7] A. Beiser, Revs. Modern Phys. **24**, 273 (1952).

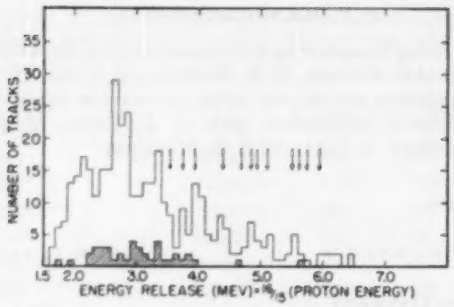

FIG. 1. Energy distribution of photoprotons (100-kev bins). Arrows indicate the energies of breaks found in the (γ,n) reaction (reference 4). The background which was subtracted is indicated by the shaded histogram.

projection of the range on to the plane of the emulsion, the angle, θ, of this projection to the beam direction, and the final depth in the emulsion reached by the track. To be accepted, the track was required to start at the surface of the emulsion, and to have a direction compatible with an origin in the irradiated part of the gas target. This latter condition required that the maximum allowable angle of dip, φ, was 23° at the front of the plate, decreasing to 11.5° at the back of the plate. The acceptable angular range in θ was 20° to 160°.

The background which arises from (n,p) reactions in the oxygen gas is negligible since the threshold for this reaction is 10.2 Mev (energy in the laboratory system). Therefore, the only source of background is due to neutrons produced in the collimator giving rise to recoil protons in the emulsion. Estimation of this background was made as follows. The emulsions were actually scanned over the angular regions $20° \leqslant \theta \leqslant 160°$ and $200° \leqslant \theta \leqslant 340°$. For both these regions the same selection rules were applied. The tracks were required to start at the surface of the emulsion, and the angle of dip was to satisfy the conditions described previously. Those tracks which were in the angular region $200° \leqslant \theta \leqslant 340°$ were taken as the background These protons could not have come from the target since their direction of motion was towards it. This method of estimating the background assumes that these recoil protons are produced symmetrically in θ about the direction of the x-ray beam. The background was approximately 11 percent of the acceptable photoproton tracks.

TREATMENT OF DATA

The energy of the proton at the surface of the emulsion was obtained from the range-energy data for Ilford emulsions given by Wilkins.[8] The energy lost by the proton in the gas between target and emulsion was calculated by using the energy loss tables of Aron, Hoffman, and Williams.[9] The energy loss formula was approximated by

$$-dE/dx = (0.1361/E)\{\ln E + 2.2239\} \text{ Mev/cm},$$

and this formula agrees with Aron's tables to within ½ percent for the range of proton energies considered. The procedure for obtaining the initial energy from the energy at the emulsion surface and the distance traveled in the gas has been described previously.[10] All protons were assumed to start at the center of the x-ray beam. The distance travelled in the gas was obtained from the angle of the track to the beam direction and the known position of the track in the plate.

Uncertainty in the measurement of proton energy is made up of three factors. They are (i) the uncertainty in locating the beginning of the track, (ii) the uncertainty in energy due to range straggling in the emulsion, and (iii) the finite thickness of the gas target. Consideration of these three factors gave a figure of ±90 kev uncertainty in energy for 3-Mev protons, and larger uncertainties for protons of lower energy.

To plot the angular distribution, the data were grouped into 20° angular intervals, according to the angle the tracks made with the x-ray beam in the laboratory system. The mean differential cross section was calculated from the number of tracks per 20° interval, by making a correction for the solid angle subtended by each interval at the position of the track. This solid angle correction factor is very closely $\langle \sin\theta \rangle_{\Delta\theta}$,[6,10] where $\langle \sin\theta \rangle_{\Delta\theta}$ is the mean value of $\sin\theta$ over the 20° interval.

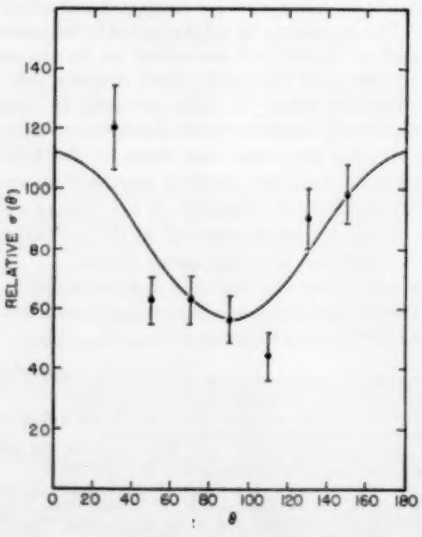

FIG. 2. The angular distribution of photoprotons. The line is 56 $(1+\cos^2\theta)$.

[8] J. J. Wilkins, Atomic Energy Research Establishment, Harwell Report G/R 664, 1951 (unpublished).

[9] Aron, Hoffman, and Williams, Atomic Energy Commission Report 663, 1949 (unpublished).

[10] B. M. Spicer, Australian J. Phys. 6, 391 (1953).

RESULTS AND DISCUSSIONS

The observed energy distribution and angular distribution of photoprotons are shown in Figs. 1 and 2.

The irradiation energy of 18.7 Mev was chosen so that only the ground state in the residual nucleus, N^{15}, was available. Protons leaving N^{15} in the 5.28- or 5.31-Mev states were not detected, since the minimum proton energy detected was 1.5 Mev. This is illustrated by the energy level diagram in Fig. 3. The magnitude of the uncertainty in proton energy forbade the definite resolution of proton groups corresponding to the excitation of discrete levels in the compound nucleus O^{16}.

Knowing that only one state of N^{15} was available in this reaction, it was possible to determine the energy of the photon causing a particular event, from the proton energy. The threshold energy for the reaction is known to be 12.11 ± 0.01 Mev from mass data.[11] We then obtain a relative cross section curve from the energy distribution shown by dividing out the relative number of photons per unit energy interval. The cross section obtained is shown in Fig. 4.

The yield of protons at 18.5 Mev was calculated from the formula

$$Y=\frac{4\pi N}{d\Omega\cdot R}\cdot\frac{1}{MV},$$

where Y is the yield of protons per mole per roentgen, R is the dose given in roentgens, V is the effective volume of the gas target (cm^3), N is the number of tracks per unit area of the emulsion, M is the number of moles/cm^2 at the gas pressure used, and $d\Omega$ is the mean solid angle at the target subtended by unit area on the emulsion.

430 tracks were found and measured on a scanned area

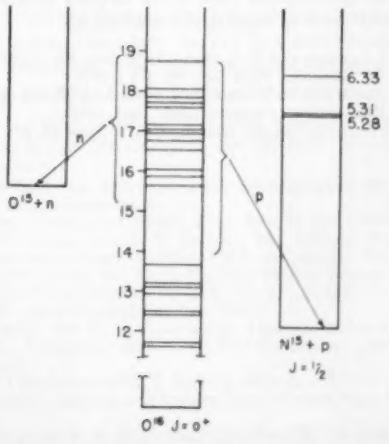

FIG. 3. Energy level diagram. The levels shown are known from other reactions. Maximum photon energy is 18.7 Mev. (γ,p) threshold is at 12.1 Mev.

[11] F. Ajzenberg and T. Lauritsen (to be published).

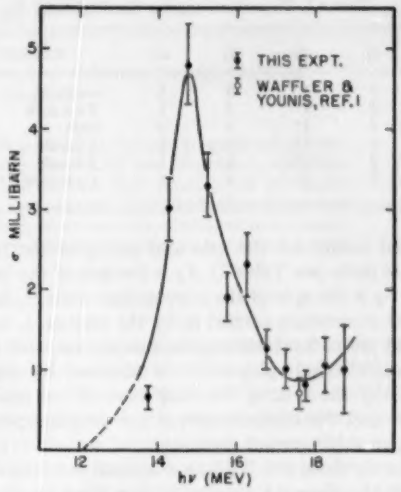

FIG. 4. Cross section for $O^{16}(\gamma,p)N^{15}$.

of 8.84 cm^2. Using this in the aforementioned formula, one finds the yield of protons at 18.7 Mev to be 4×10^4 protons per mole per roentgen. This may be compared with (γ,n) yields at 18 Mev of 5×10^3 neutrons per mole per r,[12] and 10^4 neutrons per mole per r.[13] The (γ,p) yield is expected to be higher than the (γ,n) because of its lower threshold energy.

Now

$$Y=k\int_0^{E_0}P(E,E_0)\sigma(E)dE,$$

where $P(E,E_0)dE$ is the number of photons per cm^2 per r between energies E and $E+dE$, in a spectrum of maximum energy E_0, and $\sigma(E)$ is the cross section at energy E. The k is a constant. By putting in the value of k such that the cross section is given in millibarns, and the yield in protons per mole per r, a value of 11 Mev-millibarns is obtained for $\int_{12.1}^{18.5}\sigma dE$ if the $P(E,E_0)$ is removed from the integral as $\langle P(E,E_0)\rangle_{Av}$. Having this, absolute values may be put on the cross-section curve in Fig. 4. Also shown in that figure is the cross-section value obtained by using the lithium γ rays.[1]

It should be noted that this measurement excludes the energy region where the giant resonance is expected to occur. Therefore, the cross section is expected to have a second peak at about 22 Mev, as indicated by the (γ,n) cross-section measurements of Montalbetti and Katz.[12]

The angular distribution has the form $a+b\cos^2\theta$, with a approximately equal to b. This form was also obtained when angular distributions were plotted separately for protons of energy less than 3 Mev, and for those with energy greater than 3 Mev. The angular distribution may be compared with the forms calculated[14] by using

[12] R. Montalbetti and L. Katz, Can. J. Phys. **31**, 798 (1953).
[13] G. A. Price and D. W. Kerst, Phys. Rev. **77**, 806 (1950).
[14] J. H. Smith (private communication).

TABLE I. Theoretical angular distributions.

J_A	l_γ	J_B	l_p	J_C	$\sigma(\theta)$
0^+	1	1^-	0	1	constant
0^+	1	1^-	2	1	$2+3\sin^2\theta$
0^+	1	1^+	1	0	$\sin^2\theta$
0^+	1	1^+	1	1	$1+\cos^2\theta$
0^+	2	2^+	1	1	$1+\cos^2\theta$
0^+	2	2^+	3	1	$1+6\cos^2\theta-5\cos^4\theta$

assumed values for the spin and parity of the intermediate state (see Table I). J_A is the spin of the initial state, J_B is the spin of the intermediate state, l_γ is the angular momentum carried in by the photon, l_p is the emitted proton's orbital angular momentum, and J_C is the final channel spin, which is obtained by adding vectorially the spin of the final state of the residual nucleus and the intrinsic spin of the outgoing proton. The spin of N^{15} ground state is $\frac{1}{2}^-$.

The only cases which give a distribution of the same form as the observed distribution are those for electric quadrupole absorption leading to emission of p-wave protons, and for magnetic dipole absorption, p-wave proton emission, and a final channel spin $J_C=1$. In practice, it is not possible to separate out the contributions of different final channel spins, and so the angular distribution for magnetic dipole absorption must be written $a\sin^2\theta+b(1+\cos^2\theta)$. The a and b here are both positive. The conclusion that the reaction proceeds predominantly by electric quadrupole and magnetic dipole absorption confirms the tentative conclusion drawn in the activation work of Penfold and Spicer.[4]

Using the assumption of charge independence of nuclear forces, Gell-Mann and Telegdi[5] showed that the expected threshold for the allowed, electric dipole-induced (γ,α) reaction in O^{16} is about 25 Mev. This is apparently confirmed by experiment, as Livesey and Smith[2] report a change in mechanism in this reaction at about 25 Mev. However, the isotopic spin selection rules, while forbidding the (γ,α) reaction below 19 Mev, do not forbid the (γ,p) or (γ,n) reactions in this region. In fact, the (γ,p) and (γ,n) reactions are allowed to proceed via electric dipole absorption from 13 Mev up. One must therefore seek another reason for the forbiddenness of $E1$ absorption between 13 and 19 Mev. Some possible reasons for this forbiddenness are:

(i) The number of 1^- levels in O^{16} between 13 and 18 Mev is zero or very small. This explanation does not appear reasonable since the spacing of 1^- levels is known to be 600 kev at 13 Mev,[10] and at 20 Mev is about 120 kev.[4]

(ii) The alpha-particle model for photon reactions put forward tentatively by Levinger and Bethe[15] accounts for this lack of dipole transitions. In this model, no electric dipole transitions can occur until the photon has enough energy to disrupt a particular alpha particle by a dipole transition, and this energy is about 20 Mev.

(iii) There is a selection rule, as yet unknown, which forbids electric dipole transitions in the case discussed above, and other similar cases.

The success of the alpha-particle model in accounting for most energy levels in O^{16} up to 13 Mev[16] gives reason to believe that explanation (ii) may hold in the case of the oxygen nucleus. However, similar studies of other nuclei, where the α-particle model does not have such success would help to discriminate between explanations (ii) and (iii). In this regard, it is interesting to note that photoreactions in some other nuclei do have double-peaked cross section *versus* energy curves. Examples are $Li^7(\gamma,p)$,[17] $O^{16}(\gamma,n)$,[4] $N^{14}(\gamma,n)$,[18] and $F^{19}(\gamma,n)$.[19]

ACKNOWLEDGMENTS

The author is indebted to Dr. J. H. Smith for his very considerable help in the calculation of the theoretical angular distributions, and to Dr. A. O. Hanson for many helpful discussions. Thanks are also due to Mr. H. Moore for his assistance in scanning the plates, and to T. J. Keegan and the crew of the 22-Mev betatron for their assistance in making the irradiations.

[15] J. S. Levinger and H. A. Bethe, Phys. Rev. **78**, 115 (1950).
[16] D. M. Dennison, Phys. Rev. **96**, 378 (1954).
[17] R. Rubin and M. Walter, Helv. Phys. Acta **27**, 163 (1954).
[18] L. Katz (private communication, June, 1954).
[19] Taylor, Robinson, and Haslam, Can. J. Phys. **32**, 238 (1954).

Decay Properties of U^{232}†

FRANK ASARO AND I. PERLMAN
Radiation Laboratory and Department of Chemistry, University of California, Berkeley, California

(Received March 16, 1955)

The alpha and gamma spectra of U^{232} have been studied with an alpha-particle spectrograph and gamma-ray scintillation, proportional, and coincidence counters. Alpha groups of 5.318 Mev (68 percent), 5.261 Mev (32 percent) and 5.134 Mev (0.32 percent) and gamma rays of 57.9 kev (0.21 percent), 131 kev (0.075 percent), 268 kev (0.004 percent), and 326 kev (0.004 percent) were observed. The half-life of the 58-kev first excited state of Th^{228} was found to be less than 10 microseconds. Spins and parities are assigned to the energy levels, and the results are evaluated with respect to the developing theory and systematics of complex alpha spectra and excited states of even-even nuclei.

INTRODUCTION

THE uranium isotope, U^{232}, is a beta-stable alpha emitter with a half-life of 73.6 years[1] and was first identified following its growth from the shorter-lived β^--emitter Pa^{232} which had been prepared by the $(d,2n)$ reaction on Th^{232}.[2] The alpha-particle energy has been determined by range measurement as 5.31 Mev[3] and 5.27 Mev.[4] It could be inferred that the U^{232} alpha spectrum was complex because prominent conversion electrons of an ~60-kev gamma ray were observed in coincidence with alpha tracks in a photographic emulsion.[5] An early part of the present study, in which there was found an alpha group of 58-kev lower energy than the main group, has already been reported.[6]

There has been added recent interest in the alpha spectra of even-even nuclei because they display prominently series of energy levels which have been interpreted as rotational states.[7–9] The theory of Bohr and Mottelson which explains these rotational bands as a consequence of collective motions in highly deformed nuclei predicts a simple relationship of the energy spacing between members of the band: $E_{rot} \propto I(I+1)$, where I refers to the spin which in this case is restricted to even integral numbers. As will be mentioned further in the Discussion, this simple expression applies to a limiting condition in which the rotational frequency is sufficiently slow to allow the nuclear structure to adjust adiabatically to the changing electric field. Where this situation does not apply, the rotational levels are perturbed and correction terms must be applied. It is noted that the heaviest nuclei show "pure" rotational bands and as the closed-shell region around lead is approached the perturbation becomes more and more severe. In this context, it will be seen that Th^{228} (alpha decay of U^{232}) shows a just discernible departure from the ideal case and therefore represents the entry into the "light-element" or closed-shell region.

Another aspect of note in the decay of U^{232} is the appearance of a low-lying level which does not belong to the rotational band. This particular state with spin 1, odd parity, occurs in a limited region (around 136 neutrons). It was the subject of another publication[10] and will be discussed further below.

METHODS

Preparation of source.—The U^{232} sources for the present study were prepared in two ways. In one of these, Th^{232} was bombarded with protons resulting in U^{232} by the following reactions[11]:

$$Th^{232}(p,n)Pa^{232} \xrightarrow{\beta^-} U^{232}.$$

The other method involved intensive neutron irradiation of ionium (Th^{230}):

$$Th^{230}(n,\gamma)Th^{231} \xrightarrow{\beta^-} Pa^{231}(n,\gamma)Pa^{232} \xrightarrow{\beta^-} U^{232}.$$

Inasmuch as Th^{232} was present in the irradiated ionium, U^{233} was also made by a first-order neutron capture reaction. However, its contribution to the radioactivity was quite insignificant; the alpha spectrum showed a possible peak of the U^{232} position of maximum intensity 0.06 percent relative to the U^{232} groups. The factors which produced this favorable ratio were: (1) the ionium had been considerably enriched by electromagnetic separation[12] from the initial source materials, (2) the

† This work was performed under the auspices of the U. S. Atomic Energy Commission.

[1] Sellers, Stevens, and Studier, Phys. Rev. **94**, 952 (1954).

[2] J. W. Gofman and G. T. Seaborg, The Transuranium Elements: Research Papers (McGraw-Hill Book Company, Inc., New York, 1949), Paper No. 19.14, National Nuclear Energy Series, Plutonium Project Record, Vol. **14B**, Div. IV., p. 1427.

[3] A. H. Jaffey (unpublished data, 1948).

[4] H. Kahn and G. A. Linenberger, reported in Los Alamos Scientific Laboratory Report LAMS-151, October, 1944 (unpublished).

[5] D. C. Dunlavey and G. T. Seaborg, Phys. Rev. **87**, 165 (1952).

[6] Hollander, Perlman, and Seaborg, Revs. Modern Phys. **25**, 469 (1953).

[7] A. Bohr and B. R. Mottelson, Phys. Rev. **89**, 316 (1953); **90**, 717 (1953); Kgl. Danske Videnskab. Selskab, Mat.-fys. Medd. **27**, No. 16 (1953).

[8] A. Bohr, *Rotational States of Atomic Nuclei* (Ejnar Munksgaard, Copenhagen, 1954).

[9] F. Asaro and I. Perlman, Phys. Rev. **91**, 763 (1953).

[10] Stephens, Asaro, and Perlman, Phys. Rev. **96**, 1568 (1954).

[11] We wish to thank Dr. Louis M. Slater for making this sample available to us.

[12] For typical available compositions of enriched ionium, see: Harmatz, McCurdy, and Case, Oak Ridge National Laboratory Report ORNL-1724, 1954 (unpublished). We wish to thank

TABLE I. Alpha-particle spectrograph exposures.

Exposure number	Source of U^{232}	Slit width of spectrograph source (inch)	Duration of exposure	Activity of sample (dis/minute)	Time after Th^{228} removal
134	$Th^{232}(p,n)Pa^{232} \xrightarrow{\beta^-} U^{232}$	$\frac{1}{4}\times 1$	46 hr	10^4	~1 week
245	$Io^{230}(n,\gamma)Th^{231} \xrightarrow{\beta^-} Pa^{231}$ $Pa^{231}(n,\gamma)Pa^{232} \xrightarrow{\beta^-} U^{232}$	$\frac{1}{4}\times 1$	14 hr	6×10^5	~1 month
277	Same sample as used in exposure 245	$0.018\times\frac{1}{4}$	46 hr	...	7 months
278	Same sample as used in exposure 245	$0.018\times\frac{1}{4}$	47 min	...	7 months

neutron capture cross sections[13] for Th^{230} and Pa^{231} are much larger than that for Th^{232}, (3) the half-life for U^{233} is long compared with U^{232}, and (4) the uranium was separated before all of the intermediate Pa^{233} had decayed to U^{233}.

Alpha-particle spectra.—All samples for the alpha-particle spectrograph were prepared by vacuum sublimation of the chloride onto a platinum plate which was masked to present a band 1 inch×¼ inch. This sample mounting technique, as well as the equipment and methods for taking alpha spectra, have been described in earlier reports.[14–16] As before, the alpha particles were caught on a photographic plate and the track count was plotted according to position on the plate.

Gamma-ray measurement.—Gamma-ray spectra were measured for the most part with a sodium iodide scintillation counter coupled to a 50-channel pulse-height analyzer. In some experiments a xenon-filled proportional counter was used to produce the pulse for the analyzer.

Coincidence counting methods used in this and similar studies have been described elsewhere.[10,17] Briefly, a gamma-ray pulse is fed into a 50-channel pulse-height analyzer which registers only when triggered through a gate circuit. For alpha-gamma coincidences the pulse produced by a zinc sulfide screen in optical contact with a photomultiplier tube is used to open the gate; for gamma-gamma coincidences, another sodium iodide crystal counter was used.

RESULTS

Alpha Spectrum

Four exposures, involving two U^{232} preparations, were made and the histories are given in Table I. The first measurement (Exp. 134) was made with a relatively weak sample before more active preparations had been made. Numbers 245 and 277 were moderately long exposures of an intense source aimed principally at finding low-intensity alpha groups. The more intense alpha groups register too many tracks for convenient counting. A shorter exposure (Exp. 278) was then made to get more accurate data on the abundances and energies of the most prominent groups.

As a result of these several experiments, three alpha groups were found for U^{232} as summarized in Table II. Two of these are the characteristic high-intensity groups of an even-even alpha emitter leading to the ground state and first excited state of the product. The energy of the main group was found to be 5.318 ±0.002 Mev and the second group was lower in energy by 57.2±1.2 kev. (The 5.421-Mev [18] alpha group of Th^{228}, which grew into the U^{232} sample, was used as the energy standard for these measurements.) When the differences in recoil energies from the two alpha groups are included, the first excited state is found to lie at 58.2 kev. The intensity of α_{58} was found to be 32 percent.[19]

Besides the two principal groups a weak alpha group

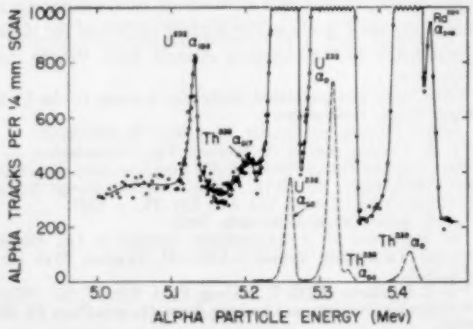

FIG. 1. U^{232} alpha spectrum with daughters partially grown in. —— Exposure 277. —— Exposure 278 (ordinate scale should be multiplied by 2).

members of the Electronuclear Research Division of Oak Ridge National Laboratory for making some enriched ionium available to us.

[13] See: *Neutron Cross-Sections*, U. S. Atomic Energy Commission Report AECU-2040 (Technical Information Division, Department of Commerce, Washington, D. C., 1952).

[14] F. L. Reynolds, Rev. Sci. Instr. **22**, 749 (1951).

[15] Asaro, Reynolds, and Perlman, Phys. Rev. **87**, 277 (1952).

[16] Asaro, Thompson, and Perlman, Phys. Rev. **92**, 694 (1953).

[17] Asaro, Stephens, Thompson, and Perlman, Phys. Rev. **98**, 19 (1955).

[18] Asaro, Stephens, and Perlman, Phys. Rev. **92**, 1495 (1953).

[19] α_{58} refers to the alpha group leading to the 58-kev state.

TABLE II. Results of spectrograph exposures.

Exposure number	α particle energy separation between α_0 and α_{188} (kev)	Separation between α_0 and α_{188} including difference in nuclear recoil (kev)	Intensity of α_{188} relative to total U^{233} α particles (%)	α decay energy separation between α_{188} and α_{131} (kev)	α decay energy separation between α_0 and α_{131} (kev)	Intensity of α_{131} relative to total U^{233} α particles (%)	α particle energy of U^{233} α_0 relative to Th^{229} α_0 (5.421 Mev) (Mev)	α particle energy of U^{233} α_{188} relative to Th^{229} α_0 (5.421 Mev) (Mev)
134	58±2	59.$_5$	31	...	...	...	...	...
245	55±4	56	35	...	189	0.3	5.317	...
277	...	...	...	129.$_5$	...	0.32±0.03	...	5.260±2
278	57.2±1.2	58.2	32±1	...	...	...	5.318±2	5.261±2
Best value	57.2	58.2	32		188	0.32	5.318	

of 0.32 percent abundance was identified as belonging to U^{232}. This group leads to a state 188 kev above the ground state. Gamma rays originating from this state and others will be described below. No other alpha groups belonging to U^{232} were noted but the limits of detection varied with the proximity to the observed groups. Over the energy range 5.07 Mev→4.83 Mev an upper limit of 0.01 percent could be set. At 4.822 Mev there was a small peak (0.06 percent of the U^{232} intensity) which is probably due to U^{233} as the energy agreement is good and it is expected that there would be some present.

The alpha spectrum of U^{232} with some of its daughter activities is shown in Fig. 1. The solid line curve was obtained from Exp. 277 in which the principal peaks were too strong to be counted. The positions and intensities of the strong groups taken from Exp. 278 are shown as the broken line curve of Fig. 1.

Gamma Rays and Decay Scheme

The partial decay scheme for U^{232} based on the present studies is shown in Fig. 2. It will be noted that a third excited level in Th^{228} is indicated by gamma radiation although the alpha group populating this state could not be seen. The experiments will be discussed in terms of the successive energy levels. Some of the gamma rays measured were extremely weak in intensity and a number of measurements of the gamma spectrum were made after repeated and varied chemical purification steps to make certain that these radiations did not arise from Th^{228} decay products. The only nonseparable substance which could have been present was U^{233} and an upper limit to its intensity could be set on the basis of the alpha spectrum.

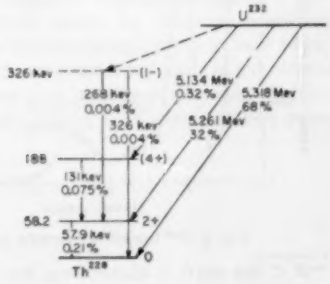

FIG. 2. U^{233} decay scheme.

The measurements on the photons included: (1) identification and intensity measurements with a scintillation spectrometer, (2) alpha-gamma and gamma-gamma coincidence determinations, (3) xenon-filled proportional counter measurements of energy. In all, 13 sets of measurements were made employing six different repurified samples of U^{233} from a common original stock.

The 58-kev state.—As indicated by the alpha spectrum, the first excited state lies at 58.2±1.2 kev and is populated directly to the extent of 32 percent. Further possible population of this state by transitions from higher states cannot be much in excess of 0.32 percent.

Several measurements with the scintillation spectrometer in which the 59.6-kev gamma ray of Am^{241} was used as an energy standard showed a peak at 57 to 58 kev. Two measurements with a xenon-filled proportional counter gave the best energy determination as 57.9±0.3 kev. The prominent Am^{241} photon also served as an intensity standard. The best determination of the intensity was 2.1×10^{-3} relative to total alpha disintegrations. The total conversion coefficient is therefore 152 which agrees well with the value 120 for the *L*-shell conversion coefficient for an *E*2 transition which was estimated from available theoretical data.[20,21] This assignment confirms the expected 2+ designation for the first excited state of Th^{228}.

This same state has been observed by others[22–24] in the beta spectrum of $MsTh_2(Ac^{228})$. Brodie[23] gave the energy of the transition as 57.0 kev and Kyles, Campbell, and Henderson[24] reported 56.75 kev. These two reports concluded that the transition is *E*2 although the conversion coefficients differed somewhat from those deduced here.

A puzzling feature of the 58-kev transition is an apparent discrepancy concerning the lifetime of the 2+

[20] Rose, Goertzel, and Swift, *Tables of Conversion Coefficients* (privately circulated).
[21] Gellman, Griffith, and Stanley, Phys. Rev. **85**, 944 (1952).
[22] D. H. Black, Proc. Roy. Soc. (London) **A106**, 632 (1944).
[23] W. D. Brodie, Proc. Phys. Soc. (London) **A67**, 265 (1954).
[24] Kyles, Campbell, and Henderson, Proc. Phys. Soc. (London) **A66**, 519 (1953).

state. Two groups[24,25] working on the beta spectrum of $MsTh_2$ have reported the lifetime of this state to be greater than 10 milliseconds. A third group has reported the lifetime to be larger than 0.5 second.[26] From the present results it is deduced that the lifetime of this state is less than 10 microseconds. In two measurements the coincidence rate between alpha particles and 58-kev gamma rays was 0.16 percent and 0.18 percent per alpha particle. These values correspond within experimental error with the above-mentioned intensity of 0.21 percent for the 58-kev photon, showing that it is in coincidence with the alpha particles within the resolving time of the coincidence circuit which was about 10 microseconds. In addition coincidences were observed between the 130-kev gamma ray and L x-rays. These L x-rays arise mainly from the conversion of the 58-kev gamma ray.

It is probable that the methods[24–26] by which delays between the events were noted could not distinguish between a long delay and a very rapid coincidence. It is to be expected[7,27] that, in a region such as this well away from closed shells, the $E2$ transitions from the first excited state would be abnormally rapid rather than slow.

The 188-kev state.—A state at this energy is defined uniquely by the existence of a U^{232} alpha group with an energy lower than the ground state transition by the appropriate amount. As already mentioned, this state is populated to the extent of about 0.32 percent.

The only gamma-ray transition observed in the present study which depopulates this state is one of 131 kev. It leads from the 188-kev state to the 58-kev state as determined by gamma-gamma coincidence measurements between 131- and 58-kev photons and between the 131-kev gamma ray and L x-rays. This situation is similar to that of other even-even nuclei among the heavy elements in which a series of states exist which are believed to belong to a rotational band and follow the sequence $0+, 2+, 4+, \cdots$. In none of these cases has a crossover transition been seen from the second even spin state to the ground state. It remains now to be seen if some of the other criteria for this sequence exist.

One of the properties of a pure rotational spectrum is that the energy spacings are proportional to $I(I+1)$, where I is the spin. The ratio of energies between the spin 4 and spin 2 states should be accordingly 20/6 or 3.33. In the present situation the ratio is 188/58 or 3.24.

If the 131-kev transition takes place between 4+ and 2+ states it must be of pure $E2$ character. Two measurements were made of the alpha-gamma coincidence rate for the 131-kev gamma ray. These gave intensities for the gamma ray of 0.05 and 0.06 percent. Two more precise measurements of the gamma spectrum gave a value of 0.075 percent for the best intensity of the 131-kev gamma ray. Inasmuch as the 188-kev state is populated to the extent of 0.32 percent the conversion coefficient becomes ~3.2. This is in good agreement with the expectations for an $E2$ transition, it is definitely too high for an $E1$ transition, and is about a factor of 3 too low for an $M1$ transition. There is some radiation observed at about 85 kev (see Fig. 3.) Although it may include scattered radiation from the 131-kev gamma ray, its abundance represents the maximum intensity of K x-rays in the decay of U^{232}. This abundance is 0.4 of the abundance of the 131-kev gamma ray, giving a maximum K conversion coefficient of 0.4. This is in good agreement with the expectations for an $E2$ transition but is a factor of 20 too low for an $M1$ transition.

A gamma-ray transition of about this energy (128 kev) was studied by Brodie[23] and by Kyles, Campbell, and Henderson[24] in the conversion electron spectrum from $MsTh_2$. As pointed out[24] the L subshell conversion ratios and the low limit set on the K conversion indicates an $E2$ transition, with which our conclusions agree. The same gamma ray (129 kev) was seen by Box and Klaiber[28] using a scintillation spectrometer.

These workers[22,24] also studied a transition of about 184 kev which they interpreted as an $M1$ transition and in their decay scheme was placed as the crossover transition from a level of this energy to the ground state for which the cascading transitions are those of 128 kev and 58 kev. In order to fit spins and parities to these conditions the sequence for the ground state and next two higher states was postulated[24] to be 0+, 2+, 1+. There are two reasons why a state at 184 kev which meets this condition cannot be the same as our 188-kev state defined by the alpha decay of U^{232}. In the first place an even-even alpha emitter cannot populate directly a state of odd spin and even parity. The other argument has to do with intensities of gamma rays. According to the data and deductions of Brodie[23] and of Kyles and co-workers,[24] the intensities of the 128-kev and 184-kev photons should be about the same. From our measurements the intensity of the 131-kev gamma ray is at least 30 times greater than a peak at 184 kev (see Fig. 3). In order to reconcile these results it is necessary to say that either there is a 1+ state at

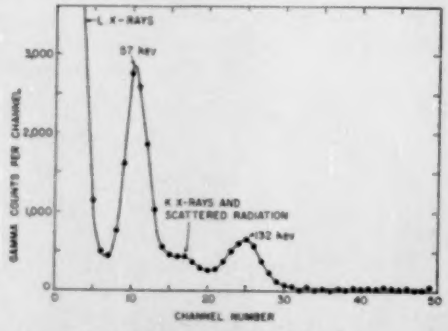

FIG. 3. U^{232} low-energy gamma spectrum.

[23] Lecoin, Perey, and Teillac, J. phys. radium **10**, 33 (1949).
[24] F. Suzor and G. Charpak, J. phys. radium **15**, 682 (1954).
[25] M. Goldhaber and A. W. Sunyar, Phys. Rev. **83**, 906 (1951).
[26] H. C. Box and G. S. Klaiber, Phys. Rev. **95**, 1247 (1954).

184-kev (populated from the beta decay of $MsTh_2$) which is different from our 188-kev state (from alpha decay of U^{232}) or the observed 184-kev transition involves higher-lying states of Th^{228} which also would not be expected to be seen in alpha decay processes. An added datum which must be considered in the over-all interpretation is the failure of Box and Klaiber[25] to observe a 184-kev photon in their scintillation counter study of $MsTh_2$. This could imply a high conversion coefficient for the 184-kev transition although it is rather difficult to set limits on the basis of their reported data.

The 326-kev state.—From the present work a level at this energy (see Fig. 2) could only be inferred from gamma-ray measurements, as the alpha-particle intensity is apparently too weak for direct detection. The evidence for the state is based on the observation of two gamma rays of 326 and 268 kev (see Fig. 4). The energy differences alone suggest transitions from a 326-kev level to the ground state and the 58-kev state, respectively.

The intensities of the two peaks as determined with the scintillation spectrometer were both about the same and amounted to about 4×10^{-3} percent of the total alpha disintegrations for each. An alpha-gamma coincidence measurement for the 268-kev gamma ray gave an intensity of 5×10^{-3} percent. Similarly, if L x-rays were used to gate the scintillation spectrometer it was found that the 268-kev gamma rays were in coincidence and the intensity came out to be 3×10^{-3} percent per alpha particle. Much less abundant coincidences with L x-rays were found for the 326-kev gamma ray. Because the L x-rays arise predominantly from the 58-kev transition it is probable that the 268-kev gamma ray goes to the 58-kev state and the 326-kev gamma ray does not. The L x-ray coincidences with the 326-kev gamma ray could be due to impurities or to the decay of still higher excited states populated by U^{232} alpha emission.

These intensity, coincidence, and energy considerations imply that a single state at 326 kev is responsible for both of these photons as shown in Fig. 2. Box and Klaiber[25] also found a pair of gamma rays differing by 58 kev and having approximately the energies seen here. Their values were 336 and 278 kev. Furthermore, they found coincidences between both of these and a gamma ray of 790 kev, which is also consistent with the supposition that both originate from a common level. However, the spectrum shown by these authors would indicate that the 336-kev gamma ray is at least twice as intense as the 278-kev gamma ray while in our measurements the 278-kev photon seemed to be somewhat more intense. This may suggest that there are two gamma

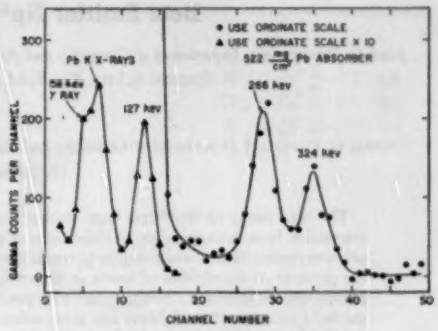

FIG. 4. U^{232} high-energy gamma spectrum.

rays of about 336 kev, one of which occupies the position as shown by us (and by Box and Klaiber) and the other is a transition between higher levels. Significantly, Kyles and co-workers[24] report conversion lines from a gamma ray of 336 kev but not from one at 278 kev.

In the absence of conversion coefficient data for our 326- and 268-kev transitions it is not possible to characterize them with certainty. We have been led to assign the 326-kev level 1− and consequently the transitions $E1$ by analogy with the well-characterized 1− levels found from other even-even alpha emitters in this region.[10]

DISCUSSION AND SUMMARY

The decay scheme for U^{232} shown in Fig. 2 bears a strong resemblance to those of other even-even alpha emitters in this region. In each case a rotational band consisting of 0+, 2+, and 4+ states is seen. In some cases the 1− state lies between the 2+ and 4+ states but for U^{232} decay it lies above the 4+ state. Just as in other cases, two $E2$ transitions are seen which cascade from the 4+ to the 2+ and 0+ (ground state). The 1− state is de-excited by competing $E1$ transitions to the 2+ and 0+ states. To be sure, further information must be obtained to get independent evidence that the transitions in question for U^{232} are indeed $E1$.

As has already been discussed, there is a partial correlation of the energy levels found in the present study from the alpha decay of U^{232} and those from the beta decay of $MsTh_2$ found by others. There are also some points of apparent disagreement. Because of the extreme complexity of the $MsTh_2$ spectrum it is not possible to resolve these difficulties readily from existing data. Some of the information worth seeking in future studies on $MsTh_2$ has been mentioned in earlier discussion.

Beta Emitter Np^{235}. I. Beta Spectroscopy*

JOHN O. RASMUSSEN, *Department of Chemistry and Radiation Laboratory, University of California, Berkeley, California*
HILDING SLÄTIS, *The Nobel Institute of Physics, Stockholm, Sweden*
AND
THOMAS O. PASSELL,† *Department of Chemistry and Radiation Laboratory, University of California, Berkeley, California*
(Received March 25, 1955)

The beta decay of Np^{235} has been studied with several beta spectrometers. In addition to the known conversion lines corresponding to transitions of energies now determined as 44.0, 102.2, 986, and 1029 kev, new conversion lines, corresponding to transitions of 942 and 927 kev were found. These transitions indicate the presence of closely spaced levels at higher excitation energies. Intensities of conversion lines and beta groups were determined and compared with previous work. Fermi-Kurie plots confirm the allowed shape of the hard beta group (1.25 Mev) and give indication of complexity in the soft beta group (0.27 Mev). The energy deviations of the ground rotational band levels from the simple rotational energy formula are discussed.

INTRODUCTION

EARLY investigations[1–4] of the decay of Np^{235} have shown a half-life of 2.1 days, a complex beta spectrum, two highly converted transitions of 43- and 103-kev energy, and two gamma rays of 983- and 1030-kev energy. The beta components were reported to have an allowed shape, 47 percent of the disintegrations belonging to the hard component, the maximum energy of which is 1272 kev, and 53 percent to the soft component of 258-kev energy.

The present paper sets forth and interprets material gained from further beta spectroscopic work on Np^{235}, some of which has been partially reported in prior notes.[5–7]

EXPERIMENTAL PROCEDURE AND RESULTS

For the Stockholm work the Np^{235} was obtained by bombarding natural uranium metal with protons of 12.5-Mev energy in the 225-cm cyclotron of the Nobel Institute of Physics,[8] and for the Berkeley work, by irradiation of Np^{237} with neutrons in the MTR reactor, Reactor Testing Station, Arco, Idaho.[9]

The neptunium activity was chemically purified by various combinations of the procedures given by Magnusson, Thompson, and Seaborg.[10]

The following types of measurements were made:

1. Beta spectroscopy with the Stockholm intermediate-image, long-lens spectrometer.[11] (Resolution ~2 percent.) (Referred to as SS.)

2. Beta spectroscopy with the Stockholm double-focusing spectrometer.[12] (Resolution 0.5 percent.) (Referred to as SD.)

3. Beta spectroscopy with the Berkeley double-focusing spectrometer.[13] (Resolution 1.2 percent.) (Referred to as BD.)

4. Electron spectroscopy of photo and Compton electrons from a (0.0005-inch) uranium metal radiator

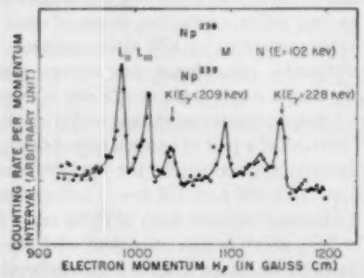

FIG. 1. Electron spectrum of Np^{235} (with some Np^{239}) in the region of the conversion lines of the 102.2-kev gamma ray. (Stockholm double-focusing spectrometer.)

* This work was supported in part by the U. S. Atomic Energy Commission.

† Present address: Phillips Petroleum Company, Idaho Falls, Idaho.

[1] Seaborg, Wahl, and Kennedy, *The Transuranium Elements: Research Papers* (McGraw-Hill Book Company, Inc., New York, 1949), National Nuclear Energy Series, Plutonium Project Record, Vol. 14B, p. 13.

[2] A. H. Jaffey and L. B. Magnusson, *The Transuranium Elements: Research Papers* (McGraw-Hill Book Company, Inc., New York, 1949), National Nuclear Energy Series, Plutonium Project Record, Vol. 14B, p. 978.

[3] Freedman, Jaffey, and Wagner, Phys. Rev. **79**, 410 (1950).

[4] J. W. Mihelich, Phys. Rev. **87**, 646 (1952).

[5] Slätis, Rasmussen, and Atterling, Phys. Rev. **93**, 646 (1954).

[6] Rasmussen, Passell, and Stephens, University of California Radiation Laboratory Unclassified Report UCRL-2585, 1954 (unpublished).

[7] T. O. Passell, Ph.D. thesis, University of California Radiation Laboratory Unclassified Report UCRL-2528, 1954 (unpublished).

[8] We are greatly indebted to Dr. Hugo Atterling, who developed and tested the special target holder for the uranium metal and who carried out the three bombardments.

[9] We express appreciation to Dr. W. B. Lewis, Dr. Richard Smith, and others at the Reactor Test Station for facilitating the irradiation.

[10] Magnusson, Thompson, and Seaborg, Phys. Rev. **78**, 363 (1950).

[11] H. Slätis and K. Siegbahn, Arkiv Fysik **1**, 339 (1949).

[12] A. Hedgran, Arkiv Fysik **5**, 1 (1952).

[13] G. D. O'Kelley, Ph.D. thesis, University of California Radiation Laboratory Unclassified Report UCRL-1243, 1951 (unpublished).

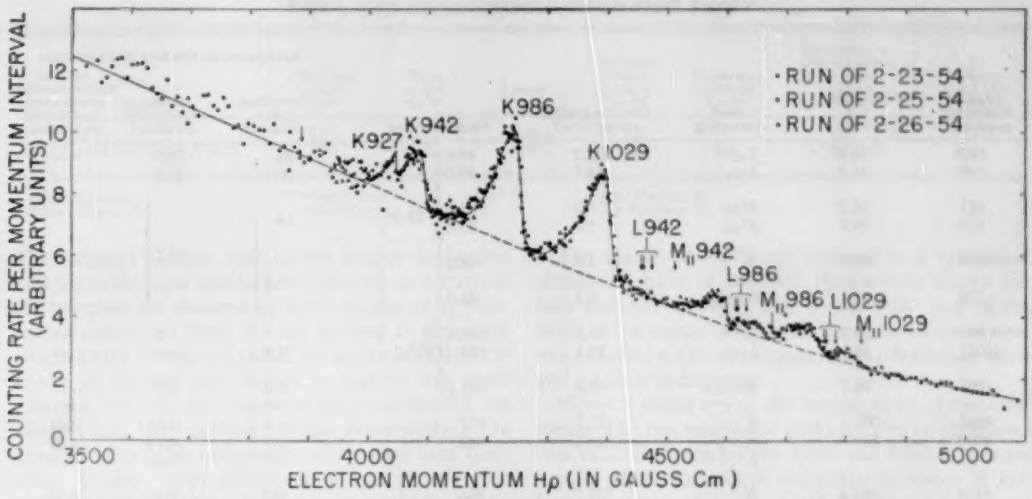

FIG. 2. The high-energy part of the Np^{239} beta spectrum. (Berkeley double-focusing spectrometer.) For interpretation of the arrows see the text.

with the Berkeley ring-focusing solenoidal spectrometer.[14] (Resolution ~2 percent.) (Referred to as BS.)

Where duplicate information was obtained, we present the best or the average of the best determinations. In general, regarding beta spectroscopic results, the energy measurements on the SD spectrometer are taken as standard, since this instrument is specifically designed for precision energy comparisons. However, the energy differences of the high-energy conversion lines determined on the BD spectrometer are preferred by virtue of the much greater source strength and consequent better counting statistics in the Berkeley work. The BD measurements were not as useful as SS and SD for the continuum and lines below 0.7 Mev (disintegration energy of Np^{239}) because of the larger admixture of the troublesome Np^{238}. The SS measurements form the basis for spectrum shape studies of the hard beta particles, as the background due to scattered electrons entering the counter is minimized by the intermediate image slit system.

Figure 1 shows the spectrum taken with the SD spectrometer in the region of the conversion lines of the 102.2-kev gamma ray. Note the lines assigned to Np^{238} present in small amount. By means of the well-known strong conversion lines of Np^{239} it was possible to make corrections for the small contamination of this activity when computing the intensities of the beta components.[15]

Figure 2 shows the spectrum taken with the BD spectrometer of the region above 3500 gauss cm. The K lines of the four high-energy gamma transitions are clearly evident. The arrows labeled for L and M lines each point to the calculated abscissa for the foot of the leading edge of the line (about 20 gauss cm to the right of the peak). The unlabeled arrow at 3887 gauss cm points to the calculated position of the K line of a transition 146 kev less energy than the most energetic gamma ray. (With the decay schemes proposed in the article[16] following this, which we refer to as paper II, it is important to search for such a transition.) There is no evidence for this line, and we can from these data say that it is less than 10 percent of the intense line K_{1030}.

The conversion line energy and intensity data are summarized in Table I. The energy figures are based on averages of the best Stockholm or Berkeley data. As the intensities are of considerable importance in constructing the decay scheme and as there is some variation in intensities obtained in various studies, Table I includes three intensity columns: one for the work of Freedman *et al.*,[3] one for Slätis *et al.*,[5] and one for the BD work previously unreported.

There is fair agreement in the intensity figures between the different investigations except for some extremely weak high-energy lines and except for the lowest energy 21.8-kev $L_{II}44$ line. At such low energies spectrometer measurements are subject to some uncertainty from counter window transmission losses. In view of the disagreement, the total intensity figure for conversion lines of the 44-kev transition has not been given much weight in the construction of a decay scheme.

It is of some interest to collect as in Table II yet other determinations of intensity of the low-energy conversion lines.[3,5,7,17,18,19] Passell[7] has measured on the BD spec-

[14] G. D. O'Kelley, California Research and Development Company Unclassified Report MTA-38, May 1954 (unpublished).

[15] Regarding the shape of the Np^{239} spectrum see H. Slätis, Arkiv Mat. Astron. Fysik **35A**, 3 (1947).

[16] Rasmussen, Stephens, Strominger, and Åström, following paper [Phys. Rev. **99**, 47 (1955)].

[17] Gellman, Griffith, and Stanley, Phys. Rev. **85**, 944 (1952).

[18] D. C. Dunlavey and G. T. Seaborg, Phys. Rev. **87**, 165 (1952).

[19] D. C. Dunlavey, unpublished results (1953) (110 electron coincidence events counted).

TABLE I. Conversion lines accompanying beta decay of Np^{238}.

Electron momentum gauss cm[a]	Electron line energy[a]	Shell converting	Electron binding energy (Pu)[b]	Gamma energy		Abundance per 100 beta disintegrations: Freedman, Jaffey, Wagner[c]	Slätis, Rasmussen, Atterling[d]	Berkeley double-focusing spectrometer (previously unreported)
503	21.8	L_{II}	22.2	44.0		38	28.7	···
549	25.9	L_{III}	18.1	44.0		20	21.0	···
671	38.2	M_{II}	5.6	43.8	44.0[e]	14		
678	39.0	M_{III}	4.6	43.6			15.2	[f]
713	42.9	N	1.4	44.3		3.2		
720	43.7	O	0.3	44.0				
991	80.1	L_{II}	22.3	102.4			1.4	···
1017	84.1	L_{III}	18.1	102.2	102.2	1.9	0.9	···
1097	96.7	$M_{II,III}$	~5.0	101.7		1.2	0.7	···
4046	805.3	K	121.7	927		···	0.05	0.04
4099	819.8	K	121.7	942		···	0.10	0.07
		L	···	···		···	0.06	···
4259	864.4	K	121.7	986		0.3	0.26	0.20
		L	···	···		···	0.13	0.06
4414	907.6	K	121.7	1029		0.3	0.22	0.20
		L	···	···		···	0.08	0.04
		M, N, O	···	···		···	0.06	0.02

[a] Calibration for 44-kev gamma lines from ThB line taken as $H_{\rho A}=534.11$ from the work of D. I. Meyer and F. H. Schmidt, Phys. Rev. **94**, 927 (1954). Calibration for 102-kev gamma lines from ThB F line taken as $H_{\rho F}=1388.56$ from the work of G. Lindström, Arkiv Fysik **4**, 1 (1951). Calibration for higher energy lines from Cs^{137} K line taken as $H_\rho=3381.3$ from the work of Lindström, Siegbahn, and Wapstra, Proc. Phys. Soc. (London) **B66**, 54 (1953). The SD measurement of absolute energy of $K_{\alpha 1}$ is used, but the energy differences to other high energy lines is taken from BD work (see reference 6).
[b] Hill, Church, and Mihelich, Rev. Sci. Instr. **23**, 523 (1952).
[c] See reference 3.
[d] See reference 5.
[e] The recent measurements of J. M. Hollander and W. G. Smith (private communication) give a best energy for this transition of 44.11 ±0.04 kev based on their work with a permanent magnet spectrograph.
[f] Berkeley measurements give the $M_{II}:M_{III}:N, O$ ratio as 1.85:1.35:1 (see reference 7).

trometer the relative intensities of these lines, using both Np^{238} and Cm^{242} samples. A very thin counter window was used and no transmission correction was made.

Dunlavey and Seaborg[18] and Dunlavey[19] have determined $L:(M+N+O)$ ratios with Cm^{242} samples by track counting in electron-sensitive photographic emulsions, and their results are presented in Table II also.

The $E2$ nature of the 44.0- and 102.2-kev transitions is clearly confirmed by comparison of the L subshell conversion results with the theoretical calculations of Gellman *et al.*[17]

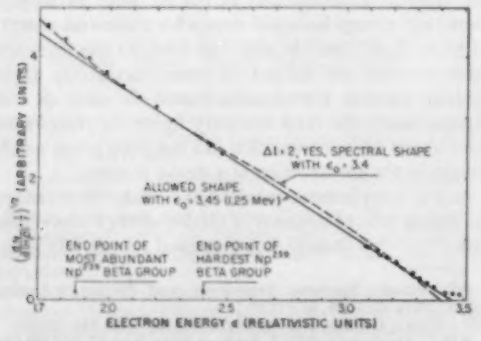
ΔI = 2, YES, SPECTRAL SHAPE WITH ϵ_0 = 3.4
ALLOWED SHAPE WITH ϵ_0 = 3.45 (0.25 Mev)
END POINT OF MOST ABUNDANT Np^{239} BETA GROUP
END POINT OF HARDEST Np^{239} BETA GROUP
ELECTRON ENERGY ε (RELATIVISTIC UNITS)
(ARBITRARY UNITS)

FIG. 3. Fermi-Kurie plot of the hard beta spectrum of Np^{238}. (Stockholm long-lens intermediate-image spectrometer.)

The hard beta spectrum was taken repeatedly in the intermediate image spectrometer in an effort to determine precisely the shape. The intermediate image spectrometer was felt to be especially suitable for spectrum shape studies, as it has a very low scattered electron background. The log ft values of the hard beta particles are in good agreement with a first forbidden $\Delta I=2$, yes, assignment, although Freedman *et al.*[3] reported an allowed spectrum shape. The reinvestigation was in part prompted by the availability of accurate tables[20] for determination of spectrum shape correction factors. These tables show that the correction factor for the $\Delta I=2$, yes spectrum shape for high atomic numbers is considerably less pronounced than the $Z=0$ approximation correction sometimes used. In the conventional Fermi-Kuri plot of Fig. 3 (where the Fermi function was obtained from the National Bureau of Standards tables)[21] are shown a straight solid line and a dashed $\Delta I=2$, yes, line calculated from the tables of Rose *et al.*[20]

[20] Rose, Perry, and Dismuke, Oak Ridge National Laboratory Report ORNL-1459, 1953 (unpublished).
[21] *Tables for the Analysis of Beta Spectra*, National Bureau of Standards Applied Mathematics Series 13 (U. S. Government Printing Office, Washington, D. C., 1952).

TABLE II. Intensities of conversion lines of the 44-kev transition.

Ratio	Freedman *et al.*[a] Np^{238}	Slätis *et al.*[b] Np^{238}	Passell[c] Cm^{242}	Berkeley double-focusing[a] Np^{238}	Dunlavey, Seaborg[d] Cm^{242}	Dunlavey re-determination by same method[e] Cm^{242}	Gellman *et al.*[f] (*E2* theoretical)
$L_{II}:L_{III}$	1.91	1.37	1.44	1.26	...	...	~1.2
$(L_{II}+L_{III}):(M+N+O)$	3.26	3.27	3.42	3.33	4.8	2.93±0.64	...

[a] See reference 3.
[b] See reference 5.
[c] See reference 7.
[d] See reference 18.
[e] See reference 19.
[f] See reference 17.

The endpoint energies were chosen to give qualitative best fits to the experimental points in each case. Parts of the spectrum are obscured by soft beta rays or by high-energy conversion lines. We are inclined to give most weight to the fit near the end of the spectrum. There the slopes of allowed and forbidden spectra are quite different, with the data agreeing much better with the allowed line. Very pertinent to the shape study is the question of possible complexity of the hard beta spectrum. If there were admixture of two groups with endpoints differing by only 44 kev, it would hardly be possible to determine their abundances by resolution of a Fermi-Kurie plot. Our belief that the hard beta spectrum consists of essentially a single group going to the 44-kev first-excited state is based on *L* x-ray—beta coincidence work reported in paper II.[16] (The contrary result previously reported[6] was shown to be in error by later experiments using the same apparatus.) The fit for the lower energy points of Fig. 3 seems better for the forbidden shape, but this may be due to an incomplete subtraction of the Np^{239} spectrum, endpoints of which are indicated by arrows in Fig. 3.

Thus, we support the conclusion of Freedman *et al.*[3] that the hard beta group has allowed shape, and we find an energy 1.25 Mev compared with their 1.272 Mev.

Figure 4 shows a Fermi-Kurie plot of the soft beta continuum from SS data after subtraction of hard beta and Np^{239} beta contributions. Parts of the spectrum are obscured by conversion lines. The Fermi-Kurie plot has a definite curvature, indicating the probable presence of more than one soft beta group, but it is not felt that the data are of sufficient accuracy to justify any resolution of the plot. The endpoint of the most energetic soft beta group seems to be about 0.27 Mev, in satisfactory agreement with the 0.258 Mev of Freedman *et al.*[3]

The intensity ratio between soft beta rays and hard beta groups was found to be 55:45 in this investigation. This ratio is in good agreement with the ratio 53:47 of Freedman *et al.*[3]

SPECTROSCOPIC MEASUREMENT OF URANIUM RADIATOR PHOTOELECTRONS

In order to study the relative intensities of the high-energy gamma rays (unresolvable by scintillation spectrometer), the spectrum of electrons ejected from a 0.0005-inch thick uranium metal radiator was studied in the Berkeley thick-lens solenoidal beta spectrometer.[16]

The sample of Np^{233} was enclosed in a cylindrical aluminum shield of sufficient thickness to absorb the beta radiation of Np^{233}, and on the plane face of the shield in the normal position for the spectrometer source was attached a disk of uranium metal 0.0005-inch thick and 0.5-inch in diameter.

Figure 5 shows one of the several series of measurements. The two prominent peaks are due to photoejection of *K* electrons by the 1029- and 986-kev gamma rays of Np^{233}. Centers of the peaks lie about 10 kev lower in energy than calculated, but this is accounted for by the thickness of the uranium radiators. Diffuse peaks due to *L* shell conversion are seen at higher energies. At energies just below the K_{986} peak the electrons due to Compton scattering events sharply rise. The Compton electrons unfortunately obscure the region of great interest where the *K* photopeaks of the weaker 941- and 925-kev gamma rays are expected. One can only say that these gamma rays are in somewhat lower intensity than the higher energy gamma rays.

The dotted lines of Fig. 5 indicate how the main peaks were resolved for determination of their relative intensities. The areas of the peaks are in the ratio $K_{1029}:K_{986} = 1:0.90$. For these energies the photoelectric absorption cross section varies nearly inversely as the square of the gamma energy.[22] Making such a correction, we obtain the gamma intensity ratio $\gamma_{1029}/\gamma_{986} = 1/0.83$. An

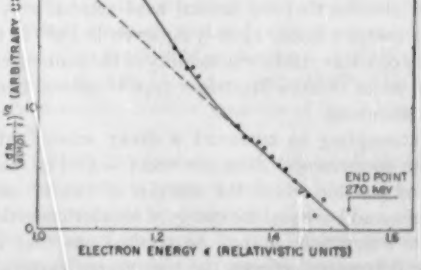

FIG. 4. Fermi-Kurie plot of the soft beta spectrum of Np^{233}. (Stockholm long-lens intermediate-image spectrometer.) Contributions from the hard beta group and from the beta spectrum of Np^{239} contamination have been subtracted out.

[22] C. M. Davisson and R. D. Evans, Revs. Modern Phys. **24**, 79 (1952).

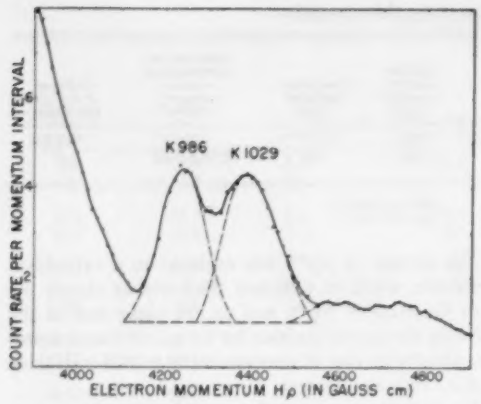

FIG. 5. Spectrum of electrons ejected from a thin uranium metal radiator by the gamma radiation of Np^{239}. (Berkeley thick-lens beta spectrometer.) Dotted lines show how the K photolines for the two most intense gamma rays were resolved for the purpose of the relative intensity determination.

effect which is difficult in our case to estimate quantitatively arises from the change in angular distribution of photoelectrons with energy.[22] The angle of the accepted electron trajectories in the solenoidal beta spectrometer with respect to the axis is between 20° and 24°, so qualitatively the effect should give higher effective transmission for the K_{1029} as compared with the K_{986} electrons. The effect should not be large with our geometries and is therefore neglected. Our ratio is to be compared with that of 1.02:1 determined by Freedman *et al.*[3]

It might be possible to observe photopeaks from the weaker gamma rays if a radiator of lower atomic number than uranium were used (increasing the energy difference between the K photoelectron energy and the Compton electron maximum), but this experiment has not been done by us.

DISCUSSION

It is obvious that the several hard gamma rays of similar energies signify close-lying levels in Pu^{239} in the vicinity of 1 Mev, and the possibility of their interpretation in terms of Bohr-Mottelson type rotational bands seems promising.

In attempting to construct a decay scheme from electron spectroscopic data, one seeks to find as many cases as possible where the energies of two or more transitions add to equal the energy of another transition. In this connection, it may be pointed out that the energy differences between the high-energy gamma K conversion lines are known much better than their absolute energies.[23] The possible sums are listed below.

$$E_{\text{hard beta}}-E_{\text{soft beta}}\approx 980 \text{ kev}; \quad E_{\gamma 986}=986 \text{ kev}; \quad (1)$$

$$E_{\gamma 1029}-E_{\gamma 986}=43._2 \text{ kev}; \quad E_{\gamma 44}=44.0 \text{ kev}; \quad (2)$$

$$E_{\gamma 986}-E_{\gamma 942}=44._8 \text{ kev}; \quad E_{\gamma 44}=44.0 \text{ kev}; \quad (3)$$

$$E_{\gamma 1029}-E_{\gamma 927}=102._3 \text{ kev}; \quad E_{\gamma 102}=102.2 \text{ kev}. \quad (4)$$

It is difficult to decide which of the gamma sums are true and which are coincidental. From the above beta spectroscopic information a simple level scheme with levels at 986 and 1073 kev was proposed,[6] accounting for all four energetic gamma rays through transitions to the known levels of 0, 44, and 146 kev. Scintillation counter coincidence studies (reported in paper II) later showed the proposed scheme to be incorrect in some respects. Hence, the decay scheme proposals and accompanying interpretation will be left to paper II.

It is of some interest to compare our values for the energies of the states of the ground rotational band with the predictions of the Bohr-Mottelson theory.[24] To a first approximation the energies should be given by $E=(\hbar^2/2\Im)I(I+1)$ with only even I values above a spin-zero base state. If one uses the first excited state energy, 44.11 kev, as determined by Hollander and Smith (private communication), the rotational quantum energy is 7.35 kev and by the simple formula the second excited state should lie at 147.0 kev. From our energy data it actually lies at 146.3 kev. The theory predicts such a deviation, and a "vibration rotation interaction" correction term of the form constant $\times I^2(I+1)^2$ subtracts from the simple energy formula. In samples of Cm^{242} the gamma transition between the 6+ and 4+ rotational states of Pu^{238} has been observed[25] and its energy measured by scintillation spectroscopy as 157±2 kev. Thus, we may check the theoretical correction term by calculating the constant using the energies of the 2+ and 4+ levels and independently using energies of the 2+ and 6+ levels. In the former case we calculate for the constant 0.0026±0.001 and in the latter, 0.0036 ±0.0015 kev. More accurate measurements of all the low-energy transition energies would be of great interest.[26]

The L-subshell conversion coefficients clearly confirm the $E2$ character of the 44- and 102-kev transitions.

The resolution of M-subshell conversion lines of the 44.0-kev transition permits some comparison with the theoretical calculations of Church and Monahan.[27] Church's threshold conversion coefficients (nonrelativistic) indicate that M shell conversion with an $E2$ transition occurs predominantly with the p electrons (M_{II},M_{III}). Such is the experimental observation here. It is interesting to note that the M_{II}:M_{III} ratio 1.37:1

[23] For a more detailed discussion on the determination of these energy differences see Rasmussen, Passell, and Stephens (reference 6).

[24] A. Bohr and B. R. Mottelson, Kgl. Danske Videnskab. Selskab, Mat.-Fys. Medd. **26**, 14 (1952), see p. 33.

[25] Asaro, Thompson, and Perlman, Phys. Rev. **92**, 694 (1953).

[26] *Note added in proof.*—Hollander and Smith have recently measured, with their permanent magnet electron spectrographs, the energies of 4+ to 2+ and 6+ to 4+ transitions in Pu^{239} as 101.9±0.3 kev and 157.7±0.5 kev, respectively. With these energies there is no discrepancy with the theoretical formula including the interaction term.

[27] E. L. Church and J. E. Monahan, Phys. Rev. **94**, 762 (1954).

is exactly equal to the $L_{II}:L_{III}$ ratio obtained by Slätis *et al.*[5]

ACKNOWLEDGMENTS

We wish to acknowledge the help of a number of persons in these investigations: Dr. Hugo Atterling and Fil. Kand, Mrs. Muusa Punnis in Stockholm and Peter Gray and Donald Strominger in Berkeley.

One of us (J.O.R.) wishes to acknowledge a fellowship from the Nobel Institute of Physics during part of this investigation.

PHYSICAL REVIEW VOLUME 99, NUMBER 1 JULY 1, 1955

Beta Emitter Np^{238}. II. Scintillation Spectroscopy and Coincidence Studies*

JOHN O. RASMUSSEN, FRANK S. STEPHENS, JR., DONALD STROMINGER, *Department of Chemistry and Radiation Laboratory, University of California, Berkeley, California*

AND

BJÖRN ÅSTRÖM, *The Nobel Institute of Physics, Stockholm, Sweden*

(Received March 25, 1955)

The relative intensities of electromagnetic radiation from Np^{238}, determined by scintillation spectroscopy, set an upper limit for K capture of $K/\text{beta} < 1$ percent.

On the basis of extensive scintillation counter coincidence measurements together with the beta spectroscopic results of the preceding article, two alternate decay schemes, differing only in minor detail, are proposed for Np^{238}. The levels of Pu^{238} involved are three close-lying ground rotational band members and a cluster of three levels near 1 Mev, two of which appear to belong to the same rotational band. Conversion coefficient determinations permit multipolarity assignment for a number of the gamma transitions and consequent spin and parity assignments for a number of excited states. Selection rules and other intensity rules involving the Bohr-Mottelson K-quantum numbers are tested, providing K-assignments for levels. There is a high degree of K-purity of those states where tests were possible. The question of possible "vibrational" character of the band near 1 Mev is discussed speculatively.

INTRODUCTION

SUPPLEMENTING the beta spectroscopic studies of Np^{238}, as reported in the preceding paper[1] (referred to here as paper I), we have carried out scintillation spectroscopic studies of the electromagnetic radiation and have also performed various coincidence studies with scintillation counting equipment. The coincidence results are of key importance in the establishment of a probable decay scheme.

SCINTILLATION SPECTROSCOPY AND THE QUESTION OF *K*-CAPTURE

The Np^{238} sample was prepared by thermal-neutron bombardment of Np^{237} in the homogeneous reactor at the University of California Radiation Laboratory, Livermore, California. The integrated neutron flux during the irradiation was sufficiently small that no significant amount of Np^{239} was formed. Chemical purification involving lanthanum fluoride precipitation followed by two TTA (thenoyltrifluoroacetone) solvent extraction steps similar to the procedures described by Magnusson, Thompson, and Seaborg[2] was made to purify the neptunium fraction from fission products and other impurities.

The 50-channel pulse-height[3] analyzer was used to study the gamma spectrum of Np^{238} from a sodium iodide scintillation crystal. This spectrum shows an unresolved photopeak near 1 Mev made up of 4 high-energy gamma rays,[1] a photopeak near 100 kev made up of 102-kev gamma and K x-rays, and a low-energy x-ray peak of about 20 kev. Scintillation spectroscopy in Stockholm showed the same peaks and no others.

The apparent resolution (ratio of energy width at half-height to photopeak energy expressed in percent) of this 1-Mev photopeak was 10.6 percent compared with 7.3 percent for the 0.84-Mev photopeak of Mn^{54} and 7.5 percent for the 1.06-Mev photopeak of Bi^{207}. This result clearly shows the composite nature of the 1-Mev peak in Np^{238}.

The 1-Mev photopeak decayed with a half-life of 2.04 days, in excellent agreement with the 2.10-day half-life previously reported by Freedman *et al.*[4]

The decay of the peak in the 100-kev region was complex. This complexity can be explained by the presence of a considerable quantity of Np^{237} and the growth of its alpha decay daughter, Pa^{233}, into the

* Much of this work was performed under the auspices of the U. S. Atomic Energy Commission.

[1] Rasmussen, Slätis, and Passell, preceding paper [Phys. Rev. 99, 42 (1955)].

[2] Magnusson, Thompson, and Seaborg, Phys. Rev. 78, 363 (1950).

[3] A. Ghiorso and A. E. Larsh, Jr., University of California Radiation Laboratory Report UCRL-2647, 1954 (unpublished).

[4] Freedman, Jaffey, and Wagner, Phys. Rev. 79, 410 (1950).

sample. The decay of the 100-kev peak was followed for 4 months, at the end of which time it was possible to calculate the component contributions due to Np^{235}, Np^{237}, and Pa^{233}.

Corrections were then made for the sodium iodide crystal efficiencies for the 1-Mev and the 100-kev photopeaks.[5] As a result, it was determined that the gamma and K x-radiation of the 100-kev region had a total intensity of 3.8 percent of the total number of unconverted gamma transitions in the 1-Mev region. Only 55 percent of the beta transitions populate the energy levels near 1 Mev in Pu^{238}.[1] Therefore, the observed intensity of the approximately 100-kev photons in the decay of Np^{239} is 2.1 percent of the total beta disintegrations. From beta spectroscopic results we can account for 0.5 percent as K x-rays from conversion of energetic gamma rays and 0.5 percent as 102-kev gamma rays (using a conversion coefficient[6] of 5). There is an excess of 1.1 percent photons not accounted for, and this figure constitutes an upper limit for possible K capture. It seems highly unlikely that the excess is in fact attributable to K capture, since the latest estimate of Glass *et al.*[7] of the available energy for electron capture (based on closed decay cycle energy balances) is 0.10 Mev, insufficient for K capture to occur at all. We attribute the excess 100-kev photons to fluorescence radiation from the Np^{237} mass in the sample.

Jaffe[8] has made a study of the L x-rays arising from the Np^{239} decay, using a Cauchois-type bent-crystal spectrometer of high resolution. His failure to find L x-rays of uranium allows him to set an upper limit of 4 percent for L_I capture and 2 percent for L_{II} capture relative to the beta transitions.

COINCIDENCE MEASUREMENTS

It is well to bear in mind what is known concerning the lowest-lying levels, as determined by studies[6] of the alpha emitter Cm^{242}. There are excited states at 44 and 146 kev with spin and parity assignments of 2+ and 4+, respectively. There are cascade $E2$ gamma transitions interconnecting these states. From the theoretical conversion coefficients of Gellman *et al.*,[9] the experimental conversion coefficients of Asaro *et al.*,[6] and the relative L:MNO conversion results discussed in paper I we estimate that the 44-kev transition is almost totally (99.9 percent) internally converted (77 percent by L_{II} and L_{III} conversion), and the 102-kev transition is approximately 83 percent converted (67 percent of the conversion electrons being from L_{II} and L_{III} orbitals). Thus, for the energetic gamma rays, those going to the ground state will be in coincidence with neither L x-rays nor 102-kev gamma rays. Of those going to the 44-kev state, about 38 percent will be in coincidence with L x-rays (assuming a fluorescence yield of 50 percent). Of those going to the 146-kev state, approximately 17 percent will be in coincidence with 102-kev gamma radiation, about 45 percent with one L x-ray, and about 11 percent with two L x-rays.

Most of the coincidence measurements were carried out with apparatus employing a sodium iodide (thallium activated) crystal and Dumont 6292 photomultiplier tube in each coincidence channel. A pulse in one channel of a height selectable by a single-channel differential discriminator generated a gate pulse which gated a 50-channel pulse-height analyzer[3] to analyze a simultaneous pulse in the other coincidence channel. The effective coincidence resolving time, $2\tau_0$, was about 7 microseconds for these experiments. The sample was placed directly between the two detectors, spaced such that the 1-inch cylindrical detector crystals each subtended about 30 percent of 4π solid angle. The detectors were shielded by lead.

The energetic gamma spectrum in coincidence with electromagnetic radiation approximately 100 kev in energy (including K x-rays and 102-kev nuclear gamma rays) was examined. In order to prevent beta particles from registering as gate counts the 100-kev radiation was observed through 691 mg/cm² of aluminum. In addition, 4 g/cm² of lead was used on the signal side of the coincidence unit, since this amount of absorber is not sufficient to cause serious attenuation of the hard gamma rays.

The curve of Fig. 1(a) shows the coincident gamma energy spectrum observed. This is to be compared with the ordinary total gamma ("singles") spectrum (solid

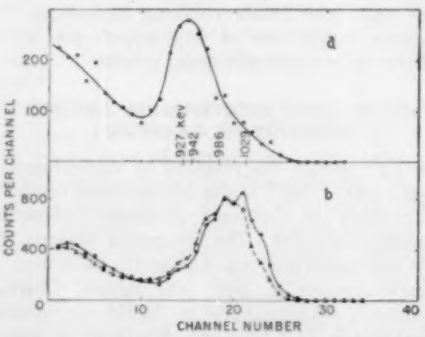

FIG. 1. Scintillation spectra (sodium iodide) of the composite 1-Mev gamma peak. Curve 1(a) is the spectrum in coincidence with ~100-kev electromagnetic radiation. Curve 1(b), dashed line, triangles, is the spectrum in coincidence with L x-radiation. Curve 1(b), solid line, circles, is the total gamma spectrum. The curves 1(b) are normalized at channel 19 (the position of the 986-kev gamma ray) to demonstrate best the differences between the curves. The marks on the baseline of 1(a) indicate the expected peak positions of the various component gamma rays, based on energy calibration with Bi^{207} and Mn^{54} standards.

[5] M. I. Kalkstein and J. M. Hollander, University of California Radiation Laboratory Report UCRL-2764, 1954 (unpublished).
[6] Asaro, Perlman, and Thompson, Phys. Rev. **92**, 694 (1953).
[7] Glass, Thompson, and Seaborg, J. Inorg. Nuc. Chem. **1**, 3 (1955).
[8] H. Jaffe, Ph.D. thesis, University of California Radiation Laboratory, Report UCRL-2537, 1954 (unpublished).
[9] Gellman, Griffith, and Stanley, Phys. Rev. **85**, 944 (1952).

line lower curve) taken at the same amplification. The shift of the peaks between the two curves is to be noted, the peak in coincidence with about 100-kev radiation lying at the low-energy side of the composite "singles" peak. We know from the beta spectroscopic results in paper I that the gamma "singles" peak consists of at least four different gamma rays of energies 1029, 986, 942, and 927 kev. From these coincidence results we conclude that γ_{942}, γ_{927}, or both, proceed to the 146-kev level. This result was reported earlier.[10] From the beta spectroscopic results we know that only the four high-energy gamma rays have enough energy for K conversion. Thus, there can be no interference in the above coincidence measurement from K x-ray-gamma coincidences.

The peak shift result for the radiation coincident with about 100-kev radiation was independently determined using another coincidence-pulse analysis apparatus with a resolving time $2\tau_0$ of about 6×10^{-8} second. With the shorter resolving time a more active sample could be used. The detection crystals were further from the sample and making a 90° angle with it. Two inches of lead shielding was placed between the crystals to minimize spurious coincidences arising from Compton scattering of gamma rays from one crystal to another. The counters were unshielded except for the one lead brick between them. Sufficient beryllium absorbers to stop completely all beta rays were used before each detector. Thus, we feel that these results, though concerning a rare coincidence process, are real and not spurious.

The energetic gamma spectrum in coincidence with L x-rays (about 18 kev) was studied with the first-mentioned coincidence equipment. In this case it was not possible to use aluminum to absorb the beta particles, as it would attenuate the L x-rays by too large a factor. Therefore 797 mg/cm² of beryllium was used on the gate side of the coincidence unit. The hard gamma rays were observed through 2.9 g/cm² of lead.

The dashed curve of Fig. 1(b) is the resulting coincidence spectrum and is plotted together with the ordinary "singles" gamma spectrum to show most clearly their differences. The curves are arbitrarily normalized to be equal at channel 19. One notes that the high-energy side of the broad "singles" peak is strongly depressed in the coincidence spectrum, a clear proof that the maximum energy gamma ray, γ_{1029}, proceeds to ground. (We shall later propose in the decay scheme section that γ_{1029} is actually two gamma rays within 2 kev of the same energy, the more intense of which goes to ground and the other to the 44-kev state. The curves of Fig. 1(b) are consistent with such an interpretation.) One also notes that the lower energy part of the "singles" peak is slightly enhanced in the L x-ray coincidence spectrum, a further confirmation of the earlier conclusion that γ_{927}, γ_{942}, or both proceed to the 146-kev state.

A determination was also made of the absolute L-gamma coincidence rate, which measurement is of great aid in establishing intensities of various radiations in the decay scheme. That is, the single-channel analyzer was set to accept pulses from the photopeak of the energetic gamma rays, and the total number of gates generated by the single-channel analyzer in a given counting time was recorded along with the integrated L x-ray coincidence peak recorded on the 50-channel analyzer. A similar measurement on alpha particle—L x-ray coincidences for Cm^{247} was made with the same geometries and absorption path (aluminum backing) for L x-rays. By comparing the results of the two measurements (knowing from alpha spectroscopy[8] that 26.3 percent of the alpha particles populate the 44-kev state and 73.7 percent, the ground state), it was possible to calculate the fraction of energetic gamma rays populating the ground state, the calculation being independent of such uncertain quantities as L fluorescence yield, L x-ray absorption loss, and detector geometry. For such a calculation we make use of the result from the beta spectroscopic work reported in paper I that the 146-kev state is populated in 3 percent of the beta disintegrations and that energetic gamma transitions occur in 55 percent of the disintegrations. Also, the conversion coefficients for the 102-kev gamma ray are used.

The result of the determination may be stated in the following two ways:

If there were no energetic gamma rays going to the 146-kev state, the result would indicate 37 percent (based on total beta disintegration) of the gamma rays going to the 44-kev state and 18 percent going to ground.

If we assume the 146-kev state is populated entirely by gamma and not by beta transitions, the proportion of high energy gamma rays going to the various states (percentage of total beta disintegrations) must be 3 percent to the 146-kev state, 32 percent to the 44-kev state, and 20 percent to ground.

A coincidence measurement similar to the preceding one was made between electrons and L x-rays, with the substitution of an anthracene crystal detector for the electrons. We wished to determine the fraction of hard beta disintegrations ($E_{max}=1.25$ Mev) which went to the various low-lying states. Electron energies including sections of the hard beta spectrum but avoiding conversion lines and the soft beta spectra ($E_{max}=0.27$ Mev) were selected by the single-channel analyzer serving as the coincidence gate generator. The ratio of L x-ray coincidence counts to gates was measured and again compared with the alpha—L x-ray results from a Cm^{242} standard in the same position. The result of such a measurement was reported[10] previously as indicating (assuming no hard beta decay to the 146-kev state) that 72 percent of the hard-beta transitions go to the 44-kev state, and 28 percent to ground. Later results showed

[10] Rasmussen, Passell, and Stephens, University of California Radiation Laboratory Unclassified Report UCRL-2585, 1954 (unpublished).

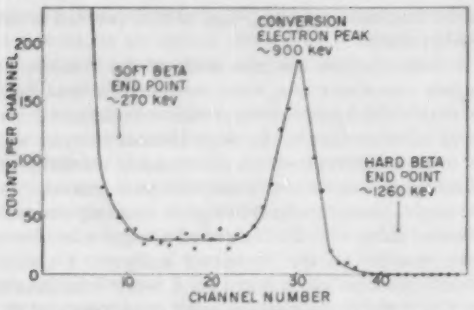

FIG. 2. Scintillation spectrum (anthracene) of electrons in coincidence with ~100-kev electromagnetic radiation.

the first report to be in error. The early measurement was made with only one sample, of relatively high activity, and there is apparently a loss in coincidence efficiency at higher counting rates in this apparatus. The later results showed a counting value of 100 percent of hard beta particles to the 44-kev state when sufficiently small samples were used. Beta-particle energies of 410 to 610 and 1020 to 1200 kev were used as gates and both intervals showed the above limit. (It should be mentioned regarding the loss effect that the L-gamma results of the preceding paragraph were checked with sources of strengths differing by a factor of four and found essentially constant.)

Engelkemeier was reported by Freedman, Jaffey, and Wagner[4] to have found coincidences between hard electrons and electromagnetic radiation of about 100-kev energy. The determination is an important one, as it bears on the question of whether a hard beta group populates the 146-kev state. Our gamma-gamma coincidence work showed that the 146-kev state is populated by energetic gamma rays, but to what fraction of its 3 percent total population was not determined. It is clear that there will be coincidences between K x-rays and energetic K conversion lines (0.5 percent of total disintegrations), but by examining the energy spectrum of electrons in coincidence with 100-kev radiation it was thought that it might be possible to find a hard beta continuum under the conversion lines. It is clear that the coincidence rate with a hard beta continuum will be about equal to the conversion line coincidence rate if all the 3 percent population of the 146-kev level were due to a hard beta group.

Figure 2 shows the results of such a measurement of the electron spectrum in coincidence with 100-kev radiation. The data are probably consistent with there being no hard beta continuum at all, but drawing in a curve for the maximum amount of hard beta continuum that could be present, one can set an upper limit that coincidences with a continuum must be less than 80 percent of coincidences with conversion electrons. The limit only tells us that the 146-kev level cannot be completely populated by the hard beta group. We shall arbitrarily assume for the later decay scheme proposals that the 146-kev level is populated entirely by energetic gamma rays and not by beta particles.

DECAY SCHEME PROPOSALS

In attempting to construct a decay scheme we start first with the ground rotational band known[5] from alpha decay fine structure studies in Cm^{242}. That is, there are levels in Pu^{238} at 0, 44.0, and 146.2 kev with spin and parity 0+, 2+, 4+, respectively. Connecting these levels are cascading $E2$ transitions, highly internally converted.

There are four high-energy gamma transitions of 927, 942, 986, and 1029 kev to account for. The L-gamma coincidence result that γ_{1029} goes to ground means there must be a level at 1029 kev. The 986-kev gamma transition is then accounted for as the transition between the 1029-kev level and the 44-kev level. The hard gamma-102-kev gamma coincidence result was that γ_{927}, γ_{942}, or both are in coincidence with 102-kev radiation, and the hard gamma-L x-ray coincidence studies (hard gamma peak shape comparisons) tend to support the conclusion that neither γ_{927} nor γ_{942} go to ground. Thus, regarding additional levels, we are left with three choices: (1) levels at 1073 and 1087 kev, (2) levels at 1073 and 986 kev, or (3) levels at 1087 and 971 kev. It is to be noted with the first two choices that there are two separate places in the decay scheme where a gamma transition of 1029 kev could occur, namely, from the 1029-kev level to ground and from the 1073-kev level to the first excited state. In order to reconcile the numerical L—gamma coincidence result that the hard gamma intensity to the ground state is 20 percent of total beta disintegrations, we can postulate that the 1029-kev gamma is indeed complex with energy difference of the two components too small for resolution even on the double-focusing beta spectrometers. Therefore, we prefer alternatives (1) and (2) for our further decay scheme discussions.

The attempt to assign intensities to all the transitions in the decay scheme is handicapped by incomplete information regarding intensities of the weaker hard gamma and soft beta transitions. Nevertheless, by using the absolute L-gamma coincidence result of 20 percent hard gamma to ground, the uranium photoconversion electron result of paper I that $\Gamma_{1029}:\Gamma_{986}=1:0.83$, and other intensities from the beta spectroscopic work (102-kev transition = 3 percent; hard beta : total soft beta = 45 : 55) and assuming intensities for γ_{927} and γ_{942} in the ratio of their K conversion lines, 1 : 2, we can calculate intensity figures for all transitions with decay scheme (1). It is obvious that the intensities of the weaker transitions as determined in this manner may be very uncertain where they are based on differences of relatively large numbers. Figure 3 shows the resulting decay scheme, where the uncertain intensities are given in parentheses. Below the intensities of the various beta groups are given their log$f t$ values, underlined.

Using the same intensity data but with the level scheme discussed as alternative (2), one obtains the decay scheme of Fig. 4. With the scheme of Fig. 4 it is possible that γ_{986} might also be complex, as there are two places in the scheme where it might occur. The purely arbitrary assumption of zero intensity for the transition from the 986-kev level to ground was made for Fig. 4.

While either decay scheme accounts for most of the data, it is appropriate to summarize the remaining inconsistencies.

First, according to the decay schemes the 44-kev transitions should occur in 80 percent of the total beta disintegrations, the percentage having been fixed by the absolute L x-ray-hard gamma coincidence rate measurement. In considerable disagreement is the figure of 65 percent from the beta spectroscopic measurements of Slätis, Rasmussen, and Atterling.[11] Even the figure of 75 percent from Freedman, Jaffey, and Wagner[4] is on the low side. Possible sources of error in the electron spectroscopic intensities could result as a consequence of the low energy of conversion lines, with uncertainty in counter window transmission corrections and resolution of peaks broadened by finite sample thickness. The ratios of intensities of conversion lines (L_{II},L_{III},M,N) determined by Slätis *et al.*[11] agree better than those of Freedman *et al.*[4] with independent determinations of Passell.[12] All these measurements are compared in Table I of the preceding paper I. The true intensity of gamma rays to ground is probably intermediate between the coincidence and the spectroscopic determinations, but in view of the disagreement between the different spectroscopic determinations we have chosen

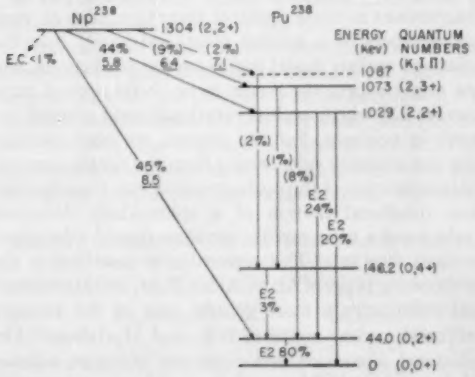

FIG. 3. Possible decay scheme (first of two alternative schemes) for Np^{238}. Radiation intensities are given as percentage of total beta disintegrations, and intensities enclosed in parentheses are indirectly determined and subject to considerable uncertainty. Below the beta group intensity figures are underlined numbers, the logft values.

[11] Slätis, Rasmussen, and Atterling, Phys. Rev. **93**, 646 (1954).
[12] T. O. Passell, Ph.D. thesis, University of California Radiation Laboratory Report UCRL-2528, 1954 (unpublished).

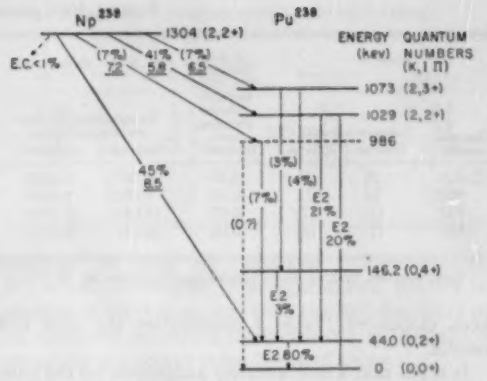

FIG. 4. Possible decay scheme (second of two alternative schemes) for Np^{238}. Radiation intensities are given as percentage of total beta disintegrations, and intensities enclosed in parentheses are indirectly determined and subject to considerable uncertainty. Below the beta group intensity figures are underlined numbers, the logft values.

to use the coincidence measurement as the basis for the decay scheme intensities.

Second, it is to be noted that the relative amounts of hard gamma and approximately 100 kev radiation as determined by scintillation pulse analysis do indicate an excess of approximately 100-kev radiation beyond that given by the proposed decay schemes. It is not reasonable on energetic grounds, as discussed earlier, to attribute this excess radiation to K capture. A related discrepancy involves an apparent excess over expectation of soft beta coincidences with approximately 100-kev radiation, as measured roughly by integration of the curve of Fig. 2. The measurement is not very quantitative, since scattering and absorption effects on the electrons in this coincidence experiment introduce uncertainties that would be hard to estimate.

Finally, regarding further work which might be profitable, we would suggest that beta spectroscopic work at even higher resolution might be fruitful, especially in the region of the high-energy conversion lines. Coincidence experiments with two beta spectrometers would be desirable. Experiments to determine the relative intensities of the weaker hard gamma rays are important. Such might lie within the range of Cauchois-type bent-crystal spectrometers, or one might study by beta spectroscopy the K photoelectrons from radiators of considerably lower atomic number than uranium. A uranium radiator was used in the experiments reported in paper I, and the K photopeaks of the weaker gamma rays lie obscured by Compton electrons of the intense gamma rays.

HARD GAMMA CONVERSION COEFFICIENTS

Using the gamma intensities from the decay schemes and the K electron line intensities from paper I, the K conversion coefficients of the hard gamma rays have

TABLE I. Hard gamma conversion coefficients.

Gamma energy	Gamma intensity (%) Scheme 1	Scheme 2	K line intensity (%) (from Berkeley double-focusing spectrometer)	Experimental K conversion coefficient Scheme 1	Scheme 2	Theoretical K conversion coefficients (interpolated from Rose *et al.*[a]) $E1$	$E2$	$M1$	$M2$	Experimental $K:L$ ratio (from Berkeley double-focusing spectrometer)	Multipolarity assignment
Σ1029	28	24	0.20	0.0071	0.0083	0.0033	0.0102	0.075	0.105	~5	$E2$
986	24	21	0.20	0.0083	0.0095	0.0035	0.0108	0.083	0.117	~3.3	$E2$
942	(2)	(7)	0.07	(0.035)	(0.010)	0.0038	0.0119	0.094	0.132	...	...
927	(1)	(3)	0.04	(0.04)	(0.013)	0.0039	0.0122	0.098	0.136	...	...

[a] Rose, Goertzel, Spinrad, Harr, and Strong, Phys. Rev. **83**, 79 (1951).

been calculated. Table I summarizes the data and results.

It is felt that a multipolarity assignment on the basis of K conversion coefficients for the two most intense hard gamma rays is justified. Despite the probable unresolved doublet nature of γ_{1029} and the consequent average meaning of its conversion coefficient, the major branch of the doublet is probably of $E2$ character, necessarily pure $E2$ since the final state has spin zero. Thus, the level at 1030 kev must have spin 2 and even parity, as the ground state is presumably 0+. The fact that the experimental conversion coefficient is smaller than the theoretical unscreened value may in part be due to experimental uncertainty and in part due to neglect of screening in the theoretical calculations. With regard to the latter point, some of the recent screened K conversion coefficients calculated by Rose and others[13] seem roughly 10 percent lower than the unscreened for $E2$ transitions of comparable energy in large-Z elements.

Within experimental uncertainty the conversion coefficient of γ_{986} indicates $E2$, although an admixture of a few percent $M1$ character could not be excluded by our data.

The uncertainties associated with the gamma radiation intensities of the weaker hard gamma rays make definite multipolarity assignments out of the question, but their orders of magnitude indicate $E2$ or mixed $E2-M1$ character as most likely. (It is apparent that with all the gamma rays the conversion coefficients might be explained by $E1-M2$ mixtures, but this explanation is not given serious consideration in view of the general rarity of that particular admixture, and the K/L ratios give experimental evidence against the $E1-M2$ interpretation.)

It is of some interest to compare the K/L conversion ratios with the earlier correlation of Goldhaber and Sunyar.[14] For gamma rays about 1 Mev and $Z=94$ their plots against Z^2/E would give a K/L ratio of about 6 for $E2$ and about 8 for $M1$ or $M2$. The lower experimental K/L ratios in the case of our $E2$ gamma rays of 1029 and 986 kev are further examples of systematic deviations to the low side for high-Z elements. Goldhaber and Sunyar[14] called attention to some such deviations, and the work of Alburger and Pryce[15] on Bi^{206} decay provides a good example of this sort of deviation. Their $E2$ gamma transitions of 880.5 and 803.3 kev have $K/(L_I+L_{II})$ ratios of about 4.7. Our K/L ratios from Table I are consistent with the $E2$ assignment in view of the considerable uncertainty in our L line intensities. From the L subshell conversion calculations of Gellman *et al.*[9] inclusion of the L_{III} conversion in K/L ratios would have virtually no effect for $M1$ transitions and less than 30 percent effect for $E2$. Thus, we are justified in comparing our K/L ratios with $K/(L_I+L_{II})$ ratios.

CONSIDERATIONS INVOLVING THE K QUANTUM NUMBERS

Two interesting observations may be made with regard to the gamma transitions occuring from the 1030-kev level. First, the rather pure $E2$ character of γ_{986}, though $M1$ is allowed, seems unusual according to lifetime estimates from the single particle lifetime formulas. Second, the absence (see paper I) of an $E2$ transition of 884-kev energy proceeding to the 4+ state at 146.2 kev seems unusual. It is concerning just such observations as these (relative transition rates to various members of a nuclear rotational band) that the deformed nuclear model makes precise predictions, and one might expect the model to be useful around mass number 238 where nuclear rotational band systems are much in evidence. For the present, we need consider only the intensity rules arising from the simple approximate separation of the nuclear motion into the relatively slow rotational motion of a spheroidally deformed nucleus and a more rapid internal motion of a deformed intrinsic structure. This separation is described in the forthcoming paper of Alaga, Alder, Bohr, and Mottelson[16] and constitutes a more general case of the strongly deformed nuclear model of Bohr and Mottelson.[17] The rotational separation introduces one quantum number in addition to I, the total angular momentum, and Π, the parity. The new quantum number is K, the projection

[13] M. E. Rose, privately circulated tables, 1954 (unpublished).
[14] M. Goldhaber and A. W. Sunyar, Phys. Rev. **83**, 906 (1951).
[15] D. E. Alburger and M. H. L. Pryce, Phys. Rev. **95**, 1482 (1954), see Fig. 10.
[16] Alaga, Alder, Bohr, and Mottelson, CERN/T/A-A-B-M-1, August 1954 [Kgl. Danske Videnskab. Selskab, Mat.-fys. Medd. (to be published)].
[17] A. Bohr and B. R. Mottelson, Kgl. Danske Videnskab. Selskab. Mat.-fys. Medd. **27**, 16 (1953).

of the total angular momentum along the nuclear symmetry axis, and the K-purity of nuclear states will depend upon how valid is the approximate separation of rotational and intrinsic structural motion. K remains the same for all members of the same rotational band and is equal to the spin of the base level of the rotational band except for an anomalous case when $K=\frac{1}{2}$. Thus, K is zero for the members of the ground rotational band as indicated in Figs. 3 and 4.

The relative rates of the electric quadrupole transitions from the 1030-kev level to the states of the ground rotational band give us a means of evaluating K for the 1030-kev level. After dividing out the fifth-power energy dependence we may obtain the ratios of reduced transition probabilities. By the theory these ratios should be simply given by vector projection factors, the squares of Clebsch-Gordan coefficients involving the K and I quantum numbers and the multipolarity L of the transition. This relation, as given by Eq. (12) of Alaga *et al.*,[16] is shown below:

$$\frac{B(L, I_i \to I_f)}{B(L, I_i \to I_f')} = \frac{\langle I_i L K_i K_f - K_i | I_i L I_f K_f \rangle^2}{\langle I_i L K_i K_f - K_i | I_i L I_f' K_f \rangle^2},$$

where the Clebsch-Gordan coefficients are in the notation of Condon and Shortley.[18] Clebsch-Gordan coefficients have been tabulated numerically by Simon.[19] Table II presents the experimental and theoretical ($K_i=0$, 1 or 2) relative reduced transition probabilities for the gamma rays from the 1030-kev level.

The assignment $K=2$ is clearly indicated for the 1030-kev level. With this assignment the absence of $M1$ character in γ_{986} finds a natural explanation. The Clebsch-Gordan coefficient vanishes when ΔK exceeds the multipolarity L, hence, dipole radiation is K-forbidden [see Alaga *et al.*,[16] Eq. (6a)].

The spacing of 44 kev between the 1029- and 1073-kev levels and the gamma radiation from the 1073-kev level suggest to us that the 1073-kev level be assigned $(2, 3+)$ as the first excited member of a rotational band based on the 1029 level. The rotational moment of inertia for this upper band is the same as that of the ground-state band within the accuracy of our measurements. The theory predicts (for pure $E2$ radiation) $B(I_i=3\to I_f=4)/B(I_i=3\to I_f=2)=0.40$. The experimental relative intensities of the gamma rays from the 1073-kev state are too uncertain to make a significant test of the reduced transition probability rules discussed above.

TABLE II. Experimental and theoretical relative reduced $E2$ transition probabilities from the 1030-kev level $(2+)$.

Final state I_f	Experimental $\frac{B(2\to I_f)}{B(2\to 0)}$ Scheme 1	Experimental $\frac{B(2\to I_f)}{B(2\to 0)}$ Scheme 2	Theoretical $\frac{B(2\to I_f)}{B(2\to 0)}$ $K_i=0$	$K_i=1$	$K_i=2$
2+ (44 kev)	1.5	1.3	1.43	0.375	1.43
4+ (146 kev)	<0.3	<0.3	2.57	1.14	0.0714

TABLE III. Beta-group energies and logft values.

Beta energy (kev)	K, spin and parity of final state	Logft Scheme 1	Logft Scheme 2
1260	0, 2+	8.5	8.5
275	2, 2+	5.8	5.8
231	(2, 3+)	(6.4)	(6.5)
217	?	(7.1)	...
or 318	?	...	(7.2)

INTERPRETATION OF BETA TRANSITIONS

The logft values of the various beta groups, as calculated using the nomograms of Moszkowski[20] are given on the decay schemes Figs. 3 and 4 as underlined numbers. They are summarized in Table III.

Freedman *et al.*[4] found an allowed spectral shape for the hard beta particle. This result was confirmed in the beta spectroscopic studies of paper I. Parts of the spectrum are obscured by soft beta groups and by conversion lines, but the assumption of allowed shape gives a satisfactory fit, whereas the assumption of the unique alpha shape ($\Delta I=2$, yes) does not. Thus, a $\Delta I=2$, yes, interpretation of the hard beta group seems ruled out.

It is somewhat surprising that the 1260- and 275-kev beta groups, which proceed to levels of the same spin and parity, should exhibit ft values different by a factor of 500. Since the relative gamma transition rates suggested that K is a fairly good quantum number, we might logically look first to the difference in K values of the final states at 44 and 1029 kev for an explanation of the great difference in logft values.

The simplest interpretation in terms of K selection rules follows from an assignment of K, I, and II of $(2, 2+)$ for Np^{238}. The transitions to ground and 146-kev state are not observed, as they are second forbidden ($\Delta I=2$, no). Though the good selection rules in I and II make the transition to the 44-kev state allowed ($\Delta I=0$, no), the selection rule[16] in the approximate quantum number K makes the transition second forbidden ($\Delta K=2$, no), and if K for the initial and final states were an absolutely good quantum number the beta transition would not be seen (log$ft\gtrsim 12$). There are evidently small admixtures of states with K values other than the principal ones in the initial state, final state or both, and for some combinations of these K impurities the change in K will be 0, or 1, permitting the transition to proceed as an allowed transition. The allowed spectrum shape of the hard beta group is a natural consequence of this interpretation.

[18] E. U. Condon and G. H. Shortley, *Theory of Atomic Spectra* (Cambridge University Press, London, 1935).

[19] Albert Simon, Oak Ridge Laboratory Report ORNL-1718, special, 1954 (unpublished).

[20] S. A. Moszkowski, Phys. Rev. **82**, 35 (1951).

With the Np^{238} (2, 2+) assignment the beta groups to the 1030- and 1073-kev levels, which are (2, 2+) and (2, 3+), respectively, should be allowed transitions by ΔK as well as ordinary selection rules. Their log ft values are a little high (5.8 and 6.5, respectively), the log ft correlations of Nordheim[21] showing all allowed transitions (21 cases) in the log ft range 4.1 to 5.7. There are, of course, cases where other factors in the nuclear rearrangement accompanying beta decay act to make allowed transitions much slower than ordinary. Such a case is our hard beta group, and de-Shalit and Goldhaber[22] have cited and discussed a number of other cases. Thus, the interpretation of our two main soft beta groups as somewhat slow allowed transitions seems not unreasonable.

The assignment of (2, 2+) for Np^{238} cannot be claimed to be unique. One might make an assignment of (2, 2−) but would then need to attribute the nonobservance of transitions to the ground state and second excited state to some unknown hindering factor. The log ft values of the 275- and 231-kev beta groups seem a little low (King and Peaslee[23] find average log ft values of 6.5 for $\Delta I = 0$, yes, and 7.5 for $\Delta I = 1$, yes transitions) for the first forbidden nature they would have in this alternate interpretation. One cannot rule out possible assignments of (3, 3±) to Np^{238}, although with such there would be some difficulty in explaining why beta transitions strongly favor the first excited state (2+) over the second excited state (4+).

An assignment of even parity to Np^{238} violates the shell-model rule that the ground states of odd-odd nuclei in this region should have odd parity, the rule following from the fact that mainly odd-parity orbitals are available for protons in the 82–126 shell and even-parity orbitals for neutrons in the shell above 126. We feel, however, that the shell-model parity rule is hardly to be trusted in the region of the heaviest elements where numerous low-energy $E1$ transitions to ground in odd-A nuclei indicate the ready availability of orbitals of both parities for odd nucleons.

CONCERNING THE POSSIBLE VIBRATIONAL NATURE OF SOME EXCITED LEVELS OF Pu^{238}

Inasmuch as the intensity rules involving K seem useful in the case of Np^{238} decay, the question is bound to be raised whether any of the high levels in Pu^{238} are "vibrational levels," as predicted by the more detailed unified model of Bohr and Mottelson.[17] The question is a difficult one to answer with the data available at present, and what follows is written in a speculative vein.

The theory predicts for spheroidal nuclei two vibrational bands, each having one quantum of vibrational excitation. The so-called beta vibrational band will have rotational band members (0, 0+), (0, 2+), (0, 4+), ···. The gamma vibrational band will have members (2, 2+), (2, 3+), (2, 4+), ···. The vibrational quantum energy may be of the order of 1 Mev for the heaviest elements. Thus, the levels in Pu^{238} of 1029 and 1073 kev with (2, 2+) and (2, 3+) assignments, respectively, might possibly be of the first gamma vibrational band, although they can equally well be purely "particle excitation" levels.

The most definitive evidence for the vibrational character of the band would be lifetime measurements of the levels. If lifetimes were found to be substantially shorter than predicted by the individual-particle lifetime formulas, this would constitute strong evidence for some vibrational character for the levels. Such measurements by ordinary electronic means seem impossible, as the expected lifetimes are so short. Following are the theoretical calculated mean lifetimes for $E2$ transitions from the (2, 3+) state at 1073 kev: single proton transition to (0, 2+) state at 44 kev, $\tau_{sp} \sim 5 \times 10^{-12}$ sec.; single phonon (vibrational transition) to 44-kev state, $\tau_{vib} \sim 3 \times 10^{-14}$ sec.; rotational transition to (2, 2+) state at 1029 kev (taking internal conversion into account), $\tau_{rotational} \sim 5 \times 10^{-11}$ sec. (Lifetime formulas of Bohr and Mottelson[17] were used.) It seems surprising that despite the great energy difference the 44-kev rotational transition could compete to the extent of about 10 percent with the 1029-kev single particle transition. From our data the presence of such competition could not quite have been determined, and we are unable to obtain any lifetime evidence in this manner.

Alaga *et al.*[16] in their discussion of the beta decay scheme of Ta^{182} cite as possible evidence for the gamma vibrational character of a band at 1222 kev the fact that the rotational moment of inertia for the band is slightly smaller (∼10 percent) than that for the ground rotational band, whereas a particle-excitation level generally has a greater rotational moment of inertia. In the case of Pu^{238}, the rotational moment of inertia of the upper band is about the same as that of the ground band and constitutes no clear evidence for or against the vibrational assignment.

The log ft values for beta decay to the 1029-kev band in Pu^{238} give further evidence bearing on the question of vibrational character. If the band were purely a gamma vibrational band with the individual nucleons remaining in paired configurations, a selection rule in the Ω quantum number[24] makes the principal soft beta transitions from (2, 2+) Np^{238} second forbidden ($\Delta\Omega = 2$, no). The observed ft values indicate the beta transitions are only about a factor of 10 slower than average for allowed transitions. Clearly the Pu^{238} band in question cannot be of very pure vibrational character, if, indeed, it has vibrational character at all. One might speculate that for some levels the separation of the intrinsic structure of the deformed nucleus into vibrational and individual particle motion is just partially valid and

[21] L. W. Nordheim, Revs. Modern Phys. **23**, 322 (1951).
[22] A. de-Shalit and M. Goldhaber, Phys. Rev. **92**, 1211 (1953).
[23] R. W. King and D. C. Peaslee, Phys. Rev. **94**, 1284 (1954).

[24] Ω is the component of total individual-particle angular momentum along the nuclear symmetry axis.

could lead to states with partial vibrational character giving enhanced $E2$ transition rates but with Ω not a very good quantum number.

ACKNOWLEDGMENTS

We wish to acknowledge helpful discussions with Dr. Aage Bohr.

We are grateful for the facilitation of neutron irradiations to Dr. W. B. Lewis and Dr. Richard Smith at the Reactor Testing Station, Arco, Idaho, and to Mr. F. L. Shon and others at the University of California Radiation Laboratory, Livermore Division. The Stockholm scintillation counter studies were aided by Professor Hilding Slätis, Dr. Hugo Atterling, and Fil. Mag. Wilhelm Forsling.

One of us (FSS) wishes to acknowledge a National Science Foundation fellowship during part of this research.

The Berkeley work was performed under the auspices of the U. S. Atomic Energy Commission.

PHYSICAL REVIEW VOLUME 99, NUMBER 1 JULY 1, 1955

Scattering of Polarized Neutrons by Heavy Nuclei*

ALBERT OKAZAKI†
University of Wisconsin, Madison, Wisconsin
(Received March 28, 1955)

The polarization of Li(p,n) neutrons emitted at a laboratory angle of 50° was measured as a function of proton energy from 2.21 to 2.40 Mev. Analysis of the polarization of the neutrons was performed by measuring the left-right asymmetry in scattering by oxygen. To determine more accurately the polarization produced in scattering by oxygen, the total cross section and angular distribution of scattered neutrons were remeasured.

Measurements of the polarization of neutrons produced in the scattering by intermediate and heavy nuclei have been continued. The results were compared with polarizations calculated by assuming the complex square-well model proposed by Feshbach, Porter, and Weisskopf and modified by the addition of a spin-orbit interaction.

INTRODUCTION

MEASUREMENTS of the polarization of neutrons produced in the scattering by intermediate and heavy nuclei have been reported previously by Adair, Darden, and Fields.[1] These measurements have been continued to study further the dependence of the polarization produced in scattering on the atomic weight. As in the previous experiment the polarization was determined by measuring the left-right asymmetry in scattering of polarized neutrons produced in the $Li^7(p,n)Be^7$ reaction. Before the polarization produced in scattering can be obtained from the measured asymmetries, the polarization of the incident neutrons must be determined. The polarization of the neutrons from the reaction was measured as a function of the incident proton energy using oxygen as the analyzer. The method of analysis has been described previously.[1]

The polarization of neutrons produced in the scattering by oxygen can be expressed in terms of the phase shifts describing the scattering. In order to obtain a more accurate determination of the phase shifts, the total cross section and the angular distributions of scattered neutrons in the energy region of the 440-kev resonance were remeasured.

SCATTERING OF NEUTRONS BY OXYGEN

The total cross section was measured by a conventional transmission experiment in which the transmission of a SnO_2 sample was compared with that of a Sn sample containing the same number of Sn nuclei per cm^2 as were present in the oxide sample. Neutrons were produced by bombarding with protons a lithium target which had a stopping power of about 6 kev for the incident protons. The observed total cross sections corrected for inscattering are plotted in Fig. 1.

Measurements of the angular distribution of neutrons scattered by oxygen were made for neutron energies 410, 438, 465, and 493 kev by a method previously described.[2] For the incident protons the lithium target used for the production of neutrons had a stopping power of 16 kev. To shield the neutron detector from neutrons coming directly from the source, a paraffin block was placed between the detector and source. In addition, the paraffin block served to collimate the neutrons so that at the sample position an area 3.7 cm wide and 6 cm high was irradiated by neutrons. The liquid oxygen scattering sample was contained in a

* Work supported by the U. S. Atomic Energy Commission and the Wisconsin Alumni Research Foundation.
† Now at Atomic Energy of Canada, Ltd., Chalk River, Ontario, Canada.
[1] Adair, Darden, and Fields, Phys. Rev. **96**, 503 (1954).
[2] M. Walt and H. H. Barschall, Phys. Rev. **93**, 1062 (1954).

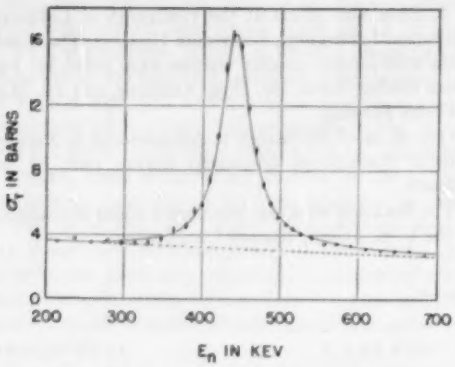

FIG. 1. The total cross section of oxygen *versus* neutron energy. The solid curve was calculated assuming resonance parameters $\Gamma = 48$ kev and $E_r = 442$ kev and S-wave scattering indicated by the dashed line.

thin-walled stainless steel cylinder 1.3 cm in diameter which was surrounded by a cylindrical piece of styrofoam 0.7 cm thick. Scattered neutrons were detected with a recoil counter having an active counting volume 2.5 cm in diameter and 10 cm long and filled with hydrogen to a pressure of 7 atmos. Upon being scattered from oxygen the neutrons lose an appreciable fraction of their energy in the laboratory system with the attendant decrease in the probability of being detected. The energy sensitivity of the counter was measured and corrections for the energy loss were applied to the data.

Making the simplifying assumption that the scattering takes place in a plane perpendicular to the axis of the scattering sample, an estimate of the effect of multiple scattering on the angular distribution was obtained by graphical means. As a check a Monte Carlo calculation similar to that described previously[2] has been performed[3] for neutron energies of 438 and 465 kev where the multiple scattering effect is most pronounced. The two methods give similar results. Since the number of scattering nuclei was not accurately known, only relative angular distributions could be determined. The observed angular distributions, which were normalized so that the integral over all solid angles gave the total cross sections, are plotted in Fig. 2.

In the energy region investigated it is expected that only S- and P-wave scattering are important. The resonance in the total cross section for a neutron energy of about 440 kev is due to an odd parity level with total angular momentum $\frac{3}{2}$ in O^{17} formed by P-wave neutrons.[4] At the resonance energy the contribution of resonance scattering to the total cross section is known and subtraction of this cross section from the observed cross section gives the potential scattering. For energies sufficiently far from the resonance energy, the scattering is mainly the result of background potential scattering which was assumed to decrease linearly with energy. An attempt was made to fit the total cross section and angular distribution measurements with various $P_{\frac{1}{2}}$ and $P_{\frac{3}{2}}$ phase shifts and S-wave phase shifts calculated from the assumed background potential scattering cross section. With a $P_{\frac{1}{2}}$ phase shift equal to zero and a $P_{\frac{3}{2}}$ resonance phase shift calculated for a resonance width of 48 kev at the resonance energy of 442 kev, good agreement with the data was obtained. The resonance phase shift was calculated by using the one-level dispersion formula[5] which takes into account the level shift. The solid line in Fig. 1 shows the calculated total cross section. In Fig. 2, the calculated angular distributions averaged over the energy spread of the incident neutrons are indicated by the curves. Reasonable agreement with the observed angular distributions was obtained for neutron energies of 410, 465, and 493 kev. Over the energy interval used in the 438-kev measurement, the angular distribution changes rapidly with energy, and inasmuch as the energy spectrum of the incident neutrons was not accurately known, the average of the calculated angular distribution could not be determined reliably.

The calculated polarization produced by the oxygen analyzer depends sensitively on the assumed $P_{\frac{1}{2}}$ phase shift. There are spin $\frac{1}{2}$, odd-parity states in O^{17} at excitation energies of 3.06 and 5.93 Mev. At the energies investigated here the contribution to the $P_{\frac{1}{2}}$ phase shifts from the latter level is less than 0.2°. The 3.06-Mev bound level probably corresponds to the 3.10-Mev state in the mirror nucleus F^{17} which has a small reduced width, and the effect of this level on the scattering is negligible. Although a good fit to the

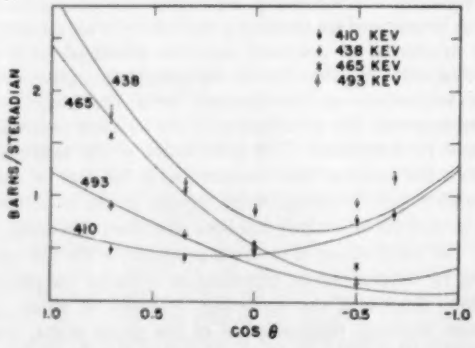

FIG. 2. Angular distribution of neutrons scattered by oxygen at neutron energies of 410, 438, 465, and 493 kev. The indicated errors include statistical errors and estimated errors in the multiple scattering corrections. The curves are the calculated distributions averaged over the neutron energy spread.

[3] The author should like to thank Dr. M. Walt of the Los Alamos Scientific Laboratory for performing the Monte Carlo calculation.

[4] C. K. Bockelman, Phys. Rev. **80**, 1011 (1950); R. K. Adair, Phys. Rev. **92**, 1491 (1953).

[5] E. P. Wigner and L. Eisenbud, Phys. Rev. **72**, 29 (1947).

total cross section and angular distribution measurements was obtained for a P-potential scattering phase shift equal to zero the measurements were not sufficiently accurate to allow the determination of a P-potential scattering phase shift less than 3°. For a neutron energy of 500 kev the hard sphere P-wave phase shift is about 6°. A calculation of the P-wave phase shift assuming the complex square well model proposed by Feshbach, Porter, and Weisskopf,[6] gives a value of less than 1°.

Using the phase shifts obtained from the total cross section and angular distribution measurements, calculations were made of the polarization produced by the oxygen analyzer.

POLARIZATION OF Li(p,n) NEUTRONS

Oxygen was used to measure the polarization of the neutrons produced in the $Li^7(p,n)Be^7$ reaction and emitted at a laboratory angle of 50° with respect to the incident proton beam. To determine the polarization of the neutrons from the reaction, the left-right asymmetry in scattering of the neutrons from oxygen was measured with the same apparatus used in the angular distribution measurements and with an experimental arrangement similar to that described previously. For a proton energy of 2.23 Mev a lithium target 65 kev thick was used and measurements of the asymmetry in scattering were performed for scattering angles of 60° and 90° c.m. All the other measurements were made with a lithium target which had a stopping power of about 35 kev for the incident protons. At proton energies of 2.27 Mev and 2.30 Mev the asymmetry was measured for six scattering angles from 45° to 120°. Measurements at the other energies investigated were made for scattering through 90°. The observed left-right asymmetries were corrected for multiple scattering and together with the calculated polarization produced by the oxygen analyzer allowed the determination of the polarization of the neutrons from the reaction. In Fig. 3,

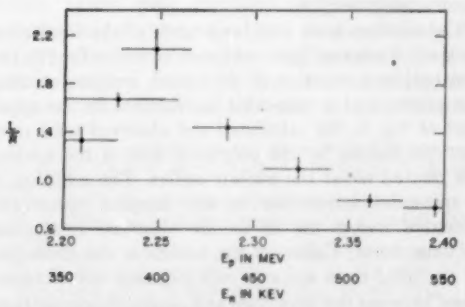

FIG. 3. Observed left-right ratios for neutron scattering at 90° c.m. by oxygen *versus* proton energy and corresponding neutron energy. The vertical lines represent standard statistical errors. The horizontal lines represent the spread in neutron energy.

[6] Feshbach, Porter, and Weisskopf, Phys. Rev. **96**, 448 (1954).

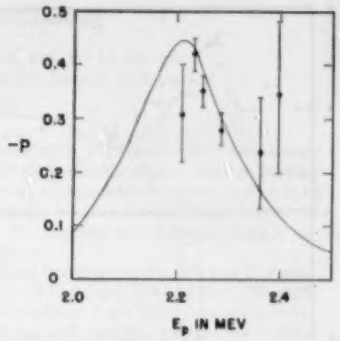

FIG. 4. Polarization of $Li^7(p,n)$ neutrons *versus* proton energy. The neutrons were emitted at 56° c.m. with respect to the incident proton beam. The solid curve is the polarization calculated by Adair for neutrons emitted at 60° c.m.

the corrected left-right asymmetries for a scattering angle of 90° are plotted as a function of the incident proton energy. As expected, the left-right scattering ratio changes from a value greater than one to a value less than one for the neutron energy at which the polarization produced in scattering by oxygen changes sign. The measured polarizations of the Li(p,n) neutrons are plotted *versus* the incident proton energy in Fig. 4. For the energies at which measurements were made for several scattering angles, the averages of the polarizations obtained for the different angles are shown.

Adair[7] has calculated the polarization of neutrons produced in the reaction as a function of the proton energy, and the calculated polarization of neutrons emitted at 60° c.m. is indicated by the solid curve in the figure. In the present experiment the measurements were made for neutrons emitted at 50° laboratory angle or 56° c.m. There is good agreement between the measurements with small statistical errors and the calculated values. The small polarization produced by the oxygen analyzer for some neutron energies results in large errors in the measured polarization of neutrons with these energies.

Willard and co-workers[8] have reported measurements of the polarization of neutrons produced in the Li(p,n) reaction and emitted at a laboratory angle of 42° with respect to the incident protons. Their results indicate a nearly constant value of 0.50 ± 0.04 for neutrons with energies from 300 to 550 kev and are larger than the values obtained in the present investigation.

POLARIZATION OF NEUTRONS SCATTERED BY HEAVY NUCLEI

The polarized neutrons from the $Li^7(p,n)$ reaction were used to measure the polarization of neutrons scattered by intermediate and heavy nuclei. In these measurements 380-kev neutrons from the reaction

[7] R. K. Adair, Phys. Rev. **96**, 709 (1954).
[8] Willard, Kington, and Bair, Phys. Rev. **95**, 1359 (1954).

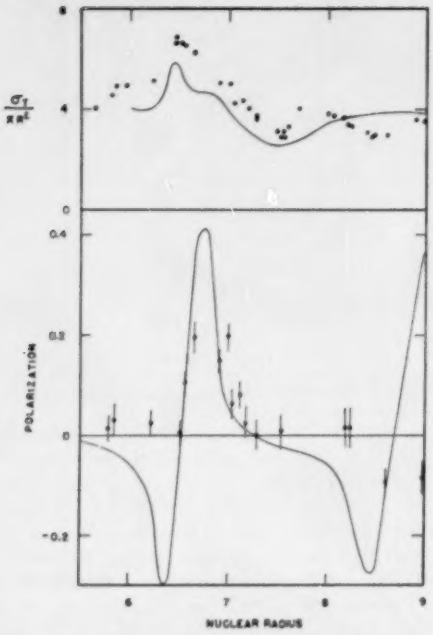

FIG. 5. In the upper part of the figure, the total cross section divided by the geometric area of the nucleus is plotted *versus* the nuclear radius in units of 10^{-13} cm. The polarization of neutrons scattered by nuclei is plotted as a function of the nuclear radius in the lower part of the figure. The nuclear radius was assumed to be $1.45A^{\frac{1}{3}}\times10^{-13}$ cm. Experimental measurements for 380-kev neutrons are shown by the points. The curves are the values calculated by using the complex square-well potential $V=[-42\times(1+0.03i)-3.0\ \mathbf{l}\cdot\mathbf{s}]$ Mev.

emitted at a laboratory angle of 50° were scattered from the element under consideration and the left-right asymmetry in scattering through 90° was observed. The polarization of the incident beam of neutrons which had an energy spread of 65 kev was 42 ± 6 percent. There is good agreement between the observed asymmetries and those previously reported. However in the previous experiment the polarization of the incident neutrons was found to be 53 ± 6 percent compared with 42 ± 6 percent measured in the present investigation. Hence the polarization produced in scattering by the intermediate and heavy nuclei was assigned a value 20 percent smaller than in the present measurements. The measured polarizations are shown in the lower part of Fig. 5 as a function of the nuclear radius which was assumed to be given by $1.45A^{\frac{1}{3}}\times10^{-13}$ cm, where A is the atomic weight. The vertical bars represent statistical errors only and do not include the uncertainty in the polarization of the incident beam. For atomic weights near 100 the polarization reaches a maximum value of about 20 percent. The lightest elements investigated, Cu and Zn, produce little polarization while the heaviest elements, Bi and U, produce small polarizations of sign opposite to that observed for the other elements.

Feshbach, Porter, and Weisskopf[6] have proposed a model in which the interaction between a neutron and a nucleus is described by a complex square-well potential $V=-42(1+0.03i)$ Mev for $r<R$. The nuclear radius R is given by $1.45A^{\frac{1}{3}}\times10^{-13}$ cm, where A is the atomic weight. While this model has been successful in reproducing qualitatively the variations of the total cross section with atomic weight and neutron energy, it does not contain a spin-dependent interaction which was shown to be present by the observed polarizations. Calculations of the polarization produced in the scattering of 378-kev neutrons were performed by assuming a spin-orbit interaction of the form $V'\ \mathbf{l}\cdot\mathbf{s}$ in addition to the complex square well potential. S and P-wave scattering were considered. The solid curve in Fig. 5 represents the polarization calculated for $V'=-3.0$ Mev. The model gives correctly the small polarizations observed for the lightest elements and also the position of the peak in the polarization though the magnitude appears to be too large. However, the model gives a large negative polarization in the region of $R=6.3\times10^{-13}$ cm whereas the measurement for Se with $R=6.23\times10^{-13}$ cm indicates little polarization. Further, large positive values are predicted for the region of U in disagreement with the observed polarization which has the opposite sign.

Recently Thomas[9] has calculated the polarization produced in scattering for a complex square-well potential and a spin-orbit interaction which is effective only at the nuclear surface where it has the form of a delta function. In these calculations neutrons with orbital angular momentum up to and including three units were considered. The results for the surface spin-orbit interaction are qualitatively the same as those obtained for the uniform spin-orbit interaction. For both spin-orbit interactions the maxima and minima in the calculated polarization occur for the same atomic weights.

Calculations have also been made of the total cross sections of intermediate and heavy elements for 378-kev neutrons as a function of the atomic weight assuming the presence of a spin-orbit interaction. In the upper part of Fig. 5, the calculated and observed total cross sections divided by the geometric area of the nucleus are plotted *versus* the nuclear radius. The addition of a spin-orbit interaction to the complex square-well potential makes the fit to the observed total cross sections worse. Failure of the models in the prediction of the total cross sections indicates that better agreement between the calculated and observed polarizations cannot be expected.

[9] R. G. Thomas (private communication).

Z-Dependence of Bremsstrahlung*

W. C. Barber, A. I. Berman,† K. L. Brown, and W. D. George
High-Energy Physics Laboratory, Stanford University, Stanford, California
(Received March 24, 1955)

The relative amounts of bremsstrahlung produced by the elements Cu, Ta, Pb, and U for incident electrons of energy 24 and 34 Mev were measured by using the $Cu^{63}(\gamma,n)Cu^{62}$ reaction as the photon detector. Because of the shape of the cross-section function, photons were detected in a comparatively narrow energy band centered at 17.5 Mev. The electron beam was monitored by a Faraday cup placed immediately behind the radiator and detector foils. Corrections were applied to account for ionization and radiation losses of the electrons, and for pair production and Compton losses of the photons.

The experimentally-determined "thin-target" cross sections relative to copper for Ta, Pb, and U, respectively, were 5.681 ± 0.13, 6.959 ± 0.16, and 8.221 ± 0.19 per atom, at 24 Mev; and 5.583 ± 0.08, 6.770 ± 0.09, and 8.172 ± 0.12 at 34 Mev. These values are from five to thirteen percent lower than the corresponding ratios calculated from the Bethe-Heitler theory (including screening and radiation produced in collision with atomic electrons). The results are consistent with a deviation from theory of $(1.54\pm0.2)\times10^{-5}\,Z^2$ percent for 24-Mev electrons, and $(1.38\pm0.14)\times10^{-5}\,Z^2$ percent for 34-Mev electrons.

INTRODUCTION

THE theory of bremsstrahlung of relativistic electrons as developed by Bethe and Heitler[1] has had numerous experimental tests which prove that it is qualitatively correct,[2,3] but some of which indicate quantitative deviations of the order of ten percent for high-Z elements.[4,5] Similar deviations have been well established in the related phenomenon of pair production and have been attributed to the failure of the Born approximation used in the theories.[6-9] Recently, Bethe, Davies, and Maximon[10,11] have published bremsstrahlung and pair-production theories based on the use of Furry wave functions, which they estimate to be correct to order mc^2/ϵ where ϵ is the energy of the final electron in bremsstrahlung or that of the less energetic electron in pair production. Their integral pair-production cross section agrees well with experiment for photon energies greater than 80 Mev and "not unreasonably" at 17.6 Mev.

Their theories indicate an important difference between bremsstrahlung and pair production such that in the limit of complete screening the bremsstrahlung cross section agrees with the Born-approximation result whereas the pair-production cross section does not. In the opposite limit of no screening, however, the new theories indicate that both the bremsstrahlung and pair-production cross sections are the same fraction lower than the result based on the Born approximation. The new integral bremsstrahlung cross section for the case of intermediate screening has not been published, but it is expected to be lower than the Born-approximation value.

The present paper came about as a result of recent measurements of the absolute (γ,n) cross sections of copper[12] and carbon.[13] It was desirable in these measurements to use a radiator having the maximum photon yield and a minimum ionization loss. This requirement is satisfied with a high-Z element; however, the deviation of the absolute bremsstrahlung cross section is expected to increase with Z. Berman and Brown[12] used a copper radiator for this reason, assuming that the deviation would not differ markedly from that which had been observed previously for pair production. Barber *et al.*[13] used both tantalum and copper radiators, and observed a discrepancy of 7 ± 2 percent in the evaluation of the $C^{12}(\gamma,n)C^{11}$ cross section based on the Bethe-Heitler theory, the tantalum yielding an apparently lower cross section.

The reaction $Cu^{63}(\gamma,n)Cu^{62}$ was chosen as a photon monitor for the present experiment because the cross-section curve has a sharp maximum at 17.5 Mev and has less than five percent of its total area above 24 Mev.[12] The primary electron energies were chosen as 24 and 34 Mev in order to gain information about the effect of energy dependence and yet keep the corrections for the degradation of energy in the finite radiator foil small.

EXPERIMENTAL TECHNIQUE

The experimental equipment and techniques employed in this experiment are identical to those described by Berman and Brown in their determination of the $Cu^{63}(\gamma,n)Cu^{62}$ absolute cross section,[12] with the exception that various materials—Cu, Ta, Pb, and U—were successively employed as radiators. In brief, the

* The research reported here was supported by the joint program of the Office of Naval Research and the U. S. Atomic Energy Commission.
† Now with Pratt and Whitney, Hartford, Connecticut.
[1] H. A. Bethe and W. Heitler, Proc. Roy. Soc. (London) **A146**, 83 (1934).
[2] J. W. Dewire and L. A. Beach, Phys. Rev. **83**, 476 (1951).
[3] Powell, Hartsough, and Hill, Phys. Rev. **81**, 213 (1951).
[4] L. H. Lanzl and A. O. Hansen, Phys. Rev. **83**, 959 (1951).
[5] C. D. Curtis, Phys. Rev. **89**, 123 (1953).
[6] A. I. Berman, Phys. Rev. **90**, 210 (1953).
[7] C. R. Emigh, Phys. Rev. **86**, 1028 (1952).
[8] R. L. Walker, Phys. Rev. **76**, 527 (1949); **76**, 1440 (1949).
[9] J. L. Lawson, Phys. Rev. **75**, 433 (1949).
[10] H. A. Bethe and L. C. Maximon, Phys. Rev. **93**, 768 (1954).
[11] Davies, Bethe, and Maximon, Phys. Rev. **93**, 788 (1954).
[12] A. I. Berman and K. L. Brown, Phys. Rev. **96**, 83 (1954).
[13] Barber, George, and Reagan, Phys. Rev. **98**, 73 (1955).

TABLE I. Results of experiment, showing major corrections.

Row	Radiator	$(E_0-\mu)=24$ Mev Cu	Ta	Pb	U	$(E_0-\mu)=34$ Mev Cu	Ta	Pb	U
1	Basic counting data	76.23±0.2	83.54±0.2	78.32±0.3	81.41±0.3	103.34±0.3	110.27±0.4	102.35±0.3	108.36±0.5
2	Integrator correction (percent)	2.40±0.2	1.50±0.2	1.34±0.2	1.38±0.2	2.14±0.2	1.45±0.2	1.10±0.2	1.15±0.2
3	Degradation corrections (percent)	6.66±1.3	5.15±1.0	4.73±0.9	4.75±1.0	2.67±0.5	2.20±0.4	2.10±0.4	2.18±0.4
4	Data after corrections	83.14±1.2	89.10±0.9	83.08±0.9	86.40±0.9	108.31±0.7	114.30±0.7	105.63±0.6	111.97±0.8
5	Effect of first foil	9.34±0.1	9.34±0.1	9.34±0.1	9.34±0.1	12.18±0.1	12.18±0.1	12.18±0.1	12.18±0.1
6	Difference Row 4 −Row 5 =effect of radiator	73.80±1.2	79.76±0.9	73.74±0.9	77.06±0.9	96.13±0.7	102.12±0.7	93.45±0.6	99.79±0.8
7	Radiator thickness (mg/cm²)	310.09±2.2	167.95±1.2	145.20±1.0	147.58±1.5	310.09±2.2	167.95±1.2	145.20±1.0	147.58±1.5
8	Yield per atom of radiator $Y_{exp}(E_0,Z)$	15.12±0.27	85.89±1.2	105.22±1.4	124.30±1.9	19.70±0.20	109.98±1.1	133.37±1.3	160.98±1.7
9	Yield per radiation length	3044±55	3012±42	2959±38	2809±42	3966±40	3857±39	3750±38	3638±40
10	Theoretical yield per atom $Y_T(E_0,Z)$ unnormalized	5.179	31.15	39.02	48.80	6.783	39.87	49.83	62.17
11	$R(E_0,Z)=C\frac{Y_{exp}(E_0,Z)}{Y_T(E_0,Z)}$	1.003±0.018	0.947±0.013	0.926±0.012	0.875±0.013	0.997±0.010	0.947±0.009	0.919±0.009	0.889±0.010

technique was to pass the external electron beam of the Mark II (38-Mev peak energy) linear accelerator through a stack of foils into a Faraday-cup electron integrator. The foil stack consisted of an 0.002-in. copper foil followed by a radiator foil of approximately 0.025 radiation length and a second 0.002-in. copper foil. To prevent errors due to variations in detector-foil thickness the same matched pairs of foils were used with the various radiators. The Cu^{62} activity (9.73-minute half-life) induced in the front and rear foils was measured with a 4π scintillation counter.

The quantity of interest is that part of the induced activity in the second foil which is due only to the photons produced in the 0.025-radiation-length radiator. The activity induced by the virtual quanta associated with the electromagnetic field of the moving electrons, by neutrons or stray gamma radiation entering with the electrons, is the same in the front as in the rear foil (except for corrections due to electron energy losses in passing through the foils). Therefore, except for minor corrections, the activity induced in the rear foil minus the activity induced in the front foil, normalized to the integrated charge, yields a quantity proportional to the number of photons produced in the front foil plus radiator. The fraction of this effect that is due to the front foil may be subtracted by reducing the data for the copper radiator first. The quantity finally determined, $Y(E_0,Z)$, is the induced activity per incident electron due to the radiator; then

$$Y_{exp}(E_0,Z)=N_r N\int_0^{E_0-\mu}\varphi_{exp}(k,E_0,Z)\sigma_{\gamma,n}(k)dk, \quad (1)$$

where k is the quantum energy, E_0 is the electron energy, N_r is the number of radiator nuclei per cm², and N is the number of Cu^{63} nuclei per cm² in the detector foil, $\sigma_{\gamma,n}(k)$ is the $Cu^{63}(\gamma,n)Cu^{62}$ cross section vs energy k, and $\varphi_{exp}(k,E_0,Z)$ is the experimental 'thin-target' integral bremsstrahlung cross section for the element Z.

From theory, and a knowledge of the shape of $\sigma_{\gamma,n}(k)$ for copper, it is possible to calculate, by numerical integration, the quantity

$$Y_T(E_0,Z)=N_r N\int_0^{E_0-\mu}\varphi_T(k,E_0,Z)\sigma_{\gamma,n}(k)dk, \quad (2)$$

where $\varphi_T(k,E_0,Z)$ is the Bethe-Heitler bremsstrahlung cross section including screening and modified by the factor $[(Z+\delta)/Z]$ to take into account the contribution of atomic electrons in producing radiation. Values of δ varying from 1.08 in the case of uranium at 24 Mev to 1.12 for copper at 34 Mev were calculated from the equations given by Wheeler and Lamb.[14] To compare experiment and theory, the ratio

$$R(E_0,Z)=CY_{exp}(E_0,Z)/Y_T(E_0,Z) \quad (3)$$

was calculated for each Z and both values of E_0. The value of the constant C was chosen arbitrarily to make the average value of $R(E_0,29)$ equal to unity.

RESULTS

The experimental results, the important experimental corrections, and the comparison with theory are shown in Table I. The quantity listed under the heading "Basic Data" (Row 1 of Table I) represents the average value of the second-foil Cu^{62} activity (corrected for multiple-scattering effects) minus the first-foil Cu^{62} activity, all divided by the observed integrated charge collected by the Faraday cup. The probable errors listed were determined from the internal consistency of fifteen bombardments made with each set of conditions. The technique of measuring the radioactivity in the foils and of measuring the integrated charge are discussed in detail by Berman and Brown.[12] The integrator correction is an experimentally determined quantity and represents the change in the observed integrated charge

[14] J. A. Wheeler and W. E. Lamb, Phys. Rev. 55, 858 (1939).

when the foils and radiators were placed in the path of the electron beam. This is due to the secondary electrons produced in the stacked foils which outweigh the loss of charge due to scattering. The degradation corrections are applied in order to compensate for both the energy loss of the electrons and the loss of photons in passing through the foils. After these corrections are applied, the resulting quantity is the "thin-target" yield due to the first foil plus radiator. The data obtained with the copper radiator are then used to determine the effect produced by the first foil (Row 5, Table I). The net effect due to the radiator alone (Row 6) is divided by the foil thickness in mg/cm² (Row 7) and multiplied by the atomic weight to give the relative yield per atom of radiator (Row 8). Estimated errors due to foil nonuniformity of 0.7 percent in the cases of Cu, Ta, and Pb, and one percent in the case of U, are added statistically at this point. The relative yield per radiation length is tabulated in Row 9 where the radiation length was computed from the formula

$$X_0=\left[\frac{4NZ(Z+1)}{137}\left(\frac{e^2}{mc^2}\right)^2 \ln 183Z^{-\frac{1}{3}}\right]^{-1}. \qquad (4)$$

The theoretical yield defined in Eq. (2) is listed in Row 10. The ratio Eq. (3) giving the comparison of experiment and theory is in Row 11.

The values of $R(E_0,Z)$ are plotted as functions of Z^2 in Fig. 1, and within experimental error they fall on straight lines. The lines plotted were obtained by least-square fitting of the four points at each value of E_0. From the straight lines it is found that $R(E_0,Z)=R_0(E_0)(1-KZ^2)$ where $K=(1.54\pm0.2)\times10^{-5}$ for $E_0=24$ Mev, and $(1.38\pm0.14)\times10^{-5}$ for $E_0=34$ Mev.

It should be noted that if the curves $\varphi_{\rm exp}$ and φ_T as functions of k were parallel over the range of k where $\sigma_{\gamma,n}(k)$ is finite, the ratio $R(E_0,Z)$ would be proportional to $\varphi_{\rm exp}/\varphi_T$. Since the curves are expected to be nearly parallel and since $\sigma_{\gamma,n}(k)$ is sharply peaked near $k=17.5$ Mev, the ratio $R(E_0,Z)$ is very nearly proportional to $\varphi_{\rm exp}(17.5,E_0,Z)/\varphi_T(17.5,E_0,Z)$.

From the definition of R, it follows then that the average value [weighted by $\sigma_{\gamma,n}(k)$] of $\varphi_{\rm exp}$ deviates from a similarly weighted φ_T and, to close approximation,

$$\frac{\varphi_T(17.5,E_0,Z)-\varphi_{\rm exp}(17.5,E_0,Z)}{\varphi_T(17.5,E_0,Z)}=KZ^2. \qquad (5)$$

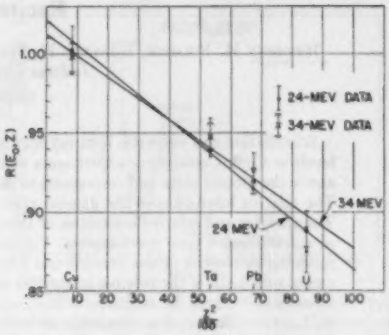

FIG. 1. The ratio $R(E_0,Z)$ of the experimental to theoretical photon yield is plotted as a function of $Z^2/100$. The results have been normalized to make the average of $R(34, 29)$ and $R(24, 29)$ equal to unity. The straight lines are least-square representations of the data.

DISCUSSION

The results of the experiment are appreciably affected by the corrections due to finite radiator thickness (Rows 2 and 3 of Table I). However, it should be emphasized that even before the corrections are applied the conclusion can be drawn that the experimental cross section relative to the Bethe-Heitler theoretical cross section decreases as a function of Z. Because of the higher ionization losses in the radiators of low Z, the effect of the thickness corrections is to increase this deviation.

It is interesting to note that the experimental deviation from the Bethe-Heitler theory is nearly the same as is observed in the case of pair production by photons of 15 to 50 Mev.[6-8] For example, Berman[6] working with photons of 19.5 Mev, expressed results in a form similar to Eq. (5) as

$$(\sigma_{\rm theor}-\sigma_{\rm exp})/\sigma_{\rm theor}=1.55\times10^{-6}Z^2,$$

for pair production. This similarity between bremsstrahlung and pair production at intermediate energies is consistent with the theories of Bethe *et al.*[10,11]

It is desirable to extend the bremsstrahlung experiments to higher initial electron energies where the screening is nearly complete. In this case, the recent theories[10,11] predict that the bremsstrahlung cross section is correctly given by the Born approximation whereas the pair-production cross section is not.

The authors wish to thank members of the staff of the High-Energy Physics Laboratory who have contributed to the completion of this research.

Excited States of Ce^{140}†

HERBERT H. BOLOTIN, CHARLES H. PRUETT, PAUL L. ROGGENKAMP,* AND ROGER G. WILKINSON
Indiana University, Bloomington, Indiana

(Received March 23, 1955)

Scintillation and magnetic beta-ray spectrometry have been applied to the study of the more important levels of Ce^{140}. Coincidence experiments verify that successive levels are at 1.60, 2.09, 2.42, and 2.53 Mev above the ground state and correspond to gamma rays of energies 1.60, 0.815, 0.490, 0.438, and 0.328 Mev. The relative intensities of the gamma rays are found to be 2.50, 1.15, 1.25, 0.15, and 1.00, respectively. The energies and relative intensities of two weak high-energy transitions have been determined by means of a scintillation pair spectrometer. Values of 2.50 ± 0.05 and 3.00 ± 0.20 Mev are obtained with corresponding intensities of one percent and 0.04 percent of the 1.60-Mev gamma-ray. The beta-ray measurements substantiate the relative intensities and end-point energies of the beta-ray groups which have been reported by others. In addition, it has been possible to estimate the internal conversion coefficients and K/L ratios. The angular correlation of four cascade pairs of the above gamma rays has been studied. The results obtained, together with the beta-ray and internal conversion data, are most consistent with the assignment 0, 2+, 4+, 3+ for the ground state and first three excited states. The assignment 0, 2+, 4+, 4+ cannot be definitely excluded.

INTRODUCTION

THE complex radiations from the decay of 40-hour La^{140} have been studied by a number of investigators. Three somewhat different decay schemes have been suggested. The decay schemes proposed by Cork and co-workers[1] and Beach, Peacock, and Wilkinson[2] were based on the beta-spectra end points and gamma-ray energies. Recently, Peacock, Quinn, and Oser[3] have reinvestigated this decay more thoroughly and have proposed a decay scheme which is consistent with the coincidence studies of Bannerman, Lewis, and Curran.[4] The present work is concerned with the major features of this decay scheme which are shown in Fig. 1. The disintegration of La^{140} has been restudied with the help of scintillation counters and a 180° magnetic spectrometer with a view to checking the disintegration scheme and assigning spins and parities of the levels. The angular correlations between several pairs of gamma rays have been measured. The results of the angular correlation of four pairs of successive gamma rays and estimations of the K/L ratios, internal conversion coefficients, and intensity ratios for the gamma transitions are presented. Assignments of spins and parities of the first three excited states of Ce^{140} are proposed.

EXPERIMENTAL PROCEDURES

Cylindrical, canned thallium-activated NaI crystals, 1 inch×1 inch, mounted on Dumont 6292 photomultiplier tubes were used to detect the gamma radiations. Aluminum disks of one-eighth inch thickness were placed over the faces of the crystals to minimize pulses due to beta rays. Pulses from each of the detectors were fed into linear amplifiers whose outputs were analyzed in fast differential discriminators. A coincidence circuit ($2\tau=10^{-7}$ sec) was used to mix the pulses from the two channels.

Aqueous and acid solutions of lanthanam chloride were prepared by chemical extraction from an equilibrium $Ba^{140}-La^{140}$ sample obtained from the Oak Ridge National Laboratory. For the angular correlation measurements the source was contained in a thin-walled cylindrical teflon source holder and was placed 6 cm from the faces of both crystals. The crystals were provided with conical lead shields of sufficient thickness to eliminate crystal-to-crystal scattering in the gamma-ray energy range under consideration. Coincidences

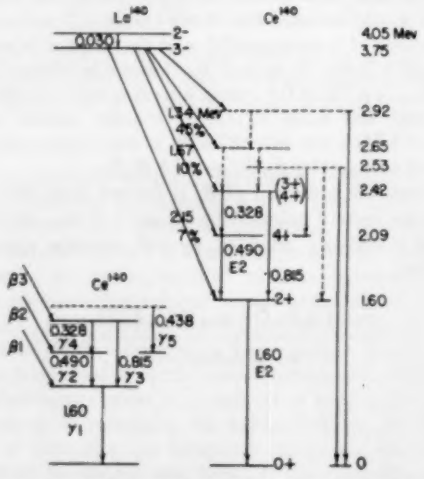

FIG. 1. Decay scheme of $La^{140}-Ce^{140}$. The relative intensities of the beta-ray groups and the energies of the gamma rays are those published by Peacock. The schematic of the decay at the lower left defines the notation used in this paper.

† Supported by the joint program of the Office of Naval Research and the U. S. Atomic Energy Commission.

* Present address: Savannah River Laboratory, E. I. duPont deNemours and Company.

[1] Cork, LeBlanc, Stoddard, Martin, Branyan, and Childs, Phys. Rev. **83**, 856 (1951).

[2] Beach, Peacock, and Wilkinson, Phys. Rev. **76**, 1624 (1949).

[3] Peacock, Quinn, and Oser, Phys. Rev. **94**, 372 (1954).

[4] Bannerman, Lewis, and Curran, Phil. Mag. **42**, 1097 (1951).

were recorded at angular intervals of 15° between 90° and 270°.

DECAY SCHEME

Although the various authors are essentially in accord as to the identification of the prominent radiations involved in the decay, the presence of a number of weaker gamma rays has lead to proposed decay schemes which are somewhat different. It seemed advisable, therefore, to check the more important features of the decay with the higher resolution scintillation equipment now available before undertaking directional correlation studies. The single crystal spectrum shown in Fig. 2 exhibits photopeaks due to the more intense gamma rays of energies 1.60, 0.815, 0.490, and 0.328 Mev (γ_1, γ_3, γ_2, and γ_4 respectively, as defined in Fig. 1). It is to be concluded that other gamma rays which have been reported in this energy region are considerably weaker, since most of the small irregularities in the

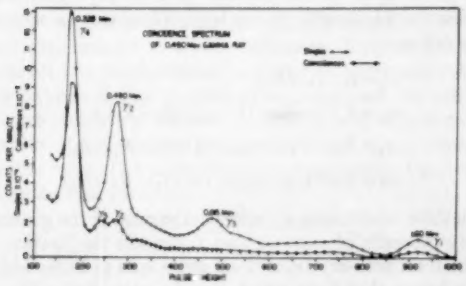

FIG. 2. Scintillation spectrum of Ce^{140} gamma rays. Circles represent the spectrum as registered by one counter. The lower curve is the coincidence spectrum obtained when the other counter is set to accept the photoelectron peak of the 0.490-Mev gamma ray.

singles curve can be ascribed to either Compton electrons or backscattering associated with the stronger radiations.

The coincidence curve shown in Fig. 2 was obtained with one channel set to accept the full photopeak due to the 0.490-Mev gamma ray while the other channel surveyed the spectrum. The curve shown in Fig. 3 resulted when the fixed channel registered the 1.60-Mev gamma ray. These coincidence curves show that the 0.490-Mev gamma ray is coupled with the 0.328-Mev radiation. The small double coincidence peak (Fig. 2) is to be expected if a weak 0.438-Mev gamma ray (γ_5) is also in cascade with the 0.490-Mev gamma ray. Moreover, γ_1 is seen to be in coincidence with γ_2, γ_3, and γ_4. Further experiments show that γ_3 is in sequence only with the 1.60-Mev radiation. The coincidence data thus indicate that γ_1 either precedes or follows a $\gamma_2-\gamma_4$ cascade pair and its γ_3 crossover. Since a delayed coincidence experiment yielded only "prompt" coincidences, the lifetime of the intermediate level of γ_2 and γ_4 is estimated to be less than 10^{-8} sec. This con-

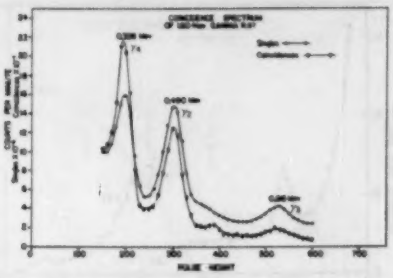

FIG. 3. Scintillation spectrum of Ce^{140} gamma rays. Triangles denote the coincidence spectrum obtained when the fixed channel was set to record the photopeak of the 1.60-Mev gamma ray.

figuration of the lower energy gamma rays receives strong support from the precise energy determinations of Hedgran and Lind.[5] They find that the sum of the energies of the cascade pair differs by only 0.20 kev from their measured value of 0.8151 Mev for γ_3. Finally, by using Bell's[6] absorption cross section curves for NaI, the relative intensities of the gamma rays have been estimated from the data shown in Figs. 2 and 3. These are listed in Table I.

Since accurate measurement of the energies and relative intensities of the weak high-energy gamma rays by usual spectrometer techniques is impracticable, a scintillation pair spectrometer was employed for this purpose. A similar three-crystal NaI(Tl) spectrometer has been described by Bair and Maienschein.[7] Pulses from the center crystal were analyzed with a differential pulse-height selector which was gated by pulses due to annihilation radiation from two side crystals. Figure 4 shows the spectrum obtained in this way. The three peaks, which appear at energies $2mc^2$ less than the gamma ray energies, are ascribed to radiations at 1.60, 2.50±0.05, and 3.0±0.2 Mev. The relative intensities calculated from the areas under the peaks and the pair

TABLE I. Gamma-ray intensities and internal-conversion data.

γ_i	γ_1: 1.60 Mev	γ_2: 0.49 Mev	γ_3: 0.815 Mev	γ_4: 0.328 Mev	γ_5: 0.438 Mev
Relative intensity of γ_i to γ_4: g_i	2.5	1.25	1.15	1.00	0.15
Ratio of conversion of γ_i to total β disintegration: R_i	0.0008	0.0040	0.00168	0.0124	0
Total conversion coefficient: α_i	0.0008	0.00831	0.00412	0.0349	···
K-conversion coefficient: α_{Ki}	0.0008	0.00732	0.00412	0.0307	···
K/L ratio	large	7.4	large	7.4	···

[5] A. Hedgran and D. Lind, Arkiv. Fysik **5**, 177 (1952).
[6] P. R. Bell, Oak Ridge National Laboratory (privately circulated tables).
[7] J. K. Bair and F. C. Maienschein, Rev. Sci. Instr. **22**, 343 (1951).

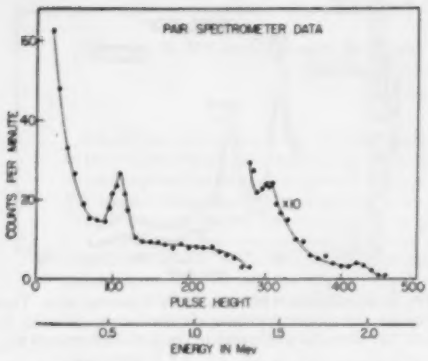

FIG. 4. Triple coincidence curve obtained with a scintillation pair spectrometer. The peaks which appear at about 0.60, 1.45, and 2.0 Mev are due to gamma rays of energies 1.60, 2.50, and 3.0 Mev. The 1.60-Mev radiation of Ce^{140} and the 2.62-Mev gamma ray of ThC″ were used for calibration.

production absorption probabilities, are 100, 1.0, and 0.04, respectively.

The beta-ray spectrum of La^{140} has been measured in a small 180° shaped field spectrometer and is in good agreement with the results of Peacock *et al.*[3] This spectrum has been resolved by Peacock into five groups having end-point energies of 2.15, 1.67, 1.34, 1.10, and 0.83 Mev. The relative intensities of these groups and the corresponding log *ft* values are listed in Table II. From these energy determinations it seems clear that the 0.328-Mev gamma ray precedes the 0.490-Mev transition. Also from the beta-ray energetics, the 1.60-Mev gamma ray must follow the 0.328−0.490 Mev cascade. The weak 0.438-Mev gamma ray (15 percent of the 0.328-Mev radiation) which is in coincidence with the 0.490-Mev gamma ray must precede it. It may be concluded that the decay scheme is substantially that of Fig. 1. Moreover, the relative intensities of the gamma rays to be expected on the basis of this scheme and the measured beta-ray intensities are in good accord with the scintillation results given in the first line of Table I.

The configuration 3− of the ground state of the La^{140}, indicated in Fig. 1, results from γ-γ and beta-gamma coincidence studies involving the radiations subsequent to the decay of Ba^{140}. Although many of the details of the Ba^{140}−La^{140} decay are still uncertain, the position of the strong 30-kev gamma ray, as shown, seems definite.[1] This assignment is supported by coincidence experiments which show that this radiation is in sequence with all of the stronger gamma rays as well as all of the higher energy beta rays. In addition, the lifetime and the 30-kev transition cannot be long with respect to the 10^{-7} sec coincidence resolving time. Since the $(d_{3/2}f_{7/2})$ shell-model configuration of the La^{140} ground state requires negative parity, a spin of at least 3− is required to explain the absence of ground-state beta transitions for both the Ba^{140}−La^{140} and La^{140}−Ce^{140} decays. A higher spin than this would not be compatible with the relatively short lifetime of the 30-kev level and the log *ft* value of 8.0 for the beta rays to this level.

INTERNAL-CONVERSION COEFFICIENTS

Reasonable estimates of the internal-conversion coefficients of the stronger transitions (γ_1, γ_2, γ_3, γ_4) can be made without detailed knowledge of the number, order, or intensities of the gamma rays which lie *above* the 2.42-Mev level. From the beta-ray spectrum the ratios R_i of the total number of conversion electrons of the particular gamma transitions γ_i to the total number of beta disintegrations have been measured (Table I). Reference to Fig. 1 shows that if the very weak 0.938, 2.5, and 3.0 Mev transitions are neglected, the *total* internal conversion coefficients of the respective gamma rays can be obtained by equating the number of conversion electrons and gamma rays arising from a given level to the number of beta rays that lead directly or indirectly to this level. These may be written as follows:

$$\alpha_1 = R_1/(1-R_1),$$
$$\alpha_2 = R_2(1+g_{32})/(1-f_2-R_3-R_2),$$
$$\alpha_3 = R_3(1+g_{43}+g_{53})/(1-f_3-R_3-R_4),$$
$$\alpha_4 = R_4(1+g_{34}+g_{54})/(1-f_4-R_3-R_4).$$

In these expressions, g_{ij} refers to the ratio of the gamma-ray intensity of γ_i to γ_j, and f_i denotes the fraction of the total beta-ray transitions which lead to levels which lie below that from which γ_i originates. From Fig. 1, it is seen that $f_2=0.07$ and $f_3=f_4=0.17$. The total internal conversion coefficients which result are listed in Table I. A check on the values of α_i may be obtained by noting that

$$\alpha_j = g_{ij}\alpha_i R_j/R_i.$$

Thus, in terms of α_4 as obtained above, the values of α_1 and α_2 agree within 10 percent of the values given in Table I.

Estimates of the K/L ratios for γ_2 and γ_4 have been made from the beta-ray spectrum. No conversion other than K conversion can be seen for γ_1 and γ_3. These values together with the corresponding values of α_K are also given in Table I.

ANGULAR CORRELATIONS

On the basis of the foregoing decay scheme, angular correlation measurements of the γ_1−γ_3, γ_1−γ_2, γ_1−γ_4

TABLE II. Beta-ray groups of La^{140}.

β group	$\beta 1$	$\beta 2$	$\beta 3$
Energy	2.15 Mev	1.67 Mev	1.34 Mev
Relative intensity	7%	10%	45%
Log *ft*	9.03	8.67	7.66

and $\gamma_2-\gamma_4$ cascades were undertaken. (The notation, as before, is described in Fig. 1.) Reference to Fig. 2 shows that the gamma rays in question are well resolved and that reliable results should be possible with the use of energy discrimination. In each correlation, singles were taken in both channels before and after the coincidence measurements to ascertain chance coincidence rates and to monitor drift in the equipment. A number of runs were taken for each correlation and a weighted average obtained after correction for decay, chance coincidences, and source asymmetry. The methods of analysis were essentially those described by Rose,[8] Klema and McGowan.[9] From the data, a least-squares fit was made of the function

$$W(\theta)=a+bP_2(\cos\theta)+cP_4(\cos\theta).$$

Finite size of the detectors necessitated correction for solid angle. These were made following the method outlined by Rose.[8]

0.815 – 1.60 Mev Correlation

The correlation between $\gamma_1-\gamma_3$ was measured with both channels set to accept the energy interval which included the γ_3 photopeak and the γ_1 photopeak. As can be seen in Fig. 2, this setting increased the coincidence efficiency without including any significant portion of the scintillation spectrum due to any other gamma rays. The analysis of the data resulted in the following function:

$$W(\theta)=1+0.0367P_2-0.025P_4,$$
$$[W(180°)-W(90°)]/W(90°)=+0.037\pm0.004.$$

1.60 – 0.490 Mev Correlation

The $\gamma_1-\gamma_2$ angular correlation was measured with one channel set to accept the γ_1 photopeak and a portion

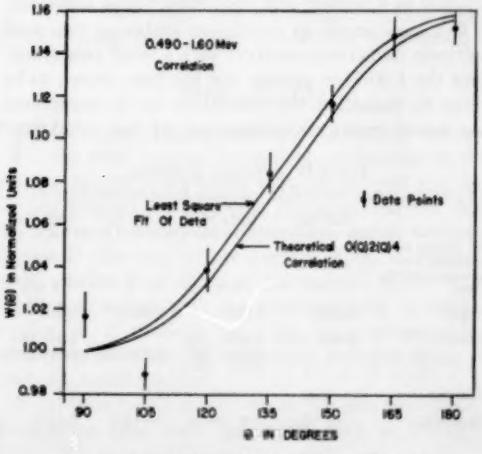

FIG. 5. Directional correlation of the 0.490- and 1.60-Mev radiations.

[8] M. E. Rose, Phys. Rev. **91**, 610 (1953).
[9] E. D. Klema and F. K. McGowan, Phys. Rev. **91**, 616 (1953).

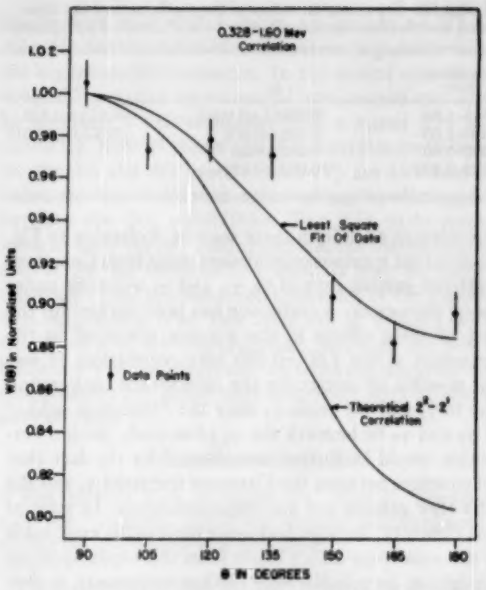

FIG. 6. Directional correlation of the 0.328- and 1.60-Mev radiations. A similar function was obtained for the angular correlation between 0.328- and the 0.490-Mev gamma rays.

of its Compton distribution, with the second channel accepting the higher side of the photopeak of γ_2. The latter setting was adopted to eliminate the effects of the weak 0.438-Mev gamma ray which was also in coincidence with γ_1. Allowance was made for the coincidences between the 1.60-Mev gamma ray and the Compton distribution of γ_3 lying under the γ_2 photopeak. The fractional number of such background coincidences was determined by extrapolation from the coincidence curve of Fig. 2 and subtracted from the data. The correction obtained in this way should be valid since the correlation described in the previous section is almost isotropic. The resulting correlation function for the $\gamma_1-\gamma_3$ cascade is

$$W(\theta)=1+0.106P_2-0.013P_4.$$

From the plot of this function shown in Fig. 5, it may be seen that the anisotropy is 0.167 ± 0.004.

0.328 – 1.60 Mev Correlation

With the channel width of one discriminator adjusted symmetrically over the photopeak of γ_4 and the other set to accept the photopeak of γ_1, as well as a portion of its Compton distribution, the angular correlation of this cascade was found to be of the form

$$W(\theta)=1-0.081P_2.$$

A plot of this function is shown in Fig. 6.

Measurements involving this cascade are not as clear-cut as the preceding ones, since the background

TABLE III. Experimental values of the coefficients of the directional correlation function $W(\theta)=1+A_2P_2(\cos\theta)+A_4P_4(\cos\theta)$.

Correlation (Mev)	A_2	A_4
0.815–1.60	0.00367±0.0054	−0.025±0.020
0.490–1.60	0.106±0.024	−0.0013±0.0019
0.328–1.60	−0.081±0.03	...
0.328–0.490	−0.092±0.020	...

coincidences arise from three sources. Reference to Fig. 2 shows that spurious coincidences result from Compton-scattered gamma rays of γ_3, γ_2, and γ_5 which lie under the γ_4 photopeak. A correction has been applied for the first of these effects in the manner described in the discussion of the 1.60−0.490 Mev correlation. It was not possible to correct for the coincidence background due to γ_2 and the weak γ_5 since the "Compton peaks" of γ_5 and γ_2 lie beneath the γ_4 photopeak. Such a correction would be further complicated by the fact that coincidences between the Compton scattered γ_2 and the 1.60-Mev gamma ray are angle-dependent. In spite of this difficulty, the sign and lower limit to the magnitude of the anisotropy which result from this experiment are thought to be reliable. Any further corrections, if they could be applied, would tend to make the measured anisotropy even more negative since the greatest contribution to the correction would come from the positive angle dependence of the $\gamma_1-\gamma_2$ coincidences.

Since a considerable number of Compton-scattered gamma rays accompanied these measurements, it might be argued that crystal-to-crystal scattering which would predominate at the 90° setting could account for the negative anisotropy. To check on this effect, a series of measurements of the well-known angular correlation of Co^{60} were made in such a way as to simulate the Compton scattering conditions which prevailed in the Ce^{140} experiment. The gamma rays of Co^{60} have energies which are in the range of the 1.60- and 0.815-Mev radiations of Ce^{140} and thus give rise to a scintillation Compton distribution which is similar to that of γ_1 and γ_3. With the differential discriminator set to accept only Compton-scattered gamma rays of Co^{60} in the 0.3–0.15 Mev region, i.e., in the range of γ_3, γ_4, and γ_5, the well established 0–2–4 correlation was obtained. It is believed, therefore, that crystal-to-crystal scattering was not present in any of the Ce^{140} experiments.

0.328−0.490 Mev Correlation

In measuring the $\gamma_2-\gamma_4$ correlation, the first and second discriminators were set on the photopeaks of the 0.328- and 0.490-Mev gamma rays, respectively. After analysis, the following correlation function was obtained:

$$W(\theta)=1-0.092P_2.$$

The same perturbations which were present in the preceding correlation are present in this case as well. Again, corrections for these effects tend to make the correlation function more negative. There is in addition, the effect of the presence of γ_1 comptons under γ_2 which together with γ_4 are rise to a negative correlation. Although correction for this effect would attenuate the observed negative anisotropy, it is felt that this perturbation is much smaller than those due to the other background contributions. As in the previous case, the experiment therefore yields the proper sign and lower limit to the magnitude of the correlation.

Table III summarizes the results of all of the directional correlation experiments. The errors indicated are statistical and do not take account of possible systematic or instrumental effects.

DISCUSSION

The experimental value of the angular correlation between the 1.60- and 0.490-Mev gamma rays is seen from Fig. 5 to agree with the theoretical 0–2–4 distribution to be expected for the first and second excited states of even-even nuclei. The estimates of α_K and the K/L ratio listed in Table IV support the $E2$ assignment for both gamma rays. Furthermore, the logft values (Table II) of the two beta groups leading to these levels from the decay of La^{140} are both in the first forbidden range, in accordance with these assignments and the spin and parity of the La^{140} ground state. The characterization of these radiations as listed in the last row of Table IV appears quite certain.

The 0.815−1.60 Mev correlation measurement is expected to be the most reliable since no correction for extraneous coincidences was necessary. The very small positive anisotropy cannot be interpreted as an attenuation of the correlation due to external field effects, since the $\gamma_1-\gamma_2$ correlation which involves the same intermediate state does not exhibit such "washing out." Therefore, the correlation cannot lead to a 0–2–4 sequence as Robinson and Madansky[10] have suggested. In fact, no theoretical correlation involving two pure multipole transitions results in such a small anisotropy. Since the 1.60-Mev gamma ray has been shown to be a pure $E2$ transition, the correlation can be interpreted if a mixed multipole assignment of the 0.815-Mev

TABLE IV. Summary of results.

	1.60 Mev	0.815 Mev	0.490 Mev	0.328 Mev
Spin change as obtained from angular correlation	2	2 or 1	2	0 or 1
α_K(exp.)	0.0008	0.0041	0.0073	0.031
α_K(theor.)	0.0007 ($E2$)	0.0028 ($E2$) 0.0044 ($M1$) 0.025 ($M3$)	0.010 ($E2$)	0.031 ($E2$) 0.044 ($M1$)
K/L(exp.)	high	high	7.4	7.4
K/L(emp.)	~10 ($E2$)	~8 ($M1$ or $E2$)	7.5 ($E2$)	8 ($M1$) 5 ($E2$)
Assignment	$E2$	$M1+E2$	$E2$	$M1$ or $M1+E2$

[10] B. L. Robinson and L. Madansky, Phys. Rev. 84, 1067 (1951).

transition is assumed. A mixing ratio of 1.8–3 percent for $E2/M1$ or 36 percent for $M3/E2$ fits the measured distribution according to assignments of 3+ or 4+, respectively, for the 2.42-Mev level.[11] Of the two possibilities, the estimated α_K listed in Table IV seems to favor the $E2-M1$ mixture. No assignment other than 3+ or 4+ is consistent with the experimental evidence. Assignment of 3+ or 4+ is in fair agreement with the logft values of $\beta 3$ given in Table II.

The two angular correlations involving the 0.328−1.60 and the 0.328−0.490 Mev gamma-ray pairs, although subject to uncertainty in magnitude, serve to corroborate the foreoing interpretation. The theoretical anisotropies to be expected for these correlations, when the spins of the levels are successively 0–2–4–3, are *negative* for both and are both given by[11]

$$W(\theta)=1-0.140P_2.$$

For the case 0–2–4–4, *positive* anisotropies are expected with the following correlation applying to both pairs:

$$W(\theta)=1+0.197P_2.$$

[11] L. C. Biedenharn and M. E. Rose, Revs. Modern Phys. **25**, 729 (1953).

In the first case (0–2–4–3), an assignment of $M1$ or $E2+M1$ for the 0.328-Mev transition is possible from the experimental correlation. In the second case (0–2–4–4), the negative experimental anisotropies can only be obtained if this transition is of a mixed $E2-M1$ character. Rose's[12] theoretical K conversion coefficients for the $E2$ and $M1$ cases (Table IV) are too close in value for the estimated value of α_K to distinguish between the two possibilities. The K/L ratio would seem to favor the $M1$ assignment and the corresponding spin of 3+ for the 2.42-Mev level. It may be further mentioned that the measured intensities of the gamma rays originating from this level are in keeping with either a 3+ or 4+ configuration. Although the possibility of 4+ is not eliminated by these experiments, the configuration 3+ seems more in keeping with all of the data of Table IV.

ACKNOWLEDGMENTS

The authors wish to thank Dr. Milo B. Sampson and the cyclotron group for several bombardments during the initial stages of this work.

[12] Rose, Goertzel, Spinrad, Harr, and Strong, Phys. Rev. **83**, 79 (1951).

PHYSICAL REVIEW VOLUME 99, NUMBER 1 JULY 1, 1955

Supermultiplets and Spin Dependent Forces*

R. W. KING
Nuclear Data Project, National Research Council, Washington, D. C.
(Received February 23, 1955)

A tentative explanation for a group of favored negatron transitions from nuclei with $N-Z=3$ is proposed on the basis of a deviation from the supermultiplet formalism due to spin-dependent forces. The experimental evidence is exhibited and discussed.

1. INTRODUCTION

THE supermultiplet formalism[1–4] provides, thus far, the most natural theoretical explanation of the striking empirical difference between favored and unfavored allowed β transitions. The empirical fact that the unfavored decays have transition matrix elements (squared) that are, on the average, about a hundred times smaller than those of the favored decays is in qualitative accord with the supermultiplet formalism insofar as it predicts that the only nonvanishing matrix elements are for transitions between states in the same supermultiplet.

Exceptions to the theory can be put into two classes. First, there exist some transitions, such as $P^{30}\rightarrow Si^{30}$, that should, according to the theory, be favored but the empirical evidence indicates that they are not. Second, there exists a small class of β transitions that should be unfavored and yet show remarkably low comparative half-lives. In particular, the supermultiplet formalism in the approximation of spin independence for nuclear forces does not permit superallowed *negatron* decay for odd-A nuclei with $A>3$. There is considerable experimental evidence from the decay of nuclei with $T_z=\frac{3}{2}$ to excited states of nuclei with $T_z=\frac{1}{2}$ that is contrary to such a restriction. It is the purpose of this note to exhibit this evidence and to propose an explanation. The point of view adopted is that the spin dependence of nuclear forces is the most likely reason for a breakdown of the usual restrictions of the supermultiplet formalism. It is shown that the experimental observations of fast negatron decay to excited states of stable odd-A nuclei with $A\lesssim 25$ can be qualitatively

* Supported by the U. S. Atomic Energy Commission.
[1] E. P. Wigner, Phys. Rev. **51**, 106 (1937).
[2] E. P. Wigner, Phys. Rev. **51**, 947 (1937).
[3] F. Hund, Z. Physik **105**, 202 (1937).
[4] E. P. Wigner, Phys. Rev. **56**, 519 (1939).

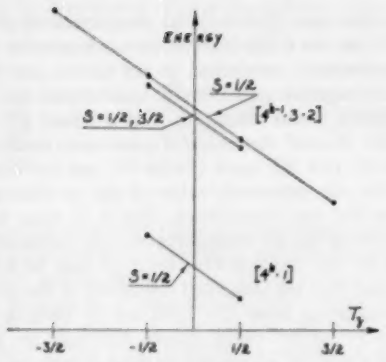

FIG. 1. Supermultiplet structure for nuclei with $A=4n+1$ or $A=4n+3$ in the approximation of spin-independent forces.

accounted for by interpreting the final states of the fast transitions as possessing components of quartet intrinsic spin states belonging to the same supermultiplet as the initial state but lower in energy because of spin-dependent forces.

2. SUPERMULTIPLET SPLITTING

In order to exhibit some of the effects of spin-dependent forces on the supermultiplets, we examine first the supermultiplet structure of odd-A nuclei under the assumption of spin-independent forces. Figure 1 gives a schematic diagram of two supermultiplets for nuclei with $A=4n+1$. The notation $[4^k\cdot 1]$ represents a core in which each space orbital has two neutrons and two protons and outside the core is one nucleon. The slope of the lines to the right is representative of Coulomb effects and accounts for positron decay within a supermultiplet after the neutron-proton mass difference has been overcome by the Coulomb energy difference. This slope to the right takes place for odd-A nuclei with $A>3$. Thus the usual criterion for super-allowed or favored-allowed β transitions (namely transitions within a supermultiplet) restricts these fast β transitions to positron decay or electron capture for odd-A nuclei with $A>3$, at least in the approximation of spin independence for nuclear forces.

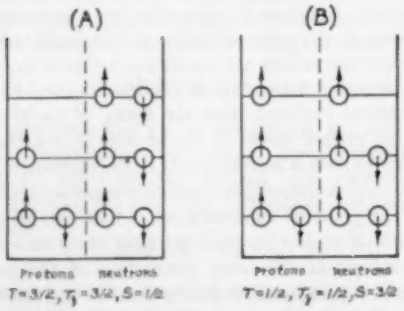

FIG. 2. Detailed structure of (A) a doublet and (B) a quartet intrinsic spin state of the $[4^{k-1}\cdot 3\cdot 2]$ supermultiplet.

As illustrated in Fig. 1, the $[4^{k-1}\cdot 3\cdot 2]$ supermultiplet contains charge multiplets with $T=\frac{1}{2}$ and $T=\frac{3}{2}$. While the states belonging to the $T=\frac{3}{2}$ charge multiplet are restricted to doublet intrinsic spin values ($S=\frac{1}{2}$), quartet values ($S=\frac{3}{2}$) are possible for $T=\frac{1}{2}$. Under the assumption of spin independence, the states ($T=\frac{3}{2}$, $T_z=\frac{1}{2}$, $S=\frac{1}{2}$), ($T=\frac{3}{2}$, $T_z=\frac{1}{2}$, $S=\frac{1}{2}$), and ($T=\frac{1}{2}$, $T_z=\frac{1}{2}$, $S=\frac{3}{2}$) belonging to the $[4^{k-1}\cdot 3\cdot 2]$ supermultiplet[5] correspond to a degenerate energy eigenvalue which exceeds the energy eigenvalue of the ($T=\frac{3}{2}$, $T_z=\frac{3}{2}$, $S=\frac{1}{2}$) state belonging to the same supermultiplet[6] by the Coulomb energy difference minus the neutron-proton mass difference. If, however, the detailed structure of the states is examined, it becomes clear that the known tendency for neutron and proton to favor the triplet intrinsic spin value is sufficient to account qualitatively for a lowering in energy of the $S=\frac{3}{2}$ states with respect to the $S=\frac{1}{2}$ states.

Figure 2 compares the detailed structure of the ($T=\frac{3}{2}$, $T_z=\frac{3}{2}$, $S=\frac{1}{2}$) state and the ($T=\frac{1}{2}$, $T_z=\frac{1}{2}$, $S=\frac{3}{2}$) state belonging to the $[4^{k-1}\cdot 3\cdot 2]$ supermultiplet. The distinguishing feature between the two states (and for that matter between (B) and any state with $S=\frac{1}{2}$ belonging to the $[4^{k-1}\cdot 3\cdot 2]$ supermultiplet) is that (B) possesses two more pairs of particles in triplet intrinsic spin states than does (A). If we denote the energy difference between a triplet and singlet state for a pair of particles in equivalent space orbits by $\Delta E_c(=)$ and that same difference for a second pair of particles in nonequivalent space orbits by $\Delta E_c(\neq)$, then the energy of the possible negatron decay between the two states of Fig. 2 can be expressed as

$$E_{\beta^-}=\Delta E_c(=)+\Delta E_c(\neq)-\Delta E_c, \qquad (1)$$

where ΔE_c is the Coulomb energy difference minus the neutron-proton mass difference. For the purposes of this discussion, ΔE_c can be approximated by the mass difference between the neutral atoms of two mirror nuclei with corresponding nuclear charge.

The term $\Delta E_c(=)$ can be estimated from odd-odd, $N=Z$ nuclei where the energy difference between the $T=0$, ground state and the lowest $T=1$, excited state is known. Although there are no direct measurements of $\Delta E_c(\neq)$, the tendency for odd-odd, $N\neq Z$ nuclei to favor triplet states speaks strongly for its positive value.

The considerations of this section can be applied in the same manner to the $A=4n+3$ decays from $T_z=\frac{3}{2}$ nuclei to $T_z=\frac{1}{2}$ nuclei (for example $C^{15}\rightarrow N^{15*}$). Thus, it can be expected that β^- transitions from nuclei having Z protons and $Z+3$ neutrons will take place to excited states of nuclei having $Z+1$ protons and $Z+2$ neutrons

[5] These states represent excited levels of nuclei such as Be^9, C^{13}, O^{17}, etc.

[6] This state represents the ground level of nuclei such as Li^9, B^{13}, N^{17}, etc.

with logft values characteristic of superallowed transitions[7] if

$$\Delta E_c < \Delta E_s(=) + \Delta E_s(\neq).$$

3. EXPERIMENTAL EVIDENCE

Table I lists the experimentally known decays of the type that fit the description given in Sec. 2. Also listed are the decays that are expected to be favored but have not been investigated or are of such small intensity as to be virtually unobservable.

The ft values are all in a slightly larger than image transition range but in a considerably smaller than unfavored range. The decay of F^{21} appears to offer the best chance of observing another favored transition. Its 5s half-life is good assurance that the transition is favored and the energy and intensity of the transition to the excited state of Ne^{21} are expected to be in the observable range. Although the $Na^{25} \rightarrow Mg^{25}$ decay *may* satisfy the conditions necessary to produce a favored transition, it seems unlikely that the intensity of the transition would be sufficient to detect even the γ following the decay (see Sec. 4).

TABLE I. Experimental evidence for favored negatron decay in nuclei with $A=4n+1$ or $A=4n+3$.[a]

A	Disintegration	Half-life (seconds)	E_{β^-} (Mev)	logft	$E_{\beta^-}+\Delta E_c$ (Mev)
9	$_3Li_6 \rightarrow {}_4Be_5^*$	0.17	7.3?	3.7	8.2
11	$_4Be_7 \rightarrow {}_5B_6^*$	particle unstable?			
13	$_5B_8 \rightarrow {}_6C_7^*$	particle unstable?			
15	$_6C_9 \rightarrow {}_7N_8^*$	2.4	3.5	3.6	5.7
17	$_7N_{10} \rightarrow {}_8O_9^*$	4.1	3.7	3.8	6.4
19	$_8O_{11} \rightarrow {}_9F_{10}^*$	29.4	2.9	4.3	5.7
21	$_9F_{12} \rightarrow {}_{10}Ne_{11}^*$	5			
23	$_{10}Ne_{13} \rightarrow {}_{11}Na_{12}^*$	40	1.2	3.8	4.7
25	$_{11}Na_{14} \rightarrow {}_{12}Mg_{13}^*$	62			

[a] For complete references see National Bureau of Standards Circular 499 (U. S. Government Printing Office, Washington, D. C., 1950), its supplements, and Nuclear Science Abstracts, Vol. 6, No. 24B (1952), Vol. 7, No. 24B (1953), Vol. 8, No. 24B (1954), and Vol. 9, No. 6B (1955).

4. CORRELATION OF EMPIRICAL EVIDENCE WITH PROPOSED INTERPRETATION

It is of interest now to correlate the values given in Table I with the proposed interpretation of these experimental results. Figure 3, shows a plot of $E_{\beta^-}+\Delta E_c = \Delta E_s(=)+\Delta E_s(\neq)$ against Z of the decaying nucleus, and also a plot of ΔE_c against Z of the decaying nucleus. This diagram demonstrates quite clearly why favored β^- transitions are not observed for $A \gtrsim 25$. The Coulomb energy difference becomes large enough to compete favorably with the energy gained by the quartet component of the final state. An extrapolated value for $E_{\beta^-}+\Delta E_c$ shows that the favored transition from Na^{25} would be of the order of 200 or 300 kev, and in view of the known complex β^- decay of Na^{25} with a highest energy component of ~3.7 Mev, it is expected that the favored transition would take place at most in only a few hundredths of a percent of the decays. It is thus not surprising that the favored transition from Na^{25} is, as yet, unobserved.

[7] Since $\Delta T \neq 0$, only Gamow-Teller matrix elements need be considered.

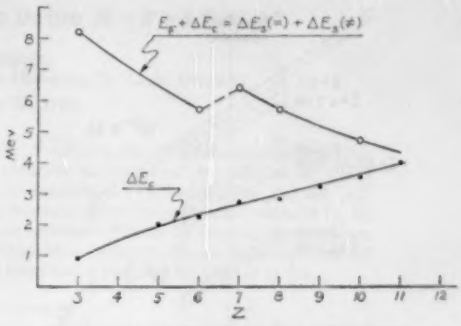

FIG. 3. Plot of $E_{\beta^-}+\Delta E_c$ and ΔE_c *vs* Z of the decaying nucleus.

It is too much to hope that the spin-dependent forces present in the nucleus are such as to permit both L and S to be good quantum numbers. We know, in fact, that this is not the case from the example of the deuteron. It is, however, reasonable to investigate the simple interpretation represented by Eq. (1) in order to determine the degree of approximation that it represents.

In Fig. 4 the values of $\Delta E_s(\neq)$ are plotted against Z of the decaying nucleus. The values of $\Delta E_s(\neq)$ have been obtained by identifying $\Delta E_s(=)$ with the energy difference between the $T=1$ and $T=0$ states of the "proper" odd-odd, $N=Z$ nucleus. It turns out that the "proper" odd-odd, $N=Z$ nucleus for both $A=4n+1$ and $A=4n+3$ decays has $A=4n+2$. For comparison a plot of $\Delta E_s(=)$ for the odd-odd, $N=Z$ nuclei is also included.

The values of $\Delta E_s(\neq)$ given in Fig. 4 are surprisingly large, but they show the same tendency to decrease with A as do the $\Delta E_s(=)$ values, and the striking feature is that $\Delta E_s(\neq)-\Delta E_s(=)$ remains at a roughly constant value of about 3 Mev. The apparent strong correlation between $\Delta E_s(=)$ and $\Delta E_s(\neq)$ speaks favorably for the model proposed. While the magnitude of

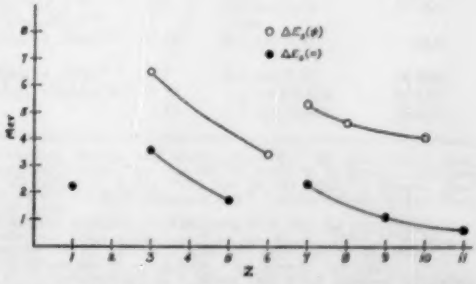

FIG. 4. Plot of $\Delta E_s(\neq)$ *vs* Z of the decaying nucleus and $\Delta E_s(=)$ *vs* Z of the appropriate $N=Z$, nucleus.

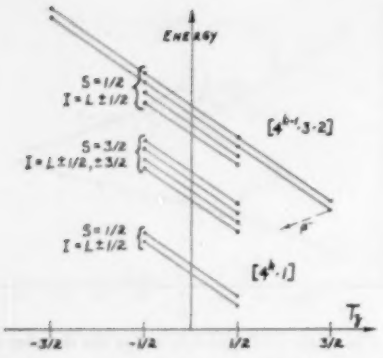

FIG. 5. Schematic representation of proposed supermultiplet splitting for nuclei with $A=4n+1$ or $A=4n+3$.

$\Delta E_s(\neq)$ strains belief, it is of some interest to speculate on the possible origin of such a difference between the two quantities. Considering the general form for a potential of the exchange type between pairs of particles, the terms that could give rise to the behavior exhibited in Fig. 4 must satisfy at least two requirements. (i) They must distinguish between singlet and triplet intrinsic spin states. (ii) They must distinguish between equivalent and nonequivalent space orbits in the sense of the supermultiplet formalism. Because of the $\sim$3 Mev difference involved, it seems reasonable to add to requirement (ii) the condition that the distinction between equivalent and nonequivalent orbits should be apparent in the exchange character and not just in the function of distance between the two particles. Two forces satisfy the above requirements—*the Heisenberg force* and *the tensor force with a Majorana exchange character*. The ordinary Wigner and Majorana forces are ruled out because they don't distinguish between triplets and singlets. The Wigner tensor force and the Bartlett force are ruled out because they don't distinguish between even and odd relative angular momentum states except in their dependence on the distance between particles.

Perhaps a more likely interpretation of the large values of $\Delta E_s(\neq)$ in Fig. 4 is the presence of an additional term in Eq. (1) which assists in lowering the final states of these fast β^- transitions. If in first approximation [the L-S approximation of Eq. (1) is schematically represented in Fig. 5] the supermultiplet is split due to spin-dependent forces, it is reasonable to assume that the same forces will couple doublet to quartet states producing further lowering of a $T_z=\frac{1}{2}$ state belonging to the $[4^{k-1}\cdot 3\cdot 2]$ supermultiplet. Such an interpretation is bolstered to some extent by Feenberg's calculations[3] of the beta-decay transition probabilities within the $[4^{k-1}\cdot 3\cdot 2]$ and $[4^{k-1}\cdot 2\cdot 1]$ supermultiplets. While the transition probabilities for Li^9, C^{15}, O^{19}, and Ne^{23} strongly suggest the predominance of quartet components in the final states of the fast β^- transitions, the decay of N^{17} makes apparent the need for a mixture of doublet and quartet components. However, in the absence of specific information as to whether the coupling of doublet and quartet states is such as to produce constructive or destructive interference terms in the transition probabilities, any specification of the final state is highly speculative.

We are in effect then forced to modify the model to permit the mixing of states within the same supermultiplet. This is neither surprising nor objectionable. A further modification of the model is of course required to explain the existence of unfavored-allowed transitions between different supermultiplets. This modification demands some mixing between different supermultiplets, but far less than that required to produce pure $j-j$ coupling if the empirical distinction between favored and unfavored transitions is to be explained. If the splitting of supermultiplets is according to the model proposed here, it is most likely that the admixtures to the $[4^k\cdot 1]$ and $[4^k\cdot 3]$ supermultiplets are the quartet states of the $[4^{k-1}\cdot 3\cdot 2]$ and $[4^{k-1}\cdot 2\cdot 1]$ supermultiplets respectively. An investigation is underway to determine if admixtures appropriate for the unfavored transitions will improve both the calculated magnetic moments for the $T_z=\frac{1}{2}$ nuclei and the image transition probabilities.

The author acknowledges with thanks the helpful conversations and correspondence he has had with E. Feenberg and D. C. Peaslee.

[3] Eugene Feenberg, following paper [Phys. Rev. **99**, 71 (1955)].

Superallowed Beta Transitions in the $N-Z=3$ Series*

EUGENE FEENBERG
Wayman Crow Laboratory, Washington University, St. Louis, Missouri
(Received February 28, 1955)

A number of fast beta transitions have been found in the $N-Z=3$ series of radioactive nuclides. King has suggested that some of these transitions (for $A<27$) occur within the lowest [4···421] or [4···432] supermultiplet; hence are superallowed (or favored). Matrix elements of $|\int\boldsymbol{\sigma}|^2$ within the [21] and [32] supermultiplets are computed with the aid of two-way displacement operators on the eigenvalues of T_3, S_z, and Y_{3z}. In the application to ${}_8O_{11}$ the only spin assignments consistent with an LS coupling interpretation of the fast transition are $I_i=5/2$, $I^*=\frac{1}{2}(S^*=\frac{1}{2})$. These are the value favored by the available experimental information. The jj coupling value of $|\int\boldsymbol{\sigma}|^2$ for the ${}_8O_{11}$ transition is too large by a factor of five.

1. INTRODUCTION

ALLOWED components with unusually small ft values have been found in the beta activity of ${}_3Li_8$, ${}_6C_9$, ${}_7N_{10}$, ${}_8O_{11}$, ${}_{10}Ne_{13}$, ${}_{11}Na_{14}$, and ${}_{12}Mg_{18}$. The available experimental information on the fast components is shown in Table I. King[1] has suggested that some of these transitions are superallowed[2] (or favored) in the sense that both final and initial states belong to the same supermultiplet (characterized by the partition symbol [4···421] or [4···432]). Figure 1 exhibits the essential qualitative features of King's interpretation based on Wigner's analysis of the supermultiplet into isobaric spin multiplets.[3] The orbital angular momentum L (a constant within the supermultiplet) couples with the spin angular momentum to give the following isobaric spin multiplets:

$$\begin{aligned}
&T=\tfrac{3}{2},\quad S=\tfrac{1}{2},\quad I=L-\tfrac{1}{2}(L>0),\quad L+\tfrac{1}{2},\\
&T=\tfrac{1}{2},\quad S=\tfrac{1}{2},\quad I=L-\tfrac{1}{2}(L>0),\quad L+\tfrac{1}{2},\\
&T=\tfrac{1}{2},\quad S=\tfrac{3}{2},\quad I=L-\tfrac{1}{2}(L>0),\quad L+\tfrac{1}{2},\\
&T=\tfrac{1}{2},\quad S=\tfrac{3}{2},\quad I=L-\tfrac{3}{2}(L>1),\quad L+\tfrac{3}{2}.
\end{aligned}\tag{1}$$

The quantum numbers $T=\frac{3}{2}$, $T_3=\frac{3}{2}$, $S=\frac{1}{2}$, $I_i=L+\frac{1}{2}$ or $L-\frac{1}{2}$ characterize the initial state. Spin-dependent forces are held responsible for displacements in energy making possible a transition within the supermultiplet from $T=T_3=\frac{3}{2}$ to $T=T_3=\frac{1}{2}$ as pictured in Fig. 1. In the following discussion the Gamow-Teller (G-T) matrix elements for all possible final states are evaluated using the pure supermultiplet description of nuclear states. Interesting correlations are observed when these results are compared with experiment. A comparison with corresponding matrix elements computed under the assumption of jj coupling throws light on the type of intermediate coupling existing in light nuclides.

* Supported in part by the joint program of the U. S. Atomic Energy Commission and the Office of Naval Research.

[1] R. W. King, Bull. Am. Phys. Soc. No. 7, 20 (1954), and preceding paper [Phys. Rev. **99**, 67 (1955)]; see also E. P. Wigner, Proceedings of the International Conference on Theoretical Physics, Kyoto and Tokyo, September, 1953 (Science Council of Japan, Tokyo, 1954).

[2] E. P. Wigner, Phys. Rev. **56**, 519 (1939).

[3] E. P. Wigner, Phys. Rev. **51**, 106 and 948 (1937).

2. UPPER LIMITS ON THE GAMOW-TELLER MATRIX ELEMENTS

The Gamow-Teller matrix element,

$$|\int\boldsymbol{\sigma}|^2=\sum_{m_f}|(\alpha_f I_f m_f;\tfrac{1}{2},\tfrac{1}{2}|\textstyle\sum\boldsymbol{\sigma}_k Q_k|\alpha_i I_i m_i;\tfrac{3}{2},\tfrac{3}{2})|^2,\tag{2}$$

is a function of the initial and final values of S, L, and T. An upper limit on $|\int\boldsymbol{\sigma}|^2$ for any choice of these quantum numbers can be computed by forming the sum

$$\sum_{\text{all}}|\int\boldsymbol{\sigma}|^2=\sum_f|(\alpha_f I_f m_f;T_f,\tfrac{1}{2}|\textstyle\sum\boldsymbol{\sigma}_k Q_k|\alpha_i I_i m_i;\tfrac{3}{2},\tfrac{3}{2})|^2,\tag{3}$$

in which *all* denotes a summation over all possible final states within the supermultiplet. The application of closure to the right-hand member of Eq. (3) yields

$$\begin{aligned}
\sum_{\text{all}}|\int\boldsymbol{\sigma}|^2&=(\alpha_i I_i m_i;\tfrac{3}{2},\tfrac{3}{2}|\textstyle\sum\boldsymbol{\sigma}_k Q_k^*\cdot\sum\boldsymbol{\sigma}_l Q_l|\alpha_i I_i m_i;\tfrac{3}{2},\tfrac{3}{2})\\
&=6(\alpha_i I_i m_i;\tfrac{3}{2},\tfrac{3}{2}|T_3|\alpha_i I_i m_i;\tfrac{3}{2},\tfrac{3}{2})\\
&=9.
\end{aligned}\tag{4}$$

Equation (A4) of the appendix is used to reduce the matrix element occurring in Eq. (4) to the explicit numerical value.

TABLE I. Low ft transitions in the $N-Z=3$ series.

Transitions	Energy (Mev)	Partial half-life	ft
${}_3Li_8\rightarrow{}_4Be_5^*$ [a]	(7.3±1)	0.17 sec	(2000–10 000)
${}_6C_9\rightarrow{}_7N_8^*$ [b]	3.5	2.4 sec	3000–4000
${}_7N_{10}\rightarrow{}_8O_9^*$ [c]	3.8	4.2 sec	6300
${}_8O_{11}\rightarrow{}_9F_{10}^*$ [d]	2.9	29.4 sec/0.70	21 000
${}_9F_{12}\rightarrow{}_{10}Ne_{11}^*$ [e]	···	5 sec	···
${}_{10}Ne_{13}\rightarrow{}_{11}Na_{12}^*$ [f]	1.18	40.2 sec/0.07	6800
${}_{11}Na_{14}\rightarrow{}_{12}Mg_{13}^*$ [d]	2.7	58.2 sec/0.45	56 000
${}_{12}Mg_{18}\rightarrow{}_{13}Al_{14}^*$ [g]	1.59	9.5 min/0.414	60 000
	1.75	9.5 min/0.582	56 000

[a] Gardner, Knable, and Moyer, Phys. Rev. **83**, 1054 (1951); Holt, Thorn, and Waniek, Phys. Rev. **87**, 378 (1952); R. K. Sheline, Phys. Rev. **87**, 557 (1952); W. F. Fry, Phys. Rev. **89**, 325 (1953); D. Reagan, Phys. Rev. **92**, 651 (1943); F. Ajzenberg and T. Lauritsen, Revs. Modern Phys. **27**, 77 (1955).

[b] Richard, Hudspeth, and Clendenin, Phys. Rev. **90**, 1272 (1954).

[c] Stephens, Halpern, and Sher, Phys. Rev. **82**, 511 (1951); L. W. Alverez, Phys. Rev. **75**, 1127 (1949); E. Hayward, Phys. Rev. **75**, 917 (1941).

[d] E. Bleuler and W. Zunti, Helv. Phys. Acta **20**, 195 (1947).

[e] E. C. Campbell and C. V. Strain, Oak Ridge National Laboratory Report ORNL, 1496, 1952 (unpublished).

[f] H. Brown and V. Perez-Mendez, Phys. Rev. **78**, 812 (1950).

[g] Daniel, Koester, and Mayer-Kuckuk, Z. Naturforsch. **8a**, 447 (1953).

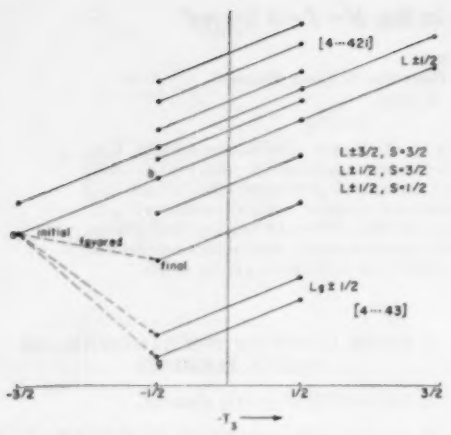

FIG. 1. Supermultiplet interpretation of a fast beta transition by an $N-Z=3$ parent nucleus. The initial state belongs to the lowest $[4\cdots421]$ supermultiplet. Spin-dependent forces split the supermultiplet into widely spaced isobaric spin multiplets. A transition within the supermultiplet then becomes energetically possible.

The $T=\frac{1}{2}$ final states may be selected by introducing the projection operator

$$P=\tfrac{1}{2}(15/4-\mathbf{T}^2) \tag{5}$$

as a factor multiplying $\sum \boldsymbol{\sigma}_k Q_k$ on the left. In this way the sum over all final states with $T=\frac{1}{2}$ is reduced to

$$\begin{aligned}\sum_{T_f=\frac{1}{2}}|f\boldsymbol{\sigma}|^2&=\sum_{\text{all}}|fP\boldsymbol{\sigma}|^2\\&=(\alpha_i I_i I_i;\tfrac{3}{2},\tfrac{3}{2}|\textstyle\sum\boldsymbol{\sigma}_k Q_k^*\cdot P\sum\boldsymbol{\sigma}_l Q_l|\alpha_i I_i I_i;\tfrac{3}{2},\tfrac{3}{2})\\&=(\alpha_i I_i I_i;\tfrac{3}{2},\tfrac{3}{2}|\,(15/2)T_3-2(T_3-1)(\mathbf{T}^2-T_3)\\&\quad-(4/3)(Y_{3x}^2+Y_{3y}^2+Y_{3z}^2)|\alpha_i I_i I_i;\tfrac{3}{2},\tfrac{3}{2})\qquad(6)\\&=8,\end{aligned}$$

with the help of Eqs. (A4) and (A5) of the appendix and the relation

$$Y_{3x}^2+Y_{3y}^2=(Y_{3x}-iY_{3y})(Y_{3x}+iY_{3y})+S_z. \tag{7}$$

To select quartet final states, the preceding calculation may be repeated employing the projection operator

$$P=\tfrac{1}{3}(\mathbf{S}^2-\tfrac{3}{4}). \tag{8}$$

Then

$$\begin{aligned}\sum_{S_f=\frac{3}{2}}|f\boldsymbol{\sigma}|^2&=\sum_{\text{all}}|fP\boldsymbol{\sigma}|^2\\&=(\alpha_i I_i I_i;\tfrac{3}{2},\tfrac{3}{2}|\textstyle\sum\boldsymbol{\sigma}_k Q_k^*\cdot P\sum\boldsymbol{\sigma}_l Q_l|\alpha_i I_i I_i;\tfrac{3}{2},\tfrac{3}{2})\\&=(\alpha_i I_i I_i;\tfrac{3}{2},\tfrac{3}{2}|\,(6T_3-8)P+4T_3-2|\qquad(9)\\&\qquad\qquad\times\alpha_i I_i I_i;\tfrac{3}{2},\tfrac{3}{2})\\&=4.\end{aligned}$$

3. EXPLICIT EVALUATION OF THE GAMOW-TELLER MATRIX ELEMENTS

The third line of Eq. (A4) is easily transformed into the matrix element relation:

$$\begin{aligned}&[2(T-1)]^{\frac{1}{2}}(\beta_f;T-1,T-2|Y_{1u}-iY_{2u}|\beta_i;T,T-1)\\&\quad-[2T]^{\frac{1}{2}}(\beta_f;T-1,T-1|Y_{1u}-iY_{2u}|\beta_i,T,T)\\&\qquad=2(\beta_f;T-1,T-1|Y_{3u}|\beta_i;T,T-1).\end{aligned}\tag{10}$$

Also

$$\begin{aligned}&\frac{(\beta_f;T-1,T-2|Y_{1u}-iY_{2u}|\beta_i;T,T-1)}{(\beta_f;T-1,T-1|Y_{1u}-iY_{2u}|\beta_i;T,T)}\\&\qquad=\frac{(T\,1\,T-1|T\,1\,T-1\,T-2)}{(T\,1\,T-1|T\,1\,T-1\,T-1)}=\left(\frac{T-1}{T}\right)^{\frac{1}{2}}.\end{aligned}\tag{11}$$

Equations (10) and (11) combine to give

$$\begin{aligned}&(\beta_f;T-1,T-1|Y_{1u}-iY_{2u}|\beta_i;T,T)\\&\quad=-(2T)^{\frac{1}{2}}(\beta_f;T-1,T-1|Y_{3u}|\beta_i;T,T-1).\end{aligned}\tag{12}$$

Equation (12) may be combined with well-known sum rules[4] to express $|f\boldsymbol{\sigma}|^2$ in the convenient forms:

$$|f\boldsymbol{\sigma}|^2_{I_i=I,\,I_f=I-1}=2TI\,|(\alpha_f,I-1,I-1;T-1,T-1|Y_{3z}|\alpha_i;I,I-1;T,T-1)|^2, \tag{13a}$$

$$|f\boldsymbol{\sigma}|^2_{I_f=I_i=I>0}=2T[(I+1)/I]\,|(\alpha_f,I,I;T-1,T-1|Y_{3z}|\alpha_i;I,I;T,T-1)|^2, \tag{13b}$$

$$|f\boldsymbol{\sigma}|^2_{I_i=I,\,I_f=I+1}=2T\frac{(I+1)(2I+3)}{2I+1}\,|(\alpha_f,I+1,I;T-1,T-1|Y_{3z}|\alpha_i;I,I;T,T-1)|^2. \tag{13c}$$

Similar formulas have been used to evaluate the G-T matrix element in the important special cases $T_i=T_f=\frac{1}{2}$ and $T_i=1$.[5]

The $_2He_4$ transition provides an interesting application for Eq. (13c). Let ψ_a and ψ_b denote the unique normalized wavefunctions belonging to $T=1$, $T_3=0$, $S=S_z=0$ and $T=T_3=0$, $S=1$, $S_z=0$ respectively. The commutator of $\mathbf{S}^2$ and Y_{3z} applied to ψ_a yields the eigenvalue equation:

$$\mathbf{S}^2(Y_{3z}\psi_a)=2(Y_{3z}\psi_a). \tag{14}$$

Similarly, Eq. (A5) of the Appendix requires

$$\mathbf{T}^2(Y_{3z}\psi_b)=2(Y_{3z}\psi_b). \tag{15}$$

[4] E. U. Condon and G. H. Shortley, *The Theory of Atomic Spectra* (Cambridge University Press, Cambridge, 1935), Chap. 3; E. Feenberg and G. E. Pake, *Quantum Theory of Angular Momentum* (Addison-Wesley Press, Cambridge, 1953), Chap. 5.

[5] M. Bolsterli and E. Feenberg, Phys. Rev. 97, 736 (1955).

Consequently,

$$Y_{3z}\psi_a=\lambda\psi_b, \quad Y_{3z}\psi_b=\lambda'\psi_a. \tag{16}$$

The relation

$$(a|Y_{3z}|b)=\lambda'(a,a)=\lambda(b,b) \tag{17}$$

implies $\lambda'=\lambda$ since ψ_a and ψ_b are normalized. Furthermore the eigenvalues of Y_{3z} are ± 1;[5] the corresponding eigenfunctions are given by suitable linear combinations of ψ_a and ψ_b:

$$Y_{3z}(a\psi_a+b\psi_b)=\pm(a\psi_a+b\psi_b), \tag{18}$$

or

$$a\lambda=\pm b, \quad b\lambda=\pm a \tag{19}$$

yielding

$$\lambda=1 \quad \text{or} \quad -1. \tag{20}$$

Thus, the squared matrix element appearing in the right hand member of Eq. (13c) has the value 1 in the ${}_2He_4$ transition; consequently $|\int\boldsymbol{\sigma}|^2=6^2$.

In the general case, the matrix elements of Y_{3z} occurring in Eq. (13) can be expressed in terms of reduced matrix elements and Racah functions.[6] The Eckart-Wigner theorem yields

$$\begin{aligned}&(I_f m;\, T_f,T_3|\, Y_{3z}|\, I_i,m;\, T_i,T_3)\\&=(2I_f+1)^{-\frac{1}{2}}(I_f;\, T_f,T_3\|\, Y_3\|\, I_i;\, T_i,T_3)\\&\qquad\times(I_i\,1\;m\;0|\,I_i\,1\;I_f\;m),\end{aligned} \tag{21}$$

$$\begin{aligned}&(S_f,m_s;\, T_f,T_3|\, Y_{3z}|\, S_i,m_s;\, T_i,T_3)\\&=(2S_f+1)^{-\frac{1}{2}}(S_f;\, T_f,T_3\|\, Y_3\|\, S_i;\, T_i,T_3)\\&\qquad\times(S_i\,1\;m_s\;0|\,S_i\,1\;S_f\;m_s),\end{aligned} \tag{22}$$

expressing matrix elements of Y_{3z} in terms of reduced matrix elements and vector addition coefficients. The Racah function appears in the relation

$$\begin{aligned}&(I_f;\, T_fT_3\|\, Y_3\|\, I_i;\, T_iT_3)\\&=(-1)^{L-1-S_i-I_f}[(2I_f+1)(2I_i+1)]^{\frac{1}{2}}\\&\quad\cdot(S_f;\, T_fT_3\|\, Y_3\|\, S_i;\, T_iT_3)W(S_fI_fS_iI_i;\, L,1),\end{aligned} \tag{23}$$

and also in the derived formula

$$\begin{aligned}&(I_f,m;\, T_f,T_3|\, Y_{3z}|\, I_i,m;\, T_i,T_3)\\&=(-1)^{L-1-S_i-I_f}[(2I_i+1)(2S_f+1)]^{-\frac{1}{2}}\\&\quad\cdot(S_f,m_s;\, T_f,T_3|\, Y_{3z}|\, S_i,m_s;\, T_i,T_3)\\&\quad\times W(S_fI_fS_iI_i;\, L,1)\frac{(I_i\,1\;m\;0|\,I_i\,1\;I_f\;m)}{(S_i\,1\;m_s\;0|\,S_i\,1\;S_f\;m_s)}\end{aligned} \tag{24}$$

expressing the matrix element of Y_{3z} in the Im space in terms of the much simpler matrix element in the Sm_s space.

In the present application we need a number of vector addition coefficients $(I_i\,1\;m\;0|\,I_i\,1\;I_f\;m)$ for $m=\frac{1}{2}(I_i+I_f-|I_i-I_f|)=I_i$ or I_f whichever is smaller:

$$\begin{aligned}&\frac{I_i}{L+\frac{1}{2}}\quad\frac{I_f}{L+\frac{1}{2}}\quad\frac{(I_i\,1\;m\;0|\,I_i\,1\;I_f\;m)}{[2L+1/2L+3]^{\frac{1}{2}}},\\&L+\tfrac{1}{2}\quad L-\tfrac{1}{2}\quad-\left[\frac{2L}{(L+1)(2L+1)}\right]^{\frac{1}{2}},\\&L-\tfrac{1}{2}\quad L+\tfrac{1}{2}\quad[2/2L+1]^{\frac{1}{2}}.\end{aligned} \tag{25}$$

The following Racah functions are also needed:

$$\begin{aligned}&W(\tfrac{1}{2},L+\tfrac{1}{2},\tfrac{1}{2},L+\tfrac{1}{2};L,1)=\tfrac{1}{2}\left[\frac{2L+3}{3(L+1)(2L+1)}\right]^{\frac{1}{2}},\\&W(\tfrac{1}{2},L-\tfrac{1}{2},\tfrac{1}{2},L+\tfrac{1}{2};L,1)=[3(2L+1)]^{-\frac{1}{2}},\\&W(\tfrac{1}{2},L+\tfrac{1}{2},\tfrac{1}{2},L-\tfrac{1}{2};L,1)=[3(2L+1)]^{-\frac{1}{2}},\\&W(\tfrac{1}{2},L-\tfrac{1}{2},\tfrac{1}{2},L-\tfrac{1}{2};L,1)=\tfrac{1}{2}\left[\frac{2L-1}{3L(2L+1)}\right]^{\frac{1}{2}},\\&W(\tfrac{3}{2},L-\tfrac{1}{2},\tfrac{1}{2},L+\tfrac{1}{2};L,1)=-\tfrac{1}{2}\left[\frac{2L-1}{6(L+1)(2L+1)}\right]^{\frac{1}{2}},\\&W(\tfrac{3}{2},L+\tfrac{1}{2},\tfrac{1}{2},L-\tfrac{1}{2};L,1)=\tfrac{1}{2}\left[\frac{2L+3}{6L(2L+1)}\right]^{\frac{1}{2}},\\&W(\tfrac{3}{2},L+\tfrac{1}{2},\tfrac{1}{2},L+\tfrac{1}{2};L,1)=-\left[\frac{L}{6(L+1)(2L+1)}\right]^{\frac{1}{2}},\\&W(\tfrac{3}{2},L+\tfrac{3}{2},\tfrac{1}{2},L+\tfrac{1}{2};L,1)=-\tfrac{1}{2}[2(L+1)]^{-\frac{1}{2}},\\&W(\tfrac{3}{2},L-\tfrac{3}{2},\tfrac{1}{2},L-\tfrac{1}{2};L,1)=\tfrac{1}{2}[2L]^{-\frac{1}{2}},\\&W(\tfrac{3}{2},L-\tfrac{1}{2},\tfrac{1}{2},L-\tfrac{1}{2};L,1)=\left[\frac{L+1}{6L(2L+1)}\right]^{\frac{1}{2}}.\end{aligned} \tag{26}$$

Two quantities remain to be evaluated:

$$\begin{aligned}K&\equiv(\tfrac{1}{2},\tfrac{1}{2};\,\tfrac{1}{2},\tfrac{1}{2}|\,Y_{1z}-iY_{2z}|\,\tfrac{1}{2},\tfrac{1}{2};\,\tfrac{3}{2},\tfrac{3}{2})\\&=-3^{\frac{1}{2}}(\tfrac{1}{2},\tfrac{1}{2};\,\tfrac{1}{2},\tfrac{1}{2}|\,Y_{3z}|\,\tfrac{1}{2},\tfrac{1}{2};\,\tfrac{3}{2},\tfrac{1}{2}),\\K'&\equiv(\tfrac{3}{2},\tfrac{3}{2};\,\tfrac{1}{2},\tfrac{1}{2}|\,Y_{1z}-iY_{2z}|\,\tfrac{1}{2},\tfrac{1}{2};\,\tfrac{3}{2},\tfrac{3}{2})\\&=-3^{\frac{1}{2}}(\tfrac{3}{2},\tfrac{1}{2};\,\tfrac{1}{2},\tfrac{1}{2}|\,Y_{3z}|\,\tfrac{1}{2},\tfrac{1}{2};\,\tfrac{3}{2},\tfrac{1}{2}).\end{aligned} \tag{27}$$

Let

$$\begin{aligned}&\psi_a\equiv\psi_{\frac{1}{2},\frac{1}{2};\,\frac{1}{2},\frac{1}{2}},\\&\psi_b\equiv\psi_{\frac{1}{2},\frac{1}{2};\,\frac{1}{2},-\frac{1}{2}}=3^{-\frac{1}{2}}(T_1-iT_2)\psi_a,\\&\psi_c\equiv\psi_{\frac{1}{2},-\frac{1}{2};\,\frac{1}{2},\frac{1}{2}},\\&\psi_d\equiv\psi_{\frac{1}{2},-\frac{1}{2};\,\frac{1}{2},-\frac{1}{2}}\\&\quad=12^{-\frac{1}{2}}(S_z-iS_y[(Y_{1z}-iY_{2z})+i(Y_{1y}-iY_{2y})]\psi_a.\end{aligned} \tag{28}$$

[6] G. Racah, Phys. Rev. **62**, 438 (1942) and **63**, 367 (1943).

TABLE II. Formulas for $|f\boldsymbol{\sigma}|^2$.

I_i	S_f	I_f	$\lvert f\boldsymbol{\sigma}\rvert^2$
$L+\frac{1}{2}$	$\frac{1}{2}$	$L+\frac{1}{2}$	$\frac{4}{3}\frac{2L+3}{2L+1}$
		$L-\frac{1}{2}$	$\frac{8}{3}\frac{2L}{2L+1}$
$L+\frac{1}{2}$	$\frac{3}{2}$	$L+\frac{1}{2}$	$2\frac{L+2}{L+1}$
		$L+\frac{1}{2}$	$\frac{4}{3}\frac{2L}{2L+1}$
		$L-\frac{1}{2}$	$\frac{2}{3}\frac{L(2L-1)}{(L+1)(2L+1)}$
$L-\frac{1}{2}$	$\frac{1}{2}$	$L+\frac{1}{2}$	$\frac{8}{3}\frac{2L+2}{2L+1}$
		$L-\frac{1}{2}$	$\frac{4}{3}\frac{2L-1}{2L+1}$
$L-\frac{1}{2}$	$\frac{3}{2}$	$L+\frac{1}{2}$	$\frac{2}{3}\frac{(L+1)(2L+3)}{L(2L+1)}$
		$L-\frac{1}{2}$	$\frac{4}{3}\frac{2L+2}{2L+1}$
		$L-\frac{3}{2}$	$2\frac{L-1}{L}$

Now

$$\begin{aligned}(b|Y_{1x}-iY_{2x}|a)&=3^{-\frac{1}{2}}(a|(T_1+iT_2)(Y_{1x}-iY_{2x})|a)\\&=3^{-\frac{1}{2}}(a|2Y_{3x}|a)=3^{-\frac{1}{2}},\\(d|Y_{1x}-iY_{2x}|a)&=12^{-\frac{1}{2}}(a|\{(Y_{1x}+iY_{2x})\\&\quad-i(Y_{1y}+iY_{2y})\}(S_x+iS_y)(Y_{1x}-iY_{2x})|a)\\&=12^{-\frac{1}{2}}(a|4T_3-4S_z|a)=-(4/3)^{\frac{1}{2}}.\end{aligned}\tag{29}$$

Also, by closure,

$$\begin{aligned}&|(b|Y_{1x}-iY_{2x}|a)|^2+|(c|Y_{1x}-iY_{2x}|a)|^2\\&\quad+|(d|Y_{1x}-iY_{2x}|a)|^2\\&\qquad=(a|(Y_{1x}+iY_{2x})(Y_{1x}-iY_{2x})|a)\\&\qquad=(a|2T_3|a)=3.\end{aligned}\tag{30}$$

Consequently,

$$\begin{aligned}|(c|Y_{1x}-iY_{2x}|a)|^2&=3-\tfrac{1}{3}-4/3\\&=4/3.\end{aligned}\tag{31}$$

Thus,

$$K^2=K'^2=4/3.\tag{32}$$

Explicit calculations with three-particle wave functions provide an instructive check on this bit of operator algebra.

The final formulas for $|f\boldsymbol{\sigma}|^2$ are collected in Table II. Some numerical values are exhibited in Table III.

4. DISCUSSION

In the decay of ${}_8O_{11}$, the assignments $I_i=5/2$, $I_f=\frac{3}{2}$ are strongly favored by the experimental evidence on beta and gamma transitions involving these states.[7] As the last column of Table III shows, these are the only assignments consistent with an LS coupling interpretation of the initial and final states. Also, $S_f=\frac{3}{2}$ is favored in agreement with King's argument based on energetic considerations. The good agreement may be illusory since two effects tending to change $|f\boldsymbol{\sigma}|^2$ are certainly present. These are (i) the occurrence of a doublet component in the (assumed) predominently quartet final state and (ii) the mixing of supermultiplets. Both effects are expected to occur as consequences of the spin dependent interaction responsible for the separation of the supermultiplet into energetically distinct isobaric spin multiplets. The first effect may either increase or decrease $|f\boldsymbol{\sigma}|^2$ while the second is likely to decrease it.

In jj coupling, the $(d_{\frac{5}{2}})^3$ configuration yields[8]

$$|f\boldsymbol{\sigma}|^2=28/25,\quad I_i=5/2,\quad I_f=\tfrac{3}{2}.$$

Thus

$$ft|f\boldsymbol{\sigma}|_{jj}^2=23\,000,$$

too large by a factor of 5.

In general, a wide range of values of the nuclear matrix element is possible depending on the relative amplitudes and phases of the doublet and quartet components in the final state wave function.

The transitions at $A=25$ and 27 may be excluded from the superallowed category, because they are only slightly faster than an average allowed transition and also because the energies fall outside the fairly regular

TABLE III. Numerical results.

Transition	L	I_i	S_f	I_f	$\lvert f\boldsymbol{\sigma}\rvert^2$	$ft\lvert f\boldsymbol{\sigma}\rvert^2$
${}_8O_{11}\rightarrow{}_9F_{10}{}^*$	2	5/2	1/2	5/2	28/15	37 000
$ft=21\,000$				3/2	32/15	45 000
			3/2	7/2	8/3	56 000
				5/2	16/15	22 000
				3/2	4/15	5600
${}_7N_{10}\rightarrow{}_8O_9{}^*$	1	1/2	1/2	3/2	32/9	22 000
$ft=6300$				1/2	4/9	2800
			3/2	3/2	20/9	14 000
				1/2	16/9	11 000
${}_{12}Mg_{13}\rightarrow{}_{13}Al_{14}{}^*$	0	1/2	1/2	1/2	4	2.4×10^5
$ft=6\times10^5$			3/2	3/2	4	2.4×10^5

[7] Jones, Phillips, Johnson, and Wilkinson, Phys. Rev. **96**, 547 (1954).

[8] E. Feenberg, *The Shell Theory of the Nucleus* (Princeton University Press, Princeton, 1955), Chap. 8.

decreasing trend exhibited by the transitions in lighter members of the $N-Z=3$ series.

APPENDIX

The function space covered by a supermultiplet is transformed into itself by the set of operators[3]:

$$\begin{aligned} S_u &= \tfrac{1}{2}\sum \sigma_u^{(k)}, \quad (u=x,y,z), \\ T_v &= \tfrac{1}{2}\sum \tau_v^{(k)}, \quad (v=1,2,3), \\ Y_{vu} &= \tfrac{1}{2}\sum \tau_v^{(k)}\sigma_u^{(k)}. \end{aligned} \tag{A1}$$

In terms of these operators,

$$\begin{aligned} \sum Q_k &= T_1 - iT_2, \\ \sum Q_k^* &= T_1 + iT_2, \\ \sum \sigma_u^{(k)} Q_k &= Y_{1u} - iY_{2u}, \\ \sum \sigma_u^{(k)} Q_k^* &= Y_{1u} + iY_{2u}. \end{aligned} \tag{A2}$$

A number of useful commutation relations obeyed by the S, T, Y operators are listed below:

$$\begin{aligned} [T_1 \pm iT_2, T_3] &= \mp(T_1 \pm iT_2), \\ [T_1 \pm iT_2, Y_{3u}] &= \mp(Y_{1u} \pm iY_{2u}), \end{aligned} \tag{A3}$$

$$\begin{aligned} [T_1 + iT_2, T_1 - iT_2] &= 2T_3, \\ [Y_{1u} \pm iY_{2u}, T_3] &= \mp(Y_{1u} \pm iY_{2u}), \\ [Y_{1u} \pm iY_{2u}, Y_{3u}] &= \mp(T_1 \pm iT_2), \\ [Y_{1u} \pm iY_{2u}, T_1 \mp iT_2] &= \pm 2Y_{3u}, \\ [Y_{1u} + iY_{2u}, Y_{1u} - iY_{2u}] &= 2T_3, \\ [Y_{1x} \pm iY_{2x}, Y_{1y} \mp iY_{2y}] &= 2iS_z, \\ [Y_{1x} \pm iY_{2x}, S_y] &= i(Y_{1z} \pm iY_{2z}), \end{aligned} \tag{A4}$$

$$\begin{aligned} &[\mathbf{S}^2, Y_{1x} \pm iY_{3x}] \\ &= -2(Y_{1x} \pm iY_{3x}) + 2i[S_x(Y_{1y} \pm iY_{3y}) \\ &\qquad - S_y(Y_{1x} \pm iY_{2x})] \\ &= 2(Y_{1x} \pm iY_{2x}) + 2i[(Y_{1y} \pm iY_{2y})S_z \\ &\qquad - (Y_{1z} \pm iY_{2z})S_y], \end{aligned} \tag{A5}$$

$$\begin{aligned} &[\mathbf{T}^2, Y_{1x} \pm iY_{3x}] \\ &= \mp 2(T_1 \pm iT_2)Y_{3x} + 2(\pm T_3 - 1)(Y_{1x} \pm iY_{2x}) \\ &= \mp 2Y_{3x}(T_1 \pm iT_2) + 2(Y_{1x} \pm iY_{2x})(\pm T_3 + 1). \end{aligned}$$

The exact analogy between the 1,2,3 and x,y,z spaces yields an image relation for every one set down in Eqs. (A3) to (A5). Thus, for example, the next to the last line of Eq. (A4) translates into

$$[Y_{1x} \pm iY_{1y}, Y_{2z} \mp iY_{2y}] = 2iT_3.$$

Two-way displacement operators have the property of displacing two eigenvalues in the set T_3', S_z', Y_{3z}' up or down by one unit while leaving the third unchanged. These operators are defined as follows in terms of two valued indices u, v, w which take on values $+1$ and -1 independently:

$$\begin{aligned} M_{uvo} &= (Y_{1x} + iuY_{2x}) + iv(Y_{1y} + iuY_{2y}), \\ M_{uow} &= (T_1 + iuT_2) + uw(Y_{1z} + iuY_{2z}), \\ M_{ovw} &= (S_x + ivS_y) + vw(Y_{3x} + ivY_{3y}). \end{aligned} \tag{A6}$$

The basic commutation relations are

$$[M_{uvo}, T_3] = -uM_{uvo}, \tag{A7}$$

$$[M_{uvo}, S_z] = -vM_{uvo}, \tag{A7}$$

$$[M_{uvo}, Y_{3z}] = 0,$$

$$[M_{uow}, T_3] = -iuM_{uow}, \tag{A8}$$

$$[M_{uow}, S_z] = 0, \tag{A8}$$

$$[M_{uow}, Y_{3z}] = -wM_{uow},$$

$$[M_{ovw}, T_3] = 0, \tag{A9}$$

$$[M_{ovw}, S_z] = -vM_{ovw}, \tag{A9}$$

$$[M_{ovw}, Y_{2z}] = wM_{ovw},$$

$$[M_{u,v,o}, M_{o,-o,w}] = 2uvwM_{uow}, \tag{A10}$$

$$[M_{u,o,w}, M_{-u,v,o}] = 2uvwM_{ovw}, \tag{A10}$$

$$[M_{o,v,w}, M_{u,o,-w}] = 2uvwM_{uvo}, \tag{A10}$$

$$[M_{uvo}, M_{u'v'o}] = (vT_3 + uS_z)(u-u')(v-v'), \tag{A11}$$

$$[M_{uow}, M_{u'ow'}] = (wT_3 + uY_{3z})(u-u')(w-w'), \tag{A11}$$

$$[M_{ovw}, M_{ov'w'}] = (wS_x + vY_{3z})(v-v')(w-w'). \tag{A11}$$

One of these displacement operators is used in constructing ψ_d in Eq. (28). The application of $M_{-1,1,0}$ to ψ_a transforms a solution with $T_3=\frac{1}{2}$, $S_z=\frac{1}{2}$ into one with $T_3=\frac{1}{2}$, $S_z=\frac{3}{2}$. Since $S_z=\frac{3}{2}$ is associated with $T=\frac{1}{2}$, the solution found in this manner belongs to $T=\frac{1}{2}$, $S=\frac{3}{2}$.

Nuclear Energy Level Fine Structure and Configuration Mixing

K. A. Brueckner, R. J. Eden,* and N. C. Francis
Indiana University, Bloomington, Indiana†

(Received March 2, 1955)

The departure of shell-model states from independent-particle states is investigated by means of transformation methods developed in previous papers. The starting point in this paper is the many-body Schrödinger equation for the nucleus in which the potential energy is assumed to arise from strong short-range two-body interactions. As a consequence the shell-model wave function cannot be a solution of this equation, however it can be related to the actual nuclear wave function by a suitably chosen transformation operator. This operator preserves the energy and angular momentum of low-lying nuclear states; hence it is possible to examine the splitting of energy levels in the shell model space. For a closed shell plus two or three particles this is shown to originate primarily from perturbations due to two-body interactions between the particles outside the shell. The methods used also give information about the nuclear wave function and provide some justification for the use of configuration mixing in determining nuclear magnetic moments. It is noted that the successes of configuration mixing based on two-body forces provide evidence that two-body correlations dominate over many-body correlations for many properties of the nucleus.

I. INTRODUCTION

THE independent-particle form of the shell model has had many successes in classifying the properties of nuclei in their ground states. These successes have suggested that small deviations from the predictions of the model, such as the departure of magnetic moments from the Schmidt lines and the splitting of energy levels, could be explained by introducing small perturbing interactions which modify the independent particle picture. Suggested interactions have been of two kinds, (1) particle-to-particle interaction usually, but not always, introduced for a small number of particles outside a closed shell, and (2) particle-to-surface coupling associated with collective motion of a core of nucleons.

At first sight it seems strange that nucleon-nucleon interactions, which appear to be strong in scattering experiments, should give rise to almost independent-particle motion in the shell model. It is perhaps even more strange that particle-to-particle interactions should be regarded as perturbations on the motion, since the model appears to require weak interactions and yet the perturbing interactions appear to be strong. In previous papers[1–3] transformation methods have been developed which relate the independent-particle model wave function to the actual wave function. In this paper the methods will be extended so that we can examine deviations from this model. In particular, we shall show that in certain approximations these deviations can be obtained by introducing particle-to-particle interactions to perturb the states of certain particles in the shell model. It should be noted that the approximations which are made do not require a weak interaction between nucleons; in fact the method which we use, even in lowest approximation, takes into account many of the strong correlations which exist in the nuclear wave function.

The general problem we wish to investigate concerns the energy level fine structure and the wave function for a nucleus which contains a few nucleons more than a closed-shell nucleus. In the independent-particle model an inert core is assumed which corresponds to the closed-shell nucleus. Then each energy level of the model will have a degeneracy arising from the different ways the angular momenta of particles outside the core can be combined to give the same total angular momentum. This degeneracy will be removed if a perturbing interaction between these particles is introduced. Such a perturbing interaction will also lead to mixing of different configurations and to modifications in the magnetic moment predicted by the model. The effects of these perturbations on the properties of the independent-particle model have been investigated by several authors,[4,5] and it is clear that these refinements of the independent-particle model represent an important step towards obtaining a model wave function which describes correctly low-energy properties of the nucleus.

The aim of this paper is to try to understand, in terms of the actual nuclear wave function, why it is that this modified independent-particle model is able to predict correctly certain nuclear properties, namely energy level splitting and magnetic moments. The starting point is the many-particle Schrödinger equation for the actual nucleus and we assume strong interactions between nucleons. The method for studying energy

* Smithson Research Fellow of the Royal Society, on leave of absence from Clare College, Cambridge, England.

† Supported in part by a grant from the National Science Foundation and the Office of Naval Research and the U. S. Atomic Energy Commission.

[1] Brueckner, Levinson, and Mahmoud, Phys. Rev. **95**, 217 (1954); K. A. Brueckner, Phys. Rev. **96**, 508 (1954); and K. A. Brueckner, Phys. Rev. **98**, 769 (1955).

[2] K. A. Brueckner and C. A. Levinson, Phys. Rev. **97**, 1344 (1955).

[3] R. J. Eden and N. C. Francis, Phys. Rev. **97**, 1366 (1955).

[4] Edmons, Flowers, and Elliott (to be published); M. H. L. Pryce, Proc. Phys. Soc. (London) **A65**, 773 (1952); D. Kurath, Phys. Rev. **91**, 1430 (1953); M. G. Redlich, Phys. Rev. **95**, 448 (1954); A. de-Shalit and M. Goldhaber, Phys. Rev. **92**, 1211 (1953); A. M. Lane (to be published).

[5] K. Ford and C. A. Levinson (to be published).

levels consists in expressing the energy of a nucleus which contains $A+2$ nucleons in terms of the energy levels of a nucleus having $A+1$ nucleons together with an additional energy. It is then shown that this additional energy can be expressed as an interaction energy if the following device is used. This device is to consider not the energy eigenvalues of the Schrödinger equation for the actual nuclei but instead the energy eigenvalues of nuclear models which are constructed to have the same energy and angular momentum as the actual nucleus for the states in which we are interested. We find that the models correspond in a certain approximation to particles moving outside an inert core.

Corresponding to a nucleus consisting of $A+1$ nucleons, we obtain a model made up of a single particle moving outside a core. There are correction terms to the energy which are small when the nucleus containing A nucleons is doubly magic (e.g., Ca^{40}), but these correction terms can be included if the energy levels of the model are taken to be the empirical energy levels of the actual nucleus. For the nucleus of $A+2$ nucleons (e.g., Ca^{42}), the model consists of two particles outside the core and we find that these particles interact both directly and via the core. The interaction via the core is found to be much smaller than the direct interaction. The energy levels without these interactions can be related to the energy levels of the single-particle-plus-core model and they are degenerate due to the different ways in which the angular momenta of the single-particle states can be combined. In our model the direct interaction term is diagonal in the states of the model so gives directly an energy shift for each state; these energy shifts serve to split the otherwise degenerate levels. We show that this level splitting is equivalent to the splitting which would be obtained by the methods of configuration mixing using a direct particle-to-particle interaction for the two particles outside the core.

In Sec. II we shall develop the consequences of an application of a simplified form of the general techniques which we have developed which is similar to the approximation used in previous papers[1] on the saturation problem. In Sec. III we shall discuss the structure and interpretation of the wave function and then show the extent to which the results of Sec. II can be related to the approximation methods of Flowers,[4] Pryce,[4] Kurath,[4] Redlich,[4] and Ford and Levinson.[5] In Sec. IV, we shall return to the exact formulation of the problem and show how various correction terms arise, what their physical significance is, and the extent to which they can be included in a simple approximation scheme following closely the methods developed in Sec. II. In Sec. V we calculate the core coupling energy for two particles outside a core interacting via the core particles. In Sec. VI we summarize our results and make some concluding remarks.

Finally we note that throughout the paper we will make use of the effect of the exclusion principle on the behavior of the particles in the nucleus and in the nuclear models. Mathematically, therefore, we should work with occupation numbers for the various states other than in terms of particle coordinates, but this would lead to a more complicated formalism and would obscure the physical discussion. Fortunately there is such a close correspondence[2] between the two methods that it is unnecessary to depart from the formulation in terms of particles, provided that we remember that the exclusion principle operates both in actual states and in intermediate states; this is the procedure adopted in this paper. It must be pointed out, however, that in actual evaluation it is necessary to make a translation from particle description to state description together with the appropriate introduction of second quantized operators.

II. DERIVATION OF ENERGY LEVEL SHIFTS IN THE COHERENT APPROXIMATION

In this section we will consider the energy levels of nuclei containing $A+1$, $A+2$, and $A+3$ nucleons. We will use an approximation which is similar to that used in reference 1, and we shall also assume that the nucleus containing A nucleons is doubly magic. These simplifications are not all necessary but are made so that we can more clearly state the main features of the method. A more detailed analysis of the approximations will be made in Sec. IV where it will be shown that the general conclusions are independent of a number of the simplifying assumptions made in the present section.

A. General Method

The Schrödinger equation for A nucleons is assumed to be

$$[\sum_{i=1}^{A} T_i+\sum_{i<j}^{A} v_{ij}]\Psi(A)=E\Psi(A). \tag{1}$$

We investigate the energy E for various numbers of nucleons, not by comparing the Schrödinger equations for the actual nuclei but by comparing the Schrödinger equations for nuclear models which are chosen to have the same energies as the actual nuclei.

The model wave function satisfies a Schrödinger equation,[3]

$$[\sum_{i=1}^{A} T_i+V_0]\Phi(A)=E\Phi(A), \tag{2}$$

and the relation between the actual nuclear wave function $\Psi(A)$ and the model wave function $\Phi(A)$ is

$$\Psi(A)=M\Phi(A), \tag{3}$$

where

$$M=1+(E-\sum_{1}^{A} T_i)^{-1}\sum_{i<j}^{A}{}' v_{ij}M, \tag{4}$$

and

$$V_0(A)=(\Phi(A),\sum_{i<j} v_{ij}M\Phi(A)). \tag{5}$$

The model wave function can be taken to be a product of single-particle wave functions,[3] each corresponding to

independent-particle motion. Thus the ground state of the model will be obtained by filling up the lowest independent-particle states according to the enclusion principle, giving a fully occupied "Fermi sea." We shall later require a model wave function which is the sum of products of independent-particle wave functions which is required to make it an eigenfunction of the total angular momentum, but for the present can be interpreted simply as a product.

To the approximation which we shall use in this section, the model operator M can be replaced by the operator F which is constructed from the following set of equations[2,3]:

$$F=1+\frac{1}{e}\sum_{i<j}^{A}{}'I_{ij}F_{ij}, \tag{6}$$

$$F_{ij}=1+\frac{1}{e}\sum_{m,n\neq i,j}{}'I_{mn}F_{mn}, \tag{7}$$

$$I_{mn}=\text{nondiagonal part of } t_{mn}, \tag{8}$$

$$t_{mn}=v_{mn}+v_{mn}\frac{1}{e}t_{mn}, \tag{9}$$

$$e=E-\sum_{i=1}^{A}T_i-\sum_{i<j}^{A}t_{eij}, \tag{10}$$

$$t_{cmn}=\text{diagonal part of } t_{mn}. \tag{11}$$

(The prime to the left of an operator indicates that matrix elements to the ground state are to be omitted.) The operators t_{ij} are the reaction matrices for the two-body interaction v_{ij} constructed in the nuclear medium; the t_{eij} are analogous to forward scattering amplitudes and the I_{ij} to incoherent scattering. The propagator "e^{-1}" describes the propagation of the nuclear particles in the nuclear medium with the effect of many-particle interactions appearing in the "potential" terms constructed from t_e.

The potential $V_0(A)$ for the model given by (5) can now be written

$$\begin{aligned}V_0(A)&=(\Phi(A),\sum_{i<j}^{A}v_{ij}F(\Phi)(A))\\&=(\Phi(A),\sum_{i<j}^{A}t_{ij}F_{ij}\Phi(A)).\end{aligned} \tag{12}$$

In deriving (12), terms of order $1/A$ compared with the leading term are neglected.[2,3] This expression for the potential can be expanded by means of (7) as a series in the incoherent reaction matrices I_{ij}. The first two terms of this series are

$$V_0(A)=(\Phi(A),\sum_{i<j}^{A}t_{ij}\Phi(A))+\sum_{i,j,k}\left(\Phi(A),I_{ij}\frac{1}{e}I_{jk}\frac{1}{e}I_{ki}\Phi(A)\right)+\cdots. \tag{13}$$

The justification for this series expansion comes essentially from the operation of the exclusion principle in the intermediate states of the last term of (13) and of higher order terms in the series; thus the intermediate states must lie above the occupied Fermi sea and this causes large energy denominators in the integrals. A more detailed and quantitative discussion of these "correction" terms will be made in Secs. IV and V. We will proceed now to consider a model for a nucleus containing $A+1$ nucleons and we make the approximation of taking for $V_0(A+1)$ only the leading term in the expansion corresponding to (13).

B. One Particle and Core

We consider the interaction of $A+1$ nucleons and separate the interaction energy into parts associated with one particle, with a core of A particles, and a remainder. The purpose of this separation is to facilitate comparison with the energies of $A+2$ and $A+3$ nucleon systems. As noted previously, we consider the energies of the corresponding nuclear models. The potential energy $V_0(A+1)$ for an $(A+1)$-nucleon system can be written down analogously to Eq. (5). It is (using primes to indicate quantities evaluated for the $A+1$ particle system)

$$V_0'(A+1)=V_0'(A)+V_1', \tag{14}$$

where $V_0'(A)$ is the potential energy of the A-particle core and V_1' is the potential energy of the $(A+1)$th particle in the field of the core.

$$V_1'=\sum_{i=1}^{A}(\Phi(A+1),t_{1i}'\Phi(A+1)). \tag{15}$$

The core potential energy V_0' is closely related to the core potential energy V_0, it is not exactly the same however for the following reasons: the addition of the $(A+1)$th particle changes the properties of the medium in which the core particles move. This change appears through a change in the core propagators e^{-1}, and also through a change in the nuclear volume. The latter effect is not explicitly present in the formalism we use, the former appears explicitly in the reaction matrices through the change

$$t_{ij}'=v_{ij}+v_{ij}\frac{1}{e'}t_{ij}', \tag{16}$$

where e' differs from e due to the presence of the $(A+1)$th particle,

$$e'=e+E_1-T_1-\sum_{i=1}^{A}t_{e1i}. \tag{17}$$

[A subscript "1" shown explicitly always denotes the $A(+1)$th particle.] We can see however that it is a reasonable approximation to neglect the difference between e' and e since the extra term $(E_1-T_1-\sum t_{e1i})$ gives zero when acting on the ground state of the

$(A+1)$th particle, thus any departures will only appear as higher order effects.

A second departure of the $A+1$ model from the A model arises from the change in radius of the model due to the presence of the extra particle. However this radius has to be chosen to minimize the total energy of the system so the core energy will not change to first order, and we will neglect the change here.

The aforementioned approximations will be investigated in more detail in Secs. IV and V where it will be shown that the neglected terms (1) appear to be small, and (2) they can be partly absorbed by taking empirical values for the single-particle energy levels. With these approximations, we find for the energy of the system of $A+1$ nucleons.

$$E(A+1)=E(A)+E_1, \tag{18}$$

where $E(A)$ is the energy of a nucleus containing A nucleons and E_1 is given by

$$E_1=V_1+(\Phi(A+1), T_1\Phi(A+1)), \tag{19}$$

$$V_1=\sum_{i=1}^{A}(\Phi(A+1), t_{1i}\Phi(A+1)). \tag{20}$$

We note that these formulas have been obtained by neglecting the following effects: (1) direct 3-particle (and higher order) couplings including third-order core polarization, (2) the change in the core propagators, (3) the change in the nuclear volume.

C. Two Particles and Core

We next consider a system of $A+2$ nucleons, which we will represent by two particles outside a core of A particles. We will try to express the energy of this system in a form equal to the sum of the energies of two particles moving without mutual interaction in the field of the core together with interaction terms which couple the two particles together and remove the degeneracy of energy levels of a system containing two noninteracting particles. The value of this form for the energy is that it facilitates comparison with the energy levels given by a single particle and a core.

The potential energy for the system of core-plus-two particles neglecting three- (or more) body correlations and also neglecting "$1/A$" terms, takes the form

$$V_0(A+2)=V_0''(A)+V_1''+V_2''+V_{12}'', \tag{21}$$

where

$$V_0''(A)=\sum_{i<j}^{A}(\Phi(A+2), t_{ij}''\Phi(A+2)), \tag{22}$$

and V_1'', V_2'' are given by expressions analogous to (20) but with the modified two-body reaction matrix t_{ij}''. The term V_{12}'' is defined by

$$V_{12}''=(\Phi(A+2), t_{12}''\Phi(A+2)). \tag{23}$$

The double primes indicate that the expressions are to be evaluated to include the effects of changes in core volume and core propagators such as those discussed for the system—one particle plus core, and the analogous changes associated with the extra two particles. These effects we will again neglect for the present and limit ourselves to noting the reasons why this is permissible: (1) the terms appear to be small as they involve three-body (or higher order) correlations which are reduced in magnitude by the operation of the exclusion principle and by other properties related to the closed-shell core, (2) some of the terms neglected here will be absorbed in the single-particle energy levels if empirical values of these are used when applying the methods, (3) the small energy shift coming from the core will not affect the relative spacing of the levels we consider. Hence we can drop the primes on the terms in (21), which means that the core energy becomes the energy of the Ath nucleus.

In this approximation the total energy of the system is

$$E(A+2)=E_1+E_2+V_{12}, \tag{24}$$

where the extra term in the energy is

$$V_{12}=(\Phi(A+2), t_{12}\Phi(A+2)). \tag{25}$$

This term will depend on the state of the two extra-core particles and thus will remove the degeneracy of the energy levels of the two particles moving without direct interaction in the field of the core.

To make this result more explicit, we next consider the form of the model wave functions $\Phi(A+2)$. Up to this point we have assumed this to be a product function; this, however, is not quite sufficient since it is not possible to form the correct functions of angular momentum in this way. We must instead choose the wave function so that it corresponds to a definite total angular momentum. We will for simplicity take the Ath nucleus to be a closed shell and assume that the model wave function $\Phi(A+2)$ is a product

$$\Phi(A+2)=\Phi(A)\phi(1,2), \tag{26}$$

where $\Phi(A)$ is a wave function for a zero angular momentum core. The outer two particles have a wave function which is the appropriate combination of shell-model wave functions to make up an eigenfunction of the total angular momentum. If for example, the state being filled by particles 1 and 2 have single-particle angular momentum j,j', then the wave function $\phi(1,2)$ will be (neglecting antisymmetrization)

$$\phi_J{}^m(1,2)=\sum_{m_1m_2} C(j, j', m_1, m_2|J, j, j', m) \times\phi_j{}^{m_1}(1)\phi_{j'}{}^{m_2}(2). \tag{27}$$

In this representation, the energy shifts given by V_{12} can be labeled by the total angular momentum, and are

$$\Delta E_{12}(J)=(\phi_J{}^m(1,2), t_{12}\phi_J{}^m(1,2)). \tag{28}$$

In Sec. IV we will consider further the interpretation of the energy shifts $\Delta E(J)$.

D. Three Particles and Core

The same techniques as those used in the preceding paragraphs can be applied to a nucleus containing $(A+3)$ nucleons. If the approximations associated with the closed-shell nucleus of A nucleons are still valid for three particles additional to the core, it will still be possible to neglect coupling via the core. However there will now be three-body correlations involving only the three outer particles and these must be taken into account in the fine structure related to the state of these three particles. Then we have to include part of the last term in (13) and the energy $E(A+3)$ will be given by

$$E(A+3)=E(A)+E_1+E_2+E_3+\langle(t_{c12}+t_{c23}+t_{c31})\rangle$$
$$+\left\langle\left(\frac{1}{e}I_{12}\frac{1}{e}I_{23}I_{31}\right)+\text{permutations}\right\rangle+\cdots. \quad (29)$$

The energy shift $\Delta E_s'$ for a given state $\phi_s(1,2,3)$ of the outer three particles is given by the last two terms of (29), where

$$\langle t_{c12}\rangle=(\phi_s(1,2,3),\, t_{12}\phi_s(1,2,3)), \quad (30)$$

$$\left\langle\frac{1}{e}I_{12}\frac{1}{e}I_{23}I_{31}\right\rangle$$
$$=\left(\phi_s(1,2,3),\, \frac{1}{e}I_{12}\frac{1}{e}I_{23}I_{31}\phi_s(1,2,3)\right). \quad (31)$$

In the next section we will consider the relation between this energy shift and that given by (28) for two particles outside a core.

III. INTERPRETATION OF THE WAVE FUNCTION; RELATION TO CONFIGURATION MIXING

In this section as in Sec. II we shall restrict ourselves to consideration of the simplified predictions of the coherent model. We shall first consider the nuclear wave function and its relation to the shell-model wave function. We will then consider the energy shifts derived in the previous section and show that these are equivalent to the energy shifts which would be the result of introducing a perturbing potential into the shell-model states.

A. Structure and Interpretation of the Wave Function

For simplicity we will consider a nucleus corresponding to one particle and a closed-shell core in the shell-model picture, since the problems we wish to discuss are all present in such a nucleus. In particular, we will discuss the relation between the nuclear wave function Ψ and the shell-model wave function Φ, and see how far the differences between the wave functions affect our interpretation of the model.

The most profound difficulty which prevents identification of Ψ with the independent-particle wave function Φ arises from the existence of strong short-range interactions between nucleons. As a consequence of these strong interactions a product wave function like Φ is nowhere near to being an approximate solution of the Schrödinger equation for the nucleus. Conversely, even for a closed-shell core it is not possible to write Ψ approximately as a product of a single-particle wave function and a core wave function and still have an approximate solution of the Schrödinger equation. Thus, if we write

$$\Psi(A+1)\doteq F_1\psi(1)\Psi(A), \quad (32)$$

we can obtain an approximate solution of the Schrödinger equation only by taking F_1 to be an operator of the form [see Eq. (6)]:

$$F_1=1+\frac{1}{e}\sum_{j=1}^{A}I_{1j}+\cdots. \quad (33)$$

Thus F_1 introduces correlations between the nucleon 1 and all the core nucleons through the incoherent operators I_{1j}. This means that $F_1\psi(1)$ appears to depend strongly on the state of the core nucleons, and cannot be simply regarded as a single-particle state. This contrasts with the shell-model interpretation that a particle outside a closed shell appears to move simply in a single-particle state (for the closed shells O^{16} and Ca^{40}).

The complicated relation between the extra nucleon and the core can be described as a polarizing effect on the core due to the strong short-range forces between the extra nucleon and the core nucleons. Therefore the nucleus would appear to consist not only of a symmetrical core plus a single-particle state but also will contain appreciable admixtures of higher excited states of the core and single particle.

We shall now attempt to relate this result to the predictions of the shell model for a "closed shell plus one" nucleus. There is no difficulty about the assignment of total angular momentum and parity, as these are invariant under the F_1 transformation. The principal difficulty of interpreting our result that the presence of the extra nucleon must lead to appreciable mixing between the single-particle and core states arises in connection with magnetic moments. If we are to avoid qualitative disagreement with experiment we must show at least that this mixing need not appreciably affect the magnetic moment.

We note first an essential difference between the Hamiltonian operator from which we deduced the mixing of states and the magnetic moment operator which seems to indicate the purity of states. The Hamiltonian is a very singular operator and slight departures from the true wave function will cause very

large deviations in the energy; in contrast, the magnetic moment operator is not singular and will be relatively insensitive to the use of an approximate wave function.

Since the magnetic moment does not depend on these very fine details of the wave function, it is sufficient to consider why it may be little affected by mixing of shell-model states, rather than trying to look at departures from the actual nuclear wave function. In the framework of the shell model the following argument has been pointed out to us by C. A. Levinson. An examination of the spins and parities of the core states of Ca^{40}, for example, shows that even if the actual wave function for 41 nucleons contains appreciable admixtures of excited core states, there will be no first order effects on the magnetic moment. This can be contrasted with the situation for the doubly magic Pb^{208} plus one nucleon where core admixtures are not only appreciable, but as has been shown by Blyn-Stoyle and Perks,[6] the mixture leads to first order corrections to the independent-particle magnetic moment, bringing it to a position approximately midway between the Schmidt lines. We note also that the foregoing argument is probably reinforced by various other special effects, including (for Ca^{40} or O^{16} plus one nucleon) the greater orthogonality of core and particle states and also the large denominators which reduce the influence of distant excited states.

The foregoing qualitative discussion indicates that it is not unreasonable to assume that the mixing of states which is required for the actual nuclear wave function to satisfy the Schrödinger equation may, for certain nuclei, have only a slight influence on the independent-particle magnetic moment. However, in using the methods discussed in the paper to compare neighboring nuclei, it would be very desirable to reinforce the aforementioned arguments that the magnetic moment of Ca^{41} should lie on the Schmidt lines by direct observation. Then one could use the empirical knowledge of the magnetic moment somewhat analogously to the empirical energy levels for predicting the properties of Ca^{42}.

We shall now proceed to consider the relation of the results of Sec. II to the methods of configuration mixing, and in our discussion we will assume that the single-particle states outside the core can be regarded as nucleon states to the extent that they have the same magnetic moments. *This does not imply that the particle states and nucleon states are not quite different with regard to other observables.*

B. Relation to Configuration Mixing

In Sec. II we have derived formulas for the energies of nuclei containing $A+1$, $A+2$, and $A+3$ nucleons in an approximation depending to some extent for its validity on the nucleus with A nucleons being a closed shell. These approximations have indicated that only the direct particle-to-particle interaction need be considered for the particles outside the core corresponding to the closed-shell nucleus. This particle-to-particle interaction leads to energy shifts in comparing the states of two and three particles outside the core with the corresponding one-particle states. These energy shifts have been derived in a form which we will now proceed to show is equivalent to the energy shift coming from introducing a perturbing potential into shell-model states.

We consider first the energy shift due to the mutual interactions for two particles moving in the average field of a core. The two-particle Schrödinger equation is

$$(H_0+v_{12})\psi=E\psi, \tag{34}$$

where

$$H_0=\sum_{i=1}^{2} T_i+\sum_{i=1}^{2} V_i, \tag{35}$$

and V_i denotes the effective core fields at the points x_i for the model. We compare this with the equation with v_{12} absent,

$$(H_0+\Delta E)\psi_0=E\psi_0. \tag{36}$$

Provided that

$$\Delta E=(\psi_0,v_{12}\psi), \tag{37}$$

the solutions are related by

$$\psi=\Omega\psi_0, \tag{38}$$

where the operator Ω is defined by the equation

$$\Omega=1+(E-H_0)^{-1\prime}v_{12}\Omega. \tag{39}$$

The energy shift ΔE is given by

$$\Delta E=(\psi_0,v_{12}\Omega\psi_0) \tag{40}$$

$$=(\psi_0,t\psi_0), \tag{41}$$

where

$$t=v_{12}+v_{12}(E-H_0)^{-1}t. \tag{42}$$

Consequently the energy shift ΔE given by (41) is the same as the energy shift ΔE_s given by (28) provided that (1) the potentials V_i in (35), are equal to the single-particle potentials given by (20), and (2) the shell model wave function ψ_0 in (41) is taken to be the same as the model wave function $\phi_s(1,2)$ in (28). With these potentials and wave functions we see that the transformation methods of Sec. II lead to an energy shift equal to that given by introducing a two-particle interaction into the shell model for two particles outside a closed shell.

In addition, the wave function ψ given by Eq. (38) can be explicitly constructed by solving Eq. (39) for the transformation operator Ω. This solution will give the admixtures of other states than the lowest independent-particle state on the wave function and can be used to determine for example the expectation value of the magnetic moment.

We consider next the formal derivation of the energy shift coming from the mutual interactions of three

[6] R. J. Blyn-Stoyle and M. A. Perks, Proc. Phys. Soc. (London) **A67**, 885 (1954).

particles moving in the average field of a core. For this system we take

$$H_0=\sum_{i=1}^{3} T_i+\sum_{i=1}^{3} V_i, \tag{43}$$

and we compare the equations

$$(H_0+\sum_{i<j}^{3} v_{ij})\psi=E\psi. \tag{44}$$

$$(H_0+\Delta E)\psi_0=E\psi_0. \tag{45}$$

Then the energy shift ΔE will be given correctly if the wave functions ψ and ψ_0 are related by

$$\psi=\Omega\psi_0=\{1+(E-H_0)^{-1}\sum v_{ij}\Omega\}\psi_0, \tag{46}$$

where Ω is defined by the set of equations

$$\Omega=1+(E-H_0)^{-1}\sum_{i<j}^{3} t_{ij}\Omega_{ij}, \tag{47}$$

$$\Omega_{ij}=1+(E-H_0)^{-1}\sum_{lm\neq ij} t_{lm}\Omega_{lm}, \tag{48}$$

$$t_{ij}=v_{ij}+v_{ij}(E-H_0)^{-1}t_{ij}, \tag{49}$$

and the energy shift is

$$\Delta E=(\psi_0,\sum_{i<j}^{3} v_{ij}\Omega\psi_0), \tag{50}$$

$$=(\psi_0,\sum_{i<j}^{3} t_{ij}\Omega_{ij}\psi_0), \tag{51}$$

$$=(\psi_0,\sum_{i<j}^{3} t_{ij}\psi_0)$$

$$+\sum_{i\neq j\neq k}^{3}\left(\psi_0, I_{ij}\frac{1}{(E-H_0)}I_{jk}\frac{1}{(E-H_0)}I_{ki}\psi_0\right)+\cdots, \tag{52}$$

where I_{ij} is as before the nondiagonal part of t_{ij}.

We see at once that this expression for ΔE corresponds to the series whose first two terms are equal to $\Delta E_s'$ given by the last two terms in (29). The leading term in (57) is simply a sum

$$\Delta E_s'''=(\phi_s(1,2,3),\{t_{12}+t_{23}+t_{31}\}\phi_s(1,2,3)). \tag{53}$$

This term can be identified by comparing it with the diagonal elements in the two-particle-plus-core system. The remaining terms in (52) or in (29) can be interpreted as arising from three-particle correlations, they are correction terms to the energy shifts for two-particle correlations which can be obtained from (53). Another way of stating this is that (53) allows for the same amount of configuration mixing in the three-particle system as in the two-particle system. An estimate of the relative importance of the three-particle correlations has been made by C. A. Levinson, who finds that taking diagonal matrix elements only in Ca^{42} [this corresponds to (53)] would lead to an error about 20 percent of the total shift predicted when all matrix elements of the interaction are considered. This can be regarded as some evidence in favor of the conclusion that two-body correlations dominate over the higher order effects.

IV. CORRECTIONS TO THE ENERGY SHIFTS OF THE COHERENT MODEL

In this section we shall make a more careful examination of the energy level fine structure in which we do not omit the various correction terms which were neglected in Sec. II. These corrections are of three types; (1) those which vanish as $1/A$ compared with the main terms in the energy, (2) those which arise from changes in the propagators as particles are added, and (3) those which arise from high-order correction terms in the energy expressions. The latter are the manifestation of third (and higher) order incoherent interaction among three (or more) particles and give the largest perturbation on the energy levels of the coherent model. We shall consider the cases of one, two, and three particles plus core and show how the corrections arise and to what extent they require changes in the formalism and interpretation of the results of Secs. II and III.

A. One Particle and Core

We consider first the interaction of a single particle with a core of A particles. The total potential energy of the system including the correction terms previously omitted is, to third order in the incoherent scattering matrices,

$$V_0(A+1)=(\Phi,\sum_{i<j} t_{ij}\Phi)+(\Phi,\sum_{i<j} I_{ij}F_{ij}\Phi)$$

$$-\left(\Phi,\sum_{i<j} I_{ij}\frac{1}{e}I_{ij}\frac{1}{e}I_{ij}\Phi\right), \tag{54}$$

where the first term is the "coherent" energy previously discussed in Secs. II and III, the second term arises from higher order incoherent terms in the energy, and the last term is a "$1/A$" correction to the total energy which can be neglected in determining the properties of the entire system but not necessarily in the fine structure of the energy levels. The sum over i, j is over all of the $A+1$ nucleons.

For convenience in comparing this expression for the energy of core plus one particle, we next break the sum up into two terms, one involving a sum only over the core particles and the remainder involving the extra particle. To make the separation possible, we take only the first nonvanishing term in the expansion of the second term of Eq. (54), i.e., we use

$$(\Phi,\sum_{i<j} I_{ij}F_{ij}\Phi)\doteq\left(\Phi,\sum_{ijk} I_{ij}\frac{1}{e}I_{jk}\frac{1}{e}I_{ki}\Phi\right), \tag{55}$$

where the restriction is to be imposed on this sum that $i\neq j\neq k$. It is now easy to carry out the desired separa-

tion into core and particle energies; we find for the core potential energy:

$$V_0(A)=(\Phi,\sum t_{ei}\Phi)+\sum\left(\Phi,I_{ij}\frac{1}{e}I_{jk}\frac{1}{e}I_{ki}\Phi\right)-\sum_{i,j,\text{core}}\left(\Phi,I_{ij}\frac{1}{e}t_{ei}\frac{1}{e}I_{ij}\Phi\right),\quad(56)$$

and for the potential energy of the extra particle in the field of the core

$$V_0(1)=(\Phi,\sum_{i,\text{core}}t_{1i}\Phi)+\sum_{ij,\text{core}}\left[\left(\Phi,I_{1i}\frac{1}{e}I_{ij}\frac{1}{e}I_{j1}\Phi\right)+\text{permutations}\right]-\sum_{i,\text{core}}\left(\Phi,I_{1i}\frac{1}{e}t_{ei}\frac{1}{e}I_{1i}\Phi\right).\quad(57)$$

In this expression for the energy of the extra particle, the first term represents the potential energy of the particle in the field of the core which is associated with coherent propagation without core excitation via the I_{ij} couplings; the second term involving the third-order combination of the I_{ij} couples the motion of particle 1 incoherently to the core with resulting excitation of the i,j pair in the core. These results are correct to all orders in the dominant coherent interaction and to third order in the incoherent interaction terms.

We note that the effects of all such correction terms as those we have considered here are automatically included if we use the empirical energy levels of the single particle plus core. Consequently the change in the formalism of Secs. II and III which arises from proper inclusion of the corrections gives rise to complication only if we wish to make a precise determination of the expected single-particle energy levels from first principles.

B. Two Particles and Core

We next consider two particles and a core and try to bring the expressions for the energy to a form in which the energies of the separate noninteracting nucleons in the field of the core is separated from the interaction terms coupling the two particles together. The latter terms act to remove the degeneracy in the energy levels of the noninteracting particles. This form for the total energy is particularly useful since it allows us to make use of the empirical observations of the one-particle levels to determine the principal contribution to the level positions and spacing.

As in the case of one extra-core particle, we start with the result for the potential energy:

$$V_0(A+2)=(\Phi',\sum_{i,j}t_{ei}'\Phi')+(\Phi',\sum_{i,j}{}'I_{ij}'F_{ij}'\Phi')-\left(\Phi',\sum_{ij}{}'I_{ij}'\frac{1}{e}t_{ij}'\frac{1}{e}I_{ij}'\Phi'\right),\quad(58)$$

where the primes indicate that in general (1) the wave function has changed as, for example, by a change in the nuclear volume and shape; (2) the primed sum over i, j includes the additional particle "2"; (3) the operators t_e' and I_{ij}' are changed from the similar operators in the one-particle case. Again we consider the last two terms as perturbations and replace in these the primed t' and I_{ij}' by the unprimed since the difference is of higher order than we are considering.

We evaluate first the principal term in the potential energy, the coherent potential energy. It is apparent in this that part of the energy shift compared with the one-particle case can come from the change in the wave function $\Phi\to\Phi'$. This effect, arising from volume and shape changes of the nucleus, has been qualitatively discussed in Sec. II. This effect is not obviously small since it can affect all of the A core particles. It also is extremely complicated in origin since it involves an understanding of the precise manner in which the core adjusts itself to the presence of the extra particle. Part of the net effect corresponds to a core polarization, but here we will examine only the effect of the change in the nuclear volume. Let us first consider the somewhat unphysical effect of fixing the nuclear volume of the A particles and adding the $(A+1)$th. The effect on the energy of this $1/A$ change on the volume per particle can be estimated from a knowledge of the rate of change of the total energy of the system with volume. It will be only a second order effect since the system saturates at the minimum of the energy *versus* density curve, and can be estimated using the saturation results of reference 1. For a nucleus of 40 nucleons it gives an energy shift for the entire nucleus which is approximately $\frac{1}{4}$ Mev. Thus the effect in this approximation is very small, furthermore it will result only in a uniform shift in all energy levels (at least those over a narrow region) and does not affect the relative level spacing which is our primary interest here.

The aforementioned argument can be reinforced if we observe the way in which the actual physical nucleus will react to the presence of an extra particle. The saturating character of the forces means that the core will change its density to keep the energy per particle constant; since the addition of the additional particle at fixed volume is equivalent to an increase in the density, the core will adjust itself to a radius sufficiently larger to compensate for the slight change in energy resulting from higher density. Consequently the already small (uniform) shift in the levels can be expected to be reduced further and can be neglected. Thus we shall in the following neglect the effects of changes in the core energy, but it will be noted that this is in no way the same as neglecting the interaction between the extra particle and the core.

In this approximation we need examine only the effects on the energy of the changed propagators in the

t_{ij}. We break the sum up into 3 terms,

$$\sum_{ij}' t_{cij}' = \sum_{ij,\text{core}} t_{cij}' + \sum_{i,\text{core}} (t_{ci1}' + t_{ci2}') + t_{12}'. \quad (59)$$

The first term in this sum is the very large core potential energy; we wish to see to what extent the core energy is affected by the simultaneous presence of two nucleons. A shift in the core energy arising from this effect would be equivalent to an additional particle-particle interaction arising from coupling through the core.

The change in t resulting from the presence of two particles is due to the change in the propagator; we have

$$t_{ij}' = v_{ij} + v_{ij}\frac{1}{e'}t_{ij}', \quad (60)$$

where

$$e' = e + e_1 + e_2 + e_{12}, \quad (61)$$

and

$$e = E_A - \sum_{i,\text{core}} T_i - \sum_{i<j,\text{core}} t_{cij}, \quad (62)$$

$$e_1 = E_1 - T_1 - \sum_{i,\text{core}} t_{ci1}, \quad (63)$$

$$e_{12} = E_{12} - t_{c12}. \quad (64)$$

We wish to relate this typical term in the core energy to the energy in the presence of only one particle for which a typical term is

$$t_{ij} = v_{ij} + v_{ij}\frac{1}{e+e_1}t_{ij}. \quad (65)$$

To develop the relation between t_{ij}' and t_{ij}, we note some simple properties of the propagators; first, we have written the total energy E of the system as a sum of energies

$$E = E_A + E_1 + E_2 + E_{12}, \quad (66)$$

where E_A is the energy of the undisturbed core, E_1 and E_2 are the total energies of particles 1 and 2, and E_{12} is the energy resulting from the interaction between particles 1 and 2. A consequence of this separation is that the term e_{12} will always be zero since the operators v_{ij} and t_{ij} act only on core particles, and t_{c12} which commutes with these operators gives E_{12} acting on the wave function of the system. We treat the remaining correction by expanding the propagator about the point where e_2 is zero, i.e., we use the identity

$$\frac{1}{e+e_1+e_2} = \frac{1}{e+e_1} - \frac{1}{e+e_1}e_2\frac{1}{e+e_1} + \cdots. \quad (67)$$

This separation is not yet complete since the second term contains in part the energy of the core in the presence of particle 2. A further expansion gives

$$\frac{1}{e+e_1+e_2} = \frac{1}{e+e_1} + \frac{1}{e+e_2} - \frac{1}{e} + \left\{\frac{1}{e}e_1\frac{1}{e}e_2\frac{1}{e} + (1\rightarrow 2)\right\}. \quad (68)$$

The last two terms then give rise to the lowest order shift in the core energy due to the simultaneous presence of two particles. Consequently we can write for the change in the core energy:

$$\Delta E = \sum_{ij}\left[v_{ij}\frac{1}{e}\left(\frac{1}{e}e_2\frac{1}{e}e_1 + \frac{1}{e}e_1\frac{1}{e}e_2\right)\frac{1}{e}t_{ij}\right]. \quad (69)$$

This term is of fourth order and therefore of higher order than the terms we have retained elsewhere; we still need to examine its structure, however, to show that the presence of the double sum over $A^2/2$ pairs of core particles does not result in an appreciable contribution to the energy.

The term e_1 can be written

$$e_1 = E_1 - T_1 - \sum_{k,\text{core}} t_{ck1}, \quad (70)$$

which vanished acting on the ground state. In addition, since v_{ij} and t_{ij} depend only on core particles, T_i commutes with them and has the value T_1^0 acting on the ground state. Thus we can write

$$e_1 = \sum_{k,\text{core}} [t_{ck1}^0 - t_{ck1}], \quad (71)$$

whereby t_{ij}^0 we mean the value that t_{ij} has acting on the ground state. We now observe that in a term such as

$$\sum_{ij} v_{ij}\frac{1}{e}\sum_k (t_{ck1}^0 - t_{ck1}), \quad (72)$$

the contribution will be zero unless i or j is equal to k, the operator t_{k1} otherwise commuting with v_{ij} to act on the ground state. Consequently the sum over i, j, k reduces to (we consider only one of the typical terms)

$$\sum_{ij} v_{ij}\frac{1}{e}(t_{ci2}^0 - t_{ci2})\frac{1}{e}(t_{ci1}^0 - t_{ci1})\frac{1}{e}t_{ij}. \quad (73)$$

The dependence on the total number of particles can now be estimated; each term in v_{ij} or t_{ij} introduces a factor $1/v$ (v the nuclear volume); the summation over a single intermediate state implied in the matrix product gives, when replaced by an integration, a factor of v. The double sum over core states gives a factor of A^2. Thus the dependence on A is of the form

$$A^2(v/v^2) \sim A^2/A^3 = 1/A, \quad (74)$$

which is the same as that of the principal energy splitting term $t_{ci2} \sim 1/A$. This additional correction term is of fourth order and in addition is small because of the cancellations occurring between t_c and t_c^0. Consequently, to the order we are calculating, we can neglect the change in the energy of the core due to the simultaneous presence of the two extra nucleons. The same arguments allow us to replace t_{ci1}' by t_{ci1} in Eq. (59).

The remaining smaller correction terms can be easily broken up into terms referring to the core and particle-

core and particle-particle interactions. Finally, combining the resulting terms which can be identified with the single-particle energies and calling them E_1 and E_2, we obtain for the energy of the A-plus-2-particle system

$$E(A+2)-E_1-E_2=t_{c12}-\left(\Phi, I_{12}\frac{1}{e}t_{c12}\frac{1}{e}I_{12}\Phi\right)$$
$$+\sum_{i,\text{core}}\left(\Phi,\left[I_{12}\frac{1}{e}I_{i2}\frac{1}{e}I_{i1}+\text{permutations}\right]\Phi\right), \quad (75)$$

which is correct to third order in the I_{ij} operators. The relative simplicity of this result is a consequence, of course, of the absorption of many of the complicated energy corrections into the single-particle energies. Each of the terms removing the degeneracy of the single-particle levels, i.e., the last three terms of Eq. (75), has the same dependence on the total number of particles, i.e., a $1/A$ dependence.

This result differs from the results of Sec. II almost entirely from the presence of the last term, the second term having a negligible effect on the energy. The last term is a coupling of particles 1 and 2 through the ith core particle, summed over the core. The resulting interaction will depend on the coordinates of particles 1 and 2 and in general be largest when the particles are close together. The interaction will also depend on the state of the core and of the extra-core particles. It can be expected to have a nonlocal character when expressed in coordinate space; in addition its spin and isotopic spin dependence will bear no simple relation to the two-body potential v_{12} which generates t_{12}. This term is in some sense analogous to the particle-particle coupling which, according to Bohr and Mottelson, is the result of interaction with the surface of the core. We shall in the next section carry out an explicit evaluation of the correction to the two-body interaction which arises from this type of particle-core coupling and show that its effect is very small.

We would now like to point out that insofar as the effects of a particle-core particle coupling can be replaced by those of an equivalent short-range two-body interaction, the net effect of the direct and core-particle interactions can be represented by a phenomenological 2-body potential. Consequently, a study of the energy-level fine structure which neglects the particle-core couplings and attempts to fit the experimental data in such an approximation will lead to an effective two-body potential which in general will differ (although possibly only slightly) from the free two-particle interaction. Stating this more recisely, if we combine all of the level splitting terms into one effective reaction matrix defined by

$$G_{c12}=t_{c12}-\left(\Phi, I_{12}\frac{1}{e}t_{c12}\frac{1}{e}I_{12}\Phi\right)$$
$$+\sum_{i,\text{core}}\left(\Phi, I_{12}\frac{1}{e}I_{2i}\frac{1}{e}I_{1i}+\text{permutations}\right), \quad (76)$$

then we can expect to find an approximately local "potential" g_{12} which will generate G_{12} according to the equation

$$G_{12}=g_{12}+g_{12}\frac{1}{e}G_{12}. \quad (77)$$

The effective potential g_{12} will then be expected to differ somewhat from v_{12}. As we shall see in the next paragraphs, the phenomenological introduction of such an effective potential to describe the net particle-particle coupling including core effects can be expected to lead to a considerable improvement in accuracy if an attempt is made to predict the energy levels of a three-particle-plus-core system making use of empirical knowledge of the core-plus-one-particle and core-plus-two-particle systems.

C. Three Particles and Core

The same techniques as those used in the preceding paragraphs can be used for the case of three extra-core particles. We shall not go through the details of the analysis since these very closely parallel the analysis of the one- and two-particle systems. The result is

$$E(A+3)=E_1+E_2+E_3+G_{c12}+G_{c13}+G_{c23}$$
$$+\left(\Phi, I_{12}\frac{1}{e}I_{23}\frac{1}{e}I_{31}\Phi\right)+\text{permutations}, \quad (78)$$

where the operators $G_{ci,j}$ are defined by equations similar to Eq. (77). Thus, if we proceed phenomenologically from the case of two extra-core particles to the three extra-core particle case, the only new terms which arise are the last of Eq. (78), those arising from incoherent coupling of the three extra-core particles. The effect of these new terms is relatively small, although not negligible, as has been pointed out in Secs. II and III. It also should be pointed out that these final correction terms in the three-particle case can be computed with sufficient accuracy from the "effective potentials" g_{ij} defined by Eqs. (76) and (77). Thus one can expect to get a high degree of accuracy in the final results if one not only uses the empirical energy levels in the one particle case but also determines the effective particle-particle coupling by examining the fine structure of the two-particle case. The errors in this procedure are quite small since they are of higher order than the leading (and dominant) terms we have considered.

V. EVALUATION OF PARTICLE-CORE COUPLING EFFECTS

We shall in this section determine the size of the correction terms defined in the previous section which originate in particle-core coupling. These terms are

$$\Delta E_{pc}=\sum_{i,\text{core}}\left[\left(\Phi, I_{12}\frac{1}{e}I_{2i}\frac{1}{e}I_{1i}\Phi\right)\right.$$
$$\left.+5\text{ permutations of }(12i)\right]. \quad (79)$$

In evaluating this correction to the interaction of particles 1, 2, we shall make certain simplifying assumptions which will allow us to make a fairly straight forward evaluation of the effect. These are: (1) the exclusion principle will be included only by requring that transitions occur to states above the Fermi limit and that particles interact only in allowed states of relative orbital momentum, (2) the wave function will be approximated by a degenerate Fermi gas of plane waves rather than the actual independent particle states of a spherical nucleus, and (3) the incoherence operators I_{ij} will be approximated by the incoherent Born approximation scattering from a Yukawa well with Serber exchange mixture. We will also approximate to the result by evaluating only a typical one of the six correction terms in Eq. (79) and multiplying the result by six.

We consider the first term of Eq. (79), written now explicitly in momentum space.

$$\Delta E_{pc}=\sum_{i,\text{core}}\sum_{\mathbf{k}_1'}\sum_{\mathbf{k}_2'}\sum_{\mathbf{k}_i'}(\mathbf{k}_1\mathbf{k}_2|I|\mathbf{k}_1'\mathbf{k}_2') \times\frac{1}{E_1+E_2-E_1'-E_2'}(\mathbf{k}_2'\mathbf{k}_i|I|\mathbf{k}_2\mathbf{k}_i') \times\frac{1}{E_1+E_i-E_1'-E_i'}(\mathbf{k}_1'\mathbf{k}_i'|I|\mathbf{k}_1\mathbf{k}_i). \quad (80)$$

For the I's, in the approximation described above, we have

$$(\mathbf{k}_3\mathbf{k}_4|I|\mathbf{k}_1\mathbf{k}_2)=\delta(\mathbf{k}_1+\mathbf{k}_2,\mathbf{k}_3+\mathbf{k}_4)\left(\frac{2\pi V_0}{\mu v}\right) \times[f(\mathbf{k}_1+\mathbf{k}_2)+f(\mathbf{k}_1+\mathbf{k}_2)], \quad (81)$$

where

$$f(\mathbf{x})=(\mu^2+x^2)^{-1}, \quad (82)$$

and V_0 is the well depth, $1/\mu$ is the well range, and $v=(4/3)\pi r_0^3 A$ is the nuclear volume.

For the energies of the particles moving in the nuclear well, we use the result derived in reference 1, that

$$E=k^2/2M^*+V,$$

where V is a constant well and M^* is an effective nucleon mass which is modified from the nucleon mass to include the effects of the quadratic momentum dependence of the actual well. In this approximation, and replacing the sums by integrals (and making use of the Kronecker delta functions over total momentum), we find

$$\Delta E_{pc}=\left[\frac{v}{(2\pi)^3}\right]^2\left(\frac{2\pi V_0}{\mu v}\right)^2(M^*)^2\int d\mathbf{k}_1'd\mathbf{k}_i \times[f(\mathbf{k}_1-\mathbf{k}_1')+f(\mathbf{k}_2-\mathbf{k}_2')] \times[f(\mathbf{k}_2-\mathbf{k}_1')+f(\mathbf{k}_i-\mathbf{k}_2)] \times[f(\mathbf{k}_1-\mathbf{k}_1')+f(\mathbf{k}_i-\mathbf{k}_1')] \times\frac{1}{[k_1^2+k_2^2-k_1'^2-(\mathbf{k}_1+\mathbf{k}_2-\mathbf{k}_1')^2]} \cdot\frac{1}{[k_1^2+k_i^2-k_1'^2-(\mathbf{k}_1+\mathbf{k}_2-\mathbf{k}_1')^2]} \quad (83)$$

with the restriction arising from the exclusion principle that

$$|\mathbf{k}_1'|\geq k_F,\quad |\mathbf{k}_2'|=|\mathbf{k}_1+\mathbf{k}_2-\mathbf{k}_1'|\geq k_F, \quad |\mathbf{k}_i'|=|\mathbf{k}_1+\mathbf{k}_i-\mathbf{k}_1'|\geq k_F. \quad (84)$$

We will also approximately include the effects of the exclusion principle by multiplying this result by the apriori probability that particles interact in even states of orbital momentum, namely $\frac{1}{2}(\frac{1}{2}\times\frac{3}{4}$ for the n-p pairs plus $\frac{1}{2}\times\frac{1}{4}$ for the like particle pairs).

We are particularly interested in the interaction between particles in the same states; thus we shall in the integral of Eq. (83) set $\mathbf{k}_1=\mathbf{k}_2$. In addition we consider particles moving in the last state filled in the Fermi gas and set $|\mathbf{k}_1|=k_F$. We shall also introduce a further approximation at this stage. We note that the momenta which enter the integrals are all quite large and that since $f(x)$ is a rapidly decreasing function of x for large x, the only term in the integrand which will contribute appreciably is that in which terms of the form $f^2(x)$ appear. A term for example of the form $f^2(\mathbf{x})f(\mathbf{x}+\mathbf{k}_i)$ will be much smaller since it is not simultaneously possible for $f^2(\mathbf{x})$ and $f(\mathbf{x}+\mathbf{k}_i)$ to be large. Consequently we drop such terms and obtain (with a change in variable in the integral)

$$\Delta E_{pc}=\frac{1}{2}\frac{v^2}{(2\pi)^6}\left(\frac{2\pi V_0}{\mu v}\right)^2M^{*2}\int d\mathbf{k}_i d\mathbf{x}\frac{f^2(\mathbf{x})}{x^2(x^2-\mathbf{k}_1\cdot\mathbf{x}-\mathbf{k}_i\cdot\mathbf{x})}, \quad (85)$$

with the restrictions

$$|\mathbf{x}-\mathbf{k}_1|\geq k_F,\quad |\mathbf{x}+\mathbf{k}_1|\geq k_F,\quad |\mathbf{x}-\mathbf{k}_i|\geq k_F. \quad (86)$$

The integration over the core variable i is, except for these restrictions, extended over the Fermi sphere of momentum. This integral cannot be carried out completely in closed form; an excellent approximation (introducing errors of less than 20 percent), however, leads to the result

$$\Delta E_{pc}=\frac{v^2}{(2\pi)^6}\left(\frac{2\pi V_0}{\mu v}\right)^2(M^*)^2(2\pi)^2\int_0^\infty f^2(x)x\,dx. \quad (87)$$

We compare this (after multiplication by six to include the other terms arising from permutations of the particles) with the diagonal term for interaction between the two surface particles,

$$\Delta E = 4\pi V_0/\mu^3 v. \tag{88}$$

The ratio is

$$\frac{\Delta E_{pc}}{\Delta E} = \frac{3}{16\pi^2}\left(\frac{M^* V_0}{\mu^2}\right)^2. \tag{89}$$

Taking $M^* = 0.54M$, $V_0/\mu = 0.252$ (corresponding to a bound state at zero energy), the final result is

$$\Delta E_{pc}/\Delta E = 0.016. \tag{90}$$

Thus the contribution to the particle-particle interaction energy which arises from particle-core-particle coupling is quite small. As pointed out in the previous section, this can be readily included by a slight modification of the effective two-body interaction or a more detailed analysis of the type carried out in this section can be made to give its effect explicitly.

VI. CONCLUSIONS

We have considered the formalism developed in treating other problems of nuclear structure and nuclear saturation, and shown how it may be extended to the more detailed problem of energy-level fine structure. We have taken as our starting point a nuclear Hamiltonian containing as interaction terms only strong short-range two-body potentials. We have then shown how the relationships among the energy levels of neighboring nuclei can be very accurately determined if use is made of empirical knowledge of energy levels of one of the nuclei and a particle-to-particle coupling is introduced. This coupling is shown to be the result to a very good approximation of direct interaction through the two-body nucleon potential, effects of coupling through the nuclear core being evaluated and shown to be small. Thus we have demonstrated the relationship between the treatment of the original many-particle Hamiltonian and the determination of details of the energy-level structure by the methods of, for example, Flowers[4] and Ford and Levinson.[5]

The remaining problem which we have considered more briefly is the character of the nuclear wave function and the effects of particle-particle and particle-core configuration mixing. These unavoidably appear in the actual nuclear wave function as a consequence of the assumed strong two-body interactions and in general will affect markedly such quantities as the nuclear magnetic moment. The configuration mixing among particles outside a simple doubly-magic core (such as Ca^{40} or O^{16}) is known to provide an explanation of the anomalies in magnetic moments; it is not obvious, however, that additional large effects will not appear due to the particle-core coupling. We have given qualitative reasons for the smallness of such effects on the magnetic moment; these reasons are (1) relative insensitivity of the magnetic moment to short-range correlations in the wave functions, (2) absence in Ca^{40} and O^{16} of core states which when mixed into the single-particle wave function can give linear changes in the magnetic moment, and (3) relatively large excitation energies and consequent nonpolarizability of the core of a doubly magic nucleus. We have also remarked, however, that the apparent purity of a state as shown by a magnetic moment on the Schmidt line cannot be regarded as evidence for a simple independent-particle nuclear wave function, but only that admixtures of other states can in certain quite special circumstances have little effect on the magnetic moment. In these special cases it also appears that arguments can be made in favor of working with a nonsingular two-body potential to perturb the shell-model states since the respulsive core of the actual two-body potential does not affect the parts of the wave function which dominate in determining energy level splitting and magnetic moments. This result is obviously related to a similar situation which exists in nucleon-nucleon scattering where, over sizeable energy intervals, many equivalent potentials give almost identical predictions of scattering.[7]

The authors would like to acknowledge many helpful discussions with Professor K. W. Ford and Dr. C. A. Levinson.

[7] See for example the discussion of the effects on high-energy processes of correlations in the nuclear ground-state wave function by Brueckner, Eden, and Francis (to be published).

Search for Double Beta Decay in Cadmium and Molybdenum*

ROLF G. WINTER†
Western Reserve University, Cleveland, Ohio
(Received March 7, 1955)

Random Wilson cloud-chamber photographs of cadmium and molybdenum foils show that the double negatron half-life is greater than or equal to 1×10^{17} years in Cd^{116} and 3×10^{17} years in Mo^{100}, and that the double positron half-life is greater than or equal to 6×10^{16} years in Cd^{106} and 4×10^{18} years in Mo^{92}. The background appears to be primarily caused by Compton electrons and photoelectrons ejecting other electrons on their way out of the foil and by photons that suffer two Compton scatterings while traversing the foil.

I. INTRODUCTION

SEVERAL paths to an experimental choice between the Dirac and Majorana neutrino theories are, in principle, possible. For instance, discovery of a neutrino magnetic moment[1] would disprove the Majorana model because electromagnetic forces would take the neutrino wave function out of the Majorana subspace.[2] On the other hand, if neutrinos from the sun contributed to the background in the inverse beta experiments of Reines and Cowan,[3] or if pile neutrinos could cause negatron emission from stable nuclei,[4] then neutrinos and antineutrinos would be equivalent in beta decay. This equivalence would probably imply the correctness of the Majorana theory, although there are alternative formalisms.[5,6] Also, the shape of the electron energy spectrum in mu-meson decay might depend on whether the two neutrinos emitted are identical or not. However, the spectrum observed seems to be consistent with either identical or different neutrinos.[7]

The most promising procedure for distinguishing between the neutrino theories is still an investigation of double beta-decay. If neutrinos and antineutrinos are not equivalent, double beta decay would involve the emission of two electrons and two neutrinos or antineutrinos, and half-lives in excess of 10^{21} years would result.[8] If neutrinos and antineutrinos are equivalent, there needs to be only one virtual neutrino which has all phase space available. Then one would expect half-lives ranging upwards from 10^{13} years depending on the form of the interaction, the energy, and the nuclear matrix elements.[9,10] If the decay is primarily to a single final state, as it should be because of the strong energy dependence of the transition probability, the sum of the energies of the electrons emitted will be constant. Unless one admits fairly artificial theories,[5,6,11,12] a demonstration of such a constant sum of energies would confirm the Majorana theory.

Lower limits ranging from 10^{14} years through 10^{19} years have been set for double beta activities of more than twenty nuclides in several investigations.[12–19] Such lower limits can never refute the Majorana theory because a large decrease in transition probabilities can result if the overlap of final and initial states is poor. The accumulation of such lower limits, however, particularly if they are above 10^{16} years, does decrease the likelihood of the neutrino being a Majorana particle.

There exists very little positive evidence for double beta decay. The Sn^{124} results of Fireman[20] have been refuted by various investigators, including Fireman himself.[19] Inghram and Reynolds[21] found evidence for the decay of Te^{130} with a half-life of about 10^{21} years, but, as has already been pointed out by Kohman,[18] the activity discovered could well be single beta decay. Fremlin and Walters[16] found a 10^{15}-year activity in Mo^{100}, but Kohman[18] found a lower limit of 10^{16} years and the present work gives a lower limit of 3×10^{17} years. McCarthy[22,23] found activities in Zr^{96} and Ca^{48} and showed that, although there are alternatives, they most probably represent double beta decays in which the two emitted negatrons carry away all of the available energy with a half-life of 6×10^{16} years. Clearly, more conclusive results are prerequisite to a final decision between Dirac and Majorana neutrinos.

* Supported by the National Science Foundation.
† Now at the Pennsylvania State University, University Park, Pennsylvania.

[1] Cowan, Reines, and Harrison, Phys. Rev. **96**, 1294 (1954).
[2] W. H. Furry, Phys. Rev. **54**, 56 (1938).
[3] F. Reines and C. L. Cowan, Phys. Rev. **92**, 830 (1953).
[4] Raymond Davis, Jr., Phys. Rev. **97**, 766 (1955).
[5] Bruno Touschek, Z. Physik **125**, 108 (1948–1949).
[6] Jayme Tiomno, Princeton University, dissertation, 1952 (unpublished).
[7] Louis Michel, Phys. Rev. **86**, 814 (1952).
[8] M. Goeppert-Mayer, Phys. Rev. **48**, 512 (1935).
[9] W. H. Furry, Phys. Rev. **56**, 1184 (1939).
[10] H. Primakoff, Phys. Rev. **85**, 888 (1952).
[11] Rolf G. Winter, Phys. Rev. **83**, 1070 (1951).
[12] Rolf G. Winter, U. S. Atomic Energy Commission Report NYO–913, September 1, 1951 (unpublished).
[13] Levine, Ghiorso, and Seaborg, Phys. Rev. **77**, 296 (1950).
[14] Mark G. Inghram and John H. Reynolds, Phys. Rev. **76**, 1265 (1949).
[15] Rolf G. Winter, Phys. Rev. **85**, 687 (1952).
[16] J. H. Fremlin and M. C. Walters, Proc. Phys. Soc. (London) **A65**, 911 (1952).
[17] Berthelot, Chaminade, Levi, and Papineau, Compt. rend. **236**, 1769 (1953).
[18] Truman P. Kohman, U. S. Atomic Energy Commission Report NYO–3626, March 1, 1954 (unpublished).
[19] E. L. Fireman and D. Schwarzer, Phys. Rev. **86**, 451 (1952).
[20] E. L. Fireman, Phys. Rev. **75**, 323 (1949).
[21] Mark G. Inghram and John H. Reynolds, Phys. Rev. **78**, 822 (1950).
[22] John A. McCarthy, Phys. Rev. **90**, 853 (1953).
[23] John A. McCarthy, Phys. Rev. **97**, 1234 (1955).

II. SELECTION OF SOURCES

Among the elements which might show double beta activity, cadmium and molybdenum seem particularly suitable for experimental investigation. The nuclide Cd^{116}, with natural abundance of 7.7 percent, has 2.6 ± 0.2 Mev, and Mo^{100}, with a natural abundance of 9.7 percent, has 2.3 ± 0.2 Mev available for double negatron emission.[24,25] In addition, Cd^{106}, with a natural abundance of 1.2 percent, has 0.8 ± 0.2 Mev available for the kinetic energy of the positrons in double positron emission.[24,25] Molybdenum also contains, with a natural abundance of 15 percent, Mo^{92}, which lies below the beta stability line and might undergo double positron decay; however, since it has a magic number of neutrons and since no adequate mass measurements exist, nothing reliable can be said about the energy available. If the neutrino is a Dirac particle, the half-lives for all four transitions are too long to be observed in the procedure described below. If the Majorana theory applies, the half-lives for Cd^{116} and Mo^{100} will be $\geq 10^{18}$ years, and the half-life of Cd^{106} will be $\geq 10^{16}$ years. Since the energy is not known for Mo^{92}, a lifetime cannot be estimated; in fact, only double K capture, or even no transition at all, may be energetically possible.

III. EXPERIMENTAL PROCEDURE

For both the cadmium and the molybdenum investigations, three foils of the material being studied were stretched across a 24-cm diameter Wilson cloud chamber. A mixture of 50 percent by volume of water and 50 percent methanol was boiled into the evacuated chamber, which was then filled to a total pressure of 1.6 atmos with argon. Stereoscopic photographs were taken of a random expansion every 30 seconds. A magnetic field of 790 gauss, made uniform to 1.5 percent over the usable region of the chamber by proper shaping of an air-core solenoid,[26] was turned on about one second before the expansion. The adjustment of the chamber was checked visually about every hundred expansions.

The pictures obtained were projected first on a screen, with the two stereoscopic views placed next to each other. Those in which two negatrons or two positrons seemed to come from the same point on the foil were marked for further study. Also, from the number and appearance of single tracks, a judgment of the acceptability of each roll of film was made: 13 percent of the photographs obtained were discarded because the appearance of the tracks and the background fog suggested doubt whether minimum-ionization electron tracks could be discerned in all parts of the chamber.

The pictures marked for further examination were projected stereoscopically through the same mirror and camera system with which they were photographed. By attempting to place a screen in the plane defined by the beginnings of both tracks, one could determine with fair precision whether the tracks came from the same point. Some difficulty arose because the layer of gas adjacent to the foil loses its supersaturation sooner than most of the chamber, so that many tracks became invisible in that layer and had to be extrapolated back to the foil. In all cases, however, it could be determined whether the tracks started within 0.4 cm of each other. When both tracks appeared to come from the same point, upper and lower bounds on their curvature, and therefore on their energy, were established. When one of the tracks was scattered too violently in the gas or was too nearly straight for meaningful measurement, the picture was discarded. Therefore, only tracks of electrons with energy between 0.1 Mev and 6 Mev could be used. For those photographs in which both tracks came from the same point and had a measurable curvature, an upper and lower bound on the sum of the energies of the two electrons, including a correction for loss in the foil, was established.

IV. CADMIUM RESULTS

For the cadmium investigation, 30 g of 0.11 g/cm² foil,[27] containing 1.2×10^{22} atoms of Cd^{116} and 1.9×10^{21} of Cd^{106}, were installed in the chamber. The probability that two electrons from one atom would travel in the illuminated region of the chamber for 4 cm was, on the average, 0.3, giving 3.6×10^{21} as the effective number of Cd^{116} nuclei and 5.7×10^{20} as the effective number of Cd^{106} nuclei.

With the foils in place and with the chamber filled and operated as for the actual double beta search, a calibrated P^{32} source was photographed. From the strength of the source and a determination of the average number of tracks seen coming from it per expansion, the sensitive time of the chamber was found to be 0.36 ± 0.08 second per photograph. Since 12 352 acceptable photographs were taken, the cadmium was examined for $(1.4\pm0.3)\times10^{-4}$ year.

In 24 cases, two negatron tracks appear to originate from the same point in the foil. To represent the results in Fig. 1, a rectangle of unit area was assigned to each event, with its base running from the minimum to the maximum total energy of the event. The solid line in Fig. 1 was obtained by adding the heights of these rectangles wherever they overlapped and gives the experimental number per unit energy as a function of the energy.

A definite indication of double beta decay would be a maximum in Fig. 1 at 2.6 Mev. No such maximum is observed, but three events contribute to the result at that location. It is interesting that the calculated background curves (see Sec. VI below) lie everywhere higher then the experimental distributions except at the high-energy end of the cadmium plot. Nevertheless, it is

[24] John T. McCarthy, Phys. Rev. **95**, 447 (1954).
[25] Richard E. Halsted, Phys. Rev. **88**, 666 (1952).
[26] Martyn H. Foss, Technical Report No. 2, Navy Contract N7 ONR-303 T.O.I. (unpublished).
[27] Obtained as 5-mil thick, 99.9 percent pure, foil from A. D. Mackay, Inc., 198 Broadway, New York 38, New York.

clear that the data do not permit a claim of a positive result. Multiplying the effective number of Cd^{116} nuclei by the time for which the cadmium was under examination and by ln2 over three, the number of events that contribute at 2.6 Mev, one finds that the double negatron half-life of Cd^{116} must be $\geq 1\times10^{17}$ years.

One double positron event was found. Its rectangle, computed as for the negatron events in the aforementioned, is shown dashed in Fig. 1. Its rather large energy range includes the available double positron energy. It is, however, entirely reasonable that the background should contribute one such event (see Sec. VI below). The double positron half-life of Cd^{106} is therefore $\geq 6\times10^{16}$ years.

V. MOLYBDENUM RESULTS

For the molybdenum investigation, 42 g of 0.13 g/cm² foil,[27] containing 2.5×10^{22} atoms of Mo^{100} and 3.9×10^{22} of Mo^{92}, were installed in the chamber. The probability of observing both electrons was again 0.3, giving 7.5×10^{21} and 1.2×10^{22} as the effective numbers of Mo^{100} and Mo^{92} nuclei.

The sensitive time of the chamber was measured with a calibrated P^{32} source as in the cadmium work and was found to be 0.54 ± 0.12 second per photograph. The higher value resulted from the use of a deeper chamber. Since 13 402 acceptable photographs were taken, the molybdenum was examined for $(2.3\pm0.5)\times10^{-4}$ year.

In 35 cases, two negatron tracks appear to originate from the same point in the foil. In Fig. 2, the results are shown in the same fashion as for cadmium in Fig. 1. No maximum is observed at 2.3 Mev, the available double negatron energy, but four of the events found straddle that energy.

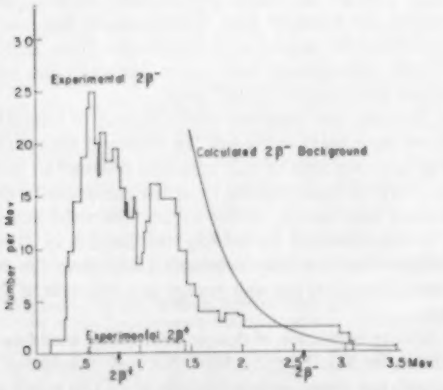

FIG. 1. Number per Mev *vs* energy, of instances in which two electrons appear to come from the same point on the Cd foil. The solid lines give the double negatron distribution. The dotted rectangle represents the one double positron event found. The smooth curve gives the estimated double negatron background. The arrows marked $2\beta^+$ and $2\beta^-$ underneath the energy scale indicate the expected double positron and double negatron energies.

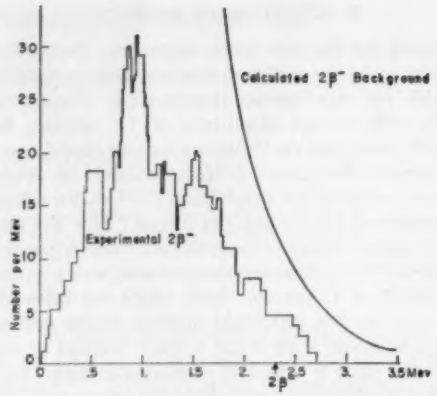

FIG. 2. Number per Mev *vs* energy, of instances in which two negatrons appear to come from the Mo foil. The smooth curve gives the estimated double negatron background. The arrow marked $2\beta^-$ underneath the energy scale indicates the expected double negatron energy.

The calculated background curve (see Sec. VI below) lies everywhere above the experimental results.

Multiplying the effective number of Mo^{100} atoms by the time for which the molybdenum was under examination and by ln2 over four, the number of events that contribute at 2.3 Mev, one finds that the double negatron half-life of $Mo^{100}\geq 3\times10^{17}$ years.

No double positron events were found. Multiplying the effective number of Mo^{92} atoms by 2.3×10^{-4} year and by 2 ln2, one finds that the double positron half-life of $Mo^{92}\geq 4\times10^{15}$ year. This result is of little significance in the absence of an estimate of the available energy.

VI. BACKGROUND

Both for the understanding of this experiment and for the planning and interpretation of other double beta experiments, it is useful to study in some detail the sources of background.

For 1869 of the cadmium pictures and 1950 of the molybdenum pictures, all single negatrons that came from the foil (presumably mostly ejected by photons arising from cosmic rays, with perhaps some due to beta-active contamination) were recorded, with their radii of curvature estimated to the nearest cm. From these single negatron distributions were obtained the expected distribution of events in which two electrons appear to emanate from the same point. Figure 3 shows the separate contributions to this background as estimated below for cadmium; for molybdenum, the curves are qualitatively similar. The sums of these contributions are superposed on the experimental distributions in Figs. 1 and 2.

A. Random Coincidence

If the origins of two single tracks happen to be less than 0.4 cm apart, the event can give the appearance

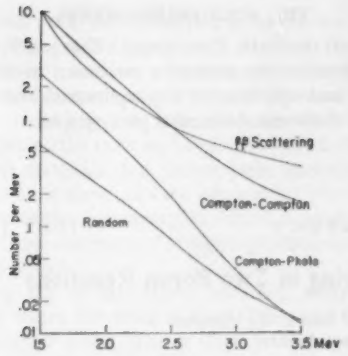

FIG. 3. Contributions in number per Mev to the estimated double-negatron background in Cd, labeled as indicated in Sec. VI.

of a double beta decay. To estimate the contribution of this effect, those pictures containing two or more negatron tracks that start anywhere in the foil were used. All possible combination of the tracks in each picture were considered. Each combination had a probability of 0.4 cm×0.4 cm, the region of distinguishability, divided by 250 cm², the total area of the foil. The distribution was then divided by two because tracks formed near the beginning of the sensitive time could be distinguished from those formed near the end by their noticeably more diffuse appearance. The result is the curve labeled *Random* in Fig. 3.

B. Negatron-Negatron Scattering

An event having the appearance of a double beta-decay results if a negatron that has been produced in the foil shares its energy with another negatron on its way out of the foil. Since a negatron starting with 0.3 Mev or less probably would have too little energy after leaving the foil for meaningful measurement, the Møller formula[28] was integrated over the energy shared from 0.3 Mev to half the energy E of the negatron considered. The resulting expression, which will then only depend on E, multiplied by the thickness of foil that the average negatron traverses, and multiplied by the number of negatrons per photograph with E, gives the expected contribution at E. The result is labeled *ββ Scattering* in Fig. 3.

C. Two Compton Scatterings, or Compton Scattering Followed by Photoelectric Emission

Whenever a single negatron was produced by Compton scattering, the residual gamma ray was capable of ejecting another negatron before leaving the foil. It was assumed that all negatrons observed were produced by photoelectric emission or by Compton scattering, and the number due to Compton scattering was computed as a function of energy. The probability that the residual photon would produce another negatron before leaving the foil was then obtained. The calculations were simplified by the assumption that, in each Compton event, the negatron received the average fraction[29] of the photon energy. In Fig. 3, the contribution due to two successive Compton scatterings is labeled *Compton-Compton*; that due to Compton scattering followed by photoelectric emission is labeled *Compton-Photo*.

D. Gas Scattering

If the apparent curvature of either one member of a negatron-positron pair, or of one part of a track going through the foil, is reversed by multiple scattering in the gas, an event giving the appearance of double beta-decay results. The magnitude of this effect was estimated by counting the number of pairs and the number of electrons passing through the foil, and then multiplying by the probability that the curvature of either branch is reversed by scattering.[30] This effect is negligible; in the 2-Mev neighborhood, the expected number of these events is 10^{-3} for either of the entire cadmium or molybdenum experiments.

E. Double Positron Background

An event with the appearance of a double positron decay could result either through gas scattering (see Sec. D), or, far more probably, through two negatrons that start elsewhere converging toward the same point on the foil. The one case found in cadmium is readily explained by the latter process.

F. Summary of Background Calculations

The estimated background suffices to explain the results obtained. Negatron-negatron scattering and two successive Compton scatterings provide the principal contributions.

The sums of all contributions superposed in Figs. 1 and 2 lie, on the whole, somewhat high and rise more rapidly as the energy goes down than the experimental distributions. This behavior might be expected, since no careful consideration of multiple scattering and total absorption of the low-energy electrons in the foil was made.

VII. CONCLUSIONS

It is intriguing that the one double positron event, and the region in which the cadmium double negatron distribution rises above the calculated background, should both occur near the expected energy. Nevertheless, the nature of the background estimates and the smallness of the number of events involved forbid any conclusions other than the setting of lower limits ranging from 10^{16} through 10^{18} years on the half-lives of the processes considered. These lifetimes are consistent

[28] Chr. Møller, Ann. Physik **14**, 569 (1932), Eq. (76).

[29] Ann T. Elms, National Bureau of Standards Circular 542, 1953 (unpublished).

[30] H. A. Bethe, Phys. Rev. **70**, 821 (1946).

with both the two-neutrino decay and with unfavored no-neutrino decay.

The background studies indicate limits on the double beta lifetimes that can be reached with expansion chambers.

VIII. ACKNOWLEDGMENTS

I wish to thank D. Connolley, C. Creager, T. Fesser, and P. Hoekstra for extensive assistance in the construction and operation of the equipment and in the scanning of the cloud-chamber photographs.

PHYSICAL REVIEW VOLUME 99, NUMBER 1 JULY 1, 1955

Scarcity of Low-Energy Levels of Be^8 Appearing in Two Boron Reactions

R. E. HOLLAND, D. R. INGLIS, R. E. MALM,* AND F. P. MOORING
Argonne National Laboratory,† Lemont, Illinois

(Received March 3, 1955)

A careful search is made for evidence of possible excited states in Be^8 in the reactions $B^{11}(p,\alpha)Be^8$ and $B^{10}(d,\alpha)Be^8$, by magnetic momentum analysis at a variety of angles and bombarding energies. In spite of observing the region corresponding to 3 to 8 Mev several times independently under different conditions, with several thousand counts per point on points spaced only about 100 kev apart, no indication was found of any of the states in this region reported by others on the basis of poorer statistics, mostly in other reactions. Each alpha-particle spectrum observed consists of a sharp ground-state peak and a broad peak of the alpha particles giving rise to the well-known 3-Mev excited state of Be^8 superposed on a continuous background from the break-up of this state and from three-particle break-up. Peaks observed near the equivalent of 10 and 11 Mev in Be^8 are identified as arising from a target impurity.

I. INTRODUCTION

THE interesting nucleus Be^8 may be expected to be especially simple because it is so light.[1] It contains just enough nucleons to make up two alpha particles. The nucleus which is twice as heavy, O^{16}, may consist of four alpha particles in a tetrahedral structure differing rather little from a sphere, and it does indeed show a strong evidence of collective motion of a body with tetrahedral symmetry, as epitomized by the alpha-particle model.[2] The even-even nucleus with mass between these two, C^{12}, appears not to follow the alpha-particle model,[1] and this may be associated both with the great difference between a triangle and a sphere and with the fact that the energy of dissociation into three alpha particles is as great as the average binding-energy of a nucleon. Although in Be^8 the possible alpha-particle structure, a line or "dumbbell," is also very different from a sphere, no energy is required to dissociate it into two alpha particles; so here again, there might be a tendency for the low states to be approximated by the alpha-particle model. In either the shell model or the alpha-particle model, or indeed in a blend of the two, the expected sequence of low-energy levels is very simple. The shell-model expectation is determined by the calculations which show in (LS) coupling a series of singlets, $^1S_0$, $^1D_2$, $^1G_4$, and similar widely-spaced levels in (jj) coupling and so also in intermediate coupling.[1] It should, however, be mentioned that states probably not belonging to the ground configuration p^n appear in the neighboring nuclei Li^7 at 6.4 Mev and C^{12} at 7.7 Mev, and might also appear in Be^8 at a comparable energy. The expectation of possible simplicity should not prejudice one, but does add interest to the experimental investigation of Be^8.

The evidence concerning the spectrum of low states in Be^8 remains conflicting. Some experiments suggest quite a number of low excited states, and other experiments, particularly those in which it has been possible to collect the most convincing statistical evidence, show only the well-known broad excited state at about 3 Mev. It is unfortunate that there are intrinsic difficulties which make it very time-consuming to collect adequate numbers of counts per point in some of the work showing the "extra" states, for the demonstration that certain other reactions do not show these states does not disprove their existence. It is always possible that an adverse matrix element is suppressing a given transition, but in the absence of some general selection rule, it becomes unlikely that this should happen at a variety of bombarding energies and angles, because a special selection that might apply for a given state of the compound nucleus or at a given angle would not be expected to apply at others. The present work is confined to reactions wherein it is not very difficult to obtain many counts per point with relatively good resolution. We have tried to vary the experimental conditions to exclude the possibility that some chance cancellation in the matrix element is hiding some of the states from us.

* Now at Bell Telephone Laboratories, Whippany, New Jersey.
† Work performed under the auspices of the U. S. Atomic Energy Commission.
[1] D. R. Inglis, Revs. Modern Phys. 25, 390 (1953).
[2] D. M. Dennison, Phys. Rev. 96, 378 (1954); J. W. Bittner and R. D. Moffat, Phys. Rev. 96, 374 (1954).

Previous work[3] on this subject up to about a year ago is summarized in the preliminary report on the present investigation[4] and in a subsequent discussion by Titterton.[5] More recently, Trail and Johnson,[6] using a counter technique for measuring neutron energies, have repeated the work on $Li^7(d,n)Be^8$. With somewhat improved statistics, but rather poor resolution, they fail to find the states at 4.09, 4.9, and 7.5 Mev inferred from the earlier photographic emulsion work on this reaction[7] and observation[8] of alpha-gamma coincidences in $Li^7(p,\gamma)Be^8$.

Among the investigations revealing some of the disputed states, the work of Cüer, Jung, and Bilwes[9,10] on $B^{10}(d,\alpha)Be^8$ seems to us to display the most impressive statistical evidence. The peaks which they considered significant consisted of at least four high points in succession isolated by a valley of at least two low points in succession. Their results suggest that the questionable states may be more easily observed near the forward direction, at least in this reaction.

II. APPARATUS AND RESULTS

Proton and deuteron beams for bombardment of B^{11} and B^{10}, respectively, were obtained from the ANL statitron at well-stabilized energies up to over 3 Mev. The energy of the alpha particles produced was analyzed by means of the 16-inch two-dimensional-focusing magnetic spectrometer previously described.[11] Targets used in some of the early work were prepared by evaporating natural boron on a thick backing, but trouble was experienced with losing the target during bombardment even with beams below 1 μa. The targets

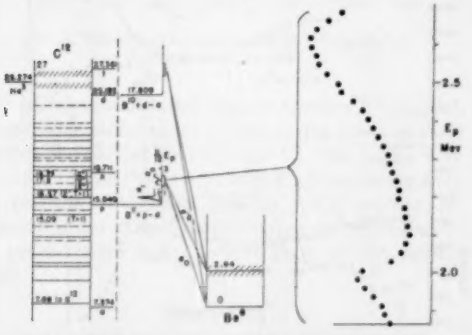

FIG. 1. Excitation curve for the reaction $B^{11}(p,\alpha)Be^8$.

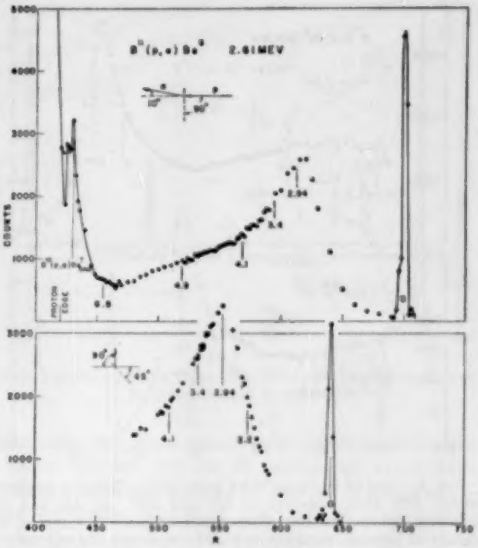

FIG. 2. Yield of alpha particles of various momenta from the reaction $B^{11}(p,\alpha)Be^8$ at a proton energy of 2.61 Mev, as observed at 10° and 90°. The numbers under the curves indicate Be^8 excitation energy in Mev.

used in most of the work were kindly prepared for us by Louis Basile by heating prepared metal backings in diborane containing either enriched B^{10} (with about 5 percent B^{11} remaining) or natural boron. The heating and gas flow had to be limited to avoid getting the targets too thick. Thick-sheet tantalum backings were simply heated by induction. Thin backings of 0.02-mil nickel foils (5×10^{-5} cm) were each held between the halves of a small nickel frame. The frame was mounted against a steel plate heated by induction, and radiation from the plate in turn heated the nickel foil. The frame fit snugly enough against the steel plate to inhibit circulation of the diborane behind the foil, but a small amount of boron was deposited on the back side of the foil.

Reaction $B^{11}(p,\alpha)Be^8$

Before investigating very carefully the distribution in energy of the product alpha particles, an excitation curve of $B^{11}(p,\alpha)Be^8$ was observed for the ground-state alpha particles, α_0, at $\theta=90°$ in the range of bombarding energies 1.9 to 2.7 Mev. The curve is shown on the right side of Fig. 1. The resonances observed at 1.98 and 2.61 Mev correspond to excited states in C^{12} at 17.76 and 18.35 Mev, agreeing with the values 17.8 and 18.39 Mev deduced from gamma-ray observations.[8] The data on the left side of Fig. 1, including the broken lines used to indicate uncertain states, were taken from reference 3. In the small insert for $B^{11}+p-\alpha$, our excitation curve is sketched on a small scale and

[3] F. Ajzenberg and T. Lauritsen, Revs. Modern Phys. **27**, 77 (1955). References are based on an advance preprint kindly supplied by the authors.
[4] R. Malm and D. R. Inglis, Phys. Rev. **92**, 1326 (1953).
[5] E. W. Titterton, Phys. Rev. **94**, 206 (1954).
[6] C. C. Trail and C. H. Johnson, Phys. Rev. **95**, 1363 (1954).
[7] Trumpy, Grotdal, and Graue, Univ. Bergen, Naturvitenskap. Rekke No. 8 (1953).
[8] E. K. Inall and A. J. F. Boyle, Phil. Mag. **44**, 1081 (1953).
[9] Cüer, Jung, and Bilwes, Compt. rend. **238**, 1405 (1954).
[10] P. Cüer and J. J. Jung, Compt. rend. **236**, 2401 (1953); also reference 3.
[11] R. Malm and D. R. Inglis, Phys. Rev. **95**, 993 (1954).

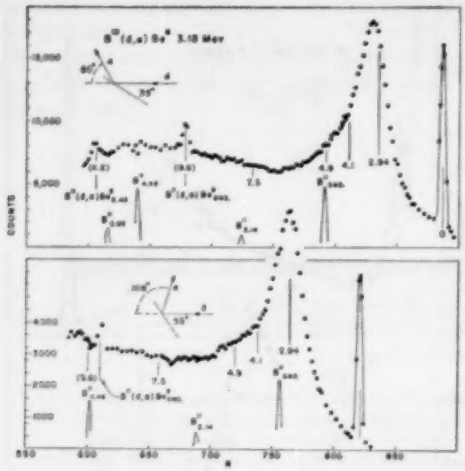

FIG. 3. Yield of alpha particles from $B^{10}(d,\alpha)Be^8$ at a deuteron energy 3.18 Mev, observed at 60° and 108°. In this and the following figures, the low sharp peaks labelled by states of B^{11} should be plotted ten times as high to represent the numbers of protons observed from the prolific competing reaction $B^{10}(d,p)B^{11}$.

compared with those previously observed[12] for energies up to 1.5 Mev for both the ground state and excited state transitions, though we have not established the factor by which to compare intensities.

Alpha-particle spectra were observed at laboratory angles of 10° and 90° for a proton bombarding energy of 2.61 Mev. The results are shown in Fig. 2 in which the abscissa is proportional to magnetic field or particle momentum. Places where one would expect to find alpha groups associated with reported levels in Be^8 are indicated in Fig. 2, labeled by the reported values of the excitation energies. Early results at 90° have been previously published.[4]

At both angles the alpha-particle spectrum showed peaks corresponding to the ground state and the 2.94-Mev excited state of Be^8. The resolution is such that the peaks of the sharp ground state each consist of four high points and in most of the regions carefully covered a peak would likewise be recognized as several successive high points.

The 10° alpha-particle spectrum shows a strong peak at a magnetic field corresponding to an excitation of Be^8 of about 7 Mev. The excitation curve of this alpha-particle group shows a resonance at a proton bombarding energy of 2.28 Mev not shown by the ground-state group α_0. We attribute this group to the reaction $B^{10}(p,\alpha)Be^7_{gnd}$. Such a group is to be expected since a natural boron (19 percent B^{10}) target was used. At 90° this group was not observed because it occurs at magnetic fields below the proton scattering edge. This group gives rise to a double peak, and the ground state also shows some indication of structure. This may be attributed to a small amount of boron on the back of the thin backing used at this angle. Confirmation of this interpretation was obtained by observing the double peak at angles near 108°.

At $\theta=65°$ and $E_p=2.61$ Mev, one hasty run was made which is not presented in a figure because the points through most of the spectrum were too widely spaced to be significant and because of the adverse circumstance that the target was only about 5 percent B^{11}, the rest being B^{10}. In it a weak peak was observed at a position equivalent to $E^x=3.61$ Mev, with an intensity about 5 percent of the ground-state peak. It is presumed to arise from another reaction but the data are insufficient to identify the target impurity.

Reaction $B^{10}(d,\alpha)Be^8$

Both thick-backed and thin-backed B^{10} targets were available, each of which had presumably about 5 percent B^{11} impurity. With these targets the reaction $B^{10}(d,\alpha)Be^8$ was observed at a variety of angles and energies in a further search for possible states of Be^8. The data shown in Figs. 3, 4, and 5 were taken with a thick-backed target, while the data in Fig. 6 were taken with a target with a thin backing (0.02-mil nickel foil). The competing reaction $B^{10}(d,p)B^{11}$ yields four groups of protons with energies in the range of interest. The protons were easily separated from the alpha particles since the sodium iodide crystal used as a detector gave considerably larger pulses for protons than for alpha particles of the same energy.

By using the known Q's for the ground-state alpha

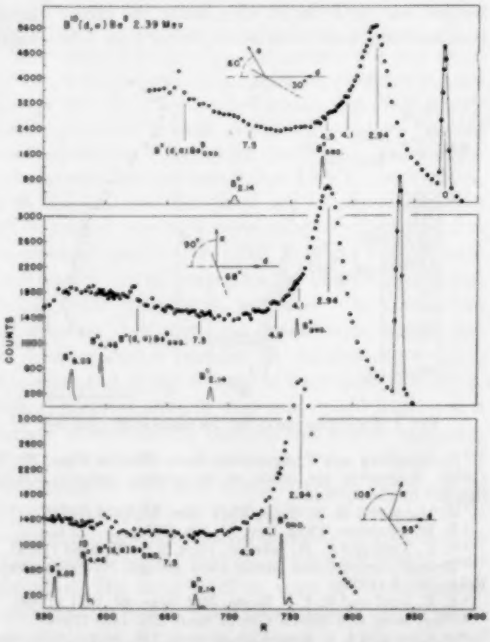

FIG. 4. Yield of alpha particles from $B^{10}(d,\alpha)Be^8$ at 2.39 Mev, observed at 60°, 90°, and 108°.

[12] Beckman, Huus, and Zupančič, Phys. Rev. **91**, 606 (1953).

particles and the $B^{10}(d,p)B^{11}$ protons, a consistent calibration of the magnet was obtained. Above an alpha energy of 15 Mev, this curve deviates from the parabola through the low-energy points by about 10 percent. This deviation occurs because the edges of the poles, where the field is measured, saturates at a lower field than the middle of the pole pieces, where the particles travel.

All of the data are consistent with this calibration to about ¼ percent except in the case of the two spectra at a bombarding energy of 3.18 Mev, shown in Fig. 3. In this figure energies according to the original calibration were satisfactory at low fields but were about one percent too high at high fields. The numbers indicating excitation energy in Be^8 were placed so as to be consistent with the $B^{10}(d,p)B^{11}$ proton groups. The source of the discrepancy has not been identified but it is felt that it does not affect the smoothness of the curves or the apparent scarcity of levels in Be^8.

Peaks corresponding to about 9.5- and 11-Mev excitation of Be^8 appeared in all of the data covering this

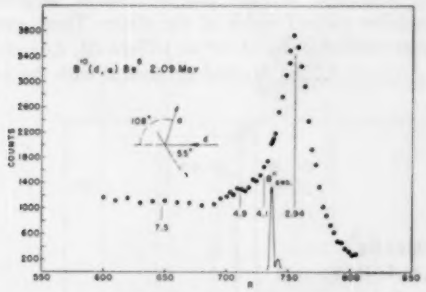

FIG. 5. Yield of alpha particles from $B^{10}(d,\alpha)Be^8$ at $E_d=2.09$ Mev, $\theta=108°$.

interval taken while studying the reaction $B^{10}(d,\alpha)Be^8$. Inconclusive evidence for a state at the lower of these energies is reported in reference 10. The peaks were identified by their variations with angle as coming from the reaction $B^{11}(d,\alpha)Be^9$ due to the 5 percent B^{11} impurity in the target, corresponding to transitions to the ground state and 2.43-Mev state of Be^9, respectively.

Discussion

All of the spectra observed show peaks due to the ground state and 2.94-Mev state of Be^8, superposed on a continuum arising from the breakup of the latter state and perhaps from direct three particle break-up. No other peaks were observed which could not be attributed to other reactions in the target. An upper limit for the intensity of another peak which would be unobserved by us is difficult to set since the accuracy of our data and the magnitude of the alpha-particle

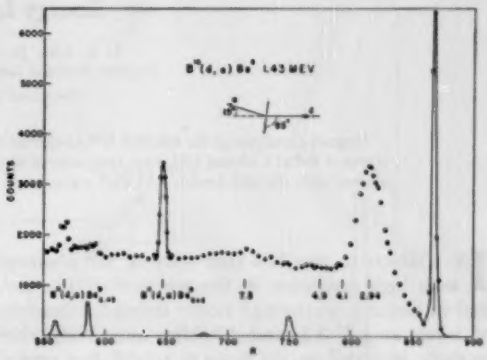

FIG. 6. Yield of alpha particles from $B^{10}(d,\alpha)Be^8$ at $E_d=1.43$ Mev near the forward direction.

continuum vary from spectrum to spectrum and place to place. We feel that for all curves, we would have detected a peak as much as 10 percent of the ground-state transition. Much of the data is considerably better than this, and in many cases in the regions where levels have been previously reported we would have observed a transition with 2 percent of the intensity of the ground-state transition. For peaks broader than the width set by our resolution, these limits would have to be increased accordingly.

In conclusion, it appears to us extremely unlikely that any systematic behavior of the matrix elements involved in the transitions should have hidden the existence of states in Be^8 in the neighborhood of 4, 5, and 7.5 Mev in Be^8. It is difficult to imagine any characteristics[13] that would distinguish these states so completely from the two lower states. We consider the weight of the accumulated evidence to favor the absence of the questionable states.

[13] The excitation curve of the reaction $B^{11}(p,\alpha)Be^8$ for the group α_1 to the broad 3-Mev state is said (see reference 3) to show the resonances at 1.98 and 2.61 Mev which we observed for the ground-state transition α_0 (Fig. 1), and in addition shows (see reference 12) a distinct resonance at 0.67 Mev not shown by α_0, at which α_1 is about 100 times as intense as α_0. Since $B^{11}+p$ (in contrast to $B^{10}+d$) can form $T=1$ states in the compound nucleus, this apparent selection has led to the suggestion (V. Telegdi, private communication) that the resonant state at 0.67 Mev has $T=1$ as is compatible with its high energy in C^{12}, and that the broad 3-Mev state of Be^8 has at least a small percentage of $T=1$, the ground state having none. (Judged by the ground state of Li^8, the lowest primarily $T=1$ state in Be^8 is expected to have $J=2$ and could thus mix with the 3-Mev state, but many other $T=1$ states are expected at slightly higher energies, some of which could mix with the ground state, and it is not clear why there should be an admixture in one and not the other. It might possibly be associated with the ground state alone being a pure alpha-particle-model state.) This proposed admixture of $T=1$ in the 3-Mev state and not in the ground state would not help explain a suppression of the questionable states relative to both. A factor 5 in the ratio α_1/α_0 is expected from the statistical factor $(2J+1)$ aside from any peculiarities of matrix elements, and the ratios of the areas under the corresponding peaks tend to be larger but for several of our curves are not much larger than this.

Energy Levels in Be^9

L. L. Lee, Jr., and D. R. Inglis
Argonne National Laboratory, Lemont, Illinois*
(Received March 3, 1955)

Magnetic analysis of the reaction $B^{11}(p,\alpha)Be^9$ at three angles verifies the existence of rather broad excited states of Be^9 at 1.75 and 3.02 Mev, the peaks of which almost vanish at 90° where the original investigation showed only the well-known 2.43-Mev state.

IN addition to the 2.43-Mev state of Be^9 observed with high resolution in the reaction[1] $B^{11}(d,\alpha)Be^9$, and in inelastic scattering,[2] rather definite indications of levels at 1.8, 3.1, and 4.9 Mev have been more recently reported[3] on the basis of scintillation crystal spectrometry in the reaction $Li^7(He^3,p)Be^9$ and[4] in $B^{10}(t,\alpha)Be^9$. Both observations were made at 90°. The possible existence of the additional levels is of interest because the intermediate-coupling interpretation[5] requires several levels in this energy region, and is consistent with having the first three excited states rather close together.

We have observed the reaction $B^{11}(d,\alpha)Be^9$ with $E_d=1.51$ Mev, as in reference 1, at three angles, analyzing the alpha energies with our two-dimensional-focusing magnetic spectrometer.[6] The procedure was similar to that used in the preceding paper. The resolution was poorer in this work than can ordinarily be obtained with this instrument because of difficulties in stabilizing the field. The data are shown in Figs. 1, 2, and 3. The ground state and 2.43-Mev state peaks appear prominently at all angles, and at 50° and 101° (lab) peaks corresponding to states at 1.75 and 3.02 Mev also appear rather clearly. At 90° they are barely discernable above background. These peaks appear to be perhaps significantly wider than the instrumental width indicated by the sharper peaks, suggesting appreciable natural width of the states. These curves indicate excited states of Be^9 at 1.75±0.02, 2.43±0.02, and 3.02±0.03 Mev, in good agreement with the work

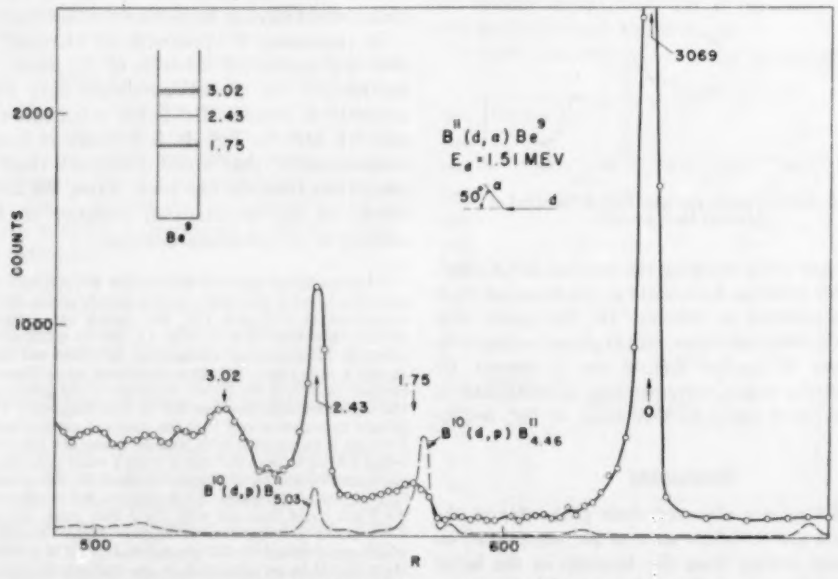

FIG. 1. Momentum analysis of $B^{11}(d,\alpha)Be^9$ at 50°. The broken line indicates protons.

* Work done under the auspices of the U. S. Atomic Energy Commission.
[1] Van Patter, Sperduto, Huang, Strait, and Buechner, Phys. Rev. **81**, 233 (1951).
[2] Browne, Williamson, Craig, and Donahue, Phys. Rev. **83**, 179 (1951); Arthur, Allen, Bender, Hausman, and McDole, Phys. Rev. **88**, 1291 (1952).
[3] Moak, Good, and Kunz, Phys. Rev. **96**, 1363 (1954).
[4] F. Ajzenberg and T. Lauritsen, Revs. Modern Phys. **27**, 77 (1955).
[5] D. R. Inglis, Revs. Modern Phys. **27**, 76 (1955).
[6] R. Malm and D. R. Inglis, Phys. Rev. **95**, 993 (1954).

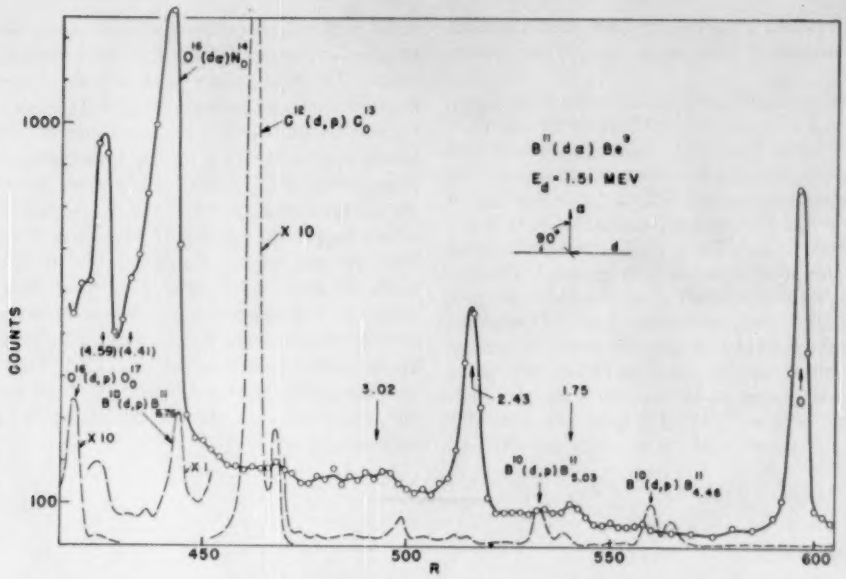

FIG. 2. Momentum analysis of $B^{11}(d,\alpha)Be^9$ at 90°.

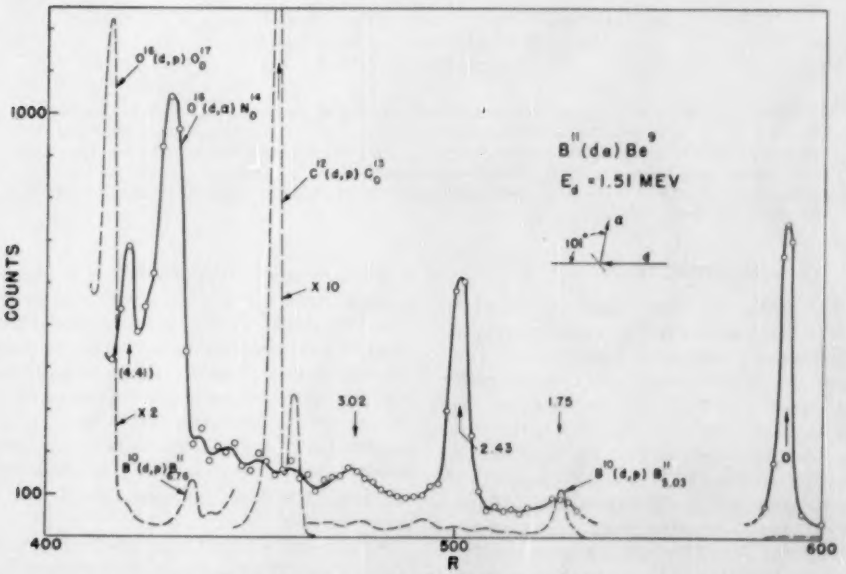

FIG. 3. Momentum analysis of $B^{11}(d,\alpha)Be^9$ at 101°.

of Moak, Good, and Kunz.[3] The apparent large natural width of the 1.75- and 3.02-Mev groups, and their low intensity, especially at 90°, explain their not having been seen by Van Patter *et al.*[1] with high resolution which enhances sharp peaks.[7]

Figures 2 and 3 show a very strong peak from $O^{16}(d,\alpha)N^{14}$. The region between this and the 3.02-Mev

[7] It has been pointed out [G. C. Phillips *et al.*, Bull. Am. Phys. Soc. **30**, No. 3, 55 (1955), not given in abstract] that the observed peak at 1.75-Mev excitation could be due to the onset of three-body breakup. While our results do not completely contradict this interpretation, we find it difficult to attribute entirely to calibration error the difference between our apparent onset of 1.56 Mev in Fig. 1 and the 1.665-Mev threshold for three-body breakup. A recent analysis by D. Kurath, more refined than in reference 5, suggests that only the first two excited states of Be^9 lie close together, which favors the three-body interpretation.

state peak exhibits a fluctuating background without enough consistency with angle to permit specific assignments.

Additional groups of particles discriminated as alphas are observed for $E_\alpha = 3.21 \pm 0.03$ Mev at 90° and $E_\alpha = 3.10 \pm 0.03$ Mev at 101° (Figs. 2 and 3). We have been unable to assign these to plausible contaminations of the natural boron target on a thick tantalum backing. If assigned to $B^{11}(d,\alpha)Be^9$, they correspond to states at 4.59 and 4.41 Mev in Be^9. These might correspond to the broad 4.9-Mev level reported in reference 3, although it seems unlikely that such groups would have been missed in the high-resolution work of reference 1. We suggest instead that they are probably spectroscopic[6] "ghosts" of the adjacent $O^{16}(d,p)O^{17}$ peaks. Such a ghost appears, for example, on the high-energy side of the $C^{12}(d,p)C^{13}$ peak at both 90° and 101°. The pulses of these peaks are discriminated in the surplus above the alpha channels and thus recorded as protons, though with more careful discrimination the ghost pulses have ordinarily been found between the larger pulses of the direct proton peak and the smaller alpha pulses, the ghost protons presumably having lost energy on scattering from the inner (small-radius) wall of the deflection chamber. Apparently in the energy region of the peaks in question the ghost pulses happen to fall just in the alpha channels, for they do not appear elsewhere. We have thus not indicated levels corresponding to these peaks in the energy level diagram shown in the small insert of Fig. 1, even as broken lines, but further investigation of the region above 4 Mev is surely needed. The deuteron scattering edge at an equivalent of about 4.6 Mev in Be^9 prevented our observation of states at higher energies.

PHYSICAL REVIEW VOLUME 99, NUMBER 1 JULY 1, 1955

Photofission of U^{238}

L. KATZ, T. M. KAVANAGH, A. G. W. CAMERON, E. C. BAILEY, AND J. W. T. SPINKS
University of Saskatchewan, Saskatoon, Canada

(Received February 7, 1955)

Chemical separation of the products resulting from photofission at various maximum bremsstrahlung energies E_0 of U^{238} serve to define the 3-dimensional yield surface $S(Y,A,E_0)$. An analysis of this surface by the photon difference method established the 3-dimensional photofission cross section surface $S(\sigma,A,h\nu)$. The peak-to-valley cross section ratio (asymmetric to symmetric fission) is examined in some detail and the results are combined with high-energy photofission data from the literature to extend our calculations and analysis to 300 Mev.

INTRODUCTION

PHOTOFISSION, the fission process induced by nuclear absorption of electromagnetic energy, has been the subject of a number of investigations. For a discussion of the earlier work in this field the review article by Spencer and Ford[1] may be consulted. The early work indicated that the cross section for photofission, $\sigma_{\gamma f}$, increased from zero at the threshold to a maximum value at about 14 Mev and decreased thereafter with increasing energy. This cross-section shape is similar to that found for other photonuclear reactions and is termed the "giant" resonance cross section.[2-4] Recent work by Duffield and Huizenga[5] has shown that this giant photofission cross section in U^{235} has a peak value of about 0.18 barn and a width of 7 Mev at half-maximum.

An examination of the photofission yield as a function of mass number, at a given photon energy shows it to have the usual double humped mass distribution. Schmitt and Sugarman[6] have studied the shape of such mass-yield curves from natural uranium when irradiated with bremsstrahlung of maximum energy $E_0 = 7$, 10, 16, 21, 48, 100, and 300 Mev. Since these curves contain contributions from all photons in the spectrum whose energy is above the photofission threshold (5.1 Mev in uranium)[7] the direct interpretation of their curves is somewhat difficult.

Richter and Coryell[8] have given photofission mass-yield curves for natural uranium at energies $E_0 = 10$ and 16 Mev. Hiller and Martin[9] published a similar curve for thorium obtained with bremsstrahlung of 69-Mev peak energy.

In line with other photonuclear investigations being carried out in our laboratory we have studied the photofission process in natural uranium as a function of

[1] R. W. Spencer and G. P. Ford, Ann. Rev. Nucl. Sci. **2**, 400 (1953).
[2] Johns, Katz, Douglas, and Haslam, Phys. Rev. **80**, 1062 (1950).
[3] B. C. Diven and G. M. Almy, Phys. Rev. **80**, 407 (1950).
[4] Montalbetti, Katz, and Goldemberg, Phys. Rev. **91**, 659 (1953).
[5] R. B. Duffield and J. R. Huizenga, Phys. Rev. **89**, 1042 (1953).
[6] R. A. Schmitt and N. Sugarman, Phys. Rev. **95**, 1260 (1954).
[7] Koch, McElhinney, and Gasteiger, Phys. Rev. **77**, 329 (1950).
[8] H. C. Richter and C. D. Coryell, Phys. Rev. **95**, 1550 (1954).
[9] D. M. Hiller and D. S. Martin, Jr., Phys. Rev. **90**, 581 (1953).

energy from threshold to 24 Mev. Sufficient measurements were taken to establish the shape of the mass-yield surface as a function of bremsstrahlung energy E_0. This surface will be designated by $S(Y,A,E_0)$ where $Y(E_0,A)$ represents the yield of mass number A resulting from a given irradiation with photons whose maximum bremsstrahlung energy is E_0. A cut through this surface at constant mass number A corresponds to the yield of this mass chain in photofission as the energy E_0 is varied. The curve so obtained is similar to the usual yield curve in photonuclear reactions and may be analyzed by the photon difference method of Katz and Cameron[10] to yield the corresponding cross section. This cross section may be written $(\sigma_{\gamma f}(h\nu))_A$. It has the "resonance" shape characteristic of photonuclear reactions and obviously must be interpreted as the cross section leading to the mass chain A in the photofission process induced by photons of energy $h\nu$.

It is now possible, with the aid of the $(\sigma_{\gamma f}(h\nu))_A$ curves, to construct a three-dimensional surface $S(\sigma,A,h\nu)$. A cut through this surface at constant $h\nu$ results in a $\sigma-A$ curve which is readily seen to be the mass yield curve which would be obtained with monochromatic photons. For this reason the $S(\sigma,A,h\nu)$ surface is of particular interest in the study of photofission. The area under the $\sigma-A$ curve obtained by cutting this surface at constant energy $h\nu$ is the total photofission cross section at that energy. It will be shown that this curve has the double humped shape characteristic of fission yield curves obtained with particle excitation.

To within the accuracy of our measurements the mass chain 115 falls in the trough of the $S(\sigma,A,h\nu)$ surface so that $(\sigma_{\gamma f})_{115}$ can be taken as representing the cross section for symmetric fission. The mass chain 139 falls near the top of the higher mass peak and can be taken as representing the cross section for asymmetric fission. The ratio

$$R(h\nu)=(\sigma_{\gamma f})_{139}/(\sigma_{\gamma f})_{115} \qquad (1)$$

is then of particular interest and is discussed at some length.

EXPERIMENTAL PROCEDURE

Thirteen-gram samples of uranyl nitrate, enclosed in a cadmium container, were irradiated in the betatron beam 28 cm in front of the electron target from which the bremsstrahlung beam originated. The dose was monitored by a 100 "r" Victoreen chamber placed in the center of an 8-cm cube of Lucite and positioned 62 cm from the electron target. After applying corrections for inverse square divergence of the beam and the angular dependance of the intensity over the finite angle subtended by the sample at the electron target, it was possible to reduce each irradiation to the same dose rate. Irradiations used lasted 10 minutes at high energy and 2 hr at low energy (~15 000 roentgens per irradiation).

The desired nuclides were isolated for counting by chemical methods and were deposited by filtration on 1-inch diameter filter papers (~9 mg/cm²). The chemical procedures followed were those outlined in the Plutonium Project Report[11] with slight modifications particularly in the cadmium procedure to include a tin scavenging step. The filter papers containing the activity were mounted in holders between two plastic films about 1 mg/cm² thick and were counted in an automatic counting device. This automatic counter was built to accommodate up to 11 samples and one standard source whose activity could be measured in sequence. In most cases decay curves were followed through several half-lives with a recorded count of 6000 disintegrations for each point on the decay curves.

Since preliminary measurements established that the $S(Y,A,E_0)$ surface as a function of E_0 is reasonably smooth, mass yield curves were taken only at betatron energies of 12, 18, and 22 Mev. Yield measurements were carried out on 12 fission product nuclides with barium separated in each case so that the activity of Ba^{139} could be used as a control activity. The 3 mass-yield curves, coupled with measurements of the yields of Cd^{115} and Ba^{139} at ~1 Mev intervals to 24 Mev, served to define the $S(Y,A,E_0)$ surface.

COMPUTATIONS

Usually, in fission yield analysis one is not concerned with the measurement of individual nuclides but rather with the total yield of each beta decay chain. For this reason computations should be based on the yield of stable isotopes at the end of the chains. However, negligable error is involved if isotopes one or two places removed from the stable nuclide are used. Since the early members of a decay chain are largely very short-lived, a two-stage decay equation will usually represent the yields with sufficient accuracy. That is, the parent of the nuclide being counted may be considered as a primary fission product and the yield $Y(E_0,A)$ of mass chain A in atoms per roentgen of irradiation per atom of U^{238} is given by

$$Y(E_0,A)=\frac{\lambda_2 N_2(\lambda_2-\lambda_1)}{\lambda_2\phi N_0}$$
$$\times\left[(1-e^{-\lambda_1 t_R})e^{-\lambda_1 t}-\frac{\lambda_1}{\lambda_2}(1-e^{-\lambda_2 t_R})e^{-\lambda_2 t}\right]^{-1}, \qquad (2)$$

where λ_1, λ_2 = the decay constants of the parent and daughter nuclides respectively; $\lambda_2 N_2$ = activity in counts/min of the daughter at time of separation from parent (corrected for counting efficiency and corrected to 100 percent chemical recovery); ϕ = x-ray intensity averaged over the uranium sample in roentgens per minute; N_0 = number of uranium atoms in the sample

[10] L. Katz and A. G. W. Cameron, Can. J. Phys. **29**, 518 (1951).

[11] D. C. Coryell and N. Sugarman, *Radiochemical Studies; The Fission Products* (McGraw-Hill Book Company, Inc., New York, 1951), National Nuclear Energy Series Plutonium Project Record, Vol. 9, Div. IV.

TABLE I. Yield of mass chains 115 and 139 in radioactive nuclei per atom U^{238} per roentgen of irradiation.

E_0 Mev	Yield $A=115$	$A=139$
8		0.37×10^{-19}
10		1.15
12	0.36×10^{-20}	2.29
13	0.68	2.85
13.5	0.74	3.53
14	1.12	3.82
15	1.35	4.83
16	1.88	4.88
18	2.97	5.45
20		6.02
20.2	3.65	6.28
22	4.22	6.23
22.5	3.93	6.47
23	4.97	
23.5		6.28
24	4.77	6.47

from which chemical separation is made; t_B = duration of irradiation; and t = decay time from end of irradiation to time of separation from the parent.

This yield is related to the cross section for photofission by the equation

$$Y(E_0,A)=\int_0^{E_0} P(h\nu,E_0)(\sigma_{\gamma f}(h\nu))_A dh\nu, \qquad (3)$$

where $P(h\nu,E_0)$ is the number of photons of energy $h\nu$ per roentgen of irradiation, falling per cm^2 of sample when the maximum bremsstrahlung energy is E_0, per Mev energy interval.

If the isotope being counted had a short-lived β-emitting daughter, then a correction was applied for the growth of this daughter subsequent to chemical separation.

The decay schemes for the 12 fission-product nuclides separated chemically for our mass-yield studies were taken from the Tables of Isotopes by Hollander, Pearlman, and Seaborg.[12] These tables contain the most recent survey of the literature and no pertinent new results on the 12 isotopes have appeared since their publication.

Corrections for self-absorption are very small since the samples were all less than 8 mg/cm^2 thick. They were calculated according to the methods of Baker and Katz.[13] Corrections for external absorption were applied under the assumption that it is exponential with the absorption coefficient given by Eq. (6) of reference 13. To obtain a backscattering correction, the data of Engelkemeir *et al.*[14] and Yaffe[15] were combined. This gave the percent backscattering from our filter paper as a function of beta energy. This correction was always less than 10 percent.

[12] Hollander, Pearlman, and Seaborg, Revs. Modern Phys. **25**, 469 (1953).
[13] R. G. Baker and L. Katz, Nucleonics **II**, No. 2, 14 (1953).
[14] Engelkemeir, Seiler, Steinberg, and Winsberg, paper 9, reference 11.
[15] L. Yaffe, *Conference on Absolute Beta Counting*, Preliminary Report No. 8 (National Research Council, Washington, D. C., 1950).

The geometric efficiency of the counting system was determined by our usual method of irradiating a copper disk in the betatron beam under standard conditions and counting the induced Cu^{62} activity. Comparison of this to the known activity for the sample in 4π geometry[10] then gave the geometric efficiency. Because of the size of the uranium sample it was necessary to apply one further correction. Suppose $I_0(h\nu)$ is the photon intensity of energy $h\nu$ falling on the sample surface, then the intensity at a distance x within the sample is

$$I_0\left(\frac{a}{a+x}\right)^2 e^{-\mu\rho x}, \qquad (4)$$

where a is the distance of the sample front from the electron target, $\mu(h\nu)$ is the mass absorption coefficient of uranyl nitrate, and ρ is the sample density. The average intensity for a sample of length b is

$$\bar{I}=\frac{I_0}{b}\int_0^b \frac{e^{-\mu\rho x}}{(1+x/a)^2}dx. \qquad (5)$$

Since in our case $a=28$ cm and $b=5.5$ cm, we can assume $x/a<1$ over the region of integration. This approximation shows the dependence of $\bar{I}/I_0$ on $(h\nu)$ is primarily through the relation $(1-e^{-\mu\rho b})/\mu\rho b$. Though μ is a strong function of $h\nu$, the variation of $\bar{I}/I_0$ with energy is less than 2 percent over the energy range involved in this work. Calculation gives $\bar{I}=0.70I_0$ and show it to be insensitive to slight variations in ρ from sample to sample.

The total yield of fissioning nuclides at a betatron operating energy E_0, per irradiated U^{238} nucleus per roentgen of irradiation is given by

$$Y(E_0)=\int_0^{238} Y(E_0,A)dA. \qquad (6)$$

We can now define the total photofission cross section by the equation

$$Y(E_0)=\int_0^{E_0} P(h\nu,E_0)\sigma_{\gamma f}(h\nu)dh\nu, \qquad (7)$$

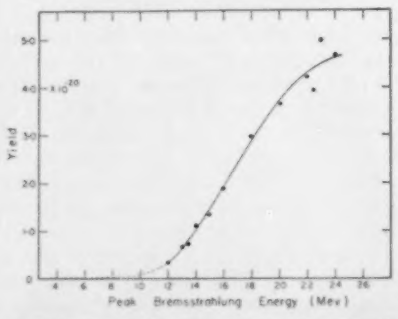

FIG. 1. Yield of mass chain 115 resulting from photofission of U^{238} as indicated by the yield of the 54-hr Cd^{115} beta-ray activity. The yield is expressed in nuclei of mass 115 per irradiated U^{238} nucleus per roentgen of irradiation.

where $P(h\nu,E_0)$ has been already defined and $\sigma_{\gamma f}(h\nu)$ is the cross section for causing fission by photons of energy $h\nu$. Substituting $Y(E_0,A)$ from Eq. (3) into (6) and inverting the order of integration, we find

$$\sigma_{\gamma f}(h\nu)=\int_0^{225}(\sigma_{\gamma f}(h\nu))_A dA. \qquad (8)$$

EXPERIMENTAL RESULTS

The measured yields of mass chains 115 and 139 (Cd^{115} and Ba^{139}) in nuclei per U^{238} nucleus per roentgen of irradiation as a function of betatron operating energy E_0 are summarized in Table I. Owing to low yield, no measurements were obtained below 12 Mev on mass chain 115 and below 8 Mev on mass chain 139. These results are plotted in Figs. 1 and 2 with the dashed parts of the curves representing a smooth extrapolation of the experimental data to low energy.

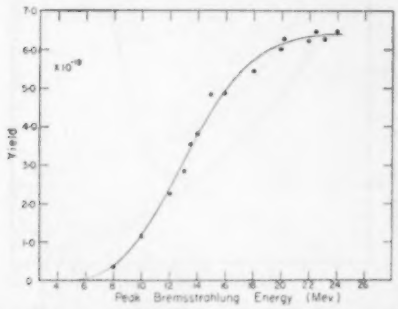

FIG. 2. Yield of mass chain 139 resulting from photofission of U^{238} as indicated by the yield of 85-min Ba^{139}. The yield is expressed in nuclei of mass 139 per irradiated U^{238} nucleus per roentgen of irradiation.

The results of our measurements on the yield of 12 mass chains at betatron operating energies of 12, 18, and 22 Mev are summarized in Table II. These yields are expressed in nuclei in each mass chain per irradiated U^{238} nucleus per roentgen of irradiation. We estimate the values given in this table to be accurate to within ±25 percent and the relative dispersion among the values plotted in Figs. 1 and 2 to be considerably less, probably 10 percent.[16] The yields are plotted in Figs. 3, 4, and 5 as circles. It was found that in all cases reflection of these points about mass 117.5 resulted in a smooth curve. This corresponds to the emission on an average of 3 neutrons per fission, in good agreement with the measurements of other workers.[6,8] The reflected points are indicated by crosses in the three figures. Few points were available for the 12-Mev curve because of the low activities of the longer-lived fission-fragment nuclides.

[16] An estimate in this relative scattering in our yield measurements can be obtained from an examination of Figs. 1 and 2. There is good reason to expect that experimental points should be on a smooth curve, and dispersion of the points from such a smooth curve indicates the accuracy to which measurements could be repeated.

TABLE II. Mass yields at constant E_0 in radioactive nuclei per atom U^{238} per roentgen of irradiation.

Mass No.	Nuclide measured	Yield $E_0=12$ Mev	$E_0=18$ Mev	$E_0=22$ Mev
77	39 hr As^{77}			0.06×10^{-19}
83	2.4 hr Br^{83}	0.15×10^{-19}	0.53×10^{-19}	0.61
89	54 day Sr^{89}		4.9	5.3
97	17 hr Zr^{97}		7.1	7.4
99	67 hr Mo^{99}		6.1	6.9
103	40 day Ru^{103}			3.9
105	4.5 hr Ru^{105}	1.0	2.3	2.6
111	7.5 day Ag^{111}		0.23	0.36
115	54 hr Cd^{115} } 43 day Cd^{115m}	0.036	0.29	0.43
138	30 min Cs^{138}		5.9	6.9
139	85 min Ba^{139}	2.4	5.6	6.3
143	33 hr Ce^{143}		5.3	5.8

This curve was drawn to have essentially the same shape as the 18- and 22-Mev curves. The double humped shape of the 18- and 22-Mev curves is quite well defined by the experimental points, and while no special attempt was made to measure the fine structure reported at masses 100 and 134[8,17,18] the high yields of Mo^{99} and Zr^{97} may be taken to indicate that it has been detected in our experiments. It will also be noted that mass 111 falls slightly below mass 115 in the 18- and 22-Mev curves. This is not in agreement with other photofission results and may be due to the difference in the absolute normalization of the mass 115 activation curve.

Peak-to-valley ratio of the fission yield curves is obtained directly from Figs. 1 and 2. This ratio is shown as curve A of Fig. 6. Schmitt and Sugarman reported values of 200, 38, 23, and 20 for this ratio at $E_0=10$, 16, 21 and 22 Mev, respectively. These values are somewhat higher than those found by us at corresponding energies, which are 150, 25, 15, and 14. The disagreement is within the combined error of both sets of measurements and is likely due to the absolute normalization of the

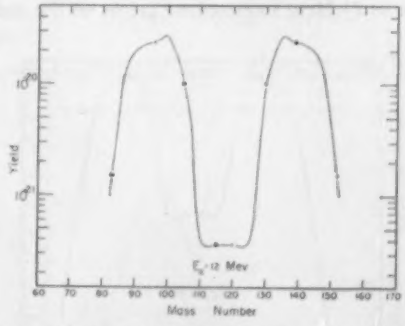

FIG. 3. Yield of mass chains 83, 105, 115, and 139 at a betatron operating energy of 12 Mev. The measurements are indicated by the circles and reflection of these about mass 117.5 are indicated by crosses. The curve drawn through these points was made to correspond in shape to those shown in Figs. 4 and 5.

[17] Glendenin, Steinberg, Inghram, and Hess, Phys. Rev. **84**, 860 (1951).

[18] D. R. Wiles and C. D. Coryell, Phys. Rev. **96**, 696 (1954).

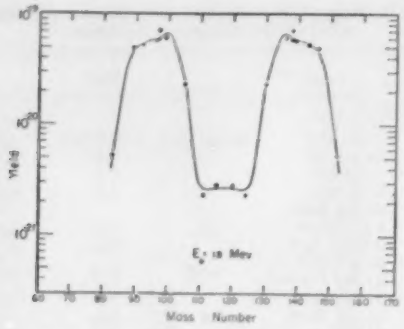

FIG. 4. Yield of mass chains 83, 89, 97, 99, 105, 111, 115, 138, 139, and 143 at a betatron operating energy of 18 Mev. The measurements are indicated by the circles and reflection of these about mass 117.5 are indicated by crosses.

mass 115 chain activation curve. The results of both investigations show a similar smooth variation of the peak-to-valley ratio with betatron operating energy. This is in strong disagreement with the results of Richter and Coryell[8] who obtained a value of 110 at $E_0=16$ Mev and predicted a sharp drop in this ratio just above 16 Mev.

In Fig. 7 we again show the peak-to-valley yield ratio, this time on a log-log plot. Our measurements are represented by the heavy line. The results of Schmitt and Sugarman[6] to 300 Mev are indicated by circles and those of Richter and Coryell[8] by crosses. The changing peak-to-valley ratio at high energy has been correctly interpreted by Schmitt and Sugarman[19] to indicate a tail on the $\sigma_{\gamma f}$ cross section. For the purpose of the analysis which will be carried out later our ratio has been extrapolated to high energy in agreement with the data of Schmitt and Sugarman. This extrapolation is indicated by the light solid line of Fig. 7.

Figures 1 to 6 serve to define the whole $S(Y,A,E_0)$ surface to 24 Mev. Intermediate points on the surface

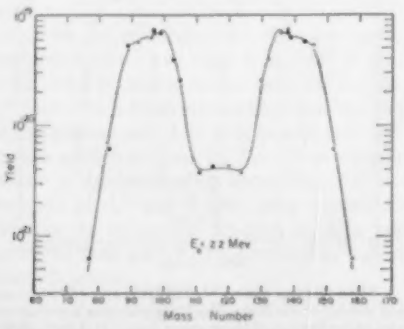

FIG. 5. Yield of mass chains 77, 83, 89, 97, 99, 103, 105, 111, 115, 138, 139, and 143 at a betatron operating energy of 22 Mev. The measurements are indicated by the circles and reflection of these about mass 117.5 are indicated by crosses.

[19] R. A. Schmitt and N. Sugarman, Phys. Rev. **89**, 1155 (1953).

were obtained, to within experimental accuracy by various cross plots of these 6 figures. This procedure naturally smooths over any fine structure detail, but does give the 3-dimensional shape of the yield surface in its broad outline.

ANALYSIS AND DISCUSSION OF EXPERIMENTAL RESULTS

Analysis of the data in Table I by the photon difference method[10] gave the photofission cross sections from threshold to 24 Mev leading to mass chains 115 and 139, that is $(\sigma_{\gamma f})_{115}$ and $(\sigma_{\gamma f})_{139}$. These cross sections are shown in Figs. 8 and 9 as a function of photon energy. The values above 24 Mev indicated in these curves were calculated by another method which will be discussed later.

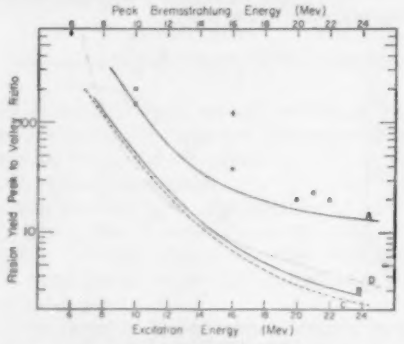

FIG. 6. Curve A: Ratio of mass 139 yield to mass 115 yield as a function of betatron operating energy (peak bremsstrahlung energy as shown on top scale). For comparison we have shown the ratio in similar measurements by Schmitt and Sugarman, reference 6 (open circles) and reference 19 (open triangle); by Richter and Coryell, reference 8 (crosses); and by Spencer, Table III, reference c (black triangle). Curve B: Ratio of photofission cross sections leading to mass chains 139 and 115 (asymmetric to symmetric fission) as a function of photon energy (bottom scale). Curve C: Asymmetric to symmetric fission yields *vs* energy of excitation as given by Hill and Wheeler, reference 21. This curve is based on the results of fission induced in various nuclides by energetic particles. Curve D: Similar to C according to Turkevich *et al.*, reference 22. Solid black circle gives ratio for thermal neutron fission of U^{235}.

The cross sections show the usual "resonance" shape characteristic of other photonuclear cross sections. $(\sigma_{\gamma f})_{115}$ reaches a maximum value of 0.73 millibarn at 18 Mev while $(\sigma_{\gamma f})_{139}$ has a maximum value of 6.8 millibarns at 14 Mev. Both cross sections have a width at half-maximum of about 9 Mev. The shift in the peak position of $(\sigma_{\gamma f})_{115}$ relative to $(\sigma_{\gamma f})_{139}$ towards higher energy by about 4 Mev is of some interest.[20]

Curve B of Fig. 6 shows the cross-section ratio $R=(\sigma_{\gamma f})_{139}/(\sigma_{\gamma f})_{115}$ as a function of photon energy. This ratio is of greater physical significance than curve A since it gives the probability ratio of asymmetric to symmetric fission as a function of nuclear excitation energy whereas curve A is the average of this ratio over

[20] Fowler, Jones, and Paehler, Phys. Rev. **88**, 71 (1952).

the bremsstrahlung spectrum. Hill and Wheeler[21] and Turkevich *et al.*[22] have drawn curves of peak-to-valley ratio against excitation energy by collecting the results of many workers on fission induced in various nuclides by energetic particles. Their results are shown as curves *C* and *D* respectively in Fig. 6. These are in excellent agreement with our results. In all cases the peak-to-valley ratio changes from approximately 150 at 8-Mev excitation to about 3 at 24-Mev excitation. (In the case of particle induced fission the excitation energy is of course the incident particle energy plus its binding energy to the target nucleus.)

It is of some interest to examine in greater detail the ratio discussed above. This examination is particularly meaningful since the present work gives the ratio for a single uranium isotope over a fairly extended energy range. It has been suggested[20] that a plot of $\ln R$ against

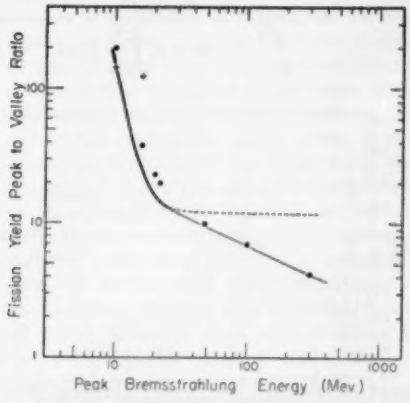

FIG. 7. Black solid line: Ratio of peak-to-valley yields taken from curve *A* of Fig. 6. Circles: Ratio of peak-to-valley yields to 300 Mev from reference 6. Light solid line: smooth extrapolation of our data to high energy. Crosses: Measurements of this ratio by Richter and Coryell, reference 8. Dashed line: Ratio which would have been obtained at high energy if symmetric and asymmetric cross-section curves had no tail beyond 24 Mev.

$(E-\Phi)^{-1}$ should yield a straight line, where R is defined above, E is the nuclear excitation energy, equal to $h\nu$ in our case, and Φ is a constant, probably the photofission threshold.[23] Fowler *et al.*[20] have collected the experimental ratios of many workers and using such a plot found a straight line to give the best fit. In Fig. 10 we

[21] D. L. Hill and J. A. Wheeler, Phys. Rev. **89**, 1102 (1953).
[22] Turkevich, Niday, and Tompkins, Phys. Rev. **89**, 552 (1953).
[23] There is some confusion as to the exact meaning of "photofission threshold." Energetically, since the U^{238} nucleus will undergo spontaneous fission, this threshold should be less than zero and we should take $\Phi=0$. On the other hand, from an experimental point of view there is some energy of excitation which is required to give a readily detectable fission rate (say one fission per hour). The exact energy assigned to this "experimental" threshold will depend only slightly on the apparatus sensitivity. Thus, in the case of U^{238}, measurements in our laboratory show that an increase in the sensitivity of the apparatus for determination of threshold by a factor of 10 lowers the "observed" threshold by less than 0.1 Mev. It can be argued that Φ should correspond to this "experimental" threshold, namely 5.1 Mev.

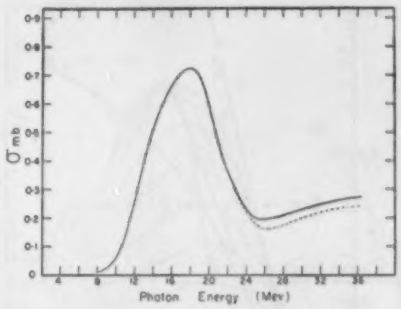

FIG. 8. Cross section for symmetric fission obtained from analysis of Fig. 1 by the photon difference method. The cross section above 24 Mev was obtained from the analysis of the ratio of Fig. 7 as outlined in the text. The dashed curve is obtained if the asymmetric cross section is assumed zero above 24 Mev.

show plots with $\Phi=0$ and 5.1 Mev, using our results from 12 to 24 Mev and using at lower energies the results obtained from neutron-induced fission in various isotopes of uranium. The results for neutron-induced fission are summarized in Table III. Our results were not felt to be sufficiently reliable below 12 Mev for this study.

For $\Phi=0$ a straight line is obtained; however, if we accept $\Phi=5.1$ we must conclude that there is a break in the curve at $h\nu=10$ Mev. If this break actually exists, one can suggest a number of reasons for it. First we notice that the break occurs at an energy where neutron emission followed by fission becomes energetically possible. The process of neutron emission may perhaps result in a changed value of R. Secondly, whatever the reason, one could suggest that there are two modes of symmetric fission and one mode of asymmetric fission. In this case we could write

$$R=\frac{(\sigma_{\gamma f})_{239}}{(\sigma_{\gamma f})_{118}'+(\sigma_{\gamma f})_{118}''}=\frac{R_1R_2}{R_1+R_2}, \tag{9}$$

where

$$R_1=(\sigma_{\gamma f})_{239}/(\sigma_{\gamma f})_{118}' \quad \text{and} \quad R_2=(\sigma_{\gamma f})_{239}/(\sigma_{\gamma f})_{118}''.$$

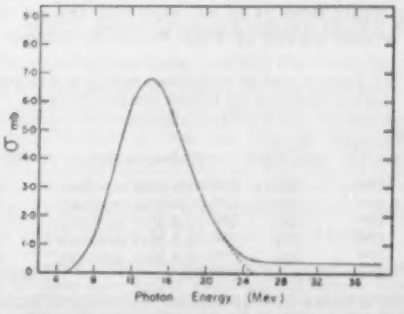

FIG. 9. Cross section for asymmetric fission obtained from analysis of Fig. 2 by the photon difference method. The cross section above 24 Mev was obtained from the analysis of the ratio of Fig. 7 as outlined in the text.

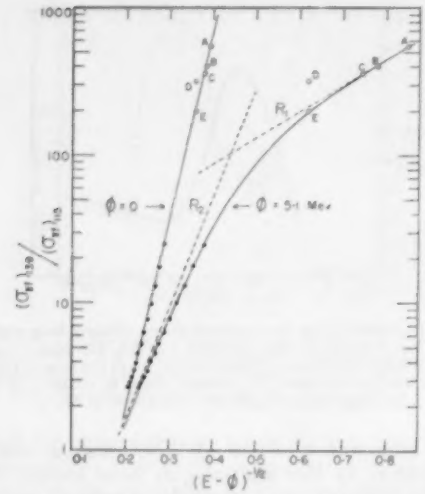

FIG. 10. Plots of the logrithm of the ratio of asymmetric to symmetric photofission cross sections as a function of $(E-\Phi)^{-\frac{1}{2}}$, where E is the excitation energy and Φ is a constant. Plots for two values of Φ are shown. Black points are values taken from curve B of Fig. 6 at 1-Mev intervals in the energy range of 12 to 24 Mev and the other points are listed in Table III; A reference a of Table III, B reference b, C and D reference c, and E reference d. For $\Phi=0$ the best fit straight line is drawn, and for $\Phi=5.1$ Mev the line drawn is $R_1R_2/(R_1+R_2)$, where R_1 and R_2 are the dashed straight lines as shown.

The primes distinguish between the two modes of symmetric fission. The solid line for $\Phi=5.1$ represents the expression $R_1R_2/(R_1+R_2)$, with R_1 and R_2 shown by the dashed straight lines in the diagram. To emphasize the agreement between our experimental data and this line, we have plotted points at 1-Mev intervals taken from the smooth curve of Fig. 6B. These procedures are entirely empirical and it is not clear whether any significance is to be attributed to the conclusions.

HIGH-ENERGY FISSION CROSS SECTION

It is possible to calculate the photofission cross section leading to symmetric and asymmetric fission in the energy region from 24 to 300 Mev with the aid of our cross section curves of Figs. 8 and 9, Schmitt and Sugarman's yield ratio as shown in Fig. 7 and the following analysis. According to Eq. (3) we can write the ratio of yields at bremsstrahlung energy E_0:

$$R(E_0)=\frac{\int_0^{E_0}P(h\nu,E_0)(\sigma_{\gamma f}(h\nu))_a dh\nu}{\int_0^{E_0}P(h\nu,E_0)(\sigma_{\gamma f}(h\nu))_s dh\nu}, \tag{10}$$

where the subscripts a and s designate the cross sections for asymmetric and symmetric fission. For energies above 24 Mev, the cross sections are not expected to be strong functions of energy and we can write

$$R(E_0)=\frac{\int_0^{24}P\sigma_a dh\nu+\bar{\sigma}_a\int_{24}^{E_0}P dh\nu}{\int_0^{24}P\sigma_s dh\nu+\bar{\sigma}_s\int_{24}^{E_0}P dh\nu}, \tag{11}$$

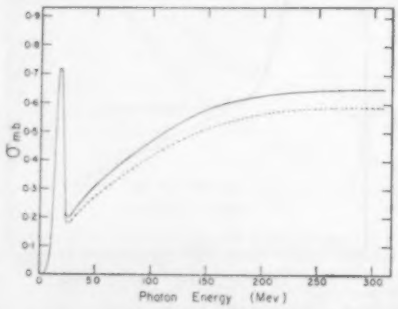

FIG. 11. Cross section for symmetric fission as shown in Fig. 8 except energy scale has been extended to 300 Mev. Calculation of the solid-line tail above 24 Mev is according to Eq. (11) as explained in the text. The dashed line shows the minimum symmetric fission cross section consistent with the data of Fig. 7.

where $\bar{\sigma}_a$ and $\bar{\sigma}_s$ are the average cross sections in the energy range 24 to E_0. In this equation the integrals can be calculated from our cross sections to 24 Mev and the Schiff[24] thin-target spectrum properly normalized.[10] $R(E_0)$ is known from the data of Schmitt and Sugarman as shown in Fig. 7. This leaves two unknowns, $\bar{\sigma}_a$ and $\bar{\sigma}_s$, and only one equation. However, their ratio can be found to a good degree of accuracy if we extrapolate the graph of Fig. 10 to a high energy (we used the curve with $\Phi=5.1$). For the first calculation we chose $E_0=29$ Mev and, by making use of the average cross section so obtained, it was next possible to calculate the average cross sections in the energy range 29–35 Mev. This process was repeated in steps of increasing size to 300 Mev. These cross-section curves are shown in Figs. 9 and 11. In Fig. 9 the tail on σ_a is indicated by the solid line. It decreases slowly from 0.3 millibarn at 35 Mev

TABLE III. Ratio of peak-to-valley cross section as a function of nuclear excitation for various uranium isotopes.

E Mev	Compound nucleus	Ratio peak/valley	Nuclear reaction	Reference
6.50	U^{239}	550	U^{238}+thermal neutrons	a
6.74	U^{239}	400	U^{238}+thermal neutrons	b
6.9	U^{239}	360	U^{238}+0.4-Mev neutrons	c
7.7	U^{239}	320	U^{238}+1.2-Mev neutrons	c
7.6	U^{239}	200	U^{238}+2.8-Mev neutrons	d
12–24	U^{239}	25–2.7	$U^{238}+h\nu$	this paper

[a] E. P. Steinberg and M. S. Freedman, Paper 219, reference 11.
[b] Steinberg, Selber, Goldstein, and Dudley, U. S. Atomic Energy Commission declassified document MDDC-1632, Jan. 6, 1948 (unpublished).
[c] P. W. Spencer, Brookhaven National Laboratory Conference Report BNL-C-9, July, 1949 (unpublished).
[d] Kebler, Steinberg, and Glendenin, Phys. Rev. **94**, 969 (1954).

[24] L. I. Schiff, Phys. Rev. **83**, 252 (1951).

to 0.1 millibarn at 300 Mev. The initial portion of the symmetric-fission cross-section tail is shown in Fig. 8 and the whole curve to 300 Mev is shown in Fig. 11. This cross section falls to approximately 0.2 millibarn at 25 Mev then rises reaching a value at 300 Mev nearly equal to the low-energy peak cross section. The two cross sections are equal at ~50 Mev, with σ_s becoming larger at the higher energies.

To get a lower limit to the magnitude of the large symmetric-fission cross-section tail, we can assume $\bar{\sigma}_a$ in Eq. (11) to be zero at all energies above 24 Mev and repeat the previous calculations. The results of such calculations is indicated by the dashed lines in Figs. 8 and 11. This is the minimum $\bar{\sigma}_s$ value consistant with experimental data and is not much different from our previous results.

At this point we wish to emphasize one fact. The σ_a and σ_s cross sections are given as functions of the *energy of excitation of the compound nucleus, not the energy of excitation when fission occurred.* These two energies are not necessarily equal since the compound nucleus may lose a considerable amount of its excitation energy by multiple neutron emission[1,25] prior to fissioning. In fact, the tail on the asymmetric fission curve, if it really exists, may simply indicate that some nuclei have become de-excited by multiple neutron emission to such an extent that fission really occurred at low energy. Similarly, the rise in the symmetric fission cross section curve above 25 Mev may indicate the appearance of a fast mode of fission which competes effectively with neutron emission, resulting in a larger fraction of the excited nuclei fissioning while still retaining a considerable portion of this energy of excitation.

3-DIMENSIONAL SHAPE OF THE PHOTOFISSION CROSS-SECTION SURFACE

Cuts at constant mass number through the 3-dimensional $S(Y,A,E_0)$ surface which was constructed from Figs. 1 to 6, gave a number of yield curves similar to these shown in Figs. 1 and 2, but at different mass numbers. These yield curves were solved by the photon difference method to give a number of $(\sigma_{\gamma f}(h\nu))_A$ cross sections curves. Finally, these curves were combined with those already discussed to define the $S(\sigma,A,h\nu)$ surface shown in Fig. 12.

Logarithmic scales were used for the cross section and energy axes of Fig. 12 in order to give the various parts of the surface proper balance. Only the heavy-mass side of $S(\sigma,A,h\nu)$ lying within the energy range 10 to 300 Mev is shown in this figure. The cuts through this surface at $A=117.5$ and $A=139$ are reproductions of the cross sections shown in Figs. 11 and 9 respectively. (Curve at mass number 139 is drawn with the high-energy tail.) None of the cross sections for the other mass numbers which were used to establish the shape of this surface are shown on the figure since to include them would have complicated the drawing.

[25] M. Lindner and R. N. Osborne, Phys. Rev. **94**, 1323 (1954).

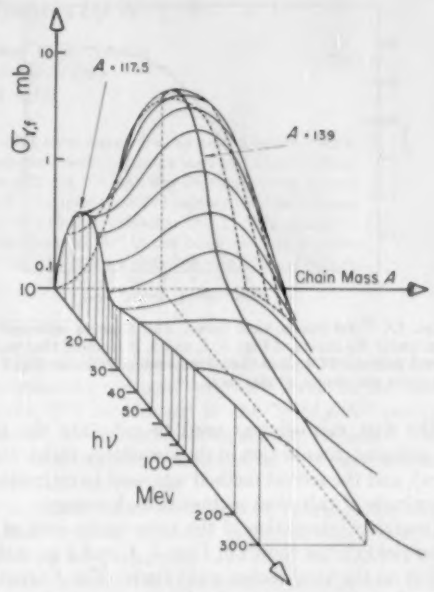

FIG. 12. The $S(\sigma,A,h\nu)$ surface. Since it is symmetric about mass number 117.5, only the higher mass side is shown. The cross sections shown in Figs. 9 and 11 are reproduced on this surface as curves at mass numbers 139 and 117.5 respectively. Note that the energy scale starts at 10 Mev on the low-energy side so that the $A=139$ curve cuts the $\sigma-A$ plane at a finite value. The shape of this surface to 24 Mev is quite well established and above this energy only the $A=117.5$ curve is known with any accuracy.

It must be pointed out that in the high-energy region only the symmetric cross section has been established with any degree of accuracy, the asymmetric cross section is known to an order of magnitude, and nothing is known of the high-energy photofission cross sections for other mass numbers.[26] From these meager data we can, however, conclude that the high-energy photofission cross section is symmetric in mass at constant photon energy, and from the analysis by Schmitt and Sugarman of their data we can take this curve to have a width at half-maximum of ~20 mass units.

TOTAL PHOTOFISSION CROSS SECTION

There are two methods by which the total photofission cross section can be calculated: (i) The total yield at any betatron energy E_0 can be calculated according to Eq. (6) and the cross section can thus be calculated from Eq. (7) by the photon difference method. (ii) According to Eq. (8), this cross section can be obtained at any energy $h\nu$ by taking the area under the curve defined by a cut in the surface of Fig. 12 at that energy.

[26] It was not possible to calculate the high-energy cross-section tails for these intermediate mass numbers from a yield curve extending to high energy, because the cross section so obtained is very sensitive to the absolute photon dose delivered to the sample at each energy. The calculation of σ_a and σ_s was made possible through the availability of the ratio of yields which are not dependent on the irradiation dose.

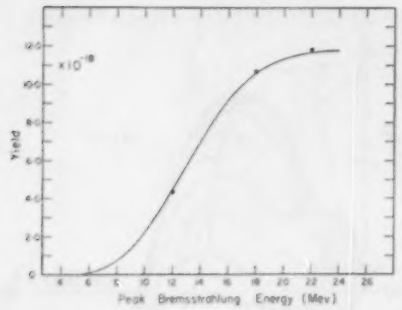

FIG. 13. Total fission yield curve. The 3 points represent the areas under the curves of Figs. 3, 4, and 5. It is found that each of these 3 points is 18.4 times the corresponding yields on Fig. 2 and this curve was drawn similar to it.

The first method was used to calculate the total photofission cross section in the low-energy region (to 24 Mev), and the second method was used to estimate the magnitude of this cross section at high energy.

Graphical integration of the areas under each of the mass-yield curves shown in Figs. 3, 4, and 5 gave three points on the total fission yield curve. The 3 areas are somewhat dependent on the precise shapes chosen for the peaks of the mass-yield curves, particularly the fine structure "hump." Since it has been established experimentally[6] that the shape of the peaks does not vary appreciably with energy, all 3 curves were drawn with the same peak shapes to within the limitations set by our experimental points. Because the area under the trough contributes very little to the total area under each curve, it would appear that the total fission yield should be closely proportional to the yield of mass 139. This was found to be true and the area in each case was found to be 18.4 times the yield of mass chain 139.

The total mass-yield curve is shown in Fig. 13 with the 3 points at 12, 18, and 22 Mev obtained by the graphical integration indicated by circles. Since this curve is identical with that for mass chain 139 shown in Fig. 2 except for the factor 18.4, the total photofission cross section, $\sigma_{\gamma f}$, to 24 Mev can be obtained directly from Fig. 9 by multiplying it by this factor. The resultant curve so obtained is shown in Fig. 14. It has a peak value of 125 millibarns at 14 Mev and an integrated cross section to 24 Mev of 1.1-Mev barns. The width at half-maximum is 8.8 Mev. These values are in good agreement with the measurements of Duffield and Huizenga.[5] They report a peak cross section of 180 millibarns situated at 14 Mev and an integrated cross section to 20 Mev of 1.2-Mev barns.

Above 150 Mev we can obtain the total photofission cross section from our values of σ_e and the estimate by Schmitt and Sugarman[6] that it has a half-width of 21 mass units. Above 150 Mev σ_e is quite constant $\sim$0.65 millibarn (see Fig. 11). We thus find $\sigma_{\gamma f}$ in this energy region to be $\sim$7 millibarn. This is in surprisingly good agreement with the average value of 7 millibarn found by Schmitt and Sugarman.[6] Below 150 Mev the symmetric cross section decreases with decreasing energy; however, the asymmetric cross section probably becomes more important, and as a first approximation we can estimate the total photofission cross section to remain constant.

Levinger and Bethe[27] and more recently Gell-Mann, Goldberger, and Thirring[28] have shown that the integrated nuclear absorption cross section for photons of all multipolarities is given by

$$\int_0^\infty \sigma_a d(h\nu) = 0.060 \frac{ZN}{A}\left(1+0.1\frac{A^2}{ZN}\right), \qquad (12)$$

where μ is the meson threshold $\sim$150 Mev, σ_a is the photon capture cross section, and the other symbols are as usually defined For U^{238} this equation gives an integrated cross section of 4.8 Mev barn. From the above analysis we can estimate the integrated total photofission cross section to 150 Mev to be 1.2 Mev barns. Duffield and Huizenga measured the integrated (γ,n) cross section in U^{238} to 20 Mev and find it to be 2.6 Mev barns. The difference of 1.0 Mev barn between the sum of these two experimental values and 4.8 Mev barns may represent the high-energy tail on the (γ,n) cross section as well as contributions from the $(\gamma,2n)$, (γ,np), (γ,p), etc., reactions.

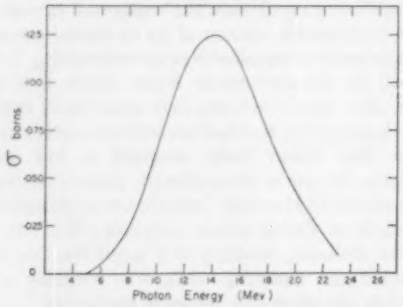

FIG. 14. Total photofission cross section as a function of photon energy. This curve can be obtained from Fig. 13 by the photon difference method, or since Fig. 13 is similar to Fig. 2 then this cross section is similar to that of Fig. 9 except that each ordinate is 18.4 times larger.

The authors would like to thank the Canadian National Research Council for financial assistance in the form of grants, and for scholarships to T.M.K. and A.G.W.C. They would also like to thank E. C. B. Pederson and H. J. King for analyzing some of the decay curves and Miss E. Shmyr and Miss R. Krehbiel for analytical assistance.

[27] J. Levinger and H. A. Bethe, Phys. Rev. **78**, 115 (1950).
[28] Gell-Mann, Goldberger, and Thirring, Phys. Rev. **95**, 1612 (1954).

Radiative Capture of Protons by N^{14}†

S. Bashkin, R. R. Carlson, and E. B. Nelson
State University of Iowa, Iowa City, Iowa
(Received March 28, 1955)

The 277-kev resonance for the production of O^{15} in its 7.61-Mev state was excited by proton bombardment of a thick TiN target. A three-crystal, scintillation spectrometer resolved gamma rays of 5.25±0.1 Mev, 6.10±0.1 Mev, and 6.65±0.15 Mev, with relative intensities of 25±6, 100, and 40±10, respectively. Direct ground state transitions have a relative intensity of less than 5. The total radiative capture yield in nitrogen is $(2.7\pm0.6)\times10^{-11}$ reaction per proton. The intensity ratio of 6.10-Mev radiation to 5.25-Mev radiation, measured with a single-crystal spectrometer, is 7±3 percent lower at 90° to the beam than at 0°. The asymmetry eliminates pure *s*-wave capture. It is concluded that the capture state has spin 5/2 and decays by dipole emission to the first three excited states of O^{15}.

INTRODUCTION

RADIATIVE capture and elastic scattering are the only nuclear reactions which can occur in the bombardment of N^{14} by protons with less than 3.1 Mev of energy. Tangen[1] has shown radiative capture to be resonant at a proton energy of 277 kev over a range of less than 2 kev. This corresponds to an excited state at 7.61 Mev in O^{15}. Duncan and Perry[2] obtained the $N^{14}(p,\gamma)O^{15}$ excitation curve by observing the positron activity from the short-lived residual nucleus. They suggested that the 277-kev resonance is excited by *s*-wave protons, giving a spin of $\frac{1}{2}^+$ or $\frac{3}{2}^+$ to the 7.61-Mev level in O^{15}.

Johnson, Robinson, and Moak[3] used a single-crystal, scintillation spectrometer to measure the energies of the gamma rays produced at the 277-kev resonance in the $N^{14}(p,\gamma)O^{15}$ reaction. The observed gamma rays were attributed to transitions from the capture state to the ground state by way of levels at 6.84 Mev, 6.19 Mev, and 5.27 Mev. Direct decays from the 7.61-Mev state to the ground state were not observed. These excited states have also been observed[4,5] in the $N^{14}(d,n)O^{15}$ reaction. Application[5] of Butler's stripping theory to the angular distributions of the neutrons in this reaction indicated that a state at about 6.8 Mev has a spin of $\frac{1}{2}^+$ or $\frac{3}{2}^+$. Assignments to the other states were less certain but included the suggestion of $\leq 5/2^-$ for a level at 7.48 Mev. The position of this level was sufficiently uncertain that it could be identical[6] with the 7.61-Mev level in O^{15}. Bent *et al.*[7] have attributed gamma rays of 6.81 Mev, 6.12 Mev, and possibly 5.26 Mev, to the reaction $N^{14}(d,n)O^{15}$.

The levels found in the foregoing experiments are in approximate correspondence with levels in the mirror nucleus, N^{15}, as located[8] in the $N^{14}(d,p)N^{15}$ reaction. However, N^{15} shows closely spaced levels near 5.3 Mev and 7 Mev which, if mirrored in O^{15}, have not been resolved in that nucleus.

The present experiment was an investigation of the absolute gamma ray and positron yields and the anisotropy of the gamma rays from the 277-kev resonance in the radiative capture of protons by N^{14}. It was hoped that these measurements would reduce the possible spin and parity assignments to the 7.61-Mev and lower excited states in O^{15}.

EXPERIMENTAL ARRANGEMENT

Protons, accelerated in a 500-kv Cockcroft-Walton accelerator and deflected through 90° by a magnetic field, struck a thick target of pressed titanium nitride powder, isolated from the vacuum pumps by a dry ice and acetone cold trap. Gamma-ray detectors were single-crystal and three-crystal scintillation spectrometers, employing NaI(Tl) crystals and RCA5819 photomultiplier tubes. The three crystal spectrometer[9] consisted of three crystals in a row, the center crystal being 2 in. long by 1½ in. in diameter and the two side crystals being 1 in. long by 1½ in. in diameter. Distance from target to nearest center-crystal face was 2½ in. The pulses from the center detector were analyzed by a 10-channel pulse-height analyzer[10] only when a triple coincidence between the three detectors occurred. By this means, pulses from the center detector were measured when a pair was produced in the center crystal and both annihilation quanta escaped. The single-crystal spectrometer consisted of the center detector of the three-crystal spectrometer and the 10-channel pulse-height analyzer. Limiters of Elmore's design[11] were used with the single-crystal spectrometer in the study of low-energy gamma rays in the presence of high-energy radiation.

† Supported in part by the U. S. Atomic Energy Commission.
[1] R. Tangen, Kgl. Norske Videnskab. Selskabs Skrifter No. 1 (1946).
[2] D. B. Duncan and J. E. Perry, Phys. Rev. **82**, 809 (1951).
[3] Johnson, Robinson, and Moak, Phys. Rev. **85**, 930 (1952).
[4] W. M. Gibson and D. L. Livesey, Proc. Phys. Soc. (London) **A60**, 523 (1948).
[5] Evans, Green, and Middleton, Proc. Phys. Soc. (London) **A66**, 108 (1953).
[6] F. Ajzenberg and T. Lauritsen, Revs. Modern Phys. **24**, 321 (1952); Revs. Modern Phys. **27**, 77 (1955). We wish to thank Professor Lauritsen for a preprint of the latter paper.
[7] Bent, Bonner, McCrary, and Sippel, Phys. Rev. **98**, 1198(A) (1955).
[8] R. Malm and W. W. Buechner, Phys. Rev. **80**, 771 (1950).
[9] Carlson, Geer, and Nelson, Phys. Rev. **94**, 1311 (1954).
[10] W. C. Johnstone, Nucleonics **11**, No. 1, 36 (1953).
[11] W. C. Elmore, Rev. Sci. Instr. **20**, 963 (1949).

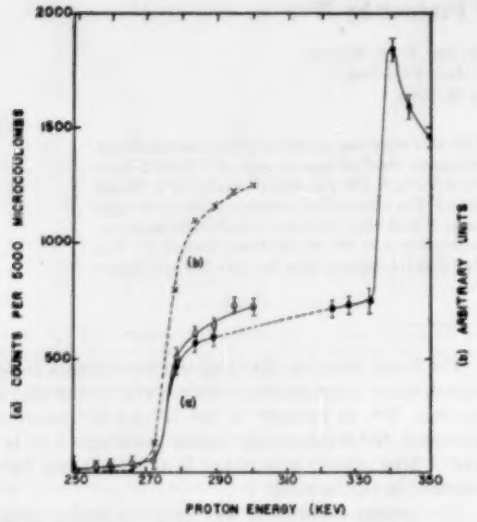

FIG. 1. (a) Yield curves of gamma rays of energy above 4.5 Mev for protons on thick TiN. Open circles obtained at outset of experiment; solid points at conclusion of experiment. (b) Yield curve of positrons for protons on thick TiN target.

GAMMA-RAY YIELDS

The solid curves of Fig. 1 illustrate the gamma-ray yield resulting from the proton bombardment of thick, titanium nitride targets for proton energies between 250 kev and 350 kev. Only gamma rays with energies in excess of 4.5 Mev were recorded in the yield curve measurements. The open points were taken at the start, and the solid points at the end, of the experiment. The good agreement of the two curves indicates that the target neither deteriorated nor accumulated any significant amount of surface contaminants during the lengthy bombardment by beams of about 100 μa. Since the O^{15} state at 7.61 Mev is less than 2 kev wide,[1] the range in proton energy over which the step in the yield curve occurs measures the inhomogeneity of the beam energy. This is estimated to be 3 kev. The absolute value of the proton energy was known to within ± 5 kev.

The peak which appears in the gamma-ray yield curve at a proton energy of 340 kev is due to a resonance for the production of 6.13-Mev gamma rays from the $F^{19}(p,\alpha\gamma)O^{16}$ reaction which was induced in fluorine contamination on the beam-defining apertures. For protons of less than 340 kev of energy, the fluorine reaction is some 900 times weaker[12] than at resonance. Its contribution to the measurements of this experiment was negligible.

The energy scale of the scintillation spectrometers was calibrated with the 6.13-Mev gamma ray from the $F^{19}(p,\alpha\gamma)O^{16}$ reaction which supplies a point at 5.11 Mev and with the 2.62-Mev gamma ray from ThC'' which supplies points at 2.62 Mev, 2.11 Mev, and 1.60 Mev. The calibration curve was linear within the accuracy of the measurement which was two percent at 6 Mev.

A single-crystal, scintillation-spectrometer survey of the gamma rays which appeared when 290-kev protons struck the target gave results in good agreement with those of Johnson, Robinson, and Moak.[3] Figure 2 shows the results of a three-crystal, scintillation-spectrometer study, at 0° to the beam, of the high-energy gamma rays arising from 295-kev proton bombardment of titanium nitride. Statistical uncertainties are given by the vertical lines. Three gamma rays are seen in Fig. 2. Their energies, which are 1.02 Mev plus the energy absorbed in the crystal, were measured as 5.25 ± 0.1 Mev, 6.10 ± 0.1 Mev, and 6.65 ± 0.15 Mev. These values agree within the experimental uncertainty with other determinations.[3,7]

In order to estimate the relative intensities of these gamma rays, the pulse-height distribution in Fig. 2 must be separated into the contributions made by each of the gamma rays. Background contributions from accidental triple coincidence and true triple coincidence from cascade decay were found to be negligible. The pulse-height distribution of the pure 6.13-Mev gamma ray from the $F^{19}(p,\alpha\gamma)O^{16}$ reaction was taken as a model for the pulse-height distributions of the three gamma rays observed above. Figure 3 shows the spectrum of Fig. 2 decomposed into its constituent parts. Figure 3 also shows the measured pulse-height distribution of the fluorine gamma ray. The relative intensities were assumed to be proportional to the relative peak heights after correcting for pair-production cross section. Choosing the intensity of the 6.10-Mev gamma

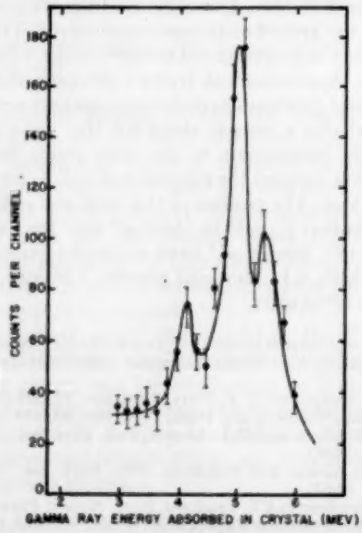

FIG. 2. Three-crystal, scintillation spectrometer analysis of gamma rays from $N^{14}(p,\gamma)O^{15}$ reaction for 295-kev protons on thick TiN.

[12] Chao, Tollestrup, Fowler, and Lauritsen, Phys. Rev. 79, 108 (1950).

ray as 100, the 5.25-Mev gamma ray has an intensity of 25±6, and the 6.65-Mev gamma ray an intensity of 40±10.

The pulse-height distribution was also measured with poorer resolution but increased detection efficiency by moving the spectrometer closer to the target. From this measurement, the intensity of the direct transition from the capture state to the ground state is estimated to be less than 5 percent that of the 6.10-Mev transition.

Comparison of the 6.10-Mev gamma-ray yield with that of the known[12] absolute yield of the fluorine gamma ray from a thick, calcium fluoride target at the 340-kev resonance, gave an absolute 6.10-Mev gamma-ray yield of $(4.5\pm1.1)\times10^{-12}$ gamma per proton for 295-kev protons on thick titanium nitride. By interpolating in the stopping power data of Warshaw[12] to obtain the stopping powers of nitrogen and titanium, and using the above relative intensities, the total absolute yield of the three $N^{14}(p,\gamma)O^{15}$ gamma rays for 295-kev protons on thick nitrogen is $(2.7\pm0.6)\times10^{-11}$ gamma per proton. Statistics, resolution, and uncertainties in the stopping powers contribute to the quoted error.

GAMMA-RAY ANISOTROPY

The possibility that the gamma rays might be distributed anisotropically was investigated with a single-crystal scintillation spectrometer placed alternately at 0° and 90° to the proton beam. The necessity of acquiring good statistics made it impossible to use the good resolution, but low efficiency, three-crystal, scintillation spectrometer. Hence the interpretation of the observed spectrum was complicated by the multiplicity of peaks produced in a single-crystal scintillation spectrometer by gamma rays of pair-producing energies. In this case, the one-escape peak of the 5.25-Mev gamma ray is not obscured by any other peaks, although there is, of course, a background due to degraded gamma rays. Similarly, the two-escape peak of the 6.10-Mev gamma ray is well isolated from other peaks, and the one-escape peak of the 6.10-Mev gamma ray is only slightly contaminated by the lower intensity, two-escape peak of the 6.65-Mev gamma ray. Consequently, the gamma rays were observed only in the energy range which encompasses those peaks.

In order to obtain an adequate yield of gamma rays a 100-μa proton beam and a $\frac{1}{4}$-in. diameter beam spot were used. The NaI(Tl) crystal of the scintillation detector was placed a distance of $2\frac{1}{2}$ in. from the target. Under these conditions an accurate measurement of the absolute angular distribution of the gamma rays could not be made. Measurements were, therefore, made on the difference in relative intensity of the 5.25-Mev and 6.10-Mev gamma rays when the angle of observation was changed from 0° to 90°. An isotropic distribution, which must follow s-wave capture and which might occur even for higher angular momentum waves, would give rise to the same ratio of intensities

[12] S. D. Warshaw, Phys. Rev. **76**, 1759 (1949).

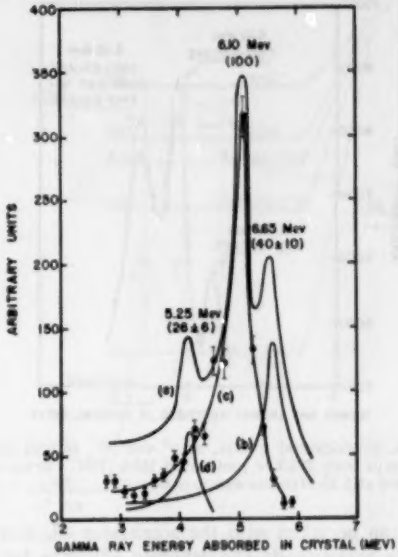

FIG. 3. Separation of high-energy spectrum of $N^{14}(p,\gamma)O^{15}$ gamma rays into individual components. (a) Total curve. (b) 6.65-Mev line. (c) 6.10-Mev line. (d) 5.25-Mev line. Points and statistics are shown for the fluorine measurement.

of the 6.10-Mev gamma rays to the 5.25-Mev gamma rays at the two angles. Unequal ratios would mean that at least one of the gamma rays under study was not distributed with spherical symmetry. The argument is not altered if the gamma rays are emitted in cascade processes.

Since the target was pressed onto a thin copper end-plate of a thin-walled brass tube and was normal to the beam, the emergent gamma rays did not traverse the same quantity of matter when viewed at 90° as when viewed at 0°. The difference in absorption of the 5.25-Mev and 6.10-Mev gamma rays emerging in the two directions was calculated and the effect on the anisotropy measurement was found to be negligible.

The 90° data were normalized to the 0° data at the one-escape peak of the 5.25-Mev gamma ray, so that any anisotropy would appear as a difference in the heights of both the one- and two-escape peaks of the 6.10-Mev gamma ray as measured at the two angles. Figure 4 shows the results. The dotted curve represents the 0° data and the solid curve, the 90° data. The 6.10-Mev gamma ray shows a definite decrease in intensity, relative to that of the 5.25-Mev radiation, as the angle of observation is altered from 0° to 90°. This decrease is estimated at 7±3 percent.

POSITRON MEASUREMENTS

There are certain advantages to measuring the absolute yield of the $N^{14}(p,\gamma)O^{15}$ reaction from the positron activity aside from the fact that it provides an independent check on the gamma ray results. Measure-

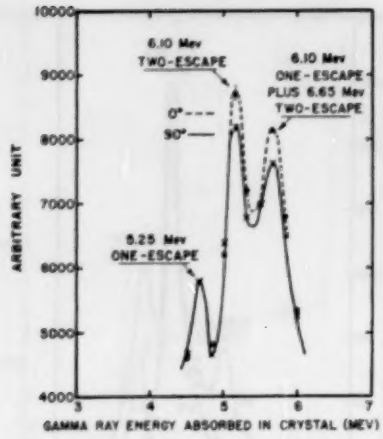

FIG. 4. Single-crystal spectra, at 0° and 90°, of high-energy gamma rays from 295-kev protons on thick TiN. Curves were normalized at 5.25-Mev one-escape peak.

ments can be taken with the accelerator off, thereby reducing background. The detection efficiency for the annihilation radiation is much greater than for the high energy gamma rays. Finally, the positron yield is greater than the yield of any one gamma ray. Disadvantages include the possible loss of O^{15} from the target, and uncertainties in the degree of saturation of the activity because of fluctuations in the beam current. Neither of these disadvantages affects the gamma-ray work.

The positron measurements necessitated knowing the O^{15} half-life. After bombarding the target for ten minutes with a 75-μa proton beam stable to ± 1 μa, the accelerator was turned off and a $\frac{3}{4}$ in. thick brass plug was inserted next to the bombarded face of the target to define the volume in which annihilation occurs. A fraction of a second was consumed by the operations which preceded starting the counters. The single-crystal scintillation spectrometer detected the annihilation radiation from the positrons. Counts in the peak of the pulse-height distribution corresponding to annihilation radiation were accumulated in 25-second intervals, separated by 5-second periods during which the data were recorded and the scaler cleared. The decay was followed for ten minutes. Semilog plots of the data were fitted with straight lines based on least squares analyses. A half-life of 121 ± 3 seconds was obtained which agrees, within experimental error, with previous measurements.[14–16] The uncertainty in the present measurement derives almost entirely from statistics.

The dotted curve of Fig. 1 shows the yield curve for the positron activity. These data represent the numbers of counts under the total absorption peak of the annihilation radiation accumulated in a 260-second interval following a ten minute bombardment of the target at each energy. The positron yield exhibits a sharp step at the same incident energy as the gamma ray yield. The rise above the resonance, which was also reported by Tangen,[1] may be due to the fact that less O^{15} escapes from the target as the bombarding energy is raised since the reaction occurs deeper in the target material.

In order to determine the absolute yield of positrons, the efficiency of the spectrometer for detecting annihilation radiation from the target was measured. The method has been previously described.[17] In this case, a Na^{22} positron source was painted in a $\frac{1}{4}$ in. diameter spot on a 2 mm thick, 1 cm^2 anthracene crystal, which was mounted on an RCA5819 photomultiplier tube. The geometry was arranged to duplicate that of the $N^{14}(p,\gamma)O^{15}$ experiment. Coincidences were counted between the positrons, as detected in the anthracene, and their annihilation radiation, as detected in a NaI(Tl) crystal. Only those pulses corresponding to the total absorption of the annihilation radiation were used to measure the desired efficiency. The Na^{22} positrons are in coincidence[6] with a 1.28-Mev gamma ray from the daughter nucleus as well as with their own annihilation radiation. Since the 1.28-Mev gamma ray produced only a small, roughly constant background over the width of the annihilation radiation total absorption peak, corrections for it were easily made.

Positrons resulting from a 10-minute bombardment by a 295-kev 3.5-μa proton beam, stable to ± 0.2 μa, were counted with the scintillation detector of known efficiency for annihilation radiation. Correcting for the stopping power of the titanium in the target in the same way as in the high energy gamma ray work, an absolute yield was obtained for a thick nitrogen target of $(2.2 \pm 0.4) \times 10^{-11}$ positron per proton. The fact that this value is lower than the value obtained from the gamma ray measurement may be due, at least partly, to the loss of O^{15} from the target during the bombardment. Tests made with beams up to 75 μa showed that the apparent yield decreased 10 percent at the highest beam strength. On this basis, the gamma-ray yield data are believed to be more reliable. These results are to be compared with the absolute yield of $(3.5 \pm 0.4) \times 10^{-11}$ positron per proton reported by Duncan and Perry.[2]

YIELDS BELOW RESONANCE

The significance of $N^{14}(p,\gamma)O^{15}$ reaction in stellar processes has been discussed by Salpeter.[18] Attempts were therefore made to measure the absolute yield for 255-kev protons by observing both the positron activity and the high energy gamma rays. The single-crystal spectrometer pulse-height distribution in the region corresponding to high energy gamma rays was meas-

[14] V. Perez-Mendez and H. Brown, Phys. Rev. **76**, 689 (1949).
[15] Sherr, Muether, and White, Phys. Rev. **75**, 282 (1949).
[16] G. T. Seaborg and I. Perlman, Revs. Modern Phys. **20**, 585 (1948).
[17] S. Bashkin and R. R. Carlson, Phys. Rev. **97**, 1245 (1955).
[18] E. E. Salpeter, Ann. Rev. Nuc. Sci. **2**, 41 (1953).

ured. The yield of high-energy gamma rays below resonance is less than 2 percent of the resonant yield. No positron activity was observed after 10-minute bombardment but the possible loss of O^{15} from the target makes an estimate of an upper limit unreliable.

DISCUSSION

The similar yield curves for the positrons and gamma rays and the measured half-life clearly identify the high energy gamma rays as originating in O^{15}. Spin and parity assignments to the capture and lower levels of O^{15} can be made on the basis of the present results together with previous work. An energy level diagram of the O^{15} nucleus is shown in Fig. 5. The three high-energy gamma rays observed in this experiment are indicated as proceeding from excited states in O^{15} at the corresponding energies. These excited states are taken to be the same states as seen in the $N^{14}(d,n)O^{15}$ work.[5] The spin of the 6.65-Mev state is thereby limited to $\frac{1}{2}^+$ or $\frac{3}{2}^+$. The ground-state spin of O^{15} is assumed to be $\frac{1}{2}^-$, like that of the ground state[6] of the mirror nucleus, N^{15}.

The thick target yield, Y, of this reaction is related to the radiative width, Γ_γ, of the narrow, well-isolated capture level, by the relation,

$$Y=(2\pi^2\lambda^2/\epsilon)\omega\Gamma_\gamma,$$

where $2\pi\lambda$ is the deBroglie wavelength of the proton at resonance, ϵ is the energy loss per atom per cm² for protons in nitrogen, and ω is a statistical weight factor equal to $(2J+1)/6$, J being the spin of the capture level. The proton width of the capture level is assumed to be much greater than the radiative width. On the basis of Fig. 5, the total absolute yield of the high-energy gamma rays is the radiative capture yield of the reaction. The present measurements result in

$$\omega\Gamma_\gamma=0.013\pm0.003 \text{ ev}$$

for the level at 7.61 Mev in O^{15}. This agrees with previous work.[19]

The capture level could have spins $\frac{1}{2}^+$ or $\frac{3}{2}^+$ if formed by s-wave proton capture; $\frac{1}{2}^-$, $\frac{3}{2}^-$, or $5/2^-$ from p-wave capture; or $\frac{1}{2}^+$, $\frac{3}{2}^+$, $5/2^+$, or $7/2^+$ from d-wave capture. Higher angular-momentum capture is unlikely. The absence of 7.6-Mev radiation rules out spins $\frac{1}{2}$ and $\frac{3}{2}$ as these would permit dipole transitions to the ground state. Such transitions would be much more intense than the observed low-energy transitions. Pure s-wave capture is also ruled out by the anisotropy observed. Since transitions to the level at 6.65 Mev make up a minimum of 25 percent of the radiative decays of the capture level, the partial width for this transition, regardless of the capture-state spin, must be at least

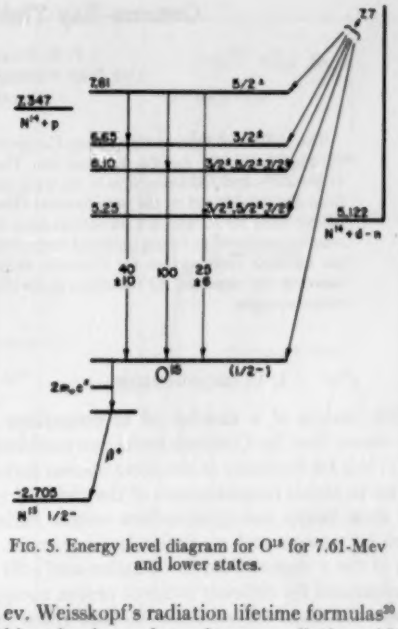

FIG. 5. Energy level diagram for O^{15} for 7.61-Mev and lower states.

0.002 ev. Weisskopf's radiation lifetime formulas[20] show that this value is much too large a radiative width for anything but a dipole transition. Consequently, the 6.65-Mev level is limited to spin $\frac{3}{2}^+$ and the 7.61-Mev level is limited to spins $5/2^+$ or $5/2^-$. If one identifies the 7.61-Mev level with that seen at 7.48 Mev in the $N^{14}(d,n)O^{15}$ experiment,[5] there is a suggestion of odd parity for the 7.61-Mev level.

Detailed consideration, using the Weisskopf radiation lifetime formulas, shows that only dipole transitions occur from the capture state to the three lowest excited states, and that there are very few transitions between those states. The experimental partial radiative widths for decay of the capture state to the states at 6.65 Mev, 6.10 Mev, and 5.25 Mev are, to within 25 percent, 0.003 ev, 0.008 ev, and 0.002 ev, respectively. Figure 5 lists all possible spin values for these states which are consistent with the present work. There is a suggestion from the $N^{14}(d,n)O^{15}$ experiment[5] that the 6.10-Mev level has odd parity and the 5.25-Mev level has even parity.

It should be noted, finally, that the discovery of multiplicity in any of the first three excited states of O^{15} would not effect the conclusions above but would simply mean that one or more of the levels in the multiplet had the spins indicated in Fig. 5.

We would like to thank Professor J. A. Jacobs for his helpful discussions of this experiment. Mr. R. C. Grimm skillfully constructed the target chambers.

[19] Woodbury, Hall, and Fowler, Phys. Rev. **75**, 1462(A) (1949).

[20] V. F. Weisskopf, Phys. Rev. **83**, 1073 (1951).

Gamma-Ray Yields from Coulomb Excitation

P. H. Stelson and F. K. McGowan
Oak Ridge National Laboratory, Oak Ridge, Tennessee
(Received March 30, 1955)

The yields of γ rays resulting from Coulomb excitation have been measured for the elements Ta, Au, Pt, Tl, Pb, Th, W, Hf, Ag, Pd, Rh, and Mo. The yields of the 137-, 166-, and 303-kev γ rays in Ta and the (277+273)- and 550-kev γ rays in Au were studied as a function of proton energy. No significant deviation from the predictions of the semiclassical theory of Alder and Winther was observed. Reduced transition probabilities for $E2$ and $M1$ transitions have been obtained from the γ-ray yields. In four cases these values may be compared to values obtained from direct half-life measurements. The good agreement indicates that the absolute cross section for Coulomb excitation is correctly given by the theory. Nuclear distortions based on the observed $E2$ transition probabilities are compared to those obtained from the observed excitation energies.

1. INTRODUCTION

THE results of a number of investigations have shown that the Coulomb excitation mechanism is a useful tool for the study of low-lying nuclear states.[1–17] We wish to report measurements of the yields of γ rays when some heavy and intermediate weight nuclei are excited by proton and α-particle bombardment. The yields of the γ rays excited in tantalum and gold have been measured for different incident proton energies to compare the observed variation to that given by the semiclassical theory of the process.[18,19] An interpretation of the γ rays observed to be excited in the various target materials is given in which locations of excited states and reduced transition probabilities are obtained. In some instances these quantities are compared to the predictions of the shell model and the collective model.[20]

2. APPARATUS

Protons and singly ionized α particles of variable energy were obtained from the 5.5-million volt ORNL electrostatic generator. A lead shield protected the experimental area from background γ rays associated with the generator and magnetic analyzer system.

In most cases targets were mounted on the target support at 45° with respect to the incident ion beam. The target support was a stainless steel tube with 0.005-inch wall thickness. By placing the detector at 230° with respect to the incident ion beam, i.e., so as to face the bombarded surface of the target, the γ rays excited by the ion beam could reach the detector without suffering appreciable attenuation from the traversal of intervening material.

It has been found that in many cases the angular distribution of the emitted γ rays is quite anisotropic so that considerable error is introduced in the determination of cross sections if this is not taken into

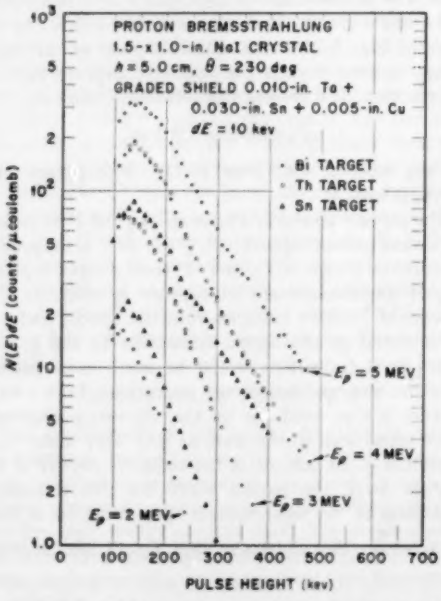

FIG. 1. Pulse-height spectra observed for proton bombardment of bismuth, thorium, and tin targets.

[1] T. Huus and C. Zupancic, Kgl. Danske Videnskab. Selskab, Mat.-fys. Medd. **28**, No. 1 (1953).
[2] C. McClelland and C. Goodman, Phys. Rev. **91**, 760 (1953).
[3] T. Huus and J. H. Bjerregaard, Phys. Rev. **92**, 1579 (1953).
[4] G. M. Temmer and N. P. Heydenburg, Phys. Rev. **93**, 351 (1954).
[5] N. P. Heydenburg, and G. M. Temmer, Phys. Rev. **93**, 906 (1954).
[6] McClelland, Mark, and Goodman, Phys. Rev. **93**, 904 (1954).
[7] J. H. Bjerregaard and T. Huus, Phys. Rev. **94**, 204 (1954).
[8] Eisinger, Cook, and Class, Phys. Rev. **94**, 735 (1954).
[9] Sherr, Li, and Christy, Phys. Rev. **94**, 1076 (1954).
[10] N. P. Heydenburg and G. M. Temmer, Phys. Rev. **94**, 1252 (1954).
[11] G. M. Temmer and N. P. Heydenburg, Phys. Rev. **94**, 1399 (1954)
[12] C. McClelland and C. Goodman, Phys. Rev. **94**, 1437 (1954).
[13] W. I. Goldburg and R. M. Williamson, Phys. Rev. **95**, 767 (1954).
[14] R. Barloutland and T. Grjebine, Compt. rend. **239**, 491 (1954).
[15] N. P. Heydenburg and G. M. Temmer, Phys. Rev. **95**, 861 (1954); G. M. Temmer and N. P. Heydenburg, Phys. Rev. **96**, 426 (1954).
[16] Cook, Class and Eisinger, Phys. Rev. **96**, 658 (1954).
[17] Simmons, Van Patter, Famularo, and Stuart, Phys. Rev. **97**, 89 (1955).
[18] K. Alder and A. Winther, Phys. Rev. **91**, 1578 (1953).
[19] K. Alder and A. Winther, Phys. Rev. **96**, 237 (1954).
[20] A. Bohr and B. Mottelson, Kgl. Danske Videnskab. Selskab, Mat.-fys. Medd. **27**, No. 16 (1953).

account. The angular distributions are of the type $A_0P_0+A_2P_2+A_4P_4$ (the P_r are Legendre polynomials) where A_0, $A_2 \gg A_4$. By placing the detector at 230° where P_2 almost vanishes one measures the coefficient A_0 which gives the cross section for the reaction.

The troublesome x-rays produced by proton bombardment were attenuated by placing a series of thin shields in front of the detector. For example, when bombarding a thallium target, a shield of 10 mils Ta, 30 mils Sn, and 5 mils Cu was used. Shields were chosen to attenuate the K x-rays by factors of 200 to 1000. No x-ray attenuation was necessary when bombarding targets with α particles.

The γ-ray detector was a thallium activated NaI crystal, $1\frac{1}{2}$ inches in diameter and 1 inch long, mounted on a DuMont type 6292 photomultiplier tube. Pulse-height spectra were measured with either a single-channel or 20-channel analyzer.[21,22] Pulse heights were converted to γ-ray energies by measuring the spectra of a series of radioactive sources which emit γ rays of well-established energies. It was found that the DuMont tube exhibited small shifts in pulse height for sources of different strength and for this reason we have assigned somewhat larger errors to the γ-ray energies than would otherwise have been the case.

The number of emitted γ rays per microcoulomb of incident particles was deduced from the pulse-height

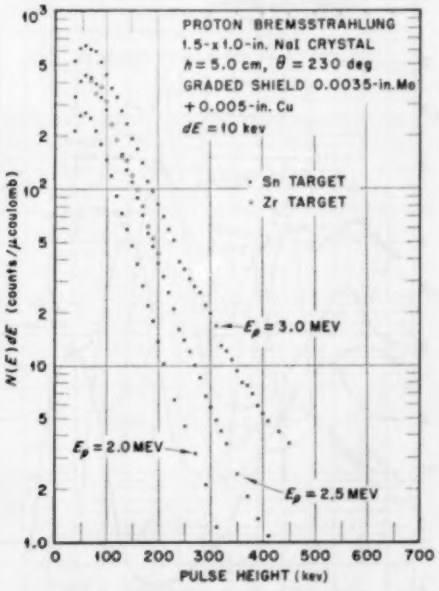

FIG. 2. Pulse-height spectra observed for proton bombardment of tin and zirconium targets.

[21] J. E. Francis and P. R. Bell, Oak Ridge National Laboratory Report ORNL-1470 (unpublished).

[22] Kelley, Bell, and Goss, Oak Ridge National Laboratory Physics Division Quarterly Progress Report ORNL-1278, 1951 (unpublished).

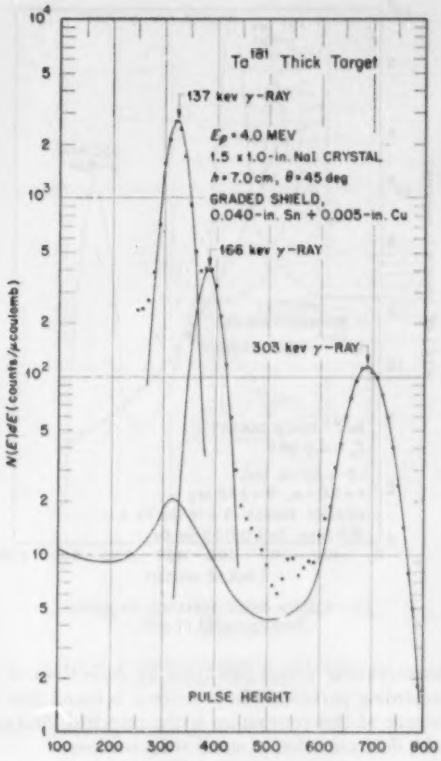

FIG. 3. Pulse-height spectrum for proton bombardment of tantalum.

spectrum using the expression

$$I=\frac{N(E_0)}{n(E_0)}\times\frac{1}{\Delta E}\times\frac{1}{\epsilon}\times\frac{1}{R_\gamma}\times\frac{1}{A_\gamma}, \qquad (1)$$

where $N(E_0)$ = the counting rate in counts per microcoulomb at the peak of the full-energy peak; $n(E_0) = 1/(\alpha_\gamma\pi^{\frac{1}{2}})$ and α_γ is the half-width of the full-energy peak at $1/e$ amplitude; ΔE = window width of the pulse-height analyzer; ϵ = detection efficiency; R_γ = ratio of the area of the full-energy peak to the total area of the pulse-height spectrum for the γ ray; and A_γ is the correction for absorption of the γ ray by material between the source and crystal.

Coincidence measurements were carried out for the thallium and gold spectra. The fast-slow coincidence circuit which was used has previously been described.[23]

3. GAMMA-RAY SPECTRA

A. Bremsstrahlung Gamma-Rays

The γ rays of discrete energy resulting from excitation of nuclear states are superimposed on a continuum of

[23] F. K. McGowan, Phys. Rev. 93, 163 (1954).

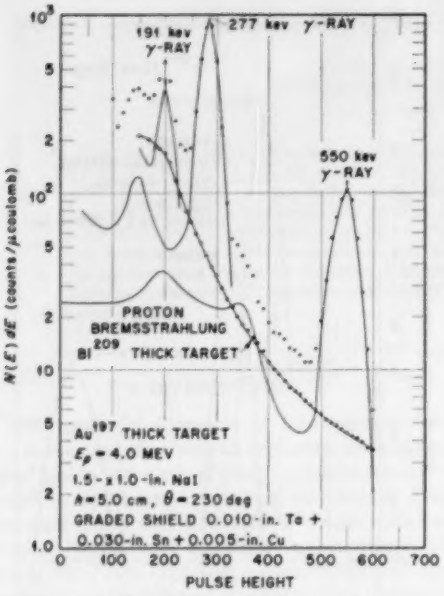
191 kev γ-RAY
277 kev γ-RAY
550 kev γ-RAY
PROTON BREMSSTRAHLUNG
Bi209 THICK TARGET
Au197 THICK TARGET
Ep = 4.0 MEV
1.5 - x 1.0 - in. NaI
h = 5.0 cm, θ = 230 deg
GRADED SHIELD 0.010-in. Ta + 0.030-in. Sn + 0.005-in. Cu
N(E) dE (counts/μcoulomb)
PULSE HEIGHT

FIG. 4. Pulse-height spectrum for proton bombardment of gold.

bremsstrahlung γ rays produced by deflections of the bombarding particles.[24] In practice it is found that the existence of this continuum is the principal limitation to the determination of small cross sections.

There are a few target materials which allow a convenient study of the continuum because of the absence of discrete γ rays. Figures 1 and 2 show spectra obtained by proton bombardment of thick bismuth, thorium, tin, and zirconium targets. Bismuth spectra are shown for incident proton energies of 2.0, 3.0, 4.0, and 5.0 Mev and tin spectra for 2.0, 2.5, and 3.0 Mev to indicate the change with proton energy.

From the practical point of view the most important information concerning the continuum is how it changes with the Z of the target material since one wants to evaluate and subtract it out for those targets in which Coulomb excitation is observed. The thorium ($Z=90$) spectrum, taken at 4.0 Mev, is seen to differ very little from the bismuth ($Z=83$) spectrum for 4.0 Mev. Similarly, the zirconium ($Z=40$) spectrum, taken at 2.5 Mev, differs very little from the tin ($Z=50$) spectrum. In fact, the spectra for tin and bismuth ($E_p=2.0$ Mev) have nearly the same shape and differ in intensity by less than a factor of two. It is concluded that proton bremsstrahlung is rather insensitive to the target Z. For target materials with $Z \geq 72$, we have used the bismuth spectrum to subtract out the continuum and for targets of intermediate Z ($42 \leq Z \leq 47$) we have used the tin and zirconium spectra.

[24] C. Zupancic and T. Huus, Phys. Rev. **94**, 205 (1954).

B. Gamma-Rays from Coulomb Excitation

Figures 3 to 12 show spectra observed when thick targets of Ta, Au, Pt, Tl, W, Ag, Pd, and Rh were bombarded by protons. Each spectrum was analyzed by first subtracting out the bremsstrahlung continuum. Then, beginning with the γ ray of highest energy, the spectrum was resolved into spectra for individual γ rays. This process sometimes required a certain amount of trial and error. The shapes of pulse-height spectra for individual gamma-rays of various energies were obtained by measuring γ rays from radioactive sources.

The pulse-height spectrum for thallium (Fig. 6) also shows the results of coincidence measurements. The window of one detector was set on the peak at 410 kev. The coincidence rate as a function of the window position of the other detector is shown.

4. GAMMA-RAY YIELDS

The γ rays we have observed when the indicated target materials were bombarded by protons and α particles are listed in Table I. Columns 3, 4, and 6 list, respectively, the bombarding particle, its incident energy, and the observed yield in number of γ rays per

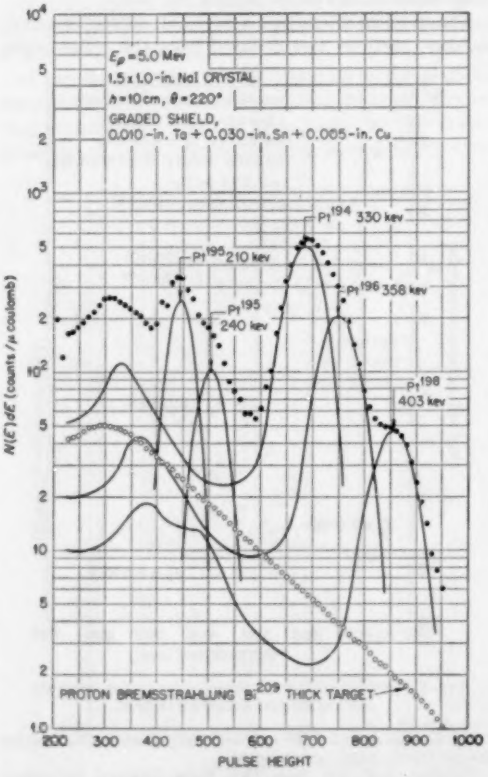
Ep = 5.0 Mev
1.5 x 1.0-in. NaI CRYSTAL
h = 10 cm, θ = 220°
GRADED SHIELD,
0.010-in. Ta + 0.030-in. Sn + 0.005-in. Cu
Pt194 330 kev
Pt195 210 kev
Pt195 240 kev
Pt196 358 kev
Pt198 403 kev
PROTON BREMSSTRAHLUNG Bi209 THICK TARGET
N(E) dE (counts/μ coulomb)
PULSE HEIGHT

FIG. 5. Pulse-height spectrum for proton bombardment of platinum.

microcoulomb. The bombarding α particles were singly ionized so that for both protons and α particles there were 6.25×10^{12} incident particles per microcoulomb. It is judged that yields have an absolute accuracy of 10 to 20 percent and that relative yields for a given γ ray have an accuracy of 5 percent. For those cases in which the errors are larger, the errors are given with the value of the yield.

Measurements of the change in the yields with proton energy were carried out for the 137-, 166-, and 303-kev γ rays in Ta^{181} using both thick and thin targets, and for the (277+273) and 550 kev γ rays in Au^{197} using a thin target. The thin targets were prepared by mounting thin foils (Ta, 10.0 mg/cm² and Au, 10.5 mg/cm²) on bismuth backings.[25] The bismuth backings were prepared by the electrodeposition of a bismuth layer approximately 100 mg/cm² thickness onto 5-mil nickel. The thin targets were mounted perpendicular to the incident beam and the detector was located in the forward direction. The yields from the thick and thin tantalum targets and the thin gold target are listed in Tables II, III, and IV, respectively.

5. INTERPRETATION AND DISCUSSION

The following formula, taken from the paper of Alder and Winther,[19] is used for the cross section for

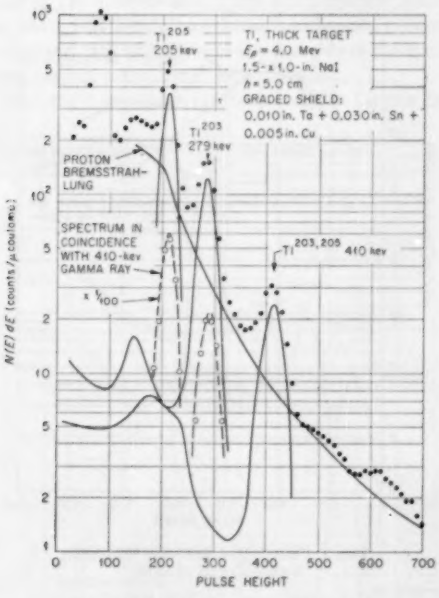

FIG. 6. Pulse-height spectrum for proton bombardment of thallium.

[25] With the arrangement in which the bismuth backing is directly behind the thin foil, the question might arise as to whether Rutherford scattering of the protons in the backing would introduce an error because some of the protons have a double traversal of the foil. An estimate of the magnitude of this effect shows that it is negligible.

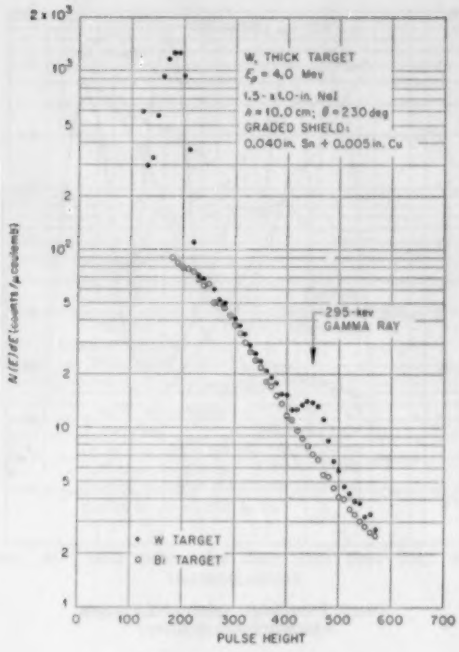

FIG. 7. Pulse-height spectrum for proton bombardment of wolfram.

electric quadropole excitation:

$$\sigma(E2)=\frac{2\pi^2m^2v_f^2}{25Z_2^2e^2\hbar^2}B(E2)g_{E2}(\xi), \tag{2}$$

where

$$\xi=\frac{Z_1Z_2e^2}{\hbar}\left[\frac{1}{v_f}-\frac{1}{v_i}\right]. \tag{3}$$

Z_1e and Z_2e are the charges of the impinging projectile and the nucleus, respectively; v_i and v_f are the initial and final relative velocities and m is the reduced mass. $B(E2)$ is the reduced transition probability for excitation by $E2$ radiation (see Bohr and Mottelson).[20] The function $g_{E2}(\xi)$ has been evaluated by Alder and Winther using numerical integration.

The $B(E2)$ for decay is obtained from the $B(E2)$ for excitation by multiplication by the factor $2I_0+1/2I+1$ where I_0 and I are the spins of the ground state and excited state." To avoid confusion the two $B(E2)$ will be written as $B(E2)_{ex}$ and $B(E2)_d$. In some cases for the odd-A nuclei the excited state may decay by $M1$ radiation. From the mixing ratio, $E2/M1$, one can then also obtain $B(M1)_d$. The values given for $B(E2)$ and $B(M1)$ are actually those for the quantities $B(E2)/e^2$ and $B(M1)/(e\hbar/2mc)^2$.

It is of interest to compare the observed values of $B(E2)$ and $B(M1)$ to those expected for transitions between states of the independent particle model.

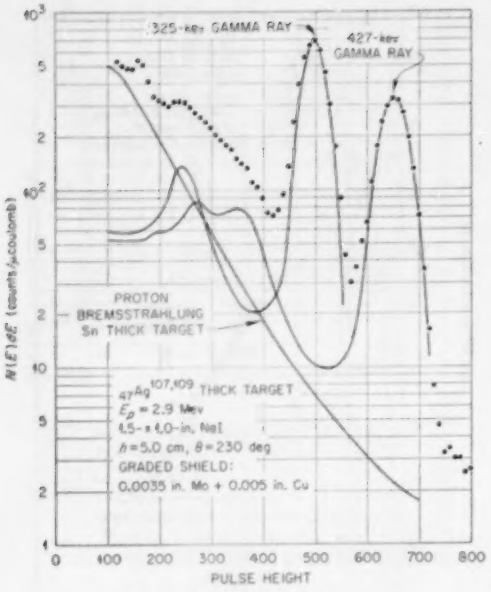

FIG. 8. Pulse-height spectrum for proton bombardment of silver.

Using the estimate given by Blatt and Weisskopf[26] one has that $B(M1)_{sp}$ is approximately unity and that $B(E2)_{sp}$ is given approximately by $(1/4\pi)|3/5R_0^2|^2$. We have taken R_0 equal to $1.44\times10^{-13}A^{1/3}$ cm.

To compare thick target γ-ray yields with theory it is necessary to integrate the theoretical cross section. One must also integrate the cross section over the foil thickness for thin targets if they are only moderately thin since the cross section may vary rapidly with energy. The yield, I, of a given γ ray is related to the cross sections for excitation by the expression

$$I=\text{const}\left[\frac{1}{1+\alpha_T}\right]\sum K_i\int_{E_1}^{E_2}\frac{\sigma_i(E)dE}{[dE/d\rho x]}, \qquad (4)$$

where α_T is the total internal conversion coefficient for the transition in question, $\sigma_i(E)$ is the cross section for the excitation of state i, K_i is the fraction of the decays of state i which give rise to the transition in question, and $dE/d\rho x$, E_1 and E_2 are the rate of energy loss and the average initial and final energies of the particles causing the excitation.

The information on rate of energy loss for the intermediate and heavy weight elements for the energies of interest is rather limited. Allison and Warshaw[27] have recently reviewed this subject for energies up to 2.0 Mev.

We have taken the values recommended by Allison and Warshaw for $dE/d\rho x$ for gold for proton energies up to 2.0 Mev. The $dE/d\rho x$ curve for gold was extended to higher energies using the results of Blaser *et al.*[28] and the shape of the $dE/d\rho x$ curve for lead which was calculated by Aron *et al.*[29] The values of $dE/d\rho x$ for elements near to gold in Z were calculated using the gold curve and the assumption that $dE/d\rho x$ in units of kev/mg/cm² varies as $Z^{-1/2}$. Curves of $dE/d\rho x$ were also constructed for α particles in gold for energies up to 5.0 Mev and for protons in silver for energies up to 5.0 Mev using information obtained by the Chicago and Copenhagen groups (see Allison and Warshaw) and Blaser *et al.*[28] These curves were used to obtain stopping powers of other elements on the assumption that $dE/d\rho x$ varies as $Z^{-1/2}$ for moderately small charges in Z.[30]

Total internal conversion coefficients (denoted by α_T) must be known to relate cross sections to observed γ-ray yields. Calculations of K-shell conversion coefficients by Rose *et al.*[31] were used for γ rays of 150 kev or higher energy. A previously discussed procedure was used to deduce theoretical values of K-shell internal conversion coefficients for γ rays with energies less than

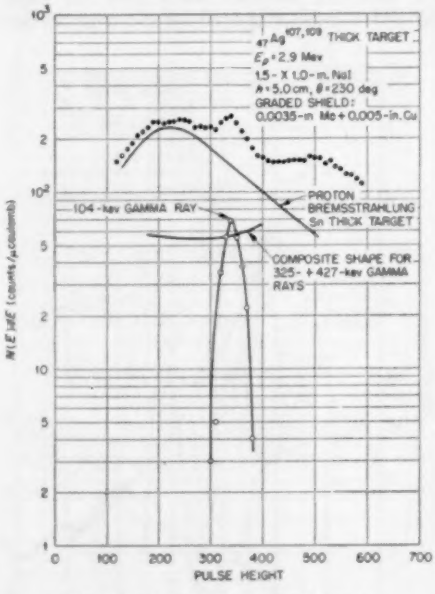

FIG. 9. Pulse-height spectrum for proton bombardment of silver.

[26] J. M. Blatt and V. F. Weiskopf, *Theoretical Nuclear Physics* (John Wiley and Sons, Inc., New York, 1952).

[27] S. K. Allison and S. D. Warshaw, Revs. Modern Phys. **25**, 779 (1953).

[28] Blaser, Boehm, Marmier, and Peaslee, Helv. Phys. Acta **24**, 3 (1951).

[29] Aron, Hoffman, and Williams, U. S. Atomic Energy Commission Report AECU-663, 1951 (unpublished).

[30] We will send to those who are interested the values we have taken for $dE/d\rho x$ for protons and α particles in gold and for protons in silver.

[31] Rose, Goertzel, Spinrad, Harr, and Strong, Phys. Rev. **83**, 79 (1951).

150 kev.[32] It was sometimes necessary to use empirical curves of K/L to obtain α_T.

Tables V and VI contain a summary of our interpretation of the γ-ray yields listed in the previous tables. The quantity

$$\int^{E_i} \frac{g_2(\xi)E'dE}{dE/d\rho x}$$

is given in kev×mg/cm². $E'=k^2[E-\Delta E/k]$ where k is $m/m+M$, E is the exciting particle energy in the laboratory system and ΔE is the energy of the excited state above the ground state. From the knowledge of the $B(E2)_{ee}$, the spins of the initial and final states and the fraction of the time the excited state decays back to the ground state by the emission of an $E2$ γ ray, it is possible to predict the lifetime of the state. These values are listed in Table VI in the column headed $T_{\frac{1}{2}}$. The $B(M1)_d$ which are listed in Table VI are obtained from the knowledge of $B(E2)_{ee}$, the $E2/M1$ value, and the spins of the initial and final states.

A. Tantalum

In agreement with others,[1,2,4,8,13] we observe three γ rays with energies of 137, 166, and 303 kev. These are interpreted to be the result of the decay of excited states at 137 and 303 kev. Huus and Zupancic[1] pointed out that the strong excitation indicates collective motion and that the ratios of the energies of the excited states suggest a rotational interpretation.

From the γ-ray yields for thick and thin targets listed

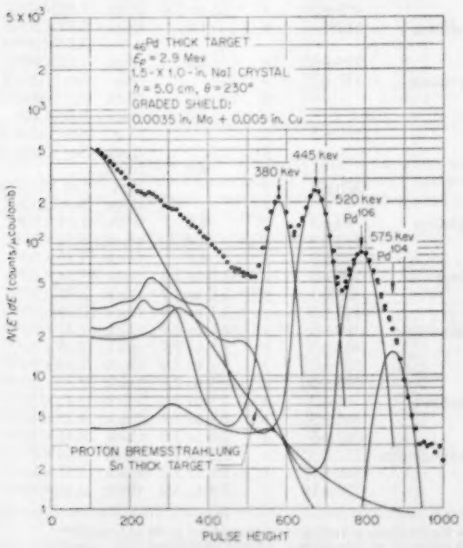

FIG. 10. Pulse-height spectrum for proton bombardment of palladium.

[32] F. K. McGowan, Phys. Rev. **85**, 151 (1952).

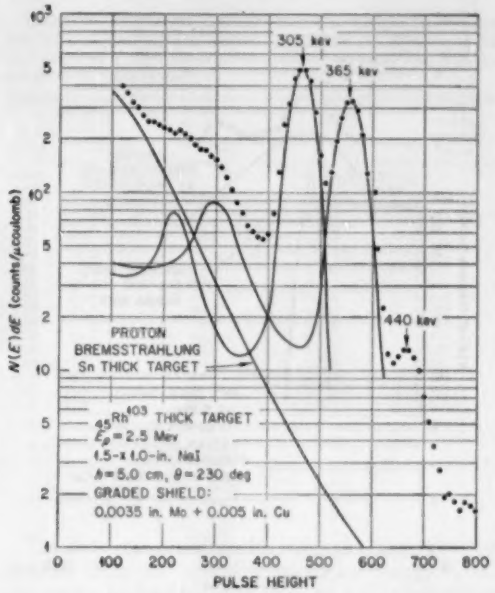

FIG. 11. Pulse-height spectrum for proton bombardment of rhodium.

in Tables II and III,[33] the value for the ratio of the number of 166- to 303-kev γ rays is found to be 1.74 ±0.10; a value which is in good agreement with those found by Goldburg and Williamson[13] and by Eisinger, *et al.*[8] The value for α_T for the 166-kev γ ray is based on the $E2/M1$ ratio deduced from angular distribution measurements.[34] Using the values α_T listed in Table V, the ratio cascades/crossovers for the 303-kev state is 3.37.

By the use of formulas (2) and (4), the $B(E2)_{ee}$ for the 137- and 303-kev states are obtained for thin and thick targets and these are listed for the different incident proton energies in Tables II and III. The constancy of the quantities $B(E2)_{ee}$ is the measure of how well the theory predicts the relative cross section provided allowances are made for experimental uncertainties. As previously stated, the relative γ-ray yields are believed to be accurate to 5 percent except for the the lowest proton energies where larger errors have been assigned. Uncertainties in the values taken for α_T will give no error to the relative values of $B(E2)_{ee}$ for the 303-kev state and will be rather unimportant for the 137-kev state where the relative $B(E2)_{ee}$ do depend on α_T because the state is fed by decay of the 303-kev state. It is estimated that the shape of the curve

[33] Since the thin target yields were observed in the forward direction a correction was applied to the values listed in Table II to take into account the angular distribution of the γ rays. An almost negligible correction was also applied to the thick target yields, which, in this case, were measured at 45°.

[34] F. K. McGowan and P. H. Stelson, following paper [Phys. Rev. **99**, 127 (1955)].

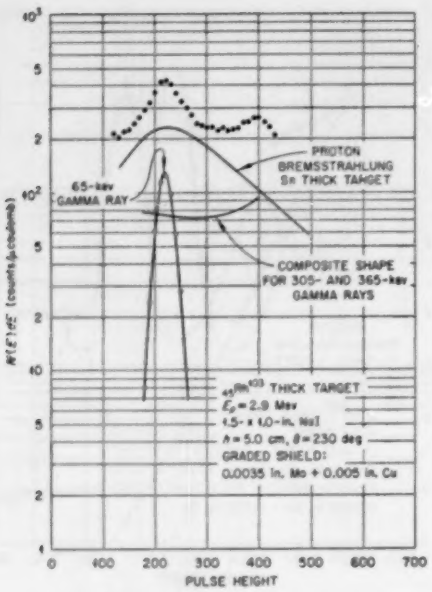
65-kev GAMMA RAY
PROTON BREMSSTRAHLUNG Sn THICK TARGET
COMPOSITE SHAPE FOR 305- AND 365-kev GAMMA RAYS
$_{45}Rh^{103}$ THICK TARGET
E_p = 2.9 Mev
1.5- x 1.0-in. NaI
h = 5.0 cm, θ = 230 deg
GRADED SHIELD:
0.0035 in. Mo + 0.005 in. Cu
PULSE HEIGHT

FIG. 12. Pulse-height spectrum for proton bombardment of rhodium.

$dE/d\rho x$ vs E_p might be in error by 10 percent. Consequently, when the target is thick or only moderately thin, a variation in $B(E2)_{ex}$ of as much as 10 percent could result from this uncertainty. It is judged that, except for the lowest proton energies, the total spread in the relative values of $B(E2)_{ex}$ caused by experimental errors (including the uncertainty in $dE/d\rho x$) is not more than 15 percent.

An inspection of the values of $B(E2)_{ex}$ indicates no significant variation. We therefore conclude that to within the accuracy of the experiment the relative cross section is correctly given by the theory. If the originally proposed expression[18] for the variable, ξ, [viz., $(\Delta E/2E)(Z_1Z_2e^2/\hbar v)$] were used instead of the expression given by (3), the variation in the $B(E2)_{ex}$ for the 303-kev state as one proceeds from low to high proton energies would amount to 35 percent. Since this is outside of the experimental errors, it is concluded that the experiment favors the expression for ξ given in formula (3). Goldburg and Williamson[19] also reached this conclusion.

Our best values of $B(E2)_{ex}$ for the 137- and 303-kev transitions are $(2.50\pm0.25)\times10^{-48}$ cm^4 and $(0.624\pm0.06)\times10^{-48}$ cm^4, respectively. These values are based on the yield from the thin target at the higher proton energies since for these cases the target is sufficiently thin that little error results from the uncertainty in the absolute value of $dE/d\rho x$. The ratio of $B(E2)_{ex}$ for the 137-kev state to the $B(E2)_{ex}$ for the 303-kev state is found to be 4.02 ± 0.20. The value of 3.89 is predicted for the rotational states of the strong coupling limit of the collective model.

By the use of the values of cascades/crossovers for the decay of the 303-kev state, the $E2/M1$ values for

TABLE I. Gamma rays observed when listed elements were bombarded by protons and/or α particles. The column headed E gives the incident particle energy in Mev. The bombarding α particles were singly ionized so that for both protons and α particles there were 6.25×10^{12} incident particles per microcoulomb.

Target material (metallic)	Gamma-ray energy E_γ (kev)	Bombarding particle	E Mev	Type of target	Yield of gamma rays per microcoulomb
Thorium	53±3	α	4.0	thick	
	760±10	p	5.0	thick	3.32×10^6
Lead	570±10	p	4.5	thick	2.96×10^5
	810±10	p	4.5	thick	4.03×10^5
Pb^{206} [a]	810±10	p	5.0	thick	4.92×10^6
Thallium	205±3	p	4.0	thick	7.72×10^6
		α	4.0	thick	2.60×10^5
	279±3	p	4.0	thick	3.90×10^6
		α	4.0	thick	4.25×10^5
	410±5	p	4.0	thick	1.50×10^6
Gold	191±3	p	4.0	thick	5.42×10^6
		α	4.0	thick	7.44×10^5
	273[b]	p	4.0	thick	6.13×10^5
		p		thin	See Table IV
	277±3	p		thin	See Table IV
		p	4.0	thick	2.86×10^6
		α	4.0	thick	3.50×10^5
	550±5	p		thin	See Table IV
		p	4.0	thick	1.16×10^6
Platinum	100±3	α	4.0	thick	
	130±3	α	4.0	thick	
	210±3	p	5.0	thick	3.57×10^5
	240±3	p	3.0, 4.0, 5.0	thick	1.67×10^5 [c]
	330±5	p	2.5 to 5.0	thick	1.35×10^6 [c]
	358±5	p	2.5 to 5.0	thick	6.38×10^5 [c]
	403±5	p	2.5 to 5.0	thick	1.89×10^5 [c]
Wolfram	112[d]	p	4.0	thick	2.87×10^5
					2.35×10^5
	295±5	p	4.0	thick	1.08×10^6
Tantalum	137±2	p		thin	See Table III
		p		thick	See Table II
		α	4.0	thick	2.05×10^5
	167±3	p		thin	See Table III
		p		thick	See Table II
		α	4.0	thick	
	303±3	p		thin	See Table III
		p		thick	See Table II
Hafnium	90±3	p	4.0	thick	1.74×10^5
	112±3	p	4.0	thick	5.33×10^5
	248±3	p	4.0	thick	1.19×10^5
Silver	104±3	p	2.1 to 2.9	thick	1.34×10^6 [e]
	325±5	p	2.1 to 2.9	thick	3.45×10^5 [e]
	427±5	p	2.1 to 2.9	thick	2.89×10^5 [e]
Palladium	380±5	p	2.1 to 2.9	thick	1.32×10^5 [e]
	445±5	p	2.1 to 2.9	thick	2.29×10^5 [e]
	520±7	p	2.1 to 2.9	thick	1.14×10^5 [e]
	575±10	p	2.1 to 2.9	thick	2.55×10^6 [e]
Thodium	65±3	p	2.1 to 2.9	thick	2.76×10^6 [e]
	305±5	p	2.1 to 2.9	thick	4.18×10^5 [e]
	365±5	p	2.1 to 2.9	thick	4.44×10^5 [e]
Molybdenum	212±3	p	2.1 to 2.9	thick	2.26×10^6 [e]
	540±7	p	2.1 to 3.0	thick	5.55×10^6 [f]
	770±10	p	2.4 to 3.0	thick	2.56×10^6 [f]

[a] Target made of radiogenic lead enriched to 88 percent Pb^{206}.
[b] Existence of this gamma ray was established from coincidence measurements.
[c] Yield for 5.0-Mev protons.
[d] Observed width too large for a single gamma ray [see McClelland *et al.* (see reference 6)].
[e] Yield for 2.9-Mev protons.
[f] Yield for 3.0-Mev protons.

the 166- and 137-kev transitions and the $B(E2)_{ex}$ for the 137- and 303-kev transitions one can calculate other reduced transition probabilities. The $B(E2)_d$ and $B(M1)_d$ for the 166-kev transition are calculated to be 3.05×10^{-48} cm^4 and 0.226, respectively. $B(M1)_d$ for the 137-kev transition is 0.105.

Bohr and Mottelson[20] have given formulas which, for transitions between rotational states, relate $B(E2)$ to the intrinsic quadrupole moment, Q_0. Similarly, the $B(M1)$ is related to the quantity $(g_\Omega-g_R)^2$ where g_Ω and g_R are the g-factors of the intrinsic and collective motions, respectively.

From the experimental values of $B(E2)$ we calculate the values of Q_0 as 7.70, 7.59, and 9.46 barns for the 137-, 303- and (least accurately known) 166-kev transitions. The close agreement of the values of Q_0 is evidence that the formulas correctly predict the relative transition probabilities.

TABLE II. Thick target yields of gamma rays of tantalum and values for $B(E2)_{ex}$. The columns headed I_{137}, I_{166}, and I_{303} give the yields in number of gamma rays per microcoulomb of protons. The $B(E2)_{ex}$ are given in units of cm^4.

E_p (Mev)	I_{137}	I_{166}	I_{303}	$B(E2)_{ex}$ 137-kev state	$B(E2)_{ex}$ 303-kev state
2.00	1.54×10^3	0.527×10^3	0.284×10^3	2.45×10^{-48}	0.711×10^{-48}
2.10	1.98	0.782	0.421	2.51	0.683
2.20	2.50	1.10	0.591	2.57	0.653
2.30	2.92	1.52	0.819	2.46	0.640
2.40	3.68	2.14	1.15	2.58	0.662
2.50	4.22	2.76	1.49	2.51	0.643
2.60	5.08	3.64	1.96	2.58	0.660
2.70	6.00	4.48	2.41	2.63	0.639
2.80	6.83	5.64	3.04	2.60	0.643
2.90	7.95	7.21	3.88	2.65	0.669
3.00	8.60	8.26	4.45	2.54	0.633
3.20	11.2	11.6	6.41	2.64	0.630
3.40	13.9	15.3	8.48	2.67	0.610
3.60	16.5	19.8	10.9	2.62	0.598
3.80	20.5	25.7	14.2	2.72	0.605
4.00	23.2	30.3	16.8	2.62	0.574
4.20	27.9	40.1	22.1	2.68	0.616
4.40	32.7	46.1	25.4	2.72	0.586
4.60	37.6	52.9	29.2	2.73	0.564
4.80	43.4	63.0	34.8	2.84	0.572

TABLE III. Thin target yields of gamma rays of tantalum and values for $B(E2)_{ex}$. The columns headed I_{137}, I_{166}, and I_{303} give the yields in number of gamma rays per microcoulomb of protons. The $B(E2)_{ex}$ are given in units of cm^4.

E_p (Mev)	I_{137}	I_{166}	I_{303}	$B(E2)_{ex}$ 137-kev state	$B(E2)_{ex}$ 303-kev state
1.43	2.44×10^2		0.60×10^2 [a]	2.75×10^{-48}	0.697×10^{-48}
1.60	4.28		3.62×10^2 [b]	2.39	0.859
1.80	7.70	2.53×10^2	11.3×10^2 [c]	2.41	0.688
2.00	11.8	5.34	28.9	2.42	0.661
2.20	16.0	11.0	57.2	2.44	0.663
2.40	20.0	17.7	100	2.40	0.637
2.60	24.7	26.2	148	2.45	0.622
2.80	30.2	38.2	211	2.53	0.622
3.00	34.2	48.5	280	2.52	0.625
3.20	37.5	59.7	341	2.46	0.622
3.40	43.3	76.5	408	2.61	0.614
3.60	47.7	86.9	480	2.61	0.620
3.80	50.5	93.9	538	2.55	0.629
4.00	54.4	105	591	2.55	0.604
4.20	57.8	118	674	2.57	0.626
4.40	59.2	123	725	2.37	0.605
4.60	64.7	133	777	2.44	0.608
4.80	70.2	143	847	2.60	0.637
5.00	72.6	156	931	2.55	0.665

[a] Relative accuracy −35 percent, +75 percent.
[b] Relative accuracy −20 percent, +45 percent.
[c] Relative accuracy ±7 percent.

TABLE IV. Thin target yields of gamma rays of gold and values for $B(E2)_{ex}$. The columns headed $I_{277+279}$ and I_{550} give the yields in number of γ rays per microcoulomb of protons. The $B(E2)_{ex}$ are given in units of cm^4.

E_p (Mev)	$I_{277+279}$	I_{550}	$B(E2)_{ex}$ 277-kev state	$B(E2)_{ex}$ 550-kev state
1.60	0.315×10^3 [a]		0.304×10^{-48}	
1.80	1.34×10^3 [b]		0.348	
2.00	3.95×10^3		0.388	
2.20	7.32	0.326×10^2 [c]	0.351	0.652×10^{-48}
2.40	13.1	1.07×10^2 [d]	0.359	0.583
2.60	19.2	2.80×10^2 [c]	0.341	0.536
2.80	27.8	6.41×10^2	0.370	0.537
3.00	35.4	11.6	0.331	0.511
3.20	44.0	19.1	0.331	0.507
3.40	54.6	29.3	0.335	0.507
3.60	64.3	40.0	0.335	0.483
3.80	75.3	52.9	0.340	0.474
4.00	83.5	66.9	0.330	0.471
4.20	93.4	83.7	0.327	0.467
4.40	103	99.9	0.335	0.467
4.60	117	118	0.345	0.466
4.80	123	135	0.338	0.462
5.00	129	156	0.328	0.471

[a] Relative accuracy ±15 percent.
[b] Relative accuracy ±7 percent.
[c] Relative accuracy ±15 percent.
[d] Relative accuracy ±10 percent.
[e] Relative accuracy ±7 percent.

The intrinsic quadrupole moment may also be deduced from the observed excitation energy.[21] Assuming the nuclear radius is given by $1.4\times10^{-13}A^{1/3}$ we calculate the values 20.7 and 20.7 barns for Q_0 for the 137- and 303-kev states, respectively. The close agreement of the Q_0 values is evidence that the relative spacing of the excited states is correctly given by the rotational interpretation. However, the absolute values of Q_0 given by excitation energy are rather different from those obtained from reduced transition probabilities.

The quantity $(g_\Omega-g_R)^2$ is calculated from the observed $B(M1)$ values for the 137- and 166-kev transitions to be (0.202) and (0.284), respectively. The 25 percent difference in the values of $(g_\Omega-g_R)^2$ is probably not outside of the experimental uncertainties. Bohr and Mottelson[20] give an expression which relates the ground state magnetic moment to the g_Ω and g_R. From the observed magnetic moment of 2.1 nm and the above values of $(g_\Omega-g_R)^2$, two solutions are obtained because the sign of the difference $(g_\Omega-g_R)$ is not known. The solutions are listed in Table VII. The theoretical estimate of g_R is Z/A or 0.40. The shell model assignment for the ground state of Ta^{181} is $g_{7/2}$. This type of state has $g_\Omega=0.50$.

B. Gold

Considerable information on the low-lying states of Au^{197} has been obtained from studies of the decay of

[21] The effective moment of inertia, $\mathcal{I}$, is obtained from the relation

$$E=\frac{\hbar^2}{2\mathcal{I}}[I(I+1)-I_0(I_0+1)].$$

Then Q_0 is obtained using the formula $\mathcal{I}=(5mA/8R_0^2Z^2)Q_0^2$, where m = the nucleon mass. [See A. Bohr, *Rotational States of Atomic Nuclei* (Ejnai Munhsgaard Forlog, Copenhagen, 1954).]

TABLE V. Summary of values of $B(E2)_{ex}$ based on the interpretation of the observed gamma-ray yields given Tables I, II, III, and IV. The first column lists the nucleus to which the gamma ray given in column 2 is assigned. Columns 3 and 4 indicate the bombarding particle and its incident energy. Columns 5 and 6 give the classification of the transition and the total internal conversion coefficient which we have used. The column headed I_1 lists the number of transitions per microcoulomb. Column 8 gives the excitation energy of the state and the column headed I_2 lists the excitations/μcoul for the state. Column 10 gives the evaluation of the integral $\int_0^E g_{E1}(\xi)E'd\xi/(dE/d\rho x)$ in units of kev×mg/cm³. The last column gives $B(E2)_{ex}$ in units of cm⁴.

Nucleus	E_γ (kev)	Bombarding particle	E (Mev)	Classification	α_T	$I_1\left(\frac{\text{transition}}{\mu\text{coul}}\right)$	Excitation (kev)	$I_2\left(\frac{\text{excitation}}{\mu\text{coul}}\right)$	$\int_0^E \frac{g_{E1}(\xi)E'dE}{dE/d\rho x}$ kev×mg/cm²	$B(E2)_{ex}$ ×10⁴⁸
$_{90}Th^{230}$	760	p	5.0	$E2$	0.017	3.38×10^{4}	760	3.38×10^{4}	3.38×10^{4}	0.13
$_{83}Pb^{207}$	570	p	4.5	$E2$	0.021	1.34×10^{4}	570	1.34×10^{4}	4.73×10^{4}	0.028[a]
$_{83}Pb^{206}$	810	p	4.5	$E2$	0.01	1.72×10^{4}	810	1.72×10^{4}	1.50×10^{4}	0.11[b]
$_{83}Pb^{206}$		p	5.0	$E2$	0.01	5.65×10^{4}	810	5.65×10^{4}	3.51×10^{4}	0.16[a]
$_{81}Tl^{205}$	205	p	4.0	$E2+M1$	0.93	2.11×10^{5}	205	1.93×10^{5}	1.33×10^{5}	0.137
	205	α	4.0	$E2+M1$	0.93	7.12×10^{5}	205	7.12×10^{5}	1.19×10^{5}	0.141
	410	p	4.0	$E2+M1$	0.14	1.81×10^{4}	615	2.11×10^{4}	1.70×10^{4}	0.117
$_{81}Tl^{203}$	279	p	4.0	0.81 $E2$+0.19 $M1$	0.22	1.61×10^{5}	279	1.46×10^{5}	1.01×10^{5}	0.135
	279	α	4.0	0.81 $E2$+0.19 $M1$	0.22	1.76×10^{5}	279	1.76×10^{5}	3.22×10^{5}	0.128
	410	p	4.0	$E2+M1$	0.14[d]	1.46×10^{4}	682	1.70×10^{4}	1.10×10^{4}	0.145
$_{79}Au^{197}$	191	p	4.0	$E2+M1$	1.09[e]	1.13×10^{5}	(191)	1.13×10^{5}	1.43×10^{5}	0.0682
	191	α	4.0	$E2+M1$	1.09[e]	1.55×10^{5}	(191)	1.55×10^{5}	1.80×10^{5}	0.0186
	191	p	4.0	$E2+M1$	1.09[e]	1.13×10^{5}	268	1.13×10^{5}	1.05×10^{5}	0.0928
	191	α	4.0	$E2+M1$	1.09[e]	1.55×10^{5}	268	1.55×10^{5}	3.98×10^{5}	0.0837
	277	α	4.0	0.57 $E2$+0.43 $M1$	0.36[e]	4.76×10^{5}	277	4.76×10^{5}	3.28×10^{5}	0.307
	277	p	4.0	0.57 $E2$+0.43 $M1$	0.36[e]	3.89×10^{5}	277	3.81×10^{5}	1.01×10^{5}	0.326
	273	p	4.0	$E2+M1$	(0.36)	8.34×10^{5}				
	550	p	4.0	$E2$	0.019	1.18×10^{5}	550	1.26×10^{5}	2.57×10^{4}	0.423
	277	p	1.6 to 5.0				277			0.334
	550	p	2.2 to 5.0				550			0.470
$_{78}Pt^{196}$	210	p	5.0	$E2+M1$	0.32[f]	1.40×10^{6}	210	1.40×10^{6}	2.87×10^{5}	0.406
					1.02[g]	2.14×10^{6}		2.14×10^{6}		0.621
	240	p	5.0	$E2$	0.20	5.93×10^{5}	240	5.93×10^{5}	2.68×10^{5}	0.184
$_{78}Pt^{194}$	330	p	4.0	$E2$	0.074	1.74×10^{6}	330	1.74×10^{6}	8.06×10^{5}	1.79
	330	p	5.0	$E2$	0.074	4.42×10^{6}	330	4.42×10^{6}	2.10×10^{5}	1.75
$_{78}Pt^{196}$	358	p	4.0	$E2$	0.060	1.21×10^{6}	358	1.21×10^{6}	7.07×10^{5}	1.43
	358	p	5.0	$E2$	0.060	2.66×10^{6}	358	2.66×10^{6}	1.94×10^{5}	1.15
$_{78}Pt^{198}$	403	p	4.0	$E2$	0.042	9.02×10^{6}	403	9.02×10^{6}	5.70×10^{5}	1.34
	403	p	5.0	$E2$	0.042	2.72×10^{6}	403	2.72×10^{6}	1.69×10^{5}	1.36
$_{74}W^{182,184,186}$	112	p	4.0	$E2$	3.16	1.40×10^{7}	112	1.40×10^{7}	1.82×10^{5}	5.44
						1.14×10^{7}		1.14×10^{7}		4.43
$_{74}W^{183}$	295	p	4.0	$E2$[h]	0.089	8.19×10^{4}	295	3.67×10^{5}	9.68×10^{4}	0.267
$_{73}Ta^{181}$	137	α	4.0	0.20 $E2$+0.80 $M1$[i]	2.09	6.33×10^{5}	137	6.33×10^{5}	5.41×10^{5}	1.98
	137	p	1.43 to 5.0	0.20 $E2$+0.80 $M1$[i]	2.09		137			2.50
	137	p	2.0 to 4.8	0.20 $E2$+0.80 $M1$[i]	2.09		137			2.62
	167	p	4.0	0.21 $E2$+0.79 $M1$	1.08	6.30×10^{5}				
	303	p	2.0 to 4.8	$E2$	0.079		303			0.578
	303	p	1.43 to 5.0	$E2$	0.079		303			0.624

[a] −40 percent, +20 percent.
[b] −35 percent, +20 percent.
[c] −40 percent, +10 percent.
[d] Wapstra, Maeder, Nijgh, and Ornstein, Physica **20**, 169 (1954).
[e] Huber, Halter, Joly, Maeder, and Brunner, Helv. Phys. Acta **26**, 591(A) (1953).
[f] Pure $E2$.
[g] Pure $M1$.
[h] See decay scheme of Murray, Boehm, Marmier, and DuMond, Phys. Rev. **97**, 1007 (1955).
[i] F. K. McGowan, Phys. Rev. **93**, 481 (1954).

Hg^{197} and Pt^{197}.[36,37] These studies reveal the following excited states: 77-kev state which decays by an $E2+M1$ transition, 268-kev state which decays predominantly by cascade through the 77-kev state (γ rays of 191 and 77 kev), 410-kev state (metastable) which decays to a 279-kev state (γ rays of 130 and279 kev).

In agreement with the work of others,[13,16] we find that under proton bombardment gold emits γ rays of 191, 277, and 550 kev. The 191- and 277-kev γ rays are also observed under α-particle bombardment. The 191-kev γ ray suggests that the 268-kev state, observed in radioactive decay of Hg^{197}, is being excited. As additional evidence in support of this conclusion, we find that the values of $B(E2)_{ex}$ calculated from the the observed yields of the γ ray for proton and α-particle bombardment differ by a factor of 4 if an excitation energy of 191 kev is assumed, whereas an excitation energy of 268 kev brings the values into fair agreement.

Since the 268-kev state decays to the 77-kev state, one expects that γ rays of 77-kev energy are also emitted. There is also the possibility that the 77-kev state is directly excited. (Radioactive decay studies indicate the state decays by an $E2+M1$ transition.) Unfortunately, γ radiation of this energy is obscured by the strong emission of K x-rays of gold which are excited by the bombarding particles. Since α-particle bombardment produces much less x-radiation than does

[36] See review article by Hollander, Perlman and Seaborg, Revs. Modern Phys. **25**, 469 (1953).
[37] J. W. Mihelich and A. de-Shalit, Phys. Rev. **91**, 78 (1953).

TABLE V.—*Continued.*

Nucleus	E_γ (kev)	Bombarding particle	E (Mev)	Classification	α_T	$I_\gamma\left(\frac{\text{transition}}{\mu\text{coul}}\right)$	Excitation (kev)	$I_\gamma\left(\frac{\text{excitation}}{\mu\text{coul}}\right)$	$\int_0^E \frac{g_{E1}(\xi)E'dE}{dE/d\rho x}$ kev×mg/cm²	$B(E2)_{ex}$ ×10⁴⁸
$_{72}Hf^{176,178,180}$	90	p	4.0	$E2$	6.1[j]	1.83×10^{7}	90	1.83×10^{7}	1.91×10^{5}	6.21
$Hf^{177,179}$[k]	112	p	4.0	$E2$[l]	3.09	6.77×10^{6}	112	6.77×10^{6}	1.81×10^{5}	2.42
$_{47}Ag^{107,109}$	104	p	2.1	$E2+M1$	0.49[m]	2.85×10^{6}				
	104	p	2.5	$E2+M1$	0.49[m]	7.13×10^{6}				
	104	p	2.9	$E2+M1$	0.49[m]	1.98×10^{7}				
	325	p	2.1	$E2+M1$	{0.018[n]}	5.90×10^{4}	325	5.61×10^{4}	4.17×10^{5}	0.225
	325	p	2.5	$E2+M1$	{0.022[o]}	1.67×10^{5}	325	1.60×10^{5}	1.17×10^{6}	0.229
	325	p	2.9	$E2+M1$		3.52×10^{5}	325	3.32×10^{5}	2.47×10^{6}	0.225
	427	p	2.1	$E2$	0.0107	3.18×10^{4}	427	3.47×10^{4}	1.53×10^{5}	0.380
	427	p	2.5	$E2$	0.0107	1.15×10^{5}	427	1.22×10^{5}	5.78×10^{5}	0.354
	427	p	2.9	$E2$	0.0107	2.92×10^{5}	427	3.12×10^{5}	1.45×10^{6}	0.360
$_{46}Pd^{110}$	380	p	2.1	$E2$	0.0143	1.58×10^{4}	380	1.58×10^{4}	2.61×10^{5}	0.989
	380	p	2.5	$E2$	0.0143	4.77×10^{4}	380	4.77×10^{4}	8.34×10^{5}	0.934
	380	p	2.9	$E2$	0.0143	1.135×10^{5}	380	1.135×10^{5}	1.91×10^{6}	0.972
$_{46}Pd^{108}$	445	p	2.1	$E2$	0.0089	9.36×10^{3}	445	9.36×10^{3}	1.36×10^{5}	1.10
	445	p	2.5	$E2$	0.0089	3.49×10^{4}	445	3.49×10^{4}	5.28×10^{5}	1.04
	445	p	2.9	$E2$	0.0089	8.65×10^{4}	445	8.65×10^{4}	1.35×10^{6}	1.03
$_{46}Pd^{106}$	520	p	2.1	$E2$	0.0057	3.13×10^{3}	520	3.13×10^{3}	6.43×10^{4}	0.766
	520	p	2.5	$E2$	0.0057	1.36×10^{4}	520	1.36×10^{4}	3.12×10^{5}	0.687
	520	p	2.9	$E2$	0.0057	4.19×10^{4}	520	4.19×10^{4}	9.16×10^{5}	0.722
$_{46}Pd^{104}$	575	p	2.5	$E2$	0.0043	6.23×10^{3}	575	6.23×10^{3}	1.90×10^{5}	0.507
	575	p	2.9	$E2$	0.0043	2.33×10^{4}	575	2.33×10^{4}	6.33×10^{5}	0.570
$_{45}Rh^{103}$	65	p	2.1	$E2+M1$	1.15[p]	7.60×10^{6}				
	65	p	2.5	$E2+M1$	1.15[p]	2.32×10^{6}				
	65	p	2.9	$E2+M1$	1.15[p]	5.94×10^{6}				
	305	p	2.1	$E2+M1$	{0.0178[q]}	9.45×10^{3}	305	8.71×10^{3}	5.34×10^{5}	0.239
	305	p	2.5	$E2+M1$	{0.023[r]}	2.05×10^{4}	305	1.83×10^{4}	1.39×10^{6}	0.193
	305	p	2.9	$E2+M1$		4.27×10^{4}	305	3.68×10^{4}	2.78×10^{6}	0.194
	365	p	2.1	$E2$	0.0157	7.15×10^{3}	365	7.91×10^{3}	3.12×10^{5}	0.371
	365	p	2.5	$E2$	0.0157	2.07×10^{4}	365	2.30×10^{4}	9.48×10^{5}	0.355
	365	p	2.9	$E2$	0.0157	4.51×10^{4}	365	5.11×10^{4}	2.09×10^{6}	0.358
$_{42}Mo^{95}$	212	p	2.1	$E2+M1$	0.036[s]	4.17×10^{3}	212	4.17×10^{3}	1.18×10^{5}	0.0416
	212	p	2.5	$E2+M1$	0.036[s]	8.25×10^{3}	212	8.25×10^{3}	2.42×10^{5}	0.0401
	212	p	2.9	$E2+M1$	0.036[s]	1.49×10^{4}	212	1.49×10^{4}	4.15×10^{5}	0.0423
$_{42}Mo^{100}$	540	p	2.4	$E2$	0.004	1.11×10^{4}	540	1.11×10^{4}	2.27×10^{5}	0.605
	540	p	2.7	$E2$	0.004	2.80×10^{4}	540	2.80×10^{4}	5.74×10^{5}	0.604
	540	p	3.0	$E2$	0.004	5.79×10^{4}	540	5.79×10^{4}	1.15×10^{6}	0.623
$_{42}Mo^{98}$	770	p	2.4	$E2$	0.001	9.00×10^{3}	770	9.00×10^{3}	2.77×10^{5}	0.394
	770	p	2.7	$E2$	0.001	3.78×10^{4}	770	3.78×10^{4}	1.11×10^{6}	0.413
	770	p	3.0	$E2$	0.001	1.07×10^{5}	770	1.07×10^{5}	3.07×10^{6}	0.423

[j] F. K. McGowan, Phys. Rev. **87**, 542 (1952).
[k] See McClelland, Massachusetts Institute of Technology Progress Report, 1954, McClelland, Mark and Goodman, Phys. Rev. **97**, 1191 (1955).
[l] McGowan, Klema, and Bell, Phys. Rev. **85**, 152 (1952).
[m] Transition taken as pure $M1$.
[n] $(E2/M1)^2 = -0.19$.
[o] $(E2/M1)^2 = -1.14$.
[p] Transition taken as pure $M1$.
[q] $(E2/M1)^2 = -0.18$.
[r] $(E2/M1)^2 = -1.17$.
[s] Medicus, Preiswerk, and Scherrer, Helv. Phys. Acta **23**, 299 (1950).

proton bombardment, the possibility of establishing the existence of this γ ray is enhanced by the use of α-particles. Heydenburg and Temmer[5] report evidence for the existence of the γ ray from a comparison of spectral shapes obtained for proton and α-particle excitation. No estimate of intensity is given.

When gold is bombarded by 4-Mev α particles, we find that the number of 191-kev transitions is less than one percent of the number of K x-rays. Hence, even when α particles are used, the number of 77-kev γ rays to be expected from the excitation of the 268-kev state is still much less than the K x-ray intensity. Direct excitation of the 77-kev state is estimated to be 30 times more probable than excitation of the 268-kev state on the assumption of equal values for $B(E2)_{ex}$. Therefore, if the $B(E2)_{ex}$ for excitation of the 77-kev is similar to that for the 268-kev, one expects an intensity of 77-kev γ rays comparable to the K x-ray intensity. To determine whether the gold K x-ray intensity were anomalously large and thereby established the existence and obtain an estimate of the yield of the 77-kev γ ray, a comparison was made of the K x-ray intensities for 4-Mev α-particles bombardment for gold and neighboring elements. An irregularity which was outside the uncertainties of the measurements was not observed. It is concluded that $B(E2)_{ex}$ for the 77-kev state is less than 0.20×10^{-48} cm⁴. The value for α_T of 5.0 was taken in obtaining this limit. Recently Sunyar[55] measured the $T_{\frac{1}{2}}$ for decay of this state by the delayed coincidence method. From his results one concludes that $B(E2)_{ex}$ is either 0.10 or

[55] A. W. Sunyar, Phys. Rev. **98**, 653 (1955).

TABLE VI. Summary of quantities obtained from the $B(E2)_{ex}$ values given in Table V. The values of $B(E2)_d$ are given in column 4 for the spin assignments of the excited states in the nuclei listed in columns 3, 2, and 1. From the values for cascades/crossovers, α_T and $E2/M1$, the values of $T_\frac{1}{2}$ and $B(M1)_d$ are calculated. The columns headed $(Q_0)_E$ and $(Q_0)_{B(E2)}$ list the values of Q_0 based on the excitation energy and the $B(E2)_d$ values, respectively. The next column gives the ratio of the two values of Q_0. The last column lists the ratio of the observed $B(E2)_d$ to that given by the single particle estimate $B(E2)_{sp}$.

Nucleus	E (kev)	I	$B(E2)_d$ $\times 10^{49}$	Cascade crossovers	$E2/M1$	$T_\frac{1}{2}$(sec)	$B(M1)_d$	$(Q_0)_E$ $\times 10^{24}$	$(Q_0)B(E2)$ $\times 10^{24}$	$\frac{(Q_0)_{B(E2)}}{(Q_0)_E}$	$\frac{B(E2)_d}{B(E2)_{sp}}$
Pb^{207}	570	5/2	0.0093		∞	1.0×10^{-10}		10.5	0.69	0.066	0.62
Pb^{204}	810	2	0.025		∞	7.70×10^{-12}		7.63	1.02	0.13	1.7
Tl^{205}	205	(3/2)	0.069		(0.27)	2.48×10^{-10}	7.6×10^{-3}	10.1	1.86	0.18	4.6
	615	(5/2)	0.039					10.1	1.40	0.14	2.6
Tl^{203}	279	3/2	0.068		4.26	3.25×10^{-10}	8.74×10^{-4}	9.43	1.91	0.20	4.6
	682	5/2	0.049	6	∞	1.12×10^{-12}		9.43	1.57	0.17	3.3
	410		1.44		0.78		2.18×10^{-1}				98
Au^{197}	277	5/2	0.223		0.56	4.11×10^{-11}	2.14×10^{-3}	(11.6)	2.55	0.22	16
	550	7/2	0.235	0.06	∞	4.43×10^{-12}		(12.7)	4.06	0.32	17
Pt^{194}	330	2	0.35		∞	3.85×10^{-11}		11.5	4.19	0.36	25
Pt^{196}	358	2	0.26		∞	3.49×10^{-11}		11.0	3.61	0.33	19
Pt^{198}	403	2	0.27		∞	1.88×10^{-11}		10.4	3.68	0.35	19
$W^{182,184,186}$	112	2	0.98		∞	7.88×10^{-10}[a]		18.9	7.02	0.37	76
Ta^{181}	137	9/2	2.00		0.25	3.78×10^{-11}	1.05×10^{-1}	20.7	7.70	0.37	160
	303	11/2	0.416	3.37	∞	1.13×10^{-11}		20.7	7.59	0.37	33
	166		3.05		0.26		2.26×10^{-1}		9.46		240
$Hf^{178,179,180}$	90	2	1.24		∞	1.08×10^{-9}		20.7	7.90	0.38	100
$Ag^{107,109}$	325	3/2	0.113[b]		0.036	4.71×10^{-12}	2.33×10^{-1}	7.05	2.38	0.34	18
	325	3/2	0.113		1.30	7.63×10^{-12}	6.46×10^{-3}		2.38		18
	427	5/2	0.122[b]	0.07	∞	2.99×10^{-11}		7.05	2.48	0.35	19
Pd^{110}	380	2	0.193		∞	3.65×10^{-11}		6.94	3.11	0.45	30
Pd^{108}	445	2	0.213		∞	1.51×10^{-11}		6.43	3.27	0.51	34
Pd^{106}	520	2	0.145		∞	1.02×10^{-11}		5.98	2.69	0.45	23
Pd^{104}	575	2	0.108		∞	8.30×10^{-12}		5.70	2.34	0.41	18
Rh^{103}	305	3/2	0.104[c]		0.032	6.28×10^{-12}	2.12×10^{-1}	7.25	2.29	0.32	17
	305	3/2	0.104		1.37	1.17×10^{-10}	4.96×10^{-3}		2.29		17
	365	5/2	0.120[c]	0.12	∞	6.39×10^{-11}		7.25	2.46	0.34	20
Mo^{100}	540	2	0.122		∞	9.48×10^{-12}		5.40	2.53	0.47	21
Mo^{97}	770	2	0.082		∞	2.54×10^{-12}		4.54	2.03	0.45	15

[a] $T_\frac{1}{2}=1.40\times10^{-9}$ sec for $E_\gamma=100$ kev.
[b] Cascade transition of 104 kev taken to be predominantly $M1$ radiation.
[c] Cascade transition of 65 kev taken to be predominantly $M1$ radiation.

0.20×10^{-43} cm^2 depending on whether the spin of the 77-kev state is $\frac{1}{2}$ or $\frac{3}{2}$.

The γ ray of 550-kev energy is not found in the radioactive decays studies. There are several reasons for believing that this γ ray results from the direct excitation of a state at 550-kev excitation energy. The yield of the γ ray as a function of proton energy is in good agreement with the prediction of the Coulomb theory when the excitation energy is taken as 550 kev (see Goldburg and Williamson,[13] Cook *et al.*,[16] and below). We were unable to establish coincidences between this γ ray and the 191- or the 277-kev γ rays. Both the large $B(E2)_{ex}$ and the angular distribution $(3/2 \xrightarrow{E2} 7/2 \xrightarrow{E2} 3/2)$ (see Goldburg and Williamson,[13] Cook *et al.*,[16] below and accompanying paper[34]) are what one might expect for collective excitations.

TABLE VII. Values of g_Ω and g_R obtained from ground state magnetic moments and the quantities $(g_\Omega-g_R)^2$.

Nucleus		Transition	$(g_\Omega-g_R)^2$	g_Ω	g_R
Ta	2.1	137	0.202	0.70	0.25
				0.50	0.95
		166	0.284	0.72	0.19
				0.48	1.02
Au	0.19	277	0.149	−0.061	0.32
				0.25	−0.14

The 277-kev γ ray is thought to result from the excitation of the excited state of this energy which is also found in radioactive decay studies. The yield of the γ ray as a function of proton energy and for α particles agrees with that predicted by the Coulomb theory when the excitation energy is taken as 277-kev (see Goldburg and Williamson,[13] Cook *et al.*,[16] and below). The $E2/M1$ value deduced from the angular distribution[34] agrees with that obtained from internal conversion measurements.

It has been pointed out that if the 550-kev state decays by cascade through the 277-kev state, the first γ ray would have an energy (273-kev) very close to the 277-kev γ ray and probably would not be resolved with a scintillation spectrometer.[13,16] Using 4-Mev protons on a thick gold target, Goldburg and Williamson[13] found that less than 10 percent of the γ rays of 277-kev energy are in coincidence. Cook *et al.*[16] found that less than 5 percent were in coincidence for 3-Mev protons on a thick target. We have established that coincidences exist. For 4-Mev protons on a thick target, it is found that 2.1 ± 0.4 percent of the 277-kev γ rays are in coincidence. From this percentage, the observed intensities and the known α_T for the 550- and 277-kev transitions it is found that 6 percent of the decays of the 550-kev state are by cascade to the 277-kev state. The value of

6 percent has some uncertainty because the α_T for the 273-kev transition is not known. We have taken α_T to be equal to that for the 277-kev transition ($E2/M1 = 0.56$). If the 273-kev transition is predominantly $M1$ or predominantly $E2$ the percentages are 7 or 5 percent, respectively.

It is also of interest to determine to what extent the 550-kev state decays to the 268-kev state. Coincidences were looked for between the 191-kev γ ray and a 282-kev γ ray (unresolved from the 277-kev γ ray). No evidence for coincidences was found. From this it is concluded that less than 0.5 percent of the decays of the 550-kev state go to the 268-kev state. It might also be mentioned that the intensity of a 473-kev γ ray which would result from the decay of the 550-kev state to the 77-kev state is less than 3 percent of the intensity of the 550-kev γ ray.

The $B(E2)_{ex}$ for the 277- and 550-kev states have been calculated from the observed thin target γ-ray yields and are listed in Table IV. The values taken for α_T and the ratio of cascades/crossovers for the 550-kev state are listed in Tables V and VI. Except for the lowest proton energies where larger errors are assigned, it is thought that the total spread in the relative values of $B(E2)_{ex}$ caused by experimental errors is not more than 15 percent. An inspection of the $B(E2)_{ex}$ values indicates no significant variation and we conclude that to within this accuracy the relative cross section is correctly given by the theory. As was the case for the 303-kev state in tantalum, one can conclude from the excitation of the gold states that the expression for ξ given by formula (3) is favored over the one originally proposed.

If the strong coupling limit of the collective model were realized in the gold nucleus one would expect to observe the strong excitation of the first two rotational states. These states should have spins of 5/2 and 7/2 and excitation energies in the proportion 5:12. The available information indicates that the 277- and 550-kev states have spins of 5/2 and 7/2, respectively. The ratio of the excitation energies is 1.99 ± 0.02 instead of the predicted value of 2.40. The values of Q_0 calculated from the excitation energies are 11.6 and 12.7 barns whereas those calculated from the $B(E2)_{ex}$ are 2.55 and 4.06 barns for the 277- and 550-kev states, respectively. The two solutions for g_0 and g_R based on the $B(M1)$ value for the 277-kev transition and magnetic moment of the ground state are given in Table VII.

C. Platinum

McClelland *et al.*[39] have shown by the use of enriched isotopes that the 330-, 358-, and 403-kev γ rays result from the excitation of Pt^{194}, Pt^{196}, and Pt^{198}, respectively. The 330- and 358-kev γ rays of Pt^{194} and Pt^{196} are also observed in radioactive decay studies. McClelland *et al.* have given values of Q_0 based on their determination of the $B(E2)_{ex}$ for the 330-, 358-, and 403-kev γ rays as 2.3, 1.7, and 1.4 barns. These are considerably smaller than the values we list and indicate differences of factors of 3.0 to 6.9 in the determination of the $B(E2)_{ex}$.

The other four γ rays of 100-, 130-, 210-, and 240-kev energy observed under proton or α-particle bombardment of natural platinum are thought to result from the excitation of Pt^{195}. The 100- and 130-kev γ rays are observed in radioactive decay to Pt^{195}.[38] The 210-kev γ ray has been assigned to Pt^{195} by McClelland *et al.*[39] from the study of the yields from enriched isotopes. They do not list the 240-kev γ ray. However, the 240-kev γ ray has also been observed by Class *et al.*[40]

D. Thallium

Thallium consists of the two isotopes Tl^{203} (29.5 percent) and Tl^{205} (70.5 percent). Radioactive decay studies give no information on excited states of Tl^{205}. Work on the decay of Hg^{203} and Pb^{203} indicate excited states in Tl^{203} at 279- and 682-kev.[30,41,42] Therefore, the 279- and 410-kev γ rays (the 682-kev state decays mainly by cascade) are believed to result from the excitation of these two levels in Tl^{203}. The 205-kev γ ray is tentatively assigned to Tl^{205}.

Coincidence measurements on the γ rays from thallium verified the fact that 410-kev γ rays are in coincidence with 279-kev γ rays. It was also found that 410-kev γ rays are in coincidence with 205-kev γ rays. This suggests that the 410-kev peak is a composite peak of two γ rays. We tentatively conclude that states of 205- and 615-kev energy are excited in Tl^{205}.

To obtain the $B(E2)_{ex}$ for the 615-kev transition in Tl^{205} we have taken α_T for the 410-kev transition to be 0.14, which is the value for the 410-kev transition in Tl^{203}. Since α_T for an $E2+M1$ transition of this energy is rather small, less than 10 percent error in $B(E2)_{ex}$ results from the fact that $E2/M1$ is not known. From the intensities of the singles and coincidence spectra one can deduce a value for α_T for the 205-kev transition. The value is 0.90 ± 0.50. An α_T of 0.90 corresponds to an $E2/M1$ value of 0.27.

Metzger and Todd[43] have determined the lifetime of the 279-kev state in Tl^{203} by the use of the resonance fluorescence method. They find the γ-ray lifetime, T_γ, is $(1.0\pm0.4)\times10^{-9}$ sec,* or $T_\frac{1}{2}$ of the state is $(5.7\pm2.3)\times10^{-10}$ sec. (We have taken $\alpha_T=0.22$ to calculate $T_\frac{1}{2}$.) This agrees with the value of 3.64×10^{-10} sec obtained from the Coulomb excitation cross section. Metzger and Todd pointed out that the lifetime is much longer than

[39] McClelland, Mark, and Goodman, Phys. Rev. **97**, 1191 (1955).

[40] Class, Cook, and Eisinger, Phys. Rev. **94**, 747 (1954).

[41] Wapstra, Maeder, Nijgh, and Ornstein, Physica **20**, 169 (1954).

[42] J. Varma, Phys. Rev. **94**, 1688 (1954).

[43] F. R. Metzger and W. B. Todd, Phys. Rev. **95**, 627 (1954).

* *Note added in proof.*—Additional measurements give a best value of $(0.6\pm0.15)\times10^{-9}$ sec. F. Metzger, private communication.

that given by the value of $B(M1)_{sp}$. The $B(M1)_d$ given in Table VI is 2000 times smaller than $B(M1)_{sp}$. In contrast, the $B(M1)_d$ for the 410-kev transition in Tl^{203} is 5 times smaller than $B(M1)_{sp}$.

The E_2 transition probabilities in the thallium isotopes are factors of 2 to 5 larger than $B(E2)_{sp}$ with the exception of the unexpectedly strong enhancement of $E2$ for the 410-kev transition in Tl^{203}. Since Tl^{203} is rather near to the double closed shell nucleus, Pb^{208}, the enhancement of an $E2$ transition probability by a factor of 100 is surprising and it is well to review the evidence for this enhancement. Wapstra *et al.*[41] and Varma[42] have studied the decay of Pb^{203} to Tl^{203}. It is found that the 682-kev state decays mostly by cascade (cascades/crossovers = 6). The measured values of α_K and $K/L+M$ for the 410-kev transition indicate that $E2$ is comparable to $M1$ (we have taken $E2/M1=0.78$). From this information it follows that $T(E2)_{410}/T(E2)_{682}=2.6$ where $T(E2)$ is the transition probability. Now taking into account the E^5 dependence of $E2$ transitions we have that $[B(E2)_d]_{410}/[B(E2)_d]_{682}=33$. The value of $[B(E2)_d]_{682}$ is determined from the Coulomb excitation cross section and it is found to be 3.3 times larger than $B(E2)_{sp}$. It then follows that $[B(E2)_d]_{410}$ is approximately 100 times larger than $B(E2)_{sp}$.†

E. Lead

Two γ rays of low yield with energies of 570- and 810-kev were observed when normal lead was bombarded with protons of 4- to 5-Mev energy. The yield of the 810-kev γ ray increased when a target of radiogenic lead enriched to 88 percent Pb^{204} was used and we therefore assign this γ ray to Pb^{206}. A γ ray of this energy is also observed in the decay of Po^{210} [38] and Bi^{206}.[44] The 570-kev γ ray is thought to result from the excitation of the first state in Pb^{207} which is known from work on the decay of Bi^{207} [38,45,46] and the $Pb^{208}(d,t)$ and $Pb^{206}(d,p)$ reactions.[47]

Delayed coincidence measurements of the half-life of the 570-kev state in Pb^{207} have shown that it is less than 4×10^{-10} sec.[45,46] From the observed $B(E2)_{ss}$ a value of $T_{\frac{1}{2}}$ of $(1.0_{-0.3}{}^{+0.4})\times10^{-10}$ sec is calculated.

Pryce[48] has emphasized that the shell model should be especially applicable to the description of the low-lying states of nuclei near to the double closed shell nucleus Pb^{208}. And it is found that the experimental information on the low lying states of Pb^{207} and Pb^{206} fits the picture of single particle neutron states to a considerable extent. The $B(E2)_d$ for the first excited states of Pb^{207} and Pb^{206} are much larger than is expected for transitions between shell model neutron states and are instead the same order magnitude as $B(E2)_{sp}$ (based on shell model proton states). Bohr and Mottelson have pointed out that in the weak coupling limit of the collective model the $B(E2)$ for transitions between neutron states may be greatly enhanced by the coupling of the states to the nuclear surface.

F. Thorium

The 53-kev γ ray, which has also been observed by Temmer and Heydenburg,[4] is thought to result from the excitation of the first rotational state in thorium. We also list a 760-kev γ ray which is observed with 5-Mev proton bombardment. However, additional work is needed to establish with certainty that this γ ray actually results from the excitation of a state in thorium. An excitation energy of 760-kev is of the order of that expected for the first vibrational state but the observed $B(E2)_{ss}$ is not as large as one would expect for this type of transition and is, instead, similar to that given by $B(E2)_{sp}$.

G. Wolfram

Other workers[3,6] have found by the use of enriched isotopes that γ rays of 100-, 112-, and 124-kev energy are excited in the isotopes W^{182}, W^{184}, and W^{186}, respectively. The 100- and 124-kev states in W^{182} and W^{186} are also known from radioactive decay measurements. It is reported[3,6] that γ rays of 46- and 103-kev energy are excited in W^{183} which is the only stable odd-A isotope of wolfram (abundance 14 percent).

For natural wolfram and an incident proton energy of 4.0 Mev we observe the spectrum shown in Fig. 7. The peak at 112 kev is too broad to be attributed to a single γ ray and it is therefore thought to be a composite line of the γ rays from the three even-A isotopes and the 103-kev γ ray from W^{183}. In calculating the average $B(E2)_{ss}$ for the even-A isotopes we have not applied a correction to account for the contribution of the 103-kev γ ray in W^{183}. This probably introduces an error of less than the natural abundance of W^{183} (14 percent).

A γ ray of 295-kev energy is also observed and we have rentatively assigned this to W^{183}. Murray *et al.*[49] have accurately measured the energies of a large number of γ rays which result from the decay of excited states of W^{183} following the β decay of Ta^{183}, and from this work they have deduced a level scheme for W^{183}. Their scheme indicates a state at 291.71 kev which decays by an $E2$ transition to the ground state. We have used their decay scheme to evaluate the $B(E2)_{ss}$ for the 291.71-kev state from the observed intensity of the 291.71-kev γ ray. One can then obtain values

† *Note added in proof.*—Recent work on the Coulomb excitation of thallium has been reported by Barloutaud, Crjebine, and Riou, Compt. rend. **240**, 1207 (1955).

[41] D. E. Alburger and M. H. L. Pryce, Phys. Rev. **95**, 1482 (1954).

[42] F. K. McGowan and E. C. Campbell, Phys. Rev. **92**, 523 (1953).

[43] D. E. Alburger and A. W. Sunyar, Bull. Am. Phys. Soc. **29**, No. 8, 28 (1954).

[47] J. A. Harvey, Can. J. Phys. **31**, 278 (1953).

[48] M. H. L. Pryce, Proc. Phys. Soc. (London) **A65**, 773 (1952).

[49] Murray, Boehm, Marmier, and DuMond, Phys. Rev. **97**, 1007 (1955).

for $B(M1)_d$ for the competing modes of decay for this state. The values for $B(M1)_d$ for the 84.70-, 82.91-, and 192.64-kev γ rays are 0.59, 0.11, and 0.0040, respectively.

Sunyar[50] has measured the half-life of the 100-kev state in W^{182} by the use of the delayed coincidence method and finds the value of 1.27×10^{-9} sec. This is in good agreement with the value of 1.40×10^{-9} sec computed from the $B(E2)_{ex}$ based on the Coulomb excitation cross section.

H. Hafnium

McClelland *et al.*[39] have shown by the use of enriched isotopes that the three even-A isotopes, Hf^{176} (5.15 percent), Hf^{178} (27.08 percent) and Hf^{180} (35.44 percent) emit γ rays of 87-, 91-, and 92-kev energy, respectively. Radioactive decay measurements[36] have indicated states at 89 and 93 kev for Hf^{176} and Hf^{180}. Therefore we interpret the line observed at 90 kev as a composite line of the three γ rays from the even-A isotopes of hafnium.

Direct measurements of the half-lives of the 89- and 93-kev states of Hf^{176} [51] and Hf^{180} [50] by the delayed coincidence method gives values of 1.35×10^{-9} sec and 1.39×10^{-9} sec, respectively. The value of 1.13×10^{-9} sec is obtained from the $B(E2)_{ex}$ based on the Coulomb excitation cross section.

Other workers[39] have investigated the excitation of states in the two odd-A isotopes, Hf^{177} and Hf^{179}, by the use of enriched isotopes and found γ rays of 114 and 235 kev for Hf^{177} and 122 and 250 kev for Hf^{179}. The peaks observed at 112 and 248 kev are therefore interpreted as composite lines from the γ rays of the odd-A isotopes.

I. Silver

Measurements of the Coulomb excitation of silver by use of enriched isotopes have been made by Heydenburg and Temmer.[15] They found that the spectra of the two isotopes (Ag^{107}, Ag^{109}) were quite similar; Ag^{107} emits γ rays of 318- and 413-kev energy and Ag^{109} emits γ rays of 305- and 400-kev energy. These results indicate that the γ rays listed as 325- and 427-kev energy are composite lines resulting from the excitation of both isotopes. In addition a rather weak γ ray of 104-kev energy was observed (see Fig. 9) which we believe to result from the cascade decay of the 427-kev state. The thick target yields were measured for 2.1-, 2.5-, and 2.9-Mev protons and it was found that the yields increased in accordance with the prediction of the Coulomb excitation theory for $E2$ transitions.

Heydenburg and Temmer found that the $B(E2)_{ex}$ were essentially the same for the two isotopes; the values are given as 0.13 and 0.22×10^{-48} cm^4 for the 325- and 427-kev transitions, respectively. Under the same assumptions (omission of internal conversions and cascade decay) our values are 0.23 and 0.34×10^{-48} cm^4. The inclusion of internal conversion and the cascade decay are rather unimportant. The values vary from 0.22 and 0.37×10^{-48} cm^4 (104-kev transition pure $M1$) to 0.23 and 0.36×10^{-48} (104-kev transition pure $E2$). The collective model[20] suggests that $B(E2)_{ex\ 427}/B(E2)_{ex\ 327}$ should be 1.5 if the spin of the 327-kev state is taken to be 3/2 and the spin of the 427-kev state is taken to be 5/2. The observed ratio is 1.6 to 1.7.

If one assumes that the $B(E2)_d$ of the 104-kev transition is comparable to those observed for the 325- and 427-kev transitions, it follows that the 104-kev transition is predominantly $M1$ ($E2/M1\cong0.01$). The value of $B(M1)$ for the 104-kev transition on the assumption of pure $M1$ is 0.86.

J. Rhodium

Heydenburg and Temmer[15] found that Coulomb excitation of rhodium results in the emission of two γ rays with energies of 295 and 357 kev. Rietjens *et al.*[52] found that several discrete γ rays are emitted in the decay of $Pd^{103} \xrightarrow{\epsilon\ \text{capture}} Rh^{103}$. Among these are two γ rays that are observed in Coulomb excitation. In addition to γ rays of 305- and 365-kev energy we also observed a 65-kev γ ray (see Fig. 12), which is believed to result from the cascade decay of the 365-kev state. A γ ray of 440-kev was also observed. However, the yield of this γ ray did not vary with proton energy in the way expected for Coulomb excitation. It is thought to be the result of a small amount of sodium impurity.

The values of $B(E2)_{ex}$ for the 305- and 365-kev transitions are given by Heydenburg and Temmer as 0.18 and 0.32×10^{-48} cm^4, respectively. Under the same assumptions (omission of internal conversion and cascade decay) our values are 0.23 and 0.32×10^{-48} cm^4. The omission of the cascade transition is more serious for rhodium than was the case for silver. Taking into account internal conversion and the cascade transition, it is found that the values vary from 0.21 and 0.36 $\times10^{-48}$ cm^4 (65-kev transition taken as pure $M1$) to 0.15 and 0.45×10^{-48} cm^4 (65-kev transition taken as pure $E2$) for the 305- and 365-kev transitions, respectively. The value of $E2/M1$ is not known for the 65-kev transition. The best agreement with the theory of Coulomb excitation; i.e., the constancy of the $B(E2)_{ex}$ for different incident proton energies for the 305- and 365-kev transitions, is obtained when the 65-kev transition is taken to be predominately $M1$. The ratio $B(E2)_{ex\ 365}/B(E2)_{ex\ 305}$ varies from 1.8 (65-kev transition $M1$) to 3.0 (65-kev transition $E2$). The ratio is expected to be 1.5 for rotational states if one assigns spin 3/2 to the 305-kev state and spin 5/2 to the 365-kev state.

If one assumes that the $B(E2)_d$ of the 65-kev transition is comparable to those observed for the 305- and

[50] A. W. Sunyar, Phys. Rev. **95**, 626 (1954).
[51] F. K. McGowan, Phys. Rev. **87**, 542 (1952).
[52] Rietjens, van den Bold, and Endt, Physica **20**, 107 (1954).

365-kev transitions, it follows that the 65-kev transition is predominantly $M1$ ($E2/M \cong 0.002$). The value of $B(M1)$ for the 65-kev transition on the assumption of pure $M1$ is 0.16.

K. Palladium

Excited states at 556-, 512-, and 430-kev in Pd^{104}, Pd^{106}, and Pd^{108}, respectively, have been found from radioactive decay studies.[36] The 575-, 520-, and 445-kev γ rays are thought to result from the excitation of these states. The 380-kev γ ray probably results from the excitation of the first excited state in Pd^{110} both because the excitation energy is a continuation of the observed trend for the other even-A isotopes of palladium and because the angular distribution exhibits a strong anisotropy characteristic of a 0–2–0 transition.

Palladium has one odd-A isotope, Pd^{105} (22 percent abundance). γ rays resulting from the excitation of this isotope are probably present. One indication of this is this is that the angular distribution of the 445- and the 380-kev γ rays are not quite in agreement with that expected for a pure 0–2–0 transition. However, a target enriched in Pd^{105} is needed to clearly identify γ rays from Pd^{105}. The values of $B(E2)_{ss}$ given for Pd^{106} and Pd^{110} are probably too large because of the contribution of γ rays from the excitation of Pd^{105}.

L. Molybdenum

The 212-kev γ ray is tentatively assigned to Mo^{94}. An excited state of this energy is observed in radioactive decay measurements.[36] Both the excitation energy and the $B(E2)_{ss}$ are smaller than those observed for other nuclei in this region.

The yield of the 540-kev γ ray varies with proton energy in agreement with the Coulomb excitation theory when an excitation energy of 540-kev is assumed. The excitation energy and the $B(E2)_{ss}$ suggest that this γ ray results from the excitation of the first excited state in Mo^{100} (9.68 percent abundance).

Radioactive decay studies indicate a first excited state of 770-kev for Mo^{96}.[36] However, the assignment of the observed 770-kev γ ray to excitation of Mo^{96} leads to a $B(E2)_{ss}$ which is somewhat larger than expected. This assignment also leads to the conclusion that no excitation is observed for Mo^{98} (24 percent abundance). We have tentatively assigned this γ ray to excitation of Mo^{98}. (Possibly both Mo^{96} and Mo^{98} have first excited states at approximately 770 kev.) Targets of enriched isotopes are required to establish with certainty the excitations of the isotopes of molybdenum.

6. CONCLUSIONS

The variation in cross section with incident proton energy has been studied for excitation of states in tantalum and gold, and no significant deviation from the variation predicted by the theory of Alder and Winther is found. In four cases the lifetimes of excited states obtained from the cross section for excitation may be compared to the lifetimes found from direct measurements using the delayed coincidences or the resonance fluorescence methods. The close agreement of the values is evidence that the theory correctly predicts the absolute cross section for excitation.

The quantities $B(E2)_d/B(E2)_{sp}$ (given in the last column of Table VI) are approximately 100 for nuclei well removed from closed shells (hafnium, tantalum, and wolfram). Platinum and gold have transitions for which $B(E2)_d/B(E2)_{sp}$ is approximately 20. The $B(E2)_d/B(E2)_{sp}$ values for thallium are approximately 3 except for the surprising case of the 410-kev transition in Tl^{203} for which it is 100. The two $E2$ transitions measured in Pb^{206} and Pb^{207} have $B(E2)_d$ values much larger than those for transitions between pure neutron states and are instead comparable to $B(E2)_{sp}$. One may interpret this as an indication of the coupling of the neutron states to the nuclear surface. The fact that $B(E2)_d/B(E2)_{sp}$ values of 20 are observed for nuclei with $47 \geq Z \geq 42$ is evidence of collective motion for states of medium weight nuclei.

The values of $B(M1)_d$ are found to be smaller than $B(M1)_{sp}$ by factors of 2 to 2000.

Even for the most highly deformed nuclei studied (hafnium, tantalum, and wolfram), the values of Q_0 based on the observed $B(E2)$ are smaller than those based on the observed excitation energy. The ratio of $(Q_0)_{B(E2)}/(Q_0)_{ss}$ is found to be rather constant. For example, $B(E2)_d$ changes by a factor of 5 for transitions in hafnium and platinum, yet there is no significant change in the ratio $(Q_0)_{B(E2)}/(Q_0)_{ss}$. The medium weight elements also have approximately the same value for this ratio as that for the heavy elements.

We thank Professor G. Breit for his interest in our work and, in particular, for suggestions concerning the analysis of the thin target yields. It is a pleasure to acknowledge the helpful discussions with Dr. M. E. Rose and Dr. L. C. Biedenharn.

Angular Distribution of Gamma Rays from Coulomb Excitation

F. K. McGowan and P. H. Stelson
Oak Ridge National Laboratory, Oak Ridge, Tennessee
(Received March 30, 1955)

The angular distributions of gamma rays with respect to the incident proton beam on a thick target have been measured for gamma rays following Coulomb excitation in $Pt^{196,198}$, Au^{197}, Ta^{181}, $Ag^{107,109}$, Pd^{106}, Pd^{108}, Pd^{110}, and Rh^{103}. The observed angular distributions deviate considerably from the semiclassical theory of angular distributions of gamma rays following Coulomb excitation given by Alder and Winther. Empirical curves of energy-dependent coefficients $a_\nu(\xi)$ for a thick target are obtained from the results for $Pt^{194,196}$ and Pd^{106}. With these empirical coefficients, information on the spin sequences and the character of the gamma transitions are deduced from the angular distribution measurements in the odd mass nuclei. The spin sequences are as follows: $7/2(E2)3/2$ and $5/2(E2+M1)3/2$ with $\delta_\gamma=-0.75$ (where $\delta_\gamma^2=E2/M1$) for the 550- and 277-kev transitions, respectively, in Au^{197}; $11/2(E2)7/2$ and $11/2(E2+M1)9/2$ with $\delta_\gamma=0.51$ for the 303- and 166-kev transitions, respectively, in Ta^{181}; $5/2(E2)1/2$ and $3/2(E2+M1)1/2$ with $\delta_\gamma=-0.19$ or -1.14 for the 427- and 325-kev transitions, respectively, in $Ag^{107,109}$; and $5/2(E2)1/2$ and $3/2(E2+M1)1/2$ with $\delta_\gamma=-0.18$ or -1.17 for the 365- and 305-kev transitions, respectively, in Rh^{103}.

1. INTRODUCTION

ALDER and Winther,[1] using a semiclassical treatment, have derived explicit expressions for the angular distribution of the gamma radiation following Coulomb excitation. They find that the angular distribution of the gamma radiation with respect to the incident particles is similar to the angular correlation between two gamma rays in cascade. The distribution function is

$$W(\theta)=1+\sum_\nu A_\nu a_\nu(\xi)P_\nu(\cos\theta), \qquad (1)$$

where the coefficients A_ν are the gamma-gamma directional angular correlation coefficients tabulated by Biedenharn and Rose[2] for the spin sequence $j_1(E2)j(L_2)j_2$ and the j's are the spins of the target nucleus, the Coulomb excited state, and the final state after gamma-ray emission, respectively. The coefficients $a_\nu(\xi)$ which depend on the excitation process through the parameter ξ have been evaluated by numerical methods for electric quadrupole excitation by Alder and Winther.

Several workers[3,4] have reported agreement between theory and experiment for the angular distribution of the 303-kev gamma ray of Ta^{181} and the 550-kev gamma ray of Au^{197}. However, our measurements have shown significant deviations from theory. For instance, the energy coefficient $a_2(\xi)$ was observed to be 17 percent smaller than theoretically expected at $E_p=4.0$ Mev for the 303-kev gamma ray in Ta^{181} on the assumption that the spin sequence is $7/2(E2)11/2(E2)7/2$. The results given in this paper suggest that the apparent agreement between theory and experiment found by the other workers is in part the result of the choice of the incident proton energy used in their experiments.

To further test the theory, the angular distributions of the gamma rays from Coulomb excited states of spin 2 have been examined. In these cases the spin of the excited state is known from gamma-gamma directional angular correlation measurements whereas the spins for the states of the odd-mass nuclei mentioned above were not known with certainty. The spin sequence $0(E2)2(E2)0$ is particularly suitable because the coefficients A_ν are large. In addition, for the cases that have been examined in these experiments, the gamma-gamma directional angular correlation measurements have shown no observable influence of extranuclear fields. This point is important for proton-gamma angular distribution measurements where a target in the solid state is necessary.

A number of other proton-gamma ray angular distributions have been measured and the results are presented. In cases for which the spin of the Coulomb excited state is known from other measurements, the energy dependent coefficients $a_\nu(\xi)$ for a thick target are tabulated. The observed deviations from theory are rather large. Finally, an interpretation of the results, in combination with the empirically determined energy-dependent coefficients, is discussed.

2. APPARATUS

The ORNL 5.5-Mv Van de Graaff accelerator was used to produce a separated beam of protons. Metallic targets which were thick to protons (the range of the protons being $\lesssim 100$ mg/cm^2) but thin for the gamma rays were oriented at 45° with respect to the incident protons. The targets ($\lesssim 100$ mg/cm^2) were prepared from thin foils or were electrodeposited onto 0.005-inch nickel. For the detection of the gamma rays, a scintillation spectrometer employing a NaI crystal 1.5 inches in diameter and 1 inch thick mounted on a DuMont 6292 photomultiplier was used. In all angular distribution experiments the front face of the crystal was located at distances 10.0 or 13.5 cm from the target. To suppress the characteristic K x-rays from the target produced by the impinging protons by factors of 10^3

[1] K. Alder and A. Winther, Phys. Rev. **91**, 1578 (1953).
[2] L. C. Biedenharn and M. E. Rose, Revs. Modern Phys. **25**, 729 (1953).
[3] Eisinger, Cook, and Class, Phys. Rev. **94**, 735 (1954); **95**, 628(A) (1954); **96**, 658 (1954).
[4] W. I. Goldburg and R. M. Williamson, Phys. Rev. **95**, 767 (1954).

to 10^6, a graded shield was placed in front of the NaI detector. The graded shields were as follows: for targets with $Z \geq 78$ the shield consisted of 0.010 inch of Ta plus 0.030 inch of Sn plus 0.005 inch of Cu; for a Ta target the shield consisted of 0.040 inch of Sn plus 0.005 inch of Cu; and for targets with $45 \leq Z \leq 53$ the shield consisted of 0.0035 inch of Mo plus 0.005 inch of Cu. Most of the data in these experiments were recorded automatically at 10° increments from 0° to 90° and from 210° to 270°. The time for the collection of a fixed number of counts was printed on a paper tape by a printing timer and the integrated current was recorded by a traffic counter. The angular positions were changed manually. To assure that the axis of rotation of the detector passed through the target, the following alignment procedure was used. The position at which the proton beam impinged on the target was located. A source of Cs^{137} of the same area as the beam was placed on the target at this position. The axis of rotation was adjusted until counting rates showed that the variation in the solid angle subtended by the detector at the target as a function of angular position was less than 0.5 percent. The position of the beam on the target was observed to remain fixed as a function of the beam energy.

3. DISCUSSION OF METHOD

Angular distribution measurements of the gamma rays were carried out with either a single-channel or a multichannel pulse-height analyzer of the ORNL design. In the measurements with a single channel the window of the analyzer was always operated to include only the full energy pulse spectrum peak of the gamma ray. In the case of the multichannel measurements, the full energy pulse spectrum peak was observed and the area of the peak was taken as a measure of the intensity. After each measurement of the intensity at an angle θ_i the intensity was measured either at $\theta=90°$ or at $\theta=0°$. In this way the intensities could be corrected for changes in gain of the detector or fractional acceptance of the window of the single-channel analyzer. In all cases, the intensities have been corrected for the bremsstrahlung continuum by measuring the intensity of the bremsstrahlung as a function of θ_i. For angular distribution measurements involving $Z \geq 73$ a Bi target electrodeposited onto nickel was used and for measurements involving $Z \sim 50$ a tin target was used. Bi and Sn targets are well suited for this purpose because of the absence of gamma rays from Coulomb excitation. We believe the extrapolation to neighboring Z will give little error since our investigations of the bremsstrahlung process show relatively little change in character with a small change in Z. In general for the measurements to be discussed below the intensity of the bremsstrahlung in the angular distributions was never more than a few percent of the gamma-ray intensity from Coulomb excitation. Finally, a correction for the attenuation of the gamma rays in the target and target backing as a function of θ_i was applied to the observed intensities. If this correction was no larger than 5 percent, a computed attenuation using the absorption cross sections taken from NBS-1003[5] was applied. If the correction was larger, the attenuation was measured directly by placing a source of gamma radiation of the same energy on the target. A least squares fit of the corrected intensities (with the appropriate weight factors) in terms of a series of Legendre polynomials,

$$W(\theta) = a_0' + a_2' P_2(\cos\theta) + a_4' P_4(\cos\theta), \qquad (2)$$

was carried out on an I.B.M. calculator. The standard deviations quoted in Table I have been obtained from Eq. (30) in a paper by Rose.[6] The values of ϵ^2, defined by Eq. (27),[6] clustered about unity indicating that nonstatistical errors were not large. A least-squares fit of each set of data in terms of a series of $\cos^{2n}\theta$ was carried out to serve as a check on the I.B.M. calculations. In Table I we tabulate $(a_\nu A_\nu)_{exp}$, which have been corrected for finite angular resolution[6] and are defined as

$$(a_\nu A_\nu)_{exp} = a_\nu / a_0.$$

4. MEASUREMENTS AND RESULTS

A. $Pt^{194,196}$

From the β decay of Ir^{194} and Au^{196}, the first excited states in Pt^{194} and Pt^{196} are known to exist at 330 and 358 kev, respectively. Directional angular correlation measurements[7–9] have verified the spin assignment of 2 for these excited states.

The differential pulse-height spectrum of the gamma radiation from platinum for $E_p = 5.0$ Mev is shown in an accompanying paper.[10] The proton-gamma angular distribution of the 330- and 358-kev gamma rays taken together has been measured for $E_p = 2.5$ to 5.0 Mev. The results are tabulated in Table I. All entries in Table I represent the mean of several determinations of the angular distribution coefficients. A comparison between theory and experiment is shown in Fig. 1. The solid curves labelled "theory" are the thick target energy-dependent coefficients $(a_\nu)_t$ deduced from the excitation cross section and the thin target coefficients a_ν given by Alder and Winther. A procedure for obtaining $(a_\nu)_t$ will be discussed in Sec. 5 The observed energy dependence of the coefficients for a thick target deviates considerably from the theory.

The second excited states in Pt^{194} and Pt^{196} are known to have spin 2.[8,9] If these states were appreciably excited by Coulomb excitation, then the observed proton-gamma angular distribution would be a com-

[5] G. R. White, National Bureau of Standards Circular NBS-1003, 1952 (unpublished).
[6] M. E. Rose, Phys. Rev. **91**, 610 (1953).
[7] J. J. Kraushaar and M. Goldhaber, Phys. Rev. **89**, 1081 (1953).
[8] R. M. Steffen, Phys. Rev. **89**, 665 (1953).
[9] Mandeville, Varma, and Saraf, Phys. Rev. **98**, 94 (1955).
[10] P. H. Stelson and F. K. McGowan, preceding paper [Phys. Rev. **99**, 112 (1955)].

TABLE I. Proton-gamma angular distribution coefficients of the terms in the expansion of the correlation function in Legendre polynomials for a thick target.

Nucleus	E_γ (kev)	E_p (Mev)	Spin sequence	$(A_2)_{\gamma\gamma}$	$(a_2A_2)_{exp}$	$(a_2)_{exp}$	$(A_4)_{\gamma\gamma}$	$(a_4A_4)_{exp}$	$(a_4)_{exp}$	$(A_3)_{exp}$	δ_γ
$_{78}Pt^{194,196}$	330 and 358	2.5	$0(E2)2(E2)0$	0.3571	0.286±0.005	0.800±0.015	1.143	−(0.078±0.010)	−(0.068±0.010)		
		3.0			0.253±0.004	0.709±0.010		−(0.062±0.006)	−(0.054±0.005)		
		3.5			0.227±0.003	0.636±0.008		−(0.026±0.008)	−(0.023±0.007)		
		4.0			0.211±0.003	0.591±0.007		−(0.013±0.004)	−(0.011±0.004)		
		4.5			0.191±0.005	0.535±0.015		−(0.007±0.008)	−(0.006±0.007)		
		5.0			0.171±0.003	0.479±0.008		0.001±0.003	0.001±0.003		
Au^{197}	550	3.5[a]	$3/2(E2)7/2(E2)3/2$	0.2186	0.176±0.006	0.80 ±0.03	0.1282	−(0.004±0.008)			
		4.0[a]			0.161±0.006	0.74 ±0.03		−(0.010±0.008)			
		5.0[a]			0.123±0.006	0.58 ±0.03		0.010±0.008			
		4.0			0.164±0.004	0.75 ±0.02		−(0.018±0.005)			
Au^{197}	277	4.0	$3/2(E2)5/2(E2+M1)3/2$		−(0.115±0.004)			0.003±0.005		−(0.21±0.01)	−(0.75±0.20)
Ta^{181}	303	4.0	$7/2(E2)11/2(E2)7/2$	0.1688	0.089±0.004	0.53 ±0.02	0.0500	−(0.006±0.004)			
Ta^{181}	166	4.0	$7/2(E2)11/2(E2+M1)9/2$		0.112±0.006			0.020±0.008		0.21±0.01	0.51 or 3.0
$Ag^{107,109}$	325	2.5	$1/2(E2)3/2(E2+M1)1/2$		−(0.282±0.004)			0.007±0.007		−(0.39±0.02)	−0.19 or −1.14
$Ag^{107,109}$	427	2.5	$1/2(E2)5/2(E2)1/2$	0.2857	0.248±0.004	0.868±0.015	0.3809	−(0.039±0.009)	−(0.102±0.024)		
Pd^{110}	380	2.1	$0(E2)2(E2)0$	0.3571	0.285±0.008	0.80 ±0.02	1.143	−(0.088±0.011)	−(0.077±0.010)		
		2.5			0.243±0.006	0.68 ±0.02		−(0.032±0.008)	−(0.028±0.007)		
		2.5			0.270±0.004	0.75 ±0.01		−(0.050±0.007)	−(0.044±0.007)		
		2.9			0.211±0.006	0.59 ±0.02		−(0.005±0.010)	−(0.005±0.009)		
Pd^{106}	445	2.5	$0(E2)2(E2)0$	0.3571	0.255±0.009	0.72 ±0.03	1.143	−(0.071±0.008)	−(0.062±0.007)		
Pd^{105}	520	2.1	$0(E2)2(E2)0$	0.3571	0.343±0.007	0.96 ±0.02	1.143	−(0.143±0.010)	−(0.125±0.009)		
		2.5			0.315±0.007	0.88 ±0.02		−(0.092±0.010)	−(0.080±0.009)		
		2.5			0.340±0.005	0.95 ±0.02		−(0.107±0.018)	−(0.094±0.017)		
		2.9			0.279±0.006	0.78 ±0.02		−(0.065±0.008)	−(0.057±0.008)		
Rh^{103}	305	1.7	$1/2(E2)3/2(E2+M1)1/2$		−(0.346±0.006)			0.006±0.007		−0.380	
		2.1			−(0.307±0.005)			0.024±0.006		−0.394	
		2.5			−(0.274±0.004)			0.019±0.006		−0.400	−0.18 or −1.17
		2.5			−(0.255±0.004)			0.007±0.004		−0.372	
		2.9			−(0.234±0.003)			0.012±0.004		−0.377	
Rh^{103}	365	1.7	$1/2(E2)5/2(E2)1/2$	0.2857	0.288±0.007	1.01 ±0.02	0.3809	−(0.046±0.009)	−(0.121±0.024)		
		2.1			0.247±0.005	0.87 ±0.02		−(0.021±0.006)	−(0.055±0.016)		
		2.5			0.224±0.004	0.78 ±0.01		−(0.027±0.005)	−(0.071±0.013)		
		2.5			0.227±0.003	0.79 ±0.01		−(0.023±0.004)	−(0.060±0.011)		
					0.200±0.002	0.70 ±0.01		−(0.012±0.003)	−(0.032±0.007)		

[a] Thin target (10.5 mg/cm²).

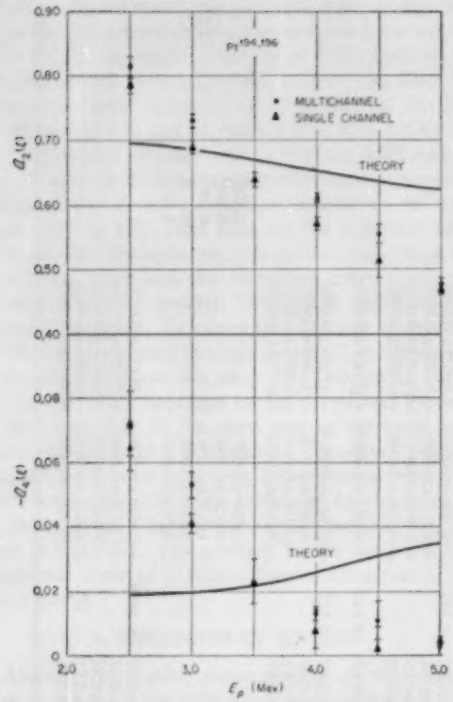

FIG. 1. Thick-target energy-dependent coefficients deduced from the angular distribution measurements of the 330-kev and 358-kev gamma rays from Pt^{196} and Pt^{198} as a function of the incident proton energy. The curves labelled "theory" are the thick-target energy-dependent coefficients deduced from the total cross section for excitation and the the thin-target coefficients given by Alder and Winther.

posite angular distribution function. Any significant excitation of the second excited states can be excluded in these isotopes for the following reasons. Recent measurements by Johns and Nablo[11] indicate that the second excited state is at 620 kev in Pt^{194}. The intensity ratio of the cascade gamma ray to the cross-over gamma ray is 3. From the differential pulse-height distribution of the gamma radiation resulting from 4.5-Mev protons incident on a thick platinum target we find that the excitation of the 620-kev state in Pt^{194} relative to the direct excitation of the 330-kev state is less than 3 percent. The contribution of 330-kev gamma rays resulting from excitation of the second excited state to the observed angular distribution function is less than 2 percent.

In Pt^{196}, the second excited state is at 688 kev and decays 99 percent of the time by a cascade gamma ray of 330 kev which is 95 percent $E2$ radiation and 5 percent $M1$ radiation.[8] Assuming the reduced transition probability for excitation of the 688-kev and 358-kev levels are equal, the yield of 330-kev gamma rays by the cascade transition in Pt^{196} relative to 330- and 358-kev gamma rays would be 5, 7, 10, and 13 percent at $E_p=3.5$, 4.0, 4.5, and 5.0 Mev, respectively. However, the reduced transition probability for the 358-kev transition in Pt^{196} is 20 times larger than independent particle theoretical estimate [see Eq. (VII. 9) given by Bohr and Mottelson].[12] Consequently, the assumption made above, i.e., that the reduced transition probability for excitation of the 682-kev state is equal to that for the 358-kev state, requires the reduced transition probability for the 330-kev cascade to be 4×10^3 times larger than the independent particle estimate and this seems rather unlikely.

[11] M. W. Johns and S. V. Nablo, Phys. Rev. **96**, 1599 (1954).

B. Au^{197}

The proton-gamma angular distributions of the 550-kev and 277-kev gamma rays in Au^{197} have been measured by several workers.[3,4] Spins of 7/2 and 5/2 for the 550-kev and 277-kev levels, respectively, were deduced from their measurements. For the 277-kev transition Goldburg and Williamson,[4] and Eisinger *et al.*[3] obtained $E2/M1=0.07$ and 0.59, respectively, by applying the energy-dependent coefficients a_ν given by Alder and Winther to their angular distribution measurements. Measurements of the proton-gamma angular distributions have been carried out for the 550-kev gamma ray in Au^{197} using thick and thin targets and for the 277-kev gamma ray in Au^{197} using a thick target. The thin target was prepared by spot-welding a thin Au foil on a Bi backing which was electrodeposited on nickel. The Bi backing served as a catcher for the protons emerging from the Au target. The results of the measurements are tabulated in Table I. The measurements for the 277-kev radiation have been treated as entirely the result of direct excitation of 277-kev level. The cascade radiation (273-, 277-kev γ rays) from the 550-kev level contributes about 4 percent to the intensity of 277-kev gamma radiation[10] at $E_p=4.0$ Mev.

C. Ta^{181}

The proton-gamma angular distribution of the 303-kev gamma ray in Ta^{181} has been measured by several workers[3,4] and a spin of 11/2 for the 303-kev level was deduced from their measurements. In addition to measurements of the proton-gamma angular distribution of the 303-kev gamma ray we have measured the proton-gamma angular distribution of the 166-kev cascade gamma ray from the 303-kev state. For the latter measurements, the window of the analyzer was set on the high energy edge of the 166-kev full pulse spectrum peak in order to exclude the detection of 137-kev gamma radiation. The results of the measurements are tabulated in Table I.

[12] A. Bohr and B. R. Mottelson, Kgl. Danske Videnskab. Selskab, Mat.-fys. Medd. **27**, No. 16 (1953).

D. $Ag^{107,109}$ and Rh^{103}

Proton-gamma angular distribution measurements have been carried out for the gamma rays in $Ag^{107,109}$ at $E_p=2.5$ Mev using thick targets of normal silver and for two gamma rays in Rh^{103} at $E_p=1.7$ to 2.9 Mev using thick targets. Since the completion of our distribution measurements, Heydenburg and Temmer[13] have reported that the two corresponding excited states in Ag^{107} and Ag^{109} differ by only a few kev. As a result the measurements for $Ag^{107,109}$ tabulated in Table I represent angular distribution coefficients of a composite angular distribution function. A comparison of the results with the observed angular distributions for the two gamma rays of Rh^{103} indicates that the angular distribution coefficients for $Ag^{107,109}$ are meaningful, i.e., the spins of the corresponding Coulomb excited states in Rh^{103}, Ag^{107}, and Ag^{109} and the character of the gamma radiation are the same.

E. Pd

Proton-gamma angular distributions have been carried out for the 445-kev gamma ray at $E_p=2.5$ Mev and for the 380-kev and 520-kev gamma rays at $E_p=2.1$ to 2.9 Mev using thick targets of palladium. A differential pulse-height spectrum of the gamma radiation from palladium produced by Coulomb excitation is shown in the accompanying paper.[10] The results of measurements are tabulated in Table I. The 520-kev gamma ray is attributed to Pd^{106} resulting from the decay of the well-known 513-kev level observed in the β-decay of Rh^{106}. From gamma-gamma directional angular correlation measurements the spins of the first and second excited states of Pd^{106} are known to be 2 and 0, respectively, and the angular correlation measurements are not disturbed by extranuclear fields.[14] The very short lifetime[10] of the intermediate state deduced from the reduced transition probability for excitation of the first excited state in Pd^{106} lends support to this latter statement. The second excited state in Pd^{106} is, of course, not excited by Coulomb excitation. As a result the angular distribution measurements of the 520-kev gamma ray serve to test the angular distribution theory for medium weight nuclei.

5. DISCUSSION OF RESULTS

In order to compare experimental angular distribution coefficients for a thick target with theory, we must evaluate the expected thick target coefficients. Now, Alder and Winther[1,15] have given both the total excitation cross section and the angular distribution of the gamma rays with respect to the incident protons for excitation by the electric quadrupole field. The differential cross section at a given energy E is

$$d\sigma(E)/d\Omega=\sigma(E)W(\theta), \tag{3}$$

where

$$\sigma(E)=\frac{4\pi^2 mB(E2)}{25Z_2^2e^2\hbar^2}E_f g_2(\xi)$$

and $W(\theta)$ is given by Eq. (1). For the differential cross section from a thick target for an incident proton energy E_i in the laboratory system, we have

$$\frac{d\sigma(E_i)}{d\Omega}\propto\int_0^{E_i}\frac{\sigma(E)W(\theta)dE}{dE/d\rho x}. \tag{4}$$

We therefore have that the expected coefficient of the Legendre polynomial P_r for a thick target is given by

$$\frac{a_r(E_i)}{a_0(E_i)}=A_r\int_0^{E_i}\frac{\sigma(E)a_r(E)dE}{dE/d\rho x}\Big/\int_0^{E_i}\frac{\sigma(E)dE}{dE/d\rho x}, \tag{5}$$

or the thick target energy-dependent coefficient is

$$[a_r(E_i)]_t=\frac{1}{A_r}\frac{a_r(E_i)}{a_0(E_i)}. \tag{6}$$

Now let us change from E to the variable ξ, where

$$\xi=\frac{Z_1Z_2e^2}{\hbar}\left(\frac{1}{v_f}-\frac{1}{v_i}\right). \tag{7}$$

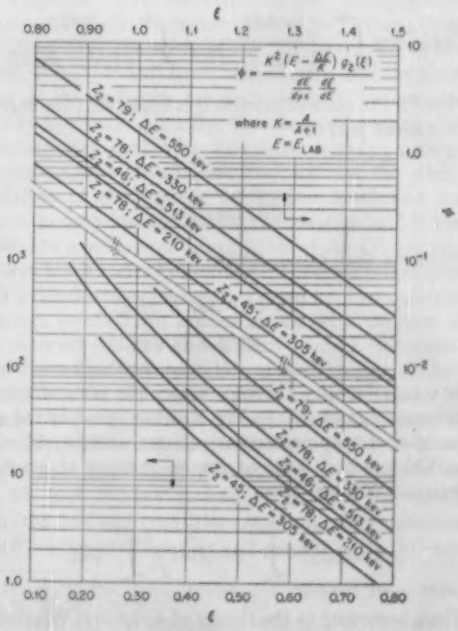

FIG. 2. The function ϕ for representative cases plotted as a function of ξ.

[13] N. P. Heydenburg and G. M. Temmer, Phys. Rev. **95**, 861 (1954).
[14] E. D. Klema and F. K. McGowan, Phys. Rev. **92**, 1469 (1953).
[15] K. Alder and A. Winther, Phys. Rev. **96**, 237 (1954).

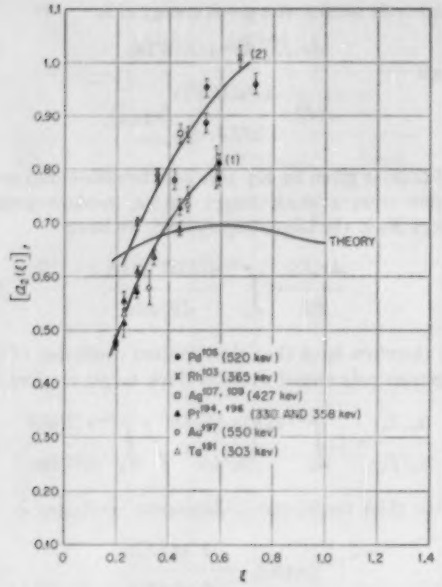

FIG. 3. Thick-target energy-dependent coefficient $a_2(\xi)$ deduced from angular distribution measurements plotted at a value of ξ corresponding to the incident proton energy on the thick target. The solid curve labelled "theory" represents the thick-target energy-dependent coefficient $[a_2(\xi_i)]_i$ as given by Eq. (9).

For any given case we have

$$[a_\nu(\xi_i)]_i=\int_\infty^{\xi_i}\frac{\sigma a_\nu d\xi}{dE/d\rho x\, d\xi/dE}\Big/\int_\infty^{\xi_i}\frac{\sigma d\xi}{dE/d\rho x\, d\xi/dE}. \quad (8)$$

Now for the cases of interest it is found that the energy-dependent part of

$$\frac{\sigma}{dE/d\rho x\, d\xi/dE}$$

which we shall call ϕ, where

$$\phi=\frac{K^2(E-\Delta E/K)g_2(\xi)}{dE/d\rho x\, d\xi/dE}$$

as a function of ξ has very nearly the same shape for different Z_2 and ΔE. In Fig. 2, ϕ has been plotted as a function of ξ for representative cases, namely; $\Delta E=200$ to 550 kev and incident proton energies of practical interest. We then have

$$[a_\nu(\xi_i)]_i=\int_\infty^{\xi_i}\phi a_\nu(\xi)d\xi\Big/\int_\infty^{\xi_i}\phi d\xi. \quad (9)$$

Thus, according to the theory of Alder and Winther, it follows that $[a_\nu(\xi_i)]_i$ vs ξ_i will be nearly an unique function. Or to put it differently, if many different cases are measured one would expect the resulting points $a_\nu(\xi_i)_{\text{exp}}$ to fall on a smooth curve as a function of ξ_i.

A comparison between theory and experiment is shown in Figs. 3 and 4 for the cases of Pt^{194,196} and Pd^{106} where the spin of the Coulomb excited state is known with reasonable certainty. The solid curves labelled "theory" represent the expected thick target energy-dependent coefficient $[a_\nu(\xi_i)]_i$ given by Eq. (9) using for a_ν the numerical calculations of Alder and Winther. For Pd^{106}, the deviations of the observed energy-dependent coefficients from theory for a thick target are even larger than they are for Pt^{194,196}. In addition the coefficient $a_2(\xi_i)_{\text{exp}}$ seems to have a Z_2 dependence over and above that contained in the parameter ξ.

The effect of multiple scattering of the protons by Rutherford scattering as they traverse a thick target on the angular distribution coefficient $[a_\nu(\xi_i)]_i$ should be discussed. Let us consider a proton-gamma angular distribution experiment, where $W(\theta_1)$ is the correlation function and $F(\theta')$ is the multiple scattering function due to Rutherford scattering. The probability that any proton from the collimated incident beam is multiple scattered through an angle θ' in the target prior to a nuclear excitation and that the resulting gamma ray is correlated to the multiple scattered proton by $W(\theta_1)$ is

$$P=\int d\Omega_1 W(\theta_1)F(\theta'). \quad (10)$$

Goudsmit and Saunderson[10] have already expressed the multiple Rutherford scattering function as a series in Legendre polynomials for the case of electrons. Their treatment is exact if one considers electrons with the same total path length in the scatterer. Thus, the coef-

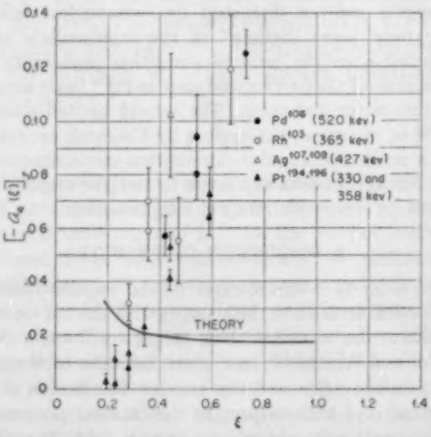

FIG. 4. Thick-target energy-dependent coefficient $a_4(\xi)$ deduced from angular distribution measurements plotted at a value of ξ corresponding to the incident proton energy on the thick target. The solid curve labelled "theory" represents the thick-target energy-dependent coefficient $[a_4(\xi_i)]_i$ as given by Eq. (9).

[10] S. Goudsmit and J. L. Saunderson, Phys. Rev. **57**, 24 (1940).

ficients G_k (coefficients of the Legendre polynomials representing the multiple Rutherford scattering function) given by Goudsmit and Saunderson should be applicable to the case of protons. A solution of this problem on the effect of multiple scattering on the proton-gamma angular distribution is similar to the effect of scattering of electrons in a conversion electron-gamma angular distribution.[17] The form of the correlation function is unchanged and each coefficient $a_\nu A_\nu$ becomes multiplied by an attenuation factor G_ν. We have evaluated the effect of multiple scattering on the thick target angular distribution coefficients by replacing $a_\nu(\xi)$ in Eq. (9) by $a_\nu(\xi)G_\nu$ and considering the case $a_\nu(\xi)$ is constant. The results are tabulated in Table II. The effect of multiple Rutherford scattering on the observed thick target energy-dependent coefficients is in the right direction but is not nearly large enough to account for the difference between curves (1) and (2) of Fig. 3. In any case the attenuation coefficients for multiple scattering are significant and should be included in the analysis of thick target angular distribution measurements. The coefficients in Table I have not been corrected for multiple Rutherford Scattering because we have no satisfactory thin target a_ν from which we could evaluate these attenuation coefficients for a thick target.

Since the deviations between theory and experiment appears to be rather large, we have chosen to analyze the remainder of the data in Table I using empirically determined energy dependent coefficients from a plot of $a_\nu(\xi_i)_{exp}$ vs ξ_i. For neighboring nuclei this method of presenting the data appears to be useful. Of the possible spin sequences that need to be considered for the 550-kev and 303-kev gamma rays in Au^{197} and Ta^{181}, respectively, on the assumption that the radiation is E2, only the spin sequences suggested originally by Eisinger *et al.*[3] and by Goldburg and Williamson[4] yield energy dependent coefficients $a_2(\xi_i)_{exp}$ that agree with the empirical $[a_2(\xi_i)]_i$ given in Fig. 3. These additional coefficients determined from the Au^{197} and Ta^{181} data are tabulated in Table I and are plotted in Fig. 3.

In general, for odd mass nuclei, the radiation from the first Coulomb excited state and the cascade radiation from the second Coulomb excited state will be $E2+M1$ radiation. In addition to inferring the spin of the excited states, information on the ratio of the quadrupole to dipole intensity is obtained from angular distribution measurements. We have applied the empirical $[a_2(\xi_i)]_i$ to our data for Au^{197} and Ta^{181} and for the indicated spin sequence in Table I. From the tabulated $(A_2)_{exp}$ for the 277-kev transition in Au^{197} one finds $\delta_\gamma = -(0.75 \pm 0.20)$ where δ_γ^2 is the ratio of the squares of the reduced matrix elements[2] and is defined as the intensity ratio (in this case) of quadrupole to dipole radiation in the gamma-ray transition. The large uncertainty in δ_γ results from the fact that

[17] S. Frankel, Phys. Rev. **83**, 673 (1951).

TABLE II. Attenuation coefficients for multiple Rutherford scattering for proton-gamma angular distributions from thick targets for the case $a_\nu(\xi)$ is constant.

Pt^{194}	$\Delta E = 330$ kev		Rh^{103}	$\Delta E = 365$ kev	
E_p(Mev)	$\bar{G}_2$	$\bar{G}_4$	E_p(Mev)	$\bar{G}_2$	$\bar{G}_4$
5.0	0.955	0.841	2.9	0.980	0.940
4.0	0.961	0.872	2.5	0.982	0.946
3.0	0.971	0.916	2.1	0.985	0.956
2.0	0.988	0.961	1.7	0.989	0.969

A_2 has a broad maximum at $\delta = -0.75$. This value of δ_γ^2 is in good agreement with that deduced from K-shell internal conversion coefficient measurements.[18] The data for the 166-kev transition in Ta^{181} lead to $\delta_\gamma = 0.51$ or 3.0. The former value agrees with the δ_γ^2 deduced from a K/L ratio measurements.[19] This sign and magnitude of δ_{166} is identical to δ_{137} of the 137-kev transition in Ta^{181}.[20]

Huus and Lunden[21] have suggested spin assignments for the Coulomb excited states in $Ag^{107,109}$ from the position of the levels using the nuclear model of Bohr and Mottelson.[12] Heydenburg and Temmer[13] have reached similar conclusions for $Ag^{107,109}$ and Rh^{103}. The signs of the angular distribution coefficients $(a_2A_2)_{exp}$ in Table I fix the level order as 1/2, 3/2, and 5/2 independent of a nuclear model. The angular distribution data for the 427-kev and 365-kev transitions in $Ag^{107,109}$ and Rh^{103}, respectively, yield additional determinations of $a_\nu(\xi_i)$ for a thick target and are plotted in Figs. 3 and 4. These additional data are in good agreement with the empirical curve deduced from the proton-gamma angular distribution measurements of Pd^{106}. Using these empirical data the spins of the 325-kev and 305-kev states in $Ag^{107,109}$ and Rh^{103}, respectively, and the character of the radiation are deduced from the angular distribution data. Actually, the observed angular distributions are composite functions, namely: proton-gamma angular distribution function for the direct excitation of the 325-kev or 305-kev levels and the proton-gamma angular distribution function for 325-kev or 305-kev gamma rays by excitation of the 427-kev and 365-kev levels and not observing the cascade transitions. This latter distribution function is not known explicitly, although we do know approximately what fraction of the observed 325-kev and 305-kev gamma rays result from direct Coulomb excitation of the 325- and 305-kev levels.[10] For the 325-kev transition in $Ag^{107,109}$ about 96 percent of the gamma rays observed are the result of direct Coulomb excitation of the 325-kev level. If we assume that the reduced $E2$ transition probabilities for the 65- and 365-kev transitions in Rh^{103} are equal, then the cascade transition must be predominantly $M1(E2/M1 = 0.002)$ or 86 to 92 percent of the 305-kev

[18] Huber, Halter, Joly, Maeder, and Brunner, Helv. Phys. Acta **26**, 591(A) (1953).
[19] T. Huus and J. H. Bjerregaard, Phys. Rev. **92**, 1579 (1953).
[20] F. K. McGowan, Phys. Rev. **93**, 471 (1954).
[21] T. Huus and A. Lunden, Phil. Mag. **45**, 966 (1954).

gamma rays result from direct Coulomb excitation of the 305-kev level. In the absence of any additional information, we have treated the data as resulting from the direct Coulomb excitation of the 305-kev level. The constancy of $(A_2)_{exp}$ for different E_γ for the 305-kev transition in Rh^{103} probably indicates that the distribution functions entering into the composite function are nearly alike.

In the treatment of the angular distribution data for the 380-kev and 445-kev gamma rays in Pd we assume that the transitions are in $_{46}Pd^{110}$ and $_{46}Pd^{108}$, respectively, as was done in the analysis of the yield data.[10] The trend of $B(E2)/e^2$ with neutron number indicated that the transitions are predominantly in these isotopes. The angular distributions indicate that transitions are predominantly of the type $2(E2)0$. The empirical coefficients $(a_2)_{exp}$ for these transitions are slightly smaller (the coefficients $(a_2)_{exp}$ for the 445-kev transition are more so than for the 380-kev transition) than those in Fig. 3 for Pd^{106}, $Ag^{107,109}$, and Rh^{103}. This is not surprising since we have not attributed any of the gamma rays to Coulomb excitation of Pd^{104} (22.23 percent).

6. CONCLUSIONS

The coefficients $a_\nu(\xi)$ are found to deviate considerably from those given by the semiclassical theory of the process. The fact that the points for heavy (or for medium weight) nuclei fall on a smooth curve indicates that the parameter ξ correctly takes into account the excitation energy and the exciting proton energy. However, from the fact that two distinct curves are obtained we conclude that the dependence on Z_2 is not correctly accounted for. Recently, Biedenharn and Class[22] have obtained an exact result for the particular case of no energy loss ($\xi=0$). The behavior of a_2 for this special case as a function of the parameter $\eta=Z_1Z_2e^2/\hbar v$ shows appreciable deviations from the classical limit. It is clear that more accurate calculations of the angular distribution coefficients a_ν are needed. Inferring spins of Coulomb excited states using a nuclear model is not very satisfying. One would prefer to arrive at the spins more directly from angular distribution measurements.

For pure multipole radiation from heavy nuclei, one might deduce the correct spin assignment from the existing calculations by Alder and Winther. However, for the medium weight nuclei the deviations between experiment and theory are larger and the deduction of the correct spin assignment would be less certain. In odd-mass nuclei, the radiation from the first Coulomb excited state and the cascade radiation from the second Coulomb excited state will in general be $E2+M1$ radiation. In addition to inferring the spin of the excited states, information on the ratio $E2/M1$ can be determined from the angular distribution measurements. A determination of this ratio demands an accurate knowledge of the coefficients a_ν.

From the results discussed in this paper, it appears possible to use empirically determined energy-dependent coefficients a_ν for a thick target to interpret angular distribution measurements involving pure or mixed multipole transitions in neighboring odd-mass nuclei.

ACKNOWLEDGMENTS

It is a pleasure to express our appreciation to Dr. M. E. Rose and Dr. L. C. Biedenharn for several stimulating discussions concerning the results. We should like to express appreciation to Buford Carter, who carried out the I.B.M. calculations and to Dr. M. H. Lietzke of the Chemistry Division for advice on the electrodeposition of bismuth.

[22] L. C. Biedenharn and C. M. Class, Phys. Rev. **98**, 691 (1955).

Observation of a 193-Millimicrosecond Metastable Level in Pu^{239}†

D. Engelkemeir and L. B. Magnusson
Chemistry Division, Argonne National Laboratory, Lemont, Illinois

(Received February 11, 1955)

A metastable level in Pu^{239} with a half-life of 193 mμsec has been observed in the beta decay of Np^{239}. This metastable state is assigned to a level 382 kev above the ground state of Pu^{239}, and appears to de-excite by parallel 61- and 105-kev *E*1 gamma transitions.

A METASTABLE level in Pu^{239} with a half-life of 193 mμsec has been observed in the beta decay of Np^{239}. Delayed coincidences were measured with a coincidence circuit similar to that described by McGowan.[1] Anthracene and sodium iodide scintillation counters served as beta and gamma detectors, respectively. Pulse-height analyzers accepted integral betas above 30 kev and integral gammas above 40 kev. Delays were introduced by means of calibrated lengths of Transradio C.22 coaxial cable or RG 65/U delay cable. A typical delay curve is shown in Fig. 1. Three measurements with RG 65/U cable gave half-lives of 192, 193, and 194 mμsec; and a single measurement with C.22 cable gave a half-life of 192 mμsec.

A search for gamma or x-radiation preceding the metastable level yielded negative results. It is estimated that the abundance of gamma transitions with energies greater than 23 kev populating the 193-mμsec level must be less than one percent of the beta disintegration rate.

The beta spectrum leading to the formation of the 193-mμsec level was measured with an anthracene scintillation spectrometer used in conjunction with the delayed coincidence circuit. A resolving time, 2τ, of 83 mμsec and a beta delay time of 111 mμsec were employed. Beta-conversion electron energy addition in the anthracene crystal was minimized by the use of a small solid angle (3.4 percent). A Kurie plot of the spectrum (Fig. 2) gives a maximum beta energy of 343 kev. This energy corresponds closely to the energies reported for the lowest-energy component in the total beta spectrum of Np^{239}. Tomlinson *et al.*[2] obtain 330 kev and Freedman *et al.*[3] 329 kev for the lowest energy component. The low-intensity tail on the curve of Fig. 2 is probably due to beta and conversion electron energy addition in the anthracene crystal. According to the decay schemes proposed by Fulbright,[4] and Asaro and Perlman[5] (Fig. 3), the 330-kev beta leads to a level in Pu^{239} which is 382 kev above the ground state. This level de-excites principally either by a 105-kev gamma transition to the 1.1-mμsec level in Pu^{239} reported by Graham and Bell[6] or by a 61-kev

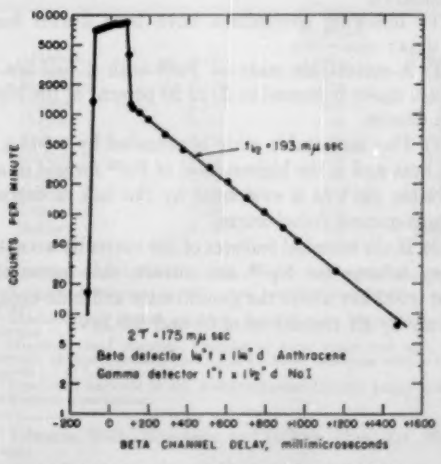

FIG. 1. Delay curve of β-γ coincidences in Np^{239}.

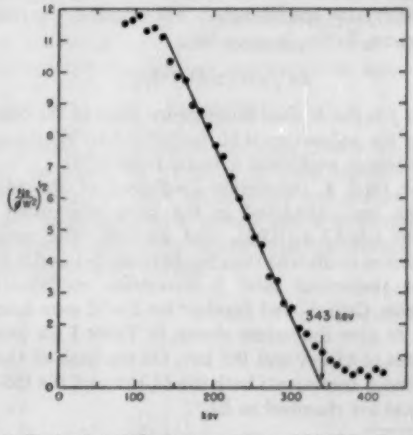

FIG. 2. Kurie plot of the beta spectrum of Np^{239} leading to the formation of the 193-mμsec level.

† Based on work performed under the auspices of the U. S. Atomic Energy Commission.

[1] F. K. McGowan, Phys. Rev. 93, 163 (1954).

[2] Tomlinson, Fulbright, and Howland, Phys. Rev. 83, 223(A) (1951).

[3] Freedman, Wagner, Engelkemeir, Huizenga, and Magnusson (private communication, 1953) reported by Hollander, Perlman, and Seaborg, Revs. Modern Phys. 25, 469 (1953).

[4] H. W. Fulbright (private communication to M. S. Freedman, February, 1952).

[5] F. Asaro and I. Perlman (private communication, November 1952) reported by Hollander, Perlman, and Seaborg, Revs. Modern Phys. 25, 469 (1953).

[6] R. L. Graham and R. E. Bell, Phys. Rev. 83, 222(A) (1951).

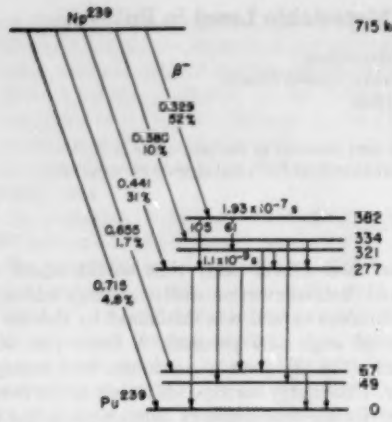

FIG. 3. Principal features of the disintegration scheme of Np^{239} (references 4 and 5) showing proposed position of the 193-mμsec level.

gamma transition. The total L conversion coefficient of the 105-kev gamma may be obtained by a comparison of the conversion electron and gamma intensities. The ratio, (a), of the number of L conversion electrons of the 105-kev gamma to the total number of K conversion electrons (from higher energy transitions) was taken from the relative intensity data of Fulbright.[4] The ratio, (b), of the number of 105-kev gammas to the total number of K x-rays was measured by Day[7] with a bent-crystal spectrometer. The total L conversion coefficient, $L\sigma/\gamma$, is given by

$$L\sigma/\gamma=(a/b)\times(1/f),$$

where f is the K shell fluorescence yield of Pu. Substituting the values: $a=0.11$, $b=0.50$, $f=0.97$, the total L conversion coefficient is found to be 0.23.

The total L conversion coefficient of the 61-kev gamma was calculated in the same way using the values: $0.066\geq a\geq 0.031$, and $b=0.08$. The total L conversion coefficient thus lies between 0.4 and 0.9.

The theoretical total L conversion coefficients of Gellman, Griffith, and Stanley[8] for $Z=92$ were interpolated to give the values shown in Table I for gamma energies of 61 kev and 105 kev. On the basis of their L conversion coefficients both the 61-kev and the 105-kev gammas are classified as $E1$.

[7] Paul Day (private communication, December, 1954).
[8] Gellman, Griffith, and Stanley, Phys. Rev. 85, 944 (1952).

From our scintillation spectrometer measurements, the absolute number of K x-rays plus 105-kev gammas was calculated to be 0.89 per disintegration. The disintegration rate of the sample was obtained from the growth of alpha activity of Pu^{239}. From the preceding data, the intensities of the unconverted 61- and 105-kev gammas are calculated to be 0.05 and 0.30, respectively, per disintegration. With the addition of the conversion electron intensities, the total number of 61 plus 105 kev transitions is found to be *ca* 0.5 per disintegration. This value is consistent with beta spectrometer measurements of the intensity of the beta branch populating the 382-kev level. The following intensities have been reported for the 330-kev beta branch: 0.52,[3] 0.47,[6] and 0.38[4] per disintegration.

A check on the assignment of the 193-mμsec metastable state to the 382-kev level was made by comparing the delayed and prompt coincidence rates in Fig. 1. If the beta and gamma detection efficiencies are assumed to be the same for delayed as for prompt events, the fraction of the total number of disintegrations which lead to the 193-mμsec metastable state is found to be 0.29. Correction for the estimated efficiencies lowers the result to *ca* 0.20 which is significantly lower than the values reported for the intensity of the 330-kev beta branch. The reason for this discrepancy is unknown.

TABLE I. Theoretical total L conversion coefficients for $Z=92$.

	61 kev	105 kev
$E1$	0.40	0.10
$E2$	140	11
$M1$	25	5.4

The following conclusions have been drawn from the data:

(1) A metastable state of Pu^{239} with a half-life of 193±4 mμsec is formed in 20 to 50 percent of the Np^{239} beta decays.

(2) This metastable state is preceded by a 343±15 kev beta and is the highest level of Pu^{239} formed in appreciable yield as is evidenced by the lack of delayed gamma-gamma coincidences.

(3) If the essential features of the currently accepted decay scheme for Np^{239} are correct, this metastable level is 382 kev above the ground state and is de-excited mainly by $E1$ transitions of 61 and 105 kev.

Photodeuteron/Photoproton Yield from Sulfur

LAURENCE S. RING, JR.
Institute for Atomic Research and Department of Physics, Iowa State College, Ames, Iowa
(Received March 16, 1955)

An investigation of the relative deuteron/proton yield from sulfur, produced by irradiation with the Iowa State College 65-Mev synchrotron, was made by employing a 12-inch, helium-filled, magnetic cloud chamber as the means of detection. The average curvature and the range of each acceptable track were measured and were used to find an experimental mass histogram that provided a clear indication of proton and deuteron groups. Analysis of the mass histogram produced a ratio of deuterons to protons of 0.19±0.04. It is estimated that the corresponding ratio for an infinitesimally thick target is 0.15±0.04.

INTRODUCTION

THE ratio of deuterons to protons ejected from nuclei excited by high-energy x-rays has been studied with several elements. Data reported so far in the literature[1–5] are summarized in Table I.

The present work to be described employed the cloud-chamber technique of Smith and Laslett[3] to determine the ratio of deuterons to protons from a thick sulfur target.

METHOD

A sulfur plate of thickness equivalent to the range of a 15-Mev proton was placed in a helium-filled, 12-inch, magnetic cloud chamber and was exposed to the collimated x-ray spectrum produced by 65-Mev electrons in the Iowa State College synchrotron. Approximately 6600 stereoscopic photographs were taken at 30-second intervals as the synchrotron was pulsed in coincidence with the cloud chamber.

The film was reprojected through the optical system of the stereoscopic camera, and 185 tracks were selected which (a) originated in the target, (b) had a minimum range of seven centimeters, (c) contained no point scattering, and (d) ended in the chamber at least one centimeter from the wall.

The stopping power of the chamber atmosphere relative to an air atmosphere was obtained by measuring the range of the 5.30-Mev alpha particles emitted from a polonium source placed in the cloud chamber. The range of each x-ray-induced track was measured and corrected to its air equivalent range by means of the measured stopping power of the cloud-chamber atmosphere. The curvature and azimuth of each track, in a pulsed magnetic field of 4000 gauss, were measured and the curvature was corrected[6] to that of a track in a plane normal to the magnetic field.

The magnetic field encompassing the cloud chamber was measured with a proton resonance device. The field was found to be uniform to less than 0.5 percent over the entire volume occupied by the chamber.

TABLE I. Reported photodeuteron/photoproton yields.

Element	Ratio	Maximum x-ray energy Mev	Reference
Beryllium	0.21[a]	310	1
Copper	0.14[a]	310	1
Copper	0.31[b]	24	2
Copper	0.76[c]	65	3
Cerium	0.05[b]	24	4
Cobalt	0.02[b]	24	5
Carbon	0.12[a]	310	1
Lead	0.24[a]	310	1
Sulfur	0.15[d]	65	present work

[a] Two-crystal telescope at 90°. Both particles have 40-Mev average energy.
[b] Obtained with nuclear emulsion. Particles were identified by grain counting.
[c] Magnetic cloud chamber. Particles in equal range and solid angle intervals. Measured protons were 1.1 to 1.8 Mev. Deuterons were in energy interval 1.2 to 2.3 Mev.
[d] Conditions identical to (c). Ratio computed for thin target based on thick target observations.

RESULTS

The range and magnetic curvature of each track were used[7] to determine its mass. A mass histogram was plotted (Fig. 1) which exhibits two well-defined peaks at the mass value of a proton and a deuteron. The experimental ratio of deuterons to protons from a thick sulfur target is 0.19±0.04.

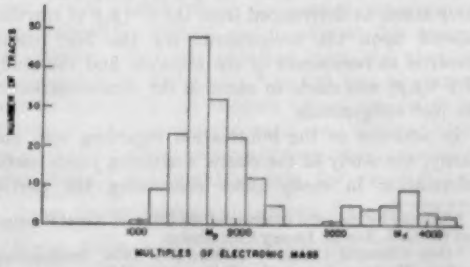

FIG. 1. Observed mass distribution of particles from sulfur. Ratio of No. of deuterons to No. of protons=0.19±0.04.

[1] Edwards, Wolfe, Silverman, and DeWire, Phys. Rev. **95**, 629 (1954).
[2] P. R. Byerly, Jr., and W. E. Stephens, Phys. Rev. **81**, 473 (1951).
[3] W. H. Smith and L. J. Laslett, Phys. Rev. **86**, 523 (1952).
[4] M. E. Toms and W. E. Stephens, Phys. Rev. **92**, 362 (1953).
[5] M. E. Toms and W. E. Stephens, Phys. Rev. **95**, 1209 (1954).
[6] R. Stokes, Phys. Rev. **84**, 991 (1951).
[7] N. Das Gupta and S. Ghosh, Revs. Modern Phys. **18**, 225 (1946).

To correct this ratio for target thickness, it was assumed that the target consisted of 63 thin lamina. An energy distribution for singly charged particles emitted from a compound sulfur nucleus[8] was attributed to each layer. Using range-energy relations[9] for sulfur, the energy distributions for protons and for deuterons that leave the thick target from each layer were determined. The contributions from all of the layers were combined to give composite energy distributions for the protons and the deuterons that emerge from the thick target.

The cloud chamber physically limited the solid angle available for particles of different ranges and therefore different energies. The range-energy relation for the cloud-chamber vapor was different for protons than for deuterons and gave a different energy range available to be measured for each type of particle. Corrections for these two effects were applied to the theoretical energy distributions of particles from the thick target. The ratio of the number of protons to the number of deuterons in the two respective energy intervals is the correction that was applied to the experimental ratio. The corrected ratio of deuterons to protons from a thin sulfur target when irradiated by 65-Mev bremsstrahlung is 0.15 ± 0.04.

The author wishes to express his gratitude to Dr. L. J. Laslett and Dr. D. J. Zaffarano for many helpful discussions and for advice during the course of this experiment.

[8] V. Weisskopf and D. Ewing, Phys. Rev. **57**, 472 (1940).
[9] J. Lindhard and M. Scharff, Phys. Rev. **85**, 1058 (1952).

PHYSICAL REVIEW VOLUME 99, NUMBER 1 JULY 1, 1955

Elastic Scattering of Protons by F^{19}†

T. S. Webb,* F. B. Hagedorn, W. A. Fowler, and C. C. Lauritsen
Kellogg Radiation Laboratory, California Institute of Technology, Pasadena, California

(Received March 21, 1955)

The differential cross section for the elastic scattering of protons by F^{19} has been measured for proton energies from 550 to 1800 kev at center-of-mass angles of 90, 125.3, and 159.8 degrees and for proton energies from 1300 to 1500 kev at 53.2, 60, 70, 80, 100, 110, and 136 degrees. Marked scattering anomalies were observed for proton energies near 669 (1^+), 843 (0^+), 873 (2^-), 935 (1^+), 1346 (2^-), 1372 (2^-), 1422 (1^+), and 1700 kev. The indicated spin and parity assignments for the corresponding levels in Ne^{20} are required by the results of this experiment or are consistent with them. Observations of the elastic scattering have also been made in the regions of 340 and 480 kev at 159.8 degrees, and no anomaly was observed in either case. The ambiguity in the choice of Γ_p/Γ has been resolved for several of the Ne^{20} levels. An approximate method of correcting the observed cross sections for the effects of finite energy resolution has been developed, and the relative stopping cross section for protons in lithium fluoride has been measured for proton energies from 400 to 1600 kev.

I. INTRODUCTION

THE study of the elastic scattering of protons by F^{19} was undertaken in connection with the recent investigations[1] at this laboratory of the low excited states in F^{19}. The spin and parity assignments for these states as determined from the $F^{19}(p,p'\gamma)$ reaction depend upon the assignments for the Ne^{20} states involved as resonances in the reaction, and the study of $F^{19}(p,p)$ was made to assist in the determination of the Ne^{20} assignments.

In addition to the information regarding spin and parity, the study of the elastic scattering yields useful information in many cases concerning the partial widths of the levels in the compound nucleus. Measurements of the reaction cross sections, $F^{19}(p,p')$ and $F^{19}(p,\alpha)$ and the total width, Γ, permit the determination of the sum and product of the proton width, Γ_p, and the reaction width, $\Gamma_\alpha+\Gamma_{p'}$. The solution of these relations yields two sets of values for Γ_p and $\Gamma_\alpha+\Gamma_{p'}$, and the size of the elastic scattering anomaly at the resonance may usually be used to resolve this ambiguity. A large anomaly generally indicates $\Gamma_p>\Gamma_\alpha+\Gamma_{p'}$ and a small anomaly, $\Gamma_p<\Gamma_\alpha+\Gamma_{p'}$.

The present article describes the experimental procedure and results, and the analysis and interpretation of these data will be discussed in the following paper.[2] Preliminary results of this experiment have been presented to the American Physical Society, and similar measurements and results have recently been reported by Dearnaley.[3]

In the course of this work, it was found desirable to

† Assisted by the joint program of the Office of Naval Research and the U. S. Atomic Energy Commission.
* Dow Chemical Company Fellow, 1953–1954; International Business Machines Corporation Fellow, 1954–1955.
[1] Peterson, Barnes, Fowler, and Lauritsen, Phys. Rev. **94**, 1075 (1954); Thirion, Barnes, and Lauritsen, Phys. Rev. **94**, 1076 (1954); Sherr, Li, and Christy, Phys. Rev. **94**, 1076 (1954) and **96**, 1258 (1954); R. F. Christy, Phys. Rev. **94**, 1077 (1954); Peterson, Fowler, and Lauritsen, Phys. Rev. **96**, 1250 (1954); and C. A. Barnes, Phys. Rev. **97**, 1226 (1955).
[2] E. Baranger, following paper [Phys. Rev. **99**, 145 (1955)].
[3] Webb, Hagedorn, Fowler, and Lauritsen, Phys. Rev. **96**, 851(A) (1954); G. Dearnaley, Phil. Mag. **45**, 1213 (1954).

investigate the effects of finite energy resolution on the observed cross sections. A discussion of this problem and a description of an approximate correction procedure are given in Appendix B.

II. EXPERIMENTAL PROCEDURE

The protons were accelerated by the 2-Mv electrostatic generator at this laboratory and were analyzed by an 80 degree electrostatic analyzer which maintained the beam homogeneous in energy to 0.05 percent. The proton beam was scattered from a thick LiF target placed at the object position of a 180-degree double-focussing magnetic spectrometer which is mounted to allow a continuously variable scattering angle from 0 to 160 degrees with respect to the incident beam direction. The scattered protons were detected by a zinc sulfide scintillation counter placed at the exit slit of the magnetic spectrometer. The energy scale of the electrostatic analyzer was calibrated by observing the gamma radiation associated with the 873 and 1372-kev resonances[4] in the $F^{19}(p,\alpha\gamma)$ reaction. The magnetic spectrometer energy calibration and the effective solid angle were then determined by observing the protons elastically scattered from copper, assuming pure Rutherford scattering. A detailed description of the calibration procedure is given in Appendix A.

LiF targets were prepared by pressing powdered LiF into a circular recess in a copper backing. The opposite face of the copper was polished so that the target could be rotated through 180 degrees to observe the scattering by copper for energy and solid angle calibration. Some evaporated LiF targets were used but it was found that for targets of sufficient thickness to mask the protons scattered from the copper backing, a few microcoulombs of bombardment would produce cracks in the LiF layer. The behavior of the pressed targets was, in general, satisfactory although new targets frequently gave high and erratic yields for the first one or two bombardments. This effect is probably due to difficulty in charge collection caused by the insulating nature of the target material before bombardment, although it could also be caused by the loss of fluorine from the target due to an initial fluorine excess or decomposition of LiF in the surface layers. As this effect was usually small (5–10 percent) and not reproducible, the equilibrium values, reached after one or two bombardments, were used. In addition to this rapid change, a slow, reproducible decrease in yield with bombardment was observed. This was probably due to decomposition of the LiF and subsequent escape of fluorine or to dilution of the surface layers by carbon and oxygen deposited during bombardment. Corrections were made for this effect by linear extrapolation to zero bombardment. This correction was usually kept to less than 5 percent by frequently changing to new target areas. Attempts were made to improve the target behavior by heating the LiF before pressing, but no noticeable improvement resulted from this treatment. The targets exhibited rapid discoloration on bombardment and would occasionally chip after long use.

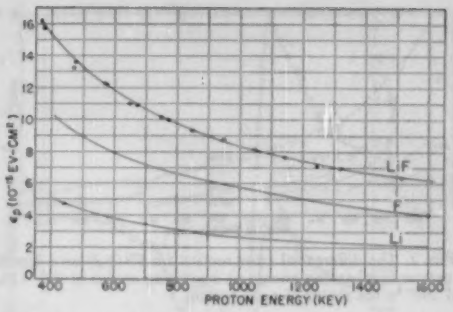

FIG. 1. The stopping cross section for protons (ϵ_p) in fluorine, lithium, and lithium fluoride in units of 10^{-15} ev-cm^2. The relative values for LiF were measured in this experiment and normalized to 8.4×10^{-15} ev-cm^2 at 1 Mev. The values for lithium are from Bader *et al.*[8] and Warters.[7] The values for fluorine are the difference between these.

Thin target yields were obtained from the thick LiF targets by observing a given interval of the momentum spectrum of the scattered protons using the magnetic spectrometer. This technique has been previously discussed by Brown *et al.*[5] and Snyder *et al.*[6] who give the appropriate expressions for obtaining the cross section and reaction energy.

The calculation of the elastic scattering cross section involves the stopping cross section for protons in the target material, and therefore a determination of this quantity was necessary. The relative stopping cross section was obtained by evaporating a thin layer of LiF on a copper backing and observing the protons elastically scattered from the copper after traversing the LiF layer.[7] The relative values were normalized to 8.42×10^{-15} ev-cm^2 at 1 Mev by assuming the stopping cross section of LiF to be the sum of the stopping cross sections for lithium and fluorine at this energy. The lithium value was obtained from the absolute measurement by Bader *et al.*[8] at 440 kev which was used to normalize the relative values measured by Warters *et al.*[7] The fluorine value was obtained from the measured proton stopping cross section for neon,[9,10] using 4-Mev alpha-particle data for neon[11,12] and

[4] Herb, Snowden, and Sala, Phys. Rev. **75**, 246 (1949). The value 1372 kev is the result of recent measurements at this laboratory by Barnes, Mills, and Hilton [C. A. Barnes, Phys. Rev. **97**, 1226 (1955)]. F. S. Mozer of this laboratory and H. B. Willard of Oak Ridge National Laboratory give 1373 kev (private communication). The previously accepted value was 1381 kev.

[5] Brown, Snyder, Fowler, and Lauritsen, Phys. Rev. **82**, 159 (1951).

[6] Snyder, Rubin, Fowler, and Lauritsen, Rev. Sci. Instr. **21**, 852 (1950).

[7] Warters, Fowler, and Lauritsen, Phys. Rev. **91**, 917 (1953).

[8] Bader, Wenzel, and Whaling (private communication).

[9] Chilton, Cooper, and Harris, Phys. Rev. **93**, 413 (1953).

[10] Reynolds, Dunbar, Wenzel, and Whaling, Phys. Rev. **92**, 742 (1953).

[11] R. W. Gurney, Proc. Roy. Soc. (London) **A107**, 340 (1925).

[12] G. Mano, Ann. Phys. **1**, 408 (1934).

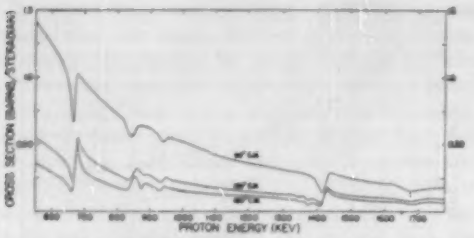

FIG. 2. The differential cross section for $F^{19}(p,p)$ as a function of proton bombarding energy at scattering angles of 90°, 125.3° and 160° in the center-of-mass system.

oxygen[11,13] to determine the value for fluorine relative to neon. This procedure was believed to be more reliable at high energies and for this reason the normalization was made at 1 Mev, the highest energy for which proton data for neon was available. Oxygen[10] and neon[9,10] proton data are both available at 600 kev, and normalization at this point gives values for LiF about 3 percent lower than those used. The final values for LiF are presented in Fig. 1, together with the values for lithium from Warters *et al.*[7] and Bader *et al.*,[8] and the values for fluorine are taken as the difference of these.[14]

The major uncertainty in the cross section values is due to the uncertainty in the value of the LiF stopping cross section which we estimate to be about 5 percent. The probable error in the solid angle (involving the ratio of the elastic scattering cross section of copper to the stopping cross section for protons in copper) is about 3 percent. The uncertainty due to target composition and behavior, estimated from the agreement of results from different targets, is also about 3 percent. This gives a probable error in the absolute values of 6 percent. In addition, the irregularity of the target surface implied by the energy resolution of the experiment (Appendix B) could introduce a systematic error in the cross section values. Rough estimates of the size of this effect indicate that it is negligible at scattering angles larger than 90 degrees but that it could increase the observed yield by 5 to 10 percent at 60 degrees.

The uncertainty in the relative cross sections is about 5 percent arising from the uncertainty in the relative stopping cross sections (4 percent) and the possible variation in the effective solid angle (3 percent). The statistical uncertainty of each point is 1–2 percent, and the current integrator reproducibility is about one percent.

III. EXPERIMENTAL RESULTS

The results of these investigations are presented as the differential cross section in Fig. 2 and as the ratio of the observed cross section to Rutherford cross section in Figs. 3 and 4. The Rutherford differential cross section can be written as

$$\frac{d\sigma_R}{d\Omega_C}=1.296\left(\frac{Z_1Z_0}{E_1}\right)^2\left(\frac{M_1+M_0}{M_0}\right)^2\csc^4\left(\frac{\theta_C}{2}\right)\times10^{-4}\frac{\text{barn}}{\text{sterad}}, \quad (1)$$

$$\frac{d\sigma_R}{d\Omega_L}=1.296\left(\frac{Z_1Z_0}{E_1}\right)^2\left[\csc^4\left(\frac{\theta_L}{2}\right)-2\left(\frac{M_1}{M_0}\right)^2+O\left(\frac{M_1}{M_0}\right)^4\right]\times10^{-4}\frac{\text{barn}}{\text{sterad}}. \quad (2)$$

For $F^{19}+p$:

$$\frac{d\sigma_R}{d\Omega_C}=0.1164\left(\frac{1}{E_1}\right)^2\csc^4\left(\frac{\theta_C}{2}\right)\frac{\text{barn}}{\text{sterad}}. \quad (3)$$

In these expressions, E_1, Z_1, and M_1 are the laboratory energy, charge, and mass respectively of the incident particle; Z_0 and M_0 apply to the nucleus at rest, and the subscripts C and L designate measurements in the center-of-mass and laboratory systems, respectively.

The cross section was measured at center-of-mass angles of 90, 125.3, and 159.8 degrees for proton energies from 550 to 1800 kev and at angles of 53.2, 60, 70, 80, 100, 110, 136 degrees for energies from 1300 to 1500 kev. The Legendre polynomials $P_1(\cos\theta)$ and $P_2(\cos\theta)$ vanish at 90 degrees and 125.3 degrees respectively. Pronounced anomalies were observed which we identify with known levels[15] of Ne^{20} at proton energies of 669,

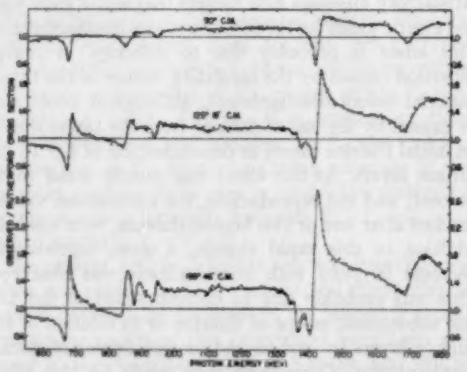

FIG. 3. Ratio of observed cross section to Rutherford cross section for the elastic scattering of protons by F^{19} at scattering angles of 90, 125.3, and 159.8 degrees in the center-of-mass system. In addition to the marked anomalies small structures are observed near 900, 1092, and 1137 kev.

[13] G. E. Gibson and H. Eyring, Phys. Rev. **30**, 553 (1927).

[14] We are indebted to W. Whaling for making available to us the collection of stopping cross sections compiled by Fuchs and Whaling, and for many valuable suggestions regarding the determination of the stopping cross section of LiF.

[15] F. Ajzenberg and T. Lauritsen, Revs. Modern Phys. **24**, 321 (1952) and Revs. Modern Phys. **27**, 77 (1955).

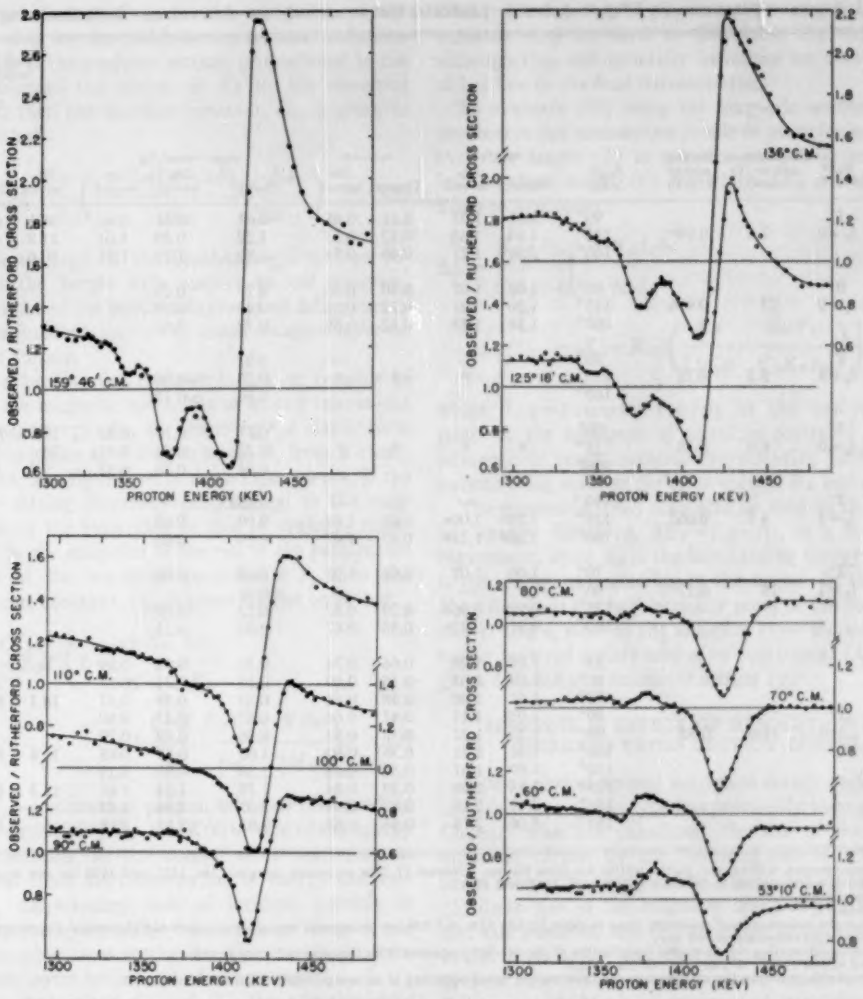

FIG. 4 Ratio of the observed cross section to Rutherford cross section in the energy range 1300 to 1500 kev at ten angles. The anomalies occur near 1346, 1372, and 1422 kev. $F^{19}(p,\alpha\gamma)$ resonance occur at 1346 and 1372 kev and an $F^{19}(p,p'\gamma)$ resonance occurs at 1422 kev. Note the absence of an anomaly near 1346 kev at forward angles and the angular variation of the 1372-kev resonance which disappears at 90 degrees.

843, 873, 935, 1346, 1372, and 1422 kev[16]; in addition a broad structure was observed in the region near 1700 kev which could be associated with one or more reported levels in this region.[15,17] There also appear to be small unresolved structures in the cross-section curve corresponding to resonances at proton energies of 900, 1092, and 1137 kev. In addition to the data shown, some investigations have been made of the regions around 340 and 480 kev. Target deterioration and carbon contamination at these energies cause a much more rapid decrease in yield with bombardment than at higher energies which makes the interpretation of these data difficult. A scattering anomaly of 10 to 20 percent of the Rutherford scattering could have been detected, however, whereas no reproducible structure was observed near either energy. The 340-kev resonance is known to correspond to a Ne^{20} state of $J=1$ and even parity,[15] and the observed reaction cross sections[15] give values of Γ_p/Γ of 0.016 or 1.0. Considering the effects of energy resolution, the larger value would be expected to give rise to an anomaly of 30 to 50 percent

[16] The resonance energies 1346 and 1422 are determined relative to the 1372-kev resonance (see reference 4). The 843-kev anomaly was incorrectly reported by Webb *et al.* and Dearnaley (reference 3) as 831 kev. The assignment 843 kev has been verified by Dearnaley (private communication).

[17] C. A. Barnes, Phys. Rev. 97, 1226 (1955).

TABLE I. Resonance parameters for $F^{19}(p,p)$. A dash (—) indicates that no anomaly was observed. σ_R = Rutherford cross section.

Resonance energy[a]	Ne^{20} J, ν, l_p	Resonance width[a] (Γ) (kev)	Partial width[a] (Γ_p/Γ)	Angle (c.m.)	σ_{max}/σ_R Theory[c]	σ_{max}/σ_R Observed	σ_{min}/σ_R Theory[c]	σ_{min}/σ_R Observed	$(\sigma_{max}-\sigma_{min})/\sigma_R$ Theory[c]	$(\sigma_{max}-\sigma_{min})/\sigma_R$ Observed	$(\sigma_{max}-\sigma_{min})/\sigma_R$ Corrected[b]	Full window width[b] ($\alpha\Gamma$) (kev) Calculated Observed	Calculated Cohen	Calculated Upper limit for surface irregularity
669	1^+			90°	1.04	1.02	0.41	0.65	0.63	0.37	0.61	14.1	4.8	16
	$l_p=0$	7.5	0.98	125°	1.64	1.35	0.42	0.55	1.22	0.80	1.01	11.8	4.1	12
				160°	2.31	1.77	0.49	0.53	1.82	1.21	1.51	10.6	3.6	10
	0^+			90°	1.03	1.07	0.80	0.86	0.23	0.21				
843	$l_p=0$	23	0.996	125°	1.20	1.27	0.72	0.88	0.48	0.39				
				160°	1.54	1.55	0.82	0.89	0.72	0.66				
	2^-			90°		—		—	0.02					
873	$l_p=1$	5.2	0.21	125°		[d]	[d]	[d]	0.26	~0.08[e]				
				160°					0.50	~0.37[e]				
	1^+			90°					0.17	0.10	0.20	17.9	6.5	18
935	$l_p=0$	8.0	0.18	125°	[d]	[d]	[d]	[d]	0.27	0.22	0.31	15	6.0	16
				160°					0.34	0.28	0.33	9.4	5.2	12
	2^-			≤110°[f]		—		—	≤0.034	—				
1346	$l_p=1$	4.5	0.067	125°	1.10[g]	1.09[g]	1.01	1.07	0.09	0.02				
				160°	1.06[g]	1.12[g]	0.87	1.07	0.19	0.05				
	2^-			70°	1.06	1.07	0.98	1.01	0.08	0.06				
1372	$l_p=1$	15	0.17	90°		—		—	≤0.02	—				
				125°	0.92[g]	0.96[g]	0.79	0.87	0.13	0.09				
				160°	0.91[g]	0.92[g]	0.55	0.67	0.36	0.25				
				53°	1.01	1.08	0.64	0.74	0.37	0.34	0.39			
				60°	1.00	1.03	0.56	0.69	0.44	0.34	0.37			
				70°	1.01	1.00	0.48	0.61	0.53	0.39	0.52	16.1	8.5	30
	1^+			80°	1.08	1.11	0.41	0.66	0.67	0.45	0.60			
1422	$l_p=0$	14.6	0.85	90°	1.23	1.27	0.37	0.58	0.86	0.69	0.79			
				100°	1.42	1.41	0.36	0.60	1.06	0.81	0.88	11.4	8.4	28
				110°	1.69	1.61	0.36	0.68	1.33	0.93	1.15			
				125°	2.15	1.98	0.39	0.64	1.76	1.34	1.47	12.3	8.0	24
				136°	2.49	2.17	0.42	0.63	2.07	1.54	1.64			
				160°	3.06	2.74	0.44	0.63	2.62	2.11	2.18	6	7.4	18

[a] Resonance energies, widths, and partial widths are from Barnes, reference 17. The resonance energies 1346, 1372, and 1422 are new determinations (see reference 4) corresponding to the older values 1355, 1381, and 1431.
[b] See appendix B.
[c] See reference 2.
[d] Values for the maximum and minimum cross sections for the 873- and 935-kev resonances are not given since the theoretical values are calculated neglecting the broad resonance at 843 kev.
[e] Obtained by subtracting the estimated contribution of the 843-kev resonance from the observed cross section.
[f] Measured at 110°, 100°, 90°, 80°, 70°, 60°, and 53.2°.
[g] The quoted values are for the maximum in the cross section curve occurring at an energy higher than the minimum.

of Rutherford scattering, and we thus conclude that Γ_p/Γ is small for this resonance.

An analysis of the scattering data has been made[2] for several of the observed resonances. This analysis, together with data from the study of the $F^{19}(p,\alpha)$ reactions,[15,18,19] allows the following spin and parity assignments to be made: 669 kev(1^+), 843 kev(0^+), 935 kev(1^+), 1372 kev(2^-), and 1422 kev(1^+). The scattering results are also consistent with the assignments[19,20]: 873 kev(2^-) and 1346 kev(2^-). Table I gives the values of $(\sigma/\sigma_R)_{max}$ and $(\sigma/\sigma_R)_{min}$ as observed in this experiment for the resonances listed above, together with the theoretical values of these quantities calculated for the assignments and proton widths given. Observed values of $(\sigma_{max}-\sigma_{min})/\sigma_R$ after correction for energy resolution effects (Appendix B) are also given in several cases. The values of Γ_p/Γ were determined from the $F^{19}(p,p')$, $F^{19}(p,\alpha)$ and $F^{19}(p,p)$ cross sections by Baranger[2] and Barnes.[17]

We wish to thank C. A. Barnes for many valuable comments and suggestions during the course of this work and the preparation of this paper and to thank E. Baranger and R. F. Christy for many illuminating discussions of the theoretical aspects of this problem.

APPENDIX A. CALIBRATION PROCEDURE

The energy scale of the electrostatic analyzer may be conveniently calibrated by observing the thick target gamma-ray yield over a proton energy range containing a sharp, symmetric resonance of known energy. In a

[18] Chao, Tollestrup, Fowler, and Lauritsen, Phys. Rev. 79, 108 (1950).
[19] Peterson, Fowler, and Lauritsen, Phys. Rev. 96, 1250 (1954).
[20] J. Seed and A. P. French, Phys. Rev. 88, 1007 (1952).

thick target excitation curve the mid-point of the observed step in the yield occurs at the resonance energy, E_R. If the analyzer setting, proportional to the potential across the plates, is S_R at the observed mid-point, then the analyzer constant, C_e, is given to first order by[6]

$$C_e=\frac{E_R}{Z_1S_R}\left(1+\frac{Z_1eV_T+\Delta E_1}{E_R}-\frac{E_R}{2M_1c^2}\right), \quad \text{(A1)}$$

where Z_1e=charge of the bombarding ion, V_T=potential of the target with respect to the analyzer, M_1=rest mass of the bombarding ion, and ΔE_1=energy loss of the incident ion in any contamination layer on the target surface.

After calibrating the analyzer it is then possible to calibrate the magnetic spectrometer at any convenient bombarding energy, E_B, by observing the elastic scattering of particles at a known angle, θ, from a clean, pure target, usually copper in these experiments. If the fluxmeter setting (inversely proportional to the magnetic field in the type used in this laboratory) corresponding to the midpoint in the rise of the momentum spectrum of the scattered particles is I, then the spectrometer constant, C_m, is given to first order by[6]

$$C_m=\frac{M_1K}{M_pZ_1^2}E_BI^2\left(1-\frac{\epsilon_2+K\epsilon_1}{K\epsilon_1}\frac{\Delta E_1}{E_B}+\frac{1-K}{K}\frac{Z_1eV_T}{E_B}+\frac{KE_B}{2M_1c^2}\right), \quad \text{(A2)}$$

where M_p=rest mass of proton, taken as the standard particle in specifying C_m, $K=K(\theta)$=ratio of the energy before scattering to the energy after scattering as determined from the conservation of energy and momentum, ΔE_1=energy loss of incident particle in contamination layers ($\Delta E_1=0$ for a "clean" target), and ϵ_1, ϵ_2=stopping cross section for the particles in contamination layers before and after scattering.

Having determined C_e and C_m, the effective solid angle is then found by observing the copper yield and assuming Rutherford cross section for copper. The appropriate formulas are given in Brown *et al.*[5]

The primary uncertainty in the energy calibrations is due to the presence of contamination layers (ΔE_1). The most effective method of avoiding this difficulty is, of course, the use of clean targets which do not become contaminated rapidly. By repeating the observation of the midpoint of the γ-ray step or momentum spectrum several times on the same target it is often possible to determine the rate of contamination and to extrapolate to zero bombardment, or to affirm that contamination is negligible. In cases where the target material is lighter than the contaminants (usually carbon) it is possible to observe the scattering peak of the contamination layer and to determine the thickness from this. Where the layer is appreciable, the magnetic spectrometer may be used to determine the thickness, although this will generally introduce an uncertainty of 1–2 kev in the final determination.

To evaluate ΔE_1 using the magnetic spectrometer, we observe the momentum profile of particles scattered from the target (T) in question and those scattered from a clean target (C) for which ΔE_1 is negligible. Then to first order:

$$\Delta E_1=\frac{K_T\epsilon_1E_B}{K_T\epsilon_1+\epsilon_2}\left[1-\frac{K_CI_C^2}{K_TI_T^2}-(K_C-K_T)\left(\frac{E_B}{2M_1c^2}-\frac{Z_1eV_T}{K_CK_TE_B}\right)\right], \quad \text{(A3)}$$

where $I_{C,T}$=fluxmeter reading at the half-intensity point in the spectrum of particles scattered by the reference or target material respectively; both observations being made at the same energy, E_B, and angle, θ.

The expression (A3) may also be used to determine the energy difference, $\Delta E_F=E_B-E_1$, in a scattering experiment. Here E_B is the bombarding energy and E_1 is the energy at scattering in the target. In this case, $K_C=K_T$, I_C is the half-intensity point of the spectrum, and ϵ_1 and ϵ_2 refer to the stopping cross section in the target material before and after scattering. (A3) then gives ΔE_F for any fluxmeter setting I_T.

APPENDIX B. EFFECT OF RESOLUTION ON OBSERVED CROSS SECTION CURVES

A discussion of several sources of energy variation in investigations of this type has previously been given by Cohen,[21] who has calculated the size of the energy variation caused by the following effects: (1) finite beam size, (2) energy variation in incoming beam, (3) finite size of the magnetic spectrometer entrance and exit windows, and (4) straggling in the energy loss in the target before and after scattering. The net result of these effects is a root-mean-square variation of about 2 kev (at 1 Mev) under typical conditions. This increases roughly linearly with energy.

Experimental estimates of the over-all energy resolution (as made by the techniques described below) indicate an energy variation which is, in many cases, somewhat larger than that calculated on the basis of (1)–(4) above, and we believe that additional factors, such as the target surface condition, are responsible for this.

No satisfactory calculations of the effect of target surface irregularity have been made, although an upper limit can be estimated by assuming that the surface is sufficiently irregular that the total energy loss in the target (as required by the experimental technique)[5] may take place either before or after scattering. Under

[21] E. R. Cohen, Ph.D. thesis, California Institute of Technology, 1949 (unpublished).

the usual target arrangement (the normal to the target surface bisecting the angle between the incident beam direction and the scattering direction), approximately half the energy loss should occur before scattering. Extreme surface roughness would lead, therefore, to a symmetric spread in the reaction energy with a half-width at half maximum of the order of the "following" depth in the target (usually less than one percent of the bombarding energy). At 1 Mev, this would give a root-mean-square variation in energy of 4–5 kev.

Microscopic examination of the LiF powder used in preparing targets for these investigations indicate that the grain size is about 10^{-4} cm which is of the order of five times the depth at which the observed scattering occurs. This suggests that the surface irregularities (assumed to be caused in part by individual crystals) are of this same order and therefore may affect substantially the energy resolution of the experiment.

Some experimental investigations of this effect have been made by observing the yield at the resonance minimum as a function of the energy loss before scattering ("following depth" in the target). By extrapolating these measurements which were made at 1422 kev at 90° to zero energy loss before scattering and using the relations derived below, these results can be used to calculate δE_F, the root-mean-square energy variation due to energy loss in the target. In a typical experiment, we find for a "following depth" of 15 kev, $\delta E_F = 3.3$ kev, while the calculated value[21] (which considers only straggling) is about 2.0 kev. The upper limit for the variation due to surface irregularities would be 8–9 kev in this case, so that a contribution of only about one-third of this would be needed to explain the observed value.

In those cases where the resonance width, Γ, is known independently from measurements of reaction cross sections, the elastic scattering data itself may be used to estimate the over-all resolution. We consider the theoretical expression for the cross section, σ, in the vicinity of a resonance:

$$\sigma = \sigma_0[1+f(x)], \tag{B1}$$

where

$$f(x) = (a+bx)/(1+x^2), \quad x = (E-E_R)/\tfrac{1}{2}\Gamma,$$

E_R is the resonance energy, and a, b, and σ_0 are approximately independent of energy and are to be determined from the experimental results where their values are needed. The observed cross section, σ', will then be

$$\sigma' = \sigma_0[1+F(x)], \tag{B2}$$

where $F(x)$ is obtained by folding $f(x)$ with the energy resolution function which is approximately independent of x over any one resonance.

In comparing the experimental results with the theoretical calculations for various spin assignments, a quantity of considerable interest is the maximum variation of the cross section over the resonance. We define

$$k = (\sigma'_{\max} - \sigma'_{\min})/(\sigma_{\max} - \sigma_{\min})$$

and wish to obtain k as a function of observable parameters of the experimental resonance curve.

For this purpose we assume a particular form of the energy distribution function, a square window of full width $\alpha\Gamma$. Using this, we then obtain a relation between $E_{\max} - E_{\min}$ and k in terms of the parameter A (or $1/A$ if $A>1$), where $A = (\sigma'_{\max} - \sigma_0)/(\sigma_0 - \sigma'_{\min})$. The additional parameter, A, is included since we treat both a and a/b as parameters to be determined from the experimental data. In principle, a, b, and σ_0 may be calculated from theoretical considerations if the assignment for the level and the potential scattering phase shift are known. These results are, however, sensitive to the choice of the latter quantity, whereas the value of k is relatively insensitive to A and hence to σ_0. We have found that a visual estimate of σ_0 (to about 5 or 10 percent) is usually satisfactory. In addition, this procedure allows the correction of the data without knowing the assignment for the level.

Carrying out the folding process, we obtain from (B1) and (B2):

$$F(x) = \frac{b}{2a}\left[c\tan^{-1}\frac{2\alpha}{1+x^2-\alpha^2} + \frac{1}{2}\log\frac{1+(x+\alpha)^2}{1+(x-\alpha)^2}\right], \tag{B3}$$

and

$$dF/dx = 0 \quad \text{at} \quad x = -c \pm [c^2+1+\alpha^2]^{\frac{1}{2}}, \tag{B4}$$

$$y = (E_{\max} - E_{\min})/\Gamma = (1+\alpha^2+c^2)^{\frac{1}{2}}, \tag{B5}$$

$$A = \frac{\tanh^{-1}(\alpha/y) - c\tan^{-1}[\alpha/(1+c^2+cy)]}{\tanh^{-1}(\alpha/y) + c\tan^{-1}[\alpha/(1+c^2-cy)]}, \tag{B6}$$

$$k = \alpha^{-1}(1+c^2)^{-\frac{1}{2}}[c\tan^{-1}(\alpha c/y) + \tanh^{-1}(\alpha/y)], \tag{B7}$$

where $E_{\max}$ and $E_{\min}$ are the proton energies for which the maximum and minimum cross sections are observed and $c = a/b$.

The effects of finite energy resolution are thus seen to be an increase in $E_{\max} - E_{\min}$ and a decrease in $\sigma'_{\max} - \sigma'_{\min}$. Our procedure involves the evaluation of the latter effect by observing the former. The parameter A is fairly insensitive to α and depends mainly on the shape of the theoretical curve (a/b). To obtain the explicit relation between k, A, and y, we first used the expression (B6) to obtain (graphically) a/b as a function of A, treating α as a parameter. We then used the relations (B5) and (B7) to obtain k as a function of y, treating A as a parameter.

An alternative procedure for obtaining k may be found by taking the product x_1x_2; from (B4) this gives

$$-x_1x_2 = \frac{(E_{\max} - E_R)(E_R - E_{\min})}{(\Gamma/2)^2} = 1+\alpha^2. \tag{B8}$$

Using (B5), (B7), and (B8) we may then obtain α, a/b, and k explicitly in terms of $E_{max}-E_R$ and $E_{min}-E_R$. The use of this method requires, however, that the resonance energy (on the energy scale of the experiment) be known with an uncertainty which is small compared to the resonance-width, Γ. In the present experiment, however, the uncertainty in the energy scale is about 3 kev, so that this condition is not well satisfied.

In cases where E_{max} or E_{min} is not clearly defined, it is possible to use A and the width at half maximum for determining k. This width is more difficult to determine than $E_{max}-E_{min}$ (both experimentally and analytically) and, except for nearly symmetric resonances, this procedure is less satisfactory.

In Table I of the text, we have given corrected values of the cross sections for comparison with the observed and theoretical values for several of the $F^{19}(p,p)$ resonances. Values for the window width, α, have been determined in many of these cases and it is found that these values are always between the values calculated using Cohen's formulation[21] and those estimated as an upper limit for target surface irregularities. The values are close to the lower limit at the higher energies (1400 kev) and large scattering angles and become larger relative to the lower limit as the energy and scattering angle are decreased. Several of these values are given in Table I.

The application of these expressions to obtain relations between experimentally determined quantities may, in part, eliminate the dependence of the results on the particular form we have taken for the resolution function. In any event, the treatment gives a useful description of the qualitative features and at least a first approximation to the quantitative aspects. In addition to the application of these results to the correction of cross sections, they should be of some value in determining resonance energies and widths from elastic scattering measurements.

PHYSICAL REVIEW VOLUME 99, NUMBER 1 JULY 1, 1955

Analysis of the Elastic Scattering of Protons from F^{19}†

ELIZABETH UREY BARANGER
Kellogg Radiation Laboratory, California Institute of Technology, Pasadena, California
(Received March 21, 1955)

An analysis of the anomalies in the elastic scattering cross section of protons on F^{19} has been carried out. The assignments 1^+ for the resonances at 669, 935, and 1422 kev, and 0^+ for the resonance at 843 kev, are required by the results of the experiment. The assignment of the resonances at 873, 1348, and 1374 kev is 2^-, with 1^- not excluded by these data alone. Unique values of the partial widths are determined for these resonances and several others in this energy range. Reduced widths are given for the various particle reactions which are observed.

IN the preceding paper, Webb, Hagedorn, Fowler, and Lauritsen[1] have discussed an experiment measuring the elastic scattering of protons by F^{19}. The present paper deals with an analysis of their experimental results. The purpose of the analysis is to determine the spins, parities, and partial widths of as many as possible of the excited states of the compound nucleus Ne^{20}. Assignments of the levels examined here, except the resonances at 843 and 1422 kev, have been determined previously by several workers using methods other than elastic scattering. They were, however, unable to determine the partial widths uniquely. Their results are summarized in a review article by Ajzenberg and Lauritsen.[2] Some preliminary work on elastic scattering was done at this laboratory by Peterson *et al.*,[3] which resulted in the assignment of the 1422-kev resonance. Recently, Dearnaley[4] has examined the elastic scattering and his results as to assignment and choice of partial widths are in agreement with ours.

In analyzing proton scattering from a nucleus such as F^{19} where reactions are also possible, certain complications arise in the formulas which have led us to use simplified and not entirely accurate forms for the scattering cross section. Thus, neglecting Coulomb effects, an arbitrary scattering amplitude associated with a given J and parity could be written as $f(e^{2i\delta}-1)$, where $f \leq 1$ and δ is arbitrary. Now in the case of a single resonance we find that $f=\Gamma_p/\Gamma$, the ratio of the elastic proton width to the total width, is independent of energy and $\cot\delta$ is linear in the energy. In the case of two overlapping resonances, however, no simple energy dependence of f and δ which is consistent with resonance theory has been found. What is needed is

† Assisted by the joint program of the Office of Naval Research and the U. S. Atomic Energy Commission.
[1] Webb, Hagedorn, Fowler, and Lauritsen, preceding paper [Phys. Rev. 99, 138 (1955)]. This paper is referred to as Paper A.
[2] F. Ajzenberg and T. Lauritsen, Revs. Modern Phys. 27, 77 (1955).
[3] Peterson, Barnes, Fowler, and Lauritsen, Phys. Rev. 94, 1075 (1954).
[4] G. Dearnaley, Phil. Mag. 45, 1213 (1954).

some expression which shows the influence of a broad resonance, where the parameters are almost energy independent on a superimposed narrow resonance. Lacking a better expression, we have used the form discussed by Blatt and Biedenharn,[5] i.e., $a_p(e^{2i(\delta_r+\varphi)}-1)+(1-a_p)(e^{2i\varphi}-1)$, where a_p is the ratio of the elastic proton width to the total width, δ_r is the resonant phase shift such that $\delta_r=-\cot^{-1}[(E-E_0)/\frac{1}{2}\Gamma]$, where E_0 is the resonance energy, and φ is a slowly varying phase shift chosen to describe the scattering amplitude off-resonance. This form is in error in that it assumes the reaction cross section to be zero off-resonance. Since the off-resonant cross section is not large, we feel that the use of the simplified form has introduced no error in interpretation.

The differential cross section for elastic scattering of s-wave protons and F^{19} (spin $\frac{1}{2}$) which form a compound state of a given J, which can be 0 or 1, can then be shown to be

$$\begin{aligned}\bar{\sigma}(\theta)=\sigma(\theta)/\sigma_R(\theta)=1-&\frac{(2J+1)}{2k\sigma_R{}^{\frac{1}{2}}}\{a_p\sin(\delta_{rJ}+\varphi_J)\\&\times\cos(\delta_{rJ}+\varphi_J+\theta_0)+(1-a_p)\sin\varphi_J\cos(\varphi_J+\theta_0)\}\\&+\frac{(2J+1)}{4k^2\sigma_R}\{a_p{}^2\sin^2(\delta_{rJ}+\varphi_J)+(1-a_p)^2\sin^2\varphi_J\\&+2a_p(1-a_p)\sin(\delta_{rJ}+\varphi_J)\sin\varphi_J\cos\delta_{rJ}\},\quad(1)\end{aligned}$$

where k is the wave number, σ_R the Rutherford cross section, and $\theta_0=(Ze^2/\hbar v)\ln\sin^2(\theta/2)$, v being the relative velocity. This expression differs from the final expression given in Blatt and Biedenharn in that we allow the phase shifts φ_J to be arbitrary parameters depending on J as well as l, the orbital angular momentum, and have not performed a sum over l.

Far from a resonance, when $\delta_r=n\pi$, this expression simplifies considerably and was used to analyze the off-resonant cross section. Since the angular dependence of the off-resonant cross section is consistent with assuming only s-wave phase shifts, we assume the higher l-wave phase shifts to be zero. The s-wave phase shifts vary over the energy region of the experiment, since the off-resonant cross section varies. It is impossible to determine from the data unique values of the individual phase shifts $\varphi_{J=0}$ and $\varphi_{J=1}$. One can only determine the expression $\varphi_{J=0}+3\varphi_{J=1}$. This is positive at low energies and negative at the higher energies. The agreement with experiment as a function of angle can be seen from Figs. 1, 2, and 3 at 570, 770, 1320, and 1520 kev. It was also checked at 1090 kev.

Since the off-resonant phase shifts can be assumed to be zero for the higher orbital angular momentum, the differential cross section for a particular J with $l>0$ is given by a Breit-Wigner formula:

$$\begin{aligned}\bar{\sigma}(\theta)=\sigma(\theta)/\sigma_R(\theta)=1-&\frac{2J+1}{k\sigma_R{}^{\frac{1}{2}}}a_p\sin\delta_{rJ}\cos(\theta_l+\delta_{rJ})\\&\times P_l(\cos\theta)+\frac{(2l+1)}{k^2\sigma_R}a_p{}^2\sin^2\delta_{rJ}\\&\times\sum_{m,M,T,R}\alpha_R{}^2\alpha_T{}^2|Y_l{}^m(\theta,\varphi)|^2\\&\times|C_{Rl}(JM;MO)C_{Tl}(JM;M-mm)|^2,\quad(2)\end{aligned}$$

where $Y_l{}^m(\theta,\varphi)$ is a spherical harmonic; $P_l(\cos\theta)$ is a Legendre polynomial; $C_{jj'}(JM;mm')$ are Clebsch-Gordan coefficients; R and T are channel spin quantum numbers; α_R is the channel spin ratio such that $\sum_R\alpha_R{}^2=1$; and

$$\theta_l=\theta_0+2\sum_{n=1}^{l}\tan^{-1}(Ze^2/\hbar vn).$$

We assume that only the lowest value of l for a given J need be included because of the rapid increase in the barrier penetration factor with l. We must add to (2) the two off-resonant s-wave contributions discussed above and also an interference term. The contribution of this interference term to $\bar{\sigma}$, which is valid either in

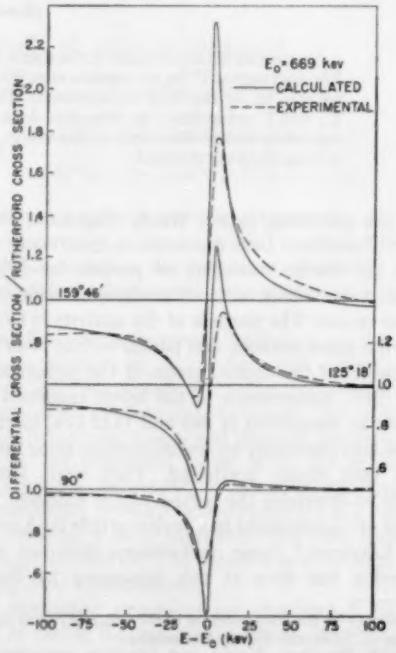

FIG. 1. The ratio of the differential cross section for the elastic scattering of protons by F^{19} to the Rutherford cross section for several center-of-mass angles as a function of the bombarding proton energy minus the resonance energy of 669 kev.

[5] J. M. Blatt and L. C. Biedenharn, Revs. Modern Phys. 24, 258 (1952).

the vicinity of an s-resonance or when no s-resonance is near, is

$$\frac{(2J+1)}{2k^2\sigma_R}P_l(\cos\theta)\alpha_{J'}{}^2 a_{pJ'}\{a_{pJ'}\sin(\delta_{rJ'}+\varphi_{J'})$$
$$\times\sin\delta_{rJ}\cos(\theta_l-\theta_0+\delta_{rJ}-\delta_{rJ'}-\varphi_{J'})$$
$$+(1-a_{pJ'})\sin\varphi_{J'}\sin\delta_{rJ}\cos(\theta_l-\theta_0+\delta_{rJ}-\varphi_{J'})\}, \quad (3)$$

where J' is the angular momentum of the s-wave resonance and J that of the other resonance. This interference term is proportional to $P_l(\cos\theta)$. There is obviously no interference between two s-waves.

We can determine the orbital angular momentum, l, by observing $\bar{\sigma}-1$ at angles θ for which $P_l(\cos\theta)=0$. When the orbital angular momentum is not zero, we have assumed φ_J to be zero, and therefore it is clear from Eq. (2) that $\bar{\sigma}-1$ should be symmetric around E_0 and positive. At this angle, the effect of the nonresonant s-wave phase shifts given in Eqs. (1) and (3) is merely to produce a constant background. Thus if $\bar{\sigma}-1$ is not symmetric and positive for any θ such that $P_l(\cos\theta)=0$, we assume that $l=0$. We thus assign $l=0$ to the resonances at 669, 843, 935, and 1422 kev. If $\bar{\sigma}-1$ is symmetric and positive at the angles where $P_l(\cos\theta)=0$ and not at other angles, we shall assume that l is given by this value. It might happen that $\bar{\sigma}-1$ could be accidentally symmetric and positive for certain values

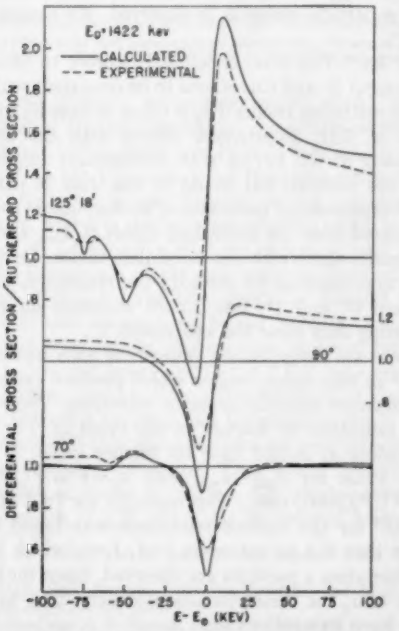

FIG. 2. The ratio of the differential cross section for the elastic scattering of protons by F^{19} to the Rutherford cross section for several center-of-mass angles as a function of the bombarding proton energy minus the resonance energy of 1422 kev.

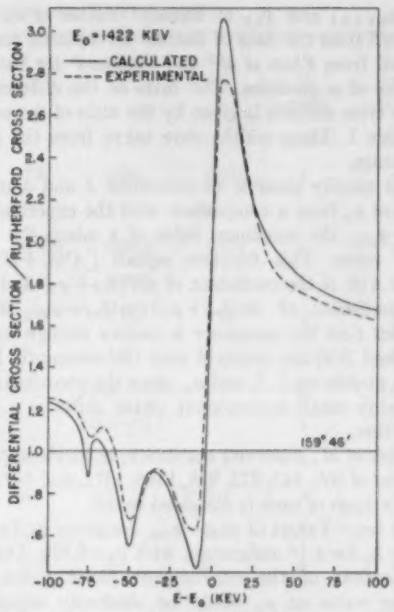

FIG. 3. The ratio of the differential cross section for the elastic scattering of protons by F^{19} to the Rutherford cross section for center-of-mass angle 159°46′ as a function of the bombarding proton energy minus 1422 kev.

of θ_l, so we must be sure that $l\neq 0$ for such a resonance. If the interference term in Eq. (2) is usually much larger than the purely resonant term, $\bar{\sigma}-1$ will essentially vanish at this angle. The resonance anomalies at 873, 1346, and 1372 kev vanish at 90°, and are not symmetric and positive at 125°, The anomalies at 1346 and 1372 kev are not symmetric and positive at 136° which is close to the angle where $P_3(\cos\theta)$ vanishes. (873 kev was not measured at this angle.) Thus at 1374 and 1348 kev, the data rules out $l=2$ and 3 and indicates $l=1$. At 873 kev, the data rule out $l=2$ and indicate $l=1$. Dearnaley[4] measured this energy region at 140.8° and his data rule out $l=3$. We examined $l=0$ for these three resonances and can also eliminate this possibility.

Next, a_p can be determined in terms of J from the reaction cross sections since

$$\sigma_r=(2J+1)\frac{\pi}{k^2}\frac{\Gamma_p\Gamma_r}{\Gamma^2}=(2J+1)\frac{\pi}{k^2}(1-a_p)a_p, \quad (4)$$

where σ_r is the sum of all reaction cross sections for protons on F^{19} and Γ_r the corresponding width. Relation (4) yields two possible values of a_p, whose sum is one. The particle reactions which occur are α-particle emission leading to states of O^{16} and inelastic proton emission leading to low states in F^{19}. We use the nota-

tion $\alpha_{0,\gamma,1,2,3}$ and $p_{1,2}$ of Barnes.[6] Values of σ_γ were obtained from the data of Barnes[6] for inelastic scattering and from Chao *et al.*[7] and Freeman[8] for the production of α particles. The ratio of the different reaction cross sections is given by the ratio of the widths in Table I. These widths were taken from the paper by Barnes.

It is usually possible to determine J and a unique value of a_p from a comparison with the experiment of $\bar{\sigma}_{\max}-\bar{\sigma}_{\min}$, the maximum value of $\bar{\sigma}$ minus the minimum value. This function equals $[A^2(\theta)+B^2(\theta)]^{\frac{1}{2}}$, where $A(\theta)$ is the coefficient of $\sin^2(\delta_{\gamma J}+\varphi_J)$ and $B(\theta)$ the coefficient of $\sin(\delta_{\gamma J}+\varphi_J)\cos(\delta_{\gamma J}+\varphi_J)$, if one assumes that the resonance is narrow enough so that $A(\theta)$ and $B(\theta)$ are constant over the resonance. It depends mainly on l, J, and a_p, since the contribution of the fairly small nonresonant phase shifts is a small correction.

Webb *et al.*, observed resonance at incident proton energies of 669, 843, 873, 935, 1346, 1372, and 1422 kev. The analysis of each is discussed below.

669 kev.—Values of $\bar{\sigma}_{\max}-\bar{\sigma}_{\min}$ are given in Table I, Paper A, for a 1^+ assignment with $a_p=0.976$. They are independent of the nonresonant phase shifts. The smaller value of a_p would be obviously impossible. $J=0$ can be eliminated since it gives values $\frac{1}{3}$ those for $J=1$. Plots of the complete resonance curves are shown in Fig. 1, where $\varphi_{J=0}$ was taken to be zero, and $\varphi_{J=1}$ to be 0.05 radian.

843 kev.—Table I of Paper A gives $\bar{\sigma}_{\max}-\bar{\sigma}_{\min}$ for a 0^+ assignment with $a_p=0.996$, where this is again independent of the nonresonant phase shifts. The smaller value of a_p and also an assignment 1^+ are impossible. The values $\bar{\sigma}_{\max}$ and $\bar{\sigma}_{\min}$ were calculated by assuming $\varphi_{J=1}=0$ and are independent of $\varphi_{J=0}$. This assignment of 0^+ agrees with the fact that α-particles leaving O^{16} in its ground state and first excited state (0^+) have been observed.

935 kev.—σ_γ is too large for Eq. (4) to be satisfied with $J=0$. $\bar{\sigma}_{\max}-\bar{\sigma}_{\min}$ is given in Table I, Paper A, with $J=1$, $a_p=0.17$ and with a nonresonant phase shift of $\varphi_{J=1}=0$ radian. If $\varphi_{J=1}=-0.19$, which is the same as the value used at 1422 kev, $\bar{\sigma}_{\max}-\bar{\sigma}_{\min}$ becomes 0.18, 0.31 and 0.41 at 90°, 125°, 160° respectively. If one subtracts from the experimental values of $\bar{\sigma}_{\max}$ and $\bar{\sigma}_{\min}$ rough experimental values of the background, the results agree quite well with the calculated ones.

1422 kev.—By using the same arguments that were used for the 669-kev resonance, this can be shown to have a 1^+ assignment with $a_p=0.85$. Plots of the complete resonance curve from 1320 kev to 1520 kev are shown in Figs. 2 and 3. The nonresonant phase shifts were chosen to be $\varphi_{J=1}=-0.19$ radian and $\varphi_{J=0}=0.09$ radian. These values of the phase shifts are not unique and no attempt was made to adjust them to give the best fit of the data.

1372 kev.—σ_γ is too large for J to be zero. The assignment $l=0$, $J=1$ is eliminated because $\bar{\sigma}_{\max}-\bar{\sigma}_{\min}$ would be observable at 90°. If l is one, J can thus be 1 or 2. The assignment 1^- cannot be eliminated because it is possible to choose channel spin ratios so that $\bar{\sigma}$ for 1^- and 2^- become approximately the same for the smaller value of a_p. However, the assignment 1^- seems unlikely since the level does not disintegrate to the ground state or the first excited state of O^{16}. It should be noted that this is not the same level as the somewhat broader level at 1367 kev which does so disintegrate.[9] The values of $\bar{\sigma}_{\max}-\bar{\sigma}_{\min}$ and of each term separately are given in Table I, Paper A, for a 2^- assignment with $a_p=0.17$ and include the effects of the strong 1^+ resonance at 1422 kev. They were calculated by using $\varphi_{J=1}=-0.19$ radian, $\varphi_{J=0}=0.09$ radian. Plots of the complete resonance curves are shown in Figs. 2 and 3.

1346 kev.—This resonance is believed to have an assignment 2^- and this is consistent with the elastic scattering if a_p has its smaller value of 0.067. For the assignments 1^+ and 0^+, which latter is possible only if the measured σ_γ is lowered 20 percent, the calculated anomaly at 90° is about 0.1. This would most probably have been observed, particularly since this region was studied very carefully. The assignment 0^- is not possible since α-particle emission is observed. We cannot rule out 1^-.

873 kev.—This level is definitely known to have the assignment 2^- and this is seen to be consistent with the elastic scattering results if a_p is taken to have its smaller value of 0.21. Interference effects with the nearby resonance at 935 kev or with nonresonant amplitudes were not included but would be less than 20 percent. If the experimental nonresonant background is roughly subtracted from the individual values of $\bar{\sigma}_{\max}$ and $\bar{\sigma}_{\min}$ the results agree with the calculated values. Using the same arguments as for the 1372 kev resonance, we can rule out 0^+ and 1^+, but cannot eliminate on elastic scattering data alone the assignment 1^-.

There are many known resonances with unknown l and J in this energy region which produce essentially no resonance anomaly in elastic scattering. These have been tabulated by Barnes[6] in his Table II. For these resonances a_p should have its smaller value. A minimum value for $\bar{\sigma}_{\max}-\bar{\sigma}_{\min}$ with $a_p=1$ is $[(2J+1)/2k\sigma_R^{\frac{1}{2}}]|P_l(\cos\theta)\cos\theta_l|$. This quantity for $l\leq 4$ at 159° or 125° for the various resonances was found to be larger than 0.3 except when $l=1$, $J=0$, which is impossible when α particles are observed. Since the larger value of a_p for these resonances is very close to 1, a_p must have its smaller value.

The reduced widths, γ^2, are given in Table I for the various resonances studied. The assignments of the

[6] C. A. Barnes, Phys. Rev. **97**, 1226 (1955). The author is indebted to Dr. Barnes for communicating his results prior to publication and for discussions concerning the partial widths of these reactions.

[7] Chao, Tollestrup, Fowler, and Lauritsen, Phys. Rev. **79**, 108 (1950).

[8] J. M. Freeman, Phil. Mag. **41**, (1950).

[9] E. B. Paul and R. L. Clarke (private communication).

TABLE I. Partial widths and reduced widths of certain $F^{19}+p$ resonances.[a]

E_{exc} (kev)	Ne^{20} J,π	Γ	Γ_p/Γ		Γ_{p0} / γ_{p0}^2	Γ_{p1} / γ_{p1}^2	Γ_{p2} / γ_{p2}^2	$\Gamma_{\alpha 0}$ / $\gamma_{\alpha 0}^2$	$\Gamma_{\alpha 1}$ / $\gamma_{\alpha 1}^2$	$\Gamma_{\alpha 2}$ / $\gamma_{\alpha 2}^2$	Γ_γ / γ_γ^2	$\Gamma_{\alpha\alpha}$ / $\gamma_{\alpha\alpha}^2$
843	0^+	23	0.996		23	~0.05	<0.01				~0.005	~0.033
					270	~3.6	<23				~0.0042	~0.0033
340	1^+	2.9	0.016		0.045	<0.0005	<0.0001	2.8	0.016	0.075	x	x
					94	<360	<10[a]	110	6.1	42	x	x
669	1^+	7.5	0.976		7.3	0.046	<0.0005	0.110	0.0004	0.025	x	x
					240	15	<10	1.5	0.027	1.6	x	x
935	1^+	8.0	0.17		1.4	3.0	<0.020	2.8	0.100	0.78	x	x
					11	125	<20	19	2.0	14	x	x
1422	1^+	14.6	0.85		12.4	2.2	≤0.035		Total <0.04		x	x
					23	14	≤ 2.8		Total <0.2		x	x
598	2^-	37	0.0012		0.043	<0.5	<0.5	37	<0.1	<0.1	x	x
					9.5	<700	<3600	180	<3	<30	x	x
873	2^-	5.2	0.21		1.1	<0.002	0.57	2.4	0.85	0.30	x	x
					36	<1.7	67	6.2	8.5	20	x	x
1346	2^-	4.5	0.067		0.3	0.3	0.6	1.8	0.45	1.05	x	x
					1.7	23	6.1	2.1	1.2	12	x	x
1372	2^-	15	0.17		2.5	0.7	1.4	9.1	0.84	0.52	x	x
					13	48	14	10	2.0	5.0	x	x

[a] The first row for each resonance is the partial width, the second row the reduced widths, all widths being given in kev. The partial width were obtained from Table II of Barnes (reference 6). An x indicates the emission is forbidden by J and π considerations.

340- and 598-kev resonances, which could not be determined by this experiment, have been determined previously.[2] γ^2 is defined as $\Gamma(2kR)^{-1}(F_l^2+G_l^2)$, where F_l and G_l are Coulomb wave functions evaluated at R, l being the lowest possible orbital angular momentum, and R is the interaction radius which is taken to be 1.41 $(A_1^{\frac{1}{3}}+A_2^{\frac{1}{3}})\times 10^{-13}$ cm, where A_1 and A_2 are the mass numbers of the two particles involved. The partial widths Γ have been given by Barnes[6] in his Table II and are repeated in our Table I. The penetration factors for the protons were obtained from the calculations of Christy and Latter.[10] For the α particles, calculations were based on the tabulations of Coulomb wave functions by Breit and his collaborators.[11] There is evidence[12,13] that the α particles are emitted with two orbital angular momenta. This would introduce a correction of about 10 percent. The single-particle reduced width, $\hbar^2/\mu R^2$, where μ is the reduced mass of the system, is 1660 kev for the protons and 390 kev for the α particles. Most of the reduced widths of the α particles are rather low, except for the large α_1 widths for the 340- and 598-kev resonances which are 28 percent and 46 percent respectively of the single-particle widths. These are much larger than usual α-particle widths. For the protons the widths at 669 and 843 kev are large, being 16 percent of the single-particle width. The reduced α_γ and α_0 widths for the resonance at 843 kev are 1.1×10^{-3} percent and 0.85×10^{-3} percent respectively of the single-particle width. As previously suggested by Barnes,[6] these low values indicate that this is a state of isotopic spin 1 of Ne^{20}. The upper limit of the reduced α widths at 1422 kev, which is 0.20 kev, is low and this may also indicate a $T=1$ state. The penetration factors, $(2kR)^{-1}(F_l^2+G_l^2)$, partially explain the branching ratios of the inelastic scattering.

The author would like to thank T. S. Webb and W. A. Fowler for many discussions concerning the interpretation of their results and to thank R. F. Christy for discussions concerning the method of analysis.

[10] R. F. Christy and R. Latter, Revs. Modern Phys. **20**, 185 (1948).
[11] Bloch, Hull, Broyles, Bouricius, Freeman, and Breit, Revs. Modern Phys. **23**, 147 (1951).
[12] J. Seed and A. P. French, Phys. Rev. **88**, 1007 (1952).
[13] Peterson, Fowler, and Lauritsen, Phys. Rev. **96**, 1250 (1954).

Double Scattering Experiment with 96-Mev Protons*

KARL STRAUCH
Harvard University, Cambridge, Massachusetts
(Received March 2, 1955)

By using 96-Mev protons, a double scattering experiment has been performed with a variety of targets and scattering angles. The observed values of the asymmetry ϵ in the intensity of the second-scattered beam are small. For instance with carbon as a first and second scatterer, and scattering angles of 20° the observed value of $\epsilon = +3.6 \pm 1.6$ percent. It is concluded that the polarization P decreases rapidly with decreasing energy below 130 Mev.

I. INTRODUCTION

DOUBLE scattering experiments performed with a variety of targets and using protons with energies of about 130 Mev and higher have shown pronounced azimuthal asymmetries ϵ in the intensity of the second scattered beam. This indicates that a high degree of polarization can be achieved by scattering of protons from nuclei. It has also been shown that the magnitude of the asymmetry ϵ and therefore of the degree of polarization increases as the scattering events become more nearly "elastic."[1]

The purpose of the investigation described here was twofold: to measure the magnitude of the asymmetry ϵ in an energy region not previously investigated, and to gain more precise information on the nature of the "elastic" events responsible for the large polarization effects. Unfortunately the second part of this program could not be carried out since the magnitude of ϵ turns out to be too small in the accessible energy region.

In previous double scattering experiments, the first scattering had been carried out inside the cyclotron tank. In this investigation, both scatterings were carried out with the external beam for the following reasons:

(1) Since nothing was known about the magnitude of the polarization below 130 Mev at the time this experiment was started, the greatest possible flexibility seemed desirable. The method used allowed the rapid variation of both the first and second scattering angles.

(2) When high-energy protons interact with a nucleus small momentum transfers are possible which leave the target nucleus in low-lying excited states.[2] One way to assure that the majority of both scattering events are truly elastic is to use a primary beam whose energy width is less than the separation between the ground and first excited state of the target nucleus. In the case of carbon, this separation is 4.4 Mev so that at the Harvard cyclotron only the external beam (energy 96 Mev, width 2 Mev) fulfills the requirement.

(3) No serious interference occurred with other experiments in progress at the same time.

The main disadvantages of the use of the external beam to carry out both scatterings arise from the small intensity of this beam. As a result, the angular resolution is relatively poor and at certain scattering angles an "inhomogeneity correction" must be applied.

II. EXPERIMENTAL ARRANGEMENT

The internal cyclotron beam is multiple coulomb scattered by an uranium target into a magnetic channel which extracts a fraction of the beam from the cyclotron (Fig. 1). After analysis and focusing by a slit system and an auxilliary magnet, a 96-Mev proton beam is available outside the shielding with an intensity of 5×10^5 protons per second per cm². It has been verified experimentally that this beam is unpolarized.

After emerging from a vacuum pipe through a defining slit, the external beam traversed an ionization chamber monitor and a brass antiscattering slit $S1$ before encountering the first target $T1$ (see Fig. 2). The first scattered beam passed through scintillation counters A and B (placed at one third the distance D from $T1$) before reaching the second target $T2$ placed at a distance D from $T1$. The line passing through the geometric centers of the targets at $T1$ and $T2$ will be called "apparatus axis;" it makes an angle θ_1 with the direction of the external proton beam. Protons scattered by $T2$ were detected by two identical telescopes 1 and 2 placed symmetrically on either side of the apparatus axis at angles of $+\theta_2$ and $-\theta_2$. The brass shields $S2$ minimized the number of protons that reached the

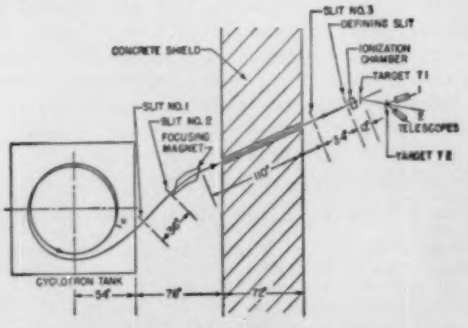

FIG. 1. Arrangement for bringing the external beam to the experimental area.

* Supported by the joint program of the Office of Naval Research and the U. S. Atomic Energy Commission.

[1] de Carvalho, Marshall, and Marshall, Phys. Rev. **96**, 1081 (1954); J. M. Dickson and D. C. Salter, Nature **173**, 946 (1954).

[2] K. Strauch and W. F. Titus, Phys. Rev. **95**, 854 (1954).

telescopes either by single scattering in $T1$ and air, or by a double scattering not involving $T2$.

The scattering and counting equipment was mounted on a platform that could be rotated around a vertical axis passing through the center of $T1$. The angles θ_1 and θ_2 could be varied with a reproducibility of better than 0.03 degrees. Target $T1$ was always placed at an angle of $90°-\frac{1}{2}\theta_1$ with respect to the external beam direction.

The telescopes 1 and 2 consisted each of 5 scintillation counters C_1 through G_1 and C_2 through G_2 spaced so that absorbers could be inserted in front of C and between F and G. The first-scattered beam was defined by the size of the external beam at $T1$ ($\frac{3}{4}$-in. width and 1-in. height) and the size of $T2$ (1 in.×4 in.); the second-scattered beams were defined by the dimensions of $T2$ and scintillators F_1 and F_2 (2 in.×4 in.) respectively. The distance between $T2$ and F_1 (or F_2) will be called d. The whole scattering and counter assembly was rigidly constructed so that even though D, d, θ_1, and θ_2 could be varied, and $T1$ and $T2$ could be rapidly removed, the apparatus was kept symmetrical around its axis to the necessary tolerances. This fact was checked experimentally by using the steep angular dependence of elastically scattered protons.

Each counter consisted of a $\frac{1}{4}$-in. thick plastic scintillator and a 1P21 photomultiplier whose output was fed directly into a diode bridge type double coincidence circuit.[3] Fast coincidence pairs AD_1, BE_1, C_1F_1, C_1G_1, AD_2, BE_2, C_2F_2, C_2G_2 were available and these were mixed in slow coincidence circuits whose output corresponded to $ABC_1D_1E_1F_1$, $ABC_1D_1E_1F_1G_1$, $ABC_2D_2E_2F_2$, and $ABC_2D_2E_2F_2G_2$ coincidences, hereafter called $A-F_1$, $A-G_1$, $A-F_2$, and $A-G_2$ coincidences respectively.

All telescope readings were normalized to a standard amount of charge collected in the ionization chamber placed in the external beam.

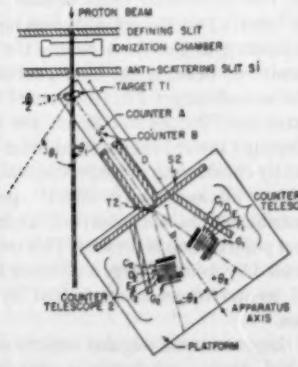

FIG. 2. The double scattering apparatus.

[3] K. Strauch, Rev. Sci. Instr. 24, 283 (1953).

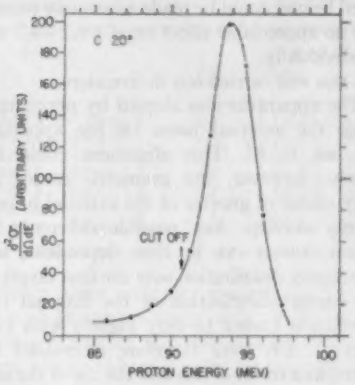

FIG. 3. Energy distribution of protons scattered at 20° from a carbon target. The intrinsic energy width of 2 Mev of the incident beam is broadened by the energy resolution of the telescope.

III. EXPERIMENTAL PROCEDURE

The use of two telescopes allowed the simultaneous measurement of two independent values of the asymmetry. Consider first telescope 1 only. The asymmetry $\epsilon(\theta_1,\theta_2)$ for a given set of first and second scattering angles θ_1 and θ_2 can be measured by keeping θ_1 constant and determining the number of double scattered protons at the angles $+\theta_2$ and $-\theta_2$. Alternately it is possible to keep θ_2 constant and to take measurements at first scattering angles of $+\theta_1$ and $-\theta_1$ (see Fig. 2). This second method turned out to be the most convenient. Readings with telescope 1 determined $\epsilon(\theta_1,\theta_2)$ as follows:

$$\epsilon(\theta_1,\theta_2)=\frac{R_1(+\theta_1,+\theta_2)-R_1(-\theta_1,+\theta_2)}{R_1(+\theta_1,+\theta_2)+R_1(-\theta_1,+\theta_2)}, \tag{1}$$

where for instance $R_1(+\theta_1, +\theta_2)$ represents the normalized double scattering counting rate of telescope 1 when the first and second scattering angles are $+\theta_1$ and $+\theta_2$ respectively (the position of telescope 1 in Fig. 2).

Another set of readings was taken simultaneously with telescope 2 from which an independent value $\epsilon(-\theta_1, -\theta_2)$ could be obtained:

$$\epsilon(-\theta_1,-\theta_2)=\frac{R_2(-\theta_1,-\theta_2)-R_2(+\theta_1,-\theta_2)}{R_2(-\theta_1,-\theta_2)+R_2(+\theta_1,-\theta_2)}. \tag{2}$$

From symmetry considerations it follows that:

$$\epsilon(\theta_1,\theta_2)=\epsilon(-\theta_1,-\theta_2) \tag{3}$$

and the final value of ϵ was obtained by taking the average of the two independent determinations.

Due to this averaging procedure, small geometric misalignments could not affect the measured value of ϵ, at least to first-order terms. Actually it is believed that all but one of the alignments (this one to be

discussed below) could be made accurately enough so as to have no appreciable effect on $\epsilon(+\theta_1, +\theta_2)$ or $\epsilon(-\theta_1, -\theta_2)$ individually.

Each run was carried out in five steps.

(1) The apparatus was aligned by photographically centering the external beam on the apparatus axis with θ_1 set to 0°. This alignment could be done accurately; however, the geometric center and the intensity center of gravity of the external beam do not necessarily overlap. Any possible difference between these two centers can be time dependent, since the beam intensity distribution over the first target depends on the energy distribution of the internal cyclotron beam which is known to vary slightly with time. The readings at $\pm\theta_1$ were therefore alternated in short cycles and as a result of this and the use of the averaging procedure just outlined the final value of ϵ is not believed to have been affected by small geometric beam fluctuations.

(2) After plateaux for all critical electronic settings had been obtained, the telescope efficiencies were rapidly compared to an accuracy of 1 percent by alternately moving each telescope into the first scattering beam by setting $\theta_2=0$.

(3) The energy of the external beam was measured with one of the telescopes set at the $\theta_2=0$ position by measuring the difference between $A-G$ and $A-F$ coincidence rates as a function of thickness of absorbers placed in front of counter C. A typical result is shown in Fig. 3. Enough absorbers were then inserted into each telescope so that $A-G_1$ and $A-G_2$ coincidences represent protons whose energy is less than about 3 Mev below the elastic peak value when both scatterings take place at the center of the targets. The required absorbers were divided into two sets placed as shown in Fig. 2 so that the $A-F_1$ and $A-F_2$ coincidence rates could have included some double scattering events in which a considerable amount of momentum was transfered during a collision.

(4) With the apparatus in position to detect double scattering events (as shown in Fig. 2), accidental and spurrious coincidences due to the high counting rates in counters A and B were measured by inserting behind B an absorber large enough to just cover the scintillator and thick enough to stop all protons. With all targets used and at all angles investigated, such coincidences were found to be negligible. These tests also indicated that no appreciable number of double scattering events of the type p-n-p were detected.

(5) For a given set of targets $T1$ and $T2$, the normalized counting rates $R_1(+\theta_1, +\theta_2)$, $R_1(-\theta_1, +\theta_2)$ and $R_2(+\theta_1, -\theta_2)$, $R_2(-\theta_1, -\theta_2)$ were then obtained by subtracting the background as follows:

$$R(\theta_1,\theta_2)=R'(\theta_1,\theta_2)-R''(\theta_1,\theta_2)-R'''(\theta_1,\theta_2), \qquad (4)$$

where $R'(\theta_1,\theta_2)$ = normalized counting rate with targets $T1$ and $T2$ in place, $R''(\theta_1,\theta_2)$ = normalized counting rate with target $T1$ in place, target $T2$ removed, and $R'''(\theta_1,\theta_2)$ = normalized counting rate with target $T1$ removed, target $T2$ in place. This method of background subtraction slightly overemphasized the importance of the background since with the target in place some of the background protons should have lost enough energy in these targets to fall below the telescope threshold. However the background was small enough so that the final value of the asymmetry ϵ was but little affected: values of ϵ obtained by the method of subtraction outlined above differed on the average by only 50 percent of the statistical uncertainty from values of ϵ obtained without any background subtraction. A set of typical data is shown in Table I. Some of the background counts were taken for shorter periods of time than the counts obtained with both scatterers in place. However in Table I all counts have been normalized to the same monitor reading.

TABLE I. Data obtained in 4 cycles with $T1$: Be, $T2$: Be, $\theta_1=\theta_2=20°$, $D=30$ in., $d=11$ in.

	$A-F$ coincidences	$A-G$ coincidences
$R_1'(20°, 20°)$	1844±43	1011±32
$R_1''(20°, 20°)$	386±28	78±13
$R_1'''(20°, 20°)$	30±9	18±8
$R_1(20°, 20°)$	1428+52	915±35
$R_1'(-20°, 20°)$	1783±42	1047±32
$R_1''(-20°, 20°)$	320±25	48+10
$R_1'''(-20°, 20°)$	15±7	6±5
$R_1(-20°, 20°)$	1448±50	993±34
$R_2'(20°, -20°)$	1516±39	954±31
$R_2''(20°, -20°)$	120±15	26±7
$R_2'''(20°, -20°)$	18±8	6±5
$R_2(20°, -20°)$	1387±42	922±32
$R_2'(-20°, -20°)$	1670±41	998±32
$R_2''(-20°, -20°)$	184±19	52±10
$R_2'''(-20°, -20°)$	6±5	3±4
$R_2(-20°, -20°)$	1480±45	943±33

IV. THE INHOMOGENEITY CORRECTION

In general, the differential cross section for elastic (and "nearly" elastic) scattering decreases rapidly with increasing scattering angle. As a result, the intensity of the first scattered beam is not homogenous over the surface of the second target $T2$: The center of gravity of protons striking $T2$ does not lie on the apparatus axis, but is deviated toward the external beam direction. As can be seen by considering the experimental geometry (Fig. 2), this "inhomogeneity effect" produces a negative contribution to the observed asymmetry ϵ, whether or not polarization is present. This contribution can be minimized by using as large a distance D between the first and second target as permitted by intensity considerations.

However, there are some angular regions over which the differential elastic scattering cross section for 96-Mev protons is essentially flat. For a light element such as carbon, such a region, centered around 8.5°,

TABLE II. Summary of experimental results.

											A−F			A−G	
T1	T2	θ_1	θ_2	D (inches)	d (inches)	E_1 (Mev)	E_1 (Mev)	E_2 (Mev)	E_2 (Mev)	Eth (Mev)	ϵ_{obs} %	ϵ %	Eth (Mev)	ϵ_{obs} %	ϵ %
C	C	8.5°	18°	60	11	86.4	14.9	68.2	9.7	10.4	−1.2±1.9	−1.2±1.9	2.5	+1.7±2.0	+1.7±2.0
C	C	15°	15°	60	14	86.6	15.5	68.1	9.6	19.6	−0.4±2.1	+0.2±2.1	2.6	+0.2±1.9	+0.7±1.9
C	C	15°	15°	30	14	86.6	15.5	68.1	9.6	19.6	+0.5±1.8	+1.8±1.8	2.6	+1.6±1.6	+3.0±1.6
C	C	20°	20°	30	11	86.6	16.0	67.6	10.0	18.9	−3.0±1.7	+2.5±1.7	3.9	−1.9±1.6	+3.6±1.6
Be	Be	20°	20°	30	11	87.3	14.2	69.7	9.3	21.0	+1.3±1.6	+4.5±1.6	3.3	−1.5±1.8	+3.1±1.8
C	Cu	8.5°	18°	60	11	86.4	14.9	63.4	20.7	11.0	+0.3±1.6	+0.3±1.6	2.2	+0.3±1.8	+0.3±1.8
Cu	Cu	26°	18°	30	11	85.7	16.3	61.7	21.2	9.9	+4.9±1.6	+4.9±1.6	3.6	+4.3±1.7	+4.3±1.7

is produced by interference between Coulomb and nuclear potential scattering. In heavier elements, a flat region exists at the top of the second diffraction maxima which in the case of copper occurs at 26°. When these special values are used for the first scattering angle θ_1, no inhomogeneity effect exists and the asymmetry due to proton polarization can be measured directly.

At other angles an "inhomogeneity correction" must be applied to the observed asymmetries. This was done by using the angular distribution of the first and second scattered beam to calculate the expected contribution to ϵ of the inhomogeneity effect, and then subtracting this contribution from the observed asymmetry ϵ. The angular distributions were measured in each case with the same targets and the same beam energy as occurred in the double scattering experiment. The magnitude of the correction can be seen from Table II. Although this is difficult to estimate, it is believed that the additional uncertainty introduced in some of the final values of ϵ by the inhomogeneity correction is at most as large as the statistical errors shown in Table II.

V. RESULTS AND DISCUSSION

Table II summarized the asymmetries obtained in this investigation. The column headings have the following meaning: $T1$ and $T2$: first and second scattering targets, θ_1 and θ_2: first and second scattering angles, D: distance between $T1$ and $T2$, d: distance between $T2$ and defining counter, E_1 and ΔE_1: average energy and spread in this energy at which the first scattering occurred due to target 1 thickness, E_2 and ΔE_2: average energy and spread in this energy at which the second scattering occured due to target 2 thickness, Eth: the lowest energy proton that was detected had an energy Eth below the elastic peak energy, ϵ_{obs}: observed value of the asymmetry, and ϵ: value of the asymmetry after inhomogeneity correction had been applied where necessary.

The most striking conclusion to be drawn from the results presented in Table II is that the asymmetry ϵ due to polarization of protons of less than 96 Mev is very small for the targets and at the angles investigated. This conclusion holds for both $A-G$ and $A-F$ coincidence events, that is events in which the majority of both scattering events were elastic and events that also included some inelastic scatterings. The errors shown are of statistical origin only. It is difficult to get accurate estimates of other sources of error but they might conceivably add up to the magnitude of the observed asymmetries.

It does not appear probable that the small size of the observed asymmetries are only due to an unfortunate choice of angles and targets. Large asymmetries have been observed with higher energy protons using the same targets and scattering at corresponding angles. The small size of the asymmetries seems to be due to the decreased energy at which the two scatterings took place in this investigation.

The asymmetry ϵ directly determines an average value of P, the polarization that would be produced by scattering an unpolarized beam on the substance in question. The average is taken over the energy region covered by the first and second scattering. For instance, with two carbon scatterers and both scattering angles at 20°, the asymmetry $\epsilon = P_1 P_2 = P_{Av}^2 = 3.6 \pm 1.6$ percent and this determines $P_{Av} = 19 + 13$ percent for carbon at 20°.

This value should be compared to $P \simeq 75$ percent obtained at 130 Mev at Harwell with carbon at 16°.[4] The magnitude of this decrease in the value of P is typical of the variation for the other target elements.

Since the observable quantity ϵ varies as $P_1 P_2$, it is much easier to measure accurately small values of P_2 by using a first scattering in which P_1 is large. This has since been done at Harwell[4] and at Chicago[5] by performing the first scattering above 100 Mev, reducing the energy of the first-scattered beam (highly polarized) by passing it through absorbers and then doing the second scattering at a lower energy. By using the Harwell results, it is possible to estimate the asymmetries that should have been observed in this experiment and the agreement is satisfactory.

It should be pointed out that Fermi's theory[6] for the polarization of elastically scattered protons correctly predicts the magnitude of the observed asymmetries. For $\theta_1 = \theta_2 = 20°$, $E_1 = 86$ Mev and $E_2 = 68$ Mev, this

[4] Dickson, Rose, and Salter (private communication, 1954).
[5] Heiberg, Kruse, Marshall, Marshall, and Solmitz, Phys. Rev. 97, 250 (1955).
[6] E. Fermi, Nuovo cimento 11, 407 (1954).

theory predicts an asymmetry of 3.8 percent or 6.5 percent depending on whether potential values determined from total neutron cross sections by Shapiro and Teem[7] or by Taylor[8] are used.

[7] I. I. Shapiro and J. M. Teem (private communication).
[8] T. B. Taylor, Phys. Rev. **92**, 831 (1953).

The author is indebted to Dr. L. Marshall and Dr. B. Rose for communicating their results before publication. Mr. J. Calame, Mr. F. Federighi, Mr. G. Gerstein, and Mr. J. Niederer helped during the long periods of data taking and greatly contributed to the success of this investigation.

PHYSICAL REVIEW VOLUME 99, NUMBER 1 JULY 1, 1955

Alternative Interpretations of Slow-Neutron Cross Sections*

O. KOFOED-HANSEN†
Columbia University, New York, New York
(Received October 26, 1954; revised manuscript received March 3, 1955)

The many-level formula of the theory of neutron resonance cross sections developed by Feshbach, Peaslee, and Weisskopf has been applied to the lowest resonances in Ag and Au. It is concluded that the approximations involved in the derivation of the usual Breit-Wigner one-level formula may lead to larger deviations in the determination of the constants in this formula than indicated by the usually applied statistical errors. In particular, in the present work a fit is obtained with a nuclear radius given as $1.47A^{\frac{1}{3}}\times10^{-13}$ cm.

INTRODUCTION

A CONSIDERABLE amount of information has been amassed in the studies of neutron capture and scattering cross sections at very low energies. The experimental data are usually interpreted in terms of the resonance formula.[1]

$$\sigma_t=\sigma_p+\sigma_s+\sigma_c$$

$$=\sum_i 4\pi R^2 g_i\left\{1+\frac{1-2\,\mathrm{Re}\,f_0}{(\mathrm{Re}\,f_1)^2+(kR-\mathrm{Im}\,f_0)^2}+\frac{-\mathrm{Im}\,f_0/kR}{(\mathrm{Re}\,f_0)^2+(kR-\mathrm{Im}\,f_0)^2}\right\} \quad (1,a)$$

$$\cong\sigma_p+\frac{\sigma_{c0}\Gamma'^2+A(E-E_0)}{4(E-E_0)^2+\Gamma'^2}+\frac{\sigma_{c0}\Gamma'^2(E_0/E)^{\frac{1}{2}}}{4(E-E_0)^2+\Gamma'^2}, \quad (1,b)$$

where σ_p (potential), σ_s' (scattering), and σ_c (capture) are $\sum_i 4\pi R^2 g_i$ times the corresponding terms in the curly bracket. The formula (1,a) is the phenomenological description of low-energy neutron cross sections. The expression is valid only when $kR\ll1$, where k is the neutron wave number and where it has been assumed that the nucleus has a relatively well-defined radius R. Because $kR\ll1$, only S-neutrons contribute to σ_t. The factors g_i are the statistical weights corresponding to the two possible spin states of the compound nucleus occurring whenever the target nucleus has a spin $\neq0$. The function f_0 is the logarithmic derivative of the radial wave function for the neutron evaluated at the nuclear radius R. f_0 has been split into its real part Re f_0 and its imaginary part Im f_0. (n,γ) reactions are responsible for the existence of the imaginary part of f_0.

In deriving the usual one-level Breit-Wigner formula (1,b) from (1,a), FPW develop Re f_0 in a Taylor series in the neutron energy E and around the resonance energy E_0 where Re $f_0=0$. In this expansion, only the first significant term is kept:

$$\mathrm{Re}\,f_0=(d\,\mathrm{Re}\,f_0/dE)_{E_0}(E-E_0)+\cdots. \quad (2)$$

In this way, the constants in (1,b) are defined by

$$\sigma_p=4\pi R^2,$$
$$\Gamma'^2=[(kR-\mathrm{Im}\,f_0)^2]_{E_0}/[(\tfrac{1}{2}d\,\mathrm{Re}\,f_0/dE)^2]_{E_0},$$
$$\sigma_{c0}\Gamma'^2=g_i 4\pi R^2\{(1/kR)_{E_0}(-\mathrm{Im}\,f_0)_{E_0}/[(\tfrac{1}{2}d\,\mathrm{Re}\,f_0/dE)^2]_{E_0}\}, \quad (3)$$
$$\sigma_{s0}\Gamma'^2=g_i 4\pi R^2/[(\tfrac{1}{2}d\,\mathrm{Re}\,f_0/dE)^2]_{E_0},$$
$$A=-g_i 16\pi R^2/(\tfrac{1}{2}d\,\mathrm{Re}\,f_0/dE)_{E_0}.$$

The validity of (2) is limited to a distance which is small compared to the level spacing. Nevertheless, the observed resonance cross sections often show an excellent agreement with the shape of (1,b) even at distances far off resonance. The experimental results are often represented in terms of the constants in (3). Here for example σ_p, the energy-independent part of the cross section, has been used in order to determine the nuclear radius[2] and it has been concluded that Ag^{107}

* This work was supported by the U. S. Atomic Energy Commission.
† On leave from the Institute for Theoretical Physics, University of Copenhagen, Copenhagen, Denmark.
[1] We use the formulation given by Feshbach, Peaslee, and Weisskopf, Phys. Rev. **71**, 143 (1947) (referred to as FPW). See also J. M. Blatt and V. F. Weisskopf, *Theoretical Nuclear Physics* (John Wiley and Sons, Inc., New York, 1952).

[2] J. Tittman and C. Sheer, Phys. Rev. **83**, 746 (1951); C. Sheer and J. Moore, Phys. Rev. **98**, 565 (1955).

and Ag^{109} have the radii 1.10 barn[1] and 0.66 barn[1] respectively, i.e., they differ by 40 percent. Also it has appeared to be difficult to reconcile the measurements of σ_t and of $(\sigma_s'+\sigma_p)/\sigma_t=\sigma_s/\sigma_t$ with the same set of constants (3). A major part of the difference between the two results is expressed in a different value for $\sigma_0=(\sigma_{c0}+\sigma_{s0})$ which comes out smaller in the σ_t measurements then in the σ_s/σ_t measurements. Thus Sheer and Moore give $\sigma_0=22\,200$ barns for the 5.19-ev level in Ag^{109}, whereas unpublished data by Wood[3] give $\sigma_0=17\,000$ barns. Here it should be emphasized that σ_0 is not obtained from an actual measurement of the maximum cross section at exact resonance since the Doppler broadening and finite resolution make this particular point uncertain. It is usually calculated together with Γ from data on several sample thicknesses using points considerably off resonance.

THEORETICAL LINE SHAPE

The argument which is stressed in the present paper is that an experimental investigation of σ_t and σ_s/σ_t in principle permits a solution of Eq. (1,a) with respect to Im f_0 and Re f_0, and therefore instead of introducing the series expansion (2) one may try to find these two magnitudes as functions of E. The method is strictly possible only when one spin state is present and only one isotope is present (see Appendix A).

Re f_0 is a monotonically decreasing function in regions where it has no poles. Also Re f_0 passes through several zeros, i.e., it is a function with a tangent-like behavior and therefore expressible as (see FPW):

$$\text{Re } f_0=-KR\tan z(E)=-KR\tan z(W), \qquad (4)$$

where K is the neutron wave number inside the range of nuclear forces corresponding to the energy W and where $z(E)$ is an increasing function of E passing through consecutive whole multiples of π at the resonances. E is the neutron energy outside the nucleus and equals $W-V_0$, where V_0 is the depth of the nuclear potential. Therefore, as an alternative approximation procedure, one may expand $z(E)$ in a power series around the resonances rather than expanding Re $f_0(E)$. This is the point of view which shall be adopted here.

FPW show that f_0 should be expressed as a function of $W+i\Gamma_r/2$, where Γ_r is the reaction width. Furthermore, a series development of $z(W)$ in order to give its imaginary part is appropriate, and thus we find

$$f_0=-KR\tan[z(E)+iq(E)], \qquad (5)$$

where q at resonance equals the reaction width multiplied by $\frac{1}{2}(dz/dE)\pi_0$. From 5 we find, when $q\ll 1$,

$$-\text{Re } f_0\cong\frac{KR\sin z\cos z}{q^2+\cos^2 z}, \qquad (6)$$

$$-\text{Im } f_0\cong\frac{KRq}{q^2+\cos^2 z}. \qquad (7)$$

[3] R. E. Wood, Phys. Rev. (to be published).

Equation (6) has the extra zeros $\cos z=0$. At these points $-\text{Im } f_0$ is very large, i.e., the denominators in (1,a) are very large and no resonances occur at these points. Apart from the immediate vicinity of such points (6) is very close to (4).

Formulas (6) and (7) are now inserted in (1,a) and the resulting expression constitutes the basis for the present alternative interpretation of low-energy neutron cross sections. We shall assume as a first approximation that $z(E)$ is a smooth function passing through consecutive integral multiples of π at the resonance energies. We then use a linear expression for

$$z(E)=(E-E_0)\pi/D,$$

where D is chosen equal to the distance to the next level.

Ag^{107} AND Ag^{109}

In order to illustrate the method suggested here, an attempt has been made to adjust the expressions involved in (1,a) to the measured σ_t and σ_s/σ_t for the lowest resonance in the element Ag,[2,4] where some of the very best measurements have been performed and where the discussion of the results have led to the aforementioned conclusions as regards the difference between the radii of Ag^{107} and Ag^{109}, respectively.

The first level (5.19 ev) in Ag^{109} is a spin 1 level. The first level (16.6 ev) in Ag^{107} is most likely a $J=0$ level.[2] Little is known about the spin of the higher levels. In order to determine a linear expression for $z(E)$ we assume, therefore, for simplicity that the first few resonances in Ag^{109} belong to the $J=1$ states and in Ag^{107} to the $J=0$ states for the compound nuclei Ag^{108} and Ag^{110}. We shall furthermore assume that the other two spin states do not contribute to σ_t apart from the potential scattering contribution $\frac{1}{4}4\pi R^2$.

With these assumptions we find immediately

$$z(E)_{109}=n\pi-0.20\pi+\pi E/26, \qquad (8)$$

which gives zeros of (4) for $E=5.2$ and 31.2, and

$$z(E)_{107}=m\pi-0.64\pi+\pi E/26. \qquad (9)$$

Having determined $z(E)$, we determine the value of KR, which to a very good approximation is found from the energy value $E_{\min}$ at which σ_s is known experimentally to have its minimum. One finds

$$KR\cong-1/\tan z(E_{\min})\cong 3.9, \qquad (10)$$

which is lower than the value predicted by FPW but still of a reasonable order of magnitude.

Finally, q is determined in the following manner. The assumption is made that KR and KRq are the same for Ag^{107} and Ag^{109}. However, this introduces an insignificant error in calculating σ_t and σ_s/σ_t from (1,a) when we are dealing with energies smaller than 10 ev.

[4] Seidl, Hughes, Palevsky, Levin, Kato, and Sjöstrand, Phys. Rev. **95**, 476 (1954).

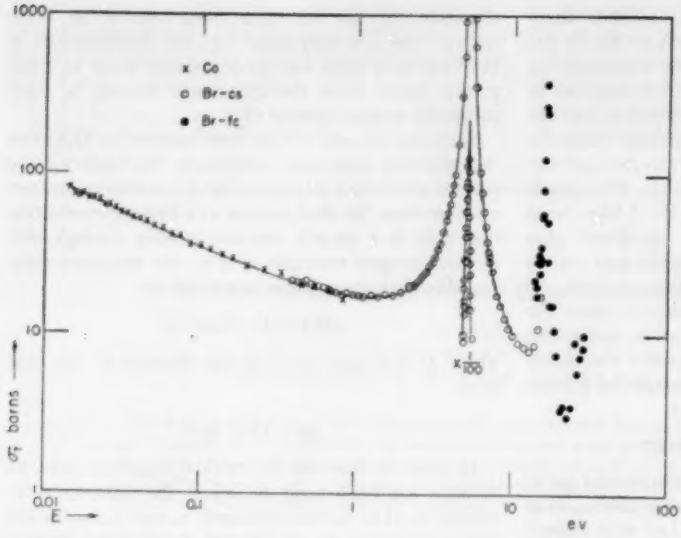

FIG. 1. The solid curve is σ_t for Ag as calculated from the formula (1,a) with the approximate expressions for Re f_0 and Im f_0 as outlined in the text. The experimental points obtained by the Columbia group and the Brookhaven fast chopper and crystal spectrometer are indicated.

We decide to use a value of the nuclear radius of

$$R=1.47\times10^{-12}A^{\frac{1}{3}}\text{ cm}. \tag{11}$$

We assume equal radii for Ag^{107} and Ag^{109}. For $A=109$ we obtain

$$4\pi R^2=6.2, \tag{12}$$

and

$$kR=[E]^{\frac{1}{2}}/650. \tag{13}$$

We then see from (1,a) that for $E=E_0$ we have

$$(\sigma_s/\sigma_t)_0\cong\frac{kR}{kR-\text{Im } f_0(E_0)}=\frac{kR}{kR+KRq}=\frac{\Gamma_n}{\Gamma}, \tag{14}$$

which gives us the value of $KRq=0.0277$ for Ag^{109} and by assumption the same for Ag^{107}. It should be noted that the total cross section at resonance is given by

$$\sigma\cong g_c\frac{4\pi R^2}{kR}\frac{1}{kR-\text{Im } f_0(E_0)}=g_c4\pi\lambda^2\frac{\Gamma_n}{\Gamma}.$$

Consequently, when Im $f_0(E_0)$ is determined from (7), $\sigma_t(E_0)$ is also fixed. The deviation between σ_t as measured this way and as measured directly is quite remarkable and makes it practically impossible to fit the 16.5-ev data together.

Now all functions are completely determined mathematically and the calculation of σ_t and σ_s/σ_t is straightforward. The results are shown in Fig. 1 and Fig. 2 together with the experimental data from references 2 and 3 and unpublished Brookhaven data.[3] The fit to the wings of the 5.2-ev resonance curve and to the σ_s/σ_t curve is better than the experimental uncertainty indicated by the authors.

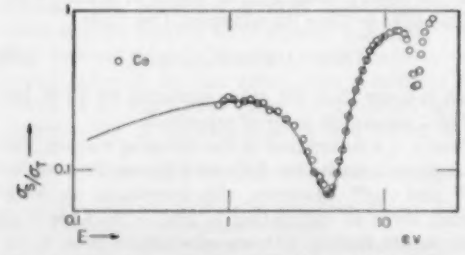

FIG. 2. The solid curve is σ_s/σ_t for Ag as calculated from the same expression used in Fig. 1. The experimental points obtained by Sheer are indicated by circles.

TABLE I. The Breit-Wigner constants for the 5.2-ev resonance in Ag^{109} as derived from the present analysis compared with those derived by applying formula (1,b).

Present analysis		Sheer	Wood
σ_p(b)	6.2		6.0±0.5
Γ(ev)	0.133	0.128±0.016	0.149±0.005
$\sigma_{c0}\Gamma^n$(ev^{n}b)	2×328	2×(44±5)	2×(366±10)
$\sigma_{s0}\Gamma^n$(ev^{n}b)	2×42		
A	2×39		2×(30±3)

Past experience has shown that it is impossible to obtain a fit of (1,b) to both these curves and with the same set of constants (3). Again, in making such fits it has been necessary to introduce different radii for Ag^{107} and Ag^{109}. In addition, the magnitude of the $1/v$ absorption at low energies has not been accounted for.

The constants (3) as derived from our expressions are given in Table I together with Sheer's data and Wood's data. Sheer analyzes his data on the additional assumption of different radii for the two isotopes as mentioned previously.

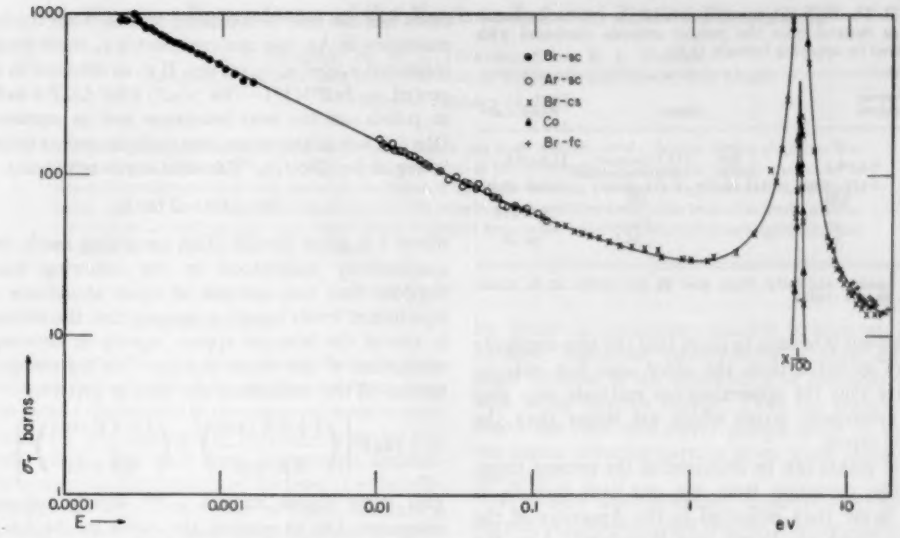

FIG. 3. The solid curve is σ_t for Au^{197} as calculated in the present approach. The points are experimental data.

Au^{197}

In the foregoing treatment of the lowest resonance in silver, one has the complication of the presence of two isotopes. In Au^{197}, only the two spin states 1 and 2 of the compound nucleus Au^{198} will introduce complications.

If we assume that the levels at 4.93 and 61.5 ev belong to the $J=2$ state and assume a linear dependence of z on E, we find

$$z(E)\cong\frac{E-4.93}{56}\pi+n\pi. \tag{16}$$

We proceed as in the case of silver and find $KR=9.2$ and by using Eq. (14) or by fitting the constant in the $1/v$ law we find $qKR=0.0305$. From the experimental value of $\sigma_s=5.8$ at $E_{\min}$, determined by $-\tan[z(E_{\min})]=1/KR$ [see Eq. (10)], we conclude that σ_s from the $J=1$ state is ~ 5.8 near the 4.93-ev resonance and we add this contribution to the σ_s we calculate from (1,a) for the $J=2$ states. The value $\sigma_s=5.8$ barns is larger than σ_p for the $J=1$ states. This is not an indication that R is larger for this state but would result from the above values of KR and q if the 80-ev state were a $J=1$ state and if another (bound) $J=1$ state appeared at about -20 ev. This is perfectly reasonable since a smooth continuation of (16) would indicate that the next $J=1$ state is the 168-ev level.

We then calculate σ_t and σ_s/σ_t from the expressions (1,a) and our formulas for Re f_0 and Im f_0 together with the semiempirical values of $z(E)$, KR, and KRq given above. The results are shown in Figs. 3 and 4. The constants (3) as derived from our mathematical expressions are given in Table II.

CONCLUSIONS

It is shown that it is possible to understand the observed σ_t and σ_s/σ_t curves for the lowest resonance in silver and gold with the same values of the constants (3) in both the σ_t and σ_s/σ_t curves. The constants derived by the present method deviate by more than the statistical errors from those used in fitting the data directly to the one-level formula. It is therefore concluded that the approximations involved in the derivation of (1,b) from (1,a) may give rise to larger deviations between (1,b) and experimental data than can be hidden in the statistical errors in the data. Therefore, care should be observed in the interpretation of Breit-Wigner constants when derived from data far off resonance. If z is assumed to be linear in E, a deviation of 1 percent between (1,a) and (1,b) occurs at a distance off resonance of about 1/25 of the distance to the next level in the same spin state. For silver, this is about 8 times Γ off resonance.

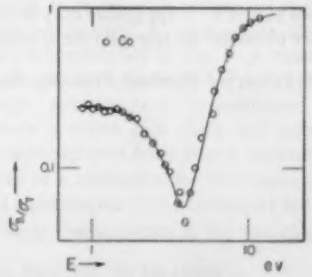

FIG. 4. The solid curve is σ_s/σ_t for Au^{197} as calculated in the present approach. The points are experimental data.

TABLE II. The Breit-Wigner constants for the 4.93-ev resonance in Au^{197} as derived from the present analysis compared with those derived by applying formula (1,b).

	Present analysis	Sheer		Wood *et al.*[a]
J	2	2	1	2
σ_p(b)	9.2 ±0.3	8.0 17.6	13.3 resonant 10.6 nonresonant	11.1 ±0.3
Γ(ev)	0.134 ±0.003	0.133 ±0.009	0.172 ±0.01	0.140 ±0.003
$\sigma_0\Gamma^N$(ev-b)	630		638	725 ±15
$\sigma_0\Gamma^N$(ev-b)	86		89.3	
A	88		84.5	96 ±8

[a] Wood, Landon, and Sailor, Phys. Rev. **98**, 639 (1955); R. E. Wood Phys. Rev. **95**, 644 (1954).

It is not our intention to claim that the new constants are more accurate than the older ones but only to emphasize that the approximation methods may give rise to systematic errors which are larger than the statistical errors.

Several points can be criticized in the present treatment. The deviation from the one-level formula is slightly larger than indicated in the Appendix of the paper by Feshbach, Porter, and Weisskopf.[5] Also, the experimentally established large variations in Γ_N are not represented by the present method.

However, the author believes that it is worthwhile to carry out experimental determinations of both σ_t and σ_s so that Re f_0 and Im f_0 can be found directly as functions of the neutron energy and subsequently be compared with theory. Preferably such experiments should be carried out on even-even isotopes with intense, low-energy resonances.

Also, it is pointed out that if more careful investigations reveal greater detail in the structure of resonance curves, one should not try to introduce constants which violate the relations between the five constants (3). If it turns out to be necessary, one should preferably introduce entirely new constants like $(dq/dE)_{E_0}$ and $(d^2z/dE^2)_{E_0}$.

The author is indebted to Professor W. W. Havens, Jr., Dr. E. Melkonian, Dr. C. Sheer, and Dr. V. Sailor for valuable discussions.

APPENDIX A

The statement that Re f_0 and Im f_0 can be found directly from σ_s and σ_t is applicable only in cases where σ_s and σ_t are obtained for one spin state only. In other cases this can lead to confusing results. Near the lowest resonance in Ag, one can construct a σ_s curve from the measured σ_t and σ_s/σ_t curves. If σ_s so obtained is interpreted as $5\pi R^2\times\frac{3}{8}(1-\langle\text{Re } f_0\rangle_{Av})^2/(\langle\text{Re } f_0\rangle_{Av})^2+4\pi R^2\times\frac{1}{8}$ at points not too near resonance and as representing $\langle\text{Re } f_0\rangle_{Av}=0$ at resonance, one finds the points indicated in Fig. 5 for $\langle\text{Re } f_0\rangle_{Av}$. The solid curve represents

$$\langle\text{Re } f_0\rangle=-2\tan 2z, \tag{17}$$

where z is given by (8). This surprising result can be qualitatively understood in the following manner. Suppose that two isotopes of equal abundance show equidistant levels in such a manner that the resonances in one of the isotopes appear exactly in between the resonances of the other isotope. The scattering cross section off the resonances will then be given by

$$\sigma_s=\tfrac{1}{2}4\pi R^2\left[\left(\frac{1+KR\tan z}{KR\tan z}\right)^2+\left(\frac{1-KR\cot z}{KR\cot z}\right)^2\right]. \tag{18}$$

This curve shows minima $\sigma_s^{\min}$ shortly before any resonance. Let us analyze the curve in the following way. We subtract $\sigma_s^{\min}$ from (18) and interpret the remainder as $\frac{1}{2}4\pi R^2(1-\langle\text{Re } f_0\rangle_{Av}^2)/\langle\text{Re } f_0\rangle_{Av}$. A simple calculation shows that we then obtain

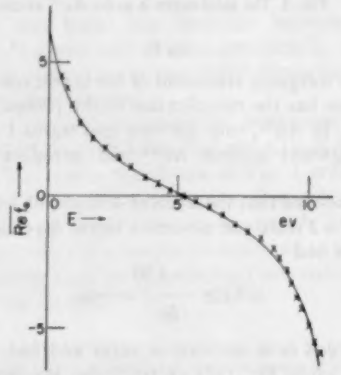

FIG. 5. The points are $\langle\text{Re } f_0\rangle_{Av}$ as calculated in the text for the lowest level in Ag. The curve represents $-2\tan 2z$.

$$\langle\text{Re } f_0\rangle_{Av}=-\tfrac{1}{2}KR\tan 2z. \tag{19}$$

Thus we see that the result (17) can be explained merely as an effect of the two contributions to the value of σ_s for silver.

[5] Feshbach, Porter, and Weisskopf, Phys. Rev. **96**, 448 (1954).

Angular Dependence of the Neutron-Induced Fission Process. II*

J. E. Brolley, Jr., W. C. Dickinson,† and R. L. Henkel
Los Alamos Scientific Laboratory, University of California, Los Alamos, New Mexico

(Received February 14, 1955)

The angular anisotropy of neutron-induced fission has been studied with a double fission chamber. For U^{235} at 7.4 Mev and Np^{237} at 14.3 Mev, the variation of the differential fission cross section was found to depend strongly on the fourth power of the cosine of the angle between the fission fragment and the neutron beam. For U^{235} a resonance-type dependence of the anisotropy on neutron energy has been observed. Qualitative indication that the light and heavy fission fragment groups have slightly different anisotropies has been obtained in the case of Np^{237} at 14.3 Mev.

INTRODUCTION

In previous work[1] it has been shown that the fragments of fission induced by 14-Mev neutrons were anisotropically distributed in the center-of-mass system. This property was observed in varying degree for five different nuclei. The data were represented approximately by angular distributions of the form $(1+A\cos^2\theta)$. To expand knowledge of this phase of fission mechanics, the present experiments have been directed to additional questions. How does the anisotropy change with the bombarding neutron energy? Do the light and heavy fragments participate equally in the process? What is the more precise form of the angular distribution? To these ends we have extended the earlier work through the use of an improved coincidence apparatus.

A theory giving information on these questions does not exist in the present literature. The collective model of Hill and Wheeler[2] and the shell-structure model of Fong[3] are recent theories which may be adapted to the interpretation of these phenomena.

EXPERIMENTAL METHODS

The early studies[1] were performed with a simple parallel-plate ionization chamber. The present experiments have utilized a collimated double fission chamber which is described in detail in the next section. In addition to providing fission rates at various angles with respect to the neutron beam it supplies the ionization spectra of the two groups of fission fragments at these angles. It also provides data for the precise study of ionization spectra from thermal neutron fission. (See Fig. 5.) The light-fragment group which has the highest energy is clearly differentiated from the heavy-fragment group by a deep valley. As the energy of the fission-inducing neutrons increases, the valley in the ionization spectrum becomes more shallow. This has been shown by Wahl[4] in ionization chamber studies at 2.5 and 14 Mev. Moreover, radiochemical studies[5] indicate a rapid increase in the probability of symmetric fission with rising neutron energy. Thus the distinction between the light and heavy groups tends to vanish as the fission inducing particle gives more energy to the reaction.

At 14-Mev neutron energy, however, the two groups are still readily identified despite the rise in the valley. At this energy one has the possibility of discerning relative changes in the angular distributions of the light and heavy groups. If the effect is marked, it would manifest itself by an increase in area of one group and decrease in area of the other in the ionization spectrum of the fragments. The angular variation of the fission cross section is given by the integral over both groups of the spectrum measured at various angles.

APPARATUS

Fission Chamber

The fission chamber described in reference 1 had several properties susceptible of improvement. Fission fragments lost a considerable fraction of their energy in traversing the long collimator passages so that the energy distribution could not be observed. Also, background pulses attributed to alpha particle pile-up, n-p and n-α reactions, and to recoiling atoms of the chamber gas were of the same magnitude as those pulses from the lowest-energy fission fragments. These effects required small but uncertain corrections to be made to the data.

To minimize these effects a collimated double fission chamber was constructed. A cross section of this chamber is shown schematically in Fig. 1. A common negative high-voltage electrode serves a Frisch grid chamber and a simple parallel-plate "coincidence" chamber. This electrode is 0.066 inch thick and honeycombed with 0.016-inch diameter holes over a one-inch diameter area to serve as a collimator for the fission fragments. The optical transmission of the collimator is 59 percent. Only coincident fission pulses in the two chambers are

* This document is based on work performed under the auspices of the U. S. Atomic Energy Commission.

† Present address: University of Indonesia, Bosscha Laboratory, Bandung, Java, Indonesia.

[1] W. C. Dickinson and J. E. Brolley, Jr., Phys. Rev. **90**, 388 (1953); J. E. Brolley, Jr. and W. C. Dickinson, Phys. Rev. **94**, 640 (1954).

[2] D. L. Hill and J. A. Wheeler, Phys. Rev. **89**, 1102 (1953).

[3] Peter Fong, Phys. Rev. **89**, 332 (1953), and privately circulated manuscript.

[4] J. S. Wahl, Phys. Rev. **95**, 126 (1954).

[5] R. W. Spence and G. P. Ford, Ann. Revs. Nuclear Sci. **2**, 399 (1953).

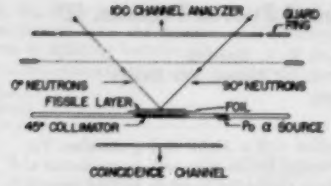

FIG. 1. Schematic cross section of double fission chamber.

counted. To attain complete symmetry between the 0° and 90° angular settings, the collimator holes are inclined at 45° to the electrode normal. The extreme angular resolution of the collimator is $9\frac{1}{4}°$ and the most probable angle of emission with respect to the collimator axis is 4°. This is poorer resolution than was employed in the first chamber but was necessary to increase the fission counting rates and to keep to a minimum the energy loss in the collimator passages of fragments entering the coincidence chamber. A foil, thin to fission fragments, upon which is evaporated a layer of fissile material, is mounted directly over the collimator area on the Frisch grid side. Whereas those fragments entering the coincidence chamber must pass through the foil and collimator passages before expending their residual energy in the chamber, the fragments entering the Frisch grid chamber lose negligible energy in the fissile layer, providing it is kept very thin. Hence an accurate fission ionization spectrum can be obtained. An identical honeycombed area, $\frac{1}{4}$ inch in diameter, adjacent to the main collimator serves to collimate Po alpha particles entering the Frisch grid chamber. These particles are emitted from a monomolecular Po film deposited electrochemically on a silver backing which is attached to the collimator plate. They are used to help calibrate the pulse-energy scale and test the equipment.

A copper-gasketed steel purifier filled with calcium chips continuously purified the chamber gas mixture (argon+CO_2). The purifier was initially outgassed for 24 hours at 200°C. With gas in the chamber the purifier was maintained at 150°C. At this temperature O_2 and H_2O contaminants were removed but the CO_2 fraction was not significantly affected.

Electronics

A block diagram of the electronic circuitry is shown in Fig. 2. Associated with every fission signal in the coincidence chamber, there is a signal produced in the Frisch grid chamber. These coincident pulses were amplified by preamplifiers with cathode follower outputs mounted directly behind the chamber and completely shielded by a cylindrical metal shell. The temperature of the preamplifiers was held constant to within one degree centigrade by a thermostatically controlled heater. After traversing RG 71/U cable to the control room, the pulse from the Frisch grid chamber, went to a Model 250 gated linear amplifier which also provided proper delay. The amplified pulse from the coincidence chamber was applied to a modified Harwell discriminator and pulse shaper having the desirable feature of generating a square wave output pulse only after the input pulse, if greater than the threshold setting, has reached its peak value. Thus the time delay of the output pulse was not a function of the amplitude of the input pulse as in the case with conventional discriminators. The output of the Harwell circuit created a 3-microsecond gate in the Model 250 amplifier, arriving about 0.2 microsecond before the pulse from the Frisch grid chamber. Output pulses from the amplifier, after an additional amplification by a window amplifier, inserted to gain distribution resolution, were analyzed by a Wilkinson type 100-channel pulse-height analyzer.[6]

For calibration, a Model 500 pulse generator was connected to feed artificial pulses to both preamplifiers so that the analyzer output could be calibrated directly in terms of millivolt input to the Frisch grid preamplifier.

Pulses in the coincidence chamber channel could be suitably delayed for the determination of the accidental coincidence rate.

Chamber Tests

In the design of the Frisch grid side of the fission chamber the paper of Bunemann, Cranshaw, and Harvey[7] was followed. The grid served to shield the collecting electrode from charges induced by the electrons and positive ions in the region of the chamber traversed by the fission fragments. The output pulse induced by the electrons moving from the grid region to the collector was closely proportional to the original number of ion pairs produced. Unfortunately, the requirement that there be no electron collection by the grid made it impossible to obtain complete shielding of the collector.

Following the notation of Bunemann *et al.*, the important parameters of our chamber are: radius of kovar

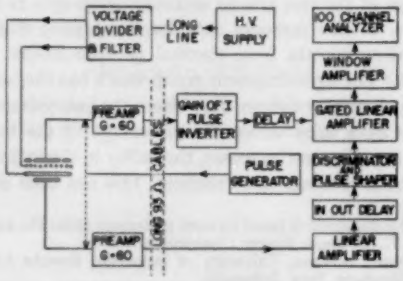

FIG. 2. Block diagram of electronics.

[6] Hiebert, Evans, and Watts, Los Alamos Scientific Laboratory Report LA-1565, April, 1953 (unpublished).

[7] Bunemann, Cranshaw, and Harvey, Can. J. Research **A27**, 191 (1949).

grid wires, $r=6.35\times10^{-3}$ cm, grid wire spacing $d=0.107$ cm, source-grid distance $a=2.60$ cm, grid-collector distance $p=1.21$ cm, $\rho=0.373$, $l=0.0174$. The inefficiency of shielding $\sigma=l/(p+l)=1.4$ percent. The minimum ratio of grid-collector to source-grid voltage to insure zero grid interception was calculated to be 1.03, corresponding to a ratio of the fields equal to 2.22.

Tests were made with monoenergetic alpha particles to compare the theoretical analysis of reference 7 with actual performance. For this work both uncollimated U^{234} and U^{235} alpha particles from a 10-microgram/cm² evaporated layer of uranium oxide and collimated Po α particles were used. An argon+5 percent CO_2 gas mixture was used at a total pressure of 900 mm Hg. This was sufficient to stop all alpha particles before reaching the grid region.

Results of measuring the pulse height of the U^{234} and Po alpha groups for different values of R, the ratio of grid-collector to source-grid voltage, are shown in Fig. 3. The theory is well confirmed since there is a noticeable increase in pulse height when R is increased from 1.0 to 1.1 but negligible difference when a further increase to 1.2 is made in R. A value of R equal to 1.1 was used in subsequent work.

The "supersaturation" effect, characteristic of argon $+CO_2$ mixtures, is observed in Fig. 3. This decrease in pulse height as the collecting voltage is increased beyond a certain point has been variously attributed to electron capture resonances in gas impurities, inelastic collisions between electrons and CO_2 molecules when the electron drift velocity reaches a certain threshold, and resonant reactions with the CO_2 molecules resulting in a breakup of the molecule and to electron attachment to one of the components. Despite this disadvantage it was found that the high electron drift velocity, low saturation voltage, and lack of hydrogen content made argon $+CO_2$ mixtures preferable for these experiments.[8]

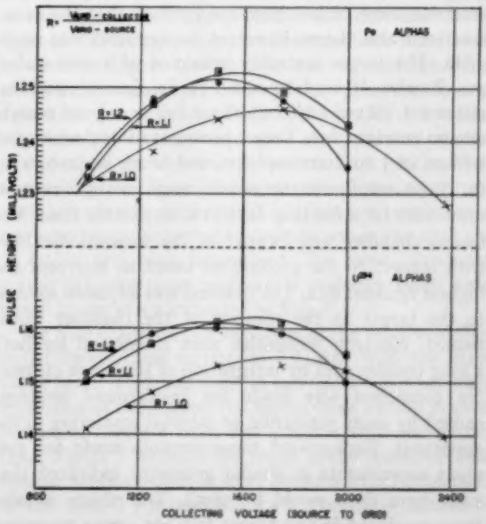

FIG. 3. Pulse height of Po and U^{234} α particles as a function of collecting voltage for different values of R.

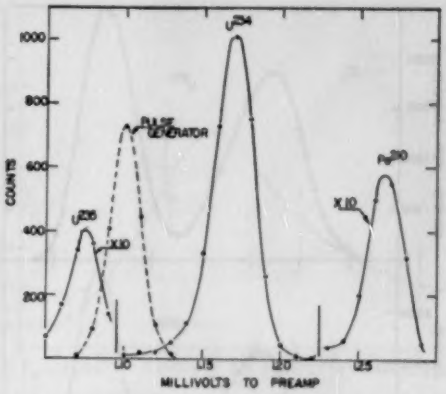

FIG. 4. Typical α pulse-height distribution. $R=1.1$ total chamber voltage, 3000.

A typical alpha pulse-height spectrum is shown in Fig. 4. The small low energy tail on the U^{234} peak is attributed to alpha particles traveling at grazing angles to the source foil. The total widths at half-maximum of the uncollimated U^{234} and collimated Po peaks are 2.56 percent and 2.22 percent respectively. The corresponding width of the pulse generator distribution is 2.14 percent. An rms subtraction of this electronic noise contribution to the widths results in "chamber" widths of 1.41 percent and 0.60 percent, respectively. It is assumed that the contribution of the pulse generator to the electronic width is negligible. The lack of 100 percent shielding efficiency and the dependence upon alpha particle trajectory of the amount of charge induced on the collector by positive ions causes the spread to be greater for the uncollimated alphas.

As a test of the over-all operation of the equipment the thermal fission spectra of U^{233} and U^{235} were observed.[9] The U^{233} and U^{235} foils were in the form of a 15-μg/cm² painted layer of U^{233} and a 10-μg/cm² evaporated layer of U^{235} respectively. The two spectra are shown in Fig. 5.

The ionization produced by a fission fragment was converted to an energy scale by comparison with the ionization produced by alpha particles. The energy obtained in this way for the most probable light and heavy fragments is called the ionization energy. This differs from the true energy because the last few Mev of the fragment energy are lost in nonionizing processes.[10] The difference between the true energy and the ionization energy is termed the ionization defect. Leachman[11]

[8] W. N. English and G. C. Hanna, Can. J. Phys. **31**, 768 (1953).
[9] Neutrons were obtained from the thermal column of the Los Alamos Water Boiler.
[10] Knipp, Leachman, and Ling, Phys. Rev. **80**, 478 (1950).
[11] R. B. Leachman, Phys. Rev. **87**, 444 (1952).

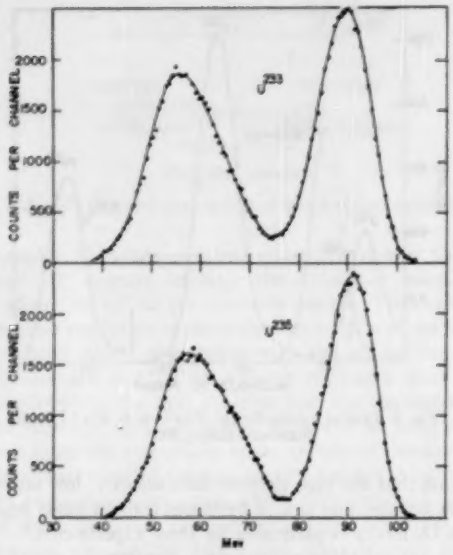

FIG. 5. U^{233} and U^{235} thermal fission spectra.

has estimated that the ionization defects in argon gas are about 5.7 and 6.7 Mev for the most probable light and heavy fragments respectively.

To compare the present values for the most probable energies of the light and heavy fragments with those obtained in the careful work of Brunton and Hanna[12] who used an argon+3 percent CO_2 mixture, it was necessary to know how the ionization defect varies with the gas mixture. Recently, ionization defect differences have been measured for a variety of gases[13] including pure argon and argon+3 percent CO_2. It was found that the defects in the mixture were 3.0 and 4.5 Mev greater than those in pure argon for the most probable light and heavy fragments respectively. If one assumes that this difference depends linearly on the percentage of CO_2 then the defects for argon+5 percent CO_2 would be 2 and 3 Mev greater than those for argon+3 percent CO_2, for the most probable light and heavy fragments respectively. To compare the measured energy values with those of Brunton and Hanna (see Table I) these energy increments have been added. Also the values have been corrected by 0.2 and 0.1 Mev respectively for fragment mean energy loss in the U^{233} and U^{235} layers. The values listed for Brunton and Hanna were corrected for source and collimator losses. The agreement would appear to be satisfactory except perhaps in the case of the heavy fragment of U^{233} where the measured value is 4.4 percent higher than those of Brunton and Hanna.

[12] D. C. Brunton and G. C. Hanna, Can. J. Research **A28**, 190 (1950).

[13] Lloyd O. Herwig and Glenn H. Miller, Phys. Rev. **95**, 413 (1954).

14-Mev Neutron Source

The source of 14-Mev neutrons was the $T(d,n)He^4$ reaction, using the atomic beam of 250-kev deuterons from the Los Alamos Cockcroft-Walton accelerator. The beam was magnetically analyzed and collimated before striking a zirconium-tritium target. The neutron flux was monitored by counting a known fraction of the alpha particles generated in the $d+T$ reaction. The error in relative neutron monitoring for various runs was about 1 percent. The active foil of the coincidence chamber was 10 cm from the target.

Data were collected in a series of symmetric, repeated runs so as to minimize the effects due to electronic drifts and deterioration of the neutron source. Since the source to foil spacing was so close, no correction was made for the small scattered-neutron backgrounds.

Other Energies

The neutron sources for the other energies were the $T(p,n)He^3$, $D(d,n)He^3$, and $T(d,n)He^4$ reactions. Protons or deuterons were accelerated by the large Los Alamos Van de Graaff generator and were precisely magnetically analyzed and controlled. The experimental area was some 20 feet from the earth so that the room-scattered and thermal-neutron background was negligible. The target assembly consisted of a thin-walled gas chamber 10 cm long and 1 cm in diameter and had either a 1/20 mil nickel entrance foil or a ½-mil molybdenum entrance foil. Target pressures of deuterium and tritium of 1 to 2 atmospheres and beam intensities up to 10 μa were used to obtain large enough neutron intensities for collecting data in a reasonable time. The fission chamber was located in the forward direction with respect to the accelerated beam to intercept the highest neutron flux. The position was adjusted as close to the target as the rotation of the chamber would permit. Neutron intensities were monitored by both a long counter and by integration of the beam current. No correction was made for background neutrons caused by room scattering or internal scattering in the apparatus. Background measurements made for previous experiments in similar geometry indicated that such corrections would be small. The effects of neutrons produced in the target foil, etc., were measured by replacing the target gas by hydrogen or vacuum.

TABLE I. Most probable fission-fragment ionization energies.

	Fragment	Brunton and Hanna	Present work
U^{233}	Light	93.0	92.0
	Heavy	56.6	59.1
U^{235}	Light	94.5	93.0
	Heavy	60.2	61.1

The errors introduced by these extraneous neutrons were negligible.

EXPERIMENTAL RESULTS

Uranium-235

The first set of data were obtained using an evaporated layer of $U^{235}O_2$, 0.5 mg/cm², on a gold backing 0.9 mg/cm². Irradiations with neutrons of various energies were performed at the large Los Alamos Van de Graaff Generator. In this study we have sought to ascertain the energy dependence of the anisotropic distribution of fragments by measuring the quantity $\sigma_f(0°, E_n)/\sigma_f(90°, E_n)$ at a number of different neutron energies. The results are compiled in Table II and graphically exhibited in Fig. 6. Data for thermal and 14-Mev neutrons are from the earlier work.[1] The energy limits indicated for E_n represent the extreme neutron energy spread intercepted by the fissile layer resulting from degradation of the accelerated charged particles in the gas target and by geometrical factors. The standard deviations indicated represent a combination of statistical errors and allowances for systematic errors. Accidental coincidences occurring during these measurements were inconsequential. The standard deviations of the angular settings probably did not exceed two degrees. Where necessary, small corrections were made to the zero-degree data to take into account the effect of the finite angular resolution of the apparatus. Recent measurements with the $T(d,n)He^4$ reaction show that additional low-energy neutrons are produced in the source when the high-energy neutrons are greater than about 20 Mev. These measurements allow an approximate calculation of the yield of these low-energy neutrons under the experimental conditions at the time the 20.4-Mev ratio was determined. The error introduced to the ratio by these neutrons is probably small compared to the error indicated in Fig. 6.

TABLE II. 0°/90° anisotropy in U^{235} fission as a function of neutron energy.

E_n (Mev)	0	2.5	4.6	7.5[a]	14.3	20.4
0°/90° Intensity ratio	0.99 ±0.05	1.02 ±0.05	1.13 ±0.06	1.36 ±0.05	1.27 ±0.08	1.11 ±0.09

[a] Average of measurements at 7.4 and 7.6 Mev.

We also observed the variation of the relative differential fission cross section at 7.4 Mev with the same fissile layer. This was done to provide a more accurate expansion of the differential fission cross section in even powers of cosine θ than was possible with the earlier data. Figure 7 portrays the result in the center-of-mass system together with a least squares fitted expansion of the form $1+A\cos^2\theta+B\cos^4\theta$. For the goodness of fit S^2, we assign the value 1.6×10^{-3}. It is clear that the fourth power of the cosine is dominant; a fact not evident in our earlier data. The least squares fit yields $\sigma_f(0°, 7.4)/\sigma_f(90°, 7.4)=1.36$ in harmony with our preceding survey.

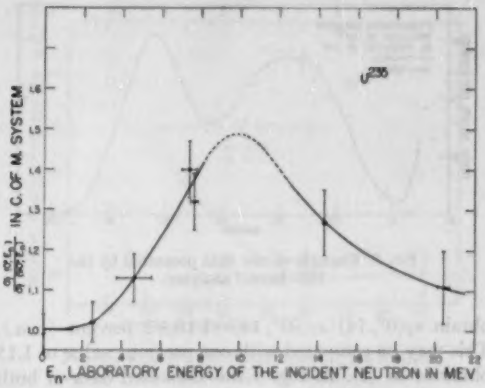

FIG. 6. Energy dependence of the anisotropy.

Neptunium-237

After completion of the U^{235} experiments a Np^{237} fissile layer was installed in the ionization chamber. This source was prepared by evaporating a deposit of $Np^{237}O_2$ to a thickness of about 60 μg/cm² on a 1.1-mg/cm² nickel foil. Irradiation of the neptunium was performed at the Los Alamos Cockcroft-Walton machine with 14.3-Mev neutrons.

The first phase of this study was the study of the fission fragment ionization spectrum at 0° (backwards) and 90°. Data were accumulated by taking many short runs at each angle until the integral count was 5000 at each position. Electronic drifts were negligible, hence the various runs were simply added. The summed data as presented by the 100-channel analyzer at 0° are illustrated in Fig. 8. The low-energy background can be removed by a short extrapolation of the spectrum into the abscissa. This correction is small and contributes a negligible error. From these measurements we

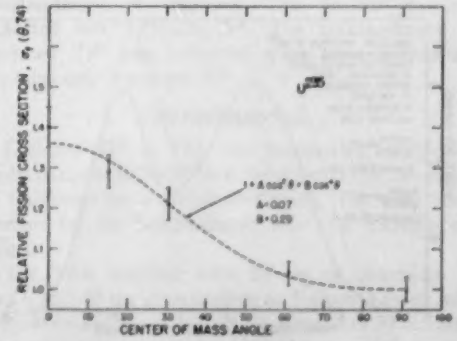

FIG. 7. Relative differential fission cross section of U^{235} at $E_n=7.4$ Mev.

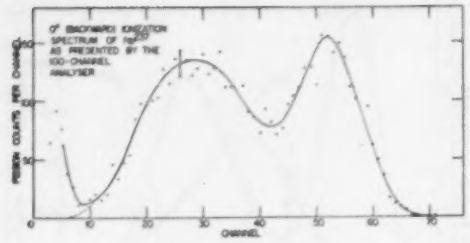

FIG. 8. Example of raw data presented by the 100-channel analyzer.

obtain $\sigma_f(0°, 14)/\sigma_f(90°, 14) = 1.16 \pm 2$ percent (c.m.). This may be compared with our previous value of 1.15 obtained in (1). In Fig. 9 the smoothed data of both positions are illustrated. The 0° (backward) curve is shifted toward lower energy because of center-of-mass motion. In order to compare the shapes more clearly, both curves were reduced to equal areas and their centroids were approximately superimposed in Fig. 10. This pattern will symmetrically invert about 90° (neglecting small center-of-mass effects); hence one sees that the heavy group tends to go forward with a somewhat higher probability than the light group. For reasons previously mentioned it is difficult to make a quantitative estimate of this effect. One may obtain a measure which is principally of qualitative significance by arbitrarily assuming that the minimum between the two groups separates them. This assumption is not strictly valid. On this premise one finds that there are about 10 percent more light fragments at 180° than at 90°. Or, inversely, at 0° there are about 10 percent more heavy fragments than at 90°, for the same total number of fissions at each angle. From the known kinetics of 14-Mev neutron-induced fission in U^{235}, one infers that center-of-mass motion can have only a relatively small influence on this phenomenon in Np^{237}. It seems probable therefore that this is a real effect in the center-of-mass system. The qualitative character, it must be re-emphasized, should be clearly borne in mind. We anticipate performing more certain experiments of this nature in the future.

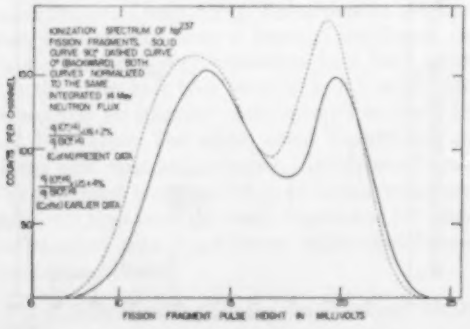

FIG. 9. Smoothed fission-fragment ionization spectra at 0° and 90°.

In the second phase of the neptunium experiments, relative differential fission cross sections at 0°, 30°, 60°, and 90° in the laboratory system were measured. Accumulation of data proceeded by short runs at chosen angles until each angle had approximately 2000 counts. As in the case of U^{235} this was an attempt to obtain a representation of the fission cross section in even powers of $\cos\theta$. The 15° point was not obtained, but as in the uranium data, one sees by inspection of Fig. 11 that the fission cross section depends principally on the fourth power of the cosine. This least squares fitted distribution is assigned a goodness of fit $S^2 = 4 \times 10^{-4}$. The fitted curve yields $\sigma_f(0°, 14)/\sigma_f(90°, 14) = 1.18$ (c.m.) in good agreement with the other measurements on neptunium.

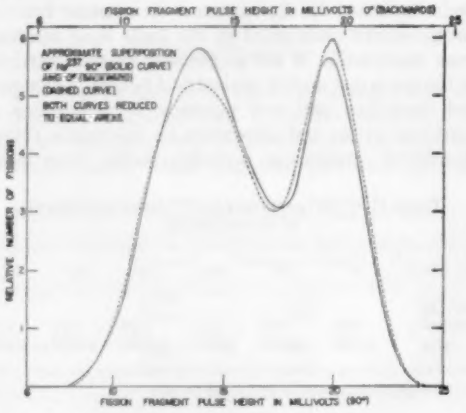

FIG. 10. Superposition of 0° and 90° ionization spectra after reduction to equal areas.

DISCUSSION

In this work, three properties of the anisotropic variation of the fission cross section were established; two being rather well founded, and one tentative. In both U^{235} and Np^{237}, at certain energies, the angular variation of the fission cross section exhibits a strong dependence on the fourth power of the cosine. The interpretation of this result is not clear but it would be instructive to compare the coefficients in both cases with the quadrupole moments of the two nuclei. This could afford insight as to how the process depended on the shape of the nucleus. Only two nuclei have been studied and therefore such conclusions may not be of a very general nature. We therefore plan to extend these studies to other fissionable nuclei.

The resonance character of energy dependence of the anisotropy seems moderately well established, though additional data are desirable, on U^{235} as well as other

nuclei. The decline of the anisotropy may well be associated with the rapidly increasing probability of symmetric fission with neutron energy.

The preponderance of heavy fragments in the forward direction likewise is susceptible of improved observation. Thus this experiment could be performed with U^{233} at 2.5-Mev neutron energy. In this region it is known that the ratio of the height of the higher-energy peak to valley minimum in the ionization spectrum is at least 3.3 whereas in the case of Np^{237} it was only about 2.

The progress of this experiment was possible only through the assistance of many of our associates. In particular we thank L. K. Schlacks for evaporating the fissile layers, R. W. Davis for untiring help in setting up the apparatus at the Cockcroft Walton machine and operating the accelerator, Group P-4 for the generous allotment of time on this accelerator, R. K. Zeigler for computational aid, and J. Waugh for graphical assistance.

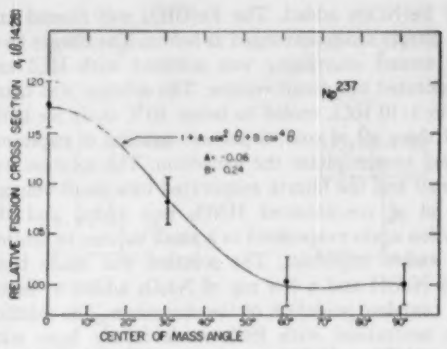

FIG. 11. Relative differential fission cross section of Np^{237} at $E_n = 14.3$ Mev.

PHYSICAL REVIEW VOLUME 99, NUMBER 1 JULY 1, 1955

Isobaric Triplet $Cr^{48}-V^{48}-Ti^{48}$*†‡

RAYMOND K. SHELINE AND JOSEPH R. WILKINSON
Department of Chemistry, Florida State University, Tallahassee, Florida

(Received February 28, 1955)

Cr^{48} has been produced by the nuclear reaction $Ti^{46}(\alpha,2n)Cr^{48}$. The gamma spectra of this nuclide have been investigated and peaks found at 118 kev and 307 kev. The two gamma rays are in coincidence and have the same intensity. The gamma rays of the daughter nuclide V^{48} have been shown to appear in the gamma spectra as Cr^{48} decays. The half-life of Cr^{48} has been determined as 24±1 hours. The energy of the Cr^{48} orbital electron capture has been shown to be approximately 1.30 Mev with a very low log *ft* value. A decay scheme for the isobaric triplet $Cr^{48}-V^{48}-Ti^{48}$ is proposed. Using the proposed decay schemes as a basis, the masses of Cr^{48} and V^{48} have been calculated to be 47.96934±22 and 47.96749±7, respectively.

INTRODUCTION

CHROMIUM-48 has been reported as an orbital electron capturing activity produced in the spallation of iron with 340-Mev protons.[1] Its half-life was reported to be 23 or 24 hours. No gamma radiations were reported for this nuclide. Cr^{48} is an even-even nucleus with an associated 0+ ground state[2] whereas V^{48}, the product nucleus, is known to have a ground state of 4+ or 5+.[3] The decay of Cr^{48} may therefore be expected to be complex with the emission of gamma rays.

This work was undertaken in an effort to produce Cr^{48} and to study its decay scheme and the decay scheme of its daughter V^{48}. Because of the great number of radionuclides produced in a spallation reaction, it was decided to attempt to produce Cr^{48} by alpha bombardment of titanium. The nuclear reaction expected was $Ti^{46}(\alpha,2n)Cr^{48}$. The bombardment of enriched Ti^{46} was indicated since normal titanium contains only 8 percent Ti^{46}.

EXPERIMENTAL

Enriched Ti^{46} as TiO_2 was bombarded by 50-Mev alpha particles in the 60-inch cyclotron at the University of California for a period of 4 hours. The total beam current for the bombardment was 12.4 microampere hours.

The TiO_2 together with 10 mg of chromium as Cr_2O_3 and 10 mg of vanadium as V_2O_5 was fused with anhydrous sodium carbonate for a period of 30 minutes. The melt was extracted with hot water and filtered. A few drops of 6*N* NaOH was added to the filtrate

* This work was supported in part by the U. S. Atomic Energy Commission.

† This paper is taken from a portion of a thesis submitted by J. R. Wilkinson to the Graduate Faculty of Florida State University in partial fulfillment of the requirements for the Ph. D. degree.

‡ A paper on the decay of Cr^{48} was presented before the New York Meeting of the American Physical Society, 1955 [van Lieshout, Greenberg, and Wu, Bull. Am. Phys. Soc. **30**, No. 1, 32 (1955)].

[1] Rudstam, Stevenson, and Folger, Phys. Rev. **87**, 358 (1952).
[2] M. G. Mayer, Phys. Rev. **78**, 16 (1950).
[3] Casson, Goodman, and Krohn, Phys. Rev. **92**, 1517 (1953).

and $Fe(NO_3)_3$ added. The $Fe(OH)_3$ was filtered and the filtrate again scavanged as before. The filtrate from the second scavenging was acidified with HCl and evaporated to a small volume. The solution was taken up in 1:10 HCl, cooled to below 10°C in an ice bath, and three ml of cold, 6 percent solution of cupferron added to precipitate the vanadium. The solution was filtered and the filtrate evaporated to a small volume. 25 ml of concentrated HNO_3 was added and the solution again evaporated to a small volume to destroy the excess cupferron. The solution was made basic with NaOH and a few mg of Na_2O_2 added to insure the complete oxidation of the chromium. The solution was neutralized with HCl, made faintly basic with NH_4OH, then faintly acid with acetic acid, and the chromium precipitated as $BaCrO_4$. The precipitate was centrifuged, washed with H_2O, and dissolved in HCl. The $BaCrO_4$ was reprecipitated by addition of NH_4OH and was again centrifuged, washed, and dissolved as before. This step was repeated five more times to purify the $BaCrO_4$. The final precipitate was mounted on thin polystyrene film and the gamma ray spectra of the chromium were investigated by scintillation techniques employing a differential and integral discriminator similar to the one previously described by Fairstein.[4]

RESULTS

The gamma-ray spectra of Cr^{48} taken as a function of time show peaks at 118-kev and 307-kev. The apparent gamma ray at 425 kev is due to the sum line of the 118-kev and 307-kev gamma rays. The 118-kev, 307-kev gamma rays and the 425-kev sum line all decay with a 23-hour half-life. No annihilation radiation was observed in the first gamma spectra of Cr^{48} taken 2 hours after the separation of vanadium. The absence of any annihilation radiation confirms the observation of Rudstam, Stevenson, and Folger[1] that Cr^{48} decays by means of orbital electron capture without positron emission.

Spectra of Cr^{48} taken at intervals of 12 to 24 hours show the growth of gamma rays at 0.99 Mev and 1.32 Mev. Gamma rays of 0.99 Mev and 1.32 Mev have previously been identified with the decay of V^{48}.[5–7] The observation of these gamma rays growing into the spectra with a 16-day half-life as the Cr^{48} gamma rays decay is a positive identification of the nuclide Cr^{48} and totally confirms the findings of Rudstam, Stevenson, and Folger.[1]

The growth of the gamma peak at 0.512-Mev is attributed to the annihilation radiation of the 0.69-Mev positron of V^{48}. The apparent gamma ray at 2.32-Mev is due largely to the sum line of the 0.99-Mev and 1.32-Mev gamma rays. The coincidence of these gamma rays is consistent with the decay scheme of V^{48}.[8] The weak peak at 2.23-Mev reported by several workers[9–10] was obscured by the 2.32-Mev sum line. Gamma spectra of Cr^{48} taken 2 hours after separation of vanadium and after an interval of 2 days are shown in Fig. 1.

The half-life of Cr^{48} was determined by means of the integrating scintillation counter. The result of these measurements is shown in Fig. 2. The half-life of 15.8 days for V^{48} is in close agreement with the half-life reported for this nuclide by Walke.[11] The half-life of Cr^{48} determined by these measurements is 24 ± 1.0 hours.

DECAY SCHEMES OF Cr^{48} AND V^{48}

The decay scheme for Cr^{48} must involve an energy level scheme in V^{48} which will permit the following: (1) an orbital electron capture to one of the excited states of V^{48}; (2) a coincidence between the 118-kev and 307-kev gamma rays; (3) very similar intensities in the 118-kev and 307-kev gamma rays.

It is highly probable that the decay of Cr^{48} to V^{48} is an allowed transition. In the first place, the parities of

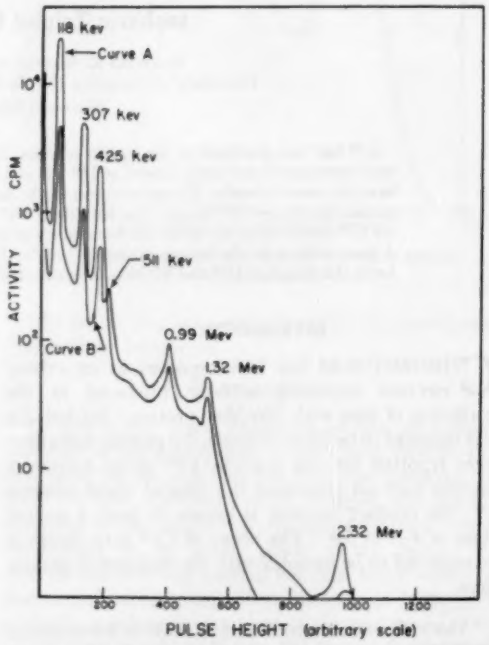

FIG. 1. The gamma spectra of Cr^{48} showing growth of V^{48} gamma rays. Curve *A* shows spectrum taken 2 hours after separation of vanadium; curve *B* shows spectrum taken 2 days after separation of vanadium.

[4] E. Fairstein, Rev. Sci. Instr. **22**, 76 (1951).
[5] W. C. Peacock and M. Deutsch, Phys. Rev. **69**, 306 (1946).
[6] Good, Peaslee, and Deutsch, Phys. Rev. **69**, 313 (1946).
[7] Robinson, Ter-Pogossian, and Cook, Phys. Rev. **75**, 1099 (1949).
[8] Ticho, Green, and Richardson, Phys. Rev. **86**, 422 (1952).
[9] M. M. Miller, Phys. Rev. **88**, 516 (1952).
[10] Roggenkamp, Pruett, and Wilkinson, Phys. Rev. **88**, 1262 (1952).
[11] H. Walke, Phys. Rev. **52**, 777 (1937).

the ground state and low-lying excited states of V^{48} will be even, as long as these particles reflect shell particle levels. Any decay of Cr^{48} to a state of 2+ or higher would result in an *ft* value high enough that an energy for the decay would have to be excessively high in order to result in a 24-hour half-life. Even if such a high energy were available, there would certainly be competition between an orbital electron capture and positron emission. Since no positron is observed, a 0+ or 1+ spin and parity must be assigned to the state to which the Cr^{48} decays.

The fact that the intensities of the 118-kev and 307-kev gamma rays are very nearly the same makes it much more probable to assume that these gamma rays are very slightly internally converted than to assume the two gamma rays are highly internally converted and to the same extent. Assuming a small amount of internal conversion, from the experimental results on gamma ray intensities, it can be said that the internal conversion of these gamma rays will be at most 5 percent. If the α_K is small, then the *K*-shell internal conversion coefficients of Rose *et al.*[12] indicate that the 118-kev gamma ray can only be an *E*1 or *M*1 transition. Because of the even parity one is led to expect for the low-lying excited states of V^{48}, the 118-kev gamma ray can only be assigned as an *M*1 transition.[13] Also, if the α_K is small, the transition possibilities for the 307-kev gamma ray can only be *E*1, *E*2, *M*1, *M*2, and *M*3. The even parity to be expected in low-lying excited states of V^{48} rules out *E*1 and *M*2. Accordingly, the 307-kev gamma ray should be *E*2, *M*1, or *M*3. The possibilities for the decay of Cr^{48} are shown in Fig. 3.

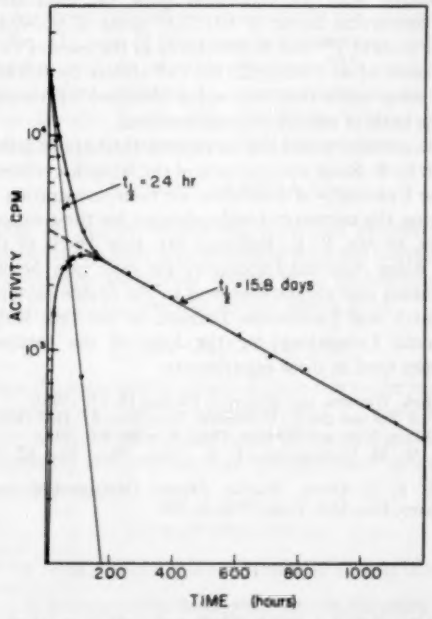

FIG. 2. The decay curve of Cr^{48} showing the growth of V^{48} in the nonequilibrium parent-daughter genetic relationship.

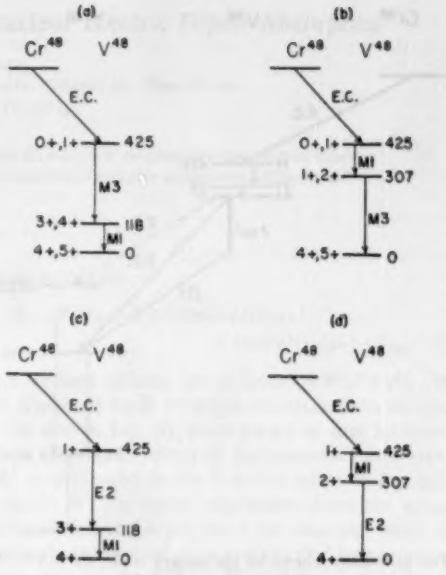

FIG. 3. Various assignments of the spins and parities of the V^{48} daughter in the Cr^{48} decay.

Recent work by van Lieshout, Greenberg, and Wu[14] has indicated the α_K for the 118-kev gamma ray is 2×10^{-2} and that for the 307-kev gamma ray is 0.6×10^{-2}. They correlated these values with the assignment of the 118-kev gamma ray as *M*1 and the 307-kev gamma ray as *E*2. The decay of Cr^{48} is thereby limited to Fig. 3(c) or (d). Some indication as to which of these two schemes actually represent the decay of Cr^{48} might be found by comparing the decay of Cr^{48} with the decay of nuclides one alpha particle on either side of Cr^{48}. Unfortunately, Fe^{52} has no gamma rays in its decay.[15] However, recent work on Ni^{56},[16] which is two alpha particles away, indicates that there is a 170-kev gamma ray from the first excited state of Co^{56} to the ground state of Co^{56}. In the decay of Ti^{44}, there is a single gamma ray of 160-kev from the first excited state of Sc^{44} to the ground state of Sc^{44}.[17] It is therefore our belief that the 118-kev gamma ray present in the decay of Cr^{48} represents the transition from the first excited state of V^{48} and that Fig. 3(c) represents the decay scheme of Cr^{48}.

[12] Rose, Goertzel, and Swift (privately circulated).
[13] M. Goldhaber and W. Sunyar, Phys. Rev. **83**, 960 (1951).
[14] van Lieshout, Greenberg, and Wu, paper presented at the New York Meeting of the American Physical Society, January, 1955 [Bull. Am. Phys. Soc. **30**, No. 1, 32 (1955)].
[15] G. Friedlander and J. M. Miller, Phys. Rev. **84**, 588 (1951).
[16] R. K. Sheline and J. R. Wilkinson (unpublished results).
[17] R. A. Sharp and R. M. Diamond, Phys. Rev. **93**, 358 (1954).

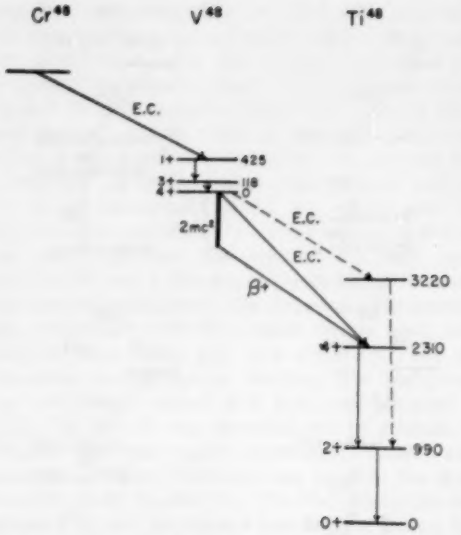

FIG. 4. A decay scheme for the isobaric triplet $Cr^{48}-V^{48}-Ti^{48}$.

Mayer, Moszkowski, and Nordheim[18] have found that the majority of allowed transitions have a log *ft* value of 5.0±0.3. However, log *ft* values for allowed transitions ranging from 4.5 to 5.9 were reported. No annihilation radiation in the gamma spectra of Cr^{48} was observed. However, due to nearby gamma rays it is only possible to set an upper limit of less than 2 percent positron emission for the decay. Using the upper limit of 2 percent positron emission and the tables of Feenberg and Trigg,[19] it is possible to calculate that the upper limit of the energy for the Cr^{48} to V^{48} transition is 1.28 Mev. From the tables of Moszkowski,[20] it is found that an energy of 1.28 Mev and a 24-hour half-life corresponds to a log *ft* value of 4.4. This is a relatively low log *ft* value even for an allowed transition. However, any higher log *ft* value would result in a positron to orbital electron capture ratio higher than we observed in our experiments. We therefore believe that the orbital electron capture energy for the Cr^{48} decay is approximately 1.30 Mev with a very low log *ft* value.

The decay of V^{48} is considered to be an allowed transition.[3] Angular correlation studies[10,21,22] of the 0.99-Mev and 1.32-Mev gamma rays indicate the spin and parity assignment of 0+, 2+, and 4+ for the ground and first two excited states of Ti^{48}.

The decay scheme of V^{48} is shown in Fig. 4. These results are in close agreement with the observation of Casson, Goodman, and Krohn.[3] The orbital electron capture from the ground state of V^{48} to the 3.22-Mev level of Ti^{48} and the 2.23-Mev gamma ray from the 3.22-Mev level of Ti^{48} to the 0.99-Mev level are shown as dotted lines in Fig. 4 since it is not possible to say from our data whether or not the 2.23-Mev gamma ray has been observed. The sum line at 2.32 Mev is slightly broader than one would normally expect and this could be atrributed to the very weak 2.23-Mev gamma-ray. It is true that the area under the 2.32-Mev sum line is approximately what one would expect for the sum line of the 0.99-Mev and 1.32-Mev gamma rays. However, the 2.23-Mev gamma ray is so weak (2 percent) that very little increase in the area under the sum line would be expected.

MASSES OF V^{48} AND CR^{48}

The mass of Ti^{48} has been reported as 47.96317±6.[22] The masses of V^{48} and Cr^{48} have been calculated on the basis of the decay scheme shown in Fig. 4. The transition energy of V^{48} is 4.02-Mev with an estimated error of ±0.028-Mev and the transition energy of Cr^{48} is 1.724-Mev with an estimated error of ±0.2-Mev. The conversion factor of 931.152[24] gives 47.96749±7 as the mass of V^{48} and 47.96934±22 as the mass of Cr^{48}. The mass of 47.96934±22 for Cr^{48} differs by 0.00087 ±22 mass units from the value obtained by Green[25] on the basis of empirical considerations.

The authors would like to express their appreciation to Dr. G. B. Rossi and the crew of the 60-inch cyclotron at the University of California for their cooperation in securing the necessary bombardments for these experiments, to Mr. P. R. Bell and Mr. Ray Davis of the Oak Ridge National Laboratory for their very helpful comments and suggestions, and to the Stable Isotopes Research and Production Division of the Oak Ridge National Laboratory for the loan of the enriched isotopes used in these experiments.

[18] Mayer, Moszkowski, and Nordheim, Revs. Modern Phys. **23**, 315 (1951).
[19] E. Feenberg and G. Trigg, Revs. Modern Phys. **22**, 399 (1950).
[20] S. A. Moszkowski, Phys. Rev. **82**, 35 (1951).
[21] Sterk, Wapstra, and Kropveld, Physica **19**, 135 (1953).
[22] P. S. Jastram and C. E. Whittle, Phys. Rev. **87**, 1133 (1952).
[23] Collins, Nier, and Johnson, Phys. Rev. **86**, 408 (1952).
[24] J. W. M. DuMond and E. R. Cohen, Phys. Rev. **82**, 555 (1951).
[25] A. E. S. Green, *Nuclear Physics* (McGraw-Hill Book Company, Inc., New York, 1955), p. 359.

Effect of Spin-Orbit Interaction on Photonuclear Electric Dipole Absorption*

SHERMAN FRANKEL
Physics Department, University of Pennsylvania, Philadelphia, Pennsylvania
(Received February 17, 1955)

The effect of a nuclear spin-orbit interaction of the form $H_1=\phi(r)\mathbf{l}\cdot\boldsymbol{\sigma}$ on photonuclear electric dipole absorption is examined. We find that the total cross section is unaffected and give expressions for the (small) effect on the average energy of absorption.

LEVINGER and Bethe[1] and others[2] have calculated the effects of exchange forces on the total electric dipole absorption cross section, $\sigma_{\rm int}=\int\sigma(E)dE$, and on the average energy of absorption, $\bar{W}=\int E\sigma(E)dE/\sigma_{\rm int}$. In view of the observed spin-orbit splitting in low-lying nuclear levels, we consider briefly the effect of a spin-orbit interaction of the form $H_1=\phi(r)\mathbf{l}\cdot\boldsymbol{\sigma}$ on electric dipole absorption. (This potential has been used by Jensen and Mayer[3] to account for observed $M1$ transition probabilities in $d_{\frac{3}{2}}\rightarrow s_{\frac{1}{2}}$ transitions which are disallowed by ordinary $M1$ operators.)

The matrix element for electric dipole transitions from the state 0 to the state n is related to the total Hamiltonian by

$$(E_n-E_0)\langle z\rangle_{0n}=\langle zH\rangle_{0n}-\langle zH\rangle_{n0}{}^*=i\hbar\langle j_z\rangle_{0n}, \quad (1)$$

where j_z satisfies the continuity equation and is derivable from the Hamiltonian according to Eq. (1). As has been pointed out previously[1,4] and is apparent in Eq. (1), any H possessing a commutator with the coordinate can in principle affect $\sigma_{\rm int}$. This condition is not, however, sufficient. $\sigma_{\rm int}$ is proportional to the oscillator strength, $\sum_n f_{0n}=\sum_n (2m/\hbar^2)(E_n-E_0)\langle z\rangle_{0n}\langle z\rangle_{0n}{}^*$. Using (1) and carrying out this sum, we obtain

$$\sum_n f_{0n}=-(m/i\hbar)\langle[j_z,z]\rangle_{00}. \quad (2)$$

Thus, for $\sigma_{\rm int}$ to be affected, it is also necessary for the *current* to have a commutator with the coordinate. The average absorption energy $\bar{W}$ is proportional to $\sum_n (E_n-E_0)f_{0n}$, which is readily shown to be

$$\sum_n (E_n-E_0)f_{0n}=2m\langle j_z{}^z\rangle_{00}. \quad (3)$$

Since the spin-orbit interaction gives rise to the current $j_z=\phi(r)(\boldsymbol{\sigma}\times\mathbf{r})_z$ which commutes with z, there is no effect on $\sigma_{\rm int}$. There should however, be an effect on $\bar{W}$. Neglecting forces other than ordinary and spin-orbit forces, we have

$$j_z=p_z/m+\phi(r)(\boldsymbol{\sigma}\times\mathbf{r})_z,$$

so that we obtain

$$\sum_n (E_n-E_0)f_{0n}=4\langle p_z{}^2/2m+\phi(r)l_z\sigma_z+\tfrac{1}{2}m\hbar^2\phi^2(r)(x^2+y^2)\rangle_{00}, \quad (4)$$

where we have utilized $(\boldsymbol{\sigma}\times\mathbf{r})_z(\boldsymbol{\sigma}\times\mathbf{r})_z=\hbar^2(x^2+y^2)$. [We have neglected Pauli Principle correlations in carrying out the sum in Eq. (4), since we are at first interested only in the explicit effect of the spin-orbit interaction on $\bar{W}$ as evidenced in the last two terms in Eq. (4).] To obtain $\bar{W}$, the above expression times the square of the effective charge[1] must be summed over the nucleons in the ground state and divided by $\sigma_{\rm int}$, which in this case is just NZ/A. Equation (4) may be rewritten as

$$\sum_n (E_n-E_0)f_{0n}=(4/3)\langle T+\phi(r)\mathbf{l}\cdot\boldsymbol{\sigma}+m\hbar^2\phi^2(r)r^2\rangle_{00}. \quad (5)$$

The first term yields the well-known result $(4/3)T_{00}$. The second term, which is just the spin-orbit energy, vanishes for closed l-shells and is a maximum at the magic numbers. Thus only a few particles will contribute via this term to $\bar{W}$. At the Mayer[5] "closed" shells ($j=l+\frac{1}{2}$), the contributions to $\bar{W}$ are

$$-\frac{8}{3}\frac{l(l+1)}{(2l+1)}\frac{Z}{NA}\Delta E \quad \text{and} \quad -\frac{8}{3}\frac{l(l+1)}{(2l+1)}\frac{N}{ZA}\Delta E$$

for neutrons and protons, respectively, where ΔE is the splitting of the $l+\frac{1}{2}$ and $l-\frac{1}{2}$ subshells. The third term may be approximated by assuming that $\phi(r)$ is essentially the (negative) constant g over the nuclear wave function, so that $\Delta E=(2l+1)\hbar^2 g$ and the third term becomes

$$\frac{4}{3}\frac{m}{\hbar^2}\left(\frac{\Delta E}{2l+1}\right)^2\overline{\langle r^2\rangle_{00}}.$$

If we use $\Delta E=2$ Mev, which is consistent with other data,[6] we find that these explicit effects of the spin-orbit interaction on $\bar{W}$ are less than a few tenths of an Mev, so that they are not important for the average energy of absorption. However, the spin-orbit interaction will still affect $\bar{W}$ implicitly in its effect on the wave function used for the Pauli Principle correlation terms, which are dominant in heavy nuclei.[2] It is also possible that terms in (3) involving spin-orbit currents and other assumed currents may not be negligible.

* This work is supported in part by the U. S. Office of Ordnance Research.

[1] J. S. Levinger and H. Bethe, Phys. Rev. **78**, 115 (1950).
[2] E. Feenberg, Phys. Rev. **49**, 328 (1936); A. J. F. Siegert, Phys. Rev. **52**, 787 (1937); J. S. Levinger and D. C. Kent, Phys. Rev. **95**, 418 (1954).
[3] J. H. D. Jensen and M. G. Mayer, Phys. Rev. **85**, 1040 (1952).
[4] J. S. Levinger, Bull. Am. Phys. Soc. **30**, No. 1, 66 (1955).
[5] M. G. Mayer, Phys. Rev. **78**, 16 (1950).

Collective Modes in Nuclei*

F. COESTER
Department of Physics, State University of Iowa, Iowa City, Iowa
(Received March 28, 1955)

The Hamiltonian of the "unified model" of Bohr and Mottelson has been derived from many-particle quantum mechanics. A point transformation in the configuration space of the N nucleons of the core introduces 6 collective coordinates describing the size and shape of the nucleus and $3N-6$ internal coordinates. The collective coordinates are essentially the components of the quadrupole moment tensor of the nucleon distribution. It is assumed that the wave function Ψ of the nucleus for the ground state and the low lying excited states can be approximated by the product $\Psi_0\Phi$ where Ψ_0 depends only on the internal coordinates of the core and Φ depends on the collective coordinates of the core and the coordinates of the external nucleons. $\Psi_0\Phi$ is treated as a trial function in the Schrödinger variational principle. For fixed Ψ_0 this yields a Schrödinger equation for Φ. The Hamiltonian in this equation is the Hamiltonian of Bohr and Mottelson plus certain correction terms. Ψ_0 influences the values of the constant parameters occurring in this Hamiltonian but not its structure. In the strong-coupling approximation the relationship between the moments of inertia of the core and the nuclear quadrupole moment is essentially the same as in the liquid drop model. This result is also independent of detailed assumptions about Ψ_0.

I. INTRODUCTION

BOHR[1-3] and Mottelson[2] have recently proposed a "unified model" of nuclear structure which has had spectacular success mainly in accounting for the rotational level structure in heavy nuclei.[3-5] The essence of this model can be stated as follows: The nucleus consists of a core which can be adequately described by a few collective coordinates plus one or several external nucleons which are treated according to the individual particle model. In the quantitative realization of this idea the liquid drop model has been used for the core and the motion of the liquid is assumed to be irrotational.

Success of the liquid drop model always raises the question: How can this success be understood from the more fundamental standpoint of quantum mechanics of the many-nucleon system? Bohr[6] has pointed out that the collective rotation of the core can be understood by applying an appropriate coordinate transformation to the many-particle description. Inglis[7] has obtained similar rotational levels from a shell model with a rotating asymmetric potential.

In this note we follow Bohr's suggestion and carry out a point transformation in the configuration space of the core which is designed to introduce explicitly the collective coordinates describing the excitations of the core and the internal coordinates describing the remaining degrees of freedom. The physical picture underlying the collective model implies that only a few degrees of freedom participate in the motions of the core. Mathematically this is expressed by the assumption that the wave function Ψ of the nucleus can be approximated by a product of a function Ψ_0 depending only on the internal coordinates and a function Φ depending on the collective coordinates and the coordinates of the external nucleons. The first factor is the same for the ground state and the low-lying excited states under consideration. This wave function shall be treated as a trial function in the Schrödinger variational principle. For a given internal wave function Ψ_0 this variational principle yields a Schrödinger equation for Φ.

The Hamiltonian in this Schrödinger equation is equivalent to the Hamiltonian of Bohr and Mottelson except for certain correction terms. Tolhoek[8] has independently investigated the relations between the Bohr-Mottelson model and the many particle problem along much the same lines. He does not, however, obtain the correction terms just mentioned.

It has been stressed by Ford[9] that the very close agreement of the theoretical and experimental energy ratios of the rotational states does not check the liquid drop model for the core. More significant is the theoretical prediction for the moment of inertia in terms of quadrupole moments and deformations deduced from isotope shifts. This prediction does not agree quantitatively with experiment.[9] In view of this situation we examine in Sec. III the influence of the correction terms in the Hamiltonian on the moment of inertia. It turns out that their effect is too small and has the wrong sign.

II. THE COLLECTIVE HAMILTONIAN

Let us consider a nuclear core with N nucleons plus $A-N$ external nucleons. The collective coordinates should describe the deformation of the core. It is convenient to take essentially the quadrupole moment of the nucleon distribution: The symmetric tensor ψ_{ik} is defined as a function of the nucleon positions by

$$\psi_{ik}=\frac{1}{2b}\sum_{\nu=1}^{N}x_i^{(\nu)}x_k^{(\nu)}-\tfrac{1}{2}\delta_{ik}. \tag{1}$$

* Supported in part by the U. S. Atomic Energy Commission.
[1] A. Bohr, Kgl. Danske Videnskab. Selskab, Mat.-fys. Medd. **26**, No. 14 (1952).
[2] A. Bohr and B. R. Mottelson, Kgl. Danske Videnskab. Selskab, Mat.-fys. Medd. **27**, No. 16 (1953).
[3] A. Bohr, *Rotational States of Atomic Nuclei* (Ejnar Munksgaards Forlag, Copenhagen, 1954).
[4] Alaga, Adler, Bohr, and Mottelson (to be published).
[5] Bohr, Froman, and Mottelson (to be published).
[6] See the appendix of reference 3.
[7] D. R. Inglis, Phys. Rev. **96**, 1059 (1954). I wish to thank Dr. Inglis for showing me his manuscript prior to publication and for several stimulating discussions about the subject of this paper.
[8] H. A. Tolhoek, Physica **21**, 1 (1955).
[9] K. Ford, Phys. Rev. **95**, 1250 (1954).

$\mathbf{x}^{(s)}$ is the position of the sth nucleon. By this definition, the trace of the tensor ψ_{ik} does not vanish identically and fluctuations in size are therefore also described by our collective coordinates. The constant b shall be defined by the condition that the expectation value of the trace $\langle\sum_i\psi_{ii}\rangle$ vanishes in the ground state. The internal coordinates describing the remaining degrees of freedom of the core are denoted by $\xi_\alpha(\mathbf{x}^{(1)}\cdots\mathbf{x}^{(N)})$, $\alpha=1\cdots 3N\text{-}6$. We assume all the ξ_α's are scalars. They need not be specified explicitly for our purposes. In the framework of our model we must assume that the wave function of the nucleus has the form

$$\Psi(\mathbf{x}^{(1)}\cdots\mathbf{x}^{(A)})=\Psi_0(\xi_1\cdots\xi_{3N-6})\times\Phi(\psi_{11}\cdots\psi_{22};\mathbf{x}^{(N+1)}\cdots\mathbf{x}^{(A)}). \quad (2)$$

The spin and isotopic spin variables have been omitted in (2) for the sake of simplicity. It is understood that Ψ_0 depends on all the spin and isotopic spin variables of the core and Φ does not. Φ does depend on the spin and isotopic spin variables of the external nucleons. Equation (2) is considered to be a trial function in the variational principle

$$\delta(\Psi,H\Psi)\equiv\delta\mathcal{H}=0, \quad (3)$$

$$(\Psi,\Psi)=1, \quad (4)$$

where we keep Ψ_0 fixed and vary Φ. Instead of expressing the Hamiltonian

$$H=-\frac{1}{2M}\sum_{s=1}^{A}\nabla^{(s)2}+\tfrac{1}{2}\sum_{r\neq s}^{A}V_{rs} \quad (5)$$

in terms of the new variables ξ_α and ψ_{ik} we find it more convenient to replace the variable ξ_α in Ψ_0 by $\xi_\alpha(\mathbf{x}^{(1)}\cdots\mathbf{x}^{(N)})$ and treat Ψ_0 as a function of $\mathbf{x}^{(1)}\cdots\mathbf{x}^{(N)}$. We have then

$$\Psi(\mathbf{x}^{(1)}\cdots\mathbf{x}^{(A)})=\Psi_0(\mathbf{x})\Phi(\psi(\mathbf{x}),\mathbf{y}), \quad (6)$$

where $\mathbf{x}$ stands for $\mathbf{x}^{(1)}\cdots\mathbf{x}^{(N)}$, $\mathbf{y}$ for $\mathbf{x}^{(N+1)}\cdots\mathbf{x}^{(A)}$ and Ψ for the six independent components ψ_{ik}. The functional to be varied is

$$\mathcal{H}=\int d\mathbf{x}\int d\mathbf{y}(1/2M)\sum_{s=1}^{A}\nabla^{(s)}\Psi^*\cdot\nabla^{(s)}\Psi+\tfrac{1}{2}\sum_{r\neq s}\Psi^*V_{rs}\Psi. \quad (7)$$

We transform the kinetic energy according to the identity

$$\int d\mathbf{x}\int d\mathbf{y}\nabla^{(s)}\Psi^*\cdot\nabla^{(s)}\Psi=\int d\mathbf{x}\int d\mathbf{y}\times\{|\Psi_0|^2\nabla^{(s)}\Phi\cdot\nabla^{(s)}\Phi^*-|\Phi|^2\Psi_0^*\nabla^{(s)2}\Psi_0+(\Psi_0\nabla^{(s)}\Psi_0^*-\Psi_0^*\nabla^{(s)}\Psi_0)\cdot\Phi^*\nabla^{(s)}\Phi\}. \quad (8)$$

If there are no accidental degeneracies Ψ_0 must be invariant under time reversal.[10] In the absence of spin variables Ψ_0 would therefore be real. In general the nucleon density matrix formed with Ψ_0 is real after the trace with respect to the spin variables has been taken. Thus the last term in (8) vanishes. From the definitions of Φ and ψ it follows that for $s\leq N$,

$$\frac{\partial\Phi}{\partial x_k^{(s)}}=i\sum_{ij}\frac{\partial\psi_{ij}}{\partial x_k^{(s)}}\pi_{ij}\Phi, \quad (9)$$

where $\pi_{ij}\equiv-\frac{1}{2}i(1+\delta_{ij})\partial/\partial\psi_{ij}$. We note further that

$$\sum_{s=1}^{N}\sum_{k}\frac{\partial\psi_{ij}}{\partial x_k^{(s)}}\frac{\partial\psi_{lm}}{\partial x_k^{(s)}}=(1/2b)\{\delta_{il}\delta_{jm}+\delta_{im}\delta_{jl}+\psi_{il}\delta_{jm}+\psi_{im}\delta_{jl}+\psi_{jl}\delta_{im}+\psi_{jm}\delta_{il}\}. \quad (10)$$

We can write $\mathcal{H}$ in the form

$$\mathcal{H}=\int d\mathbf{x}\int d\mathbf{y}\int d\psi\delta(\psi-\psi(\mathbf{x}))\Big\{-\frac{1}{2M}\sum_{s=1}^{N}\times(\Psi_0^*\nabla^{(s)2}\Psi_0)|\Phi|^2+(1/2Mb)|\Psi_0|^2\sum_{ijk}(\delta_{ik}+2\psi_{ik})\times(\pi_{ij}\Phi)^*(\pi_{kl}\Phi)+(1/2M)\sum_{r=N+1}^{A}|\Psi_0|^2\times\nabla^{(r)}\Phi^*\cdot\nabla^{(r)}\Phi+\Psi_0^*\Phi^*\tfrac{1}{2}\sum_{r\neq s}^{A}V_{rs}\Psi_0\Phi\Big\}, \quad (11)$$

where $d\psi\equiv d\psi_{11}d\psi_{22}d\psi_{33}d\psi_{12}d\psi_{23}d\psi_{13}$. The ψ's are integration variables. $\psi(x)$ is defined by (1). The normalization integral is written accordingly

$$\int d\mathbf{x}\int d\mathbf{y}\int d\psi\delta(\psi-\psi(\mathbf{x}))|\Psi_0|^2|\Phi|^2=1. \quad (12)$$

Varying Φ for fixed Ψ_0 we obtain the Schrödinger equation for Φ.

$$(H_c+H_{\text{int}}+H_p-E)\Phi=0, \quad (13)$$

where H_c is the collective Hamiltonian of the core, H_p is the Hamiltonian of the external nucleons and H_{int} is the interaction between collective modes of the core and the external nucleons.

$$H_{\text{int}}=(1/D(\psi))\sum_{r>N}\sum_{s\leq N}\int d\mathbf{x}\delta(\psi-\psi(\mathbf{x}))\times\Psi_0^*V_{rs}\Psi_0-\sum_{r>N}V_p(\mathbf{x}^{(r)}), \quad (14)$$

where

$$D(\psi)=\int d\mathbf{x}\delta(\psi-\psi(\mathbf{x}))|\Psi_0|^2, \quad (15)$$

and

$$V_p(\mathbf{x}^{(r)})=(1/D(0))\sum_{s=1}^{N}\int d\mathbf{x}\delta(\psi(\mathbf{x}))\Psi_0^*V_{rs}\Psi_0 \quad (16)$$

is the potential energy of the rth external nucleon in

[10] E. P. Wigner, Gött. Nachr. 31, 546 (1932).

the field of the undeformed core.

$$H_p=-(1/2M)\sum_{r>N}\nabla^{(r)2}+\tfrac{1}{2}\sum_{r\neq r'>N}V_{rr'}+\sum_{r>N}V_p(\mathbf{x}^{(r)}). \quad (17)$$

The collective Hamiltonian H_c is

$$H_c=(1/2Mb)[1/D(\psi)]\sum_{ijk}\pi_{ij}(\delta_{jk}+\psi_{jk})D(\psi)\pi_{jk}$$
$$-[1/2MD(\psi)]\int d\mathbf{x}\delta(\psi-\psi(\mathbf{x}))\sum_{s=1}^{N}$$
$$\times\Psi_0^*\nabla^{(s)2}\Psi_0+\tfrac{1}{2}\sum_{s\neq s'}^{N}[1/D(\psi)]$$
$$\times\int d\mathbf{x}\delta(\psi-\psi(\mathbf{x}))\Psi_0^*V_{ss'}\Psi_0. \quad (18)$$

The normalization condition on Φ is

$$\int d\psi\int d\mathbf{y}D(\psi)|\Phi|^2=1. \quad (19)$$

In order to bring the collective Hamiltonian into a useful form we transform the Schrödinger equation (13) according to $D^{\frac{1}{2}}\Phi\to\Phi$, $D^{\frac{1}{2}}HD^{-\frac{1}{2}}\to H$ and use the operator identity:

$$D^{-\frac{1}{2}}\sum_{ijk}\pi_{ij}(\delta_{jk}+2\psi_{jk})D\pi_{ki}=D^{-\frac{1}{2}}\sum_{ijk}\pi_{ij}(\delta_{jk}+2\psi_{jk})\pi_{jk}D^{\frac{1}{2}}$$
$$-\sum_{ijk}(\delta_{jk}+2\psi_{jk})D^{-\frac{1}{2}}(\pi_{ij}\pi_{ki}D^{\frac{1}{2}})-\frac{1}{iD}(\sum_i\pi_{ii}D). \quad (20)$$

The parentheses in $(\pi_{ii}D)$ and similar expressions indicate that the differentiation operates only on D and not on anything else. H_p and H_{int} are not affected by this transformation.

$$H_c=T_c+V_c, \quad (21)$$

where

$$T_c=(1/2Mb)\sum_{ij}\pi_{ij}\pi_{ij}+(1/Mb)\sum_{ijk}\pi_{ij}\psi_{jk}\pi_{ki}, \quad (22)$$

and

$$V_c=-(1/2Mb)(\sum_{ijk}(\delta_{jk}+2\psi_{jk})D^{-\frac{1}{2}}(\pi_{ij}\pi_{ki}D^{\frac{1}{2}})$$
$$-iD^{-1}(\sum_i\pi_{ii}D))$$
$$-[1/2MD(\psi)]\int d\mathbf{x}\delta(\psi-\psi(\mathbf{x}))\sum_{s=1}^{N}\Psi_0^*\nabla^{(s)2}\Psi_0$$
$$+\tfrac{1}{2}\sum_{s\neq s'}^{N}D^{-1}(\psi)\int d\mathbf{x}\delta(\psi-\psi(\mathbf{x}))\Psi_0^*V_{ss'}\Psi_0. \quad (23)$$

We assume further that $|\psi_{ik}|\ll 1$ in regions where Φ is appreciably different from zero and expand in powers of ψ.

$$V_c(\psi)=\bar{V}_c+c_0\sum_i\psi_{ii}+\tfrac{1}{2}c'(\sum_i\psi_{ii})^2+\tfrac{1}{2}c\sum_{ij}\psi_{ij}^2. \quad (24)$$

$$H_{\text{int}}=-k'(\mathbf{y})(\sum_i\psi_{ii})-\sum_{r=N+1}^{A}k_r(\mathbf{y})\sum_{ij}\psi_{ij}$$
$$\times(x_i^{(r)}x_j^{(r)}-\tfrac{1}{3}|\mathbf{x}^{(r)}|^2\delta_{ij})|\mathbf{x}^{(r)}|^{-2}. \quad (25)$$

The constants c_0, c', and c are the expansion coefficients obtained by expanding (23) in powers of ψ. They are, of course, functionals of Ψ_0. Similarly k' and k are ψ-independent coefficients arising in the expansion of (14).

Our Hamiltonian can now be easily compared to that of Bohr if we introduce instead of the Cartesian components ψ_{ik} the trace $\bar{\psi}=\sum_i\psi_{ii}$ and the spherical tensor α_μ, $\mu=0,\pm1,\pm2$

$$\alpha_0=(4\pi/5)^{\frac{1}{2}}(\psi_{33}-\tfrac{1}{3}\bar{\psi}),$$
$$\alpha_{\pm1}=\mp(8\pi/15)^{\frac{1}{2}}(\psi_{31}\mp i\psi_{32}), \quad (26)$$
$$\alpha_{\pm2}=(8\pi/15)^{\frac{1}{2}}\{\tfrac{1}{2}(\psi_{11}-\psi_{22})\mp i\psi_{12}\}.$$

V_c, H_{int} and the first term of T_c in (22) are then separated in terms depending on $\bar{\psi}$ only and terms depending on the α's only. The latter are identical with Bohr's Hamiltonian for $\lambda=2$ if we define constants B and C as $B=(15/8\pi)Mb$ and $C=(15/8\pi)c$. The terms depending on $\bar{\psi}$ can also be derived from the liquid drop model for the core if one allows density fluctuations of the liquid.[11]

We have thus derived the Hamiltonian of Bohr's unified model from many particle quantum mechanics with the assumption (2). This derivation yields a correction term

$$(1/Mb)\sum_{ijk}\pi_{ij}\psi_{jk}\pi_{ki} \quad (27)$$

in the kinetic energy. As long as one treats the constants B, C, etc., as empirical parameters this term is the only new feature. However, from an appropriate assumption for Ψ_0 we can in principle arrive at an independent evaluation of these constants.

In investigating the same problem Tolhoek[8] uses collective coordinates $\alpha_{\lambda\mu}$ defined by

$$\alpha_{\lambda\mu}=(1/\lambda B_\lambda)\sum_{s=1}^{N}r^{(s)\lambda}Y_\lambda^\mu(\vartheta_s\varphi_s)^*, \quad (28)$$

and obtains exactly Bohr's Hamiltonian without correction terms of the form (27), [$\alpha_{2\mu}$ in (28) is the same as α_μ in (26)].[12] From (23) and (24), we see that D does not appear in the Hamiltonian except through the constants c and c'. Tolhoek's arbitrary restriction $D=1$ therefore does not affect the result as long as no attempt is made to calculate the strength of the restoring forces from (23).

[11] G. Wentzel, Lectures on Strong Coupling Meson Theory, Appendix, University of Rochester, 1954 (unpublished).

[12] Such correction terms are implicitly contained in Tolhoek's Eq. (5.12) but disappear in the reduction from (5.12) to (5.13).

III. SOLUTION OF THE SCHRÖDINGER EQUATION IN THE STRONG COUPLING APPROXIMATION

We wish to discuss the influence of the correction terms (27) in the strong coupling approximation. The approximations involved and the results in the lowest order are the same as those of Bohr[1-2] and Ford[13]; we find it convenient, however, to use different variables in which zero order wave functions can be written down in closed form.[14] In order to separate the vibrational and the rotational degrees of freedom we express the Hamiltonian in terms of the eigenvalues of ψ, q_1 q_2 q_3, and the Euler angles which specify the orientation of the principle axes of ψ. It is convenient to express the derivatives with respect to the Euler angles in terms of the components, Q_1 Q_2 Q_3, of the angular momentum of the core in the direction of the principle axes of ψ. They are related to the π_{ik} by

$$Q_\kappa = i\sum_{ik}[Q_\kappa,\psi_{ik}]\pi_{ik}. \tag{29}$$

$$\psi_{ik} = \sum_{\kappa=1}^{3} S_{i\kappa}S_{k\kappa}q_\kappa,$$

where $S_{i\kappa}$ is the orthogonal matrix which transforms ψ to principle axes. Since

$$\begin{aligned}[Q_\kappa,q_\kappa']&=0,\\ [Q_1,S_{k1}]&=0,\end{aligned} \tag{30}$$

$$[Q_1,S_{k2}] = -iS_{k3}, \tag{31}$$

and all cyclic permutations of (31), we have

$$\sum_{ik}S_{i3}S_{k3}\pi_{ik} = \tfrac{1}{2}(q_2-q_3)^{-1}Q_1. \tag{32}$$

With (32) we find the Hamiltonian in the new variables

$$\begin{aligned}H_c = &-(1/2Mb)\Bigg[\sum_{\kappa=1}^{3}\frac{\partial}{\partial q_\kappa}(1+q_\kappa)\frac{\partial}{\partial q_\kappa}\\ &+(q_3-q_1)^{-1}\left\{(1+2q_3)\frac{\partial}{\partial q_3}-(1+2q_2)\frac{\partial}{\partial q_2}\right\}\\ &+(q_3-q_1)^{-1}\left\{(1+2q_3)\frac{\partial}{\partial q_3}-(1+2q_1)\frac{\partial}{\partial q_1}\right\}\\ &+(q_1-q_2)^{-1}\left\{(1+2q_1)\frac{\partial}{\partial q_1}-(1+2q_2)\frac{\partial}{\partial q_2}\right\}\Bigg]\\ &+(1/4Mb)[(1+q_3+q_2)(q_3-q_2)^{-2}Q_1^2\\ &+(1+q_3+q_1)(q_3-q_1)^{-2}Q_2^2\\ &+(1+q_1+q_2)(q_1-q_2)^{-2}Q_3^2]\\ &+\tfrac{1}{2}c\sum_\kappa q_\kappa^2+\tfrac{1}{2}c'(\sum_\kappa q_\kappa)^2+c_0\sum_\kappa q_\kappa,\end{aligned} \tag{33}$$

The interaction Hamiltonian is

$$H_{\rm int} = -k'(\mathbf{y})\sum_\kappa q_\kappa - \sum_{r=N+1}^{A} k_r(y)\sum_{\kappa=1}^{3} q_\kappa(n_\kappa^{(r)2}-\tfrac{1}{3}), \tag{34}$$

where $\mathbf{n}^{(r)}\equiv\mathbf{x}^{(r)}/|\mathbf{x}^{(r)}|$. n_κ is the component of $\mathbf{n}$ in the direction of the "body fixed" axis κ.

For the sake of simplicity we shall assume only one external nucleon from now on. The discussion could easily be generalized to cover more nucleons. The strong coupling approximation is characterized by the assumption that Φ is an eigenstate of $\mathbf{I}^2$, I_3, $\mathbf{j}^2$, j_3 where $\mathbf{I}$ is the total angular momentum of the nucleus, $\mathbf{j}$ is the angular momentum of the external nucleon and I_3, j_3 are components in the direction of the "body fixed" 3-axis. Let K and Ω be the eigenvalues of I_3 and j_3 respectively. For the low-lying states $K=\Omega$. k' and k are replaced by constants $\bar{k}'$ and $\bar{k}$. The diagonal part of the Hamiltonian in this representation is

$$H = H_{\rm vib}^0 + H_{\rm vib}' + H_{\rm rot}, \tag{35}$$

where

$$\begin{aligned}H_{\rm vib}^0 = &-(1/2Mb)\Bigg[\sum_\kappa\frac{\partial^2}{\partial q_\kappa^2}+(q_3-q_2)^{-1}\left(\frac{\partial}{\partial q_3}-\frac{\partial}{\partial q_2}\right)\\ &+(q_3-q_1)^{-1}\left(\frac{\partial}{\partial q_3}-\frac{\partial}{\partial q_1}\right)\\ &+\frac{1}{(q_1-q_2)}\left(\frac{\partial}{\partial q_1}-\frac{\partial}{\partial q_2}\right)\Bigg]+\tfrac{1}{2}c\sum_\kappa q_\kappa^2\\ &+\tfrac{1}{2}c'(\sum_\kappa q_\kappa)^2+(c_0-\bar{k}')\sum_\kappa q_\kappa+\bar{k}(q_3-\tfrac{1}{3}\sum_\kappa q_\kappa)\\ &\times(3\Omega^2-j(j+1))[4j(j+1)]^{-1}.\end{aligned} \tag{36}$$

$H_{\rm vib}'$ is the vibrational part of the correction term (27)

$$\begin{aligned}H_{\rm vib}' = &-(1/Mb)\Bigg\{\sum_\kappa\frac{\partial}{\partial q_\kappa}q_\kappa\frac{\partial}{\partial q_\kappa}+(q_3-q_2)^{-1}\left(q_3\frac{\partial}{\partial q_3}\right.\\ &\left.-q_2\frac{\partial}{\partial q_2}\right)+(q_3-q_1)^{-1}\left(q_3\frac{\partial}{\partial q_3}-q_1\frac{\partial}{\partial q_1}\right)\\ &+(q_1-q_2)^{-1}\left(q_1\frac{\partial}{\partial q_1}-q_2\frac{\partial}{\partial q_2}\right)\Bigg\}.\end{aligned} \tag{37}$$

It is neglected in the following since it has no effect on the moment of inertia in our approximation. In order to retain it without inconsistency we would have to include third order terms from the potential energy. The rotational energy has the form

$$\begin{aligned}H_{\rm rot} = &\tfrac{1}{2}\mathcal{I}^{-1}\{I(I+1)-(K^2+\Omega^2)+j(j+1)\\ &-(-1)^{I-j}(j+\tfrac{1}{2})(I+\tfrac{1}{2})\delta_{\Omega 1}\delta_{\kappa 1}\}\end{aligned} \tag{38}$$

where the moment of inertia $\mathcal{I}$ is given by

$$\begin{aligned}\mathcal{I}^{-1} = &(1/4Mb)\{(1+q_3+q_2)(q_3-q_2)^{-2}\\ &+(1+q_3+q_1)(q_3-q_1)^{-2}\}.\end{aligned} \tag{39}$$

[13] K. Ford, Phys. Rev. **97**, 29 (1953).

[14] The mathematical procedures are very similar to those used by Wentzel, reference 11.

H_{vib}^0 is treated as the zero order Hamiltonian, H_{rot} is a perturbation. The variables in H_{vib}^0 can be separated by introducing q^0, q, and q' as follows

$$\begin{aligned} q^0 &= \textstyle\sum_\nu q_\nu, \\ q &= q_1 - \tfrac{1}{2}(q_1+q_2), \\ q' &= (3/8)^{\frac{1}{2}}(q_1-q_2). \end{aligned} \tag{40}$$

In these variables H_{vib}^0 is separated if q'^2 remains small compared to q^2 and can be neglected. We have then

$$\begin{aligned} H_{\text{vib}}^0 = &-(3/2Mb)\left\{\frac{\partial^2}{\partial q^{02}}+\tfrac{1}{3}\left(\frac{\partial^2}{\partial q^2}+\frac{2}{q}\frac{\partial}{\partial q}\right)\right. \\ &\left.+\tfrac{1}{4}\left(\frac{\partial^2}{\partial q'^2}+\frac{1}{q'}\frac{\partial}{\partial q'}\right)\right\}+\tfrac{1}{2}(c'+\tfrac{1}{4}c)q^{02} \\ &+(c_0-\bar{k}')q^0+\tfrac{1}{2}cq'^2+\tfrac{1}{2}cq^2 \\ &+\bar{k}[(3\Omega^2-j(j+1))/6j(j+1)]q. \end{aligned} \tag{41}$$

The eigenfunctions of this Hamiltonian are of the form

$$\Phi_{\text{vib}} = q^{-1}\chi(q)\chi'(q')\chi^0(q^0), \tag{42}$$

where the χ's are harmonic oscillator wave fuuctions. Since b was defined by the condition $\langle q^0\rangle = 0$ we must have $c_0 = \bar{k}'$. Our approximations require the following relations between the parameters: The expectation value $\bar{q}$ of q is

$$\bar{q} = (\bar{k}/c)[(j(j+1)-3\Omega^2)/4j(j+1)]. \tag{43}$$

Because of the expansion of the potential energy in powers of the q's all matrix elements of the q's must be small compared to one. We must have $|\bar{q}| \ll 1$ or $|\bar{k}/c| \ll 1$. The conditions $\langle q'^2\rangle \ll 1$, $(q-\bar{q})^2 \ll 1$ and $\langle q^{02}\rangle \ll 1$ imply

$$(Mbc)^{\frac{1}{2}} \gg 1, \tag{44}$$

and

$$[Mb(c+3c')]^{\frac{1}{2}} \gg 1. \tag{45}$$

The existence of a rotational spectrum requires that the vibration rotation interaction be small

$$\langle (q-\bar{q})^2\rangle \ll \bar{q}^2, \tag{46}$$

or

$$(Mbc)^{\frac{1}{2}} \gg c^2/\bar{k}^2. \tag{47}$$

From (47) follows $q'^2 \ll \bar{q}^2$ which was used above. If these relations hold the expectation value of the moment of inertia (39) can be written in the form

$$\begin{aligned} \langle \mathcal{I}^{-1}\rangle = (1/2Mb\bar{q}^2)\{1+\tfrac{1}{3}\bar{q} \\ +3\langle (q-\bar{q})^2\rangle \bar{q}^{-2}+2\langle q'^2\rangle \bar{q}^{-2}\}. \end{aligned} \tag{48}$$

The correction terms in (46) all decrease the moment of inertia. Neglected terms are of the order $\bar{q}^3$, $\langle q'^2\rangle^2\bar{q}^{-4}$ or smaller. In principle off-diagonal matrix elements of the Hamiltonian with respect to K and Ω contribute correction terms in second-order perturbation theory. It is easy to see, however, that their effect is small compared to the corrections given in (48).[15]

IV. DISCUSSION

It should be emphasized that our results are independent of detailed assumptions about the structure of the core. The structure of the collective Hamiltonian and the expression (48) for the moment of inertia do not depend on the internal wave function Ψ_0. The essential assumptions of our model are the definition (1) of the collective coordinates together with the separation of the wave function (2). Here as with the liquid drop model the deformations must be small enough to allow an expansion of the potential energy in powers of the deformation. This is necessary to arrive at any quantitative conclusions. The assumption of a small vibration-rotation interaction (46) appears inescapable where pure rotational spectra are observed. Not much progress can be expected from further investigation of Ψ_0 in the present model, since with the assumptions just stated one cannot hope to fit experimental moments of inertia and quadrupole moments no matter what Ψ_0 is. The reason for this lies probably in the fundamental assumptions (1) and (2). We notice in particular that our collective coordinates are additive in the nucleons of the core. Correlations between different nucleons in the core are therefore not included in the collective modes. Brueckner *et al.*[16] have pointed out that there is good experimental evidence for strong correlations. The magnitude of the experimental moments of inertia may also be evidence in favor of such correlations. An improvement of our model is being sought in two directions. (a) One may generalize the model to allow for a possible difference between charge and mass distribution in the core. (b) One can investigate alternative definitions of collective coordinates which would not be additive in the individual nucleons. One might, of course, also try to retain (1) and modify (2) as follows[17]:

$$\Psi = \Psi_0(\xi_1 \cdots \xi_{3N-6} q_1 q_2 q_3)\Phi(\varphi\vartheta\chi\mathbf{y}), \tag{49}$$

but then the model gives hardly any predictions without the full knowledge of Ψ_0.

I wish to thank Professor G. Wentzel for his continued interest in this problem and many helpful discussions.

[15] See A. Bohr, reference 1, Sec. V, 4.
[16] Brueckner, Eden, and Francis (preprint).
[17] See A. Bohr, reference 3, Appendix.

Energy Available for Beta Decay of Nd^{150}

BENJAMIN G. HOGG
Department of Physics, Royal Military College of Canada, Kingston, Ontario, Canada
(Received February 10, 1955)

A study of the beta-decay systematics at mass number 150 suggests that the mass-spectrographically determined $Nd^{150}-Sm^{150}$ difference of 4.6 ± 0.8 Mev is too high. If the recent value of $Pm^{150}-Sm^{150}=5.3\pm0.15$ Mev is used with a graphically estimated value of 4.0 Mev for the $Nd^{150}-Sm^{150}$ difference, then single beta decay of Nd^{150} is energetically impossible.

THE possibility of beta decay of Nd^{150} has been suggested by Kohman[1] and experimentally sought by Mulholland and Kohman.[2] No activity was found and a lower limit of 2×10^{15} years was placed on the half-life for such a decay.

Recently a measurement of the total energy of beta decay of Pm^{150} has been made,[3] giving a $Pm^{150}-Sm^{150}$ mass difference of 5.3 ± 0.15 Mev. The $Nd^{150}-Sm^{150}$ mass difference has previously been measured mass spectrographically,[4] and a value of 4.6 ± 0.8 Mev obtained. The large error in this last measurement precludes any final statement on the single beta decay of Nd^{150}, since as Mrs. Kistiakowsky Fischer points out,[3] the energy available for decay by this mode is now -0.7 ± 1.0 Mev or a maximum possible energy of decay of 0.3 Mev.

If one treats the beta-decay energy systematics in a manner similar to that of Way and Wood[5] and plots energy difference for double beta decay or the energy of two successive disintegrations against mass number A, then one obtains what appear to be straight lines. The resulting curve for the Nd–Sm nuclides plus the immediate neighbor curves for Ce–Nd and Sm–Gd, are shown in Fig. 1. The values which are used to construct these curves are taken from the compilation of King[6] and represent the best beta-decay data available. The two points, with errors indicated, are from the mass spectrographic data of Hogg and Duckworth. Except for the discontinuity at 82 neutrons in the Ce–Nd family all the lines are reasonably straight and depend little on whether the energy difference is for odd-A or even-A nuclides.

The $Nd^{150}-Sm^{150}$ energy difference at mass number 150 as read from the straight line is 4.0 Mev, which still

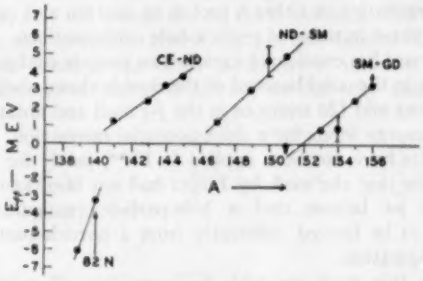

FIG. 1. The energies of two successive beta disintegrations are plotted against the mass number for three families. The circles are beta-decay data taken from reference 6 and the circles with errors are mass spectrographic values taken from reference 4. Arrows on the circles indicate that more energy is possible in such decays.

lies within the experimental error of the mass spectrographic value of 4.6 ± 0.8 Mev. If one considers this value of 4.0 Mev to represent the $Nd^{150}-Sm^{150}$ mass difference, and even if one allows an error as large as ±0.8 Mev, then the $Nd^{150}-Pm^{150}$ mass difference would now be -1.3 ± 1.0 Mev which leaves no possibility for the single beta decay of Nd^{150}.

[1] T. P. Kohman, Phys. Rev. **73**, 16 (1948).
[2] G. I. Mulholland and T. P. Kohman, Phys. Rev. **85**, 144 (1952).
[3] V. Kistiakowsky Fischer, Phys. Rev. **96**, 1549 (1954).
[4] B. G. Hogg and H. E. Duckworth, Can. J. Phys. **32**, 65 (1954).
[5] K. Way and M. Wood, Phys. Rev. **94**, 119 (1954).
[6] R. W. King, Revs. Modern Phys. **26**, 327 (1954).

Energy Levels of Pb^{208}

G. E. TAUBER
Department of Physics, Western Reserve University, Cleveland, Ohio
(Received February 21, 1955)

The various hole-particle configurations in the neighborhood of the doubly magic nucleus $Z=82$, $N=126$ have been investigated and applied to the excited states of Pb^{208}. For a particle-particle interaction of the form $V=(mP+nQ)V(|\mathbf{r}_1-\mathbf{r}_2|)$, where P denotes Majorana and Q Bartlett forces, the energy levels have been calculated in the L-S and j-j limit both for a delta-type and Gaussian potential with various ranges and compared with the experimental results.

I. INTRODUCTION

RECENT experimental work by Elliott[1] indicates that the excited states of Pb^{208} do not follow the simple $I=0, 2, 4$ rule found for most even-even nuclei,[2] but have spins ranging between 3 and 6 and odd parity. According to the shell model,[3] Pb^{208} is a doubly "magic" nucleus and its lowest excited levels would arise from the excitation of either a proton or neutron and could be treated in terms of particle-hole configurations.

Pryce[4] has considered various two particle configurations in the neighborhood of the double closed shell 82 protons and 126 neutrons in the j-j limit and obtained the energy levels for a delta-potential interaction. His results have not been applied to Pb^{208}, partly for the reason that the work by Elliott had not been known. Also we believe that a hole-particle configuration has to be treated differently from a particle-particle configuration.

In this work we wish to investigate all possible particle-hole configurations which could play a part in the excited states of Pb^{208}. A general particle-particle interaction of the form $V=(mP+nQ)V(|\mathbf{r}_1-\mathbf{r}_2|)$, where P denotes the Majorana and Q Bartlett forces, has been assumed and the energy levels in the L-S and j-j limit obtained for all possible configurations. Finally the energy levels have been calculated for both a delta-type and a Gaussian potential with various ranges. Comparing our results with the experimental data for the spins and energy levels of the excited states of Pb^{208} we are able to rule out certain configurations and determine the strengths of the others.

II. CONFIGURATION

From tables of shell structures[5] we find that the following hole-particle configurations are possible[6]:

(a) excitation of a neutron

$$3p_{1/2}^{-1}2g_{9/2},\ 3p_{1/2}^{-1}i_{11/2},\ 2f_{5/2}^{-1}2g_{9/2}, \tag{1}$$

(b) excitation of a proton

$$3s_{1/2}^{-1}1h_{9/2},\ 3s_{1/2}^{-1}2f_{7/2},\ 2d_{3/2}^{-1}1h_{9/2}. \tag{1a}$$

The corresponding L-S configurations and J-values are shown in Table I.

In order to calculate the L-S limit energies we make use of the theorem on nearly closed configurations,[7] according to which the direct integral of nearly closed configurations is simply the negative of the corresponding particle configurations apart from a constant term.[8] Applying the sum rule it is found that the triplet states are equal to the singlet ones

$$^3J=^1J=J. \tag{2a}$$

Most of the necessary results have been given in the literature,[9] and the others can readily be found with the help of Racah's formulas.[10] The Bartlett operator Q interchanges the spins, which in the case of hole-particle configurations (where one introduces the spin

TABLE I. J values and L-S states for various two-particle configurations.

Configuration	J	L-S states
$p_{1/2}g_{9/2}$	5	^3H ^1H ^3G
	4	^3H ^3G ^1G ^3F
$p_{1/2}i_{11/2}$	6	^3J ^3I ^1I ^3H
	5	^3I ^3H ^1H
$f_{5/2}g_{9/2}$	7	^3J ^1J ^3I
	6	^3J ^3I ^1I ^3H
	5	^3I ^3H ^1H ^3G
	4	^3H ^3G ^1G ^3F
	3	^3G ^3F ^1F ^3D
	2	^3F ^3D ^1D ^3P
$s_{1/2}h_{9/2}$	5	^3H ^1H
	4	^3H
$s_{1/2}f_{7/2}$	4	^3F
	3	^3F ^1F
$d_{3/2}h_{9/2}$	6	^3J ^3I ^1I ^3H
	5	^3I ^3H ^1H ^3G
	4	^3H ^3G ^1G ^3F
	3	^3G ^3F ^1F

[1] L. G. Elliott (unpublished communication).
[2] M. Goldhaber, Phys. Rev. **90**, 600 (1953).
[3] M. G. Mayer, Phys. Rev. **74**, 235 (1948); **75**, 1969 (1949); **78**, 16 (1950).
[4] M. H. L. Pryce, Proc. Phys. Soc. (London) **65**, 773 (1952).
[5] P. F. A. Klinkenberg, Revs. Modern Phys. **24**, 63 (1952).
[6] We exclude those which would give rise to positive parity. Strictly speaking the partially filled shells (in the L-S limit) should also be considered, such as $1h_{11/2}$, $1i_{13/2}$.
[7] E. U. Condon and G. H. Shortley, *The Theory of Atomic Spectra* (Cambridge University Press, Cambridge, 1951), Chap. 13.
[8] G. E. Tauber and T. Y. Wu, Phys. Rev. **94**, 1307 (1954).
[9] Reference 7, Chap. VII, and G. H. Shortley and B. Freed, Phys. Rev. **54**, 739 (1938).
[10] G. Racah, Phys. Rev. **61**, 186 (1942).

of the "missing" particle) results in the fact that all triplet states vanish and the singlet states are twice the value of the direct integral, as

$$^3Q+{}^1Q={}^3J+{}^1J=2J \qquad (2b)$$

from the sum-rule. For convenience sake we have summarized the ones we need (see Table I) in Table II. In the case of the exchange (Majorana) integrals, the effect of the spin is to make the triplet states equal to the singlet ones,

$$^3P={}^1P=P. \qquad (2c)$$

They can be calculated with the help of a simple formula,[11]

$$P=-g_LG^L,\ g_L=[(2l_1+1)(2l_2+1)/2L+1]C_{l_1l_2L} \qquad (3)$$

first given by Shortley,[12] and are summarized in Table III. The fact that there is this difference between particle and hole configurations makes us believe that

TABLE II. Energies in the *LS* limit for Bartlett (*Q*) interactions.

Configuration	State	*Q*	
pg	^1H	$-2F_0-56F_2$	$F_0=F^0$
	^1G	$-2F_0+154F_2$	$F_2=(1/385)F^2$
pi	^1I	$-2F_0+22F_2$	$F_0=F^0$
	^1H	$-2F_0-14F_2$	$F_2=(1/55)F^2$
fg	^1J	$-2F_0-280F_2-84F_4-8F_6$	
	^1I	$-2F_0+210F_2+406F_4+90F_6$	$F_0=F^0$
	^1H	$-2F_0+318F_2-578F_4-2150F_6$	$F_2=(1/1155)F^2$
	^1G	$-2F_0+188F_2-78F_4+1350F_6$	$F_4=(3/11\,011)F^4$
	^1F	$-2F_0-60F_2+598F_4-2340F_6$	$F_6=(1/11\,269.4)F^6$
	^1D	$-2F_0-230F_2+286F_4+2574F_6$	
sh	^1H	$-2F_0$	$F_0=F^0$
sf	^1F	$-2F_0$	$F_0=F^0$
dh	^1I	$-2F_0+66F_2+72F_4$	
	^1H	$-2F_0+70F_2-168F_4$	$F_0=F^0$
	^1G	$-2F_0+0F_2+182F_4$	$F_2=(1/273)F^2$
	^1F	$-2F_0-104F_2-78F_4$	$F_4=(1/819)F^4$

hole-particle configurations should be treated differently than particle-particle configurations and from first principles.

The transformation to the j-j limit then proceeds in the ordinary manner. The energy in the j-j limit in terms of the L-S energies is given by

$$E_J=\alpha^1E(J)+\beta^3E(J)+\gamma^1E(J+1)+\delta^1E(J-1), \qquad (4)$$

where the coefficients α, β, γ, and δ have been given by Racah[13] and again by Pryce.[4] The expressions occurring in our work are given in Table IV.

[11] Only alternate states, those with $L=l_1+l_2,\ l_1+l_2-2,\cdots |l_1-l_2|$ have nonvanishing G coefficient as $C_{l_1l_2L}$ vanishes if the triangular conditions $|l_1-l_2|\leq L\leq l_1+l_2;\ L+l_1+l_2=2g$ are not met.

[12] G. H. Shortley and B. Freed, reference 9.

[13] G. Racah, Physica **16**, 651 (1950).

TABLE III. Energies in the *LS* limit for Majorana (*P*) interactions.

Conf.	State		*P*
pg	$^3F=^1F$	$-12\,G_3$	$G_3=(1/49)G^3$
	$^3H=^1H$	$-15\,G_5$	$G_5=(1/121)G^5$
pi	$^3J=^1J$	$-7\,G_7$	$G_7=(1/75)G^7$
	$^3H=^1H$	$-18\,G_5$	$G_5=(1/121)G^5$
fg	$^3J=^1J$	$-49\,G_7$	$G_7=(1/429)G^7$
	$^3H=^1H$	$-180\,G_5$	$G_5=(1/1573)G^5$
	$^3F=^1F$	$-18\,G_3$	$G_3=(1/77)G^3$
	$^3P=^1P$	$-4\,G_1$	$G_1=(1/3)G^1$
sh	$^3H=^1H$	$-\,G_5$	$G_5=(1/11)G^5$
sf	$^3F=^1F$	$-\,G_3$	$G_3=(1/7)G^3$
dh	$^3J=^1J$	$-7\,G_7$	$G_7=(1/65)G^7$
	$^3H=^1H$	$-10\,G_5$	$G_5=(1/97)G^5$
	$^3F=^1F$	$-50\,G_3$	$G_3=(1/137)G^3$

III. ENERGY LEVELS

The contribution to the energy consists of three parts, *viz.*, the energy due to the interaction with the core, the spin-orbit interaction and the central interaction between the extra particles. As none of the parameters occurring is known, we are only able to

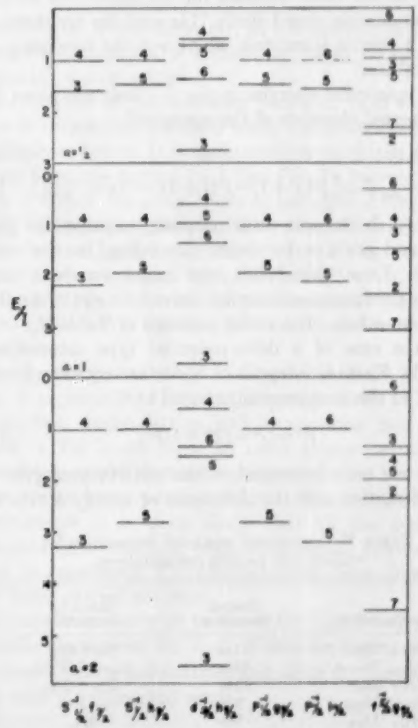

FIG. 1. Energy levels for delta-type potential. The levels are plotted in terms of the parameter I [Eq. (8)] for the various hole-particle configurations listed and for three values of a as indicated. The numbers indicate the spins of the levels (all having $-\pi r$ parity).

TABLE IV. Transformation of energies JJ to LS.

Configuration	J	
$p_{1/2}g_{9/2}$	5	$E_5=(5/15)\,{}^1E(5)+(6/15)\,{}^3E(5)+(4/15)\,{}^3E(4)$
	4	$E_4=(4/27)\,{}^1E(4)+(4/15)\,{}^3E(4)+(11/1215)\,{}^3E(5)+(140/243)\,{}^3E(3)$
$p_{1/2}i_{11/2}$	6	$E_6=(7/39)\,{}^1E(6)+(25/234)\,{}^3E(6)+(120/169)\,{}^3E(7)+(11/3042)\,{}^3E(5)$
	5	$E_5=(1/3)\,{}^1E(5)+(5/18)\,{}^3E(5)+(7/18)\,{}^3E(6)$
$f_{5/2}g_{9/2}$	7	$E_7=(3/7)\,{}^1E(7)+(24/49)\,{}^3E(7)+(4/49)\,{}^3E(6)$
	6	$E_6=(20/63)\,{}^1E(6)+(640/1323)\,{}^3E(5)+(15/637)\,{}^3E(7)+(56/351)\,{}^3E(5)$
	5	$E_5=(2/9)\,{}^1E(5)+(64/135)\,{}^3E(5)+(20/297)\,{}^3E(6)+(13/55)\,{}^3E(4)$
	4	$E_4=(1/7)\,{}^1E(4)+(16/35)\,{}^3E(4)+(26/315)\,{}^3E(5)+(20/63)\,{}^3E(3)$
	3	$E_3=(5/63)\,{}^1E(3)+(80/189)\,{}^3E(4)+(4/49)\,{}^3E(5)+(550/1323)\,{}^3E(3)$
	2	$E_2=(2/63)\,{}^1E(2)+(64/189)\,{}^3E(2)+(11/189)\,{}^3E(3)+(4/7)\,{}^3E(1)$
$s_{1/2}h_{9/2}$	5	$E_5=(5/11)\,{}^1E(5)+(6/11)\,{}^3E(5)$
	4	$E_4={}^3E(5)$
$d_{3/2}h_{9/2}$	6	$E_6=(7/55)\,{}^1E(6)+(3/110)\,{}^3E(6)+(120/143)\,{}^3E(7)+(9/1430)\,{}^3E(5)$
	5	$E_5=(13/55)\,{}^1E(5)+(39/550)\,{}^3E(5)+(819/1210)\,{}^3E(6)+(48/3025)\,{}^3E(4)$
	4	$E_4=(18/55)\,{}^1E(4)+(81/550)\,{}^3E(4)+(416/825)\,{}^3E(5)+(7/330)\,{}^3E(3)$
	3	$E_3=(2/5)\,{}^1E(3)+(3/10)\,{}^3E(3)+(3/10)\,{}^3E(4)$

make qualitative guesses and compare the results for the different configurations.

For a simple harmonic potential the energy is given by

$$E=h\nu(2n+l), \tag{5}$$

which, in our case, becomes for configurations with a neutron outside closed shells $11h\nu$ and $9h\nu$ for those in which a proton is excited, where ν is the frequency of the oscillator.

The spin-orbit energies in the j-j limit are given by the diagonal elements of the operator[14]

$$(A|H|A)=\sum\zeta_{nl}d_i\left[j^i(j^i+1)-l^i(l^i+1)-s^i(s^i+1)/2\right], \tag{6}$$

where ζ_{nl} is the spin-orbit coupling, negative for particles and positive for holes (according to the shell model). From this result one might conclude that certain configurations require lower energies of excitation than others. The result is shown in Table V.

In the case of a delta-potential type interaction, both the F and G integrals of Slater are equal and connected to the fundamental integral by[15]

$$F^k=G^k=(2k+1)F^0. \tag{7}$$

As we are only interested in the relative strengths of the interaction and the difference of energy levels we define two parameters

$$I=mF^0, \quad a=n/m, \tag{8}$$

and try to find a reasonable value for a to match the experimental data. (Of course I can also differ from configuration to configuration as F^0 depends on the radial wave function). The energy levels for the delta-type interaction are plotted for different values of a and configurations in Fig. 1.

For the Gaussian (or any other) potential and simple harmonic oscillating wave functions the generalized Slater integrals can be expressed in terms of Talmi integrals[16] defined by

$$I_l=N_l^2\int_0^\infty \exp(-\nu r^2)r^{2l+2}V(r)dr, \tag{9}$$

with the help of simple relations.[15] For a Gaussian type of potential, the Talmi integrals are given by[17]

$$I_l=V_0\left[\lambda^2/(1+\lambda^2)\right]^{l+\frac{1}{2}}, \tag{10}$$

where $\lambda=r_0\sqrt{\nu}$; r_0 is the range of the nuclear forces and ν is related to the range of the wave function. We have obtained the energy levels for three values of λ, *viz.*, $\lambda=\frac{1}{2}$, $\frac{3}{4}$ and 1 which roughly correspond to nuclear ranges of 1.0, 1.5, and 2.0×10^{-13} cm for an acceptable value of ν. The constants m and n have been obtained from free-nucleon scattering data,[17] and the energy levels for the three values of λ plotted in Fig. 2.

TABLE V. Central and spin orbit interactions for various hole particle configurations.

Configuration	Central interaction	Spin orbit interaction
$3p_{1/2}{}^{-1}2g_{9/2}$	$11h\nu$	$\zeta_{1p}+2\zeta_{1g}$
$3p_{1/2}{}^{-1}1i_{11/2}$	$11h\nu$	$\zeta_{1p}-(7/2)\zeta_{1i}$
$2f_{5/2}{}^{-1}2g_{9/2}$	$11h\nu$	$2\zeta_{1f}+2\zeta_{1g}$
$3s_{1/2}{}^{-1}1h_{9/2}$	$9h\nu$	$-3\zeta_{1h}$
$3s_{1/2}{}^{-1}1f_{7/2}$	$9h\nu$	$\frac{1}{2}\zeta_{1f}$
$2d_{3/2}{}^{-1}1h_{9/2}$	$9h\nu$	$\frac{1}{2}\zeta_{1d}-3\zeta_{1h}$

IV. COMPARISON WITH EXPERIMENTAL RESULTS

The energy levels obtained by Elliott are shown in Fig. 3. It is seen that the lowest excited level has a spin $I=3$, which might indicate that a proton is excited into an s or d state (see Figs. 1 and 2). That it is

[14] Reference 7, Chap. 10.
[15] I. Talmi, Helv. Phys. Acta **25**, 185 (1952).
[16] Reference 8, Appendix I. In applying those results they had to be generalized for $n\neq0$, as the radial wave function consists of several terms (see reference 15).
[17] G. E. Tauber and T. Y. Wu, Phys. Rev. **93**, 295 (1954), Table II.

more probable to excite a proton than a neutron may also be inferred from the fact that there is a difference of $2\hbar\nu$ in the central energy due to the core (see Table V). As none of the configurations contains all the levels present we have to assume that more than one configuration plays a role in the level scheme. In order to differentiate between the various configurations we might consider the spin-orbit interaction. Nothing is known *a priori* about the magnitude of the spin-orbit parameter ζ_{nl} except that it is negative and increases with increasing l and n. From this and the results in Table V it follows that $2d_{3/2}^{-1}1h_{9/2}$ is definitely lower than $3s_{1/2}^{-1}1h_{9/2}$ and may or may not be lower than $3s_{1/2}^{-1}1h_{9/2}$. Similarly, $3p_{1/2}^{-1}2g_{9/2}$ is lower than $3p_{1/2}^{-1}\times 1i_{11/2}$ and probably also lower than $2f_{5/2}2g_{9/2}$.

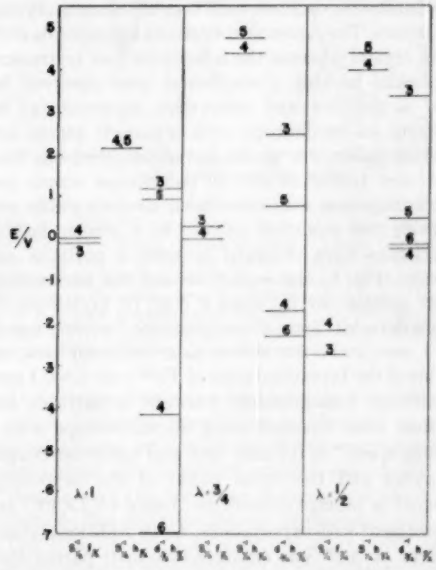

FIG. 2. Energy levels for Gaussian potential. The levels are plotted in terms of the parameter V_0 [Eq. (10)] for the various hole-particle configurations listed and for three values of λ as indicated. The numbers indicate the spins of the levels (all having $-\pi$ parity).

Thus in the case of the delta-potential interaction between the extra particles (Fig. 1) a possible scheme would be:

$$\begin{aligned} I=3:&\quad d_{3/2}h_{9/2},\\ I=5:&\quad s_{1/2}h_{9/2}\quad\text{or}\quad p_{1/2}g_{9/2},\\ I=4:&\quad s_{1/2}h_{9/2}\quad\text{or}\quad p_{1/2}g_{9/2},\\ I=5:&\quad d_{3/2}h_{9/2},\\ I=6:&\quad d_{3/2}h_{9/2}, \end{aligned} \tag{11}$$

with a ratio of n/m of the order of 2. The strength of the interaction can then be determined by fitting the

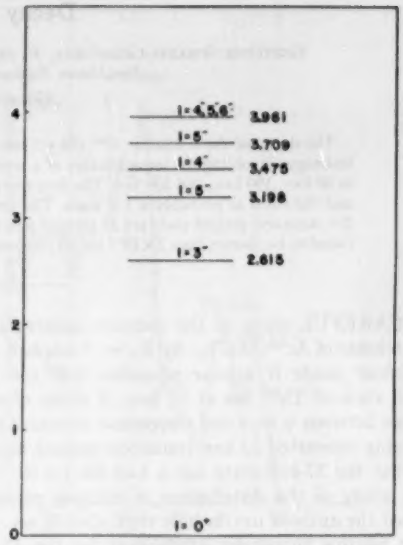

FIG. 3. Energy levels of Pb^{208} (according to Elliott). Energy levels are given in Mev and spins and parity indicated.

experimental levels. However, as the number of undetermined parameters is sufficiently large, no new information can be gained.

In the case of the Gaussian potential (and for the type of interaction assumed here) the situation is not as simple as before. It is again possible to obtain as the lowest level one having $I=3$ (see Fig. 2), but not possible to obtain the other levels in the right order. This might indicate that the Gaussian potential is not the one to be used here, but a different, say, a Yukawa type potential as suggested by Lee-Whiting[18] or that the particular type of interaction and constants assumed, while applicable to light nuclei[17] are not the ones to be used here.

In the light of all this, we can conclude in stating that it is possible to obtain the energy levels of Pb^{208} for certain configurations and interactions, but that based on the levels alone an exact evaluation of the parameters would be meaningless, due to the fact that there are so many parameters and all could be fitted. Furthermore it is quite likely that all the possible configurations enter and that configuration interaction must be considered. Calculations along these lines are now being carried out here.

In conclusion we wish to thank Dr. Lee-Whiting for valuable discussions, Dr. L. G. Elliott for letting us see his results before publication, and Miss A. Dranse for help with the numerical work.

[18] We are indebted to Dr. Lee-Whiting for private communications on this point.

Decay of U^{232} (74 yr)*

GERTRUDE SCHARFF-GOLDHABER, E. DER MATEOSIAN, G. HARBOTTLE, AND M. MCKEOWN
Brookhaven National Laboratory, Upton, New York

(Received March 11, 1955)

The decay of the α emitter U^{232} (74 yr) was studied by means of γ-ray scintillation counters and by a technique involving the impregnation of a scintillating crystal with this source. Excited states were found at 60 kev, 190 kev, and 330 kev. The first two are interpreted as rotational states of character 2+ and 4+ and the third as probably a 1− state. The branching ratio for transitions from the 330-kev state to the 2+ state and ground state are 57 percent and 43 percent respectively. The half-life of the 60-kev state was found to be shorter than 2×10^{-8} sec, in contrast to earlier reports based on a study of the β^- decay of Ac^{228}.

A CAREFUL study of the complex disintegration scheme of Ac^{228}($MsTh_2$) by Kyles, Campbell, and Henderson[1] made it appear plausible that the first excited state of Th^{228} lies at 57 kev. A study of coincidences between γ rays and conversion electrons from the highly converted 57-kev transition seemed to indicate that the 57-kev state has a half-life $\tau>10^{-7}$ sec, and a study of the distribution of electron pulses in time led the authors to conclude that $\tau>0.01$ sec.

The relative conversion coefficients for the 57 kev transition in the L_I, L_{II}, and L_{III} shells determined by Brodie[2] identify this transition as $E2$ if interpreted on the basis of Rose's[3] recent results on L conversion coefficients. This spin and parity assignment and also the energy fit well into the pattern of first excited states of even-even nuclei.[4] However, an $E2$ transition of this energy is expected to be faster even than a one-particle transition ($\tau<10^{-8}$ sec).

Recently Dunlavey and Seaborg[5] reported that a highly converted γ ray of about 60 kev follows the α emission of U^{232} in 31 percent of all disintegrations. It seems probable that this transition is identical with that following the β decay of Ac^{228}, and therefore we chose U^{232}, with its presumably very simple disintegration scheme, to search for the half-life of the first excited state of Th^{228}. As a first step we incorporated, by a method previously described,[6] a small amount of the U^{232} source[7] (kindly supplied by Dr. M. H. Studier of the Argonne National Laboratory) into a NaI(Tl) crystal which was then attached to a photomultiplier tube. If the 60-kev transition had a half-life $\tau>1$ μsec, which is the resolving time of the crystal, we would have observed pulses corresponding to conversion electrons from this transition, in addition to the α-ray pulses. No such pulses were observed, implying that $\tau<1$ μsec. We also prepared a U^{232} source mounted on 1 mg/cm² pliofilm and studied coincidences between two scintillation counters with thin anthracene crystals as detectors. The conversion electrons impinged directly on the crystal whereas the α particles had to traverse the pliofilm backing. Coincidences were observed between α particles and conversion electrons (a) by triggering an oscilloscope with α-particle pulses and observing pulses due to the conversion electrons from the 57-kev transition on the oscilloscope screen and (b) by triggering with conversion electron pulses and observing the α-particle pulses. In a similar fashion coincidences were observed between α particles and L x-rays (Fig. 1) and α particles and the unconverted 60-kev gamma ray by using a NaI(Tl) crystal as the photon detector. Since the oscilloscope "writing speed" was 1 μsec/inch, the above data indicated that the half-life of the 1st excited state of Th^{228} was $<\sim0.1$ μsec. Coincidence measurements between α particles and electrons were repeated using an oscilloscope with a "writing speed" of 0.2 μsec/inch and again the triggering pulses and the signal pulses of the oscilloscope appeared in prompt coincidence, hence $\tau<2\times10^{-8}$ sec, in agreement with expectations. As an additional check, a source of Ac^{228} was separated from its parent Ra^{228}

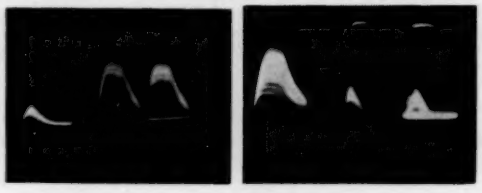

(a) (b)

FIG. 1. $\alpha-L$ x-ray coincidences in U^{232}. (a) The first pulse reading from left to right is the L x-ray pulse from detector 1 with which the oscilloscope is triggered during the coincidence run. The second pulse is self-triggered and shows α-particle pulses in detector 2. The third pulse is the α-particle pulse in detector 2 shown while the oscilloscope was being triggered by the L x-ray pulse of detector 1. (b) The roles of the α and L x-ray pulses were reversed and again the first pulse shows the triggering pulse (α particle in detector 2), the second pulse shows the L x-rays in detector 1, self-triggered, and the third pulse shows coincidences between the triggering pulse and the signal (L x-ray in detector 1).

* Work performed under the auspices of the U. S. Atomic Energy Commission.

[1] Kyles, Campbell, and Henderson, Proc. Phys. Soc. (London) **A66**, 519 (1953).

[2] W. D. Brodie, Proc. Phys. Soc. (London) **A67**, 265 (1954).

[3] Rose, Goertzel, and Swift (private communication).

[4] G. Scharff-Goldhaber, Phys. Rev. **90**, 587 (1953); P. Stähelin and P. Preiswerk, Nuovo cimento **10**, 1149 (1953).

[5] D. C. Dunlavey and G. T. Seaborg, Phys. Rev. **87**, 165 (1952).

[6] Scharff-Goldhaber, der Mateosian, Goldhaber, Johnson, and McKeown, Phys. Rev. **83**, 480 (1951).

[7] The U^{232} sources were separated from their decay products immediately before use. The samples contained, however, a 30-fold excess (in weight) of U^{233}.

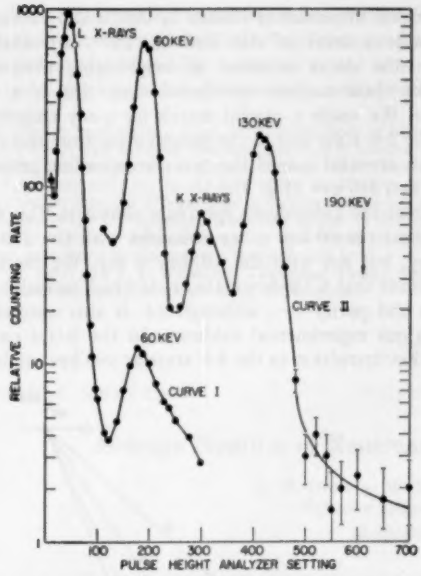

FIG. 2. Photon spectrum of U^{232} ($E \leq 200$ kev). Curve I, taken with a 1 cm^3 NaI(Tl) crystal with a Be window, shows the relative intensities of the 60-kev gamma rays and L x-rays. Curve II was taken with a (3 $cm)^3$ NaI(Tl) crystal. It shows the relative intensities of the 60-kev and 130-kev gamma rays and the K x-rays. The bump on the right side of the 60-kev peak in curve I was due to Bi K x-rays accompanying the decay of Pb^{212}, a daughter product of U^{232}. This residue of Pb^{212} was removed from the source by a repurification before Curve II was taken.

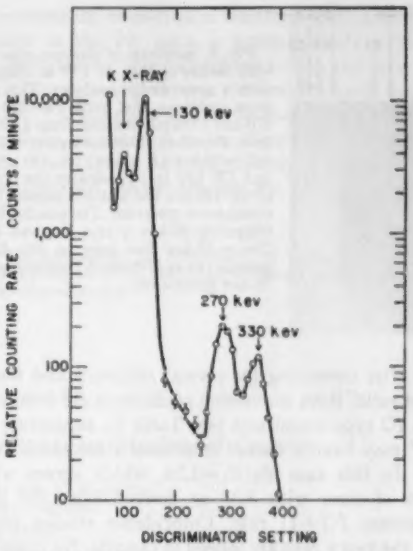

FIG. 3. Photon spectrum of U^{233} ($E \leq 400$ kev). Two well-resolved gamma rays are seen at 270 kev and 330 kev in addition to K x-rays and the 130-kev gamma ray. This run was made with the (3 $cm)^3$ NaI(Tl) crystal and a source of U^{233} which had been repurified to reduce the concentration of daughter products in the sample. The 159-, 239-, and 320-kev gamma-ray lines of Te^{123}, Pb^{212}, and Cr^{51}, respectively, were used to calibrate the energy scale.

and coincidences were observed between β particles and L x-rays; from this experiment we obtained an upper limit of 0.2 μsec for the lifetime of any electromagnetic transition strongly converted in the L shell. Since most of the L x-rays are due to the conversion of the 57-kev transition, this supports the results obtained with U^{232}.

The complete photon spectrum of the U^{232} source was investigated with a NaI(Tl) scintillation counter equipped with a single-channel pulse-height analyzer (Figs. 2 and 3). In the low-energy region unconverted γ rays of 60 ± 3 kev were seen as well as strong L x-rays, some K x-rays, and 130-kev gamma rays (Fig. 2). Assuming that practically all of the L x-rays are due to the conversion of the 60-kev transition, and applying a factor of 0.50 for the L-shell fluorescence yield,[8] we obtain a value of 120 for the L conversion coefficient of the 60-kev transition. We further find for the K conversion coefficient of the 130-kev transition a value of

TABLE I. Internal conversion coefficients and transition probabilities of γ rays from U^{233}.

Energy of γ rays (kev)	Assumed character of transition	Obs. rel. intensities of unconverted γ rays	Conversion coefficients[a] α_K	α_L	α_M	α_{tot}	Computed rel. int. of transitions	No. of transitions per 100 α's
60	$E2$	*1.00*	···	97 120[c]	32[b]	129	130	32
130	$E2$	0.51	0.36 0.38[c]	2.40	0.8[b]	3.56	2.3	0.57[d]
270	$E1$	0.037	0.035	0.005	···	0.04	0.039	0.0096
330	$E1$	0.028	0.022	0.003	···	0.025	0.029	0.0070

[a] Extrapolations of data in tables privately circulated by Rose *et al.* (reference 3).
[b] α_M was estimated to be $\frac{1}{4}$ of α_L. This agrees with measurements made by Brodie (reference 2).
[c] Experimentally determined values. See text.
[d] After these experimental results had been obtained, it was learned from a report by Rasmussen (reference 13) that Asaro, Stephens, and Perlman (private communication), by investigating the α spectrum of U^{233}, had also observed a 190-kev level. The α branch leading to this level was found to be 0.3 per 100 α's, in fair agreement with our result.

[8] B. B. Kinsey, Can. J. Phys. **A26**, 404 (1948).

FIG. 4. Spectrum of photons coinciding with 60-kev γ rays of U^{232} as displayed with a gray wedge analyzer. This spectrum indicates that both the 330- and 270-kev γ transitions arise from a 330-kev level. Prominent lines are seen at ~35 kev (a), ~90 kev (K x-rays) (c), 130 kev (d), and 270 kev (e); f indicates the position of the 330-kev line which is missing in the coincidence spectrum. The position of the triggering 60-kev γ rays is given by b. The ~35-kev line may be the 42-kev gamma ray of U^{232} which coincides with a 56-kev gamma ray.

0.38 after correcting for crystal efficiency and fluorescence yield. Both conversion coefficients are compatible with $E2$ type transitions (see Table I), suggesting that Th^{228} may have a second rotational state (4+) at 190 kev. In this case $E_2/E_1=3.16$, which agrees within limits of error with 3.33 as derived from the Bohr-Mottelson $I(I+1)$ rule. Coincidence studies proved that the two γ rays are indeed in cascade. No cross-over gamma ray of 190-kev energy was seen; had it been present to the extent of 1 percent of the unconverted 130-kev transitions, it would have been detected.

The ratio of the unconverted gamma rays $N_{\gamma 130}:N_{\gamma 60}\approx 1:2$. If one uses the theoretical conversion coefficients for $E2$ transitions and the latest value[9] for the percentage of α transitions going to the ground state (68 percent), one finds that per 100 α transitions there are 32 transitions of 60 kev and 0.57 transitions of 130 kev. The details of the calculations are given in Table I.

These two transitions seem to be identical with the 56.75- and 127.5-kev transitions, respectively, observed by Kyles and collaborators[1] in the decay of Ac^{228}. These authors also observed a 184.2 kev transition, identified as $M1$, on the basis of its K/L ratio, with an intensity ~1.2 times that of the 127.5-kev transition. It was assumed to be the cross-over transition from the second excited state of Th^{228}. Our results concerning the missing cross-over transition in the decay of U^{232} (<1 percent of 130-kev transitions) show that the 184.2-kev line is not the cross-over transition from the second excited state.

TABLE II. Alpha-branching ratios for U^{232}.

α energy (Mev)	Decay prob. (10^{-11} sec^{-1})	Theoretical branching ratio (without spin correction) R_T	Experimental branching ratio R_E	Experimental forbiddenness factor R_E/R_T	Theoretical spin correction factor
5.318[a]	8.3	0.680[a]	0.680	1	1 ($l=0$)
5.258	3.8	0.310	0.314	1	0.64 ($l=2$)
5.128	0.62	0.0505	0.0057	0.11	0.23 ($l=4$)
4.988	0.086	0.0070	0.00017	0.24	0.8 ($l=1$)

[a] See reference 9.

[9] F. Asaro and I. Perlman, Revs. Modern Phys. **26**, 456 (1954).

Recent unpublished studies by Asaro and Perlman[10] indicate a level of 330 kev in Th^{228}. By analogy with the decay schemes of neighboring even-even nuclei these authors concluded that this is a 1− state. We made a careful search for γ-ray transitions to the 2+ state and to the ground state from this level which revealed indeed the two corresponding peaks of 270 and 330 kev (Fig. 3).

From the coincidence spectrum shown in Fig. 4 we see that the 60-kev γ ray coincides with the 270-kev γ ray, but not with the 330-kev γ ray. We therefore conclude that a 330-kev state exists which probably has spin and parity 1−, although 2+ is also compatible with our experimental evidence. In the latter case a 140-kev transition to the 4+ state at 190 kev might be

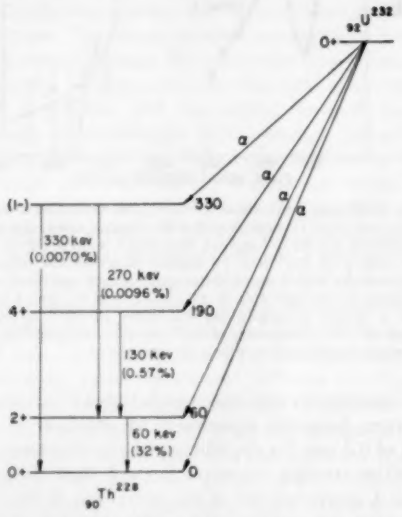

FIG. 5. Proposed disintegration scheme of U^{232}. The spin assignments of the 60-kev and 190-kev states are based on the measured internal conversion coefficients, whereas the spin assignment of the 330-kev state is tentatively made following Stephens, Asaro, and Perlman's systematics. (See reference 10.) However, an assignment of 2+ for this state is also compatible with the experimental evidence. From the experimentally determined relative intensities the number of transitions per alpha particle (in percent) were computed by using the value reported by Dunlavey and Seaborg (see references 5 and 9) for the 60-kev transition.

expected. A weak transition of this energy cannot be excluded on the basis of our experiments, since it would be masked by the 130-kev γ ray. The relative intensities of the 330- and 270-kev γ rays are $I_{\gamma 330}/I_{\gamma 270}=0.76$. The data used for the calculation of the absolute transition probabilities, assuming that both transitions are $E1$ transitions, are given in Table I. It follows that 57 percent of the transitions from this level go to the 2+ state and 43 percent to the ground state.[11]

[10] See Stephens, Asaro, and Perlman, Phys. Rev. **96**, 1568 (1954).

[11] It seems worthwhile mentioning here that H. B. Box and G. S. Klaiber [Phys. Rev. **95**, 1247 (1954)], who studied the

In Table II, α-particle branching ratios derived from theoretical transition probabilities[12] are compared with the experimental branching ratios calculated from the observed γ-ray intensities. In agreement with previous observations on even-even α emitters the α transition intensity to the 2+ state is approximately equal to that predicted by theory without taking the spin correction into account, whereas the transitions to the 4+ state and 1− state are reduced by factors 0.11 and 0.24 respectively, in contrast to the theoretical spin correction factors 0.23 and 0.84 respectively.[13]

The proposed decay scheme for U^{233} is shown in Fig. 5.

unconverted γ rays emitted from Ac^{229}, found lines of 278 and 336 kev, which they assigned to transitions from a 336-kev level to the first excited state and ground state of Th^{229}. However, their Fig. 3 indicates that in the Ac^{229} decay the 336-kev line is much stronger than the 278-kev line, in contrast to the intensity ratio found in the U^{233} spectrum. This may be due to the superposition of a 347-kev line corresponding to a transition from a 404 kev, postulated by the authors, to the 57-kev level.

[12] J. M. Blatt and V. F. Weisskopf, *Theoretical Nuclear Physics* (John Wiley and Sons, Inc., New York, 1952), p. 575.

[13] J. O. Rasmussen, Jr., University of California Radiation Laboratory Report UCRL-2431 (unpublished), and E. L. Church, private communication.

PHYSICAL REVIEW VOLUME 99, NUMBER 1 JULY 1, 1955

Average Number of Neutrons per Spontaneous Fission of Cm^{244}†

G. H. Higgins, W. W. T. Crane, and S. R. Gunn
Radiation Laboratory, Livermore, California

(Received February 28, 1955)

The average number of neutrons per fission, ν, for Cm^{244} has been measured by the manganous sulphate moderator-absorber system. The value 2.60 ± 0.11 has been determined.

A SAMPLE of Cm^{244} was purified by ion-exchange techniques and electroplated on a platinum foil of about 20 cm^2 area. The foil was rolled tightly and the heat output from it was measured calorimetrically. The calorimeter used was of the steady-state resistance bridge type used at the Mound Laboratory.[1] The accuracy of the present measurement was about one percent. A small portion of the original sample was pulse analyzed and the fraction of Cm^{242} was measured and the total heat output was corrected for the contribution from this source. From the alpha disintegration energy and half-lives for alpha emission and spontaneous fission,[2] the number of fissions in the sample was determined.

The number of neutrons emitted from the sample was determined by placing it at the center of a tank containing a saturated solution of manganous sulphate. After the Mn^{56}, which was produced by the capture of a neutron by Mn^{55}, was in equilibrium with the neutrons from the sample, the activity in the solution was determined with an immersion counter. The efficiency of the tank and counter system was measured by finding the ratio of counter events to neutrons from several calibrated polonium-beryllium sources. Since the tank was infinitely large to the polonium-beryllium neutron spectrum, no correction for spectral differences was necessary.

Corrections were made for the contribution to the number of neutrons from the spontaneous fission of Cm^{242}, using the value of $\nu=3.0\pm0.3$ determined by Barclay and Whitehouse.[3] This correction amounted to about 0.8 percent. An upper limit for the contribution from neutrons produced by the alpha particles on low-Z elements was determined by preparing a sample of Cm^{242} in the same manner and measuring an apparent ν in the same system. The value determined was 3.68, as compared with 3.0 measured by coincidence methods, and since the ratio of decay by alpha emission to decay by spontaneous fission is about twenty-five times larger for Cm^{242} than for Cm^{244}, and the energy of the alpha particles emitted by Cm^{244} is about 0.4 Mev lower than those of Cm^{242}, the error introduced from this source is estimated as about one percent. While the precision of the measurements is ±1 percent, the accuracy of the standards may be in error by as much as 3 percent.

We are deeply indebted to S. G. Thompson for supplylng the source material and wish to express our thanks to J. Harper and L. Mann for their help with the electronic equipment.

† This work was performed under the auspices of the U. S. Atomic Energy Commission.

[1] Eichelberger, Jordan, Orr, and Parks, Atomic Energy Commission Declassified Document AECD-3515 (unpublished) and other Mound Laboratory reports.

[2] Hollander, Perlman, and Seaborg, Revs. Modern Phys. **25**, 469 (1953).

[3] F. R. Barclay and W. J. Whitehouse, Proc. Phys. Soc. (London) **A66**, 447 (1953).

Bombardment Energy and Fission Product Yield Pattern for Protons on Natural Uranium and U^{235}

W. H. Jones,* A. Timnick,† J. H. Paehler, and T. H. Handley
Oak Ridge National Laboratory, Oak Ridge, Tennessee

(Received October 25, 1954; revised manuscript received March 14, 1955)

Relative fission yields of ten nuclides produced by proton-induced fission of natural uranium and U^{235} were determined at several proton energies in the range 12 to 20 Mev. The expected trend toward symmetric fission at increased energies is observed. A statistical relation is used to correlate this shift in fission symmetry with the excitation energy of the compound nucleus.

A NUMBER of investigations in recent years[1–7] support the conclusion that symmetric fission is increasingly favored at higher excitation energies of the compound nucleus. This laboratory has previously reported a preliminary study[8] of the influence of bombardment energy on the proportions of Mo^{99}, Ag^{111}, and Ba^{140} formed during proton-induced fission of uranium. Those results led to a more extensive series of experiments, including the work on natural uranium[9] and U^{235}, herewith described, and similar studies now in progress on U^{233}, Th^{232}, and Th^{230}.

The target assembly, Fig. 1, consists of four foils of natural uranium, or two foils of electrodeposited U^{235}, each about 25×6 mm in size, interleaved with calculated thicknesses[10] of aluminum to form a stack. One bombardment was also made with two foils of electrodeposited natural uranium. The thickness of the pure natural uranium foil was 11 mg/cm², while the thickness of the electrodeposited natural uranium and the U^{235} was of the order of 4 mg/cm². Special purity aluminum was used as a base for the deposits. The foil stack was attached inside the target head against the 11-mil-thick aluminum window, directly in contact with the cooling water. This head was then positioned to intercept the internal proton beam near the maximum radius of the 86-inch fixed-frequency proton cyclotron.[11] The usual bombardment was 100 μa for an hour. Detuning of the beam was helpful in avoiding "burning" and crumbling of the uranium foils.

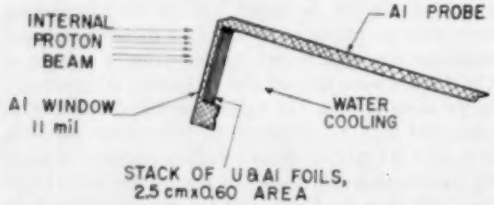

FIG. 1. Target assembly for proton bombardment of uranium foils.

The beam energy was determined in separate bombardment runs by producing the (p,n) and $(p,2n)$ reactions of Cu^{63} in a stack of copper foils.[11] Computation from known excitation curves[12] and the range-energy relations[10] for protons in copper gave 20.5±1.0 Mev as the beam energy. The energy of the protons reaching each uranium foil in the target stack was calculated from the beam energy thus established and the range-energy curves in aluminum and uranium. For bombardments of pure natural uranium, the first three foils were arranged to receive energies of ~18, 15, and 12 Mev, respectively, while the fourth foil was set beyond the proton range as a check on neutron fission background. For the electrodeposited natural uranium and U^{235}, two foils were arranged to receive energies of 20 and 16 Mev in a series of bombardments. In another series of bombardments of two foils of electrodeposited U^{235}, the first foil received 12 Mev, while the second was set beyond the proton range. The neutron fission background proved insignificant.

After the activity induced by a given bombardment run was allowed to diminish overnight, the target was disassembled and, in the case of the pure natural uranium, each foil was dropped into an individual flask containing nitric acid and silver as a carrier (the latter because of its strong absorption on glass). When dissolution was complete, the contents were diluted to 100 ml, and measured aliquots were used for determination, by radiochemical and counting methods, of the relative amount of each of the chosen fission products. The electrodeposited natural uranium and U^{235} foils were dropped into individual beakers containing nitric acid and warmed until active effervescence ceased. Each resulting solution was decanted, with its rinsings, to a volumetric flask.

* Research Participant from Emory University, Emory University, Georgia.
† On leave from Michigan State College, East Lansing, Michigan, 1952.
[1] P. R. O'Connor and G. T. Seaborg, Phys. Rev. **74**, 1189 (1948).
[2] A. S. Newton, Phys. Rev. **75**, 17 (1949).
[3] R. H. Goeckermann and I. Perlman, Phys. Rev. **76**, 628 (1949).
[4] R. W. Spence, U. S. Atomic Energy Commission Report AECU-645 (1949) (unpublished).
[5] A. Turkevich and J. B. Niday, Phys. Rev. **84**, 52 (1951).
[6] H. A. Tewes and R. A. James, Phys. Rev. **88**, 860 (1952).
[7] J. S. Wahl, Phys. Rev. **95**, 126 (1954).
[8] Fowler, Jones, and Paehler, Phys. Rev. **88**, 71 (1952).
[9] Tentative results presented at the 1953 Washington meeting; Jones, Paehler, Handley, and Timnick, Phys. Rev. **91**, 486 (1953).
[10] Aron, Hoffman, and Williams, U. S. Atomic Energy Commission Report AECU-663 (1949) (unpublished).
[11] R. S. Livingston, Nature **170**, 221 (1952).
[12] S. N. Ghoshal, Phys. Rev. **80**, 939 (1950); Blaser, Bohm, Marmier, and Peaslee, Helv. Phys. Acta **23**, 3 (1950).

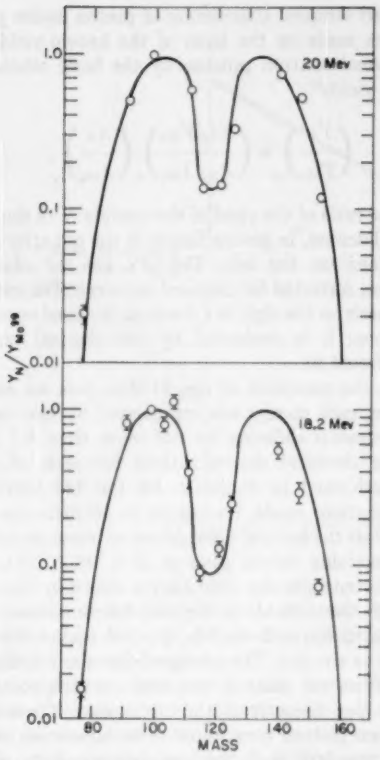

FIG. 2. Relative fission yields for natural uranium, 20 and 18.2 Mev.

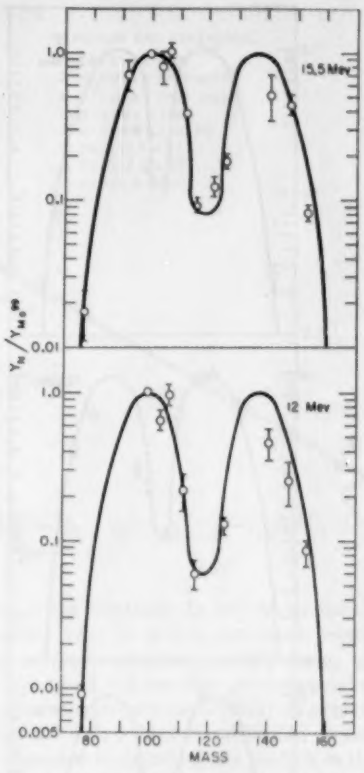

FIG. 3. Relative fission yields for natural uranium, 15.5 and 12 Mev.

On the basis of considerations of medium half-life, suitable intervals of mass, and practicability of the chemistry involved, the isotopes selected were, As^{77}, Y^{91}, Mo^{99}, Ru^{103}, Ag^{111}, Cd^{115}, Sn^{125}, Ba^{140}, Nd^{147}, and Sm^{153}. For most of these, the chemical procedures used were no departure from the standard methods described by Meinke,[13] the exceptions being molybdenum and the rare earths. For molybdenum, the ether extraction steps proved both tedious and inefficient; the use of silver nitrate as a final precipitant has been criticized.[14] The method adopted employs repeated α-benzoin-oxime[15] precipitations, a combination of scavenging operations, and final precipitation with lead nitrate.

The insoluble fluorides of the rare earths were isolated from the other elements present, then redissolved in a mixture of boric acid and concentrated nitric acid. After several scavengings,[16] the rare earths were precipitated as hydroxides, dissolved in hydrochloric acid and the solution introduced onto a column of Dowex-50 cation exchange resin, 250–500 mesh. This column, some 2 cm in diameter and 90 cm long, was maintained at 100°C by a steam jacket, after the design of Ketelle and Boyd.[17] A 5 percent solution of citric acid, kept sterile with a little phenol and adjusted very carefully with ammonia to *p*H 3.40, was used as the eluant. At this operating temperature an eluant throughput of 150 ml per hour was achieved by placing the reservoir two floors above the exchange column and reinforcing all connections. The receiving vessels were placed on a turntable controlled by an interval timer so set that each consecutive vessel received the column output for 30 minutes. Once routinized, this installation would dependably separate overnight the yttrium, samarium, and neodymium, in that order. Each was then precipitated as the oxalate, and the precipitate washed, transferred, and ignited to the oxide.

All precipitates in this work were bonded into stainless steel planchets by the addition of a trace of

[13] W. W. Meinke, U. S. Atomic Energy Commission Report AECD-2738 (1949) (unpublished).

[14] N. E. Ballou *Radiochemical Studies: The Fission Products* (McGraw-Hill Book Company, Inc., New York, 1951), Paper No. 257, National Nuclear Energy Series, Plutonium Project Record Vol. 9, 1538.

[15] Another point not adequately made in the literature is the apparent instability of the 2 percent alcoholic solution of α-benzoin-oxime used as precipitant. Old solutions precipitate very poorly; two weeks is suggested as the age limit for this reagent.

[16] Reference 14, p. 1673.

[17] B. H. Ketelle and G. E. Boyd, J. Am. Chem. Soc. **69**, 2800 (1947).

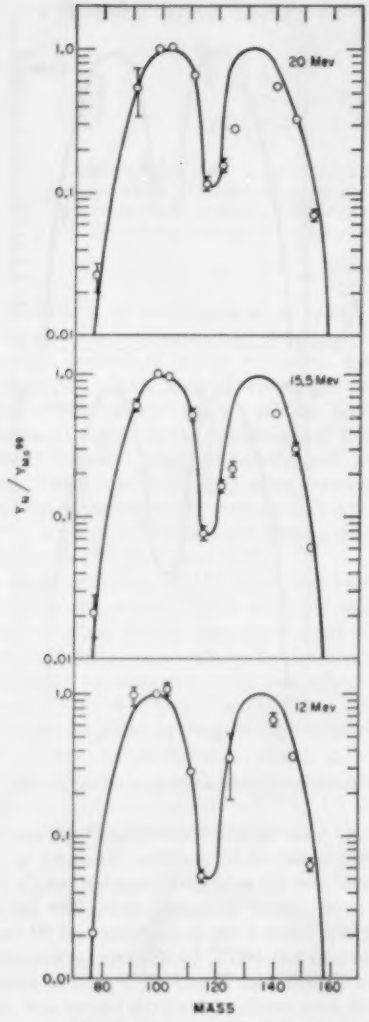

FIG. 4. Relative fission yields for uranium-235, 20, 15.5, and 12 Mev.

shellac to the alcohol used in transferring. These planchets were filed by number and their activities were counted at intervals of one, three, or seven days, over a period of several half-lives. For the most part, the resulting log-rate plots showed insignificant contamination, and the curves could be extrapolated to zero time with confidence. Mixed half-lives were involved in only three cases: Ru^{103}(40 day) *vs* Ru^{106}(365 day); Cd^{115}(54 hr) *vs* Cd^{115}(43 day); and Sn^{123}(27 hr) *vs* Sn^{132}(130 day) *vs* Sn^{125}(10 day).

As a basis for yield calculations, thermal neutron runs were made by exposing similar uranium foils in a nuclear reactor, followed by radiochemical and counting operations identical with those used for the cyclotron-irradiated samples. Calculation of proton fission yields was then made on the basis of the known yields[18] of the thermal neutron process, by the basic relation of relative yields[19]

$$\left(\frac{Y_N}{Y_{Mo}}\right)_p = \left(\frac{Y_N/Y_{Mo}}{A_N/A_{Mo}}\right)_n \left(\frac{A_N}{A_{Mo}}\right)_p.$$

Here the ratio of the yield of the nuclide N to the yield of molybdenum, in proton fission, is the quantity being determined on the left. The A's are the observed activities, corrected for chemical recovery. The complex parenthesis on the right is a constant for fixed operating conditions; it is evaluated by the thermal neutron runs referred to.

With the exception of the 20-Mev data on natural uranium, each energy was represented by two to four bombardments differing by not more than 0.7 Mev, and the chemical determinations for each of these were performed in duplicate. Of the 183 individual determinations made, the results in 16 instances were rejected on the basis of unexplained extreme deviations. The remaining values gave at 20.0, 18.2, 15.5, and 12.0-Mev energies the yield curves shown in Figs. 2–4, in which the ordinate is the molybdenum-based yield ratio found for each nuclide, plotted against its mass number as abscissa. The average difference of individual values from the mean is indicated for each point if it exceeds the diameter of the circle used. These mean deviations plotted were found to be approximately 0.8 of the standard deviation, as determined by checks made in a number of representative cases. The fit of

TABLE I. Fission product yields, percent.

Natural uranium					Uranium-235			
Mass	Proton energy, Mev				Mass	Proton energy, Mev		
	20	18.2	15.5	12		20	15.5	12
75;161	0.02	0.02	0.02	0.01	75;159	0.04	0.03	0.03
77;159	0.09	0.07	0.08	0.05	77;157	0.12	0.09	0.09
79;157	0.23	0.19	0.16	0.13	79;155	0.23	0.18	0.20
81;155	0.39	0.39	0.32	0.28	81;153	0.42	0.34	0.37
83;153	0.62	0.71	0.59	0.51	83;151	0.69	0.61	0.68
85;151	0.95	1.11	1.04	1.04	85;149	1.01	0.92	1.16
87;149	1.43	1.65	1.70	1.71	87;147	1.52	1.37	1.92
89;147	1.94	2.37	2.39	2.38	89;145	1.90	1.97	2.55
91;145	2.50	3.02	3.00	3.32	91;143	2.47	2.51	3.51
93;143	3.01	3.66	3.70	4.04	93;141	3.00	3.03	4.09
95;141	3.52	4.04	4.21	4.66	95;139	3.59	3.47	4.35
97;139	4.07	4.36	4.49	5.02	97;137	4.08	3.89	4.39
99;137	4.63	4.64	4.68	5.18	99;135	4.48	4.18	4.39
101;135	4.63	4.64	4.68	5.13	101;133	4.48	4.18	4.26
103;133	4.54	4.50	4.49	4.77	103;131	4.48	4.06	4.00
105;131	4.44	4.32	4.07	4.04	105;129	4.44	3.72	3.34
107;129	4.12	3.90	3.56	3.11	107;127	4.08	3.26	2.77
109;127	3.66	3.06	3.00	2.23	109;125	3.63	3.20	2.09
111;125	2.73	1.81	1.68	1.14	111;123	2.91	2.13	1.25
113;123	1.13	0.52	0.51	0.47	113;121	1.79	0.68	0.29
115;121	0.64	0.45	0.41	0.32	115;119	0.51	0.31	0.23
117;119	0.62	0.42	0.39	0.31	117;117	0.51	0.31	0.23
118;118	0.61	0.42	0.39	0.31				

[18] Reference 14, Appendix B, p. 2003.
[19] Reference 14, Part V, 1368 (1951).

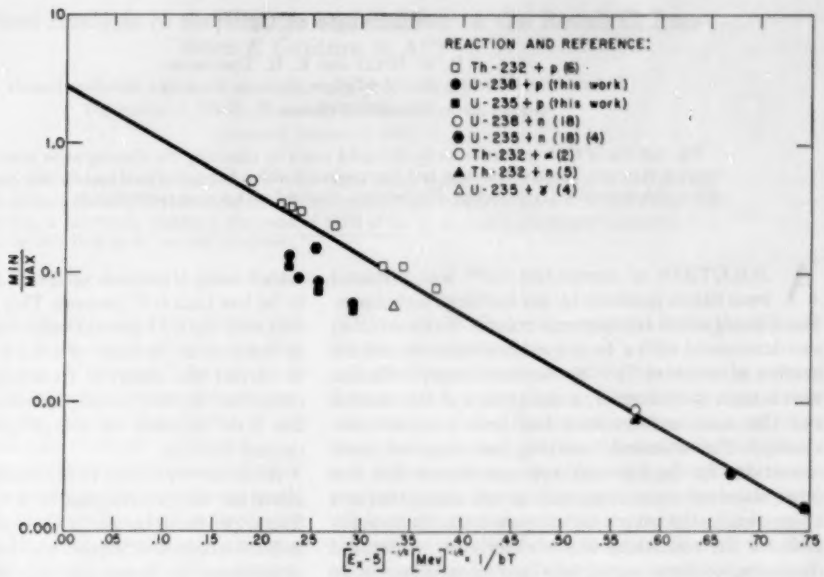

FIG. 5. Fission symmetry as a function of excitation energy.

these points is not always good, as seen, but it is considered that the yield distribution picture at these energies is fairly represented.

In completing these curves the assumptions of symmetric yield and no fine structure were adhered to. Mirror points, though not shown on the completed figures, were equally weighted in their construction, with the curves reflected on mass 118 for natural uranium, and on 117 for U^{235}. With mirror points omitted, partial failure of the above assumptions seems suggested; these assumptions have nevertheless been retained on the basis of inconclusive evidence to the contrary.

For percentage yields, the yield ratios from each of these curves were summed over the complete range from mass 75 to the midpoint. A factor was determined for bringing this total to 100 percent, and each curve was converted from yield ratios to percentage yields by applying its factor. From the resulting curves (not shown), Table I was obtained by reading for the odd mass numbers the percentage yields thus averaged.

A statistical approach to the fission process[8,20] predicts how the relative mass distribution changes with nuclear excitation energy. For interpreting along these lines the observed trend toward symmetric fission at higher energies, the relation plotted in Fig. 5 was formulated. Here the logarithmic ordinate is the minimum-to-maximum yield ratios, as taken from both our work and from other nuclear fission reactions as recorded in the literature. In setting up the abscissa, the quantity (E_x-5) is first evaluated, where E_x is the sum of the bombarding particle energy plus the energy with which it is bound in the compound nucleus. The binding energies are calculated from semiempirical mass tables.[21] The 5 Mev is subtracted as being the energy expended in distorting the nucleus to the point of fission; this value correlates with the γ-ray fission threshold of about 5 Mev. The square root of this (E_x-5) is thus of the nature of nuclear temperature, and the abscissa, with its negative exponent, is proportional to the reciprocal temperature of the distorted nucleus. When the proportionality constant is evaluated on the basis of energy level densities as estimated by Weisskopf,[22] the straight line as drawn corresponds to the relation

$$Y_{\min}/Y_{\max} = 2.8 \exp[-2.9/T].$$

Since the relative probability of two states differing in energy by an amount ΔE is $\exp[-\Delta E/T]$, it is thus suggested that 2.9 Mev is the additional energy required to produce symmetrical, in preference to asymmetrical fission.

The authors wish to acknowledge the original suggestions and continued interest of J. L. Fowler of this Laboratory. Authors W. H. Jones and A. Timnick are grateful for the opportunity of participating in this cooperative program.

[20] P. Fong, Phys. Rev. **89**, 332 (1953).

[21] N. Metropolis and G. Reitwiesner, U. S. Atomic Energy Commission Report NP-1980, 1950 (unpublished).

[22] V. F. Weisskopf (private communication to J. L. Fowler).

Half-Life of Cs^{137}†

D. M. WILES AND R. H. TOMLINSON
Department of Chemistry, Hamilton College, McMaster University, Hamilton, Canada
(Received February 28, 1955)

The half-life of Cs^{137} was found to be 26.6±0.4 years by observing the disintegration rate of a known number of atoms. The disintegration rate was measured with a 4π proportional counter and the number of atoms was determined from isotope dilution data obtained with a mass spectrometer.

A SOLUTION of carrier-free Cs^{137} was prepared from fission products by ion exchange techniques. The disintegration rate per unit volume of this solution was determined with a 4π proportional counter and the number of atoms of Cs^{137} by means of isotope dilution with a mass spectrometer; a description of the counter and the mass spectrometer has been reported previously.[1] The observed counting rate required small corrections for background and coincidence loss but other standard corrections such as self-absorption and absorption in the source mount were found to be negligible for the conditions of this experiment. A detailed discussion of these corrections has been given in an earlier paper[1] on the half-life of Sr^{90}.

Additional corrections to the measured counting rates were necessary in the case of Cs^{137}. In its decay scheme the gamma radiation from the isomeric state of Ba^{137} (2.6-min half-life) is not in coincidence with the beta emission. Hence the observed counting rates were corrected for the contribution of conversion electrons and for secondary electrons produced by the gamma radiation. The correction for the conversion electrons was made assuming 92 percent decay to metastable Ba^{137} [2] and an internal conversion coefficient of 0.118.[3] In order to correct for secondary electrons the gamma-radiation efficiency of the brass proportional counter was estimated using aluminum sandwich techniques and found to be less than 0.27 percent. This compares reasonably well with the 0.15 percent value obtained from the data of Bradt *et al.*[4] A value of a 0.2 percent has been used to correct the observed counting rate and, since the correction is itself small, an uncertainty in its value has little influence on the probable error of the calculated half-life.

TABLE I. Concentration and counting rate values for Cs^{137} solution.

Concentration in μg per ml	Counts per sec per ml ×10⁻³ [a]
0.0310	1.298
0.0315	1.305
0.0320	1.307
0.0311	1.297
0.0314	1.303
av 0.0314±0.0004	1.300
	1.308
	av 1.303±0.004
Corrected for internal conversion electrons and for secondary electrons	1.174±0.004
Corrected for Cs^{134} contribution	1.139±0.004

[a] Corrected for coincidence loss and background.

A further correction to the counting rate was made to allow for the contribution of 2.3-year Cs^{134} formed in fission products by an (n,γ) reaction with Cs^{133}. Two sodium iodide scintillation spectrometers were used in coincidence to determine this contamination of the sample. With these spectrometers, the coincidence rate due to the 0.605- and 0.796-Mev cascade gamma rays of Cs^{134} was compared under conditions of known geometry with the single-channel counting rate due to the 0.661-Mev gamma ray of Cs^{137}. The ratio of these rates, together with the latest decay schemes,[2,5] gives a correction of 3.0±0.5 percent to the observed beta activity.

From the data in Table I a value of 26.6±0.4 years is obtained for the half-life of Cs^{137}, where the limits of precision include only the uncertainties in the counting rate and concentration determinations. This is considerably lower than the currently accepted value of 33±2 years[6] calculated from comparison of the mass spectrometric ratios of Cs^{133}/Cs^{137} in fission products differing up to 5.4 years in age. More recent studies of similar ratios have been made in this laboratory with fission products up to 8 years old and these results give a half-life of 26±1 years.[7] Any variation in the relative yields of the samples compared by this method would materially affect the calculated half-life. Both the 26- and 33-year values were obtained by comparison of different fission-product samples and hence depend on the assumption that changes in the relative fission yields due to different irradiation conditions are small. Nevertheless it is felt that the 26-year value based on completely independent measurements does support the 26.6-year half-life found in this investigation.

The authors are grateful to Dr. M. W. Johns and I. R. Williams for their co-operation in making the scintillation spectrometer studies.

† This research was supported financially by the National Research Council of Canada and the Research Council of Ontario.
[1] D. M. Wiles and R. H. Tomlinson, Can. J. Phys. **33**, 133 (1955).
[2] L. M. Langer and R. J. D. Moffat, Phys. Rev. **82**, 635 (1951).
[3] M. A. Waggoner, Phys. Rev. **80**, 489 (1950).
[4] H. Bradt *et al.*, Helv. Phys. Acta. **19**, 77 (1946).
[5] Keister, Lee, and Schmidt, Phys. Rev. **97**, 45 (1955).
[6] Wiles, Smith, Horsley, and Thode, Can. J. Phys. **31**, 419 (1953).
[7] Melaika, Parker, Petruska, and Tomlinson (unpublished).

Theoretical Analysis of the Charge Distribution on the Recoil Cl Ions from K Capture in A^{37}†

R. A. RUBENSTEIN* AND J. N. SNYDER
Department of Physics, University of Illinois, Urbana, Illinois

(Received January 5, 1955)

An analysis of the charge spectrum of the recoil Cl ions which result from K capture in A^{37}, recently measured by Kofoed-Hansen, is made using recently computed Auger transition rates. It is shown that this charge spectrum, a previously measured fluorescence yield of 0.1 in Cl, and a previously measured K/L capture ratio of 0.92/0.08 in A^{37} are not consistent.

KOFOED-HANSEN has recently investigated[1] the distribution-in-charge of the recoil chlorine ions from the nuclear reaction $A^{37}+e^- \rightarrow Cl^{37}+\nu$ (K or L capture). The refined experimental techniques used permitted observation of the relative abundances of the variously charged recoil ions (Column A, Table I).

Recent measurements by Snell and Pleasonton[2] agree with Kofoed-Hansen's results in that doubly or quadruply charge ions seem to occur about half as frequently as triply charged ions. However, a preliminary estimate of the number of single-charged ions occurring appears to be less than that found by Kofoed-Hansen.

According to Kofoed-Hansen, 65±5 percent of the captures are accompanied by a K-series Auger electron. Since the K-series fluorescence yield of chlorine is about 0.1,[3] initial K vacancies in the recoil atoms are about 90 percent efficient for the production of such electrons. Hence, the above observation implies that a fraction $p_K \sim 0.65/0.9 \sim 0.75$ of the chlorine atoms are formed with a vacancy in the K-shell.

However, Pontecorvo, Kirkwood, and Hanna[4] have reported that the reaction in question proceeds by K capture with probability ~0.92. If this be so, then a fraction 0.17 of the recoil atoms with K-vacancies ($0.92-0.75 \sim 0.17$) are unaccounted for in the Kofoed-Hansen experiment.

TABLE I. Distribution-in-charge of the recoil chlorine ions.

Charge on final ion	A Experimental relative abundance[b]	Theoretical relative abundances for various distributions of initial vacancies in the recoil atom[a]: B $0.75K$ $0.25L_I$	C $0.75K$ $0.08L_I$ $0.17L_{II,III}$	D $0.92K$ $0.08L_I$
1	0.26±0.03	0.10	0.27	0.11
2	0.13±0.04	0.31	0.13	0.16
3	0.38±0.04	0.39	0.39	0.49
4	0.18±0.02	0.15	0.15	0.18
5	0.04±0.01	0.04	0.04	0.05
6	0.01±0.01	0.00	0.00	0.00
Average charge	2.64±0.08	2.69	2.50	2.87

[a] See reference 9.
[b] See reference 1.

A possible process that might account for the missing K-vacancies by transferring them into L-vacancies is "shake-up". If the K capture occurs in a time short compared to atomic periods, the electronic wave function (which was an eigenfunction appropriate to the original nuclear charge) cannot change appreciably and will have the same shape after the capture. However, it will not be an eigenfunction appropriate to the new nuclear charge but will be instead some linear combination of such eigenfunctions. One of these eigenfunctions represents the residual atom with an L-vacancy rather than a K-vacancy. Order of magnitude estimates of the probability of this effect render it highly suspect as an explanation of the missing K-vacancies. In the first place, present theoretical estimates of such a process[5,6] are too small to account for such a large fraction of the events. In the second place, even if such shake-up did occur, the electron captures in question would have been indistinguishable from L captures in the Pontecorvo, Kirkwood, and Hanna (PKH) experiment, and would have been reported as such, since the energy given up by the atom during shake-up is carried off by the neutrino and the recoil ion which thus have energies appropriate to L rather than K capture.

The above discrepancy between the PKH measurements and the Kofoed-Hansen experiment further manifests itself in the latter's distribution-in-charge. The appearance of multiply charged chlorine ions in that experiment is due to the reorganization of the atom with an original K- or L-vacancy formed in the nuclear reaction by subsequent Auger effects,[7,8] each Auger process contributing one unit of positive charge to the final ion.

A new theoretical treatment of the Auger effect[9] using the techniques available with modern high-speed digital computers has been carried out for argon ($Z=18$), krypton ($Z=36$), and silver ($Z=47$). A Hartree self-consistent field method was used to obtain better approximations to the electronic wave functions in atoms

† Assisted in part by the Office of Naval Research.
* Now at Shell Development Company, Houston, Texas.
[1] O. Kofoed-Hansen, Phys. Rev. **96**, 1045 (1954).
[2] A. H. Snell and F. Pleasonton, Phys. Rev. **97**, 246 (1955).
[3] Broyles, Thomas, and Haynes, Phys. Rev. **89**, 715 (1953).
[4] Pontecorvo, Kirkwood, and Hanna, Phys. Rev. **75**, 982 (1949).
[5] J. S. Levinger, Phys. Rev. **90**, 11 (1953).
[6] A. Migdal, J. Phys. (U.S.S.R.) **4**, 423 (1914).
[7] M. L. Perlman and J. A. Miskel, Phys. Rev. **91**, 899 (1953).
[8] E. P. Cooper, Phys. Rev. **61**, 1 (1942).
[9] R. A. Rubenstein and J. N. Snyder (to be published).

TABLE II. Transition probabilities in argon calculated from theory.[a]

$P_r(K\rightarrow L_{II,III})=0.122$	$P_r(K\rightarrow M)=0.009$
$P(K\rightarrow L_I^2)=0.061$	$P(K\rightarrow L_I M)=0.032$
$P(K\rightarrow L_I L_{II,III})=0.199$	$P(K\rightarrow L_{II,III}M)=0.082$
$P(K\rightarrow L_{II,III}^2)=0.498$	$P(L_I\rightarrow L_{II,III}M)=1.00$
$P(L_{II,III}\rightarrow M^2)=1.00$	

Probabilities marked with the subscript r represent radiative transitions. All others are Auger processes. K stands for a vacancy in the K shell, L_I for a vacancy in the L_I shell, $L_{II,III}$ for a vacancy in either the L_{II} or L_{III} shell, and M for a vacancy in any M shell.

[a] See reference 9.

with vacancies. With these wave functions the matrix elements for Auger transitions and radiative transitions were computed.

The results of these computations have been expressed in Table II as a list of probabilities for the several transitions. Each entry is the ratio of the transition rate for the given process to the total rate for *all* processes originating in the same level. Only the important transitions are shown in Table II.

The resulting set of Auger and radiative transition probabilities makes it possible to compute the relative probability of occurrence of the different charged ions that can arise as a result of Auger cascades starting from either an initial K-vacancy or an initial L-vacancy. Column D of Table I gives the charge distribution to be expected if the initial vacancy distribution is $0.92K$, $0.08L_I$ as measured by PKH. This is inconsistent with Kofoed-Hansen's observed charge distribution.

However, it can be argued from the Kofoed-Hansen data and from reasonable assumptions about the atomic reorganization process, that the above discrepancy cannot be explained simply by a reassignment of the L/K ratio such as to yield K capture with 75 percent probability, L capture with 25 percent probability, i.e., that the unexplained 17 percent of the recoil ions could not have been formed in a state with an L_I-vacancy as would necessarily have been the case were they products of L-capture reactions (the subscript indicates in which subshell of the L shell the vacancy occurs). The recent theoretical investigation[9] of the Auger effect shows that it is reasonable to assume:

(1) Almost every L_I-vacancy is filled by a Coster-Kronig transition[10] of the type $L_I\rightarrow L_{II,III}M$, in which an L_I-vacancy is destroyed while an M-vacancy and either an L_{II}- or an L_{III}-vacancy is created with the ejection of an Auger electron. The matrix element for this transition is anomalously large compared with ordinary Auger transitions because of considerable overlap between the $2s$ and $2p$ electronic functions.[9,10] This transition is energetically allowed in chlorine,[8] and the assumption that it occurs with unit probability is borne out by the excellent agreement of the theoretical with the experimental abundance for triply and quadruply charged ions (Table I, columns A, B, and C). If this assumption were incorrect, the theory would lead to underestimate of these abundances.

(2) Every $L_{II,III}$-vacancy is filled by an Auger process, since radiation rates are much smaller than Auger transition rates in the L shell.

(3) No mechanism exists whereby an M-vacancy may be filled by an Auger process.[11]

The above arguments are relatively insensitive to the numerical values of the theoretically computed Auger transition rates; if they be granted, then a chlorine atom which is formed with an L_I- or $L_{II,III}$-vacancy will always lead to a doubly- (or singly-) charged final ion.

Thus, if the K and L captures occur with relative probability 0.75 and 0.25, respectively, then one would expect to observe doubly-charged ions with *at least* 0.25 probability since L capture involves only the L_I electron. (The theoretical distribution based on an L/K ratio of 0.25/0.75 is shown in Table I, column B.) Kofoed-Hansen observes doubly-charged ions only 13 percent of the time.

The Kofoed-Hansen experiment agrees well with the theory if one assumes that all of the extra 17 percent of the recoil atoms lead to singly-charged final ions (e.g., if they are formed with an $L_{II,III}$-vacancy). This case is shown in Table I, column C.

It can therefore be concluded that the Kofoed-Hansen experiment seems to contradict the earlier PKH measurement of the L/K ratio; on the other hand, a simple revision of this ratio is not in itself sufficient to explain the observed distribution-in-charge of the final ions.

[10] E. H. S. Burhop, *The Auger Effect* (Cambridge University Press, Cambridge, England, 1952).

[11] The possibility that surface effects in Kofoed-Hansen's apparatus may have degraded some of the higher charged ions into lower charged ones has been neglected.

Manganese Thermal Neutron Activation Cross Section

J. DeJuren and J. Chin
National Bureau of Standards, Washington, D. C.
(Received March 17, 1955)

The thermal activation cross section of manganese has been remeasured and found to be $\sigma_{act}=13.1_9\pm0.3_9$ barns (standard error). This value, combined with previous values, yields a "best average value" of $13.2_7\pm0.2$ barns.

BECAUSE of its characteristic response to neutrons, manganese is often used for the calibration of thermal neutron densities. The precision of absolute calibrations is limited by the experimental error (2.2 percent) in the value of the thermal neutron activation cross section of manganese. The following measurement was carried out in order to reduce the error in the cross section value to less than 2.0 percent.

The thermal neutron activation cross section of manganese has been determined by measuring the absolute activity of a sample of manganese sulfate solution irradiated in a known thermal neutron flux. A small cell, containing about 3.5 ml of manganese sulfate solution and a 2.0×3.4 cm^2 manganese foil, was placed in a graphite column three or four centimeters from a ten-curie Po-Be neutron source (Fig. 1). At this distance from the source the thermal neutron density is of sufficient magnitude and uniformity to provide enough activity for 4π counting of an aliquot of the activated manganese sulfate solution. The diagonal positioning of the foil used to calibrate the neutron density insures that the foil and solution sample the same average neutron density, regardless of the attenuation throughout the cell.

After irradiation for several hours the cell was removed and 0.200 ml of the solution was pipetted onto a quarter-mil mylar film and the absolute activity was determined with a 4π proportional flow counter (only the manganese activity is present). Then the foil was 2π counted in the same counter. After correction for decay, the ratio of the manganese sulfate activity, $C_{4\pi}$, to the foil activity, A_s, for the unknown flux is obtained. Next the cadmium difference activity for the foil was measured in the NBS standard thermal neutron density[1] (originally calibrated with boron). This measurement calibrates the manganese foil activity, A_s, in terms of the known thermal neutron density, n.

The manganese thermal neutron activation cross section is then determined from the equation

$$C_{4\pi}\times A_s/A_c=n\bar{v}\sigma N,$$

where N is the number of manganese nuclei in the 0.200 ml manganese sulfate aliquot, and σ is the manganese activation cross section at $\bar{v}=2.2\times10^5$ cm/sec.

Two sets of measurements were taken for each of the activities, and the result obtained is

$$\sigma_{act}=13.1_9\pm0.3_9 \text{ barns (standard error).}$$

Most of the error stems from the uncertainty in $n(\pm2$ percent). The 4π data, including absorption correction, should be accurate to ±0.7 percent.

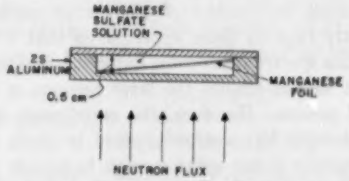

FIG. 1. Cell geometry during irradiation.

This result agrees well with the "best average value" of 13.4 ± 0.3 barns for the activation cross section and 13.2 ± 0.4 barns for the absorption cross section listed in Supplement 2 of the Neutron Cross Section Compilation.[2] When all three are combined, the error is reduced to 0.2 barn (1.5 percent).

A more detailed description of the preparation and use of thin manganese sulfate sources will appear in a later paper describing the absolute calibration of a neutron source.

[1] J. DeJuren and H. Rosenwasser, J. Research Natl. Bur. Standards **52**, 93 (1954).

[2] *Neutron Cross Sections*, Atomic Energy Commission Report AECU-2040 (Technical Information Division, Department of Commerce, Washington, D. C., 1952).

Nuclear Spin and Magnetic Moment of 3.1-hr Cs^{134m}†

L. S. GOODMAN AND S. WEXLER
Argonne National Laboratory, Lemont, Illinois
(Received March 16, 1955)

The nuclear spin, hyperfine structure constant and magnetic moment of the excited isomer 3.1-hr Cs^{134m} were determined by means of the atomic beam magnetic resonance method. The intensity of the active species was measured by deposition of the beam on a cold surface and subsequent counting. A spin of $8(\hbar)$, a hfs $\Delta\nu = 3684.3 \pm 0.5$ Mc/sec, and a nuclear moment of 1.10 ± 0.01 nm were found. The nuclear magnetic moment proved to be positive in sign.

I. INTRODUCTION

IN recent years there has been a rising interest in the direct determination of nuclear spins and moments of radioactive isotopes. This interest has stemmed from advances in the understanding of nuclear structure as evidenced in such contributions as the shell model, beta-ray theory, and isomeric decay systematics.

One of the most fruitful methods of performing these measurements has been the atomic beam magnetic resonance method, developed for stable nuclides by Rabi and his co-workers.[1] A variation of the technique, introduced by Zacharias,[2] greatly increased the sensitivity of the method and led to the first atomic beam measurements on artificially produced active species.[3] The isotopic enrichment of the active nuclides was sufficiently high in these experiments that a conventional mass spectrometer could differentiate signals from adjacent masses despite the large amount of inactive material present. However, the enrichment of radioactive isotopes by neutron capture in chain reacting piles generally is not great enough to permit use of a mass spectrometer. In these cases measurement of the activity in the deposited beam may be resorted to, as was first demonstrated in the determination of the nuclear constants of Na^{24} and K^{42}.[4] All told, the nuclear properties of approximately twelve radioactive nuclides have been determined by atomic beam methods.[5-6] The active species selected for study have, up till now, been exclusively beta emitters, and the results obtained have accordingly served as tests of the predictions of the shell-model and beta-ray theories.

It was therefore desirable to measure the nuclear spin and magnetic moment of an excited isomer, since the results would be of interest with regard to the formulation of decay schemes based on semiempirical[7] and theoretical[8] properties of gamma emission. The 3.1-hr nuclide Cs^{134m} was chosen because (a) it could be prepared in sufficiently high specific activity by neutron capture that its beam intensity may be measured by condensation and subsequent counting, and (b) the excellent detector available for the inactive Cs^{133} atoms in the beam made easy the calibration of the magnetic field. The well-known "flop-in" nuclear resonance experiment of Zacharias[2] was followed with an apparatus, which though similar in magnet geometry to an M.I.T. machine,[3] contained several modifications necessary for working with relatively short-lived activities.

II. THEORY OF THE METHOD

Although the principles of the method have been described in detail elsewhere,[1-3,9] for the sake of clarity we will review its salient features. The experiment is based on the observation of transitions between magnetic substates in the Zeeman structure of the hyperfine levels of an atom in an external magnetic field. In the absence of an external field the angular momentum of the nucleus, I (in units of $\hbar$), is coupled to that of the surrounding electrons, so that for an atom of electronic state $J=\frac{1}{2}$ the total angular momentum of the atom, F, is either $I+\frac{1}{2}$ or $I-\frac{1}{2}$. Since the electronic and nuclear spins may be coupled in two different ways, the magnetic moments associated with them will interact so that the energy of the atom will have either of two values, the difference between the states being the hyperfine structure separation $\Delta W = h\Delta\nu$. Splitting of each of the hyperfine levels occurs when the atom is in an external magnetic field, as shown in Fig. 1, which describes some of the energy states of an atom with arbitrary nuclear spin I and $J=\frac{1}{2}$. Coupling of the nuclear and electronic spins is preserved in fields of low strengths, and the splitting is linear with field and equal between adjacent m_F sublevels. The difference in energy between the substates farthest apart in the $F=I+\frac{1}{2}$ hyperfine level ($m_F=F$ and $m_F=-F$) is, neglecting the nuclear moment, just that due to the orientation of the electronic magnetic moment parallel and antiparallel to the external field, i.e., $2g_J J\mu_0 H$

† Work performed under the auspices of the U. S. Atomic Energy Commission.
[1] Rabi, Zacharias, Millman, and Kusch, Phys. Rev. **53**, 318 (1938); see also Kusch, Millman, and Rabi, Phys. Rev. **57**, 765 (1940), and later papers.
[2] J. R. Zacharias, Phys. Rev. **61**, 270 (1942).
[3] Davis, Nagle, and Zacharias, Phys. Rev. **76**, 1068 (1949).
[4] E. H. Bellamy and K. F. Smith, Phil. Mag. **44**, 33 (1953).
[5] Jaccarino, Bederson, and Stroke, Phys. Rev. **87**, 676 (1952).
[6] A. Lemonick and F. M. Pipkin, Phys. Rev. **95**, 1356 (1954).
[7] M. Goldhaber and A. W. Sunyar, Phys. Rev. **83**, 906 (1951).
[8] Rose, Goertzel, Spinrad, Harr, and Strong, Phys. Rev. **83**, 79 (1951).
[9] J. B. M. Kellogg and S. Millman, Revs. Modern Phys. **18**, 323 (1946).

(where g_J is the Landè g-factor, J the electronic angular momentum, μ_0 the Bohr magneton, and H the magnetic field). Since this energy is divided by $2F+1$ equally separated levels into $2F$ intervals, the Zeeman splitting of adjacent substates is $g_J J\mu_0 H/F$. For an $S_{\frac{1}{2}}$ electronic state the frequency representing this energy difference is:

$$\nu_0=\frac{\mu_0 H}{hF}=\frac{1.400H}{I+\frac{1}{2}}\ \text{Mc/sec}. \tag{1}$$

However, owing to the use of the Zacharias conditions[2] for refocusing the beam, only those transitions between substates are observed in which there is a reversal in sign of the effective electronic magnetic moment. Referring again to Fig. 1, we see that we are limited to the $F=I+\frac{1}{2}$; $m_F=-F\leftrightarrow m_F=-(F-1)$ transition at low external fields and low frequencies. The assignment of the nuclear spin is a straightforward procedure, for it is only necessary to search for a single resonance corresponding to one of the various possible values of $F=I+\frac{1}{2}$ in a known external magnetic field.

If, however, the nuclear spin of the isotope under study is large and/or the hfs rather small, the finite width of the radiofrequency resonance in this experiment may not permit resolution of the ν_0's for adjacent possible values of I at fields where the splitting is still linear. In this case the observation of a single resonance does not allow an unambiguous spin assignment. It is necessary to observe transitions in higher fields where the low frequency resonance deviates from Eq. (1). Under these conditions a better approximation for the $F=I+\frac{1}{2}$; $-F\leftrightarrow-(F-1)$ transition is[3]

$$\nu=1.400\frac{H}{F}+\left(1.400\frac{H}{F}\right)^2\frac{2I}{\Delta\nu}. \tag{2}$$

Measurement of the resonance frequencies at two settings of the external field will then permit calculation of the magnitude of the nuclear spin and an approximate value of the hfs. The external magnetic field is determined by observing the same transition in an atom of known nuclear constants, in our case, the inactive isotope Cs^{133} present in the beam.

In increasingly higher external fields the decoupling of the nuclear and electronic spins becomes greater and the splitting of the sublevels departs from the description of Eq. (2). The behavior of the hyperfine structure in an external magnetic field is completely described for $J=\frac{1}{2}$ by the Breit-Rabi equation,[10] which incidentally is the basis for the plot in Fig. 1 for arbitrary I and positive nuclear moment. After the nuclear spin has been assigned by the procedure indicated above, an accurate determination of hyperfine structure separation is carried out by observing the $F=I+\frac{1}{2}$; $m_F=-F\leftrightarrow m_F=-(F-1)$ transition in successively larger fields until the Paschen-Back effect is strong. The hfs

[10] G. Breit and I. I. Rabi, Phys. Rev. **38**, 2082 (1931).

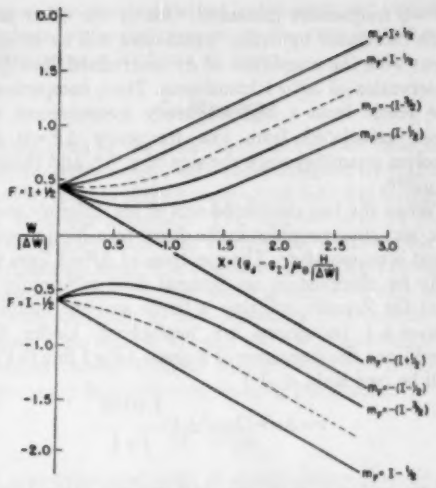

FIG. 1. Diagram showing variation with magnetic field of hyperfine substates of an atom with electronic angular momentum $J=\frac{1}{2}$ and nuclear spin I. The nuclear moment is assumed positive. There are $2(I+\frac{1}{2})+1$ substates in the $F=I+\frac{1}{2}$ hyperfine level, of which five are shown, and $2(I-\frac{1}{2})+1$ substates in the $F=I-\frac{1}{2}$, of which only three are drawn. The separation of adjacent sublevels has not been drawn to scale.

is then calculated for each of the frequencies ν found by the use of the Breit-Rabi equation, which, for the low-frequency transition observed, may be put in the form[11]

$$\Delta\nu(\text{Mc/sec})=\frac{(\nu-g_I k)(g_J k-\nu)}{\nu-g_I k-(g_J-g_I)k/(2I+1)}, \tag{3}$$

where $k=\mu_0 H/h$, a constant of the external field, and g_I is the nuclear g-factor ($=-\mu_I/I$). A value for g_I of Cs^{134m}, sufficiently accurate for inclusion in Eq. (3), is obtainable from the Fermi-Segrè relation,[12]

$$\Delta\nu_{134m}/\Delta\nu_{133}=\frac{(2I_{134m}+1)g_I^{134m}}{(2I_{133}+1)g_I^{133}}, \tag{4}$$

where one takes the approximate $\Delta\nu_{134m}$ derived in Eq. (2). Use is made of the known nuclear constants of the stable isotope Cs^{133}:[13] $\Delta\nu=9192.76$ Mc/sec, $I=7/2(\hbar)$, $\mu_I=2.575$ nm. The more precise $\Delta\nu_{134m}$'s thus calculated yield better values of g_I^{134m} by introducing the former back into Eq. (4). From the improved g-factors the magnetic moment of Cs^{134m} (μ_I^{134m}) is readily calculated in nuclear magnetons from $\mu_I=-g_I I$.

The sign of the nuclear moment may be decided upon from the calculation of the magnitude of the hfs. Taking g_I^{134m} first positive and then negative, we may compute from Eq. (3) two different values of $\Delta\nu$ for each of the

[11] S. Millman and P. Kusch, Phys. Rev. **58**, 438 (1940).
[12] E. Fermi and E. Segrè, Z. Physik **82**, 729 (1933).
[13] H. Taub and P. Kusch, Phys. Rev. **75**, 1481 (1949); V. W. Cohen, Phys. Rev. **46**, 713 (1934); Kusch, Millman, and Rabi, Phys. Rev. **55**, 1176 (1939).

$\Delta F=0$ frequencies measured. One or the other set of such calculated hyperfine separations will be in agreement with the magnitude of $\Delta\nu$ determined directly by observation of $\Delta F=1$ transitions. Thus, comparison of the result from a high-frequency measurement with those calculated from low frequency $\Delta F=0$ data resolves unambiguously the sign of g_I^{134m}, and therefore of μ_I^{134m}.

When the two calculated sets of hfs differ by several Mc/sec, great precision in the direct transition measurement is unnecessary. The spectrum of $\Delta F=1$ lines need only be observed in an external field sufficiently low that the Zeeman splitting is linear and the individual $\Delta m_F=\pm 1$ transitions are unresolved. Under these conditions the frequency of a given $\Delta F=1$ line in Cs^{134m} will be (see Rabi *et al.*[1])

$$\nu=\Delta\nu+(2m_F'\pm 1)\frac{1.400H}{I+\frac{1}{2}}, \tag{5}$$

where m_F' can have any half-integral value between $(I-\frac{1}{2})$ and $-(I-\frac{1}{2})$. Since m_F' varies only in jumps of one, the spacing between adjacent lines in the unresolved pattern is constant. With the exception of the $F=I+\frac{1}{2}$, $m_F=-(I+\frac{1}{2})\leftrightarrow F=I-\frac{1}{2}$, $m_F=-(I-\frac{1}{2})$ transition, which is not observed in this experiment, and the $F=I+\frac{1}{2}$, $m_F=(I+\frac{1}{2})\leftrightarrow F=I-\frac{1}{2}$, $m_F=(I-\frac{1}{2})$, each line is the superposition of two transitions. Thus if the number of possible $\Delta F=1$ transitions is large, i.e. I is high, the unresolved pattern should be symmetrical in shape, the center being very close to the frequency of the hyperfine structure constant.

An estimate may be made of the width of the unresolved pattern. From Eq. (5) neglecting the finite resolution of the apparatus, we find the frequency difference between extreme lines is $4I(1.400H)/(I+\frac{1}{2})$ or $4I\nu_0$. If the external magnetic field is such that the Zeeman splitting is 50 kc/sec, the width will be approximately 1.6 Mc/sec when I is taken as $8(\hbar)$. The actual width, however, would be somewhat greater because of the short time of the atom in the rf field and because of the adding up of tails from adjacent resonances.

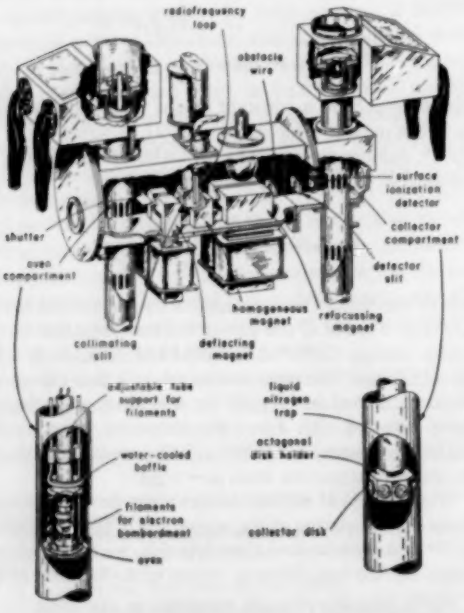

FIG. 2. Artist's sketch of atomic beam apparatus. Only the important components are shown. Many of the details, such as the pumping systems, inside section walls and hydraulic lifts have been left out to avoid confusion.

III. APPARATUS

A. General Plan of Apparatus

The atomic beam magnetic resonance apparatus constructed for this experiment was patterned after the M.I.T. machine described by Davis, Nagle, and Zacharias.[3] A cut-away artist's sketch appears in Fig. 2. The usual inhomogeneous deflecting and refocusing fields, with gradients parallel and in the same direction, are on either side of the homogeneous field in which transitions between the magnetic sublevels take place. Atoms emerging from the oven pass from the oven compartment through an isolation chamber into the main section housing the magnets and detectors. Depending on the velocities of the atoms, the angles from the normal at which they leave the oven, and the gradient of the deflecting field, certain ones will be focused on the collimating slit and pass into the gap containing the homogeneous and oscillating radiofrequency fields. Only those atoms which in the overlapping fields undergo transitions involving a change in sign of their effective magnetic moments at high field are refocused onto the detector slit, lying, like the oven and collimating slits, on the neutral axis of the beam. Atoms not suffering such transitions are deflected away from the detector by the two inhomogeneous magnets.

Radiofrequency power to effect the transitions was introduced through a vertical copper "hairpin," two cm along the beam, situated between the poles of the uniform field magnet. The oscillating field produced was mainly parallel to the beam and at right angles to the static field. A "pickup" coil mounted in the vicinity of the hairpin served to give a measure of the power of the oscillating field. The rf signal picked up by the coil was rectified by a crystal, and the resultant current measured with a microammeter. For the low-frequency studies a Kovar seal made a satisfactory vacuum lead through for the rf. In the measurements of the $\Delta F=1$ transitions, which occurred at relatively high frequencies, an Andrews Corporation gas barrier seal, matched to $\frac{7}{8}$-inch air dielectric coaxial line, was used, and was found to be negligibly lossy while being quite satisfactory vacuum-wise.

The widths of all the slits defining the beam—oven, collimating and detector—were each 0.010 inch. The obstacle wire measured 0.015 inch.

A conventional type of surface ionization detector, mounted through a flange in the side of the apparatus and situated directly behind the detector slit, served to measure the Cs^{132} intensity in the beam. The detector rode on a carriage which could be moved out of the path of the beam without disturbing the vacuum. Positive ion currents to the cylindrical collector plate were amplified by a vibrating reed electrometer.

The active Cs^{134m} component was measured by condensing the beam on one-inch diameter copper disks ($\frac{1}{16}$-inch thick), which were held by spring clamps on the faces of a brass octagon attached to the bottom of a liquid nitrogen trap. These disks were washed with water, alcohol, and ether before being used. If a disk showed radioactive contamination it was first etched in dilute HCl. No other surface treatment was necessary. The long tube containing the collector was rotated in o-ring gaskets so as to position each of eight disks in turn behind the collector slit. Vertical movement of the tube was effected by hydraulic lifts. A drybox attached around the tube above the apparatus made it possible to bring the cold octagon and trap through vacuum locks into a dry helium atmosphere for the changing of disks. Measurement of the activity was made by placing each disk in a windowless G-M flow counter containing a 98 percent He-2 percent Isobutane gas mixture.

B. Vacuum System

The vacuum housing consisted of a brass box 12 in. wide, $13\frac{3}{4}$ in. high, and 55 in. long, supported by an aluminum Unistrut frame. Walls of the box, $\frac{3}{4}$ in. thick on sides and top and 1 in. on bottom, were either welded together and then tinned on the inside or screwed together and silver soldered. Components inside the housing were introduced through appropriately cut holes in the four sides and held on by flanges bolted to the apparatus. o-ring gaskets, greased with Apiezon T, formed the vacuum seals.

Evacuation of the apparatus was performed by two 6-in. oil diffusion pumps attached to the main chamber, and one 4-in. pump each on the isolation and oven compartments. The four pumps were backed by a 4-in. booster pump which evacuated into a mechanical pump. Each of the four primary pumps was attached to the side of the vacuum housing through a water-cooled 4-in. baffle valve and a large, cylindrical liquid nitrogen trap. An auxiliary system consisting of 2-in. tubing and valves evacuated by a large mechanical pump served the dual purposes of roughing down the chambers and tubes and of maintaining a vacuum between o-ring pairs in which shafts leading into the apparatus were rotated. A vacuum of less than 10^{-6} mm pressure was readily attained in the main and isolation chambers, while the pressure in the oven section was usually between 10^{-6} and 10^{-5} mm.

C. Magnets

Dimensions of the pole pieces of the two deflecting magnets were identical with those designed by Nagle[14]; however, the gap of the homogeneous field was increased to $\frac{1}{2}$ in. in our apparatus. The pole pieces of all three magnets were bolted onto a brass bar, which served to maintain alignment. The magnetic circuits were brought out through the vacuum wall via flanged o-ring seals and were energized by high-resistance coils outside the housing. This scheme allowed the use of electronically regulated current supplies and obviated the need for large storage batteries and charging equipment.

D. Oven

A cold-rolled steel oven of simple design (Fig. 3) sat on a tripod in the oven tube (Fig. 2), two of whose legs constituted a tantalum-tungsten thermocouple, with the oven forming the junction. This scheme allows monitoring of oven temperatures from 100 to over 1500°C. The tripod was mounted on a carriage installed on a base in the long oven tube. Controls for fine adjustment (such as direction, tilt and traverse position of the oven slit) entered through the top flange of the tube and were connected to the carriage by means of flexible rods.

The heating system was designed to be relatively universal; electron bombardment from thoriated tungsten filaments was decided upon. For Cs metal, of course, just the radiation from the filaments give adequate heating. The heating and temperature monitoring designs had the added advantage of not requiring connections to the oven block itself, which contained a radioactive source. Introducing the active Cs metal into the oven was done in a He-filled drybox attached to the oven tube above the apparatus. Like the collector, this tube was moved vertically through vacuum locks by hydraulic lifts.

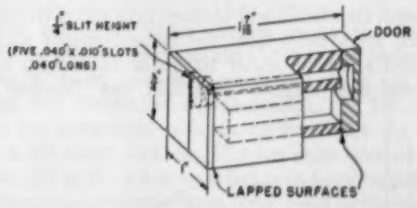

FIG. 3. Cold-rolled steel oven for Cs metal. Two quartz capsules are placed in the cavity and then partially crushed. The lapped door and slit jaws are held onto the block by screws not indicated in the drawing.

[14] D. E. Nagle, thesis, Massachusetts Institute of Technology, 1948 (unpublished).

E. Radio-Frequency Equipment

For study of the low-frequency $\Delta F=0$ transitions, the General Radio Type 805-C signal generator (50 kc/sec to 50 Mc/sec) was used. A conventional, one stage, tuned power amplifier, with a 2E26 tube, was used to enhance the transition probability in this frequency region. In the region extending up to 300 Mc/sec a Hewlett-Packard Model 608 A was employed; a Spencer-Kennedy Model 202 wide band amplifier used with this oscillator gave some improvement in the refocused beam intensity. $\Delta F=1$ transitions were excited by a Sperry reflex klystron, Model 2K-42, powered by a Polytechnic Research and Development Company Type 801 A supply.

Frequencies less than 150 Mc/sec were measured by a Berkeley Frequency Meter, Model 5570, with a range extender, Model 5575. The instrument is capable of accuracies of one part in 10^7. In the present work, however, no effort was made to measure frequencies to better than 1 kc/sec. For measurement of frequencies higher than 150 Mc/sec, the signal from the H–P 608 A was crystal mixed with that from the G–R 805 C, the output frequency of which was determined by the Berkeley meter. The 600-kc/sec beat was detected with a NC-125 receiver, which was calibrated at that point. The same technique worked well in the measurement of the klystron frequency, in which case the Hewlett-Packard 608 A served as the local oscillator and a Hallicrafters Model S-36 A as receiver for the 33-Mc/sec beat between the 25th harmonic of the H–P and the signal from the klystron. To decide whether the klystron frequency was higher or lower than that of the local oscillator harmonic, the signal from the pickup loop was measured to within 15 Mc/sec by means of a crystal rectifier and variable tuning stub arrangement. Drift of the H–P 608 A (about 1 kc/sec) and fluctuation of the power level of the klystron allowed about 40 kc/sec uncertainty in the klystron frequency.

IV. PRELIMINARY ALIGNMENT AND PROCEDURE

After optical alignment of the slits with a telescope, a sodium beam was brought up, deflected with the inhomogeneous magnets, and refocused by applying a resonant combination of uniform field and rf frequency. Strong stray fields from the inhomogeneous magnets induced a field of about 100 gauss in the gap of the uniform field magnet. This field was "bucked out" when necessary by reversing the current in the magnet winding of the homogeneous field. The magnitudes of the two deflecting fields and the positions of the collector and oven slits were varied over wide ranges so as to obtain the maximum signal to background ratio. This ratio was thereby improved by a factor of two to three over that found with the arrangement suggested by optical alignment alone.

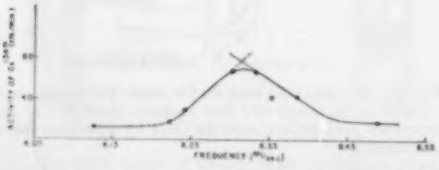

FIG. 4. Typical resonance curve observed for $F=I+\frac{1}{2}$; $m_F=-F\leftrightarrow m_F=-(F-1)$ transitions.

Cesium metal, distilled from a mixture of Ca chips and CsCl, was sealed under vacuum in small quartz vials; each capsule contained about 350 mg of material. The 3.1-hr Cs^{134m} isomer was produced by irradiation for several hours in a thermal neutron flux of about 1.5×10^{13}/sec/cm² available in the heavy water reactor at this laboratory. In a given run two such irradiated vials were partially crushed in the oven, situated in the helium atmosphere of the drybox, and the closed oven was placed on the tripod in the raised oven tube. This loading usually lasted over seven hours. The tube was then lowered through vacuum locks so as to bring the oven into position. After the cesium beam was stabilized by adjusting the oven temperature, the obstacle wire was moved into position and the deflecting magnets were energized. The homogeneous field was set by observing the low-frequency $\Delta F=0$ line in Cs^{133}, using the hot-wire detector. The collecting disks were lowered through vacuum locks, cooled to liquid nitrogen temperature, and brought into position.

TABLE I. Observed transition frequencies for Cs^{134m} and Cs^{133} and calculated hfs $\Delta\nu_{134m}$ (Mc/sec).

ν_{133}	ν_{134m}	$\Delta\nu_{134m}$ if μI pos	$\Delta\nu_{134m}$ if μI neg
9.365±0.010	4.480±0.015		
17.220±0.010	8.295±0.020		
43.940±0.010	21.934±0.020		
90.937±0.010	48.403±0.010	3681±5	3698±5
164.105±0.030	97.140±0.025	3682±1	3689±1
282.845±0.020	201.666±0.020	3684.3±0.5	3695.0±0.5

Search for the $\Delta F=0$ transition in active Cs^{134m} was then made by varying the rf, usually in 50–100 kc/sec steps, and exposing one of the disks to the beam for a definite time (usually five minutes) with each frequency setting. Recalibration of the homogeneous field was conducted between deposition periods. After collection of the beam on all eight disks, the collector tube was raised into the drybox and the disks were removed for counting. the 100-kev conversion electron activity on each was measured in a windowless flow type G–M counter. The disks were each counted at least twice and the decay rates at a common time determined for plotting of a resonance curve. On the following day each disk was again counted to be sure of the absence of possible 2-yr Cs^{134} contamination from handling the collectors. When a resonance was found, the search of the frequency region was repeated. The observation of a given $\Delta F=0$ transition in Cs^{134m} provided values of

$\Delta\nu_{134m}$ and g_I^{134m} from which the frequency region to be searched at higher external field could be calculated.

In the direct determination of the hyperfine structure constant the homogeneous magnetic field was set to produce a Zeeman splitting in Cs^{134m} of approximately 50 kc/sec. A search was then conducted for a broad refocused intensity in the frequency regions suggested by the two $\Delta\nu$'s calculated from the low-frequency data. The reflex klystrom was varied in 500-kc/sec steps, and its output kept constant to within 40 kc/sec for the duration of each beam collection period.

V. CALCULATIONS AND RESULTS

The measured frequencies of the $F=I+\frac{1}{2}$; $m_F=-F\leftrightarrow m_F=-(F-1)$ transitions in the Cs^{134m} isomer are listed in Table I with the corresponding lines of Cs^{133} used to measure the magnitude of the external field. Observations were first made in sufficiently low magnetic field to preserve largely the coupling of the electronic and nuclear spins, and then extended gradually to higher fields in which the decoupling of the angular momenta and the very small direct interaction of the nuclear magnetic moment with the applied field measurably affect the magnitude of the Zeeman splitting. From the theoretical discussion it is clear that we are interested in extracting the following information about 3.1-hr Cs^{134m} from the data: the nuclear spin I (in units of $\hbar$), the hyperfine structure separation (in Mc/sec), the nuclear magnetic moment (in nuclear magnetons), and the sign of the moment.

The two lowest frequency resonances (a typical curve appears in Fig. 4) observed in Cs^{134m}, 4.480 and 8.295 Mc/sec (Table I), were introduced in Eq. (2) to evaluate the nuclear spin and to give an approximate value for the hyperfine structure constant. A nuclear angular momentum of $8(\hbar)$ and a $\Delta\nu\approx 3600$ Mc/sec come out of the calculation. These values were confirmed by the measurements at higher frequencies. From the approximate $\Delta\nu$ so found and the Fermi-Segrè relation [Eq. (4)], a sufficiently accurate g_I was evaluated for use in the Breit-Rabi equation [Eq. (3)]. More accurate hyperfine structure constants were then calculated for each of the resonances found at progressively higher rf signals. The frequencies of the observed transitions are assembled in Columns 1 and 2 of Table I along with their estimated errors, these assumed to be due only to the uncertainty in estimating the exact position of the resonance. As pointed out under *Theory of Method*, either of two values for $\Delta\nu$ is the correct one depending on whether the nuclear magnetic moment is parallel or antiparallel to the spin. Thus the correct hfs is most nearly 3684.3 $\pm$0.5 Mc/sec (Column 3, Table I) if the moment is positive and 3695.0$\pm$0.5 Mc/sec (Column 4) if negative. Although the consistency of the $\Delta\nu$ values so calculated can sometimes[1-3] indicate which of the two signs is to be taken, this was not the case here, and only the

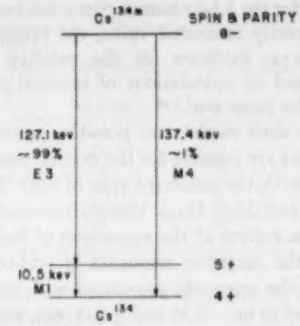

FIG. 5. Decay systematics of Cs^{134m} [Sunyar, Mihelich, and Goldhaber (see reference 17)].

measurement of the direct hyperfine transition in Cs^{134m} could settle the question. Because of the conveniently low frequency of the hfs, $\Delta F=1$ transitions could be looked for with available equipment. Operating in an external magnetic field so low as to permit observation only of the unresolved lines, we found a broad resonance, about 2.5 Mc/sec wide at half-maximum, centered at 3684.5$\pm$0.5 Mc/sec, while no indication of a resonance was seen in the neighborhood of 3695 Mc/sec. Therefore, we conclude that the hyperfine structure constant of 3.1-hr Cs^{134m} is 3684.5$\pm$0.5 Mc/sec and the nuclear magnetic moment is positive. Finally, from the Fermi-Segrè formula $\mu_I^{134m}=+1.10\pm0.01$ nm.

Substantially the same values for the nuclear constants of Cs^{134m} reported here and in preliminary notes[15] were obtained by Cohen and Gilbert[16] in a similar, but independent experiment at the Brookhaven National Laboratory.

VI. DISCUSSION

For some time it had been assumed that 3.1-hr Cs^{134m} decayed by emission of a single γ ray of 127-kev (an $E3$ transition) to a 2.3-yr Cs^{134} ground state. However, as a consequence of the preliminary measurements on the spin of the excited isomer, Sunyar, Mihelich, and Goldhaber[17] (Fig. 5) reinvestigated this decay and found a previously undetected 10.5-kev gamma following the 127-kev transition. These authors presented evidence for the decay systematics of the Cs^{134m} isomer presented in Fig. 4. From conversion coefficient data, and empirical and theoretical considerations, the 127.1-kev γ ray was considered to be an $E3$ transition, the 10.5 kev an $M1$ decay, and the 137.4-kev cross over an $M4$. As the spin of the 2.3-yr state has been found to be $4(\hbar)$ by direct measurement using atomic beam techniques,[4,5] the decay systematics of the Cs^{134m} transitions favor a

[15] L. S. Goodman and S. Wexler, Phys. Rev. **95**, 570 (1954); **97**, 242 (1955).
[16] V. W. Cohen and D. A. Gilbert, Phys. Rev. **95**, 569 (1954); **97**, 243 (1955).
[17] Sunyar, Mihelich, and Goldhaber, Phys. Rev. **95**, 570 (1954).

spin of 8($\hbar$) for the 3.1-hr isomer. Since this result agrees with the directly measured value, the present experiment serves as evidence for the validity of decay schemes based on calculations of internal conversion coefficients by Rose *et al.*[8,18]

From the shell model two possible proton-neutron configurations are possible for the excited isomer Cs^{134m} compatible with the measured spin of 8($\hbar$). These are[19] $1g_{7/2}$, $1h_{11/2}$, and $2d_{5/2}$, $1h_{11/2}$. Using a two-nucleon wave function, one arrives at the expression of Bellamy and Smith[4] for the magnetic moments of odd-odd nuclei, from which the moments associated with these states are calculated to be -0.36 and $+2.90$ nm, respectively. Possibly a mixed configuration, as suggested by de-Shalit and Goldhaber,[20] of these two states may account for the measured result of $+1.10$ nm.[21]

An empirical method for estimating moments of odd-odd nuclei stems from proposals[22] that the spin contributions to the magnetic moment of the odd nucleons are suppressed from their respective free particle values when the neutron and proton are in the nucleus. Following this suggestion, we may take the effective intrinsic moment of the odd neutron and odd proton in Cs^{134m} to be -1.4 and 1.5 nm, respectively, using the graph prepared by Bloch.[22] Introducing these values into the same two-nucleon calculations, we find fair agreement with experiment in the result of $+0.8$ nm computed for the $g_{7/2}$, $h_{11/2}$ configuration. The $d_{5/2}$, $h_{11/2}$ proton-neutron configuration gives the much higher value of $+2.1$ nm for the nuclear moment.

ACKNOWLEDGMENTS

We wish to thank J. A. Dalman for his ingenious design work and assistance in performing the experiments, H. W. Ostrander for his design of many parts of the apparatus, and M. Hamermesh, D. E. Nagle, and D. Kurath for stimulating discussions.

[18] Rose, Goertzel, and Swift (privately circulated tables).
[19] Mayer, Moszkowski, and Nordheim, Revs. Modern Phys. **23**, 315 (1951).
[20] A. de-Shalit and M. Goldhaber, Phys. Rev. **92**, 1211 (1953).
[21] The suggestion of a mixed configuration in Cs^{134m} was first made by Cohen and Gilbert, reference 15.
[22] F. Bloch, Phys. Rev. **83**, 839 (1951); H. Miyazawa, Progr. Theoret. Phys. (Japan) **6**, 263 (1951); A. de-Shalit, Helv. Phys. Acta **24**, 296 (1951).

PHYSICAL REVIEW VOLUME 99, NUMBER 1 JULY 1, 1955

Cosmic-Ray Intensity above the Atmosphere at High Latitudes*†

L. H. Meredith,‡ J. A. Van Allen, and M. B. Gottlieb
Department of Physics, State University of Iowa, Iowa City, Iowa
(Received October 29, 1954; revised manuscript received April 8, 1955)

The total charged particle cosmic-ray intensity above the atmosphere has been measured with thin-walled Geiger counters (total effective stopping power of apparatus and residual atmosphere 0.5 g/cm² of aluminum) carried in balloon-launched rockets at geomagnetic latitudes 54.3° N, 62.1° N, 71.9° N, and 86.7° N. The respective values of unidirectional particle intensity averaged over the upper hemisphere are: $J=0.44\pm0.01$, $\leq 0.50\pm0.05$, $\leq 0.50\pm0.05$, and $=0.48\pm0.01$ (cm² sec sterad)$^{-1}$. These results are consistent with the complete or nearly complete absence of primary cosmic rays having a magnetic rigidity less than 1.7×10^9 volts.

I. INTRODUCTION

A. Purpose

THE purpose of this investigation was to make an absolute measurement of the total intensity of charged primary cosmic rays down to the lowest feasible value of magnetic rigidity R—in this case down to a value of R of about 0.2×10^9 volts.

The intensity of low-rigidity cosmic rays is of interest for several reasons, *viz.*: (a) They may constitute a significant portion of the primary beam. (b) The presence or absence of low-rigidity primaries may provide a crucial test of any proposed mechanism for the astrophysical origin and propagation of cosmic rays. (c) A specific aspect of (b) may be a definitive test of the magnitude of the magnetic dipole moment of the sun. (d) It is of aeromedical interest to know the radiation intensity which will be encountered in flight at high altitudes and in the vicinity of the earth.

B. Necessary Geographic Location

The theoretical properties of the geomagnetic field as a magnetic spectrometer are summarized by Alpher.[1] A special feature of the theory is that the critical value of magnetic rigidity R_c, which a particle must possess in order to reach the top of the atmosphere at a specified location, diminishes with increasing geomagnetic lati-

* Based on the doctoral dissertation of L. H. M. (June, 1954).
† Assisted by joint program of the Office of Naval Research, the U. S. Atomic Energy Commission, and the Navy Bureau of Aeronautics; and by the Research Corporation.
‡ Present address: U. S. Naval Research Laboratory, Washington 25, D. C.

[1] R. A. Alpher, J. Geophys. Research **55**, 437 (1950).

tude λ and approaches zero as λ approaches 90° north or south. For vertical incidence at high latitudes, the critical value of magnetic rigidity is given to good accuracy by the Störmer relation:

$$R_c = 14.8 \cos^4\lambda, \quad (1)$$

where R_c is measured in units of 10^9 volts (i.e., in Bv).

It is therefore important to make experimental measurements at the highest possible latitudes in order to extend knowledge of the low-rigidity portion of the primary spectrum.

In the present paper, geomagnetic latitudes[2,3] in the centered-dipole representation are denoted by λ'; and in the eccentric-dipole representation, by λ.

C. Necessary Altitude

While the earth's magnetic field determines the geographic position at which measurement of the intensity of any low-rigidity primaries must be made, absorption by the earth's atmosphere determines the minimum altitude necessary.[4,5]

Present-day balloon techniques seldom provide measuring conditions at an atmospheric pressure depth of less than 10 g/cm². This depth is equal to the ionization range of a vertically arriving proton of 0.46-Bv rigidity, for example. A useful summary of the limitations of balloon-borne apparatus can be obtained as follows: The ionization ranges h of stripped nuclei of specified rigidity and of various atomic numbers Z can conveniently be obtained from the graphs of Rossi.[6] Then the minimum magnetic rigidity R_c which a particle must possess to arrive vertically at a specified geomagnetic latitude λ can be calculated with Eq. (1). By means of these two sets of data one can then list the geomagnetic latitude at which the value of R_c for vertical incidence corresponds to the air range h for vertical travel down through the residual atmosphere to the apparatus. Such a listing (Table I) may be said to give the geomagnetic latitude "equivalent" to a given atmospheric depth (or absorber thickness).

On the reasonable assumption that primaries of these low values of rigidity (and energy) are unable to make their existence evident (as by production of long range secondaries) at depths greater than their ionization ranges, it is evident from Table I that it is fruitless with present day balloon techniques to attempt measurements on the proton component of the primary beam at latitudes higher than 65°; or on the heavy components, at latitudes higher than about 52–56°, depending upon the value of Z.

TABLE I. Geomagnetic latitudes such that R_c for vertical incidence corresponds to ionization range h for representative stripped nuclei.

Primary nucleus \ h	0.5 g/cm²	10 g/cm²	20 g/cm²
H	70°	65°	63°
He	66	60	58
N	64	56	54
Mg	63	55	52
Ca	62	53	50
Fe	61	52	48

In particular, there is no reasonable prospect that balloon measurements will extend the known primary spectrum to magnetic rigidities less than 0.5 Bv for any component.[4]

II. EXPERIMENTAL MATTERS

A. Attainment of High Altitudes

In order to extend knowledge of the primary spectrum to lower rigidities we have employed the Iowa balloon-launched rocket ("rockoon") technique.[5,7]

B. Nature of the Apparatus

In choosing between a single Geiger counter and a Geiger counter coincidence telescope for these measurements we were led to adopt the former by several practical considerations:

(a) The angular motion of free-flying rockets in a near vacuum is usually complex and unpredictable. For this reason it is necessary to provide auxiliary instrumentation—such as a magnetometer and an array of photoelectric cells—for continuous aspect measurement in order to be able to interpret directional measurements.[8] Such complexity entails considerable technical difficulty of achievement in the small pay-volume and pay-load available.

(b) The statistical accuracy of telescope data from a brief rocket flight, after necessary subdivision into intervals of azimuthal and zenith angles, is not high.

(c) The stopping power of a telescope is almost inevitably several times greater than that of a single counter.

(d) Single Geiger counters have been shown to provide reliable absolute measurements of total charged particle intensity. A statistical accuracy of about 1 percent in the intensity above the appreciable atmosphere can be obtained in a typical rocket flight. Furthermore, a single Geiger counter is a sufficiently isotropic detector that it is unnecessary to know its orientation during

[2] S. Chapman and J. Bartels, *Geomagnetism* (The Clarendon Press, Oxford, 1940), Vol. 2.

[3] Vestine, Laporte, Lange, Cooper, and Hendrik, Carnegie Institution of Washington Publication 578, 1947 (unpublished); and Vestine, Laporte, Lange, and Scott, Carnegie Institution of Washington Publication 580, 1947 (unpublished).

[4] J. A. Van Allen and S. F. Singer, Nature **170**, 62 (1952).

[5] J. A. Van Allen, Nuovo cimento **10**, 630 (1953), a preliminary account of part of the present work.

[6] B. Rossi, *High-Energy Particles* (Prentice-Hall, Inc., New York, 1952), pp. 40, 41.

[7] J. A. Van Allen and M. B. Gottlieb, *Rocket Exploration of the Upper Atmosphere*, edited by R. L. F. Boyd and M. J. Seaton (Pergamon Press, London, 1954), pp. 53–64.

[8] J. A. Van Allen, *Physics and Medicine of the Upper Atmosphere*, edited by C. S. White and O. O. Benson, Jr., (University of New Mexico Press, Albuquerque, 1952), pp. 412–431.

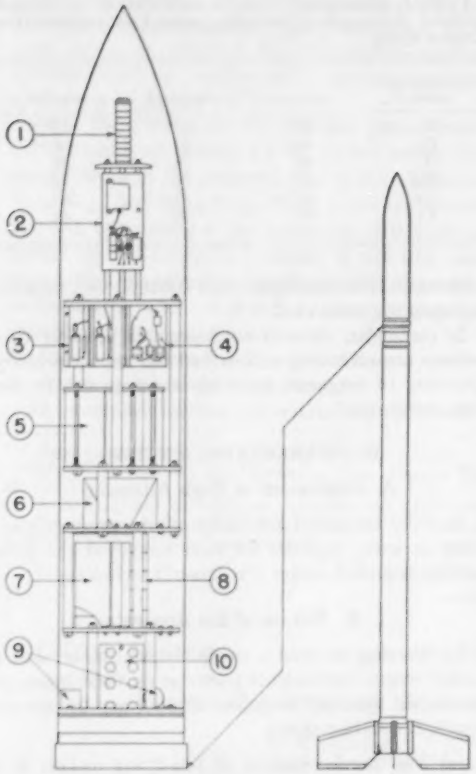

FIG. 1. Physical arrangement of equipment in the rocket. Diameter of nose shell was 6.5 inches. 1. Single Victoreen 1B85 Geiger Counter. 2. Thin fiber plate and cathode follower. 3. Scale-of-thirty-two circuit. 4. Variable frequency audio-oscillator (sub-carrier oscillator) which frequency modulates the radio transmitter. 5, 6, 7, 8, and 9. Miscellaneous batteries for circuit power. 10. Radio telemetering transmitter.

the high-altitude portion of the rocket flight, where the incidence of the radiation is only mildly anisotropic.

C. Geometric Factor of the Geiger Counter

The Victoreen 1B85 Geiger counter was selected for these measurements principally because of its thin wall (30 mg/cm² of aluminum).

The average unidirectional intensity over the upper hemisphere is defined by

$$J=\frac{1}{2\pi}\int_0^{2\pi}\int_0^{\pi/2} J(\theta,\varphi)\sin\theta d\theta d\varphi, \qquad (2)$$

wherein $J(\theta,\varphi)$ is the unidirectional intensity at zenith angle θ, azimuthal angle φ, and where it is understood that any upward moving radiation is arbitrarily assigned to the θ, φ of its reversed trajectory.

The counting rate N of a Geiger counter may be written as

$$N=\epsilon GJ. \qquad (3)$$

The efficiency is denoted by ϵ and the geometric factor G is, in general, a function of the angular distribution of the radiation, the orientation of the counter, and its effective length l and effective diameter a.

The value of G for a cylindrical counter of any orientation in a field in which the unidirectional intensity is isotropic over one hemisphere, zero over the other is

$$G_{iso}=0.5\pi^2 al(1+a/2l). \qquad (4)$$

It is easily shown that, for the observed angular distributions of radiation above the atmosphere at various latitudes and for the l/a ($\sim$3.5) of our counters, the quantity

$$N/\epsilon G_{iso} \qquad (5)$$

does not differ from the true J by as much as 1 percent in a typical rocket flight. Hence we are justified in using Eq. (3) with $G=G_{iso}$ for the calculation of J from the observed counting rate N on the high altitude plateau.[9–11] This simplification does not obtain, of course, within the lower atmosphere where the angular distribution of radiation intensity is markedly anisotropic.

In order to calculate J from N we then must know a, l, and ϵ. It has been found by other investigators[12,13] that the effective diameter of a Geiger counter is within 0.01 cm of its physical inside diameter. The physical inside diameter of the 1B85's was measured to be 1.91±0.01 cm and the effective diameter was taken to be

$$a=1.91\pm0.02 \text{ cm}. \qquad (6)$$

The effective lengths of individual Geiger counters and their efficiencies were determined experimentally.[14] A tabulation of effective lengths and of the quantity ϵG_{iso} is given in Table II.

In view of the earlier discussion, J above the atmosphere was calculated from the observed counting rates on the high-altitude plateau by using Eq. (3) with $G=G_{iso}$. The corrections for counter dead-time and loss of counts in the circuits were negligible.

It was necessary to use a different set of instrumentation for each rocket flight as no recovery was attempted. The individual sets were intercompared by measuring the counting rate of each set when a standard radioactive source was placed a standard distance from it. The counting rates of the individual sets were proportional to the effective length of the Geiger counter used within the statistical uncertainty of 0.5 percent.

[9] J. A. Van Allen and H. E. Tatel, Phys. Rev. **73**, 245 (1948).
[10] Gangnes, Jenkins, and Van Allen, Phys. Rev. **75**, 57 (1949).
[11] G. J. Perlow and C. W. Kissinger, Phys. Rev. **81**, 552 (1951).
[12] J. C. Street and R. H. Woodward, Phys. Rev. **46**, 1029 (1934).
[13] K. Greisen and N. Nereson, Phys. Rev. **62**, 316 (1942).
[14] Miscellaneous experimental details are described by L. H. Meredith, Doctoral Dissertation, State University of Iowa, 1954 (unpublished).

D. Radio Telemetering System

Throughout the balloon-borne phase and the free-flight phase of the rocket's flight, the counting rate of the Geiger counter was transmitted to a receiving station on the launching ship[15] by a radio telemetering system. The Geiger counter pulses were fed directly to a cathode follower and from this to a scale of thirty-two circuit.[16] Pulses from this scaler were used to shift the frequency of a 3900-cps subcarrier oscillator. The oscillator output then frequency modulated a 76 megacycle per second rf transmitter. The transmitting antenna consisted of two portions of the rocket itself: the nose shell (about 36 in. in length) was electrically insulated from the afterbody. The transmitter was arranged to produce an rf potential difference between these two portions, giving a quite suitable radiation pattern with cylindrical symmetry about the rocket axis.

At the receiving station the rf signal was received by a directional two-stack Yagi antenna and fed to a Clarke Instrument Company 167-J high quality FM receiver. The receiver's audio-frequency output was put through a band-pass filter to a discriminator. This discriminator yielded a voltage pulse for each transient audio-frequency shift. These pulses were amplified by a Brush Electronics Company BL-905 amplifier and then recorded on the moving paper strip of a Brush BL-202 inking oscillograph. A simultaneous recording was made on the same paper strip of time signals which occurred at five second intervals. This telemetering system was similar to that described by Coor.[17]

E. Physical Arrangement

The physical arrangement of the equipment in the rocket is shown in Fig. 1. The equipment was mounted on circular plates which were $\frac{3}{8}$ in. thick. The upper three of these plates were of Dow metal while the lower one, which supported the lead storage battery, was of steel. The plates were supported by $\frac{1}{2}$ in. diameter brass posts. To prevent corona the nose shell was sealed pressure-tight with an "O"-ring to maintain sea-level pressure throughout flight.

TABLE II. Effective lengths and geometric factors of Geiger counters.

Flight number	Counter effective length (cm)	ϵG_{geo} (cm² steradian)
White Sands	6.70±0.08	70.7±1.1
S.U.I.-2	6.60±0.08	69.8±1.1
S.U.I.-4	6.60±0.08	69.8±1.1
S.U.I.-5	6.60±0.08	69.8±1.1
S.U.I.-23	6.20±0.08	66.1±1.1

[15] The U. S. Coast Guard Cutter Eastwind (WAGB-279), an icebreaker.

[16] Rugged subminiature tubes (Raytheon CK5678's) were used in a circuit adapted from one kindly sent us by J. A. Simpson.

[17] T. Coor, Doctoral Dissertation, Princeton University, 1948 (unpublished).

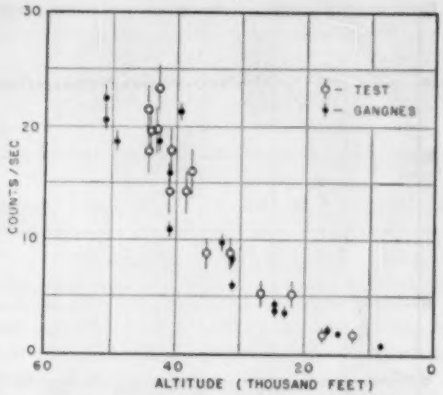

FIG. 2. Comparison of test flight results (open circles) of present equipment at White Sands, New Mexico with previous results (solid circles) at same location. See text and reference 10.

From Fig. 1, it can be seen that the Geiger counter was located at the apex of the instrumentation and was well isolated from any masses of material. The polystyrene supporting disk at the lower end of the counter was 2 in. in diameter and 0.2 in. in thickness. The aluminum nose shell was 0.050 in. in thickness. These thicknesses were judged to be the minimum values sufficient to provide the necessary strength.

Minimum thicknesses were desired for two reasons. The first was to reduce the contribution of locally produced secondaries to the measured counting rate. In this connection it should be mentioned that the body of the rocket subtended less than 2 percent of the total solid angle seen by the Geiger counter. The second was to reduce to the lowest practical value the amount of material which a particle must traverse before reaching the active volume of the Geiger counter. It was for this latter purpose that thin walled Victoreen 1B85 Geiger counters were selected. By means of detailed path length calculations on the exact physical arrangement it was found that the minimum thickness of material which a particle had to traverse to reach the active volume of the counter was 0.4 g/cm². With the rocket in nose-up aspect 90 percent of the radiation experienced a path length of less than 0.5 g/cm²; whereas in nose-down aspect, 60 percent experienced a path length less than 0.5 g/cm². Hence we adopted 0.5 g/cm² of aluminum as the effective apparatus thickness.

F. Preliminary Flights

An initial test firing of one complete set of instrumentation was made in a Deacon rocket nearly identical with those later to be used in the flights at northern latitudes. The rocket was launched from a short tower mounted on the ground at the White Sands Proving Ground. The firing was conducted by the staff of the Naval Ordnance Missile Test Facility at 0645 M.S.T. on June 26, 1952. Operation of the equipment was

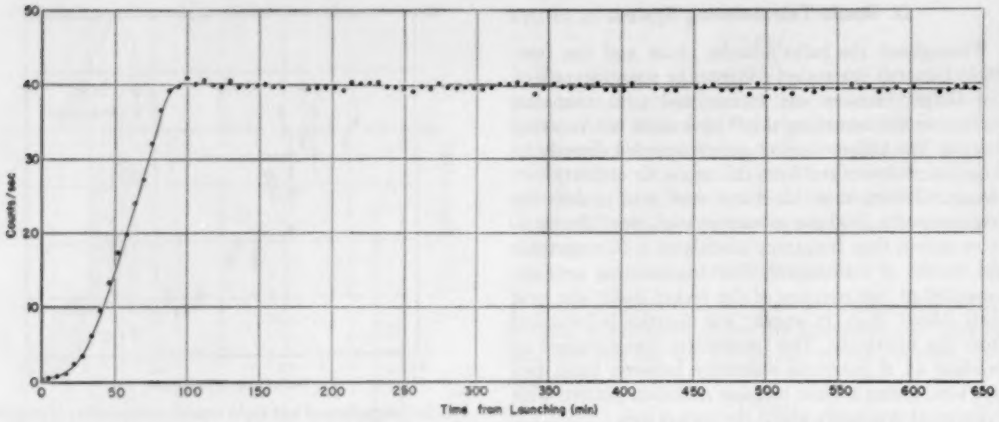

FIG. 3. Counting rate data obtained in a balloon-rocket flight in which the rocket failed to fire. $\lambda = 87°$ N. S.U.I.-2 of August 24, 1952.

satisfactory. The observed counting rate of the Geiger counter as a function of altitude is shown in Fig. 2; tracking data furnished by the N.O.M.T.F. were used in converting the observed counting rate *vs* time data to an altitude above sea level basis.

Also shown for comparison on Fig. 2 are similar data previously obtained by Gangnes, Jenkins, and Van Allen[10] at the same location. These previous results, obtained with a single Geiger counter of different dimensions, were normalized on an absolute basis to the size of a 1B85 counter by using the appropriate geometric factors. There is seen to be satisfactory agreement between the two sets of data.

A flight test on how long the entire system would operate properly on the batteries used was obtained in a balloon rocket flight made at $\lambda = 87°$. In this flight the rocket failed to fire due to a defective firing circuit. Figure 3 shows the results obtained. It can be seen that

FIG. 4. Chart showing geographic location of rockoon flights.

TABLE III. General flight data.

Flight No.	S.U.I.-2	S.U.I.-4	S.U.I.-5	S.U.I.-23
Geographic latitude and longitude of balloon launching	77° 31′ N 73° 30′ W	77° 32′ N 73° 29.5′ W	77° 21′ N 73° 29′ W	44° 33′ N 57° 03′ W
Geomagnetic latitude of balloon launching				
(a) Per centered dipole	88.5°	88.5°	88.5°	56.5°
(b) Per eccentric dipole	86.7°	86.7°	86.7°	54.3°
Time of rocket firing	Rocket did not fire. Balloon launched at 0334 G.C.T.	0830 G.C.T.	1917 G.C.T.	1510 G.C.T.
Date	24 Aug. 1952	29 Aug. 1952	29 Aug. 1952	3 Sept. 1953

for nine hours the counting rate was nearly constant at 39.5 counts/second. The small counting rate decrease was attributed to a slow descent of the balloon and rocket. During this period the rocket altitude was about 21.3 km (45 g/cm²). This flight also demonstrated the adequacy of the arrangements for maintaining the temperature of the rocket in the range of proper operability. In addition, the data are of value for comparison with data from subsequent rocket flights.

The termination of the data was caused by the fading of the transmitter signal. This could have been caused by the passage of the apparatus over the radio horizon or by a transmitter battery failure. In either case Fig. 3 shows the system could operate on the batteries used for at least 10.7 hours after launching. The complete system was set in operation about a half hour before launching. For the flights in which the rocket fired the total time of operation of the equipment was an hour and a half to two hours. The system then had a safety factor in its length of operation of about six.

III. RESULTS

A. General Flight Data

The locations of the launchings of the "rockoon" flights are shown in Fig. 4. In this figure, the number

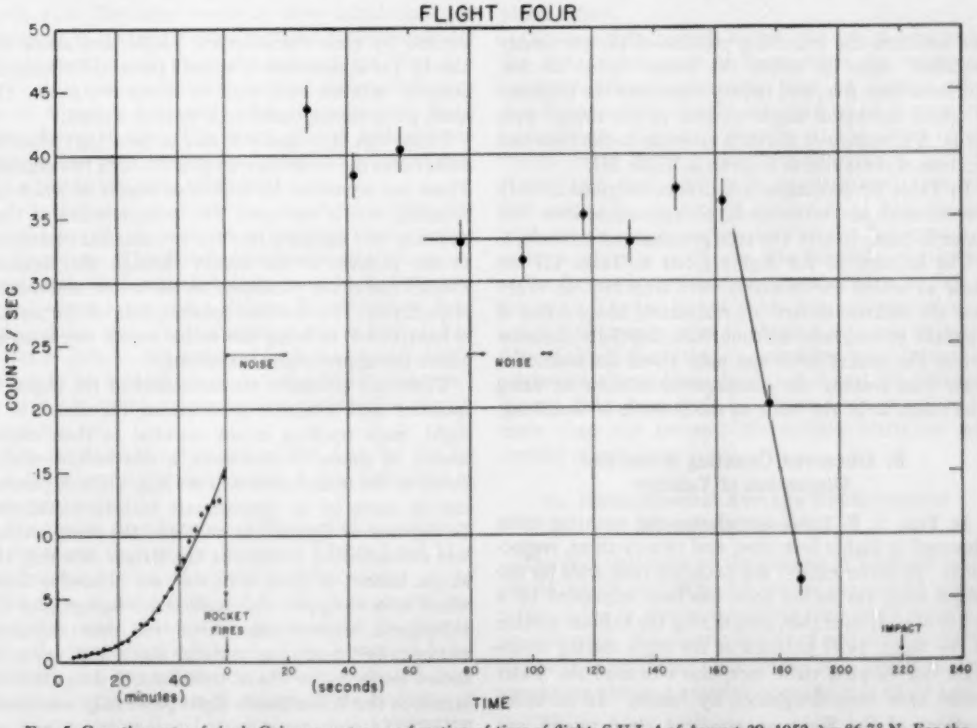

FIG. 5. Counting rate of single Geiger counter as a function of time of flight. S.U.I.-4 of August 29, 1952. λ = 86.7° N. For the first 54 minutes the rocket was being lifted by a General Mills Type 551 balloon. The remainder of the data was recorded during flight of the rocket to high altitude and return to the sea. Note 60-fold expansion of time scale during latter period.

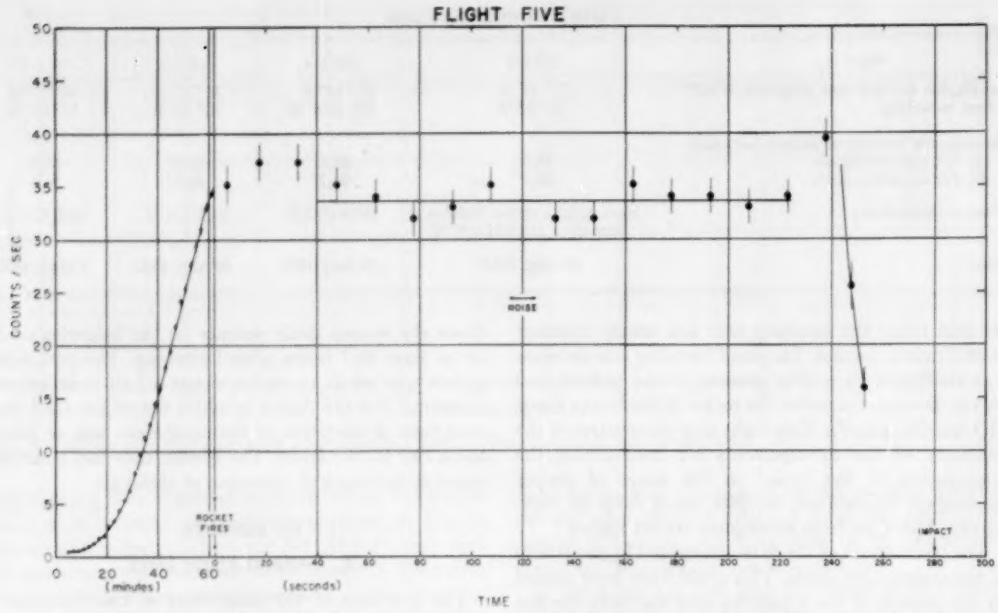

FIG. 6. Counting rate of single Geiger counter as a function of time of flight. S.U.I.-5 of August 29, 1952. $\lambda = 86.7°$ N. Rocket fired at 62 minutes after release of rocket-balloon system from ship.

two indicates the launching position of the previously described flight in which the rocket failed to fire. Numbers four, five, and twenty-three give the locations at which successful single counter rocket firings were made. A summary of the data relevant to the time and location of these flights is given in Table III.

In Table III geomagnetic latitudes are given in both the centered- and eccentric-dipole approximations. The latter is taken to give the true geomagnetic latitude, λ.

The latitude of the flights given in Table III are those at which the rockoons were launched. In every case the rockoon drifted approximately along a line of constant geomagnetic latitude. Also, the flight duration before the rocket fired was only about an hour. For these two reasons the geomagnetic latitude of firing was taken to be the same as the latitude of launching.

B. Observed Counting Rates and Discussion of Validity

In Figs. 5, 6, and 7 are shown the counting rates observed in flights four, five, and twenty-three, respectively. To better exhibit the data, the time scale for the period after the rocket fired has been expanded by a factor of sixty over that used during the balloon portion of the flight. Brief portions of the flight during which noise due to poor radio reception obscured the scaler pulses have been designated by "noise." In all other portions of the flight an excellent clear record was obtained. That all the pulses were from the scaler was verified by their characteristic height and shape and also by the appearance of a small pulse of the opposite polarity between each scale of thirty-two pulse. This small pulse corresponded to a scale of sixteen.

From Figs. 5, 6 and 7 it can be seen that after the rocket fires the counting rate goes through two maxima. These are separated by a plateau region in which the counting rate is constant. The interpretation of these counting rate curves is that the two maxima correspond to the passage of the rocket through the Regener-Pfotzer transition maximum on the ascent and descent respectively. The constant counting rate on the plateau is interpreted[9] as being due to the cosmic ray intensity above the appreciable atmosphere.

Under the primitive circumstances of the flights no facilities were available for tracking the rocket in its flight. Such tracking is not essential to these experiments, of course. Nonetheless, a worthwhile validity check on the time duration of the high-altitude plateaus can be made by an approximate ballistic calculation. In the case of flights four and five, the firing altitude was estimated by comparing the Geiger counting rate at the instant of firing with the rate in similar flights which were equipped with radio sonde barographs. The subsequent altitude-time curve was then calculated numerically[18] assuming vertical flight and using the rocket performance characteristics and drag data obtained in the White Sands flight previously mentioned.

[18] The authors are indebted to Mr. E. C. Ray and Mr. R. M. Missert for these calculations.

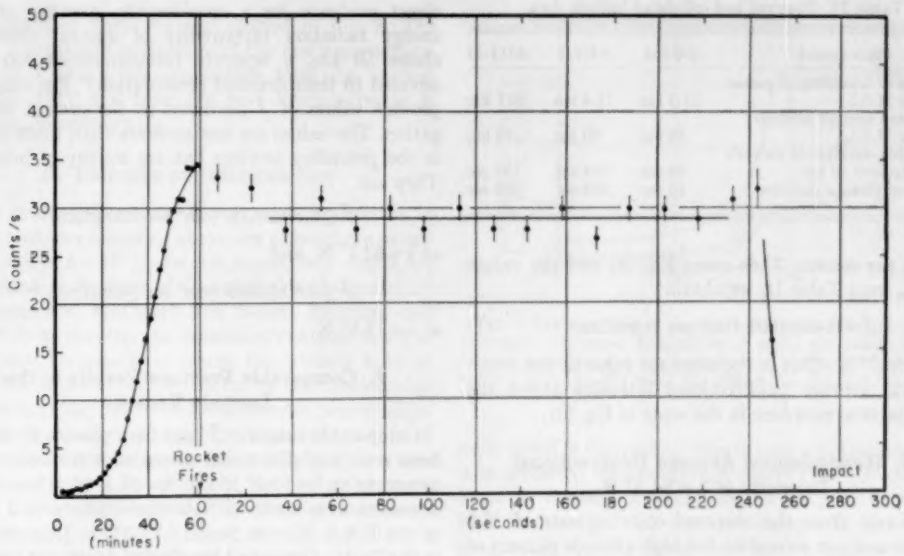

FIG. 7. Counting rate of single Geiger counter as a function of time of flight. S.U.I.-23 of September 3, 1953. $\lambda = 54.3°$ N. Rocket fired at 62 minutes after release of rocket-balloon system from ship.

The firing altitude of Flight 23 was known from radio sonde data. Pertinent results of these calculations are tabulated in Table IV. Also included in this table are the observed plateau durations as found from Figs. 5, 6 and 7. It is evident that the observed plateau durations are in adequate agreement with the calculated flight time above 50 km. The onset of the high-altitude plateau has been previously found[10] to occur at just this altitude (at lower latitudes).

A further over-all check was made by plotting the distribution of time intervals between successive pulses on the plateau. This distribution was in excellent agreement with that expected from a scale-of-thirty-two circuit whose input was a Poisson distribution of individual pulses with constant average rate of arrival; and it was in definite disagreement with the broader distribution to be expected from any significant occurrence of bursts of corona, microphonism, intermittent circuit operation, etc.

The satisfactory agreement of the data for the up and down legs of the flight is also a good indication of trustworthiness.

The greater time duration of the transition maximum on the ascent than on the descent of Flights 5 and 23 is attributable to lack of precision of knowledge of the firing time of the rocket and to the three second accelerative period of the rocket on the ascent. No sharply defined telemetering indication of the instant of firing occurred; the firing time was crudely estimated from the more rapid time-rate-of-change of the intensity of the rf telemetering signal which occurs during the rocket phase of the flight. A precise determination of the firing time is, of course, not essential to the accuracy of the plateau data.

Our own data provide no information as to whether the flights were made at times when the cosmic-ray intensity differed appreciably from its average value. But Simpson[19] has kindly informed us of the neutron intensities at Climax, Colorado, at the times of our flights. These neutron intensities are given in Table V. Neher and Forbush[20] have demonstrated that the fluctuations in the rate of ionization at high balloon altitudes are closely correlated with the fluctuations in neutron intensity at Climax. The fractional fluctuation of the former is two to three times as great as that of the latter. The last line of Table V was calculated using a factor of three in order to obtain a generous estimate. Thus Table V shows that our omnidirectional intensities above the atmosphere (Flights 4, 5 and 23) probably do not differ from their long term average values by more than one percent. No explicit correction was applied to our data.

C. Hemispherical Average Unidirectional Intensity at $\lambda = 86.7°$ N

The counting rates on the plateau of Flights 4 and 5 are 33.3 ± 0.8 and 33.6 ± 0.5 counts per second respectively, being in agreement within their small statistical uncertainties. (Geometric factors of respective counters identical.) Combining these results with proper relative weight we obtain a plateau counting rate of 33.5 ± 0.4

[19] J. A. Simpson (private communication).
[20] H. V. Neher and S. E. Forbush, Phys. Rev. **88**, 889 (1952).

TABLE IV. Observed and calculated ballistic data.

Flight number	S.U.I.-4	S.U.I.-5	S.U.I.-23
Altitude of launching of rocket above M.S.L.	11.0 km	17.4 km	20.1 km
Calculated summit altitude above M.S.L.	55 km	90 km	98 km
Calculated duration of rocket's flight above 50 km	64 sec	181 sec	198 sec
Measured plateau duration	76 sec	184 sec	200 sec

counts per second. Then using Eq. (3) and the values of ϵG_{∞} from Table II, we obtain

$$J=0.48\pm0.01 \text{ (cm}^2 \text{ sec steradian)}^{-1} \quad (7)$$

at $\lambda=86.7°$ N. This is the absolute value of the hemispherical average unidirectional intensity above the appreciable atmosphere in the sense of Eq. (2).

D. Hemispherical Average Unidirectional Intensity at $\lambda=54.3°$ N

Similarly, from the observed counting rate of 28.8 $\pm$0.4 counts per second on the high-altitude plateau of Flight 23, we obtain

$$J=0.44\pm0.01 \text{ (cm}^2 \text{ sec steradian)}^{-1} \quad (8)$$

at $\lambda=54.3°$ N. The errors indicated in (7) and (8) encompass statistical counting errors and errors in knowledge of ϵG_{∞}.

E. Hemispherical Average Unidirectional Intensity at $\lambda=62.1°$ N and $\lambda=71.9°$ N

Two other successful rockoon flights (S.U.I.-20 and S.U.I.-13) of identical apparatus were made during the 1953 expedition. The flights at $\lambda=62.1°$ N and 71.9° N respectively were made in the auroral zone. Inasmuch as the results of these flights have provided direct evidence for a considerable intensity of low-energy radiation (apparently of auroral character) above 50 km, a separate communication has been devoted to their detailed presentation.[21] But they also provide values of J pertinent to the present investigation. The values are less accurate than those quoted in the preceding sections but are worthy of inclusion. They are

$$J\leq0.50\pm0.05 \text{ (cm}^2 \text{ sec steradian)}^{-1} \quad (9)$$

at $\lambda=62.1°$ N, and

$$J\leq0.50\pm0.05 \text{ (cm}^2 \text{ sec steradian)}^{-1} \quad (10)$$

at $\lambda=71.9°$ N.

F. Comparable Previous Results in this Latitude Region

Comparable values of J have been previously derived from results of directional coincidence telescope measurements at $\lambda=52.2°$ N and $\lambda=59.3°$ N. These measurements were made with Aerobee rockets on a cruise of the U.S.S. Norton Sound (AV-11) in January, 1950 in the Pacific Ocean and the Gulf of Alaska.[5] Apparatus stopping powers were about 3 g/cm^2 of copper and aluminum. The results were:

$$J=0.31\pm0.03 \text{ (cm}^2 \text{ sec steradian)}^{-1} \quad (11)$$

at $\lambda=52.2°$ N, and

$$J=0.41\pm0.03 \text{ (cm}^2 \text{ sec steradian)}^{-1} \quad (12)$$

at $\lambda=59.3°$ N.

IV. SUMMARY AND DISCUSSION

A. Tabular Summary of Observed Data

The values of J above the atmosphere (7), (8), (9), (10), (11), (12) and others previously reported[10,22] are

TABLE V. Neutron intensity data at Climax, Colorado (after Simpson).[a]

Flight No.	S.U.I.-2	S.U.I.-4	S.U.I.-5	S.U.I.-23
Firing time	Aug. 24, 1952 (See Table III)	Aug. 29, 1952 0830 G.C.T.	Aug. 29, 1952 1917 G.C.T.	Sept. 3, 1953 1510 G.C.T.
Average neutron intensity during hour of measurement	0530 to 1330: 3550	0800 to 0900: 3593	1900 to 2000: 3597	1500 to 1600: 3627[b]
Long term average hourly rate[c]	3589.8	3589.8	3589.8	3639.7[b]
Percent difference between neutron intensity during flight and average value	−1.1%	+0.09%	+0.20%	−0.35%
Presumed percent difference between measured and average charged particle intensities above atmosphere	−3.3%	+0.3%	+0.6%	−1.0%

[a] See reference 19.
[b] These rates were measured with a different pile than that in use during Flights 2, 4, and 5. The rate has, however, been normalized to the pile used at the time of Flights 2, 4, and 5. This normalization has an uncertainty of ±0.5 percent.
[c] For Flights 2, 4, and 5 this rate was obtained by averaging the neutron intensity for the period July 24–September 1, 1952. For Flight 23 the rate was the average neutron intensity for the period spanned by ±20 days of the firing day.

[21] Meredith, Gottlieb, and Van Allen, Phys. Rev. 97, 201 (1955).
[22] J. A. Van Allen and A. V. Gangnes, Phys. Rev. 78, 50 (1950).

summarized in Table VI and plotted in Fig. 8. The reader is cautioned to distinguish the raw experimental value of J above the atmosphere from the vertical intensity $J(0°)$ and from the best direct estimate of the primary intensity J_P.

B. Remarks on Interpretation

It is evident that there is only a slight increase in total cosmic-ray intensity above the atmosphere as one goes north of $\lambda=55°$ N. In this respect our results are concordant with those of Carmichael and Dymond,[33] Pomerantz and McClure[34] and Neher, Peterson, and Stern.[35] In particular, the ionization chamber work of Neher and his associates places the latitude knee at $\lambda'=58°$ N or $\lambda=57°$ N. By virtue of the considerably reduced stopping power of our apparatus plus residual atmosphere (total of 0.5 g/cm²) in contrast to that of previous balloon investigators (10 to 15 g/cm²), it is now possible to extend considerably and to make more certain the low-rigidity end of the primary cosmic-ray spectrum.

Several general points should be noted:

(1) The interpretation of all gross "latitude effects" into information pertaining to the rigidity (or energy) spectrum of the primary radiation has essential dependence on geomagnetic theory.[1] If presently accepted geomagnetic theory is found to contain important omissions or errors then the interpretation will be correspondingly in error.

(2) Our measurements are limited in temporal extension and may not provide a full picture of long term conditions.

(3) Single Geiger counters measure effectively the omnidirectional intensity. Hence the observed values of J previously reported comprise comparable contributions from primary radiation and from secondary radiation (atmospheric "albedo"). That is, we may write

$$J=J_P+J_A, \tag{13}$$

where the subscripts P and A denote primary and albedo radiation respectively.

(4) Total intensity measurements such as the present ones are of no useful significance with respect to heavy primaries ($Z>2$) due to the low relative intensity of heavies in the primary beam. Rather, they pertain to the major components—protons and alpha particles. A separate investigation of the low-rigidity end of the spectra of heavy primaries is reported elsewhere.[36]

(5) Even if there is a cutoff in the spectra of the principal components of the primary radiation at a magnetic rigidity $R_{\min}$—corresponding to the geomagnetic cutoff in the vertical direction at some latitude λ—it is predicted by geomagnetic theory that J_P will continue to increase substantially as one goes to higher latitudes than λ. This expected increase is due to the progressive opening up of the "earth's shadow cone." At latitudes such as $\lambda=55°$ the shadow cone is responsible for much higher values of R_c at large zenith angles than the vertical value. Only at $\lambda=90°$ does R_c go to zero for all θ and φ.

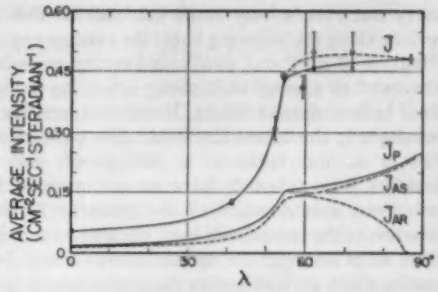

FIG. 8. Summary plot of observed total unidirectional intensity (averaged over upper hemisphere) J above the atmosphere at various latitudes, and the analysis into primary radiation J_P, splash albedo J_{AS}, and re-entrant albedo J_{AR}. $J=J_P+J_{AS}+J_{AR}$. See Sec. IV of text.

(6) For analytical purposes it is helpful to consider the albedo radiation at any point above the atmosphere to be divided into two categories: (a) "splash albedo," upward moving secondary radiation arising from nuclear collisions of primaries in the atmosphere and (b) "re-entrant albedo," downward moving secondary radiation of the same origin which has been unable to escape from the earth's field and which is therefore returning to the atmosphere.

(7) The intensity of splash albedo is calculable, in principle, from data on the angular distribution and intensities of primaries, on the cross sections for interaction, on the multiplicity, angular distribution, energies and nature of the secondaries, etc. Unfortunately, the existing experimental data are still too meager to permit a satisfactory calculation. Nonetheless, it is illuminating

TABLE VI. Observed unidirectional intensity above the atmosphere averaged over upper hemisphere.

Geomagnetic latitude—λ	J (cm² sec steradian)⁻¹	Reference
0	0.053±0.002	a
41° N	0.120±0.009	b
52.2° N	0.31 ±0.03	c
54.3° N	0.44 ±0.01	d
59.3° N	0.41 ±0.03	c
62.1° N	0.50 ±0.05	e
71.9° N	0.50 ±0.05	e
86.7° N	0.48 ±0.01	d

[a] See reference 22.
[b] See references 9, 10, 11.
[c] See reference 5.
[d] See present paper.
[e] See reference 21.

[33] H. Carmichael and E. G. Dymond, Proc. Roy. Soc. (London) **A171**, 321 (1939).
[34] M. A. Pomerantz and G. W. McClure, Phys. Rev. **86**, 536 (1952) and references to previous work therein.
[35] Neher, Peterson, and Stern, Phys. Rev. **90**, 655 (1953).
[36] Ellis, Gottlieb, and Van Allen, Phys. Rev. **95**, 147 (1954).

to carry out even a very crude calculation. This we have done along the following lines: the average angular distribution of grey and minimum-ionizing secondary tracks and their average multiplicity according to high-altitude balloon data of Salant, Hornbostel, and Blau[27] were adopted; the interaction mean free path of primaries in air was taken to be 100 g/cm²; and all secondaries were taken to have an air range of 150 g/cm². From consideration of the generally forward collimation of the secondaries in an elementary act, it is evident that most of the splash albedo arises from primaries which are incident on the atmosphere at large zenith angles. By the same token, the intensity of the splash albedo is a minimum in the vertical direction; its intensity at large zenith angles is several times greater. In a specific calculation for isotropic incidence of primaries, we find that the contribution of albedo (splash) to the average intensity above the atmosphere is

$$J_{AS}=0.3J_P. \tag{14}$$

The bulk of the contribution comes from primaries arriving at zenith angles greater than 60°.

(8) The fate of the splash albedo in the earth's magnetic field is either return to the top of the atmosphere (thus becoming re-entrant albedo) or escape to infinity. In a valuable discussion of this matter Treiman[28] has shown that all splash albedo which originates at latitude λ and which does not satisfy the geomagnetic conditions for escape will return to the atmosphere at approximately the same latitude (in either the same or opposite hemisphere of the earth), the breadth of the zone of re-entry being dependent on the magnetic rigidity of the radiation and on the angle of "emission." In a typical case this zone has a width of one or two degrees of latitude. Treiman conjectures that the re-entrant albedo returns more or less isotropically. Yet it is possible to see that in some simple cases (e.g., near the equator) that albedo which leaves at a large zenith angle will likewise return at a large zenith angle. Thus, it is reasonable to believe that there is some persistence of direction, though the tendency is toward isotropy of re-entry. In view of the essential lack of interchange of albedo from one latitude to another and in consideration of the magnetic rigidities of typical secondaries one may conclude that approximately the ratio

$$J_{AR}/J_{AS}=1 \quad \text{for} \quad \lambda<55°, \tag{15}$$

wherein the subscript AR denotes albedo (re-entrant), and the subscript AS, albedo (splash). Toward higher latitudes, the ratio of J_{AR}/J_{AS} progressively diminishes due to increasing ease of escape from the geomagnetic field until

$$J_{AR}=0, \quad \text{at} \quad \lambda=90°. \tag{16}$$

These considerations are essential to our interpretation of the variation of J with λ.

(9) The total unidirectional intensity above the atmosphere *in the vertical direction* contains the least contribution of albedo, and therefore represents the best simply observable approximation to the true primary intensity at any latitude. Absolute measurements of the vertical unidirectional intensity above and near the effective top of the atmosphere have been reported by a number of workers.[29–31] The results of these measurements can be well represented[31] by the integral number-rigidity spectrum:

$$J(>R)=0.48R^{-1.1}, \quad 2 \text{ Bv}\leq R\leq 15 \text{ Bv}, \tag{17}$$

where $J(>R)$ gives the intensity in units of (cm² sec steradian)$^{-1}$ of particles whose magnetic rigidity exceeds $R(\equiv pc/Ze)$ Bv. Or, in the corresponding range of energy[29] (making the approximation $Z/A=1$ for all constituents),

$$J(>E)=0.37E^{-0.9}, \tag{18}$$

where E is kinetic energy in Bev and the units of J are as in (17).

It is a matter of great importance to determine experimentally the fraction of the vertical unidirectional intensity which is albedo. The experimental difficulties are formidable; but there are several investigations[32,33] at $\lambda'=40°$, 41° which make it reasonable to assume that about 0.85 of the total vertical unidirectional intensity is true primary radiation and about 0.15 of the total is albedo of splash and re-entrant types. We shall make the further tentative assumption that this proportion is independent of latitude.

C. First Trial Interpretation: No Spectral Cutoff

On the basis of the foregoing considerations it is assumed specifically that the integral primary spectrum is given by

$$J_P(>R)=0.41R^{-1.1}, \tag{19}$$

or by

$$J_P(>E)=0.31E^{-0.9}. \tag{20}$$

For a first trial interpretation it is further assumed that there is *no spectral cutoff*—e.g., spectra (19) and (20) continue to hold below the rigidity, or energy, for which they have been determined and do, indeed, hold for $R\to 0$, or $E\to 0$. Then, by using the details of geomagnetic theory and the range limitations of our apparatus, it is possible to calculate the expected latitude dependence of observable J_P. The effective apparatus

[27] J. Hornbostel (private communication).
[28] S. B. Treiman, Phys. Rev. **91**, 957 (1953).
[29] Winckler, Stix, Dwight, and Sabin, Phys. Rev. **79**, 656 (1950).
[30] M. Vidale and M. Schein, Nuovo cimento **8**, 1 (1951).
[31] J. A. Van Allen and S. F. Singer, Phys. Rev. **78**, 819 (1950); **80**, 116 (1950).
[32] S. E. Golian and E. H. Krause, Phys. Rev. **71**, 918 (1947); G. J. Perlow and J. D. Shipman, Phys. Rev. **71**, 325 (1947); Perlow, Davis, Kissinger, and Shipman, Phys. Rev. **88**, 321 (1952).
[33] J. R. Winckler and K. Anderson, Phys. Rev. **93**, 596 (1954).

thickness was 0.5 g/cm² of aluminum. This corresponds to the ionization range of a proton of kinetic energy 19 Mev or magnetic rigidity 0.19 Bv. The hemispherical average *primary* intensity, in the sense of Eq. (2) and as observable with our apparatus was calculated omitting any contribution from albedo. Such calculations give a lower limit of the total J to be expected under the prevailing assumption. The results of these calculations are that the extrapolated spectrum (19) leads to a lower limit of the expected intensity at $\lambda=87°$ of about *five times* that observed, and that the extrapolated spectrum (20) leads to a lower limit of expected intensity about *seventeen times* that observed.

Hence, without further refinement, we conclude that the assumptions of this section—namely no low-rigidity spectral cutoff and no change of spectral form at low rigidities—are overwhelmingly false.

D. Second Trial Interpretation: Sharp Spectral Cutoff at $R=1.7$ Bv

The assumption is now made that the integral primary spectrum is given by

$$\begin{aligned} &J_P(>R)=0.41R^{-1.1}, \quad 1.7 \text{ Bv}\leq R<\infty\,; \\ &J_P(>R)=(0.41)(1.7)^{-1.1}=0.23, \quad R\leq 1.7 \text{ Bv}. \end{aligned} \tag{21}$$

The foundations for this assumption are to be found in reference 31.

For simplicity of calculation, the spectral assumption of this section has been formalized in Eqs. (21) to a perfectly sharp break at $R=1.7$ Bv (vertical geomagnetic cutoff at $\lambda=54°$). It may well be that a rounding of the spectrum from 1.8 to 1.2 Bv, and then a complete flatness below 1.2 Bv, for example, are more natural and may be supported eventually by more detailed experiments in the appropriate latitude range.

The resulting curve of expected J_P *vs* λ is plotted in Fig. 8.

Also shown in Fig. 8 are two dashed curves representing the latitude dependence of J_{AS} and J_{AR}. At latitudes less than 55° it was assumed that $J_{AR}=J_{AS}$. (This is equivalent to the assumption that all albedo particles have a magnetic rigidity less than 1.6 Bv.) And, of course,

$$J=J_P+J_A=J_P+J_{AS}+J_{AR}. \tag{22}$$

North of $\lambda=55°$, a continuation of the J_{AS} curve has been estimated by assuming that J_{AS} is proportional to the intensity of primary radiation arriving at zenith angles greater than 60°. Finally, the curve of J_{AR} north of 55° has been drawn so that

$$J_{AR}=J-J_P-J_{AS}. \tag{23}$$

The fall-off of J_{AR} north of 55° is seen to be generally plausible; and in fact J_{AR} falls to nearly zero at $\lambda=90°$, as it must, though this requirement was nowhere introduced in the analysis.

It seems most remarkable that the true fall-off of J_{AR} with latitude should occur in just such a way as to so nearly compensate for the concurrent increase of J_P+J_{AS}. There is, however, a suggestion of an upward bulge in the measured values of J in the vicinity of $\lambda=70°$. If this bulge persists in more accurate measurements (which are currently underway), it may be related to the similar one reported by Neher *et al.*[25] and may simply reflect the imperfection of the above mentioned cancellation.

A specific prediction of the foregoing interpretation is that the *vertical* intensity above the atmosphere at $\lambda=90°$ is 0.29 (cm² sec sterad)$^{-1}$. No experimental evidence on this matter is available as yet.

Figure 8 and the foregoing discussion demonstrate that the experimental results are consistent with a primary spectrum which is sharply cut off at $R=1.7$ Bv [Eq. (21)].

In view of fundamental uncertainties in the higher rigidity portion of the primary spectrum, in the production of albedo, and in the details of geomagnetic theory, it is very difficult to make a precise conclusion as to the absence of primaries of magnetic rigidity less than about 1.7 Bv. Nonetheless, Fig. 8 presents the physical situation as presently understood and is probably substantially correct.

V. ACKNOWLEDGMENTS

The authors are indebted for important assistance to Lt. Malcolm S. Jones, Jr., U.S.N, formerly of the Office of Naval Research, and to Dr. R. A. Ellis, Jr., Mr. J. G. Sentinella, and Mr. L. F. Blodgett of this laboratory.

The rocket flights were made possible by the cooperation of a number of agencies of the U.S. Navy and the U.S. Coast Guard and in particular by the officers and men of the U.S.C.G.C. Eastwind, from which the flights were launched. The full-hearted support and patience of Captain O. A. Peterson, U.S.C.G., captain of the Eastwind during the difficult pioneer flight operations of the summer of 1952, are especially appreciated.

Balloon launching operations were supervised by engineers of the General Mills Aeronautical Laboratories.

Photoproduction of Positive Pions in Hydrogen-Magnetic Spectrometer Method*

R. L. Walker, J. G. Teasdale, V. Z. Peterson, and J. I. Vette
California Institute of Technology, Pasadena, California

(Received March 7, 1955)

Positive pions produced in a cold, high-pressure hydrogen gas target by the 500-Mev bremsstrahlung of the CalTech synchrotron, have been analyzed by a large magnetic spectrometer. The photoproduction cross section has been measured as a function of photon energy at laboratory angles of 12.5°, 30°, 51°, 73°, 104°, 140°, and 180°. The energy region covered depends somewhat on the angle, but is typically from 200 to 470 Mev. From these excitation curves the angular distribution of the photopions in the center of momentum system is obtained for various photon energies, and these angular distributions are analyzed in the form $A+B\cos\theta+C\cos^2\theta$. The angular distribution has a backward maximum at low energies and a forward maximum at high energies, the coefficient B changing sign at about 340 Mev. The total cross section shows a striking maximum near 290 Mev, of magnitude 205×10^{-28} cm², and falls off above the maximum faster than λ^3.

INTRODUCTION

THE nature of the interaction between pions and nucleons may be investigated most directly, perhaps, by measurements of the scattering of pions by nucleons. Many such pion-nucleon scattering experiments have been performed, and the results analyzed in terms of scattering phase shifts.[1,2] The analysis does not yield unique results, and the problem of deciding which phase shifts are probably the correct ones has been extensively investigated by de Hoffmann, Metropolis, Alei, and Bethe.[2–4]

A closely related process is photopion production, which involves the interaction between photons and the two particles, pion and nucleon, as well as the interaction between pion and nucleon themselves.

The first measurements of the photoproduction of positive pions in hydrogen were those of Steinberger and Bishop[5] at Berkeley. They measured the cross section at 90° in the laboratory between photon energies 170 and 320 Mev, using targets of polyethylene and carbon, and making a subtraction to obtain the cross section in hydrogen. The pions were identified by requiring a delayed coincidence from the $\pi-\mu-e$ decay. The pion energy was obtained from its range in aluminum absorber placed between target and counter. Steinberger and Bishop found that the excitation curve at 90° seemed to reach a maximum near 290 Mev and was either flat or starting to decrease between 280 and 310 Mev. They also measured the angular distribution at 255 Mev between 60° and 160° in the center of mass system, and found a maximum in the backward hemisphere. These results have been verified in succeeding work.

Further measurements of photopion production in hydrogen have been made at Berkeley by White, Jacobson, and Schulz[6] and by Jarmie, Repp, and White.[7]

The most extensive measurements to date in the region 200 to 300 Mev have been those performed at Cornell with a double focusing magnetic analyser, and targets of polyethylene and carbon.[8] The Cornell group finds that the angular distribution at 200, 235, and 265 Mev is peaked in the backward hemisphere in agreement with the data of Steinberger and Bishop. The cross section increases with energy in this region.

The behavior of the photopion production near threshold is of considerable interest, and has been extensively investigated at Illinois using photographic plates to detect positive mesons produced in a liquid hydrogen target.[9] Measurements at low energies have also been made at CalTech using photographic plates[10] and at the Massachusetts Institute of Technology using counter techniques involving a $\pi-\mu-e$ decay detection scheme[11] and a $\pi-\mu$ detection scheme.[12]

When the present experiments were begun, in June, 1953, we were especially interested in finding the behavior of the angular distribution above 300 Mev. The suggestion[13] that there might be a resonant interaction between pion and nucleon in a $P_{\frac{3}{2}}$ state of isotopic spin $\frac{3}{2}$ was consistent with pion-nucleon scattering data, and could perhaps explain the marked peak in the photoproduction of neutral pions at 90°, near 300 Mev.[14]

* This work was supported in part by the U. S. Atomic Energy Commission.

[1] See, for example: Anderson, Fermi, Martin, and Nagel, Phys. Rev. **91**, 155 (1953).

[2] For a review of the experimental data and analysis, and a list of references to the original work, see the forthcoming book: H. A. Bethe and F. de Hoffmann, *Mesons and Fields* (Row, Peterson, and Company, Evanston), Vol. 2.

[3] de Hoffmann, Metropolis, Alei, and Bethe, Phys. Rev. **95**, 1586 (1954).

[4] H. A. Bethe and F. de Hoffmann, Phys. Rev. **95**, 1100 (1954).

[5] J. Steinberger and A. S. Bishop, Phys. Rev. **86**, 171 (1952).

[6] White, Jacobson, and Schulz, Phys. Rev. **88**, 836 (1952).

[7] Jarmie, Repp, and White, Phys. Rev. **91**, 1023 (1953).

[8] Jenkins, Luckey, Palfrey, and Wilson, Phys. Rev. **95**, 179 (1954).

[9] G. Bernardini and E. L. Goldwasser, Phys. Rev. **94**, 729 (1954); Phys. Rev. **95**, 857 (1954).

[10] Vincent Peterson and I. George Henry, Phys. Rev. **96**, 850 (1954).

[11] Goldschmidt-Clermont, Osborn, and Winston, Phys. Rev. **91**, 468 (1953).

[12] G. S. Janes and W. L. Kraushaar, Phys. Rev. **93**, 900 (1954).

[13] K. Brueckner, Phys. Rev. **86**, 106 (1952).

[14] Walker, Oakley, and Tollestrup, Phys. Rev. **89**, 1301 (1953).

Calculations of photoproduction based on this idea had already been given by Brueckner and Watson.[15] If such a resonant interaction exists, one might expect the forward-backward asymmetry in the photopion production, which must arise from an interference between even and odd states, presumably S and P, to change sign at energies above the resonance. We find that this does, in fact, occur, and that the total cross section falls off very rapidly at energies above 300 Mev as might be expected from the resonance idea.

METHOD

Since the photoproduction of a pion in hydrogen is a two-body process, a measurement of the energy and angle of the emitted meson determines uniquely the energy k of the photon producing the reaction

$$\gamma+p\rightarrow\pi^{+}+n. \tag{1}$$

This fortunately makes it possible to measure the cross section at a specific photon energy in spite of the continuous bremsstrahlung spectrum from a synchrotron. The present experiment consists of counting the number of mesons produced at a given angle as a function of the meson energy, measured with a magnetic spectrometer. From the laws of conservation of energy and momentum, it is easy to find the following relation between the photon energy k and the pion momentum p_π, and angle θ_π.

$$k=\frac{m_pE_\pi-\frac{1}{2}(m_\pi^2-m_n^2+m_p^2)}{m_p-E_\pi+p_\pi\cos\theta_\pi}, \tag{2}$$

where m_π, m_p, and m_n are the masses of pion, proton, and neutron, respectively,[16] and $E_\pi=(p_\pi^2+m_\pi^2)^{\frac{1}{2}}$ is the total energy of the pion. The range of photon energies, Δk, corresponding to the range of momentum, Δp_π, accepted by the spectrometer, may be found by multiplying Δp_π by the factor,

$$\frac{\partial k}{\partial p_\pi}=\frac{p_\pi(m_p+k)-kE_\pi\cos\theta_\pi}{E_\pi(m_p-E_\pi+p_\pi\cos\theta_\pi)}. \tag{3}$$

The differential cross section $\sigma(\theta)$ is related to the observed counts C per standard beam monitor reading through the formula

$$C(k)=\sigma(\theta)\Delta\Omega N(k)\Delta k N_H R(k), \tag{4}$$

where $\Delta\Omega$ is the solid angle accepted by the spectrometer. $N(k)\Delta k$ is the number of photons of mean energy k within an energy interval Δk in the Bremsstrahlung beam. This number is known from an absolute beam calibration to be discussed later. N_H is the number of target hydrogen atoms per cm^2. $R(k)$ is a correction factor for the effect of decay of the pions before reaching the counters. It will be discussed in a later section. The preliminary reports of the present data[17] made use of a rough calculation of the decay correction, and differ a little from the final results reported here.

The values of k and Δk obtained from the simple formulas (2) and (3) have been corrected for energy loss of the pions in the walls of the target, as will be discussed in the next section.

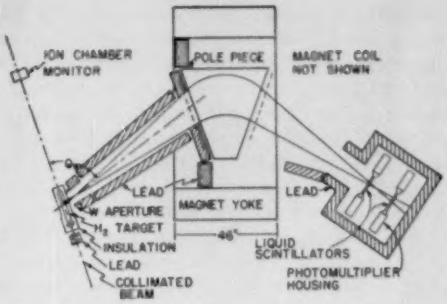

FIG. 1. Diagram of the magnetic spectrometer and the gas target.

APPARATUS

The experimental arrangement is shown in Fig. 1. The photopions are produced in a high-pressure hydrogen gas target located about 8 meters from the internal synchrotron target. The beam is collimated to 3.8 cm in diameter at the target by a primary lead collimator which is backed up by successively larger holes in two other lead collimators, the final one located immediately in front of the target. The hydrogen gas is contained at about 2000 psi in a bomb 2 inches in diameter and 17 inches long with 0.030-inch steel walls. This is connected to a liquid nitrogen reservoir, and surrounded by about 1.5 inches of styrafoam insulation, so that the hydrogen can be cooled to about 95°K, resulting in a typical gas density of 0.030 g cm^{-3}.

The density is obtained from a pressure measurement accurate to about one percent, and a temperature measurement of approximate accuracy three percent. The temperature is read at the two ends of the bomb with thermocouples, the reference junction being in the liquid nitrogen reservoir, at the temperature 77°K.

The thicknesses of the steel target walls, the styrafoam insulation, and the air path between target and magnet are not negligible in stopping power for the mesons. Thus a small correction must be made for energy loss of the pions before they enter the magnet. This correction shifts the photon energy k calculated from formula 2 by 4 to 12 Mev, depending on the meson angle and energy. This energy loss also influences the momentum range Δp_π accepted by the spectrometer, and thus the photon interval Δk. The resulting correction to the cross section amounts to only 1 to 3 percent in general, but becomes as high as 12 percent at lowest energies.

[15] K. Brueckner and K. M. Watson, Phys. Rev. **86**, 923 (1952).
[16] A positive pion mass of 139.6 Mev/c^2 was used in the calculations.
[17] Walker, Teasdale, and Peterson, Phys. Rev. **92**, 1090(A) (1953).

The energy analysis of the pions emitted at a given angle is made with a conventional magnetic analyser having wedge-shaped pole pieces as shown in Fig. 1. Two geometrical arrangements were used, one capable of measuring higher energy mesons than the other. The "short-focus" arrangement (shown in Fig. 1) has a focal distance (from the edge of the pole piece to the focal point) of 170 cm and a radius of curvature of 72 cm. This is suitable for measuring mesons of energies up to 200 Mev, using the maximum magnetic field of 15 000 gauss. A second "long-focus" arrangement has a focal distance of 254 cm, a radius of curvature of 98 cm, and can be used for meson energies up to 300 Mev. Neither arrangement is double focusing although in both some "focusing" in the vertical direction occurs in the fringe field of the magnet.[18]

The fringe field has been measured as a function of distance from the pole tip edge, and its effect on the path of the particles is included in the relation between particle momentum and magnetic field. The field was calibrated as a function of magnet current by means of a proton resonance magnetometer.

The counters are high enough for the short-focus arrangement to cover the full vertical height of the "image" as limited by a three-inch vertical aperture at the magnet entrance. This is not quite true for the long-focus arrangement. Thus, a correction to the solid angles for the long-focus measurements was made for the pions missing the counters above or below. This correction of 6 ± 3 percent was determined experimentally by counting protons from the target with the normal 3-inch magnet aperture and with an aperture decreased to 2 inches, for which the counters are definitely high enough.

The momentum resolution of the spectrometer is determined mainly by the width of the counters which is 9 inches. This gives a momentum range Δp accepted of approximately $\Delta p = (0.090)p$ for both long- and short-focus arrangements. The solid angle of acceptance is determined by the lead aperture at the magnet entrance. It varied from 0.002 to 0.011 steradian in the present experiments. The effective length of target seen by the spectrometer is defined by tungsten lined slits placed at the focal point of the magnet and as near to the target as possible. These slits, and the edges of the magnet aperture were tapered to minimize the uncertainties arising from slit penetration.

Mesons are counted by two large scintillation counters in coincidence. Each is a liquid scintillation cell of dimensions 6×9×1 inches, viewed by two RCA 5819 photomultipliers connected to the two ends of the cell by short Lucite light pipes. These counters are enclosed in lead shielding 4 inches thick on all sides, and additional lead shielding is placed along the sides of almost the entire meson path as shown in Fig. 1.

It was appreciated too late, unfortunately, that some mesons which scatter from this shielding pass through the counters, so a 10 percent correction must be made for this scattering. The experimental information for this correction is given in item C3 under "Errors."

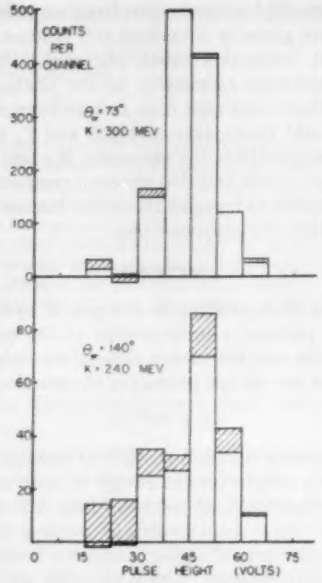

FIG. 2. Pulse-height spectra from the front counter, showing the pion peak. Background, as measured with the magnetic field of the spectrometer reversed, is shown by the cross-hatched areas. The two spectra are chosen from among the best and the worst obtained during the experiment.

Pulses from the two counters are amplified with amplifiers having rise times of about 0.07 μsec and delay line clippers giving pulses about 0.5 μsec long. These trigger pulse shaping circuits which form the inputs to a coincidence circuit with resolving time of 0.1 μsec. The coincidence circuit output is used to gate an 8-channel pulse-height analyzer which measures the pulse-height in the front counter. This is helpful in separating counts caused by mesons from background counts. Sample pulse-height spectra are shown in Fig. 2, the two curves having been chosen from the best and worst obtained during the experiment. This pulse-height analysis can be used at low energies to help distinguish mesons from electrons. Chance coincidence counts are monitored by a duplicate coincidence circuit having a 1-μsec delay in one input. The chance coincidences were 1 to 6 percent of the true counts in general, but in some cases became as high as 15 percent.

IDENTIFICATION OF PIONS

The magnet directs all particles having the appropriate momentum into the counters, and it is necessary to count from these only the number of pions, or in practice, pions plus decay muons. Discrimination against protons is very simple since protons of the same momenta

[18] See for example E. Segrè, *Experimental Nuclear Physics* (John Wiley and Sons, Inc., New York, 1953), Chapter by K. T. Bainbridge, pp. 576 ff.

as the pions observed in these experiments have very much smaller ranges than the pions. Thus a small thickness of lead absorber between the two counters prevents any coincidences from protons. Discrimination against positrons is more difficult, except at the lowest energies, where the ionization of pions in the first counter is appreciably above minimum, so that the pion pulse height peak is shifted above that of electrons. However, since one may expect the numbers of high-energy electrons and positrons to be about equal, it is easy to subtract the positron background by making a measurement with the magnetic field reversed. Fortunately, these negative field backgrounds were not high for most of the measurements, although they become large at the extreme angles. The magnitude of these backgrounds is given in Table I. At 12.5° no slits could be used at the target so the ends of the bomb were in view of the magnet, and the electron background was quite serious. The electron counts could be reduced to 25 to 50 percent for the high-energy points by using 5 cm of lead absorber between the two counters. For the lower energies where the mesons could not safely penetrate this thickness of absorber, no measurements could be made.

Incidentally, the procedure of subtracting electron backgrounds taken with the magnetic field reversed also eliminates counts which might arise from the possible production of positive and negative pion pairs. This experiment measures the cross section for single pion production.

The number of high-energy electrons emitted from the hydrogen target at angles of 30° or more is small, of course, because the usual shower processes of pair production, bremsstrahlung, Compton scattering, and electron scattering, occur at very small angles in hydrogen. In fact, it seems likely that most of the electrons which we do observe at the central angles originate from π^0 decay photons converted in the target wall or elsewhere.

As a test of the fact that the counts observed are actually caused by mesons, we measured the absorption curve in lead for the particles being counted (with the electron background subtracted). One such range curve is reproduced in Fig. 3. This shows that most of the particles have the range corresponding to pions, al-

TABLE I. Negative field backgrounds.

Lab angle	Negative field counting rate/π^+ counting rate Low-energy region	Central energies	High energies
12.5° L.F.*	1.0 –2.0	0.5 –0.8	0.23–0.4
30° S.F.	0.4 –0.6	0.07–0.4	0.04–0.07
30° L.F.	0.30–2.0	0.13–0.30	0.18–0.27
51° S.F.	0.10–0.26	0.04–0.10	0.04–0.06
51° L.F.	0.06–0.13	0.04–0.10	0.07–0.10
73° S.F.	0.09–0.17	0.04–0.06	0.04–0.05
104° S.F.	0.03–0.06	0.02–0.04	0.03–0.10
140° S.F.	0.15–0.46	0.10–0.30	0.30–0.36
180° S.F.	1.0 –1.6	1.3	2.7 –3.4

* L.F. and S.F. indicate long- and short-focus arrangements, respectively.

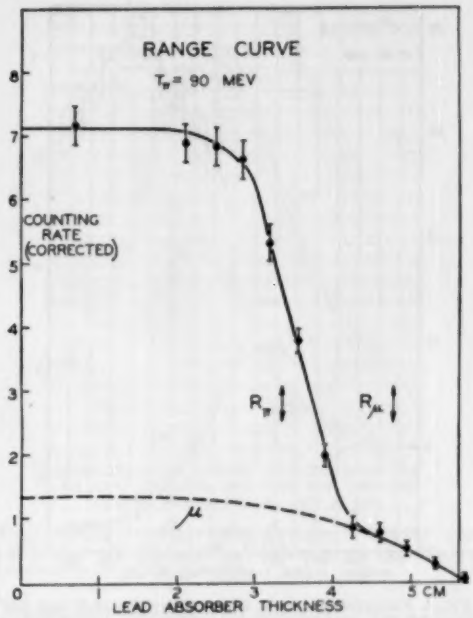

FIG. 3. Range curve for the particles observed at 73° with momentum corresponding to 90-Mev pions. The tail is probably due to muons from $\pi-\mu$ decay in flight. The curve marked μ indicates the fraction of counts expected to come from muons according to the calculations made for the decay correction. The pion counting rate has been corrected for nuclear absorption in the lead absorber.

though a tail of longer-range particles is present. This tail is expected since we have no good way to separate decay muons from the pions. Corrections for $\pi-\mu$ decay involve a calculation of the number of muons counted compared to the number of pions. The height of the dashed curve marked μ in Fig. 3 is taken from these decay correction calculations, which are described in a later section.

The range curve of Fig. 3 has been corrected for nuclear absorption of the pions in the lead absorber. In fact, all the data taken for the cross-section measurements have been corrected for nuclear absorption in the target walls, in the front counter, and in the lead absorber (if any) between the two counters. The absorption cross sections assumed were "geometrical," corresponding to a mean free path of 160 g cm^{-2} of lead, for example. This nuclear absorption correction factor amounts to 0.95 to 0.90 in most of the present measurements, but is 0.62 for the 12.5° data.

INCIDENT PHOTON SPECTRUM

To obtain the absolute differential cross section from the number of counts observed, one must know the number of photons in the collimated beam per unit energy range at energy k. This number, the $N(k)$ of Eq. (4), is normalized to a standard beam monitor reading, as are the observed counts, C. The beam

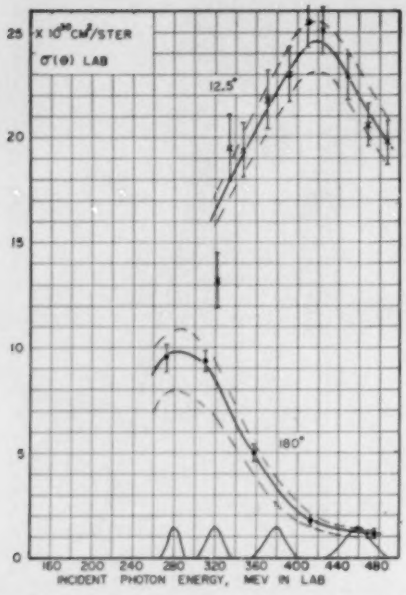

FIG. 4. Excitation curves at laboratory angles 12.5° and 180°, taken with the long-focus arrangement (crosses) and short-focus arrangement (circles), respectively. The differential cross section in the laboratory system is plotted as a function of photon energy. The resolution functions shown at the bottom are approximately correct for both sets of data.

monitor is an air ionization chamber similar to the one designed at Cornell, with one-inch-thick copper walls in which a shower is generated, the shower maximum falling approximately at the ion collection region. The ionization charge produced by the beam is integrated by a circuit which is similar to those described by Lewis and Collinge[19] and by Littauer.[20] The charge collected from this chamber is very nearly proportional to the total energy in the synchrotron beam, independent of the synchrotron energy. (The constant of proportionality is 10 or 12 percent less at 500 Mev than at 300.) In addition to this feature, the thick walls of the chamber make it insensitive to its nearby surroundings. For example, the reading is very little affected by stacks of lead behind or at the sides of the chamber.

The calibration of the synchrotron beam, i.e., the measurement of the total energy in the beam corresponding to a given charge collected from this ion chamber, has been made by two methods in this laboratory. One involves a measure of the total energy liberated in a shower produced in aluminum, by a method similar to that of Blocker, Kenney, and Panofsky.[21] This was done by J. C. Keck. The other consisted of measuring the photon spectrum $N(k)$ with a pair spectrometer whose absolute efficiency is known. These measurements will be described elsewhere.[22] The shape of the photon spectrum observed with the pair spectrometer agrees with the theoretical Bremsstrahlung shape within the experimental accuracy of three or four percent. Each of the two beam calibration methods has an estimated accuracy of about 5 percent, but the results disagree unfortunately by 15 percent. The pair spectrometer calibration gives $Q=4.75\times10^{18}$ Mev/coulomb. The shower method gives $Q=4.12\times10^{18}$. Thus until further work is done to clear up this discrepancy, we use $Q=4.44\times10^{18}$ Mev per coulomb at STP for these experiments.[23]

The photon spectrum $N(k)$ near the upper end, i.e., near the synchrotron energy, E_0, depends on how the electron beam of the synchrotron is "spilled out." In these counter experiments, the beam was spread out for about 15 milliseconds at the peak of the magnetic field, giving a duty cycle of 0.015. This results in a spread of electron energies of about 15 Mev, and a resulting region of uncertainty at the upper end of the spectrum. From the pair spectrometer measurements, taken under these same conditions, we conclude that measurements at energies 450 Mev or below, with resolution similar to that of the present experiments, are not influenced by

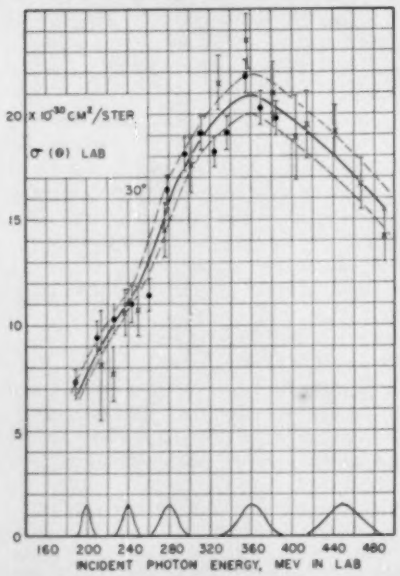

FIG. 5. Excitation curve at laboratory angle 30°. The points shown by crosses in this data and in the 51° data of Fig. 6 were obtained with the long-focus arrangement. The points indicated by circles in all the excitation curves were obtained with the short-focus arrangement.

[19] I. A. D. Lewis and B. Collinge, Rev. Sci. Instr. **24**, 1113 (1953).
[20] Raphael Littauer, Rev. Sci. Instr. **25**, 148 (1954).
[21] Blocker, Kenney, and Panofsky, Phys. Rev. **79**, 419 (1950).
[22] D. H. Cooper, thesis, California Institute of Technology, 1954 (unpublished).
[23] This corresponds to 3.91×10^{18} Mev/coulomb at 300 Mev, compared to the Cornell calibration of 3.71×10^{18}. For this reason alone, our cross sections would be 5 percent lower than those measured at Cornell (and Illinois).

the uncertainties of the upper end of the bremsstrahlung spectrum. The synchrotron energy E_0 as measured with the pair spectrometer is 500 to 505 Mev.

180° DATA

Some relatively uncertain measurements were made at a meson angle of 180°, and since the conditions applying to these measurements are somewhat special, they are described in this section. Obviously the photon beam must pass through the spectrometer magnet before hitting the target so that background troubles are apt to become serious.

This background was reduced as much as possible by appropriate lead shielding, and by evacuating the magnetic field region of the spectrometer. The beam entered and left this region through long evacuated tubes capped with thin aluminum windows. Even with these precautions, the backgrounds were as high or higher than the meson counting rates. Furthermore, if mesons were to come through the cylindrical target wall at a very small angle, the effective wall thickness would be quite large. Thus, the magnet entrance aperture was reduced to 8.4 cm in diameter so that only mesons coming through the hemispherical end cap of the target would be accepted. Nevertheless, this geometry makes the measurement rather sensitive to scattering effects in the bomb walls. Fragmentary calculations of a portion of these scattering effects have been made and gave no corrections for this portion. However, it seems likely that the scattering effects would increase the flux of pions out of the ends of the target, and thus give cross sections that are too high since no corrections have been made. A somewhat arbitrary error of $+10$, -20 percent has been assigned for this effect. Thus, the 180° cross sections are probably good as upper limits, but they have not been included in the least squares fits of the angular distributions. Good measurements at 180° could probably be made using a liquid hydrogen target.

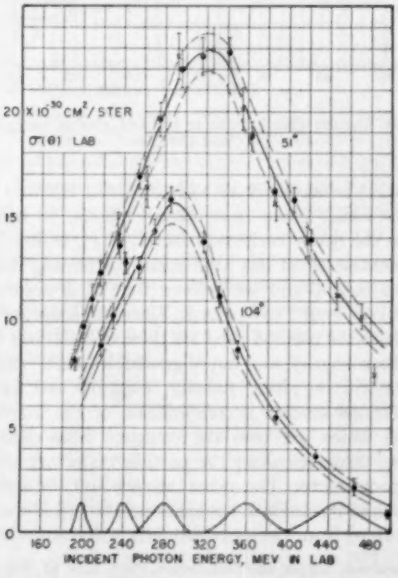

FIG. 6. Excitation curves at laboratory angles 51° and 104°. The resolution curves are for the 51° data. Those for the 104° data are approximately 15 percent wider at low energy and 50 percent wider at high energy.

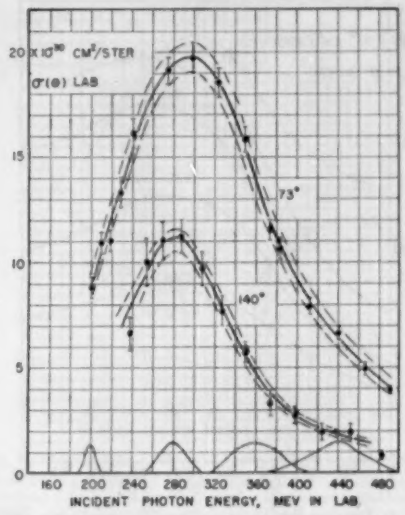

FIG. 7. Excitation curves at laboratory angles 73° and 140°. The resolution curves are for the 73° data. Those for the 140° data are approximately 25 percent narrower.

RESULTS

The differential cross section as a function of energy at each of the laboratory angles measured, is shown in Figs. 4, 5, 6, and 7. These cross sections are calculated, using relation 4, from the observed counting rates after making the various corrections already mentioned.

The data of Figs. 4 to 7 have been analyzed to obtain angular distributions in the center of momentum system at energies from 200 to 470 Mev, in 30 Mev intervals. These angular distributions are shown in Figs. 8, 9, and 10. The points shown are simply the cross sections taken from the solid curves of Figs. 4 to 7, converted to the center of momentum system and plotted at the center of momentum angle. The errors include both random statistical errors and systematic errors which affect the shape of the angular distributions.

The solid curves of Figs. 8, 9, and 10 are derived from a least-squares fit of the data to the form

$$\sigma(\theta) = A + B\cos\theta + C\cos^2\theta. \tag{5}$$

The values of the coefficients A, B, and C thus obtained are given in Fig. 11. The most striking feature of the angular distributions is the shift from a backward maximum at low energies to a forward maximum at high

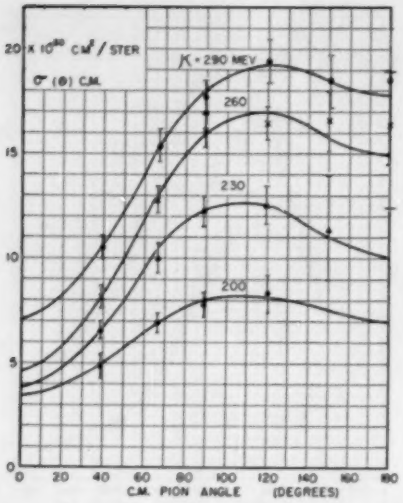

FIG. 8. Angular distributions. The differential cross section in the center of momentum system is given as a function of the c.m. pion angle for incident photon energies 200, 230, 260, and 290 Mev in the laboratory. The errors on the points represent both the random statistical errors, and those systematic errors which affect the shape of the angular distribution. The solid curves are obtained from least squares fits of the angular distributions to the form $\sigma(\theta)=A+B\cos\theta+C\cos^2\theta$.

energies. This is described, of course, by the coefficient B changing sign near 340 Mev.

The total cross section,

$$\sigma=4\pi(A+C/3), \tag{6}$$

is given in Table II. The total cross section divided by the square of the incident photon wavelength λ in the c.m. system is shown as a function of the photon energy in Fig. 12.

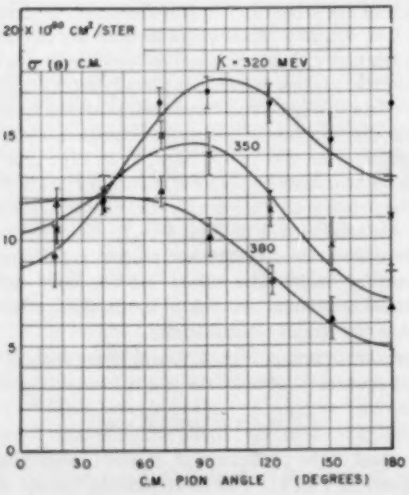

FIG. 9. Angular distributions at incident photon energies 320, 350, and 380 Mev.

DECAY CORRECTIONS

The distance between the target and counters in the magnetic spectrometer is long, so that the pions have an appreciable probability of decaying before reaching the counters. If one assumes the mean life for $\pi-\mu$ decay $\tau=(2.55\pm0.11)\times10^{-8}$ sec,[24–26] it is a simple matter to calculate the fraction of pions which arrive at the counters before decay. This is plotted as the curves marked R_π in Figs. 13 and 14. If a pion decays before reaching the counters, the decay muon may still pass through the two counters and be recorded. Furthermore, the counters will be traversed by some muons from the decay of pions which themselves would not have been counted, either because they have the wrong energy or direction of emission from the target. Since our counters cannot in general tell the difference between pions and

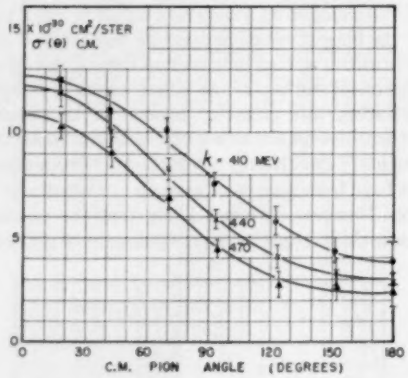

FIG. 10. Angular distributions at incident photon energies 410, 440, and 470 Mev.

muons, it is necessary to add to R_π the fraction R_μ of counts which come from decay muons, in order to obtain the decay correction factor, $R(k)$, of Eq. (4). A considerable effort has been spent calculating this correction factor, and we believe that it is accurate in general to about 5 to 7 percent. Since a description of the details of the method used for these calculations would be rather lengthy, and not of general interest,[27] only the results will be given, namely, Figs. 13 and 14. The calculations involve a computation of the number of muons which get into the counters from decays at various distances along the particle trajectory through the spectrometer. This takes into account the spectrum of pions at the angle of the spectrometer, (this spectrum is obtained from the measurements, using a preliminary

[24] Jacobson, Schulz, and Steinberger, Phys. Rev. **81**, 894 (1951).
[25] C. E. Wiegand, Phys. Rev. **83**, 1085 (1951).
[26] Durbin, Loar, and Havens, Phys. Rev. **88**, 179 (1952).
[27] A description of the procedure used in these calculations is available for those interested.

value for the decay corrections); the $\pi-\mu$ decay dynamics, both in energy and angle; geometrical properties of the spectrometer; and the fact that the muons will not count if their range is too small to get into the second counter. Fortunately, the decay position making the greatest contribution to the muon counting rate is at the source, where the calculation is both simple and accurate, involving simply a conversion of the observed pion spectrum to a spectrum of decay muons.

ERRORS

The errors have been classified into three types: (All errors quoted are intended to be standard statistical errors).

(A) *Errors in the absolute cross section* which are independent of meson energy and angle.

(1) Beam calibration: 7 percent.

(2) Average H_2 gas density: 3 percent.

(3) Part of the $\pi-\mu$ decay correction, R: 4 percent.

(4) Part of the correction for scattering from the lead shielding: 4 percent.

(5) Error in the momentum range, Δp, accepted by the spectrometer: 2 percent.

TABLE II. Total cross sections in units 10^{-30} cm². The errors are obtained from the least-squares fits of the angular distributions. Errors of type A are not included.

k (Mev) =	200	230	260	290	320
$\sigma(\mu b)$ =	89±7	133±6	175±5	204±5	192±5
k (Mev) =	350	380	410	440	470
$\sigma(\mu b)$ =	158±5	125±4	102±3	84±3	68±3

The resulting over-all error in absolute values of the cross sections is about 10 percent.

(B) *Random statistical errors* which fluctuate from point to point. These are indicated as errors on the individual points in the excitation curves of Figs. 4, 5, 6, and 7. They are mainly counting errors arising from the limited numbers of counts, and from uncertainty in the determination of upper and lower limits for the meson peaks such as shown in Fig. 2. However, included in these random errors are the effects of those variations in the temperature of the ion chamber monitor, the target gas density, and the synchrotron energy, which could not be corrected.

(C) *Systematic errors which vary smoothly* from point to point on an excitation curve or angular distribution. These are indicated on the excitation curves by dashed curves on either side of the solid one. These errors include the following:

(1) Part of the $\pi-\mu$ decay correction error: 2 to 6 percent (typically 4 percent).

(2) Error in the nuclear absorption cross section: 10 percent of the absorption cross section. This amounts to an error in the correction factor of 1 to 2 percent except for the 12.5° data where it is 5 percent.

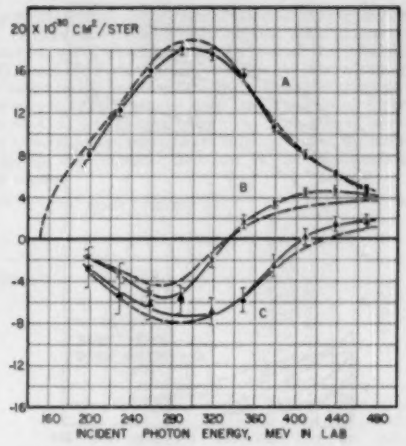

FIG. 11. Coefficients A, B, and C obtained by a least-squares fit of the angular distribution to the form $\sigma(\theta)=A+B\cos\theta+C\cos^2\theta$. The dashed curves give the "average" experimental coefficients of Table III, taking into account all the data shown in Fig. 15.

(3) Error in the correction for scattering from the lead shielding: 3 percent. This correction was measured experimentally at $\theta_\pi=49°$ by taking data with the lead shielding very far apart and comparing to the counts obtained with the shielding normal. This gave the following results for this scattering correction:

$$k=200 \text{ Mev: } 1.092\pm0.070,$$
$$k=300 \text{ Mev: } 1.089\pm0.029,$$
$$k=400 \text{ Mev: } 1.126\pm0.024.$$

This shows no definite or sensible variation with energy, so a uniform correction of 10 percent has been applied to all the data.

(4) Slit penetration errors: 1 to 2 percent.

(5) Uncertainties in the angle $\theta_\pi(\pm1°)$ and in meson

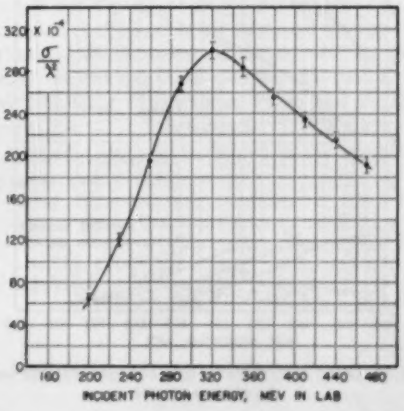

FIG. 12. The total cross section σ divided by λ^2. $2\pi\lambda$ is the c.m. photon wavelength.

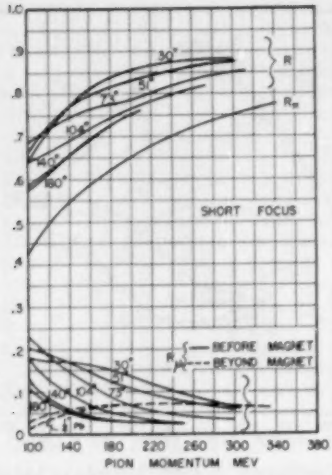

FIG. 13. Decay corrections for data obtained with the short-focus arrangement. See section on decay corrections.

momentum (±1 percent) as they affect the cross section: 1 to 3 percent.

(6) Uncertainty in solid angle because the counters are not sufficiently high: 3 percent for long-focus measurements only.

COMPARISON WITH OTHER EXPERIMENTS

An experiment described in an accompanying paper has been done in this laboratory[23] by using a counter telescope to measure these same cross sections. These two experiments are completely independent except for the beam monitor and the hydrogen target gas density. (The two sets of data were taken simultaneously, using the same target.) Furthermore, the two experiments have different difficulties in general. For example, the effects of $\pi-\mu$ decay are large for the magnet experiment, especially at low energies, but are quite unimportant for the telescope experiment. On the other hand, corrections for nuclear absorption in the stopping material become large for the telescope data, especially at high energies, but are not very important for the magnet data.

The data obtained by the two methods agree well in their general features, but differ some in detail. At low energies, the magnet data are low compared to the telescope data in the forward direction, and high in the backward direction. At high energies, the magnet data are considerably higher in the forward direction. These differences result in a smaller coefficient B of the $\cos\theta$ term in the angular distribution for the telescope data than for the magnet data. This may be seen in Fig. 15, where the curves of Fig. 11 giving the coefficients A, B, and C are reproduced together with the corresponding curves from the telescope experiment.

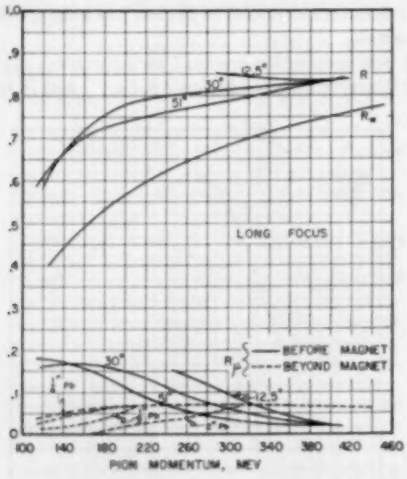

FIG. 14. Decay corrections for data obtained with the long-focus arrangement.

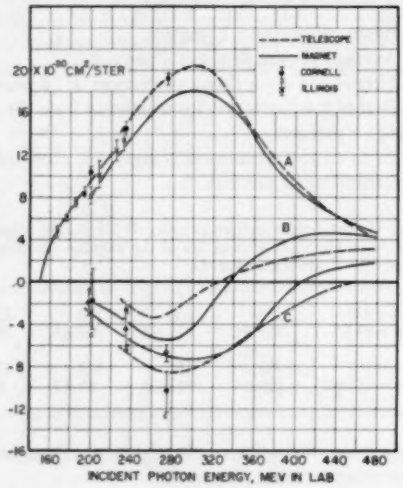

FIG. 15. Comparison with other experiments. The solid curves are reproduced from Fig. 11 for the present experiment. The dashed curves are the corresponding ones from the telescope data of Tollestrup, Keck, and Worlock. The Cornell data of Jenkins, Luckey, Palfrey, and Wilson (see reference 8) are shown by the circle points; and the Illinois data of Bernardini and Goldwasser (see reference 9) are shown by the crosses and solid curve for A at low energies.

The data of Jenkins, Luckey, Palfrey, and Wilson[8] at Cornell are also compared to the present data in Fig. 15 by giving the coefficients A, B, and C from the Cornell experiment. The agreement with the present data is reasonably good.

The low-energy 90° measurements of Bernardini and Goldwasser[9] are also shown in Fig. 15. These were ob-

[23] Tollestrup, Keck, and Worlock, following paper [Phys. Rev. 99, 220 (1955)].

tained with the Illinois betatron by using photographic plate detection and a liquid hydrogen target. These data fit rather well onto the coefficient A of the present experiment.

For use in comparison with theory, we have tried to draw an average experimental curve for all the data shown in Fig. 15, for each of the three coefficients. The curve for A follows the values of Bernardini and Goldwasser at low energy, then the average of the CalTech magnet and telescope data at high energy. The curves for B and C are essentially the average of the magnet and telescope data. All three curves are given an energy dependence at threshold expected theoretically, i.e., approximately $(k-k_0)^{\frac{1}{2}}$, $(k-k_0)$, and $(k-k_0)^{\frac{1}{2}}$ for A, B, and C, respectively. k_0 is the threshold photon energy 151 Mev. These curves are shown in Fig. 11 by dashed curves, and values of the average A, B, and C are given in Table III at 30-Mev intervals.

TABLE III. Average experimental values of the coefficients A, B, and C in the center-of-momentum angular distribution: $\sigma(\theta)=A+B\cos\theta+C\cos^2\theta$. These averages include all the data shown in Fig. 15, from CalTech, Cornell, and Illinois. The errors are estimates based on the accuracy of individual experiments and on the degree of consistency among different experiments. Since these values of A, B, and C have been taken from smooth curves, the values at neighboring energies are correlated, and the errors indicate merely the estimated accuracy of the coefficients in this energy region.

k (Mev)	A	B (units 10^{-30} cm²/sterad)	C
170 Mev	5.2±0.5		
200	9.3±0.5	−1.8±1.0	−3.3±1.6
230	13.1±0.5	−3.0±0.9	−5.7±1.0
260	16.9±0.5	−4.3±1.0	−7.4±1.0
290	18.9±0.5	−3.8±1.2	−7.9±0.9
320	18.4±0.5	−1.1±0.9	−7.2±0.9
350	15.3±0.5	+1.1±0.6	−5.4±0.9
380	11.3±0.4	+2.5±0.6	−3.0±0.7
410	8.2±0.4	+3.2±0.8	−0.8±0.8
440	6.2±0.3	+3.5±0.7	+0.4±0.8
470	4.7±0.3	+3.7±0.6	+1.0±0.8

INTERPRETATION

Several more or less phenomenological descriptions of pion photoproduction have been given.[15,29–32] Most of these relate the photoproduction to pion nucleon scattering since the pion-nucleon interaction plays a dominant role. Chew[31] has used a cutoff form of meson theory to calculate the photoproduction as well as the scattering. The most satisfactory theory at present for comparison with experiment is the phenomenological one of Gell-Mann and Watson,[32] as extended recently by Watson.[34] This (and also the other theories) gives a description in terms of photoproduction into states of definite angular momentum and isotopic spin. Thus a full comparison with experiment must treat the production of charged and neutral pions together. Such an analysis is being prepared in collaboration with K. M. Watson, so not much analysis of the positive pion cross sections will be given here. However, it seems clear that the most striking features of the data may be explained by the idea of a resonance[19,15] in the pion nucleon interaction in the state of angular momentum and isotopic spin $\frac{3}{2}$.

One of these features is, of course, the rapid decrease in the cross section above 320 Mev, appreciably faster than λ^2. The other is the change in the angular distribution from a backward maximum at low energies to a forward maximum at high energies. In a simple "resonance" theory[32] the coefficient B of the $\cos\theta$ term contains a factor $[\cos(\alpha_{33}-\alpha_3)+2\cos(\alpha_{33}-\alpha_1)]$, where α_{33}, α_3, and α_1 are the phase shifts for pion nucleon scattering in the $T=J=\frac{3}{2}$ p-state, and the two s-states of isotopic spin $T=\frac{3}{2}$ and $T=\frac{1}{2}$, respectively. According to the choice of phase shifts made by Bethe and de Hoffmann,[4] in which a resonance is indicated by α_{33} going through 90°, the above factor changes sign at about 340 Mev. This agrees very well with the energy at which our coefficient B goes through zero.

ACKNOWLEDGMENTS

We are indebted to all the members of the synchrotron laboratory for contributions to this experiment, especially to Dr. R. F. Bacher for continual interest in the experiment and discussion of the results. Dr. M. L. Sands, D. C. Oakley, D. H. Cooper, and Paul Donoho helped take some of the data. These and Dr. R. V. Langmuir, Dr. A. V. Tollestrup, Dr. J. C. Keck, and our chief engineer, Bruce Rule, helped in the operation of the synchrotron.

[29] B. T. Feld, Phys. Rev. **89**, 330 (1953).
[30] M. Ross, Phys. Rev. **94**, 454 (1954).
[31] Geoffrey F. Chew, Phys. Rev. **95**, 1669 (1954).
[32] K. M. Watson, Phys. Rev. **95**, 228 (1954).
[33] M. Gell-Mann and K. M. Watson, Ann. Rev. Nuc. Sci. **4**, 219 (1954).
[34] K. M. Watson, Lectures at California Institute of Technology during the summer, 1954 (unpublished).

Photoproduction of Positive Pions in Hydrogen-Counter Telescope Method*

A. V. Tollestrup, J. C. Keck, and R. M. Worlock
California Institute of Technology, Pasadena, California

(Received March 7, 1955)

The excitation functions for positive pion production from hydrogen have been obtained in the energy region from 230 Mev to 450 Mev and at laboratory pion angles of 24°, 38°, 53°, 73°, 93°, 115°, 140°, and 160°. The pions are detected and identified by measuring their range and ionization in a scintillation counter telescope. The above data are analyzed to give the angular distributions in the center-of-momentum system, and a least-squares analysis made to determine coefficients in $\sigma(\theta)=A+B\cos\theta+C\cos^2\theta$. The total cross section shows a peak at 300 Mev of magnitude 2.20×10^{-28} cm². The coefficient B passes through a maximum negative value at 250 Mev and then passes through zero at 325 Mev and remains positive up to the highest energy measured.

I. INTRODUCTION

THE operation of the CalTech synchrotron has made it possible to obtain data on the photoproduction of positive mesons from hydrogen in the energy region from 200 Mev to 500 Mev and thus considerably extend the region over which the cross section has been measured. The measurements reported here consist of excitation curves at pion angles of 24°, 38°, 53°, 73°, 93°, 115°, 138°, 160° in the laboratory system and from these curves the angular distributions in the c.m. system at photon energies of 230, 260, 290, 320, 350, 380, 410, 440, and 470 Mev are derived. Previous measurements of this process[1] have been done at 300 Mev and below and have left undecided the question as to whether or not the $T=\frac{3}{2}$, $J=\frac{3}{2}$ state plays a predominant role in the photoproduction as predicted by strong coupling theory.[2]

At the time this experimental program was undertaken it was realized that it would be possible to perform the measurements by either of two methods. In both methods the incident photon energy must be calculated from a knowledge of the pion energy and the dynamics of the reaction studied. This energy can be inferred either by measuring the pion range in a scintillation counter telescope or by measuring the pion momentum by means of deflecting magnets.[3] The second method is described in the preceding paper and is hereafter referred to as the "magnet method." These two techniques are subject to quite different systematic errors and tend to complement each other. For instance, the magnet method at low energies required corrections for slit edge scattering and penetration and also rather large decay corrections due to the long flight path traversed by the mesons. The telescope was subject to these effects only to a very limited extent, and at low energies all of the corrections to the data were small and amenable to exact calculation. However, at high energy the telescope method suffers from rather big corrections due to the large interaction of the pions with the material in which their range is being measured. The final results of the two experiments do not agree in complete detail, and tend to indicate that undetected systematic errors still exist in either or both of the experiments. These details will be discussed further at the end of the paper. On the other hand, the agreement between the experiments is such that no doubt is left about the over-all behavior of the process and a good comparison with existing theories is possible.

II. EXPERIMENTAL METHOD

(a) Collimation

The bremsstrahlung beam from an internal 0.016-in. thick strip of copper is first collimated by a ½-in. hole in a 12-in. thick lead block located 12 ft from the copper target. This primary collimation is followed by two secondary collimators which are of such a size and aligned in such a way that they do not intercept the direct beam. One of these secondary collimators is located in a concrete wall which shields the experimental area from the machine and the final one is just in front of the high pressure hydrogen target and arranged so as to shield the walls of the steel target cylinder from x-rays, as shown in Fig. 1. The beam at the target is 1½ in. in diameter.

(b) Target

The high-pressure hydrogen target is a steel cylinder 17 in. long by 2 in. in diameter which is filled with gas to a pressure of 2000 lb and cooled to a liquid nitrogen temperature. The walls of the target, through which the mesons had to pass, consisted of 0.030 in. of steel and 1½ in. styrofoam insulation. The loss of energy experienced by the mesons in passing through the gas and the target wall was taken into account when computing the range of the meson. The temperature was measured at the two ends of the target by means of thermocouples and the average value was used in com-

* This work was supported in part by the U. S. Atomic Energy Commission.

[1] J. Steinberger and A. S. Bishop, Phys. Rev. **86**, 171 (1952); White, Jacobson, and Shalz, Phys. Rev. **88**, 836 (1952); Jarmie, Repp, and White, Phys. Rev. **91**, 1023 (1953); Jenkins, Luckey Palfrey, and Wilson, Phys. Rev. **95**, 179 (1954); White, Jakobson, and Repp, Bull. Am. Phys. Soc. **29**, No. 8, 21 (1954).

[2] K. Brueckner and K. M. Watson, Phys. Rev. **86**, 928 (1952).

[3] Walker, Teasdale, Peterson, and Vette, preceding paper [Phys. Rev. **99**, 210 (1955)].

puting the density.[4] Generally, a value of about 0.03 g/cm³ was obtained with an accuracy of ±3 percent.

(c) Monitor

The monitor was a thick ionization chamber and the problem of its calibration is described in reference 3.

(d) Detector

The bremsstrahlung beam striking the hydrogen target produced a cylindrical source of mesons. The detector first had to identify the particle counted as a meson and secondly define its angle and energy in order that the energy of the photon producing the meson could be calculated from the dynamics of the reaction. Figure 1 shows how this was accomplished. The four scintillation counters numbered from 1 to 4 are connected in such a way that a particle producing a pulse simultaneously in C_1, C_2, C_3, but not in C_4 has its pulse height measured in C_2. A_1, A_2, and A_3 are blocks of copper of adjustable thickness and hence only those particles were accepted which had a range between $R=C_1+A_1+C_2+A_2$ and $R+\Delta R=C_1+A_1+C_2+A_2+C_3+A_3$. The energy was then deduced from the range-energy curves for mesons in copper.[5] The number

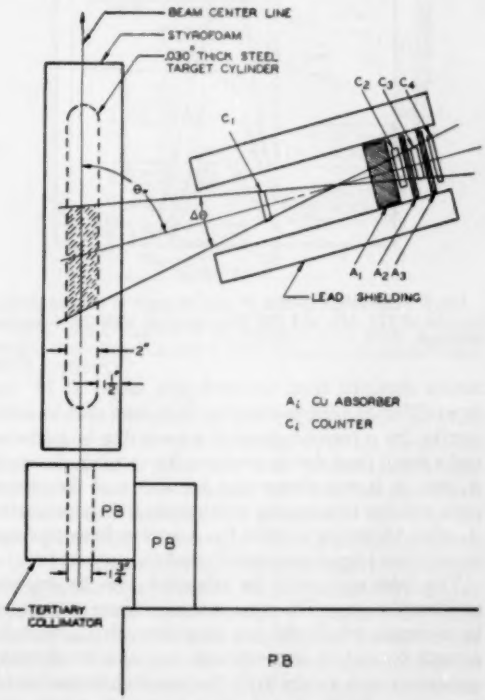

FIG. 1. Plan view of target and telescope.

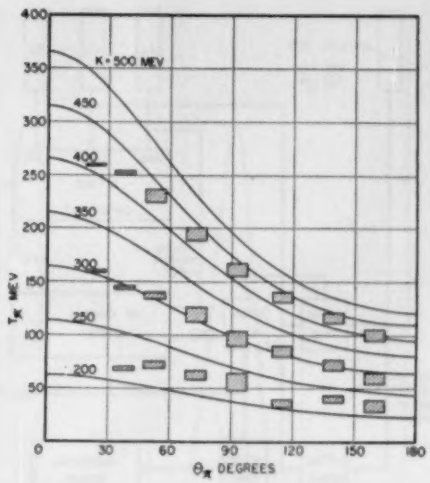

FIG. 2. Kinematics of charged pion production. The shaded areas indicate resolution of the telescope at typical points. The width of a rectangle is the half-width of the telescope angular resolution function and the height is the pion energy interval accepted.

of photons contributing to the reaction is then given by

$$N(\gamma)=N(k)\Delta k=N(k)\frac{\partial k}{\partial E_\pi}\frac{\partial E_\pi}{\partial R}\Delta R, \qquad (1)$$

where $N(k)$ = number of photons/Mev in the bremsstrahlung spectrum.

The angular resolution function was triangular in shape with a width at half-maximum of $\Delta\theta=a/l$, where a was the width of counters C_1 and C_3 and l is their spacing. Thus 75 percent of the counts occur within this half-angle which in general was about 10°. Figure 2 shows a summary of this information. The graph is one of the T_π *vs* θ_π in the laboratory for various fixed photon energies. Since the telescope defines a ΔT_π and a $\Delta\theta_\pi$ as indicated above, rectangles ΔT_π high by $\Delta\theta_\pi/2$ wide may be plotted on a $T_\pi-\theta_\pi$ graph representing the resolution of the telescope. A few representative rectangles are shown in Fig. 2 from which it may be seen that the photon energy interval accepted was 25 Mev or less.

The number of mesons counted by the telescope per coulomb collected on the beam integrator is given by the expression

$$N_\pi(\theta)=N_H N(k)\Delta k\int_{\Omega\tau}\frac{d\sigma}{d\Omega_{lab}}d\Omega d\tau, \qquad (2)$$

where N_H is the number of hydrogen atoms per cm³, $N(k)$ is the number of photons of energy k per Mev per coulomb collected on the ion chamber, and the integral is over the coordinates describing the counter and the volume of the target. It is possible to carry this integral out exactly, but it has been found more convenient to

[4] Johnston, Bezman, Rubin, Swanson, Corak, and Rifkin, U. S. Atomic Energy Commission Report MDDC-850 (unpublished).
[5] Aron, Hoffman, and Williams, U. S. Atomic Energy Commission Report AECU-663 (unpublished).

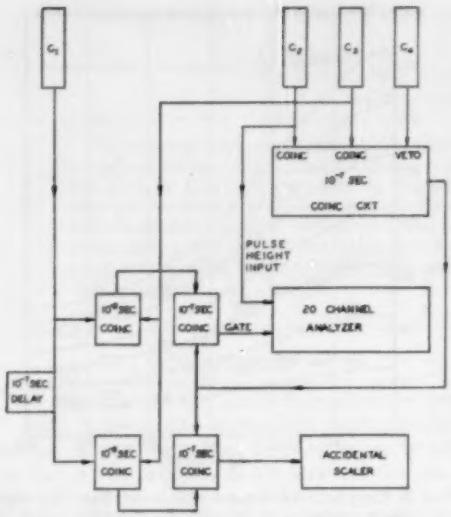

FIG. 3. Block diagram of electronics for 4-counter telescope.

use a series expansion:

$$N_\pi(\theta)=\frac{N_H a^3 h N(k)\Delta k}{lc\sin\theta}(1+\alpha+\cdots)\frac{d\sigma(\theta)}{d\Omega_{\text{lab}}}. \qquad (3)$$

Here a is the width of the counters C_1 and C_2, h is the height of counter C_3, c the distance from the center of C_3 to the point where the axis of the telescope intersects the beam axis, and l is the distance from C_1 to C_3. The term α involves the squares of the ratios of beam radius, h, and a to the distance c. These terms have been calculated and amount to 0.5 percent for θ equal to 160° and are smaller at other angles.

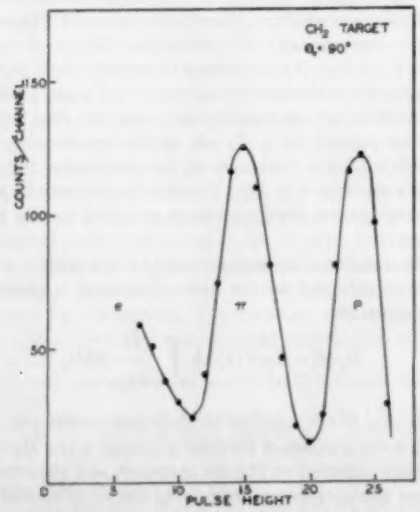

FIG. 4. Pulse-height spectrum from CH_2 target at lab angle of 90°, showing peaks due to electrons, mesons, and protons.

In the course of the experiment three different telescope arrangements were used. The first had the electronics arranged as shown in a block diagram in Fig. 3. The counters are numbered as in Fig. 2. The pulses from counters C_1 and C_2 were put into a fast coincidence circuit with a resolving time of 10^{-8} sec. These counters defined the solid angle and in addition the presence of C_1 made the telescope insensitive to γ rays converted by the copper absorbers which were placed between C_1 and C_2. If in addition to a fast coincidence between C_1 and C_3 a slow coincidence was recorded between C_2 and C_3, then the gate to the 20-channel pulse-height analyzer was opened and the pulse height in counter C_2 was recorded. A typical pulse-height spectrum from a CH_2 target is shown in Fig. 4 and it is seen that the three peaks representing electrons, π mesons, and protons are easily resolved. Figure 5 shows typical

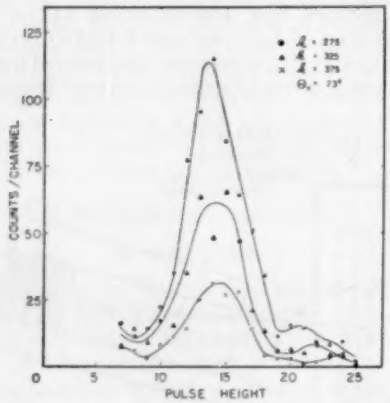

FIG. 5. Pulse-height spectra at pion lab angle of 73° and photon energies of 275, 325, and 375 Mev obtained with the 4-counter telescope.

results obtained from the hydrogen target at 73° for three different photon energies. It is seen that in addition to the π mesons, there is a peak due to electrons and a small peak due to protons. By varying absorbers A_1 and A_2 it was shown that the source of the proton peak was due to π mesons which made a star in absorber A_1 after triggering counter C_1. A proton from this star would then trigger counters C_2 and C_3.

The telescope could be triggered also by various accidental events. The most serious of these was caused by a meson which did not pass through C_1, but did actuate C_2 and C_3 properly and was also accidentally coincident with a pulse in C_1. To provide information for correction of this type of event, an accidental channel was constructed by sending the delayed pulses from C_1 through electronic circuits identical with those through which the nondelayed pulses traveled. The accidental channel was then aligned in such a way that it had the

same counting rate as the true channel when both channels received delayed pulses from C_1. The continuous monitoring of the accidental events not only provided the data for the necessary corrections, but also enabled one to adjust the experimental conditions such that the corrections never became large.

At the forward angles of 24° and 38° the structure of the telescope was modified. At these angles C_1, which must be biased to count minimum ionization particles, counted at an excessive rate due to electrons produced in the ends of the bomb and scattered into the telescope. Hence, counter C_1 was replaced by wolfram slits and these slits in conjunction with counter C_2 then defined the angular acceptance of the telescope. In addition, a $\pi-\mu$ decay scheme was constructed to help identify the mesons. The block diagram of the

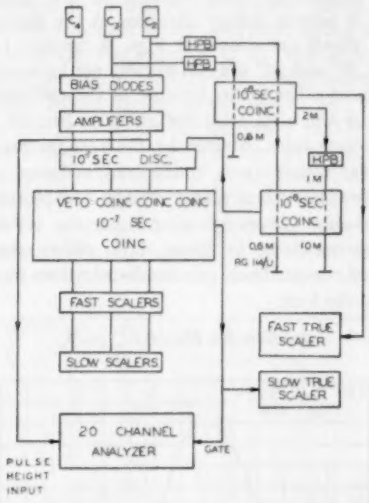

FIG. 6. Block diagram of electronics in $\pi-\mu$ decay detection scheme. Cable length in meters. HPB indicates a Hewlett Packard 460-B amplifier.

electronics is shown in Fig. 6. It may be seen that a fast coincidence was required between counters C_2 and C_3. This coincidence pulse was then formed into a gate signal 0.1 μsec in duration and delayed by about 15 m μsec and then put into coincidence with any delayed pulse from counter C_3. This, it should be noted, reduced the detection efficiency, since only the μ mesons falling in the delay interval were detected. The copper absorber A_3 was removed and a special 1-in. thick counter built for C_3 which then defined the ΔR of the telescope. The output of this second fast coincidence circuit was then combined with the slower electronics to gate the pulse-height analyzer on counter C_2. Thus, not only was a $\pi-\mu$ decay required, but the dE/dx of the particle was also measured in counter C_2. Figure 7 shows the pulse-height spectrum recorded in counter C_2. The complete lack of peaks corresponding to electrons

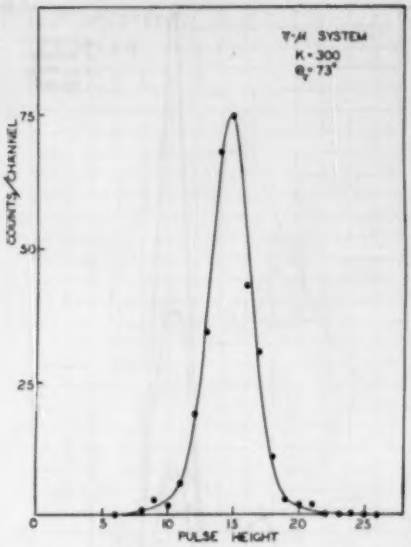

FIG. 7. Pulse-height spectrum at pion lab angle of 73°, and photon energy of 300 Mev using $\pi-\mu$ decay identification system. Electrons would have fallen in the interval between 0 and 10 and protons between 20 and 25 on the pulse-height scale.

or protons indicates the system was identifying π mesons in a very satisfactory fashion. The efficiency of this system was then obtained by calibrating it against the previous telescope at 73° and 300 Mev. The statistical accuracy of this calibration was (±3 percent).

At 38° the excitation curve obtained with the $\pi-\mu$ telescope was 20 percent higher than with the other telescope at energies above 300 Mev and even higher than this at lower energies. A check at 53° did not display this effect and it is felt that here the counting rates were low enough so that the first telescope was operating properly. The counting rates obtained with the $\pi-\mu$ method were only about a sixth those that could have been obtained by the previous system because of the small ΔR which the 1-in. liquid cell presented and also because of the reduced efficiency of detecting the μ-decay pulse. This resulted in larger statistical errors in the data at these two angles.

Finally, the 160° data were obtained at a considerably later time than the rest of the data. This was due in part to the necessity of turning the hydrogen target end for end in order to reach this extreme angle with the counters. In the meantime, the telescope was rebuilt with plastic scintillators in place of the previous liquid cells. When the telescope was reassembled, wolfram slits were placed in front of counter C_1 and thus the slits and counter C_3 defined the angular acceptance of the telescope. The excitation curve was then run at 160°, and as a check the 73°, 115°, and 140° curves were re-run. When the data were reduced, it was discovered that they produced results 20 percent higher than were

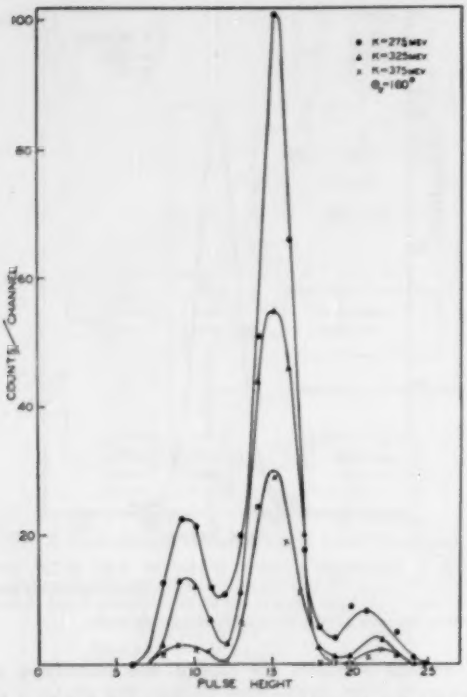

FIG. 8. Pulse-height spectra obtained at pion lab angle of 160° and photon energies of 275, 325, and 375 Mev.

previously obtained. Calculations indicated that scattering and slit-edge penetration could account for only half of this effect. However, it was felt that there were other systematic errors in the absolute value of these data and consequently the data at 73°, 115°, and 140° were compared with the previous data to obtain a normalization factor for the 160° results. A least-square analysis was made to obtain the normalizing constant, and gave 0.820 ± 0.013. The new data, when thus normalized and plotted, interlaced the old data nicely and showed no indication of systematic deviations in either energy or angle. Figure 8 shows typical pulse-height curves obtained in counter C_2 at 160° for three different photon energies.

III. RESULTS

The differential cross sections in the laboratory system *vs* photon energy obtained in the manner described above are shown in Figs. 9 through 12. The data at 38° and 24° are statistically not as accurate as the data at other angles because of the calibration required by the $\pi-\mu$ telescope and also because of the low counting rates obtained by the $\pi-\mu$ method.

Angular distributions in the center-of-mass system at 30-Mev intervals of photon energy were plotted from the excitation curves by using either the actual data or approximations to these data rather than the smoothed curves. These angular distributions were then fitted to the form

$$d\sigma/d\Omega = A + B\cos\theta + C\cos^2\theta, \qquad (4)$$

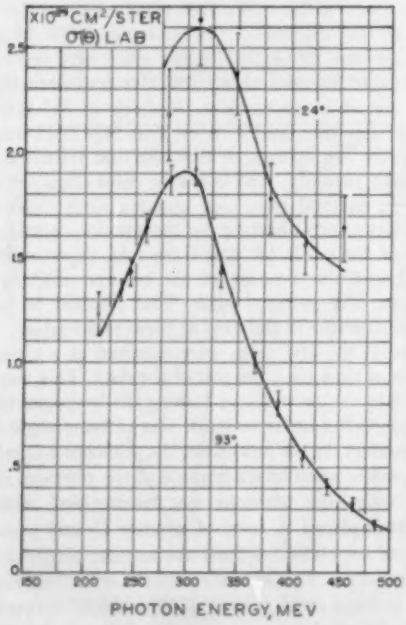

FIG. 9. Laboratory cross section as function of incident photon energy at pion lab angles of 24° and 93°.

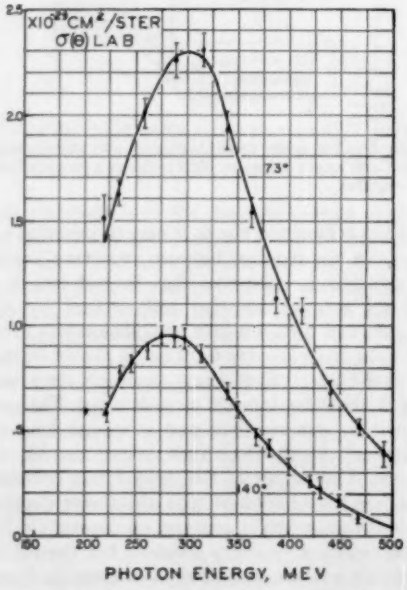

FIG. 10. Laboratory cross section as function of incident photon energy at pion lab angles of 73° and 140°.

by means of a least-squares analysis. The weighting of the input data in this analysis included both statistical errors plus estimates of those systematic errors that effect the relative values of the input data. The results of this analysis are shown in Figs. 13 to 15 where the solid curves are calculated from Eq. (4) using the least squares values for A, B, and C. A plot of these coefficients *versus* energy is shown in Fig. 16 and their values at 30-Mev intervals are listed in Table I. The total cross section curve is shown in Fig. 17 as computed from

$$\sigma(k)=4\pi(A+C/3), \tag{5}$$

and values are listed in Table I.

IV. DATA CORRECTION

(a) Absorption Correction

The largest correction to the data was due to absorption of the π mesons in the copper stopping material of the telescope. For instance, at 73°, 300-Mev photon energy 32 percent of the incident mesons interacted in the copper before coming to rest and at 24°, 450-Mev photon energy this number increased to 77 percent. Although this correction is rather large, it can be accurately made if the value of the mean free path of mesons in copper is known. The measurement of the π^- interaction cross section in copper has been made at 85 Mev[6] as well as 113 and 137 Mev.[7] Since the measurements all agree within the accuracy of the experi-

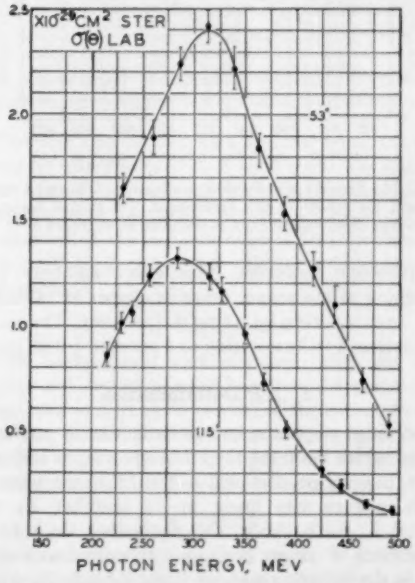

FIG. 11. Laboratory cross section as function of incident photon energy at pion lab angles of 53° and 115°.

[6] Chedester, Isaacs, Sachs, and Steinberger, Phys. Rev. 82, 958 (1951).
[7] R. L. Martin, Phys. Rev. 87, 1052 (1952).

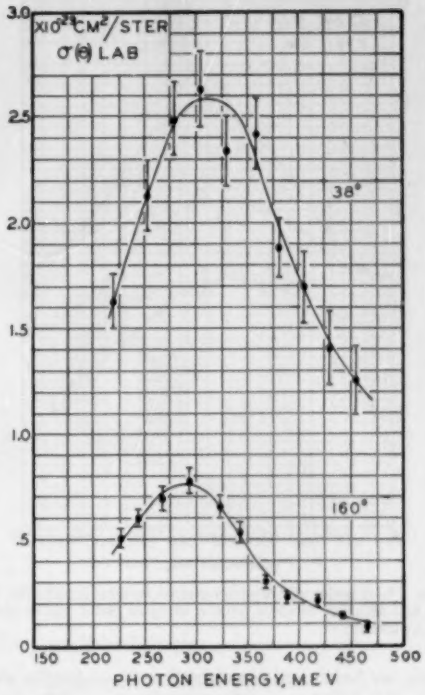

FIG. 12. Laboratory cross section as function of incident photon energy at pion lab angles of 38° and 160°.

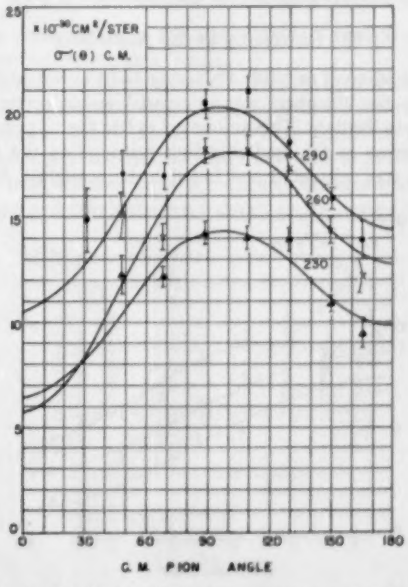

FIG. 13. Angular distribution curves in c.m. system for 230-, 260-, and 290-Mev incident photon energies. Solid curves are the least-square fit.

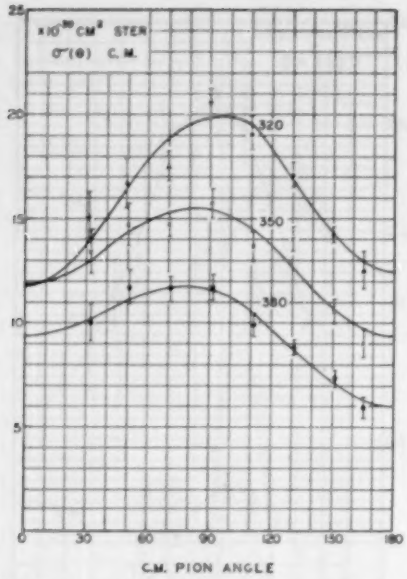

FIG. 14. Angular distribution curves in c.m. system for 320-, 350-, and 380-Mev incident photon energies. Solid curves are the least-square fit.

ments, we have used a weighted average for the mean free path of 12.1 cm with an uncertainty of 5 percent. The maximum uncertainty in the absorption correction amounts to 7 percent at 24° and 450 Mev and is reduced to 2.5 percent at 300 Mev and 73°.

(b) Scattering in the Absorbers

The effect of multiple scattering and shadow scattering in the absorbers was calculated and a correction made to the data. This amounted to less than 3 percent. Scattering in the lead shielding surrounding the telescope was calculated and found to be negligible. Scattering corrections in the bomb wall and in the front counter, when used, were assumed to be negligible due to the fact that scattering into the telescope tends to cancel scattering out of the telescope. To test this hypothesis absorber was shifted from position A_1 to a position in front of counter C_1. No effect could be detected up to $\frac{7}{16}$ in. of copper at a meson energy of 65 Mev. This was an excellent test since the amount of scattering material was always much less than this amount.

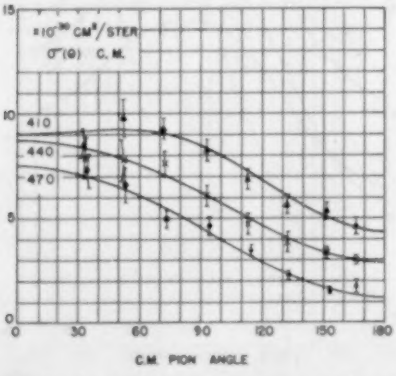

FIG. 15. Angular distribution curves in c.m. system for 410-, 440-, and 470-Mev incident photon energies. Solid curves are the least-square fit.

(c) Range Energy Relation

Meson ranges in copper were obtained from the proton range energy relation given by Aron.[5] These ranges were corrected for multiple scattering in the absorbers in order to obtain the projected ranges which the telescope measures. This effect amounts to a shortening of the meson range in copper as calculated from Aron's curves by about 1.5 percent. The ranges were assumed to be accurate to 1 percent +0.01 cm.

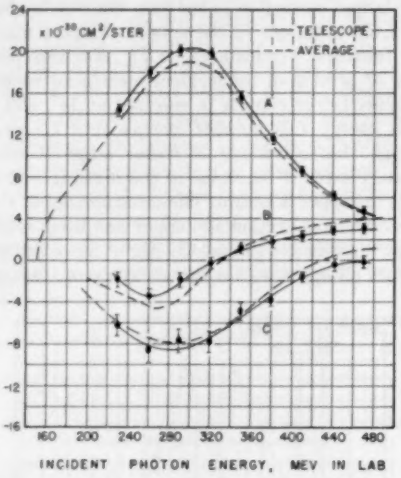

FIG. 16. Angular distribution coefficients. The solid curves represent the results of this experiment. The dotted curves are the average of all experiments as obtained in reference 3.

(d) ΔR Determination

The range of photon energies effective in producing mesons which actuated the telescope was, as indicated above, directly proportional to the ΔR of the telescope which in turn was made up of absorber A_2 plus counter 3. As a check, the equivalent thickness in centimeters of copper of C_3 was experimentally measured in the following manner. The counts in the meson peak were observed as absorber A_3 was varied from 0 up to $\frac{1}{4}$ in. of copper in 5 steps while adjusting absorber A_2 to keep the mean range constant. The data when plotted should give a straight line which has an inter-

cept with the absorber A_3 axis equal to the equivalent thickness of counter 3. The results are shown in Fig. 18 where a least-squares fit to the data has been made. The equivalent thickness of the counter thus measured is 0.285 ± 0.015 cm copper, whereas the calculated value was 0.275 which is equal to the measured value within the statistical accuracy of the experiment. Since ΔR was composed of the counter plus the absorber A_3, the error is less than the statistical uncertainty of the above experiment and was given the value of ± 2 percent.

(e) Accidentals and Dead-Time Correction

As has been described above, the accidental events were monitored simultaneously with the real events by means of delayed channels. This correction amounted to less than 5 percent in general, but in a few exceptional cases rose to 15 percent. In addition a few counts were missed because of dead-time losses caused by the veto counter C_4 being accidentally triggered in coincidence with a true event. This effect was corrected for and amounted to less than 3 percent in general, but again in a few cases got as high as 15 percent.

TABLE I. Results obtained by a least-squares determination of the coefficients A, B, and C in Eq. (4) of the text. Also in the last column is listed the total cross section as computed from Eq. (5).

k (Mev)	A	B	C	Total
	(units 10^{-29} cm²/sterad)			
230	1.43 ±0.03	−0.167 ±0.058	−0.619 ±0.095	15.30 ±0.33
260	1.79 ±0.04	−0.348 ±0.073	−0.862 ±0.120	18.80 ±0.40
290	2.02 ±0.04	−0.183 ±0.061	−0.768 ±0.110	22.05 ±0.38
320	1.99 ±0.04	−0.035 ±0.056	−0.782 ±0.095	21.70 ±0.36
350	1.55 ±0.04	+0.122 ±0.051	−0.489 ±0.089	17.43 ±0.34
380	1.16 ±0.03	+0.172 ±0.042	−0.388 ±0.074	12.90 ±0.30
410	0.85 ±0.026	+0.232 ±0.037	−0.176 ±0.059	9.89 ±0.26
440	0.625 ±0.031	+0.292 ±0.042	−0.042 ±0.062	7.64 ±0.29
470	0.461 ±0.021	+0.311 ±0.037	−0.022 ±0.050	5.68 ±0.24

The veto counter had an additional effect for which it was necessary to correct. A valid count was discarded when the π meson correctly triggered the telescope, but then the resulting decay electron activated the veto counter within the resolving time of the slow coincident circuits. This effect has been calculated to be 6 percent ± 2 percent.

(f) Backgrounds

The backgrounds were obtained with the target empty and typically were less than 10 percent, but sometimes as high as 30 percent of the counts from the gas. The geometry of the telescope was always such that the steel ends of the target were excluded from the region contributing counts to the telescope.

V. ERRORS

A summary of the assumed errors is given below. These are divided into two classes. The first are errors which are independent of energy and angle and hence affect the absolute value of all the results. These errors are not included in the results shown on any of the graphs or in the results quoted in Table I.

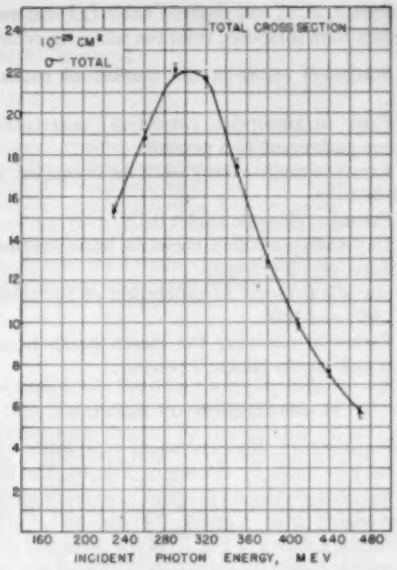

FIG. 17. Total cross section, for $\gamma + p \rightarrow \pi^+ + n$.

They are the following:

(1) Beam calibration: 7 percent.
(2) H_2 gas density: 3 percent.
(3) ΔR: 2 percent.
(4) Solid angle: 2 percent.
(5) μ decay actuating veto counter: 2 percent.

The combination of the above yields 8 percent as the error in absolute cross section.

In addition to the above, there exists both systematic errors which vary with angle as well as the random statistical errors. These errors were combined into a weighting factor which varied from point to point when the least squares fit of the angular distributions were made, and this is the error shown on the curves for the

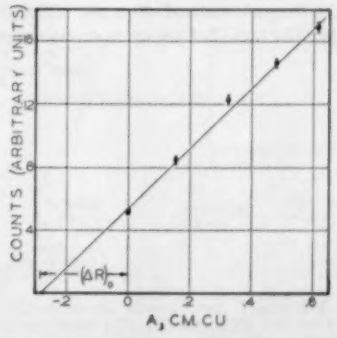

FIG. 18. Counting rate as function of absorber A_3. The line represents the least-square fit to the points. The intercept with the abscissa gives the equivalent thickness of counter C_3.

coefficients A, B, C, and given in Table I. These weighting factors were composed from the following errors:

(1) Statistical errors in the number of counts recorded.

(2) Error in absorption correction: uncertainty in mean free path equal to 5 percent.

(3) Errors in range-energy relations in copper: 1 percent +0.01 cm.

(4) Error in telescope angle: 0.7°.

(5) Day-to-day random errors in beam calibration, gas density, etc: 2 percent.

(6) Statistical factor in calibration of the telescope at 24°, 38°, and 160°.

(7) Errors in resolving the meson peaks from the electron and proton peaks: 2 percent.

VI. DISCUSSION OF RESULTS

A comparison of this experiment with other experiments may be made by examining Fig. 16. The dotted curve was obtained by an attempt to average all of the data available from Cornell, Illinois, and CalTech. These data are shown in Fig. 15 of the preceding paper.[3] In the energy region considered in this paper the dotted curve is essentially an average of the telescope results and the magnet results. Therefore the difference between the two experiments is about double the difference between the two curves of Fig. 16. It is seen that there is a reasonable agreement between this experiment and the magnet experiment on the A and C coefficients, but that there is quite a disagreement on the B coefficient. This shows up in a detailed comparison of the angular distribution curves where it is found that the magnet method gives results that are high compared to the telescope for either forward angles at photon energies higher than 380 Mev or backward angles at energies in the neighborhood of 290 Mev. In the region of $\theta_{c.m.}$ equal to 90°, the experiments agree quite well with each other and also with the Cornell and Illinois results at lower energy.

As has been pointed out, the telescope data are subject to large absorption corrections at high energies, whereas the magnet method does not suffer from this uncertainty. The fact that the cross sections agree quite well at 73° up to 450-Mev photon energy would seem to indicate that we make this correction accurately up to a meson energy of 200 Mev. This disagreement at forward angles involving meson energies higher than this cannot be due to errors in the absorption correction. This is because a pion interaction cross section in copper of twice geometrical would have to be used in order to make the two experiments agree in this region. In the backward hemisphere the telescope has high counting rates and in general the backgrounds and corrections to the data are small. On the other hand, the decay corrections for the magnet method become rather large at low meson energies. Thus, to a certain extent the two methods tend to complement each other.

The energy at which B reverses sign is found to be 325 Mev as compared to 335 Mev obtained in the magnet experiment. If one assumes a simple resonance theory as Watson[8] has done, one finds that B should pass through zero when

$$[\cos(\alpha_{33}-\alpha_3)+2\cos(\alpha_{33}-\alpha_1)]=0, \qquad (6)$$

where α_{33}, α_3, and α_1, are the phase-shifts obtained in the analysis of meson scattering experiments. If one uses the phase shifts as calculated by Bethe and deHoffmann,[9] the above quantity equals zero at 340 Mev. Thus, these experiments conform quite well to the predictions of this set of phase shifts. A more detailed comparison with the phenomenological theory of Watson and Gell-Mann[8] is in preparation and will be published at a later date.

ACKNOWLEDGMENTS

The authors wish to acknowledge the help and support received from all members of the synchrotron laboratory during the progress of this experiment. We are indebted particularly to Dr. R. F. Bacher. Also, Dr. R. V. Langmuir, Dr. J. G. Teasdale, Dr. R. L. Walker, Dr. D. C. Oakley, and Mr. B. H. Rule assisted in running the machine.

[8] K. M. Watson, lectures at CalTech during the summer of 1954; M. Gell-Mann and K. M. Watson, Ann. Rev. Nuc. Sci. 4, 219 (1954).

[9] H. A. Bethe and F. deHoffmann, Phys. Rev. 95, 1100 (1954).

Heavy Mesons Produced by 2.2- and 3.0-Bev Protons*

R. D. Hill,† E. O. Salant, and M. Widgoff‡
Brookhaven National Laboratory, Upton, New York

(Received March 24, 1955)

Emulsions were traversed by radiations from a target bombarded by either 2.2-Bev or 3.0-Bev protons. Analyses of tracks of twelve heavy mesons that came to rest in the emulsions are presented. The stopped heavy mesons produced secondaries showing that 2 were tau mesons, 1 was a negative K meson, and 9 were positive K mesons. Grain count, scattering and range measurements served to determine K-meson masses; the average of 6 positive K mesons that could be measured well was $(965\pm15)m_e$. Evidence is given, from comparison with existing $p\beta$-blob density curves, that one K^+ secondary is a muon or electron, while another K^+ secondary is a pion. If, in the latter case, it is assumed that the K^+ decays into a charged and a neutral pion, the mass of the K^+ is found to be $(945\pm20)m_e$ and the Q of the decay (207 ± 9) Mev, the same, within experimental error, as for θ^0.

INTRODUCTION

DURING the past year and a half, the heavy mesons θ^0, τ, K^-, and K^+ have all been produced, either by 2.2- or 3-Bev protons, or by 1.5-Bev pions, at the Cosmotron.[1–4]

Although data on heavy mesons have been accumulating rapidly in cosmic-ray observations,[5] such data do not often include knowledge of the nature and energy of the producing particle. Such knowledge is available in accelerator experiments, which have the further advantage that a known, localized target can be used, and emulsions can be so placed that radiations from the target traverse them in planes approximately parallel to their surfaces. This arrangement makes for easier scanning and longer K-meson tracks than does the arrangement in which the emulsion itself is the target.

The target was in the straight section of the Cosmotron, and the path of its radiations to the detecting emulsions was entirely in this field-free region. Magnetic analysis of the radiations from the target has also been done, but this paper reports only those experiments in which the K mesons were not magnetically selected.

EXPERIMENTAL ARRANGEMENTS

Stacks of 24 strips of 2 in.×3 in. 400μ Ilford G5 nuclear emulsions were exposed at either of two positions outside the Cosmotron vacuum chamber, as illustrated in Fig. 1(a), or inside the vacuum chamber, adjacent to a target, mounted as shown in Fig. 1(b). For each exposure, the target, held on a plunging ram, was kept in a position shielded from the proton beam for most of the Cosmotron's accelerating cycle. At the end of each cycle, the target was plunged into a position such that it was struck only by protons of full energy. Exposures were limited by the number of background tracks which arose from: (i) pions and protons coming directly from the target, (ii) stars produced in the emulsion and surrounding material by secondaries from the target. It was found that satisfactory scanning with a 20× dry objective could be carried out on emulsions which had a flux of the order of 10^4 minimum ionizing track per cm^2.

For the emulsion stacks exposed as shown in Fig. 1(a), particles entering the emulsions from the target penetrated the 0.47-inch thick steel wall of the Cosmotron. This served to reduce the intensity of evaporation particles from disintegrations in the target, and to slow

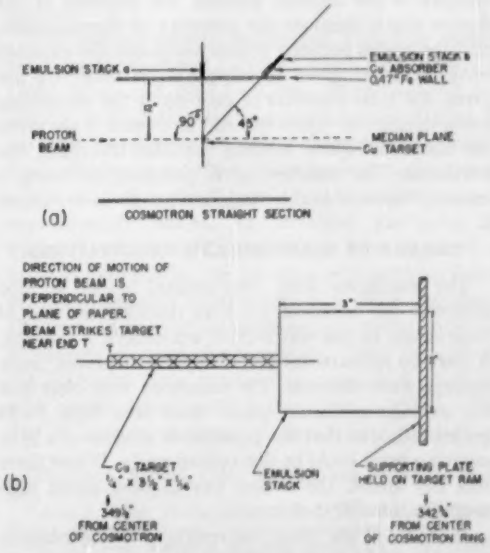

FIG. 1. Experimental arrangement. Figure 1(a) shows the positions of emulsions *LT2*, *LT3* and *LT5*, relative to the target and the proton beam of the Cosmotron. Figure 1(b) shows the method of mounting emulsions *LT7* and *LT11*, for exposures inside the vacuum chamber of the Cosmotron.

* Work performed under the auspices of the U. S. Atomic Energy Commission.

† Now at the University of Illinois, Urbana, Illinois.

‡ Now at Harvard University, Cambridge, Massachusetts.

[1] Fowler, Shutt, Thorndike, and Whittemore, Phys. Rev. **93**, 861 (1954).

[2] J. Hornbostel and E. O. Saland, Phys. Rev. **93**, 902 (1954).

[3] Hill, Salant, and Widgoff, Phys. Rev. **94**, 1794 (1954); **95**, 1699 (1954).

[4] Hill, Salant, Widgoff, Osborne, Pevsner, Ritson, Crussard, and Walker, Phys. Rev. **94**, 797 (1954).

[5] C. F. Powell, Nuovo cimento **11**, Suppl. 2, 165 (1954).

TABLE I. Summary of exposures.

Exposure code number	Exposure details	Number of protons in circulating beam (approximate)	Flux of lightly ionizing particles	Number of K particles observed
LT 3a	2.2 Bev Fig. 1(a) 90°	0.8×10^{9}	2×10^{4}/cm²	0
LT 2b	2.2 Bev Fig. 1(a) 45°	0.7×10^{9}	5×10^{3}/cm²	1
LT 5a	3.0 Bev Fig. 1(a) 90°	1.2×10^{9}	3×10^{4}/cm²	8
LT 5b	3.0 Bev Fig. 1(a) 45°	1.9×10^{9}	4×10^{3}/cm²	1
LT 7	3.0 Bev Fig. 1(b) 90°	4.7×10^{9}	5×10^{4}/cm²	2
LT 11	2.2 Bev Fig. 1(b) 90°	8.8×10^{9}	5×10^{4}/cm³	0

down the K particles. Several exposures, e.g., those at 45° to the proton beam, were made with additional absorbers between the target and the emulsions. These absorbers were used to reduce the energies of the K particles emitted in the forward direction so that some would come to rest in the emulsion stack. The stacks exposed inside the vacuum chamber were shielded from the target by $\frac{5}{32}$ in. of Cu; however, evaporation tracks made the plates difficult to scan in the area adjacent to the target.

Table I gives a summary of the exposures. The energies of the incident protons, the numbers of the figures which illustrate the geometry of the exposures, and the angles between proton beam and the detected secondaries are given in column 2. In column 3 are given the total numbers of protons in the circulating beam during the exposures, and in column 4 are given the fluxes of lightly ionizing particles traversing the emulsions. The numbers of K particles, including τ mesons, observed in the emulsions, are given in column 5.

DETAILS OF SCANNING AND OBSERVATIONS

The emulsions were area-scanned under a 20× objective for tracks of particles reaching the end of their range. In this way σ stars, π-μ decays, μ-e decays, K-particle interactions and decays, and proton track endings were observed. The emulsions were clear and the average minimum grain count was high (~38 grains/100μ), so that the presence or absence of a light outgoing track could be determined easily. Where there was any doubt, the ending was checked under high magnification (90× objective).

In Table II are given the results of this systematic scanning. Column 2 gives the area scanned for each stack. Columns 3–6 give the numbers of light-meson endings. Column 4 includes both one-prong σ stars, and those π-μ events in which the μ did not decay in the stack. Column 8 gives the number of K mesons found in the area listed in column 2. Columns 7 and 9 give, for π mesons and K particles, respectively, the approximate limits within which the particle energies must lie when they leave the target, in order for them to come to rest in the part of the emulsion which was scanned. These limits were calculated with the assumption that the particles traversed the absorber between target and emulsion in a straight line, and entered the emulsion through the edge of the stack.

In addition to the K particles listed in Table II, several were found in random scanning of some areas of the plates: two ($K7$ and $K9$) in *LT5a* and two, including one τ meson, in *LT7*. No systematic scanning has yet been done on the *LT7* and *LT11* stacks.

A check was made of the direction of entry of the π mesons that stopped in the emulsions, and it was found that more than three-fourths came from the direction of the target.

In Table III are given some of the details of the K-particle tracks observed. Columns 2–4 give, respectively, the total track length in the emulsion stack, the average track length per emulsion strip, and the maximum track length in a single strip. Column 5 shows whether the particle entered through the edge of the stack, in which case the particle could have come directly from the target, or through one of the 2-inch ×3-inch surfaces of the stack, in which case the K particle must have undergone scattering, or must have been produced in surrounding material by secondaries. The tracks of all the K particles which entered the stack through the edge facing the target lay within the angular spread of the beam from the target. Column 6 gives the energy of the particle on entering the emulsion. For the particles coming from the target direction, the energies on leaving the target have been calculated on the assumption that they traveled straight through the intervening absorber. These values are given in column 7.

Of the K particles listed here, $K1$ made a small star at the end of its range, and was thus identified as a K^- particle; $\tau1$ and $\tau2$ were identified as such because at the end of their range they underwent the characteristic decay into three coplanar charge light mesons; the remaining mesons $K2$ to $K10$ each came to rest in the emulsion and gave rise to a lightly ionizing particle, with no other visible secondary, and are phenomenologically identified as K^+ particles which have decayed.

We believe that the scarcity of K^- stars relative to K^+ endings is not due to scanning inefficiency. About $\frac{1}{4}$ of K^- stars have, in addition to 1 or more black prongs, a fast particle.[6] Our efficiency for finding and identifying such stars is appreciably higher than for finding K^+ endings, hence the ratio of K^+ mesons to star-forming K^- mesons should be even higher than the present observations indicate.

[6] J. Hornbostel and E. O. Salant, Phys. Rev. 98, 218 (1955).

TABLE II. Results of systematic area scanning.

Exposure code number	Area scanned (cm^2)	Number of light meson track endings: σ stars, 2 or more prongs	1-prong σ stars and π-μ events	π-μ-e	μ-e	Observable π-meson energy interval (Mev)	Number of K particles found in systematic scanning	Observable K-particle energy interval (Mev) (approximate)
LT 3*a* (2.2 Bev, 90°)	15.0	105	317	133	173	70–100	0	120–150
LT 2*b* (2.2 Bev, 45°)	62.0	192	551	213	357	160–195	1	260–300
LT 5*a* (3.0 Bev, 90°)	53.4	255	775	250	504	45–90	6	80–145
LT 5*b* (3.0 Bev, 45°)	27.3	38	114	34	98	160–195	1	260–300

Any comparison of rates of K-particle production at different energies and different angles that can be made from the data given in Tables I and II is uncertain, partly because of the small number of K particles observed, and partly because of uncertainties in the relative intensities of the different exposures. Neither the number of stopping pions and muons, nor the flux of lightly ionizing particles, assumed to consist mostly of light mesons, can be used as a measure of exposure intensity, since the cross section for production of these mesons is not known as a function of angle and primary energy. The circulating-beam monitor cannot be used reliably in a quantitative way at the low intensities used for the exposures, although it was used as a guide in timing them. Thus, there is no basis for a quantitative comparison of yields at different energies. There is no evidence for an appreciable change in the yield at 45° in going from a primary energy of 2.2 Bev to 3.0 Bev; at 90°, although many more K mesons were found at 3.0 Bev than at 2.2 Bev, it should be noted that the observable energies were higher and the energy interval was narrower at 2.2 Bev.

The same uncertainty in relative intensities does not apply to comparison of the numbers N of K mesons observed at 45° and 90°, with incident 3.0-Bev protons. The exposures at the two angles were for the most part simultaneous; the 45° plates were exposed somewhat longer to compensate, to some extent, for the smaller solid angle subtended. After correction for solid angle, relative exposure as measured by the circulating beam monitor, and area scanned, the ratio is $N(90°)/N(45°) = 1.8_{-1.5}{}^{+0.4}$. The error is the statistical standard deviation. The loss by decay is not significantly different at the two positions, if a lifetime equal to the lower limit 5×10^{-9} sec given by Astbury *et al.*[7] is assumed.

The expected value of this ratio has been calculated by Sternheimer,[8] by assuming that K mesons are produced in reactions of the type $p+\text{nucleon}\rightarrow\Lambda^0+K+\text{nucleon}$, with target nucleons having energies that follow a Gaussian distribution with an average energy of 20 Mev. Two possible angular distributions of the K particles in the center-of-mass system have been considered: one is isotropic, and the other varies as $\cos^2\theta$. For each of these, two possible distributions in energy have been assumed: one, f_1, is proportional to the relativistic phase space factor times a constant matrix element; the other, f_2, is proportional to the phase space factor times $p_K{}^2$, where p_K is the momentum of the K particle in the center-of-mass system. Of these, only the isotropic distribution, with the energy distribution f_1, seems inconsistent with the measured ratio.

MASSES OF K PARTICLES

One of the most important questions associated with K particles is whether the particles with different charges and decay properties have the same or different masses.

The most accurately determined K-particle masses are those of the θ^0 and τ mesons which have masses of $(966\pm10)m_e$ and $(965.5\pm0.7)m_e$, respectively.[9,10] Although, individually, the measured masses of most K particles are distributed widely throughout the range from $\sim800m_e$ to $\sim1300m_e$, there appears to be general acceptance[11] that the K-particle mass probably lies at approximately $1000m_e$. In particular, the group of workers[12] at l'Ecole Polytechnique have reported a value of $(913\pm20)m_e$ for the mass of S particles found in their cosmic-ray experiments with cloud chambers. However, in spite of the improvement in statistics and techniques of mass measurements, there are still in the literature some outstanding cases of K particles with masses significantly higher than $\sim1000m_e$. The first K particle observed at Bristol was reported to

[7] Astbury, Buchanan, Chippindale, Millar, Newth, Page, Rytz, and Sahiar, Phil. Mag. 44, 242 (1953).

[8] R. S. Sternheimer, Phys. Rev. 93, 642 (1954), Brookhaven Internal Reports RS-41, RS-42, RS-44, RS-46 (unpublished) and private communication.

[9] Thompson, Burwell, Cohn, Huggett, and Karzmark, Phys. Rev. 95, 661(A) (1954).

[10] Amaldi, Fabri, Hoang, Lock, Scarsi, Touschek, and Vitale, Nuovo cimento 12, Suppl. 2 (Padua Conference), 419 (1954).

[11] C. F. Powell, Report of Bagnères Conference, p. 222 (1953); Nuovo cimento 11, Suppl. 2, 165 (1954).

[12] Gregory, Lagarrigue, Leprince-Ringuet, Muller and Peyrou, Nuovo cimento 11, 292 (1954); L. Leprince-Ringuet, Proceedings of the Fourth Annual Rochester Conference (University of Rochester Press, Rochester, 1954).

TABLE III. Details of K-particle tracks.

K particle and stack in which it was found	Total track length in stack (mm)	Average track length per emulsion strip (mm)	Max. length in a single strip (mm)	Surface at which particle entered stack	Energy of particle when it entered emulsion (Mev)	Approximate energy of particle when it left target (Mev)
$K1$ LT 2b	31.5	6.5	11.3	edge facing target	78	275
$K2$ LT 5a	45.1	3.8	9.3	edge facing target	96	125
$K3$ LT 5a	21.3	3.0	9.1	edge facing target	62	100
$K4$ LT 5a	42.5	2.8	9.1	edge facing target	93	120
$K5$ LT 5b	10.4	0.95	1.5	edge facing target	42	260
$K6$ LT 5a	13.5	2.7	4.0	edge facing target	48	90
$K7$ LT 5a	9.4	3.1	3.7	2 in.×3 in. surface	38	...
$K8$ LT 5a	21.8	3.6	6.8	edge facing target	62	100
$K9$ LT 5a	18.2	2.6	4.2	2 in.×3 in. surface	57	...
$K10$ LT 7	4.1	4.1	4.1	2 in.×3 in. surface	24	...
$\tau 1$ LT 5a	33.9	17.0	17.5	edge facing target	82	115
$\tau 2$ LT 7	1.2	1.2	1.2	2 in.×3 in. surface	12	...

have a mass of approximately $1300m_e$,[13] and another of 1300–$1400m_e$ was reported[14] at Paris. There are also, apart from the observed stopping K particles, the jet-produced K particles, discovered by Daniel and Perkins[15] and reinvestigated by Fowler and Perkins,[6] which have a mass of approximately $1450m_e$.

Because the tracks of the K mesons we observed were generally more than 1 cm long, the particle mass was usually most conveniently and precisely determined by grain density-range measurements. In several cases, masses were also determined by the method of scattering-range.

(1) Masses Determined by the Method of Grain Density Range

Owing to the comparatively heavy development of our emulsions, which had a minimum grain count of ~38 grains per 100μ, the average grain density of K-particle tracks at 12 mm residual range was approximately 100 grains per 100μ, and at 24 mm approximately 80 per 100μ. No grain counts were made at residual ranges less than 1 cm because of the high grain density.

Of the twelve K particles tabulated in Table III, eight gave tracks from which masses were measured by the method of grain density range. The tracks were grain-counted in those emulsions for which a reasonably long segment of track existed and for which the residual range was as large as possible. In the same emulsions, under the same conditions of counting and as nearly as possible at the same time, measurements of grain density range were made on π mesons, and, in a few cases, μ mesons, with which the measurements of the K particles were compared. Pions and muons were used for calibration because our emulsions contained large numbers of them, and in general they could be found satisfactorily close (~1 cm or less) to the region in which the K mesons were being counted. In each case, in order to be certain that the calibration particles had not decayed or interacted in flight, it was required that at least one of the calibrating tracks be that of a π^+ meson which decayed into a muon of approximately 600μ range, the standard range of muons from pions which have come to rest. Usually only those calibrating tracks that were sufficiently long in one emulsion (the one being studied) were accepted. The calibrating tracks were grain-counted over an interval of grain density that included the K-particle grain density in the plate. In order to reduce the possibility of systematic errors, each K-particle mass was determined against at least two calibrating tracks in a given emulsion strip, and, whenever possible, similar measurements were made in more than one strip of the stack.

When the grain densities of the K particle and its calibrating tracks had been determined, a plot was made, for each type of particle (K, π, or μ meson), of y, the logarithm of grain density per mm of tracks, *vs* x, the logarithm of the residual range R, and a least

[13] C. O'Ceallaigh, Phil. Mag. **42**, 1032 (1951); S. von Friesen, Proceedings of the Bagnères Conference, 1953 (unpublished), p. 128; C. F. Powell, Nuovo cimento **11**, Suppl. 2, 165 (1954).

[14] L. Leprince-Ringuet, Proceedings of the Fourth Annual Rochester Conference (University of Rochester Press, Rochester, 1954), p. 72.

[15] R. Daniel and D. Perkins, Proc. Roy. Soc. (London) **A221**, 351 (1954).

squares line, $y=a+bx$, was fitted to each set of points. All of these lines should have the same slope, and, in fact, the fitted slopes were found to agree with each other within the statistical errors. The average, $\bar{b}$, of these slopes, weighted according to their statistical errors, was determined. A new line was then drawn for each type of particle, by passing a line of slope $\bar{b}$ through the center of gravity, $\bar{x}=\sum_i w_i x_i/\sum_i w_i$, $\bar{y}=\sum_i w_i y_i/\sum_i w_i$, of each set of points, where the w_i are the statistical weights of the individual points x_i, y_i. The K-particle mass was determined from the ratio of the ranges at equal grain density of the K track and calibration track. For example, if one takes $y=\bar{y}_\tau$ as the constant grain density line, then

$$\frac{M_K}{M_\tau}=\frac{R_0}{\bar{R}_\tau}=\frac{\exp x_0}{\exp \bar{x}_\tau}, \tag{1}$$

where

$$x_0=(\bar{y}_\tau-\bar{y}_K)/\bar{b}+\bar{x}_K, \tag{2}$$

and the statistical standard error is given by

$$\frac{\epsilon(R_0)}{R_0}=\left[\frac{1}{\bar{b}}\frac{(0.76)^2}{N_\tau}+\frac{1}{\bar{b}}\frac{(0.76)^2}{N_K}+\frac{(\bar{y}_\tau-\bar{y}_K)^2}{\bar{b}}\sigma^2(\bar{b})\right]^{\frac{1}{2}}. \tag{3}$$

Here N_τ and N_K are the total counted numbers of π-meson and K-meson grains, respectively, and $\sigma^2(\bar{b})$ is the statistical error in the weighted average slope $\bar{b}$. Similarly, one can obtain M_K/M_μ.

Of course, the ratio obtained by taking the range intercepts with any line of constant grain density will be the same, but the error will be changed somewhat from that given above. It is necessary to limit the range and grain density interval over which one fits a straight line, as the slope of the lng *vs* ln$R$ line is not constant over large intervals. Usually, points representing a grain density variation of not more than 10 grains per 100μ were fitted by a single line. The slope is then rather poorly determined by the points, since the range interval covered is small. It is, therefore, desirable, in order to minimize the importance of the slope in determining the range intercepts, to choose calibration tracks such that their $\bar{y}$ will be as close as possible to $\bar{y}_K$.

The results of the mass determinations by the method of grain density-range are given in Table IV. The values given there were obtained by using $m_\tau=273.4m_e$ and $m_\mu=207.0m_e$.[16] Column 2 gives the range intervals and the emulsion strip numbers in which the mass determinations were made; column 4 gives the number and kind of calibrating tracks used; columns 3 and 5 give the total numbers of grains counted in K-particle and calibrating tracks, respectively. In column 6 are given the K-particle mass values determined separately for each emulsion strip, with the standard statistical errors found by means of Eq. (3). Column 7 gives the weighted average mass value and standard statistical error for each particle. In most of the cases where the same K particle was measured in two emulsions, the mass values are in agreement within the statistical errors; differences might be an indication of errors arising from nonstatistical sources such as irregularities in the emulsion.

The masses given in Table IV, including those of negative ($K1$), positive ($K2$, $K3$, $K4$, $K6$, $K8$, $K9$) and τ mesons, are in satisfactory agreement with one another, within limits of about $70m_e$. The value of the τ-meson mass is also in accord with the value of $965.5m_e$,[10] determined from the three-pion decay of the τ meson. The weighted average value of the K^+-particle mass, obtained from the K^+ masses given in Table IV, excluding $\tau 1$, is $(965\pm15)m_e$. The error given is the standard statistical error. It should be noted that the decay products of the K^+ mesons have not been identified in most cases, and that several different decay schemes are probably represented. Thus this average does not represent the mass of any particular species of K particle.

(2) Masses Determined by the Method of Scattering-Range

There are two approaches to the measurement of masses by the method of scattering-range: for long tracks, constant cell lengths can be used to measure the scattering at large residual range, while for short tracks, measurements can be made by using constant sagitta methods.[17]

The masses of several of the K particles have been measured by one or both of these means.

Tracks that were long and flat, in the emulsion strips where the residual ranges were large, were suitable for constant cell-length measurements. The track of $\tau 1$ satisfied the requirements very well, and since the mass of the τ meson is well known, the other K-particle masses were obtained by comparing the scattering measurements on them with those made on the τ-meson track, in the following way.

From 119 cells of 100μ length, the mean scattering angle for the τ meson in the residual range interval from 17.5 mm to 29.9 mm was measured to be $0.216°\pm0.013°$. This value was obtained from the mean second differences measured with 100μ and 200μ cells, by using the noise elimination technique of Menon, O'Ceallaigh, and Rochat.[18] The error is the statistical error determined by the number of independent 200μ cells, as defined by O'Ceallaigh and Rochat.[19] By using the known mass of the τ particle and the effective residual

[16] Smith, Birnbaum, and Barkas, Phys. Rev. **91**, 765 (1953).

[17] Biswas, George, and Peters, Proc. Indian Acad. Sci. **38**, 418 (1953); Dilworth, Goldsack, and Hirschberg, Nuovo cimento **11**, 113 (1954).

[18] Menon, O'Ceallaigh, and Rochat, Phil. Mag. **42**, 932 (1951).

[19] C. O'Ceallaigh and O. Rochat, Phil. Mag. **42**, 1050 (1951).

TABLE IV. K-particle masses determined by the method of grain density vs range.

K particle	Residual range interval (mm) and emulsion strip in which grain count was made	Total grains counted in K-particle track	Kind and number of calibrating tracks	Total grains counted in calibrating tracks	K-particle mass values (m_e)	Weighted average values of K-particle mass (m_e)
$K1$	15.2–19.9 (2b.15)	3733	4π 2μ	7577	970±55	980±30
	19.9–27.4 (2b.16)	5410	2π 1μ	8266	985±35	
$K2$	10.8–20.1 (5a.10)	8988	4π	15028	955±30	940±25
	20.1–23.9 (5a.11)	3079	4π	9168	910±40	
$K3$	12.0–21.0 (5a.16)	9253	3π	11630	1005±35	1005±35
$K4$	16.1–23.1 (5a.19)	5897	3π	11957	965±30	975±25
	23.1–32.2 (5a.20)	6788	3π	6266	1010±60	
$K6$	11.0–13.4 (5a.17)	2545	3π	9637	955±70	955±70
$K8$	14.3–19.3 (5a.23)	4641	3π	8624	950±40	975±40
	19.8–22.2 (5a.24)	2022	2π	4532	1305±145	
$K9$	13.8–16.3 (5a.23)	2344	3π	8624	950±45	950±45
$\tau 1$	10.0–16.6 (5a.11)	6611	2π	6723	970±65	955±25
	19.4–29.5 (5a.10)	8948	2π	8378	955±30	

range R, defined by Gottstein and Mulvey[20] as

$$R=\left[\frac{0.15(R_2-R_1)}{R_1^{-0.15}-R_2^{-0.15}}\right]^{0.87},$$

where R_2 and R_1 are the ranges at the beginning and end of the interval measured, a value of K_s, the scattering constant in the equation $p\beta=K_s/\bar{\alpha}_{100}$, may be obtained by trial and error, from the universal curves of $p\beta/R$ vs β and p/Mc vs β. From the above data, a value of K_s equal to (25.8±1.5) (Mev/c)-degree was thus derived. Although this value in no way represents an improved determination of the scattering constant, it is nevertheless a direct and independent check of the scattering method. The masses of $K1$, $K2$ and $K4$, on which scattering measurements could be made at approximately the same residual range as for $\tau 1$, have been determined by using the value of 25.8 (Mev/c)-degree for the scattering constant. The values of the masses, together with the range intervals in which the measurements were made, the effective residual ranges and the mean scattering angles, are given in Table V. In all cases, the mean scattering angles were determined as in the case of $\tau 1$,[18] and the errors in the mass values are those which arise from the statistical errors in $\bar{\alpha}_{100}$.[19]

Values of K-particle masses measured by constant sagitta methods, with the variable cell length schemes of Biswas, George, and Peters[17] and of Fay, Gottstein, and Hain[21] are given in Table VI.

The mass values determined by scattering with cells of constant length (Table V) are in agreement, within the errors, with those obtained from grain density measurements (Table IV). The mass values determined by constant-sagitta scattering methods (Table VI) do not seem to be consistent with the results of the other methods; except in the case of $K1$, they are considerably higher. We believe that the constant-sagitta methods are not reliable for the short track lengths we have used; the results have been found to be inconsistent from

[20] K. Gottstein and J. H. Mulvey, Phil. Mag. 42, 1089 (1951).

[21] Fay, Gottstein, and Hain, Nuovo cimento 11, Suppl. 2, 234 (1954).

one part of a track to another, and from one cell length scheme to another. It also seems possible that there is a systematic error, which could arise from a variation of the scattering constant with range, at small residual range.

The best mass determinations are those based on grain density measurements, which yield an average of $(965\pm15)m_e$. The determinations from scattering are of considerably lower statistical accuracy. Inclusion of the constant cell length scattering values with the grain density values does not change the average mass, and also does not improve the accuracy. Inclusion of the constant-sagitta results as well increases the average mass to $1000m_e$, again with no significant improvement in accuracy. Because of the inconsistencies of these constant-sagitta measurements, the final average mass, obtained by omitting them, is accordingly taken to be $(965\pm15)m_e$.

NATURE OF CAPTURE OR DECAY OF K PARTICLES

The manner in which K particles are captured or decay is of prime interest in the study of these particles. In the following sections, the capture of one K^- particle, the decays of two τ mesons and of four K^+ particles are analyzed.

(1) Capture of a K^- Meson

An illustration of the star produced by the capture of $K1$ is shown in Fig. 2. The center of the star shows considerable evidence of low-energy electron tracks, probably from Auger electrons associated with the capture of the K^- into the emulsion atom, although it cannot be certain that they are not merely background tracks. There is no evidence either for a recoil track of for a high-energy electron ($\gtrsim$50 kev). However, the last section of the K^- track is so dense that the existence of a short recoil track in the backward direction, obscured by the incoming track, could not be ruled out.

Of the two visible outgoing tracks, one has a low grain density and is 2.14 mm long in the first emulsion strip, 1.04 mm in the adjacent strip. The particle then produced in flight a star of two black tracks. The other outgoing particle from the K^- star was heavily ionizing and traveled a total of 969μ in three emulsion strips before coming to rest.

Scattering measurements were made on both the outgoing tracks from the K^- star. The heavily ionizing particle was found to have range and $p\beta$ corresponding to those of a proton emitted with an energy of (13.5 $\pm$0.5) Mev. The lightly ionizing particle had a $p\beta$ of (125$\pm$30) Mev/c which is consistent with either a pion of (75$\pm$25) Mev or a proton of (62$\pm$15) Mev.

Grain density measurements on the light track showed a small variation from 1.64 to 1.71 times minimum in passing along the track from the K^- star to the secondary star. These grain density measurements are consistent with a pion of (50$\pm$5) Mev or a proton of (300$\pm$20) Mev. We must conclude from the consistency of scattering and grain density data that the lightly ionizing particle was a pion of approximately 50 Mev.

TABLE V. K-particle masses determined by method of scattering vs range, with constant length cells of 100μ and 200μ and scattering constant of 25.8 (Mev/c)-degree.

K particle	Residual range interval (mm)	Effective residual range (mm)	Mean scattering angle $\bar{\alpha}_{200}$ (degrees)	Mass (m_e)
$\tau1$	17.5–29.9	23.2	0.216	965.5 (standard)
$K1$	19.8–27.2	23.2	0.216	970$\pm$240
$K2$	20.2–27.3	23.4	0.208	1040$\pm$270
$K4$	23.1–32.2	27.4	0.205	881$\pm$200

The angle between the outgoing pion and proton tracks was measured on a tilting stage microscope to be 135°$\pm$2°.

A point of particular interest in the analysis of K^- stars is their characteristically low energy.[22–24] In the present K^- star there is direct evidence of only 203 Mev of emitted energy (including the pion rest energy), whereas the energy available from complete conversion of the K^- particle is approximately 500 Mev.

Any scheme suggested to account for this star must predict the emission of a 50-Mev charged pion. It is not necessary to account specifically for the 13-Mev proton, which could result from evaporation. The products of K capture may include hyperons[6,25,26] (the hyperons Λ and Σ, of rest energy 1115 Mev and 1190 Mev, respectively, will be considered presently), but, since there is no such track in the star, any charged hyperon must be regarded as reabsorbed within the parent nucleus, a process discussed by Goldhaber.[26] Various schemes will now be discussed.

Consider, first, capture of a K^- meson by a single nucleon N at rest in a nucleus. Let the process be limited to the production of two particles and let these

TABLE VI. K-particle masses determined by the method of scattering vs range, with constant sagitta.

K particle	Residual range interval (mm)	Mass[a] (m_e)	Mass[b] (m_e)
$K1$	0–2.1	1090$\pm$300	800$\pm$180
	0–11.3	800$\pm$130	750$\pm$110
$K2$	0–3.6	1380$\pm$300	1450$\pm$290
$K3$	0–4.2	...	1430$\pm$260
$K7$	0–2.5	...	1540$\pm$340
$K10$	0–4.0	1320$\pm$290	1100$\pm$200

[a] See reference 17.
[b] See reference 21.

[22] Lal, Pal, and Peters, Proc. Indian Acad. Sci. **38**, 398 (1953).
[23] J. Hornbostel and E. O. Salant, Phys. Rev. **93**, 902 (1954).
[24] C. F. Powell, Nuovo cimento **11**, Suppl. 2, 165 (1954).
[25] H. DeStaebler, Jr., Phys. Rev. **95**, 1110 (1954).
[26] M. Goldhaber, Phys. Rev. **92**, 1279 (1953); see also R. H. Dalitz, Phys. Rev. **94**, 1046 (1954).

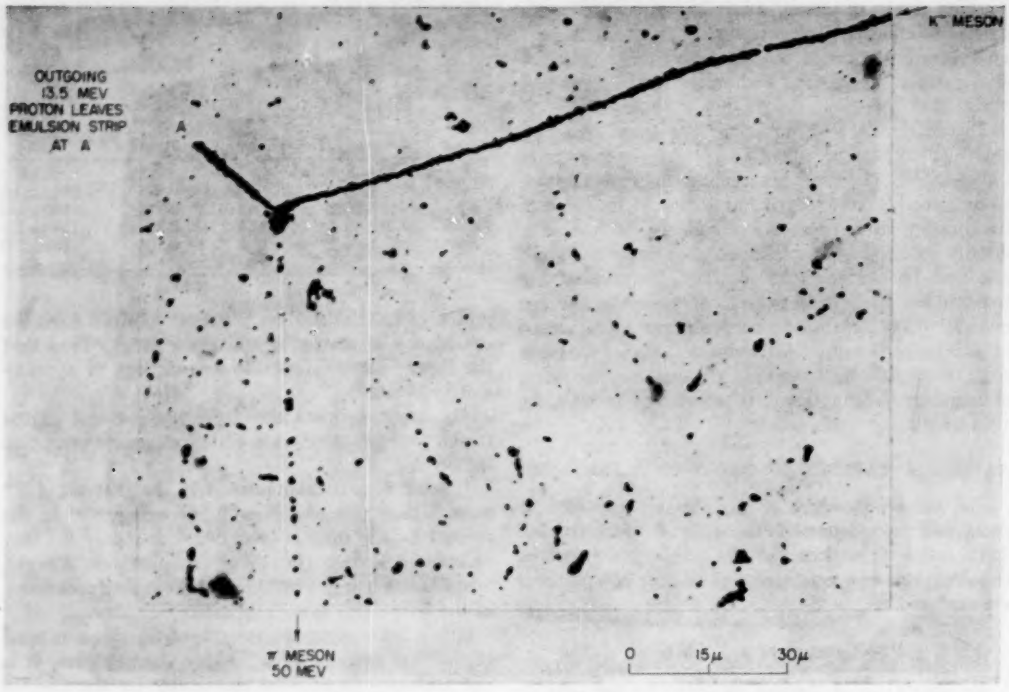

FIG. 2. Star produced by capture of K^- meson. A K^- meson coming from the right is shown stopping and producing a two-prong star of a π meson and a proton.

two particles emerge without interacting with any of the nucleons of the nucleus.

In the following reactions, where the Q values are in Mev,

$$K^-+N\rightarrow\pi^-+N+353, \quad (1)$$

$$K^-+N\rightarrow\pi^-+\Lambda^0+178, \quad (2)$$

$$K^-+N\rightarrow\pi^-+\Sigma^0+102, \quad (3)$$

the kinetic energies of the pions are 280 Mev for (1), 150 Mev for (2) and 87 Mev for (3), each inconsistent with the observed pion energy. It is to be noted that the K-meson rest energy is too low to produce a pion in addition to a cascade particle (rest energy $\sim$1315 Mev).

However, if the target nucleon is not at rest, then, as a consequence of Fermi energy, the pion of reaction (3) might be observed with 50 Mev, but not the pion of the first two reactions.

But even with a stationary nucleon, a 50-Mev pion can be obtained if any one of the other limitations is dropped. If the pion makes collisions with the other nucleons of the nucleus, it could lose enough energy. If the K-meson capture involves more than one nucleon, or produces more than two particles, as in

$$K^-+N+N\rightarrow\pi^-+N+N+353, \quad (1a)$$

$$K^-+N\rightarrow\pi^-+\pi^0+N+219, \quad (1b)$$

$$K^-+N+N\rightarrow\pi^-+\Lambda^0+N+178, \quad (2a)$$

momenta and energies can be balanced so as to accomplish the desired result.

An interesting alternative is the case discussed by Goldhaber,[26] where a hyperon (produced in K-meson capture) is trapped within the nucleus and subsequently emits a pion. Because its traversal time of a nucleus is much briefer than its lifetime, the hyperon must come to rest long before its break-up. But a Λ^0 decaying at rest yields only a 32-Mev pion; consequently a bound Λ^0 would not explain our K star. On the other hand, trapping of a Σ, produced in the reaction

$$K^-+N\rightarrow\pi^0+\Sigma^-+102 \quad (4)$$

would yield a 95-Mev charged pion, which, by collisions with nucleons, could emerge with 50 Mev. Similarly, a cascade particle, produced without an additional pion, could, if it decayed within the nucleus, yield a charged pion of the observed energy.

Thus it is apparent that many different schemes could

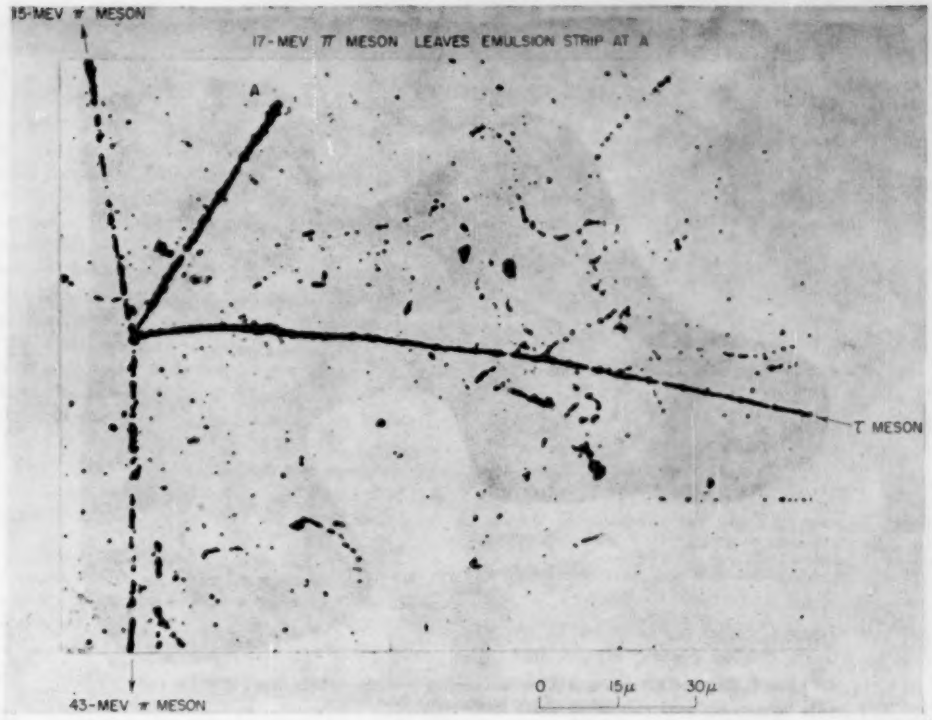

FIG. 3. Decay of τ meson. A τ meson coming from the right is shown decaying at rest into three coplanar charged π mesons.

account for our K^- star. Only reactions (1), (2) and (3) with all of the restrictions initially noted must be rejected, and (3) is acceptable with plausible Fermi energy.

So far, no account has been taken of the recent ideas of Pais and Gell-Mann and of Goldhaber, which restrict the possible products of K-meson capture.[26,27] Reactions (1), (1a), and (1b) are ruled out. In their schemes, any Σ particle in the presence of nuclear matter is transformed into a Λ^0, which then decays. Since, as we have seen, the decay of a Λ^0 will not yield a sufficiently energetic pion, neither will be Σ. Hence decay of the trapped Σ of reaction (4) will not do.

Consequently, if the theoretical restrictions are valid, the only mechanism that could yield the observed K star is the production of a charged pion and a hyperon, according to reactions (2a) or (3). The schemes of Pais and Gell-Mann and of Goldhaber forbid the formation of a cascade particle from K^- capture.

(2) Decay of τ Mesons

An illustration of the decay of $\tau 1$ is shown in Fig. 3. The details of the $\tau 1$-meson decay have already been given[3] and they are here merely summarized, together with those of $\tau 2$, in Table VII.

It is noteworthy that the ratio of the numbers of τ mesons and other K mesons, $\frac{1}{3}$, is the same as the ratio reported in cosmic rays.

(3) Decay of K^+ Mesons

A typical K^+ decay, $K2$, is shown in Fig. 4. Of the nine K^+ particles, five had secondary tracks which were too steep for reliable scattering measurements, as the track length per emulsion strip was 1 mm or less. Of the four secondary tracks considered suitable for measurement, $K2$ averaged 3.1 mm per strip; $K3$, 2.3 mm per strip; $K7$, 4.1 mm per strip; and $K10$ had a track length of 52.5 mm in a single strip. A preliminary report of $K10$ has been given.[28] None of the secondary tracks ended in the emulsion.

Grain and blob counts, as well as scattering measurements, were made on the four selected tracks. In order to obtain the ratio of the grain or blob density of a segment of track to the plateau grain or blob density, the plateau density in the neighborhood of each track segment was determined by blob- or grain-counting electrons from μ-e decays. The grain- and blob-count

[27] M. Gell-Mann and A. Pais, Proc. Glasgow Conference, July, 1954 (to be published); also private communication. M. Goldhaber (private communication).

[28] Hill, Salant, and Widgoff, Phys. Rev. 98, 247(A) (1955).

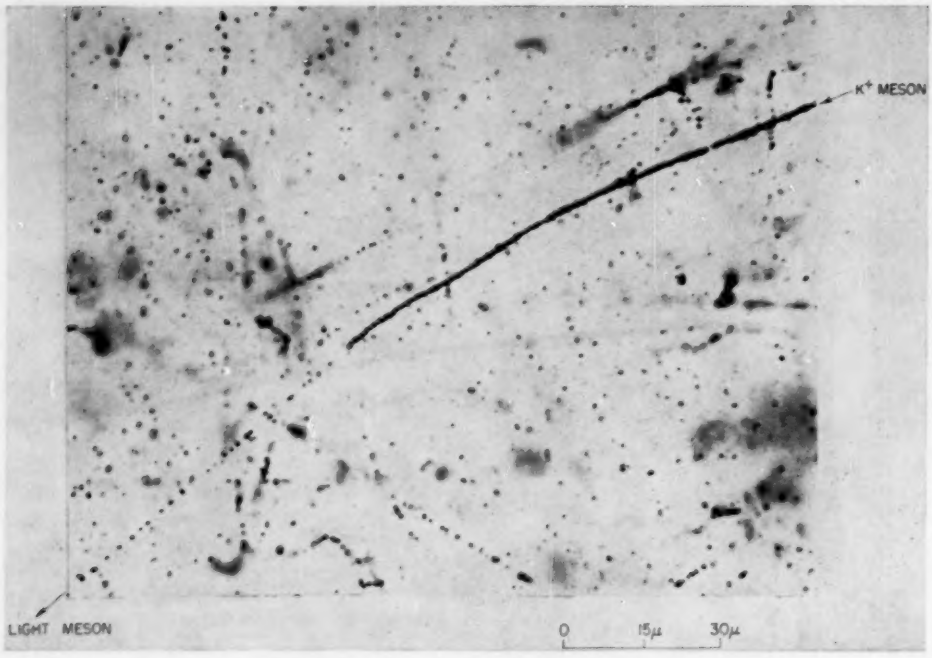

FIG. 4. Decay of K^+ meson. A K^+ meson coming from the right is shown stopping and decaying into an outgoing light meson.

histograms for a particular emulsion, *LT5a7*, are shown in Fig. 5. Figure 5(a) shows a histogram of the grain counts of electrons from μ-e decays; Fig. 5(b) shows a histogram of blob counts of the same electrons. The distribution of the blob counts can be seen to be narrower, probably because blob counting is less liable to subjective errors. It thus appears to be advantageous to use blob rather than grain counting for tracks of near-minimum ionization.

The calibration counting was done on long tracks which showed relatively little scattering, and the electrons used probably all had energies of about 10 Mev or more. The blob count thus obtained has been taken to be the plateau blob count, b_{plat}.

The scattering and blob density measurements on the decay-product track of *K*10 were made over the first 4.9 cm of its range. The last 0.35 cm of the track in the emulsion approached the edge of the plate and was not measured because of the possibility of distortion. The primary cell length used in the scattering measurements was 100μ, and the mean scattering angle, $\bar{\alpha}_{100}=0.171° \pm 0.006°$, was obtained from the 100μ and 200μ values of the mean second difference by using the noise elimination technique of Menon, O'Ceallaigh, and Rochat.[18] If one uses the value[20] 24.3 (Mev/c)-deg for the scattering constant, as is consistent with the measured ratio, $b/b_{\text{plat}}=1.18$, of average blob density to plateau blob density, one obtains for the average $p\beta$ of the track a value of (139±8) Mev/c.

TABLE VII. Details of τ-meson decays.

τ meson	π mesons (charge where known)	Pion energies (Mev)	Lengths pion tracks (mm)	Relative angles (degrees)	Q value (Mev)
$\tau 1$	$\pi 1^+$	15.4	4.9	61.3	75.6±1.0
	$\pi 2$	16.8	4.6	150.0	
	$\pi 3$	43.4	8.1		
$\tau 2$	$\pi 1$	34	1.95	126.2	79±12
	$\pi 2$	24	0.47	131.3	
	$\pi 3$	21	0.27		

It was apparent that the scattering angle increased with distance from the origin of the track. For the purpose of analysis, the track was therefore divided into six segments and the mean scattering angle, $\bar{\alpha}_{100}$, computed for each segment. The segment with the largest scattering was ~3.5 mm long, each of the other segments ~9 mm. The values so obtained are given in Table VIII.

The blob density was measured along the whole length of the track and showed a significant increase with distance from the origin. The measured blob densities for the six sections of the track under con-

[20] Bristol curves, based on work of L. Voyvodic and E. Pickup (private communication).

sideration are also shown in Table VIII. The total numbers of blobs counted in each section were of the order of 3000, so that the statistical mean deviations in blob densities are of the order ± 0.6 blobs per 100μ. The tracks of fast electrons in close proximity to the K-secondary track showed slight local variations (~ 3 percent) in plateau blob density. The values of b^* are the blob densities corrected for these local variations. The ratios of b^* to b_{plat} are given in the final column of Table VIII.

Each of the secondary outgoing tracks of $K2$, $K3$, and $K7$ mesons was scattered in three adjacent emulsions. In order to indicate the possible degree of accuracy of the scattering measurements, the separate mean second scattering differences are shown in Table IX. It is seen from these values that, with the possible exception of the case $K7$, the constancy of both $\bar{D}_{100\mu}$ and $\bar{D}_{200\mu}$, as well as the ratio $\bar{D}_{200\mu}/\bar{D}_{100\mu}$, is not very good. No correction for distortion was made because the numbers of independent second differences of both positive and negative signs were always approximately the same. The values of $\bar{\alpha}_{100}$ were obtained by using the noise elimination procedure.

TABLE VIII. Summary of scattering and blob density measurements for the secondary track of $K10$.

Distance of midpoint of track segment from origin (mm)	$\bar{\alpha}_{100}$ (degrees)	$p\beta$ (Mev/c)	b^* (blobs per 100μ)	b^*/b_{plat} ($b_{\text{plat}}=29.5\pm0.3$)
4.35	0.148 ± 0.022	163 ± 24	33.0 ± 0.6	1.12 ± 0.03
13.05	0.143 ± 0.020	170 ± 23	34.2 ± 0.6	1.16 ± 0.03
21.75	0.151 ± 0.020	161 ± 21	34.8 ± 0.6	1.18 ± 0.03
30.45	0.181 ± 0.025	134 ± 19	35.3 ± 0.6	1.20 ± 0.03
39.70	0.213 ± 0.028	114 ± 15	37.0 ± 0.6	1.25 ± 0.03
46.75	0.240 ± 0.045	101 ± 19	37.3 ± 0.7	1.26 ± 0.04
Whole track	0.174 ± 0.010	139 ± 8	34.8 ± 0.3	1.18 ± 0.01

Blob counting on the outgoing tracks showed no significant variation from one emulsion to another. The ratios b^*/b_{plat} are given in the final column of Table IX. The errors quoted are the standard deviations based on the numbers of grains counted.

The values of b^*/b_{plat}, from Tables VIII and IX are plotted as a function of $p\beta$ in Fig. 6.

For various reasons, enough pion tracks for good blob count-$p\beta$ calibration in the relevant emulsion strips have not yet been obtained. While the search for the appropriate tracks is still going on, it was regarded as instructive to compare the measured values of the K secondaries with pion ionization-$p\beta$ curves obtained in other laboratories. These curves are drawn solid in Fig. 6, from the values given by (a) Daniel *et al.*,[30] (b) the group at the University of Padua,[31] and (c) Fleming and Lord.[32] The muon curves in Fig. 6 are derived in the usual way from the pion curves. In cases (a) and (b), the plateau blob densities were obtained from blob counts of pair electrons of energy >10 Mev and from primaries of high energy stars. For (a), the value is ~ 19 per 100μ, for (b) 22 per 100μ. The plateau blob density for (c), obtained from μ-decay electrons, was 30 per 100μ. Values of $p\beta$ were determined, in (a) and (b) by scattering measurements, in (c) by the more precise magnetic measurement of momentum of selected pion beams.

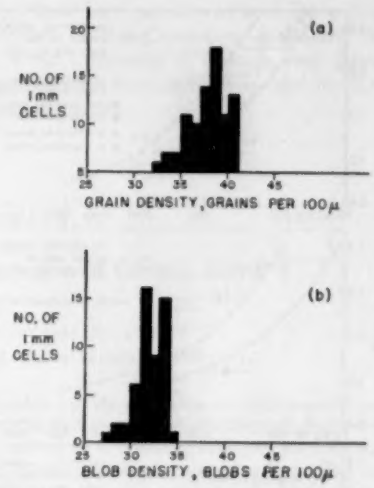

FIG. 5. Histograms of blob and grain densities. Figure 5(a) shows a histogram of grain counts on high energy electrons from μ-e decays. Figure 5(b) shows a similar histogram of blob counts on the same electrons as were used in obtaining Fig. 5(a).

The secondaries of $K3$ and $K7$ are consistent with either the π or μ calibration curves.

In all three calibrations, the $K2$ secondary agrees with the μ but not with the π curve. It cannot be excluded, however, that any of the secondaries $K2$, $K3$, or $K7$ is an electron.

TABLE IX. Scattering and blob density determinations for secondary tracks of $K2$, $K3$, and $K7$ mesons.

K particle	Length scattered (mm) (emulsion number)	$D_{100\mu}$ (μ)	$D_{200\mu}$ (μ)	$\bar{\alpha}_{100}$ (degrees)	$p\beta$ (Mev/c)	b^*/b_{plat}
$K2$	2.5 (6)	0.0340	0.0980	0.182	134 ± 18	1.02 ± 0.03
	4.1 (7)	0.0331	0.1025			
	1.6 (8)	0.0202	0.0395			
$K3$	2.4 (8)	0.0211	0.0639	0.131	186 ± 30	0.99 ± 0.04
	2.1 (9)	0.0201	0.0830			
	1.4 (10)	0.0239	0.0354			
$K7$	4.1 (22)	0.0281	0.0739	0.127	192 ± 22	1.02 ± 0.03
	4.2 (23)	0.0251	0.0583			
	3.3 (24)	0.0243	0.0587			

[30] Daniel, Davies, Mulvey, and Perkins, Phil. Mag. **43**, 753 (1952).
[31] Padua group (private communication by G. T. Zorn).
[32] J. R. Fleming and J. J. Lord, Phys. Rev. **92**, 511 (1953).

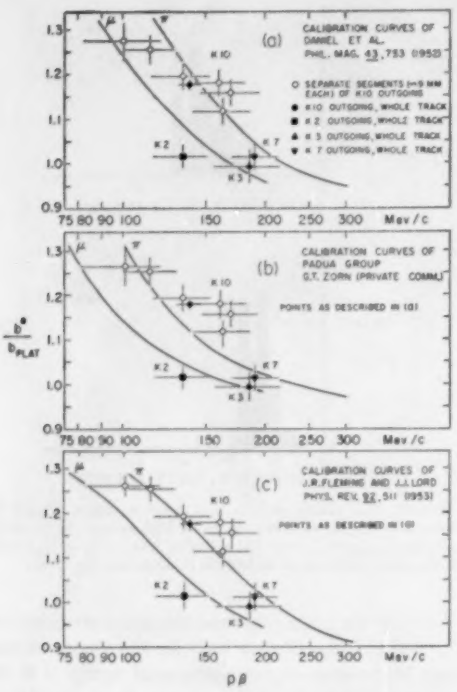
(a)
CALIBRATION CURVES OF DANIEL ET AL. PHIL. MAG. 43, 753 (1953)
(b)
CALIBRATION CURVES OF PADUA GROUP G.T. ZORN (PRIVATE COMM.)
(c)
CALIBRATION CURVES OF J.R. FLEMING AND J.J. LORD PHYS. REV. 92, 511 (1953)
K10
K2
K3
K7
75 80 90 100 150 200 250 300 Mev/c
pβ

FIG. 6. Plots of blob densities *vs* $p\beta$-values for the outgoing light mesons of K^+ mesons: $K2$, $K3$, $K7$, and $K10$. Figures 6(a), 6(b), and 6(c) show these data plotted relative to the π- and μ-meson curves of Daniel *et al.*, the Padua Group, and Fleming and Lord, respectively.

In all three calibrations, the $K10$ secondary for $p\beta \geq 134$ is consistent with the π but not with the μ curve. For $p\beta = 114$, $K10$ is consistent with the π curves but not with the μ curves of (b) and (c), while it could be just as well associated with either curve of calibration (a). The less precise point at $p\beta = 101$ could lie either on the π or μ curves of (b) and (c), and better on the μ than on the π curve of (a).

The fit of the higher $p\beta$ points to all π calibration curves and failure of those points to fit the μ curves are evidence that the $K10$ secondary is a pion. The discrepancy between the low $p\beta$ points and the Daniel π curve arises because the $K10$ points lie on a flatter curve. Since the plateau density in the Brookhaven plates is 29.5 and in the Daniels plates only 19, this greater flatness is not surprising in view of saturation effects. The Padua plates have plateau density 22, and curve (b) also is steeper than the $K10$ curve. The plateau density of the Fleming-Lord plates is the same as for the Brookhaven plates (and both were determined in the same way, from μ-decay electrons) and the slopes of the $K10$ and (c) curves are quite consistent with each other.

The point representing the average $p\beta$, (139 ± 8) Mev/c, and average blob density of the entire $K10$ track is consistent with the π curves but not with the μ curves of all three calibrations. The average $p\beta$ of $K2$ is (134 ± 18) Mev/c. Hence it can be stated that, at approximately the same $p\beta$, the blob density of $K10$ is 20 percent higher than the blob density of $K2$. This supports the evidence for identifying the $K10$ secondary as a pion.

If one accepts this evidence that the $K10$ secondary is a pion, one finds, from the $p\beta$ measurements and the known rate of energy loss in emulsion, its $p\beta$, momentum and kinetic energy at emission as 165 ± 7 Mev/c, 198 ± 7 Mev/c and 102 ± 6 Mev, respectively.

That positive K mesons might decay into two light mesons, a positive pion and a neutral secondary, was first suggested by Menon and O'Ceallaigh,[32] who observed five cases in which the $p\beta$ of the decay particle was approximately constant and lay between 162 and 187 Mev/c. A similar case was later observed by Bonetti *et al.*,[34] who determined the $p\beta$ of the decay particle as 200 ± 33 Mev/c.

It was mentioned in the preliminary report[28] that, if the $K10$ decay is represented by

$$K^+ \rightarrow \pi^+ + \pi^0 + Q,$$

then (with masses[16,35] $m_{\pi^+} = 273.4 m_e$ and $m_{\pi^0} = 263.7 m_e$) $Q = 207\pm9$ Mev and the mass of the $K10$ primary is $(945\pm20)m_e$.

The primary track $K10$ was not long enough to make possible a precise direct measurement of its mass; the values obtained by constant sagitta scattering methods and given in Table VI are not inconsistent with the value deduced from the assumed decay.

Thus the event $K10$, the recent Princeton cloud-chamber observation,[36] and two recent K^+ decays in emulsions[37] are very similar. The K-meson mass and the Q agree closely[9] with the mass and Q of the θ^0, which decays into two charged pions.

Since it is not certain that the $K10$ primary came directly from the target, nothing significant can be said about its lifetime.

ACKNOWLEDGMENTS

We are indebted more than we can say to Mrs. M. Hall and the other scanners, Mrs. M. Bracker, Mrs. B. Cozine, and Mrs. A. Lea. We take pleasure in thanking Mrs. M. Carter, Mr. J. Smith, and Mr. J. Quinn for

[32] M. G. K. Menon and C. O'Ceallaigh, Proc. Roy. Soc. (London) **A221**, 292 (1953).
[34] Bonetti, LeviSetti, Panetti, and Tomasini, Proc. Roy. Soc. (London) **A221**, 318 (1953).
[35] W. Chinowsky and J. Steinberger, Phys. Rev. **93**, 586 (1954).
[36] Hodson, Ballam, Arnold, Harris, Rau, Reynolds, and Treiman, Phys. Rev. **96**, 1089 (1954).
[37] Baldo, Belliboni, Sechi, and Zorn, Nuovo cimento **12**, Suppl. 2 (Padua Conference), 220 (1954).

preparing and processing the emulsions, Dr. R. Sternheimer for informative discussions of the theoretical aspects of K-particle production, and Dr. M. Goldhaber, Dr. J. Hornbostel, and Dr. G. Zorn for helpful criticisms and suggestions. And of course the exposures would not have been possible without the willing and able services of the Cosmotron Staff. Dr. Marcel Schein of the University of Chicago very generously sent us a precision stage which was used for the scattering measurements.

PHYSICAL REVIEW VOLUME 99, NUMBER 1 JULY 1, 1955

Hydromagnetic Waves and the Acceleration of Cosmic Rays*

EUGENE N. PARKER
Department of Physics, University of Utah, Salt Lake City, Utah
(Received January 27, 1955; revised manuscript received March 15, 1955)

The large amounts of energy necessary for the acceleration of cosmic rays throughout the galaxy introduces a serious transport problem. The hydrodynamic and hydromagnetic equations are investigated from the viewpoint of energy propagation. It is shown that, with the galactic model of Fermi and Chandrasekhar, the observed motions of the interstellar gas reduce to hydromagnetic waves, which are, as it turns out, the most effective means of energy transport. A consideration of the interaction of charged particles with hydromagnetic waves shows that it is the fluid velocity, and not the wave velocity, that is responsible for the acceleration of cosmic rays by Fermi's mechanism.

We calculate the the dissipation of hydromagnetic waves in the interstellar medium, and the variation of amplitude and wavelength of such waves with changes in density and large-scale field intensity. It is then shown that the galaxy is no more than one percent efficient in the acceleration of cosmic rays because of the tremendous viscous losses in the interstellar medium, and that there is no hydromagnetic mechanism that can convert the observed large-scale low-velocity fluctuations in the interstellar medium to the required small-scale high-velocity motions.

MORRISON, Olbert, and Rossi[1] have discussed the necessary conditions for accelerating, by Fermi's mechanism,[2,3] the cosmic-ray particles observed at the earth. The energy they require for the acceleration comes directly from the irregular motions of the gas clouds in the spiral arms of the galaxy. So much energy is needed to accelerate the cosmic-ray particles that the clouds would lose their irregular motions in a period of time of the order of only 10^6 years. There seem to be only two sources of energy of sufficient magnitude to supply the clouds for significant periods of time: One is the gravitational energy of the galaxy as a whole; and the other is the nuclear energy continually liberated in the interior of stars. Though it is not clear as to how the gravitational energy of the galaxy can excite the small scale cloud motions, Oort[4] and Spitzer[5] have recently proposed a mechanism whereby the O and B stars can transfer large amounts of energy to the motions of the gas clouds: The O and B stars, with their enormous surface temperatures, ionize and explode the gas clouds near whose centers they are formed.

The average life of a cosmic-ray particle based on collision length is of the order of 4×10^7 years. Morrison *et al.* find, however, that before the particle escapes from the galaxy a life of no more than 4×10^6 years can be tolerated in view of the observed mass spectrum. Since the energy density of cosmic rays is about the same as starlight, *viz.* 5×10^{-13} erg/cm^3,[6] they require 3×10^{-27} erg/cm^3/sec for the acceleration of cosmic rays, instead of only 3×10^{-28} erg/cm^3/sec based on the lifetime of 4×10^7 years.

Now, whatever the source of the energy maintaining the irregular motions of the gas clouds, whether it be Oort's mechanism alone or this mechanism in conjunction with other sources, there must be some means for propagating the irregular motion from the relatively localized sources of supply, *viz.*, the O and B complexes. The bodily transport of kinetic energy by the moving clouds themselves is very inefficient because the transfer to other clouds is through the inelastic collisions between clouds. We are led to consider the possibility of more efficient transport processes, and toward this end we shall now decompose the equations of hydrodynamics and hydromagnetics into components according to the manner in which they propagate.

I. HYDRODYNAMICS

It is well known that for suitable boundary conditions there exist functions $\mathbf{A}(\mathbf{r})$ and $\varphi(\mathbf{r})$, where $\mathbf{r}$ represents the position vector, such that any analytic vector function $\mathbf{v}(\mathbf{r})$ may be expressed[7] as

$$\mathbf{v}(\mathbf{r})=\nabla\times\mathbf{A}(\mathbf{r})-\nabla\varphi(\mathbf{r}),\quad \nabla\cdot\mathbf{A}(\mathbf{r})=0. \tag{1}$$

Taking the curl and the divergence of this expression,

* This work was supported by the Office of Naval Research.
[1] Morrison, Olbert, and Rossi, Phys. Rev. **94**, 440 (1954).
[2] E. Fermi, Phys. Rev. **75**, 1169 (1949).
[3] E. Fermi, Astrophys. J. **119**, 1 (1954).
[4] J. H. Oort, Bull. Astron. Soc. Netherlands **12**, 177 (1954).
[5] J. H. Oort and L. Spitzer, Jr., Astrophys. J. **121**, 6 (1955).
[6] T. Dunham, Jr., Am. Phil. Soc. **81**, 277 (1939).
[7] C. F. Sommerfeld, *Mechanics of Deformable Bodies* (Academic Press, Inc., New York, 1950), p. 147.

we find that

$$\nabla\times\mathbf{v}(\mathbf{r})=\nabla\times[\nabla\times\mathbf{A}(\mathbf{r})]=-\nabla^2\mathbf{A}(\mathbf{r}), \quad (2)$$

$$\nabla\cdot\mathbf{v}(\mathbf{r})=-\nabla^2\varphi(\mathbf{r}). \quad (3)$$

The solutions of (2) and (3) are

$$\mathbf{A}_1(\mathbf{r})=\frac{1}{4\pi}\int\frac{d^3\mathbf{r}'}{|\mathbf{r}-\mathbf{r}'|}\nabla\times\mathbf{v}(\mathbf{r}'), \quad (4)$$

$$\varphi_1(\mathbf{r})=\frac{1}{4\pi}\int\frac{d^3\mathbf{r}'}{|\mathbf{r}-\mathbf{r}'|}\nabla\cdot\mathbf{v}(\mathbf{r}'). \quad (5)$$

We designate as characteristic solutions the solutions of the homogeneous equations

$$\nabla^2\mathbf{A}_0(\mathbf{r})=0, \quad \nabla^2\varphi_0(\mathbf{r})=0. \quad (6)$$

We decompose $\mathbf{v}(\mathbf{r})$ into three parts, the *transverse*, *longitudinal*, and *characteristic* components, defined as

$$(\mathrm{tr})\mathbf{v}(\mathbf{r})=\nabla\times\mathbf{A}_1(\mathbf{r}), \quad (\mathrm{lo})\mathbf{v}(\mathbf{r})=-\nabla\varphi_1(\mathbf{r}),$$
$$(\mathrm{ch})\mathbf{v}(\mathbf{r})=\nabla\times\mathbf{A}_0(\mathbf{r})-\nabla\varphi_0(\mathbf{r}), \quad (7)$$

where

$$\nabla\times\mathbf{v}(\mathbf{r})=\nabla\times(\mathrm{tr})\mathbf{v}(\mathbf{r}), \quad \nabla\cdot\mathbf{v}(\mathbf{r})=\nabla\cdot(\mathrm{lo})\mathbf{v}(\mathbf{r}),$$
$$\nabla^2(\mathrm{ch})\mathbf{v}(\mathbf{r})=0. \quad (8)$$

(4), (5), and (6) yield a unique representation of $\mathbf{v}(\mathbf{r})$ when the boundary conditions are suitably specified.

We next consider the orthogonality of the three components of the velocity over a given region of space; we shall show that it depends only on the boundary conditions. Moreover, if we choose $(\mathrm{ch})\mathbf{v}=0$ over the surface of the region, $(\mathrm{ch})\mathbf{v}$ vanishes everywhere within the region because it satisfies Laplace's equation (8). From (7), using some well-known vector identities,

$$\int dV(\mathrm{tr})\mathbf{v}\cdot(\mathrm{lo})\mathbf{v}$$
$$=-\int dV(\nabla\times\mathbf{A}_1)\cdot\nabla\varphi_1=-\int dV\nabla\cdot(\mathbf{A}_1\cdot\nabla\varphi_1)$$
$$=+\int d\mathbf{S}\cdot\mathbf{A}_1\times(\mathrm{lo})\mathbf{v}; \quad (9)$$

$$\int dV(\mathrm{lo})\mathbf{v}\cdot(\mathrm{ch})\mathbf{v}$$
$$=-\int dV\nabla\varphi_1\cdot\nabla\times\mathbf{A}_0+\int dV\nabla\varphi_1\cdot\nabla\varphi_0$$
$$=-\int dV\nabla\cdot(\mathbf{A}_0\times\nabla\varphi_1)+\int dV\nabla\cdot(\varphi_1\nabla\varphi_0)$$
$$=-\int d\mathbf{S}\cdot(\mathbf{A}_0\times\nabla\varphi_1)+\int d\mathbf{S}\cdot\varphi_1\nabla\varphi_0$$
$$=+\int d\mathbf{S}\cdot\nabla\times(\varphi_1\mathbf{A}_0)-\int d\mathbf{S}\cdot(\mathrm{ch})\mathbf{v}\varphi_1$$
$$=-\int d\mathbf{S}\cdot(\mathrm{ch})\mathbf{v}\varphi_1; \quad (10)$$

$$\int dV(\mathrm{ch})\mathbf{v}\cdot(\mathrm{tr})\mathbf{v}$$
$$=\int dV\nabla\times\mathbf{A}_0\cdot\nabla\times\mathbf{A}_1-\int dV\nabla\varphi_0\cdot\nabla\times\mathbf{A}_1$$
$$=\int dV\{\nabla\cdot[\mathbf{A}_1\times(\nabla\times\mathbf{A}_0)]+\mathbf{A}_1\cdot\nabla\times(\nabla\times\mathbf{A}_0)\}$$
$$-\int dV\nabla\cdot(\mathbf{A}_1\times\nabla\varphi_1)$$
$$=\int d\mathbf{S}\cdot\mathbf{A}_1\times(\mathrm{ch})\mathbf{v}. \quad (11)$$

Thus, orthogonality of the three components may be achieved in a finite space by suitable choice of boundary conditions.

The resolution of $\mathbf{v}$ into characteristic, transverse, and longitudinal components separates in a clear way the motions of the fluid according to their means of propagation:

The characteristic component, satisfying Laplace's equation, is a potential type field, and, barring singularities within the region, is propagated by potential gradients of external origin.

The transverse component is propagated convectively with velocities of order $\mathbf{v}$, as represented in $(\mathbf{v}\cdot\nabla)\mathbf{v}$; correspondingly the analysis of incompressible turbulence into Fourier components or "waves" is a purely formal device.

The longitudinal velocity is in part a potential flow of internal origin, as indicated by (23) below, and in part a wave motion propagating with the velocity of sound [see (24) and (28) below]. As we shall show, however, for low Mach number the acoustical radiation is usually of such low-energy density that the net energy transport may be neglected.

To demonstrate these statements, we start from the hydrodynamic equation,

$$\partial\mathbf{v}/\partial t=-(1/\rho)\nabla p-(\mathbf{v}\cdot\nabla)\mathbf{v}+(\nu/3)\nabla(\nabla\cdot\mathbf{v})+\nu\nabla^2\mathbf{v}, \quad (12)$$

and the equation of continuity,

$$(1/\rho)D\rho/Dt=-\nabla\cdot\mathbf{v}, \quad (13)$$

where D/Dt is the substantial derivative $\partial/\partial t+(\mathbf{v}\cdot\nabla)$. In terms of $(\mathrm{tr})\mathbf{v}$, $(\mathrm{lo})\mathbf{v}$, and $(\mathrm{ch})\mathbf{v}$, they may be written

$$\partial\mathbf{v}/\partial t=-(1/\rho)\nabla p-(\mathbf{v}\cdot\nabla)\mathbf{v}$$
$$+(4\nu/3)\nabla[\nabla\cdot(\mathrm{lo})\mathbf{v}]+\nu\nabla^2(\mathrm{tr})\mathbf{v}, \quad (14)$$

$$(1/\rho)D\rho/Dt=-\nabla\cdot(\mathrm{lo})\mathbf{v}. \quad (15)$$

To obtain equations for the individual components we first note that $(\mathrm{ch})\mathbf{v}$ can be computed from (8). To obtain an equation for $(\mathrm{tr})\mathbf{v}$, we take the curl of (14). Using the vector identity $\nabla\times[(\mathbf{v}\cdot\nabla)\mathbf{v}]=-\nabla\times[\mathbf{v}\times(\nabla\times\mathbf{v})]$, we obtain the usual vorticity diffusion equation

$$D\boldsymbol{\omega}/Dt=(\boldsymbol{\omega}\cdot\nabla)\mathbf{v}-\boldsymbol{\omega}\nabla\cdot(\mathrm{lo})\mathbf{v}+\nu\nabla^2\boldsymbol{\omega}, \quad (16)$$

where

$$\omega=\nabla\times\mathbf{v}=\nabla\times(\mathrm{tr})\mathbf{v}=-\nabla^2\mathbf{A}_1. \tag{17}$$

To obtain (lo)$\mathbf{v}$ we note that at low Mach numbers $|(\mathrm{lo})\mathbf{v}|\ll|(\mathrm{tr})\mathbf{v}|+|(\mathrm{ch})\mathbf{v}|$. Thus, omitting all terms in (lo)$\mathbf{v}$ we take the divergence of (12) and obtain

$$\nabla^2 p=-\rho\nabla\cdot[(\mathbf{v}\cdot\nabla)\mathbf{v}]+O[(\mathrm{lo})\mathbf{v}]. \tag{18}$$

Using the vector identity

$$\nabla\cdot[(\mathbf{v}\cdot\nabla)\mathbf{v}]=\nabla^2(v^2/2)-\nabla\cdot(\mathbf{v}\times\boldsymbol{\omega})+O[(\mathrm{lo})\mathbf{v}], \tag{19}$$

we obtain

$$\nabla^2 p=-\nabla^2(\rho v^2/2)+\rho\nabla\cdot(\mathbf{v}\times\boldsymbol{\omega})+O[(\mathrm{lo})\mathbf{v}] \tag{20}$$

$$=-\nabla^2(\rho v^2/2)+\rho\omega^2-\mathbf{v}\cdot(\nabla\times\boldsymbol{\omega})+O[(\mathrm{lo})\mathbf{v}]. \tag{21}$$

(20) or (21) gives p in terms of $\mathbf{v}$. If we denote the speed of sound by C, so that

$$C^2=dp/d\rho, \tag{22}$$

then (15) may be rewritten to give the velocity potential[1] of the longitudinal component

$$\nabla^2\varphi_1=(1/\rho C^2)Dp/Dt. \tag{23}$$

Finally, consider the portion of φ_1, or (lo)$\mathbf{v}$ that is acoustical radiation. Suppose that we write p as the sum of two parts, Π and π. Let π represent the weak pressure fluctuations responsible for accelerating (lo)$\mathbf{v}$ in flows of low Mach number; then $\pi\ll\Pi$. It follows that the dynamical equation for (lo)$\mathbf{v}$ or φ_1 may be written

$$(D/Dt)(\mathrm{lo})\mathbf{v}=-(D/Dt)\nabla\varphi_1=-(1/\rho)\nabla\pi \tag{24}$$

if we neglect the dissipation of (lo)$\mathbf{v}$ by viscosity. The operator $(D/Dt)\nabla$ may be written as $\nabla(\partial/\partial t)$ plus terms representing the transport of (lo)$\mathbf{v}$ from one place to another by (tr)$\mathbf{v}$ and (ch)$\mathbf{v}$. Such terms are scattering terms and in the sequel will be indicated only by (s.t.). They are of no particular interest for our purpose and may be found elsewhere.[8] Thus (24) may be rewritten as

$$\nabla(\partial\varphi_1/\partial t)=(1/\rho)\nabla\pi+(\mathrm{s.t.}), \tag{25}$$

and, neglecting the scattering terms and variations in ρ, we have

$$\partial\varphi_1/\partial t=\pi/\rho+(\mathrm{s.t.}). \tag{26}$$

Thus, (23) may be rewritten as

$$\nabla^2\varphi_1-\frac{1}{C^2}\frac{\partial^2\varphi_1}{\partial t^2}=\frac{1}{\rho C^2}\frac{D\Pi}{Dt}+\frac{1}{C^2}\left[\frac{1}{\rho}\frac{D\pi}{Dt}-\frac{1}{\rho}\frac{\partial^2\varphi_1}{\partial t^2}\right]+(\mathrm{s.t.})$$

$$=\frac{1}{\rho C^2}\frac{D\Pi}{Dt}+\frac{1}{\rho C^2}\left(\frac{D\pi}{Dt}-\frac{\partial\pi}{\partial t}\right)+(\mathrm{s.t.})$$

$$=\frac{1}{\rho C^2}\frac{D\Pi}{Dt}+(\mathrm{s.t.}). \tag{27}$$

The solution of (27) is

$$\varphi_1=\Box^{-2}\left[\frac{1}{\rho C^2}\frac{D\Pi}{Dt}\right], \tag{28}$$

where $\Box^{-2}$ represents the retarded integral. It can be shown[8] that $\Box^{-2}$ is just the operation singling out the Fourier components of Π for which $C|\mathbf{k}|=\omega$, and so, as is also clear from (27), (28) gives the radiative portion of (lo)$\mathbf{v}$. $\mathbf{k}$ represents the wave vector, of magnitude $2\pi/\lambda$. The relation (27) or its equivalent was obtained previously by Lighthill[9] and by Parker[8] by a much more lengthy derivation.

Denoting the particle velocity associated with the acoustical radiation by $\mathbf{u}(\mathbf{r},t)$, we use (28) to compute the radiation at a large distance $\mathbf{R}$ from a source. Then

$$\mathbf{u}=-\nabla\varphi_1=+\frac{1}{4\pi\rho C^2}\nabla\int\frac{dV'}{|\mathbf{R}-\mathbf{r}'|}\left[\frac{D\Pi}{Dt}\right]_{[t-|\mathbf{R}-\mathbf{r}'|/C]} \tag{29}$$

$$=-\frac{\mathbf{e}_r}{4\pi\rho C^3}\int\frac{dV'}{|\mathbf{R}-\mathbf{r}'|}\left[\frac{\partial}{\partial t}\frac{D\Pi}{Dt}\right]_{[t-|\mathbf{R}-\mathbf{r}'|/C]}+O(R^{-2}). \tag{30}$$

To estimate the energy radiated by a single eddy of scale L, we note from (21) that the fluctuation in p is of the order of

$$\delta p\sim\rho v^2.$$

The characteristic time is L/v, so that

$$\frac{D\Pi}{Dt}\sim\frac{\rho v^3}{L},\quad \frac{\partial}{\partial t}\left(\frac{D\Pi}{Dt}\right)\sim\frac{\rho v^4}{L^3}. \tag{31}$$

(30) gives

$$|\mathbf{u}(\mathbf{R})|\sim v(L/R)(v/C)^2. \tag{32}$$

(23) gives

$$|\mathbf{u}(\mathbf{R})|\sim|(\mathrm{lo})\mathbf{v}|\,(v/C) \tag{33}$$

for the radiation from the volume L^3 of the eddy. Thus the ratio of $\mathbf{u}$ to the transverse velocity is of the order of the cube of the Mach number for turbulent flows; only the fraction v/C of (lo)$\mathbf{v}$ is radiation. If, on the other hand, we were to consider a forced periodic flow where the amplitude of the motion of each individual particle is of the order of l and make $l\ll L$, it is easily shown that $\partial\mathbf{v}/\partial t\gg(\mathbf{v}\cdot\nabla)\mathbf{v}$; $\mathbf{u}(\mathbf{R})$ may then be *very* much larger than the result given in (33).

To understand why in the case of turbulence only so small a fraction of (lo)$\mathbf{v}$ is radiation, we note that the characteristic frequency, for turbulence and the associated longitudinal velocity, is

$$\omega\sim(2\pi/L)v\sim kv,$$

where k is the wave number, of the order of $2\pi/L$. But for acoustical radiation $kC=\omega$. Thus ω is too low by a factor of v/C to give radiation.

[8] E. N. Parker, Phys. Rev. **90**, 240 (1953).
[9] M. J. Lighthill, Proc. Roy. Soc. (London) **211**, 564 (1954).

II. HYDROMAGNETICS

Let us next consider the generation of hydromagnetic waves. Such waves are a form of transverse motion, as we shall show presently, and we may therefore expect that they will appear in more copious quantities than the longitudinal acoustical waves. It will moreover be shown that in the presence of a strong, large-scale magnetic field essentially all of the fluid motion may be represented as a hydromagnetic wave field.

To illustrate the nature of hydromagnetic or Alfvén waves, consider the hydromagnetic equations for a perfect fluid.

$$\partial\mathbf{B}/\partial t=\nabla\times(\mathbf{v}\times\mathbf{B}),\quad \partial\mathbf{v}/\partial t+(\mathbf{v}\cdot\nabla)\mathbf{v} =-(1/\rho)\nabla p+(1/\mu\rho)(\nabla\times\mathbf{B})\times\mathbf{B}. \quad (34)$$

Let the large-scale field be a uniform field

$$\mathbf{B}_0=B_0\mathbf{e}_x,$$

where $\mathbf{e}_x$ represents a unit vector in the x direction, and let us introduce a magnetic disturbance $\mathbf{b}=b\mathbf{e}_y$ as a result of the velocity $v\mathbf{e}_y$. The assumption of the parallelism of $\mathbf{v}$ and $\mathbf{b}$ is based upon the well-known theorem that for infinite conductivity the magnetic field is carried bodily with the fluid particles. The hydromagnetic equations reduce rigorously to

$$\partial b/\partial t=B_0\partial v/\partial x,\quad \partial v/\partial t=(B_0/\mu\rho)\partial b/\partial x -(1/\rho)\nabla(p+b^2/2\mu). \quad (35)$$

Taking the divergence of the equation for $\partial v/\partial t$ we obtain for the present, incompressible case,

$$\nabla^2(p+b^2/2\mu)=0. \quad (36)$$

$p+b^2/2\mu$ has no singularities. Its Laplacian vanishes, and hence it is equal to a constant. The equation for $\partial v/\partial t$ reduces to

$$\partial v/\partial t=(B_0/\mu\rho)(\partial b/\partial x). \quad (37)$$

Eliminating either b or v between (35) and (37) results in the homogeneous wave equation

$$\partial^2 v/(\partial x)^2-(\mu\rho/B_0^2)\partial^2 v/\partial t^2=0, \quad (38)$$

and the same equation for b, satisfied by transverse Alfvén waves.[10]

Let us now consider the problem of general hydromagnetic motions. For low Mach numbers (lo)$\mathbf{v}$ is small and was investigated in the previous section. Thus, we shall omit (lo)$\mathbf{v}$ from our discussion.

(ch)$\mathbf{v}$ must be zero since it satisfies Laplace's equation and vanishes on the boundaries. The divergence of the magnetic field $\mathbf{B}$ is zero, so that (lo)$\mathbf{B}$ vanishes identically. Consider now a large region filled with a homogeneous incompressible inviscid fluid with a large electrical conductivity σ. Across the region, let there be some large-scale irrotational magnetic field $\mathbf{B}=$(ch)$\mathbf{B}$. Such a field will be in equilibrium, exerting no forces on the fluid since the ponderomotive force $(\nabla\times\mathbf{B})\times\mathbf{B}$ vanishes. $\partial\mathbf{B}/\partial t$ is zero wherever $\mathbf{v}$ vanishes; furthermore, (ch)$\mathbf{B}$ satisfies Laplace's equation and hence ∂(ch)$\mathbf{B}/\partial t$ vanishes everywhere. In the vicinity of the center of the region let the fluid be in motion, interacting with $\mathbf{B}$ so that $\partial\mathbf{B}/\partial t\neq 0$ and $\nabla\times\mathbf{B}\neq 0$. We now may set

$$\mathbf{v}=(\mathrm{tr})\mathbf{v},\quad \mathbf{B}=(\mathrm{ch})\mathbf{B}+(\mathrm{tr})\mathbf{B}. \quad (39)$$

Using (39), Eqs. (34) for $\mathbf{v}$ and $\mathbf{B}$ may be written

$$\partial(\mathrm{tr})\mathbf{B}/\partial t=\nabla\times[(\mathrm{tr})\mathbf{v}\times(\mathrm{ch})\mathbf{B}] +\nabla\times[(\mathrm{tr})\mathbf{v}\times(\mathrm{tr})\mathbf{B}], \quad (40)$$

$$\partial(\mathrm{tr})\mathbf{v}/\partial t=-[(\mathrm{tr})\mathbf{v}\cdot\nabla](\mathrm{tr})\mathbf{v}-(1/\rho)\nabla p +(1/\mu\rho)[\nabla\times(\mathrm{tr})\mathbf{B}]\times(\mathrm{ch})\mathbf{B} +(1/\mu\rho)[\nabla\times(\mathrm{tr})\mathbf{B}]\times(\mathrm{tr})\mathbf{B}. \quad (41)$$

We now take the curl of (40) and (41) so as to eliminate p. We define the vectors $\boldsymbol{\omega}$ and $\boldsymbol{\Omega}$ as the curls of the velocity and magnetic field, respectively,[11]

$$\boldsymbol{\omega}=\nabla\times(\mathrm{tr})\mathbf{v},\quad \boldsymbol{\Omega}=\nabla\times(\mathrm{tr})\mathbf{B}. \quad (42)$$

Using standard vector identities we readily obtain

$$\partial\boldsymbol{\Omega}/\partial t=\nabla\times\{[(\mathrm{ch})\mathbf{B}\cdot\nabla](\mathrm{tr})\mathbf{v}-[(\mathrm{tr})\mathbf{v}\cdot\nabla](\mathrm{ch})\mathbf{B}\} +\nabla\times\{\nabla\times[(\mathrm{tr})\mathbf{v}\times(\mathrm{tr})\mathbf{B}]\}, \quad (43)$$

$$\partial\boldsymbol{\omega}/\partial t=(1/\mu\rho)\{[(\mathrm{ch})\mathbf{B}\cdot\nabla]\boldsymbol{\Omega}+(\boldsymbol{\Omega}\cdot\nabla)(\mathrm{ch})\mathbf{B}\} +(1/\mu\rho)\nabla\times[\boldsymbol{\Omega}\times(\mathrm{tr})\mathbf{B}]+\nabla\times[(\mathrm{tr})\mathbf{v}\times\boldsymbol{\omega}]. \quad (44)$$

We have assumed that (ch)$\mathbf{B}$ is a large-scale field. This implies that derivatives of ln(ch)$\mathbf{B}$ are small compared to derivatives of ln(tr)$\mathbf{B}$ and ln(tr)$\mathbf{v}$. Neglecting the derivatives of (ch)$\mathbf{B}$, (43) and (44) reduce to

$$\partial\boldsymbol{\Omega}/\partial t=[(\mathrm{ch})\mathbf{B}\cdot\nabla]\boldsymbol{\omega}+\nabla\times\nabla\times[(\mathrm{tr})\mathbf{v}\times(\mathrm{tr})\mathbf{B}], \quad (45)$$

$$\partial\boldsymbol{\omega}/\partial t=(1/\mu\rho)[(\mathrm{ch})\mathbf{B}\cdot\nabla]\boldsymbol{\Omega}+(1/\mu\rho)\nabla\times[\boldsymbol{\Omega}\times(\mathrm{tr})\mathbf{B}] +\nabla\times[(\mathrm{tr})\mathbf{v}\times\boldsymbol{\omega}]. \quad (46)$$

Differentiating (46) with respect to t and using (45) to eliminate $\partial\boldsymbol{\Omega}/\partial t$, we obtain

$$\partial^2\boldsymbol{\omega}/\partial t^2-(1/\mu\rho)[(\mathrm{ch})\mathbf{B}\cdot\nabla]^2\boldsymbol{\omega} =\mathbf{F}[(\mathrm{ch})\mathbf{B},(\mathrm{tr})\mathbf{B},(\mathrm{tr})\mathbf{v}], \quad (47)$$

where $\mathbf{F}$ represents the sum of a rather large number of terms; the terms are nonlinear in (tr)$\mathbf{B}$ and (tr)$\mathbf{v}$ and are of order zero or one in (ch)$\mathbf{B}$.

Since we are already neglecting derivatives of (ch)$\mathbf{B}$, we may rotate the coordinate axes without further loss

[10] H. Alfvén, *Cosmical Electrodynamics* (Oxford University Press, London, 1950).

[11] It is possible to carry through the development in terms of (tr)$\mathbf{v}$ and (tr)$\mathbf{B}$ instead of their curls. The procedure of first taking the curls is considerably simpler; it was suggested to the author by Dr. A. Schlüter. $\boldsymbol{\omega}$ and $\boldsymbol{\Omega}$ determine (tr)$\mathbf{v}$ and (tr)$\mathbf{B}$. (ch)$\mathbf{B}$ is, of course, independent of $\boldsymbol{\Omega}$.

of generality, so that, at least locally,

$$(\mathrm{ch})\mathbf{B}=\mathbf{e}_z B_0. \tag{48}$$

Then (47) reduces to the inhomogeneous wave equation,

$$\partial^2\omega/\partial t^2-(1/C^2)\partial^2\omega/\partial x^2=\mathbf{F}[B_0,\ (\mathrm{tr})\mathbf{B},\ (\mathrm{tr})\mathbf{v}], \tag{49}$$

where $C=B_0(\mu\rho)^{-\frac{1}{2}}$ is the velocity of propagation. In like manner it can be shown that Ω satisfies an equation of the same form.

Thus, we have shown that hydromagnetic motions in the presence of a strong field B_0 may be represented by a super-position of hydromagnetic or Alfvén waves. The term on the right-hand side represents the interaction (or creation and annihilation) of the component waves through the nonlinear terms of the hydromagnetic equations. The nonlinear terms result in dispersion and scattering, as well as a lack of complete equipartition of energy between $(\mathrm{tr})\mathbf{v}$ and $(\mathrm{tr})\mathbf{B}$.

If $(\mathrm{ch})\mathbf{B}$ is of the same order or is smaller than $(\mathrm{tr})\mathbf{B}$, then $\mathbf{F}$ is of the same order as the individual terms on the left hand side of (49); $\mathbf{F}$ is so complicated that in this case the hydromagnetic wave formulation implied by (49) becomes of formal interest only. But, on the other hand, if $|(\mathrm{ch})\mathbf{B}|\gg|(\mathrm{tr})\mathbf{B}|$, then (49) reduces to a homogeneous wave equation, $\mathbf{F}$ becoming small as compared to the individual terms on the left-hand side. In this case

$$B_0^2/2\mu\gg\rho v^2/2. \tag{50}$$

The energy density of $(\mathrm{tr})\mathbf{B}$ will at least not exceed the order of magnitude of the energy density of $(\mathrm{tr})\mathbf{v}$ and so

$$\rho[(\mathrm{tr})\mathbf{v}]^2,\quad [(\mathrm{tr})\mathbf{B}]^2/\mu\ll B_0^2/\mu. \tag{51}$$

Terms of zero and first order in $(\mathrm{ch})\mathbf{B}$ will be smaller than second-order terms. The terms of which $\mathbf{F}$ is composed, therefore, can presumably be made smaller in order of magnitude than the term $[(\mathrm{ch})\mathbf{B}\cdot\nabla]^2\omega$ in (47), so that in place of (49) we have the homogeneous wave equation

$$\partial^2\omega/\partial x^2-(1/C^2)\partial^2\omega/\partial t^2=0. \tag{52}$$

To justify this presumption, we note that $\mathbf{F}$ may be written

$$\begin{aligned}\mathbf{F}[(\mathrm{ch})\mathbf{B},\ (\mathrm{tr})\mathbf{B},\ (\mathrm{tr})\mathbf{v}]&=(1/\mu\rho)[(\mathrm{ch})\mathbf{B}\cdot\nabla]\\ &\{\nabla\times\nabla\times[(\mathrm{tr})\mathbf{v}\times(\mathrm{tr})\mathbf{B}]\}+(1/\mu\rho)(\partial/\partial t)\nabla\\ &\times[\Omega\times(\mathrm{tr})\mathbf{B}]+(\partial/\partial t)\nabla\times[(\mathrm{tr})\mathbf{v}\times\omega].\end{aligned} \tag{53}$$

Since in the general case (52) implies that a hydromagnetic field may be regarded as a superposition of interacting hydromagnetic waves, we specialize to a single wave, of characteristic frequency ν. From (52) we see that the characteristic length is C/ν. Thus, in order of magnitude we may write

$$|\nabla|\sim\nu/C,\quad |\omega|\sim(\nu/C)|(\mathrm{tr})\mathbf{v}|,$$
$$|\Omega|\sim(\nu/C)|(\mathrm{tr})\mathbf{B}|. \tag{54}$$

(53) then gives the order of magnitude of $\mathbf{F}$ as

$$|\mathbf{F}|\sim\frac{\nu^3}{C}(\mathrm{tr})v\left[\frac{(\mathrm{tr})B}{B_0}\right]\times\left\{1+\frac{(\mu\rho)^{-\frac{1}{2}}(\mathrm{tr})B}{(\mathrm{tr})v}+\frac{(\mathrm{tr})v}{(\mu\rho)^{-\frac{1}{2}}(\mathrm{tr})B}\right\}. \tag{55}$$

The individual terms on the left-hand side of (47) are both of the order of $(\nu^2/C)(\mathrm{tr})v$. Thus $\mathbf{F}$ is smaller by a factor $(\mathrm{tr})B/B_0$, and we have justified (52).

Had we assumed, on the other hand, that there were solutions in which the characteristic length was independent of B_0, we would have arrived at the trivial result that $\omega=0$.

Lüst and Schlüter[12] have demonstrated an interesting type of propagation of hydromagnetic disturbances which is not included in the above development because the fluid which is propagated is not penetrated by the large-scale magnetic field. Imagine a classical vortex ring in a field-free inviscid fluid. Such a ring propagates parallel to its axis and with a velocity of the same order as the fluid velocity. The interior and the exterior of the ring are isolated from each other in that no flow lines connect them. By adding rotation around the axis of the ring and making minor adjustments in the configuration of the velocity within the ring, it is possible to make the velocity $\mathbf{v}$ parallel to its curl. Schlüter then shows that it is possible to introduce a magnetic field $\mathbf{B}$ which is everywhere proportional and parallel to $\mathbf{v}$. And just as the ring is isolated from its surroundings by $\mathbf{v}$, so is the magnetic field within the ring not connected with the surroundings. Further $\nabla\times(\mathbf{v}\times\mathbf{B})$ and $(\nabla\times\mathbf{B})\times\mathbf{B}$ both vanish. Hence the initial condition that $\mathbf{v}$, $\mathbf{B}$, and $\nabla\times\mathbf{B}$ are all parallel is preserved, since $\partial\mathbf{B}/\partial t$ vanishes, and the field exerts no force on the fluid. The result is that the vortex ring propagates according to the hydrodynamic equations in the absence of a magnetic field and carries with it its internal magnetic field. It is very likely, however, that this type of solution of the hydromagnetic equations is of less physical interest in our present context than the wave solutions derived previously.

III. ENERGY TRANSPORT IN THE GALAXY

We have investigated the transport of mechanical energy through a fluid in the weak-field or hydrodynamic limit and in the strong-field or hydromagnetic limit. We shall now attempt to decide which of the several transport processes predominates in the arms of the galaxy.

Consider hydrodynamic transport: There is the bodily transport of energy by $(\mathrm{tr})\mathbf{v}$ and $(\mathrm{ch})\mathbf{v}$, in which the energy is transported with the velocity of the fluid motions. There is the transport of energy by acoustical

[12] R. Lüst and A. Schlüter, Z. Astrophys. 34, 263 (1954).

waves at the velocity of sound: If the Mach number of the fluid motion is small, the acoustical transport velocity is large compared to the fluid velocity, but the acoustical energy density is so small that the net transport is low; if the fluid motion greatly exceeds the velocity of sound, the motion is essentially a system of strong shock waves, and energy is transported at a velocity of the same order as the fluid velocity. Thus, in the hydrodynamic case the transport of significant amounts of energy is essentially bounded by the order of magnitude of the fluid velocity.

The observed[13] irregular gas velocities in the spiral arm of the galaxy are of the order of 5 km/sec, which is essentially an upper limit on the hydrodynamic transport velocity. The motion is, incidently, highly supersonic in many regions because the temperature[14] is of the order of 50 or 100°K except near early type stars. The velocity of sound is, accordingly, of the order of 1–2 km/sec.

Consider next hydromagnetic transport: For the hydromagnetic or strong-field limit we have shown that the equations reduce to a homogeneous wave equation, (52), giving a wave velocity $B_0(\mu\rho)^{-\frac{1}{2}}$ which is also the group velocity, since there is no dispersion of these waves. In the spiral arm of the galaxy in the vicinity of the sun, $B_0 \sim 6\times10^{-6}$ gauss[15] and $\rho\sim2\times10^{-24}$ g/cm^3,[16] corresponding to one hydrogen atom per cm^3. $B_0(\mu\rho)^{-\frac{1}{2}}$ is then about 12 km/sec. We see that $B_0(\mu\rho)^{-\frac{1}{2}}$ exceeds the fluid velocity of 5 km/sec. This demonstrates that the magnetic field in the spiral arm, which is now generally assumed to exist, is a strong field in the sense of (50), justifying the use of (52), and that hydromagnetic transport dominates hydrodynamic transport.

IV. ACCELERATION OF COSMIC RAYS

With the observed magnetic fields in the spiral arms of the galaxy, which are strong in the sense given to this term in (50), the irregular motions may be regarded as hydromagnetic or Alfvén waves with weak mutual interaction. There are, of course, gravitational fields in the spiral arms due to the large-scale variations in the distribution of matter. These fields will complicate the propagation of the hydromagnetic waves and will make possible gravitational waves of various kinds,[17,18] but it does not seem that they can alter the essentials of the problem. Thus, the problem of the acceleration of cosmic rays reduces essentially to a consideration of the interaction of a cosmic-ray particle with a hydromagnetic wave.

Consider, then, the motion of a particle with charge q, rest mass m_p, and velocity $\mathbf{w}$ moving in a region filled with a conducting fluid with velocity $\mathbf{v}(\mathbf{r},t)$. The velocity of the fluid is everywhere assumed to be small compared to the speed of light, c, though, of course, w may be comparable to c. Since we are interested only in the accelerating mechanism, we shall neglect dissipative losses due to the rapid passage of the particle through the fluid. A discussion of the energy losses may be found in the literature.[1]

Elsasser[19] has shown that the electric field associated with the fluid is related to the magnetic field by

$$\mathbf{E}=-(\mathbf{v}\times\mathbf{B})[1+O(1/R_m)]. \tag{56}$$

R_m is the magnetic Reynolds number; $1/R_m$ goes to zero in the limit of infinite electrical conductivity of the fluid. The electric field $\mathbf{E}'$ in the frame of reference moving with the fluid is

$$\mathbf{E}'=(\mathbf{E}+\mathbf{v}\times\mathbf{B})[1+O^2(v/c)]=O(1/R_m) \tag{57}$$

and so may be made vanishingly small. Thus (57) rules out the possibility of accelerations by an induced static electric field.

There remains Fermi's mechanism[2,3] wherein the acceleration is brought about through the cumulative effect of many essentially random fluctuations of small-scale fields, rather than by a continuous acceleration in a large-scale field. From (56) we have the rate at which the field does work on the particle as

$$dW/dt=q\mathbf{w}\cdot\mathbf{E}=-q\mathbf{w}\cdot(\mathbf{v}\times\mathbf{B}). \tag{58}$$

Since the magnetic field $\mathbf{B}_0$ in the spiral arm of the galaxy exceeds the energy density of the fluid motions, the fluid motions satisfy the homogeneous wave equation (52). Under the same assumptions, Eqs. (45) and (46), from which (52) was derived, reduce to

$$\partial(\mathrm{tr})B_i/\partial t=B_0\partial(\mathrm{tr})v_i/\partial x_1,$$
$$\partial(\mathrm{tr})v_i/\partial t=(B_0/\mu\rho)\partial(\mathrm{tr})B_i/\partial x, \tag{59}$$

where $i=(1,2,3)$. From (52) we see that $(\mathrm{tr})\mathbf{v}$ may be written in the form

$$(\mathrm{tr})v_\alpha=f_\alpha(x_1\pm Ct)h_\alpha(x_2,x_3) \quad (\alpha=1,2,3) \tag{60}$$

(without summation convention for α). Putting (60) into (59), we find that

$$(\mathrm{tr})v_\alpha=\pm(C/B_0)(\mathrm{tr})B_\alpha, \quad (\alpha=1,2,3), \tag{61}$$

that is, the fluid velocity and the perturbation field are parallel.

Writing the magnetic field, by (39), as

$$\mathbf{B}=\mathbf{B}_0+(\mathrm{tr})\mathbf{B}, \tag{62}$$

(58) reduces to

$$dW/dt=-q\mathbf{w}\cdot(\mathbf{v}\times\mathbf{B}_0)=-qw_\perp v_\perp B_0, \tag{63}$$

where $\mathbf{v}_\perp$ and $\mathbf{w}_\perp$ represent the components of $\mathbf{v}$ and $\mathbf{w}$ perpendicular to $\mathbf{B}_0$. We see that dW/dt depends on the components of the particle velocity $\mathbf{w}$ and the fluid

[13] A. Blaauw, B. A. N. **11**, 405 (1952).
[14] M. Savedoff and L. Spitzer, Astrophys. J. **111**, 593 (1950).
[15] S. Chandrasekhar and E. Fermi, Astrophys. J. **118**, 113 (1953).
[16] J. H. Oort, Astrophys. J. **116**, 233 (1952).
[17] S. Chandrasekhar and E. Fermi, Astrophys. J. **118**, 116 (1953).
[18] H. L. Helfer, Astrophys. J. **119**, 34 (1954).
[19] W. M. Elsasser, Phys. Rev. **95**, 1 (1954).

velocity $\mathbf{v}$ which are perpendicular to $\mathbf{B}_0$, and does not depend directly on the velocity of propagation of the hydromagnetic waves or on the perturbation field (tr)$\mathbf{B}$.

The time τ over which the acceleration occurs is of the order of the reciprocal of the cyclotron frequency ω, or

$$\tau \sim \omega^{-1} = (m_p/qB_0)(1-w^2/c^2)^{-\frac{1}{2}}, \tag{64}$$

where m_p is the rest or proper mass of the particle. Thus

$$\Delta W \equiv \int dt(dW/dt) \sim (dW/dt)\tau \sim w_\perp v_\perp m_p(1-w^2/c^2)^{-\frac{1}{2}}. \tag{65}$$

If we limit ourselves to extreme relativistic particles so that $w_\perp$ is a sizeable fraction of c, then

$$\Delta W/W \sim v_\perp/c. \tag{66}$$

W represents the total energy of the particle, $m_p c^2(1-w^2/c^2)^{-\frac{1}{2}}$.

Collisions where $\mathbf{w}_\perp$ and $\mathbf{v}_\perp$ have opposite sense initially (head-on collisions) are more probable than where they have the same sense (overtaking collisions) by a factor

$$\kappa = (w_\perp + v_\perp)/(w_\perp - v_\perp) = 1 + 2v_\perp/w_\perp + O^2(v_\perp/w_\perp). \tag{67}$$

Since ΔW is an odd function of the product $w_\perp v_\perp$, it follows that the mean energy gain per interaction is

$$\langle \Delta W \rangle_{\text{av}} = (\kappa - 1)\,|\Delta W| = 2mv_\perp^2, \qquad \langle \Delta W \rangle_{\text{av}}/W = 2(v_\perp/c)^2. \tag{68}$$

We see from this that the same rate of acceleration is obtained whether we regard the galactic magnetic field as containing moving magnetic clouds[2,3] or whether we regard the irregular magnetic fields and fluid motions as hydromagnetic waves propagating along the field. In addition we have been able to show in a general way that it is the fluid velocity $v_\perp$ perpendicular to $\mathbf{B}_0$, rather than the velocity of propagation of the hydromagnetic waves or the fluid velocity parallel to $\mathbf{B}_0$ which is responsible for the acceleration. The perturbation field (tr)$\mathbf{B}$ contributes indirectly, of course, in that it constitutes the magnetic inhomogeneities responsible for the reflection of the particles as they spiral along $\mathbf{B}_0$. Thus, if (tr)$\mathbf{B}/\mathbf{B}_0$ became too small, there would be little or no reflection, and no acceleration of charged particles.

Let us summarize the essentials of the above hydromagnetic treatment of the acceleration of cosmic-ray particles in the arms of the galaxy: We have adopted the model of the galactic magnetic field used by Chandrasekhar and Fermi.[15,17] The field is assumed to be fairly uniform, threading lengthwise through the gas making up the spiral arm of galaxy, like the string in a string of beads. We postulate that irregular motions are generated in the gas clouds in the spiral arms. Oort's mechanism of ejection of gas clouds from near O and B stars may be largely responsible for these motions. The gas motions are propagated from their regions of origin as hydromagnetic waves along the relatively intense magnetic field in the arms. Cosmic-ray particles are accelerated by the magnetic field carried by the fluid velocity of these waves, in a manner equivalent to Fermi's mechanism. The galactic magnetic field serves only as a conduit along which flows, in the form of hydromagnetic waves, the very large quantity of energy required for the particle acceleration. The energy transmitted in this way by the galactic field may be many times the energy of the field itself. Using the estimates of the acceleration energy given by Morrison *et al.* we find that a galactic field of 6×10^{-6} gauss has an energy density corresponding to only about $(3/2)\times10^7$ years of cosmic-ray acceleration. This is to be compared with the period of galactic rotation of 2×10^8 years.

V. PROPAGATION OF HYDROMAGNETIC WAVES

The propagation of hydromagnetic waves in a homogeneous large-scale field has been discussed at length in the literature[20,21] and need not be repeated here in detail.

For hydromagnetic waves in a homogeneous field B_0, the fluid velocity v_i and the magnetic field b_i of the waves are related by

$$v_i = \pm(C/B_0)b_i, \tag{69}$$

where C is the wave velocity $B_0(\mu\rho)^{-\frac{1}{2}}$ in mks units. v_i and b_i satisfy

$$\partial^2(v_i,b_i)/(\partial x_1)^2 - (1/C^2)\partial^2(v_i,b_i)/\partial t^2 = 0, \tag{70}$$

$$\partial(v_i,b_i)/\partial x_i = 0. \tag{71}$$

Without loss of generality we have chosen the large-scale field to be in the $i=1$ direction.

When the large-scale field is not intense compared to the field of the waves, we have motions which are hydrodynamic in character in addition to hydromagnetic waves, (70). But when the large-scale field is intense, the wave solution represents the complete solution of the hydromagnetic equations.

In order to investigate dissipation of hydromagnetic waves due to the fluid viscosity ν and the magnetic viscosity, $\nu_m = 1/\mu\sigma$, where σ is the conductivity, we shall restrict ourselves to plane polarized waves. Let

$$v_i = \delta_{i2}v, \quad b_i = \delta_{i2}b, \tag{72}$$

where δ_{i2} is the Kronecker delta. v and b are assumed to be functions only of x_1. Then, in a homogeneous field the hydromagnetic equations reduce to

$$\frac{\partial b}{\partial t} = B_0\frac{\partial v}{\partial x_1} + \nu_m\frac{\partial^2 b}{(\partial x_1)^2}, \qquad \frac{\partial v}{\partial t} = \frac{B_0}{\mu\rho}\frac{\partial b}{\partial x_1} + \nu\frac{\partial^2 v}{(\partial x_1)^2}. \tag{73}$$

[20] S. Lundquist, Phys. Rev. **76**, 1805 (1949).
[21] S. Lundquist, Arkiv. Fysik. **5**, 297 (1952).

(73) is readily solved if $\nu_m = \nu$ or if either ν_m or ν is negligible. If $\nu_m \ll \nu$, we differentiate the second equation with respect to t and use the first to eliminate $\partial b/\partial t$:

$$\frac{\partial^2 v}{\partial t_2} = C^2 \frac{\partial^2 v}{(\partial x_1)^2} + \nu \frac{\partial^3 v}{(\partial x_1)^2 \partial t}.$$

A similar equation is obtained for b if $\nu \ll \nu_m$. If $\nu_m = \nu$, the symmetrized form[4] of the equations may be used.[21,22]

We assume solutions of the form $\exp i(\omega t + kx)$. If ν and ν_m are small enough that the waves are not seriously damped in distances of the order of one wavelength, then the distance l over which the amplitude will decay by a factor of e is

$$l = \begin{cases} 2C^3/\nu\omega^2 & \text{if } \nu_m \ll \nu \\ C^3/\nu\omega^2 & \text{if } \nu_m = \nu \\ 2C^3/\nu_m\omega^2 & \text{if } \nu_m \gg \nu. \end{cases} \tag{74}$$

An analytical treatment of the propagation of hydromagnetic waves in an inhomogeneous field is complicated and has been deferred to the appendix. It will be sufficient for the present to assume, after Alfvén,[10] that, in a region where the fluid density and the large-scale magnetic field B_0 are slowing varying functions of position, reflection is negligible, and the energy transport of the hydromagnetic waves is parallel to the field. Since the wave is a harmonic motion, the kinetic energy density $\rho v^2/2$ and the magnetic energy density $b^2/2\mu$ are equal. The energy flux per unit area is $\Phi = C\rho v^2$, which might be written

$$\Phi = B_0\mu^{-\frac{1}{2}}\rho^{+\frac{1}{2}}v^2 = B_0\mu^{-\frac{1}{2}}\rho^{-\frac{1}{2}}b^2.$$

If the flow of energy is everywhere parallel to B_0, then Φ is proportional to B_0 and $\rho^{+\frac{1}{2}}v^2$ and $\rho^{-\frac{1}{2}}b^2$ must be independent of position. Then $v \alpha \rho^{-\frac{1}{2}}$ and $b \alpha \rho^{+\frac{1}{2}}$, and both v and b are independent of B_0.

In their discussion of the motions of the interstellar medium necessary to give general acceleration of cosmic ray particles over the galaxy, Morrison, Olbert, and Rossi[1] concluded that velocity fluctuations of 120 km/sec over distances of the order of 1 light year were needed. In terms of our hydromagnetic wave formulation this means velocity amplitudes of the order of 120 km/sec and a wavelength of 2 light yr. The large-scale magnetic field along the spiral arm of the galaxy is of the order of 6×10^{-6} gauss. With one hydrogen atom[23] per cm^3, the velocity of propagation is 12 km/sec. The period of a wave for which $\lambda = 2$ light yr is only 5×10^4 years and the displacement amplitude is of the order of 3 light yr. The dissipation of hydromagnetic waves in the interstellar medium (neglecting compressibility effects) is due primarily to the viscosity of the fluid.[19] In regions of neutral hydrogen the temperature is of the order of 100°K. With one hydrogen atom per cm^3, the mean free path is 10^{15} cm or 70 a.u. The kinematic viscosity is of the order of 0.5×10^{20} cm^2/sec. The decay length for waves for which $\lambda = 2$ light yr is 5×10^9 light yr. In a region of ionized hydrogen, ν is larger by a factor of ten so that the decay length is 5×10^8 light yr.

VI. DYNAMICAL REQUIREMENTS

The observations[24] of the Doppler shift in the absorption lines of the interstellar medium detect velocity fluctuations of the order of 5 km/sec with a scale of 100 parsecs (1 parsec = 3.24 light years). Oort[4] and Spitzer[5] have shown that the radiation from early type stars ($T > 8000$°K) may disrupt[25] the interstellar gas structures sufficiently to produce these velocity fluctuations, as well as to supply the energy for the acceleration of cosmic rays, each requiring about 10^{-27} erg/cm^3/sec.

The interstellar medium, composed largely of neutral hydrogen, at 100°K,[14] strongly absorbs radiation beyond the Lyman limit, becoming ionized as a result. Ionized hydrogen, which under these conditions will have a temperature of the order of 10 000°K, does not strongly absorb ultraviolet radiation. Hence there is usually a sharp division between the region of ionized gas and the cool neutral gas. The ionized region about an early type star is called the *Strömgren sphere.*

Oort and Spitzer point out that in passing by an *O*, *B*, or *A* star, the side of a gas cloud facing the star will be rapidly ionized and heated, the temperature and pressure increasing by a factor of as much as 100. The hot layer expands rapidly, exposing a fresh cool layer underneath. The gas cloud rockets away from the star, achieving velocities up to 30 or 40 km/sec. It is also pointed out that a number of *O*-stars formed simultaneously within a large cloud will explode the cloud, producing fragments with velocities of the order of 30 km/sec.

Estimates indicate that the mechanism is barely adequate, and, indeed, if we assume the rapid acceleration requirements of Morrison *et al.* the mechanism may be too weak to supply the cosmic-ray acceleration energy. The expanding clouds around *O* associations have velocities of the order of 30 km/sec and diameters of the order of 100 parsecs. So far as the author is aware, the expansion mechanism is the only process yet conceived that has possibilities as a significant source of energy for the motions of the interstellar medium. The rotation of the galaxy is a huge reservoir of mechanical energy, and we shall find it convenient to use as a standard of comparison, but there is at present no obvious way in which this energy can be converted to the relatively small-scale motions of the interstellar medium.

The question before us now is whether there is sufficient energy available to maintain the motions of the

[23] W. M. Elsasser, Phys. Rev. **79**, 183 (1950).
[25] J. H. Oort, Astrophys. J. **116**, 233 (1952).
[24] A. Blaauw, B. A. N. **11**, 405 (1952).
[25] F. D. Kahn, B. A. N. **12**, 187 (1954).

interstellar medium, required for the acceleration of cosmic rays throughout the galaxy, and whether there is a process which might transform the relatively large-scale low velocity motions resulting from the mechanism of Oort and Spitzer into the required short-wavelength high-velocity fluctuations.

A. Dissipation by Compressibility

Consider first the dissipation of motions of the order of 120 km/sec with a scale of 1 light yr. The galactic magnetic field is relatively weak (corresponding to 12 km/sec) and the motions are tremendously supersonic. The thermal velocity of the hydrogen atoms composing the interstellar medium is of the order of 1.6 km/sec (100°K). Thus, if such velocity fluctuations exist, they are either purely plane polarized shear waves (plane hydromagnetic waves) or else they are shock waves. To assume the former is admittedly artificial, but, if the latter, then the characteristic time of dissipation is of the order of the time required to travel one or two light yr at 120 km/sec, no more than 5×10^3 years.

Now 120 km/sec and one hydrogen atom per cm^3 is an energy density of 3×10^{-10} erg/cm^3. If the shock wave fluctuations last even 10^4 yr, an energy input of 10^{-21} erg/cm^3 sec is required to maintain them, which is to be compared with the energy available from the disruption of gas clouds by early type stars, and needed to accelerate cosmic rays, both of the order of 10^{-27} erg/cm^3 sec.

To compare this energy consumption with the energy of rotation of the galaxy, we note that the mass of the gas in the spiral arms of the galaxy is comparable to the mass of the stars there. 120 km/sec is about half the velocity of rotation of the spiral arms. Hence 120 km/sec small-scale fluctuations of the interstellar medium would contain at any one time about $\frac{1}{4}$ as much kinetic energy as the rotation of the star and gas system composing the spiral rms of the galaxy. There would be enough energy in the galactic rotation to maintain the fluctuations for only 4×10^4 years! Clearly, then, one cannot expect to maintain such a system of shock waves.

B. Dissipation by Viscosity

Assume that the 120 km/sec velocity fluctuations are plane polarized *shear* waves. Then, in the hydromagnetic equations the nonlinear terms $v_j\partial v_i/\partial x_j$, $v_j\partial b_i/\partial x_j$, etc., vanish identically and we have just the hydromagnetic wave equation, (70). As was shown earlier, the amplitude of hydromagnetic waves with a wavelength of 2 light yr, or $\frac{3}{4}$ psc, will decay by a factor of e after propagating 5×10^3 light yr. With a velocity of propagation of 12 km/sec, this gives a decay time of 4×10^{13} sec (1.3×10^6 yr) and amounts to a dissipation of 0.8×10^{-25} erg/cm^3/sec. The rotational energy of the galaxy would be sufficient to supply the motions for 10^9 years or about five rotations of the galaxy. The dissipation still exceeds by a factor of 100 the energy going into the acceleration of cosmic rays, and available from the mechanism of Oort and Spitzer.

C. Transformation of Velocity and Length

Consider the transformation of large-scale velocity fluctuations in the interstellar medium to violent small-scale waves. The above energy considerations eliminate all possibilities except that the small scale motions be plane polarized hydromagnetic waves (and even this artificial case dissipates energy a hundred times more rapidly than it seems to be available). The hydromagnetic waves satisfy a linear wave equation, so that there are no nonlinear effects to which we might appeal to break up large-scale motions into fluctuations of smaller scale, as for instance in turbulence. We have only the variation of the velocity amplitude as $\rho^{-\frac{1}{2}}$ and the wavelength as $B_0\rho^{-\frac{1}{2}}$, discussed in the previous section. But decreasing ρ to increase the velocity increases rather than decreases the wavelengths; B_0 would have to decrease by a factor of 800 to reduce the wavelength from 30 psc to 2 light yr while increasing the velocity amplitude from 30 km/sec to 120 km/sec.

D. Galactic Acceleration of Cosmic Rays

We conclude that even under almost ideal conditions there is not sufficient energy available to maintain the velocity fluctuations in the interstellar medium necessary (as determined by Morrison *et al.*[6]) for the acceleration of cosmic rays throughout the galaxy; the galaxy, because of its high internal viscosity, is less than one percent efficient in accelerating cosmic rays. Nor does there exist a general hydromagnetic mechanism capable of reducing the scale and increasing the velocity of the motions to the required 1 light yr and 120 km/sec. It would seem, then, that we have difficulty with the assumption that cosmic rays are accelerated throughout the galaxy by collisions with randomly moving magnetic fields.

Consider, then, a later proposal by Fermi[3] that the cosmic rays are accelerated in magnetic "traps." Two hydromagnetic waves of sufficiently large amplitude as to reflect all particles are assumed to be approaching each other along the magnetic field in the spiral arm. The particles caught between them will be accelerated at a very high rate because they experience only head-on collisions. Equation (66) gives the energy gain per collision as

$$\Delta W/W \approx v_\perp/c$$

for relativistic particles. $v_\perp$ represents the component of the fluid velocity perpendicular to the galactic magnetic field. Thus, because all the collisions are head-on, $\Delta W/W$ is larger by a factor of $v_\perp/c$ than when the acceleration is by collision with randomly moving clouds. If we assume fluid velocities in the interstellar medium of 10 km/sec, then $\Delta W/W$ is of the order of

10^{-4}. The calculations of Morrison *et al.*[1] would then require that the diffusion length be 12 light yr. Though 12 light yr is still a little small and 10 km/sec may be just a little large to agree with observations,[24] they are certainly close enough as to no longer be entirely out of the question. The energy dissipation, which is proportional to v^2/λ^2, is smaller by a factor 10^4 than before; the magnetic trap operates at an efficiency of better than 50 percent, so far as losses to viscosity are concerned, and the mechanism of Oort and Spitzer may be adequate as a source of energy.

The remaining difficulties must not be minimized, however. Fermi's magnetic trap accelerates particles until their motion parallel to the magnetic field allows them to penetrate one or the other of the inhomogeneities forming the jaws of the trap. Further acceleration depends on the motion parallel to the field being deflected by sharp magnetic inhomogeneities—hydromagnetic shock waves[26,27]—into a direction perpendicular to the field, whereupon the particle may again be caught in a trap and accelerated. The dearth of observations of hydromagnetic shock waves prevents further comment on this particular aspect of the problem. Unfortunately it is not at all clear that traps in which the jaws are opening rather than closing will not reduce the average of $\Delta W/W$ to v^2/c^2, just as for acceleration by collisions of the cosmic ray particles with randomly moving hydromagnetic waves. If $\Delta W/W \approx v^2/c^2$ or less, we are back to the difficulties discussed above.

The difficulties with the acceleration of cosmic rays throughout the galaxy leave open several possibilities. On the one hand, there may be galactic acceleration mechanisms which are more efficient than Fermi's. On the other hand, with the present meager knowledge of stellar magnetic fields, cosmic rays may be of more local origin than the galaxy, originating either in the vicinity of the solar system or in some anomalous region in the galaxy. It is interesting to note that the result of Singer's calculations[28,29] on the proportion of He^3 and He^4 found in certain meteorites is not inconsistent with the assumption that the cosmic-ray intensity has been much lower over the last 7×10^7 yr than it is today.

APPENDIX

Hydromagnetic Equations in an Inhomogeneous Field

Thus far we have not treated quantitatively the effects of the variations of the large-scale field; we will now consider analytically the effect of slow spatial variation of the large-scale field and of the density of the conducting fluid. Introducing these variations as small perturbations on the homogeneous case, the asymptotic form of the complete solution of the hydromagnetic equations (in the limit as we go to intense large-scale fields) may still be represented as hydromagnetic waves, though the amplitude and form of the waves may vary during propagation, and the magnetic and velocity fields of the waves will no longer be exactly parallel, as they are in the homogeneous field case.

1. Coordinates

Consider a large-scale magnetic field B_i which varies slowly with the orthogonal position coordinates x^j. Let the field be in the $i=1$ direction and have symmetry about the $x^2=0$ plane and about the $x^3=0$ plane. The x^1-axis will lie along a line of force. We fix our attention on the region within a distance a of the x^1-axis. Finally we assume that within the region of radius a the field intensity does not vary in the direction normal to the field. Choosing the coordinate x^1 to lie everywhere along the field, the coordinates x^2 and x^3 are everywhere perpendicular to the field, and to each other.

Using the above coordinate system it follows that

$$B^i(x^j)=\delta^{i1}B(x^1), \tag{1}$$

where δ^{ij} is the Kronecker delta. The lines of force become the coordinate lines $x^2=$ constant, $x^3=$ constant.

Since the coordinates x^i are orthogonal, g_{ij} is a diagonal tensor and its determinant g is just the product of the diagonal terms. Further $g^{11}=1/g_{11}$, etc. $\sqrt{g_{22}}$ and $\sqrt{g_{33}}$ become a direct measure of the separation of the lines of force in the x^2 and x^3 directions respectively. Since the spacing of the lines of force is independent of x^2 and x^3, it follows that g_{22} and g_{33} are both independent of x^2 and x^3, varying only with x^1.

The divergence of B^i is identically zero. Thus

$$B_{;i}{}^i=0, \tag{2}$$

where the semicolon represents covariant differentiation, defined by

$$B_{;j}{}^i=\partial B^i/\partial x^j+\Gamma_{kj}{}^iB^k. \tag{3}$$

$\Gamma_{jk}{}^i$ is a Christoffel symbol of the second kind defined as

$$\Gamma_{jk}{}^i=\Gamma_{kj}{}^i=\tfrac{1}{2}g^{ir}(\partial g_{rj}/\partial x^k+\partial g_{kr}/\partial x^j-\partial g_{jk}/\partial x^r). \tag{4}$$

Using (3), together with the identity

$$\Gamma_{ji}{}^i=\tfrac{1}{2}(1/g)(\partial g/\partial x^j), \tag{5}$$

(2) becomes

$$\partial B/\partial x^1+(B/2g)(\partial g/\partial x^1)=0. \tag{6}$$

Integrating, we obtain the familiar result,

$$B(x^j)\sqrt{g(x^k)}=B(0)\sqrt{g(0)}. \tag{7}$$

Or, in other words, the tensor density constructed from $B^i(x^j)$ is independent of position.

(7) may be written as

$$B(x^j)\sqrt{g_{11}(x^k)}=B_0\sqrt{g(0)}[g_{22}(x^1)g_{33}(x^1)]^{-\frac{1}{2}}. \tag{8}$$

[26] F. deHoffmann and E. Teller, Phys. Rev. **80**, 692 (1952).
[27] H. L. Helfer, Astrophys. J. **117**, 177 (1953).
[28] S. F. Singer, Phys. Rev. **90**, 168 (1953).
[29] S. F. Singer, Astrophys. J. **119**, 291 (1954).

The right-hand side is a function only of x^1. The left-hand side represents the physical component of the magnetic field, i.e., $(g_{ij}B^iB^j)^{\frac{1}{2}}$, which we assumed to be independent of x^2 and x^3. Thus our coordinates are consistent with (2).

Consider g_{11}. For convenience we put $g_{11}=1$ on the x^1-axis so that x^1 is a direct measure of distance along the axis. In general $g_{11}\neq 1$ off the x^1-axis since the surfaces $x^1=$constant are not planes where the large-scale field is varying with x^1. Thus, the two surfaces $x^1=b$ and $x^1=b+\epsilon$ will have a separation ϵ at the x^1-axis; away from the axis the separation will be less than ϵ if the field is curving away from the axis and greater than ϵ if the field is bending toward the axis. The separation of the two surfaces is given at all points by $\epsilon\sqrt{g_{11}}$.

Confining our attention to the $x^3=0$ plane for the moment, we let $s(d)$ represent the distance, measure along a surface $x^1=$constant, from the x^1-axis to $x^2=d$, $x^3=0$. Then the angle between the surfaces $x^1=b$ and $x^1=b+\epsilon$ at $x^2=d$, $x^3=0$ is $-\epsilon\partial^2 s/(\partial x^1)^2+O^2(d)$. The surfaces are parallel at the x^1-axis and are portions of spheres to the order considered. Thus, their separation at $x^2=d$, $x^3=0$ has increased from the ϵ at the x^1-axis to $\epsilon-(s/2)\epsilon\partial^2 s/(\partial x^1)^2$. Hence

$$\sqrt{g_{11}}=1-(s/2)\partial^2 s/(\partial x^1)^2+O^4(d), \tag{9}$$

and

$$g_{11}=1-s\partial^2 s/(\partial x^1)^2+O^4(d), \tag{10}$$

where $s=x^2\sqrt{g_{22}}$. More generally we write

$$s^2=(x^2)^2g_{22}+(x^3)^2g_{33},$$

and drop the restriction of (10) to the $x^3=0$ plane.

It is readily shown with g_{11} given by (10) that up to and including terms $O^2(x^2,x^3)$ all components of the Riemann curvature tensor vanish. Thus to $O^2(x^2,x^3)$ our space is Euclidean, covariant differentiation is commutative, and we are taking into account the longer transit along lines of force off the x^1-axis due to their curvature and slope.

Finally, in our discussion of coordinates, let us compute the Christoffel symbols associated with the g_{ij} we have constructed. We introduce the conventions that we do not sum over repeated Greek indices and that the indices α,β,γ are not equal. From the fact that g_{ij} is a diagonal tensor we find that

$$\Gamma_{\beta\gamma}{}^{\alpha}=0,\ \Gamma_{\beta\alpha}{}^{\alpha}=\tfrac{1}{2}g_{\alpha\alpha}{}^{-1}\partial g_{\alpha\alpha}/\partial x^{\beta},$$
$$\Gamma_{\beta\beta}{}^{\alpha}=-\tfrac{1}{2}g_{\alpha\alpha}{}^{-1}\partial g_{\beta\beta}/\partial x^{\alpha},\ \Gamma_{\alpha\alpha}{}^{\alpha}=\tfrac{1}{2}g_{\alpha\alpha}{}^{-1}\partial g_{\alpha\alpha}/\partial x^{\alpha}. \tag{11}$$

From the fact that g_{22} and g_{33} depend only on x^1, we have

$$\Gamma_{22}{}^{2}=\Gamma_{32}{}^{2}=\Gamma_{22}{}^{3}=\Gamma_{23}{}^{3}=\Gamma_{32}{}^{3}=\Gamma_{33}{}^{3}=0.$$

Thus, the only nonvanishing components of $\Gamma_{jk}{}^{i}$ are those for which at least two of the indices i,j,k are equal and at least one equals unity.

It is readily shown that the only nonvanishing components of $B_{;j}{}^{i}$ are $B_{;1}{}^{\alpha}$ and $B_{;\alpha}{}^{\alpha}$:

$$B_{;1}{}^{1}=+(1/\sqrt{g_{11}})\partial(B\sqrt{g_{11}})/\partial x^1,$$
$$B_{;1}{}^{2}=-(B/2g_{22})\partial g_{11}/\partial x^2,$$
$$B_{;1}{}^{3}=-(B/2g_{33})\partial g_{11}/\partial x^3,$$
$$B_{;2}{}^{2}=+(B/2g_{22})\partial g_{22}/\partial x^1,$$
$$B_{;3}{}^{3}=+(B/2g_{33})\partial g_{33}/\partial x^1.$$

For our calculations we need derivatives of the velocity and magnetic field of the wave only with respect to x^1, i.e., $v_{;1}{}^{i}$ and $b_{;1}{}^{i}$. Thus

$$v_{;1}{}^{1}=\frac{\partial v^1}{\partial x^1}+v^i\frac{1}{2g_{11}}\frac{\partial g_{11}}{\partial x^i},\qquad v_{;1}{}^{2}=\frac{\partial v^2}{\partial x^1}-\frac{v^1}{2g_{22}}\frac{\partial g_{11}}{\partial x^2}+\frac{v^2}{2g_{22}}\frac{\partial g_{22}}{\partial x^1},$$
$$v_{;1}{}^{3}=\frac{\partial v^3}{\partial x^1}-\frac{v^1}{2g_{33}}\frac{\partial g_{11}}{\partial x^3}+\frac{v^3}{2g_{33}}\frac{\partial g_{33}}{\partial x^1},$$

with similar expressions for $b_{;1}{}^{i}$.

1. Hydromagnetic Equations

If the vector $\mathbf{B}$ represents the complete magnetic field, (wave plus large-scale components), then in mks units the hydromagnetic equations in the absence of dissipation may be written

$$\partial\mathbf{B}/\partial t=-(\mathbf{v}\cdot\nabla)\mathbf{B}+(\mathbf{B}\cdot\nabla)\mathbf{v}-\mathbf{B}\nabla\cdot\mathbf{v}, \tag{12}$$

$$\partial\mathbf{v}/\partial t=-(1/\rho)\nabla(p+B^2/2\mu)+(1/\mu\rho)(\mathbf{B}\cdot\nabla)\mathbf{B}-(\mathbf{v}\cdot\nabla)\mathbf{v} \tag{13}$$

in vector notation. $\mathbf{v}$ represents the fluid velocity. If $\mathbf{v}$ is less than the speed of sound, then $\partial\rho/\partial t\cong 0$ and

$$\nabla\cdot(\rho\mathbf{v})\cong 0. \tag{14}$$

If ρ varies slowly with position, then $\nabla\cdot\mathbf{v}$ is small and we put

$$\nabla(p+B^2/2\mu)=0.$$

If we represent the wave fields by v^i and b^i, then the contravariant components of $\mathbf{B}$ become B^i+b^i, where B^i is the large-scale field discussed above. In the limit as $g_{ij}B^iB^j$ goes to infinity, (12) and (13) reduce asymptotically to

$$\partial b^i/\partial t=-v^jB_{;j}{}^{i}+B^jv_{;j}{}^{i}+B^iv^j\rho_{,j}/\rho+O(b^a/B), \tag{15}$$

$$\partial v^i/\partial t=(1/\mu\rho)(b^jB_{;j}{}^{i}+B^jb_{;j}{}^{i})+O(b^a/B), \tag{16}$$

using (14) to eliminate $v_{;i}{}^{i}$ from (15).

Differentiating (16) with respect to t and using (15) to eliminate $\partial b^i/\partial t$, we obtain a tensor equation in v^i alone. However, it turns out to involve less algebra if we write out separately each component of (15) and

(16) before carrying out the elimination. We obtain

$$\frac{\partial b^1}{\partial t}=B\frac{\partial v^1}{\partial x^1}-v^1\frac{\partial B}{\partial x^1}+v^1B\frac{1}{\rho}\frac{\partial \rho}{\partial x^1}+\frac{Bv^2}{2g_{11}}\frac{\partial g_{11}}{\partial x^2}+\frac{Bv^3}{2g_{11}}\frac{\partial g_{11}}{\partial x^3},$$
$$\frac{\partial b^2}{\partial t}=B\frac{\partial v^2}{\partial x^1},\quad \frac{\partial b^3}{\partial t}=B\frac{\partial v^3}{\partial x^1}, \tag{17}$$

and

$$\frac{\partial v^1}{\partial t}=\frac{1}{\mu\rho}\left[\frac{\partial}{\partial x^1}(Bb^1)+\frac{Bb^1}{g_{11}}\frac{\partial g_{11}}{\partial x^1}+\frac{Bb^2}{2g_{11}}\frac{\partial g_{11}}{\partial x^2}+\frac{Bb^3}{2g_{11}}\frac{\partial g_{11}}{\partial x^3}\right],$$
$$\frac{\partial v^2}{\partial t}=\frac{B}{\mu\rho}\left[\frac{\partial b^2}{\partial x^1}-\frac{b^1}{g_{22}}\frac{\partial g_{11}}{\partial x^2}+\frac{b^2}{g_{22}}\frac{\partial g_{22}}{\partial x^1}\right], \tag{18}$$
$$\frac{\partial v^3}{\partial t}=\frac{B}{\mu\rho}\left[\frac{\partial b^3}{\partial x^1}-\frac{b^1}{g_{33}}\frac{\partial g_{11}}{\partial x^3}+\frac{b^3}{g_{33}}\frac{\partial g_{33}}{\partial x^1}\right].$$

We see that the equations for the $i=2$ and the $i=3$ components are of exactly the same form; we shall henceforth omit the equation for the $i=3$ components since it can be obtained directly from the $i=2$ equations by replacing the indices 2 by 3.

Differentiating (18) with respect to t and using (17) to eliminate the $\partial b^i/\partial t$, we obtain

$$\frac{\partial^2 v^1}{\partial t^2}=C^2\left\{\frac{\partial^2 v^1}{(\partial x^1)^2}+\frac{\partial v^1}{\partial x^1}\left(\frac{1}{B}\frac{\partial B}{\partial x^1}+\frac{1}{g_{11}}\frac{\partial g_{11}}{\partial x^1}+\frac{1}{\rho}\frac{\partial \rho}{\partial x^1}\right)\right.$$
$$+\frac{\partial v^2}{\partial x^1}\left(\frac{1}{g_{11}}\frac{\partial g_{11}}{\partial x^2}\right)+\frac{\partial v^3}{\partial x^1}\left(\frac{1}{g_{11}}\frac{\partial g_{11}}{\partial x^3}\right)$$
$$-v^1\left[\left(\frac{1}{B}\frac{\partial B}{\partial x^1}\right)^2+\frac{1}{B}\frac{\partial^2 B}{(\partial x^1)^2}-\frac{2}{B}\frac{\partial B}{\partial x^1}\frac{1}{\rho}\frac{\partial \rho}{\partial x^1}\right.$$
$$\left.-\frac{1}{\rho}\frac{\partial^2 \rho}{(\partial x^1)^2}+\left(\frac{1}{\rho}\frac{\partial \rho}{\partial x^1}\right)^2+\frac{1}{B}\frac{\partial B}{\partial x^1}\frac{1}{g_{11}}\frac{\partial g_{11}}{\partial x^1}\right]$$
$$+v^2\left[\frac{1}{B}\frac{\partial B}{\partial x^1}\frac{1}{g_{11}}\frac{\partial g_{11}}{\partial x^2}+\frac{1}{2g_{11}}\frac{\partial^2 g_{11}}{\partial x^1\partial x^2}\right]$$
$$\left.+v^3\left[\frac{1}{B}\frac{\partial B}{\partial x^1}\frac{1}{g_{11}}\frac{\partial g_{11}}{\partial x^3}+\frac{1}{2g_{11}}\frac{\partial^2 g_{11}}{\partial x^1\partial x^3}\right]\right\}, \tag{19}$$

$$\frac{\partial^2 v^2}{\partial t^2}=C^2\left\{\frac{\partial^2 v^2}{(\partial x^1)^2}-\frac{\partial v^1}{\partial x^1}\frac{1}{g_{22}}\frac{\partial g_{11}}{\partial x^2}+\frac{\partial v^2}{\partial x^1}\left(\frac{1}{B}\frac{\partial B}{\partial x^1}+\frac{1}{g_{22}}\frac{\partial g_{22}}{\partial x^1}\right)\right.$$
$$+v^1\left(\frac{1}{B}\frac{\partial B}{\partial x^1}\frac{1}{g_{22}}\frac{\partial g_{11}}{\partial x^2}\right)-v^2\left(\frac{1}{2g_{11}g_{22}}\frac{\partial g_{11}}{\partial x^2}\frac{\partial g_{11}}{\partial x^2}\right)$$
$$\left.-v^3\left(\frac{1}{2g_{11}g_{22}}\frac{\partial g_{11}}{\partial x^2}\frac{\partial g_{11}}{\partial x^3}\right)\right\}. \tag{20}$$

3. *Solution of the Hydromagnetic Equations*

The solution of (19) and (20) may be constructed from a linear superposition of terms of the form

$$v^i(x^j,t)=\psi^i(x^j)\exp(i\omega t). \tag{21}$$

Then

$$\frac{\partial^2\psi^1}{(\partial x^1)^2}+\frac{\partial\psi^1}{\partial x^1}\left(\frac{1}{h(1)}\frac{\partial h(1)}{\partial x^1}+\frac{1}{\rho}\frac{\partial \rho}{\partial x^1}\right)+\frac{\partial\psi^2}{\partial x^1}\left(\frac{1}{g_{11}}\frac{\partial g_{11}}{\partial x^2}\right)$$
$$+\frac{\partial\psi^3}{\partial x^1}\left(\frac{1}{g_{11}}\frac{\partial g_{11}}{\partial x^3}\right)+\psi^1\left[\frac{\omega^2}{C^2}-\left(\frac{1}{B}\frac{\partial B}{\partial x^1}\right)^2-\frac{1}{B}\frac{\partial^2 B}{(\partial x^1)^2}\right.$$
$$+\frac{2}{B}\frac{\partial B}{\partial x^1}\frac{1}{\rho}\frac{\partial \rho}{\partial x^1}+\frac{1}{\rho}\frac{\partial^2 \rho}{(\partial x^1)^2}-\left(\frac{1}{\rho}\frac{\partial \rho}{\partial x^1}\right)^2-\frac{1}{B}\frac{\partial B}{\partial x^1}\frac{1}{g_{11}}\frac{\partial g_{11}}{\partial x^1}\Big]$$
$$+\psi^2\left[\frac{1}{B}\frac{\partial B}{\partial x^1}\frac{1}{g_{11}}\frac{\partial g_{11}}{\partial x^2}+\frac{1}{2g_{11}}\frac{\partial^2 g_{11}}{\partial x^2\partial x^3}\right]$$
$$+\psi^3\left[\frac{1}{B}\frac{\partial B}{\partial x^1}\frac{1}{g_{11}}\frac{\partial g_{11}}{\partial x^3}+\frac{1}{2g_{11}}\frac{\partial^2 g_{11}}{\partial x^1\partial x^3}\right]=0, \tag{22}$$

$$\frac{\partial^2\psi^2}{(\partial x^1)^2}-\frac{\partial\psi^1}{\partial x^1}\left(\frac{1}{g_{22}}\frac{\partial g_{11}}{\partial x^2}\right)+\frac{\partial\psi^2}{\partial x^1}\left(\frac{1}{h(2)}\frac{\partial h(2)}{\partial x^1}\right)$$
$$+\psi^1\left[\frac{1}{B}\frac{\partial B}{\partial x^1}\frac{1}{g_{22}}\frac{\partial g_{11}}{\partial x^2}\right]+\psi^2\left[\frac{\omega^2}{C^2}-\frac{1}{2g_{11}g_{22}}\left(\frac{\partial g_{11}}{\partial x^2}\right)^2\right]$$
$$-\psi^3\frac{1}{2g_{11}g_{22}}\frac{\partial g_{11}}{\partial x^2}\frac{\partial g_{11}}{\partial x^3}=0, \tag{23}$$

where

$$h(1)=g_{11}B=B_0\sqrt{g_0(g_{11}/g_{22}g_{33})^{\frac{1}{2}}},$$
$$h(2)=g_{22}B=B_0\sqrt{g_0(g_{22}/g_{33}g_{11})^{\frac{1}{2}}}, \tag{24}$$

etc. $h(2)$ and $h(3)$ represent the eccentricity of the cross section of any given tube of flux in the large-scale field.

We shall restrict ourselves to hydromagnetic waves of sufficiently high frequency that the wavelength, λ, is small compared to the characteristic scale of variation, L, of the large-scale magnetic field, $\lambda/L\ll 1$. Then $\partial\psi^i/\partial x^1\sim\psi^i O(1/\lambda)$, $\partial^2\psi^i/(\partial x^1)^2\sim\psi^i O(1/\lambda^2)$;

$$(1/B)(\partial B/\partial x^1)\sim O(1/L),\ (1/B)[\partial^2 B/(\partial x^1)^2]\sim O(1/L^2); \tag{25}$$
$$g_{11}\sim 1+O(s^2/L^2),\ \partial g_{11}/\partial x^1\sim O(s^2/L^3),$$
$$\partial g_{11}/\partial x^2\sim O(s/L^2).$$

s represents distance from the x^1-axis. If we use the expression for g_{11} given in (10), we will be neglecting terms in (22) and (23) of the order of (ψ^i/λ^2) times $(\lambda/L)(s/L)^2$.

(22) and (23) must be solved simultaneously with (14), which may be written as

$$(\rho\psi^i)_{,i}=0, \quad \text{or} \quad \frac{\partial}{\partial x^i}(\rho\sqrt{g}\psi^i)=0. \tag{26}$$

To effect a solution we note that (22) and (23) may both be written as

$$\frac{\partial^2\psi^\alpha}{(\partial x^1)^2}+\frac{\partial\psi^\alpha}{\partial x^1}\left[\frac{1}{h(\alpha)}\frac{\partial h(\alpha)}{\partial x^1}+\frac{\delta^{1\alpha}}{\rho}\frac{\partial\rho}{\partial x^1}\right]+\psi^\alpha\frac{\omega^2}{C^2}=\frac{\psi^i}{\lambda^2}O^2\left(\frac{\lambda}{L}\right), \tag{27}$$

and (26) as

$$\frac{\partial}{\partial x^i}(\rho\psi^i)+\rho\psi^1\left[\frac{1}{\sqrt{g_{22}}}\frac{\partial\sqrt{g_{22}}}{\partial x^1}+\frac{1}{\sqrt{g_{33}}}\frac{\partial\sqrt{g_{33}}}{\partial x^1}\right]=\frac{\rho\psi^i}{\lambda}O^2\left(\frac{\lambda}{L}\right). \tag{28}$$

Suppose now that when $t=0$, ψ^1 and ψ^3 vanish, so that we have a plane polarized wave. ψ^1 and ψ^2 will not remain zero at all subsequent times, but the terms generating them from ψ^2 are of second order in λ/L or smaller. Thus there will be a period of time of the order of L/C following $t=0$ when ψ^1 and ψ^3 are small compared to ψ^2. During this time (27) and (28) reduce to

$$\frac{\partial^2\psi^2}{(\partial x^1)^2}+\frac{\partial\psi^2}{\partial x^1}\frac{1}{h(2)}\frac{\partial h(2)}{\partial x^1}+\psi^2\frac{\omega^2}{C^2}=\frac{\psi^2}{\lambda^2}O^2\left(\frac{\lambda}{L}\right), \tag{29}$$

$$\frac{\partial\psi^2}{\partial(x^2)}=\frac{\psi^2}{\lambda}O^2\left(\frac{\lambda}{L}\right). \tag{30}$$

Applying the WKB approximation to (29) we write

$$\psi^2=\exp\sum_{n=0}^{\infty}R_n \tag{31}$$

where the subscript denotes the order in λ/L. (30) implies that

$$\frac{\partial R_n}{\partial(x^2)}=\frac{R_n}{\lambda}O^2\left(\frac{\lambda}{L}\right), \tag{32}$$

since ρ does not vary in the x^2-direction. Using primes to denote differentiation with respect to x^1, (29) becomes

$$\sum R_n''+(\sum R_n')^2+(\sum R_n')h'(2)/h(2)+\omega^2/C^2=O^2(\lambda/L).$$

Equating to zero terms of the same order in λ/L we obtain

$$(R_0')^2+\omega^2/C^2=0,$$

$$R_0''+2R_0'R_1'+R_0'h'(2)/h(2)=0.$$

Thus

$$R_0'=\pm i\omega/C, \quad R_0=\pm i\omega\int dx^1/C; \tag{33}$$

$$2R_1=-\ln R_0'-\ln h(2). \tag{34}$$

(31) gives

$$(\sqrt{g_{22}}v^2)=A(\rho_0/\rho)^{\frac{1}{4}}\exp\left[i\omega\left(t\pm\int dx^1/C\right)\right], \tag{35}$$

where A is a constant and ρ_0 is the density at $x=0$. From (17) we obtain

$$(\sqrt{g_{22}}b^2)=\pm A(\mu\rho_0)^{\frac{1}{4}}(\rho/\rho_0)^{\frac{1}{4}}\times\exp\left[i\omega\left(t\pm\int dx^1/C\right)+i\delta\right], \tag{36}$$

where δ represents the difference in phase between the velocity and magnetic field of the wave;

$$\delta=\frac{C}{\omega}\left(\frac{1}{\sqrt{g_{22}}}\frac{\partial\sqrt{g_{22}}}{\partial x^1}+\frac{1}{4}\frac{1}{\rho}\frac{\partial\rho}{\partial x^1}\right).$$

$\sqrt{g_{22}}v^2$ and $\sqrt{g_{22}}b^2$ represent the physical components of the velocity and magnetic field of the waves. We note that the amplitudes are independent of B and are proportional to $\rho^{\pm\frac{1}{4}}$ respectively. This result was first obtained by Alfvén by assuming that the energy transport of the waves is always parallel to the magnetic field. Our calculations have justified Alfvén's assumption under rather general conditions. A still more general solution of (22) and (23) is difficult, but the fact that the geometry of a single pulse will change as B varies, implies that $|\sqrt{g_{22}}v^2|/|\sqrt{g_{33}}v^3|$ is not independent of x^1, and so the components cannot individually be proportional only to $\rho^{-\frac{1}{4}}$. One expects to find defocussing, and possibly focussing, effects upon solving the equations to a higher approximation.

Photoproduction of Mesons in Deuterium

JOHN CHAPPELEAR*
Department of Physics, Indiana University, Bloomington, Indiana
(Received March 23, 1955)

The corrections from multiple scattering of the photoproduced meson to the usual impulse approximation to the elastic photoproduction cross section for neutral mesons in deuterium have been computed. The result obtained for gamma-ray energies of 285 Mev and 345 Mev is a depression of the cross section of about a factor of two at all angles and at both energies. This is in qualitative accord with experiment.

1. INTRODUCTION

THE theory of neutral photomeson production in deuterium has been considered by many authors.[1-4] These treatments were phenomenological and based on the impulse approximation; they therefore neglected the possibility of a final state interaction of the photoproduced meson with the deuteron. Since the meson-nucleon interaction is quite strong, it is expected that the cross section will be considerably modified. This interaction can be described as the consequence of multiple scattering, and has been treated in connection with scattering of mesons in deuterium.[5] In this paper we shall extend previous calculations to include the corrections to the impulse approximation which arise from this effect.

The method to be described retains the phenomenological features of the previous calculations by the following assumptions; first, a transition operator is used which yields a $(2+3\sin^2\theta)$ distribution for π^0 production from hydrogen. The physical basis for choosing this transition operator is the assumption that π^0 production takes place in the state with $I=\frac{3}{2}$ and $J=\frac{3}{2}$;[6] the distribution predicted seems to be in accord with experiment.[7] Following this model it is assumed that the scattering also has a resonance in this state. The parameters of the theory then may be determined by comparison with the measured transition amplitudes for photoproduction and scattering in hydrogen. Second, off-the-energy-shell scattering has been neglected. It will be seen that the nature of this approximation is such as to lead us not to expect agreement of more than qualitative nature between the theoretical and experimental results. There are several reasons for this neglect. First, there is some reason to believe that the range of the corrections due to multiple virtual scattering is less than that due to multiple real scattering, and therefore that most of the correction comes from the latter. Second, the present state of meson theory does not allow reliable predictions of the behavior of the scattering amplitudes off the energy shell. Since our treatment is phenomenological, it seems best to omit this type of calculation. Third, the difficulties of solving the multiple scattering problem including virtual mesons are very considerable, since numerical solution of coupled integral equations is required.

The procedure for the calculation is quite straightforward. A formal solution to the Schrödinger equation for the problem is constructed following the method of Chew and Goldberger[8] and of Watson[9] and making use of approximations similar to the impulse approximation to simplify the results. Finally the formal solution is evaluated in terms of the known expressions for the operators which are involved. The elastic differential cross section is computed for photoproduction of π^0 mesons. From these results it is also easy to obtain the usual impulse approximation to the cross section, so that the effects of the multiple scattering can readily be seen. The graphs and numerical results are discussed in Sec. III.

2. FORMAL METHODS

Notation: Let the two nucleons be numbered 1 and 2.

$h_{1,2}$ = interaction terms in the Hamiltonian between the meson field and the nucleon field.

$H_{1,2}$ = interaction terms in the Hamiltonian between the meson and nucleon fields and the radiation field.

$h=h_1+h_2$.

$H=H_1+H_2$.

$\mathcal{H}_0$ = the sum of the free-field Hamiltonians.

$\mathcal{H}'=h+H$.

$\mathcal{H}$ = the total Hamiltonian $=\mathcal{H}_0+\mathcal{H}'$.

ψ = the solution to the Schrödinger equation for the problem.

ϕ = the initial state (a deuteron plus a gamma ray).

$\frac{1}{a}=\frac{1}{E-\mathcal{H}_0+i\epsilon}$, the Green's function for the problem.

$T=\mathcal{H}'+\mathcal{H}'\frac{1}{a-\mathcal{H}'}\mathcal{H}'$, the transition operator for the problem.

* Now with Shell Development Company, Exploration and Production Research Division, Houston, Texas.

[1] N. C. Francis, Phys. Rev. **89**, 766 (1953).
[2] M. Lax and W. Feshbach, Phys. Rev. **88**, 509 (1952).
[3] G. F. Chew and H. Lewis, Phys. Rev. **84**, 779 (1951).
[4] Saito, Wantanabe, and Yamaguchi, Progr. Theoret. Phys. (Japan) **7**, 103 (1952).
[5] K. A. Brueckner, Phys. Rev. **89**, 834 (1953).
[6] K. A. Brueckner and K. M. Watson, Phys. Rev. **86**, 923 (1952).
[7] E. U. DeWire and G. Silverman, Phys. Rev. **94**, 756(A) (1954).
[8] G. F. Chew and M. L. Goldberger, Phys. Rev. **87**, 778 (1952).
[9] K. M. Watson, Phys. Rev. **89**, 575 (1953).

$t_i=h_i+h_i\frac{1}{a-h_i}h_i$, the transition operator for scattering at nucleon i.

$$T_i=h_i+H_i+(h_i+H_i)\frac{1}{a-h_i-H_i}(h_i+H_i)$$

$$\simeq\left[1+h_i\frac{1}{a-h_i}\right]H_i\left[1+\frac{1}{a-h_i}h_i\right],$$

if one neglects terms not linear in H_i, the transition operator for photomeson production from the ith nucleon alone.

We start from the Schrödinger equation for the problem written symbolically in integral form:

$$\psi=\psi_0+\frac{1}{a}\mathcal{K}'\psi. \tag{2.1}$$

A formal solution to the Schrödinger equation can be written, following the method of Chew and Goldberger,[8] as

$$\psi=\left[1+\frac{1}{a}T\right]\phi, \tag{2.2}$$

where the transition operator T is, to terms linear in the weak gamma-ray interaction H_i,

$$T=\left[1+h\frac{1}{a-h}\right]H\left[1+\frac{1}{a-h}h\right]. \tag{2.3}$$

We now wish to replace the interaction Hamiltonians which appear in this expression by the related (and observable) transition operators for scattering and photoproduction on a single nucleon. To do this, we proceed in the following way: first, using the definitions for T_i, we find that Eq. (2.2) for T is formally equivalent to

$$T=\left[1+h\frac{1}{a-h}\right]\left[\left[1+h_1\frac{1}{a-h_1}\right]^{-1}\right.$$
$$\times T_1\left[1+\frac{1}{a-h_1}h_1\right]^{-1}+\left[1+h_2\frac{1}{a-h_2}\right]^{-1}$$
$$\left.\times T_2\left[1+\frac{1}{a-h_2}h_2\right]^{-1}\right]\left[1+\frac{1}{a-h}h\right]. \tag{2.4}$$

We introduce our first approximation by assuming that

$$\{1+[1/(a-h_1)]h_1\}^{-1}\{1+[1/(a-h)]h\}$$

and

$$\{1+[1/(a-h_2)]h_2\}^{-1}\{1+[1/(a-h)]h\}$$

are equal to 1. Physically, this means that we neglect one nucleon's influence on the photoproduction at the other nucleon before the gamma ray is absorbed. The exchange of these virtual mesons also serves to bind the deuteron, and we will include this effect by using the correct deuteron wave function. Next, eliminating the meson-nucleon interaction terms h_i by a series of formal manipulations, we are led to the result,

$$T=a\left[1-\frac{1}{a}t_1\frac{1}{a}t_2\right]^{-1}\left[\frac{1}{a}T_1+\frac{1}{a}t_1\frac{1}{a}T_2\right]+(1\rightleftarrows2). \tag{2.5}$$

We can interpret this equation for T physically. If the denominator were expanded in a power series, the first terms in the expansion would be T_1 and T_2, the usual impulse approximation. The next two terms are $t_1(1/a)T_2$ and $t_2(1/a)T_1$. These terms represent the first correction to the impulse approximation due to one scattering at the other nucleon after photoproduction. The other terms represent all higher order corrections of this type.

3. COMPUTATION

We assume that the scattering takes place in P states and that photoproduction takes place in S and P states as predicted in reference 5. Accordingly, we choose a form for t_i in momentum space:

$$\langle q|t_i|q'\rangle=b_i\mathbf{q}\cdot\mathbf{q}'e^{-i(\mathbf{q}-\mathbf{q}')\cdot\mathbf{r}_i}, \tag{3.1}$$

where b_i is a matrix in charge space and is also dependent on energy. We have also a momentum representation for T_i,

$$\langle q|T_i|\phi\rangle=(\alpha_i+\boldsymbol{\gamma}_i\cdot\mathbf{q})e^{-i(\mathbf{q}-\mathbf{K})\cdot\mathbf{r}_i}, \tag{3.2}$$

where α_i and $\boldsymbol{\gamma}_i\cdot\mathbf{q}$ are matrices in charge space which contain the spin and energy dependence of the photoproduction transition matrix $|\phi\rangle$ is the initial state of the system containing a gamma ray of momentum $\mathbf{R}$ and two nucleons at $\mathbf{r}_1$ and $\mathbf{r}_2$. The vector $\mathbf{q}$ is the momentum of the photoproduced meson.

To solve our problem we need a representation of the inverse operator $[1-(1/a)t_1(1/a)t_2]^{-1}$ which appears in Eq. (2.5). Let

$$y=\left[1-\frac{1}{a}t_1\frac{1}{a}t_2\right]^{-1}. \tag{3.3}$$

Then we find that y satisfies the integral equation

$$y=1+y\frac{1}{a}t_1\frac{1}{a}t_2. \tag{3.4}$$

In momentum space $1/a$ is diagonal.

$$\left\langle q\left|\frac{1}{a}\right|q'\right\rangle=\frac{1}{E-\omega+i\epsilon}\delta(\mathbf{q}-\mathbf{q}'). \tag{3.5}$$

We find from Eqs. (3.1) and (3.5) that the matrix element of $t_1(1/a)t_2$ is

$$\left\langle q\left|\frac{1}{t_1-t_2}\right|q'\right\rangle=-e^{-i(\mathbf{q}\cdot\mathbf{r}_1-\mathbf{q}'\cdot\mathbf{r}_2)}\mathbf{q}\cdot\nabla_R\mathbf{q}'\cdot\nabla_R \times\int b_1b_2\frac{d^3q}{(2\pi)^3}\frac{e^{i\mathbf{q}\cdot\mathbf{R}}}{E-\omega+i\epsilon}, \quad (3.6)$$

where $\mathbf{R}=\mathbf{r}_1-\mathbf{r}_2$. In evaluating this integral we shall retain only the contribution from the pole on the energy shell, i.e., we suppose that b_1 and b_2 have no poles which contribute appreciably to the integral. This is equivalent to the assumption that the scatterings on the energy shell give the principal contribution to the correction due to multiple scattering. The evaluation is then elementary and we find that

$$\left\langle q\left|\frac{1}{t_1-t_2}\right|q'\right\rangle=e^{-i(\mathbf{q}\cdot\mathbf{r}_1-\mathbf{q}'\cdot\mathbf{r}_2)}\left[\frac{\omega_E}{2\pi}\right] \times b_1b_2\mathbf{q}\cdot\nabla_R\mathbf{q}'\cdot\nabla_R\frac{e^{iq_ER}}{R}. \quad (3.7)$$

We have introduced q_E as the momentum vector which conserves energy with the incident gamma ray and $\omega_E=(q_E^2+u^2)^{\frac{1}{2}}$. Where no confusion can result, q_E will often be called q. If we introduce the functions f and g defined by

$$f(R)=-\frac{1}{R}\frac{d}{dR}\frac{e^{iqR}}{R}, \quad (3.8)$$

and

$$g(R)=\frac{1}{R}\frac{d}{dR}f(R), \quad (3.9)$$

we obtain

$$\left\langle q\left|\frac{1}{t_1-t_2}\right|q'\right\rangle=b_1b_2\frac{\omega_E}{2\pi}(f\mathbf{q}\cdot\mathbf{q}'+g\mathbf{q}\cdot\mathbf{R}\mathbf{q}'\cdot\mathbf{R}). \quad (3.10)$$

This result can be substituted in Eq. (3.4). We introduce an auxiliary function,

$$\mathbf{S}(q)=\int\langle q|y\mathbf{q}'e^{-i\mathbf{q}'\cdot\mathbf{r}_1}|q'\rangle\frac{d^3q'}{(2\pi)^3}. \quad (3.11)$$

We find the equation for $\mathbf{S}$ by operating on Eq. (3.4).

$$\mathbf{S}=\mathbf{q}e^{-i\mathbf{q}\cdot\mathbf{r}_1}+\mathbf{S}\left[\frac{\omega_E}{2\pi}\right]b_1b_2\cdot\int\frac{d^3q'}{(2\pi)^3} \times(f\mathbf{q}'+g\mathbf{R}\mathbf{q}'\cdot\mathbf{R})\frac{e^{-i\mathbf{q}'\cdot\mathbf{R}}}{E-\omega'+i\epsilon}. \quad (3.12)$$

If we perform the integration and put $c_i=-(\omega_E/2\pi)b_i$ we find that

$$\mathbf{S}=\mathbf{q}e^{-i\mathbf{q}\cdot\mathbf{r}_1}+\mathbf{S}c_1c_2f^2+\mathbf{S}\cdot\mathbf{R}(2fg+g^2R^2)c_1c_2\mathbf{R}. \quad (3.13)$$

We can solve for $\mathbf{S}$ by scalar multiplication by $\mathbf{R}$. The resulting equation for $\mathbf{S}\cdot\mathbf{R}$ is

$$\mathbf{S}\cdot\mathbf{R}=\frac{1}{1-c_1c_2h^2}\mathbf{q}\cdot\mathbf{R}e^{-i\mathbf{q}\cdot\mathbf{r}_1}, \quad (3.14)$$

where we have introduced the abbreviation

$$h=f+R^2g. \quad (3.15)$$

By substitution in Eq. (3.13) we obtain an equation for $\mathbf{S}$. The solution for $\mathbf{S}$ is

$$\mathbf{S}=\frac{1}{1-f^2c_1c_2}e^{-i\mathbf{q}\cdot\mathbf{r}_1}\mathbf{q}+\mathbf{R}\frac{\mathbf{q}\cdot\mathbf{R}}{R^2}e^{-i\mathbf{q}\cdot\mathbf{r}_1} \times\left[\frac{1}{1-h^2c_1c_2}-\frac{1}{1-f^2c_1c_2}\right]. \quad (3.16)$$

If we define

$$P(q)=\int\langle q|ye^{-i\mathbf{q}'\cdot\mathbf{r}_1}|q'\rangle\frac{d^3q'}{(2\pi)^3}, \quad (3.17)$$

a similar calculation shows that

$$P=e^{-i\mathbf{q}\cdot\mathbf{r}_1}-i\mathbf{q}\cdot\mathbf{R}\frac{e^{-i\mathbf{q}\cdot\mathbf{r}_1}}{1-h^2c_1c_2}fhc_1c_2. \quad (3.18)$$

From Eq. (3.14) we see that

$$\langle q|T|\phi\rangle=\int\frac{d^3q'}{(2\pi)^3}\langle q|y|q'\rangle\left[\langle q'|T_1|\phi\rangle + \int\frac{d^3q''}{(2\pi)^3}\langle q'|t_1|q''\rangle\frac{1}{E-\omega''+i\epsilon}\langle q''|T_2|\phi\rangle\right]. \quad (3.19)$$

Using the definitions of T_1 and T_2, we finally obtain

$$\begin{aligned}\langle q|T|\phi\rangle=&\left(1-i\mathbf{q}\cdot\mathbf{R}\frac{1}{1-h^2c_1c_2}fhc_1c_2\right)\alpha_1e^{i(\mathbf{K}-\mathbf{q})\cdot\mathbf{r}_1}\\ &+\left\{\frac{1}{1-f^2c_1c_2}\mathbf{q}\cdot\boldsymbol{\gamma}_1+\frac{1}{R^2}\left(\frac{1}{1-h^2c_1c_2}\right.\right.\\ &\left.\left.-\frac{1}{1-f^2c_1c_2}\right)\times\mathbf{q}\cdot\mathbf{R}\boldsymbol{\gamma}_1\cdot\mathbf{R}\right\}e^{i(\mathbf{K}-\mathbf{q})\cdot\mathbf{r}_1}\\ &+\left\{i\mathbf{q}\cdot\mathbf{R}\frac{1}{1-h^2c_1c_2}fc_1\alpha_2-\left[\frac{1}{1-f^2c_1c_2}fc_1\mathbf{q}\cdot\mathbf{r}_2\right.\right.\\ &+\frac{1}{R^2}\left(\frac{h}{1-h^2c_1c_2}-\frac{f}{1-f^2c_1c_2}\right)\\ &\left.\left.\times c_1\mathbf{q}\cdot\mathbf{R}\boldsymbol{\gamma}_1\cdot\mathbf{R}\right]\right\}e^{i(\mathbf{K}\cdot\mathbf{r}_2-\mathbf{q}\cdot\mathbf{r}_1)}+(1\rightleftarrows2). \quad (3.20)\end{aligned}$$

To compute the elastic cross section for π^0 production we must average $\langle q|T|\phi\rangle$ over the square of the deuteron wave function.[1] We perform the average over the angles of $\mathbf{R}$ and introduce

$$\mathbf{l}=\tfrac{1}{2}(\mathbf{K}-\mathbf{q}), \tag{3.21}$$

and

$$\mathbf{m}=\tfrac{1}{2}(\mathbf{K}+\mathbf{q}). \tag{3.22}$$

Then Eq. (3.20) can be written as

$$\begin{aligned}\langle q|T|\phi\rangle=&\left(1-\mathbf{q}\cdot\nabla_l\frac{fh}{1-h^2c_1c_2}c_1c_2\right)\alpha_1\frac{\sin lR}{lR}\\&+\left[\frac{1}{1-f^2c_1c_2}\mathbf{q}\cdot\boldsymbol{\gamma}_1-\frac{1}{R^2}\left(\frac{1}{1-h^2c_1c_2}\right.\right.\\&\left.-\frac{1}{1-f^2c_1c_2}\right)(\mathbf{q}\cdot\nabla_l)(\boldsymbol{\gamma}_1\cdot\nabla_l)\Big]\frac{\sin lR}{lR}\\&+\left\{-\frac{f}{1-f^2c_1c_2}\mathbf{q}\cdot\nabla_m c_1\alpha_2-\left[\frac{f}{1-h^2c_1c_2}c_1\mathbf{q}\cdot\boldsymbol{\gamma}_2\right.\right.\\&-\frac{1}{R^2}\left(\frac{h}{1-h^2c_1c_2}-\frac{f}{1-f_{\mathcal{S}}c_1c_2}\right)c_1(\mathbf{q}\cdot\nabla_m)\\&\left.\left.\times(\boldsymbol{\gamma}_2\cdot\nabla_m)\right]\right\}\times\frac{\sin mR}{mR}+(1\rightleftarrows2).\end{aligned} \tag{3.23}$$

We now compute the isotopic spin dependence of the transition operator. This is done in the Appendix. The results are

$$c_1=b\begin{bmatrix}2 & \sqrt{2}\\ \sqrt{2} & 1\end{bmatrix}, \tag{3.24}$$

and

$$c_2=b\begin{bmatrix}2 & -\sqrt{2}\\ -\sqrt{2} & 1\end{bmatrix}. \tag{3.25}$$

We also compute $\mathbf{q}\cdot\boldsymbol{\gamma}_1$ and $\mathbf{q}\cdot\boldsymbol{\gamma}_2$ in the appendix [Eqs. (5.8) and (5.9)].

The states used as basis vectors for this representation are the two states of the meson—two nucleon system with total isotopic spin equal to unity; b is $\lambda^3e^{i\delta}\sin\delta$. To obtain this result we have introduced the assumption that scattering takes place in the state with isotopic spin equal to three halves. If we introduce dimensionless variables

$$\mathbf{x}=\mathbf{q}R, \tag{3.26}$$

$$\mathbf{y}=\mathbf{K}R, \tag{3.27}$$

$$\mathbf{w}=\mathbf{m}R, \tag{3.28}$$

$$\mathbf{z}=\mathbf{l}R, \tag{3.29}$$

then the transition matrix element for elastic π^0 production can be shown to be

$$\begin{aligned}\langle q|T_{MS}|\phi\rangle=&\frac{1}{K}\frac{2\pi}{(12)^{\frac{1}{2}}}\frac{v}{(wq)^{\frac{1}{2}}}\left\{\left[\left(\frac{\sin z}{z}+f\frac{\sin w}{w}\right)\right.\right.\\&\times\frac{1}{1-f^2}+\frac{1}{2}\left(\frac{1}{1-h^2}-\frac{1}{1-f^2}\right)\\&\times[-2a(z)+\mathbf{x}\cdot\mathbf{z}b(z)]-\frac{1}{2}\left(\frac{h}{1-h^2}\right.\\&\left.\left.-\frac{f}{1-f^2}\right)[-2a(w)+\mathbf{x}\cdot\mathbf{w}b(w)]\right]\\&\times[x_1(1)+x_1(2)]-\frac{i}{2}\frac{y}{x}(\boldsymbol{\sigma}_1+\boldsymbol{\sigma}_2)\cdot\boldsymbol{\varepsilon}\\&\times\left[\mathbf{x}\cdot\mathbf{z}\left(\frac{1}{1-h^2}-\frac{1}{1-f^2}\right)b(z)\right.\\&\left.\left.+\mathbf{x}\cdot\mathbf{w}\left(\frac{h}{1-h^2}-\frac{f}{1-f^2}\right)b(w)\right]\right\}.\end{aligned} \tag{3.30}$$

The various symbols used in the equation are defined as follows: v is a term which contains part of the energy dependence of the cross section. Its value is determined by comparison with the π^0 production cross section in hydrogen. The functions f, g, and h are functions now of x, and are redefined as

$$f(x)=\frac{e^{i(x+\delta)}}{x}\sin\delta, \tag{3.31}$$

$$g(x)=-\frac{1}{x}\frac{d}{dx}f(x), \tag{3.32}$$

$$h(x)=f(x)+x^2g(x). \tag{3.33}$$

We have also (reference 6):

$$x_i=\frac{1}{qK}\{2\mathbf{q}\cdot(\mathbf{K}\times\boldsymbol{\varepsilon})-i\boldsymbol{\sigma}_i\cdot[\mathbf{q}\times(\mathbf{K}\times\boldsymbol{\varepsilon})]\}. \tag{3.34}$$

Finally,

$$a(z)=-\frac{1}{z}\frac{d}{dz}\frac{\sin z}{z}, \tag{3.35}$$

and

$$b(z)=-\frac{1}{z}\frac{d}{dz}a(z). \tag{3.36}$$

The usual impulse approximation is obtained by putting $\delta=0$. Then $f=h=0$. We find that

$$\langle q|T_{IA}|\phi\rangle=\frac{1}{K}\frac{2\pi}{(12)^{\frac{1}{2}}}\frac{v}{(\omega q)^{\frac{1}{2}}}\frac{\sin z}{z}[x_1(1)+x_1(2)]. \tag{3.37}$$

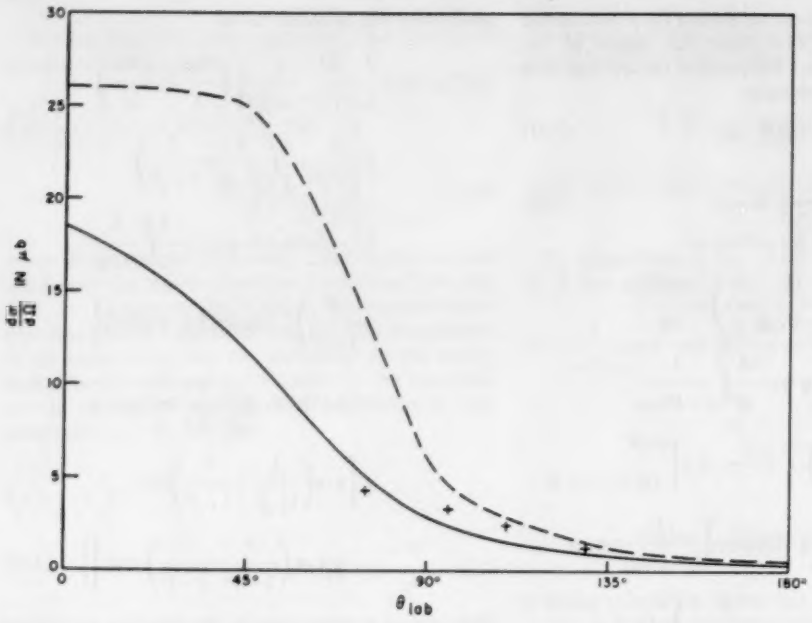

FIG. 1. Photoproduction cross section as a function of emitted meson angle in the laboratory system at a gamma-ray energy of 285 Mev. The dashed line is the impulse approximation, the solid line is the impulse approximation with multiple scattering corrections, and the crosses are experimental points from Silverman *et al.* (reference 10).

In obtaining these results we have made use of the assumption of reference 6, that photoproduction of neutron mesons takes place in a state with $J=\frac{3}{2}$ (magnetic dipole). We have not included contributions from production of charged mesons in S-states. This contribution has been evaluated numerically and found to be small. We introduce a simplified form of $\langle q|T_{MS}|\phi\rangle$.

$$\langle q|T_{MS}|\phi\rangle=\frac{1}{K}\frac{2\pi}{(12)^{\frac{1}{2}}}\frac{v}{(\omega q)^{\frac{1}{2}}}\times[A[x_1(1)+x_1(2)]+B(\sigma_1+\sigma_2)\cdot\epsilon]. \quad (3.38)$$

Let the averages over $\varphi_D^2(R)$ be denoted by $\bar{A}$, $\bar{B}$, and $\langle(\sin z)/z\rangle_{Av}$. Then the cross section is

$$\frac{d\sigma_{MS}}{d\Omega}=\frac{|v|^2}{9}\frac{1}{K^2}[|\bar{A}|^2(5\sin^2\theta+2)+|\bar{B}|^2-2\cos\theta\,\mathrm{Re}(A^*B)]. \quad (3.39)$$

We obtain the usual impulse approximation by averaging and squaring Eq. (3.37). We find

$$\frac{d\sigma_{IA}}{d\Omega}=\frac{|v|^2}{9}\frac{1}{K^2}(5\sin^2\theta+2)[\langle(\sin z)/z\rangle_{Av}]^2. \quad (3.40)$$

If we use the Hulthén wave function,

$$\varphi_D(R)=\left(\frac{28}{9}\alpha\right)^{\frac{1}{2}}\left(\frac{e^{-\alpha R}-e^{-7\alpha R}}{R}\right), \quad (3.41)$$

where $\alpha=45.5$ Mev, we find that

$$\langle(\sin z)/z\rangle_{Av}=\frac{28}{9}\frac{\alpha}{l}\left[-\tan^{-1}\left(\frac{2\alpha}{l}\right)+2\tan^{-1}\left(\frac{8\alpha}{l}\right)-\tan^{-1}\left(\frac{14\alpha}{l}\right)\right]. \quad (3.42)$$

The functions $\bar{A}$ and $\bar{B}$ must be evaluated numerically. This was done at gamma-ray energies of 285 and 345 Mev. These energies correspond to meson phase shifts for scattering of about 45° (135 Mev) and 90° (200 Mev). In Fig. 1 we show the results of the calculation in the laboratory system at $K=285$ Mev. The experiments of Silverman *et al.*[7] are also plotted. We see that the multiple scattering tends to depress the cross section by roughly the same amount at all angles. The magnitude of the cross section was fixed by fitting to the π^0 cross section in hydrogen.[10]

In Fig. 2 we also plot the results at $K=345$ Mev in the center-of-mass system. The results are approximately the same, a depression of the cross section at all angles.

We have also computed the cross section for a transition operator which yields a $\sin^2\theta$ distribution for π^0 production in hydrogen. The result is shown in Fig. 3 for $K=285$ Mev. The correction factor due to multiple scattering is about the same as in Fig. 1.

[10] A. Silverman and M. Stearns, Phys. Rev. **88**, 1225 (1952).

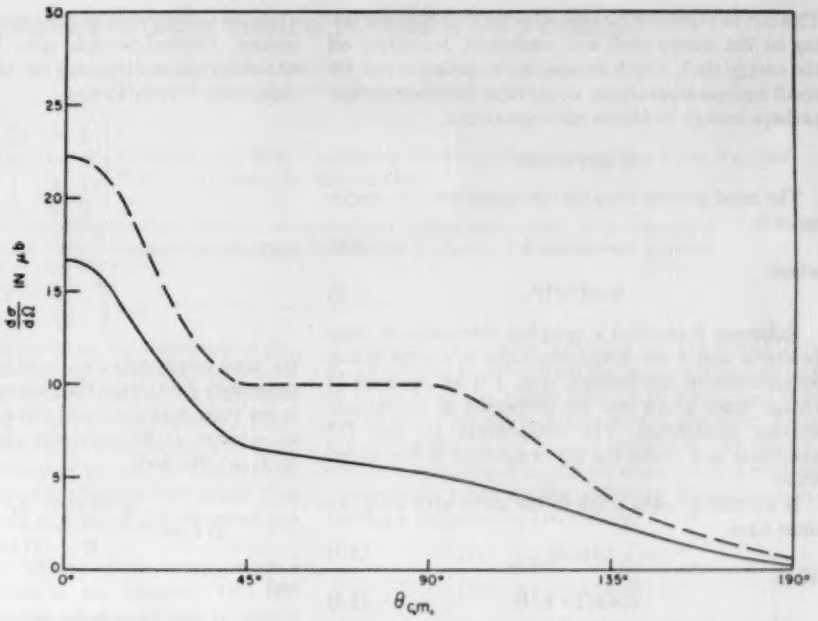

FIG. 2. Photoproduction cross section as a function of emitted meson angle in the center-of-mass system at a gamma-ray energy of 345 Mev. The significance of the curves is the same as in Fig. 1.

4. CONCLUSIONS

The possibility that the observed depression of the photoproduction cross section for mesons in deuterium can be explained in part by inclusion of the effects of multiple scattering in the calculations seems to be substantiated by these results. We see that measurement of the differential cross section at angles further forward is suggested, in order to look for a quantitative check on the theory. We also see that little information can be obtained as to what order of radiative transition is involved from measurements at these energies. The quantitative agreement with experiment is only fair.

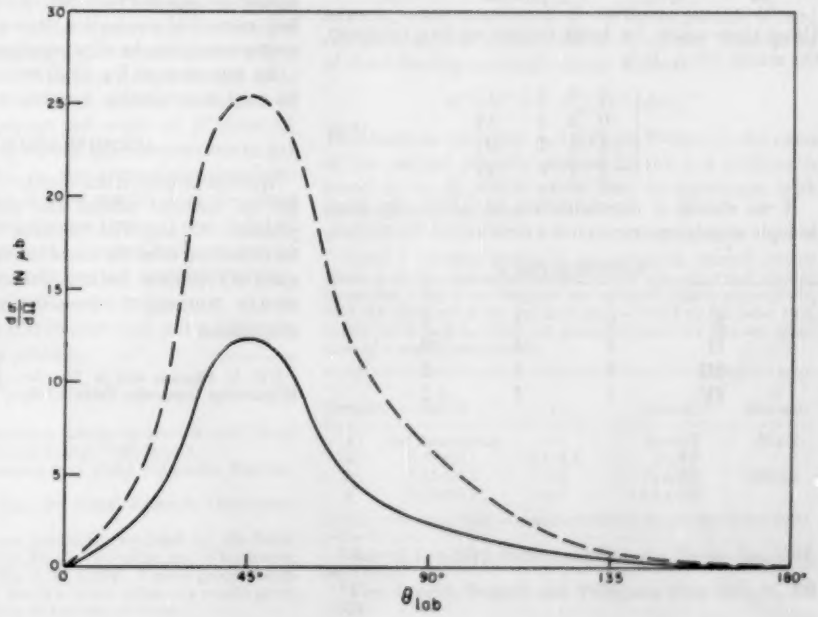

FIG. 3. Photoproduction cross section as a function of emitted meson angle in the laboratory system at 285 Mev with a transition operator yielding a $\sin^2\theta$ distribution. The significance of the curves is the same as in Fig. 1.

This can be explained by remembering that only scattering on the energy shell was considered. Scattering off the energy shell, which is expected to be important for small nucleon separations, would raise the cross section, perhaps enough to obtain such agreement.

5. APPENDIX

The most general form for the operators c_i in charge space is

$$c_i = a + b\boldsymbol{\tau}_i \cdot \mathbf{I}, \tag{5.1}$$

where

$$\mathbf{I} = i\mathbf{U} \times \mathbf{U}^\dagger. \tag{5.2}$$

Reference 8 contains a complete discussion of these points. a and b are scalar functions in charge space, independent of the isotopic spin. $\mathbf{I}$ is an operator in charge space which has the properties of an isotopic angular momentum. The components U_i and $U_i^\dagger$ annihilate and create the ith component of the meson wave.

If scattering takes place in the state with $I=\frac{3}{2}$, we must have

$$a = 2b. \tag{5.3}$$

Then

$$c_i = b(2 + \boldsymbol{\tau}_i \cdot \mathbf{I}). \tag{5.3}$$

To obtain a representation for c_i we choose a set of basis vectors as follows:

Representation 1

I	$t_0^0 w_1^0$	2 nucleon singlet $+\pi^0$
II	$t_1^0 w_1^0$	2 nucleon triplet $+\pi^0$
III	$t_1^{-1} w_1^1$	2 neutrons $+\pi^+$
IV	$t_1^1 w_1^{-1}$	2 protons $+\pi^-$

Using these states for basis vectors we can construct the matrix for c_1. It is

$$c_1 = \begin{pmatrix} 2 & 0 & 1 & -1 \\ 0 & 2 & 1 & 1 \\ 1 & 1 & 1 & 0 \\ -1 & 1 & 0 & 1 \end{pmatrix}. \tag{5.5}$$

If we choose a representation in which the total isotopic angular momentum is a constant of the motion,

Representation 2

	t	l	I
I	0	1	1
II	1	1	0
III	1	1	1
IV	1	1	2

where t = isotopic spin of 2 nucleons; l = isotopic spin of mesons; I = total isotopic spin. We can transform c_1 into this representation by use of the Clebsch-Gordan coefficients.[11] Then we find

$$c_1 = \begin{pmatrix} 2 & 0 & \sqrt{2} & 0 \\ 0 & 0 & 0 & 0 \\ \sqrt{2} & 0 & 1 & 0 \\ 0 & 0 & 0 & 3 \end{pmatrix}. \tag{5.6}$$

Similarly we obtain

$$c_2 = \begin{pmatrix} 2 & -\sqrt{2} \\ -\sqrt{2} & 1 \end{pmatrix}. \tag{5.7}$$

We need retain only two rows and columns (the two states with $I=1$) since the photoproduction takes place in the state with $I=1$ and the scattering operators do not change I. We can also compute $\langle q|T_1|\phi\rangle$ and $\langle q|T_2|\phi\rangle$. We find

$$\langle q|T_1|\phi\rangle = \frac{e^{-i(\mathbf{q}-\mathbf{K})\cdot\mathbf{r}_1}}{K} \frac{2\pi}{(12)^{\frac{1}{2}}} \frac{x_1(1)v}{(\omega_q)^{\frac{1}{2}}} \begin{bmatrix} 1 \\ 1/\sqrt{2} \end{bmatrix} \tag{5.8}$$

and

$$\langle q|T_2|\phi\rangle = \frac{e^{-i(\mathbf{q}-\mathbf{K})\cdot\mathbf{r}_2}}{K} \frac{2\pi}{(12)^{\frac{1}{2}}} \frac{x_1(2)v}{(\omega_q)^{\frac{1}{2}}} \begin{bmatrix} 1 \\ -1/\sqrt{2} \end{bmatrix}. \tag{5.9}$$

This result is obtained by writing a transition operator which leads to the results of reference 6, and then computing the matrix elements for it in representation 2. To obtain this result we have assumed that production in S states does not contribute. This is not correct, but numerical evaluation shows that this neglect is unimportant for the π^0 production cross section.

By reference to Eq. (3.2) we can obtain $\boldsymbol{\gamma}_i \cdot \mathbf{q}$ which we need in computing our cross section.

ACKNOWLEDGMENTS

We wish to extend our thanks to Dr. K. A. Brueckner for his constant advice and encouragement on this problem. We also wish to thank Dr. A. C. G. Mitchell for extending to us the use of the facilities of the Department of Physics at Indiana University. We are indebted to Dr. Norman C. Francis for many illuminating discussions.

[11] E. U. Condon and G. Shortley, *Theory of Atomic Spectra* (Cambridge University Press, London, 1935).

Production of Heavy Unstable Particles in a p-p Collision*

M. M. Block,† *Nucleonics Division, Naval Research Laboratory, Washington, D. C.*
E. M. Harth,‡ *Duke University, Durham, North Carolina*

and

W. B. Fowler, R. P. Shutt, A. M. Thorndike, and W. L. Whittemore, *Brookhaven National Laboratory, Upton, New York*

(Received February 14, 1955)

A hydrogen-filled diffusion cloud chamber was exposed to a 2.7-Bev proton beam. In a collection of 202 p-p collisions, there was one event interpreted as the associated production of a hyperon and a K-meson, via the reaction $p+p\rightarrow\Lambda^{+}+K^{+}+n$.

AN event best interpreted as the simultaneous production of a K-meson and a hyperon in a proton-proton interaction was recently observed in a diffusion cloud chamber exposed to an external beam of 2.7-Bev protons[1] from the Brookhaven Cosmotron. The cloud chamber contained hydrogen gas at 20 atmospheres and was located in a magnetic field of 9500 gauss. This event was found among a total of 202 observed p-p collisions.

Figure 1 shows the collision of the beam proton i with a hydrogen nucleus in the chamber. Two fast positively charged particles, a and b, are seen to emerge from the collision. The emission of at least one neutral particle is required since tracks i, a, and b are not coplanar. Table I gives the measured momenta, ionization estimates and angles in the laboratory system. The momenta were determined with a Cooke microscope at low magnification. Track a was too short to permit a momentum measurement.

Particle b, after a path length of $\sim$6 cm, is seen to decay through an angle of 12.5 degrees into the charged particle b' which is probably a pion or muon, but might be as heavy as a proton. The decay angle is such as to rule out π-μ decay. Particle a travels $\sim$3 cm and apparently decays through an angle of 2° into a'. Although this angle is small, the measurements are reproducible to $\pm$0.5° in the three-dimensional reprojection system used for the spatial analysis. Since the estimated ionization changes from $\sim$1 to 1.5–2.5 at the point of the 2° break, this further lends support to the hypothesis that a is indeed an unstable particle. On the basis of its ionization and momentum, a' was identified as a proton; this implies that a is a hyperon.

The two-body decay scheme,

$$\Lambda^{+}\rightarrow p+\pi^{0}+Q, \tag{1}$$

is assumed for a, with a Q-value of 115 Mev.[2] This decay scheme together with the measured momentum of a' leads to the values 1.02$\pm$0.16 Bev/c and 0.46 $\pm$0.13 Bev/c for the momentum of a, the latter value being ruled out on the basis of ionization. The identification of a as a hyperon, and the assumption of nucleon conservation leads to the following alternatives involving a single neutral secondary:

$$\text{(Ia)}\quad p+p\rightarrow\Lambda^{+}+n+K^{+},$$
$$\text{(Ib)}\quad p+p\rightarrow\Lambda^{+}+\pi^{0}+\Lambda^{+},$$

where n is a neutron. On the assumption of the scheme (Ia), M_b, the mass of b, may now be computed from the energy and momentum conservation laws, using the computed momentum of a and the measured momentum of b. One obtains M_b=0.51$\pm$0.10 Bev, in good agreement with the K-meson mass of $\sim$500 Mev.

Since there is a large uncertainty in the measurement of the momentum of b, it is of interest to utilize the more accurate momentum of the decay particle b', and calculate p_b, the momentum of b, on the assumption of the following two-body decay scheme:

$$K^{+}\rightarrow\pi^{+}+\pi^{0}+Q(217\text{ Mev}).^{3}$$

This leads to the value p_b=0.87$\pm$0.19 Bev/c; the mass of the neutral particle emitted in the p-p collision is found to be M_n=0.93$\pm$0.04 Bev, in agreement with the mass of a neutron.

TABLE I. Directly observable parameters of charged secondaries; p is the measured momentum, I the estimated specific ionization; θ and ϕ are the polar and azimuth angles, respectively, with the direction of the incident proton taken as the polar axis, except for $\theta_{a'}$ and $\theta_{b'}$ which are measured from the forward directions of a and b, respectively.

Particle	p (Bev/c)	I	θ (degrees)	ϕ (degrees)
a	not measurable	$\sim$1	24$\pm$0.5	30$\pm$2
a'	0.57$\pm$0.1	1.5–2.5	2$\pm$0.5	
b	0.83$\pm$0.5	$\sim$1	16$\pm$0.5	180$\pm$3
b'	0.73$\pm$0.1	$\sim$1	12.5$\pm$0.5	

* This research was supported jointly by the Office of Naval Research and the U. S. Atomic Energy Commission.

† On military leave of absence from Duke University, Durham, North Carolina.

‡ On leave of absence from the Naval Research Laboratory, Washington, D. C.

[1] A value of 2.6 Bev was previously reported for the beam energy: Block, Harth, Fowler, Shutt, Thorndike, and Whittemore, Bull. Am. Phys. Soc. **29**, No. 7, 33 (1954). A more precise beam analysis indicated that 2.7 Bev is a better value; the results given here are relatively insensitive to the precise value.

[2] Bonetti, Levi-Setti, Panetti, and Tomasini, Nuovo cimento **10**, 345 (1953).

[3] Kim, Burwell, Huggett, and Thompson, Phys. Rev. **96**, 229 (1954).

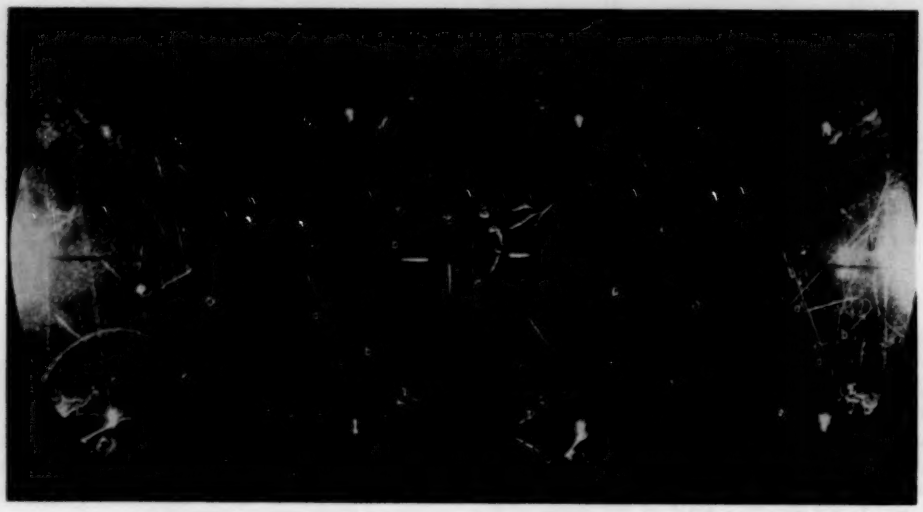

FIG. 1. Stereoscopic view of incoming proton i interacting in the hydrogen gas to produce tracks a and b. Tracks a' and b' are interpreted as decay fragments of a and b, respectively. The pictures have been retouched to make the event visible in the reproduction.

If a similar calculation is carried out for scheme (Ib), it is found that this alternative can be ruled out because energy and momentum cannot simultaneously be conserved if there is creation of two hyperons and a pion with the observed momenta and angles of emission.

We now wish to consider the possibility that a is a proton, and that both the 2° break between a and a', and the apparent change in ionization are spurious; the momentum of a' is taken as representative of the momentum of this particle. The following interpretations of the event may now be investigated:

$$\text{(IIa)} \quad p+p\rightarrow p+\Lambda^0+K^+,$$
$$\text{(IIb)} \quad p+p\rightarrow p+n+K^+,$$
$$\text{(IIc)} \quad p+p\rightarrow p+\pi^0+\Lambda^+.$$

Proceeding as before, scheme (IIa) leads to a mass value of $M_b=0.58\pm0.13$ Bev for particle b, which is compatible with the K-meson mass. Scheme (IIb) yields a mass of 0.70 ± 0.15 Bev for b; this mass is somewhat high for a K-meson, but the interpretation cannot be ruled out.

Assumption (IIc) leads to the following alternatives:

$$\Lambda^+\rightarrow\pi^++n+115 \text{ Mev},$$

or

$$\Lambda^+\rightarrow p+\pi^0+115 \text{ Mev}.$$

The first decay scheme leads to computed momenta for b that are incompatible with the measured momentum. If we assume the latter decay scheme, energy and momentum conservation is violated using the measured momenta and angles. Thus, (IIc) is ruled out.

In summary, if the interpretation is made in terms of particles of established masses, there remain the three possibilities:

$$\text{(Ia)} \quad p+p\rightarrow\Lambda^++K^++n,$$
$$\text{(IIa)} \quad p+p\rightarrow p+K^++\Lambda^0,$$
$$\text{(IIb)} \quad p+p\rightarrow p+K^++n.$$

All interpretations imply that the K-meson observed in this event is a boson. The first two are cases of associated production of heavy unstable particles. However, (Ia) is very strongly favored by the arguments given in identifying a as a hyperon, as well as by the high degree of compatibility of all measured quantities with this interpretation. It is therefore suggested that the event represents an example of the simultaneous production of a hyperon and a K-meson in a proton-proton collision.

A transformation of the event into the center-of-mass system of the colliding protons has been carried out on the basis of interpretation (Ia). The results are given in Table II. The laboratory value $p_a=1.02$ Bev/c, as derived from the two-body decay scheme (1), was used.

TABLE II. Transformation into c.m. system of colliding protons, based on interpretation: $p+p\rightarrow\Lambda^++K^++n$.

	$\bar{p}$ (Bev/c)	$\bar{E}$ (Bev)	$\bar{\theta}$ (degrees)	$\bar{\phi}$ (degrees)
Hyperon (a)	0.59	1.33	136	30
K-meson (b)	0.165	0.53	111	180
Neutron	0.53	1.08	34	248

A value for p_b in the laboratory system was then determined which was kinematically consistent with a mass of 500 Mev for the K-meson. This momentum turns out to be 0.56 Bev/c, which is well within the limits of error given for p_b.

The interpretation of the event as the simultaneous production of a K-meson and a hyperon is in accord with the predictions of Pais[4] and Gell-Mann[5] that heavy unstable particles are produced in pairs.

The authors wish to express their appreciation to Mr. M. Blevins of Duke University for aiding in the computations.

[4] A. Pais, Phys. Rev. **86**, 663 (1952).
[5] M. Gell-Mann, Phys. Rev. **92**, 833 (1953).

PHYSICAL REVIEW VOLUME 99, NUMBER 1 JULY 1, 1955

Disintegration of Aluminum by Protons in the Energy Range 0.4 to 3.0 Bev*

G. Friedlander, J. Hudis, and R. L. Wolfgang
Chemistry Department, Brookhaven National Laboratory, Upton, New York

(Received March 11, 1955)

Excitation functions for the production of Na^{24}, Na^{22}, F^{18}, $O^{15}(?)$, N^{13}, C^{11}, and Be^{7} in proton bombardments of Al have been measured from 0.4 to 3.0 Bev. The formation cross sections have strikingly small energy dependence, and this feature is discussed in the light of possible energy transfer mechanisms. The absolute cross-section values are based on a calibration method (suggested by A. Turkevich) which is discussed. It is based on measurements of gross radioactivity in copper irradiated at various energies and on the assumption that the fraction of inelastic collisions with copper nuclei that lead to radioactive products is independent of proton energy from 0.3 to 3 Bev. The validity of this assumption is examined.

WHEN proton beams with kinetic energies up to 3 Bev became available in the Brookhaven Cosmotron, it seemed desirable to extend radiochemical studies of nuclear reactions into this new range of bombarding energies. In an initial survey the yields of many radioactive products from the bombardment of a few selected target elements in different mass regions were measured at a given energy (usually 2.2 Bev) and compared with similar data at lower energies.[1-3] For target elements of medium[2] and high[3] Z the product yield distributions at 2.2-Bev bombarding energy were found to differ markedly from those observed with 300- to 400-Mev protons. For low-Z targets such as carbon[4] and aluminum[1] the most striking observation was the relatively slight difference between the cross sections in the two energy regions. In the present paper we report more detailed data on the excitation functions for the production of several radioactive nuclides in the bombardment of aluminum with protons in the energy range from 0.4 to 3.0 Bev.

The products studied include Na^{24}, Na^{22}, F^{18}, N^{13}, C^{11}, and Be^{7}. The production of all these nuclides from aluminum was investigated previously at lower proton energies. Hintz and Ramsey[6] published excitation functions for the formation of Na^{24}, Na^{22}, and F^{18} with protons of kinetic energies up to 120 Mev. Marquez and Perlman[6] and Marquez[7] reported cross sections for the production from aluminum of all six of the aforementioned nuclides by 335-Mev and 420-Mev protons, respectively.

EXPERIMENTAL

The irradiations were all carried out in the circulating beam of the Cosmotron. The proton energy was varied by variation of the turn-off time for the rf accelerating voltage. To prevent bombardment by stray protons of lower than the desired energy the targets were rammed into the bombardment position at the end of each acceleration cycle as previously described.[2] Circulating proton beams of about 10^{10} protons per pulse and a repetition rate of 12 pulses per minute were used in most of this work. Bombardments of one to two minutes' duration were found to produce adequate counting rates of the short-lived activities investigated: 15.0-hr Na^{24}, 112-min F^{18}, 20.5-min C^{11}, 10-min N^{13}, and some 2-min activity, probably largely O^{15}. The yields of 53-day Be^{7} and 2.6-year Na^{22} were studied in aluminum samples irradiated up to a few hours.

Bombardments were carried out at a number of proton energies between 0.4 and 3.0 Bev. At each energy the yields of the various product activities were determined relative to the yield of Na^{24}. The excitation function for the $Al^{27}(p,3pn)Na^{24}$ reaction was measured in a separate set of experiments as described below.

* Research performed under the auspices of the U. S. Atomic Energy Commission.
[1] Wolfgang, Sugarman, and Friedlander, Phys. Rev. **94**, 775 (1954).
[2] Friedlander, Miller, Wolfgang, Hudis, and Baker, Phys. Rev. **94**, 727 (1954).
[3] Sugarman, Duffield, Friedlander, and Miller, Phys. Rev. **95**, 1704 (1954).
[4] R. L. Wolfgang and G. Friedlander, Phys. Rev. **96**, 190 (1954).
[6] N. M. Hintz and N. F. Ramsey, Phys. Rev. **88**, 19 (1952).
[6] L. Marquez and I. Perlman, Phys. Rev. **81**, 953 (1951).
[7] L. Marquez, Phys. Rev. **86**, 405 (1952).

The targets were made up of 0.00025-in. or 0.003-in. aluminum foils of purity >99.9 percent. Earlier experiments[8] had shown that recoil losses of Na^{24}, F^{18}, and C^{11} from 0.00025-in. aluminum foils are quite serious; but such losses were found to be negligible for all the nuclides investigated except for Be^7 if only the center two foils of a stack of six 0.00025-in. foils were used for the activity measurements. For the runs in which the Be^7 yields were studied, 0.003-in. target foils were used after Dr. N. Sugarman had shown in a preliminary irradiation of a stack of 0.003-in. foils that the recoil loss of Be^7 from such foils is less than a few percent.

The relative cross sections for the formation of Na^{24}, F^{18}, C^{11}, N^{13}, and "the 2-min activity" [$O^{15}(?)$] were determined by analysis of the gross decay curves of the irradiated 0.0005-inch aluminum foils (two 0.00025-inch layers) measured with end-window gas-flow proportional counters. The analysis into 15.0-hour, 112-minute and 20.5-minute components presented no difficulties and their relative intensities are thought to be known to ± 5 percent. The intensities of the 10-minute N^{13} and 2-minute $O^{15}(?)$ activities have somewhat larger uncertainties; checks between different runs and between duplicate decay curve analyses carried out by different individuals[9] indicate that these intensities may have probable errors of about ± 20 percent. The effects of absorption in the 1.2 mg cm^{-2} counter window and of self-absorption and self-scattering in the 0.0005-inch (3.5 mg cm^{-2}) foils were thought to be sufficiently small to be taken as equal for the different β emitters. However, a correction had to be made for the different back-scattering of electrons and positrons[10] from the thick aluminum sample backings. Since the samples were counted in very nearly 2π geometry, Seliger's data for 2π geometry were used, and all β^+-counting rates were multiplied by $1.42/1.27=1.12$ to make them directly comparable with the Na^{24} counting rates. The over-all counting efficiency for Na^{24} in our standard arrangement was determined by Dr. J. B. Cumming by a $\beta-\gamma$ coincidence calibration of Na^{24} induced in aluminum foils by n,α reaction. For the 0.0005-inch foils this over-all counting efficiency was found to be 0.506, for the 0.003-inch foils it was 0.459.

The Na^{22}/Na^{24} ratios were determined in irradiated 0.003-inch aluminum foils by β-decay measurements over several months. In the proportional counters used the counting efficiency for Be^7 was found to be so low as to make the contribution of Be^7 activity to the measured counting rates negligible. Long-lived activities produced from impurities in the aluminum foil were found not to be a serious source of error. The counting efficiency for Na^{22} with the proportional counter arrangement used was established in a separate experiment, in which the absolute disintegration rate of a much stronger Na^{22} sample was determined by a $\beta-\gamma$ coincidence measurement. For this calibration measurement the Na^{22} was produced in a 0.003-inch aluminum foil by bombardment with 380-Mev protons at the Nevis cyclotron.

The Be^7 yields were determined with chemically separated beryllium samples. The target was dissolved in HCl and, after addition of Be and Na carriers, $Al(OH)_3$ and $Be(OH)_2$ were precipitated with NH_3. The hydroxides were dissolved in HCl, the bulk of the aluminum removed as $AlCl_3 \times 6H_2O$ by the addition of HCl gas and ether, and $Be(OH)_2$ (and some $Al(OH)_3$) precipitated with NH_3. This precipitate was dissolved in glacial acetic acid, and beryllium was purified by repeated extractions of its basic acetate into chloroform, and finally ignited to BeO for mounting.

The radiochemical purity of the Be^7 samples was checked by decay measurements and by determination of the pulse height distribution with a grey-wedge scintillation spectrometer. The absence of β activity served as an additional criterion of purity. The Be^7 activities were counted with NaI scintillation counters calibrated as follows. A stronger Be^7 source was counted in the same geometry, and also intercompared with a calibrated Na^{22} standard by means of a scintillation spectrometer. This intercomparison involved measurement of the areas under the 0.48-Mev peak of Be^7 and the 0.51-Mev annihilation peak of Na^{22}. The small difference in counting efficiency at these two energies was neglected. The relative areas were converted to relative disintegration rates by means of published decay scheme information (11 percent abundance[11] of 0.48-Mev γ rays in Be^7; 90 percent β^+ emission[12] in Na^{22}).

In one run the relative yields of Be^7 and Na^{22} were checked by comparison of the γ activities of chemically separated samples with calibrated scintillation counters. For this purpose the sodium fraction was obtained by evaporation of the filtrate from the $Al(OH)_3+Be(OH)_2$ precipitate, followed by a NaCl precipitation.

RESULTS

For each bombardment, the disintegration rates of the nuclides measured were converted to relative formation cross sections by means of the appropriate corrections for length of bombardment and, where chemical separations were performed, for chemical yields.[13] In Table I these relative cross sections are given, normalized at each proton energy to the Na^{24} yield taken as unity. On the basis of estimates of the various sources of error in the experiments, the probable errors of the yields in Table I are thought to be about ± 30 percent for N^{13} and "O^{15}," ± 15 percent for Be^7, and ± 10 percent for the others.

[8] R. Wolfgang and G. Friedlander, Phys. Rev. **94**, 775 (1954).
[9] Dr. F. S. Rowland kindly participated in these check analyses.
[10] H. H. Seliger, Phys. Rev. **88**, 408 (1952).
[11] R. M. Williamson and H. T. Richards, Phys. Rev. **76**, 614 (1949).
[12] R. Sherr and R. H. Miller, Phys. Rev. **93**, 1076 (1954).
[13] Dr. R. W. Stoenner kindly carried out the Na chemical-yield determination.

ABSOLUTE CROSS SECTION OF THE REACTION $Al^{27}(p,3pn)Na^{24}$

In order to convert the relative yields shown in Table I to absolute cross sections, it is necessary to know the formation cross section for at least one product as a function of bombarding energy. For convenience, the product chosen was Na^{24}; its activity is easily measured without chemical separation in irradiated aluminum foils, and its formation cross section has been the subject of several studies at synchrocyclotron energies.[5–7,14,15]

Since no external proton beam of sufficient intensity for activation experiments has been available at the Cosmotron, and since a direct, absolute determination of the number of protons striking an internal target is quite difficult, a somewhat indirect method was resorted to for the absolute cross section measurements. The technique was proposed and first applied with 2.2-Bev protons by Turkevich.[16] Since it has formed the basis of all the cross-section measurements made to date on proton-induced nuclear reactions at the Cosmotron, it is discussed here in some detail.

Turkevich's beam calibration method is based on the assumption that, for a target element of medium atomic weight such as copper, that fraction of all the inelastic collisions which leads to the formation of radioactive products stays approximately constant with bombarding energy over a wide energy range. Then, if the total inelastic cross section of, say, copper is known as a function of energy, the production of gross radioactivity in copper foils by protons of various energies serves as a measure of the relative beam intensities at these energies; furthermore, the measurements can be put on an absolute basis if the production of gross radioactivity in copper is determined at a proton energy of about 0.4 Bev where it may be calibrated directly against some known reaction cross section.

TABLE I. Product yields relative to the Na^{24} yield taken as unity at each proton energy.

Proton energy (Bev)	Na^{22}	F^{18}	O^{15} [a]	N^{13}	C^{11}	Be^{7}
0.39[b]	1.89					
0.41		0.65[c]		~0.07	0.27[c]	
0.6	1.78	0.64	0.6	~0.08	0.31	
1.0	1.59[c]	0.7[c]			0.5[c]	0.71
1.4	1.87	0.62	0.7	~0.15	0.52	0.77
1.6	1.38					
1.8	1.81					
2.2	1.37	0.66[c]	0.6[c]	~0.17[c]	0.57[c]	1.18[d]
3.0	1.66[c]	0.65	0.7	~0.11	0.61	1.08

[a] The 2-min activity observed is here considered to be O^{15}.
[b] Nevis cyclotron bombardment.
[c] Mean of two or more runs.
[d] In this run a Be^7/Na^{22} ratio of 0.88 was independently determined by scintillation spectrometry on the unseparated Al target. This corresponds to a Be^7 yield of 1.21 relative to Na^{24}. In another 2.2-Bev bombardment an approximate Be^7 yield of 0.83 (relative to Na^{24}) was found by comparison of chemically separated Be and Na samples.

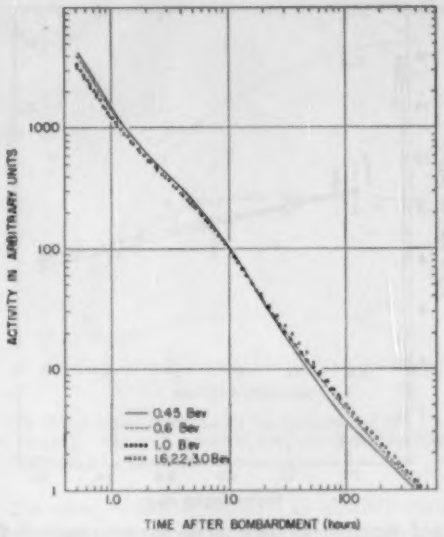

FIG. 1. Gross decay curves of copper foils bombarded with protons of various energies. The curves are normalized at 10 hours after bombardment.

The basic assumption that the ratio of the cross section for formation of radioactive products to the total inelastic cross section of copper is independent of proton energy in the range from about 0.3 to 3 Bev is plausible in view of the experimental data on the yield distributions of spallation products formed from copper. With respect to the stability line, the formation cross sections of the spallation products show very similar patterns at 2.2-Bev[3] and at 340-Mev[17] proton energy, the largest cross sections at both energies being near stability. The yield distribution as a function of mass number, on the other hand, changes quite strongly with bombarding energy,[2] so that the individual product cross sections can by no means be thought to remain constant. Yet the gross activity produced at each energy apparently represents a sufficiently large statistical assembly of half-lives that the gross decay curves of copper foils bombarded at various energies have very similar shapes. This is seen in Fig. 1 which shows on a log-log plot the decay curves of copper foils bombarded for 2 to 5 minutes with protons of various energies between 0.45 and 3.0 Bev. The foils were measured with β-proportional counters. The curves can all be represented approximately by a straight line on the log-log plot, corresponding to the equation $A_t = A_1 t^{-1.31}$, where A_t and A_1 are the activities t hours and 1 hour, respectively, after the end of bombardment. From $t=0.5$ hr to $t=400$ hr no experimental points deviate by more than $\pm$ 20 percent from this line. On the basis of the

[14] Birnbaum, Crandall, Millburn, and Pyle, Phys. Rev. (to be published).
[15] Stevenson, Hicks, and Folger (private communication).
[16] A. Turkevich, Phys. Rev. **94**, 775 (1954).
[17] Batzel, Miller, and Seaborg, Phys. Rev. **84**, 671 (1951).

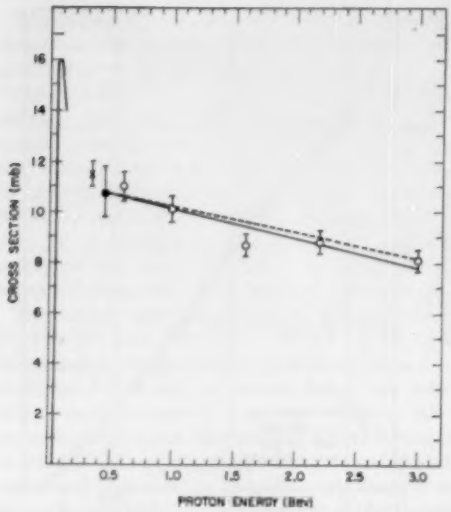

FIG. 2. Excitation function of the reaction $Al^{27}(p,3pn)Na^{24}$. The open circles are the cross sections determined in the present paper, the solid circle is from reference 7, the cross from reference 14, and the curve at low energies from reference 5. The solid line is a least squares fit to the points at $E_p \geq 0.45$ Bev. The dashed line has been the basis of the cross-section scale used for nuclear reactions studied with the Cosmotron.

similarity of all the gross decay curves the following additional assumption was considered reasonably justified: Not only the total number of active atoms formed (which would be hard to measure in practice), but the number N_{ac} of decays over a limited time, such as between 0.5 hr and 400 hr after bombardment, and observed in a β-proportional counter, is approximately proportional to the total number of inelastic events in the copper target. For each run, N_{ac} was determined by graphical integration under the decay curve (on linear scale!) between 0.5 and 400 hr. If a modified activation cross section, σ_{ac}, is defined as the cross section for production of these N_{ac} atoms and σ_{in} is the inelastic cross section for protons on copper, then the assumption may be stated in the form

$$\sigma_{ac}/\sigma_{in} = C, \tag{1}$$

where C is a constant independent of proton energy.

We now turn to the question of the energy dependence of σ_{in}. Actually, very few measurements are available. Kirschbaum[18] reported values of σ_{in} for copper of 746 ± 45, 667 ± 31, and 608 ± 22 mb with protons of 185, 240 and 305 Mev. A measurement[19] at a proton energy of 1.6 Bev gave a value of 680 ± 50 mb, and an inelastic cross section of 674 ± 34 mb has been reported for 1.4-Bev neutrons.[20] Both these direct measurements and the energy dependence of the elementary p-p and n-p cross sections[21] indicate that σ_{in} goes through a minimum in the vicinity of 400 Mev. For the present purpose it has been assumed that σ_{in} for copper stays essentially constant from 0.8 to 3 Bev (as do the total p-p and p-n cross sections[21]) and that

$$\sigma_{in}{}^{>0.8} = 1.15\sigma_{in}{}^{0.45} = 1.07\sigma_{in}{}^{0.6}, \tag{2}$$

where the superscripts are the proton energies in Bev. Any errors due to the assumptions of Eq. (2) are probably small compared with those introduced by the assumptions of the previous paragraph.

Experiments were carried out at 0.45, 0.60, 1.0, 1.6, 2.2, and 3.0 Bev. All bombardments were short compared with 0.5 hr. In each run a 0.003-inch aluminum foil and, downstream from it, three thicknesses of 0.001-inch copper foil were bombarded. After bombardment, an area of 1 or 2 cm^2 was cut out of the center of the foil stack. Only the middle Cu foil was used for the decay measurement and determination of N_{ac}; the other two foils served to compensate for the recoil losses of active nuclei from the middle foil. The Na^{24} activity in the Al foil was measured as described earlier and from it was deduced the number N_{Na} of Na^{24} atoms produced by the bombardment.

If the numbers of Al and Cu atoms in the foils are n_{Al} and n_{Cu}, respectively, and if σ_{Na} is the cross section for the production of Na^{24} from Al, then at each proton energy

$$\sigma_{ac} n_{Cu}/N_{ac} = \sigma_{Na} n_{Al}/N_{Na}. \tag{3}$$

N_{ac}, N_{Na}, n_{Cu}, and n_{Al} are measured quantities. At 0.45-Bev proton energy σ_{Na} is known from Marquez' work[7] as 10.8 mb; with the use of this value $\sigma_{ac}{}^{0.45}$ was calculated from the 0.45-Bev run to be 54.6 mb. Then, according to Eqs. (1) and (2), $\sigma_{ac}{}^{0.6} = 58.5$ mb and $\sigma_{ac}{}^{>0.8} = 62.8$ mb. Now σ_{Na} may be evaluated at each bombarding energy from Eq. (3). The values of σ_{Na} so obtained are shown in Table II and Fig. 2. In the figure the literature values for σ_{Na} at lower energies[5,7,14] are also shown. The solid line of Fig. 2 is a least-squares fit to the points for $E_p \geq 0.45$ Bev. It does not differ significantly from the dotted line drawn through Marquez's 0.45-Bev point and Turkevich's[16] value of 9.0 mb at 2.2 Bev. This dotted line has been the basis for all proton cross sections at Cosmotron energies reported to date and will continue to be used until a more reliable absolute determination of the cross-section scale is made.

The estimated probable errors of ± 5 percent shown

TABLE II. Cross section for the reaction $Al^{27}(p,3pn)Na^{24}$ as a function of proton energy (based on Marquez' value of 10.8 mb at 0.45 Bev).

E_p (Bev)	0.60	1.0	1.6	2.2	3.0
σ (mb)	11.0	10.1	8.7	8.8	8.1

[18] A. J. Kirschbaum, University of California Radiation Laboratory Report UCRL-1967, 1952 (unpublished).
[19] R. B. Duffield and G. Friedlander (unpublished).
[20] Coor, Hill, Hornyak, Smith, and Snow, Phys. Rev. **98**, 1369 (1955).
[21] Chen, Leavitt, and Shapiro (to be published).

on the points in Fig. 2 do not include any estimate of the error in the basic assumption of the method [Eq. (1)]. Such an estimate is difficult to make at this time. To date the only direct evidence on this point comes from the data on copper spallation by 2.2-Bev protons.[2] The cross sections for copper spallation products were based on the value 9.0 mb for the reaction $Al(p,3pn)Na^{24}$ at 2.2 Bev. On this basis the sum of all the measured cross sections for radioactive products of $A>10$ is about 180 mb (the value for V^{49} in reference 2 should be lowered from 27 mb to about 15 mb on the basis of a recent redetermination[22] of the V^{49} half-life). The dependence of the formation cross sections on A and Z indicates that the measured values must represent about one-quarter of the total inelastic cross section, in good agreement with the measured values of σ_{in} ($\approx$675 mb)[19,20] based on transmission data. It is difficult to see how the estimate of 0.25 for the fraction of σ_{in} represented by the measured cross sections can be in error by more than $\pm$30 percent. This then may be assigned as the limit of error on the absolute values of the $Al(p,3pn)$ cross sections in Table II and Fig. 2.

DISCUSSION

On the basis of the $Al(p,3pn)$ cross section discussed in the preceding section, the relative yields of Table I may now be converted into production cross sections. The results are summarized in Figs. 3 and 4 together with the 0.42-Bev data of Marquez.[7] Except for their Be^7 point, the 0.34-Bev measurements of Marquez and Perlman[6] are not included because, according to Marquez,[7] the cross sections reported in reference 6 were calculated without proper corrections for β-ray absorption losses.

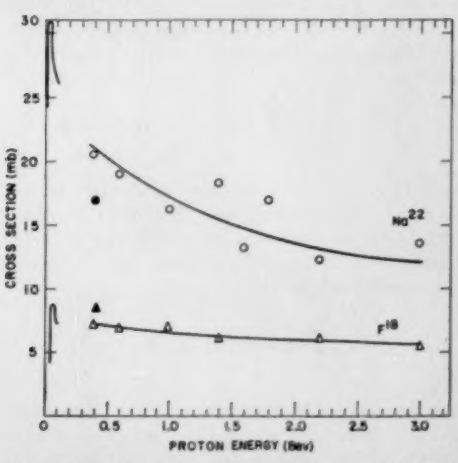

FIG. 3. Excitation functions for the formation of Na^{22} and F^{18} from Al. Data from reference 5 (curve for $E_p<0.12$ Bev) and reference 7 (solid points at 0.42 Bev) are included.

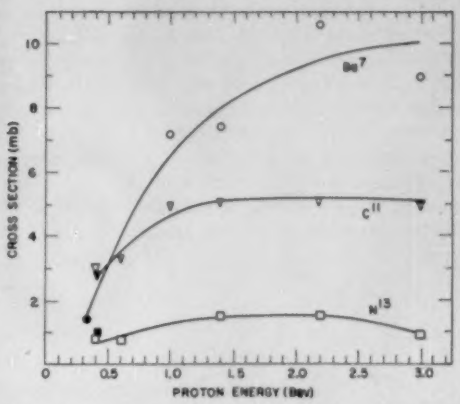

FIG. 4. Excitation functions for the formation of N^{13}, C^{11}, and Be^7 from Al. The solid points at 0.42 Bev are from Marquez (reference 7).

The main feature of the data is certainly the relatively slight energy dependence of the cross sections studied. If we assume that, with the possible exception of Be^7, the products observed are formed by evaporation processes following deposition of excitation energy, then the data indicate remarkably little change in the spectrum of these energy depositions with change in proton energy from 0.4 to 3 Bev. The gradual change in the shapes of the excitation functions from Na^{24} and Na^{22} through F^{18} and N^{13} to C^{11} indicates that, with increasing bombarding energy, the spectrum of excitation energies shifts slowly towards higher values. It is not clear whether the shape of the Be^7 excitation function should be ascribed entirely to this trend. Other mechanisms probably contribute to the formation of Be^7 as will be discussed below.

The rather high cross section for Be^7 formation above 1 Bev is of interest. In the spallation of copper[2] and of heavier elements[3] with 2.2-Bev protons a peak in the yield-vs-mass curve about 20 mass numbers below the target mass has been observed, and one might therefore be tempted to interpret the high yield of Be^7 as evidence for a similar peak in aluminum spallation. In the heavier elements the peak has been ascribed to a high probability for the transfer of hundreds of Mev to the struck nucleus by the reabsorption of π mesons produced in the same nucleus. This mechanism should be less important in aluminum than in copper because of the larger ratio of meson mean free path to nuclear radius. The absolute magnitude of the Be^7 cross section may thus be somewhat large to be accounted for in this manner. It is very likely that evaporation of Be^7 aggregates from excited nuclei (or perhaps some other direct ejection mechanism) makes at least some contribution to the Be^7 formation cross sections. This is indicated by the fact[23] that at Bev energies Be^7 is

[22] W. S. Lyon, Phys. Rev. 97, 121 (1955).

[23] Hudis, Baker, and Friedlander, Phys. Rev. 95, 612 (1954).

formed in high cross section from heavier target nuclei also, where it can hardly be a spallation residue.

It may be noted that, over the entire energy range, the N^{13} formation cross section is strikingly low compared to the other cross sections. In view of the similarity between C^{11}, N^{13}, O^{15}, and F^{18} as regards their positions relative to β stability and their β-decay energies, these low cross sections for N^{13} are, at first sight, surprising. Following a suggestion by Dr. D. H. Wilkinson, we attribute this apparent anomaly to the fact that all excited states of N^{13} are unstable with respect to heavy-particle emission[24] whereas each of the other nuclides observed has a number of excited states which can be de-excited by gamma emission only.

It is a pleasure to express our gratitude to the Cosmotron operating staff for carrying out the bombardments. Miss G. Vedder and Mrs. N. Hamilton helped with the activity measurements.

[24] F. Ajzenberg and T. Lauritsen, Revs. Modern Phys. **24**, 321 (1952).

PHYSICAL REVIEW VOLUME 99, NUMBER 1 JULY 1, 1955

Elastic Photoproduction of π^0 Mesons from Deuterium*

B. WOLFE,† A. SILVERMAN, AND J. W. DEWIRE
Laboratory of Nuclear Studies, Cornell University, Ithaca, New York
(Received January 12, 1955)

The average differential cross section for the reaction $\gamma+d \rightarrow \pi^0+d$ has been measured for photons between 250 and 300 Mev at four angles. A difference measurement with deutero-paraffin and normal paraffin targets was employed. The recoil deuterons were detected by a counter telescope which discriminated against protons by recording the product of the energy and the specific ionization loss of the particles. The reaction was further identified by demanding a coincidence between the deuteron pulse and a pulse from a photon counter placed at an angle corresponding to the direction of the π^0. The values of the differential cross section for various angles of the π^0 in the laboratory system are as follows:

$\theta(\pi^0)$	$d\sigma/d\Omega$ (10^{-30} cm²/steradian)	$\theta(\pi^0)$	$d\sigma/d\Omega$ (10^{-30} cm²/steradian)
76°	4.2±0.6	110°	2.5±0.4
93°	3.2±0.5	130°	1.2±0.3

The stated errors are the standard statistical errors and apply to the relative cross sections at the various angles. The absolute cross-section scale is subject to an experimental error of 25 percent. The measured cross sections are in agreement with theoretical calculations based on the impulse approximation, with the assumption of equal amplitudes for π^0 production from the proton and neutron and constructive interference.

INTRODUCTION

NEUTRAL pi mesons can be produced by the photon bombardment of deuterium in either of two reactions, the elastic process

$$\gamma+d=\pi^0+d$$

in which the deuteron recoils as a unit, and the inelastic process

$$\gamma+d=\pi^0+p+n$$

in which the deuteron is broken up into its component nucleons. A study of these two reactions together with a knowledge of the π^0 production from hydrogen,

$$\gamma+p=\pi^0+p,$$

can lead to information about the relative properties of the photoproduction from protons and neutrons.

An exact theoretical calculation of meson photoproduction from deuterium is beyond the scope of present-day physics although some approximate calculations based on simplified meson theories have been made.[1,2] To simplify the problem, one can make use of the impulse approximation, which states that meson production in a nucleus may be treated as the sum of interactions with the individual nucleons.[3–6] By using this method it has been shown[5] that the cross section for the elastic production of a π^0 meson with a deuteron recoil of momentum D may be written, neglecting spin effects, as

$$\sigma_{el}=|A_n+A_p|^2\left(\int\psi_0^2\exp(\tfrac{1}{2}i\mathbf{D}\cdot\mathbf{R})d\mathbf{R}\right)^2, \quad (1)$$

where A_n is the amplitude for π^0 production from the neutron, A_p is the amplitude for π^0 production from the proton, $\psi_0(R)$ is the ground-state deuteron wave function, and $\mathbf{R}$ is the relative coordinate between neutron and proton. The quantity

$$\left|\int\psi_0^2\exp(\tfrac{1}{2}i\mathbf{D}\cdot\mathbf{R})d\mathbf{R}\right|^2$$

can be interpreted as the probability that the deuteron will stick together if one of the nucleons is given an impulse D. In the same notation, the cross section of a

* Assisted by the joint program of the Office of Naval Research and the U. S. Atomic Energy Commission.
† Now at Eastman Kodak Company, Rochester, New York.
[1] Heckrotte, Henrich, and Lepore, Phys. Rev. **85**, 490 (1952).
[2] N. C. Francis and R. E. Marshak, Phys. Rev. **85**, 496 (1952).
[3] G. F. Chew, Phys. Rev. **80**, 196 (1950).
[4] M. Lax and H. Feshbach, Phys. Rev. **81**, 189 (1951).
[5] G. F. Chew and H. W. Lewis, Phys. Rev. **84**, 779 (1951).
[6] M. Lax and H. Feshbach, Phys. Rev. **88**, 509 (1951).

free proton is given by

$$\sigma_p = A_p^2.$$

The total cross section from deuterium (elastic plus inelastic) is given by

$$\sigma_d = A_n^2 + A_p^2 + 2 \operatorname{Re} A_n^* A_p \int \psi_0^2 \exp(i\mathbf{D}\cdot\mathbf{R}) d\mathbf{R}. \quad (2)$$

The last term of (2) is small except at threshold or for forward angles of π^0 production. For other cases the ratio σ_d/σ_p is a measured of the relative size of A_n and A_p. This ratio has been measured by Cocconi and Silverman[7] and by Andre[8] who find values of σ_d/σ_p close to 2 over a wide range of angle and energy. This result implies that $A_n^2 = A_p^2$. Adopting this equality and referring to (1), one can readily see that the elastic cross section is extremely sensitive to the relative phase of A_n and A_p. If $A_n = A_p$ (constructive interference) σ_{el} is relatively large but if $A_n = -A_p$ (destructive interference) σ_{el} is zero, in the aforementioned approximation.

To be more precise, the experiments show that A_n and A_p do not differ by more than 25 percent. If we assume this difference, then the elastic cross section can vary by a factor of 32 depending on whether one assumes constructive or destructive interference. Since this ratio is so large, it is apparent that an experimental measurement of the cross section of the elastic process should clearly distinguish between constructive and destructive interference.

EXPERIMENTAL PROCEDURE

1. Counter Geometry

The process $\gamma + d = \pi^0 + d$ is an elastic process in the sense that there are only two bodies involved at any one time. Therefore a measurement of the energy and angle of emission of one of the products completely determines the energy and angle of the other product and the energy of the photon that initiates the event. In this experiment the angle and energy of the recoil deuteron were measured. The target was deuterated paraffin 2 mm thick and the background count was observed from a normal paraffin target of the same chemical composition. In order to reduce this background, the process was further identified by demanding a coincidence between the deuteron counter and a photon counter placed in the direction of emission of the π^0. Figure 1 shows the experimental geometry for the case of π^0 emission at 110° and recoil deuteron at 28° to the direction of the incoming photon.[9]

The photon beam intensity was monitored by a thick-wall ionization chamber which had been calibrated

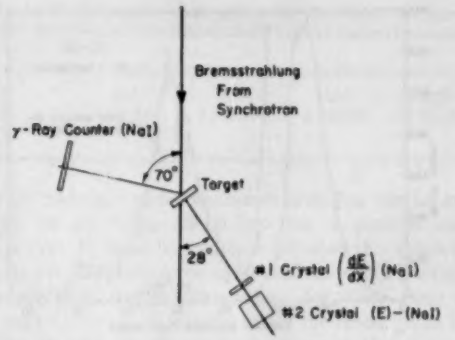

FIG. 1. Experimental arrangement showing γ-ray beam, target, deuteron detector and γ-ray counter. There is a $\frac{1}{4}$-in. Pb converter between the target and γ-ray detector (not shown).

previously[10] in terms of effective quanta in the bremsstrahlung spectrum.[11] The current from the monitor chamber was integrated electronically[12] to give the number of effective quanta accumulated during a run. From the measured spectrum[10] the number of incident photons could be computed.

The efficiency of the photon counter was kept constant throughout the experiment at each of the four angles studied. However, its absolute efficiency was not known, so that the measurements gave only the relative cross sections at each angle. To obtain the absolute cross section the measurement was repeated at one angle without the requirement of a photon coincidence. Recoil deuterons alone were detected and it was assumed that all deuterons of the required energy and angle in the $DC_2 - CH_2$ difference came from π^0 production.

2. Deuteron Detector

The deuteron counter telescope had to be capable of identifying deuterons against a proton background which sometimes exceeded the deuteron rate by a factor of ten. This was done by using a scintillation counter telescope consisting of a thin sodium iodide counter to measure the energy loss dE/dx of the particle and a thick sodium iodide counter in which the particle stopped and gave a pulse proportional to its energy E. The pulse heights in the two counters were multiplied electronically, the product EdE/dx being approximately proportional to $M^{0.8}Z^2E^{0.2}$, where M and Z are the mass and charge of the particle. Such a pulse spectrum would be expected to give good separation between protons and deuterons. This technique is described in

[7] G. Cocconi and A. Silverman, Phys. Rev. **88**, 1230 (1952).
[8] C. C. Andre, University of California Radiation Laboratory Report 2425, November, 1953 (unpublished).
[9] All angles in this article refer to the laboratory frame.
[10] Corson, DeWire, McDaniel, and Wilson, *The Cornell 300-Mev Synchrotron* (Cornell University Press, Ithaca, 1953).
[11] The number of effective quanta Q is related to the spectrum $N(W)$ by $QW_0 = \int_0^{W_0} WN(W)dW$, where W_0 is the maximum energy of the spectrum.
[12] R. M. Littauer, Rev. Sci. Instr. **25**, 148 (1954).

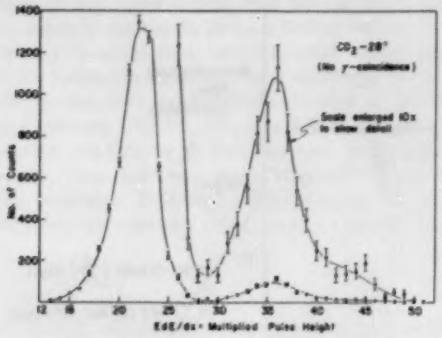

FIG. 2. The product (EdE/dx) pulse-height distribution from a deutero-paraffin target. No γ-ray coincidence was required. The peak at smaller pulse heights is due to protons and the one at larger pulse heights to deuterons. The calculated ratio of the two pulse heights is 1.7 and equals the measured ratio within the experimental error. There is some evidence for a triton group at the large pulse-height side of the deuteron distribution.

detail elsewhere,[18] and hence no further details will be given here.

The particle resolution of the deuteron counter is illustrated in Fig. 2 where the pulse-height spectrum from a deutero-paraffin target is shown. No photon coincidence was required in this run. In the measurements involving a coincidence with a photon the proton-deuteron separation was not so marked; an error of 10 percent was incurred in determining the number of deuteron counts in the spectrum. This error is included in the final errors in cross section.

At each angular setting the energy limits on the deuteron counter were adjusted to accept deuterons from bombarding photons of energies between 250 and 300 Mev. This was done by setting upper and lower biases on the energy pulse from the large crystal. The energy scale was established by observing the maximum pulse height obtained from the crystal exposed to protons, using the known thickness of the crystal and its corresponding proton energy.

Figure 3 shows the calculated effective bombarding photon spectrum at each angle where the experiment was performed. The ordinates are proportional to the product of the photon flux and the effective target thickness; hence the integrals under the curves are proportional to the number of incident photons per effective quantum multiplied by the number of target deuterons from which detectable events arise.

3. π^0 Detector

The emission of a π^0 meson was observed by counting one of the decay photons in a photon counter placed in the direction of emission of the π^0. The counter consisted of a one-cm thick NaI crystal preceded by a $\frac{1}{4}$-inch Pb converter and a 2-inch carbon plate to absorbe low-energy charged particles. The crystal was 10 cm in diameter. The associated electronic circuit was biased so that a particle was required to lose 3 Mev in the crystal to be recorded.

The kinematics of the elastic process are such that the angle of emission of the π^0 is determined almost completely by the angle of the deuteron, independent of energy over a rather large range. Because of the relativistic contraction in the π^0 decay process, the efficiency of the π^0 counter is enhanced when it is placed directly in the path of the high-energy π^0.

Even though the photon counter provides no data on the kinematics of the π^0 production process, its use presents two advantages: (1) The reaction is more clearly defined. (2) The recoil deuterons from the carbon in the targets are nearly entirely eliminated. This provides a considerable improvement in the statistics of subtracting the count from the normal paraffin target.

On the other hand, the use of the photon counter involves the distinct disadvantage that it is very difficult to measure its absolute efficiency for counting π^0 mesons. This efficiency is the product of two factors, the first being the probability that at least one of the decay photons strikes the counter, the second the probability that a photon striking the counter will be counted. The first factor was calculated directly from the kinematics of the π^0 decay and varied from 0.59 at 76° for the π^0 to 0.40 at 130°. The second factor, the so-called intrinsic efficiency, cannot be computed with any confidence and requires a rather elaborate pro-

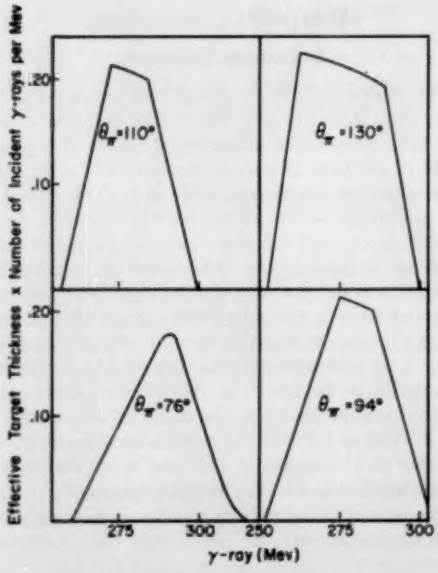

FIG. 3. Effective incident photon spectrum at each angle. The ordinates are proportional to the photon flux and effective target thickness. The integrals under the curve yield the quantity (Ni) used in the calculation of the absolute cross section (see text).

[18] Wolfe, Silverman, and DeWire, Rev. Sci. Instr. (to be published).

cedure to measure it. Instead of this factor was determined, and the absolute cross section scale established, by repeating the run at 110° for the π^0 without the photon counter. The ratio of the difference counting rates divided by the computed first factor then gives the value of the intrinsic efficiency. This procedure implies that all the deuterons in the correct energy range in the D-paraffin, H-paraffin difference come from the elastic π^0 production. The intrinsic efficiency was found to be 0.78±0.18. This value is consistent with the efficiency of a similar counter used by Silverman and Stearns[14] in measuring the photoproduction of π^0 mesons from hydrogen. Its efficiency was determined by using the 170-Mev monoenergetic photons from the Cornell synchrotron.[15]

EXPERIMENTAL RESULTS

1. Calculation of the Cross Section

At each angle the value of the differential cross section was computed from the experimental data using the following formula:

$$\left.\frac{d\sigma}{d\Omega}\right|_{\pi^0} = \frac{C d\Omega_D/d\Omega_{\pi^0}}{\Delta\Omega_D (Nt)\epsilon f},$$

where $d\sigma/d\Omega|_{\pi^0}$ is the cross section per steradian in the lab system; C is the number of counts in the D-paraffin, H-paraffin difference per 10^{11} effective quanta; $\Delta\Omega_D$ is the solid angle subtended by the deuteron counter; $d\Omega_D/d\Omega_{\pi^0}$ is computed from the tables of Malmberg and Koester,[16] (Nt) is the product of the number of incoming photons per 10^{11} effective quanta and the effective thickness of the target in deuterons per cm²—it is found from the integrals of the curves in Fig. 3 and the monitor reading; ϵ is the intrinsic efficiency, measured to be 0.78; and f is the probability that a π^0 decay photon strikes the photon counter. Numerical values used in this formula are given in Table I.

2. Values of the Cross Section

The differential cross sections measured in this experiment are given in Table II. The quoted errors are the standard statistical errors including the uncertainty in separating the pulses due to protons and deuterons. It must be remembered that the absolute values are all based on the additional run at $\theta(\pi^0)=110°$ taken without the photon counter, for which there is an uncertainty of 25 percent. Thus the errors given in Table II refer to the relative values at the various angles and there is an additional 25 percent uncertainty in the absolute cross section scale.

TABLE I. Numerical data used in computing the cross section. The various terms are discussed in the text. The number of counts C and the product (Nt) are normalized to 10^{11} effective quanta.

Deuteron angle	42.5°	35°	28°	20°
Photon counter angle	76°	97°	106°	128°
$\Delta\Omega_D$(sterad)	0.00087	0.00089	0.00089	0.00112
C	7.5±0.8	8.1±0.8	5.8±0.7	3.9±0.8
f	0.59	0.56	0.53	0.42
$d\Omega_D/d\Omega_{\pi^0}$	0.296	0.245	0.209	0.184
(Nt) $(10^{23}$ cm$^{-2})$	1.38	1.67	1.36	1.78

TABLE II. Differential cross section for the elastic photoproduction of π^0 mesons from deuterium for various angles of emission of the π^0.

$\theta(\pi^0)$	76°	93°	110°	130°
$d\sigma/d\Omega|_{\pi^0}$ $(10^{-30}$ cm$^2)$	4.2±0.6	3.2±0.5	2.5±0.4	1.2±0.3

3. Auxiliary Measurements

A number of additional experiments were performed to test the assumption that the recorded counts actually came from the elastic π^0 production process. These were:

(*a*) Preliminary measurements were made with targets of D_2O and H_2O 0.5 cm thick. The results were in agreement with those quoted above. At 115° for the π^0 (30° for the deuteron) the cross section was observed to be 2.4 microbarns per steradian with an uncertainty of about 30 percent.

(*b*) Using the water targets and the same biases as in (*a*), the deuteron counter was moved from 30° to 60°. At this angle no deuterons could be expected from the elastic production. The D_2O rate at 30° was 44±4 events per 10^{11} effective quanta while the rate at 60° was 5±2. The H_2O rate at 30° was 12±2.

(*c*) At the 30° position a one-cm carbon absorber was placed in front of the telescope. Such an absorber is just sufficient to exclude a deuteron from the elastic process from the energy acceptance interval of the counter. The D_2O-H_2O difference rate without absorber was 18±2 per 10^{11} effective quanta. The D_2O rate with absorber was 2.4±1.4.

(*d*) With the deuteron counter at 30°, the synchrotron energy was reduced from 315 Mev to 250 Mev. At this energy no deuteron with sufficient energy to be recorded should be produced. When this was done the difference counting rate dropped from 18±2 to 0.5±2 counts per 10^{11} effective quanta.

Measurement (*d*) gives an indication of the possible contribution of the deuteron Compton effect ($\gamma+d=\gamma+d$) to our experiment. This process would record in our counting system in a similar way to the elastic π^0 production. If indeed we had been measuring only the Compton process at the higher energy then it is estimated that the counting rate at 250 Mev would have been about 7 per 10^{11} effective quanta. This estimate is made on the basis of a constant Compton cross section between 210 and 280 Mev.

[14] A. Silverman and M. Stearns, Phys. Rev. **88**, 1225 (1952).
[15] J. W. Weil and B. D. McDaniel, Phys. Rev. **86**, 582 (1952).
[16] J. H. Malmberg and L. J. Koester, Jr., *Tables of Nuclear Reaction Kinematics at Relativistic Energies* (Physics Department, University of Illinois, Urbana).

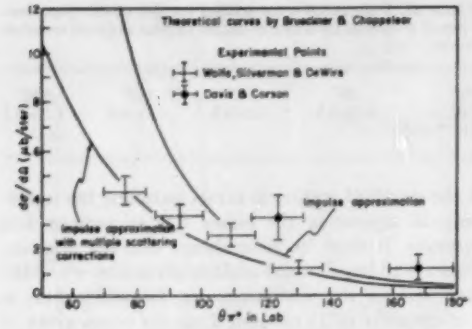

FIG. 4. Experimental results together with those of Davis and Corson. The solid curves are calculated by Brueckner and Chappelear using the impulse approximation with and without multiple scattering corrections.

Ernstene, Keck, and Tollestrup[17] have performed an experiment to measure the deuteron Compton effect. Their results, when applied to our experiment, indicate that the Compton effect is probably less than 15 percent of the elastic production.

DISCUSSION OF RESULTS

Our experimental results are plotted in Fig. 4. The curves are the results of calculations of Brueckner and Chappelear.[18,19] The upper curve is the result from the impulse approximation if one assumes a $2+3\sin^2\theta$ center-of-mass distribution of π^0 mesons from free protons and constructive interference, $A_n=A_p$. The lower curve is based on a modification of the impulse approximation which takes into account the scattering of the outgoing π^0 by the other nucleon of the deuteron.[20] The experimental points fit the corrected curve better, although except for the point at 76° the data are compatible with either curve.

There is some uncertainty in the theoretical curve at large π^0 angles where the deuteron comes off with high energy. The probability that the deuteron comes off bound is then dependent on the high-momentum components in the deuteron wave function, which are not too accurately known. Other uncertainties in the theoretical curves arise from a lack of knowledge of the relative magnitude of the spin flip and non-spin flip processes in π^0 production, and to the lack of precise information on the values of A_n and A_p. In view of these uncertainties, the excellent agreement between theory and experiment may be fortuitous. However the experimental results do rule out the possibility that the interference between neutron and proton waves is destructive, for this would give cross sections of the order of 1/30 the measured cross section or less. On the other hand, the experiment is not sufficiently sensitive to point definitely to constructive interference. For instance, a phase difference of 90° between A_n and A_p would lead to cross sections only a factor of two below the measured values. More reliable comparison with the impulse approximation could be made if the experimental cross sections were known in the forward direction since the recoil momentum of the deuteron is low and the form factor can be calculated more reliably. However, measurements in this region would have required a thinner target and the counting rates were very low. Further, the detection of deuterons of very low energy becomes difficult by this method since the first crystal must be made thin compared with the range of the deuteron.

Two other experimental results[8,21] confirm the main conclusion of this paper. Davis and Corson[21] have measured the elastic π^0 production from deuterium by detecting recoil deuterons in photographic plates after magnetic analysis. Their results are shown in Fig. 4 and are seen to be in reasonable agreement with the results of this paper. Andre[8] has measured the ratio of the total cross sections (elastic+inelastic) for hydrogen and deuterium near threshold. His measured ratio at 90° laboratory angle is

$$\frac{(d\sigma/d\Omega)_D}{(d\sigma/d\Omega)_H}=4.2\pm1.3.$$

From Eq. (2) one finds that the calculated ratio is 3.2 for constructive interference and 0.8 for destructive interference.

We wish to thank K. A. Brueckner and J. Chappelear for permission to quote their results prior to publication. We are also indebted to R. H. Dalitz for several discussions concerning the theoretical implications of this work.

[17] Ernstene, Keck, and Tollestrup (private communication).
[18] K. A. Brueckner, Phys. Rev. 89, 834 (1953).
[19] K. A. Brueckner and J. Chappelear (private communication).
[20] At the most forward angle the theoretical curves are changed only by a few percent if a $\sin^2\theta$ distribution is used instead of a $2+3\sin^2\theta$ distribution. At 130°, however, the theoretical values decrease by about 35 percent.
[21] H. L. Davis and D. R. Corson, following paper [Phys. Rev. 99, 273 (1955)].

Elastic Photoproduction of π^0 Mesons from Deuterium at 270 Mev*

H. L. Davis† and D. R. Corson
Laboratory of Nuclear Studies, Cornell University, Ithaca, New York

(Received January 12, 1955)

The cross section for the process $\gamma+d\rightarrow\pi^0+d$ has been measured by observing the recoil deuteron. The recoil was first analyzed by a uniform magnetic field and then allowed to pass through a nuclear emulsion. The following values were obtained for the absolute cross section for π^0 production at a photon energy of 270 Mev and π^0 laboratory angles 124° and 168°: $d\sigma/d\Omega(124°)=3.2\pm0.9$ μb/steradian and $d\sigma/d\Omega(168°)=1.3\pm0.5$ μb/steradian. The fact that the cross section is the same order of magnitude as the cross section for the production of π^0's from hydrogen is evidence that constructive interference exists between the π^0 production from the proton and the π^0 production from the neutron. On the basis of approximate theories of meson production from deuterium, a lower limit is deduced for the isotropic part of the angular distribution of π^0's photoproduced from hydrogen.

INTRODUCTION

THE π^0 mesons produced by the interaction of γ rays with deuterium come from two processes:

$$\gamma+d\rightarrow\pi^0+n+p, \quad (1)$$

$$\gamma+d\rightarrow\pi^0+d. \quad (2)$$

As discussed in the previous paper[1] the magnitude of the cross section for process (2) (often referred to as the "elastic" process) should be quite sensitive to the relative phase between the complex amplitudes for π^0 production from the neutron and from the proton. A measurement of the cross section should be able to distinguish between constructive and destructive interference of these amplitudes.

In addition to the information available from the absolute magnitude of the elastic cross section, some information concerning the angular distribution of the π^0 production from hydrogen may be obtained by observing the variation of the deuteron cross section with meson angle. Using the impulse approximation Chew and Lewis[2] have shown that, in the case of elastic production from deuterium, the angular distribution of the π^0 in the center-of-mass system will be proportional to $F(\theta)I^2(d)$. $F(\theta)$ is closely related to the angular distribution for π^0 production from a free proton. In particular, $F(\theta)=2+5\sin^2\theta$ if the free proton distribution is $2+3\sin^2\theta$ (the latter distribution being appropriate for π^0 production in a $J=\frac{3}{2}$ state). $I^2(d)$ is an integral involving only the ground-state wave function of the deuteron and is a function of the recoil deuteron momentum. It represents the probability that the recoiling proton and neutron remain together in the form of a deuteron. By using calculated values of $I^2(d)$, the observed angular variation of the elastic production from deuterium may be related directly to $F(\theta)$, and hence to the angular distribution for production from the free proton.

The absolute cross section of the elastic process has been measured at Cornell University at gamma-ray energies near 270 Mev by two groups using different methods. Both groups used the Cornell 315-Mev synchroton as the source of gamma rays and identified the process of interest by detecting the recoil deuteron. The first group, Wolfe, Silverman, and DeWire,[1] measured the absolute cross section at a meson angle of 110° in the laboratory by detecting the recoil deuteron with a scintillation counter telescope. In addition, they determined the relative cross sections at 130°, 110°, 93°, and 76° by observing one of the decay gamma rays of the π^0 meson in coincidence with the recoil deuteron. Their experiment is described in detail in the preceding paper.[1] The second method of measuring the cross section is the subject of this paper. In this method, the recoil deuterons were first analyzed by a uniform magnetic field and then detected by a nuclear emulsion. The absolute cross section was determined at deuteron recoil angles of 4° and 22° in the laboratory, corresponding to meson laboratory angles of 168° and 124°.

EXPERIMENTAL METHOD

The deuterium target consisted of a thin piece (0.37 g/cm^2) of heavy paraffin (CD_2). The effect of the carbon was subtracted by measurement of the recoil deuterons from a pure carbon target.

The momentum and angle of emission of the recoils were determined by the arrangement shown in Fig. 1. The experimental target and emulsion were situated in a uniform magnetic field of 18.2 kilogauss. The deuteron recoils produced in the target by the gamma-ray beam traversed a 40° arc before passing through a 200-micron nuclear emulsion inclined at an angle of 45° with the horizontal plane of the experimental system. Measurements on the track of a given recoil determined (1) the position at which the recoil entered the emulsion and (2) the horizontal incident angle of the recoil trajectory. For a recoil issuing from a point target these two observations uniquely determine both the momentum

* Supported by the joint program of the Office of Naval Research and the U. S. Atomic Energy Commission.

† Now at Pratt and Whitney Aircraft Company, East Hartford, Connecticut.

[1] Wolfe, Silverman, and DeWire, preceding paper [Phys. Rev. 99, 268 (1955)].

[2] G. F. Chew and H. W. Lewis, Phys. Rev. 84, 779 (1951).

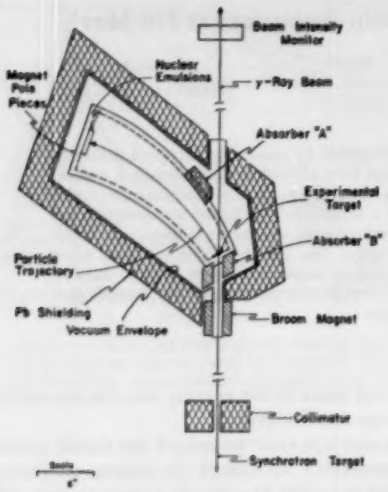

FIG. 1. Experimental arrangement (top view), showing γ-ray beam, target, magnet poles and nuclear emulsion detector. Target, recoil particle path, and emulsion are all inside a vacuum chamber maintained at fore-pump pressure.

and the angle of emission of the recoil. We assume that the deuteron recoils from the deuterium were all produced by the process $\gamma+d\rightarrow\pi^0+d$. Since this is a two-body interaction, the recoil momentum and emission angle determine the energy and angle of the π^0 and the energy of the incident photon. In Fig. 2, the deuteron energy is shown as a function of laboratory angle for an incident photon of 270 Mev. Actually, the finite size of the target introduces an uncertainty in the momentum and emission angle associated with a given track in the emulsion. The uncertainty in momentum was about ± 5 percent and the uncertainty in angle of emission was $\pm 2°$.

The assumption concerning the identity of the recoils presupposes that (1) no other process produces deuteron recoils from deuterium in a significant quantity and (2) that the recoil particles which are not deuterons may be distinguished from the recoil deuterons. With regard to (1), at the gamma-ray energies we are dealing with, the only competing process to be considered seriously is the nuclear Compton effect: $\gamma+d\rightarrow\gamma'+d$. The absolute cross section for this process has not yet been measured; however, Ernstene, Keck and Tollestrup[3] have performed an experiment which sets an upper limit on this cross section. They suggest that the yield of recoil deuterons from the Compton effect is not more than a few percent of the yield from the elastic process at a deuteron laboratory angle of 50°. Even if one assumes a pessimistic angular distribution for the Compton cross section (i.e., one containing a large $\cos^2\theta$ term), their result places an upper limit for Compton effect contribution to our total yield of 4 percent and 10 percent at the 124° and 168° points, respectively.

Concerning (2), at the gamma-ray energies of interest, protons are the only other charged particles which can be photoproduced from deuterium with sufficient momentum to be observed in our system. Tracks made by protons and deuterons of the same momentum were easily separated because their grain densities differ by a factor of three. For this purpose Ilford C2 emulsions have a convenient sensitivity. In the momentum interval of interest, protons have energies greater than 50 Mev while deuterons have energies between 30 Mev and 60 Mev. In C2 emulsions the maximum energy which a particle can have and still produce an observable track is about 50 Mev for protons and about 100 Mev for deuterons. Therefore, in the selected momentum interval, proton tracks were nearly invisible while deuteron tracks were easily recognized. Figure 3 shows tracks of different particles all having the same $H\rho$.

Heavier particles, such as tritons or alpha particles, can be produced only in the carbon and therefore subtract out in the CD_2-C difference.

In order to obtain a valid CD_2-C difference, it is necessary that the scanning efficiency be the same for both the CD_2 and the C tracks. This condition was insured by using the same emulsion to detect the recoils from both targets. The tracks caused by recoils from one target were made distinct from the tracks belonging to the other target by rotating the emulsion plane 180° about its perpendicular axis when the targets were changed. Under the microscope the scanner sees the tracks from one target travel up the field of view and the tracks from the other target travel down the field of view as he racks down into the emulsion. Since both sets of tracks occur in the same block of emulsion and are scanned simultaneously, there should be no difference in scanning efficiency. Simultaneous scanning also reduces the total scanning time.

Other essential features of the experimental arrange-

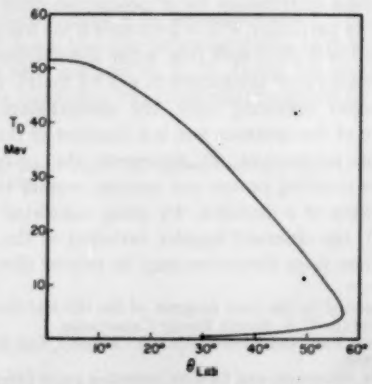

FIG. 2. Deuteron recoil energy as a function of laboratory angle for "elastic" processes produced by a 270-Mev γ ray.

[3] Ernstene, Keck, and Tollestrup (private communication).

ment shown in Fig. 1 are the absorber A, the clearing magnet, and the vacuum envelope. Absorber A prevents particles from traveling from target to emulsion through the fringe field. The clearing magnet sweeps charged particles from the beam before they reach the experimental target, thereby considerably reducing the electron background in the emulsion. The vacuum envelope allows one to evacuate to forepump pressure the entire target-plate system as well as a part of the synchrotron beam path on either side of the target. The removal of the air reduces the background and is mandatory at the 4° position where electrons produced from the air behind the target may reach the emulsion.

Auxiliary experiments were performed to determine the no-target background and the amount of scattering-in. The no-target background was observed directly by exposing an emulsion in the usual experimental arrangement without the experimental target in position. No tracks which had acceptable values of incident angle and track length were found in this emulsion. Consequently an upper limit of 5 percent may be placed on the no-target background contribution to the total yield from the CD_2 target. In taking the difference between the CD_2 and C yields, the no-target background should subtract out, so no significant error is anticipated from this source.

Deuterons coming from the target may scatter from the polefaces of the magnet and strike the emulsion. Since the solid angle subtended at the target by the magnet polefaces is much larger than that subtended by the emulsion it seemed possible that the scattering-in from the polefaces might produce a serious error in the experiment. The scattering-in was observed directly by placing an absorber between the target and the emulsion in such a way that the emulsion was shielded from the target but both target and emulsion still had an unobstructed view of the poleface area. Thus, any particles which originated in the target and still reached the emulsion must have been scattered from the polefaces or other adjacent material. The number of such tracks was small enough to place an upper limit of 7 percent on the contribution of scattered-in tracks to the total number of CD_2-C difference tracks. In addition, about half of the exposures were made with "antiscattering-in" baffles on the polefaces. These baffles prevented scattering-in from a significant fraction of the poleface area. The results with and without the baffles in place were found to agree within the statistical uncertainty, confirming our direct observation that the scattering-in was not a large effect.

COLLECTION AND EVALUATION OF THE DATA

The scanners recorded only those tracks (about 3300 total were finally acceptable) with incident horizontal angles corresponding to momenta falling within limits set by the selected gamma ray energy interval. (At both emission angles the effective gamma energy interval was chosen to be 270±30 Mev. The deuteron recoils

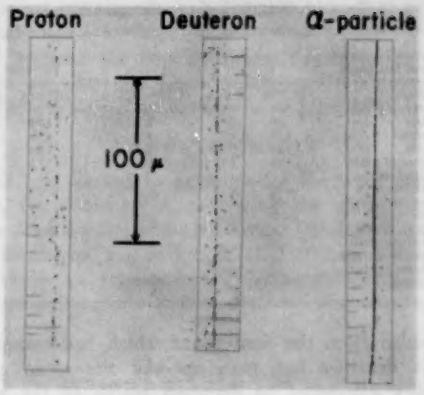

FIG. 3 Examples of proton, deuteron, and α-particle tracks all having the same momentum near the minimum of the acceptable momentum interval when they enter the emulsion at the top.

produced by these gamma rays via the elastic π^0 process had energies 40±10 Mev at 22°±4° and 50±10 Mev at 4°±4° in the laboratory.) The following information was recorded for each acceptable track: (1) α', the projection of the horizontal incident angle on the emulsion plane, (2) the xy coordinates of the track at the air surface, (3) the direction of travel of the track in the field of view, (4) the estimated gain density, and (5) Δy, the y component of the projected track length on the emulsion plane. The measurement of α' for a given track had a random uncertainty of ±1° (the total interval of acceptance was about 10° wide). The systematic error in the measurement of α', however, was not greater than 0.2°. Δy and the xy coordinates were determined with negligible uncertainty. The estimated grain density assigned to each track was subject to an estimated 30 percent total uncertainty. Coincidence scanning indicated that the absolute scanning efficiency was better than 95 percent.

The distribution of the values of Δy and the estimated grain densities were investigated for the two groups of tracks obtained from each emulsion. The Δy distribution agreed in each instance with that expected for tracks made by recoils traveling directly from the target to the emulsion. The estimated grain densities were plotted as a function of the angle α', the plots showing the expected decrease in grain density with increasing momentum. The grain densities of tracks from CD_2 and tracks from C corresponding to the same momentum were found to be the same. The absolute values of the grain densities were in good agreement with grain densities of tracks known to be made by deuterons of the same energy. (The latter tracks were observed in 400μ emulsions exposed in the same experimental arrangement but at a dip angle of 5°. Since it was possible to observe both momentum and range the particle mass could be determined.) All tracks were

TABLE I. Summary of experimental data.

Deuteron lab angle	22°			4°	
Meson lab angle	124°			168°	
Emulsion No.	2C140	2C124	2C104–2C110	2C132A	2C145
Uncorrected N_D	126	695	433	236	415
totals N_C	89	301	296	183	343
Corrected N_D'	126	693	453	236	433
totals N_C'	88	500	290	183	345
Differences ΔN	38	193	163	53	88
Standard deviation of differences	±15	±35	±27	±20	±28
Normalized ΔN^*	67	80	95	37	44
differences	±26	±14	±16	±14	±14
$d\sigma/d\Omega$ at 270 Mev (cm² per steradian per incident photon per target nucleus)		$(3.2\pm0.9)\times10^{-30}$		$(1.3\pm0.5)\times10^{-30}$	

excluded from the final count which had estimated grain densities less than one-half the mean grain density attributed to deuteron tracks at the same incident angle. Since, for the same momentum, the grain density of proton tracks is only one-third that of deuteron tracks and since the estimated grain densities are accurate to within 30 percent, this selection procedure insured that all the deuterons and none of the protons were included in the final count.

Before the CD_2-C subtraction was performed some small corrections were applied to the total number of tracks N_D from the heavy paraffin, and to the total number of tracks N_C from the carbon. The corrections adjusted for errors arising from (1) the difference in energy loss of the recoils in the CD_2 and C targets, (2) a small difference in the amount of carbon in the two targets, and (3) any difference existing in angle of inclination of the emulsion during the CD_2 and C target runs. These corrections were never more than 5 percent each and, since they tend to cancel, the total correction was even less. In Table I the original totals N_D and N_C, the corrected totals N_D' and N_C' and the difference $\Delta N=N_D'-N_C'$ are shown for the various emulsions scanned. The differences ΔN^* are the ΔN's normalized to correspond to the same emulsion area and synchrotron exposure. ΔN^*, therefore, should be the same for all the emulsions at the same deuteron recoil angle. The ΔN^*'s were averaged at each of the two major angles to give the final cross sections shown in Table I. The uncertainties indicated in the final results represent the standard deviation of the total experimental uncertainty. The various contributions to the total uncertainty are shown in Table II. The ratio of the cross section at the two angles is independent of the uncertainties in synchrotron energy, the standard ion chamber calibration, and the number of target nuclei per cm³. The value of the ratio with its standard deviation is $R(168°/124°)=0.41\pm0.12$.

TABLE II. Contributions to total experimental error.

Source	Percent uncertainty in final cross section 124°	168°
Statistical	12	24
No. of photons	9	9
No. of target nuclei	5	5
Solid angle	2	2

Our results and those of Wolfe *et al.*[1] are compared in Fig. 4 of the preceding paper with the theoretical curves calculated by Brueckner and Chappelear for the elastic π^0 process. The calculations assume constructive interference and a $(2+3\sin^2\theta)$ distribution in the center-of-mass system. The upper curve was calculated by using the impulse approximation; the lower curve was obtained in the same way except that corrections arising from the multiple scattering of the π^0 by the nucleon system were taken into account. It is apparent that both experiments are compatible with the theoretical angular distribution. Our absolute values are considerably higher than the theoretical curves and higher than Wolfe, Silverman, and DeWire's experimental values. However, in view of the uncertainties of both measurements and of the calculations as well, no particular significance should be attached to this apparent disagreement.

CONCLUSIONS

Two pieces of information are obtained from the experiment: (1) the order of magnitude of the absolute value of the cross section and (2) the ratio of the cross sections at 124° and 168°. Our result for (1) is in agreement with that found by Wolfe *et al.*, and we confirm their conclusion that the interference is constructive for elastic π^0 production near 300 Mev.[4]

Result (2), the ratio of the cross sections at 124° and 168° is, as we have pointed out, related to the angular distribution of the π^0 production from hydrogen. If this latter distribution is represented by $G(\theta)$, then in the impulse approximation the angular distribution for the elastic production from deuterium at a given γ-ray energy has the form $(d\sigma/d\Omega)\sim F(\theta)I^2(\theta)$, where $F(\theta)$ is closely related to $G(\theta)$ but with a relatively smaller isotropic part, and $I^2(\theta)$ is the probability that the deuteron remains bound after the π^0 production. Accepting this qualitative picture of the process, and taking $G(\theta)=a+b\sin^2\theta$, we may use our data to set a lower limit on a/b, the relative isotropic part of the angular distribution for π^0's photoproduced from the free proton, by the following arguments:

(1) The deuteron is less likely to remain bound when it recoils with higher momentum, i.e., when it goes more forward and the meson goes more backward (168°). So without using any detailed calculation of $I^2(\theta)$ we can safely say that $I^2(168°)\leq I^2(124°)$, and we will use the extreme value $I^2(168°)=I^2(124°)$ leading to a minimum a/b in our limit calculation.

(2) The effect of scattering by the "spectator" nucleon is not known for sure, but the qualitative features of the calculation by Brueckner and Chappelear[5]

[4] C. C. Andre [University of California Radiation Laboratory Report No. 2425, 1953 (unpublished)] also found constructive interference for the elastic cross section near threshold at 150 Mev.

[5] See the preceding paper for discussion of the theoretical curves [Wolfe, Silverman, and DeWire, Phys. Rev. 99, 268 (1955)].

show that, in the laboratory angle interval of interest, the primary effect is to suppress the cross section and not to change the angular distribution. Consequently we ignore the effect of such scattering in calculating a minimum a/b.

(3) The isotropic part of the free proton angular distribution will, if anything, be larger than the isotropic part of the elastic deuteron angular distribution (before modification by the deuteron form factor). Again we take the extreme case of no difference in the two distributions in calculating a lower limit for a/b.

On the basis of these arguments, and using our measured cross-section ratio $R(168°/124°)=0.41\pm0.12$, we calculate $a/b\geq 0.35^{+0.23}_{-0.08}$.

If we take the impulse approximation at its face value, use Chew and Lewis[2] values for $I^2(\theta)$, and make no scattering corrections, we calculate $a/b=0.80^{+0.70}_{-0.25}$.

ACKNOWLEDGMENTS

We are pleased to acknowledge the assistance of Mrs. Carol Sienko in processing the emulsions, of Mrs. Jane Loeffler and Mrs. Louise Cahill in scanning the emulsions, and of Dr. R. H. Dalitz in discussing the theoretical implications of the measurement.

PHYSICAL REVIEW VOLUME 99, NUMBER 1 JULY 1, 1955

Energy Distribution of γ Rays from π^0 Decay*

R. M. STERNHEIMER
Brookhaven National Laboratory, Upton, New York
(Received March 7, 1955)

It is shown that the γ-ray energy distribution resulting from the decay of π^0 mesons produced in a target bombarded by a high-energy particle beam is related in a simple manner to the differential π^0 production cross section, for sufficiently high energies of the γ's ($\gtrsim$500 Mev). An expression is obtained for the π^0 production cross section in terms of the γ-ray energy distribution. This result is extended to the case of an arbitrary two-body decay, for which an expression is obtained for the production cross section of the primaries in terms of the energy distribution of the secondaries emitted in the decay.

I. INTRODUCTION

INFORMATION about the π^0 meson production in a target bombarded by a high-energy particle beam can be obtained from a measurement of the energy distribution of the γ rays from the π^0 decay at various angles to the beam. At incident energies in the range of 200–400 Mev,[1] the interpretation of the γ-ray spectrum is very complicated, because at each angle of observation, a wide range of angles of the π^0's is involved. However, with increasing energy of the incident particles and of the resulting γ rays from π^0 production, the maximum possible angle between the observed γ and the decaying π^0 becomes very small, and it can be assumed that the π^0 differential production cross section remains approximately constant over the small range of π^0 angles involved. It will be shown that in this high-energy region (γ energy$\gtrsim$500 Mev), the π^0 cross section can be expressed in a simple manner in terms of the γ-ray energy spectrum. A similar expression will also be obtained for an arbitrary two-body decay for the production cross section of the primaries in terms of the energy distribution of the secondaries which are emitted in the decay.

II. RELATION BETWEEN π^0 PRODUCTION CROSS SECTION AND γ-RAY ENERGY SPECTRUM

The velocity v_π of the π^0 in the laboratory system is related as follows[2] to the laboratory angle ψ between the observed γ and the π^0:

$$\bar{k}=\gamma_\pi k(1-v_\pi\cos\psi), \tag{1}$$

where k is the energy of the γ-ray in the laboratory system, $\bar{k}$ is its energy in the π^0 rest system, and $\gamma_\pi=(1-v_\pi^2)^{-\frac{1}{2}}$. Upon squaring Eq. (1) and solving for v_π, one obtains

$$v_\pi=\frac{k^2\cos\psi\pm\bar{k}(\bar{k}^2-k^2\sin^2\psi)^{\frac{1}{2}}}{k^2\cos^2\psi+\bar{k}^2}. \tag{2}$$

The total energy E_π of π^0 is given by

$$E_\pi=\frac{m_\pi(k^2\cos^2\psi+\bar{k}^2)}{k[\bar{k}\pm\cos\psi(\bar{k}^2-k^2\sin^2\psi)^{\frac{1}{2}}]}, \tag{3}$$

where m_π = mass of π^0. It is seen that for a given ψ, there are in general two values of E_π. Moreover, since the expression under the radical must be positive, ψ is

* Work performed under the auspices of the U. S. Atomic Energy Commission.

[1] See, for example, A. Silverman and M. Stearns, Phys. Rev. **88**, 1225 (1952); G. Cocconi and A. Silverman, Phys. Rev. **88**, 1230 (1952); Goldschmidt-Clermont, Osborne, and Scott, Phys. Rev. **89**, 329 (1953); Phys. Rev. **97**, 188 (1955); Walker, Oakley, and Tollestrup, Phys. Rev. **89**, 1301 (1953); Marshall, Marshall, Nedzel, and Warshaw, Phys. Rev. **88**, 632 (1952); R. H. Hildebrand, Phys. Rev. **89**, 1090 (1953).

[2] It is assumed that the units are such that $c=1$.

$\leqq\psi_{max}$, where ψ_{max} is given by

$$\psi_{max}=\sin^{-1}(\bar{k}/k). \tag{4}$$

ψ_{max} becomes very small at high energies k; thus $\psi_{max}=7.8°$ for $k\approx 500$ Mev, and 3.9°, for $k=1$ Bev. Hence the spectrum of γ rays above $\sim$500 Mev depends only on the production cross-section for π^0 at about the same angle as the angle of observation of the γ rays. This result is not inconsistent with the fact that π^0 mesons of all energies emit some γ rays at large angles to their direction of motion, and even backwards, because these large angle γ's have low energy in the laboratory system ($\lesssim$100 Mev). Equation (4) corresponds to the case in which the γ ray is emitted at right angles to the direction of π^0 in the π^0 rest system. The transverse momentum in the laboratory system is then $\bar{k}$, so that: $\sin\psi=\bar{k}/k$.

Figure 1 shows E_γ *vs* ψ for photon energies $k=200$, 400, 600, and 800 Mev. The lower branch of the curves corresponds to the + sign in Eq. (3); the upper branch corresponds to the − sign. The smallest E_γ is obtained for $\psi=0°$ and is given by

$$E_{\gamma,\min}=k(1+\bar{k}^2/k^2), \tag{5}$$

which approaches k as k is increased. For $\psi=\psi_{max}$, we have $E_\gamma=2k$. The largest E_γ is $E_{\gamma,max}=\infty$, and is obtained for $\psi=0°$ on the upper branch of the curves.

We now obtain an expression for $P(k,\theta_\gamma)$, the number of γ rays per unit energy interval dk and per unit solid angle at an angle θ_γ to the incident beam, in terms of $f(E_\pi,\theta_\pi)$, the differential π^0 production cross section per unit energy interval dE_π and per unit solid angle at an angle θ_π to the beam (see Fig. 2). The number of γ rays in a small energy interval dk can be written

$$P(k,\theta_\gamma)dk=nN\sum\int d\theta_\pi\int d\varphi_\pi f(E_\pi,\theta_\pi)\times\sin\theta_\pi(2/4\pi)JdE_\pi, \tag{6}$$

where n = number of incident particles, N = number of target nuclei per cm², φ_π = azimuthal angle of π^0, $(2/4\pi)$ is the number of γ rays per steradian in the π^0 rest system, and J is the Jacobian for the transformation from the π^0 rest system to the laboratory. In Eq. (6), the integrations extend over the regions of θ_π and φ_π which contribute to the γ intensity at θ_γ (i.e., for which $\psi\leqq\psi_{max}$); dE_π is the interval of E_π corresponding to dk at (θ_π,φ_π); the sum refers to the fact that there are, in general, two such intervals for given values of θ_π and φ_π for which $\psi\leqq\psi_{max}$. Equation (6) can be evaluated more conveniently by using the direction of the γ as the polar axis. We have $J=\partial\cos\bar{\psi}/\partial\cos\psi$, where $\bar{\psi}$ is the angle between π^0 and γ in the π^0 rest system. One obtains

$$P(k,\theta_\gamma)=nN\sum\int_0^{\psi_{max}}f(E_\pi,\theta_\gamma)\frac{\partial E_\pi}{\partial k}\left(\frac{2}{4\pi}\right)\frac{\partial\cos\bar{\psi}}{\partial\cos\psi}\times(2\pi)\sin\psi d\psi. \tag{7}$$

Here $f(E_\pi,\theta_\gamma)$ has been used instead of $f(E_\pi,\theta_\pi)$ on the assumption that ψ_{max} is small enough so that $f(E_\pi,\theta_\pi)$ does not vary appreciably over the range of θ_π. Thus Eq. (7) is valid for $k\gtrsim 500$ Mev (where $\psi_{max}=7.8°$), although it may hold with reasonable accuracy down to $k\sim$200 Mev ($\psi_{max}\sim 20°$). An exception may occur near the forward direction[3] if $f(E_\pi,\theta_\pi)$ near $\theta_\pi=0°$ varies rapidly over a region of angles of the order of ψ_{max}.

In order to obtain $\partial\cos\bar{\psi}/\partial\cos\psi$, we note that

$$\cos\bar{\psi}=(\cos\psi-v_\pi)/(1-v_\pi\cos\psi). \tag{8}$$

Differentiation of (8) gives

$$\frac{\partial\cos\bar{\psi}}{\partial\cos\psi}=\frac{1}{\gamma_\pi^2(1-v_\pi\cos\psi)^2}=\frac{\bar{k}^2}{k^2}. \tag{9}$$

Since ψ and $\bar{k}^2/k^2$ are small, we set $\cos\psi\approx 1$ in Eq. (3) and neglect $\bar{k}^2$ in comparison with k^2, except in the term $\bar{k}^2-k^2\sin^2\psi$. As shown below, the resulting errors

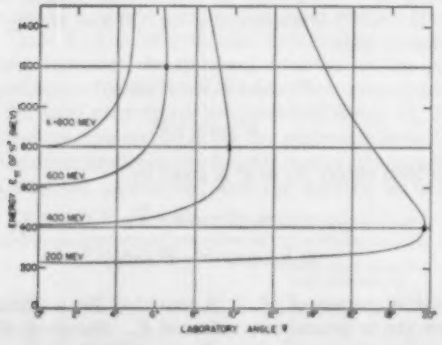

FIG. 1. Total energy E_π of π^0 as a function of the angle ψ between π^0 and γ for various γ energies k. The crosses correspond to the maximum angle ψ_{max}.

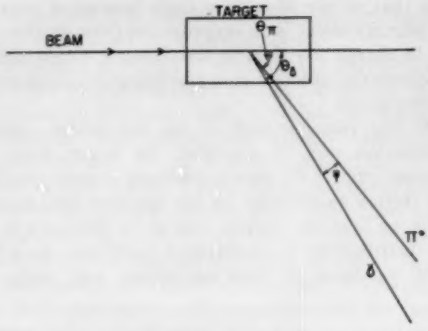

FIG. 2. Relationship between the angles involved in Eqs. (6) and (7). The lines marked π^0 and γ indicate the directions of motion of the π^0 meson and the γ ray.

[3] This possibility was pointed out to the author by Dr. M. H. Ross.

are very small above $k=500$ Mev. Equation (3) becomes

$$E_\pi=\frac{m_\pi k}{\bar{k}\pm(\bar{k}^2-k^2\sin^2\psi)^{\frac{1}{2}}}. \tag{10}$$

From Eq. (10), one finds

$$\sin\psi d\psi=4(\bar{k}^2/E_\pi^3)[1-1/(2x)]dE_\pi, \tag{11}$$

$$\frac{\partial E_\pi}{\partial k}=\frac{1}{x(2x-1)}, \tag{12}$$

where $x=k/E_\pi$. Upon inserting (9), (11), and (12) into (7), one obtains

$$P(k,\theta_\gamma)=2nN\int_k^\infty \frac{f(E_\pi,\theta_\gamma)}{E_\pi}dE_\pi. \tag{13}$$

It may be noted that the integral over ψ of Eq. (7) has been transformed into an integral over E_π by means of (11). Upon differentiating both sides of (13), one obtains

$$\frac{\partial P(k,\theta_\gamma)}{\partial k}=-\frac{2nNf(k,\theta_\gamma)}{k}, \tag{14}$$

which gives

$$f(k,\theta_\gamma)=-\frac{k}{2nN}\frac{\partial P(k,\theta_\gamma)}{\partial k}. \tag{15}$$

Equation (15) gives the production cross section in terms of the number of γ rays observed.[4] We note that the argument (k,θ_γ) of f refers to the energy and angle of the π^0, i.e., the expression for f at a given energy and angle involves $k\partial P/\partial k$ evaluated at the same energy and angle. Equation (15) implies that $\partial P/\partial k<0$ in the region of validity of this equation. This also follows directly from (13), since P is an integral from k to ∞ over a positive function. As mentioned previously, the preceding treatment is valid only for high γ energies ($k\gtrsim 500$ Mev), although it may give a reasonably accurate estimate down to $k\sim 200$ Mev. At still lower energies, it is not legitimate to replace $f(E_\pi,\theta_\pi)$ by $f(E_\pi,\theta_\gamma)$ in Eq. (6). In this case, the γ-ray spectrum involves an integral over the production cross section for a wide range of angles θ_π, and it is probable that a measurement of $P(k,\theta_\gamma)$ at several angles θ_γ would be necessary to determine $f(E_\pi,\theta_\pi)$ for any given θ_π. Moreover, the procedure for solving Eq. (6) for f would then be very complicated.[5]

[4] A similar expression has been obtained by Carlson, Hooper, and King [Phil. Mag. 41, 701 (1950)] for the energy spectrum of π^0 mesons irrespective of angle in terms of the γ-ray spectrum.

[5] For the case of π^0 mesons produced by γ rays in hydrogen, Borsellino has obtained an expression for the energy distribution of the decay γ rays, $P(k,\theta_\gamma)$, on the assumption that the π^0 production cross section in the center-of-mass system of the γ and the proton is proportional to $A\cos\bar{\theta}_\pi+B$, where $\bar{\theta}_\pi$ = center-of-mass angle of π^0 [see G. Cocconi and A. Silverman, Phys. Rev. 88, 1230 (1952)].

In order to test the validity of the approximation made by using Eq. (10) for E_π, the integrand of Eq. (13) was evaluated exactly for $k=400$ Mev and 800 Mev. The exact integrand which replaces $[nNf(E_\pi,\theta_\gamma)]\times(2/E_\pi)$ of Eq. (13) is given by

$$I=[nNf(E_\pi,\theta_\gamma)]\left\{\sin\psi\frac{\partial\psi}{\partial E_\pi}\frac{\partial E_\pi}{\partial k}\frac{k^3}{\bar{k}^3}\right\}. \tag{16}$$

The exact expressions for $\partial E_\pi/\partial k$ and $\partial\psi/\partial E_\pi$ as obtained from Eq. (3) were calculated for the complete range of ψ, and the resulting values of the curly bracket of Eq. (16) were compared with the approximate value $2/E_\pi$. For $k=400$ Mev, $2/E_\pi$ is smaller than the exact value by an amount which decreases from 6 percent to 2 percent as ψ increases from 0° to $\psi_{\max}(=9.7°)$ along the lower branch of the E_π vs ψ curve (corresponding to the range of E_π from 411 Mev to 800 Mev). For the upper branch of the E_π vs ψ curve, the error is of the order of 2 percent. For $k=800$ Mev, the underestimate is $\lesssim 2$ percent for the lower branch of the E_π vs ψ curve. These errors are quite small and of the expected order of magnitude, being somewhat less than m_π^2/k^2.

In Eq. (13), the lower limit of the integral was taken as k. If the exact expression for $E_{\pi,\min}$ [Eq. (5)] is used, one obtains

$$P(k,\theta_\gamma)=2nN\int_{k(1+\bar{k}^2/k^2)}^\infty \frac{f(E_\pi,\theta_\gamma)}{E_\pi}dE_\pi. \tag{17}$$

Differentiation of (17) gives

$$\frac{\partial P(k,\theta_\gamma)}{\partial k}=-2nN\frac{f[k(1+\bar{k}^2/k^2),\theta_\gamma]}{k(1+\bar{k}^2/k^2)}\frac{d}{dk}\left[k\left(1+\frac{\bar{k}^2}{k^2}\right)\right]. \tag{18}$$

Since $\bar{k}^2/k^2\ll 1$, Eq. (18) becomes

$$f[k(1+\bar{k}^2/k^2),\theta_\gamma]=-\left(1+\frac{2\bar{k}^2}{k^2}\right)\frac{k}{2nN}\frac{\partial P(k,\theta_\gamma)}{\partial k}. \tag{19}$$

Upon replacing k by $k(1-\bar{k}^2/k^2)$ on both sides of Eq. (19), one finds

$$f(k,\theta_\gamma)=-\frac{k}{2nN}\left(1+\frac{\bar{k}^2}{k^2}\right)\frac{\partial P[k(1-\bar{k}^2/k^2),\theta_\gamma]}{\partial k}. \tag{20}$$

Equation (20) may be compared with (15). Both the presence of $(1+\bar{k}^2/k^2)$ and the fact that $\partial P/\partial k$ is evaluated at a smaller γ energy $[k(1-\bar{k}^2/k^2)$ instead of $k]$ contribute to increase $f(k,\theta_\gamma)$, since it is expected that $|\partial P/\partial k|$ increases with decreasing k. On the other hand, the underestimate of the integrand of Eq. (13) tends to give a value of f which is too high. Hence the replacement of the exact lower limit $E_{\pi,\min}$ by k is probably compensated to some extent by the use of the approximate integrand in Eq. (13). It can be concluded

that the accuracy of Eq. (15) is of the same order and possibly somewhat better than the maximum errors of 6 percent and 2 percent in the integrand which were found for $k=400$ Mev and 800 Mev, respectively.

Swartz and DeWire[6] have made measurements of the γ-ray spectrum at 90° to the proton beam of the Brookhaven Cosmotron, at proton energies of 1, 2, and 3 Bev. If one assumes a target nucleon Fermi energy of 25 Mev, the cutoff energy of the γ rays is 471, 659, and 766 Mev, respectively, for the three proton energies. The observed spectra[5] at the three energies show a maximum at $\sim$100 Mev and extend up to energies in the range 300–600 Mev. At 100 Mev, $\psi_{\max}=42.5°$, and the above treatment does not apply. However, near the upper end of the spectrum ($k\gtrsim 300$ Mev), Eq. (15) can be used to give an estimate of the π^0 production cross section. For forward angles of observation ($\theta_\gamma\lesssim 45°$), Eq. (15) applies over a wider range of energies, since the cutoff k is then of order 1–3 Bev.

III. EXTENSION TO GENERAL TWO-BODY DECAY

It seems of interest to extend Eq. (15) to the case of an arbitrary two-body decay. The result may be of interest in cases of the decay of unstable particles in which it is easier to detect the secondaries than the primaries. As an example, one may consider the possibility of counter experiments to detect the θ^0 particles, in which the energy distribution of the π^+ and π^- mesons is measured.

We consider secondary particles of total energy[7] E in the laboratory system, which are moving at an angle θ to the incident beam. By a derivation similar to that of Eq. (3), one finds that the laboratory total energy E_p of the primary particle is related as follows to E and to the angle ψ between primary and secondary:

$$E_p=\frac{m_p(p^2\cos^2\psi+\bar{E}^2)}{E\bar{E}\pm p\cos\psi(\bar{p}^2-p^2\sin^2\psi)^{\frac{1}{2}}}, \tag{21}$$

where p=momentum of secondary in laboratory system, m_p=mass of primary particle, $\bar{E}$ and $\bar{p}$ are the (constant) energy and momentum, respectively, of the secondary in the rest system of the primary. Equation (21) shows that ψ must be $\leqq\psi_{\max}$, where

$$\psi_{\max}=\sin^{-1}(\bar{p}/p). \tag{22}$$

E_p is double-valued for $\psi<\psi_{\max}$. These results are similar to those obtained for the π^0 decay [see Eq. (4) and Fig. 1].

The number of secondaries $P(E,\theta)$ per unit energy interval and per steradian is given by

$$P(E,\theta)=2\pi nN\sum\int_0^{\psi_{\max}} f(E_p,\theta_p)\times(\partial E_p/\partial E)(1/4\pi)J\sin\psi d\psi, \tag{23}$$

where $f(E_p,\theta_p)$ is the differential cross section for producing primaries of energy E_p at an angle θ_p to the incident beam; J=Jacobian; the factor (2π) comes from the integration over the azimuthal angle; $(1/4\pi)$ gives the number of decays per steradian in the rest system,[8] and the sum sign indicates summation over the two branches of the E_p vs ψ curve. In the following, it is assumed that E is sufficiently high so that $\psi_{\max}$ is small ($\lesssim 10°$) and $f(E_p,\theta_p)$ can be replaced by $f(E_p,\theta)$, i.e., f can be evaluated at the angle of the secondary. Following the same procedure as in Sec. II, we set $\cos\psi\approx 1$ in Eq. (21), and neglect $\bar{E}^2$ and $\bar{p}^2$ in comparison with E^2 and p^2, except in the term $\bar{p}^2-p^2\sin^2\psi$. In this approximation, the difference between p and E is also neglected. Equation (21) becomes

$$E_p=\frac{m_pE}{\bar{E}\pm(\bar{p}^2-E^2\sin^2\psi)^{\frac{1}{2}}}. \tag{24}$$

Upon introducing

$$x\equiv E/E_p, \tag{25}$$

Eq. (24) gives

$$\sin^2\psi=E^{-2}(2m_p\bar{E}x-m_p^2x^2-m^2), \tag{26}$$

$$\sin\psi d\psi=(m_p^2/E_p^3)[1-\bar{E}/(m_px)]dE_p, \tag{27}$$

$$\frac{\partial E_p}{\partial E}=\frac{m_p\bar{E}x-m^2}{m_px^2(m_px-\bar{E})}, \tag{28}$$

where m=mass of secondary particle.

The Jacobian J is given by $d\cos\bar{\psi}/d\cos\psi$, where $\bar{\psi}$ is the angle between primary and secondary in the rest system. By a straightforward calculation, one finds

$$J=\frac{p^2}{\gamma_p\bar{p}(p-v_pE\cos\psi)}, \tag{29}$$

where v_p=velocity of primary and $\gamma_p=(1-v_p^2)^{-\frac{1}{2}}$. Equation (29) is exact. We now make the approximation used above, of treating terms such as m^2/E^2 and m_p^2/E^2 as small compared to 1. One obtains by means of (26):

$$E=(p^2+m^2)^{\frac{1}{2}}\approx p[1+m^2/(2p^2)], \tag{30}$$

$$v_p\approx 1-m_p^2/(2E_p^2), \tag{31}$$

$$\cos\psi\approx 1-\psi^2/2\approx 1-(2m_p\bar{E}x-m_p^2x^2-m^2)/(2p^2). \tag{32}$$

[6] C. E. Swartz and J. W. DeWire, Bull. Am. Phys. Soc. **30**, No. 1, 25 (1955), and private communication.

[7] Throughout this section, letters without a subscript refer to the secondaries; letters with subscript p refer to the primaries. Unbarred quantities pertain to the laboratory system, while barred quantities pertain to the rest system of the decaying particle.

[8] It is assumed that the decay is isotropic in the rest system of the primary particle.

Upon inserting (30)–(32) into (29), one finds

$$J=\frac{\bar{p}^2 m_p x}{\bar{p}(m_p\bar{E}x-m^2)}. \tag{33}$$

Upon substituting (27), (28), and (33) in Eq. (23), one obtains

$$P(E,\theta)=\frac{nNm_p}{2\bar{p}}\int_{E_{p,\min}}^{E_{p,\max}}\frac{f(E_p,\theta)}{E_p}dE_p, \tag{34}$$

where $E_{p,\min}$ and $E_{p,\max}$ are the minimum and maximum values of E_p, given by

$$E_{p,\min}=m_pE/(\bar{E}+\bar{p})\equiv\alpha E, \tag{35}$$

$$E_{p,\max}=m_pE/(\bar{E}-\bar{p})\equiv\beta E, \tag{35a}$$

where α and β are coefficients defined by (35) and (35a). Upon differentiating both sides of (34), one obtains

$$\frac{\partial P(E,\theta)}{\partial E}=-\frac{nNm_p}{2\bar{p}E}[f(\alpha E,\theta)-f(\beta E,\theta)]. \tag{36}$$

It is convenient to introduce ρ and $Q(E,\theta)$ defined by

$$\rho\equiv\beta/\alpha=(\bar{E}+\bar{p})/(\bar{E}-\bar{p}), \tag{37}$$

$$Q(E,\theta)\equiv-\frac{2\bar{p}E}{nNm_p}\frac{\partial P(E,\theta)}{\partial E}. \tag{38}$$

Equation (36) can be written

$$Q(E,\theta)=f(\alpha E,\theta)-f(\beta E,\theta). \tag{39}$$

$Q(E,\theta)$ can be obtained from the observed intensity of secondaries. In order to solve Eq. (39) for f in terms of Q, we note that

$$Q(\rho E,\theta)=f(\alpha\rho E,\theta)-f(\alpha\rho^2E,\theta), \tag{40}$$

and there are similar equations for $Q(\rho^jE,\theta)$ for $j\geq 2$. It is seen that $f(\alpha E,\theta)$ is given by

$$f(\alpha E,\theta)=Q(E,\theta)+Q(\rho E,\theta)+Q(\rho^2E,\theta)+\cdots. \tag{41}$$

Since $\alpha>1$, $Q(E,\theta)$ involves only values of $f(E_p,\theta)$ for $E_p>E$. In view of $\rho>1$, the sum of Eq. (41) will therefore have a finite number of terms, limited by the energy of the incident beam. Thus if j_m is the largest j for which $Q(\rho^jE,\theta)>0$, we have

$$f(E,\theta)=\sum_{j=0}^{j_m}Q(\rho^jE/\alpha,\theta). \tag{42}$$

This equation gives the differential production cross section f in terms of Q, which in turn is related to the energy distribution of the secondaries by Eq. (38). In Eq. (42), E and θ are the energy and angle of the primary. The errors involved in the use of (42) are of order $(m_p\alpha/E)^2$, i.e., m_p^2 divided by the square of the lowest energy of the secondary for which Q must be evaluated.

As an example, for the θ^0 decay, $\bar{E}=247$ Mev and $\bar{p}=204$ Mev/c give $\alpha=1.095$, $\beta=11.5$, and $\rho=10.5$. Equation (42) becomes

$$f(E,\theta)=Q(0.913E,\theta)+Q(9.58E,\theta)+\cdots. \tag{42a}$$

It is seen that for 3-Bev incident protons, in the region of validity of the formula ($E\gtrsim 1.5$ Bev), only the first term of (42a) is present. As a check on the approximations made in the integrand of (34), $(\partial E_p/\partial E)J\times\sin\psi(\partial\psi/\partial E_p)$ was calculated exactly [using (21) and (29)] for pions of kinetic energy 2 Bev arising from θ^0 decay. For the lower branch of the E_p vs ψ curve, it was found that the approximate value $m_p/(\bar{p}E_p)$ of Eq. (34) underestimates the exact value by $\lesssim 5$ percent. This is approximately $m_p^2/E^2=0.053$.

Equation (42) can also be used for the pions from Λ^0 decay. In this case, $\alpha=4.10$, $\beta=15.5$, and $\rho=3.78$ give

$$f(E,0)=Q(0.244E,\theta)+Q(0.922E,\theta)+Q(3.49E,\theta)+\cdots. \tag{42b}$$

For the $\pi-\mu$ decay, we have $\alpha=1$, $\beta=\rho=1.71$, so that

$$f(E,\theta)=Q(E,\theta)+Q(1.71E,\theta)+Q(2.91E,\theta)+\cdots. \tag{42c}$$

IV. CONCLUSIONS

It has been shown that the differential cross section for π^0 production by a high-energy beam incident on a target can be obtained directly from a measurement of the energy distribution of the decay γ rays at various angles to the beam. This result is given by Eq. (15), which holds when the total energy of the π^0 is $\gtrsim 500$ Mev, although it may give reasonable estimates down to ~ 300 Mev. The energy distribution of the γ rays can be measured with a total absorption γ-ray spectrometer[9] of the type used by Swartz and DeWire.[6] Hence in this high-energy region, the experimental arrangement and interpretation are expected to be less complicated than at bombarding energies in the range[1] of 200–400 Mev, where it is advantageous to observe coincidences of the decay γ rays or the range of the recoil protons for the case of photoproduction in hydrogen. Equation (15) is obviously independent of the nature of the incident particles which produce the π^0's. However, this treatment is not applicable to the low-energy end of the π^0 spectrum.

The results for the π^0 decay have been extended to a general two-body decay, for possible application to counter experiments to detect K mesons or hyperons.[10] In this case, Eqs. (38) and (42) give the differential production cross section of the primaries in terms of the energy distribution of the secondaries arising from the decay.

I would like to thank Dr. J. W. DeWire, Dr. M. H. Ross, and Dr. C. E. Swartz for helpful discussions.

[9] A. Kantz and R. Hofstadter, Phys. Rev. **89**, 607 (1953); R. S. Foote and H. W. Koch, Rev. Sci. Instr. **25**, 746 (1954); R. M. Sternheimer, Atomic Energy Commission Reports AECU-2982, 2983, and 2984 (unpublished).

[10] S. L. Ridgway and G. B. Collins, Phys. Rev. **98**, 247(A) (1955).

Associated Photons in *K*-Particle Decays Observed with a Multiplate Cloud Chamber*

H. COURANT†
Department of Physics and Laboratory for Nuclear Science, Massachusetts Institute of Technology, Cambridge, Massachusetts
(Received March 11, 1955)

The existence of photons among the decay products of *K*-mesons is confirmed [see Bridge, Courant, DeStaebler, and Rossi, Phys. Rev. **91**, 1024 (1953)]. If these photons arise through a two-body decay process, it is not possible to assume that they are produced directly as the neutral product; however, they can be accounted for quite naturally by assuming that the neutral product is a π^0-meson. The frequency with which the photons are observed is low and for this reason it is not possible to interpret all the decay events observed in the cloud chamber in terms of a single two-body decay process in which the neutral particle is a π^0-meson. The statistical arguments leading to this conclusion are given.

I. INTRODUCTION

RECENT observations of *K*-particles by means of multiplate cloud chambers have been reported by the Ecole Polytechnique[1] and the M. I. T. groups.[2,3] The general features of the events and a bibliography of previous work will be found in these two publications. In this paper we consider *K*-particles which stop in the cloud chamber and so decay at rest. This type of decay is classified phenomenologically as an *S*-event. To identify such an event we have required either (a) that the charged secondary product traverse at least 10 g cm^{-2} of lead without multiplication, or (b) that the neutral decay product be detected.

In all of the analysis which follows, we assume in each case a two-body decay scheme (however, not necessarily the same decay scheme for all events). The main justification of this assumption is that the range spectrum of the charged secondaries of the decay events does not contain many short-range cases. These would be expected if the decay process were a three-body one.

The experimental data consist of 33 *S*-events, all of which were obtained using a plate assembly of 11 lead plates, each 1.1 radiation lengths thick. Among these 33 examples, we have found 9 in which there is an electron cascade close to the point of decay. The present paper presents a study of this particular phenomenon. Additional details concerning the events as well as some more recent data obtained with a different plate assembly have been reported previously.[3]

II. ELECTRON CASCADES

Figures 1, 2, and 3 are pictures of *S*-particle decay events in which a related electron cascade is observed. In Fig. 1 (25178), the decay occurs in the fourth plate from the top, and the electron cascade manifests itself as a spray of five electrons emerging directly from the plate of decay in a general direction opposite to that of the charged decay product.

In Fig. 2 (32531), the decay occurs in the sixth plate, and the electron cascade is seen to emerge from the seventh plate. The nonionizing link between the point of decay and the plate where materialization occurs is strong evidence that the cascade is initiated by a photon. In this case the direction of the photon is

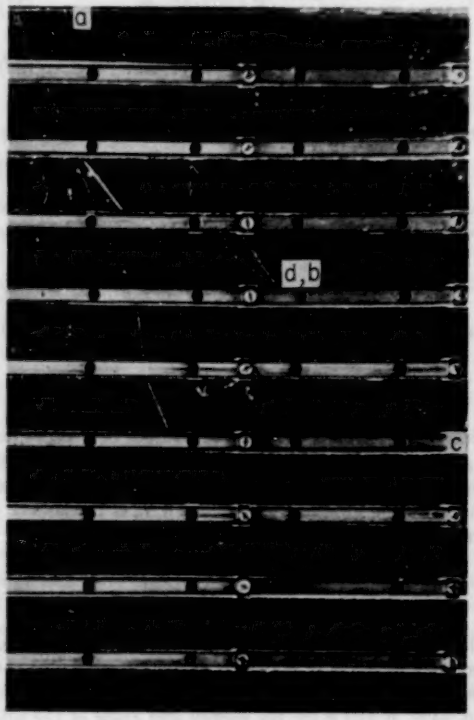

FIG. 1. Example of associated *S*-event and electron cascade. *a* is the point at which the *K*-meson enters the chamber; *b* is the point of decay; *c* is the point at which the charged secondary leaves the chamber; and *d* is the point at which the electron cascade is initiated.

* This work was supported in part by the joint program of the Office of Naval Research and the U. S. Atomic Energy Commission.
† Now at Laboratoire de Physique del'Ecole Polytechnique, Paris, France.
[1] Gregory, Lagarrigue, Leprince-Ringuet, Muller, and Peyrou, Nuovo cimento **11**, 292 (1954).
[2] Bridge, Peyrou, Rossi, and Safford, Phys. Rev. **90**, 921 (1953).
[3] Bridge, Courant, Dayton, DeStaebler, Rossi, Safford, and Willard, Nuovo cimento **12**, 81 (1954).

$180°\pm5°$ from the line of flight of the charged decay product.

Figure 3 (2877), is similar to Fig. 2 in that there is a nonionizing link between the point of decay and the point where materialization occurs. In this case, however, the angle between the trajectory of the photon and that of the charged decay product is $155°\pm5°$.

Before discussing the significance of the observation of the electron cascades, it is necessary to establish unambiguously that the observed cascades are related to the S-particle decays. To do this we must evaluate the probability of chance association, i.e., the probability of finding an unrelated electron cascade that has the characteristics of direction, proximity, and general behavior which might lead us to identify it erroneously as a manifestation of the neutral decay product.

For this purpose we have examined the pictures exhibiting S-particle decay and counted the number of cascades observed anywhere in the chamber. Each of these electron cascades shows a general direction of propagation, and we assume that the origin of the initiating photon must be somewhere within a cone of $15°$ half-angle from this inferred line of propagation.

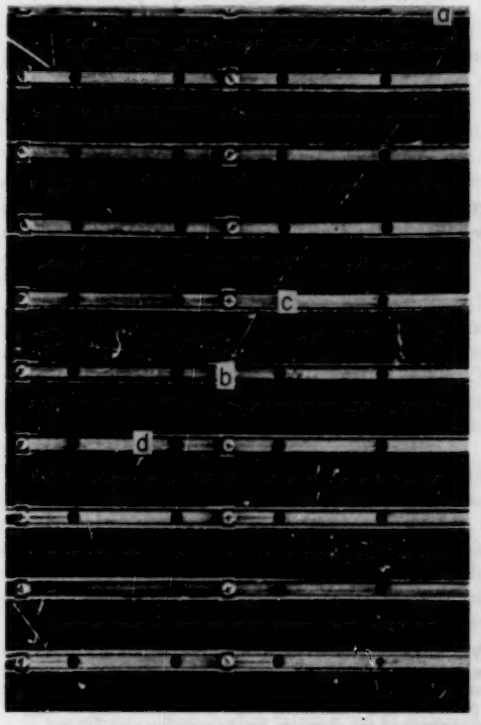

FIG. 2. Example of associated S-event and electron cascade. a is the point at which the K-meson enters the chamber; b is the point of decay; c is the point at which the charged secondary leaves the chamber; and d is the point at which the electron cascade is initiated.

Furthermore, we assume that the origin of the initiating photon must be within two radiation lengths (2 plates of our chamber) from the point where the electron cascade is observed. In this manner we define a volume of material in the cloud chamber in which a fortuitous S-event would erroneously be associated with the electron cascade.

To obtain the probability for a chance association between an electron cascade and an S-particle decay we take the ratio of the volume of material available for making such an association and that available for the S-event to be observed at all. This ratio has a value of 0.0013, and it is a measure of the probability that there be a chance association between a particular S-event and an electron cascade. This figure is based on 31 suitable examples of S-decay in which related electron cascades might have been observed if they had occurred. The probability that all nine of our cases of cascades associated with S-decay are due to chance is

$$P=(0.0013)^9=10^{-26}.$$

This is the probability that none of the observed cascades are causally related to the phenomenon of S-decay. The probability that some of our nine cases are not genuine is

$$P=1-(1-0.0013)^{31}=0.04.$$

It therefore seems likely that most of our events which have been identified as exhibiting electron cascades in association with S-particle decay have been correctly interpreted on this point.

III. NEUTRAL PARTICLE AS π^0-MESON

In this section, we investigate the possibility that the observed electron cascades originate from the decay photons of π^0-mesons under the assumption that the π^0-meson is produced in a two-body decay process. To do this we compare the observed angular distribution of the photons with that expected under the above assumptions.

We define φ as the angle between the trajectory of the charged decay product and that of the observed photon. Let ϑ^* be the angle between the direction of the photon and the direction of flight of the π^0-meson as viewed in the frame of reference in which the π^0-meson is at rest. The angles φ and ϑ^* are related by the expression

$$-\gamma_0\tan\varphi=\sin\vartheta^*/(\cos\vartheta^*+\beta_0),$$

where β_0 is the velocity of the π^0-meson in the laboratory system, and $\gamma_0=1(1-\beta_0^2)^{\frac{1}{2}}$.

It is evident from the above relation that the photon which in the frame of reference of the π^0-meson is emitted in a forward direction ($0°\leqslant\vartheta^*\leqslant90°$) will appear in the laboratory within a cone of semi-apex angle $\vartheta_0=\tan^{-1}[1/(\gamma_0\beta_0)]$. For the purpose of graphically presenting the angular probability distribution of

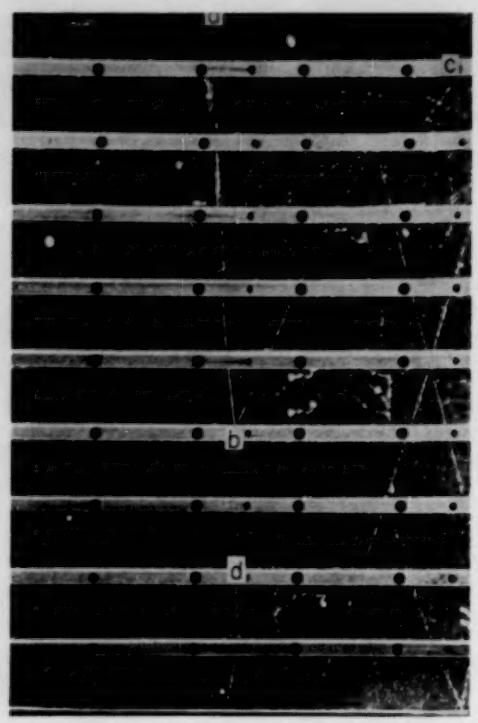

FIG. 3. Example of associated S-event and electron cascade. a is the point at which the K-meson enters the chamber; b is the point of decay; c is the point at which the charged secondary leaves the chamber; and d is the point at which the electron cascade is initiated.

π^0-meson decay photons as observed in the laboratory, we define the variable x as follows: $x=\gamma_0 \tan\vartheta$. Let us construct a cone of semi-apex angle ϑ with the trajectory of the neutral decay particle as its axis. Consider the circle defined by the intersection of such a cone of height γ_0 with a plane normal to its axis. The value of the variable $x(\vartheta)$ then is equal to the radius of this circle. We define $W(x)dx$ as the probability that the variable x lie in dx at x. $W(x)dx$ can be considered as the probability that a photon traverse the above-mentioned circle in a ring of width dx at the radius x. Figure 4 shows the differential probability distribution $W(x)$ of the forward photon ($0°\leqslant\vartheta^*\leqslant 90°$) from the decay of a π^0-meson of momentum $p_{\pi^0}=200$ Mev/c. (In this case, our definition gives $x=1.78\tan\vartheta$.)

Although the cone containing all photons emitted in the forward direction has a semiapex angle of 34° (for $p_{\pi^0}=200$ Mev/c), graphical integration of $W(x)$ leads to the result that half of these photons are contained in a coaxial cone of semi-apex angle 20°.

In the analysis which follows, only the first seven of the nine observed decay photons are employed. This is due to the fact that the last two cases were added to our collection after the statistical analysis had been performed, and that the determination of the angle φ in one of them is not very precise.

In the frame of reference where the π^0-meson is at rest, the differential angular probability distribution for the forward-going decay photon is

$$W^*(\vartheta^*)d\vartheta^*=\sin\vartheta^* d\vartheta^*.$$

Since $W^*(\vartheta^*)d\vartheta^*=d(-\cos\vartheta^*)$, we introduce the variable z according to the definition $z=\cos\vartheta^*$. The resulting distribution is the rectangular distribution, i.e., it has a constant value in the range $0\leqslant z\leqslant 1$, and the value zero elsewhere.

We now define the quantity K_n as follows:

$$K_n=\sum_{i=1}^{n} z_i.$$

Since z_i can assume any value between 0 and 1, it is clear that K_n may have values between 0 and n.

In what follows, we will need the differential distribution W_n of K_n. It can be shown that the probability $W_n(K_n)dK_n$ of finding K_n in dK_n is given by[4,5]

$$W_n(K_n)dK_n=\frac{dK_n}{(n-1)!}\sum_{r=0}^{m}(-1)^r\binom{n}{r}(K_n-r)^{n-1},$$

for values of K_n between m and $m+1$, where

$$\binom{n}{r}=n!/(n-r)!r!$$

is the rth binomial coefficient of the power n. The probability function $W_7(K_7)$ is shown in Fig. 5. One sees that it has a maximum at $K_7=3.5$, which is thus

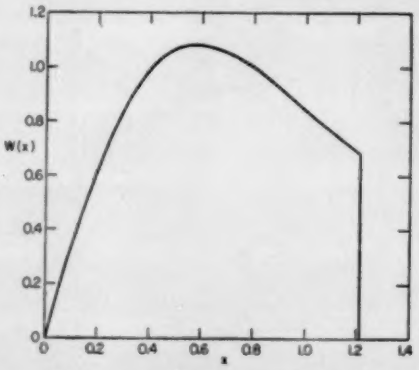

FIG. 4. The differential probability $W(x)$ that in the laboratory the more energetic photon emitted in the decay of a π^0-meson of momentum 200 Mev/c has a particular value of x. The variable x is related to ϑ, the laboratory angle between the line of flight of the photon and the π^0-meson, by the equation $x=1.78\tan\vartheta$.

[4] M. G. Kendall, *The Advanced Theory of Statistics* (Charles Griffin and Company Ltd., London, 1952), Vol. 1, p. 240 ff.
[5] H. Cramer, *Mathematical Methods of Statistics* (Princeton University Press, Princeton, 1951), p. 244 ff.

TABLE I. The experimentally observed values of K_7 and the corresponding values of $P(\Delta K_7)$ computed as described in the text for several values of π^0-momentum, p_{π^0} (Mev/c). $P(\Delta K_7)$ represents the *a priori* probability that K_7 deviates from the most probable value by at least the amount observed.

S-particle with photon	Space angle φ (in lab system)	$z_i=\cos\vartheta_i^*$ $p_{\pi^0}=150$	$p_{\pi^0}=200$	$p_{\pi^0}=250$	$p_{\pi^0}=300$	$p_{\pi^0}=350$	$p_{\pi^0}=400$	$p_{\pi^0}=450$
1	180°	1.000	1.000	1.000	1.000	1.000	1.000	1.000
2	178°	0.999	0.998	0.997	0.995	0.994	0.993	0.991
3	178°	0.999	0.998	0.997	0.995	0.994	0.993	0.991
4	157°	0.567	0.392	0.210	0.000	0.000	0.000	0.000
5	140°	0.000	0.170	0.340	0.456	0.566	0.607	0.677
6	155°	0.510	0.318	0.120	0.000	0.120	0.170	0.240
7	162°	0.708	0.588	0.470	0.340	0.210	0.120	0.000
	$K_7=\sum_1^7 z_i$	4.78	4.46	4.13	3.79	3.88	3.88	3.89
	$P(\Delta K_7)$	0.1	0.2	0.4	0.6	0.6	0.6	0.6

the most likely value of K_7. We can now compute the function

$$P(\Delta K_7)=\int_0^{\bar{K}_7-\Delta K_7} W(K_7')dK_7' + \int_{\bar{K}_7+\Delta K_7}^{7} W(K_7')dK_7'.$$

This function represents the total probability of finding for $\sum_1^7 z_i$ a value that deviates from the most probable value, $\bar{K}_7$, ($\bar{K}_7=3.5$) by more than a given amount, ΔK_7.

In Table I, we have tabulated the experimental values of K_7 and the corresponding calculated values of $P(\Delta K_7)$ for six different assumed values of p_{π^0}. As explained above, the values of $P(\Delta K_7)$ given in Table I represent the *a priori* probability of finding a value of K_7 which deviates from the most probable value as much or more than does the experimental value. If $P(\Delta K_7)$ is sufficiently small we may conclude that the experimentally observed angular distribution is not related to that on which the probability calculations are based. It is seen that the angular distribution of the photons observed in the cloud chamber is consistent with that expected from π^0-mesons of momentum between 150 and 400 Mev/c.

We should point out that when we transform the observed angles into the rest system of the π^0-meson some of the photons were emitted with $\vartheta^*>90°$, i.e., in the backward cone. The number of these cases varies with the assumed value of p_{π^0}. In these events the value of z_i for the forward photon was used in the analysis. The estimated errors in the measurement of the space angles would allow the quantity $P(\Delta K_7)$ to vary by as much as ± 0.3 for $p_{\pi^0}=150$ Mev/c. This does not alter the conclusions of the analysis.

If the electron cascades are interpreted in terms of a π^0-meson, one might expect to detect both photons occasionally. However, in the nine cases of S-decay where related photons have been detected we have not seen evidence for a second photon which could possibly be the other photon from the decay of the π^0-meson. We have examined each of these nine cases to determine the trajectory of this second photon (assuming a momentum of 200 Mev/c for the π^0-meson) and then calculated the probability for this photon to be detected. We find that because of the geometry of our nine events the likelihood of detecting the second photon is essentially zero in all cases. Thus the fact that we have not observed the second photon from the decay of a π^0-meson in any of our examples is entirely consistent with the assumption that the observed photons originate in the decay of π^0-mesons created in the S-events.

We should emphasize here that the treatment of this section is merely a test to see whether our data would fit the hypothesis of a π^0-meson as a decay product in two-body decay. Our data may in fact fit some other hypothesis equally well. For example, a three-body decay in which one of the neutral particles is a photon may well be possible. However, the two-body decay scheme which has a single photon as the neutral product is certainly ruled out.

IV. PROBABILITY OF DETECTING π^0-MESON AS DECAY PRODUCT

In this section, we now examine the hypothesis that a π^0-meson is created in each of our 33 examples of S-decay.

We shall approach this problem from the point of view that the number of cases in which we have detected a photon is small compared to the number of cases we would expect to see under the assumption that a π^0-meson is created in each decay event.

Thus, our treatment of the data is to be an attempt to account for the small number of photons observed in our collection of 33 examples. We shall consistently use approximations which underestimate the probability of detecting photons, and which exaggerate the number of observed photons which should be included in the analysis. If this biased approach yields the result that our data are not compatible with the hypothesis that a

TABLE II. Numerical values of b_m and q_m for 33 S-events. b is the detection probability for an electron cascade and $q_m = 1 - b_m$.[a]

m	b_m	q_m	m	b_m	q_m	m	b_m	q_m
1*	0.00	1.00	12	0.38	0.62	23	0.67	0.33
2	0.00	1.00	13*	0.39	0.61	24*	0.69	0.31
3	0.00	1.00	14	0.39	0.61	25	0.69	0.31
4	0.06	0.94	15*	0.48	0.52	26	0.74	0.26
5	0.10	0.90	16	0.48	0.52	27*	0.75	0.25
6*	0.19	0.81	17	0.51	0.49	28	0.75	0.25
7	0.20	0.80	18	0.51	0.49	29	0.76	0.24
8	0.29	0.71	19*	0.52	0.48	30	0.82	0.18
9	0.29	0.71	20	0.55	0.45	31*	0.87	0.13
10*	0.38	0.62	21	0.63	0.37	32	0.87	0.13
11	0.38	0.62	22	0.66	0.34	33	0.95	0.05

[a] The numbers indicated by a star (*) correspond to examples in which associated electron cascades were found.

π^0-meson is created in each decay, we may certainly conclude that the premise is incorrect.

In proceeding with the analysis of the individual events, this over-all approach has the following direct consequences:

(a) We shall accept as *bona fide* examples of associated electron cascades those cases in which the charged secondary from the decay is not under observation in the cloud chamber for a range sufficient to identify the event independently as an S-event (the charged secondary should be observed to penetrate at least 10 g cm^{-2} of lead within the illuminated region of the chamber[1]). Among our examples one case falls into this category.

(b) Although the analysis is based on the detection only of the forward photon (which is more energetic), we shall accept as examples of associated electron cascades those cases in which we have detected the backward-going photon. Among our examples two cases fall into this category.

(c) The evaluation of the probability of detecting the forward photon in each of our 33 cases is based on an assumed momentum of 200 Mev/c of the π^0-meson. This is the lowest value that one can ascribe to the momentum of the π^0-mesons if one assumes that the sample is homogeneous. For in one case, the charged secondary penetrates 85 g cm^{-2} of lead before it leaves the chamber, and if it is a π-meson, its momentum exceeds 200 Mev/c. A decrease in this momentum increases the apex angle of the cone in which the decay photons must lie, and, since the portion of the cone that is found in the illuminated region of the cloud chamber usually decreases with increasing apex angle, the probability of finding the decay photon in the cloud chamber decreases with decreasing energy of the π^0-meson.

To determine the probability that we should see n associated electron cascades among the 33 examples of S-decay in our collection, we must first calculate the probability for detecting the photon in each case. This calculation must take into account the following: (1) the particular geometry of the event; (2) the probability that a photon will undergo materialization; and (3) the probability that at least one of the created electrons will emerge from the plate where materialization occurs. We shall outline the method used for this calculation by considering the above points in order.

(1) *Geometry considerations.*—In each case we have estimated the fraction of decay photons which were available for materialization in the illuminated region of the cloud chamber. This fraction in general has a new value for each lead plate which is to be considered.

(2) *Materialization probability.*—The materialization probability of the photon was evaluated for each lead plate on the basis of the estimated average angle of incidence of the photon to the plate. The energy of the photon was taken as 100 Mev. The materialization probability in lead for this photon is 0.6 per radiation length.

(3) *Probability of observing at least one of the electrons.*—This part of the calculation takes into account the probability of catastrophic (radiative) energy loss by the electrons of the first generation in the cascade.[6] In most cases this results in a value of the electron detection probability of about 0.95.

The evaluation of the photon-detection probability as outlined above is consistent with the general approach detailed at the beginning of this section. In part 1 of this outline, we have made the assumption that the photon probability density is roughly constant within the π^0-meson decay cone. This approximation results in an exaggeration of the probability density along the periphery of the cone in which the photons lie. The consequence of this is to overestimate slightly the probability that the photon leave the illuminated region of the cloud chamber, thus causing the likelihood of detection by materialization to be underestimated. In part 2, we base the materialization probability on that

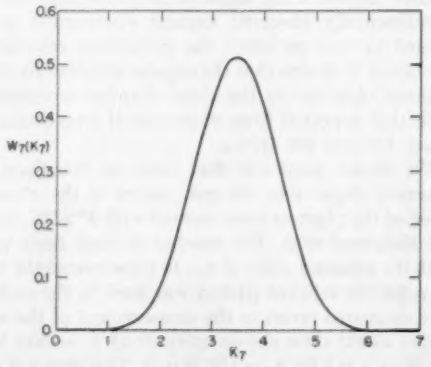

FIG. 5. The differential probability $W_7(K_7)$ plotted *versus* K_7.

[6] This calculation was performed by H. C. DeStaebler and has been adjusted to give agreement with R. R. Wilson's Monte Carlo histories of photon-initiated electron cascades in lead. Professor Wilson kindly lent us the original histories; see H. C. DeStaebler, Jr., Massachusetts Institute of Technology thesis, 1954 (unpublished).

for a photon of 100-Mev energy. The energy of the decay-photon from a π^0-meson of momentum 200 Mev/c varies from 121 Mev to 221 Mev within the cone. Since the materialization probability increases with increasing energy we thus underestimate the over-all materialization probability.

We now define the quantity b_m as the overall probability to observe an electron cascade in the picture of the mth decay event, and the quantity

$$q_m = 1 - b_m,$$

representing the probability of *not* observing an electron cascade in the mth picture. The quantities b_m and q_m of each of our 33 S-particle decays are tabulated in Table II.

The product

$$(b_1+q_1)(b_2+q_2)\cdots(b_{32}+q_{32})(b_{33}+q_{33})$$

is equal to one, since each term (b_m+q_m) is equal to one. If we express this product as a polynomial we may

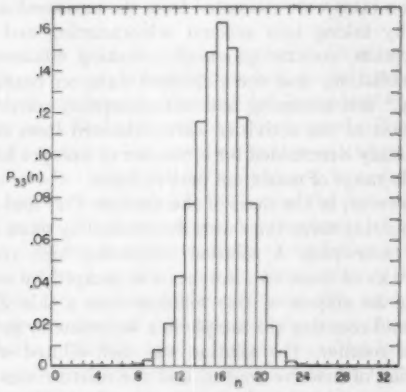

FIG. 6. The probability of observing exactly n electron cascades in the experimental data as a function of n.

interpret the sum of all terms having dimensions $b^n q^{33-n}$ as the probability that we should find n examples of associated electron cascades among our 33 events. Thus by arranging the terms appropriately we may find the numerical value of $P_{33}(n)$, which we define as the probability of detecting n associated photons among our 33 S-particles.

TABLE III. Numerical values of the quantity $P_{33}(n)$, the probability of observing exactly n electron cascades in the sample of 33 S-events.

n	$P_{33}(n)$	n	$P_{33}(n)$	n	$P_{33}(n)$
1	6.44×10^{-11}	12	4.31×10^{-3}	23	2.24×10^{-4}
2	2.01×10^{-9}	13	7.70×10^{-3}	24	5.47×10^{-4}
3	3.71×10^{-8}	14	1.16×10^{-1}	25	1.04×10^{-4}
4	4.76×10^{-7}	15	1.45×10^{-1}	26	1.50×10^{-5}
5	4.40×10^{-6}	16	1.63×10^{-1}	27	1.58×10^{-6}
6	3.09×10^{-5}	17	1.51×10^{-1}	28	1.10×10^{-7}
7	1.70×10^{-4}	18	1.18×10^{-1}	29	4.56×10^{-9}
8	7.52×10^{-4}	19	7.73×10^{-2}	30	8.23×10^{-13}
9	2.72×10^{-3}	20	4.26×10^{-2}	31	~0
10	8.15×10^{-3}	21	1.94×10^{-2}	32	~0
11	2.05×10^{-3}	22	7.32×10^{-3}	33	~0

Table III gives the numerical values obtained for $P_{33}(n)$, and Fig. 6 shows these values plotted. By inspection of Fig. 6 or Table III, it is apparent that we should have seen about 16 cascades among our 33 S-decay events. Instead, we only found 9 cases of associated cascades, a number which deviates by 7 units from the expected value. The total probability of a deviation equal or larger than 7 is

$$\sum_{1}^{9} P_{33}(n)+\sum_{23}^{33} P_{33}(n)=3.3\times10^{-3}.$$

Thus the hypothesis that each of our events has given rise to a π^0-meson as the neutral decay product is ruled out.

V. CONCLUSIONS

We have presented conclusive evidence that electron cascades are related to the S-decays in the events in which they were observed (Sec. II). We have shown that the observed cascades *may* be due to the creation of a π^0-meson as the neutral decay product (Sec. III). We have shown that our data are *not* consistent with the assumption that a π^0-meson is created in each decay (Sec. IV).

The author wishes gratefully to acknowledge the discussion, guidance, and other assistance generously given by members of the M.I.T. cosmic-ray group.

Nuclear Reactions of Copper with Various High-Energy Particles*

G. H. Coleman† and H. A. Tewes
Radiation Laboratory, University of California, Livermore, California
(Received December 17, 1954; revised manuscript received January 31, 1955)

A study of the spallation of copper by 90-Mev neutrons, 90-Mev protons, 190-Mev protons, and 190-Mev deuterons has been made. Radiochemical methods have been employed to determine absolute cross sections for the production of a number of nuclides produced by the interaction of these high-energy particles with copper.

OVER the past several years, the spallation of a number of elements by high-energy particles has been studied.[1–6] However, in almost all cases, the energies of the particles used in producing the spallation reaction have been sufficiently high that the method whereby the struck nucleus is excited prior to spallation is not clear-cut. Charge exchange or other noncapture processes appear to account for the greater part of the excitation, whereas compound nucleus formation is relatively unimportant. A further complicating factor is the appreciable transparency of nuclei to high-energy incident particles. Hence, it was felt that a study should be made of relatively low-energy spallation, where the compound nucleus mechanism plays a more important role in the formation of the "spalling" nucleus.

Unfortunately, the programmatic study of spallation reactions which was originally contemplated could not be carried out; however, a limited research program on the spallation of natural copper (Cu^{63} and Cu^{65}) has been completed. This paper reports on the results of several irradiations which were made on the Berkeley 184-inch cyclotron with 90-Mev neutrons and 90-Mev protons, at which energy the compound nucleus mechanism may be considered more important in the formation of the "spalling" nucleus than is the case at higher energies. To facilitate comparisons between intermediate and high-energy spallation, several additional irradiations of copper were carried out, using 190-Mev protons and 190-Mev deuterons.

After each irradiation the target was dissolved, appropriate carriers were added, and one or more elements were separated by chemical procedures which were, in most cases, similar to those used by Batzel.[7] In all charged-particle bombardments, the Na^{24} produced in aluminum monitor foils was used to determine the absolute beam intensities. In all neutron runs a copper fraction was isolated, and the Cu^{64} was used as an internal monitor to ascertain relative beam intensities. Subsequently, the cross section for the formation of Cu^{64} by 90-Mev neutrons was found by the use of carbon monitor foils, where the $C^{12}(n,2n)C^{11}$ cross section is known. The cross sections used for all monitor reactions are given in Table I.

Activities of beta-emitting nuclides were measured with thin-window halogen-filled GM counters, all of which were cross calibrated. In most cases, disintegration rates were estimated from the measured activities by taking into account self-scattering and self-absorption, counter geometry, counting efficiency of the radiation, and the published data on branching decay.[8] Self-scattering and self-absorption corrections for most of the activities were estimated from curves previously determined for a number of isotopes having a wide range of maximum beta energies.

However, in the cases of the nuclides Cu^{64} and Cu^{61}, all counting corrections were determined by more accurate techniques. A solution containing high specific activities of these two isotopes was assayed by evaporating an aliquot of this solution onto a thin Zapon film and counting the sample in a 4π geometry proportional counter. The solution was then diluted with a solution of inactive copper, and the mixture was used to prepare a series of counting samples with varying weights. The counting data from these samples were subsequently used in the determination of relatively precise self-scattering and self-absorption corrections.

The cross sections measured in this investigation are listed in Table II. The absolute values reported for Cu^{64} and Cu^{61} are accurate to approximately ± 5 percent. The relative values reported for all other nuclides should

Table I. Cross sections (in mb) used for monitor reactions.

Reaction	90 Mev	190 Mev	Reference
$C^{12}(n,2n)C^{11}$	22		a
$Al^{27}(p,3pn)Na^{24}$	9.2	9.2	b
$Al^{27}(d,\alpha p)Na^{24}$		21.8	c

* This work was performed under the auspices of the U. S. Atomic Energy Commission.
† Present address: Department of Chemistry, University of California at Los Angeles, Los Angeles 24, California.
[1] D. H. Templeton, Ann. Revs. Nuclear Sci. **2**, 93 (1953).
[2] J. W. Meadows, Phys. Rev. **91**, 885 (1953).
[3] R. W. Fink and E. O. Wiig, Phys. Rev. **94**, 1357 (1954).
[4] R. E. Bell, Phys. Rev. **95**, 651(A) (1954).
[5] E. Belmont and J. M. Miller, Phys. Rev. **95**, 1554 (1954).
[6] R. W. Fink and E. O. Wiig, Phys. Rev. **96**, 185 (1954).
[7] Batzel, Miller, and Seaborg, Phys. Rev. **84**, 671 (1951).

[a] E. M. McMillan and H. F. York, Phys. Rev. **73**, 262 (1948); Birnbaum, Crandall, Millburn, and Pyle (to be published); Schecter, Crandall, Millburn, and Ise, Phys. Rev. **97**, 184 (1955).
[b] Stevenson, Hicks, and Folger, University of California Radiation Laboratory Report UCRL-4371 (to be published).
[c] Batzel, Crane, and O'Kelley, Phys. Rev. **91**, 939 (1953).

[8] Decay schemes used are those given in Hollander, Perlman, and Seaborg, Revs. Modern Phys. **25**, 469 (1953).

TABLE II. Cross sections (in mb) for the formation of nuclides in the bombardment of copper.

	90-Mev neutrons	90-Mev protons	90-Mev protons[a]	190-Mev protons	190-Mev deuterons	190-Mev deuterons[b,c]	340-Mev protons[b]	370-Mev neutrons[d]
Zn^{65}		9[e]	12	2	21[e]	1.4	1.1	
Zn^{63}		7[e]	7.1	2[e]	14[e]	1.0	0.8	
Cu^{64}	98	39	55	24	40	37	23	58.6
Cu^{62}	135	98[e]	120	42[e]	83	69	48	37.1
Cu^{61}	50	56.4	65	30	46	~30[f]	23	15.4
Cu^{60}	5	6[e]		8[e]	10	9		
Ni^{65}	2				0.4[e]	1.2		0.88
Ni^{57}	0.3	0.8		1.3[e]	1.3[e]	2.6	1.8	0.54
Co^{62}	2							
Co^{61}	15	2		2[e]	7.4[e]	4	5	3.78
Co^{58}	0.5	0.6[g]		1.4	2.6[e]	1.0	2.3	0.415
Fe^{59}	0.16	0.30[e]		0.16[e]	0.30[e]	2.2	1.7	1.24
Fe^{52}	0.003	0.007		0.10	0.11	0.1	0.2	0.134
Mn^{54}	3	0.8		1.6	2.5	5	2.5	2.51
Mn^{52}	0.14[g]	0.1[e,g]		0.4[e,g]	0.8[g]	4	7	4.68
Mn^{51}	0.03			0.3[e]	0.6	1.3	1.6	0.76
Cr^{49}	0.006	0.01[e]		0.7[e]	0.9[e]	0.5	0.9	0.35
V^{48}	0.1[e]	0.02[e]		2.6[e]	2.9[e]	1.6	0.7	

[a] Calculated from results given in reference 2.
[b] Calculated from results given in reference 7.
[c] Cross sections in this column were recalculated by the authors.
[d] From reference 9.
[e] Based on a single run.
[f] Reported by W. H. Hutchin as 38 mb (see reference 7).
[g] Cross section for Mn^{52m} only.

be accurate to ±25 percent; however, those cases in which only one determination was made have been noted. Some results obtained by Meadows,[2] Batzel, Miller, and Seaborg[7] and Marquez[9] are also listed to provide a reasonably complete picture of copper spallation studies below 400 Mev. It should be noted that the cross section quoted by Miller for the formation of Cu^{61} in the 190-Mev deuteron bombardment of copper was only a rough estimate. Since all spallation product yields reported by him were expressed relative to this isotope, the authors arbitrarily used the production cross section for Cu^{61} determined in the present work to recalculate Miller's results. Inasmuch as Meadows did not apply backscattering corrections to his data, the agreement between his cross sections and those reported in this paper is satisfactory.

It can be seen that the cross sections of most of the proton-initiated spallation reactions are quite similar at 190 Mev and 340 Mev. Apparently, the excitation of the target nucleus is not greatly enhanced by increasing the energy of the incident protons above 190 Mev. However, reduction of the particle energy to 90 Mev produces the expected decrease in the production of the lighter spallation products. This effect is shown by both neutrons and protons, thereby indicating that the nature of the impinging nucleon is of only secondary importance. It is to be noted that the cross section for the production of Cu^{64} is appreciably higher in 90-Mev neutron spallation than it is in 90-Mev proton spallation. Although this effect may reflect a real difference in the $(n,2n)$ and (p,pn) reaction cross sections on Cu^{65}, it is possible that in the case of neutron spallation a small background of low-energy neutrons could produce an appreciable amount of Cu^{64} by means of the $Cu^{63}(n,\gamma)$ reaction. A comparison between the production of Cu^{64} in the spallation of copper with 340-Mev protons and 370-Mev neutrons indicates that a somewhat similar situation exists in this energy region.

In a comparison of the spallation produced by 190-Mev protons and 190-Mev deuterons, the smaller average energy per nucleon and hence the smaller transparency of the struck nucleus to deuterons should be manifested by an increased production of those nuclides which are formed predominantly in spallation induced by 90-Mev particles. This expected effect is markedly displayed by the data given in Table II.

A more detailed analysis of the results reported in this paper does not appear to be warranted because of the incomplete nature of these results. A further complication in the interpretation of experimental data lies in the lack of uniqueness in the method of production of any given spallation product; i.e., in almost all cases the nuclide may have resulted from the interaction of a bombarding particle with either Cu^{63} or Cu^{65}.

ACKNOWLEDGMENTS

We wish to thank Mr. James T. Vale and the group operating the 184-inch cyclotron for the irradiations performed in the course of these studies; we should also like to acknowledge the invaluable help of Mrs. E. King in the analysis of much of the counting data.

[9] L. Marquez, Phys. Rev. 88, 225 (1952).

Interaction of Nonlocal and Local Fields*

WILLIAM DONALD SCHULZ
Columbia University, New York, New York†

(Received October 28, 1954)

A system of a scalar nonlocal (meson) field and a spinor local field is considered. Through the introduction of an invariant projection operator the interaction term is chosen with close consideration to the angular momentum properties of the nonlocal field. When the interaction is so chosen that the system is restricted to spin zero mesons, the system is shown to be equivalent to a system of local fields in nonlocal interaction. The convergence properties introduced by the nonlocal field are always due to form invariant functions even when higher spin mesons are allowed in the theory. The close relationship of this theory to that of local fields in nonlocal interaction means that all the quantization difficulties of the latter are present here also.

1. INTRODUCTION

IT has been proposed by Yukawa[1] that one construct a nonlocal field equation by substituting an internal coordinate operator for the mass constant in ordinary field theory. This gives a "mass spectrum" and internal coordinate functions which it is hoped would act as convergence factors. In particular, Yukawa proposed an "oscillator model" free-meson field operator of the following form ($\hbar=c=1$),

$$F=F^{\rm ex}+(F^{\rm int})^2, \quad F^{\rm ex}=-\partial^2/\partial X_\mu\partial X_\mu, \tag{1.1}$$

$$F^{\rm int}=\frac{\lambda}{\sqrt{2}}\left(-\frac{\partial^2}{\partial r_\mu\partial r_\mu}+\frac{r_\mu r_\mu}{\lambda^4}\right). \tag{1.2}$$

This paper will consider the interaction of a scalar nonlocal field, whose free-field equation is

$$F\phi(X,r)=0 \tag{1.3}$$

with an ordinary spinor field. With a little attention as to how spinor indices are summed in relation to the labels of the arguments of the fields, form functions, and S functions, one can convert all of the equations to the pseudoscalar case. Actually the summation over spinor indices is never explicitly considered so the choice of whether ϕ is scalar or pseudoscalar depends entirely upon the choice made for the form function appearing in the interaction Lagrangian.

Tentatively, then, we wish to consider a system of the sort

$$L=L_1+L_2+L_I,$$

$$L_1=\int\mathfrak{L}_1(Xr)dXdr, \quad L_2=\int\mathfrak{L}_2(x)dx,$$

$$L_I=\int\mathfrak{L}_I(\bar\psi(x'),\phi(X''r''),\psi(x'''))dx'dX''dr''dx'''.$$

The integrations are over all space time and $dx=dx_1dx_2dx_3dx_0$, etc., as usual.

$$\mathfrak{L}_1=-\frac{1}{2}\frac{\partial\phi}{\partial X_\mu}\frac{\partial\phi}{\partial X_\mu}-\frac{\lambda^2}{4}\left\{\frac{\partial^2\phi}{\partial r_\mu\partial r_\nu}\frac{\partial^2\phi}{\partial r_\mu\partial r_\nu}+\frac{2}{\lambda^4}\left(2r_\mu\frac{\partial\phi}{\partial r_\mu}\phi+r_\nu^2\frac{\partial\phi}{\partial r_\mu}\frac{\partial\phi}{\partial r_\mu}\right)+\frac{r_\mu^2r_\nu^2}{\lambda^8}\phi^2\right\}. \tag{1.4}$$

$$\mathfrak{L}_2=-\frac{1}{2}\bar\psi(x)\gamma_\mu\frac{\partial\psi(x)}{\partial x_\mu}+\frac{1}{2}\frac{\partial\bar\psi}{\partial x_\mu}\gamma_\mu\psi(x)-\bar\psi M\psi(x). \tag{1.5}$$

$$\mathfrak{L}_I'=-g\bar\psi(x')f(x',X'',r'',x''')\phi(X''r'')\psi(x'''). \tag{1.6}$$

There is a prime on the $\mathfrak{L}_I$ in Eq. (1.6) since we will make a slightly different choice for $\mathfrak{L}_I$ later on. The form function $f(x',X'',r'',x''')$ may be a δ function if so desired. For example, Yukawa[1] used an interaction of the form (1.6), where

$$f(x',X'',r'',x''')=\delta(X''-\tfrac{1}{2}(x'+x''))\delta(r''-(x'-x''')). \tag{1.7}$$

The introduction of the form function actually simplifies the analysis since it makes apparent the relation of this theory to the theory of local fields in nonlocal interaction and allows one to use techniques developed there.[2,3]

For convenience, introduce the eight-vector

$$\zeta_\mu\sim(X_1X_2X_3X_4r_1r_2r_3r_4), \quad d\zeta=dXdr;$$

then, if we take the variation

$$\delta L=0,$$

where the variation of the fields, and also $\delta(\partial\phi/\partial\zeta_\mu)$, vanishes on the boundary as usual, we get the field

* Submitted in partial fulfillment of the requirements for the degree of Doctor of Philosophy, in the faculty of Pure Science, Columbia University.

† Now at University of California Radiation Laboratory, Livermore, California.

[1] H. Yukawa, Phys. Rev. **91**, 415 and 416 (1953).

[2] C. Bloch, Kgl. Danske Videnskab. Selskab, Mat.-fys. Medd. **27**, No. 8 (1952).

[3] P. Kristensen and C. Møller, Kgl. Danske Videnskab. Selskab, Mat.-fys. Medd. **27**, No. 7 (1952).

equations

$$\frac{\partial^2}{\partial\zeta_\mu\partial\zeta_\nu}\frac{\partial\mathfrak{L}_1}{\partial\phi_{\mu\nu}}-\frac{\partial}{\partial\zeta_\mu}\frac{\partial\mathfrak{L}_1}{\partial\phi_\mu}+\frac{\partial\mathfrak{L}_1}{\partial\phi}=-\int\frac{\partial\mathfrak{L}_I'(x',\zeta,x'')}{\partial\phi(\zeta)}dx'dx''' \tag{1.8}$$

$$-\frac{\partial}{\partial x_\mu}\frac{\partial\mathfrak{L}_2}{\partial\psi_\mu}+\frac{\partial\mathfrak{L}_2}{\partial\psi}=-\int\frac{\partial\mathfrak{L}_I'(x,\zeta'',x''')}{\partial\bar{\psi}(x)}d\zeta''dx'''$$

$$-\frac{\partial}{\partial x_\mu}\frac{\partial\mathfrak{L}_2}{\partial\psi_\mu}+\frac{\partial\mathfrak{L}_2}{\partial\psi}=-\int\frac{\partial\mathfrak{L}_I'(x',\zeta'',x)}{\partial\psi(x)}dx'd\zeta'',$$

where $\phi_\mu=\partial\phi/\partial\zeta_\mu$, $\psi_\mu=\partial\psi/\partial x_\mu$, etc., or more explicitly

$$F\phi(\zeta)=\int\frac{\partial\mathfrak{L}_I'}{\partial\phi(\zeta)}dx'dx''',$$

$$\left(\gamma_\mu\frac{\partial}{\partial x_\mu}+M\right)\psi(x)=\int\frac{\partial\mathfrak{L}_I'}{\partial\bar{\psi}(x)}d\zeta''dx''', \tag{1.9}$$

$$\left(-\gamma_\mu^T\frac{\partial}{\partial x_\mu}+M\right)\bar{\psi}(x)=\int\frac{\partial\mathfrak{L}_I'}{\partial\psi(x)}dx'd\zeta''.$$

2. NONLOCAL FIELD OPERATOR

If we examine some of the properties of the operator F we will quickly see some difficulties. F^{int} is made up of four separable harmonic oscillator operators. Thus the eigensolutions of F^{int} can be written as the product of four simple harmonic oscillator solutions. Let

$$h_{n_i}(r_i)=N_{n_i}H_{n_i}\left(\frac{r_i}{\lambda}\right)\exp(-r_i^2/2\lambda^2),\ n_i=0,1,\cdots, \tag{2.1}$$

where $H_{n_i}(r_i/\lambda)$ are the Hermite polynomials and N_{n_i} is a normalizing factor, then

$$\left(-\frac{d^2}{dr_i^2}+\frac{r_i^2}{\lambda^4}\right)h_{n_i}(r_i)=\frac{2n_i+1}{\lambda^2}h_{n_i}(r_i). \tag{2.2}$$

If

$$\Gamma_n(r)=\prod_{i=0}^{3}h_{n_i}(r_i), \tag{2.3}$$

then

$$F^{\text{int}}\Gamma_n(r)=\kappa_s\Gamma_n(r), \tag{2.4}$$

$$\kappa_s=\sqrt{2}(s+1)/\lambda,\quad s=n_1+n_2+n_3-n_0. \tag{2.5}$$

There is an infinite degeneracy for a given eigenvalue κ_s and it will turn out later, principally for reasons of angular momentum, that the eigensolutions in the form given by (2.3) are not the most advantageous to use. Thus let us separate F^{int} in spherical coordinates in 3 space so that the spherical harmonics enter in. Define

$$p=n_1+n_2+n_3; \tag{2.6}$$

also

$$\chi_n(r)=R_{pl}(\rho)\mathcal{Y}_{lm}(\theta\varphi)h_{n_0}(r_0), \tag{2.7}$$

where ρ is the magnitude of $\mathbf{r}$ and

$$\mathbf{J}^2(\theta\varphi)\mathcal{Y}_{lm}(\theta\varphi)=l(l+1)\mathcal{Y}_{lm}(\theta\varphi), \tag{2.8}$$

$$\mathbf{J}^2(\theta\varphi)=-\left\{\frac{1}{\sin\theta}\frac{\partial}{\partial\theta}\left(\sin\theta\frac{\partial}{\partial\theta}\right)+\frac{1}{\sin^2\theta}\frac{\partial^2}{\partial\varphi^2}\right\}. \tag{2.9}$$

Then

$$F^{\text{int}}\chi_n(r)=\kappa_s\chi_n(r) \tag{2.10}$$

leads to

$$\left\{\frac{1}{\rho^2}\frac{\partial}{\partial\rho}\left(\rho^2\frac{\partial}{\partial\rho}\right)-\frac{l(l+1)}{\rho^2}-\frac{\rho^2}{\lambda^4}+\frac{2p+3}{\lambda^2}\right\}R_{pl}=0. \tag{2.11}$$

The solutions $R_{pl}(\rho)$ are orthonormal functions of the form

$$R_{pl}(\rho)=N_{pl}H_{pl}(\rho/\lambda)\exp(-\rho^2/2\lambda^2), \tag{2.12}$$

where N_{pl} is a normalizing factor and $H_{pl}(\eta)$ is a polynomial in η of degree p. For the case $l=p$, $H_{pl}(\eta)$ is particularly simple, being just η^p. The relation

$$\int_0^\infty R_{pl}(\rho)R_{p'l}(\rho)\rho^2d\rho=\delta_{pp'} \tag{2.13}$$

gives us for this special case:

$$R_{pp}(\rho)=\left(\frac{2^{p+2}}{1\cdot3\cdot5\cdots(2p+1)\lambda^3\pi^{\frac{1}{2}}}\right)^{\frac{1}{2}}\left(\frac{\rho}{\lambda}\right)^p\exp(-\rho^2/2\lambda^2).$$

For a given p, l has the range

$$l=p,\ p-2,\ p-4,\ \cdots\begin{cases}0 & p\text{ even}\\ 1 & p\text{ odd}\end{cases}. \tag{2.14}$$

This is all we will say about the function $R_{pl}(\rho)$, since all that will be used in this paper are the relations (2.13) and (2.14).

The eigenfunctions of F can now be written

$$\varphi_{kn}(\zeta)=e^{ikX}\chi_n(r), \tag{2.15}$$

$$F\varphi_{kn}(\zeta)=(k^2+\kappa_s^2)\varphi_{kn}(\zeta). \tag{2.16}$$

The free field solutions of F are obtained by requiring $k^2+\kappa_s^2=0$, which gives the interpretation of $|\kappa_s|$ as a mass.

Consider the Green's functions of the F operator

$$F_\zeta G_{A,R}(\zeta,\zeta')=-\delta(\zeta-\zeta'), \tag{2.17}$$

$$G_{A,R}(\zeta,\zeta')=\sum_n\Delta_{A,R}^s(X-X')\chi_n(r)\chi_n^*(r'). \tag{2.18}$$

$\Delta_{A,R}^s(X-X')$ is the usual advanced or retarded function with mass constant κ_s^2, i.e.,

$$\Delta_{A,R}^s(X-X')=-\frac{1}{(2\pi)^4}\int\frac{e^{ik(X-X')}}{k^2+\kappa_s^2}dk, \tag{2.19}$$

where the contour is to be taken below or above the singularities in the k_0 plane to produce the advanced or retarded functions respectively. In general a G function can be defined for every type of Δ function, for example (and for later use)

$$G(\zeta,\zeta')=\sum_n \Delta^s(X-X')\chi_n(r)\chi_n^*(r'), \quad (2.20)$$

where

$$\Delta(X-X')=\frac{i}{(2\pi)^3}\int \delta(k^2+\kappa_s^2)\epsilon(k)e^{ik(X-X')}dk, \quad (2.21)$$

$$\epsilon(k)=k_0/|k_0|. \quad (2.22)$$

We can now write the integral equation for $\phi(\zeta)$. Using the convention of letting

$$\xi\sim(x',\zeta'',x'''), \quad d\xi=dx'd\zeta''dx''',$$

we get

$$\phi(\zeta)=\phi^{in}(\zeta)+\int G_R(\zeta,\zeta'')\frac{\partial \mathfrak{L}_I'(\xi)}{\partial\phi(\zeta'')}d\xi, \quad (2.23)$$

where $\phi^{in}(\zeta)$ is the "incoming field" and satisfies the free field equation. As a first approximation substitute the incoming fields in the integral,

$$\phi(\zeta)=\phi^{in}(\zeta)+\phi^{(1)}(\zeta)+\cdots,$$

$$\phi^{(1)}(\zeta)=\sum_{p l m n_0}\chi_n(r)\int\Delta_R^s(X-X')\chi_n^*(r'')\frac{\partial \mathfrak{L}_I'^{in}(\xi)}{\partial\phi(\zeta'')}d\xi$$

a multifold infinite number of integrals even in this first approximation. Nor is there any reason to expect the terms in this series to decrease in magnitude since the degree of the polynomials in ρ and r_0 increases with p and n_0 respectively.

If we are to do anything at all it seems some of these mass states must be eliminated.

3. PROJECTION OPERATOR

Let us introduce a relativistic invariant projection operator into the theory, into the interaction Lagrangian first of all.

$$\mathfrak{L}_I=-g\bar\psi(x')f(\xi)[P_l\cdot\phi(\zeta'')]\psi(x'''), \quad (3.1)$$

where for example P_l can be defined as

$$P_l\varphi_{kn}(\zeta)=\begin{cases}\varphi_{kn}(\zeta) & s=a,b,c,\cdots\\ 0 & s\neq a,b,c,\cdots\end{cases} \quad (3.2)$$

since s is an invariant label under a Lorentz transformation. That is, a eigenfunction belonging to κ_s transforms into an eigenfunction belonging to κ_s since F^{int} is invariant under the Lorentz group. Thus the separation of an arbitrary function into two parts by P,

$$g(\zeta)=Pg(\zeta)+(1-P)g(\zeta)$$

is an invariant separation. There is no mixing of the two parts under a Lorentz transformation, i.e., P is a relativistic invariant operator.

Projection operators are Hermitian operators; thus we have the property

$$\int g_1(\zeta)[Pg_2(\zeta)]d\zeta=\int[P^c g_1(\zeta)]g_2(\zeta)d\zeta, \quad (3.3)$$

where $g_1(\zeta)$ and $g_2(\zeta)$ are arbitrary functions and P^c operates on the complex conjugate base function set, in our example

$$P^c\varphi_{kn}^*(\zeta)=\begin{cases}\varphi_{kn}^*(\zeta) & s=a,b,c,\cdots\\ 0 & s\neq a,b,c,\cdots\end{cases}. \quad (3.4)$$

We wish $P\phi(\zeta)$ to be real, this means we must require

$$P^c=P. \quad (3.5)$$

This is true for our example since taking the complex conjugate of $\varphi_{kn}(\zeta)$ does not affect the s label in any way; i.e., the subset of functions $\varphi_{kn}(\zeta)$ labeled by a s contains the complex conjugate functions $\varphi_{kn}^*(\zeta)$ also.

$P\phi(\zeta)$ is considered then as the physical field which we let interact with the spinor field. $(1-P)\phi(\zeta)$ represents a nonphysical part of the field which we wish to eliminate from the theory.

In order to derive the desired field equations, the general variational principle must be modified so that only variations which commute with the projection operator are allowed. Then with the aid of properties (3.3) and (3.5), δL_I becomes

$$\delta L_I=\int\Big\{-g\int f(x,\zeta'',x''')[P\phi(\zeta'')]\times\psi(x''')d\zeta''dx''\Big\}\delta\bar\psi(x)dx$$

$$+\int\Big\{-g\int\bar\psi(x')f(x',\zeta'',x)\times[P\phi(\zeta'')]dx'd\zeta''\Big\}\delta\psi(x)dx$$

$$+\int\Big\{-gP_l\int\bar\psi(x')f(x',\zeta,x''')\times\psi(x''')dx'dx'''\Big\}\delta\phi(\zeta)d\zeta,$$

which gives the equations of motion,

$$F\phi(\zeta)=-gP_l\int\bar\psi(x')f(x',\zeta,x''')\psi(x''')dx'dx''',$$

$$\left(\gamma_\mu\frac{\partial}{\partial x_\mu}+M\right)\psi(x)$$

$$=-g\int f(x,\zeta'',x''')[P\phi(\zeta'')]\psi(x''')d\zeta''dx''', \quad (3.6)$$

$$\left(-\gamma_\mu{}^T\frac{\partial}{\partial x_\mu}+M\right)\bar{\psi}(x)$$

$$=-g\int\bar{\psi}(x')f(x'_\beta\zeta'',x)[P\phi(\zeta'')]dx'd\zeta''.$$

The integral equation for $\phi(\zeta)$ is then

$$\phi(\zeta)=P_\zeta\phi^{\text{in(out)}}(\zeta)+g\int G_{R(A)}(\zeta_\beta\zeta'')P_{\zeta''}\times\int\bar{\psi}(x')f(\xi)\psi(x''')d\xi, \quad (3.7)$$

where $P_\zeta\phi^{\text{in(out)}}(\zeta)$ has been chosen as the incoming (outgoing) $\phi(\zeta)$ field since $P\phi(\zeta)$ is considered as the physical field and there is no sense putting nonphysical fields into the theory if you do not have to. The integral equation for $\phi(\zeta)$ becomes by using (3.3) and (3.5) again

$$\phi(\zeta)=P_\zeta\phi^{\text{in(out)}}(\zeta)+g\int[P_{\zeta''}G_{R(A)}(\zeta_\beta\zeta'')]\times\psi(x')f(\xi)\psi(x''')d\xi. \quad (3.8)$$

From the form of $G_{R(A)}(\zeta_\beta\zeta'')$, we see immediately that

$$P_{\zeta'}G_{R(A)}(\zeta_\beta\zeta'')=P_\zeta G_{R(A)}(\zeta_\beta\zeta''), \quad (3.9)$$

and thus

$$\phi(\zeta)=P_\zeta\left[\phi^{\text{in(out)}}(\zeta)+g\int G_{R(A)}(\zeta_\beta\zeta'')\bar{\psi}(x')f(\xi)\psi(x''')d\xi\right], \quad (3.10)$$

$$\phi(\zeta)=P\phi(\zeta).$$

Consequently, the nonphysical fields have been entirely eliminated from the theory. The integral equations are now

$$\begin{aligned}P\phi(\zeta)&=P\phi^{\text{in(out)}}(\zeta)+g\int[PG_{R(A)}(\zeta_\beta\zeta'')]\times\bar{\psi}(x')f(\xi)\psi(x''')d\xi,\\ \psi(x)&=\psi^{\text{in(out)}}(x)+g\int S_{R(A)}(x-x')f(\xi)\times[P\phi(\zeta'')]\psi(x''')d\xi,\\ \bar{\psi}(x)&=\bar{\psi}^{\text{in(out)}}(x)+g\int\bar{\psi}(x')f(\xi)\times[P\phi(\zeta'')]S_{A(R)}(x'''-x)d\xi.\end{aligned} \quad (3.11)$$

The definition of P that was given in (3.2) is not sufficient to allow much progress to be made toward solving the above equations. Due to the infinite degeneracy of the $\varphi_{kn}(\zeta)$ for a given s, $PG_{R(A)}(\zeta_\beta\zeta'')$ will still contain an infinite sum over mass states.

What other invariant labels are available? An examination of Eq. (2.16) shows that k^2 is an invariant label. This k^2 invariant will be of use later on but it is no help with the present problem where we are concerned with the mass states.

Actually, P has to be defined with respect to a different function set. Up to now our internal and external states have been entirely unconnected. Physically it is reasonable, in fact desirable, to require that the internal state depend on the external state. If mass states containing $\mathcal{Y}_{lm}(\theta\varphi)$ functions are going to be associated with particles of spin l, it is in the rest frame that the particle should be in an eigenstate of angular momentum operators. This rest frame exists only for k timelike since if the particle is at rest in this frame the first 3 components of k must vanish. The Lorentz transformation accomplishing this is given by

$$a_{ij}{}^{(k)}=_{k^2<0}\begin{bmatrix}1+\left(\frac{k_1}{K_a}\right)^2 & \frac{k_1k_2}{K_a{}^2} & \frac{k_1k_3}{K_a{}^2} & \frac{k_1k_4}{K_b}\\ \frac{k_1k_2}{K_a{}^2} & 1+\left(\frac{k_2}{K_a}\right)^2 & \frac{k_2k_3}{K_a{}^2} & \frac{k_2k_4}{K_b}\\ \frac{k_1k_3}{K_a{}^2} & \frac{k_2k_3}{K_a{}^2} & 1+\left(\frac{k_3}{K_a}\right)^2 & \frac{k_3k_4}{K_b}\\ \frac{-k_1k_4}{K_b} & \frac{-k_2k_4}{K_b} & \frac{-k_3k_4}{K_b} & \frac{-k_4{}^2}{K_b}\end{bmatrix}, \quad (3.12)$$

$$K_a{}^2=(-k^2)^{\frac{1}{2}}[(-k^2)^{\frac{1}{2}}+|k_0|], \quad K_b=|k_0|(-k^2)^{\frac{1}{2}}.$$

Note that

$$a_{ij}{}^{(-k)}=a_{ij}{}^{(k)}, \quad (3.13)$$

$$k_i{}^0=a_{ij}{}^{(k)}k_j, \quad k^0\sim\left(0,0,0,\frac{k_4(-k^2)^{\frac{1}{2}}}{|k_0|}\right). \quad (3.14)$$

Direct verification is the easiest way to show that this $a_{ij}{}^{(k)}$ matrix has the desired properties. If we restrict ourselves to pure velocity transformations, then this is a unique transformation.

Thus a function set can be defined as follows.

$$k^2<0, \quad \varphi_n(k,\zeta)=\exp(ik^0X^0)\chi_n(r^0), \quad (3.15)$$

where

$$k_i{}^0=a_{ij}{}^{(k)}k_j, \quad X_i{}^0=a_{ij}{}^{(k)}X_j, \quad r_i{}^0=a_{ij}{}^{(k)}r_j, \quad (3.16)$$

since $a_{ij}{}^{(k)}$ is a Lorentz transformation, we still have

$$F\varphi_n(k,\zeta)=(k^2+\kappa_n{}^2)\varphi_n(k,\zeta); \quad (3.17)$$

also

$$F^{\text{int}}\chi_n(k,r)=\kappa_n\chi_n(k,r), \quad (3.18)$$

where

$$\varphi_n(k,\zeta)=e^{ikX}\chi_n(k,r); \quad \chi_n(k,r)=\chi_n(r^0). \quad (3.19)$$

Thus for this new function set, k^2 and s are still good invariant labels.

Consider now a pair of invariant "coupling operators."

$$F_1^{\text{coup}}=-\left(\frac{\partial^2}{\partial X_\mu\partial r_\mu}\right)^2+\frac{1}{\lambda^4}\left(r_\mu\frac{\partial}{\partial X_\mu}\right)^2 \tag{3.20}$$

$$\begin{aligned}F_2^{\text{coup}}=&-\frac{\partial^2}{\partial X_\beta{}^2}\left(-r_\mu{}^2\frac{\partial^2}{\partial r_\nu{}^2}+r_\mu r_\nu\frac{\partial^2}{\partial r_\mu\partial r_\nu}+2r_\mu\frac{\partial}{\partial r_\mu}\right)\\&+\left(r_\mu\frac{\partial}{\partial X_\mu}\right)^2\frac{\partial^2}{\partial r_\nu{}^2}+r_\mu{}^2\left(\frac{\partial^2}{\partial X_\nu\partial r_\nu}\right)^2\\&-2r_\mu r_\nu\frac{\partial^4}{\partial X_\mu\partial X_\beta\partial r_\beta\partial r_\nu}-2r_\mu\frac{\partial^3}{\partial X_\mu\partial X_\nu\partial r_\nu}.\end{aligned} \tag{3.21}$$

F_1^{coup} was originally introduced by Yukawa into the free nonlocal field equation in an attempt to eliminate the infinite degeneracy (1). This approach led to difficulties when the interaction with other fields was considered. Here we will just use these coupling operators to establish invariant labels.

$$\begin{aligned}F_1^{\text{coup}}\varphi_n(k,\zeta)=&\left\{-\left(\frac{\partial^2}{\partial X_\mu{}^0\partial r_\mu{}^0}\right)^2+\frac{1}{\lambda^4}\left(r_\mu{}^0\frac{\partial}{\partial X_\mu{}^0}\right)^2\right\}\\&\times\exp(ik^0X^0)\chi_n(r^0)\\=&-(k_0{}^0)^2\left\{\frac{-\partial^2}{\partial r_0{}^{02}}+\frac{r_0{}^{02}}{\lambda^4}\right\}\exp(ik^0X^0)\chi_n(r^0)\\=&-(k_0{}^0)^2\left\{\frac{1}{\lambda^2}(2n_0+1)\right\}\exp(ik^0X^0)\chi_n(r^0)\\=&\frac{k^2}{\lambda^2}(2n_0+1)\varphi_n(k,\zeta),\quad k^2<0.\end{aligned} \tag{3.22}$$

This shows n_0 is an invariant label and since p is equal to $s+n_0$, p is also an invariant label.

Similarly for F_2^{coup}

$$\rho_\mu{}^0\sim(r_1{}^0,r_2{}^0,r_3{}^0)$$

$$\begin{aligned}F_2^{\text{coup}}\varphi_n(k,\zeta)=(k_0{}^0)^2\Bigg(&-(\rho_\mu{}^0)^2\frac{\partial^2}{\partial\rho_\nu{}^{02}}\\&+\rho_\mu{}^0\rho_\nu{}^0\frac{\partial^2}{\partial\rho_\mu{}^0\partial\rho_\nu{}^0}+2\rho_\mu{}^0\frac{\partial}{\partial\rho_\mu{}^0}\Bigg)\varphi_n(k,\zeta).\end{aligned}$$

Upon rearranging the parenthesis, one finds it is equal to

$$\begin{aligned}\mathbf{J}^2(\theta^0\varphi^0)=-\Bigg\{&\left(\rho_2{}^0\frac{\partial}{\partial\rho_2{}^0}-\rho_3{}^0\frac{\partial}{\partial\rho_3{}^0}\right)^2\\&+\left(\rho_2{}^0\frac{\partial}{\partial\rho_1{}^0}-\rho_1{}^0\frac{\partial}{\partial\rho_2{}^0}\right)^2+\left(\rho_1{}^0\frac{\partial}{\partial\rho_2{}^0}-\rho_2{}^0\frac{\partial}{\partial\rho_1{}^0}\right)^2\Bigg\};\end{aligned}$$

thus

$$k^2<0,\quad F_2^{\text{coup}}\varphi_n(k,\zeta)=-k^2l(l+1)\varphi_n(k,\zeta), \tag{3.23}$$

which shows l is an invariant label also.

The application of the coupling operators can be considered as "auxiliary conditions" on the free field solutions. The requirement that the free field solutions be eigenfunctions of F_1^{coup} and of F_2^{coup} with specified values of n_0 and l tells you what linear combinations of the degenerate solutions of $F\phi=0$ are to be considered as representing physical states. The presence of the projection operator in the interaction then insures that the interaction is self-consistent with the auxiliary conditions.

At any rate, for $k^2<0$ the $\varphi_n(k,\zeta)$ provide the extra invariant mass state labels that are needed if the infinite sum over mass states in the Green's function is to be reduced to a finite sum. Thus, for example, if we specify $n_0=0$, $p=2$, $l=2$ for $k^2<0$ and set the rest of the function set equal to zero, this leaves us $m=-2$, $-1, 0, 1, 2$, just five mass states which, as will be shown later, describe a particle of spin 2.

$$k^2\geqslant 0.$$

For $k^2>0$ a Lorentz transformation can be found such that

$$k_i{}^0=b_{ij}{}^{(k)}k_j,\quad k^0=((k^2)^{\frac{1}{2}},0,0,0),$$

and if one defines [going back to the functions defined in (2.3)],

$$k^2>0,\ \Gamma_n(k,r)=\Gamma_n(r^0)=\prod_{i=0}^{3}h_{n_i}(b_{ij}{}^{(k)}r_j),$$

then the functions

$$\exp(ikX)\Gamma_n(k,r)$$

are eigenfunctions of both F and F_1^{coup} with invariants s and n_1. However, the addition of n_1 to the invariant labels does not help since $s-n_1=n_2+n_3-n_0$ and there still are an infinite set of n_2, n_3, and n_0 values for given s, n_1 values. The $k^2=0$ case is more complicated than this and just as unsatisfactory.

What we really need to make invariant is n_0. If the $k^2<0$ case is examined, it is seen that $h_{n_0}(r_0{}^0)$ has a form invariant argument,

$$h_{n_0}(r_0{}^0)=h_{n_0}\left(\frac{-k_0k_\mu r_\mu}{|k_0|(-k^2)^{\frac{1}{2}}}\right)\quad k^2<0$$

and that this is apparently the reason (it is a sufficient condition anyway) that n_0 be an invariant. It can easily be shown that one cannot construct a Lorentz transformation such that $r_0{}^0$ is a form invariant function of k and r when $k^2\geqslant 0$. Only by considering eigenfunctions of F^{ins} which diverge at infinity were we able to produce a relativistic invariant label equivalent to n_0. These solutions, of course, are of no use.

Final Definition of the Function Set

Thus it seems the best that can be done is to define the projection operator with respect to the following base function set.

$$\varphi_n(k,\zeta)=\exp(ik^0X^0)\chi_n(r^0), \tag{3.24}$$

where

$$k_i^0=a_{ij}{}^{(k)}k_j,\quad X_i^0=a_{ij}{}^{(k)}X_j,\quad r_i^0=a_{ij}{}^{(k)}r_j,$$
$$a_{ij}{}^{(k)}=\delta_{ij}\quad\text{for}\quad k^2\geq 0,$$

and $a_{ij}{}^{(k)}$ as given in (3.12) for $k^2<0$. This gives the invariant labels

$$\begin{matrix} k^2,\ \mathfrak{p},\ l,\ n_0,\ s & \text{for} & k^2<0 \\ k^2,\ s & \text{for} & k^2\geq 0. \end{matrix} \tag{3.25}$$

Then

$$P\varphi_n(k,\zeta)=\left\{\begin{matrix} 0 \\ \text{or} \\ \varphi_n(k,\zeta) \end{matrix}\right\} \tag{3.26}$$

depending on the values of the invariants listed in (3.25).

Observe that according to (3.13)

$$\chi_n(-k,r)=\chi_n(k,r). \tag{3.27}$$

Actually what has been shown with the establishment of $\mathfrak{p}$, l, n_0 as invariants for $k^2<0$ is that under an arbitrary Lorentz transformation

$$X_\mu'=a_{\mu\nu}X_\nu,\quad r_\mu'=a_{\mu\nu}r_\nu,$$

$$\varphi_{pln_0m'}(k',\zeta')=\sum_{m''=-l}^{+l}\int dk''C_{m'',m'}{}^{(pln_0)}(k'',k')\times\varphi_{pln_0m''}(k'',\zeta), \tag{3.28}$$

where the $C_{m'',m'}{}^{(pln_0)}(k'',k')$ are infinite-dimensional unitary representations of the Lorentz group.

It is easily shown that

$$C_{m'',m'}{}^{(pln_0)}(k'',k')=\delta(k''-k)d_{m'',m'}{}^{(pln_0)}(k,k'), \tag{3.29}$$

where

$$k_\nu=a_{\mu\nu}k_\mu' \tag{3.30}$$

and

$$d_{m'',m'}{}^{(pln_0)}(k,k')=\int\chi_{pln_0m''}{}^*(k,r)\chi_{pln_0m'}(k',r)dr; \tag{3.31}$$

thus

$$\chi_{\substack{pln_0m'\\ k'^2<0}}(k',r')=\sum_{m=-l}^{+l}d_{mm'}{}^{(pln_0)}(k,k')\chi_{pln_0m}(k,r). \tag{3.32}$$

For the case $l=m=0$ *and* $k^2<0$, the function $\chi_n(k',r')$ transforms into the function $\chi_n(k,r)$ under a Lorentz transformation. Thus these particular $\chi_n(k,r)$ must be form invariant functions of the four vectors k and r.

4. GREENS FUNCTIONS

In order to apply the redefined P operator to the various G functions, these functions must be expressed in terms of the new function set $\varphi_n(k,\zeta)$.

Introduce the principal value function $\bar{\Delta}^s(X)$,

$$\bar{\Delta}^s(X)=\frac{-1}{(2\pi)^4}\mathcal{P}\int\frac{e^{ikX}}{k^2+\kappa_s{}^2}dk; \tag{4.1}$$

then

$$\begin{aligned}\Delta_R{}^s(X)&=\bar{\Delta}^s(X)-\tfrac{1}{2}\Delta^s(X),\\ \Delta_A{}^s(X)&=\bar{\Delta}^s(X)+\tfrac{1}{2}\Delta^s(X),\end{aligned} \tag{4.2}$$

so that we can write

$$\begin{aligned}G_R(\zeta,\zeta')&=\bar{G}(\zeta,\zeta')-\tfrac{1}{2}G(\zeta,\zeta'),\\ G_A(\zeta,\zeta')&=\bar{G}(\zeta,\zeta')+\tfrac{1}{2}G(\zeta,\zeta').\end{aligned} \tag{4.3}$$

Let

$$\Lambda_s(r,r')=\sum_q\chi_{sq}(r)\chi_{sq}{}^*(r'), \tag{4.4}$$

q representing the indices remaining in n after s is specified,

$$G(\zeta,\zeta')=\sum_s\frac{i}{(2\pi)^3}\int\delta(k^2+\kappa_s{}^2)\epsilon(k)\times e^{ik(X-X')}\Lambda_s(r,r')dk, \tag{4.5}$$

and similarly for all the other G functions.

Consider how $\Lambda_s(r,r')$ transforms under a Lorentz transformation,

$$r_i^0=a_{ij}r_j,\quad \chi_{sq}(r^0)=\sum_{q'}C_{q'q}\chi_{sq'}(r), \tag{4.6}$$

since s is an invariant for the $\chi_n(r)$ functions, $C_{q'q}$ is a unitary matrix, therefore

$$\begin{aligned}\sum_q\chi_{sq}(r^0)\chi_{sq}{}^*(r'^0)&=\sum_{qq'q''}C_{q'q}C_{q''q}{}^*\chi_{sq'}(r)\chi_{sq''}{}^*(r)\\ &=\sum_{q'}\chi_{sq'}(r)\chi_{sq'}{}^*(r'),\\ \Lambda_s(r^0,r'^0)&=\Lambda_s(r,r').\end{aligned} \tag{4.7}$$

Thus $\Lambda_s(r,r')$ is form invariant and can be written as

$$\Lambda_s(r,r')=\Lambda_s(r^0,r'^0)=\sum_q\chi_{sq}(k,r)\chi_{sq}{}^*(k,r'). \tag{4.8}$$

The individual terms in the sum depend on k but not the total sum over q.

$$G(\zeta,\zeta')=\sum_s\frac{i}{(2\pi)^3}\int\delta(k^2+\kappa_s{}^2)\epsilon(k)e^{ik(X-X')}\times[\textstyle\sum_q\chi_{sq}(k,r)\chi_{sq}{}^*(k,r')]dk.$$

Take the sum over q outside,

$$G(\zeta,\zeta')=\frac{i}{(2\pi)^3}\sum_n\int\delta(k^2+\kappa_s{}^2)\epsilon(k)\times\varphi_n(k,\zeta)\varphi_n{}^*(k,\zeta')dk \tag{4.9}$$

and $G(\zeta,\zeta')$ is expressed in terms of the desired base function set. Similarly,

$$\bar{G}(\zeta,\zeta')=\frac{-1}{(2\pi)^4}\sum_n\mathcal{P}\int\frac{\varphi_n(k,\zeta)\varphi_n{}^*(k,\zeta')}{k^2+\kappa_s{}^2}dk. \tag{4.10}$$

Since $\bar{G}$ contains $k^2\geq 0$, in order to reduce $PG_{A,R}$ to

a finite sum we must require that

$$P\varphi_n(k,\zeta)=0 \quad \text{for} \quad k^2\geqslant 0.$$

This is a little strange but there does not seem to be any way of getting around this requirement. One of the consequences of this is that it is possible to have virtual mesons in zero mass states but not real ones. That is, κ_s is equal to zero for s equal to -1, thus $P\phi^{in}(\zeta)$ cannot contain $s=-1$ states since k and s are related by $k^2+\kappa_s^2=0$ and thus $k^2=0$ for $s=-1$ in $P\phi^{in}(\zeta)$. However, $G_{A,R}(\zeta,\zeta')$ has states with $k^2<0$ and $s=-1$ [in $\bar{G}(\zeta,\zeta')$], so $s=-1$ can appear here. Of course, we can just require $P\varphi_n(k,\zeta)=0$ for $s=-1$ and forget about this oddity.

5. CONSERVATION EQUATIONS

Energy-momentum, charge, and angular momentum tensors which are constants of collision can be found by the usual method of considering the properties of the Lagrangian under different variations. Constants of the motion can also be found exactly as in the theory of local fields in nonlocal interaction.[4] Angular momentum is the case of most interest, so the calculation of this as a constant of collision will be gone through in some detail.

Consider a variation

$$x\rightarrow x+\delta x, \quad \zeta\rightarrow\zeta+\delta\zeta, \tag{5.1}$$

where the δx and $\delta\zeta$ correspond to that produced by an infinitesimal Lorentz transformation, then

$$\delta x_\mu=\epsilon_{\mu\nu}x_\nu, \quad \delta\zeta_\mu=E_{\mu\nu}\zeta_\nu \tag{5.2}$$

where

$$E_{\mu\nu}=\begin{pmatrix}\epsilon_{\mu\nu} & 0\\ 0 & \epsilon_{\mu\nu}\end{pmatrix}, \tag{5.3}$$

$$\epsilon_{\mu\nu}=-\epsilon_{\nu\mu}, \quad E_{\mu\nu}=-E_{\nu\mu}.$$

Define

$$d\sigma_\mu(x)\sim(dx_2dx_3dx_0,\ \cdots,\ dx_1dx_2dx_3/i)$$

and

$$d\sigma_\mu(\zeta)\sim(d\tau d\sigma_\nu(X),\ dXd\sigma_\lambda(\tau));$$

then under this variation,

$$\begin{aligned}\delta L=&\int d\sigma_\mu(\zeta)\mathfrak{L}_1\delta\zeta_\mu+\int d\sigma_\mu(x)\mathfrak{L}_2\delta x_\mu\\&+\int d\sigma_\mu(\zeta'')\mathfrak{L}_I\delta\zeta_\mu''dx'dx'''\\&+\int d\sigma_\mu(x')\mathfrak{L}_I\delta x_\mu'd\zeta''dx'''\\&+\int d\sigma_\mu(x''')\mathfrak{L}_I\delta x_\mu'''dx'd\zeta''\end{aligned} \tag{5.4}$$

as is intuitively quite reasonable and can be shown directly without much trouble.[5] Actually the surface integrals containing $\mathfrak{L}_I$ all vanish by the usual argument of turning the interaction on and off adiabatically. Furthermore, it must be assumed that $\phi(\zeta)$ vanishes as r, including r_0, goes to infinity and thus all surface integrals over r space also vanish and we are left with

$$\delta L=\int d\sigma_\nu(X)d\tau\mathfrak{L}_I\delta X_\nu+\int d\sigma_\nu(x)\mathfrak{L}_I\delta x_\nu. \tag{5.5}$$

However, for reasons of symmetry we will keep all the terms appearing in (5.4) in the following manipulations. Convert all surface integrals to volume integrals by using

$$\int d\sigma_\mu(x)g(x)\delta x_\mu=\int dx\delta x_\mu\frac{\partial g(x)}{\partial x_\mu}.$$

δL_I becomes then

$$\begin{aligned}\delta L_I=&-g\int\bar{\psi}_\mu(x')\delta x_\mu'f(\xi)[P\phi(\zeta'')]\psi(x''')d\xi\\&-g\int\bar{\psi}(x')f(\xi)[P\phi(\zeta'')]\psi_\mu(x''')\delta x_\mu'''d\xi\\&-g\int\bar{\psi}(x')f(\xi)\delta\zeta_\mu''\frac{\partial}{\partial\zeta_\mu''}[P\phi(\zeta'')]\psi(x''')d\xi,\end{aligned} \tag{5.6}$$

since

$$\left(\epsilon_{\mu\nu}x_\nu'\frac{\partial}{\partial x_\mu'}+\epsilon_{\mu\nu}x_\nu'''\frac{\partial}{\partial x_\mu'''}+E_{\mu\nu}\zeta_\nu''\frac{\partial}{\partial\zeta_\mu''}\right)f(\xi)=0.$$

Here is where the symmetry of this development is most useful, for since

$$E=1+E_{\mu\nu}\zeta_\nu\partial/\partial\zeta_\mu$$

is the generating operator of an infinitesimal Lorentz transformation, then it is seen E must commute with P directly from the definition of P. Thus it follows immediately that

$$[\delta\zeta_\mu\partial/\partial\zeta_\mu,\ P_I]=0,$$

and thus

$$\begin{aligned}\delta L_I=&-g\int\bar{\psi}_\mu(x')\delta x_\mu'f(\xi)[P\phi(\zeta'')]\psi(x''')d\xi\\&-g\int\bar{\psi}(x')f(\xi)[P\phi(\zeta'')]\psi_\mu(x''')\delta x_\mu'''d\xi\\&-g\int d\zeta''\phi_\mu(\zeta'')\delta\zeta_\mu''\\&\times\left\{P_{I''}\int\bar{\psi}(x')f(\xi)\psi(x''')dx'dx'''\right\}.\end{aligned} \tag{5.7}$$

[4] W. Pauli, Nuovo cimento **10**, 635 (1953); J. Rzewuski, Nuovo cimento **10**, 784 (1953).

[5] E. Hill, Revs. Modern Phys. **23**, 253 (1951).

Consider now δL_1:

$$\delta L_1=\int d\zeta\left\{\frac{\partial^e \mathfrak{L}_1}{\partial\zeta_\mu}\delta\zeta_\mu+\frac{\partial\mathfrak{L}_1}{\partial\phi}\phi_\mu\delta\zeta_\mu+\frac{\partial\mathfrak{L}_1}{\partial\phi_\nu}\phi_{\nu\mu}\delta\zeta_\mu+\frac{\partial\mathfrak{L}_1}{\partial\phi_{\nu\lambda}}\phi_{\nu\lambda\mu}\delta\zeta_\mu\right\},\quad(5.8)$$

where $\partial^e\mathfrak{L}_1/\partial\zeta_\mu$ is the derivative of $\mathfrak{L}_1$ with respect to its explicit dependence on ζ.

Writing

$$\frac{\partial\mathfrak{L}_1}{\partial\phi_\nu}\phi_{\nu\mu}\delta\zeta_\mu=\frac{\partial}{\partial\zeta_\nu}\left(\frac{\partial\mathfrak{L}_1}{\partial\phi_\nu}\phi_\mu\delta\zeta_\mu\right)-\frac{\partial}{\partial\zeta_\nu}\left(\frac{\partial\mathfrak{L}_1}{\partial\phi_\nu}\right)\phi_\mu\delta\zeta_\mu-\frac{\partial\mathfrak{L}_1}{\partial\phi_\nu}\phi_\mu E_{\mu\nu},$$

$$\frac{\partial\mathfrak{L}_1}{\partial\phi_{\nu\lambda}}\phi_{\nu\lambda\mu}\delta\zeta_\mu=\frac{\partial}{\partial\zeta_\nu}\left[\frac{\partial\mathfrak{L}_1}{\partial\phi_{\nu\lambda}}\frac{\partial}{\partial\zeta_\lambda}(\phi_\mu\delta\zeta_\mu)-\frac{\partial}{\partial\zeta_\lambda}\left(\frac{\partial\mathfrak{L}_1}{\partial\phi_{\nu\lambda}}\right)\phi_\mu\delta\zeta_\mu\right]+\frac{\partial^2}{\partial\zeta_\lambda\partial\zeta_\nu}\left(\frac{\partial\mathfrak{L}_1}{\partial\phi_{\nu\lambda}}\right)\phi_\mu\delta\zeta_\mu-2\frac{\partial\mathfrak{L}_1}{\partial\phi_{\nu\lambda}}\phi_{\nu\mu}E_{\mu\lambda}$$

this gives

$$\delta L_1=\int d\zeta\left\{\frac{\partial\mathfrak{L}_1}{\partial\phi}-\frac{\partial}{\partial\zeta_\nu}\frac{\partial\mathfrak{L}_1}{\partial\phi_\nu}+\frac{\partial^2}{\partial\zeta_\nu\partial\zeta_\lambda}\frac{\partial\mathfrak{L}_1}{\partial\phi_{\nu\lambda}}\right\}\phi_\mu\delta\zeta_\mu+\int d\zeta\left\{\frac{\partial^e\mathfrak{L}_1}{\partial\zeta_\mu}\delta\zeta_\mu-\frac{\partial\mathfrak{L}_1}{\partial\phi_\nu}\phi_\mu E_{\mu\nu}-2\frac{\partial\mathfrak{L}_1}{\partial\phi_{\nu\lambda}}\phi_{\nu\mu}E_{\mu\lambda}\right\}+\int d\sigma_\nu(\zeta)\left\{\frac{\partial\mathfrak{L}_1}{\partial\phi_\nu}\phi_\mu\delta\zeta_\mu+\frac{\partial\mathfrak{L}_1}{\partial\phi_{\nu\lambda}}\frac{\partial}{\partial\zeta_\lambda}(\phi_\mu\delta\zeta_\mu)-\frac{\partial}{\partial\zeta_\lambda}\left(\frac{\partial\mathfrak{L}_1}{\partial\phi_{\nu\lambda}}\right)\phi_\mu\delta\zeta_\mu\right\}.\quad(5.9)$$

Note that the last two terms containing $\partial\mathfrak{L}_1/\partial\phi_{\nu\lambda}$ in the surface integral will both vanish since they will appear only in surface integrals over r space.

Consider now the invariance of $\mathfrak{L}_1$ under an infinitesimal Lorentz transformation at a fixed space-time point of the field

$$\Delta\mathfrak{L}_1=0,\quad\Delta\phi=0,$$

$$\Delta\mathfrak{L}_1=\frac{\partial^e\mathfrak{L}_1}{\partial\zeta_\mu}\delta\zeta_\mu+\frac{\partial\mathfrak{L}_1}{\partial\phi_\nu}\Delta\phi_\nu+\frac{\partial\mathfrak{L}_1}{\partial\phi_{\nu\lambda}}\Delta\phi_{\nu\lambda},$$

$$\Delta\phi_\nu=\frac{\partial\phi(\zeta)}{\partial\zeta_\nu'}-\frac{\partial\phi(\zeta)}{\partial\zeta_\nu},\quad\frac{\partial}{\partial\zeta_\nu'}=\frac{\partial}{\partial\zeta_\nu}-E_{\mu\nu}\frac{\partial}{\partial\zeta_\mu};$$

thus

$$\Delta\phi_\nu=-E_{\mu\nu}\phi_\mu;$$

similarly,

$$\Delta\phi_{\nu\lambda}=-E_{\mu\nu}\phi_{\mu\lambda}-E_{\mu\lambda}\phi_{\mu\nu},$$

$$\Delta\mathfrak{L}_1=\frac{\partial^e\mathfrak{L}_1}{\partial\zeta_\mu}\delta\zeta_\mu-\frac{\partial\mathfrak{L}_1}{\partial\phi_\nu}E_{\mu\nu}\phi_\mu-2\frac{\partial\mathfrak{L}_1}{\partial\phi_{\nu\lambda}}E_{\mu\lambda}\phi_{\mu\nu}=0.$$

Thus the second integral over $d\zeta$ vanishes also leaving only

$$\delta L_1=\int d\zeta\{-F\phi\}\phi_\mu\delta\zeta_\mu+\int drd\sigma_\nu(X)\left\{\frac{\partial\mathfrak{L}_1}{\partial\phi_\nu}\phi_\mu\delta\zeta_\mu\right\}.\quad(5.10)$$

Repeating the process that leads to Eq. (5.9), one obtains for

$$\delta L_2=\int dX\left\{\frac{\partial\mathfrak{L}_2}{\partial\psi^\sigma}-\frac{\partial}{\partial X_\tau}\frac{\partial\mathfrak{L}_2}{\partial\psi_\tau^\sigma}\right\}\psi_\mu^\sigma\delta X_\mu-\int dX\frac{\partial\mathfrak{L}_2}{\partial\psi_\tau^\sigma}\psi_\mu^\sigma\epsilon_{\mu\nu}+\int d\sigma_\nu(X)\frac{\partial\mathfrak{L}_2}{\partial\psi_\nu^\sigma}\psi_\mu^\sigma\delta X_\mu.\quad(5.11)$$

Then the invariance of $\mathfrak{L}_2$ and $\mathfrak{L}_I$ under a Lorentz transformation at a fixed space-time point of the fields $\psi^\sigma(X)$ gives

$$\Delta\mathfrak{L}_2=\Delta\mathfrak{L}_I=0,\quad\Delta\psi^\sigma\neq0;$$

so, we have

$$\int\Delta\mathfrak{L}_2dX+\int\Delta\mathfrak{L}_Id\xi=0,$$

which leads, using the field equations, to

$$\int dX\frac{\partial\mathfrak{L}_2}{\partial\psi_\tau^\sigma}\psi_\mu^\sigma\epsilon_{\mu\tau}=\int dX\frac{\partial}{\partial X_\tau}\left(\frac{\partial\mathfrak{L}_2}{\partial\psi_\tau^\sigma}\Delta\psi^\sigma\right),$$

substitution of which into (5.11) produces,

$$\delta L_2=\int dX\left\{\frac{\partial\mathfrak{L}_2}{\partial\psi^\sigma}-\frac{\partial}{\partial X_\tau}\frac{\partial\mathfrak{L}_2}{\partial\psi_\tau^\sigma}\right\}\psi_\mu^\sigma\delta X_\mu+\int d\sigma_\nu(X)\left\{\frac{\partial\mathfrak{L}_2}{\partial\psi_\nu^\sigma}\psi_\mu^\sigma\delta X_\mu-\frac{\partial\mathfrak{L}_2}{\partial\psi_\nu^\sigma}\Delta\psi^\sigma\right\}.\quad(5.12)$$

Now combine δL_1, δL_2, and δL_I as given by (5.10), (5.12), and (5.7) and use the field equations again, then

$$\delta L=\int drd\sigma_\nu(X)\left\{\frac{\partial\mathfrak{L}_1}{\partial\phi_\nu}\phi_\mu\delta\zeta_\mu\right\}+\int d\sigma_\nu(X)\left\{\frac{\partial\mathfrak{L}_2}{\partial\psi_\nu^\sigma}\psi_\mu^\sigma\delta X_\mu-\frac{\partial\mathfrak{L}_2}{\partial\psi_\nu^\sigma}\Delta\psi^\sigma\right\}.\quad(5.13)$$

Subtract this expression for δL from the expression

given for δL in (5.5)

$$\int d\sigma_\nu(X)\left\{\int\left[-\frac{\partial \mathfrak{L}}{\partial \phi_\nu}\phi_\mu\delta\gamma_\mu+\mathfrak{L}_1\delta X_\nu\right]dr - \frac{\partial \mathfrak{L}_2}{\partial \psi_{\nu,\sigma}}\psi_{\mu,\sigma}\delta X_\mu+\mathfrak{L}_2\delta X_\nu+\frac{\partial \mathfrak{L}_2}{\partial \psi_{\nu,\sigma}}\Delta\psi^\sigma\right\}=0. \quad (5.14)$$

Express as a coefficient of $\epsilon_{\mu\lambda}$ using the definitions,

$$\Delta\psi^\sigma=\frac{i}{2}S_{\mu\lambda}{}^{\sigma\rho}\psi^\rho\epsilon_{\mu\lambda}, \quad (5.15)$$

$$t_{\nu\mu}=\int\left[-\frac{\partial \mathfrak{L}_1}{\partial(\partial\phi/\partial X_\nu)}\frac{\partial\phi}{\partial X_\mu}+\delta_{\nu\mu}\mathfrak{L}_1\right]dr - \frac{\partial \mathfrak{L}_2}{\partial \psi_{\nu,\sigma}}\psi_{\mu,\sigma}+\delta_{\nu\mu}\mathfrak{L}_2. \quad (5.16)$$

Then

$$\int d\sigma_\nu(X)\left\{t_{\nu\mu}\epsilon_{\mu\lambda}X_\lambda+\frac{i}{2}\frac{\partial \mathfrak{L}_2}{\partial \psi_{\nu,\sigma}}S_{\mu\lambda}{}^{\sigma\rho}\psi^\rho\epsilon_{\mu\lambda} - \int\frac{\partial \mathfrak{L}_1}{\partial \phi_\nu}\frac{\partial\phi}{\partial r_\mu}\epsilon_{\mu\lambda}r_\lambda\right\}=0, \quad (5.17)$$

which yields the conservation equation

$$\int d\sigma_\nu(X)\left\{(t_{\nu\mu}X_\lambda-t_{\nu\lambda}X_\mu)+\frac{i}{2}\frac{\partial \mathfrak{L}_2}{\partial \psi_{\nu,\sigma}}(S_{\mu\lambda}{}^{\sigma\rho}-S_{\lambda\mu}{}^{\sigma\rho})\psi^\rho - \int\frac{\partial \mathfrak{L}_1}{\partial(\partial\phi/\partial X_\nu)}\left(r_\lambda\frac{\partial}{\partial r_\mu}-r_\mu\frac{\partial}{\partial r_\lambda}\right)\phi dr\right\}=0. \quad (5.18)$$

By repeating the previous argument for the much simpler case of a variation where

$$\delta x_\mu=\epsilon_\mu, \quad \delta X_\mu=\epsilon_\mu, \quad \delta r_\mu=0,$$

i.e., a displacement of the external coordinates only, then the following energy-momentum conservation equation is obtained

$$\int d\sigma_\nu(X)t_{\nu\mu}=0, \quad (5.19)$$

where, however, it must be required that $f(\xi)$ is invariant under this variation, i.e.,

$$\left(\frac{\partial}{\partial x_\mu'}+\frac{\partial}{\partial X_\mu''}+\frac{\partial}{\partial x_\mu'''}\right)f(\xi)=0. \quad (5.20)$$

Thus there is no trouble in interpreting Eq. (5.18). The first term represents the external angular momentum, the second gives the spin from the spinor particles, and the third gives the contribution from the internal state of the scalar particles. This last will be investigated more later on.

Charge conservation,

$$\int d\sigma_\nu(X)\bar\psi\gamma_\nu\psi=0, \quad (5.21)$$

follows directly from the invariance of the Lagrangian under

$$\psi\to e^{i\alpha}\psi, \quad \bar\psi\to e^{-i\alpha}\bar\psi.$$

The previous conservation equations have all given constants of collision. One can take the constants of collision and add an interaction term to them so as to produce constants of the motion as shown in (4). Thus, for the simplest case, if we define

$$Q=Q^0+Q^{\rm int},$$

where

$$Q^0=-i\int\bar\psi\gamma_0\psi d^3X;$$

then the requirements

$$\frac{dQ}{dX_0}=0, \quad Q^{\rm int}(\pm\infty)=0$$

lead to

$$Q^{\rm int}(X_0)=\tfrac{1}{2}\int[\epsilon(X-x')-\epsilon(X-x'')]\mathfrak{L}_I(\xi)d\xi,$$

where $\epsilon(x)$ is $+$ or -1 as $x_0>0$ or <0. However, the previously calculated constants of collision are all that are needed in this discussion.

6. QUANTIZATION

As in nonlocal interaction of local field theory, the system can be quantized by defining the commutation relations of the incoming free fields. Thus, for the spinor fields one has the usual relations,

$$\begin{aligned}\{\psi^{\rm in}(x),\psi^{\rm in}(x')\}&=\{\bar\psi^{\rm in}(x),\bar\psi^{\rm in}(x')\}=0,\\ \{\psi^{\rm in}(x'''),\bar\psi^{\rm in}(x')\}&=-iS(x'''-x'),\\ [\psi^{\rm in}(x),\phi^{\rm in}(\zeta)]&=[\bar\psi^{\rm in}(x),\phi^{\rm in}(\zeta)]=0.\end{aligned} \quad (6.1)$$

The obvious choice for the commutation relation of the nonlocal field is

$$[\phi^{\rm in}(\zeta),\phi^{\rm in}(\zeta')]=-iG(\zeta,\zeta'), \quad (6.2)$$

and indeed this is what will be used. This commutation relation corresponds to a $\phi^{\rm in}(\zeta)$ of the form,

$$\phi^{\rm in}(\zeta)=\frac{1}{(2\pi)^{\frac{1}{2}}}\sum_n\int\frac{d^3k}{(2k_0{}^s)^{\frac{1}{2}}}[a_{kn}\varphi_n(k^s,\zeta) + a_{kn}{}^*\varphi_n{}^*(k^s,\zeta)], \quad (6.3)$$

$$\left.\begin{aligned}[a_{kn},a_{k'n'}{}^*]&=\delta(\mathbf{k}-\mathbf{k}')\delta_{nn'},\\ [a_{kn},a_{k'n'}]&=[a_{kn}{}^*,a_{k'n'}{}^*]=0,\end{aligned}\right\} \quad (6.4)$$

$$k^s\sim(\mathbf{k},ik_0{}^s), \quad k_0{}^s=(\mathbf{k}^2+\kappa_s{}^2)^{\frac{1}{2}} \quad (6.5)$$

exactly what one expects from analogy with local field theory.

If the definition

$$\pi^{\text{in}}(\zeta)=\frac{\partial\phi^{\text{in}}(\zeta)}{\partial X_0} \tag{6.6}$$

is made, then

$$[\phi^{\text{in}}(\zeta),\pi^{\text{in}}(\zeta')]=-i\sum_s \frac{\partial\Delta(X-X')}{\partial X_0}\bigg|_{X_0=X_{0'}} \Lambda_s(r,r')$$

$$=i\delta(\mathbf{X}-\mathbf{X}')\delta(r-r') \tag{6.7}$$

since

$$\frac{\partial\Delta(X-X')}{\partial X_0}\bigg|_{X_0=X_{0'}}=-\delta(\mathbf{X}-\mathbf{X}').$$

This points up the fact that for the free nonlocal field there is no trouble in setting up a classical Hamiltonian field formulation where X_0 is treated as the nonsymmetric time variable and r is treated on a par with $\mathbf{X}$, as is indicated in relation (6.7). The quantum-mechanical Schrödinger representation can then be constructed by assuming the usual commutation relations and the Schrödinger equation.

Consider now the nonlocal energy-momentum four vector for the free field.

$$\mathrm{P}_\nu=-i\int t'_{4\nu}d^3X. \tag{6.8}$$

A symmetrized expression must be taken for $t'_{\mu\nu}$.

$$t'_{\mu\nu}=\frac{1}{2}\int\left\{\frac{\partial\phi}{\partial X_\mu}\frac{\partial\phi}{\partial X_\nu}+\frac{\partial\phi}{\partial X_\nu}\frac{\partial\phi}{\partial X_\mu}\right.$$

$$\left.-\delta_{\mu\nu}\left(\frac{\partial\phi}{\partial X_\lambda}\frac{\partial\phi}{\partial X_\lambda}+\phi(F^{\text{int}})^2\phi\right)\right\}dr. \tag{6.9}$$

The substitution of the incoming field as given in (6.3) into the expression for P_ν leads to the expected result that

$$\mathrm{P}_\nu{}^{\text{in}}=\frac{1}{2}\sum_n\int d^3k k_\nu(a_{\mathbf{k}n}{}^*a_{\mathbf{k}n}+a_{\mathbf{k}n}a_{\mathbf{k}n}{}^*). \tag{6.10}$$

In the process of attaining this expression, use was made of the fact that

$$\int\chi_n(k,r)\chi_{n'}(k',r)dr=0=\int\chi_n{}^*(k,r)\chi_{n'}(k',r)dr. \tag{6.11}$$
$$s\neq s' \qquad\qquad s\neq s'$$

That is, k and k' merely specify Lorentz transformations. Thus if $\chi_{n'}(k',r)$ is expressed in terms of the functions $\chi_{n''}(k,r)$, then $s''=s'$ since s is an invariant label for all k and the integrals in (6.11) are zero from orthogonality.

Define

$$L_{\lambda\mu}=r_\lambda\partial/\partial r_\mu-r_\mu\partial/\partial r_\lambda. \tag{6.12}$$

From Eq. (5.18) a symmetrized internal angular momentum operator can be written as follows,

$$I_{\lambda\mu}=\frac{1}{2}\int\left\{\frac{\partial\phi}{\partial X_0}L_{\lambda\mu}\phi+[L_{\lambda\mu}\phi]\frac{\partial\phi}{\partial X_0}\right\}d^3Xdr, \tag{6.13}$$

which becomes, upon substitution of ϕ^{in},

$$I_{\lambda\mu}{}^{\text{in}}=\frac{i}{2}\sum_{\substack{nn'\\ s=s'}}\int d^3k\int\chi_n{}^*(k,r)L_{\lambda\mu}\chi_{n'}(k,r)dr$$

$$\times(a_{\mathbf{k}n}{}^*a_{\mathbf{k}n'}+a_{\mathbf{k}n'}a_{\mathbf{k}n}{}^*). \tag{6.14}$$

The reduction of $I_{\lambda\mu}{}^{\text{in}}$ to this form requires the use of

$$\int\chi_n(k,r)L_{\lambda\mu}\chi_{n'}(k',r)dr=0$$
$$s\neq s'$$

$$=\int\chi_n{}^*(k,r)L_{\lambda\mu}\chi_{n'}(k',r)dr. \tag{6.15}$$
$$s\neq s'$$

This follows from the fact that $(1+\sum_{\lambda<\sigma}\epsilon_{\lambda\sigma}L_{\lambda\sigma})$ acting on $\chi_{n'}(k',r)$ generates an infinitesimal Lorentz transformation under which s' is an invariant label. Thus $L_{\lambda\mu}\chi_{n'}(k',r)$ must be expressible as a linear combination of base functions which are labeled by s'. Then using (6.11) we get (6.15).

Particle states can thus be defined in the usual manner by letting creation operators $a_{\mathbf{k}n}{}^*$ operate on the free field vacuum. These states are eigenstates of $\mathrm{P}_\nu{}^{\text{in}}$ and describe a partical in a spin state l, m. For example, if the vacuum fluctuation angular momentum is dropped,

$$I_{21}{}^{\text{in}}a_{\mathbf{k}-\theta,n}{}^*|0\rangle=ma_{\mathbf{k}-\theta,n}{}^*|0\rangle, \tag{6.16}$$

since

$$L_{21}=-\partial/\partial\varphi.$$

The substitution of $P\phi(\zeta)$ for $\phi(\zeta)$ produces the commutation relation

$$[P_\zeta\phi(\zeta),P_{\zeta'}\phi(\zeta')]=-iP_\zeta G(\zeta,\zeta') \tag{6.17}$$

and will just cause the summations over n and n' in the expressions for $\mathrm{P}_\nu{}^{\text{in}}$ and $I_{\lambda\mu}{}^{\text{in}}$ to be restricted to the "physical states," i.e., those not set to zero by P.

While discussing operator properties it might be worthwhile to mention that although

$$f^*(x',\xi'',x''')=f(x''',\xi'',x') \tag{6.18}$$

is a sufficient condition to insure that L_f is a Hermitian operator, it is not always necessary. The functions $\varphi_n(k,\zeta)$ have a parity $(-)^{l+n_\theta}$ under the reflection r to $-r$. Thus one could require

$$P\phi(X,-r)=P\phi(X,r) \quad\text{or}\quad P\phi(X,-r)=-P\phi(X,r),$$

depending on the choice of P. For these cases, the condition on $f(\xi)$ becomes

$$f^*(x',\xi'',x''')=f(x''',X'',\pm r'',x'),$$

or

$$f^*(x',\xi'',x''')=\pm f(x''',X'',\pm r'',x'),$$

respectively.

7. INTERACTING SYSTEM IN TERMS OF EQUIVALENT LOCAL FIELDS

Let

$$\phi(\xi)=\sum_n\int\phi_n(k)\varphi_n(k,\xi)dk, \tag{7.1}$$

and since $\phi(\xi)$ is Hermitian,

$$\phi(\xi)=\sum_n\int\phi_n^*(k)\varphi_n^*(k,\xi)dk. \tag{7.2}$$

"Equivalent local fields" can be defined by

$$\phi_n(x)=\int\phi_n(k)e^{ikx}dk. \tag{7.3}$$

Since

$$G(\xi,\xi')=\sum_n\int\Delta^s(k)\varphi_n(k,\xi)\varphi_n^*(k,\xi')dk, \tag{7.4}$$

one readily finds

$$[\phi_n^{\text{in}}(x),\phi_{n'}^{\text{in}*}(x')]=-i\delta_{nn'}\Delta^s(x-x'). \tag{7.5}$$

For the Greens functions, we have similarly

$$G_{A,R}(\xi,\xi')=G_{A,R}^*(\xi,\xi')$$

$$=\sum_n\int\Delta_{A,R}^{s*}(k)\varphi_n^*(k,\xi)\varphi_n(k,\xi')dk. \tag{7.6}$$

Substitute (7.1), (7.2), and (7.6) into the integral equations (3.11). One can take account of the projection operator by simply considering that the quantities $\phi_n(k)$ and $\varphi_n(k,\xi)$ vanish for those values of n and k that the P operator sets to zero.

$$\begin{aligned}
\phi_n^*(k)&=\phi_n^{\text{in(out)}*}(k)+g\Delta_{R(A)}^{s*}(k)\int\varphi_n(k'',\xi'')\\
&\quad\times\delta(k-k'')\bar\psi(x')f(\xi)\psi(x''')dk''d\xi,\\
\psi(x)&=\psi^{\text{in(out)}}(x)+g\sum_n\int S_{R(A)}(x-x')f(\xi)\\
&\quad\times\phi_n(k)\varphi_n(k'',\xi'')\delta(k-k'')\psi(x''')dkdk''d\xi,\\
\bar\psi(x)&=\bar\psi^{\text{in(out)}}(x)+g\sum_n\int\bar\psi(x')f(\xi)\phi_n(k)\\
&\quad\times\varphi_n(k'',\xi'')\delta(k-k'')S_{A(R)}(x'''-x)dkdk''d\xi.
\end{aligned} \tag{7.7}$$

Let

$$\delta(k-k'')=\int\frac{e^{ikx'-ik''x''}}{(2\pi)^4}dx'', \tag{7.8}$$

and define

$$f_n(x',x'',x''')=\int f(\xi)\varphi_n(k'',\xi'')\frac{e^{-ik''x''}}{(2\pi)^4}dk''d\xi''; \tag{7.9}$$

so then

$$\begin{aligned}
\phi_n^*(x)&=\phi_n^{\text{in(out)}*}(x)+g\int\Delta_{R(A)}^s(x-x'')\bar\psi(x')\\
&\quad\times f_n(x',x'',x''')\psi(x''')dx'dx''dx''',\\
\psi(x)&=\psi^{\text{in(out)}}(x)+g\sum_n\int S_{R(A)}(x-x')\\
&\quad\times f_n(x',x'',x''')\phi_n(x'')\psi(x''')dx'dx''dx''',\\
\bar\psi(x)&=\bar\psi^{\text{in(out)}}(x)+g\sum_n\int\bar\psi(x')f_n(x',x'',x''')\\
&\quad\times\phi_n(x'')S_{A(R)}(x'''-x)dx'dx''dx'''.
\end{aligned} \tag{7.10}$$

Choose P such that

$$P\varphi_n(k,\xi)=0 \quad\text{for}\quad l\neq 0 \quad\text{and}\quad k^2\geqslant 0,$$

i.e., consider only spin zero mesons. It was shown at the end of Sec. 3 that $\chi_n(k,r)$ is a form invariant function of k and r for this case. It follows from this that $f_n(x',x'',x''')$ is a form invariant function of x', x'' and x''' and also that $\phi_n(x)$ transforms like a scalar field. We also have $\phi_n^*(x)=\phi_n(x)$ for $l=0$. In short, Eqs. (7.10) and (7.5) become identical with those for a collection of scalar local fields, each with its own mass value $|\kappa_n|$ and form function $f_n(x',x'',x''')$, in nonlocal interaction with a spinor local field.

Thus it is evident that on the question of convergence this theory will go as far as, and no further than, the theory of local fields in nonlocal interaction. It is true that for higher spin states the $f_n(x',x'',x''')$ are no longer form invariant, however the exponential part of $\chi_n(k,r)$,

$$\chi_n(k,r)=N_{pl}H_{pl}(\rho^0/\lambda)\mathcal{Y}_{lm}(\theta^0\varphi^0)N_{n0}H_{n0}(r_0^0/\lambda)$$
$$k^2<0$$
$$\times\exp\left\{-\frac{1}{2\lambda^2}\left[r_n^2+\frac{2(kr)^2}{-k^2}\right]\right\}$$

is a form invariant function of k and r. Since this is where any convergence factors must come from it is seen that the noninvariance properties of the $f_n(x',x'',x''')$ are not of such a form as to aid in the problem of convergence.

8. CONCLUSION

Having defined the commutation relations of the incoming fields, the commutation relations of the outgoing fields are determined by the field equations. Following Hayashi,[6] the outgoing fields can be split up

[6] C. Hayashi, Progr. Theoret. Phys. Japan **10**, 533 (1953); and Progr. Theoret. Phys. Japan **11**, 226 (1954).

into two parts,

$$P\phi^{\text{out}}=P\phi_A{}^{\text{out}}+P\phi_B{}^{\text{out}}, \quad \psi^{\text{out}}=\psi_A{}^{\text{out}}+\psi_B{}^{\text{out}},$$

such that the fields $\psi_A{}^{\text{out}}$ and $P\phi_A{}^{\text{out}}$ satisfy the same commutation relations as the incoming fields. Then a unitary matrix, M, can be defined as

$$M^{-1}\psi^{\text{in}}M=\psi_A{}^{\text{out}}, \quad M^{-1}P\phi^{\text{in}}M=P\phi_A{}^{\text{out}}.$$

One would like to say that this M matrix corresponds to the Heisenberg S matrix. However, the relation of this M matrix to the classical conservation equations is not very clear, especially since the fields $P\phi_B{}^{\text{out}}$ and $\psi_B{}^{\text{out}}$ do not vanish in general. The situation would be improved if they did vanish in general. Hayashi[6] in his latest investigations of local fields in nonlocal interaction seems to be proceeding in this direction, that is, making the out fields obey the same commutation relations as the in fields by modifying the equations of motion. In general, if the quantization difficulties are cleared up for local fields in nonlocal interaction, one can expect that those of the present theory will also be cleared up.

I wish to acknowledge my indebtedness to Professor H. Yukawa with respect to the over-all contents of this paper and to Professor N. Kroll for suggesting the attack which was used on angular-momentum conservation.

PHYSICAL REVIEW VOLUME 99, NUMBER 1 JULY 1, 1955

Renormalization in the New Tamm-Dancoff Theory of Meson-Nucleon Scattering*†

R. H. DALITZ,‡ *Laboratory of Nuclear Studies, Cornell University, Ithaca, New York*

AND

F. J. DYSON, *Institute for Advanced Studies, Princeton, New Jersey*

(Received December 24, 1954)

The new Tamm-Dancoff equations for meson-nucleon scattering are set up in the lowest approximation and it is shown how explicit nonphysical singularities may be avoided in these equations. The particle self-energies appearing in the integral equation are renormalized, but the resulting modified propagator for the system then has a nonphysical singularity. For the states $T=j=\frac{1}{2}$, the vertex and self-energy expressions generated by the uncrossed graph are considered. The renormalized vertex may be constructed by the successive solution of two one-dimensional integral equations, the finite part of the self-energy then being obtained by quadratures. Vertex renormalization is uncertain to a constant factor in the $S_{\frac{1}{2}}$ state, and the $S_{\frac{1}{2}}$ theory therefore depends on two parameters. No numerical results are obtained, owing to a number of difficulties found in this theory—a comparison is made between these difficulties and those of the corresponding Bethe-Salpeter equation.

I. INTRODUCTION

SOME preliminary calculations of phase shifts for meson-nucleon scattering have recently been reported[1] for the relativistic π-meson theory with pseudoscalar coupling, based on the simplest Tamm-Dancoff approximation to the meson-nucleon system. This approximation omits all amplitudes describing the system except those directly coupled to the one-meson one-nucleon amplitude in consequence of the interaction between the meson and nucleon fields. For this amplitude an integral equation was obtained. In addition to terms describing the interaction between the meson and nucleon of this amplitude, the integral equation contained a number of divergent terms, representing the self-energies of the particles and the change in the energy of the vacuum state which result from the interaction between the meson and nucleon fields. The interaction kernel in this integral equation is clearly the most important term physically since it accounts for the scattering process, while these other terms simply describe various kinds of correction to the motion. Since these corrections could not be evaluated in this Tamm-Dancoff theory, self-energy terms were simply omitted and calculations were carried through for the $T=\frac{3}{2}$, $S_{\frac{1}{2}}$, and $P_{\frac{1}{2}}$ states of the meson-nucleon system. Although this lowest-order Tamm-Dancoff theory represents a drastic approximation to the complete γ_5 theory, very considerable success was obtained in accounting for the striking behavior of the phase-shift[2] δ_{33} in terms of one parameter, the coupling constant $G^2/4\pi$. For the $S_{\frac{1}{2}}$ state, the linear behavior of the phase shift δ_3 for high momenta could be understood in terms of the strong repulsive interaction obtained

* Assisted by the joint program of the Office of Naval Research and the U. S. Atomic Energy Commission.

† Presented as a post-deadline paper at the Washington meeting of the American Physical Society, April, 1954.

‡ On leave of absence from the Department of Mathematical Physics, University of Birminghan, England.

[1] Dyson, Ross, Salpeter, Schweber, Sundaresen, Visscher, and Bethe, Phys. Rev. 95, 1644 (1954). This paper will be referred to as D3.

[2] De Hoffmann, Metropolis, Alei, and Bethe, Phys. Rev. 95, 1586 (1954); R. L. Martin, Phys. Rev. 95, 1606 (1954).

in the Tamm-Dancoff theory, the departures at lower momenta being attributed to some weak attractive interaction not included in the theory at the present stage.

Experiments on meson-nucleon scattering have now determined these and other phase shifts over a wide range of energies. The cross sections are relatively insensitive to certain phase shifts, notably the $T=\frac{1}{2}$, P-phase shifts δ_{11} and δ_{13}, for which it can only be said that they are small. However, in addition to the phases δ_3 and δ_{33}, the behavior of the $T=\frac{1}{2}$, $S_{\frac{1}{2}}$ phase δ_1 now appears to be fairly well established.[3]

In the Tamm-Dancoff theory, the interaction kernel contains one term (the uncrossed graph) which is effective only for the $T=\frac{1}{2}$, $j=\frac{1}{2}$ meson-nucleon states. This is a consequence of the fact that these states have the same isotopic spin, angular momentum, and parity as the state of one stationary nucleon or of one antinucleon. Although the integral equation has a finite form, it has no finite solution for these states, since this additional term generates new self-energy divergences in an implicit way. However this interaction term gives an important contribution to the scattering processes and cannot consistently be omitted. No means were available for the treatment of this problem and no calculations were made for these states in the previous work.

In order to avoid the presence of the vacuum self-energy term in the integral equation, a new Tamm-Dancoff (N.T.D.) method has been proposed[4] in which the amplitudes are based on the physical vacuum state rather than the bare-particle vacuum state. In the integral equation obtained with the corresponding Tamm-Dancoff approximation, no vacuum self-energy term appears, the energy of the system being measured relative to that of the physical vacuum, and the particle self-energies appearing have a form which is now closely related to that of the covariant theory.[5] In this N.T.D. theory, the positive and negative frequency states were treated symmetrically, and a new difficulty appeared, namely the presence of unphysical singularities in the N.T.D. amplitudes. The avoidance of these singularities clearly required the statement of a further boundary condition expressing the fact that the state with respect to which the N.T.D. amplitudes are defined is really the physical vacuum state.

The purpose of the present investigation was to inquire to what extent the existing phase-shift calculations could be improved by the inclusion of particle self-energy corrections, and supplemented by their extension to the $T=\frac{1}{2}$, $j=\frac{1}{2}$ states. In Sec. II, the N.T.D. equations for the problem are set up in the simplest Tamm-Dancoff approximation and it is found possible in this approximation, by the use of the boundary condition mentioned above, to give a set of equations which have no nonphysical singularities. This requires, however, that the theory no longer be symmetrical between positive and negative frequencies. The renormalization of the self-energies appearing in the integral equation itself is carried out in Sec. III, where it is found that a further nonphysical singularity appears in consequence of this achievement. In Sec. IV, the renormalization of the vertex and self-energy parts generated by the uncrossed graph (see Fig. 1) is carried through, and the evaluation of their finite parts by the solution of finite integral equations and by finite integration processes is discussed. The Tamm-Dancoff method has the attraction that it is numerically calculable since all the operations appropriate may be handled by standard numerical techniques. Except at one point (vertex renormalization in the $T=\frac{1}{2}$, $S_{\frac{1}{2}}$ state), the N.T.D. theory suffers no disadvantage from its lack of formal covariance, apart from the algebraic complexity of the equations finally obtained. This is emphasized in the final Sec. V, where the difficulties preventing calculation of phase shifts with this theory are discussed, and a comparison is made with the corresponding situation in the lowest approximation for the Bethe-Salpeter equation.

II. NEW TAMM-DANCOFF EQUATIONS FOR MESON-NUCLEON SCATTERING

For the interaction of the meson and nucleon fields, the Hamiltonian has the form

$$H=H_0+H_I, \tag{1}$$

where H_0 is the free particle Hamiltonian and

$$H_I=G\int\psi^*\gamma\tau_a\psi\phi_a d_3x. \tag{2}$$

In this expression (2), γ denotes the Dirac matrix $i\beta\gamma_5$, and

$$\psi(r)=(2\pi)^{-\frac{3}{2}}\int d_3p\sum_s b_{ps}u e^{ip\cdot r},$$

$$\psi^*(r)=(2\pi)^{-\frac{3}{2}}\int d_3p\sum_s b^*_{ps}u^* e^{-ip\cdot r}, \tag{3}$$

$$\phi_a(r)=(2\pi)^{-\frac{3}{2}}\int d_3k(2\omega_k)^{-\frac{1}{2}}(a_{ka}+a^*_{-ka})e^{ik\cdot r}.$$

The spinor u satisfies the equation

$$(\alpha\cdot p+\beta M)u=\pm E_p u, \tag{4}$$

with $E_p=(M^2+p^2)^{\frac{1}{2}}$, according as u refers to a nucleon or an antinucleon state. These spinors are normalized

[3] H. A. Bethe and F. de Hoffmann, Phys. Rev. **95**, 1100 (1954); J. Orear, Phys. Rev. **96**, 176 (1954).
[4] F. J. Dyson, Phys. Rev. **90**, 994 (1953) and Phys. Rev. **91**, 1543 (1953). The latter paper will be referred to as D2.
[5] F. J. Dyson, Phys. Rev. **91**, 421 (1953) (this paper will be referred to as D1); W. M. Visscher, Phys. Rev. **96**, 788 (1954).

to the relation

$$u^*u=1. \tag{5}$$

The projection operators $\Omega^{\pm}(p)$ given by

$$\Omega^{+}(p)=\sum_{u+}uu^*, \quad \Omega^{-}(p)=\sum_{u-}uu^*, \tag{6}$$

may then be expressed in the form

$$\Omega^{\pm}(p)=[E_p\pm(\alpha\cdot p+\beta M)]/2E_p. \tag{7}$$

Consider now a physical state Ψ of one meson and one nucleon in interaction, and the physical vacuum state Ψ_0. For any product P of the emission and absorption operators b, b^*, a, and a^* of (3), we will use the notation

$$\langle P\rangle\equiv\langle\Psi_0|P|\Psi\rangle. \tag{8}$$

Denoting the physical energy of the state Ψ (relative to the vacuum state) by ϵ, then

$$\begin{aligned}\epsilon\langle P\rangle&=\langle[P,H]\rangle\\&=\langle[P,H_0]\rangle+\langle[P,H_I]\rangle.\end{aligned} \tag{9}$$

By expressing P as a sum of terms in normal order, i.e., of terms in which all creation operators stand to the left of the annihilation operators, every $\langle P\rangle$ may be written as a linear sum of the "new Tamm-Dancoff" amplitudes $\langle C(N)A(N')\rangle$.

Consider first the amplitude

$$\langle b_{-qu}a_{qu}\rangle. \tag{10}$$

For this, the Eq. (9) now leads to

$$(\epsilon-\omega_q-\eta_{-qu}E_q)\langle b_{-qu}a_{qu}\rangle=\langle[b_{-qu}a_{qu},H_I]\rangle, \tag{11}$$

where η_{-qu} takes the value $+1$ for a positive energy spinor and -1 for a negative energy spinor. With H_I replaced by expression (2), the right-hand side of (11) becomes

$$\begin{aligned}&G(2\pi)^{-\frac{1}{2}}\int\int d_3p d_3k(2\omega_k)^{-\frac{1}{2}}\sum_w\sum_v(v^*\gamma_\tau\gamma_\beta w)\\&\times\langle[b_{-qu}a_{qu},(a_{k\alpha}+a^*_{-k\alpha})b^*_{p+k,v}b_{pw}]\rangle.\end{aligned} \tag{12}$$

The commutator appearing in (12) is now brought to normal form, in order to express (12) in terms of the N.T.D. amplitudes. Equation (11) then becomes

$$\begin{aligned}&(\epsilon-\omega_q-\eta_{-qu}E_q)\langle b_{-qu}a_{qu}\rangle\\&=G(2\pi)^{-\frac{1}{2}}\Big[(2\omega_q)^{-\frac{1}{2}}\theta_{-qu}\sum_w(u^*\gamma_\tau a w)\langle b_{0w}\rangle\\&+(2\omega_q)^{-\frac{1}{2}}\int d_3p\sum_w\sum_v(v^*\gamma_\tau a w)\langle b_{-qu}b^*_{p-q,v}b_{pw}\rangle\\&+\int d_3k(2\omega_k)^{-\frac{1}{2}}\sum_w(u^*\gamma_\tau\beta w)\\&\times\langle a_{qa}(a_{k\beta}+a^*_{-k\beta})b_{-q-k,w}\rangle\Big],\end{aligned} \tag{13}$$

where $\theta_{-qu}=(1+\eta_{-qu})/2$ with the values $+1$ for a positive energy spinor u, 0 for a negative energy spinor.

It is now necessary to obtain similar equations for the various N.T.D. amplitudes appearing on the right-hand side of (13). In this way, successively, an infinite set of N.T.D. equations may be built up. At this point however, in analogy to the Tamm-Dancoff approximation made in the previous calculations[1] of meson-nucleon scattering, this set of equations will be approximated by omitting each N.T.D. amplitude depending on four or more creation or absorption operators. With this approximation the two-meson amplitudes of (13) are given by the following equations:

$$\begin{aligned}&(\epsilon-\omega_q-\omega_k-E_{q+k})\langle a_{qa}a_{k\beta}b_{-q-k,w}\rangle\\&=G(2\pi)^{-\frac{1}{2}}\theta_{-q-k,w}\sum_u\{(w^*\gamma_\tau a u)(2\omega_q)^{-\frac{1}{2}}\langle a_{k\beta}b_{-ku}\rangle\\&+(\omega^*\gamma_\tau\beta u)(2\omega_k)^{-\frac{1}{2}}\langle a_{qa}b_{-qu}\rangle\},\end{aligned} \tag{14}$$

$$\begin{aligned}&(\epsilon+\omega_q+\omega_k+E_{q+k})\langle a^*_{-qa}a^*_{-k\beta}b_{-q-k,w}\rangle\\&=G(2\pi)^{-\frac{1}{2}}\bar\theta_{-q-k,w}\sum_u\{(w^*\gamma_\tau a u)(2\omega_q)^{-\frac{1}{2}}\langle a^*_{-k\beta}b_{-ku}\rangle\\&+(\omega^*\gamma_\tau\beta u)(2\omega_k)^{-\frac{1}{2}}\langle a^*_{-qa}b_{-qu}\rangle\},\end{aligned} \tag{15}$$

$$\begin{aligned}&(\epsilon+\omega_q-\omega_k-\eta_{-q-k,w}E_{q+k})\langle a^*_{-qa}a_{k\beta}b_{-k-q,w}\rangle\\&=G(2\pi)^{\frac{1}{2}}\sum_u\{\bar\theta_{-q-k,w}(w^*\gamma_\tau a u)(2\omega_q)^{-\frac{1}{2}}\langle a_{k\beta}b_{-ku}\rangle\\&+\theta_{-q-k,w}(w^*\gamma_\tau\beta u)(2\omega_k)^{-\frac{1}{2}}\langle a^*_{-qa}b_{-qu}\rangle\},\end{aligned} \tag{16}$$

where $\bar\theta_{pu}=(1-\theta_{pu})$.

For this last Eq. (16), there arises the question discussed in D2, the possibility that an unphysical singularity may occur in the amplitude $\langle a^*_{-qa}a_{k\beta}b_{-k-q,w}\rangle$. For a positive spinor w, the factor multiplying this amplitude in (16) may vanish, since there exist infinitely many k, for a given q, for which

$$\epsilon+\omega_q-\omega_k-E_{q+k}=0. \tag{17}$$

Such a singularity in $\langle a^*_{-qa}a_{k\beta}b_{-k-q,w}\rangle$ would mean that, in coordinate space, this amplitude would have a finite value at infinity. This would imply the existence of a real process resulting in one meson, one nucleon and minus-one meson. Such a process would only be possible here if a real meson were present in the comparison state Ψ_0. In the present problem, however, this is not the case, since the comparison state Ψ_0 is the physical vacuum.[6] The amplitude $\langle a^*_{-qa}a_{k\beta}b_{-q-k,w}\rangle$ must therefore be finite even for momenta satisfying Eq. (17). For fixed q and positive w, the right-hand side of (16) must vanish for every k satisfying (17); thus

$$\sum_u(w^*\gamma_\tau\beta u)\langle a^*_{-qa}b_{-qu}\rangle=0 \tag{18}$$

[6] The N.T.D. equations which have been set up have the same form for any comparison state Ψ_0. It is only at this point that the nature of the comparison state is invoked to provide an additional condition on the amplitudes which are to describe the physical situation. The boundary condition which had been proposed in D2 is not correct, since the principal value singularity still allows a standing wave at infinity.

for an infinite set of positive energy spinors $w_+(-k-q)$. From this it follows[7] that (since γ and τ_β are non-singular)

$$\sum_u u\langle a^*_{-qu}b_{-qu}\rangle=0. \tag{19}$$

The spinors u form a complete set, so that

$$\langle a^*_{-qu}b_{-qu}\rangle=0, \tag{20}$$

for all q, α, u. From (15) and (16), it then follows that

$$\langle a^*_{-qu}a^*_{-k\beta}b_{-q-k,w}\rangle\equiv 0, \tag{21}$$

and that, for positive w,

$$\langle a^*_{-qu}a_{k\beta}b_{-q-k,w}\rangle=0. \tag{22}$$

For the three-nucleon amplitude of (13), the N.T.D. equation is

$$\begin{aligned}&(\epsilon-\eta_{-qu}E_q+\eta_{p-q,v}E_{p-q}-\eta_{pw}E_p)\langle b_{-qu}b^*_{p-q,v}b_{pw}\rangle\\&\quad=G(2\pi)^{-\frac{1}{2}}\{(2\omega_q)^{-\frac{1}{2}}(w^*\gamma\tau_\alpha v)\langle b_{-qu}(a_{q\alpha}+a^*_{-q\alpha})\rangle\\&\quad\times(\theta_{pw}\tilde\theta_{p-q,v}-\tilde\theta_{pv}\theta_{p-q,w})+(2\omega_p)^{-\frac{1}{2}}(u^*\gamma\tau_\beta v)\\&\quad\times\langle b_{pw}(a_{-p\alpha}+a^*_{p\alpha})\rangle(\tilde\theta_{-qu}\theta_{p-q,v}-\theta_{-qu}\tilde\theta_{p-q,v})\}.\end{aligned} \tag{23}$$

From this, it follows at once that

$$\langle b_{-qu}b^*_{p-q,v}b_{pw}\rangle=0 \tag{24}$$

when the spinors u, v, w are all positive or all negative. Consider next the equation (23) for u positive and v, w negative [recalling Eq. (20)],

$$\begin{aligned}&(\epsilon-E_p-E_{p-q}-E_q)\langle b_{-qu}b^*_{p-q,v}b_{pw}\rangle\\&\quad=-G(2\pi)^{-\frac{1}{2}}(2\omega_p)^{-\frac{1}{2}}(u^*\gamma\tau_\alpha w)\langle b_{pw}a_{-p\alpha}\rangle.\end{aligned} \tag{25}$$

For this amplitude it is again necessary to invoke the boundary condition that Ψ_0 is the physical vacuum state since, for every p, the energy factor on the left of (25) vanishes for infinitely many q. From reasoning similar to that given above, this leads to the condition that, for w negative,

$$\langle b_{pw}a_{-p\alpha}\rangle=0. \tag{26}$$

From (23), it now follows that the amplitude $\langle b_{-qu}b^*_{p-q,v}b_{pw}\rangle$ is zero except when one (and only one) of u, v, w refers to a negative energy state. For these nonzero components, Eq. (23) reduces to

$$\begin{aligned}&(\epsilon+E_q+E_{p-q}-E_p)\langle b_{-qu}b^*_{p-q,v}b_{pw}\rangle\\&\quad=G(2\pi)^{-\frac{1}{2}}(2\omega_p)^{-\frac{1}{2}}(u^*\gamma\tau_\alpha w)\langle b_{pw}a_{-p\alpha}\rangle,\end{aligned} \tag{27}$$

$$\begin{aligned}&(\epsilon-E_q-E_{p-q}-E_p)\langle b_{-qu}b^*_{p-q,v}b_{pw}\rangle\\&\quad=G(2\pi)^{-\frac{1}{2}}\{(2\omega_q)^{-\frac{1}{2}}(w^*\gamma\tau_\alpha v)\langle b_{-qu}a_{q\alpha}\rangle\\&\qquad+(2\omega_p)^{-\frac{1}{2}}(u^*\gamma\tau_\alpha v)\langle b_{pw}a_{-p\alpha}\rangle\},\end{aligned} \tag{28}$$

$$\begin{aligned}&(\epsilon-E_q+E_{p-q}+E_p)\langle b_{-qu}b^*_{p-q,v}b_{pw}\rangle\\&\quad=-G(2\pi)^{-\frac{1}{2}}(2\omega_p)^{-\frac{1}{2}}(w^*\gamma\tau_\alpha v)\langle b_{-qu}a_{q\alpha}\rangle,\end{aligned} \tag{29}$$

where (27), (28), and (29) in turn refer to the cases u, v, and w negative.

For the remaining amplitude of (13), the N.T.D. equation is

$$\begin{aligned}&(\epsilon-\eta_{0w}M)\langle b_{0w}\rangle=G(2\pi)^{-\frac{1}{2}}\int d_3k\sum_u\theta_{-ku}\\&\qquad\times(w^*\gamma\tau_\alpha u)(2\omega_k)^{-\frac{1}{2}}\langle b_{-ku}a_{k\alpha}\rangle,\end{aligned} \tag{30}$$

taking account of Eqs. (20).

These equations now form the complete set of Tamm-Dancoff equations in the present approximation. For each nonzero amplitude on the right of (13), there is an equation expressing this amplitude in terms of $\langle a_{p\alpha}b_{-pu}\rangle$. Substituting these expressions in Eq. (13) then gives an equation for $\langle a_{p\alpha}b_{-pu}\rangle$ alone. The use made of the fact that Ψ_0 is the physical vacuum state has ensured that this equation will contain no unphysical singularities. The equation obtained is

$$\begin{aligned}&(\epsilon-\omega_p-E_p)\langle a_{p\alpha}b_{-pu}\rangle=\Big\{(T_N+T_m)\langle b_{-pu}a_{p\alpha}\rangle\\&\qquad+\frac{G^2}{16\pi^3}\int\frac{d_3k}{(\omega_p\omega_k)^{\frac{1}{2}}}(u^*[C(p,k)Q'_{\alpha\beta}\\&\qquad+D(p,k)Q_{\alpha\beta}]w)\langle b_{-pw}+a_{p\beta}\rangle\Big\},\end{aligned} \tag{31}$$

where S_N, S_m, $C(p,k)$, and $U(p,k)$ are defined as follows:

$$\begin{aligned}T_N=\frac{3G^2}{16\pi^3}\Big\{u^*\int&\frac{d_3k}{\omega_k}\Big(\frac{\gamma\Omega^+(-p-k)\gamma}{\epsilon-\omega_p-\omega_k-E_{p+k}}\\&+\frac{\gamma\Omega^-(-p-k)\gamma}{\epsilon-\omega_p+\omega_k+E_{p+k}}\Big)u\Big\},\end{aligned} \tag{32}$$

$$\begin{aligned}T_m=\frac{G^2}{16\pi^3}\frac{2}{\omega_p}\int d_3k\ \mathrm{Sp}[&\gamma\Omega^+(-k)\gamma\Omega^-(-p-k)]\\&\times\Big(\frac{1}{\epsilon-E_p-E_k-E_{p+k}}-\frac{1}{\epsilon-E_p+E_k+E_{p+k}}\Big),\end{aligned} \tag{33}$$

$$C(p,k)=\frac{\gamma\Omega^+(-p-k)\gamma}{\epsilon-\omega_p-\omega_k-E_{p+k}}-\frac{\gamma\Omega^-(-p-k)\gamma}{\epsilon-E_p-E_k-E_{p+k}}, \tag{34}$$

$$D(p,k)=\frac{\gamma\Omega^+(0)\gamma}{\epsilon-M}+\frac{\gamma\Omega^-(0)\gamma}{\epsilon+M}=\gamma\frac{1}{\epsilon-\beta M}\gamma. \tag{35}$$

The quantities Q', Q occurring in (31) are discussed in D3. In particular $Q_{\alpha\beta}=\tau_\alpha\tau_\beta$, $Q'_{\alpha\beta}=\tau_\beta\tau_\alpha$, and (Q',Q) have the eigenvalues (2,0) for $T=\frac{3}{2}$ states, and $(-1,3)$ for $T=\frac{1}{2}$ states.

It is of interest now to compare this equation with the corresponding equation of the old Tamm-Dancoff theory [Eq. (10) of D3]. Owing to the use of amplitudes relating to the physical vacuum state rather

[7] If $Q=-k-q$, then the vectors Q satisfying (17) lie on a complete surface enclosing the origin. If $(w^*(Q)A)=0$, then $\Omega^+(Q)A=0$. From this, $[(E_Q-\beta M)/Q+\alpha\cdot Q/Q]A=0$. If this expression is integrated over the surface, then the last term vanishes, and one finds $A=0$.

than to the bare vacuum state, there is no vacuum self-energy term in the present equation, the energy of the state being referred directly to the energy of the real vacuum. The graphs corresponding to the terms appearing in Eq. (31) are given in Fig. 1. In these graphs the + sign refers to normal particles and the − sign to the minus-particles, borrowed from the vacuum state. If a + line goes forward, it corresponds to a plus particle, if backward then to a plus antiparticle (of positive energy), while a − line going forward corresponds to a minus antiparticle, backward to a minus particle. Thus graphs (a) and (b) correspond to the nucleon and meson self-energy terms T_N and T_m. In these the (+) terms do not differ from the corresponding terms in the old Tamm-Dancoff equation, but the energy denominators of the (−) terms differ just in the way necessary for a close correspondence with the self-energy expressions of the covariant theory (see references 5 and Sec. III). The crossed graphs (c) and (d) are unchanged; the numerical calculations previously reported for the $T=\frac{3}{2}$, $S_{\frac{1}{2}}$ and $P_{\frac{1}{2}}$ states therefore need no modification in the approximation in which the self-energy graphs (a) and (b) are neglected. The uncrossed graph differs again only in the (−) term, the energy denominator $1/(E+M)$ replacing the previous more complicated denominator $1/(E-E_p-\omega_p-M-E_k-\omega_k)$; this term is effective only for the $T=\frac{1}{2}$, $S_{\frac{1}{2}}$ state, the modification being sufficient to permit carrying through all renormalization necessary for this state.

For the wave function $\psi(k)$ of the system we define

$$\psi(k)=(\omega_k)^{\frac{1}{2}}\sum_{u+}u\langle b_{-k\sigma}a_{k\alpha}\rangle. \tag{36}$$

Suppressing the isotopic spin suffices, Eq. (31) now becomes

$$(\epsilon-\omega_p-E_p)\psi(p)=\left\{(T_N+T_m)\psi(p)+\Omega^+(-p)\frac{G^2}{16\pi^3}\times\int\frac{d_3k}{\omega_k}[Q'C(p,k)+QU(p,k)]\psi(k)\right\}. \tag{37}$$

It is now required to find a solution $\psi(k)$ of the form

$$\psi(k)=\psi_0(k)+P\frac{1}{\epsilon-\omega_k-E_k}f(k), \tag{38}$$

where $\psi_0(k)=\delta(\epsilon-\omega_k-E_k)f_0(k)$. If $f_0(k)$ is an eigenfunction of angular momentum j, parity w, and isotopic spin T, then the phase shift δ_{jwT} for the meson-nucleon scattering in this state is given by

$$\tan\delta_{jwT}=-\pi f(l)/f_0(l), \tag{39}$$

where $\epsilon-\omega_l-E_l=0$.

III. SELF-ENERGY GRAPHS

The contributions of the meson and nucleon self-energy graphs of Fig. 1 to the integral equation for meson-nucleon scattering have been given in Eqs. (32) and (33). Consider first the nucleon self-energy S_N. The expression (32) may be rewritten in the following form:

$$T_N(p)=-\frac{M}{E_p}\left\{\bar v(p)\left(\frac{3G^2}{16\pi^3}\int\frac{Md_3k}{E_{p+k}\omega_k}\left[\frac{\gamma_5\Lambda^+(-p-k)\gamma_5}{\epsilon-\omega_p-\omega_k-E_{p+k}}-\frac{\gamma_5\Lambda^-(p+k)\gamma_5}{\epsilon-\omega_p+\omega_k+E_{p+k}}\right]\right)v(p)\right\}, \tag{40}$$

where $\Lambda^\pm$ are the covariant projection operators, related to the $\Omega^\pm$ by

$$\Lambda^\pm(\pm p)=\pm\frac{E_p}{M}\Omega^\pm(p)\beta, \tag{41}$$

and $\bar v(p)=(M/E_p)^{\frac{1}{2}}u^*(p)\beta$, $v(p)=(M/E_p)^{\frac{1}{2}}u(p)$.

It was pointed out in D1 that this second-order self-energy expression, obtained with the N.T.D. theory, is related to the self-energy Σ_2 of the covariant theory in the following way:

$$T_N(p)=\frac{M}{E_p}\bar v(p)\Sigma_2(P)v(p), \tag{42}$$

where

$$\Sigma_2(P)=-\frac{3G^2}{(2\pi)^4}\int\frac{d_4k}{k^2-\mu^2}\left(\gamma_5\frac{1}{\mathbf{P}-\mathbf{k}-M}\gamma_5\right), \tag{43}$$

and P is the four-vector $(\Delta+E_p, -p)$, $\Delta=\epsilon-\omega_p-E_p$. For a momentum p on the energy shell $\Delta=0$, (43) represents the self-energy of a free nucleon. This relationship (42) has been demonstrated by Visscher[5] and in D1, by using an adaptation of Cini's method[6] (old Tamm-Dancoff theory) to the N.T.D. theory. It may also be verified directly by integration of (43) over the variable k_0, the result (40) being obtained after a little rearrangement.

The covariant self-energy Σ_2 has the following form

$$\Sigma_2(P)=\delta M+A(\mathbf{P}-M)+\Sigma_c(\mathbf{P}), \tag{44}$$

where the finite part Σ_c is given by the integral

$$\Sigma_c(\mathbf{P})=-\frac{3G^2}{16\pi^2}\int_0^1 dx\left[[M-(1-x)\mathbf{P}]\ln\frac{\phi(P^2)}{\phi(M^2)}+(\mathbf{P}-M)\frac{2M^2x^2(1-x)}{\phi(M^2)}\right], \tag{45}$$

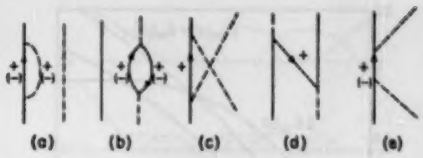

FIG. 1. The graphs responsible for meson-nucleon scattering in the new Tamm-Dancoff theory.

[6] M. Cini, Nuovo cimento **10**, 526 and 614 (1953).

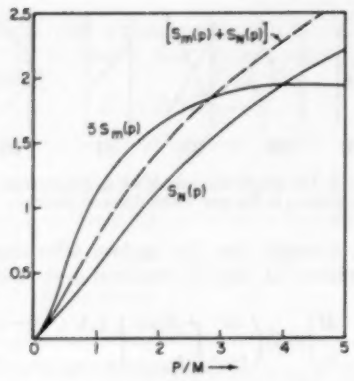

FIG. 2. The self-energy functions $S_N(p)=G^2R_N(p)$ and $S_m(p)=G^2R_m(p)$, plotted for $G^2/4\pi=13$ and $\epsilon=M$.

with $\phi(P^2)=(1-x)\mu^2+xM^2-x(1-x)P^2$. In the expression (40) for T_N, only the expectation value of Σ_2 in the state $v(p)$ is needed. This is obtained by replacing $\mathbf{P}-M$ by $\Delta E_p/M$ and P^2 by $M^2+\Delta(\Delta+2E_p)$ in (44) and (45). If we take $\mu=0$ in the integral (45), then

$$\frac{M}{E_p}\bar{v}(p)\Sigma_2(P)v(p)=\frac{M\delta M}{E_p}+A\Delta+G^2R_N\Delta, \quad (46)$$

where

$$R_N=-\frac{3}{32\pi^2}\frac{\Delta}{E_p}\frac{M^2-E_p(\Delta+2E_p)}{M^2+\Delta(\Delta+2E_p)}$$
$$\times\left[\frac{\Delta(\Delta+2E_p)}{M^2+\Delta(\Delta+2E_p)}\ln\left(\frac{-\Delta(\Delta+2E_p)}{M^2}\right)-1\right]. \quad (47)$$

According to its definition, $R_N(p)$ vanishes on the energy shell $\Delta=0$. $R_N(p)$ is plotted in Fig. 2 as function of p for $\epsilon=M$.

The first term of (46) may be brought to the left of Eq. (37) to be absorbed as a correction to the nucleon mass. If one neglects $T_m(p)$ for the present, the infinite constant A gives rise to a coupling constant renormalization when the remainder of $T_N(p)$ is brought to the left of (37), this equation then taking the form

$$(\epsilon-\omega_p-E_p)(1-G_1^2R_N(p))\psi(p)$$
$$=\frac{G_1^2}{16\pi^3}\Lambda^+(-p)\int\frac{d_3k}{\omega_k}(Q'C(p,k)+QU(p,k))\psi(k), \quad (48)$$

where the renormalized coupling constant is $G_1^2=G^2/(1-A)$. The nucleon self-energy divergence which appears explicitly in the integral equation (37) may therefore be renormalized satisfactorily, the integral equation being brought to the finite form (48), where the propagator for the system $(\epsilon-E_p-\omega_p)^{-1}$ is now replaced by a modified propagator $[(\epsilon-\omega_p-E_p)\times(1-G_1^2R_N(p))]^{-1}$.

However it is also necessary to consider the meson self-energy $T_m(p)$. This is also closely related with the corresponding self-energy expression in the covariant theory, in fact

$$T_m(p)=-\frac{1}{2\omega_p}\Omega(Q^2) \quad (49)$$

where Ω is the meson self-energy in lowest approximation,

$$\Omega(Q^2)=\frac{2G^2}{(2\pi)^4}\int d_4k$$
$$\times\mathrm{Sp}[\gamma_5(Q+\tfrac{1}{2}k-M)^{-1}\gamma_5(Q-\tfrac{1}{2}k-M)^{-1}], \quad (50)$$

and Q is the four-vector $(\Delta+\omega_p, p)$. This relationship has been established by Visscher[5] using the Cini method for the N.T.D. theory, and may readily be verified by integration of (50) over k_0. $\Omega(Q^2)$ is then written in the form

$$\Omega(Q^2)=\delta(\mu^2)+B(Q^2-\mu^2)+\Omega_C(Q^2). \quad (51)$$

The function $\Omega_C(Q^2)$ is well known, and for the value of Q appropriate we will write it in the form

$$\Omega_C(Q^2)=-2\omega_pG^2R_m(p)\Delta, \quad (52)$$

where, neglecting terms of order $(\mu/M)^2$ in $R_m(p)$,

$$R_m(p)=-\frac{1}{2\pi^2}\frac{\Delta+2\omega_p}{2\omega_p}\left\{1-\left(\frac{\Delta(\Delta+2\omega_p)-4M^2}{\Delta(\Delta+2\omega_p)}\right)^{\frac{1}{2}}\right.$$
$$\left.\times ar\sinh\left(\frac{(-\Delta(\Delta+2\omega_p))^{\frac{1}{2}}}{2M}\right)\right\}. \quad (53)$$

The function $R_m(p)$ is plotted in Fig. 2 for $\epsilon=M$. It also vanishes on the energy shell $\Delta=0$ (by definition) and is generally small compared with the nucleon term $R_N(p)$.

It must be remarked here that the second (infinite) term of (51) is not proportional to Δ as is appropriate for a coupling constant renormalization in the Tamm-Dancoff theory, but is given by $B\Delta(\Delta+2\omega_p)$. Since the meson field satisfies the Klein-Gordon equation rather than a linear equation, such a result is difficult to avoid in any prescription based on the covariant theory. A true mass and coupling-constant renormalization in the Tamm-Dancoff theory requires the subtraction of a term $C+D\Delta$ from the expression $T_m(p)$ of (33); however no such subtraction can succeed in making $T_m(p)$ finite. The N.T.D. method has led to a well-defined calculation of the finite part of the meson self-energy graph, closely related to that of the covariant theory, but it fails in so far as the interpretation of the infinite parts is concerned.

If the infinite parts of $R_m(p)$ are simply omitted, the integral equation takes the form (48) with $\{(\epsilon-\omega_p-E_p)\times[1-G_1^2(R_N(p)+R_m(p))]\}^{-1}$ as the propagator for the system. In view of the difficulty just mentioned, this procedure is not as convincing as it might have been, but there is still one further point to be made. According to their definition, both $R_m(p)$ and $R_N(p)$ must vanish on the energy shell $E_p+\omega_p=\epsilon$. For very large p, they have the following asymptotic forms:

$$R_N(p)\sim\frac{3}{32\pi^3}\left(\ln\left(\frac{2p\epsilon}{M^2}\right)-1\right),$$
$$R_m(p)\sim\frac{\epsilon}{8\pi^2 p}\left(\ln\left(\frac{2p\epsilon}{M^2}\right)-2\right). \tag{54}$$

The second factor of the modified propagator therefore must have a singularity at some high momentum p, for all G^2, since $[R_N(p)+R_m(p)]$ ranges from 0 to $+\infty$. For $G^2/4\pi=13$ and $\epsilon=M$, this singularity lies at $p=1.3M$.

Such a singularity is not physically reasonable. Its existence would imply the presence of a corresponding singularity in the wave function of the meson-nucleon state, whose interpretation would require the presence of waves of very high momentum at infinity, although the ingoing meson-nucleon waves have energy ϵ. This would be possible only if some bound system[9] could be formed with rest mass far below that of the nucleon. This is clearly not the case, and this singularity must be regarded only as a consequence of the approximations made in setting up the present N.T.D. theory. Despite the success of the N.T.D. method in relating the self-energy graphs of the integral equations to self-energy expressions of the covariant theory, the presence of this singularity prevents the use of this renormalization method for calculating self-energy corrections to the calculations of D3 for the $T=\frac{3}{2}$ states.

IV. RENORMALIZATION PROBLEM FOR THE STATES $T=1/2$, $j=1/2$

A further renormalization problem arises for the $S_{\frac{1}{2}}$ and $P_{\frac{1}{2}}$ states of isotopic spin $T=\frac{1}{2}$, since they respectively have the same spin, parity, and isotopic spin as the minus-one-anti-nucleon state and the one nucleon state. In Eq. (37), $Q=3$ for the $T=\frac{1}{2}$ states and the term $U(p,k)$ becomes effective. The integral equation now has no finite solution: this may be recognized most readily by attempting to solve the integral equation as a power series in G^2, by iteration from $\psi_0(k)$. The successive terms correspond to graphs built up from the basis graphs of Fig. 1, and two typical graphs

FIG. 3. Typical graphs generated by the kernels $C(p,k)$ and $U(p,k)$ of Eq. (55).

are shown in Fig. 3. Graphs in which the uncrossed graph $U(p,k)$ has operated at least once have a structure of the type (b), and the vertices and self-energy parts thus generated require renormalization.

Consider then the integral equation (38). It will be convenient to use the covariant projection operators (41) and the equation then takes the form

$$(\epsilon-\omega_p-E_p)\psi(p)=G_\epsilon^2(p)\Lambda^+(-p)\frac{M}{E_p}\left\{\int\frac{d_3k}{\omega_k}Q'H(p,k)\psi(k)+\gamma_5\frac{Q\beta}{\epsilon-\beta M}\int\gamma_5\psi(k)\frac{d_3k}{\omega_k}\right\}, \tag{55}$$

where

$$H(p,k)=-\frac{M}{E_{p+k}}\left\{\frac{\gamma_5\Lambda^+(-p-k)\gamma_5}{\epsilon-\omega_p-\omega_k-E_{p+k}}+\frac{\gamma_5\Lambda^-(p+k)\gamma_5}{\epsilon-E_p-E_k-E_{p+k}}\right\}, \tag{56}$$

and we have written $G_\epsilon^2(p)$ in place of $F_\epsilon(p)G^2/16\pi^2$, where the factor $F_\epsilon(p)$ arises from any (nonsingular) modification of the propagator $(\epsilon-\omega_p-E_p)^{-1}$ of the system due to particle self-energy effects. If these are neglected, $F_\epsilon(p)$ is to be replaced by unity. Since the kernel $H(p,k)$ lies between positive energy projection operators, its form may be simplified to

$$H(p,k)=H_-(p,k)(1+\beta)/2+H_+(p,k)(1-\beta)/2, \tag{57}$$

where

$$H_\pm(p,k)=\frac{1}{2E_{p+k}}\left\{\frac{\mp(E_p+E_k-E_{p+k})+M}{\epsilon-\omega_p-\omega_k-E_{p+k}}+\frac{\mp(E_p+E_k+E_{p+k})+M}{\epsilon-E_p-E_k-E_{p+k}}\right\}. \tag{58}$$

For the $T=\frac{1}{2}$ states, Q and Q' take the values $3,-1$.

A solution of the form (39),

$$\psi(p)=\psi_0(p)+\frac{P}{\epsilon-\omega_p-E_p}f(p) \tag{59}$$

is now required. Consider first the function $g(p)$ which

[9] T. D. Lee [Phys. Rev. **95**, 1329 (1954)] has recently studied a special meson theory in which the Tamm-Dancoff approximation used here is actually exact. Complete solutions are obtained, and it is found that the modified propagator has a pole of this kind, when there exists a bound state lying below the energies of the quanta of the individual fields.

is the solution of

$$g(p)=G_\epsilon^2(p)\Big[B_\epsilon(p)+\Lambda^+(-p)\frac{M}{E_p}\int\frac{d_3k}{\omega_k}Q'H(p,k)\times\frac{P}{\epsilon-\omega_k-E_k}g(k)\Big], \quad (60)$$

where $B_\epsilon(p)$ is the Born approximation amplitude

$$B_\epsilon(p)=\Lambda^+(-p)\frac{M}{E_p}\int\frac{d_3k}{\omega_k}Q'H(p,k)\psi_0(k). \quad (61)$$

Procedures for the approximate solution of this Eq. (60) have been discussed in D3 and we shall not consider this problem further here.

By substitution of (59) in the Eq. (55) and use of the Eq. (60), it will be found that the complete function $f(p)$ is now given by

$$f(p)=g(p)+G_\epsilon^2(p)\frac{M}{E_p}\Lambda^+(-p)\Gamma_\epsilon(p)\chi, \quad (62)$$

where $\Gamma_\epsilon(p)$ is the solution of the equation

$$\Gamma_\epsilon(p)=\gamma_5+\frac{G^2}{16\pi^3}\int\frac{d_3k}{\omega_k}Q'H(p,k)P_\epsilon(k)\frac{M}{E_k}\times\Lambda^+(-k)\Gamma_\epsilon(k), \quad (63)$$

and

$$\chi=\frac{Q\beta}{\epsilon-\beta M}\int\gamma_5\psi(k)\frac{d_3k}{\omega_k}. \quad (64)$$

In (63) the notation

$$P_\epsilon(k)=F_\epsilon(k)\frac{P}{\epsilon-\omega_k-E_k} \quad (65)$$

has been used, so that $P_\epsilon(k)$ now represents the modified propagator of the theory. It is useful also to define the adjoint $\Gamma_\epsilon^\dagger(p)$ of $\Gamma_\epsilon(p)$, satisfying the equation

$$\Gamma_\epsilon^\dagger(p)=\gamma_5+\frac{G^2}{16\pi^3}Q'\int\frac{d_3k}{\omega_k}\Gamma_\epsilon^\dagger(k)\Lambda^+(-k)\frac{M}{E_k}\times P_\epsilon(k)H(k,p). \quad (66)$$

After substitution of (59) (62) in Eq. (64), the following equation is obtained for the spinor:

$$\chi=\frac{Q\beta}{\epsilon-\beta M}\int\frac{d_3k}{\omega_k}\gamma_5\times\left(\phi(k)+\frac{G^2}{16\pi^3}P_\epsilon(k)\frac{M}{E_k}\Lambda^+(-k)\Gamma_\epsilon(k)\chi\right), \quad (67)$$

where

$$\phi(k)=\psi_0(k)+\frac{P}{\epsilon-\omega_k-E_k}g(k). \quad (68)$$

With use of (66), the first integral on the right of (67) becomes

$$\begin{aligned}\int\frac{d_3k}{\omega_k}\gamma_5\phi(k)&=\int\frac{d_3q}{\omega_q}\Gamma_\epsilon^\dagger(q)\phi(q)-\frac{G^2}{16\pi^3}\int\int\frac{d_3q}{\omega_q}\Gamma_\epsilon^\dagger(q)\Lambda^+(-q)\\&\quad\times\frac{M}{E_q}P_\epsilon(q)Q'H(q,k)\phi(k)\frac{d_3k}{\omega_k}\\&=\int\frac{d_3q}{\omega_q}\Gamma_\epsilon^\dagger(q)\phi(q)-\int\frac{d_3q}{\omega_q}\Gamma_\epsilon^\dagger(q)\frac{P}{\epsilon-\omega_q-E_q}g(q)\\&=\int\frac{d_3q}{\omega_q}\Gamma_\epsilon^\dagger(q)\psi_0(q), \quad (69)\end{aligned}$$

and the solution χ of Eq. (67) may be written

$$\chi=\frac{Q\beta}{\epsilon-\beta M-Q\beta S(\epsilon)}\int\frac{d_3q}{\omega_q}\Gamma_\epsilon^\dagger(q)\psi_0(q), \quad (70)$$

where

$$S(\epsilon)=\int\gamma_5\frac{m d_3k}{E_k\omega_k}P_\epsilon(k)\Lambda^+(-k)\Gamma_\epsilon(k). \quad (71)$$

The function $\Gamma_\epsilon(p)$ is the vertex operator of the present theory and corresponds to the sum of all vertex graphs of the type shown in Fig. 3(b). Its definition by Eq. (63) is purely formal, as $\Gamma_\epsilon(p)$ is an infinite quantity. The function $S(\epsilon)$ is the self-energy expression resulting from joining the outgoing meson and nucleon lines of the vertex $\Gamma_\epsilon(p)$, i.e., it corresponds to the sum of all simple self-energy graphs of the type shown in Fig. 3(b). It is now necessary to discuss the renormalization of $\Gamma_\epsilon(p)$ and $S(\epsilon)$ and the calculation of their finite parts.

(a) Vertex Operator

Only matrix elements of $\Gamma_\epsilon(p)$ leading to a positive energy spinor are effective in Eq. (63) and in the expression (62) owing to the presence of the projection operator $\Lambda^+(-p)$. It is therefore appropriate to reduce (63) to two-component form. We now define the two-component function $\Delta_\epsilon(p)$ by the relation

$$\Delta_\epsilon(p)=\tfrac{1}{2}(1+\beta)\Lambda^+(-p)\Gamma_\epsilon(p). \quad (72)$$

The matrix element appearing in (62) may be expressed in terms of this function by

$$\Lambda^+(-p)\Gamma_\epsilon(p)=\left(1-\frac{\gamma_5\sigma\cdot p}{E_p+M}\right)\Delta_\epsilon(p). \quad (73)$$

Now the spinor χ on which $\Delta_\epsilon(p)$ will operate in (62) corresponds to a state of zero momentum (since the system is being treated in c.m. system). From parity

conservation, χ is a positive frequency spinor if the incident system is in a $p_{\frac{1}{2}}$ state, a negative frequency spinor if in an $S_{\frac{1}{2}}$ state. In zero approximation, then, $\Delta_\epsilon(p)$ may be reduced to

$$\Delta_\epsilon^{(1)}(p)=\frac{1+\beta}{2}\left[\frac{E_p+M}{2M}\gamma_0+\frac{\sigma\cdot p}{2M}\right]. \tag{74}$$

Clearly only the first of these terms is effective for the $S_{\frac{1}{2}}$ state, in which case the spinor χ standing to the right of $\Delta_\epsilon(p)$ has negative frequency, and only the second for the $p_{\frac{1}{2}}$ state, χ then being a positive frequency spinor. From considerations of rotational invariance and of parity, the function $\Delta_\epsilon(p)$ will have the general form

$$\Delta_\epsilon(p)=\frac{1+\beta}{2}\left[\frac{E_p+M}{2M}V_S(p)\gamma_0+V_P(p)\frac{\sigma\cdot p}{2M}\right], \tag{75}$$

where $V_S(p)$ and $V_P(p)$ are scalar functions. Corresponding to the adjoint operator $\Gamma_\epsilon^\dagger(p)$, an operator $\Delta_\epsilon^\dagger(p)$ is defined

$$\begin{aligned}\Delta_\epsilon^\dagger(p)&=\Gamma_\epsilon^\dagger(p)\Delta^+(-p)\frac{1+\beta}{2}\\&=\left[\frac{E_p+M}{2M}V^\dagger{}_S(p)\gamma_0+V^\dagger{}_P(p)\frac{\sigma\cdot p}{2M}\right]\frac{1+\beta}{2}.\end{aligned} \tag{76}$$

To obtain equations separately for $V_S(p)$ and $V_P(p)$, we proceed from Eqs. (63) and (73), whence

$$\begin{aligned}\Delta_\epsilon(p)=\Delta_\epsilon^{(1)}(p)&+\frac{G^2}{16\pi^3}Q'\int\frac{d_3q}{E_q\omega_q}\Delta_\epsilon^{(1)}(p)\\&\times\left(H_+(p,q)\frac{1-\beta}{2}+H_-(p,q)\frac{1+\beta}{2}\right)P_\epsilon(q)\\&\times\left(1-\frac{\gamma_0\sigma\cdot q}{E_q+M}\right)\Delta_\epsilon(q).\end{aligned} \tag{77}$$

The integral on the right of (77) may now be simplified to

$$\begin{aligned}&\frac{1+\beta}{2}\frac{G^2}{16\pi^3}Q'\int\frac{d_3q}{E_q\omega_q}\left(\frac{E_p+M}{2M}\right)\\&\times\left(H_-(p,q)-\frac{\sigma\cdot p\sigma\cdot q}{(E_p+M)(E_q+M)}H_+(p,q)\right)P_\epsilon(q)\Delta_\epsilon(q).\end{aligned}$$

Substitution of (75) for $\Delta_\epsilon(p)$, and comparison of terms on either side gives equations for V_S and V_P separately:

$$\begin{aligned}V_S(p)=1+\frac{G^2}{8\pi^3}Q'\int\frac{q^2dq}{E_q\omega_q}\frac{d\Omega_q}{4\pi}&\\\times\left[H_-(p,q)-\frac{p\cdot q}{(E_p+M)(E_q+M)}H_+(p,q)\right]&\\\times P_\epsilon(q)(E_q+M)V_S(q),&\end{aligned} \tag{78a}$$

$$\begin{aligned}V_P(p)=1+\frac{G^2}{8\pi^3}Q'\int\frac{q^2dq}{E_q\omega_q}\frac{d\Omega_q}{4\pi}&\\\times\left[\frac{p\cdot q}{pq}H_-(p,q)-\frac{pq}{(E_p+M)(E_q+M)}H_+(p,q)\right]&\\\times P_\epsilon(q)\frac{q(E_p+M)}{p}V_P(q).&\end{aligned} \tag{78b}$$

We will write these equations in the form

$$V_a(p)=1+\frac{G^2}{16\pi^3}Q'\int dqL_a(\epsilon,p,q)V_a(q), \tag{79}$$

the kernels $L_a(\epsilon,p,q)$ being obtained by integrating (78) over the angles of q. In terms of the symmetric function $K_a(\epsilon,p,q)$ obtained by averaging the square bracket of (78) over the angle between p and q they are given by

$$\begin{aligned}L_S(\epsilon,p,q)&=\frac{q^2}{E_q\omega_q}(E_q+M)U_S(\epsilon,p,q)P_\epsilon(q),\\L_P(\epsilon,p,q)&=\frac{q^3}{E_q\omega_q}\frac{E_p+M}{p}U_P(\epsilon,p,q)P_\epsilon(q).\end{aligned} \tag{80}$$

The function $U_a(\epsilon,p,q)$ has been calculated in D3 with the result

$$\begin{aligned}U_S(\epsilon,p,q)&=(A-2M)K_0(C)+(\epsilon-M)K_0(B)\\&\quad+\frac{pq}{(E_p+M)(E_q+M)}(AK_1(C)+(\epsilon+M)K_1(B)),\\U_P(\epsilon,p,q)&=(A-2M)K_1(C)+(\epsilon-M)K_1(B)\\&\quad+\frac{pq}{(E_p+M)(E_q+M)}(AK_0(C)+(\epsilon+M)K_0(B)),\end{aligned}$$

in which

$$\begin{aligned}A&=E_p+\omega_p+E_q+\omega_q+M-\epsilon,\\B&=E_p+E_q-\epsilon,\\C&=\omega_p+\omega_q-\epsilon.\end{aligned}$$

The K_0 and K_1 functions are explicitly:

$$K_0(x)=\frac{1}{2pq}\ln\left(\frac{\bar{E}+x+R}{\bar{E}+x-R}\right),$$

$$K_1(x)=-\frac{1}{2pq}(M^2+p^2+q^2-x^2)K_0(x)+\frac{1}{2pq}\left(1-\frac{x}{\bar{E}}\right),$$

with $\bar{E}=(E_{p+q}+E_{p-q})/2$, $R=pq/\bar{E}$.

It is now necessary to find an equation for the direct calculation of the finite part of V_S and of V_P. The renormalized function $V_a^R(\epsilon,p)$ is related to $V_a(\epsilon,p)$ by

$$V_a^R(\epsilon,p)=Z_a^{-1}V_a(\epsilon,p). \tag{81}$$

Equation (79) then becomes

$$V_a^R(\epsilon,\not{p})=1+\left[\frac{G^2}{16\pi^2}Q'\int dqL_a(\epsilon,\not{p},q)V_a^R(\epsilon,q)-\left(1-\frac{1}{Z_a}\right)\right]. \quad (82)$$

The renormalized $V_a^R(\epsilon,\not{p})$ may be defined by the condition

$$V_a^R(M,0)=1 \quad (83)$$

from which it follows that Z_a is to be chosen

$$\frac{1}{Z_a}=1-\frac{G^2}{16\pi^2}Q'\int dqL_a(\epsilon,0,q)V_a^R(M,q). \quad (84)$$

From Eqs. (82) and (84), we may now construct a finite integral equation for $V_a^R(M,\not{p})$:

$$V_a^R(M,\not{p})=1+\frac{G^2}{16\pi^2}Q'\int dq\times(L_a(M,\not{p},q)-L_a(M,0,q))V_a^R(M,q). \quad (85)$$

This is an integral equation whose solution may be obtained by standard numerical methods. It may readily be verified that the dominant term of $L_a(M,\not{p},q)$ for large q is independent of $\not{p}$, so that the subtraction does lead to cancellation of the divergent terms of the integral. This requirement is, of course, essential for the success of this renormalization scheme, and the fact that it is met here provides a strong check on the appropriateness of the N.T.D. equations for the problem at hand.

When $V_a^R(M,\not{p})$ is known, the complete function is $V_a^R(\epsilon,\not{p})$ given by

$$V_a^R(\epsilon,\not{p})=V_a^R(M,\not{p})+\frac{G^2}{16\pi^2}Q'W_a(\not{p}), \quad (86)$$

where $W_a(\not{p})$ satisfies the equation

$$W_a(\not{p})=\int dq(L_a(\epsilon,\not{p},q)-L_a(M,\not{p},q)V_a^R(M,q)+\frac{G^2}{16\pi^2}Q'\int dqL_a(\epsilon,\not{p},q)W_a(q). \quad (87)$$

In the physical case ($Q'=-1$) these kernels correspond to attractive interactions,[10] and the vertex functions $V_a^R(\epsilon,\not{p})$ may be shown (Appendix B) to decrease as a negative power of $\not{p}$ for large $\not{p}$. The integral in (84), logarithmically divergent in Born approximation (where $V_a^R(\epsilon,\not{p})=1$), is now convergent and it may be shown (Appendix B) that, in fact,[11] $1/Z_a=0$. It should be remarked that, in this theory, the expressions for Z_S and Z_P are quite different; this is a consequence of the asymmetry between the positive and negative frequency states included in the theory, required by the considerations of Sec. II.

In the covariant theory, the renormalized vertex operator $\Gamma_5^R(\not{p}',\not{p})$ may be defined by the condition

$$\mathrm{Lim}_{\not{p}'\to\not{p}}[\bar{u}(\not{p}')\Gamma_5^R(\not{p}',\not{p})u(\not{p})]/[\bar{u}(\not{p}')\gamma_5 u(\not{p})]=1, \quad (88)$$

where $\not{p}$ is the four-momentum of a real nucleon. It is to be noted that this condition only makes a direct statement concerning the diagonal elements of $\Gamma_5^R(\not{p}',\not{p})$—the nondiagonal elements of $\Gamma_5^R(\not{p}',\not{p})$ between positive and negative frequency states, are, of course, well-determined by this condition and are definite, but unknown, functions of $G^2/4\pi$. In the $p_{\frac{1}{2}}$ state, V_P involves the diagonal element of $\Gamma_\epsilon(q)$ and the renormalization procedure (83) adopted is the direct analog of (88), the four-momentum $\not{p}$ being chosen $(M,0)$. However, in the $S_{\frac{1}{2}}$ state, the nondiagonal element of $\Gamma_\epsilon(q)$ is effective and V_S should be renormalized not to unity, but to a value whose magnitude we are at present unable to determine. V_S^R and Z_S are therefore each undetermined to a constant factor. This inability to relate V_S to the diagonal elements of $\Gamma_\epsilon(q)$ is again a consequence of the lack of symmetry between positive and negative frequency states in the theory.

(b) Self-Energy Graphs

Consider now the calculation of the finite part of the self-energy $S(\epsilon)$ of (70). As Salam[12] has emphasized, there occur overlap divergences in these self energy parts, which require careful consideration. However Ward[13] has shown how these difficulties may be avoided by a special method which we shall adapt to the present case.

Consider then the derivative[14] of $S(\epsilon)$,

$$\frac{d}{d\epsilon}S(\epsilon)=\frac{G^2}{16\pi^3}\int\frac{Md_3k}{E_k\omega_k}\gamma_5\left(\frac{dP_\epsilon(k)}{d\epsilon}\Lambda^+(-k)\Gamma_\epsilon(k)+P_\epsilon(k)\Lambda^+(-k)\frac{d\Gamma_\epsilon(k)}{d\epsilon}\right). \quad (89)$$

[10] $L_S(\epsilon,\not{p},q)$ is $(-\frac{1}{2})$ times the interaction kernel for the $T=\frac{1}{2}$, $S_{\frac{1}{2}}$ state, known to correspond to a strong repulsion. Similarly for the kernel $L_P(\epsilon,\not{p},q)$.

[11] This result implies that, for the case of physical interest, $V_a^R(\epsilon,\not{p})$ satisfies the homogeneous part of Eq. (79). Edwards (Phys. Rev. **90**, 284 (1953)) has also pointed this out in his study of a covariant vertex function, based on a different approximation. The solution of this homogeneous equation is uncertain to a factor $A(\epsilon)$. Only $A(M)$ is specified by the boundary condition (83), and $A(\epsilon)$ must be obtained by comparison of the asymptotic forms obtained for energies ϵ and M. The numerical solution of a singular homogeneous integral equation requires great care in the region of high momenta, whereas the Eqs. (85), (87) are well-behaved and stable in this respect. It should also be noted that, for positive Q' (i.e., a repulsive interaction), the renormalized vertex function is still well-defined by Eqs. (85), (87), but does not satisfy the homogeneous equation.

[12] A. Salam, Phys. Rev. **82**, 217 (1951).

[13] J. C. Ward, Proc. Phys. Soc. (London) **A64**, 54 (1951).

[14] The derivative of a principal value integral $\int\phi(\not{p})P_\epsilon(\not{p})d\not{p}$ with respect to the position of the singularity will be denoted symbolically by $\int\phi(\not{p})(dP_\epsilon(\not{p})/d\epsilon)d\not{p}$. Its evaluation will be discussed in Appendix A.

Substituting for γ_k the expression given in Eq. (66) and using the derivative of (63), namely

$$\frac{d\Gamma_\epsilon(q)}{d\epsilon}=\frac{G^2}{16\pi^3}Q'\int\frac{d_3k}{E_k\omega_k}$$
$$\times\left(\left[\frac{dH(\epsilon,q,k)}{d\epsilon}P_\epsilon(k)+H(\epsilon,q,k)\frac{dP_\epsilon(k)}{d\epsilon}\right]\Lambda^+(-k)\Gamma_\epsilon(k)\right.$$
$$\left.+H(\epsilon,q,k)P_\epsilon(k)\Lambda^+(-k)\frac{d\Gamma_\epsilon(k)}{d\epsilon}\right), \quad (90)$$

it will be found that

$$\frac{dS(\epsilon)}{d\epsilon}=\frac{G^2}{16\pi^3}\int\frac{Md_3k}{E_k\omega_k}\Gamma_\epsilon^\dagger(k)\Lambda^+(-k)\frac{dP_\epsilon(k)}{d\epsilon}\Lambda^+(-k)\Gamma_\epsilon(k)$$
$$+\left(\frac{G^2}{16\pi^3}\right)^2Q'\int\int\frac{M^2d_3pd_3q}{E_p\omega_pE_q\omega_q}\left[\Gamma_\epsilon^\dagger(p)\Lambda^+(-p)P_\epsilon(p)\right.$$
$$\left.\times\frac{dH(\epsilon,p,q)}{d\epsilon}P_\epsilon(q)\Lambda^+(-q)\Gamma_\epsilon(q)\right]. \quad (91)$$

This may now be expressed in terms of $V_S{}^R$ and $V_S{}^P$ by substituting (73), (75), and (81). After some reduction, this becomes

$$\frac{dS(\epsilon)}{d\epsilon}=\frac{1-\beta}{2}Z_S{}^2\Lambda_S+\frac{1+\beta}{2}Z_P{}^2\Lambda_P, \quad (92)$$

where Λ_S and Λ_P are given by

$$\Lambda_\alpha(\epsilon)=\frac{G^2}{8\pi^3}\int\frac{k^2dk}{M\omega_k(E_k+M)}\frac{dP_\epsilon(k)}{d\epsilon}|v_\alpha(k)|^2$$
$$+\left(\frac{G^2}{8\pi^3}\right)^2Q'\int\int\frac{q^2dq}{E_q\omega_q}\frac{p^2dp}{E_p\omega_p}$$
$$\times\left(\bar v_\alpha(q)P_\epsilon(q)\frac{dK_\alpha(\epsilon,q,p)}{d\epsilon}P_\epsilon(p)v_\alpha(p)\right), \quad (93)$$

and β may be taken as $+1$ for the $p_{\frac{1}{2}}$ state ($\alpha=P$), -1 for the $S_{\frac{1}{2}}$ state ($\alpha=S$). The functions $v_\alpha(p)$ are given by $v_S(p)=(E_p+M)V_S{}^R(p)$ and $v_P(p)=pV_P{}^R(p)$. The quantities Λ defined by Eq. (93) each have the structure of a vertex. The first term of Λ diverges less than linearly. The second term is convergent over p and q integrations separately, and diverges less than linearly for the joint integration. The quantity $\Lambda(\epsilon)-\Lambda(\beta M)$ is therefore a convergent integral if the integrands are subtracted before the integration. The self-energy $S_\alpha(\epsilon)$ is then, on integration of (92)

$$S_\alpha(\epsilon)=S_\alpha(\beta M)+(\epsilon-\beta M)Z_\alpha{}^2\Lambda_\alpha(\beta M)$$
$$+Z_\alpha{}^2\int_{\beta M}^{\epsilon}(\Lambda_\alpha(\epsilon')-\Lambda_\alpha(\beta M))d\epsilon'. \quad (94)$$

The last integral of (94) represents the finite part of the self energy $S_\alpha(\epsilon)$ after renormalization—we shall denote this finite part by $(G^2/16\pi^3)S_\alpha{}^R(\epsilon)$. Of the other terms, the first represents a correction to the nucleon mass and the second produces a coupling-constant renormalization at certain points.

The final expression for $f(p)$ is now

$$f(p)=g(p)+\frac{G_2{}^2}{16\pi^3}\frac{M}{E_p}F_\epsilon(p)\Lambda^+(-p)\Gamma_\epsilon(p)$$
$$\times\frac{Q\beta}{\epsilon-\beta M-(G_2{}^2/16\pi^3)Q\beta S_\alpha{}^R(\epsilon)}$$
$$\times\int\frac{d_3k}{\omega_k}\Gamma_\epsilon{}^{R\dagger}(k)\psi_0(k), \quad (95)$$

where $G_2{}^2$ is the renormalized coupling constant $G^2Z_\alpha{}^2/(1-Z_\alpha{}^2\Lambda_\alpha(\beta M))$. At all other places in this expression, where the coupling constant occurs implicitly, the unrenormalized coupling constant G^2 is effective. This corresponds to the appearance of $G_2{}^2$ only at the points marked with a cross on the graph (b) of Fig. 1. For an approximate theory, such as the present one, it is not to be expected that a renormalization scheme can be obtained which is complete and consistent at every point. What is significant is that, with the N.T.D. method, the finite parts of all divergent expressions have been identified uniquely and it has been shown that the infinite parts occurring in self-energy and vertex terms may be interpreted as mass and coupling constant renormalizations. For the $p_{\frac{1}{2}}$ state, it would be natural to identify G_2 with G, which corresponds simply to dropping all infinite terms. However, for the $S_{\frac{1}{2}}$ state, the renormalized vertex function is uncertain to a constant factor—if a finite vertex operator is defined corresponding to some standard condition such as (83), this uncertainty is transferred to an uncertainty in G_2. For the $S_{\frac{1}{2}}$ state, therefore, the two coupling constants G and G_2 are to be considered as quantities to be determined independently from comparison with experiment.

To obtain the phase shift, only the large components of $f(p)$ are needed. For the $S_{\frac{1}{2}}$ state, taking $\psi_0(p)=\delta(\epsilon-\omega_p-E_p)$,

$$f_S{}^+(p)=g_S{}^+(p)-\frac{G_2{}^2}{4\pi^2}\frac{E_p+2M}{3E_p}V_S{}^R(p)$$
$$\times\frac{3}{\epsilon+M+(3G_2{}^2/16\pi^3)S_S{}^R(\epsilon)}\frac{l(E_l+M)}{2M\epsilon}V^\dagger{}_S{}^R(l). \quad (96a)$$

For the $p_{\frac{1}{2}}$ state, $\psi_0(q)$ is $\delta(\epsilon-\omega_p-E_p)\sigma\cdot p/p$ and

$$f_{P^+}(p)=g_{P^+}(p)+\frac{G_2^2}{4\pi^2}\frac{1}{2E_p}V_{P^R}(p)$$

$$\times\frac{3}{\epsilon-M-(3G_2^2/16\pi^2)S_{P^R}(\epsilon)}\frac{p^2}{2M\epsilon}V^{\dagger}{}_{P^R}(l). \quad (96b)$$

The phase shift is then given by expression (39).

V. DISCUSSION

It is of interest to summarize in this section the various difficulties which have appeared in the course of this work, and to compare the situation with that for the corresponding covariant Bethe-Salpeter equation. In lowest approximation for meson-nucleon scattering, this equation may be written

$$(\mathbf{p}-M-\Sigma_2(\mathbf{p}))(q^2-\mu^2-\Omega_2(q^2))\phi(p,q)$$

$$=\frac{G^2}{(2\pi)^4}\int d_4k\left(\gamma_5\frac{Q'}{\mathbf{p}-\mathbf{k}-M}\gamma_5\right.$$

$$\left.+\gamma_5\frac{Q}{\mathbf{p}+\mathbf{q}-M}\gamma_5\right)\phi(p+q-k,k). \quad (97)$$

This equation goes a little beyond the lowest approximation in that the use of the modified propagators corresponds to the inclusion of some terms of order G^4. For Eq. (97) a consistent coupling constant renormalization is not strictly possible since a product of propagators occurs, but it is reasonable to simply drop the infinite parts of Σ_2 and Ω_2. However, as Feldman[15] has pointed out, the modified nucleon propagator $[\mathbf{p}-M-\Sigma_2(\mathbf{p})]^{-1}$ has a pole in the complex p_0-plane, which probably has the consequence that (99) has no finite solution in its present form. In Sec. III, it has been remarked that the modified propagator in the Tamm-Dancoff theory also has a nonphysical pole, which prevents its use in the scattering calculations. The physical interpretation of the pole is quite different in the two cases and it appears most probable that there is no simple relationship between them. Each of these situations illustrates that approximations to the modified propagators may be used only with caution, and only when they contain no singularities beyond those required by the physical processes possible. Both in (37) and (97) then, the presence of a spurious pole prevents the use of the appropriate modified propagators in the theory.

For the $T=\frac{1}{2}$ states, the calculation of a covariant renormalized vertex may be reduced to the solution of a finite integral equation in a manner similar to that developed in Sec. IIIa, and the self-energy renormalization procedure may be followed through according to the method of Ward.[13] However the difficulty in the covariant theory is that reliable solutions cannot be obtained for these four-dimensional integral equations at present, especially as numerical techniques are inadequate to deal with integral equations involving several variables. The advantage of the N.T.D. theory is that all these operations involve the solution of one-dimensional integral equations by standard techniques. The advantage of the covariant theory is that it includes both positive and negative frequencies; the vertex renormalization is then well-determined in that the relation between the renormalized vertices effective for the $S_{\frac{1}{2}}$ state and for the $p_{\frac{1}{2}}$ state is known explicitly. For the graphs generated from (97), only an incomplete renormalization is possible, of course, in that the renormalization of each coupling constant is not independent of its position in the graphical structure. This situation also holds in the N.T.D. schemes; it is not a serous matter since the important thing is to calculate the finite parts corresponding to a given graph. The difficulty for the N.T.D. scheme is that, in the $S_{\frac{1}{2}}$ state, the uncertainty in the vertex renormalization involves essentially the introduction of a new parameter in the theory.

Both the B-S and the N.T.D. theories have the defect of not satisfying the symmetry principle of Goldberger and Gell-Mann,[16] that to every uncrossed graph generated in the theory a corresponding crossed graph should be included. One consequence of this symmetry principle is that the difference between the $T=\frac{3}{2}$ and $T=\frac{1}{2}$ scattering lengths at zero momentum must approach zero in the limit of vanishing meson mass. If this feature of the complete γ_5 theory is not present in the approximate calculations of S-state scattering, it may well be that the difference in slope calculated may reflect the approximations of the method rather than the content of the complete theory. This defect will exist in any strict Tamm-Dancoff theory, and this suggests the direction in which any further modifications of the noncovariant theory should tend.

In a more complete theory, one may expect that equations of the type (37) may be obtained, but with a far more complicated kernel. The modification to the S-state kernel used here may be expected to be quite different from that for P-state kernels, so that a comparison of (37) with experimental results may well lead to effective coupling constants different for S- and P-states. A practical difficulty (see Appendix A) in the use of the considerations of Sec. IV is that for the $T=\frac{1}{2}$, $j=\frac{1}{2}$ states the integral equations (60) and (85) have satisfactory solutions only if $G^2/4\pi$ is less than 6.7. This is certainly not a deep difficulty since for reasonable coupling strengths the unsatisfactory character of the solution only shows up for very large momenta (say $p>10M$) where the Tamm-Dancoff kernel could not be regarded as a reasonable approximation.

[15] G. Feldman, Proc. Roy. Soc. (London) **A223**, 112 (1954).

[16] M. Goldberger and M. Gell-Mann, Proceedings of the Rochester Conference (University of Rochester, Rochester, 1954).

Several more general criticisms of the N.T.D. method, made recently, should also be mentioned here. Symanzig[17] has considered the soluble case of the anharmonic oscillator and has shown that the N.T.D. amplitudes do not diminish with increasing complexity of the amplitude considered but may even increase exponentially, although the old Tamm-Dancoff amplitudes describing an excited state of this system do diminish satisfactorily. It seems possible that this lack of convergence may be a general feature of the N.T.D. method and that the equations considered here could not be regarded as the first approximation in a converging sequence of equations. Renormalization of explicit self-energy expressions occurring in higher approximations of the theory have been considered by Taylor[18] who concludes that these expressions do not have the structure necessary for the success of the renormalization procedure. The effect of these objections on the present theory is not yet clear however, but it seems probable that the equations studied here should still provide a first approximation to the more extended theory.

VI. ACKNOWLEDGMENTS

In conclusion, we wish to express our appreciation to Professor H. A. Bethe for discussions of the problems raised in this work.

APPENDIX A. CALCULATION OF DERIVATIVES OF PRINCIPAL VALUE INTEGRALS

The derivative of the following integral $I_\epsilon(k)$,

$$I_\epsilon(k)=\int_0^\infty P_\epsilon(k)\phi(k)dk \tag{A1}$$

with respect to energy ϵ, is to be calculated. $P_\epsilon(k)$ is singular at $k=l$, where $\epsilon=\omega_l+E_l$, so that (A1) is to be understood as a principal value integral. We may write

$$P_\epsilon(k)=A_\epsilon(k)/(k-l). \tag{A2}$$

The differentiation of $I_\epsilon(k)$ then leads to

$$\frac{dI_\epsilon(k)}{d\epsilon}=\int_0^\infty \frac{1}{(k-l)}\frac{dA_\epsilon(k)}{d\epsilon}\phi(k) + \frac{dl}{d\epsilon}\left[\frac{d}{dl}\int_0^\infty \frac{1}{k-l}A_\epsilon(k)\phi(k)dk\right]. \tag{A3}$$

The first term of (A3) is a principal value integral again, so that only the square bracket need be considered. The principal value integral appearing there may be given by the average of the integrals along two contours from 0 to $+\infty$ in the complex plane, are passing above $k=l$, the other below. Then for these contours C, the square bracket becomes simply

$$\int_C \frac{1}{(k-l)^2}B(k)dk, \tag{A4}$$

where $B(k)=\phi(k)A_\epsilon(k)$. Making use of the integral

$$\int_{-\infty}^{\infty} dk/(k-l)^2=0,$$

(A4) may be rearranged to give the following explicitly finite expression

$$\int_0^l \frac{B(l+x)-2B(l)+B(l-x)}{x^2}dx + \int_{2l}^\infty \frac{B(k)}{(k-l)^2}dk+\frac{2B(l)}{l}, \tag{A5}$$

suitable for numerical computations.

APPENDIX B. BEHAVIOR OF THE FUNCTIONS $g(p)$ AND $V_R(\epsilon,p)$ FOR LARGE p

Consider first the function $g(p)$ satisfying Eq. (60). The states $S_{\frac{1}{2}}$ and $P_{\frac{1}{2}}$ are of special interest in the present work, and our detailed remarks will be confined to this case. Only the large components $g_\alpha{}^+(p)$ of $g_\alpha(p)$ need be considered, and the integral equation for $g_\alpha{}^+(p)$ has been given in D3. With the notation of the present paper,

$$g_\alpha{}^+(p)=\frac{G^2}{8\pi^2}Q'B_\alpha(p)+\frac{G^2}{8\pi^2}Q'\int dkL_\alpha(\epsilon,p,k)g_\alpha{}^+(k), \tag{B1}$$

where $L_\alpha(\epsilon,p,k)$ is given by Eq. (80) and $B_\alpha(p)$ is obtained from the integral of (B1) by replacing $P_\epsilon(k)$ of L_α by $\delta(\epsilon-\omega_k-E_k)$ and $g_\alpha{}^+(k)$ by 1.

Now for $p\gg k$,

$$L_\alpha(\epsilon,p,k)\sim\frac{k^2}{E_k\omega_k}\frac{E_k\pm M}{\epsilon-\omega_k-E_k}\frac{1}{p}+O\left(\frac{1}{p^2}\right), \qquad B_\alpha(p)\sim\frac{l}{\epsilon}\frac{E_l\pm M}{p}+\cdots, \tag{B2}$$

where the + sign refers to the S-state, the − sign to the P-state. If p and k are comparable, and large compared with M, $L_\alpha(\epsilon,p,k)$ is given by the following expression. With $a>b\gg M$,

$$L_\alpha(\epsilon,a,b)\simeq L_\alpha(\epsilon,b,a)\simeq\left[-\frac{a+b}{ab}\ln\frac{a+b}{a}+\frac{1}{2}\frac{a+b}{a^2}\right]. \tag{B3}$$

In the integral equation (B1), consider the ranges of integration $k\gtrless X$, where $X\gg M$. Then for $p\gg X$, the

[17] K. Symanzig, Gottingen Dissertation, March, 1954 (unpublished).
[18] J. Taylor, Phys. Rev. 95, 1313 (1954).

integral up to $k=X$ and the term $B_a(p)$ are each of form $1/p$, while the kernel is homogeneous for $k>X$. This integral equation is therefore singular at infinity and not of the Fredholm type. Such equations, homogeneous for large momenta, characteristically have solutions with an asymptotic form $\sim p^\lambda$. If $\lambda>-1$, the integration for $X<k<\infty$ may be extended down to $k=0$ using the asymptotic form of the kernel, with error of lower order, and this term (being homogeneous) reproduces the form p^λ with a coefficient depending on λ. This term is dominant on the right of (B1), and equating this with $g_a^+(p)$ gives the following equation for λ:

$$\frac{16\pi^2}{G^2}=-Q'D(\lambda), \tag{B4}$$

where

$$D(\lambda)=\frac{\pi\,\mathrm{cosec}\pi\lambda}{\lambda(1+\lambda)}-\frac{1}{\lambda^2}-\frac{1}{(1+\lambda)^2}+\frac{1}{2\lambda(1+\lambda)}+\frac{3}{2(\lambda-1)(2+\lambda)}.$$

This derivation of (B4) is valid only for $-1<\lambda<0$, $D(\lambda)$ is singular at $\lambda=0$ and $\lambda=-1$. In Born approximation, the asymptotic form of $g_a^+(p)$ corresponds to $\lambda=-1$, and, for $T=\frac{1}{2}$, $j=\frac{1}{2}$ states ($Q'=-1$), the value of λ increases with increasing G^2 until it reaches $\lambda=-\frac{1}{2}$ at $G^2/4\pi=3\pi/(3\pi-8)\sim 6\cdot 7$. At this critical value of G^2, the function $g(p)$ is no longer normalizable for large p. For G^2 beyond this critical value, the value of λ is complex, of the form $\lambda=-\frac{1}{2}\pm iu$—the equation no longer has a uniquely defined solution, and no solutions are normalizable. Such a critical value $G_c^2(j)$ exists for every attractive meson-nucleon state, but owing to the centrifugal repulsion, $G_c^2(j)$ increases with increasing j, being about[19] 26.9 for $j=\frac{3}{2}$.

For the $T=\frac{3}{2}$, $j=\frac{1}{2}$ states, Eq. (B4) has no solution in the range $-1<\lambda<0$. However it may be shown that the asymptotic form of the solution is still p^λ, where $\lambda<-1$ and is given by the same Eq. (B4). For these states, as G^2 is increased, the value of λ decreases from $\lambda=-1$, and the solution decreases faster than Born approximation for large p.

The function $V_a^R(M,p)$ is defined by the integral Eq. (85). In Born approximation $V_a^R(M,p)$ is asymptotically constant. For definite G^2, $V_a^R(M,p)$ may be expected to have asymptotic form p^λ, where λ may be either $\lambda\lesssim 0$.

If $\lambda<0$, then the integrals on the right of (86) are separately convergent, and in the limit $p\to\infty$, the equation becomes

$$1-\frac{G^2}{8\pi^2}Q'\int dk L_a(M,0,k)V_a^R(M,k)=0. \tag{B5}$$

This implies that $1/Z_a=0$, and that $V_a^R(M,p)$ satisfies the homogeneous part of integral equation (79). For this equation, it is easily shown the dominant part of the integral comes from the asymptotic region, so the value of λ is again given by Eq. (B4). This equation does in fact give a negative λ for the physical case $Q'=-1$. As G^2 increases from zero, λ decreases from zero to negative values, reaching $\lambda=-\frac{1}{2}$ for $G^2=G_c^2$. For this attractive interaction, then, $V_a^R(\epsilon,p)$ decreases more and more rapidly with p, as the interaction becomes stronger.

For $\lambda>0$, more care would be needed. With Eq. (85), the dominant terms on the right come from large momenta k and the asymptotic form of $L_a(M,0,k)$ must now be included. When this is done, the calculation may be carried through as above, with the result that Eq. (B4) is valid again for positive λ. Hence, for a repulsive interaction, the value of λ runs from zero along the right-hand branch of the function $D(\lambda)$, and $V_a^R(M,p)$ increases as p increases. For this case integral (B5) diverges and $1/Z_a=\infty$. The function $V_a^R(M,p)$ now does not satisfy the homogeneous part of the integral equation (80)—in fact, this homogeneous integral equation now has no solution, in general.

For this case, it is necessary to examine also Eq. (87). Since $L_a(\epsilon,q,k)$ is independent of ϵ for large k, the dominant part of the inhomogeneous term in (87) has the asymptotic form $\sim X(\epsilon)p^{\nu-1}$, corresponding to asymptotic form p^ν for $V_a^R(M,p)$. If the function $W_a(k)$ is $\sim k^\mu$ for large k, the form of (87) requires $\mu<0$ and a comparison of dominant terms requires $\mu=\nu-1$. $W_a(k)$ then has asymptotic form $A(\epsilon)q^{\nu-1}$, where

$$A(\epsilon)\left(1+\frac{G^2}{16\pi^2}D(\nu-1)\right)=X(\epsilon). \tag{B6}$$

The difference between $V_a^R(\epsilon,p)$ and $V_a^R(M,p)$ is therefore of one order lower than the separate vertex-functions. This is of importance since the renormalization procedure adopted would not otherwise succeed.

[19] H. A. Bethe and F. J. Dyson, Phys. Rev. **90**, 372 (1953). See also H. A. Bethe and F. de Hoffmann, *Mesons and Fields* (Row, Peterson, and Company, Evanston, 1955), Vol. 2.

Decay of Spin-Zero Mesons into Two Leptons*

HIRONARI MIYAZAWA† AND REINHARD OEHME
Institute for Nuclear Studies, University of Chicago, Chicago, Illinois
(Received March 9, 1955)

The following general theorem is formulated: The matrix element for the decay of spin-zero mesons with mass m into two leptons with masses μ_1 and μ_2 respectively contains only terms proportional to μ_1/m and μ_2/m, if in the open polygonal arc of lepton lines the number of matrices γ_μ plus the number of internal lines (S_F-functions) is odd. There can also be terms proportional to μ_i/m if virtual leptons with $\mu_i \neq \mu_1, \mu_2$ appear in the arc. Application of this theorem to the reaction $\pi^0 \to e^+ + e^-$ leads to a ratio of the one pair to the two pair decay of the order $(\mu_e/m_{\pi^0})^2 \sim 10^{-8}$. *A priori* one would expect this ratio to be of the order one. Furthermore, the theorem provides a more general basis for the discussion of the relative probability of the reactions $\pi \to \mu + \nu$ and $\pi \to e + \nu$.

THE recent development of bubble chambers makes it possible to detect higher order decays of pions into leptons. Therefore it might be of interest to study processes like

$$\pi^0 \to e^+ + e^-, \quad \pi^0 \to e^+ + e^- + e^+ + e^-, \quad \pi^+ \to e^+ + \nu, \quad \text{etc.}$$

It is the purpose of this note to show, on the basis of general principles, that in many cases the transition probability for the decay of spin-zero mesons into two leptons is reduced by a factor of the order $(\mu/m)^2$, where μ is the mass of the heaviest lepton emitted and m is the meson mass. The matrix element for a process of this kind can be written in the general form[1]

$$M(p,q) = \bar{\psi}_1(p) F(p,q) \psi_2(q) \phi(q-p). \tag{1}$$

Here $\phi(q-p)$ is the wave function of the decaying spin zero meson having four-momentum $q-p$, and $\bar{\psi}_1(p)$ and $\psi_2(q)$ are the corresponding wave functions of the emitted leptons. They obey the Dirac equations

$$i\bar{\psi}_1(p)\mathbf{p} = -\mu_1 \bar{\psi}_1(p), \quad i\mathbf{q}\psi_2(q) = -\mu_2 \psi_2(q),$$

where we use the notation $\mathbf{A} \equiv \gamma_\mu A_\mu = -i\beta\alpha_\kappa A_\kappa + i\beta A_0$ and $\bar{\psi} \equiv \psi^\dagger \gamma_4$; μ_1 and μ_2 are the masses of the emitted leptons. $F(p,q)$ is a spinor matrix which transforms as a scalar or pseudoscalar function depending on the relative parity of $\bar{\psi}_1(p)\psi_2(q)$ and $\phi(q-p)$. If a, b, etc., are scalar functions of $p^2 = -\mu_1^2$, $q^2 = -\mu_2^2$, and $pq = \frac{1}{2}(m^2 - \mu_1^2 - \mu_2^2)$, we can write the 4×4 spinor matrix $F(p,q)$ for reasons of covariance in the form

$$F(p,q) = \begin{cases} a + bm^{-1}\mathbf{p} + cm^{-1}\mathbf{q} + dm^{-2}(\mathbf{qp} - \mathbf{pq}) \\ \gamma_5\{a' + b'm^{-1}\mathbf{p} + c'm^{-1}\mathbf{q} + d'm^{-2}(\mathbf{qp} - \mathbf{pq})\}. \end{cases} \tag{2}$$

The first row is for scalar F and the second for pseudoscalar F. Introducing this into Eq. (1) we obtain by use of the Dirac equation

$$M = \begin{cases} \left[a + ib\frac{\mu_1}{m} + ic\frac{\mu_2}{m} + 2d\frac{\mu_1\mu_2 + pq}{m^2}\right] \\ \qquad \times \bar{\psi}_1(p)\psi_2(q)\phi(q-p) \\ \left[a' - ib'\frac{\mu_1}{m} + ic'\frac{\mu_2}{m} - 2d'\frac{\mu_1\mu_2 + pq}{m^2}\right] \\ \qquad \times \bar{\psi}_1(p)\gamma_5\psi(q)\phi(q-p). \end{cases} \tag{3}$$

We observe that the terms in F which are linear in γ_μ lead in the matrix element M to contributions proportional to the lepton masses. These contributions vanish for $\mu_1 \to 0$, $\mu_2 \to 0$, provided the coefficients do not become infinite in this limit. A behavior like that would be very unusual and can be excluded in all applications discussed below. If, for a special decay process, the function $F(p,q)$ contains only terms involving products of odd numbers of matrices γ_μ besides those which are *a priori* proportional to μ_1 or μ_2, it can be reduced to

$$F(p,q) = \begin{cases} bm^{-1}\mathbf{p} + cm^{-1}\mathbf{q} + f_1 m^{-1}\mu_1 + f_2 m^{-1}\mu_2 \\ \gamma_5(b'm^{-1}\mathbf{p} + c'm^{-1}\mathbf{q} + f_1' m^{-1}\mu_1 + f_2' m^{-1}\mu_2). \end{cases} \tag{4}$$

The corresponding matrix element therefore contains only terms proportional to the lepton masses μ_1 and μ_2. Here we have made the assumption that the open polygonal arc of lepton lines contains no internal lines corresponding to spin one half particles with masses different from μ_1 and μ_2. Thus every internal lepton line is associated with a propagation function

$$S_F(k) = (i\mathbf{k} - \mu)/(k^2 + \mu^2),$$

where μ is either μ_1 or μ_2. After having performed the integrations over intermediate momenta, the four vector k_μ must be of the form $k_\mu = x(m,\mu_1,\mu_2)p_\mu + y(m,\mu_1,\mu_2)q_\mu$. We see that every S_F-function introduces a term proportional to γ_μ and a term which is *a priori* proportional to μ_1 or μ_2. For the applications it is only important that the masses of the virtual leptons in the open polygonal are smaller or of the same order of magnitude than those of the final particles.

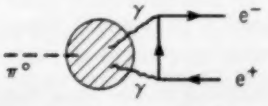

FIG. 1. Graph of order α^2 for the process $\pi^0 \to e^+ + e^-$.

* Supported in part by the U. S. Atomic Energy Commission.
† On leave of absence from the University of Tokyo, Tokyo, Japan.
[1] R. Oehme, Z. Naturforsch. **7a**, 55 (1952).

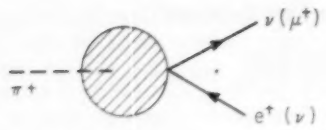

FIG. 2. Graph for the reactions $\pi^+ \to e^+ + \nu$ and $\pi^+ \to \mu^+ + \nu$.

On the basis of these arguments we can formulate the theorem: "The matrix element for the decay of spin-zero mesons with mass m into two leptons with masses μ_1 and μ_2 respectively contains only terms proportional to μ_1/m and μ_2/m, if in the open polygonal arc of lepton lines the number of matrices γ_μ at vertices plus the number of internal lines (S_F-functions) is odd. Should the lepton arc contain internal lines corresponding to virtual spin-one-half particles with masses μ_i being unequal to μ_1 and μ_2, then the matrix element contains also terms proportional to μ_i/m."

As a first application of this theorem we consider the reaction $\pi^0 \to e^+ + e^-$. We assume only that the π^0 meson has spin zero and that the interaction occurs via the electromagnetic field, i.e., that the pair is produced by virtual photons. No specific assumption about the meson-photon interaction is necessary. Under these conditions the matrix element of first order in the fine structure constant α vanishes identically.[2] The process involving two virtual photons is in principle possible, but we have $N(\gamma_\mu)+N(S_F)=$odd. (See Fig. 1.) Therefore, according to the theorem formulated above, the matrix element is proportional to μ_e/m_{π^0} and the transition probability contains the factor

$$(\mu_e/m_{\pi^0})^2\alpha^4.$$

One can easily see that $N(\gamma_\mu)+N(S_F)=$odd is independent of the number of virtual photons involved. Thus the contributions to the matrix element which are of higher order in α must be also proportional to μ_e/m_{π^0}. We conclude that the reaction $\pi^0 \to e^+ + e^-$ is less probable by a factor of the order 10^{-5} than the decay into two pairs, for which Kroll and Wada[3] find

$$(\pi^0 \to e^+ + e^- + e^+ + e^-)/(\pi^0 \to \gamma + \gamma) \approx 3.5 \times 10^{-5}.$$

For the ratio of one pair to double γ decay we obtain

$$r \equiv (\pi^0 \to e^+ + e^-)/(\pi^0 \to \gamma + \gamma) \sim 10^{-9}.$$

The measurements of Lindenfeld, Sachs, and Steinberger[4] lead to an upper limit of 5×10^{-4} for this ratio.

The only direct coupling between pseudoscalar π^0-mesons and electrons for which the above theorem is not applicable is: $i\bar{\psi}_e \gamma_5 \psi_e \phi_{\pi^0}$. If we assume this hypothetical interaction to be about as strong as the Fermi coupling for β decay, it would lead to a ratio r of the order 10^{-6}.

Let us further consider the decay of a charged π meson into a μ meson and a neutrino and into an electron (positron) and a neutrino. Assuming that both processes are caused by the same interaction (see Fig. 2), one would expect from the difference of phase spaces a ratio

$$R \equiv (\pi \to e + \nu)/(\pi \to \mu + \nu) \sim 3.3,$$

whereas experimentally one finds that $R \lesssim 10^{-4}$.[5]

We can write the matrix element for both reactions in the form (1). If the coupling to the lepton field is such that the number of γ_μ matrices contained in F is odd, we find, according to our theorem,

$$R \sim 3.3(\mu_e/\mu_\mu)^2 \sim 10^{-4}.$$

This result does not depend on whether the interaction is direct or occurs via nucleon pairs or other intermediate fields. We assume only that the charged π meson has spin zero and that the μ meson and the neutrino have spin one-half. Terms proportional to μ_ν/μ_μ have been neglected, because μ_ν is zero or at least small compared with μ_e. We see that vector and pseudovector lepton couplings lead to a ratio R which is compatible with the experimental limit. All other lepton couplings give in general $R \gtrsim 1$. Of course there are other selection rules which forbid both reactions under certain assumptions about the intermediate fields and couplings.[6] Application of the generalized Furry theorem for intermediate closed nucleon loops leads in some cases to a simultaneous reduction of both decay processes by a factor of the order α^2.[7]

A ratio R of the order 10^{-4} for pseudovector lepton couplings has been found by several authors.[8] They have calculated the matrix elements for both decay processes in first order of the meson nucleon coupling, assuming that the interaction occurs via an intermediate nucleon field. According to our theorem this result holds in a more general sense. We finally remark that for some of the lepton couplings which lead to a ratio $R \sim 10^{-4}$ the reaction $\pi \to e + \nu + \gamma$ should be more probable by a factor of the order $(m_\pi/\mu_e)^2\alpha \sim 10^2$ than the decay $\pi \to e + \nu$. For the process $\pi \to e + \nu + \gamma$ our theorem is not applicable.

We are indebted to Professor G. Wentzel for interesting discussions. Thanks are also due to Professor V. Telegdi and Dr. S. Cohen for helpful comments.

[2] See reference 1; for vector mesons this is the most probable decay process.

[3] U. M. Kroll and W. Wada, Phys. Rev. **98**, 1355 (1955).

[4] Lindenfeld, Sachs, and Steinberger, Phys. Rev. **89**, 531 (1953).

[5] S. Lokanathan and J. Steinberger (private communication via J. Steinberger); H. Friedman and J. Rainwater, Phys. Rev. **81**, 644 (1951).

[6] See, for example, C. N. Yang and J. Tiomno, Phys. Rev. **79**, 485 (1950).

[7] C. B. van Wyck, Phys. Rev. **80**, 487 (1950); A. Pais and R. Jost, Phys. Rev. **87**, 871 (1952). R. Oehme, in *Kosmische Strahlung*, edited by W. Heisenberg (Springer-Verlag, Berlin, 1953), p. 557.

[8] For a survey of the literature and for references see L. Michel, in *Progress in Cosmic Ray Physics*, edited by G. J. Wilson (Interscience Publishers, Inc., New York, 1952), pp. 176–181. More recently, M. Gell-Mann and V. Telegdi have made calculations on this subject (unpublished; private communication from V. Telegdi).

Reduction of Relativistic Two-Particle Wave Equations to Approximate Forms. III*

W. A. BARKER,† *Physikalisches Institut, Eidgenössische Technische Hochschule, Zürich, Switzerland*

AND

F. N. GLOVER,‡ *Physics Department, Saint Louis University, St. Louis, Missouri*

(Received November 12, 1954)

The interaction between two fermions of charge $\epsilon_{\rm I}$ and $\epsilon_{\rm II}$ and intrinsic magnetic moment $\mu_{\rm I}$ and $\mu_{\rm II}$ is described by a sixteen-component wave equation of the Breit type. The method of reduction of two-particle wave equations, as given in two previous papers by Chraplyvy, is used to convert this equation to an approximate four-component Pauli equation. A simple perturbation calculation is used to determine the contribution of the intrinsic magnetic moments to the fine and hyperfine structure of hydrogen and positronium.

1. INTRODUCTION

IN two previous papers,[1] referred to hereafter as I and II, the Foldy-Wouthuysen canonical transformation[2] was generalized by Chraplyvy to the two-body problem both for the singular case of equal masses as well as for the case of unequal masses. We consider here several applications using, except where noted, the terminology and notation of I and II.

Four-component one-body relativistic equations of the Dirac type or sixteen-component two-body equations of the Breit type may now be reduced to two- or four-component approximate equations of the Pauli type by the Foldy-Wouthuysen method or by the procedure of expressing the small components of the spinor ψ in terms of its large components.[3] In Sec. 2, the differences between these methods are brought out in a discussion of a familiar one-body example which we shall have occasion to refer to later as the limiting case of a two-body problem.

In Sec. 3, we compare the Hermitian part of a three-dimensional Bethe-Salpeter equation with the corresponding Breit equation by applying the two-body transformation of I to both.

In Secs. 4 and 5, the Breit interaction between two fermions of charge $\epsilon_{\rm I}$ and $\epsilon_{\rm II}$ is amplified to include intrinsic magnetic moment and virtual annihilation terms. The resulting equations are converted to the Pauli representation by means of the two-body transformation. It is then a simple matter to calculate the contribution of the intrinsic magnetic moments to the fine and hyperfine structure of hydrogen and positronium.

2. THE HYDROGEN ATOM: ONE-BODY TREATMENT

Essentially the same differences exist between the results of the Foldy-Wouthuysen and the "large component" methods of reduction when applied to either the one or the two-body problem. Although these differences have been discussed qualitatively before,[1,2] a simple quantitative comparison may be of interest. We consider the hydrogen atom, approximated as a one-body problem.

The exact solution for the energy E of the Dirac equation[4] for hydrogen,

$$(\beta m+\boldsymbol{\alpha}\cdot\mathbf{p}-e^2/r)\psi=i\partial\psi/\partial t, \tag{1}$$

may be expanded in ascending powers of the fine structure constant α.

$$E=m-\frac{m\alpha^2}{2n^2}-\frac{m\alpha^4}{2n^4}\left[\frac{n}{j+\frac{1}{2}}-\frac{3}{4}\right]+\cdots. \tag{2}$$

If the Foldy-Wouthuysen transformation is applied to Eq. (1), one obtains

$$H'\psi'=\left\{\beta m+\frac{\beta p^2}{2m}-\frac{e^2}{r}-\frac{\beta p^4}{8m^3}+\frac{\pi e^2}{2m^2}\delta(\mathbf{r})+\frac{e^2}{8m^2}\boldsymbol{\sigma}\cdot\left(\frac{\mathbf{r}}{r^3}\times\mathbf{p}-\mathbf{p}\times\frac{\mathbf{r}}{r^3}\right)+\cdots\right\}\psi', \tag{3}$$

where H' is obviously Hermitian and ψ' is still a four-component spinor. This equation may be separated into two two-component equations referring to positive and

TABLE I. One-body relativistic energy level corrections in Eq. (3).

Operator	Expectation value	
$-\frac{p^4}{8m^3}$	$-\frac{m\alpha^4}{2n^4}\left(\frac{n}{l+\frac{1}{2}}-\frac{3}{4}\right)$	
$\frac{\pi e^2}{2m^2}\delta(\mathbf{r})$	$\frac{m\alpha^4}{2n^3}\delta_{0l}$	
$\frac{e^2}{4m^2}\boldsymbol{\sigma}\cdot\frac{\mathbf{r}}{r^3}\times\mathbf{p}$	$\frac{m\alpha^4}{2n^3}\frac{1}{(2l+1)(l+1)}$	$j=l+\frac{1}{2}$, $l\neq 0$
	$-\frac{m\alpha^4}{2n^3}\frac{1}{l(2l+1)}$	$j=l-\frac{1}{2}$

* This work was supported in part by the Office of Scientific Research, Air Research and Development Command, U. S. Air Force.

† On leave of absence from St. Louis University during the academic years 1953–1955.

‡ Present address: Woodstock College, Woodstock, Maryland.

[1] Z. V. Chraplyvy, Phys. Rev. **91**, 388 and **92**, 1310 (1953).

[2] L. L. Foldy and S. A. Wouthuysen, Phys. Rev. **78**, 29 (1950).

[3] Other reduction methods exist. See R. A. Ferrell, thesis, Princeton University, Princeton, New Jersey, 1951 (unpublished).

[4] Units are chosen so that $\hbar=c=1$.

negative energy states respectively by the simple prescription of replacing β by $+1$ or -1. The resulting equation for the electron in positive energy states is just the Schrödinger equation for the hydrogen atom plus relativistic correction terms whose contribution to the energy may be readily calculated by perturbation theory.[5] The three relativistic energy level corrections given in Table I combine to give the $m\alpha^4$ term in the expansion of the Sommerfeld fine structure formula, Eq. (2).

If, on the other hand, one uses the "large component" method[6] to reduce Eq. (1), one obtains

$$\left\{\frac{p^2}{2m}-\frac{e^2}{r}-\frac{p^4}{8m^3}+\frac{\pi e^2}{m^2}\delta(\mathbf{r})+\frac{ie^2}{4m^2}\frac{\mathbf{r}}{r^3}\cdot\mathbf{p}+\frac{e^2}{4m^2}\boldsymbol{\sigma}\cdot\frac{\mathbf{r}}{r^3}\times\mathbf{p}+\frac{ie^2}{4m^2}\boldsymbol{\sigma}\cdot\nabla\times\frac{\mathbf{r}}{r^3}\right\}\chi=i\frac{\partial\chi}{\partial t}. \quad (4)$$

Clearly the "Hamiltonian" operating on the two large components χ is not Hermitian. Comparing Eqs. (4) and (3) for positive energy states we find that the kinetic energy relativistic correction and spin-orbit terms appear in both, but instead of one term affecting the S states there are now two. However, since

$$\left\langle\frac{\pi e^2}{m^2}\delta(\mathbf{r})+\frac{ie^2}{4m^2}\frac{\mathbf{r}}{r^3}\cdot\mathbf{p}\right\rangle=\left\langle\frac{\pi e^2}{2m^2}\delta(\mathbf{r})\right\rangle=\frac{m\alpha^4}{2n^3}\delta_{0l}, \quad (5)$$

where $\langle A\rangle$ denotes the expectation value of A, we see that the relativistic energy level corrections again add to give exactly the $m\alpha^4$ term in Eq. (2).

In the two-body problem, there is no exact solution available by which to check approximate solutions. One would again expect the two reduction methods to give the same result for the energy levels. Given a choice, however, certainly the method which leads to a Hermitian Hamiltonian is more satisfactory.

3. TWO-BODY EQUATIONS

In I, Chraplyvy has shown that a two-body Hamiltonian written in the form

$$H=\beta^{\mathrm{I}}m_{\mathrm{I}}+\beta^{\mathrm{II}}m_{\mathrm{II}}+(\mathcal{E}\mathcal{E})+(\mathcal{E}\mathcal{O})+(\mathcal{O}\mathcal{E})+(\mathcal{O}\mathcal{O}), \quad (6)$$

where $(\mathcal{E}\mathcal{E})$, $(\mathcal{E}\mathcal{O})$, $(\mathcal{O}\mathcal{E})$, and $(\mathcal{O}\mathcal{O})$ represent even-even, even-odd, odd-even, and odd-odd terms, may be transformed into an even-even operator[7]

$$\begin{aligned}H_{TR}=&\beta^{\mathrm{I}}m_{\mathrm{I}}+\beta^{\mathrm{II}}m_{\mathrm{II}}+(\mathcal{E}\mathcal{E})+\frac{\beta^{\mathrm{I}}}{2m_{\mathrm{I}}}(\mathcal{O}\mathcal{E})^2\\&+\frac{\beta^{\mathrm{II}}}{2m_{\mathrm{II}}}(\mathcal{E}\mathcal{O})^2-\frac{\beta^{\mathrm{I}}}{8m_{\mathrm{I}}^3}(\mathcal{O}\mathcal{E})^4-\frac{\beta^{\mathrm{II}}}{8m_{\mathrm{II}}^3}(\mathcal{E}\mathcal{O})^4\\&+\frac{1}{8m_{\mathrm{I}}^2}[[(\mathcal{O}\mathcal{E}),(\mathcal{E}\mathcal{E})],(\mathcal{O}\mathcal{E})]\\&+\frac{1}{8m_{\mathrm{II}}^2}[[(\mathcal{E}\mathcal{O}),(\mathcal{E}\mathcal{E})],(\mathcal{E}\mathcal{O})]\\&+\frac{\beta^{\mathrm{I}}\beta^{\mathrm{II}}}{4m_{\mathrm{I}}m_{\mathrm{II}}}[[(\mathcal{O}\mathcal{E}),(\mathcal{O}\mathcal{O})]_+,(\mathcal{E}\mathcal{O})]_+\\&+\frac{\beta^{\mathrm{I}}m_{\mathrm{I}}-\beta^{\mathrm{II}}m_{\mathrm{II}}}{2(m_{\mathrm{I}}^2-m_{\mathrm{II}}^2)}(\mathcal{O}\mathcal{O})^2+\cdots. \quad (7)\end{aligned}$$

If $(\mathcal{E}\mathcal{E})$, $(\mathcal{E}\mathcal{O})$, $(\mathcal{O}\mathcal{E})$, and $(\mathcal{O}\mathcal{O})$ are Hermitian, it is evident that H_{TR} is Hermitian.

The Hermitian part of the three-dimensional Bethe-Salpeter equation[8] written in coordinate space is

$$\begin{aligned}H\Psi(\mathbf{r})=&(H_{\mathrm{I}}+H_{\mathrm{II}}+\tfrac{1}{2}[\{\Lambda_+^{\mathrm{I}}\Lambda_+^{\mathrm{II}}-\Lambda_-^{\mathrm{I}}\Lambda_-^{\mathrm{II}}\},U_B(\mathbf{r})]_+)\\&\times\Psi(\mathbf{r})=E\Psi(\mathbf{r}), \quad (8)\end{aligned}$$

where

$$\begin{aligned}&H_{\mathrm{I}}\equiv\beta^{\mathrm{I}}m_{\mathrm{I}}+\boldsymbol{\alpha}^{\mathrm{I}}\cdot\mathbf{p}, \quad H_{\mathrm{II}}\equiv\beta^{\mathrm{II}}m_{\mathrm{II}}-\boldsymbol{\alpha}^{\mathrm{II}}\cdot\mathbf{p},\\&\Lambda_\pm^{\mathrm{I}}\equiv\frac{E_{\mathrm{I}}\pm H_{\mathrm{I}}}{2E_{\mathrm{I}}}, \quad \Lambda_\pm^{\mathrm{II}}\equiv\frac{E_{\mathrm{II}}\pm H_{\mathrm{II}}}{2E_{\mathrm{II}}},\\&E_{\mathrm{I}}\equiv+(m_{\mathrm{I}}^2+p^2)^{\frac{1}{2}}, \quad E_{\mathrm{II}}\equiv+(m_{\mathrm{II}}^2+p^2)^{\frac{1}{2}},\\&U_B(\mathbf{r})\equiv\frac{\epsilon_{\mathrm{I}}\epsilon_{\mathrm{II}}}{r}\left(1-\frac{\boldsymbol{\alpha}^{\mathrm{I}}\cdot\boldsymbol{\alpha}^{\mathrm{II}}}{2}-\frac{(\boldsymbol{\alpha}^{\mathrm{I}}\cdot\mathbf{r})(\boldsymbol{\alpha}^{\mathrm{II}}\cdot\mathbf{r})}{2r^2}\right).\end{aligned} \quad (9)$$

If we replace the Casimir projection operators in the curly brackets in Eq. (8) by 1, we obtain the well-known Breit equation.

$$\begin{aligned}H\Psi(\mathbf{r})=&\left\{\beta^{\mathrm{I}}m_{\mathrm{I}}+\boldsymbol{\alpha}^{\mathrm{I}}\cdot\mathbf{p}+\beta^{\mathrm{II}}m_{\mathrm{II}}-\boldsymbol{\alpha}^{\mathrm{II}}\cdot\mathbf{p}\right.\\&\left.+\frac{\epsilon_{\mathrm{I}}\epsilon_{\mathrm{II}}}{r}\left(1-\frac{\boldsymbol{\alpha}^{\mathrm{I}}\cdot\boldsymbol{\alpha}^{\mathrm{II}}}{2}-\frac{(\boldsymbol{\alpha}^{\mathrm{I}}\cdot\mathbf{r})(\boldsymbol{\alpha}^{\mathrm{II}}\cdot\mathbf{r})}{2r^2}\right)\right\}\\&\times\Psi(\mathbf{r})=E\Psi(\mathbf{r}). \quad (10)\end{aligned}$$

Equation (10) is in the form of Eq. (6) with

$$(\mathcal{E}\mathcal{E})=\epsilon_{\mathrm{I}}\epsilon_{\mathrm{II}}/r, \quad (\mathcal{O}\mathcal{E})=\boldsymbol{\alpha}^{\mathrm{I}}\cdot\mathbf{p}, \quad (\mathcal{E}\mathcal{O})=-\boldsymbol{\alpha}^{\mathrm{II}}\cdot\mathbf{p}, \quad (11)$$

and

$$(\mathcal{O}\mathcal{O})=-\frac{\epsilon_{\mathrm{I}}\epsilon_{\mathrm{II}}}{r}\left(\frac{\boldsymbol{\alpha}^{\mathrm{I}}\cdot\boldsymbol{\alpha}^{\mathrm{II}}}{2}+\frac{(\boldsymbol{\alpha}^{\mathrm{I}}\cdot\mathbf{r})(\boldsymbol{\alpha}^{\mathrm{II}}\cdot\mathbf{r})}{2r^2}\right).$$

In order to write Eq. (8) in the form of Eq. (6), we evaluate the anticommutator, retaining only those terms in the expansion which contribute to the desired accuracy. The result is

[5] W. A. Barker and Z. V. Chraplyvy, Phys. Rev. **89**, 446 (1953). See also E. U. Condon and G. H. Shortley, *The Theory of Atomic Spectra* (Cambridge University Press, New York, 1951).

[6] See, for example, E. L. Hill and R. Landshoff, Revs. Modern Phys. **10**, 87 (1938).

[7] See I, Eq. (7). The additional terms in (7) which arise if $(\mathcal{O}\mathcal{E})$ and $(\mathcal{E}\mathcal{O})$ do not commute make no contribution to the desired accuracy in any of the cases treated in this paper.

[8] E. E. Salpeter, Phys. Rev. **87**, 328 (1952).

$$(\mathcal{SS})=\frac{\epsilon_1\epsilon_{II}}{2r}(\beta^I+\beta^{II})-\frac{\epsilon_1\epsilon_{II}}{8}\left(\frac{\beta^I}{m_I^2}+\frac{\beta^{II}}{m_{II}^2}\right)\left[p^2,\frac{1}{r}\right]_+, \quad (12a)$$

$$(\mathcal{OS})=\boldsymbol{\alpha}^I\cdot\mathbf{p}+\epsilon_1\epsilon_{II}\left(\frac{1}{4m_I}+\frac{1}{8m_{II}}\right)\times\left[\boldsymbol{\alpha}^I\cdot\mathbf{p},\frac{1}{r}\right]_+ +\frac{i\epsilon_1\epsilon_{II}}{8m_{II}}\boldsymbol{\alpha}^I\times\boldsymbol{\sigma}^{II}\cdot\left[\mathbf{p},\frac{1}{r}\right]_+ +\frac{\epsilon_1\epsilon_{II}}{8m_{II}}\times\left[\mathbf{p}\cdot,\frac{\mathbf{r}(\boldsymbol{\alpha}^I\cdot\mathbf{r})}{r^3}\right]_+ +\frac{i\epsilon_1\epsilon_{II}}{8m_{II}}\boldsymbol{\sigma}^{II}\cdot\left[\mathbf{p}\times,\frac{\mathbf{r}(\boldsymbol{\alpha}^I\cdot\mathbf{r})}{r^3}\right]_+, \quad (12b)$$

$$(\mathcal{SO})=-\boldsymbol{\alpha}_{II}\cdot\mathbf{p}-\epsilon_1\epsilon_{II}\left(\frac{1}{4m_{II}}+\frac{1}{8m_I}\right)\left[\boldsymbol{\alpha}^{II}\cdot\mathbf{p},\frac{1}{r}\right]_+ -\frac{i\epsilon_1\epsilon_{II}}{8m_I}\boldsymbol{\alpha}^{II}\times\boldsymbol{\sigma}^I\cdot\left[\mathbf{p},\frac{1}{r}\right] -\frac{\epsilon_1\epsilon_{II}}{8m_I}\left[\mathbf{p}\cdot,\frac{\mathbf{r}(\boldsymbol{\alpha}^{II}\cdot\mathbf{r})}{r^3}\right]_+ -\frac{i\epsilon_1\epsilon_{II}}{8m_I}\boldsymbol{\sigma}^I\cdot\left[\mathbf{p}\times,\frac{\mathbf{r}(\boldsymbol{\alpha}^{II}\cdot\mathbf{r})}{r^3}\right]_+. \quad (12c)$$

Here

$[\mathbf{A}\cdot,\mathbf{B}]_+\equiv\mathbf{A}\cdot\mathbf{B}+\mathbf{B}\cdot\mathbf{A}$ and $[\mathbf{A}\times,\mathbf{B}]_+\equiv\mathbf{A}\times\mathbf{B}+\mathbf{B}\times\mathbf{A}$.

The elimination of a leading $(\mathcal{OO})$ term[9] is a consequence of

$$[\beta^I,\boldsymbol{\alpha}^I]_+=[\beta^{II},\boldsymbol{\alpha}^{II}]_+=0. \quad (13)$$

The $(\mathcal{OO})$ terms in the Breit interaction, $U_B(\mathbf{r})$, are changed into $(\mathcal{SO})$ and $(\mathcal{OS})$ terms respectively when acted on by $\boldsymbol{\alpha}^I\cdot\mathbf{p}$ and $\boldsymbol{\alpha}^{II}\cdot\mathbf{p}$ in (8). Expressions (11) and (12) are manifestly Hermitian.

We may now apply the prescription (7) and transform the Hamiltonians in (8) and (10) into even-even operators. Neglecting contributions of order $m\alpha^6$ and higher the result for (8) is

$$(H_{TR})=\beta^Im_I+\beta^{II}m_{II}+\frac{\beta^Ip^2}{2m_I}+\frac{\beta^{II}p^2}{2m_{II}}-\frac{\beta^Ip^4}{8m_I^3}-\frac{\beta^{II}p^4}{8m_{II}^3} +(\beta^I+\beta^{II})\frac{\epsilon_1\epsilon_{II}}{2r}-(\beta^I+\beta^{II})\frac{\pi\epsilon_1\epsilon_{II}\delta(\mathbf{r})}{4} \times\left(\frac{1}{m_I^2}+\frac{1}{m_{II}^2}\right)-(\beta^I+\beta^{II})\frac{\epsilon_1\epsilon_{II}}{8r^3} \times\left(\frac{\boldsymbol{\sigma}^I}{m_I^2}+\frac{\boldsymbol{\sigma}^{II}}{m_{II}^2}\right)\cdot(\mathbf{r}\times\mathbf{p})+(\beta^I+\beta^{II})\frac{\epsilon_1\epsilon_{II}}{4m_Im_{II}} \times\left\{\frac{1}{r}p^2+\mathbf{r}\left(\frac{\mathbf{r}}{r^3}\cdot\mathbf{p}\right)\cdot\mathbf{p}-\frac{1}{r^3}(\boldsymbol{\sigma}^I+\boldsymbol{\sigma}^{II})\cdot(\mathbf{r}\times\mathbf{p})\right\} +(\beta^I+\beta^{II})\frac{\epsilon_1\epsilon_{II}}{8m_Im_{II}}\left\{\frac{\boldsymbol{\sigma}^I\cdot\boldsymbol{\sigma}^{II}}{r^3}-\frac{3(\boldsymbol{\sigma}^I\cdot\mathbf{r})(\boldsymbol{\sigma}^{II}\cdot\mathbf{r})}{r^5} -\frac{8\pi}{3}\boldsymbol{\sigma}^I\cdot\boldsymbol{\sigma}^{II}\delta(\mathbf{r})\right\}+\cdots. \quad (14)$$

[9] There are $(\mathcal{OO})$ terms which contribute to higher order.

On the other hand, one obtains the following transformed Hamiltonian[10] from the Breit equation (10):

$$(H_{TR})=\beta^Im_I+\beta^{II}m_{II}+\frac{\beta^Ip^2}{2m_I}+\frac{\beta^{II}p^2}{2m_{II}}-\frac{\beta^Ip^4}{8m_I^3}-\frac{\beta^{II}p^4}{8m_{II}^3} +\frac{\epsilon_1\epsilon_{II}}{r}-\frac{\pi\epsilon_1\epsilon_{II}\delta(\mathbf{r})}{2}\left(\frac{1}{m_I^2}+\frac{1}{m_{II}^2}\right)-\frac{\epsilon_1\epsilon_{II}}{4r^3} \times\left(\frac{\boldsymbol{\sigma}^I}{m_I^2}+\frac{\boldsymbol{\sigma}^{II}}{m_{II}^2}\right)\cdot(\mathbf{r}\times\mathbf{p})+\frac{\beta^I\beta^{II}\epsilon_1\epsilon_{II}}{2m_Im_{II}} \times\left\{\frac{1}{r}p^2+\mathbf{r}\left(\frac{\mathbf{r}}{r^3}\cdot\mathbf{p}\right)\cdot\mathbf{p}-\frac{1}{r^3}(\boldsymbol{\sigma}^I+\boldsymbol{\sigma}^{II})\cdot(\mathbf{r}\times\mathbf{p})\right\} +\frac{\beta^I\beta^{II}\epsilon_1\epsilon_{II}}{4m_Im_{II}}\left\{\frac{\boldsymbol{\sigma}^I\cdot\boldsymbol{\sigma}^{II}}{r^3}-\frac{3(\boldsymbol{\sigma}^I\cdot\mathbf{r})(\boldsymbol{\sigma}^{II}\cdot\mathbf{r})}{r^5} -\frac{8\pi}{3}\boldsymbol{\sigma}^I\cdot\boldsymbol{\sigma}^{II}\delta(\mathbf{r})\right\}+\frac{\beta^Im_I-\beta^{II}m_{II}}{2(m_I^2-m_{II}^2)}\epsilon_1^2\epsilon_{II}^2 \times\left\{\frac{3}{2r^3}-\frac{\boldsymbol{\sigma}^I\cdot\boldsymbol{\sigma}^{II}}{r^2}+\frac{(\boldsymbol{\sigma}^I\cdot\mathbf{r})(\boldsymbol{\sigma}^{II}\cdot\mathbf{r})}{2r^4}\right\}+\cdots. \quad (15)$$

The spinor on which H_{TR} operates in (14) and (15) has 16 components. We may separate out two four-component wave equations in which both particles are in positive or negative energy states by setting $\beta^I=\beta^{II}=1$ or $\beta^I=\beta^{II}=-1$ respectively. The other two possibilities corresponding to $\beta^I=-\beta^{II}=\pm1$, yield four-component wave equations in which one particle is in a positive energy state and the other is in a negative energy state.

Several differences between (14) and (15) should be emphasized:

(a) The e^4 terms in (15) responsible for the disagreement between the predicted and observed values of the fine structure of helium[11] are not present in (14). These terms in (15) come from the $(\mathcal{OO})^2$ term in (7). There are no $(\mathcal{OO})$ terms in (12) as a result of the fundamental anticommutation relations (13) and hence no e^4 terms appear in (14).

(b) When both particles are in negative energy states $(\beta^I=\beta^{II}=-1)$ all the terms in Eq. (14) are equal in magnitude but opposite in sign to the terms obtained when both particles are in positive energy states $(\beta^I=\beta^{II}=1)$. If one particle is in a positive energy state and the other in a negative energy state, all interaction terms in (14) vanish. The same behavior is not exhibited by Eq. (15).

(c) In particular when $\epsilon_1\epsilon_{II}=-e^2$, there are bound negative energy states in the case of Eq. (14), but there are no bound negative energy states in the case of Eq. (15).

[10] There is one incorrect numerical factor and several misprints in I, Eq. (8), which have been rectified in Eq. (15). See Appendix A for Errata to I and II.

[11] See G. Breit, Phys. Rev. **36**, 383 (1930) and **39**, 616 (1932).

(d) If the mass of one of the particles is assumed to be so large that it becomes an immovable supplier of field for the other particle, i.e. $m_{\rm I}\to\infty$ or $m_{\rm II}\to\infty$, then Eq. (15) goes over into Eq. (3). The Breit equation (10) from which (15) is obtained goes over into the Dirac equation (1) if we let the velocity operator ($\boldsymbol{\alpha}^{\rm I}$ or $\boldsymbol{\alpha}^{\rm II}$) of the immovable particle go to zero. These limiting processes do *not* cause (14) and (8) to go over into (3) and (1).

All of the differences between (14) and (15) are due to the presence of the Casimir projection operators in (8) and their absence in (10). This difference between these two two-body equations stems from the manner in which they were derived. Equation (8) is a specialized form of the Bethe-Salpeter equation derived from hole theory. The Breit equation (10) was derived from the single-electron form of quantum electrodynamics.

The results of this section confirm and elaborate points which have been made previously by Bethe,[12] Brown and Ravenhall,[13] and Salpeter.[14]

4. THE HYDROGEN ATOM: TWO-BODY TREATMENT INTRINSIC MAGNETIC MOMENT TERMS

The possibility of amplifying the Breit interaction to include intrinsic magnetic moment terms has previously been considered by Breit and Meyerott.[15] They found that there is no objection in principle to this generalization of Pauli's idea[16] to the two-body problem.

In the treatment which follows, intrinsic magnetic moment terms are added to the Breit interaction for the electron as well as for the proton. A quantum electrodynamic explanation exists for the electron's intrinsic magnetic moment, but no similar fundamental explanation has yet been advanced to account quantitatively for the proton's intrinsic magnetic moment. Here the intrinsic moments are both placed on the same phenomenological footing.

Our fundamental wave equation is of the form of Eq. (8) with $U_B(\mathbf{r})$ replaced by $U_B(\mathbf{r})+U_{IM}(\mathbf{r})$ where

$$U_{IM}(\mathbf{r})=\frac{\epsilon_{\rm I}\epsilon_{\rm II}}{2m_{\rm I}}\mu_{\rm I}\left(i\beta^{\rm I}\boldsymbol{\alpha}^{\rm I}\cdot\frac{\mathbf{r}}{r^3}-\beta^{\rm I}\boldsymbol{\sigma}^{\rm I}\cdot\boldsymbol{\alpha}^{\rm II}\times\frac{\mathbf{r}}{r^3}\right)$$
$$-\frac{\epsilon_{\rm I}\epsilon_{\rm II}}{2m_{\rm II}}\mu_{\rm II}\left(i\beta^{\rm II}\boldsymbol{\alpha}^{\rm II}\cdot\frac{\mathbf{r}}{r^3}-\beta^{\rm II}\boldsymbol{\sigma}^{\rm II}\cdot\boldsymbol{\alpha}^{\rm I}\times\frac{\mathbf{r}}{r^3}\right)$$
$$+\beta^{\rm I}\beta^{\rm II}\frac{\epsilon_{\rm I}\epsilon_{\rm II}\mu_{\rm I}\mu_{\rm II}}{4m_{\rm I}m_{\rm II}}\left\{\frac{\boldsymbol{\sigma}^{\rm I}\cdot\boldsymbol{\sigma}^{\rm II}}{r^3}-\frac{3(\boldsymbol{\sigma}^{\rm I}\cdot\mathbf{r})(\boldsymbol{\sigma}^{\rm II}\cdot\mathbf{r})}{r^5}\right.$$
$$\left.-\frac{8\pi}{3}\boldsymbol{\sigma}^{\rm I}\cdot\boldsymbol{\sigma}^{\rm II}\delta(\mathbf{r})\right\}. \quad (16a)$$

Applying the same procedure as before, we find that Eq. (14) is augmented by terms of precisely the same form as terms already appearing in that equation; namely,

$$(H_{IM})_{TR}=-\frac{(\beta^{\rm I}+\beta^{\rm II})}{4}\pi\epsilon_{\rm I}\epsilon_{\rm II}\delta(\mathbf{r})\left(\frac{2\mu_{\rm I}}{m_{\rm I}^2}+\frac{2\mu_{\rm II}}{m_{\rm II}^2}\right)$$
$$-\frac{(\beta^{\rm I}+\beta^{\rm II})}{8r^3}\epsilon_{\rm I}\epsilon_{\rm II}\left(\frac{2\mu_{\rm I}\boldsymbol{\sigma}^{\rm I}}{m_{\rm I}^2}+\frac{2\mu_{\rm II}\boldsymbol{\sigma}^{\rm II}}{m_{\rm II}^2}\right)\cdot(\mathbf{r}\times\mathbf{p})$$
$$-\frac{(\beta^{\rm I}+\beta^{\rm II})}{4m_{\rm I}m_{\rm II}r^3}\epsilon_{\rm I}\epsilon_{\rm II}(\mu_{\rm I}\boldsymbol{\sigma}^{\rm I}+\mu_{\rm II}\boldsymbol{\sigma}^{\rm II})\cdot\mathbf{r}\times\mathbf{p}$$
$$+\frac{(\beta^{\rm I}+\beta^{\rm II})\epsilon_{\rm I}\epsilon_{\rm II}}{8m_{\rm I}m_{\rm II}}(\mu_{\rm I}+\mu_{\rm II}+\mu_{\rm I}\mu_{\rm II})$$
$$\times\left\{\frac{\boldsymbol{\sigma}^{\rm I}\cdot\boldsymbol{\sigma}^{\rm II}}{r^3}-\frac{3(\boldsymbol{\sigma}^{\rm I}\cdot\mathbf{r})(\boldsymbol{\sigma}^{\rm II}\cdot\mathbf{r})}{r^5}\right.$$
$$\left.-\frac{8\pi}{3}\boldsymbol{\sigma}^{\rm I}\cdot\boldsymbol{\sigma}^{\rm II}\delta(\mathbf{r})\right\}. \quad (16b)$$

If we amplify (10) rather than (8) by $U_{IM}(\mathbf{r})$ we obtain the same result as (16)b for both particles in positive energy states ($\beta^{\rm I}=\beta^{\rm II}=+1$). It is just the reduced Hamiltonian obtained by setting $\beta^{\rm I}=\beta^{\rm II}=+1$ in Eqs. (14) and (16b) which we are concerned with in determining the bound state energy levels of hydrogen.

It is convenient[17] to write the operator for the binding energy $W=H_{RED}-m_{\rm I}-m_{\rm II}$ explicitly in terms of the reduced mass μ. If we identify $m_{\rm I}$ with the electron mass m and $m_{\rm II}$ with the proton mass M, then $1/\mu=1/m+1/M$ and $\epsilon_{\rm I}\epsilon_{\rm II}=-e^2$. Let

$$W=W_0+W_1+W_2+W_3+W_4, \quad (17)$$

where

$$W_0=p^2/2\mu-e^2/r, \quad (18)$$

$$W_1=-\frac{p^4}{8\mu^3}+\frac{\pi e^2}{2\mu^2}\delta(\mathbf{r})+\frac{e^2}{4\mu^2}\boldsymbol{\sigma}^{\rm I}\cdot\frac{\mathbf{r}}{r^3}\times\mathbf{p}, \quad (19)$$

TABLE II. Contributions to $\langle W_2\rangle$ in Eq. (20).

Operator	Expectation value
$-\frac{e^2}{2mM}\frac{1}{r}p^2$	$\frac{\mu^3\alpha^4}{2mMn^4}-\frac{\mu^3\alpha^4}{mMn^3(l+\frac{1}{2})}$
$-\frac{e^2}{2mM}\mathbf{r}\left(\frac{\mathbf{r}}{r^3}\cdot\mathbf{p}\right)\cdot\mathbf{p}$	$\frac{\mu^3\alpha^4}{2mMn^4}-\frac{\mu^3\alpha^4}{2mMn^3(l+\frac{1}{2})}+\frac{\mu^3\alpha^4}{mMn^3}\delta_{0l}$
$\frac{3p^4}{8m^3M}$	$-\frac{9\mu^4\alpha^4}{8m^3Mn^4}+\frac{3\mu^4\alpha^4}{2m^3M(l+\frac{1}{2})n^3}$
$\frac{3p^4}{8mM^3}$	$-\frac{9\mu^4\alpha^4}{8mM^3n^4}+\frac{3\mu^4\alpha^4}{2mM^3(l+\frac{1}{2})n^3}$
$-\frac{\pi e^2}{mM}\delta(\mathbf{r})$	$-\frac{\mu^3\alpha^4}{mMn^3}\delta_{0l}$

[12] H. Bethe, *Handbuch der Physik* (Verlag Julius Springer, Berlin, 1933), Vol. 24, 1, p. 375.
[13] G. E. Brown and D. G. Ravenhall, Proc. Roy. Soc. (London) **A208**, 552 (1951).
[14] Reference 8. See especially the discussion on p. 331.
[15] G. Breit and R. Meyerott, Phys. Rev. **72**, 1023 (1947).
[16] W. Pauli, *Handbuch der Physik* (Verlag Julius Springer, Berlin, 1933), Vol. 24, Part 1, p. 232.
[17] This treatment follows that of W. E. Lamb, Jr., Phys. Rev. **85**, 259 (1952) and K. Bechert and J. Meixner, Ann. Physik **22**, 525 (1935).

TABLE III. Lamb shift contributions from W_3, Eq. (21).

Operator	Expectation value		Energy increase in Mc/sec $2^2S_{\frac{1}{2}}$	$2^2P_{\frac{1}{2}}$	$2^2P_{\frac{3}{2}}$
$\mu_1\frac{\pi e^2}{m^2}\delta(\mathbf{r})$	$\mu_1\frac{\mu^3\alpha^4}{m^2n^3}\delta_{0l}$		+50.065		
$\mu_{11}\frac{\pi e^2}{M^2}\delta(\mathbf{r})$	$\mu_{11}\frac{\mu^3\alpha^4}{M^2n^3}\delta_{0l}$		+0.023		
$\mu_1\frac{e^2}{2m\mu r^3}\boldsymbol{\sigma}^{\mathrm{I}}\cdot(\mathbf{r}\times\mathbf{p})$	$\mu_1\frac{\mu^3\alpha^4}{mn^3l(l+1)(2l+1)}$	$j=l+\frac{1}{2}$ $l\neq 0$			+8.349
	$-\mu_1\frac{\mu^3\alpha^4}{mn^3l(2l+1)}$	$j=l-\frac{1}{2}$		−16.697	
$-\frac{e^2}{4M^2r^3}\boldsymbol{\sigma}^{\mathrm{I}}\cdot(\mathbf{r}\times\mathbf{p})$	$-\frac{\mu^3\alpha^4}{2M^2n^3(l+1)(2l+1)}$	$j=l+\frac{1}{2}$ $l\neq 0$			−0.001
	$+\frac{\mu^3\alpha^4}{2M^2n^3l(2l+1)}$	$j=l-\frac{1}{2}$		+0.002	

$$W_2=-\frac{e^2}{2mM}\frac{1}{r}p^2-\frac{e^2}{2mM}\mathbf{r}\left(\frac{\mathbf{r}\cdot\mathbf{p}}{r^3}\right)\cdot\mathbf{p}+\frac{3p^4}{8m^2M}+\frac{3p^4}{8mM^2}-\frac{\pi e^2}{mM}\delta(\mathbf{r}), \quad (20)$$

$$W_3=\frac{\pi e^2}{m^2}\mu_1\delta(\mathbf{r})+\frac{\pi e^2}{M^2}\mu_{11}\delta(\mathbf{r})+\frac{e^2}{2m^2}\mu_1\boldsymbol{\sigma}^{\mathrm{I}}\cdot\frac{\mathbf{r}}{r^3}\times\mathbf{p}+\frac{e^2}{2mM}\mu_1\boldsymbol{\sigma}^{\mathrm{I}}\cdot\frac{\mathbf{r}}{r^3}\times\mathbf{p}-\frac{e^2}{4M^2}\boldsymbol{\sigma}^{\mathrm{I}}\cdot\frac{\mathbf{r}}{r^3}\times\mathbf{p}, \quad (21)$$

$$W_4=-\frac{e^2}{4mM}(1+\mu_1)(1+\mu_{11})\left\{\frac{\boldsymbol{\sigma}^{\mathrm{I}}\cdot\boldsymbol{\sigma}^{\mathrm{II}}}{r^3}-\frac{3(\boldsymbol{\sigma}^{\mathrm{I}}\cdot\mathbf{r})(\boldsymbol{\sigma}^{\mathrm{II}}\cdot\mathbf{r})}{r^5}-\frac{8\pi}{3}\boldsymbol{\sigma}^{\mathrm{I}}\cdot\boldsymbol{\sigma}^{\mathrm{II}}\delta(\mathbf{r})\right\}+\frac{e^2}{2mM}(1+\mu_{11})\boldsymbol{\sigma}^{\mathrm{II}}\cdot\frac{\mathbf{r}}{r^3}\times\mathbf{p}+\frac{e^2}{4M^2}(1+2\mu_{11})\boldsymbol{\sigma}^{\mathrm{II}}\cdot\frac{\mathbf{r}}{r^3}\times\mathbf{p}. \quad (22)$$

W_0 is the Schrödinger Hamiltonian for a particle of mass μ, charge $-e$ in a Coulomb field whose potential is e/r. We now tabulate all the individual contributions to the energy levels, determined by treating W_1, W_2, W_3, and W_4 as perturbations of the Balmer energy levels: $\langle W_0\rangle=-\mu\alpha^2/2n^2$.

W_1 consists of the relativistic correction terms which are familiar in the reduction of the Dirac equation (1). The individual contributions to W_1 may be obtained from Table I simply by replacing m there by μ.

The last three terms of W_2 are corrections which occur as a result of writing W in terms of the reduced mass. The expectation value of W_2 is obtained without approximation from the addition of the individual contributions in Table II:

$$\langle W_2\rangle=-\mu^3\alpha^4/8mMn^3. \quad (23)$$

The first four terms of W_3 yield the contributions of the intrinsic electron and proton magnetic moments to the Lamb shift. The last term of W_3 arising as a result of writing W in terms of μ, makes a very small contribution to the Lamb shift. The expectation values of these operators as well as the numerical values for the $2^2S_{\frac{1}{2}}$, $2^2P_{\frac{1}{2}}$, and $2^2P_{\frac{3}{2}}$ states of hydrogen are given in Table III.

In a review paper[18] on the Lamb shift, Salpeter pointed out that the contribution of the electron's intrinsic magnetic moment ($\sim\alpha/2\pi$) for an infinitely heavy nucleus is given by $\frac{1}{2}L$, where the Lamb constant $L=\alpha^3\,\mathrm{Ry}_\infty c/3\pi$, and that the correct factor accounting for the finite mass of the nucleus is not $\sim(1-3m/M)$ and had not as yet been calculated. From Table III, we see that the contribution from $\mu_1=(\alpha/2\pi)(1-5.946\alpha/\pi)$ may be written $\sim+\frac{3}{4}L(1-3m/M)(1-5.946\alpha/\pi)$ from the term affecting the S states and $\sim-\frac{1}{4}L(1-2m/M)\times(1-5.946\alpha/\pi)$ from the term affecting the P states. These combine to increase the separation of the $2^2S_{\frac{1}{2}}-2^2P_{\frac{1}{2}}$ states by $\sim+\frac{1}{2}L(1-11m/4M)(1-5.946\alpha/\pi)=66.78$ Mc/sec, of which -0.10 Mc/sec is due to the mass correction and -0.94 Mc/sec to the fourth order intrinsic magnetic moment of the electron.[19] Corrections of this order are now of interest since the experimental accuracy in Lamb shift measurements is ±0.10 Mc/sec.[20]

The contribution of the proton's intrinsic magnetic moment to the Lamb shift agrees with that calculated by Salpeter[18] and is still not measurable. It should be pointed out that the normal Dirac moment of the proton as well as that of the electron have been taken into account in these calculations and that their combined contribution to the Lamb shift is represented by the fifth term in W_3 and amounts to -0.002 Mc/sec.

In the case of hydrogen, the hyperfine structure splitting is small compared to the fine structure splitting. The operator for the hyperfine energy, W_4, includes all

[18] E. E. Salpeter, Phys. Rev. **89**, 92 (1953).
[19] R. Karplus and N. M. Kroll, Phys. Rev. **77**, 536 (1950).
[20] Triebwasser, Dayhoff, and Lamb, Phys. Rev. **89**, 98 (1953).

terms which depend on the nuclear spin operator $\mathbf{i}=\boldsymbol{\sigma}^{II}/2$. Because of the tensor interaction, l is not a good quantum number. We restrict our attention, however, to the S and P states. Since there are no matrix elements of W_4 connecting these two states, we may consider the diagonal elements for a given l.

S states.—The expectation value of W_4 for the S states is given simply by

$$\langle W_4\rangle=\frac{2\pi\alpha}{3mM}(1+\mu_I)(1+\mu_{II})\langle\boldsymbol{\sigma}^I\cdot\boldsymbol{\sigma}^{II}\delta(\mathbf{r})\rangle, \quad (24)$$

which leads to the S state hyperfine splitting,

$$\Delta W_S=\frac{8}{3}\frac{\mu^3\alpha^4}{mMn^3}(1+\mu_I)(1+\mu_{II}). \quad (25)$$

This is in agreement with Lamb,[17] but does not, of course, take into consideration a number of effects treated in quantum electrodynamic calculations.[21]

P states.—It is convenient to write W_4 for $l\neq 0$ in terms of $\mathbf{i}$, $\mathbf{s}=\boldsymbol{\sigma}^I/2$ and $\mathbf{l}=\mathbf{r}\times\mathbf{p}$.

$$W_4=\frac{e^2}{mM}(1+\mu_I)(1+\mu_{II})\frac{1}{r^3}\left\{\frac{3\mathbf{i}\cdot\mathbf{rs}\cdot\mathbf{r}}{r^2}-\mathbf{i}\cdot\mathbf{s}\right\}$$
$$+\frac{e^2}{mM}(1+\mu_{II})\frac{1}{r^3}\mathbf{i}\cdot\mathbf{l}+\frac{e^2}{2M^2}(1+2\mu_{II})\frac{1}{r^3}\mathbf{i}\cdot\mathbf{l}. \quad (26)$$

Equation (26) is of the same form as the hyperfine energy operator for $l\neq 0$ as treated in Bethe's Handbuch article[22] and recently reviewed by Lamb,[17] but it includes additional small contributions. It is, therefore, a simple matter to determine the expectation value of W_4 for the $P_{\frac{1}{2}}$ and $P_{\frac{3}{2}}$ states.

$$P_{\frac{1}{2}}\colon\langle W_4\rangle=\frac{\mu^3\alpha^4}{9n^3}\left\{\frac{(1+\mu_I)(1+\mu_{II})}{mM}+\frac{1+\mu_{II}}{mM}\right.$$
$$\left.+\frac{1+2\mu_{II}}{2M^2}\right\}\langle 2f(f+1)-3\rangle, \quad (27)$$

$$P_{\frac{3}{2}}\colon\langle W_4\rangle=\frac{\mu^3\alpha^4}{18n^3}\left\{-\frac{(1+\mu_I)(1+\mu_{II})}{5mM}+\frac{1+\mu_{II}}{mM}\right.$$
$$\left.+\frac{1+2\mu_{II}}{2M^2}\right\}\langle 2f(f+1)-9\rangle, \quad (28)$$

where $\mathbf{f}=\mathbf{i}+\mathbf{j}$. The $P_{\frac{1}{2}}$ and $P_{\frac{3}{2}}$ state hyperfine splittings are

$$\Delta W_{P_{\frac{1}{2}}}=\frac{4\mu^3\alpha^4}{9n^3Mm}\left\{(1+\mu_{II})(2+\mu_I)+\frac{m(1+2\mu_{II})}{2M}\right\}$$
$$=59.096\text{ Mc/sec for } n=2, \quad (29)$$

and

$$\Delta W_{P_{\frac{3}{2}}}=\frac{4\mu^3\alpha^4}{9n^3Mm}\left\{\frac{(1+\mu_{II})(4-\mu_I)}{5}+\frac{m(1+2\mu_{II})}{2M}\right\}$$
$$=23.626\text{ Mc/sec for } n=2. \quad (30)$$

These results are to be compared with earlier theoretical expressions given by Lamb[23]:

$$\Delta W_{P_{\frac{1}{2}}}=\frac{8\mu^3\alpha^4}{9mMn^3}(1+\mu_{II});$$
$$\Delta W_{P_{\frac{3}{2}}}=\frac{16}{45}\frac{\mu^3\alpha^4}{mMn^3}(1+\mu_{II}), \quad (31)$$

which are the leading terms in (29) and (30). The electron's intrinsic magnetic moment increases the hyperfine splitting of the $2^2P_{\frac{1}{2}}$ and $2^2P_{\frac{3}{2}}$ states by $+0.034$ Mc/sec and -0.007 Mc/sec respectively. The Dirac and intrinsic magnetic moment of the proton (2nd term in curly brackets in Eqs. (29) and (30)) increase the hyperfine splitting of both P states by 0.013 Mc/sec. Corrections of this order should now be considered, inasmuch as $2P$-state hyperfine splittings are now known experimentally to within 0.20 Mc/sec,[20] and more precise results are to be expected.

5. POSITRONIUM

Again we consider a wave equation of the form of Eq. (8) with the Breit interaction amplified to include the first-order single quantum virtual annihilation exchange interaction,[24] $U_A(\mathbf{r},\mathbf{r}')$ as well as the intrinsic magnetic moment terms Eq. (16a). For positronium $m_I=m_{II}=m$; $\mu_I=\mu_{II}\sim\alpha/2\pi$, and

$$U_A(\mathbf{r},\mathbf{r}')=-(\pi e^2/m^2)(\gamma_j c)\delta(\mathbf{r})\delta(\mathbf{r}')(c^{-1}\gamma_j). \quad (32)$$

The pair creation matrices $\gamma_j c$ and the pair annihilation matrices $c^{-1}\gamma_j$ are defined by the relation:

$$\bar{\psi}(\gamma_j c)(c^{-1}\gamma_j)\psi=\bar{\psi}_{kK}(\gamma_j c)_{Kk}(c^{-1}\gamma_j)_{K'k'}\psi_{k'K'},$$
$$j=1,2,3,$$
$$k,K=1,2,3,4, \quad (33)$$

with $\bar{\psi}=\psi^*\gamma_0$; $c=\gamma_0\gamma_2=c^{-1}$; $\gamma_j=\beta\alpha_j$; $\gamma_0=\beta$. Clearly U_A is even-even.

[21] R. Arnowitt, Phys. Rev. **92**, 1002 (1953), has made the latest calculation on the hyperfine splitting of the S states. This and earlier calculations by R. Karplus and A. Klein, Phys. Rev. **85**, 972 (1952); N. M. Kroll and F. Pollock, Phys. Rev. **86**, 876 (1952) and E. E. Salpeter and W. A. Newcomb, Phys. Rev. **87**, 150 (1952), have been used together with the experimental value, known to an accuracy of ± 0.0003 Mc/sec, to calculate precision values of the fine structure constant.

[22] Reference 12, p. 386.

[23] Reference 17, Sec. 56, and W. E. Lamb, Jr., and R. C. Retherford, Phys. Rev. **79**, 549 (1950).

[24] R. Karplus and A. Klein, Phys. Rev. **87**, 848 (1952); see Eqs. (3.5) and (5.3).

In I, Chraplyvy has shown that for $m_I = m_{II}$, there is no finite transformation which will convert a two-body Hamiltonian containing $(\mathcal{O}\mathcal{O})$ terms into an $(\mathcal{E}\mathcal{E})$ operator. We may still use Eq. (7) for positronium, however, since the Casimir projection operators eliminate $(\mathcal{O}\mathcal{O})$ terms to the order considered. [See Eq. (12).] If we amplify the Breit equation (10) rather than Eq. (8) by $U_A(\mathbf{r},\mathbf{r}')$, we must apply the more general prescriptions of II. In either case we obtain the same result for both particles in positive energy states (apart from the e^4 terms discussed in Sec. 2).

Separating out the four-component wave equation for both particles in positive energy states allows us to write the energy corresponding to the interaction (32) in two equivalent ways:

$$\begin{aligned} V_A &= (\pi e^2/m^2)\psi^*(0)_{uU}\{(\sigma_3)_{Uu}(\sigma_3)_{U'u'}+\delta_{Uu}\delta_{U'u'} \\ &\qquad +(\sigma_1)_{Uu}(\sigma_1)_{U'u'}\}\psi(0)_{u'U'} \\ &= (\pi e^2/m^2)\psi^*(0)_{uU}\{\tfrac{3}{2}\delta_{uu'}\delta_{UU'} \\ &\qquad +\tfrac{1}{2}\boldsymbol{\sigma}_{uu'}\cdot\boldsymbol{\sigma}_{UU'}\}\psi(0)_{u'U'}, \end{aligned} \tag{34}$$

where $u, U = 1, 2$. In the second form of Eq. (34), the Pauli matrices refer to the individual particles I, II. Hence we may say that in the Pauli representation, the virtual annihilation exchange interaction is given by

$$(U_A)_{REP} = \frac{\pi e^2}{m^2}(\tfrac{3}{2}+\tfrac{1}{2}\boldsymbol{\sigma}^{\mathrm{I}}\cdot\boldsymbol{\sigma}^{\mathrm{II}})\delta(\mathbf{r}). \tag{35}$$

In the case of positronium (unlike hydrogen), the hyperfine and fine structure splittings are of the same order of magnitude and l is a good quantum number in spite of the tensor interaction.[25] Therefore, we regroup the various terms contributing to the positronium binding energy $V = H_{REP} - 2m$ in a slightly different way than was done for hydrogen. Let

$$V = V_0 + V_1 + V_2 + V_3 + V_4, \tag{36}$$

where

$$V_0 = p^2/m - e^2/r, \tag{37}$$

$$V_1 = -\frac{p^4}{4m^3} + \frac{5\pi e^2}{2m^2}\delta(\mathbf{r}) - \frac{e^2p^2}{2m^2r} - \frac{e^2}{2m^2}\mathbf{r}\left(\frac{\mathbf{r}}{r^3}\cdot\mathbf{p}\right)\cdot\mathbf{p}, \tag{38}$$

$$V_2 = \frac{3e^2}{2m^2r^3}\mathbf{S}\cdot\mathbf{l}, \quad \text{where} \quad \mathbf{S} = \tfrac{1}{2}(\boldsymbol{\sigma}^{\mathrm{I}}+\boldsymbol{\sigma}^{\mathrm{II}}), \tag{39}$$

$$V_3 = \mu_1\left\{\frac{2\pi e^2}{m^2}\delta(\mathbf{r}) + \frac{e^2}{m^2r^3}\mathbf{S}\cdot\mathbf{l}\right\}, \tag{40}$$

$$V_4 = -\frac{e^2}{4m^2}(1+\mu_1)^2\left\{\frac{\boldsymbol{\sigma}^{\mathrm{I}}\cdot\boldsymbol{\sigma}^{\mathrm{II}}}{r^3} - \frac{3(\boldsymbol{\sigma}^{\mathrm{I}}\cdot\mathbf{r})(\boldsymbol{\sigma}^{\mathrm{II}}\cdot\mathbf{r})}{r^5} - \frac{8\pi}{3}\boldsymbol{\sigma}^{\mathrm{I}}\cdot\boldsymbol{\sigma}^{\mathrm{II}}\delta(\mathbf{r})\right\} + \frac{\pi e^2}{2m^2}\boldsymbol{\sigma}^{\mathrm{I}}\cdot\boldsymbol{\sigma}^{\mathrm{II}}\delta(\mathbf{r}). \tag{41}$$

We now write the contributions of V_1, V_2, V_3, and V_4 to the energy levels, determined, as in the case of hydrogen, by treating them as perturbations on the Balmer energy levels $\langle V_0\rangle = -m\alpha^2/4n^2$.

V_1, which includes a part of the virtual annihilation exchange interaction, consists of kinetic energy and orbital terms. It is spin-independent and hence contributes equally to the singlet and triplet states.

$$\langle V_1\rangle = \frac{11m\alpha^4}{64n^4} + \frac{7m\alpha^4}{16n^3}\delta_{0l} - \frac{m\alpha^4}{4n^3(l+\frac{1}{2})}. \tag{42}$$

The spin-orbit interaction V_2 depends on the total spin S. It does not contribute to either the singlet or S states.

$$\langle V_2\rangle^t = \frac{3m\alpha^4}{16n^3l(l+\frac{1}{2})(l+1)}(1-\delta_{0l}) \times \begin{cases} l, & j=l+1 \\ -1, & j=l \\ -(l+1), & j=(l-1). \end{cases} \tag{43}$$

V_3 gives the contribution of the intrinsic magnetic moments of the electron and positron to the Lamb shift. Using $\mu_1 = \mu_{II} \sim \alpha/2\pi$, we get

$$\langle V_3\rangle = \frac{m\alpha^5}{8\pi n^3}\delta_{0l} + \frac{m\alpha^5(1-\delta_{0l})}{16\pi n^3l(l+\frac{1}{2})(l+1)} \times \begin{cases} l, & j=l+1 \\ -1, & j=l \\ -(l+1), & j=(l-1). \end{cases} \tag{44}$$

All spin-spin interactions are given by V_4. The $\delta(\mathbf{r})$ terms affect only the S states

$$\begin{aligned} \langle V_4\rangle_{l=0} &= \frac{7\pi\alpha}{6m^2}\left(1+\frac{4\alpha}{7\pi}\right)\langle(2S^2-3)\delta(\mathbf{r})\rangle \\ &= -\frac{7m\alpha^4}{16n^3}\left(1+\frac{4\alpha}{7\pi}\right) \text{ for } {}^1S_0 \text{ states} \\ &= \frac{7}{48}\frac{m\alpha^4}{n^3}\left(1+\frac{4\alpha}{7\pi}\right) \text{ for } {}^3S_1 \text{ states.} \end{aligned} \tag{45}$$

The remaining terms for $l \neq 0$ are zero for the singlet

[25] A detailed proof is given in reference 3.

states.

$$\langle V_4\rangle_{l\neq 0}=-\frac{e^2}{4m^2}\left(1+\frac{\alpha}{\pi}\right)\left\langle\frac{\boldsymbol{\sigma}^{\mathrm{I}}\cdot\boldsymbol{\sigma}^{\mathrm{II}}}{r^3}-\frac{3(\boldsymbol{\sigma}^{\mathrm{I}}\cdot\mathbf{r})(\boldsymbol{\sigma}^{\mathrm{II}}\cdot\mathbf{r})}{r^5}\right\rangle$$

$$=\frac{m\alpha^4(1-\delta_{0l})}{16n^3l(l+\frac{1}{2})(l+1)}\left(1+\frac{\alpha}{\pi}\right)$$

$$\times\begin{cases}-\dfrac{l}{2l+3}, & j=l+1\\ 1, & j=l\\ -\dfrac{(l+1)}{2l-1}, & j=(l-1).\end{cases}\qquad(46)$$

Adding $\langle V_0\rangle$, $\langle V_1\rangle$, $\langle V_2\rangle$, $\langle V_3\rangle$, and $\langle V_4\rangle$ the binding energy for the singlet and triplet states is

$$\langle V\rangle^s=-\frac{m\alpha^2}{4n^2}+\frac{11m\alpha^4}{64n^4}-\frac{m\alpha^4}{4n^3(l+\frac{1}{2})}+\frac{m\alpha^5}{8\pi n^3}\delta_{0l},\qquad(47)$$

$$\langle V\rangle^t=-\frac{m\alpha^2}{4n^2}+\frac{11m\alpha^4}{64n^4}-\frac{m\alpha^4}{4n^3(l+\frac{1}{2})}+\frac{7m\alpha^4}{12n^3}\delta_{0l}$$

$$+\frac{m\alpha^4(1-\delta_{0l})}{8n^3(l+\frac{1}{2})}\begin{cases}\dfrac{3l+4}{(2l+3)(l+1)}, & j=l+1\\ \dfrac{-1}{l(l+1)}, & j=l\\ \dfrac{-3(l-1)}{l(2l-1)}, & j=l-1\end{cases}$$

$$+\frac{m\alpha^5}{8\pi n^3}\delta_{0l}+\frac{m\alpha^5(1-\delta_{0l})}{16\pi n^3l(l+\frac{1}{2})(l+1)}$$

$$\times\begin{cases}\dfrac{2l(l+1)}{(2l+3)}, & j=l+1\\ 0, & j=l\\ \dfrac{-2l(l+1)}{(2l-1)}, & j=l-1.\end{cases}\qquad(48)$$

The $m\alpha^4$ terms in Eq. (47) and Eq. (48) agree with those of Ferrell.[26] The only $m\alpha^5$ terms considered in our calculation are those arising from the intrinsic magnetic moments of the electron and positron. Recently Fulton and Martin[27] have calculated all the corrections of order α^5 to the $n=2$ energy levels of positronium using a quantum electrodynamic method. It is possible to identify[28] the intrinsic magnetic moment contribution in their final expressions. These are found to agree with the results of our phenomenological treatment.

We are indebted to Professor Z. V. Chraplyvy for suggesting this problem and for numerous valuable discussions. One of us (W. A. B.) would like to express his appreciation to Professor W. Pauli for his encouragement and comments, and to Dr. A. Thellung, Dr. R. Jost, and Dr. P. Martin for helpful discussions.

APPENDIX A

Errata to I

In Eq. (4), the first minus sign should be replaced by a plus sign.

On p. 389, the second display formula in the middle of the left column should read:

$$(\Omega\psi)_{kK}=\sum_{n,N}\eta_{knN}\omega_{KN}\psi_{nN}.$$

In Eq. (7j), the numerical coefficient should be $\frac{1}{8}$ (rather than $\frac{3}{16}$).

In Eq. (8b), the denominator of the last term should be $2m_1c$.

In Eq. (8e), first line, the minus sign between the terms should be replaced by a plus sign; the curly brackets of the second line should read

$$\left\{-\frac{i(\mathbf{r}\cdot\mathbf{p}_1)}{r^3}+4\pi i\delta(\mathbf{r})(\mathbf{r}\cdot\mathbf{p}_1)+\frac{2\boldsymbol{\sigma}^{\mathrm{II}}\cdot(\mathbf{r}\times\mathbf{p}_1)}{r^3}\right\}.$$

The last term of Eq. (8e) should be $(8\pi/3)(\boldsymbol{\sigma}^{\mathrm{I}}\cdot\boldsymbol{\sigma}^{\mathrm{II}})\delta(\mathbf{r})$.

In Eq. (8f), the curly brackets should read

$$\left\{\frac{3}{r^3}-\frac{2(\boldsymbol{\sigma}^{\mathrm{I}}\cdot\boldsymbol{\sigma}^{\mathrm{II}})}{r^3}+\frac{(\boldsymbol{\sigma}^{\mathrm{I}}\cdot\mathbf{r})(\boldsymbol{\sigma}^{\mathrm{II}}\cdot\mathbf{r})}{r^4}\right\}.$$

Errata to II

On p. 1131, the last formula of the left column should begin with $\alpha_y^{\mathrm{II}}\alpha_z^{\mathrm{I}}$.

In Eq. (6c), the subscript at the end of the second term should be *oo* (rather than *oe*).

[26] R. A. Ferrell, Phys. Rev. **84**, 858 (1951). The details are given in Dr. Ferrell's thesis, reference 3.

[27] T. Fulton and P. C. Martin, Phys. Rev. **93**, 903 (1954); **95**, 811 (1954).

[28] We are indebted to Dr. Martin for an interesting discussion on the relationship between their work and ours.

Functional Integrals and Adiabatic Limits in Field Theory*

S. DESER†
Institute for Advanced Study, Princeton, New Jersey
(Received March 26, 1955)

The behavior of a system of coupled fields as some of the particles become very heavy is investigated. By means of a technique expressing the relevant exact Green's functions as functional integrals, the limiting process need only be performed for bare one-particle propagators to get the result for the exact functions. It is shown that the resultant propagators are those for the remaining finite masses moving in external fields generated by the heavy particles acting as static point sources. The situation in which the coupling to the intermediate fields has no simple nonrelativistic limit is also discussed.

I.

THE behavior of a coupled system of fields as some of the particle masses are taken much greater than the others is always supposed to approach in such a limit that of a reduced system, in which the heavy particles act as static sources of the fields to which they are coupled. It is the purpose of this note to supply a proof of this adiabatic limiting assumption.

By use of a technique expressing the relevant propagation functions as functional integrals, the desired limiting process need only be performed in one simple part of the exact expressions, to include all radiative corrections and interactions, at once.

We shall, for simplicity, consider the coupling of several fermions via a boson field (of zero or finite mass) and with various (scalar, vector, etc.) couplings. Since the limit considered is essentially one in which the heavy particle becomes nonrelativistic, couplings which have no simple behavior in this limit [such as $ps(ps)$] present difficulties which will be discussed separately.

II.

The technique to be employed is one which stems both from Feynman's formulation as path integrals,[1] and Schwinger's functional derivative equations[2] for the propagators in field theory, and expresses them as functional integrals over all possible prescribed external boson field distributions.

We shall not here derive the basic expressions for Green's functions, since an independent derivation (for the case neglecting vacuum polarization effects) has already been published.[3] Concerning ourselves first with this approximate case, we may write for the Green's function for one fermion interacting with a boson field and in the presence of an external, prescribed field ϕ,

$$G_+'(x,x';\phi)=\frac{1}{N}\int G_+(x,x';\Omega)\times\exp\Big[-\tfrac{1}{2}i\int(\phi+\Omega)(y)\Delta_+^{-1}(y,y')\times(\Omega+\phi)(y')(dy)(dy')\Big]\delta\Omega, \tag{1}$$

$$N=\int\exp\Big[-\tfrac{1}{2}i\int\Omega\Delta_+^{-1}\Omega(dy)(dy')\Big]\delta\Omega,$$

where Δ_+ is the Green's function for the boson field (which may have finite or zero mass).

G_+ satisfies the equation of a bare particle in an external field Ω:

$$(\gamma p+m+g\Gamma\Omega)G_+=1. \tag{2}$$

Γ represents the various elementary couplings, and Ω may be a vector, pseudoscalar, etc.

It may also be proved that in general, the exact n-fermion, r-boson Green's function is in this approximation[4]:

$$G_{n,r}'(x_1\cdots x_n,x_1'\cdots x_n';\eta_1\cdots\eta_r;\phi)=\frac{i^{[r/2]}}{N}\int G_+(x_1,x_1';\Omega)\cdots G_+(x_n,x_n';\Omega)\Omega(\eta_1)\cdots\Omega(\eta_r)\times\exp\Big[-\tfrac{1}{2}i\int(\phi+\Omega)\Delta_+^{-1}(\phi+\Omega)(dy)(dy')\Big]\delta\Omega, \tag{3}$$

suitably antisymmetrized in the fermion variables. Thus, all effects of interaction and radiative corrections are taken care of in the sum over possible distributions of virtual quanta (as represented by the external field Ω), weighted by exponential, the action integral for the boson field.

Equation (3) for $r=0$ follows directly from the functional differential equations for G_n, for example, as

* An abstract of some of this work was presented at the Pacific Northwest American Physical Society meeting, July, 1954 [Phys. Rev. **96**, 843A (1955)].

† F. B. Jewett Fellow.

[1] R. P. Feynman, Phys. Rev. **80**, 440 (1950); **84**, 108 (1951).

[2] J. Schwinger, Proc. Natl. Acad. Sci. U. S. **37**, 452 (1951).

[3] S. F. Edwards and R. E. Peierls, Proc. Roy. Soc. (London) **A224**, 24 (1954).

[4] Inner products are always understood between the vectors Γ and Ω, and with the tensor Δ^{-1}.

given in reference 2. That is, just as the result (1) arose from the formal integration of the equation

$$[\gamma p+m+g\Gamma(\langle\phi\rangle-\delta/\delta J)]G_+'=1, \tag{4}$$

integration of the analogous one for n fermions,

$$[\gamma_1 p+m+g\Gamma_1(\langle\phi\rangle-\delta/\delta J)]_1 G_n'(x_1\cdots x_n,x_1'\cdots x_n') = G_{n-1}'(x_2\cdots x_n;x_2'\cdots x_n'), \tag{5}$$

yields the desired result. Remembering that to include r mesons,[5] one must apply the operator $\delta/\delta J=\Delta_+\delta/\delta\phi$ r times to $G_{n,0}$, the result follows for that case as well.

Perturbation theory emerges immediately if one inserts the Born approximation series for the G_+'s, and integrates the resultant expressions formally.

The value of the formulation just given for our purpose is apparent. The mass parameters appear only in the G_+'s, that is, bare particle Green's functions. There a limit such as $m\to\infty$ may be taken very easily. To illustrate the general proof, consider the two-body problem,[6]

$$G_{+12}(x_1x_2,x_1'x_2';0) = (1/N)\int G_+(x_1,x_1';\Omega)G_+(x_2x_2';\Omega) \times\exp\left[-\tfrac{1}{2}i\int\Omega\Delta_+^{-1}\Omega(dy)(dy')\right]\delta\Omega. \tag{6}$$

Let us suppose m_2 very large; then $G_+(x_2,x_2';\Omega)=(x_2|\,(\gamma p+m_2+g\Gamma\Omega)^{-1}|\,x_2')$ can be given explicitly for couplings with nonrelativistic limit ($\Gamma=1,\gamma_\mu$). The solution of the limiting equation,

$$(p_0-m_2-g\Omega)G_+=1, \tag{7}$$

is

$$G_+'(2)=-i\delta(\mathbf{r}_2-\mathbf{r}_2')\theta(t_2-t_2') \times\exp\left[-im_2(t_2-t_2')-ig\int_{t_2'}^{t_2}\Omega(\mathbf{r}_2,t)dt\right], \tag{8}$$

$$\theta(x)=\begin{cases}1, & x>0\\ 0, & x<0\end{cases}.$$

Setting this into Eq. (6), absorbing the phase factor $\exp[-im_2(t_2-t_2')]$ into the definition of G_{+12}, and letting the source times get very large,

$$G_{+12}\to\exp[\tfrac{1}{2}ig^2V(0)(t_2-t_2')](1/N)\int G_+(x_1,x_1';\Omega) \times\exp\left\{-\tfrac{1}{2}i\int[\Omega(x)+gV(\mathbf{r})\delta(t)\delta(\mathbf{r}-\mathbf{r}_2)]\Delta_+^{-1} \times[\Omega(x')+gV(\mathbf{r}')\delta(t')\delta(\mathbf{r}'-\mathbf{r}_2)](dx)(dx')\right\}\delta\Omega, \tag{9}$$

$$V(r)=e^{-\mu r}/r \text{ or } 1/r.$$

The $\exp[\frac{1}{2}ig^2V(0)(t_2-t_2')]$ factor outside represents the well-known self-energy of a static source, and is also an irrelevant phase factor; comparing this expression with Eq. (1), we see that particle 1 moves in an effective static external field $\phi=V(\mathbf{r}-\mathbf{r}_2)$, or otherwise stated, it propagates in a region with a static point source (current) located at $\mathbf{r}_2$. This proof is of course the same for $G_{n,r}$ in the limit as any of the n particles become heavy and are therefore representable as fixed δ-function currents. In particular, had we taken in our illustration m_1 going to infinlty as well, we would have obtained the old result for the energy of a system of two fixed sources exchanging bosons. In this trivial limit, the functional integration is immediately performed. The energy consists of a self term $\frac{1}{2}g^2V(0)$ for each particle, and an interaction term $g_1g_2V(\mathbf{r}_1-\mathbf{r}_2)$.

The cases discussed in the foregoing were of a type for which the coupling approached a definite nonrelativistic limit. In the case of γ_5 or $\gamma_5\gamma_\mu$ coupling the situation is more complicated. At first glance, the heavy particle no longer interacts with the field in the limit, since a large component reduction of γ_5 or $\gamma_5\gamma_\mu$ brings a $1/m_2$ factor into the coupling, and the equation for G_+ reduces to the form

$$\left(p_0-m-g\frac{\boldsymbol{\sigma}\cdot\nabla}{m}\phi\right)G_+=1. \tag{10}$$

A new coupling constant $f=g/m_2$ may be defined, of course, and if taken finite in the limit, the usual gradient coupling arises, so that the heavy nucleon acts as a source of the form[7] $\boldsymbol{\sigma}\cdot\nabla\delta(\mathbf{r}_2)$, in the weak coupling approximation, where noncommutativity of the σ's is neglected.

However, the equation[8]

$$(p_0-m-g\gamma_5\phi)G_+=1 \tag{11}$$

[5] S. Deser and P. C. Martin, Phys. Rev. **96**, 1075 (1953).

[6] G_+ can also be written symbolically as an ordered proper-time integral, $G_+=\int ds\,\exp[-s(\gamma p+m+g\Gamma\Omega)]$, and so G_{+12} could be represented as a double integral of this sort; however, this does not make solution any simpler.

[7] The singularity of the potential obtained, is, of course, due to the passage to the state limit. Inclusion of recoil reduces the singularity; see for example, L. Van Hove, Phys. Rev. **75**, 1519 (1949).

[8] An alternate procedure is to perform a Foldy transformation on Eq. (11), and then do the functional integrals.

may be solved directly, and since $\gamma_s^2=-1$, we have

$$\begin{aligned} G_+ &= -i\delta(r-r_2)\theta(t_2-t_2') \\ &\quad\times\exp\left[-im(t_2-t_2')-i\gamma_s g\int\Omega(r_2,t)dt\right] \\ &= -i\delta(r-r_2)\theta(t_2-t_2')\exp[-im(t_2-t_2')] \\ &\quad\times\left[\cos g\int\Omega-\gamma_s\sin g\int\Omega\right], \end{aligned} \tag{12}$$

and the first part remains in the limit to act as effective source of a field resembling the scalar one.[9] The $\cos g\int\Omega$ term may be rewritten as $\frac{1}{2}[\exp(g\int\Omega)+\exp(-g\int\Omega)]$. The first part alone is the scalar result, while the second half, which will in general also contribute, represents a source at the same point, but with opposite charge. Thus, the propagator for the remaining particles is a superposition of two such terms. If we consider the special case of the G_+' of particle 2 by itself, then, since the boson action is even, the two terms have the same integral, and all the results are as in the scalar case. This is not surprising, since the field effects can only enter in even powers in the nucleon propagator, and since only the self-field exists, ϕ_s^2 and $(i\gamma_5\phi_{ps})^2$ are of course identical. In the many-particle Green function, however, there are other meson field sources around; while the above remarks still hold for those effects which are even as well in the other Ω's, it is no longer the case when odd terms from other particles enter. Then the parity counts and the superposition results.

III.

We turn now to the complete problem, including closed loops. In this case, the action function of the boson field is not so simple; the Δ_+' is itself a functional of Ω, and in fact satisfies equations:

$$(k^2+\mu^2)\Delta_+'=1+ig\frac{\delta}{\delta J}\mathrm{tr}(\sum\Gamma_i G_{+i}'), \tag{13}$$

the sum extending over the various fermion fields. It is to be expected that our results still remain, since the heavy particles become more and more difficult energetically to create and therefore their closed loops will not appear. In fact, since, as we have seen, the limiting behavior for $G_+[\phi]$ is one in which negative-energy states vanish, there can be no heavy pair creation.

Thus, in the limit as $m\to\infty$, the vacuum polarization effects due to the heavy particles disappear and they merely act once again as static point sources of the field. However, the field thus generated is no longer the simple Y, but one modified by the vacuum polarization of the finite-mass particles, that is, $\phi(x)=\int_{-\infty}^{\infty}\Delta_+'(x-x_2)dt_2$, where Δ_+' satisfies Eq. (13), but omitting the effect of the heavy field. Of course, the complete problem with closed loops can only be stated implicitly in closed form; that is, while an expression for G_+ can be written down, it is purely formal, being actually a transcendental functional integral equation rather than the much simpler Eq. (1).

Thus, we may still write

$$G_+'[0]=\int\delta\Omega G_+(\Omega)\exp\left[-\tfrac{1}{2}i\int\Omega T\Omega(dy)(dy')\right] \tag{14}$$

T itself depends on G_+ and is defined through

$$\begin{aligned} &\exp\left[-\tfrac{1}{2}i\int\Omega T\Omega(dy)(dy')\right] \\ &\quad=\int\delta J\exp\left[i\int J\Omega(dy)+i\int^{\phi}\Delta_+^{-1}[\phi']\phi'\delta\phi'\right] \end{aligned} \tag{15}$$

and $\phi=\int^J\Delta_+[J']\delta J'$, which reduces to the usual result when Δ_+ is independent of ϕ.

In this form, the parameter m enters in a fashion which precludes any proof as to the limiting behavior of G_+'. However, as was stated above, it is evident that there can be no vacuum polarization of the heavy field, since it loses its negative-energy components.[10] Alternatively, had we written the vacuum polarization contribution in the form $G_+'[0]=\int\delta\Omega G_+(\Omega)\exp[-\frac{1}{2}i\times\int\Omega\Delta_+^{-1}\Omega(dy)(dy')-iL'(\Omega)]$ where $\exp[-iL'(\Omega)]$ is the contribution from closed loops, and used the formal Fredholm series result, say, for $\exp[-iL']$, we would have observed that each term vanishes due to the $\theta(t)$ factor in the $G_+[0]$ to be inserted in the series. $\theta(t)$, of course, just states that negative energy states have been dropped.

I wish to thank Dr. Robert Oppenheimer and the Institute for Advanced Study for their hospitality, and Dr. R. L. Arnowitt for interesting conversations.

[9] Similar results have been obtained previously by J. V. Lepore, Phys. Rev. **87**, 209 (1952).

[10] Had the γ_0 been kept in Eq. (11), negative energy states would have entered, but the equation could not then be solved. However, with "relativistic" couplings, the question whether one or another reduction is the more accurate only has meaning with reference to the full recoil solution.

Letters to the Editor

PUBLICATION of brief reports of important discoveries in physics may be secured by addressing them to this department. The closing date for this department is five weeks prior to the date of issue. No proof will be sent to the authors. The Board of Editors does not hold itself responsible for the opinions expressed by the correspondents. Communications should not exceed 600 words in length and should be submitted in duplicate.

Possible Mathematical Formulation of the Gell-Mann Model for New Particles

BERNARD D'ESPAGNAT AND JACQUES PRENTKI
CERN, Geneva, Switzerland
(Received May 13, 1955)

GELL-MANN and Pais[1] have recently proposed several schemes for describing the existence and interactions of hyperons and heavy mesons. One of these is essentially a refined version of a hypothesis originally proposed by Gell-Mann[2] and by Nakano and Nishijima.[3] As has been pointed out by the authors,[1] this particular model does not appear at first sight to be the most attractive for theorists, mainly because it involves an apparent arbitrariness in the choice of the relation Q *versus* I_3 for the various particles. On the other hand, it is perhaps the model best fitted for the interpretation of present experimental evidence.

In view of these facts, we wish to point out in this note that an equivalent but more axiomatic formulation of the Gell-Mann rules is possible. The theory will be developed in a three-dimensional isotopic spin space. As is well known,[4] in such a space it is possible to define two kinds of spinors which differ by their symmetry properties with respect to an oriented plane. If ξ, ξ' denote spinors of the first kind and η, η' spinors of the second kind, the true scalars that can be formed with these quantities are $\xi'^{*T}\xi$, $\eta'^{*T}\eta$, $\eta'^{T}\tau_2\xi$, $\xi'^{T}\tau_2\eta$, where the superscripts * and ^{T} mean "imaginary conjugate" and "transposed", respectively. Families of particles are now defined by their transformation properties in Lorentz and isotopic spin space. In Table I different fields are so defined, the list being obviously not limitative. We postulate only that family A contains the nucleons and family δ the π mesons.

TABLE I. Several types of fields.

	Lorentz space	Isotopic space	
ψ_A	spinor	spinor of first kind	$\mathfrak{N}$
ψ_B	spinor	spinor of second kind	Ξ
ψ_a	spinor	no spin (scalar)	Λ
ψ_b	spinor	spin 1 (pseudo-vector)	Σ
φ_Δ	no spin	spinor of first kind	θ
φ_δ	no spin	spin 1 (pseudo-vector)	π

The other correspondences given in column 4 are not postulated; they will follow [with respect to interactions, charges Q, and relation $Q(I_3)$] from the mathematical formulation.

Along with Lorentz invariance, the invariance with respect to rotations *and reflections* in isotopic space will be postulated for strong interactions. The most general Lagrangian that follows from these assumptions is easily constructed. For the interaction part, terms like

$$\bar{\psi}_a\varphi_\Delta{}^{*T}\psi_A, \quad \bar{\psi}_b\varphi_\Delta{}^{*T}\tau\psi_A, \quad \bar{\psi}_a\psi_B{}^T\tau_2\varphi_\Delta, \cdots$$

appear, together with others of the same general form which for the sake of brevity will not be written.

Let us define the operator

$$U=\int d\tau[\bar{\psi}_A{}^T\beta\psi_A-\bar{\psi}_B{}^T\beta\psi_B - i(\pi_\Delta{}^T\varphi_\Delta-\pi_\Delta{}^{*T}\varphi_\Delta{}^*)]. \quad (1)$$

It can be verified that U commutes with the total Hamiltonian containing the fields of Table I.[5] U is therefore a constant of the motion. On the other hand the conservation of fermions is respected and, of course, I^2 and I_3 are constants. The latter can be written

$$\begin{aligned}2I_3=&n(A)-n(\bar{A})-n(A')+n(\bar{A}')+n(B)\\&-n(\bar{B})-n(B')+n(\bar{B}')+2[n(b)-n(\bar{b})-n(b')\\&+n(\bar{b}')]+n(\Delta)-n(\bar{\Delta})-n(\Delta')+n(\bar{\Delta}')\\&+2[n(\delta)-n(\delta')], \quad (2)\end{aligned}$$

where A and A' refer to different charge states of the nucleon, etc., and the bars refer to the antiparticles; while

$$\begin{aligned}U=&n(A)-n(\bar{A})+n(A')-n(\bar{A}')-n(B)+n(\bar{B})\\&-n(B')+n(\bar{B}')+n(\Delta)-n(\bar{\Delta})+n(\Delta')-n(\bar{\Delta}').\end{aligned}$$

One sees that the constant $I_3+\frac{1}{2}U$ is, for known particles (nucleons and π mesons), equal to the charge Q and can thus be considered as a general definition of this quantity.[6] The eigenvalues of U give therefore the desired relation between charge and I_3. In particular, $Q=I_3+\frac{1}{2}$ for one quantum of the ψ_A or φ_Δ fields, while $Q=I_3$ for ψ_a, ψ_b, and φ_δ; and finally $Q=I_3-\frac{1}{2}$ for ψ_B field quanta. The correspondence given in Table I, column 4 between the field families ψ_A, ψ_B, etc., and the observed particles $\mathfrak{N}$, Ξ, etc., is therefore justified as far as charge is concerned. On the other hand, it can be verified that the postulate of complete invariance leads to an interaction Lagrangian which allows only the virtual processes given by the Gell-Mann rules. The equivalence is therefore complete.

A fact which is perhaps of some significance is that, in such a straightforward generalization of the ordinary formalism, the Ξ field appears as a spinor of the second kind in isotopic space when the nucleon field is taken as a spinor of the first kind. As a practical rule, one

may point out that instead of the conservation of Q and I_3 one may of course use the conservation of Q and U. Possible reactions (including electromagnetic) will therefore be obtained by requiring (a) the usual conservation of fermions, (b) the conservation of charge, (c) the use of the following rule: denote by "isofermions" the nucleons, the θ, and the anti-Ξ, and by "anti-isofermions" the antinucleons, the anti-θ (charge conjugated), and the Ξ; then *the number of isofermions minus the number of anti-isofermions must be conserved.*

[1] M. Gell-Mann and A. Pais. Proceedings of the Glasgow Conference on Nuclear and Meson Physics, 1954 (to be published), p. 342. See also A. Pais, Phys. Rev. **86**, 663 (1952); Physica **19**, 869 (1953); Progr. Theoret. Phys. (Japan) **10**, 457 (1953); Proc. Natl. Acad. Sci. U. S. **40**, 484, 835 (1954).

[2] M. Gell-Mann, Phys. Rev. **92**, 833 (1953).

[3] T. Nakano and K. Nishijima, Prog. Theoret. Phys. (Japan) **10**, 581 (1953).

[4] E. Cartan, *Leçons sur la théorie des spineurs* (Hermann & Cie, Paris, 1938), Vol. I, especially Chap. III.

[5] Other choices of fields also leading to a constant U are possible; they give the same physical results. (1) is obtained from the invariance of the total Lagrangian with respect to the transformation $\psi_A \to \psi_A e^{i\alpha}$, $\psi_B \to \psi_B e^{-i\alpha}$, $\varphi_\Delta \to \varphi_\Delta e^{i\alpha}$.

[6] Some considerations on the total Lagrangian show that this assumption is indeed the most natural one.

Bevatron *K*-Mesons*

ROBERT W. BIRGE, ROY P. HADDOCK, LEROY T. KERTH, JAMES R. PETERSON, JACK SANDWEISS,† DONALD H. STORK, AND MARIAN N. WHITEHEAD

Radiation Laboratory, University of California, Berkeley, California

(Received May 9, 1955)

TO facilitate the search for K-mesons from the Bevatron, two of us (L.T.K. and D.H.S.) have suggested the use of a strong-focusing spectrometer (Fig. 1),[1] consisting of a magnetic quadrupole focusing lens[2] followed by an analyzing magnet. Particles of any desired momentum can be brought to a focus, forming an image of the target at a point behind the analyzing magnet. Emulsion stacks are placed at this point. With this arrangement we have found examples of four types of heavy mesons first established in cosmic-ray work.[3] Particles of different mass can be separated according to their ranges in emulsion. For particles of momentum 360 Mev/c, the range of K's is 4.6 times the range of the protons, and pions pass through the emulsion stack at minimum ionization.

A stack of 107 Ilford G.5600-μ pellicles,[4] 3.5 in. by 3.5 in., has been exposed so that 114-Mev K-particles stopped in the center of the stack. The proper time of flight for such particles from the target to the emulsion is about 10^{-8} sec.

This stack has been scanned in a swath across the direction of the meson flux for tracks lying in the plane of the emulsion whose ionization is visibly greater than minimum. Particles stopping in the stack (beyond the position of the swath) have masses less than 1200 m_e. Particles that go all the way through the stack have masses less than 800 m_e.

The tracks are followed until they stop and the endings are examined for decays. To date 300 decays have been observed. Twenty of these are π^+ mesons whose unique decay into three charged pions is readily identifiable. Among the others, all of which decay into one lightly ionizing secondary, only those with a secondary that is flat or with an ionization obviously higher than minimum have been categorized. Three examples have been found of what is assumed to be the alternate decay of the π into one charged and two neutral pions, with the pion stopping in the emulsion stack. Two events decay into low-energy muons (less than 55 Mev) and are presumably examples of the κ or $K_{\mu 3}$.

To establish the existence of the $K_{\pi 2}(\theta^+,\chi^+)$ or of the $K_{\mu 2}$ mesons, either very large emulsions are needed to stop the long-range secondary or else very accurate measurements of the multiple scattering and the ionization must be made. Measurements on four fortuitously flat secondaries at a distance of 5 cm from the decay point revealed that three of the primaries were $K_{\pi 2}$'s and one presumably a $K_{\mu 2}$, as determined by the tentative identification of the secondary as a high-energy muon. Excellent calibration on grain count is available from the π mesons of known energy traversing the same region of the emulsions. From the number of K-mesons found here compared to the number found at about 25 cm from the target,[5] it is unlikely that the mean life of any of the K's seen is less than 3×10^{-9} sec.

In the initial exposure, the momentum resolution as determined from the proton ranges allows a mass determination to $\pm 40\, m_e$ on each K-meson. With a few exceptions, all particles with lightly ionizing secondaries fall within a distribution of this width centered about 20 m_e below the average for τ mesons plotted separately (Fig. 2). In a subsequent exposure the momentum resolution has been improved. The scattered points on the high-mass side of the main distribution may be due to particles that suffered inelastic collisions, or scattered off the channel. A

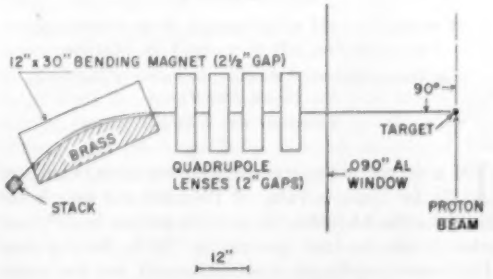

FIG. 1. Strong-focusing spectrometer.

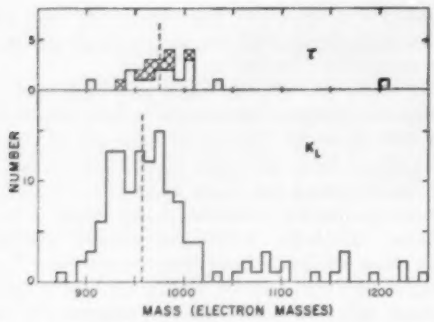

FIG. 2. Mass distributions: Upper histogram represents τ mesons. Crossed squares refer to τ's found nonsystematically. Lower histogram is made up of particles decaying into a single lightly ionizing secondary.

comparison of the measured τ meson mass of (974 ± 6) m_e with the accepted value[3] of $966\,m_e$ indicates a possible systematic error.

This work was done with the encouragement and guidance of Professor Chaim Richman. Most of the scanning was performed by Mrs. Beverly Baldridge, Miss Irene d'Arche, Mrs. Marilynn Harbert, Mrs. Edith Goodwin, and Miss Kathryn Palmer.

It is with pleasure that we acknowledge the help and advice in nuclear emulsion techniques given us by Professor Powell's group at Bristol. The assistance of the Bevatron crew, under the direction of Dr. Edward J. Lofgren, and their skillful operation of the machine are greatly appreciated.

* This work was performed under the auspices of the U. S. Atomic Energy Commission.
† National Science Foundation Predoctoral Fellow.
[1] Kerth, Stork, Birge, Haddock, and Whitehead, Bull. Am. Phys. Soc., Vol. 30, No. 3, 41 (1955).
[2] Courant, Livingston, and Snyder, Phys. Rev. **88**, 1190 (1952).
[3] Padua Conference, Nuovo cimento **11**, Suppl. No. 2 (1954).
[4] Birge, Kerth, Richman, Stork, and Whetstone, University of California Radiation Laboratory Report No. UCRL-2690, September, 1954 (unpublished).
[5] Proceedings of the 5th Rochester Conference (to be published).

14-Mev (n,α) Cross Sections in Zirconium. I*

J. E. BROLLEY, JR., M. E. BUNKER, D. R. F. COCHRAN, R. L. HENKEL, J. P. MIZE, AND J. W. STARNER

Los Alamos Scientific Laboratory, University of California, Los Alamos, New Mexico

(Received May 2, 1955)

IN a survey of neutron-induced reactions, Paul and Clarke[1] quote a value of 194 ± 107 mb as a lower limit for the 14.5-Mev (n,α) cross section in Zr^{90}, and 63 ± 25 mb for this process in Rh^{103}. Brolley and Dickinson[2] conducted a direct search for the alpha particles from these elements using neutrons of about 14.3 Mev in an attempt to observe any variation in barrier height with angle. In this work the valuable help of the nuclear plate and Cockcroft-Walton groups is gratefully recognized. Their study indicated considerably smaller cross sections than reported by Paul and Clarke. The problem has been re-examined using several different methods by A. Armstrong and J. E. Brolley, Jr., F. L. Ribe and R. W. Davis, and the present authors. In the following Letters the results and the compatibility of the several experiments are discussed by A. Armstrong and J. E. Brolley, Jr., and F. L. Ribe and R. W. Davis.

We have bombarded various samples of normal zirconium metal with neutrons of average energy 14.1 and 14.9 Mev produced by the Cockcroft-Walton machine. Strontium was chemically separated from the zirconium and counted with a Na(Tl)I crystal whose sensitivity was known for the γ radiations from Sr^{87m} and Sr^{91}. Table I presents the results.

The standard deviations indicated are essentially those of counting. The Zr^{90} cross sections apply to the production of the isomer only. The diminution of these

TABLE I. (n,α) cross section in mb. Neutron energy, E_n, in Mev.

E_n	14.1	14.9
Zr^{90}	3.1 ± 0.2	3.0 ± 0.2
Zr^{94}	4.9 ± 0.6	3.9 ± 0.5

cross sections with increasing neutron energy may possibly be associated with competition from the $(n,2n)$ process. These cross-section values fall markedly below the trend of $\sigma_{obs}/\sigma_{calc}$ cited by Paul and Clarke. Though all nuclei in these processes have magic numbers or near magic numbers of neutrons (50), the (n,α) cross sections of neighboring nuclei are not sufficiently well established to discern a correlation with neutron number. We are indebted to R. W. Davis for invaluable help in the irradiations.

* Research performed under the auspices of the U. S. Atomic Energy Commission.
[1] E. B. Paul and R. L. Clarke, Can. J. Phys. **31**, 267 (1953).
[2] J. E. Brolley and W. C. Dickinson (unpublished).

14-Mev (n,α) and (n,p) Cross Sections in Zirconium. II*

A. H. ARMSTRONG AND J. E. BROLLEY, JR.

Los Alamos Scientific Laboratory, University of California, Los Alamos, New Mexico

(Received May 2, 1955)

FURTHER confirmation of a low value for the (n,α) cross section for zirconium bombarded by 14.1-Mev neutrons has been obtained in still another experiment, in which nuclear plates were used as detectors of the reaction products.

A collimated beam of 14.1-Mev neutrons from the $H^3(d,n)He^4$ reaction was incident upon a 4-mil normal zirconium target at the center of a nuclear-plate camera.[1]

Ilford *E*-1 plates were placed around the periphery of the camera floor, with their long axes coinciding with radii extending from the center of the base of the camera. Two runs were made, one with the target in position and the other a background run without the target.

Equivalent areas on run and corresponding background plates were analyzed at eight camera positions such that the angles made by the reaction particles with the direction of the incident neutron beam extended from 17.5° to 128°. Measurements were made of all tracks longer than 10 microns entering the surface of the emulsion in directions consistent with target-detector geometry. The tracks were further identified, from grain density, as proton or α-particle tracks. Thus data for the (n,p) cross section were obtained at the same time as those for the (n,α) cross section.

The value obtained for the (n,α) cross section integrated from 17.5° to 128° is 10 ± 10 mb for reaction α particles of energy greater than 3 Mev. Since in these calculations it is assumed that all the stable isotopes of normal zirconium contribute to the observed reaction particles, the value given is one-half the upper limit for Zr^{90}.

A preliminary value for the (n,p) cross section obtained from this experiment is 180 ± 70 mb, which is in fair agreement with that given by Paul and Clarke.[2] The energies of essentially all the observed reaction protons are below 6 Mev.

* Work performed under the auspices of the U. S. Atomic Energy Commission.

[1] Allred, Armstrong, and Rosen, Phys. Rev. **91**, 90 (1953).

[2] E. B. Paul and R. L. Clarke, Can. J. Phys. **31**, 267 (1953).

14-Mev (n,α) Cross Section in Zirconium. III*

F. L. Ribe and R. W. Davis

Los Alamos Scientific Laboratory, University of California, Los Alamos, New Mexico

(Received May 2, 1955)

A DIRECT measurement of the yield of alpha particles produced by bombarding normal zirconium with 14.1-Mev neutrons has confirmed the smallness of the Zr^{90} and Zr^{94} (n,α)-reaction cross sections observed by the activation measurements of Brolley *et al.* reported in the first of the preceding letters.

A one-mil foil of zirconium metal was bombarded with monoenergetic neutrons from the $H^3(d,n)He^4$ reaction, and the alpha particles were detected by means of a counter telescope, consisting of two proportional counters and a NaI(Tl) scintillator, described in detail elsewhere.[1] The counters were biased to a lower limit of ionization energy loss so that alpha particles of energies $\leq$18 Mev were detected, while protons and deuterons of energies $\geq$0.8 and 1.6 Mev were excluded.

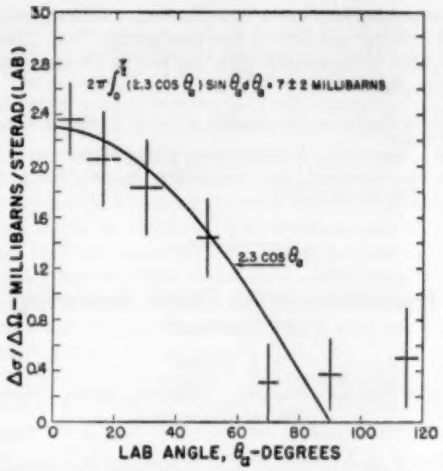

FIG. 1. Differential cross section for the yield of alpha particles of energies greater than six Mev from normal zirconium bombarded by 14.1-Mev neutrons.

At each telescope angle the scintillator pulse-height spectrum was observed between alpha-particle energies of 6 and 18 Mev. Background was measured by exposing a platinum blank to the telescope. The energy spectrum at zero and 15 degrees was peaked at its upper limit of 17 Mev and decreased to zero at about 10 Mev. Between 10 and six Mev, no alpha particles were observed. At larger angles, up to 115 degrees, yields were too low for significant spectrum determinations.

The measured differential cross section of Fig. 1 has been fitted somewhat arbitrarily to a cosine function whose integral over the forward hemisphere is 7 ± 2 millibarns. This is of course a weighted average of the (n,α) cross sections of the five stable isotopes of zirconium for alpha particles of energies greater than six Mev. However, the upper-limit value of the cross section for alpha particles of energies as low as three Mev found by Armstrong and Brolley[2] indicates that there is no significant contribution to the yield in the energy region from three to six Mev. The degree of agreement of both of these values with those of Brolley *et al.* for the Zr^{90} and Zr^{94} cross sections precludes a large yield of alpha particles below both the 3- and 6-Mev energy limits such as would be necessary to account for the large $Zr^{90}(n,\alpha)$ cross section of 194 millibarns found by Paul and Clarke. The fact that our value is somewhat larger than that of Brolley *et al.* is probably due to the fact that transitions to the ground state of Sr^{87}, as well as to the isomeric state, contributed to our yield. In addition, there are contributions from the other three isotopes of normal zirconium.

A separate search gave no indication, within statistics, of a yield of protons of energies greater than about five Mev, in agreement with the results of Armstrong and Brolley.

* Work done under the auspices of the U. S. Atomic Energy Commission.

[1] F. L. Ribe and J. D. Seagrave, Phys. Rev. **94**, 934 (1954).

[2] A. H. Armstrong and J. E. Brolley, Jr., preceding Letter [Phys. Rev. **99**, 330 (1955)].

Resonances in the Elastic Scattering of Protons*

B. B. KINSEY†

Radiation Laboratory, University of California, Berkeley, California

(Received May 6, 1955)

THE purpose of this note is to report the existence of nuclear resonances of an unusual type in carbon and oxygen. These resonances were found during a search for anomalies in the elastic scattering of protons using the 32-Mev linear accelerator of this laboratory. The apparatus was that used by Eisberg and Igo.[1] The protons scattered elastically from a thin target (about 20 mg/cm^2) were detected by a plastic scintillator and counted after pulse-height analysis. The experimental procedure consisted in fixing the angle of scattering near the first minimum of the diffraction pattern and plotting the counting rate against the energy of the incident proton beam, which was altered by absorption in polystyrene. Smooth variations of the counting rate with the proton energy were found with most targets. These variations correspond to the slow displacement of the maxima and minima of the diffraction pattern. In carbon and in oxygen, however, the smooth curve is interrupted by a sharp peak which rises about 20 percent above the mean counting rate in its immediate vicinity. In carbon, the energy of the peak is 22.5±0.3 Mev; the width at half-maximum is about 1.5 Mev. The results obtained with a polystyrene foil of about 15 mg/cm^2 are shown in Fig. 1. The effect on the diffraction pattern is shown in Fig. 2; the minimum is filled in near the peak of the resonance and regains its normal shape within 1 Mev on either side of it. The oxygen resonance was first found in a comparison of the elastic scattering of silicon and silica. The data shown in Fig. 3 were obtained with a gaseous target. The peak is at 18.6±0.3 Mev, and the width is about 1.3 Mev. The oxygen resonance is well marked for angles near the minimum of the diffraction pattern but is too small to be detected when the counting rate, at other angles, rises much above this minimum value. In carbon and oxygen no other resonance was found in a proton energy range of 14 to 31.5 Mev. A search for similar resonance in B, N, F, Al, Si, S, Ca, Fe, and Cu, over the same energy range, gave no result. This does

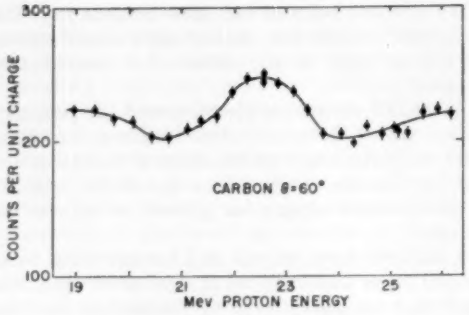

FIG. 1. Resonance in the elastic scattering of protons from carbon at 60°.

not exclude the existence of resonances in these nuclei, for the method is effective only for resonances which are neither too narrow (less than 200 kev) nor too broad (more than 3 Mev). The measured widths are close to the natural widths for they are large compared with both the proton energy loss in the targets—400 kev and 100 kev, for carbon and oxygen, respectively—and the spread in energy of the proton beam—about 100 kev.[2]

It is unlikely that the resonances found in carbon and oxygen are size resonances, because they are much sharper than would be expected theoretically and because no resonance was found in nitrogen, which lies intermediate in atomic weight. Now in carbon there is no anomaly in the cross section[3] of the $C^{12}(p,pn)C^{11}$ reaction near 23 Mev. The observed effect, therefore, demonstrates, in a narrow energy range, an increase in the probability of elastic re-emission of the proton. This is a characteristic to be expected of a single-particle state. It is unlikely, however, that the

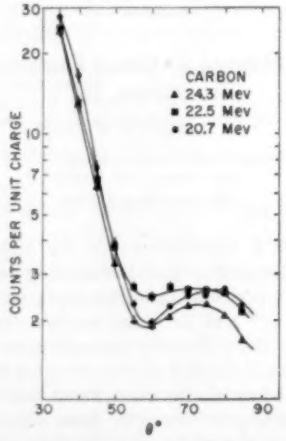

FIG. 2. Angular distribution of protons scattered elastically from carbon, at the peak of the resonance (squares), and above (triangles) and below it (circles).

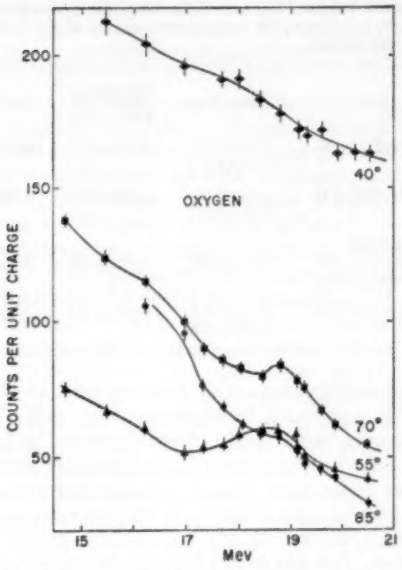

FIG. 3. Resonance in the elastic scattering of protons from oxygen at various angles.

resonance is caused by a state with an independent existence at this high excitation energy; it is more probable that its characteristics are distributed over many levels of the usual kind.

The author is much indebted to Mr. Robert Watt and Lt. Troy Stone for assistance in these measurements; to Dr. R. Finke for advice and discussion; to Mr. William Gantz for assistance with electronics; and to Professor E. O. Lawrence and the U. S. Atomic Energy Commission for the privilege of working at the Radiation Laboratory.

* This work was done under the auspices of the U. S. Atomic Energy Commission.

† Now at Atomic Energy Research Establishment, Harwell, England.

[1] R. M. Eisberg and G. Igo, Phys. Rev. **93**, 1039 (1954).

[2] Alvarez, Bradner, Franck, Gordon, Gow, Marshall, Oppenheimer, Panofsky, Richman, and Woodyard, Rev. Sci. Instr. **26**, 111 (1955).

[3] Aamodt, Peterson, and Phillips, Phys. Rev. **88**, 739 (1952).

Systematics of Neutron Capture Cross Sections*

B. G. HARVEY

Radiation Laboratory, University of California, Berkeley, California

(Received April 25, 1955)

THERE appears to exist a rough correlation between the neutron cross sections of heavy (*trans*-lead) nuclei and the binding energy of the captured neutron. In Fig. 1 the sum of capture and fission cross section (where fission occurs) for each nuclide is plotted against the neutron binding energy.[1]

The correlation is best for the even-even nuclides. Odd-even nuclei, forming odd-odd compound nuclei, have larger cross sections for a given binding energy than even-evens which form even-odd compound nuclei. Conversely, even-odd nuclei, which form even-even compound nuclei, appear to have smaller cross sections than might be expected. The cross sections of Pb^{208} and Bi^{209} are unusually low, which is presumably a consequence of their closed-shell configurations. The singular position of both Bk^{249} and Cf^{250} might be connected in some unexplained way with the minor closed shell at 152 neutrons.[2]

To a rough approximation, the thermal capture cross section is given by $\sigma_{th}=(\xi^2\Gamma_{rad}/D)\times 1100$ barns[3,4] where $\xi^2\approx 1$, and D is the level distance in ev in the compound nucleus. For heavy nuclei, Γ_{rad} is always close to 0.1 ev. Very roughly, therefore, $\sigma_{th}=110/D$.

For nuclei of comparable type, D, and therefore σ_{th}, will be determined mainly by the excitation of the compound nucleus, and hence by the neutron binding energy. The separation of different nuclear types in Fig. 1 suggests that the level density of the compound nucleus decreases in the order odd-odd nuclei > even-odd > even-even, which is not unexpected.

However, the rate of increase of σ with binding energy E is much greater than expected from a semiempirical

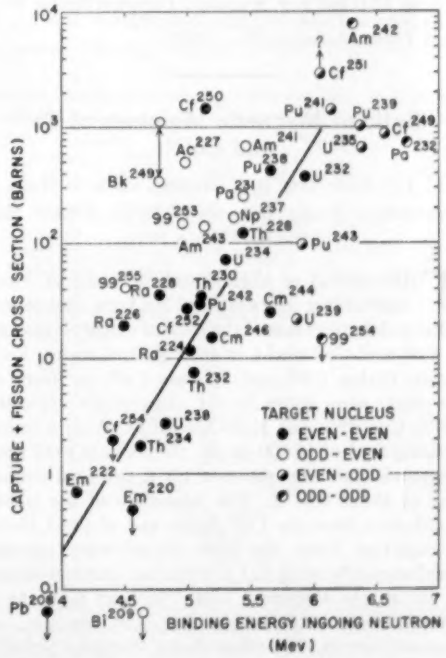

FIG. 1. Neutron cross sections of the *trans*-lead nuclides.

level spacing formula of the type $1/D=C\exp(2E\sqrt{a})$, using reasonable values of the coefficients c and a. The cross sections plotted in Fig. 1 are, however, not thermal neutron values, but in most cases were measured with a reactor neutron energy distribution. Corrections for epithermal resonance capture will be generally much greater for nuclei with big cross sections whose resonances are closer to thermal energies.[4] This should increase the slope of the line, but the effect is probably not very large.

There seems to be a tendency for cross sections to reach a limiting value of a few thousand barns, regardless of how large the binding energy may be. This phenomenon might be due to the level separation D becoming equal to, or even less than Γ_{rad}. The problem may then be treated by continuum theory, giving $\sigma=4\pi kK\lambda^2/(k+K)^2$, K being of the order of 10^{12} cm^{-1}, λ and k the wavelength and wave number of the neutron, and R the nuclear radius. For reactor neutrons, $\lambda=10^{-8}$ to 10^{-9} cm, which gives $\sigma\approx10^2$ to 10^4 barns, in reasonable agreement with the experimental results.

It is a pleasure to acknowledge the interest of Glenn T. Seaborg, Stanley G. Thompson, and Albert Ghiorso in this work.

* This work was performed under the auspices of the U. S. Atomic Energy Commission.
[1] Glass, Thompson, and Seaborg, J. Inorg. and Nuc. Chem. **1**, 3 (1955).
[2] Ghiorso, Thompson, Higgins, Harvey, and Seaborg, Phys. Rev. **95**, 293 (1954).
[3] J. M. Blatt and V. F. Weisskopf, *Theoretical Nuclear Physics* (John Wiley and Sons, Inc., New York, 1952).
[4] D. Bogart, Nucleonics **10**, 36 (1952).

Ratio of Magnetic Moments of Co^{58} and Co^{60}†

J. C. Wheatley,* D. F. Griffing, and R. D. Hill
Department of Physics, University of Illinois, Urbana, Illinois
(Received May 6, 1955)

THE method of aligning cobalt nuclei in Tutton salts at low temperatures[1] has been used to make a direct determination of the ratio of magnetic moments of Co^{58} and Co^{60} nuclei in their ground states. Radioactive 72-day Co^{58} and 5.2-year Co^{60}, in microcurie amounts, were grown in the same single crystals of (20% Cu, 80% Zn) $K_2(SO_4)_2\cdot6H_2O$. With a demagnetizing field of 10 000 gauss, the crystals were cooled from an initial temperature of 1.3°K to a final temperature of about 0.03°K. The intensities of the 805-kev γ radiation from the Co^{58} decay and of the 1.33-Mev γ radiation from the Co^{60} decay were measured simultaneously using NaI scintillation counters situated at 90° to the alignment axis. The heat input to the crystals was estimated to be ~10 erg/min, and observations could be taken during warm-up periods of about two hours. Least-squares parabolic curves of the percentage increase of counting rates at 90° *vs* $(1/T^*)^2$ were fitted to all experimental data. These final curves for Co^{58} and Co^{60} are shown in Fig. 1.

TABLE I. Values of the ratio of the magnetic moments of Co^{58} and Co^{60}, $\mu_{Co^{58}}/\mu_{Co^{60}}$, for various assumptions of the Co^{58} and Co^{60} decay schemes.

Co^{60} \ Co^{58}	$2(\beta1)2(\gamma2)0$	50% mixture $2(\beta1)2(\gamma2)0$ $2(\beta0)2(\gamma2)0$	$2(\beta0)2(\gamma2)0$
$5(\beta1)4(\gamma2)2(\gamma2)0$	1.10±0.03 (1.00±0.17)	0.89±0.03	0.76±0.02
$4(\beta1)4(\gamma2)2(\gamma2)0$	1.06±0.03 (1.00±0.17)	0.85±0.03	0.73±0.02
50% mixture $4(\beta1)4(\gamma2)2(\gamma2)0$ $4(\beta0)4(\gamma2)2(\gamma2)0$	1.11±0.03	0.89±0.03	0.76±0.02
$4(\beta0)4(\gamma2)2(\gamma2)0$	1.16±0.03 (1.09±0.19)	0.93±0.03	0.80±0.02

In our experiment, since the Co^{58} and Co^{60} nuclei are aligned in the same crystals, and therefore experience the same internal magnetic fields, the ratio $(\mu/I)_{58}/(\mu/I)_{60}$ evaluated at any temperature should be a constant. This was in fact found to be the case within the limits of the experimental errors. This method of determination depends neither on the evaluation of the ratio of magnetic temperature, T^*, to the thermodynamic temperature, nor upon the absolute evaluation of the internal magnetic field acting on the cobalt nuclei. The ratio of the magnetic moments, however, can be obtained only by assuming certain definite decay schemes of Co^{58} and Co^{60}.

We assume the ground state of Co^{60} to have a spin of either 4 or 5,[2] and to decay to the 2.50-Mev excited state of Ni^{60} according to any of the following schemes[3]: (a) $5(\beta1)4(\gamma2)2(\gamma2)0$; (b) $4(\beta0)4(\gamma2)2(\gamma2)0$; (c) a 50% mixture of $4(\beta0)4(\gamma2)2(\gamma2)0$ and $4(\beta1)4(\gamma2)2(\gamma2)0$; and (d) $4(\beta1)4(\gamma2)2(\gamma2)0$. We assume the ground state of Co^{58} to hvae a spin of 2,[4] and

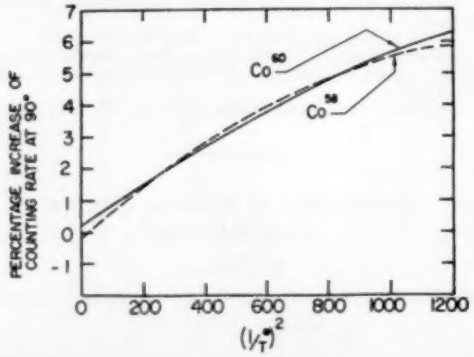

FIG. 1. Least-squares parabolic variation of the experimental increase of counting rates at 90° of 805-kev γ ray of Co^{58} and 1.33-Mev γ ray of Co^{60} *vs* $(1/T^*)^2$ (T^* is the magnetic temperature). The standard deviation of the experimental points is approximately ±0.3 percent for both curves.

to decay to the 805-kev excited state of Fe^{58} according to one of the following schemes: (1) $2(\beta 1)2(\gamma 2)0$; (2) a 50% mixture of $2(\beta 1)2(\gamma 2)0$ and $2(\beta 0)2(\gamma 2)0$; and (3) $2(\beta 0)2(\gamma 2)0$.

The angular distributions of the γ radiation following the beta decays of both Co^{58} and Co^{60} have been calculated for the above modes of decay as functions of temperature.[5] We have used the computations of Cox *et al.*[5] in order to determine the ratio of μ_{58}/μ_{60} from our data, and the results are given in Table I.

Measurement of the absolute values of the magnetic moments of Co^{58} and Co^{60} have already been made by the Oxford and Leiden groups. Daniels *et al.*[6] have measured $\mu_{58}=3.5\pm0.3$ nm and have observed the Co^{58} decay to be consistent with pure *G-T* selection rules. Bleaney *et al.*[1] have determined the magnetic moment of Co^{60} for various assumptions of the Co^{60} decay scheme. Bu using their values for μ_{60} and that of Daniels *et al.* for μ_{58}, the values shown in parentheses in Table I are obtained for the ratio μ_{58}/μ_{60}. Our values are in good agreement with the ratios deduced in this manner from the absolute values. The value of $\mu_{60}=4.3\pm0.2$ nm observed by Poppema *et al.*,[7] when used with the value of μ_{58} observed by Daniels *et al.*,[6] gives $\mu_{58}/\mu_{60}=0.82\pm0.08$. This ratio, when compared with the values of Table I, is not consistent with any of the modes of the Co^{60} beta decay considered and at the same time a Gamow-Teller type of beta decay of Co^{58}. Our determination of the μ_{58}/μ_{60} ratio, however, does not decide between the two sets of μ_{60} measurements, but it shows that the separate measurements of μ_{58} and μ_{60} by the Oxford workers are internally consistent.

We are indebted to the University of Illinois low-temperature group for the availability of the liquid helium supply and to Dr. D. Mapother for many suggestions concerning liquid helium problems. To Dr. R. P. Hudson of the National Bureau of Standards, Washington, D. C., we are indebted for many valuable suggestions concerning adiabatic demagnetization techniques. We are also grateful to Mr. G. de Pasquali for performing chemical separations and analyses.

† Assisted by joint program of Office of Naval Research and the U. S. Atomic Energy Commission.

* At present on leave at Kamerlingh Onnes Laboratory, Leiden, Holland.

[1] Daniels, Grace, and Robinson, Nature **168**, 780 (1951); Bleaney, Daniels, Grace, Halban, Kurti, Robinson, and Simon, Proc. Roy. Soc. (London) **A221**, 170 (1954).

[2] M. Deutsch and G. Scharff-Goldhaber, Phys. Rev. **83**, 1059 (1951).

[3] We use the notation $5(\beta 1)4(\gamma 2)2(\gamma 20)$ to indicate that a nucleus of spin 5 undergoes β decay which carries 1 unit of angular momentum, to form a nucleus of spin 4 which then emits a γ ray which carries 2 units of angular momentum. . . .

[4] K. Strauch, Phys. Rev. **79**, 487 (1950).

[5] J. A. Spiers, National Research Council of Canada Publication No. 1925 (unpublished); N. R. Steenberg, Proc. Phys. Soc. (London) **A65**, 791 (1952); Cox, DeGroot, and Hartogh, Physica **19**, 1119 (1953).

[6] Daniels, Grace, Halban, Kurti, and Robinson, Phil. Mag. **43**, 1297 (1952).

[7] Poppema, Steenland, Beun, and Gorter, Physica **21**, 233 (1955).

Measurements on *K*-Particles from the Bevatron*

WARREN W. CHUPP, GERSON GOLDHABER, SULAMITH GOLDHABER, STEPHEN J. GOLDSACK,† JOSEPH E. LANNUTTI, FRANCES M. SMITH, AND FRANCIS H. WEBB

Radiation Laboratory, Department of Physics, University of California, Berkeley, California

(Received May 9, 1955)

AS an initial step in the study of *K*-particles, stacks of nuclear emulsions have been exposed at the Bevatron in two positions. (a) *Exposure in the direct proton beam* (proton energies 4.8 and 5.7 Bev): For this purpose the stacks were mounted on a plunging probe with a "lip target."[1] This probe assembly was plunged into the vacuum chamber during the last part of the accelerating cycle. (b) *Exposure to secondaries emitted at 90° to the target* (proton energies 4.8 and 6.1 Bev): Stacks were placed in a re-entrant well at a distance of about 10 inches from the target. (Time of flight for *K*-particles observed is about 10^{-9} sec.) A 0.1-inch aluminum wall was the only intervening material.

In 2.5 cm^3 of emulsion scanned to date, 35 *K*-particles and five τ mesons have been found. In Table I, mass measurements on 22 of these *K*-particles and three τ mesons are given. The mass measurements were obtained (a) by grain count *vs* range in the region of 1 to 3 cm residual range,[2] and (b) by "opacity" measurements[3] for short *K*-particle track lengths in the region of 0.5 to 1.5 cm residual range. Each of the above measurements was directly calibrated against protons. For

TABLE I. Measurements on *K*-particles and their secondaries.

	Mass m_θ			Secondary		
Particle	Ionization range	Const. sagitta	Dip angle	$p\beta$	b/b_p	I/I_0
K_1 [a]	1010±30 [c]	895±230	28°	...	...	
K_2 [a]		700±180	0°	189±25	0.89±0.04	
K_3 [a]	815±70 [c]	940±280	44°	...	...	
K_4 [a]	934±30 [c]	880±230	4.5°	185±20	1.14 ±0.06	
K_5 [a]	962±30 [c]	880±200	26°	150±30	~1.	
K_6 [a]	947±100 [c]	1460±370	56°	...	...	
K_7 [a]	820±60 [c]	...	17°	...	...	
K_8 [a]	875±40 [c]	1010±280	0°	86±8	0.968±0.04	
K_9 [a]	975±50 [c]	1320±380	no secondary found			
K_{10} [a]	988±45 [d]		7°	135±22		1.16±0.05
K_{11} [a]	938±125 [d]					
K_{12} [a]		795±190				
K_{13} [a]	846±75 [d]		18°			
K_{14} [a]	1035±70 [d]	690±170	17°			2.48±0.05
K_{15} [a]	1035±80 [d]		43°			
K_{16} [a]	941±40 [d]		18°			
K_{17} [a]	836±65 [d]		82°			
K_{18} [a]	875±70 [d]		63°			
K_{19} [a]	927±45 [d]		26°			
K_{20} [a]	901±45 [d]		24°			
K_{21} [b]	881±65 [d]		3°	160±20		1.19±0.03
K_{22} [b]		1280±330		135±24		1.17±0.07
			Q value (Mev)			
τ_1 [a]	...	...	82.8±6			
τ_2 [a]	...	1220±420	78.1±3			
τ_3 [b]	982±45 [d]	...	78.0±5			
τ_4 [b]	932±45 [d]	...	...			
τ_5 [a]	...	...	71.3±3			

[a] Found in wall exposure giving a time of flight of about 10^{-9} sec.
[b] Found in the direct proton beam. Time of flight is $1\times10^{-10}-3\times10^{-10}$ sec.
[c] Grain count *vs* range.
[d] Opacity (reference 3) *vs* range.

quick identification of K-particles, a constant sagitta measurement was carried out over the last 7 mm of residual range using the $P1$ cell scheme of Biswas *et al.*[4] with the cell scheme fed automatically into the microscope.[5] The weighted average of all mass measurements gives $936\,m_e \pm 11\,m_e$ for the K-particles observed. The measurements were checked for internal-external consistency and were found to be consistent. The mass value quoted above would indicate the presence of K-particles in our sample (presumably the $K_{\mu 2}$[6]) of a mass lighter than the τ mass ($965\,m_e$). As the ionization-range methods are the only ones contributing appreciably to the weighted average, a further possible systematic error cannot be excluded, however. We do not feel, therefore, that a mass different from the τ-meson mass is necessarily established by these measurements.

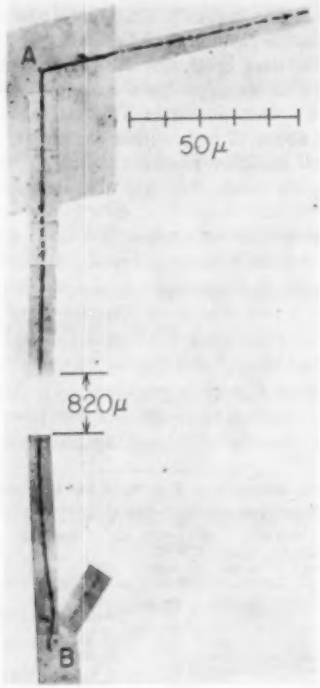

FIG. 1. Elastic scattering of K_1 from light element. K_1 scatters at A and decays at B into lightly ionizing secondary.

Multiple-scattering and ionization measurements were carried out on secondaries with dip angles less than 10°. The secondary of K_8 was identified to be an electron of 60 ± 6 Mev.[7] Table II gives the results of the blob count and multiple-scattering measurements on the secondary of K_8. Column 6, Table II gives the measured blob density for the secondary. For comparison we give in Column 7 the expected grain density for a μ meson corresponding to the measured $p\beta$. From this comparison it is clear that a much lighter particle (i.e., electron) is present. The secondary of K_{14} can be interpreted as being either a π from the alternate decay of the τ meson ($\tau^+ \rightarrow 2\pi^0 + \pi^+$) or a slow μ from the decay of a $K_{\mu 2}$. K_9 is a case where no secondary was found; there was also no Auger electron found in conjunction with this event. All the other secondaries are consistent with L-mesons or electrons. K_1 (see Fig. 1) undergoes an elastic scattering from a light nucleus (with visible recoil) in the emulsion. The scattering angle is $79° \pm 1°$ and the recoil angle is $55° \pm 5°$ with the incident direction. The residual range of the K_1 particle after the scattering is 960μ, corresponding to an energy of about 10.5 Mev, which is well above the Coulomb barrier.

Of the 35 K-particles found to date, 34 (presumably positive) decayed into single charged secondaries. Only one, K_9, can be interpreted to be negative since no secondary has been found. No K-particles giving rise to stars at the end of the range have been found in this survey.

We are greatly indebted to Edward J. Lofgren and the Bevatron crew for their help and patience in carrying out the exposures. We also wish to thank Miss S. Livingston, Mrs. L. Shaw, and Mrs. C. Toche for their help and painstaking work in scanning the emulsions.

TABLE II. Measurements on K_8 secondary.

Plate	Length per plate (mm)	Distance from decay point (mm)	Average dip angle	$p\beta$ Mev/c	b/b_p	Expected g/g_p for μ meson
8–18	8.9	2.2	~0°	56±8	0.968±0.04	1.50
8–18	···	6.7	5°	37±5	0.960±0.04	1.97
8–17	2.6	9.5	13°	38±8	0.947±0.05	1.93
8–16	1.9	12.5	17.5°	31±7	0.88 ±0.05	2.24
8–15	1.5	14.1	22°	38±10	1.01 ±0.09	1.93
8–14	1.1	15.4	29°	28±8	1.05 ±0.10	2.42
8–13	0.9	16.4	32.5°	29±10	~1	2.34
8–12	0.4	17.0	55°	10±4	~1	···

* This work was done under the auspices of the U. S. Atomic Energy Commission.
† Assisted by the Office of Naval Research; now at the Physics Department, University of Birmingham, Birmingham, England.
[1] E. McMillan, Rev. Sci. Instr. **22**, 117 (1951).
[2] M. Tchang-Fong Huang, Compt. rend. 238, 1790 (1954).
[3] The "opacity" A is given by $A = 1 - G$, where G is the integral gap length. H. H. Heckman (private communication).
[4] Biswas, George, and Peters, Proc. Indian Acad. Sci. **38**, 418 (1953).
[5] S. J. Goldsack and G. Goldhaber, Phys. Rev. **98**, 284(A) (1955). Further details on the cell-scheme mechanism will be published elsewhere.
[6] Leprince-Ringuet, Proceedings of the Fifth Rochester Conference on High-Energy Physics, 1955 (to be published).
[7] The first example of this type of decay was found by Friedlander, Keef, Menon, and Van Rossum, Phil. Mag. **45**, 1043 (1954). From this and further cases reported at the 1955 Rochester High-Energy Conference, a three-body decay process can be inferred.

Nuclide 99^{254}†

B. G. Harvey, S. G. Thompson, G. R. Choppin, and A. Ghiorso

Radiation Laboratory, University of California, Berkeley, California

(Received May 9, 1955)

THE nuclide 99^{254} has previously been reported[1,2] and found to decay[2,3] with a half-life of 36 hours by emission of β^- particles. Further investigation has revealed the existence of another isomer of 99^{254} which decays almost entirely by emission of alpha particles. The 36-hour isomer has been found to exhibit electron-capture branching to produce Cf^{254}.

1. *The long-lived isomer.*—Samples of the 20-day 6.6-Mev alpha-emitting 99^{253} subjected to neutron bombardment were shown by alpha pulse analysis to contain a nuclide emitting 6.44±0.01 Mev alpha particles. This new alpha radioactivity showed no decrease in intensity during 3 months, so that the nuclide responsible for it must have a half-life longer than about 2 years.

Chemical purification of the 99^{253} by the method of ion-exchange elution, using Dowex-50 cation resin and ammonium α-hydroxy-isobutyrate as eluant,[4] showed that the 6.44-Mev alpha emitter could not be separated from element 99.

Its assignment, based on the systematics of alpha radioactivity,[5,6] was most logically to mass 254. This assignment was confirmed by collecting recoil nuclei from a very thin sample of the new alpha emitter. These daughter nuclei were shown to decay, by emission of β^- particles, with a half-life of approximately 3 hours. This radiation is characteristic of Bk^{250}.[7]

The absence of any 7.2-Mev alpha particles of 100^{254} [1,2,3,8] in equilibrium with this long-lived isomer of 99^{254} shows that the partial half-lives of the latter species for both β^- decay and isomeric transition to the 36-hour isomer are more than 100 times longer than the alpha half-life. It is perhaps more likely that the 36-hour isomer is the metastable state, and it will be convenient provisionally to refer to it as 99^{254m}.

2. *Electron capture in* 99^{254m}.—Preliminary experiments[9] showed that a californium isotope decaying by spontaneous fission, with no detectable emission of alpha particles, grew into very carefully purified samples containing 99^{253}, 99^{254}, 99^{254m}, and 99^{255}. The californium exhibited a half-life of 85±15 days. This observation has since been repeated and confirmed with much larger amounts of activity.

The californium isotope responsible for such a short-lived spontaneous fission decay is most likely of even mass, and is therefore probably Cf^{254}, since Cf^{250} and Cf^{252} are already known.[7,10,11] Some Cf^{256} might have been formed by electron capture decay of the (unknown) nuclide 99^{256}, which might have been present in the sample. However, 99^{256} is expected to be short-lived,[12] and any Cf^{256} produced by its electron-capture decay would have been removed in the initial purification of the 99 sample. Samples containing only 99^{253} and 99^{254} exhibit only a very small spontaneous fission activity. The Cf^{254} must therefore grow from the 36-hour 99^{254m}, by the electron-capture process, and not from the 99^{254}. The amount of Cf^{254} produced by a known amount of 99^{254m} gave a value of 1000 for the ratio of β^- decay to electron capture.

† This work was performed under the auspices of the U. S. Atomic Energy Commission.

[1] Harvey, Thompson, Ghiorso, and Choppin, Phys. Rev. **93**, 1129 (1954).
[2] Fields, Studier, Mech, Diamond, Friedman, Magnusson, and Huizenga, Phys. Rev. **94**, 209 (1954).
[3] Choppin, Thompson, Ghiorso, and Harvey, Phys. Rev. **94**, 1080 (1954).
[4] Choppin, Harvey, and Thompson (unpublished work).
[5] Perlman, Ghiorso, and Seaborg, Phys. Rev. **77**, 26 (1950).
[6] Ghiorso, Thompson, Higgins, and Harvey, Phys. Rev. **95**, 293 (1954).
[7] Ghiorso, Thompson, Choppin, and Harvey, Phys. Rev. **94**, 1081 (1954).
[8] Studier, Fields, Diamond, Mech, Friedman, Sellers, Pyle, Stevens, Magnusson, and Huizenga, Phys. Rev. **93**, 1428 (1954).
[9] Ghiorso, Harvey, Choppin, and Thompson (unpublished work).
[10] Diamond, Magnusson, Mech, Stevens, Friedman, Studier, Fields, and Huizenga, Phys. Rev. **94**, 1083 (1954).
[11] Thompson, Ghiorso, Harvey, and Choppin, Phys. Rev. **93**, 908 (1954).
[12] Glass, Thompson, and Seaborg, J. Inorg. and Nuclear Chem. **1**, 3 (1955).

Absorption Experiments Involving Heavy Mesons

T. D. Lee

Columbia University, New York, New York

(Received May 10, 1955)

THE purpose of this note is to point out that several interesting properties of some of these new elementary particles may be obtained by performing certain absorption experiments.

Absorption of K^- *by deuteron.*—We consider the following reactions:

$$K^- + d \rightarrow \Sigma^0 + \pi^- + p, \qquad (A_1)$$

$$K^- + d \rightarrow \Sigma^- + \pi^0 + p, \qquad (A_2)$$

$$K^- + d \rightarrow \Sigma^- + p. \qquad (B_1)$$

The reactions (A_1) and (A_2) are of interest because they may give a direct verification as to whether in the strong interactions of these new particles the total isotopic spin is a good quantum number or not. It may be emphasized that while *charge independence* has become a fundamental principle used in almost all recent theoretical analyses of these particles,[1] no evidence as to its validity concerning these particles has yet been established. We note that if the total

isotopic spin is conserved and if we assume that (a) there exists no charged particle of about the same mass as Λ^0 and (b) there exists no doubly charged particle of about the same mass as either Σ^- or K^-, then from the known reactions,[2]

$$\pi^- + p \rightarrow \Lambda^0 + K^0,$$
$$\pi^- + p \rightarrow \Sigma^- + K^+,$$

it is necessary to assume that the isotopic spin values for these particles are

$$I_\Lambda = 0, \quad I_K = \tfrac{1}{2}, \quad \text{and} \quad I_\Sigma = 1,$$

which is precisely the Gell-Mann scheme.[3] Thus, charge independence would imply that the differential cross sections for the above reactions (A_1) and (A_2) are the same.

$$\sigma(A_1) = \sigma(A_2).$$

On the other hand, information concerning the spins of K^- and Σ^- can be obtained by performing the reaction (B_1) together with its inverse reaction:

$$\Sigma^- + p \rightarrow K^- + d. \qquad (B_2)$$

From the principle of detailed balance the ratio of cross sections for these two reactions gives immediately the ratio $(2J_K+1)/(2J_\Sigma+1)$ with J_K and J_Σ as the spins of K^- and Σ^-, respectively.

Charge independence may also be verified by other reactions from K^- and d. However, they all involve some reactions with too many neutral particles as resultants, which make these reactions much harder to detect.

Absorption of K^- by He^4 or C^{12}.—It is also possible to verify the validity of charge independence by examining the absorption of K^- by He^4. We consider the following reactions:

$$K^- + He^4 \rightarrow \Sigma^0 + H^3, \qquad (C_1)$$
$$K^- + He^4 \rightarrow \Sigma^- + He^3, \qquad (C_2)$$
$$K^- + He^4 \rightarrow \Lambda^0 + H^3 + \pi^0, \qquad (D_1)$$
$$K^- + He^4 \rightarrow \Lambda^0 + He^3 + \pi^-, \qquad (D_2)$$
$$K^- + He^4 \rightarrow \Sigma^0 + He^3 + \pi^-, \qquad (E_1)$$
$$K^- + He^4 \rightarrow \Sigma^- + He^3 + \pi^0. \qquad (E_2)$$

If charge independence were true, the differential cross sections of the above reactions are related by

$$\sigma(C_2) = 2\sigma(C_1),$$
$$\sigma(D_2) = 2\sigma(D_1),$$
$$\sigma(E_1) = \sigma(E_2).$$

The same relations between these reactions still hold if one uses C^{12} instead of He^4 and adds two α particles to the right-hand sides of the above reactions.

The author wishes to thank Professor J. Steinberger, Professor R. Serber, and Professor C. N. Yang for discussions.

[1] See A. Pais, Proceeding of the Fifth Annual Rochester Conference on High-Energy Physics (to be published) for a review of these analyses.
[2] Fowler, Shutt, Thorndike, and Whittemore, Phys. Rev. **93**, 861 (1954).
[3] M. Gell-Mann, Phys. Rev. **93**, 933 (1953).

Further Observations of Negative K Mesons*

J. Hornbostel and E. O. Salant
Brookhaven National Laboratory, Upton, New York
(Received May 16, 1955)

CONTINUED examination of the emulsions for which observations of negative K mesons have been reported[1] has revealed 22 such particles producing stars at the end of their range. Measurements of the masses of those particles are presented below.

The experimental arrangement was like that sketched earlier,[2] but with the following differences: the proton energy was 2.8 Bev, the collimator aperture was narrowed to 1 inch, the mesons incident on the emulsions were emitted at $(4\pm1)°$ to the proton beam, and a magnet M (10 000 gauss) was interposed between the collimator and the stack of emulsions. The masses of the K^- mesons have been determined from their initial momenta and their ranges in the emulsions.

The mean momentum p of the meson beam was established in two ways. One way depended on measurements of the Cosmotron's magnetic field and the locations and orientations of target and collimator. This gave (310 ± 4) Mev/c for p; the error is due mainly to uncertainty in the value of the Cosmotron's field strength. The other way depended on the deflection of the negative pion beam by the magnet M; for this the collimator was narrowed to $\frac{1}{4}$ inch and the deflection was measured by locating the displaced pion beam in the emulsions. The correlation between p and deflection was established by the wire method to an accuracy of 0.5 percent. This procedure gave (316 ± 4) Mev/c for p; the error is due mainly to the statistical uncertainty in locating the beam's center in the emulsions.

An average of the two methods is taken, namely $p=(313\pm3)$ Mev/c. The average spread in momentum is ±8 Mev/c.

The emulsions were conditioned before packing in an atmosphere of 60 percent relative humidity. The spread in K^- ranges is entirely consistent with a unique mass value and the average spread in momentum. The average range of the K^- mesons is (45.8 ± 0.8) mm, a figure that includes a small allowance for packing material and a correction for distortion. Masses were computed with the range-energy relationship of

Baroni, Castagnoli, Cortini, Franzinetti, and Manfredini corrected for the different type and density of our emulsions.[3]

The average value of the K^- mass is found to be $(931\pm24)m_e$. The stated error is a standard deviation, calculated from the following contributions: from uncertainty in momentum, 16 m_e; from uncertainties in range, due to (a) statistical uncertainty in average range, 8 m_e, (b) emulsion distortion, 10 m_e, (c) uncertainty of moisture content, 7 m_e; from inaccuracy of range-energy relation, 9 m_e.

Clearly, the value is not accurate enough to decide whether the mass of these K^- mesons is or is not the same as the τ mass 965.5 m_e.[4] It is consistent with the recent $K_{\mu 2}$ mass, 941 m_e.[5]

Besides these K^- mesons coming to rest, five making stars in flight have been identified, giving a collision mean free path of 20 cm, in approximate agreement, as noted previously,[1] with the geometrical mean free path (27 cm). Although tracks possibly due to ρK mesons (K particles that stop without producing visible products[6]) have also been observed in these emulsions, they do not appear numerous enough to alter that agreement significantly.

We take pleasure in acknowledging our indebtedness to the Cosmotron staff, to R. M. Sternheimer for computing the Cosmotron trajectories; to W. L. Homer for surveying the relevant positions, to J. W. Quinn for help in the experiments, and to M. Bracker, B. M. Cozine, A. C. Lea, J. D. Leek, and E. R. Medd for microscopy.

* Work performed under the auspices of the U. S. Atomic Energy Commission.

[1] J. Hornbostel and E. O. Salant, Phys. Rev. **98**, 218 (1955).
[2] J. Hornbostel and E. O. Salant, Phys. Rev. **93**, 902 (1954).
[3] Baroni, Castagnoli, Cortini, Franzinetti, and Manfredini (unpublished); preprint circulated by CERN, Geneva.
[4] Report of Committee on τ Mesons, Nuovo cimento **12**, Suppl. 2, 419 (1954).
[5] L. Leprince-Ringuet, Proceedings of the Fifth Rochester Conference on High Energy Physics, 1955 (to be published), p. 105.
[6] Report of Committee on K Particles, Nuovo cimento **12**, Suppl. 2, 433 (1954).

PHYSICAL REVIEW VOLUME 99, NUMBER 1 JULY 1, 1955

Proceedings of the American Physical Society

Minutes of the 1955 Spring Meeting of the Ohio Section at Ohio Wesleyan University, Delaware, Ohio, April 22 and 23, 1955

THE regular spring meeting of the Ohio Section of the American Physical Society was held at Ohio Wesleyan University, Delaware, Ohio, on Friday and Saturday, April 22 and 23, 1955. Friday morning was spent in viewing and judging the projects prepared by high school students of the state for the Junior Ohio Academy of Science. About one-third of the projects were in the field of physics. It is hoped that this attention will encourage these students to follow this interest in college.

The subject for discussion on Friday afternoon, "Recent Developments in the Application of Nuclear Energy," proved of such wide interest that the sections of physics and chemistry of the Ohio Academy of Science joined in our meeting. This gave us large numbers for the following invited papers: "Principles of Reactor Operation" by R. J. Stephenson, College of Wooster; "Disposal of Radioactive Wastes" by F. C. Mead, Jr., The Monsanto Chemical Company; "Radioactive Isotopes in Medicine" by G. W. Callendine, Jr., Ohio State University Medical Center; and "Food Sterilization by Radiation" by R. F. Robinson, The Battelle Memorial Institute, Columbus, Ohio.

On Saturday morning, eleven contributed papers were presented. No abstracts were provided for the following three: "Radio Detection of Meteors Using Standard Laboratory Equipment" by Horace T. Castillo, Wright Air Force Development Center; "A Study of the Spectroscopic Binary 5 Lacertae" by Philip C. Stanger, Ohio Wesleyan University; and "The Air Force Institute of Technology Engineering Curriculum" by William J. Price, U. S. Air Force Institute of Technology.

This being the annual business meeting of the Ohio Section, the following officers were chosen for the year 1955–1956; Chairman, Richard N. Thayer, Lamp Development Laboratory, General Electric Company, Cleveland, Ohio; Vice-Chairman, Edward S. Foster, Jr., University of Toledo, Toledo, Ohio; and Secretary-Treasurer, Leon E. Smith, Denison University, Granville, Ohio.

Abstracts of eight contributed papers follow.

Leon E. Smith, *Secretary*
The Ohio Section
American Physical Society
Granville, Ohio

Gamma-Ray Yield from Natural Silicon Bombarded with Protons.* MILTON R. SEILER, JOHN N. COOPER, AND J. C. HARRIS, *Ohio State University.*—An investigation of the gamma-ray yield produced by the bombardment of natural silicon with protons has been undertaken for proton energies between 400 and 1200 kev. Natural silicon is composed of three stable isotopes of mass numbers 28, 29, and 30 which have relative abundances of 0.92, 0.05, and 0.03, respectively. Proton captures by these nuclei yield P^{29}, P^{30}, and P^{31}. Of these the first two are unstable and decay by positron emission. Data have been taken with both thick and thin targets of SiO prepared by vacuum evaporation. Prominent gamma-ray resonances were observed for proton energies of 414, 500, 622, 675, 698, 703, 732, 760, 778, 944, and 989 kev. The two lowest resonances are in excellent agreement with the data of Tangen[1] who investigated proton capture resonances at energies up to 500 kev. Work is currently in progress on the bombardment of separated silicon-29.

* Supported in part by the U. S. Atomic Energy Commission through a contract with the Ohio State University Research Foundation.
[1] R. Tangen, Kgl. Norske Videnskab. Selskab, Skrifter NR 1 (1946).

Technique for the Detection of Nuclear Resonances by Observing Residual Radioactivity.* ROBERT T. SMITH, JR., J. C. HARRIS, AND JOHN N. COOPER, *Ohio State University.*—Apparatus has been designed, constructed, and tested for the detection of weak nuclear resonances leading to radioactive products. It is used for the study of short-lived positron emitters produced by proton capture. The apparatus utilizes a rotating target and a photomultiplier detector. Preliminary measurements have been made on Al^{25} and Al^{26} formed by bombarding magnesium with protons. Compared with apparatus previously used here[1] for studying these reactions, the new apparatus has many advantages. Counting efficiency is greatly improved by substituting the photomultiplier for a Geiger counter since a larger solid angle is used, there is less positron loss by absorption, and the scintillation detector is more sensitive. The rotating target permits the use of larger beam currents. Furthermore, a mathematical treatment reveals that the rotating target technique permits detection of a larger fraction of the total number of radioactive nuclei formed than does the technique of building up an equilibrium concentration and then counting decays over several half-lives.

* Supported in part by the U. S. Atomic Energy Commission through a contract with the Ohio State University Research Foundation.
[1] Taylor, Russell, and Cooper, Phys. Rev. **93**, 1056 (1954).

Emission Constant of Ac^{227}. G. R. GROVE AND L. N. RUSSELL,* *Monsanto Chemical Company.*†—The emission constant of actinium was determined. The emission content is defined as the number of roentgens per hour at one meter of gamma radiation from a one-curie source. Activity of the sample was 655 Mc, determined by repeated calorimeter measurements over a period of about 180 days which is the time required for the secular equilibrium to be established. Purity of the sample was established by pulse-height analysis and absorption-coincidence counting. The dosage rates at various distances from the source were measured with a calibrated Victoreen *r*-meter. After corrections for scattering and leakage of the meter were made a value of 225 mr/hr/curie at one meter was obtained. The accuracy of this value is believed to be of the order of 5%.

* Present address: Ohio Wesleyan University.
† Monsanto Chemical Company operates for the U. S. Atomic Energy Commission.

Gaseous Thermal Diffusion. G. R. GROVE, K. W. FOSTER, AND R. E. VALLEE, *Monsanto Chemical Company.**—Several thermal columns were designed and are being used in a study of the effects of variations of the parameters of the theory of the thermal diffusion process.[1] These columns are 12 feet long with access ports spaced 12 inches apart, and they have inside diameters ranging from 1.00 to 1.61 inches. An electrically-heated molybdenum center wire was used to provide a radial temperature gradient for each column with the outer wall temperature held constant by means of water cooling. Preliminary data for the transport coefficients and shape factors of the columns have been obtained. The time and pressure dependence of the separation factor of each column were determined for mixtures of hydrogen and helium and for natural neon. The isotopic constituents of the separated gas mixtures were determined by mass-spectrometric analyses and the results are in good quantitative agreement with the parameters of the theory. Also resulting values for the thermal diffusion constants at a center-wire temperature of 900°C are within reasonable agreement with theoretical values although a temperature dependence has been observed.

* Monsanto Chemical Company operates for the U. S. Atomic Energy Commission.
[1] R. C. Jones and W. H. Furry, Revs. Modern Phys. **18**, 151 (1946).

Use of Characteristic Curves in the Study of Electrochemical Systems. FREDERICK H. GILES, *Bowling Green State University.*—When current flow is initiated through an electrolytic cell, the transient effects, as well as the steady-state conditions, show a dependence upon the parameters of potential and resistance external to the cell. Voltage and current data, obtained by using varied settings of the external parameters, may then be plotted in a manner analogous to the familiar i *vs* V curves employed in vacuum tube analysis. These "characteristic curves" can then be used to predict the behavior of the current and potential in any subsequent transient, as well as to give direct information concerning the source and size of any potentials and resistances which arise in the cell after current flow has begun. Data obtained using copper anodes in phosphoric acid illustrate the procedure.

Stability of the Transuranic Elements. R. KLINGENSMITH, E. DALLY, AND G. ARFKEN, *Miami University.*—The alpha, beta, and fission stability of the nuclides through $Z = 106$ have been studied by extrapolating the results of alpha and spontaneous fission systematics. Nuclear masses have been calculated for the even-even nuclides, the beta stable region determined, and partial half-lives predicted.

Use of Clays for Disposal of Radioactive Wastes. WILLIAM L. R. RICE, *U. S. Air Force Institute of Technology.*—It is proposed to use clay minerals to dispose of radioactive waste solutions. The solutions would be contacted with the clay and the radioactive ions adsorbed on the clay by an ion-exchange process. Following adsorption, the ions would be firmly bound within the clay by heat treatment to give a ceramic substance impervious to the action of leaching solutions.[1]

A study was made of the optimum conditions for adsorption of lanthanum on montmorillonite clay. It was found that three important variables are lanthanum concentration, clay-to-water ratio, and *p*H of solution. Optimum conditions for adsorption on montmorillonite occur at a clay concentration of about 5000 ppm and at a solution *p*H of about 5.0. The adsorption increases with increasing lanthanum concentration, becoming constant at saturation of the clay.

Preliminary results are encouraging and would indicate that the clay technique would be an inexpensive and efficient method for disposal of radioactive wastes.

[1] Ginell, Martin, and Hatch, Nucleonics 12, 14–18 (1954).

Relative Stability of Even-Numbered Isobars. J. D. KURBATOV AND J. W. DOWNS,* *Ohio State University.*—The nuclear energy of even-numbered isobars has been evaluated from disintegration data of intermediate odd-odd radioactive nuclei and from masses of stable isobars. The survey showed that eight species for which the decay scheme is well estab-

lished, disintegrate by positron and electron emission. These provide information for nuclear energy differences. The stable isobars of these mass numbers are the nuclei which best compensate Coulomb and symmetry energies, such that the difference between nuclear energies is the smallest. For all other stable isobars for which experimental data are available now the nuclear energy difference is higher. The following general characteristics were established: (1) Stable isobar series of the same $T\xi$ have smaller nuclear energy content for the higher Z-species than the isobars of higher $T\xi$ for mass numbers less than the mass number of the intermediate odd-odd species, which decays by two modes. (2) Series of stable isobars of the same $T\xi$ with mass numbers higher than the intermediate odd-odd radioactive nucleus, which disintegrate by two modes, have higher nuclear energy content for the higher Z than the isobars with higher $T\xi$. For example, the nuclear energy of $_{31}Ge^{70}$ is less than that of $_{30}Zn^{70}$. The isobar $_{33}As^{74}$ disintegrates by two modes into Ge^{74} and Se^{74}. The nuclear energy of $_{36}Kr^{78}$ is higher than that of $_{34}Se^{78}$.

* Major J. W. Downs, U. S. Air Force at present assigned to Ohio State University for graduate study.

Minutes of the 1955 Spring Meeting of the New York State Section at Buffalo, May 13 and 14, 1955

THE thirty-third meeting of the New York State Section was held at Buffalo, New York, on May 13 and 14, with The University of Buffalo and Roswell Park Memorial Institute acting jointly as hosts to about 100 registrants. The Friday morning session was devoted to two invited papers and six contributed papers; the Friday afternoon session was devoted to three invited papers. In the evening, following dinner and the business meeting, members of the section joined with the University of Buffalo Chapter of Sigma Xi for a lecture on "Crashes" by Mr. Edward Dye, a member of the research staff of Cornell Aeronautical Laboratory in Buffalo.

The Saturday morning session was held at Roswell Park Memorial Institute. Three papers by members of the Institute staff preceded a tour of the research laboratories.

At the business meeting, the following officers were elected for two-year terms: Chairman, Harold E. Way, Union College; Vice-Chairman, George W. Hazzard, General Electric Research Laboratory; Secretary, Darin H. Tomboulian; Treasurer, William I. Caldwell, Taylor Instrument Company. Elected to the Executive Committee for four-year terms were Monica Healea, Vassar College, and Kenneth Moore, Rensselaer Polytechnic Institute; for a two-year term, to fill the vacancy resulting from the election of Hazzard to the vice-chairmanship, Oran Miller, Eastman Kodak Company.

Titles of the invited papers, and abstracts of the contributed papers, are listed below.

L. W. PHILLIPS, *Secretary*
New York State Section
The University of Buffalo
Buffalo 14, New York

Invited Papers

Education of Physicists in an Engineering World. G. W. HAZZARD, *General Electric Research Laboratory.*

Information Theory—Bit by Bit. E. T. WELMERS, *Bell Aircraft Corporation.*

New Sintered-Plate Nickel-Cadmium Storage Battery. L. GRANT HECTOR, *The Sonotone Corporation.*

Sun and Cosmic Rays. P. MORRISON, *Cornell University.*

Monte Carlo Methods for the Study of Cell Populations. J. G. HOFFMAN, *Roswell Park Memorial Institute.*

Electronic Stopping Power and Radiation Damage. N. A. BAILY, *Roswell Park Memorial Institute.*

Magnetic Susceptibilities of Biological Material. D. L. WOERNLEY, *Roswell Park Memorial Institute.*

Flying-Spot Microscope and Its Application to the Study of Cell Sizes. H. C. BOX, *Roswell Park Memorial Institute,* AND A. RUSSEK, *The University of Buffalo.*

Contributed Papers

A Systematic g-Shift for Free Electrons. J. G. CASTLE, JR., *The University of Buffalo.*—Free-electron spin-resonance absorption in thermal carbon blacks has been observed and can be attributed to conduction carriers. The single line spectra of such blacks have much sharper lines than those of soft carbon powder[1] and as such are more suitable for studying g-values and line shapes. The lines are symmetric, closely Lorentz-shaped, and show an intensity of absorption similar to those in soft carbons, namely, zero at $Ht = 1400°C$, and readily observed magnitude for Ht-values from 1600°C to 3000°C. However, the line width and g-value have a striking dependence on Ht, going from 2 gauss and 2.004 at 1600°C to about 8 gauss and 2.014 at 3000°C. It is expected that the strong g-shift is due to spin-orbit coupling for the conduction carriers in the carbon blacks.

[1] J. G. Castle, Jr., Phys. Rev. **95**, 846 (1954).

Using the Snooperscope Tube with the Spectrometer. DONALD E. DEAN, *New York State College for Teachers.*—The purpose of this instrument is to demonstrate visually to the student the near ultraviolet and infrared as a continuation of the visible spectrum. When constructing the instrument a jeweler's eyepiece was first mounted to the tube in a hard rubber shell and focused on the fluorescent screen of the infrared tube. Next the ocular and crosshairs of the spectrometer were removed. By use of the filter holder of the tube and a cylindrical adapter of hard rubber, the tube was mounted to the telescope of the spectrometer. A Sola 3000-volt gas-tube transformer was used for a high potential between photoemissive and fluorescent screens. Both a thin glass mounted grating and a prism were used for dispersion. When a Variac transformer was used to reduce continually the brightness of a projection lamp, the visible portion of the spectrum com-

pletely dissappeared before the infrared. A sodium lamp gave several lines in the infrared and a mercury lamp a strong line in the ultraviolet.

An Attempt to Geometrize Electromagnetic Theory. R. H. PENFIELD, *Harpur College.*—In recent work Einstein has considered g_{ik}'s which are neither symmetric nor antisymmetric. However, when one considers the line element $ds^2=g_{ik}dx^i dx^k$, the antisymmetric part makes no contribution to the line element and therefore does not affect the geodesics. Therefore, it seemed desirable to investigate whether equations similar to Maxwell's could be obtained from the requirement that the g_{ik}'s should be completely antisymmetric and the $dx^i dx^k$ should anticommute. By restricting the affine connection two of Maxwell's equations can be obtained readily. However, it appears that the two remaining equations are not contained in the theory mainly due to the nonsymmetric nature of Maxwell's equations.

A Transmission-Line Demonstration. M. J. PRYOR, *New York State College for Teachers.*—In this demonstration a comparison is made between transmission of electrical energy at generated and at stepped up potentials. The purpose is to vividly show the advantage of transformer use at the time when transformers are first discussed in class. The potentials used are such that the exhibit is set up and left for the students to operate. A projection-lamp transformer connected to the service line substitutes for a six-volt ac generator. Two pairs of lines lead directly from the "generator" to a six-volt, 18-ampere projection lamp which is the load. Two other pairs of lines are "high-tension lines" with the potential at 120 volts. Transformers like the first one mentioned, produce the step-up and step-down in the "generated" potential. These lines, in turn, operate the same lamp. The lamp is observed to be completely lighted with wire but one twenty-fifth the cross section of wire which was unsatisfactory for direct transmission. In class use the differences in brilliance give graphic evidence of the difference in effectiveness. For individual inspection, there are meters which give current and potential at each important position in the transmission system. Little difference results from having all lines connected to the lamp. This makes it possible to operate the entire demonstration from the "generator" position.

Fused Silica Dielectric Measurements at Low Frequencies. J. P. SACKINGER, *Corning Glass Works.*—Measurements have been made of the dielectric constant and loss tangent at low frequencies on several samples of Corning fused silica and one sample of fused quartz. All measurements are taken at room temperature. A value of 3.64 ± 0.07 is found for the dielectric constant for all samples. No change in dielectric constant is found between 100 cycles and 20 kilocycles per second. Values of loss tangent range from about 1×10^{-4} to 1.5×10^{-4} for Corning fused silica samples. The effects of various electrode materials and methods of application on loss tangent data will be discussed.

Kinetic Analysis of Thyroidal Iodide Trapping and Binding in the Human Subject. ROSALYN S. YALOW AND SOLOMON A. BERSON, *Veterans Administration Hospital*—The kinetics of tracer mixing in multicompartmental systems has been presented in its theoretical aspects by Sheppard and Householder[1] and several special cases have been reviewed by Solomon.[2] This type analysis cannot be applied to open multicompartmental systems in which available data is limited to only two compartments. This report describes a graphic method for analysis of transfer rates between a terminal and its adjacent compartment from observations restricted to these two compartments in an otherwise unconstrained multicompartmental system. This method is applied to the determination of the rates of thyroidal iodide trapping and binding *in vivo*. The outflux rate constant, λ_{TP}, is given by the relation $\lambda_{TP}=(dT'/dt)/(P'T_s-T')-(dR/dt)/R$, where T' is total thyroidal radioactivity, P' is concentration of plasma radioactivity, T_s is the ratio, T'/P', at distribution equilibrium, and R is the total radioactivity remaining in the body at any time t. Results indicate that iodide trapping is the rate limiting process in thyroidal iodide accumulation.

[1] C. W. Sheppard and A. S. Householder, J. Appl. Phys. **22**, 510 (1951).
[2] A. K. Solomon, J. Clin. Invest. **28**, 1297 (1949).

CONTENTS—continued

Letters to the Editor:

Possible Mathematical Formulation of the Gell-Mann Model for New Particles . . . . . Bernard d'Espagnat and Jacques Prentki 328

Neutron K^0-Mesons . . . . . Robert W. Birge, Roy P. Haddock, Leroy T. Kerth, James R. Peterson, Jack Sandweiss, Donald H. Stork, and Marian N. Whitehead 329

14-Mev (n,α) Cross Sections in Zirconium. I . . . . . J. E. Brolley, Jr., M. E. Benker, D. R. F. Cochran, R. L. Henkel, J. P. Minn, and J. W. Starner 330

14-Mev (n,α) and (n,p) Cross Sections in Zirconium. II . . . . . A. H. Armstron and J. E. Brolley, Jr. 330

14-Mev (n,α) Cross Section in Zirconium. III . . . . . F. L. Ribe and R. W. Davis 331

Resonances in the Elastic Scattering of Protons . . . . . B. B. Kinsey 332

Systematics of Neutron Capture Cross Sections . . . . . B. G. Harvey 333

Ratios of Magnetic Moments of Cs^{133} and Cs^{135} . J. C. Wheatley, D. F. Griffing, and R. D. Hill 334

Measurements on K-Particles from the Bevatron . . . . . Warren W. Chupp, Gerson Goldhaber, Sulamith Goldhaber, Stephen J. Goldsack, Joseph E. Lannutti, Frances M. Smith, and Francis H. Webb 335

Isotope 59^{144} . . . . . B. G. Harvey, S. G. Thompson, G. R. Choppin, and A. Ghiorso 337

Absorption Experiments Involving Heavy Mesons . . . . . T. D. Lee 337

Further Observations of Negative K Mesons . . . . . J. Hornbostel and E. O. Salant 338

Proceedings of the American Physical Society:

Minutes of the 1955 Spring Meeting of the Ohio Section at Ohio Wesleyan University, Delaware, Ohio, April 22 and 23, 1955 339

Minutes of the 1955 Spring Meeting of the New York State Section at Buffalo, May 13 and 14, 1955 341